



cells

Special Issue Reprint

Molecular and Cellular Mechanisms of Cancers

Glioblastoma II

Edited by
Javier S. Castresana and Bárbara Meléndez

mdpi.com/journal/cells



Molecular and Cellular Mechanisms of Cancers: Glioblastoma II

Molecular and Cellular Mechanisms of Cancers: Glioblastoma II

Guest Editors

Javier S. Castresana
Bárbara Meléndez



Basel • Beijing • Wuhan • Barcelona • Belgrade • Novi Sad • Cluj • Manchester

Guest Editors

Javier S. Castresana
Department of Biochemistry
and Genetics
University of Navarra
Pamplona
Spain

Bárbara Meléndez
Department of Pathology
Virgen de la Salud Hospital
Toledo
Spain

Editorial Office

MDPI AG
Grosspeteranlage 5
4052 Basel, Switzerland

This is a reprint of the Special Issue, published open access by the journal *Cells* (ISSN 2073-4409), freely accessible at: www.mdpi.com/journal/cells/special_issues/glioblastoma.II.

For citation purposes, cite each article independently as indicated on the article page online and using the guide below:

Lastname, A.A.; Lastname, B.B. Article Title. <i>Journal Name</i> Year , <i>Volume Number</i> , Page Range.
--

ISBN 978-3-7258-2936-1 (Hbk)

ISBN 978-3-7258-2935-4 (PDF)

<https://doi.org/10.3390/books978-3-7258-2935-4>

© 2024 by the authors. Articles in this book are Open Access and distributed under the Creative Commons Attribution (CC BY) license. The book as a whole is distributed by MDPI under the terms and conditions of the Creative Commons Attribution-NonCommercial-NoDerivs (CC BY-NC-ND) license (<https://creativecommons.org/licenses/by-nc-nd/4.0/>).

Contents

About the Editors	vii
Preface	ix
Javier S. Castresana and Bárbara Meléndez Glioblastoma Biology, Genetics and Possible Therapies Reprinted from: <i>Cells</i> 2023 , <i>12</i> , 2063, https://doi.org/10.3390/cells12162063	1
Natali Joma, Issan Zhang, Germanna L. Righetto, Laura McKay, Evan Rizzel Gran and Ashok Kakkar et al. Flavonoids Regulate Redox-Responsive Transcription Factors in Glioblastoma and Microglia Reprinted from: <i>Cells</i> 2023 , <i>12</i> , 2821, https://doi.org/10.3390/cells12242821	5
Hera Hasan, Mohammad Afzal, Javier S. Castresana and Mehdi H. Shahi A Comprehensive Review of miRNAs and Their Epigenetic Effects in Glioblastoma Reprinted from: <i>Cells</i> 2023 , <i>12</i> , 1578, https://doi.org/10.3390/cells12121578	25
Carolin Kubelt, Dana Hellmold, Daniela Esser, Hajrullah Ahmeti, Michael Synowitz and Janka Held-Feindt Insights into Gene Regulation under Temozolomide-Promoted Cellular Dormancy and Its Connection to Stemness in Human Glioblastoma Reprinted from: <i>Cells</i> 2023 , <i>12</i> , 1491, https://doi.org/10.3390/cells12111491	50
Paola Schildhauer, Philipp Selke, Christian Scheller, Christian Strauss, Rüdiger Horstkorte and Sandra Leisz et al. Glycation Leads to Increased Invasion of Glioblastoma Cells Reprinted from: <i>Cells</i> 2023 , <i>12</i> , 1219, https://doi.org/10.3390/cells12091219	72
Freya R. Weth, Lifeng Peng, Erin Paterson, Swee T. Tan and Clint Gray Utility of the Cerebral Organoid Glioma ‘GLICO’ Model for Screening Applications Reprinted from: <i>Cells</i> 2022 , <i>12</i> , 153, https://doi.org/10.3390/cells12010153	92
Upasana Kapoor-Narula and Nibedita Lenka Elucidating the Anti-Tumorigenic Efficacy of Oltipraz, a Dithiolethione, in Glioblastoma Reprinted from: <i>Cells</i> 2022 , <i>11</i> , 3057, https://doi.org/10.3390/cells11193057	107
Danijela Drakulic, Marija Schwirtlich, Isidora Petrovic, Marija Mojsin, Milena Milivojevic and Natasa Kovacevic-Grujicic et al. Current Opportunities for Targeting Dysregulated Neurodevelopmental Signaling Pathways in Glioblastoma Reprinted from: <i>Cells</i> 2022 , <i>11</i> , 2530, https://doi.org/10.3390/cells11162530	128
Takuichiro Hide, Ichiyo Shibahara, Madoka Inukai, Ryota Shigeeda and Toshihiro Kumabe Ribosomes and Ribosomal Proteins Promote Plasticity and Stemness Induction in Glioma Cells via Reprogramming Reprinted from: <i>Cells</i> 2022 , <i>11</i> , 2142, https://doi.org/10.3390/cells11142142	180
Marie Geraldine Lacore, Caroline Delmas, Yvan Nicaise, Aline Kowalski-Chauvel, Elizabeth Cohen-Jonathan-Moyal and Catherine Seva The Glycoprotein M6a Is Associated with Invasiveness and Radioresistance of Glioblastoma Stem Cells Reprinted from: <i>Cells</i> 2022 , <i>11</i> , 2128, https://doi.org/10.3390/cells11142128	203

Swalih P. Ahmed, Javier S. Castresana and Mehdi H. Shahi Role of Circular RNA in Brain Tumor Development Reprinted from: <i>Cells</i> 2022 , <i>11</i> , 2130, https://doi.org/10.3390/cells11142130	217
Tuyen T. Dang, Megan Lerner, Debra Saunders, Nataliya Smith, Rafal Gulej and Michelle Zalles et al. XRN2 Is Required for Cell Motility and Invasion in Glioblastomas Reprinted from: <i>Cells</i> 2022 , <i>11</i> , 1481, https://doi.org/10.3390/cells11091481	245
Mathew Lozinski, Nikola A. Bowden, Moira C. Graves, Michael Fay, Bryan W. Day and Brett W. Stringer et al. Transcriptomic Profiling of DNA Damage Response in Patient-Derived Glioblastoma Cells before and after Radiation and Temozolomide Treatment Reprinted from: <i>Cells</i> 2022 , <i>11</i> , 1215, https://doi.org/10.3390/cells11071215	259
Francesca Lessi, Sara Franceschi, Mariangela Morelli, Michele Menicagli, Francesco Pasqualetti and Orazio Santonocito et al. Single-Cell Molecular Characterization to Partition the Human Glioblastoma Tumor Microenvironment Genetic Background Reprinted from: <i>Cells</i> 2022 , <i>11</i> , 1127, https://doi.org/10.3390/cells11071127	274
Eno I. Essien, Thomas P. Hofer, Michael J. Atkinson and Nataša Anastasov Combining HDAC and MEK Inhibitors with Radiation against Glioblastoma-Derived Spheres Reprinted from: <i>Cells</i> 2022 , <i>11</i> , 775, https://doi.org/10.3390/cells11050775	292
Urszula Hohmann, Christoph Walsleben, Chalid Ghadban, Frank Kirchhoff, Faramarz Dehghani and Tim Hohmann Interaction of Glia Cells with Glioblastoma and Melanoma Cells under the Influence of Phytocannabinoids Reprinted from: <i>Cells</i> 2022 , <i>11</i> , 147, https://doi.org/10.3390/cells11010147	313
Li-Wei Sun, Shao-Hsuan Kao, Shun-Fa Yang, Shang-Wun Jhang, Yi-Chen Lin and Chien-Min Chen et al. Corosolic Acid Attenuates the Invasiveness of Glioblastoma Cells by Promoting CHIP-Mediated AXL Degradation and Inhibiting GAS6/AXL/JAK Axis Reprinted from: <i>Cells</i> 2021 , <i>10</i> , 2919, https://doi.org/10.3390/cells10112919	331
Feng-Cheng Pai, Hsiang-Wei Huang, Yu-Ling Tsai, Wen-Chiuan Tsai, Yu-Chen Cheng and Hsin-Han Chang et al. Inhibition of FABP6 Reduces Tumor Cell Invasion and Angiogenesis through the Decrease in MMP-2 and VEGF in Human Glioblastoma Cells Reprinted from: <i>Cells</i> 2021 , <i>10</i> , 2782, https://doi.org/10.3390/cells10102782	346

About the Editors

Javier S. Castresana

Javier S. Castresana is a Professor of Genetics at the University of Navarra, Pamplona, Spain. He previously worked for three years at Karolinska Institute as a predoctoral student; for two years at Harvard Medical School as a postdoctoral student; and for five years at the Spanish Scientific Research Council as a senior researcher. He is interested in glioblastoma genetics and epigenetics, with a special focus on brain tumor stem cell characterization.

Bárbara Meléndez

Bárbara Meléndez is a researcher at the Molecular Pathology Research Unit, Department of Pathology, Virgen de la Salud Hospital, Toledo, Spain. She is interested in brain tumor genetics and epigenetics.

Preface

The fight against glioblastoma is continuous since its life expectancy is 12 to 15 months after diagnosis. The genetics and epigenetics of the tumor are not the only important factors in minimizing the devastating impact of glioblastoma; other therapeutic approaches that can be used alone or in combination with some of the current therapies should be considered. Currently, temozolomide is the chemotherapy agent par excellence, used against glioblastoma when there is no expression of the MGMT enzyme. In this Special Issue, different pathways and new targets were explored, along with epigenetic possibilities for therapy like the inhibition of HDAC and the role of miRNA and circular RNA, tumor cell dormancy, cancer stem cells, and other approaches, to try to better understand and possibly combat glioblastoma.

Javier S. Castresana and Bárbara Meléndez

Guest Editors

Glioblastoma Biology, Genetics and Possible Therapies

Javier S. Castresana ^{1,*}  and Bárbara Meléndez ²¹ Department of Biochemistry and Genetics, University of Navarra School of Sciences, 31008 Pamplona, Spain² Molecular Pathology Research Unit, Virgen de la Salud Hospital, 45005 Toledo, Spain; bmelendez@sescam.jccm.es* Correspondence: jscastresana@unav.es

Glioblastoma is the most aggressive intracranial tumor. Current treatment consists of surgery, radiotherapy, and chemotherapy (temozolomide). Resistance to radiotherapy and chemotherapy are frequent. Temozolomide is preferably used in patients who do not express MGMT. Temozolomide induces the formation of O6-methylguanine in DNA. MGMT repairs this DNA damage. Therefore, glioblastoma cells become resistant to temozolomide when MGMT expression ensures the repair of damaged DNA by temozolomide. On the contrary, if MGMT is not expressed, the DNA damage caused by temozolomide will not be repaired, and glioblastoma cells will die, that is, glioblastoma cells will be sensitive to temozolomide.

Lack of MGMT expression is associated with the hypermethylation of the MGMT promoter. Therefore, in clinical practice, an immunohistochemical approach is used to detect patients who do not express MGMT in glioblastoma biopsies, being these patients the ones who could benefit the most from MGMT expression laboratory assays [1].

Due to chemotherapy resistance, various combinations of drugs with temozolomide are being tested. The sensitization to temozolomide in previously resistant cells can be seen, thanks to the intervention of a second compound [2].

Bioactive compounds are also tested in order to prove their possible inhibitory activity of cell growth or migration in glioblastoma [3–5]. Sun et al. [3] demonstrated the antimetastatic potential of corosolic acid in glioblastoma cells by inhibiting the JAK2/MEK/ERK axis.

Kapoor-Narula and Lenka [4] demonstrated the anticancer effect of Oltipraz, a synthetic dithiolethione present in many vegetables, by decreasing the glioma cancer stem cells content in favor of differentiating GFAP+ glioma cells, together with the suppression of neurospheres formation. Even in vivo treatment with Oltipraz ectopically suppressed glioblastoma tumors xenografted in mice.

Several articles have revealed a preliminary positive effect of cannabinoids against glioblastoma [6–8]. Hohmann et al. [5] did not reach the same clear conclusions: on the one hand, they saw that cannabinoids increased the size of glioblastoma spheroids, but on the other hand, migration was unaffected.

Another way of intervention against glioblastoma is the direct attack of its brain tumor stem cells, trusting that such cells are the initiators and/or maintainers of the tumor, as well as being the cells that make the tumor resistant to chemotherapy and radiotherapy. In this sense, there are promising findings, such as those published by Lacore et al. [9], who blocked the M6a glycoprotein by siRNA, leading to a decrease in cell proliferation and invasion, as well as to an increase in radiosensitivity in glioblastoma stem cells.

Also, trying to target the stem cell component of this tumor, Essien et al. [10] assayed a combined treatment of an HDAC and an MEK inhibitor, together with radiation, detecting a bigger decay in the expression of stem cell markers Nestin and SOX2 than with the standard treatment of temozolomide and radiation. Other studies have shown the efficacy of epigenetically inhibiting HDAC in glioblastoma cells [11–15], even preferentially targeting the cancer stem cell compartment [16,17].



Citation: Castresana, J.S.; Meléndez, B. Glioblastoma Biology, Genetics and Possible Therapies. *Cells* **2023**, *12*, 2063. <https://doi.org/10.3390/cells12162063>

Received: 4 August 2023

Accepted: 10 August 2023

Published: 14 August 2023



Copyright: © 2023 by the authors. Licensee MDPI, Basel, Switzerland. This article is an open access article distributed under the terms and conditions of the Creative Commons Attribution (CC BY) license (<https://creativecommons.org/licenses/by/4.0/>).

Tumor cell dormancy complicates cancer therapy [18]. Cells that have metastasized to other organs remain in a quiescent state even for years, after which the cells might be newly activated and capable of originating the true metastatic disease. Every effort to understand the life cycle of tumor cell dormancy [19,20], the possible similarities found between tumor dormant cells and tumor stem cells [21,22], and, even more important, the sensitization of dormant cells to chemotherapy [23] are of great importance to overcome metastatic disease. Glioblastoma almost never metastasizes outside of the brain. Rather, it invades into the brain, but also develops tumor cell dormancy [20,22,24] capable of producing recurrent tumors several months after complete surgical resection, radiotherapy, and temozolomide treatments. Therefore, research has also been conducted on how glioblastoma dormant cells induced by temozolomide treatment can develop stem cell characteristics: Kubelt et al. [24] reported in this Special Issue about a possible connection between temozolomide-induced glioblastoma cell dormancy and the development of stem-like characteristics in glioblastoma cells.

Several other articles of this Special Issue concentrate on inhibiting specific targets with the idea of inhibiting or reducing cell proliferation, migration, and invasion. Then, Pai et al. [25] revealed that the inhibition of FABP6 (a bile acid carrier protein) reduced invasion and angiogenesis in glioblastoma cells by decreasing MMP-2 and VEGF. Secondly, the expression of XRN2, a 5'-3' exoribonuclease, was shown to be associated with cell migration and the invasion of glioblastoma cells [26]; therefore, inhibition of XRN2 expression might be a strategy to treat glioblastoma. And thirdly [27], it was revealed that the role of the Warburg effect in cancer cells, which turns on aerobic glycolytic processes and methylglyoxal synthesis, finally provokes a general glycation pattern that leads to the invasion of glioblastoma cells, a mechanism that might be disrupted by deglycating agents.

Another approach to combat glioblastoma might be the possibility of targeting specifically well-known pathways like Sonic Hedgehog, Wnt, Notch, TGFbeta, and others [28]. In such a way, single-cell studies [29], transcriptome analysis [30], and organoid models [31] are good approaches to define a holistic picture of glioblastoma.

Two reviews dealing about the epigenetic role of miRNA [32] and of circular RNA [33] in relation with different pathways that promote glioblastoma lead us into the last known category of epigenetic control, apart from histone methylation, histone acetylation, and DNA gene promoter methylation, all of them playing a role in the genesis of glioblastoma [34,35].

Finally, a new way of leading glioblastoma cells to differentiation is proposed by Hide et al. [36] based on ribosomes and ribosomal protein S6 administered to glioblastoma cells. Those cells might then be differentiated into reprogrammed glioblastoma stem cells with the possibility of the further differentiation of normal cells.

In summary, this second Special Issue on the Molecular and Cellular Mechanisms of Glioblastoma presents 16 articles dealing on the biology, genetics, and possible treatments against this devastating disease. Pathways to gliomagenesis and new targets have been explored, together with epigenetic possibilities like the inhibition of HDAC and the role of miRNA and circular RNA, tumor cell dormancy, cancer stem cells, and other approaches, to try to better understand and possibly combat glioblastoma.

Funding: This project was funded by a grant from the Fundación Universidad de Navarra, Pamplona, Spain.

Conflicts of Interest: The authors declare no conflict of interest.

References

1. Lalezari, S.; Chou, A.P.; Tran, A.; Solis, O.E.; Khanlou, N.; Chen, W.; Li, S.; Carrillo, J.A.; Chowdhury, R.; Selfridge, J.; et al. Combined analysis of O6-methylguanine-DNA methyltransferase protein expression and promoter methylation provides optimized prognostication of glioblastoma outcome. *Neuro Oncol.* **2013**, *15*, 370–381. [CrossRef] [PubMed]
2. Tomar, M.S.; Kumar, A.; Srivastava, C.; Shrivastava, A. Elucidating the mechanisms of Temozolomide resistance in gliomas and the strategies to overcome the resistance. *Biochim. Biophys. Acta Rev. Cancer* **2021**, *1876*, 188616. [CrossRef]



3. Sun, L.W.; Kao, S.H.; Yang, S.F.; Jhang, S.W.; Lin, Y.C.; Chen, C.M.; Hsieh, Y.H. Corosolic Acid Attenuates the Invasiveness of Glioblastoma Cells by Promoting CHIP-Mediated AXL Degradation and Inhibiting GAS6/AXL/JAK Axis. *Cells* **2021**, *10*, 2919. [CrossRef] [PubMed]
4. Kapoor-Narula, U.; Lenka, N. Elucidating the Anti-Tumorigenic Efficacy of Oltipraz, a Dithiolethione, in Glioblastoma. *Cells* **2022**, *11*, 3057. [CrossRef]
5. Hohmann, U.; Walsleben, C.; Ghadban, C.; Kirchhoff, F.; Dehghani, F.; Hohmann, T. Interaction of Glia Cells with Glioblastoma and Melanoma Cells under the Influence of Phytocannabinoids. *Cells* **2022**, *11*, 147. [CrossRef] [PubMed]
6. Rupperecht, A.; Theisen, U.; Wendt, F.; Frank, M.; Hinz, B. The Combination of $\Delta(9)$ -Tetrahydrocannabinol and Cannabidiol Suppresses Mitochondrial Respiration of Human Glioblastoma Cells via Downregulation of Specific Respiratory Chain Proteins. *Cancers* **2022**, *14*, 3129. [CrossRef]
7. Milian, L.; Mata, M.; Alcacer, J.; Oliver, M.; Sancho-Tello, M.; Martín de Llano, J.J.; Camps, C.; Galbis, J.; Carretero, J.; Carda, C. Cannabinoid receptor expression in non-small cell lung cancer. Effectiveness of tetrahydrocannabinol and cannabidiol inhibiting cell proliferation and epithelial-mesenchymal transition in vitro. *PLoS ONE* **2020**, *15*, e0228909. [CrossRef]
8. Marcu, J.P.; Christian, R.T.; Lau, D.; Zielinski, A.J.; Horowitz, M.P.; Lee, J.; Pakdel, A.; Allison, J.; Limbad, C.; Moore, D.H.; et al. Cannabidiol enhances the inhibitory effects of delta9-tetrahydrocannabinol on human glioblastoma cell proliferation and survival. *Mol. Cancer Ther.* **2010**, *9*, 180–189. [CrossRef]
9. Lacore, M.G.; Delmas, C.; Nicaise, Y.; Kowalski-Chauvel, A.; Cohen-Jonathan-Moyal, E.; Seva, C. The Glycoprotein M6a Is Associated with Invasiveness and Radioresistance of Glioblastoma Stem Cells. *Cells* **2022**, *11*, 2128. [CrossRef]
10. Essien, E.I.; Hofer, T.P.; Atkinson, M.J.; Anastasov, N. Combining HDAC and MEK Inhibitors with Radiation against Glioblastoma-Derived Spheres. *Cells* **2022**, *11*, 775. [CrossRef]
11. De La Rosa, J.; Urdiciain, A.; Zazpe, I.; Zelaya, M.V.; Meléndez, B.; Rey, J.A.; Idoate, M.A.; Castresana, J.S. The synergistic effect of DZ-NEP, panobinostat and temozolomide reduces clonogenicity and induces apoptosis in glioblastoma cells. *Int. J. Oncol.* **2020**, *56*, 283–300. [CrossRef]
12. Chang, H.H.; Chang, Y.Y.; Tsai, B.C.; Chen, L.J.; Chang, A.C.; Chuang, J.Y.; Gean, P.W.; Hsueh, Y.S. A Selective Histone Deacetylase Inhibitor Induces Autophagy and Cell Death via SCNN1A Downregulation in Glioblastoma Cells. *Cancers* **2022**, *14*, 4537. [CrossRef] [PubMed]
13. Uddin, M.S.; Mamun, A.A.; Alghamdi, B.S.; Tewari, D.; Jeandet, P.; Sarwar, M.S.; Ashraf, G.M. Epigenetics of glioblastoma multiforme: From molecular mechanisms to therapeutic approaches. *Semin. Cancer Biol.* **2022**, *33*, 100–120. [CrossRef] [PubMed]
14. Kunadis, E.; Lakiotaki, E.; Korkolopoulou, P.; Piperi, C. Targeting post-translational histone modifying enzymes in glioblastoma. *Pharmacol. Ther.* **2021**, *220*, 107721. [CrossRef]
15. Chen, R.; Zhang, M.; Zhou, Y.; Guo, W.; Yi, M.; Zhang, Z.; Ding, Y.; Wang, Y. The application of histone deacetylases inhibitors in glioblastoma. *J. Exp. Clin. Cancer Res.* **2020**, *39*, 138. [CrossRef]
16. Nakagawa-Saito, Y.; Saitoh, S.; Mitobe, Y.; Sugai, A.; Togashi, K.; Suzuki, S.; Kitanaka, C.; Okada, M. HDAC Class I Inhibitor Domatinostat Preferentially Targets Glioma Stem Cells over Their Differentiated Progeny. *Int. J. Mol. Sci.* **2022**, *23*, 8084. [CrossRef]
17. Reddy, R.G.; Bhat, U.A.; Chakravarty, S.; Kumar, A. Advances in histone deacetylase inhibitors in targeting glioblastoma stem cells. *Cancer Chemother. Pharmacol.* **2020**, *86*, 165–179. [CrossRef] [PubMed]
18. Gomis, R.R.; Gawrzak, S. Tumor cell dormancy. *Mol. Oncol.* **2017**, *11*, 62–78. [CrossRef] [PubMed]
19. Phan, T.G.; Croucher, P.I. The dormant cancer cell life cycle. *Nat. Rev. Cancer* **2020**, *20*, 398–411. [CrossRef]
20. Adamski, V.; Hattermann, K.; Kubelt, C.; Cohrs, G.; Lucius, R.; Synowitz, M.; Sebens, S.; Held-Feindt, J. Entry and exit of chemotherapeutically-promoted cellular dormancy in glioblastoma cells is differentially affected by the chemokines CXCL12, CXCL16, and CX3CL1. *Oncogene* **2020**, *39*, 4421–4435. [CrossRef]
21. Hen, O.; Barkan, D. Dormant disseminated tumor cells and cancer stem/progenitor-like cells: Similarities and opportunities. *Semin. Cancer Biol.* **2020**, *30*, 157–165. [CrossRef]
22. Adamski, V.; Hempelmann, A.; Flüh, C.; Lucius, R.; Synowitz, M.; Hattermann, K.; Held-Feindt, J. Dormant glioblastoma cells acquire stem cell characteristics and are differentially affected by Temozolomide and AT101 treatment. *Oncotarget* **2017**, *8*, 108064–108078. [CrossRef] [PubMed]
23. Carlson, P.; Dasgupta, A.; Grzelak, C.A.; Kim, J.; Barrett, A.; Coleman, I.M.; Shor, R.E.; Goddard, E.T.; Dai, J.; Schweitzer, E.M.; et al. Targeting the perivascular niche sensitizes disseminated tumour cells to chemotherapy. *Nat. Cell Biol.* **2019**, *21*, 238–250. [CrossRef]
24. Kubelt, C.; Hellmold, D.; Esser, D.; Ahmeti, H.; Synowitz, M.; Held-Feindt, J. Insights into Gene Regulation under Temozolomide-Promoted Cellular Dormancy and Its Connection to Stemness in Human Glioblastoma. *Cells* **2023**, *12*, 1491. [CrossRef]
25. Pai, F.C.; Huang, H.W.; Tsai, Y.L.; Tsai, W.C.; Cheng, Y.C.; Chang, H.H.; Chen, Y. Inhibition of FABP6 Reduces Tumor Cell Invasion and Angiogenesis through the Decrease in MMP-2 and VEGF in Human Glioblastoma Cells. *Cells* **2021**, *10*, 2782. [CrossRef]
26. Dang, T.T.; Lerner, M.; Saunders, D.; Smith, N.; Gulej, R.; Zalles, M.; Towner, R.A.; Morales, J.C. XRN2 Is Required for Cell Motility and Invasion in Glioblastomas. *Cells* **2022**, *11*, 1481. [CrossRef]
27. Schildhauer, P.; Selke, P.; Scheller, C.; Strauss, C.; Horstkorte, R.; Leisz, S.; Scheer, M. Glycation Leads to Increased Invasion of Glioblastoma Cells. *Cells* **2023**, *12*, 1219. [CrossRef] [PubMed]

28. Drakulic, D.; Schwirtlich, M.; Petrovic, I.; Mojsin, M.; Milivojevic, M.; Kovacevic-Grujicic, N.; Stevanovic, M. Current Opportunities for Targeting Dysregulated Neurodevelopmental Signaling Pathways in Glioblastoma. *Cells* **2022**, *11*, 2530. [CrossRef] [PubMed]
29. Lessi, F.; Franceschi, S.; Morelli, M.; Menicagli, M.; Pasqualetti, F.; Santonocito, O.; Gambacciani, C.; Pieri, F.; Aquila, F.; Aretini, P.; et al. Single-Cell Molecular Characterization to Partition the Human Glioblastoma Tumor Microenvironment Genetic Background. *Cells* **2022**, *11*, 1127. [CrossRef]
30. Lozinski, M.; Bowden, N.A.; Graves, M.C.; Fay, M.; Day, B.W.; Stringer, B.W.; Tooney, P.A. Transcriptomic Profiling of DNA Damage Response in Patient-Derived Glioblastoma Cells before and after Radiation and Temozolomide Treatment. *Cells* **2022**, *11*, 1215. [CrossRef]
31. Weth, F.R.; Peng, L.; Paterson, E.; Tan, S.T.; Gray, C. Utility of the Cerebral Organoid Glioma 'GLICO' Model for Screening Applications. *Cells* **2022**, *12*, 153. [CrossRef] [PubMed]
32. Hasan, H.; Afzal, M.; Castresana, J.S.; Shahi, M.H. A Comprehensive Review of miRNAs and Their Epigenetic Effects in Glioblastoma. *Cells* **2023**, *12*, 1578. [CrossRef] [PubMed]
33. Ahmed, S.P.; Castresana, J.S.; Shahi, M.H. Role of Circular RNA in Brain Tumor Development. *Cells* **2022**, *11*, 2130. [CrossRef]
34. Montella, L.; Cuomo, M.; Del Gaudio, N.; Buonaiuto, M.; Costabile, D.; Visconti, R.; Di Risi, T.; Vinciguerra, R.; Trio, F.; Ferraro, S.; et al. Epigenetic alterations in glioblastomas: Diagnostic, prognostic and therapeutic relevance. *Int. J. Cancer* **2023**, *153*, 476–488. [CrossRef] [PubMed]
35. Romani, M.; Pistillo, M.P.; Banelli, B. Epigenetic Targeting of Glioblastoma. *Front. Oncol.* **2018**, *8*, 448. [CrossRef]
36. Hide, T.; Shibahara, I.; Inukai, M.; Shigeeda, R.; Kumabe, T. Ribosomes and Ribosomal Proteins Promote Plasticity and Stemness Induction in Glioma Cells via Reprogramming. *Cells* **2022**, *11*, 2142. [CrossRef]

Disclaimer/Publisher's Note: The statements, opinions and data contained in all publications are solely those of the individual author(s) and contributor(s) and not of MDPI and/or the editor(s). MDPI and/or the editor(s) disclaim responsibility for any injury to people or property resulting from any ideas, methods, instructions or products referred to in the content.

Article

Flavonoids Regulate Redox-Responsive Transcription Factors in Glioblastoma and Microglia

Natali Joma ¹, Issan Zhang ¹, Germanna L. Righetto ^{1,2}, Laura McKay ³, Evan Rizzel Gran ¹, Ashok Kakkar ³ and Dusica Maysinger ^{1,*}

¹ Department of Pharmacology and Therapeutics, McGill University, 3655 Promenade Sir-William-Osler, Montreal, QC H3G 1Y6, Canada; natali.joma@mail.mcgill.ca (N.J.); issan.zhang@mail.mcgill.ca (I.Z.); germanna.righetto@mail.utoronto.ca (G.L.R.); evan.gran@mail.mcgill.ca (E.R.G.)

² Structural Genomics Consortium, University of Toronto, 101 College St, Toronto, ON M5G 1L7, Canada

³ Department of Chemistry, McGill University, 801 Sherbrooke St W, Montreal, QC H3A 0B8, Canada; laura.mckay@mail.mcgill.ca (L.M.); ashok.kakkar@mcgill.ca (A.K.)

* Correspondence: dusica.maysinger@mcgill.ca

Abstract: The tumor microenvironment (TME) has emerged as a valuable therapeutic target in glioblastoma (GBM), as it promotes tumorigenesis via an increased production of reactive oxygen species (ROS). Immune cells such as microglia accumulate near the tumor and its hypoxic core, fostering tumor proliferation and angiogenesis. In this study, we explored the therapeutic potential of natural polyphenols with antioxidant and anti-inflammatory properties. Notably, flavonoids, including fisetin and quercetin, can protect non-cancerous cells while eliminating transformed cells (2D cultures and 3D tumoroids). We tested the hypothesis that fisetin and quercetin are modulators of redox-responsive transcription factors, for which subcellular location plays a critical role. To investigate the sites of interaction between natural compounds and stress-responsive transcription factors, we combined molecular docking with experimental methods employing proximity ligation assays. Our findings reveal that fisetin decreased cytosolic acetylated high mobility group box 1 (acHMGB1) and increased transcription factor EB (TFEB) abundance in microglia but not in GBM. Moreover, our results suggest that the most powerful modulator of the Nrf2-KEAP1 complex is fisetin. This finding is in line with molecular modeling and calculated binding properties between fisetin and Nrf2-KEAP1, which indicated more sites of interactions and stronger binding affinities than quercetin.

Keywords: microglia; glioblastoma; tumor microenvironment; reactive oxygen species; oxidative stress; natural polyphenols; fisetin; quercetin; redox-responsive transcription factors



Citation: Joma, N.; Zhang, I.; Righetto, G.L.; McKay, L.; Gran, E.R.; Kakkar, A.; Maysinger, D. Flavonoids Regulate Redox-Responsive Transcription Factors in Glioblastoma and Microglia. *Cells* **2023**, *12*, 2821. <https://doi.org/10.3390/cells12242821>

Academic Editors: Javier S. Castresana and Bárbara Meléndez

Received: 2 November 2023
Revised: 29 November 2023
Accepted: 7 December 2023
Published: 12 December 2023



Copyright: © 2023 by the authors. Licensee MDPI, Basel, Switzerland. This article is an open access article distributed under the terms and conditions of the Creative Commons Attribution (CC BY) license (<https://creativecommons.org/licenses/by/4.0/>).

1. Introduction

Glioblastoma multiforme (GBM) is an aggressive brain cancer of glial origin. Its heterogeneity and propensity for treatment resistance (innate or acquired) are significant challenges in the clinics [1,2]. The GBM microenvironment contains a significant proportion of tumor-associated macrophages (TAMs) and microglia (40–50%) [3–5]. Microglia are immunological surveyors of the brain, which respond to signals and stressors with a repertoire of neurotrophic factors and inflammatory mediators [6–8]. Under maladaptive conditions, microglia can excessively release pro-inflammatory cytokines, damage-associated molecular patterns (DAMPs), and reactive oxygen species (ROS), contributing to neuroinflammation and redox imbalance [6]. The pharmacological modulation of microglia has the potential to reduce injury in neurodegenerative disorders, brain injury, and cancer [1,4,5,9–11].

One of the key dysregulated factors in GBM is high mobility group box 1 (HMGB1) [6,12]. HMGB1's activity is influenced by its cellular localization, oxidative state, and post-translational modifications, such as acetylation, methylation, and phosphorylation [13].

HMGB1 mediates inflammatory responses by binding to receptors like RAGE (receptor for advanced glycation end products) and TLRs (Toll-like receptors). Extracellular HMGB1 can activate immune cells, including microglia, and promote tumor invasiveness, resistance, and immunosuppression [14,15]. HMGB1 interacts with various cellular factors, including heat shock protein 72 (HSP72), a chaperone known for mediating resilience against oxidation, inflammation, and other stressors [16–18].

Another critical redox-responsive factor in inflammation is transcription factor EB (TFEB), the primary regulator of lysosomes [19]. Under conditions of stress, TFEB translocates to the nucleus, signaling increased lysosomal biogenesis and function. This translocation is mediated by an upstream transcription factor, nuclear factor erythroid-derived-2-like 2 (Nrf2). Under homeostasis, Nrf2 remains bound to Kelch-like ECH-associated protein 1 (KEAP1). However, in response to stress, Nrf2 dissociates from KEAP1, leading to enhanced antioxidant defenses and oxidative stress regulation [20].

Flavonoids, known for their therapeutic activity against a range of diseases, including cancer, cardiovascular disease, and neurodegenerative disorders [21], exhibit varying effects on cells and organs. These differences can be in part attributed to the complexity of human tissues and the diversity of cellular responses, particularly in the brain [22–24]. These differences are particularly noticeable when comparing cancer cells with non-transformed cells. Many polyphenols display cytoprotective properties in normal cells and cytotoxic effects in cancer cells (e.g., GBM) [25,26]. These findings prompted the investigation of potential interactions between natural polyphenols (fisetin and quercetin) and several molecular targets, focusing on microglia as sensitive responders in the GBM microenvironment.

The treatment of microglia and GBM using natural compounds represents an attractive approach to undermine the supportive role of TAMs in the GBM microenvironment by targeting multiple dysregulated pathways in inflammation. However, the interaction between flavonoids with transcription factors implicated in cell functions was not previously explored. Here, we examined the modulatory effects of fisetin and quercetin on major stress-responsive factors (TFEB, Nrf2, KEAP1, HSP72, and HMGB1) in human microglia and GBM cells [27–31]. These agents were selected because of their documented anti-inflammatory properties [21,32,33].

The aim of this study was to establish the differential effects of natural polyphenols in human microglia and GBM cells. We first evaluated the toxicity of the polyphenolic compounds and their capacity to modulate (i) reactive oxygen species (ROS) and (ii) the abundance and location of HMGB1 and TFEB. We then investigated protein–protein interactions of Nrf2, KEAP1, HSP72, and HMGB1 in parallel with molecular docking to reveal interactions between the polyphenols and proteins of interest. This study should advance the current understanding of the selected natural compounds as differential modulators of microglia and GBM.

2. Materials and Methods

2.1. Cell Culture

The HMC3 human microglia (CRL-3304) and U251N human glioblastoma cells were originally obtained from the American Type Culture Collection. Unless otherwise specified, cells were maintained in Dulbecco's Modified Eagle Medium (DMEM, 11965084, Thermo Fisher Scientific, Ottawa, ON, Canada) supplemented with 5% (*v/v*) fetal bovine serum (Wisent, St-Jean-Baptiste, QC, Canada) and 1% (*v/v*) Penicillin–Streptomycin (Thermo Fisher Scientific, Ottawa, ON, Canada) at 37 °C with 5% CO₂ and 95% relative humidity.

2.2. Mitochondrial Metabolic Activity (MTT)

Cells were seeded at 50,000 cells per well in 24-well plates (Sarstedt, Montreal, QC, Canada) and cultured for 24 h before treatment. Cells were washed twice with phosphate-buffered saline (PBS) before treatment with increasing concentrations of fisetin (5, 15, 25, 50, 100 µM; Cayman Chemical Company, Ann Arbor, MI, USA) or quercetin (5, 15, 25, 50, 100 µM; Cayman Chemical Company, Ann Arbor, MI, USA) in serum-deprived DMEM

for 24 h. Cells were then incubated with 0.5 mg/mL MTT (Millipore-Sigma, Oakville, ON, Canada) at 37 °C. The medium was removed, and cells were lysed with dimethylsulfoxide (DMSO, Millipore-Sigma, Oakville, ON, Canada) before colorimetric measurements at 595 nm (Spark 10M, Tecan, Männedorf, Switzerland).

2.3. Lactose Dehydrogenase (LDH) Assay

Cells were seeded and treated for the MTT assay. At the end of treatment, the medium was collected and centrifuged at 14,000 rpm for 5 min at 4 °C to remove cell debris. The supernatant was then used according to the instructions of the Cytotoxicity Detection Kit (Roche, Mississauga, ON, Canada). In short, medium samples were pipetted in triplicate in a 96-well plate (Sarstedt, Montreal, QC, Canada) and incubated with the kit reagent for 30 min at room temperature in the dark. Colorimetric measurements were made at 492 nm (Spark 10M).

2.4. Cell Counting

Confluent monolayer cell cultures of 70–80% were detached using 0.05% trypsin–EDTA, seeded in 96-well cell culture plates (Sarstedt) at 2500 cells per well, and cultured for 24 h. Cells were treated with increasing concentrations of TMZ (0.001, 0.5, 1, 10, 50, and 100 µM) +/– fisetin (IC₅₀ = 10 µM) for 72 h. Nuclei were labeled with Hoechst 33342 (10 µM, Thermo Fisher Scientific) for 30 min. Cells were imaged using a fluorescence microscope (Leica DMI4000B) with the UV filter at 10× magnification.

2.5. CellROX Assay

Cells were seeded at 7000 cells per glass coverslip and cultured for 24 h. Cells were washed twice with phosphate-buffered saline before treatment. Cells were treated with fisetin (25 µM) or quercetin (25 µM) with or without buthionine sulfoximine (BSO, 100 µM, Millipore-Sigma, Oakville, ON, Canada) or SARS-CoV-2 spike protein (SMT1-1, 5 µM, National Research Council Canada, Ottawa, ON, Canada). Following treatment, cells were incubated for 30 min at 37 °C with CellROX Deep Red (5 µM, Thermo Fisher Scientific, Burlington, ON, Canada) to detect intracellular oxidative stress. Cell nuclei were labeled with Hoechst 33342 (10 µM, Thermo Fisher Scientific, Burlington, ON, Canada). Cells were rinsed in phenol-free DMEM once and imaged using a fluorescence microscope with the CY5 filter at 20× magnification (Leica DMI 4000B, Richmond Hill, ON, Canada).

2.6. Immunocytochemistry

Cells were seeded at 7000 cells/coverslip on glass coverslips and cultured for 24 h before treatment. Following treatment, cells were fixed in 4% paraformaldehyde (10 min), permeabilized with 0.1% Triton X-100 (*v/v*, 10 min, Sigma-Aldrich, St. Louis, MO, USA), blocked in 10% goat serum (*v/v*, 1 h, Thermo Fisher Scientific) in PBS, and incubated with primary antibodies overnight at 4 °C, namely rabbit anti-TFEB (1:500, Sigma-Aldrich, SAB4503154-100UG) or rabbit anti-HMGB1 acetyl-Lys12 (1:500, MyBioSource, MBS9404216, San Diego, USA). Cells were washed in PBS three times and incubated with secondary antibodies for 1 h at room temperature: goat anti-rabbit Alexa Fluor 647 (1:500, Thermo Fisher, A21244). Cells were washed with PBS; nuclei and F-actin were labeled with Hoechst 33342 (10 µM, 10 min) and F-actin with 1:400 Alexa Fluor® 488 Phalloidin (Invitrogen, Burlington, ON, Canada), respectively. After three more washings with PBS, coverslips were mounted on microscope slides using Aqua-Poly/Mount (Polysciences, Warrington, PA, USA). Samples were imaged using a fluorescence microscope (Leica DMI4000B, Leica), and intracellular fluorescence was analyzed in ImageJ. The nuclear and/or cytoplasmic fluorescence of TFEB and acetylated HMGB1 for each cell was measured and normalized to the nuclear or cytoplasmic area. The background fluorescence was subtracted.

2.7. GBM Tumoroid Preparation

U251N tumoroids were prepared using the hanging drop method [34]. Drops of 5000 cells in 20 μ L medium were pipetted onto the inner side of the lid of a 100 mm Petri dish (Thermo Fisher Scientific). The lid was quickly flipped 180° to cover the Petri dish filled with 20 mL PBS. Hanging drops were cultured at 37 °C for 48 h to allow tumoroids to form. Tumoroids were then gently scooped into a medium-filled Petri dish coated with 2% agarose and cultured for 48 h. Tumoroids were implanted in agarose gel. The gels were covered with 100 μ L DMEM with or without treatment. Tumoroids were imaged using light microscopy immediately after implantation on day 0 and day Tumor size (area) was measured using ImageJ.

2.8. Molecular Docking

The crystal structures of HMGB1 (PDB: 1AAB), HSP72 bound to ADP (PDB ID: 5BN9), and KEAP1 bound to Nrf2 (PDB ID: 3WN7) were selected for docking analysis because of their high resolution and overall high-quality scores among the proteins deposited in the Protein Data Bank for each target. Prior to the docking, Pymol (The PyMOL Molecular Graphics System, Version 1.2r3pre, Schrödinger, and LLC) was used to edit the protein structures and delete any undesired ligands or binding partners. The SwissDock web server was used for molecular docking, and well-characterized binding pockets were defined as regions of interest [35]. In the case of HSP72 and KEAP1, the docking was restricted to the binding region of the compound co-crystallized with the proteins. For the apo HMGB1 structure, previous docking and NMR information of protein binding to glycyrrhizin and salicylic acid was used to define the likely binding region for the natural compounds [36–38]. The software UCSF Chimera (version 1.14.0) was used to analyze the docking results and curate the most promising binding modes for each molecule [39]. Binding modes with the most favorable energy (low DG) and making more contact with the protein binding region were chosen for further analysis. The software LigPlot+ (version 2.2.8) was used to investigate the characteristics of protein-ligand binding, such as contacting amino acids and interaction strengths [40]. PyMol software (version 2.4.0) was used to create 3D representations of the results observed on LigPlot+ for the binding modes with a higher number of contacting amino acids and a higher number of hydrogen bonds and hydrophobic contacts for each natural compound analyzed.

2.9. Proximity Ligation Assay

Cells were seeded at 7000 cells per glass coverslip and cultured for 24 h before treatment. At the end of treatment, cells were washed twice with PBS, fixed with 4% paraformaldehyde (10 min, Millipore-Sigma, Oakville, ON, Canada), and then permeabilized with 0.1% Triton X-100 (*v/v*), 10 min (Millipore-Sigma, Oakville, ON, Canada). Blocking was performed for 1 h following instructions from the Duolink kit (Thermo Fisher Scientific, Oakville, ON, Canada). Samples were incubated with primary antibodies (rabbit anti-Nrf2, Abcam, Toronto, ON, Canada, 1/500; mouse anti-KEAP1, Proteintech, Rosemont, Illinois, USA, 1/500; rabbit anti-HMGB1, Abcam, Toronto, ON, Canada, 1/500; mouse anti-HSP70, Abcam, Toronto, ON, Canada, 1/500) overnight at 4 °C in a humidified chamber. Samples were then washed and processed for proximity ligation following the manufacturer's recommendations. Nuclei were labeled for 10 min with Hoechst 33342 (10 μ M), and actin was labeled for 20 min with Phalloidin Alexa Fluor 488 (1/400, Thermo Fisher Scientific, Oakville, ON, Canada). Samples were imaged using a fluorescence microscope (Leica DMI 4000B).

2.10. Western Blot

Cells were seeded at 300,000 cells per dish in 35 mm cell culture dishes (Thermo Fisher Scientific, Oakville, ON, Canada) and cultured for 24 h. Cells were treated in serum-deprived conditions for 24 h, after which cells were washed twice with cold PBS on ice. Cells were harvested with cell scrapers and centrifuged at 2500 rpm and 4 °C for

3 min, resuspended in lysis buffer (RIPA) supplemented with complete inhibitors (Roche, Mississauga, ON, Canada) and incubated for 30 min on ice. Cell lysates were centrifuged at 14,000 rpm and 4 °C for 30 min, after which the supernatants were used for SDS-PAGE after protein quantification following instructions from the Pierce BCA assay (Thermo Fisher Scientific, Oakville, ON, Canada). Samples were normalized to 15 µg protein per lane and boiled for 5 min at 95–100 °C in the presence of Laemmli buffer. Samples were loaded onto 10% bis-acrylamide gels and run at 100 V for 30 min and then 120 V for 1 h. Proteins were transferred onto PVDF membranes (Bio-Rad, Saint-Laurent, QC, Canada) at 250 mA for 90 min on ice. Blots were blocked in 5% BSA-TBS-T (Wisent, St-Jean-Baptiste, QC, Canada) for 1 h at room temperature and then incubated with primary antibodies in 5% BSA-TBS-T overnight at 4 °C (mouse anti-KEAP1, Abcam, 1/4000; mouse anti-HSP70, Abcam, 1/4000; rabbit anti-HMGB1, Abcam, 1/4000; mouse anti-beta-tubulin, Cell Signaling, Burlington, ON, Canada). Blots were washed three times for 10 min in TBS-T and then incubated with secondary antibodies in 5% BSA-TBS-T (goat anti-mouse HRP, Bio-Rad, 1/5000; goat anti-rabbit HRP, Bio-Rad, 1/5000, Saint-Laurent, QC, Canada) for 1 h at room temperature. Blots were washed three times in TBS-T for 10 min and then incubated with chemiluminescent substrate (Clarity, Bio-Rad, Saint-Laurent, QC, Canada) before imaging with Imager 600 (Amersham, Oakville, ON, Canada). Band density was analyzed in ImageJ (version 2.14.0).

2.11. Statistical Analysis

Data are presented as mean and standard deviation (SD) (mean ± SD). Statistical significance was determined using a two-way analysis of variance (ANOVA), followed by Tukey's multiple comparison test. *p*-values less than 0.05 were considered significant. Experiments were repeated independently at least three times. Statistical analysis and graph representations were performed using GraphPad Prism (version 10.0.0).

3. Results

3.1. GBM Cells Are More Sensitive to Fisetin and Quercetin Compared to Microglia

Our study focuses on two well-studied flavonoids, fisetin and quercetin, known for their potential pharmacological relevance. Specifically, these natural compounds have shown remarkable anti-cancer effects in numerous selected *in vitro* and *in vivo* systems [41]. The physicochemical properties of fisetin and quercetin are summarized in Table 1.

Table 1. Physicochemical properties of natural products investigated.

	Molecular Mass (g mol ⁻¹)	Water Solubility (mg mL ⁻¹)	Topological Polar Surface Area (Å ²)	Number of H-Bond Donors	Number of H-Bond Acceptors	λ _{max} in Water (nm)
Fisetin (C ₁₅ H ₁₀ O ₆)	286.24	0.01	107	4	6	360
Quercetin (C ₁₅ H ₁₀ O ₇)	302.23	0.06	127	5	7	557

We first compared the cytotoxicity of the selected natural compounds on the mitochondrial metabolic activity (MTT) and lactate dehydrogenase (LDH) release of microglia and GBM cells. Cells were cultured with increasing concentrations of fisetin or quercetin (0, 5, 15, 25, 50, 100 µM). These compounds had minimal impact on the viability of microglia (Figure 1A). Fisetin and quercetin reduced GBM cell viability in a dose-dependent manner, indicating differential cytotoxicity in these cell types (Figure 1B).

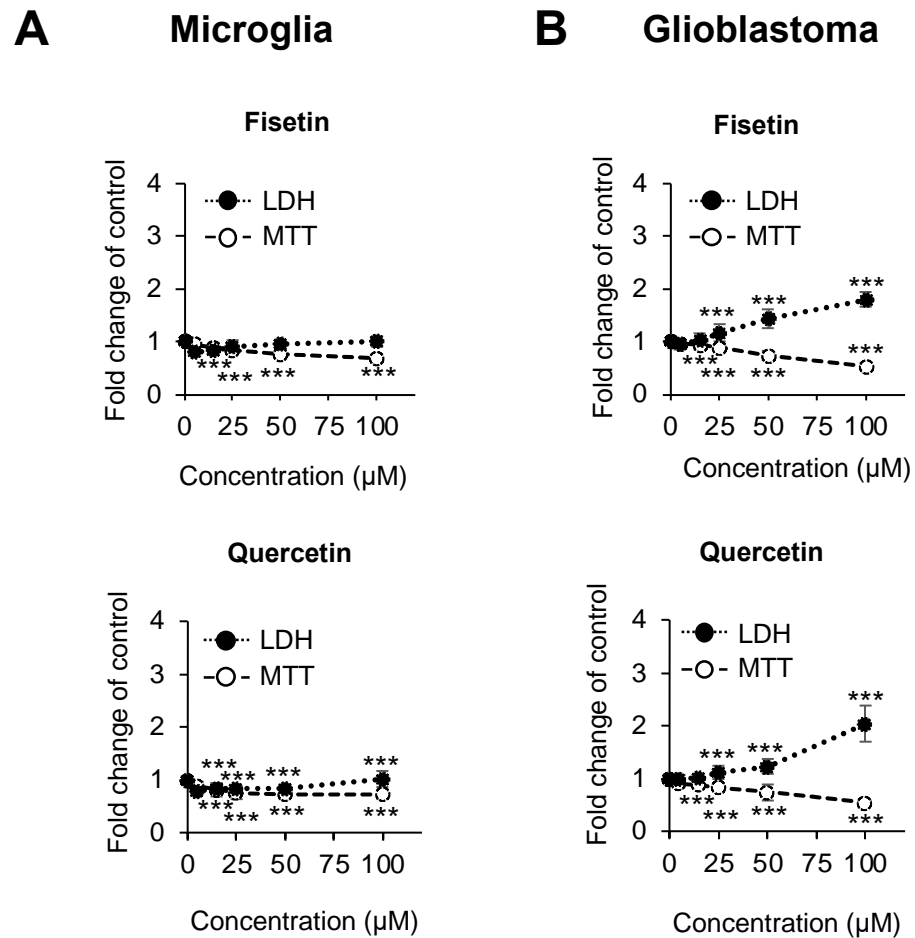


Figure 1. Dose-dependent lactate dehydrogenase (LDH) release and mitochondrial metabolic activity (MTT) in response to fisetin and quercetin. (A) Human microglia and (B) GBM cells were treated with increasing concentrations of selected compounds (0, 5, 15, 25, 50, 100 μM for fisetin and quercetin) for 24 h in serum-deprived conditions. Culture medium was used to assess LDH release, and cellular mitochondrial metabolic activity was measured using the MTT assay. Shown are the average fold change in LDH or MTT compared to the mean of the untreated control (set to 1) \pm SD from at least 3 independent experiments. (***) $p < 0.001$.

3.2. Combination of Fisetin and Temozolomide Synergistically Inhibits GBM Survival

While natural compounds may not directly induce cancer cell death, they have the potential to improve the potency of GBM treatment when combined with anti-cancer drugs, such as temozolomide (TMZ). We assessed the effect of combination treatment with fisetin and TMZ by cell counting and MTT assay, followed by calculating the combination index (CI). The combination of fisetin and TMZ at their respective IC₅₀ concentrations proved to be more effective than either compound alone. When 10 μM fisetin was combined with 30 μM TMZ, there was a 70% reduction in GBM cell viability after 72 h (Figure 2A). Notably, the CI value for the fisetin-TMZ combination was 0.00013 ($C < 1$), indicating a synergistic effect.

Subsequently, we conducted additional testing of these selected compounds on GBM tumoroids, which serve as a more relevant model *in vivo*. Given that tumoroids are more drug-resistant than monolayer cultures, we used a higher concentration of fisetin (25 μM). In line with results obtained from monolayer cultures, the combination of fisetin and TMZ resulted in a reduction in tumoroid area, whereas treatment with individual compounds did not noticeably impact tumor size (Figure 2B).

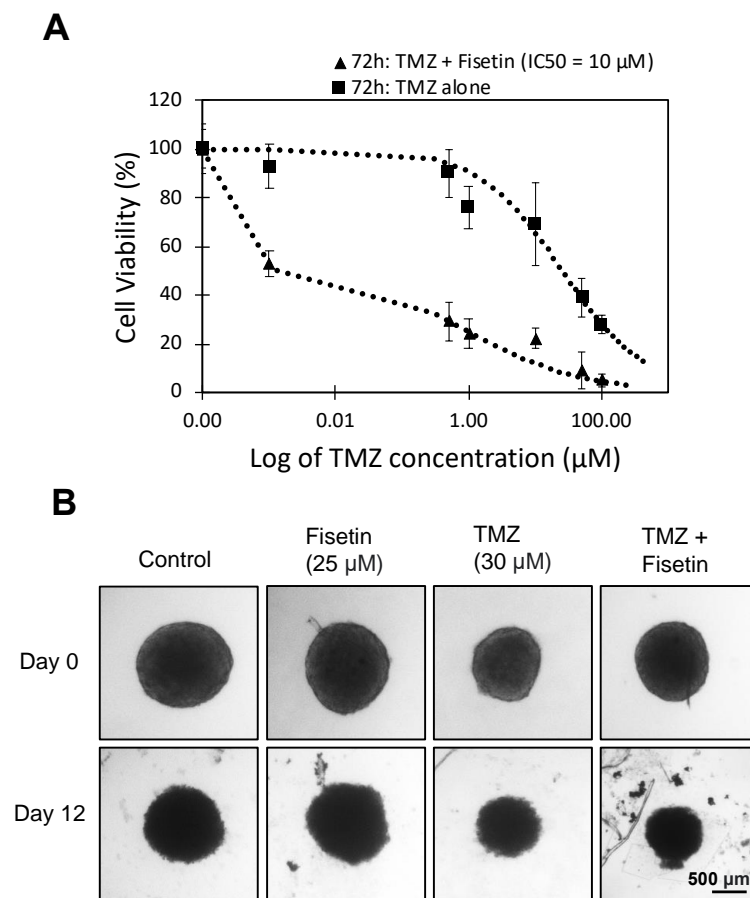


Figure 2. Dose-dependent effect in response to fisetin and TMZ. **(A)** Dose-dependent decrease in cell viability (72 h) with the combination of a fixed concentration of fisetin (10 μM) and increasing concentration of TMZ (0.001, 0.5, 1, 10, 50, and 100 μM). Each point represents the mean from three independent experiments normalized to the untreated control. Cell viability was measured by counting Hoechst 33342-labeled nuclei imaged using a fluorescence microscope. **(B)** Representative micrographs of GBM tumoroids treated with TMZ (30 μM) +/- fisetin (25 μM) on day 0 and day 12. Tumor size (area) was calculated using ImageJ.

3.3. Fisetin Reduces Oxidative Stress in GBM and Microglia

Many natural compounds have been shown to modulate oxidative stress, which is sustained differently in normal and transformed cells. Oxidative stress enhances cancer cell invasiveness and supports glioblastoma stem cell maintenance [42], contributing to treatment resistance and tumor recurrence [43]. Environmental stressors like chemicals, pollutants, and radiation are known triggers for oxidative stress [44]. Previously, we established that microglia could be activated by lipopolysaccharide (LPS), an element of Gram-negative bacterial cell walls [45]. In this study, we investigated the antioxidant effects of fisetin and quercetin in both microglia and GBM cells when subjected to exogenous stressors, namely L-buthionine sulfoximine (BSO) (Figure S1) or SARS-CoV-2 spike protein (SMT1-1) (Figure 3).

To confirm the effects on ROS status, we detected changes in intracellular ROS using the fluorescent probe CellROX. Fisetin and quercetin proved most efficient at decreasing ROS levels in microglia (Figure S1A) back to control or lower, whereas only fisetin exhibited effectiveness in GBM cells (Figure S1B). These findings align with previous studies using BSO in combination treatment with natural compounds such as curcumin to kill GBM [46].

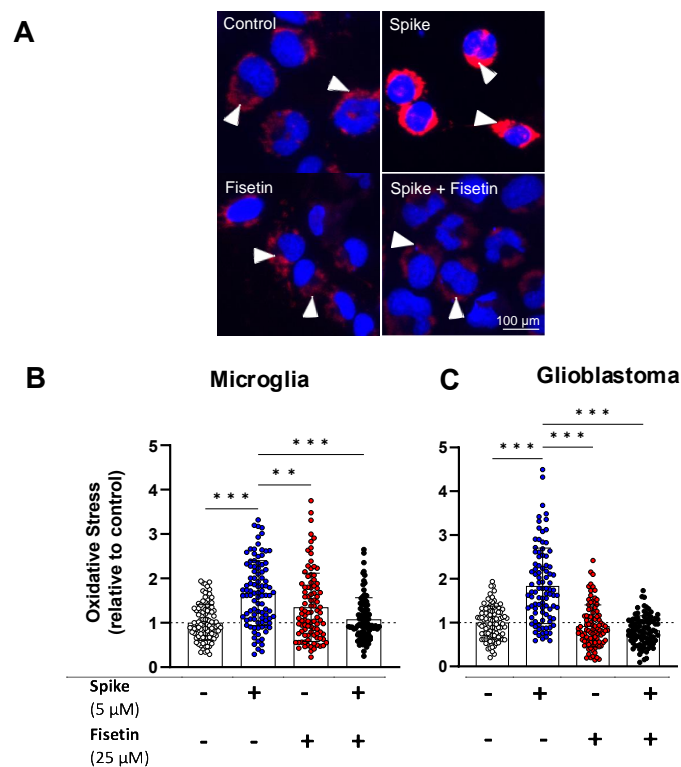


Figure 3. Oxidative stress in human microglia and GBM cells treated with fisetin +/- spike. Microglia and GBM cells were treated with spike (5 μ M), fisetin (25 μ M), or a combination of spike and fisetin for 24 h in serum-free media. (A) Representative fluorescence micrographs of microglia loaded with CellROX Deep Red (red) and imaged using a fluorescence microscope. Nuclei (blue) were labeled with Hoechst 33342. The arrowheads represent intracellular ROS. Scale bar = 100 μ m. Shown are the normalized intracellular fluorescence values to the mean of the untreated control (set to 1) for (B) microglia and (C) GBM. Dotted lines represent the mean of the control group normalized to 1. Statistical analysis was assessed using two-way ANOVA, followed by Tukey's multiple comparison test. At least 90 cells from three independent experiments were analyzed. Mean \pm SD. (** $p \leq 0.01$, *** $p \leq 0.001$).

We found that spike increased ROS production in both microglia (Figure 3A,B) and GBM cells (Figure 3C). Nevertheless, spike-mediated oxidative stress was significantly attenuated after treating microglia and GBM cells with fisetin (Figure 3B,C). These results show that fisetin treatment normalized ROS levels back to control and suppressed spike-induced oxidative stress in both cell types, indicating a lack of cell type-specific effects of fisetin on ROS modulation.

3.4. Fisetin Increases TFEB Abundance in Stressed Microglia

An important redox-sensitive transcription factor that is altered by oxidative stress is transcription factor EB (TFEB). TFEB regulates the expression of genes that are essential for lysosomal biogenesis and enzymatic activities, including the protease cathepsin B. Normally, TFEB is mainly located in the cytosol; however, under stress, TFEB is translocated to the nucleus, where it promotes the expression of multiple target genes involved in autophagy (Figure 4A) [47]. We used immunocytochemistry (ICC) to evaluate the abundance of nuclear and cytosolic TFEB in microglia and GBM cells treated with fisetin, spike, or their combination. We found that fisetin increased the abundance of TFEB in both the nucleus and cytosol of stressed microglia (Figure 4B,C). Notably, the increase in TFEB levels was less pronounced in GBM cells (Figure 4D).

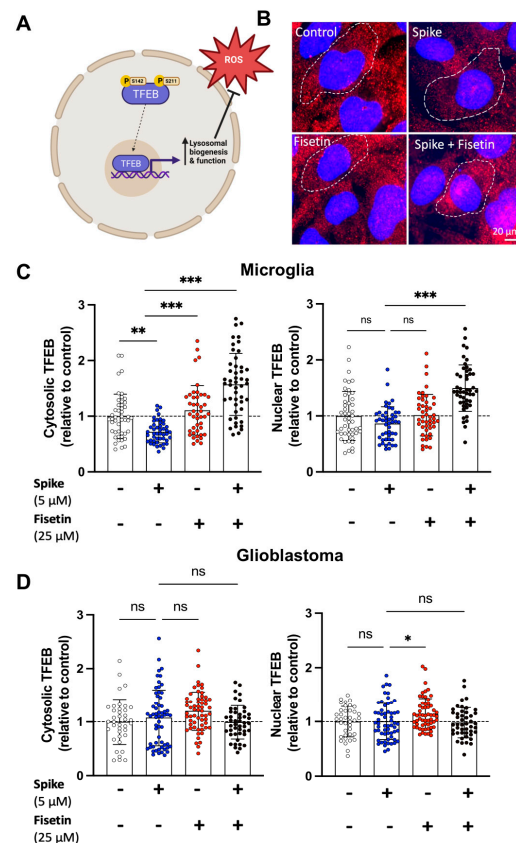


Figure 4. TFEB in human GBM cells and microglia treated with fisetin +/- spike. GBM cells and microglia were treated with spike (5 μM), fisetin (25 μM), or a combination of spike and fisetin for 24 h in serum-free media. (A) TFEB undergoes dephosphorylation under conditions of stress, where it is free to translocate to the nucleus and upregulate transcription of lysosomal biogenesis and function. (B) Microglia were labeled for TFEB (red) using rabbit anti-TFEB (1:500) and imaged using a fluorescence microscope. Nuclei were labeled with Hoechst 33342 (blue). Scale bar = 20 μm. Shown are the normalized intracellular fluorescence values to the mean of the untreated control (set to 1) in (C) human microglia and (D) GBM cells. Dotted lines represent the mean of the control group normalized to 1. Statistical analysis was assessed using two-way ANOVA, followed by Tukey's multiple comparison test. At least 40 cells from three independent experiments were analyzed. Mean ± SD. (ns—nonsignificant, * $p \leq 0.05$, ** $p \leq 0.01$, *** $p \leq 0.001$).

3.5. Fisetin Decreases Cytosolic acHMGB1 Abundance in Microglia, but Not in GBM

Another key transcription factor that is redox-responsive is high mobility group box 1 (HMGB1). HMGB1 normally localizes to the nucleus, where it can undergo post-translational modifications, including acetylation (Figure 5A). In response to oxidative stress, it translocates to the cytoplasm and is released in the extracellular space as an alarmin [48]. We used ICC to assess the levels of nuclear and cytosolic acetylated HMGB1 (acHMGB1) in microglia and GBM cells treated with fisetin, spike, or their combination. Fisetin +/- spike significantly reduced cytosolic acHMGB1 in microglia (Figure 5B,C). Interestingly, fisetin did not affect the abundance of cytosolic acHMGB1 in GBM cells (Figure 5D).

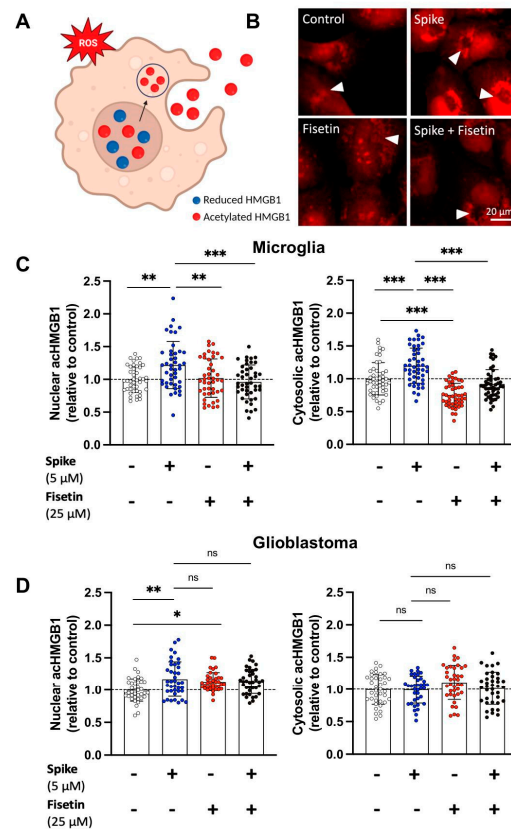


Figure 5. acHMGB1 in human GBM cells and microglia treated with fisetin +/- spike. GBM cells and microglia were treated with spike (5 μ M), fisetin (25 μ M), or a combination of spike and fisetin for 24 h in serum-free media. (A) Under stress, acHMGB1 translocates to the cytoplasm and can be released into the extracellular space as an alarmin. (B) Microglia were labeled for acHMGB1 (red) and imaged using a fluorescence microscope. Scale bar = 20 μ m. The arrowheads represent cytosolic acHMGB1. Shown are the normalized intracellular fluorescence values to the mean of the untreated control (set to 1) in (C) human microglia and (D) GBM cells. Dotted lines represent the mean of the control group normalized to 1. Statistical analysis was assessed using two-way ANOVA, followed by Tukey’s multiple comparison test. At least 40 cells from three independent experiments were analyzed. Mean \pm SD. (ns—nonsignificant, * $p \leq 0.05$, ** $p \leq 0.01$, *** $p \leq 0.001$).

3.6. Molecular Docking

To examine the effects of each natural compound on selected target proteins, we used in silico modeling to calculate binding affinities between proteins and natural compounds in parallel to experimental investigations using proximity ligation assays. The in silico data is depicted graphically (Figures S2 and S3). The calculated binding energies and contact residues are presented in Tables 2 and 3.

Table 2. Parameters of fisetin binding to target proteins.

Target	ΔG (Kcal mol ⁻¹)	Hydrophobic Contacts	Hydrogen Bonds	Number of Contacting Residues	Residues in Common with Known Ligand
KEAP 1	−9.1	5	5	10	9
HSP72	−7.9	9	1	10	9
HMGB1	−8.1	3	1	4	2

Table 3. Parameters of quercetin binding to target proteins.

Target	ΔG (Kcal mol ⁻¹)	Hydrophobic Contacts	Hydrogen Bonds	Number of Contacting Residues	Residues in Common with Known Ligand
KEAP 1	−9.1	8	7	13	10
HSP72	−7.2	5	2	7	5
HMGB1	−6.2	6	1	7	3

Cellular ROS is regulated by several factors, including Nrf2, a primary regulator of antioxidant defenses. Under homeostatic conditions, KEAP1 is bound to Nrf2, sequestering the complex in the cytosol. Under oxidative stress, however, the interaction of KEAP1 with Nrf2 is weakened, and thus Nrf2 translocates to the nucleus, activating genes encoding antioxidant, anti-inflammation, and autophagy proteins [49]. HMGB1 is also sensitive to ROS, which causes changes in its intracellular location and post-translational modifications. In turn, HSP72 can serve as a chaperone for proteins modified or damaged by ROS.

3.7. Fisetin and Quercetin Can Bind to KEAP1, HSP72 and HMGB1

We first investigated if the modulation of Nrf2, HMGB1, and HSP72 could be explained by direct binding of fisetin to the proteins of interest. To restrict the analysis to binding regions with biological relevance, we focused docking on protein regions previously reported as involved in the binding with other compounds or proteins. For HSP72, we focused on the ATP binding pocket, as it is known to bind not only ATP but also other competitive inhibitors [50]. Although there is a lack of structural information on HMGB1 bound to small molecules, biophysical analyses have suggested that its N- and C-terminus regions (box A and B) are involved in the binding of the natural compounds glycyrrhizin and salicylic acid [25,37,38]. Therefore, the box A region was considered in our docking. In the case of KEAP1, the central channel of the protein formed by its beta-propeller folding has been shown to bind different compounds and the protein Nrf2 [51–55].

In silico analyses indicated that fisetin could bind all the proteins of interest with different strengths and predicted binding energies (Figure S2 and Table 2). Fisetin had the highest number of hydrophobic contacts and hydrogen bonds when docked to KEAP1 and HSP72 protein structures, with 10 contacting residues for each protein (Table 2). In addition, both proteins had favorable binding energies to fisetin, with ΔG of −9.1 kcal/mol and −7.9 kcal/mol for KEAP1 and HSP72, respectively. Although fisetin docking to HMGB1 has a similar binding energy ($\Delta G = -8.1$ kcal/mol) compared to other targets, the number of contacts between the compound and protein target is considerably lower (Table 2). This small number of contacts with the compound is related to the overall surface of HMGB1, which has shallow pockets in the box A region (Figure S2F).

Quercetin, similar to fisetin, is also predicted to bind to all three protein targets (Figure S3). The interaction with KEAP1 presented the most favorable binding energy (−9.1 kcal/mol) and the highest number of contact residues (Table 3). Binding energies were observed to be comparable to that of fisetin (Tables 2 and 3), and differences in the number of contacting residues were small. Fisetin and quercetin have similar structures (Table 1), featuring a three-ring backbone formed by two benzene rings separated by a pyran ring [56]. The presence of one additional hydroxyl group on quercetin is the major difference between the two molecules.

3.8. Modulation of Protein Targets in Microglia and Glioblastoma Cells

Distinctions between microglia and glioblastoma imply differences in their protein function and interactions. Fisetin and quercetin did not markedly change the protein levels of HMGB1, HSP72, or KEAP1 in microglia and glioblastoma (Figure S4), but did modulate key protein–protein interactions (Figure 6). Results from proximity ligation assays show that fisetin significantly impacts Nrf2-KEAP1 interaction in microglia, whereas it is most

effective in enhancing HMGB1-HSP72 interaction in glioblastoma (Figure 6). Overall, these findings support the need for combining in silico modeling with experimental approaches, as each of them contributes to a more complete picture of the biological effects of flavonoids.

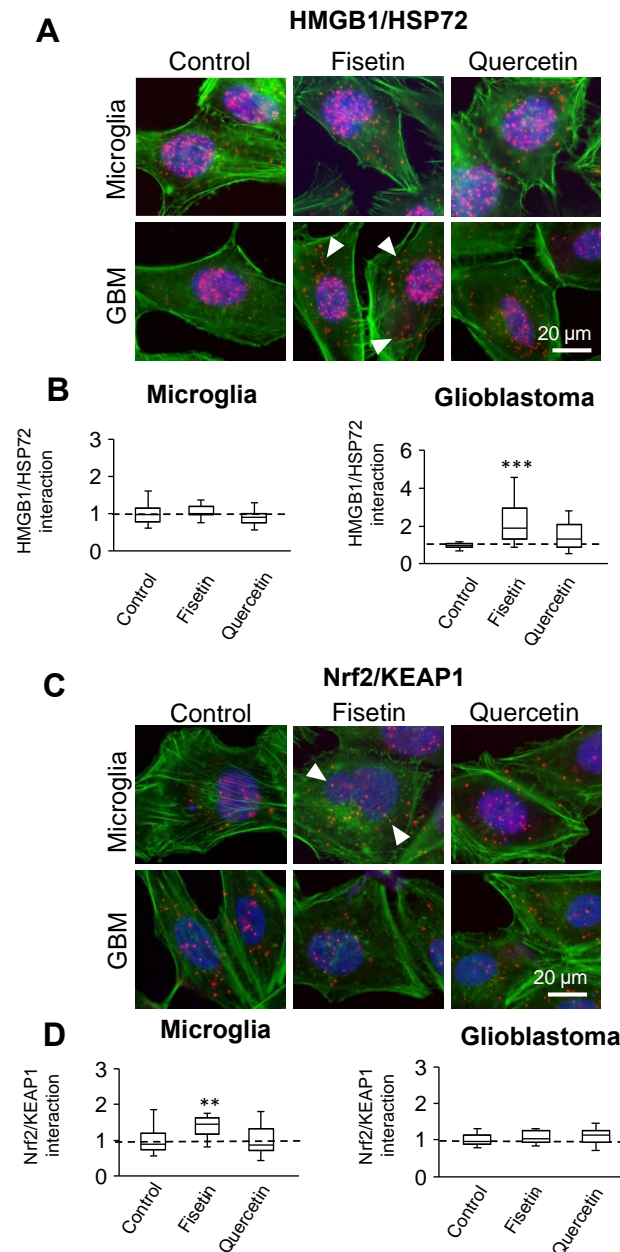


Figure 6. Nrf2-KEAP1 and HMGB1/HSP72 protein–protein interactions detected using proximity ligation assays. Interactions between (A,B) Nrf2-KEAP1 and (C,D) HMGB1/HSP72 in microglia and

glioblastoma treated with fisetin (25 μ M) or quercetin (25 μ M) for 24 h in serum-deprived media. Shown are representative fluorescence micrographs with protein interactions (red dots) in cells labeled for actin (green) and nuclei (blue). The arrowheads indicate protein–protein interactions. Shown are the distribution of the number of interactions per cell as fold change in the untreated control (set to 1), with the minimum value, 25th to 75th percentiles, and maximum values indicated. Box blots show the median, 25–75% quartiles, minimum and maximum values. Dotted line represents the mean of the control normalized to 1. At least 60 cells from three independent experiments were analyzed. (** $p < 0.01$; *** $p < 0.001$).

4. Discussion

The results obtained from these studies offer insights into the mechanisms of action of fisetin and quercetin within cerebral tumor cells of glioblastoma and microglia, a common central macrophage in the TME. GBM microenvironment plays a pivotal role in tumorigenesis, primarily the generation of ROS. ROS can significantly impact the quantity and quality of non-cancer cells in the vicinity, such as microglia, by modulating redox-responsive transcription factors, including TFEB, Nrf2, HSP72, and HMGB1. The response to treatment observed in microglia and GBM supports the hypothesis that polyphenols exert their differential effects by interacting with redox-responsive factors.

Polyphenols are widely studied bioactive compounds in pharmacology and life sciences and are popularly used in cosmetics, as dietary supplements, and as therapeutics [57–62]. A number of studies suggested their potential health benefits in cardiovascular disease, diabetes, and neurodegenerative diseases [32,33,63,64]. They can downregulate inflammation and protect non-cancerous cells against oxidative stress [65,66]. Flavonoids can also inhibit cancer cell proliferation and angiogenesis [67–69] with striking cell-type-dependent effects [68,70–73]. Although their effectiveness in different cell types is well documented, mechanistic data are still sparse. In this study, we compared the effects of fisetin and quercetin in immortalized microglia and transformed GBM cells. GBM cells were more sensitive to the natural compounds, showing pronounced concentration-dependent decreases in mitochondrial metabolic activity, as well as significantly higher LDH release (Figure 1).

Fisetin, a commonly found dietary flavonoid, has recently gained attention for its antioxidant properties and its potential to prevent a broad range of life-threatening diseases [74]. Our study shows that fisetin significantly decreases oxidative stress in both non-neoplastic (microglia) and neoplastic (GBM) cells (Figure 3). Similar to its analog quercetin, fisetin influences numerous biological processes that may contribute to its senolytic effects [75]. For example, due to its hydrophobic nature, fisetin can penetrate and accumulate within cell membranes, where it exerts antioxidant and anti-inflammatory effects [76]. Additionally, fisetin induces apoptotic effects in senescent cells by suppressing Bcl-2 family members and other components of the senescence-associated secretory phenotype (SASP) network [77]. Importantly, fisetin has shown even greater senotherapeutic activity than quercetin in both animal and human tissues [76]. Currently, fisetin is the subject of several clinical trials for various cancers and age-related diseases, including osteoarthritis, coronavirus infections, frail elderly syndrome, and chronic kidney diseases [78]. As a result, the clinical potential of fisetin, in terms of its safety, tolerability, and efficacy, could potentially be harnessed in medicine.

Many natural compounds possess the ability to target multiple molecules, making them valuable candidates for cancer treatment. However, the precise molecular interactions between cellular proteins and neuroprotective polyphenols remain poorly characterized. Our *in silico* analysis, focusing on KEAP1, HSP72, and HMGB1, suggests that fisetin and quercetin can bind to biologically relevant binding pockets within these proteins. Among these interactions, KEAP1 demonstrates the most favorable binding energy and the highest number of contacts with fisetin and quercetin (Tables 2 and 3). This observation aligns with the structural characteristics of KEAP1, known for its large central channel typical of WD-repeat proteins [79]. Several co-crystal structures of KEAP1 have implied interactions within its central channel, involving Nrf2 and various small molecules [51–53,80–83].

Nrf2 plays a pivotal role in the production of endogenous antioxidants in response to oxidative stress [84,85]. In normal physiological conditions, Nrf2 interacts with the KEAP1 protein in the Kelch domain of KEAP1 and undergoes cytosolic degradation [86]. When mild to moderate oxidative stress occurs, the Nrf2-KEAP1 complex dissociates, allowing Nrf2 to translocate to the nucleus. This stimulates the upregulation of antioxidant-responsive genes such as HO-1 and NQO1, thereby enhancing the production and release of endogenous antioxidants like GSH, SOD, and catalase to mitigate oxidative stress [86,87]. Flavonoids have been reported to interfere with Nrf2-KEAP1 protein–protein interactions in the cytosol, preventing the spontaneous degradation of Nrf2. These flavonoids competi-

tively bind with the KEAP1 protein at the Nrf2 binding site, resulting in the translocation of Nrf2 to the nucleus. This activation of Nrf2 subsequently triggers the upregulation of antioxidant genes like GSH, SOD, and catalase [88]. Increased Nrf2-KEAP1 interaction following fisetin treatment is thus in line with lower intracellular ROS (Figures 3 and 6).

Fisetin and quercetin also displayed favorable binding energies with HMGB1, although the number of contacts is lower than for KEAP1 (Tables 2 and 3). HMGB1 is primarily found in the nucleus, but upon stress, it is translocated to the cytosol, where it can be post-translationally modified (acetylated, oxidized, and methylated) [89–93]. HMGB1 can be secreted to the extracellular space via active secretion or passive release by necrotic cells [94–98]. Once in the extracellular environment, it can act as a paracrine factor and interact with receptors, particularly RAGE, thereby activating key signaling pathways that regulate cell growth, differentiation, motility, and death [97,99]. The interaction between HMGB1 and RAGE has been suggested to promote the proliferation and invasion of various tumor cells [99]. Interestingly, we found that fisetin does not affect acHMGB1 abundance and translocation in GBM. On the other hand, fisetin reduces cytosolic acHMGB1 levels in microglia but does not affect nuclear acHMGB1 abundance (Figure 5). This suggests that fisetin modulates the release of acHMGB1 in immune cells and, in turn, reduces the exacerbated inflammation in the TME. Bassi et al. showed that glioma cells contain HMGB1 predominantly in the nucleus and cannot secrete it constitutively or upon stimulation. However, necrotic glioma cells can release HMGB1 after it has translocated from the nucleus to the cytosol [100]. These findings suggest that HMGB1 is acting as an autocrine factor that promotes the growth and migration of tumor cells.

All compounds had comparable binding energies with HSP72, whereas fisetin was predicted to have the greatest number of contacting residues. Fisetin fits deeply into the HSP72 binding pocket, contacting at least three residues at the bottom (Figure S2E). Ser275 was shown as essential for HSP72 to bind ATP and other compounds via hydrogen bonds [101]. HSP72 and its family respond to cellular stressors in both normal and transformed cells [102] and can interact with other stress-responsive proteins, including HMGB1 [103]. HMGB1-HSP72 modulation via fisetin in GBM (Figure 6) is relevant for therapeutic approaches, as HSP70 proteins contribute to drug resistance in many cancers [104–107].

Despite the promising results of flavonoids against various cancer types, their application in cancer treatment is hindered by issues such as low solubility, poor absorption, and rapid metabolism [108]. To overcome these limitations, nanocarriers have been developed to enhance the bioavailability of flavonoids [88]. Both *in vitro* and *in vivo* studies have shown potential anticancer activity of flavonoid nanoparticles against A549 lung cancer cells, B16F10 melanoma cells, MCF-7 breast cancer cells, HepG2 liver cancer cells, and CT26 colorectal cancer cells [88]. Various types of flavonoid nanocarriers are currently employed in cancer therapy, including polymeric nanoparticles [109], nanocapsules [110], metallic nanoparticles such as gold [111], and solid lipid nanocarriers [112]. We propose incorporating fisetin into polymeric soft nanoparticles to improve its solubility, stability, and sustained delivery, all while retaining its biological activity (Figure S5).

Our docking and biological studies aimed at relating potential interactions between fisetin and quercetin with modulations of the protein targets in human cells. The differential effects of the natural compounds depend on the cell type, target protein, and their location, which is often determined by interacting partners and post-translational modifications. Our studies introduce a complementary approach to the development of new therapeutics for GBM, leveraging the simultaneous targeting of multiple intracellular proteins (e.g., transcription factors) whose effects depend on their location and interaction partners. Such an approach could result in more favorable patient outcomes compared to standard therapeutic interventions.

5. Conclusions

Current therapeutic approaches with polyphenols in different pathologies, including GBM, are limited and mainly target the tumor itself. We support the proposed approach that altering the cells in the tumor microenvironment is essential and can contribute to improved patient outcomes. Taken together, the presented studies show differential effects of fisetin and quercetin in microglia and glioblastoma cells. Molecular modeling combined with experimental data suggests that combination with other natural compounds (e.g., docosahexaenoic acid) [113] is warranted and that alternative therapeutic interventions could be developed aiming at differential disruptions of protein–protein interactions in glioblastoma itself and its surrounding microenvironment, comprising microglia, peripheral macrophages, astrocytes, vasculature, etc. In addition to binding energy and contact residues, the affinity and specificity of these interactions need to be further investigated. Future studies using biophysical and structural biology methods will be fundamental to advance our understanding of the proteins-compounds interactions described in this study. Nonetheless, this study suggests direct binding of fisetin and quercetin to the binding pockets of KEAP1, HSP72, and HMGB1. We suggest that experimental approaches, particularly with human organoids consisting of several cell types—transformed and non-transformed—would offer acceptable testing paradigms for future therapeutics. Such experimental models using human cells combined with single-cell transcriptomics and single-nucleus transcriptomics could offer new paths to uncover better treatments for GBM [114].

Supplementary Materials: The following supporting information can be downloaded at <https://www.mdpi.com/article/10.3390/cells12242821/s1>, Figure S1: Modulation of intracellular oxidative stress induced by buthionine sulfoximine (BSO) using selected natural compounds; Figure S2: Docking analyses of fisetin binding to target proteins; Figure S3: Docking analyses of quercetin binding to target proteins; Figure S4: Protein levels of KEAP1, HSP72 and HMGB1 in human microglia and glioblastoma cells; Figure S5: Physical properties of fisetin-loaded self-assembly.

Author Contributions: Conceptualization, D.M. and A.K.; investigation, N.J., I.Z., G.L.R., L.M. and E.R.G.; writing—original draft preparation, N.J. and I.Z.; writing—review and editing, N.J., I.Z., G.L.R., L.M., E.R.G., A.K. and D.M.; supervision, D.M. and A.K.; funding acquisition, D.M. and A.K. All authors have read and agreed to the published version of the manuscript.

Funding: This research was funded by the Natural Sciences and Engineering Research Council of Canada (RGPIN 2020-07011) (RGPIN-2023-03565).

Data Availability Statement: Data are contained within the article.

Acknowledgments: We thank Qiaochu Zhang for her assistance in preparing Table 1. The graphical abstract was created with BioRender.com (accessed on 6 December 2023).

Conflicts of Interest: The authors declare no conflict of interest.

References

- Matias, D.; Balça-Silva, J.; da Graça, G.C.; Wanjiru, C.M.; Macharia, L.W.; Nascimento, C.P.; Roque, N.R.; Coelho-Aguiar, J.M.; Pereira, C.M.; Dos Santos, M.F.; et al. Microglia/Astrocytes–Glioblastoma Crosstalk: Crucial Molecular Mechanisms and Microenvironmental Factors. *Front. Cell. Neurosci.* **2018**, *12*, 235. [CrossRef] [PubMed]
- Shergalis, A.; Bankhead, A., 3rd; Luesakul, U.; Muangsins, N.; Neamati, N. Current Challenges and Opportunities in Treating Glioblastoma. *Pharmacol. Rev.* **2018**, *70*, 412–445. [CrossRef] [PubMed]
- Geribaldi-Doldán, N.; Fernández-Ponce, C.; Quiroz, R.N.; Sánchez-Gomar, I.; Escorcía, L.G.; Velásquez, E.P.; Quiroz, E.N. The Role of Microglia in Glioblastoma. *Front. Oncol.* **2021**, *10*. [CrossRef] [PubMed]
- Gutmann, D.H.; Kettenmann, H. Microglia/Brain Macrophages as Central Drivers of Brain Tumor Pathobiology. *Neuron* **2019**, *104*, 442–449. [CrossRef] [PubMed]
- Hambardzumyan, D.; Gutmann, D.H.; Kettenmann, H. The role of microglia and macrophages in glioma maintenance and progression. *Nat. Neurosci.* **2016**, *19*, 20–27. [CrossRef]
- Gülke, E.; Gelderblom, M.; Magnus, T. Danger signals in stroke and their role on microglia activation after ischemia. *Ther. Adv. Neurol. Disord.* **2018**, *11*, 1756286418774254. [CrossRef]
- Masuda, T.; Sankowski, R.; Staszewski, O.; Prinz, M. Microglia Heterogeneity in the Single-Cell Era. *Cell Rep.* **2020**, *30*, 1271–1281. [CrossRef]
- Prinz, M.; Jung, S.; Priller, J. Microglia Biology: One Century of Evolving Concepts. *Cell* **2019**, *179*, 292–311. [CrossRef]
- Donat, C.K.; Scott, G.; Gentleman, S.M.; Sastre, M. Microglial Activation in Traumatic Brain Injury. *Front. Aging Neurosci.* **2017**, *9*, 208. [CrossRef]
- Simpson, D.S.A.; Oliver, P.L. ROS Generation in Microglia: Understanding Oxidative Stress and Inflammation in Neurodegenerative Disease. *Antioxidants* **2020**, *9*, 743. [CrossRef]
- Liu, H.; Sun, Y.; Zhang, Q.; Jin, W.; Gordon, R.E.; Zhang, Y.; Wang, J.; Sun, C.; Wang, Z.J.; Qi, X.; et al. Pro-inflammatory and proliferative microglia drive progression of glioblastoma. *Cell Rep.* **2021**, *36*, 109718. [CrossRef] [PubMed]
- Rosciszewski, G.; Cadena, V.; Auzmendi, J.; Cieri, M.B.; Lukin, J.; Rossi, A.R.; Murta, V.; Villarreal, A.; Reinés, A.; Gomes, F.C.A.; et al. Detrimental Effects of HMGB-1 Require Microglial-Astroglial Interaction: Implications for the Status Epilepticus -Induced Neuroinflammation. *Front. Cell. Neurosci.* **2019**, *13*, 380. [CrossRef] [PubMed]
- Andersson, U.; Tracey, K.J.; Yang, H. Post-Translational Modification of HMGB1 Disulfide Bonds in Stimulating and Inhibiting Inflammation. *Cells* **2021**, *10*, 3323. [CrossRef] [PubMed]
- Ou, A.; Ott, M.; Fang, D.; Heimberger, A.B. The Role and Therapeutic Targeting of JAK/STAT Signaling in Glioblastoma. *Cancers* **2021**, *13*, 437. [CrossRef]
- Rapoport, B.L.; Steel, H.C.; Theron, A.J.; Heyman, L.; Smit, T.; Ramdas, Y.; Anderson, R. High Mobility Group Box 1 in Human Cancer. *Cells* **2020**, *9*, 1664. [CrossRef]
- Campisi, J.; Leem, T.H.; Fleshner, M. Stress-induced extracellular Hsp72 is a functionally significant danger signal to the immune system. *Cell Stress Chaperones* **2003**, *8*, 272–286. [CrossRef]
- Fujii, K.; Idogawa, M.; Suzuki, N.; Iwatsuki, K.; Kanekura, T. Functional Depletion of HSP72 by siRNA and Quercetin Enhances Vorinostat-Induced Apoptosis in an HSP72-Overexpressing Cutaneous T-Cell Lymphoma Cell Line, Hut78. *Int. J. Mol. Sci.* **2021**, *22*, 11258. [CrossRef]
- Matokanovic, M.; Barisic, K.; Filipovic-Grcic, J.; Maysinger, D. Hsp70 silencing with siRNA in nanocarriers enhances cancer cell death induced by the inhibitor of Hsp90. *Eur. J. Pharm. Sci.* **2013**, *50*, 149–158. [CrossRef]
- Napolitano, G.; Ballabio, A. TFEB at a glance. *J. Cell Sci.* **2016**, *129*, 2475–2481. [CrossRef]
- Ngo, V.; Duennwald, M.L. Nrf2 and Oxidative Stress: A General Overview of Mechanisms and Implications in Human Disease. *Antioxidants* **2022**, *11*, 2345. [CrossRef]
- Batra, P.; Sharma, A.K. Anti-cancer potential of flavonoids: Recent trends and future perspectives. *3 Biotech* **2013**, *3*, 439–459. [CrossRef] [PubMed]
- Atanasov, A.G.; Waltenberger, B.; Pferschy-Wenzig, E.-M.; Linder, T.; Wawrosch, C.; Uhrin, P.; Temml, V.; Wang, L.; Schwaiger, S.; Heiss, E.H.; et al. Discovery and resupply of pharmacologically active plant-derived natural products: A review. *Biotechnol. Adv.* **2015**, *33*, 1582–1614. [CrossRef] [PubMed]
- Forman, H.J.; Zhang, H. Targeting oxidative stress in disease: Promise and limitations of antioxidant therapy. *Nat. Rev. Drug Discov.* **2021**, *20*, 689–709. [CrossRef] [PubMed]
- Harvey, A.L.; Edrada-Ebel, R.; Quinn, R.J. The re-emergence of natural products for drug discovery in the genomics era. *Nat. Rev. Drug Discov.* **2015**, *14*, 111–129. [CrossRef] [PubMed]
- Choi, J.; Moquin, A.; Bomal, E.; Na, L.; Maysinger, D.; Kakkar, A. Telodendrimers for Physical Encapsulation and Covalent Linking of Individual or Combined Therapeutics. *Mol. Pharm.* **2017**, *14*, 2607–2615. [CrossRef] [PubMed]
- Newman, D.J.; Cragg, G.M. Natural products as sources of new drugs over the nearly four decades from 01/1981 to 09/2019. *J. Nat. Prod.* **2020**, *83*, 770–803. [CrossRef] [PubMed]
- Berman, A.Y.; Motechin, R.A.; Wiesenfeld, M.Y.; Holz, M.K. The therapeutic potential of resveratrol: A review of clinical trials. *NPJ Precis. Oncol.* **2017**, *1*, 35. [CrossRef]
- Jia, S.; Xu, X.; Zhou, S.; Chen, Y.; Ding, G.; Cao, L. Fisetin induces autophagy in pancreatic cancer cells via endoplasmic reticulum stress- and mitochondrial stress-dependent pathways. *Cell Death Dis.* **2019**, *10*, 1–15. [CrossRef]

29. Maysinger, D.; Moquin, A.; Choi, J.; Kodiha, M.; Stochaj, U. Gold nanourchins and celastrol reorganize the nucleo- and cytoskeleton of glioblastoma cells. *Nanoscale* **2017**, *10*, 1716–1726. [CrossRef]
30. Rauf, A.; Imran, M.; Khan, I.A.; Ur-Rehman, M.; Gilani, S.A.; Mehmood, Z.; Mubarak, M.S. Anticancer potential of quercetin: A comprehensive review. *Phytother. Res.* **2018**, *32*, 2109–2130. [CrossRef]
31. Aalinkel, R.; Bindukumar, B.; Reynolds, J.L.; Sykes, D.E.; Mahajan, S.D.; Chadha, K.C.; Schwartz, S.A. The dietary bioflavonoid, quercetin, selectively induces apoptosis of prostate cancer cells by down-regulating the expression of heat shock protein. *Prostate* **2008**, *68*, 1773–1789. [CrossRef] [PubMed]
32. Anhê, F.F.; Desjardins, Y.; Pilon, G.; Dudonné, S.; Genovese, M.I.; Lajolo, F.M.; Marette, A. Polyphenols and type 2 diabetes: A prospective review. *PharmaNutrition* **2013**, *1*, 105–114. [CrossRef]
33. Cao, H.; Ou, J.; Chen, L.; Zhang, Y.; Szkudelski, T.; Delmas, D.; Daglia, M.; Xiao, J. Dietary polyphenols and type 2 diabetes: Human Study and Clinical Trial. *Crit. Rev. Food Sci. Nutr.* **2018**, *59*, 3371–3379. [CrossRef] [PubMed]
34. Del Duca, D.; Werbowetski, T.; Del Maestro, R.F. Spheroid Preparation from Hanging Drops: Characterization of a Model of Brain Tumor Invasion. *J. Neuro-Oncol.* **2004**, *67*, 295–303. [CrossRef] [PubMed]
35. Grosdidier, A.; Zoete, V.; Michielin, O. SwissDock, a protein-small molecule docking web service based on EADock DSS. *Nucleic Acids Res.* **2011**, *39*, W270–W277. [CrossRef] [PubMed]
36. Choi, H.W.; Tian, M.; Song, F.; Venereau, E.; Preti, A.; Park, S.-W.; Hamilton, K.; Swapna, G.V.T.; Manohar, M.; Moreau, M.; et al. Aspirin's Active Metabolite Salicylic Acid Targets High Mobility Group Box 1 to Modulate Inflammatory Responses. *Mol. Med.* **2015**, *21*, 526–535. [CrossRef]
37. Mollica, L.; De Marchis, F.; Spitaleri, A.; Dallacosta, C.; Pennacchini, D.; Zamai, M.; Agresti, A.; Trisciuglio, L.; Musco, G.; Bianchi, M.E. Glycyrrhizin Binds to High-Mobility Group Box 1 Protein and Inhibits Its Cytokine Activities. *Chem. Biol.* **2007**, *14*, 431–441. [CrossRef]
38. Paudel, Y.N.; Khan, S.U.; Othman, I.; Shaikh, M.F. Naturally Occurring HMGB1 Inhibitor, Glycyrrhizin, Modulates Chronic Seizures-Induced Memory Dysfunction in Zebrafish Model. *ACS Chem. Neurosci.* **2021**, *12*, 3288–3302. [CrossRef]
39. Pettersen, E.F.; Goddard, T.D.; Huang, C.C.; Couch, G.S.; Greenblatt, D.M.; Meng, E.C.; Ferrin, T.E. UCSF Chimera? A visualization system for exploratory research and analysis. *J. Comput. Chem.* **2004**, *25*, 1605–1612. [CrossRef]
40. Laskowski, R.A.; Swindells, M.B. LigPlot+: Multiple ligand–protein interaction diagrams for drug discovery. *J. Chem. Inf. Model.* **2011**, *51*, 2778–2786. [CrossRef]
41. Zeng, Y.; Song, J.; Zhang, M.; Wang, H.; Zhang, Y.; Suo, H. Comparison of In Vitro and In Vivo Antioxidant Activities of Six Flavonoids with Similar Structures. *Antioxidants* **2020**, *9*, 732. [CrossRef] [PubMed]
42. Olivier, C.; Oliver, L.; Lalier, L.; Vallette, F.M. Drug Resistance in Glioblastoma: The Two Faces of Oxidative Stress. *Front. Mol. Biosci.* **2021**, *7*. [CrossRef] [PubMed]
43. Costa, A.; Scholer-Dahirel, A.; Mechta-Grigoriou, F. The role of reactive oxygen species and metabolism on cancer cells and their microenvironment. *Semin. Cancer Biol.* **2014**, *25*, 23–32. [CrossRef] [PubMed]
44. Pizzino, G.; Irrera, N.; Cucinotta, M.; Pallio, G.; Mannino, F.; Arcoraci, V.; Squadrito, F.; Altavilla, D.; Bitto, A. Oxidative Stress: Harms and Benefits for Human Health. *Oxid. Med. Cell. Longev.* **2017**, *2017*, 8416763. [CrossRef] [PubMed]
45. Baghbanbashi, M.; Yong, H.W.; Zhang, I.; Lotocki, V.; Yuan, Z.; Pazuki, G.; Maysinger, D.; Kakkar, A. Stimuli-Responsive Miktoarm Polymer-Based Formulations for Fisetin Delivery and Regulatory Effects in Hyperactive Human Microglia. *Macromol. Biosci.* **2022**, *22*, e2200174. [CrossRef] [PubMed]
46. Zhang, I.; Cui, Y.; Amiri, A.; Ding, Y.; Campbell, R.E.; Maysinger, D. Pharmacological inhibition of lipid droplet formation enhances the effectiveness of curcumin in glioblastoma. *Eur. J. Pharm. Biopharm.* **2016**, *100*, 66–76. [CrossRef]
47. Martina, J.A.; Puertollano, R. TFEB and TFE3: The art of multi-tasking under stress conditions. *Transcription* **2016**, *8*, 48–54. [CrossRef]
48. Yu, Y.; Tang, D.; Kang, R. Oxidative stress-mediated HMGB1 biology. *Front. Physiol.* **2015**, *6*, 93. [CrossRef]
49. Ong, A.J.S.; Bladen, C.E.; Tigani, T.A.; Karamalakakis, A.P.; Evason, K.J.; Brown, K.K.; Cox, A.G. The KEAP1–NRF2 pathway regulates TFEB/TFE3-dependent lysosomal biogenesis. *Proc. Natl. Acad. Sci. USA* **2023**, *120*. [CrossRef]
50. Jones, A.M.; Westwood, I.M.; Osborne, J.D.; Matthews, T.P.; Cheeseman, M.D.; Rowlands, M.G.; Jeganathan, F.; Burke, R.; Lee, D.; Kadi, N.; et al. A fragment-based approach applied to a highly flexible target: Insights and challenges towards the inhibition of HSP70 isoforms. *Sci. Rep.* **2016**, *6*, 34701. [CrossRef]
51. Fukutomi, T.; Takagi, K.; Mizushima, T.; Ohuchi, N.; Yamamoto, M. Kinetic, Thermodynamic, and Structural Characterizations of the Association between Nrf2-DLGex Degron and Keap1. *Mol. Cell. Biol.* **2014**, *34*, 832–846. [CrossRef]
52. Hörer, S.; Reinert, D.; Ostmann, K.; Hoevens, Y.; Nar, H. Crystal-contact engineering to obtain a crystal form of the Kelch domain of human Keap1 suitable for ligand-soaking experiments. *Acta Crystallogr. Sect. F Struct. Biol. Cryst. Commun.* **2013**, *69*, 592–596. [CrossRef] [PubMed]
53. Ontoria, J.M.; Biancofiore, I.; Fezzardi, P.; Ferrigno, F.; Torrente, E.; Colarusso, S.; Bianchi, E.; Andreini, M.; Patsilnakos, A.; Kempf, G.; et al. Combined Peptide and Small-Molecule Approach toward Nonacidic THIQ Inhibitors of the KEAP1/NRF2 Interaction. *ACS Med. Chem. Lett.* **2020**, *11*, 740–746. [CrossRef] [PubMed]
54. Wu, S.-Y.; Watabe, K. The roles of microglia macrophages in tumor progression of brain cancer and metastatic disease. *Front. Biosci.* **2017**, *22*, 1805–1829. [CrossRef] [PubMed]

55. Zhong, M.; Lynch, A.; Muellers, S.N.; Jehle, S.; Luo, L.; Hall, D.R.; Iwase, R.; Carolan, J.P.; Egbert, M.; Wakefield, A.; et al. Interaction Energetics and Druggability of the Protein–Protein Interaction between Kelch-like ECH-Associated Protein 1 (KEAP1) and Nuclear Factor Erythroid 2 Like 2 (Nrf2). *Biochemistry* **2019**, *59*, 563–581. [CrossRef] [PubMed]
56. Rashid, M.I.; Fareed, M.I.; Rashid, H.; Aziz, H.; Ehsan, N.; Khalid, S.; Ghaffar, I.; Ali, R.; Gul, A.; Hakeem, K.R. Flavonoids and Their Biological Secrets. *Plant Hum. Health* **2019**, *2*, 579–605. [CrossRef]
57. Manach, C.; Mazur, A.; Scalbert, A. Polyphenols and prevention of cardiovascular diseases. *Curr. Opin. Infect. Dis.* **2005**, *16*, 77–84. [CrossRef]
58. Michalska, M.; Gluba, A.; Mikhailidis, D.P.; Nowak, P.; Bielecka-Dabrowa, A.; Rysz, J.; Banach, M. The role of polyphenols in cardiovascular disease. *Med. Sci. Monit. Int. Med. J. Exp. Clin. Res.* **2010**, *16*, RA110–RA119.
59. Pandey, K.B.; Rizvi, S.I. Plant polyphenols as dietary antioxidants in human health and disease. *Oxid. Med. Cell. Longev.* **2009**, *2*, 270–278. [CrossRef]
60. Panzella, L. Natural Phenolic Compounds for Health, Food and Cosmetic Applications. *Antioxidants* **2020**, *9*, 427. [CrossRef]
61. Quiñones, M.; Miguel, M.; Aleixandre, A. Beneficial effects of polyphenols on cardiovascular disease. *Pharmacol. Res.* **2013**, *68*, 125–131. [CrossRef] [PubMed]
62. Zillich, O.V.; Schweiggert-Weisz, U.; Eisner, P.; Kersch, M. Polyphenols as active ingredients for cosmetic products. *Int. J. Cosmet. Sci.* **2015**, *37*, 455–464. [CrossRef] [PubMed]
63. Ebrahimi, A.; Schluessener, H. Natural polyphenols against neurodegenerative disorders: Potentials and pitfalls. *Ageing Res. Rev.* **2012**, *11*, 329–345. [CrossRef] [PubMed]
64. Silva, R.F.M.; Pogačnik, L. Polyphenols from Food and Natural Products: Neuroprotection and Safety. *Antioxidants* **2020**, *9*, 61. [CrossRef] [PubMed]
65. Hussain, T.; Tan, B.; Yin, Y.; Blachier, F.; Tossou, M.C.; Rahu, N. Oxidative Stress and Inflammation: What Polyphenols Can Do for Us? *Oxid. Med. Cell. Longev.* **2016**, *2016*, 7432797. [CrossRef] [PubMed]
66. Shakoor, H.; Feehan, J.; Apostolopoulos, V.; Platat, C.; Al Dhaheri, A.S.; Ali, H.I.; Ismail, L.C.; Bosevski, M.; Stojanovska, L. Immunomodulatory Effects of Dietary Polyphenols. *Nutrients* **2021**, *13*, 728. [CrossRef] [PubMed]
67. Asensi, M.; Ortega, A.; Mena, S.; Feddi, F.; Estrela, J.M. Natural polyphenols in cancer therapy. *Crit. Rev. Clin. Lab. Sci.* **2011**, *48*, 197–216. [CrossRef]
68. Mahbub, A.; Maitre, C.; Haywood-Small, S.L.; McDougall, G.J.; Cross, N.A.; Jordan-Mahy, N. Differential Effects of Polyphenols on Proliferation and Apoptosis in Human Myeloid and Lymphoid Leukemia Cell Lines. *Anti-Cancer Agents Med. Chem.* **2013**, *13*, 1601–1613. [CrossRef]
69. Maiuolo, J.; Gliozzi, M.; Carresi, C.; Musolino, V.; Oppedisano, F.; Scarano, F.; Nucera, S.; Scicchitano, M.; Bosco, F.; Macri, R.; et al. Nutraceuticals and Cancer: Potential for Natural Polyphenols. *Nutrients* **2021**, *13*, 3834. [CrossRef]
70. Cháirez-Ramírez, M.H.; de la Cruz-López, K.G.; García-Carrancá, A. Polyphenols as Antitumor Agents Targeting Key Players in Cancer-Driving Signaling Pathways. *Front. Pharmacol.* **2021**, *12*. [CrossRef]
71. Miccadei, S.; Di Venere, D.; Cardinali, A.; Romano, F.; Durazzo, A.; Foddai, M.S.; Fraioli, R.; Mobarhan, S.; Maiani, G. Antioxidative and Apoptotic Properties of Polyphenolic Extracts from Edible Part of Artichoke (*Cynara scolymus* L.) on Cultured Rat Hepatocytes and on Human Hepatoma Cells. *Nutr. Cancer* **2008**, *60*, 276–283. [CrossRef] [PubMed]
72. Mileo, A.M.; Di Venere, D.; Abbruzzese, C.; Miccadei, S. Long Term Exposure to Polyphenols of Artichoke (*Cynara scolymus* L.) Exerts Induction of Senescence Driven Growth Arrest in the MDA-MB231 Human Breast Cancer Cell Line. *Oxidative Med. Cell. Longev.* **2015**, *2015*, 1–11. [CrossRef] [PubMed]
73. Prakash, M.D.; Stojanovska, L.; Feehan, J.; Nurgali, K.; Donald, E.L.; Plebanski, M.; Flavel, M.; Kitchen, B.; Apostolopoulos, V. Anti-cancer effects of polyphenol-rich sugarcane extract. *PLOS ONE* **2021**, *16*, e0247492. [CrossRef] [PubMed]
74. Zhang, H.; Zheng, W.; Feng, X.; Yang, F.; Qin, H.; Wu, S.; Hou, D.-X.; Chen, J. Nrf2–ARE Signaling Acts as Master Pathway for the Cellular Antioxidant Activity of Fisetin. *Molecules* **2019**, *24*, 708. [CrossRef] [PubMed]
75. Zhu, Y.I.; Tchkonja, T.; Pirtskhalava, T.; Gower, A.C.; Ding, H.; Giorgadze, N.; Palmer, A.K.; Ikeno, Y.; Hubbard, G.B.; Lenburg, M.; et al. The Achilles’ heel of senescent cells: From transcriptome to senolytic drugs. *Ageing Cell* **2015**, *14*, 644–658. [CrossRef] [PubMed]
76. Zhu, Y.; Doornebal, E.J.; Pirtskhalava, T.; Giorgadze, N.; Wentworth, M.; Fuhrmann-Stroissnigg, H.; Niedernhofer, L.J.; Robbins, P.D.; Tchkonja, T.; Kirkland, J.L. New agents that target senescent cells: The flavone, fisetin, and the BCL-XL inhibitors, A1331852 and A1155463. *Ageing* **2017**, *9*, 955–963. [CrossRef] [PubMed]
77. Schafer, M.J.; White, T.A.; Iijima, K.; Haak, A.J.; Ligresti, G.; Atkinson, E.J.; Oberg, A.L.; Birch, J.; Salmonowicz, H.; Zhu, Y.; et al. Cellular senescence mediates fibrotic pulmonary disease. *Nat. Commun.* **2017**, *8*, 14532. [CrossRef] [PubMed]
78. Chaib, S.; Tchkonja, T.; Kirkland, J.L. Cellular senescence and senolytics: The path to the clinic. *Nat. Med.* **2022**, *28*, 1556–1568. [CrossRef]
79. Schapira, M.; Tyers, M.; Torrent, M.; Arrowsmith, C.H. WD40 repeat domain proteins: A novel target class? *Nat. Rev. Drug Discov.* **2017**, *16*, 773–786. [CrossRef]
80. Lo, S.-C.; Li, X.; Henzl, M.T.; Beamer, L.J.; Hannink, M. Structure of the Keap1:Nrf2 interface provides mechanistic insight into Nrf2 signaling. *EMBO J.* **2006**, *25*, 3605–3617. [CrossRef]





81. Ma, B.; Lucas, B.; Capacci, A.; Lin, E.Y.-S.; Jones, J.H.; Dechantsreiter, M.; Enyedy, I.; Marcotte, D.; Xiao, G.; Li, B.; et al. Design, synthesis and identification of novel, orally bioavailable non-covalent Nrf2 activators. *Bioorganic Med. Chem. Lett.* **2019**, *30*, 126852. [CrossRef] [PubMed]
82. Padmanabhan, B.; Tong, K.I.; Ohta, T.; Nakamura, Y.; Scharlock, M.; Ohtsuji, M.; Kang, M.-I.; Kobayashi, A.; Yokoyama, S.; Yamamoto, M. Structural Basis for Defects of Keap1 Activity Provoked by Its Point Mutations in Lung Cancer. *Mol. Cell* **2006**, *21*, 689–700. [CrossRef] [PubMed]
83. Pallesen, J.S.; Narayanan, D.; Tran, K.T.; Solbak, S.M.; Marseglia, G.; Sørensen, L.M.E.; Høj, L.J.; Munafò, F.; Carmona, R.M.C.; Garcia, A.D.; et al. Deconstructing Noncovalent Kelch-like ECH-Associated Protein 1 (Keap1) Inhibitors into Fragments to Reconstruct New Potent Compounds. *J. Med. Chem.* **2021**, *64*, 4623–4661. [CrossRef] [PubMed]
84. Canning, P.; Sorrell, F.J.; Bullock, A.N. Structural basis of Keap1 interactions with Nrf2. *Free Radic. Biol. Med.* **2015**, *88*, 101–107. [CrossRef] [PubMed]
85. Tebay, L.E.; Robertson, H.; Durant, S.T.; Vitale, S.R.; Penning, T.M.; Dinkova-Kostova, A.T.; Hayes, J.D. Mechanisms of activation of the transcription factor Nrf2 by redox stressors, nutrient cues, and energy status and the pathways through which it attenuates degenerative disease. *Free Radic. Biol. Med.* **2015**, *88*, 108–146. [CrossRef] [PubMed]
86. Satta, S.; Mahmoud, A.M.; Wilkinson, F.L.; Yvonne Alexander, M.; White, S.J. The role of Nrf2 in cardiovascular function and disease. *Oxid. Med. Cell. Longev.* **2017**, *2017*, 9237263. [CrossRef] [PubMed]
87. Clifford, T.; Acton, J.P.; Cocksdge, S.P.; Davies, K.A.B.; Bailey, S.J. The effect of dietary phytochemicals on nuclear factor erythroid 2-related factor 2 (Nrf2) activation: A systematic review of human intervention trials. *Mol. Biol. Rep.* **2021**, *48*, 1745–1761. [CrossRef]
88. Khan, J.; Deb, P.K.; Priya, S.; Medina, K.D.; Devi, R.; Walode, S.G.; Rudrapal, M. Dietary Flavonoids: Cardioprotective Potential with Antioxidant Effects and Their Pharmacokinetic, Toxicological and Therapeutic Concerns. *Molecules* **2021**, *26*, 4021. [CrossRef]
89. Andersson, U.; Yang, H.; Harris, H. High-mobility group box 1 protein (HMGB1) operates as an alarmin outside as well as inside cells. In *Seminars in Immunology*; Academic Press: New York, NY, USA, 2018; pp. 40–48.
90. Andersson, U.; Tracey, K.J. HMGB1 Is a Therapeutic Target for Sterile Inflammation and Infection. *Annu. Rev. Immunol.* **2011**, *29*, 139–162. [CrossRef]
91. Chen, R.; Kang, R.; Tang, D. The mechanism of HMGB1 secretion and release. *Exp. Mol. Med.* **2022**, *54*, 91–102. [CrossRef]
92. Deng, M.; Scott, M.J.; Fan, J.; Billiar, T.R. Location is the key to function: HMGB1 in sepsis and trauma-induced inflammation. *J. Leukoc. Biol.* **2019**, *106*, 161–169. [CrossRef] [PubMed]
93. Tang, Y.; Zhao, X.; Antoine, D.J.; Xiao, X.; Wang, H.; Andersson, U.; Billiar, T.R.; Tracey, K.J.; Lu, B.; Papatheodorou, A.; et al. Regulation of Posttranslational Modifications of HMGB1 During Immune Responses. *Antioxid. Redox Signal.* **2016**, *24*, 620–634. [CrossRef]
94. Bianchi, M.E. Significant (re)location: How to use chromatin and/or abundant proteins as messages of life and death. *Trends Cell Biol.* **2004**, *14*, 287–293. [CrossRef]
95. Müller, S.; Ronfani, L.; Bianchi, M.E. Regulated expression and subcellular localization of HMGB1, a chromatin protein with a cytokine function. *J. Intern. Med.* **2004**, *255*, 332–343. [CrossRef] [PubMed]
96. Raucci, A.; Palumbo, R.; Bianchi, M.E. HMGB1: A signal of necrosis. *Autoimmunity* **2007**, *40*, 285–289. [CrossRef] [PubMed]
97. Ulloa, L.; Messmer, D. High-mobility group box 1 (HMGB1) protein: Friend and foe. *Cytokine Growth Factor Rev.* **2006**, *17*, 189–201. [CrossRef] [PubMed]
98. Yang, H.; Wang, H.; Czura, C.J.; Tracey, K.J. The cytokine activity of HMGB1. *J. Leukoc. Biol.* **2005**, *78*, 1–8. [CrossRef]
99. Bierhaus, A.; Humpert, P.M.; Morcos, M.; Wendt, T.; Chavakis, T.; Arnold, B.; Stern, D.M.; Nawroth, P.P. Understanding RAGE, the receptor for advanced glycation end products. *J. Mol. Med.* **2005**, *83*, 876–886. [CrossRef]
100. Bassi, R.; Giussani, P.; Anelli, V.; Colleoni, T.; Pedrazzi, M.; Patrone, M.; Viani, P.; Sparatore, B.; Melloni, E.; Riboni, L. HMGB1 as an autocrine stimulus in human T98G glioblastoma cells: Role in cell growth and migration. *J. Neuro-Oncol.* **2007**, *87*, 23–33. [CrossRef]
101. Ambrose, A.J.; Chapman, E. Function, Therapeutic Potential, and Inhibition of Hsp70 Chaperones. *J. Med. Chem.* **2021**, *64*, 7060–7082. [CrossRef]
102. Zhao, K.; Zhou, G.; Liu, Y.; Zhang, J.; Chen, Y.; Liu, L.; Zhang, G. HSP70 Family in Cancer: Signaling Mechanisms and Therapeutic Advances. *Biomolecules* **2023**, *13*, 601. [CrossRef] [PubMed]
103. Tang, D.; Kang, R.; Xiao, W.; Jiang, L.; Liu, M.; Shi, Y.; Wang, K.; Wang, H.; Xiao, X. Nuclear Heat Shock Protein 72 as a Negative Regulator of Oxidative Stress (Hydrogen Peroxide)-Induced HMGB1 Cytoplasmic Translocation and Release. *J. Immunol.* **2007**, *178*, 7376–7384. [CrossRef] [PubMed]
104. Gupta, R.; Sharma, D. Evolution of Magnetic Hyperthermia for Glioblastoma Multiforme Therapy. *ACS Chem. Neurosci.* **2019**, *10*, 1157–1172. [CrossRef] [PubMed]
105. Hermisson, M.; Strik, H.; Rieger, J.; Dichgans, J.; Meyermann, R.; Weller, M. Expression and functional activity of heat shock proteins in human glioblastoma multiforme. *Neurology* **2000**, *54*, 1357–1365. [CrossRef] [PubMed]
106. Iglesia, R.P.; Fernandes, C.F.d.L.; Coelho, B.P.; Prado, M.B.; Escobar, M.I.M.; Almeida, G.H.D.R.; Lopes, M.H. Heat Shock Proteins in Glioblastoma Biology: Where Do We Stand? *Int. J. Mol. Sci.* **2019**, *20*, 5794. [CrossRef] [PubMed]
107. Sha, G.; Jiang, Z.; Zhang, W.; Jiang, C.; Wang, D.; Tang, D. The multifunction of HSP70 in cancer: Guardian or traitor to the survival of tumor cells and the next potential therapeutic target. *Int. Immunopharmacol.* **2023**, *122*, 110492. [CrossRef]

108. Dobrzynska, M.; Napierala, M.; Florek, E. Flavonoid Nanoparticles: A Promising Approach for Cancer Therapy. *Biomolecules* **2020**, *10*, 1268. [CrossRef] [PubMed]
109. Prabhu, H.R.; Patravale, V.B.; Joshi, M.D. Polymeric nanoparticles for targeted treatment in oncology: Current insights. *Int. J. Nanomed.* **2015**, *10*, 1001–1018.
110. Kothamasu, P.; Kanumur, H.; Ravur, N.; Maddu, C.; Parasuramrajam, R.; Thangavel, S. Nanocapsules: The Weapons for Novel Drug Delivery Systems. *Bioimpacts* **2012**, *2*, 71–81. [CrossRef]
111. Jain, S.; Hirst, D.G.; O’Sullivan, J.M. Gold nanoparticles as novel agents for cancer therapy. *Br. J. Radiol.* **2012**, *85*, 101–113. [CrossRef]
112. Mu, H.; Holm, R. Solid lipid nanocarriers in drug delivery: Characterization and design. *Expert Opin. Drug Deliv.* **2018**, *15*, 771–785. [CrossRef] [PubMed]
113. Dierge, E.; Debock, E.; Guilbaud, C.; Corbet, C.; Mignolet, E.; Mignard, L.; Bastien, E.; Dessy, C.; Larondelle, Y.; Feron, O. Peroxidation of n-3 and n-6 polyunsaturated fatty acids in the acidic tumor environment leads to ferroptosis-mediated anticancer effects. *Cell Metab.* **2021**, *33*, 1701–1715.e5. [CrossRef] [PubMed]
114. Yeo, A.T.; Rawal, S.; Delcuze, B.; Christofides, A.; Atayde, A.; Strauss, L.; Balaj, L.; Rogers, V.A.; Uhlmann, E.J.; Varma, H.; et al. Single-cell RNA sequencing reveals evolution of immune landscape during glioblastoma progression. *Nat. Immunol.* **2022**, *23*, 971–984. [CrossRef] [PubMed]

Disclaimer/Publisher’s Note: The statements, opinions and data contained in all publications are solely those of the individual author(s) and contributor(s) and not of MDPI and/or the editor(s). MDPI and/or the editor(s) disclaim responsibility for any injury to people or property resulting from any ideas, methods, instructions or products referred to in the content.

Review

A Comprehensive Review of miRNAs and Their Epigenetic Effects in Glioblastoma

Hera Hasan ¹, Mohammad Afzal ², Javier S. Castresana ³ and Mehdi H. Shahi ^{1,*}

¹ Interdisciplinary Brain Research Centre, Faculty of Medicine, Aligarh Muslim University, Aligarh 202002, India; herahasanoofficial786@gmail.com

² Department of Zoology, Faculty of Life Sciences, Aligarh Muslim University, Aligarh 202002, India; ma.afzal1235@gmail.com

³ Department of Biochemistry and Genetics, University of Navarra School of Sciences, 31008 Pamplona, Spain; jscastresana@unav.es

* Correspondence: mehdihayat.md@amu.ac.in

Abstract: Glioblastoma is the most aggressive form of brain tumor originating from glial cells with a maximum life expectancy of 14.6 months. Despite the establishment of multiple promising therapies, the clinical outcome of glioblastoma patients is abysmal. Drug resistance has been identified as a major factor contributing to the failure of current multimodal therapy. Epigenetic modification, especially DNA methylation has been identified as a major regulatory mechanism behind glioblastoma progression. In addition, miRNAs, a class of non-coding RNA, have been found to play a role in the regulation as well as in the diagnosis of glioblastoma. The relationship between epigenetics, drug resistance, and glioblastoma progression has been clearly demonstrated. *MGMT* hypermethylation, leading to a lack of *MGMT* expression, is associated with a cytotoxic effect of TMZ in GBM, while resistance to TMZ frequently appears in *MGMT* non-methylated GBM. In this review, we will elaborate on known miRNAs linked to glioblastoma; their distinctive oncogenic or tumor suppressor roles; and how epigenetic modification of miRNAs, particularly via methylation, leads to their upregulation or downregulation in glioblastoma. Moreover, we will try to identify those miRNAs that might be potential regulators of *MGMT* expression and their role as predictors of tumor response to temozolomide treatment. Although we do not impact clinical data and survival, we open possible experimental approaches to treat GBM, although they should be further validated with clinically oriented studies.

Keywords: glioblastoma; miRNA; temozolomide; epigenetics; DNA methylation



Citation: Hasan, H.; Afzal, M.; Castresana, J.S.; Shahi, M.H. A Comprehensive Review of miRNAs and Their Epigenetic Effects in Glioblastoma. *Cells* **2023**, *12*, 1578. <https://doi.org/10.3390/cells12121578>

Academic Editor: Luiz Otavio Penalva

Received: 18 April 2023

Revised: 1 June 2023

Accepted: 5 June 2023

Published: 7 June 2023



Copyright: © 2023 by the authors. Licensee MDPI, Basel, Switzerland. This article is an open access article distributed under the terms and conditions of the Creative Commons Attribution (CC BY) license (<https://creativecommons.org/licenses/by/4.0/>).

1. Introduction

The CNS5 Classification and Glioblastoma

Glioblastoma, according to the 2021 WHO (World Health Organization) Classification of Tumors of the Central Nervous System, or CNS5 classification [1], is an *IDH* wild-type glioma. Previous classifications considered glioblastoma as primary (*IDH* wild type) and secondary (*IDH* mutant) [2]. CNS5 classification has simplified the subdivisions of adult-type diffuse gliomas, dividing them into three tumor types: astrocytoma (*IDH* mutant), oligodendroglioma (*IDH* mutant and 1p/19q codeletion), and glioblastoma (*IDH* wild type).

Glioblastoma, according to the CNS5 classification, is defined as a diffuse astrocytic WHO grade 4 glioma, *IDH* wild type, and H3 wild type, that has one or more of the following histological or genetic features: microvascular proliferation, necrosis, *TERT* promoter mutation, *EGFR* amplification, and +7/−10 chromosome and copy-number changes at chromosomes 7 (gains and amplifications) and 10 (losses) [1,2].

Despite the availability of a plethora of aggressive treatments and conventional therapies, such as chemotherapy, radiotherapy, and surgical resection, glioblastoma (GBM) is

still irremediable, obnoxiously fatal, and almost invariably leads to patient death. GBM stem cells (GSCs) constitute a subpopulation of GBM cells that contribute to the failure of conventional treatments, as they are highly tumorigenic but relatively quiescent cells, which make them resistant to conventional therapies [3]. Some idiosyncrasies of GBM have been identified, which make GBM a very particular entity, separated from the rest of gliomas. GBM exhibit central necrosis and microvascular proliferation, are highly infiltrative, and rarely display extracranial metastases; they are exceptionally invasive, and their rate of migration is so high that they are spread far away from their origin and even extend across the contralateral brain hemisphere, making complete surgical resection of GBM achingly complicated. GBM is highly vascularized and presents a high mutation rate and significant genetic instability that contributes to intra-tumor heterogeneity, which complicates therapy [4]. By understanding the biology and the cellular origin of GBM, the daunting task of developing potential novel approaches for treating this disease might be achieved.

Epigenetics is broadly defined as the study of heritable aberrations in gene expression without any change in DNA sequence [5]. Moreover, the reversible nature of epigenetic modification has engendered an endeavor to develop more progressive novel therapeutic approaches aiming to combat GBM [6]. Epigenetic modification plays a critical role in the transformation of normal to malignant cells via a complex interplay with genetic alterations, impacting critical cellular processes involved in the progression of glioma, such as DNA repair, apoptosis, and cell invasion and proliferation, which profoundly contribute to the catastrophic disruption of normal cells, transforming them to high-grade glioma cells [7]. DNA methylation and histone modification are the two classic most important types of epigenetic modification. However, recently, the role of non-coding RNA, such as miRNAs, and their epigenetic modifications are on the road to discovering more reliable and novel prognostic and predictive GBM biomarkers [8].

MicroRNAs (miRNAs) are small non-coding endogenous RNAs, typically 21 to 23 nucleotides long. They exert their regulatory effect post-transcriptionally by regulating a large number of genes through silencing the expression of specific mRNAs, a process called RNA interference (RNAi). Additionally, miRNAs can regulate the expression of a plethora of genes that play a key role in cancer. For example, EZH2, a chromatin modifier, has been reported to be regulated directly by miR-205, miRNA-101, and miR-26a [9]. miRNAs play crucial roles in GBM progression either by acting as oncogenic miRNAs via silencing tumor suppressor genes or by acting as tumor suppressors. Moreover, several miRNAs involved in GBM development have been observed to be methylation sensitive, which can be a potential target to develop mRNA-based therapies for GBM [8].

2. DNA Methylation

DNA methylation is a type of epigenetic modification that plays a key role in the regulation of chromatin structure, genome imprinting, and gene expression [10]. Most studies based on DNA methylation as an epigenetic mark predominantly focuses on methylation of a cytosine residue followed by a guanine, a reaction in which a methyl group is covalently transferred to the 5'-position of cytosine, forming 5-methyl cytosine (5mC), which occurs via an enzyme called DNA methyl transferase (DNMT) [7]. DNMT family consists of 5 members: DNMT1, DNMT2, DNMT3a, DNMT3b, and DNMT3L [7]. Among them, DNMT1 specifically targets hemi-methylated DNA, while DNMT3a and DNMT3b are involved in the de novo methylation of unmethylated substrates [6,7].

DNA methylation usually inhibits the transcription of eukaryotic genes, particularly when it occurs in their promoters. DNMTs transfer methyl residues from SAM (S-adenosyl methionine) to DNA, thus preventing the binding of transcription factors to the promoter region of target genes. DNA methylation usually targets CpG islands, which are clusters of CpG dinucleotides that are found in the promoter regions in nearly half of all human genes [7]. CpG islands are genomic regions of 200 base pairs with a 50% GC content of total nucleotides and a CpG ratio > 0.6 [10]. CpG islands are hypomethylated under standard

physiological conditions [6], which correlates with active gene expression, whereas CpG islands of tumor cells have been found to be hypermethylated in DNA repair genes and tumor suppressor genes involved in cell proliferation and progression, which results in transcriptional silencing of these genes [6].

2.1. DNA Methylation in GBM

Cancer-specific DNA methylation is characterized by the global loss of methylation accompanied by gene promoter hypermethylation. Specific CpG hypermethylation of tumor suppressor gene promoters resulting in transcriptional silencing is the most widely studied epigenetic aberration in GBM [7,11]. While hypomethylation takes place in the repetitive region of the DNA that might be responsible for genomic instability contributing to tumor growth [7], hypermethylation of the *MGMT* (*O*⁶-methylguanine-DNA methyltransferase) promoter leads to *MGMT* epigenetic silencing in about 40% of GBM, which correlates with a better response to temozolomide (TMZ) treatment with an increase in median survival time [7,10].

However, the link of *MGMT* hypermethylation with a positive response to TMZ is not always guaranteed, as not all the cases of GBM with methylated *MGMT* exhibit a promising response to TMZ [7]; additionally, there are cases of better response to TMZ treatment in a patient with unmethylated *MGMT* promoter. This led us to contemplate miRNAs as a different regulatory mechanism that might regulate *MGMT* expression [11]. A negative correlation between miRNA and *MGMT* expression has been reported [12], something we will discuss later separately in this paper.

Besides this, there is another common epigenetic marker of glioma, 5hmC (DNA-5-hydroxymethylcytosine), which results from oxidation of 5mC, a reaction catalyzed via TET protein, an event of alteration of methyl status of DNA, reported in several patients with GBM. 5hmC has been reported to be negatively correlated with cell proliferation and grades of tumors. Hence, 5hmC can be considered a marker of good prognosis in GBM [7,13].

2.2. DNA Methylation: Its Role in Regulation of Metabolism in GBM

DNA methylation has been reported to be involved in the modification of genes related to glycolysis in GBM. DNA-methylating enzymes exert their regulatory effect on metabolic target genes, either via methylating DNA in introns or in the promoter region, thus silencing the expression of these genes.

2.3. PKM2

This enzyme controls the synthesis of pyruvate, the last metabolite of the glycolytic pathway. Hypomethylation at intron 1 of the *PKM* gene has been observed to exhibit a positive correlation with GBM. Additionally, *PKM2* is under the regulation of miR-7, miR-326, and Let miR-7. Hence, *PKM2* might be a useful target for several cancer-suppressing drugs [14].

2.4. LDHA

LDHA gene codes for lactate dehydrogenase, a glycolytic enzyme. Epigenetic silencing of this gene via hypermethylation of their promoter region has been documented in *IDH*-mutant GBM, according to classifications previous to CNS5 [14,15]. However, even silencing *LDHA* by siRNA inhibited proliferation, induced apoptosis, and increased chemosensitivity to temozolomide in GBM (CNS5 definition) cells [16].

2.5. HK2

HK2 gene codes for hexokinase that catalyzes the rate-limiting step of glycolysis: phosphorylating glucose to glucose-6-phosphate. Aberration in the methylation status of this gene either via hypermethylation or hypomethylation of CpG islands within intron 1 has been reported in GBM cell lines or tumors [14]. Predominantly, hypomethylation has

been found to be a frequent event in GBM compared to normal cells [14,17]. Several studies authenticate the *HK2* overexpression contribution to tumor growth with a drug-resistant phenotype [17]. Additionally, *HK2* has been observed to be silenced epigenetically in normal cells, while its overexpression in GBM is a consequence of hypomethylation of its promoter region [17]. Decitabine (a cytosine analog) is a potent DNMT inhibitor that recovers *HK2* expression in GBM, something that may prolong patients' mean survival time [14].

Hence, these reports suggest the significance of DNA methylation in determining the possible outcome of GBM and provide insights into the highly intertwined relationship between metabolic and epigenetic regulation and their combined contribution in deciding the fate of tumor progression in GBM [17]. Thus, by understanding the complex interplays between these regulatory bodies, it will be possible to develop novel therapies which might remarkably enhance the efficacy of treatment in GBM.

3. miRNA

MicroRNAs (miRNAs/miRs) are small non-coding RNAs of 19–22 nucleotides long [12,18] profoundly involved in post-transcriptional regulation of expression of a plenitude of genes either via sequence-specific repression of mRNA [12] or mRNA degradation. The first miRNA was discovered in *Caenorhabditis elegans* in 1993 [19]. miRNAs play a pivotal role as modulators of cellular homeostasis and regulate several major cellular processes, such as proliferation, migration, cell cycle progression, and apoptosis [19,20]. Dysregulation of miRNA unequivocally has been associated with a wide range of clinical conditions, such as cancer, neurodegenerative diseases, and cardiovascular diseases. Additionally, aberrant miRNA expression has been reported to play a key predictive factor in the progression, development, and sustainment of GBM [21], either by miRNAs acting as oncogenes, silencing tumor-suppressing genes, or by themselves as tumor suppressors [22].

3.1. miRNA Biogenesis

miRNA biogenesis can progress through two pathways: canonical and non-canonical. Among them, the canonical pathway is the most important one related to miRNA biogenesis and maturation [23]. The first step of the canonical pathway concerns the synthesis of pri-miRNA from the genome by the enzyme RNA polymerase III/II followed by its subsequent cleavage into pre-miRNA through a microprocessor complex consisting of Drosha-DGCR8 complex [19,23,24]. Drosha is a nuclear RNase III enzyme that cleaves hairpin loop sequences in pri-miRNA [24], resulting in the production of ~70 nucleotides (nt) pre-miRNA bearing a 2 nt 3' overhang [23]. After the completion of these initial steps in the nucleus, pre-miRNA is shuttled out of the nucleus into the cytoplasm by a nuclear transporter protein Ran/GTP/Exportin-5 (XPO5) for final processing via Dicer enzyme and TARBP2 [25,26]. Dicer is an RNAase III endonuclease that cleaves a pre-miRNA into a mature miRNA duplex [25]. The final step that marks the end of miRNA biogenesis is a load of either the 3p or 5p strand of the mature miRNA duplex, depending on their thermodynamic stability, into the Argonaute (AGO) protein, making functional miRISC (miRNA-induced silencing complex) [23] recognize the 3'-UTR of a target gene and result in translational suppression or degradation of mRNA via a phenomenon called RNA interference [20]. Approximately, 50% of all protein-coding human genes are regulated by miRNAs. Therefore, any alteration in their miRNA expression might result in clinical diseases, such as cancer and others [27].

3.2. miRNA in GBM

GBM is characterized by aberrations in miRNA expression. miRNAs either act as oncogenes or tumor suppressors and exert a major impact on oncogenic processes involving gliomagenesis, such as regulation of angiogenesis, metabolic pathways, and associated enzymes, or by regulating GSC (glioma stem cell) differentiation in GBM. miRNAs can regulate around 3% of all genes of glioma tumors and 30% of coding genes. Interestingly,

one miRNA can control the expression of 100 mRNA associated with GBM [13]. miRNAs target metabolic reprogramming, a critical hallmark of GBM [28], which results in increased aerobic glycolysis in GBM compared to normal brains. Aerobic glycolysis is controlled by oncogenic signaling pathways and tumor suppressor genes; aberration in any of these genes may alter the expression of metabolic enzymes and the activity of metabolic transporters [28]. Expression of these glycolytic regulators and metabolic genes is targeted by miRNAs, such as miR-144, miR-155, miR-34a, and others [14]. Some miRNAs also act as epigenetic regulators of GSC in GBM and may contribute to GBM heterogeneity during tumor formation. Some examples are miR-451 and miR-1275, which impede cell proliferation in GSC, while miR-137 enhances proliferation and inhibits apoptosis. miRNAs also contribute significantly to the regulation of angiogenesis, another significant hallmark of GBM, by inducing molecules, such as cytokines, metalloproteinase, and growth factors, such as VEGF or EGFR [20]. Thus, several potential drugs can be developed, and valuable therapeutic targets can be determined for GBM treatment if we do a meticulous analysis of miRNA expression patterns. In this review article, we will make a compendium of miRNAs known to be upregulated or downregulated in the GBM (Tables 1 and 2). Additionally, we will present their different roles in gliomagenesis.

3.3. Upregulated miRNA

miR-21

miRNA-21 was the first one reported as an oncogenic miRNA with an anti-apoptotic activity significantly contributing to the progression of GBM. It is highly upregulated in most tumors, particularly in GBM [21]. Thus, by downregulating miR-21 with subsequent caspase activation, the miR-21 anti-apoptotic effect can be reversed, which will ultimately aid in enhancing overall survival in GBM patients [6]. miR-21 is a key inhibitor of PTEN and p53, and an activator of EGFR, Cyclin D1, and AKT-2 [29]. Other targets of miR-21 are proteoglycan, SPOCK1, and transcription regulators, such as RB1CC1 [7].

miR-21 enhances EGFR expression by repressing PPAR alpha and VHL, with subsequent activation of beta-catenin and AP-1. Therefore, the silencing of miR-21 expression will decrease the oncogenic activity of EGFR, BCL2, and cyclin D, and it will lead to the upregulation of tumor suppressor proteins, such as Bax, p21, TGFBR2, or p53 [30]. Apart from having pro-proliferative activity, miR-21 also promotes tumor invasion and migration [31], as it induces tumor invasion by targeting regulators of matrix metalloproteinase, such as RECK (reversion inducing cysteine-rich protein with Kazal motifs) and TIMP3 (tissue inhibitor of metalloproteinase) [24,30]. Finally, it has been reported that miR-21 silencing can be used as a therapy in the treatment of TMZ-resistant GBM patients [30].

3.4. miR-10b and miR-10a

These are oncogenic miRNAs commonly overexpressed in GBM [29]. miR-10a exhibits chemoresistance [31], while miR-10b significantly promotes GBM cell proliferation, invasion, migration, and EMT (epithelial–mesenchymal transition) [18], and it also imparts an oncogenic effect on GSC cells [31]. miR-10b expression levels correlate with clinical and WHO tumor grades [32]. miR-10b targets are cell cycle inhibitors [7], such as CDKN1A and CDKN2A, BIM, BCL2, TEAP2C, and PTEN, an antagonist of the PI3K pathway [14,18,31]. It promotes GBM cell invasion by enhancing RhoC (Ras homolog gene family member C) and uPAR (Urokinase-type plasminogen activator receptor) expression via modulation of HOXD10 expression [18]. Thus, miR-10b inhibition along with the co-targeting of PTEN and activation of p53 will lead to the induction of apoptosis as well as to cell cycle arrest and suppression of GBM cell invasion and migration [18,31].

3.5. miR-10b-miR-21

miR-10b and miR-21 complex co-inhibition are reported to be associated with cell cycle arrest with a considerable reduction in GBM cell migration [33].

3.5.1. miR-10b and miR-222

miR-10b and miR-222 together contribute to oncogenic activity in GBM and are associated with poor survival [34]. Synergistically, they promote tumor progression and cell proliferation by targeting PTEN, which activates the p53 antitumor signaling pathway by suppressing MDM2, a key inhibitor of p53 [18,34]. They also regulate apoptosis in a p53/PTEN-independent manner directly by modulating the expression of BIM, an apoptotic initiation factor [34]. Thus, miR-10b and miR-222 can be potential therapeutic targets for the treatment of GBM [34].

3.5.2. miR-9

miR-9 overexpression in GBM with poor overall prognosis has been widely reported [14,29,35]. It promotes tumor cell proliferation, migration, and inflammation; it also indirectly regulates KRAS via targeting NF1, a KRAS inhibitor [14,35]. Overexpressed miR-9 has been observed to be positively correlated with GSC differentiation, thereby conferring chemoresistance to GBM [35]. miR-9 also induces TMZ resistance in CD133+ cells; therefore, miR-9 upregulation is an indicator of poor survival [35,36]. Additionally, miR-9, when upregulated, downregulates tumor suppressor gene *PTCH1*, which results in the activation of the SHH signaling pathway, thus reducing tumor cell death [36].

3.5.3. miR-221/222

miR221/222 overexpression is associated with the increase in tumor growth and other major hallmarks of cancer, such as proliferation, migration, invasion, and angiogenesis. It has an oncogenic influence on GBM, and it correlates with poor survival [7,12,18]. miR-221/222 cluster promotes all these malignant properties by increasing MMP2, MMP3, and VEGF along with its target Akt signaling pathway [12,18]. Other targets of miR-221/222 are PTEN, TIMP3, E2F3, and PUMA [12,37]. The miR-221/222 cluster displays anti-apoptotic activities by inhibiting *PUMA*, which is a proapoptotic gene, or by co-targeting the *PTEN* gene [30,37]. They also promote tumor cell proliferation by targeting the p27Kip1 cell cycle inhibitor [7], a member of cyclin-dependent kinase inhibitors that do not let the phase transition of cells from the G1 to the S phase. Thus, by downregulating the expression of the miR-221/222 cluster, tumor proliferation and growth can be controlled [13,37].

3.5.4. miR-26a

This miRNA is overexpressed in high-grade GBM, and its expression is associated with the degree of malignancy [38]. It acts as an oncogene by binding to the 3' UTR of PTEN, leading to PTEN protein inhibition. MiR-26a overexpression in glioma cells circumvents the need for loss of heterozygosity of PTEN to promote tumor formation [7,14,29]. miR-26a expression has been found to be directly upregulated by MYC oncogene [38].

3.5.5. miR-17-92 Cluster

The expression of this miRNA cluster has been reported to be exceptionally higher in GBM than in normal healthy brain tissue. It employs its oncogenic effect on high-grade glioma and its elevated expression level associated with the aggressiveness of the tumor [8]. miR-17-92 higher expression correlates with GBM [39] and with GSC regulation [24]. It promotes GSC differentiation and exhibits an anti-apoptotic effect. It targets tumor suppressor genes and cell cycle inhibitors, such as *PTEN* and *CDKN1A* [8]. Thus, inhibiting or lowering the expression level of this cluster may promote a longer survival rate in GBM patients [30].

3.5.6. miR-148a

This miRNA promotes exosome-induced GBM, cell proliferation, and metastasis [40]. It has been acknowledged as one of the significant GBM-associated risky miRNAs by TCGA (The Cancer Genome Atlas) [40]. miR-148a level has been found to be excessively elevated in the serum of patients with GBM compared to normal healthy participants [40]. miR-148a

exerts its oncogenic influence by directly targeting *CADM1* (cell adhesion molecule 1), which is a tumor suppressor gene that inhibits cell motility and tumor proliferation [18,40]. Thus, by decreasing *CADM1* and protein levels, miR-148a increases STAT 3 pathway activity and causes glioma cell proliferation and metastasis [18,40].

3.5.7. Other Upregulated miRNA in GBM

miR-221, miR-125, miR-182, miR-196, miR-30, miR-143, miR-494-3p, miR-96a/96b, miR-182, miR-210, miR-503, and miR-378 have all been reported to be upregulated in GBM and contribute to gliomagenesis.

miR-221 targets cell cycle inhibitors [7] and promotes proliferation as well as potentially enhancing GBM cell migration and invasiveness [39].

miR-125 is an oncogenic miRNA and promotes the proliferation of GBM cells by targeting the anti-apoptotic gene *BMF* [29].

miR-182 and miR196 are both elevated in GBM [29]. miR-182 enhances the aggressiveness of glioma cells by targeting *USP15*, *TNIP1*, *CYTL2*, and *OPTN*, which disrupts the negative feedback loop of NF- κ B. On the other hand, miR-196 increases glioma cell proliferation and poor survival in GBM patients [29].

miR-30 and miR-486 are oncogenic miRNAs and promote angiogenesis [29]. miR-30 is overexpressed in GSC, and it enhances its tumorigenicity by silencing *SOCS3* (suppressor of cytokine signaling 3) along with inducing the JAK/STAT3 pathway [41]. It also induces resistance to glioma cells against TRAIL protein as well as inhibits apoptosis by binding to the 3'UTR of caspase 3 [41]. miR-30 has been observed to be negatively correlated with the survival of glioma patients [41].

miR-143 promotes glioma cell differentiation by targeting *HKII* [14]. miR-451 is an oncogenic miRNA; it upregulates in GBM and contributes to tumorigenesis by targeting the *LKB39-AMPK* pathway [14].

miR-495-3p promotes proliferation, migration, and invasion by targeting the P13K/AKT tumor-suppressing signaling pathway [13]. miR-96a and 96b are oncogenic miRNAs that contribute to the poor overall survival of glioma patients [13]. miR-93 promotes angiogenesis and tumor growth [13]. miR-503 is upregulated in GBM and inhibits apoptosis by targeting *PACD4* [18]. miR-378 targets *VEGFR2* and promotes tumor growth and angiogenesis [18,20]. miR-201 is an oncogenic miRNA, significantly elevated in the serum of glioma patients. It is associated with high-grade glioma and poor overall survival [42]. The major target of miR-201 is HIF (hypoxia-inducible factors 1 and 2). It induces cell proliferation and inhibits apoptosis [18,42]. Thus, it can be considered as a potential circulating biomarker but not preferable for early detection of glioma [42].

3.6. Downregulated miRNAs

3.6.1. miR-31

It plays a pivotal role in tumor suppression by inhibiting invasion and migration via targeting the *RDX* gene (Radixin) [29].

3.6.2. miR-124

miRNA-124 has a low expression in high-grade glioma [43]. Its overexpression lowers *SNAI2* levels, which results in suppression of GSCs invasiveness and of other stem-like traits that contribute to GBM malignancy [29]. It also induces cell cycle arrest directly by targeting *CDK4*, *CDK6*, and cyclin D. Hence, miR-124 inhibits glioma cell growth [43].

3.6.3. miR-34

miR-34a is downregulated in GBM, and, if expressed in tumor cells, it causes suppression of cell proliferation and invasion, controls GSC differentiation, stem-like traits, and cell cycle arrest by targeting *Notch1*, *Notch2*, *CDK6*, *EGFR*, and *c-Met* [13,44]. They also promote apoptosis by targeting *Bcl-2* [45,46].

miR-34c-3p and miR-34c-5p present very low expression in high-grade glioma, which indicates that these miRNAs have a tumor-suppressing impact on gliomagenesis [44]. Overexpression of these miRNAs results in the suppression of tumor invasion [46]. miR-34c-3p targets Notch2 and lowers its expression, inhibiting cell proliferation and promoting S-phase arrest, along with the activation of apoptotic pathways [44]. miR-34c-5p expression correlates with a decrease in Notch1 and Notch2 levels, which results in the inhibition of cell proliferation. Targets of miR-34c-5p other than Notch1/Notch2 are CDK6 and EGFR [44].

3.6.4. miR-302-367 Cluster

This miRNA targets GICs (glioma-initiating cells), which confer resistance to glioma cells against TMZ treatment, as well as inhibits the CXCR4 receptor, which, in turn, disrupts the SHH signaling pathway, thus resulting in preventing tumor progression [14]. This cluster of tumors suppressing miRNAs, when expressed in GBM cells, targets transformation-related proteins required for the maintenance of tumor stemness by suppressing the expression of reprogramming factors, such as SOX2, Myc, KLF4, and OCT3/4, and transcription factors, such as SALL2 and OLIG2. Along with this, they enhance the expression of tumor suppressor genes, such as *UCH1*, *PEA15*, and *MYBBP1A*. miR-302-367 cluster induces differentiation of glioma cells by suppressing the expression of stem-like genetic programming by inhibiting PI3K/AKT and STAT3 signaling pathways [47].

3.6.5. miR-181

miR-181 is a family of four members (miR181a, miR-181b, miR-181c, and miR-181d), all of which are downregulated in GBM [21,48]. Among them, a significant reduction in expression levels of miR-181a and 181b has been observed in high-grade gliomas. These two members of miR-181 are routinely employed in distinguishing high-grade gliomas from low-grade gliomas [21]. miR-181a suppresses GSC-induced stemness and other tumorigenic effects via targeting CD133 and BMI1 stemness-related markers [21]. miR-181c expression decreases in GBM due to the absence of CTCF with concomitant epigenetic silencing by DNA methylation [9]. miR-181d forms a cluster with miR-181c on chromosome 19, and it is downregulated in GBM. miR-181d regulates the WNT signaling pathway by targeting the *CREBBP* gene [48]. Its expression level negatively correlates with IGF-1 in GBM [48,49]. IGF-1 promotes tumor progression by inhibiting miR-181d with modulating cytokines secretion, with a concomitant increase in cytokines level [49]. miR-181d, therefore, exhibits a profound correlation with IGF-1-associated cytokines. These upregulated chemokines in GBM, such as C-C chemokine receptor type 1 (CCR1) and interleukin (IL-1b) are the direct targets of 181d tumor-suppressing activity [49]. The other important targets of miR-181d for tumor suppression are Bcl-2 and KRAS [49]. Thus, through a meticulous assessment of the expression level status of IGF-1 and miR-181d in GBM tissues, the overall survival rate in a GBM patient might be determined [49].

3.6.6. miR-219-5p and miR-219-1-3p

Downregulation of these miRNAs correlates with the increase in glioma cell proliferation. Their overexpression causes a reduction in tumor growth [13].

3.6.7. miR-1

miR-1 has a tumor-suppressing activity in GBM cells, as it has been observed that it inhibits the proliferation and migration of GBM cells when expressed ectopically [18,21,50]. Additionally, upon expression in glioma cells, they enhance the sensitivity of GBM cells toward TMZ induce apoptosis [50].

3.6.8. miR-370-3p

miR-370-3p is downregulated in both high- and low-grade glioma [12]. They suppress cell proliferation and migration by regulating the WNT signaling pathway via targeting the 3'UTR of β -catenin whose stabilization is pre-required for activation of WNT signaling [12].

Other targets of miR-370-3p are FOXO1 (forkhead box O1 in humans), FOXM1, and TGF β (Transforming growth factor β) [51]. Therefore, miR-370-3p can be used as a potential target in the development of anti-GBM therapy [51].

3.6.9. miR-328

miR-328 lower expression suggests a poor overall survival rate in patients with GBM [21]. The downregulation of miR-328 in GBM tissues contributes to proliferation and tumor growth by enhancing cell division. miR-328 anti-proliferative activity can be used as a potential therapeutic target for GBM therapy [52].

3.6.10. miR-375

miR-375 is an anti-proliferative miRNA whose downregulation aids in the progression of glioma cell tumorigenesis by facilitating its cell proliferation, invasion, and migration [18,53].

3.6.11. miR-137

This is a tumor-suppressing miRNA that, on expression, provides protection from tumor progression by inhibiting angiogenesis via inhibition of EZH2 (enhancer of zeste homology2), a key proliferation-inducing factor [18,20]. Thus, low expression of this miRNA often correlates with poor prognosis [18,20].

3.6.12. miR-128

This miRNA has a prolific role as a tumor-suppressing factor. Its low expression is associated with high-grade glioma. Therefore, miR-128 can be used to distinguish between low- and high-grade glioma [21]. miR-128 induces its tumor-suppressing effect, such as anti-proliferative and anti-metastasis effects, by inhibiting tumor-associated signaling pathways, such as WNT, ERK, EGFR, IGF1R, or BCL2 [13,18,24,54]. miR-128 induces apoptosis via caspase activation [21]. It suppresses GSC's self-renewable capacity by targeting SUZ12, E2F3, and BMI1 [24,54]. miR-128 reduces tumor cell growth by targeting PDGFRA and EGFR and controls angiogenesis by inhibiting P70S6K1 kinase [55].

3.6.13. miR-7

miR-7 is downregulated in low-grade gliomas [14]. Consequently, the EGFR expression level increases, inducing upregulation of PKM2 via NF- κ B activation, thus contributing to glioma tumorigenesis [13,14]. The other target of miR-7 is the AKT/PI3K signaling pathway [13].

Table 1. List of upregulated miRNAs in GBM.

miRNA	Target	Expression	Function	Reference
miR-21	PTEN, p53, VH1, PPAR α , TIMP3, RECK, SPOCK1, RB1CC1	Up	Tumor Growth (+), regulate EGFR/AKT signaling, Cell invasion (+), Cell proliferation (+), Apoptosis (–)	[7,24,29,30]
10b	p-53, CDKN1A, CDKN2A, BIM, BCL2, TEAP2C, HOXD10, uPAR, R4OC	Up	Promotes cell cycle, Cell invasion (+)	[14,18,31]
miR-10b/222	p53/PTEN, BIM	Up	Apoptosis (+), Cell Proliferation (+)	[18,34]
miR-9	NF1, PTCH1P	Up	Cell proliferation (+), Cell migration (+), Inflammation (+), Resistance to chemotherapy (+), Apoptosis (–)	[14,35,36]

Table 1. *Cont.*

miRNA	Target	Expression	Function	Reference
miR-221/222	PTEN, MMP2, MMP3, BEGF, PUMA, E2F3, TIMP3, P27KiP1	Up	Tumor growth (+), Apoptosis (–), Proliferation (+), Angiogenesis (+), Migration (+), Invasion (+)	[7,12,18,30,37]
miR-26a	PTEN	Up	Tumor growth (+)	[7,14,29]
miR-148a	CADM1	Up	Cell proliferation (+), Metastasis (+)	[18,40]
miR-125	BMF	Up	Apoptosis (–)	[29]
182	USPI5, TNIP1, CMTLD	Up	GBM aggressiveness (+), Disrupt negative feedback loop of NF-KB	[29]
miR-196		Up	Cell proliferation (+), Poor survival	[29]
miR-30	SOCS3, JAK/STAT3, TRAIL Protein	Up	GSC differentiation (+), Apoptosis (–)	[41]
miR-143	HKII	Up	Cell differentiation (+)	[14]
miR-145	LKB 39- AMPK pathway	Up	Tumor growth (+)	[14]
miR-495-3p	PTEN/AKT pathway	Up	Migration (+), Proliferation (+), Invasion (+)	[13]
miR-503	PACDA	Up	Apoptosis (+)	[18]
miR-93		Up	Angiogenesis (+), Tumor growth (+)	[13]
miR-378	VEGFR2	Up	Angiogenesis (+), Tumor growth (+)	[18,20]
miR-201	HIF1, HIF2	Up	Apoptosis (–), Cell proliferation (+)	[18,42]

Table 2. List of downregulated miRNA in GBM.

miRNA	Target	Expression	Function	Reference
miR-31	Radixin	Down	Invasion (–), Migration (–)	[29]
miR-124	SNA12, CDKA, CDK6, Cyclin D	Down	Cell cycle arrest (+), GSCs invasiveness (–)	[29,43]
miR-34a	Notch 1, Notch 2, CDK6, EGFR, C-met, BCI-2	Down	Cell proliferation (–), Invasion (–), GSCs differentiation (–), Cell cycle arrest (+)	[13,44–46]
miR-34c-3p	Notch 2	Down	S-phase arrest (+), Proliferation (–), Apoptosis (+)	[44]
miR-34c-5p	Notch 1, Notch 2, CDK6, EGFR	Down	Cell proliferation (–)	[44]
miR-302-367 cluster	GIC, CXRC4, PI3K/AKT pathway, STAT3 pathway, SALL2, OLIG2, SOX2, CM γ C, KLF4, OCT3/4, UCH1, MYBBP1A, PEAL5	Down	Tumor growth (–), GSC stemness (–)	[14,47]
miR-181	CDI33, BMI1, WNT signaling pathway, CCR1,	Down	GSC stemness (–)	[21]
(a) miR-181a (c) miR-181d	IL-1b, BCI-2, K-Ra5	Down	Tumor growth (+)	[48,49]
(b) miR-181c	TGFBR1 TGFBR2, TGFBRAP1	Down	Cell invasion (–), Proliferation (–)	[56]
miR-219-5p miR-219-1-3p		Down	Tumor growth (–), Proliferation (–)	[13]

Table 2. Cont.

miRNA	Target	Expression	Function	Reference
miR-1		Down	Sensitize GBM to TMZ, Apoptosis (+)	[50]
miR-328		Down	Proliferation (–)	[52]
miR-375		Down	Proliferation (–), Invasion (–), Migration (–)	[53]
miR-137	EZH2	Down	Angiogenesis (–), Proliferation (–)	[18,20]
miR-128	WNT, BRK, EGFR, IGF1R, BCL2, 5UZI2, BIM1, EZF3, PDGFRA	Down	Apoptosis (+), Proliferation (–), Metastasis (–), Angiogenesis (–), GSCs Renewability (–)	[13,24,54,55]
miR-7	PKM2, EGFR, AKT/PI3K pathway	Down	Tumor Growth (–)	[13,14]

4. miRNA and DNA Methylation: An Epigenetic Interplay in GBM

The complex epigenetic interplay between miRNA and DNA methylation has lately appeared to be quite intriguing to researchers. The monitoring of epigenetic changes during tumor progression can be quite useful to assess the efficacy of any epigenetic therapy, which might be used in combination with other established anti-tumor therapies in order to enhance their sensitivity and subdue the tumor-induced resistance against these therapies [57].

miRNA can either get modulated by epigenetic regulation or can, in turn, regulate those epigenetic modulators via feedback mechanisms. Thus, the epigenetic machinery and miRNA interaction can be considered potential targets for tumor therapies [57]. Most miRNAs are downregulated in GBM as a result of hypermethylation in the CpG island of their promoter region, a phenomenon of miRNA silencing via DNA methylation. There are plenty of miRNAs in GBM that are regulated epigenetically via DNA methylation.

miR-29a, miR-29b, and miR-29c constitute the miRNA-29 family of tumor-suppressing miRNAs that directly target DNA methyl transferases, such as DNMT3a and DNMT3b. As a result of this interaction, DNA methylation is repressed, hence suppressing tumor progression of glioma cells [58,59]. miR-185 and miR-153 are tumor suppressors, which, when overexpressed in glioma cells inhibit DNMT1, induce hypomethylation, and inhibit tumorigenesis [7,21].

miR-211 promotes apoptosis by targeting MMP9 with concomitant activation of caspase-9/caspase-3 to inhibit tumor invasion. It has been reported to be downregulated in GBM due to epigenetic silencing via hypermethylation in its promoter region [58]. Other tumor suppressor miRNAs, such as miR-204, miR-145, miR-137, miR-124, miR-127, miR-219-1, and miR-181c, have been reported to be subjected to epigenetic silencing via DNA methylation in GBM. Among these, miR-181c epigenetic regulation in GBM has been profoundly studied and widely mentioned in the research literature.

miR-181c is a tumor suppressor miRNA that is under-expressed in GBM due to DNA-methylation-induced repression. Its expression level inversely correlates with tumor invasion and proliferation [58]. miR-181c expression is regulated via CTCF and DNA methylation. CTCF is an 11-zinc finger highly conserved nuclear protein [12,13,31], which protects miR-181c repression from DNA methylation by binding to its CpG island region of their promoter. Thus, the absence of CTCF and the gain of DNA methylation together contributes to the downregulation of miR-181c in glioma cells [58].

miR-204 targets SOX4, a stem transcription factor, and prevents cell invasion. This miRNA is downregulated in GBM via DNA methylation [58]. miR-23 is another tumor-suppressing miRNA that causes cell cycle arrest but has been found to be inactivated epigenetically [58]. miR-137 inhibits GSC differentiation, but it is under-expressed in tumor cells and GSCs cells as a consequence of hypermethylation in their promoter region [58,60].

miR-124 aberrant expression induced by epigenetic silencing is responsible for uncontrolled cell growth, as miR-124 hypermethylation prevents it from causing cell cycle arrest at Go/G1 phase [43]. miR-127 and miR-219-1 are tumor-suppressing miRNAs that have lower levels of expression in GBM than in healthy brains due to hypermethylation in their promoter region [8]. Thus, the understanding of these epigenetic networks and their interaction with different miRNAs involved in GBM might be quite useful to establish new reliable and precise approaches for the diagnosis and treatment of GBM.

5. miRNA and Epigenetic Modifications in TMZ Response and Drug Resistance

The main obstacle in current GBM treatment is the resistance to radiotherapy and chemotherapy (TMZ), which profoundly limits the effectiveness of these therapies. TMZ is the first-line chemotherapeutic agent, currently considered the standard therapeutic option for the treatment of GBM. However, this therapy is often susceptible to many resistance-inducing factors which limit its efficacy. miRNA and epigenetic modification greatly influence the TMZ response to GBM treatment. Thus, in order to predict and improve these therapeutic responses in GBM patients, it is necessary to elucidate the mechanisms by which miRNA and epigenetic factors control the outcome of GBM therapies, and even more specifically, it is essential to understand which factors and regulatory mechanisms influence and determine the response to TMZ in GBM patients.

5.1. Epigenetic Modulation and TMZ Response

MGMT is a DNA repair system considered a major contributor to TMZ resistance in GBM [61,62]. MGMT induces resistance to TMZ by removing a methyl group from O₆-methylguanine, which results in the neutralization of TMZ-induced DNA damage, thus reducing the overall cytotoxic effect of TMZ [62]. Therefore, MGMT methylation status is often considered an important predictor of TMZ treatment response [6,62].

The epigenetic silencing of the MGMT gene via hypermethylation at the CpG islands of its promoter results in the inactivation of the MGMT gene, which correlates with enhanced TMZ efficacy along with better prognosis in GBM patients [6,58]. Therefore, it is essential to understand the epigenetic changes taking place during gliomagenesis in order to predict better outcomes after novel and conventional therapies.

5.2. miRNA and TMZ Response

Besides their particular epigenetic actions, miRNAs have been reported to play important roles in TMZ resistance [61] (Table 3). Several miRNAs have been observed to play regulatory roles in TMZ response: miR-195, miR-130a, miR-181a, miR-221, miR-21, miR-210, miR-222, and miR-10a. Apart from these, there are several other miRNAs that have been reported to be involved in MGMT regulation [62]. Upregulation of miR-370-3p, miR-603, miR-221/222, and miR-648 and downregulation of miR-181d, miR-370-3p, and miR-142-3p results in the inhibition of MGMT suppression, therefore, conferring chemoresistance to GBM cell against TMZ treatment [62]. The downregulation of miR-221/222 via antagomiRs treatment has been shown to increase the sensitivity of GBM cells to TMZ as well as promote apoptosis by restoring the p53 pathway [55,63]. We have also noted the following:

- a. miR-21 in an oncogenic miRNA that contributes to drug resistance. Its downregulation enhances chemotherapy efficacy against human GBM cells [63]. miR-21 is often considered a potential biomarker for TMZ resistance [18]. Therefore, silencing miR-21 with simultaneous TMZ treatment can markedly enhance the apoptosis of cancer cells and, therefore, increase the median survival time of patients with TMZ-resistant GBM [18].
- b. miR-181d has also been identified as a predictor of TMZ response and patient survival [49]. It was experimentally proved that transfecting miR-181d into GBM cells caused MGMT expression decay, which is associated with good prognosis and overcoming of resistance. So, miR-181d positively associates with TMZ response and

- patient survival [18,63]. Another miRNA of the same family, miR-181c, is involved in TMZ resistance, as it is suppressed in a patient with GBM who showed a positive response to radiotherapy/TMZ treatment [64].
- c. miR-195 and miR-10a are reported to be overexpressed in GBM cells having low sensitivity to TMZ; therefore, downregulation of these miRNAs can significantly improve TMZ response and survival chance [55].
 - d. miR-124, miR-134, and miR-128 induce their antitumor activity synergistically by inhibiting GSC proliferation and promoting an effective response of radiotherapy and chemotherapy against GBM [63].
 - e. miR-370-3p, a negative regulator of *MGMT*, has been reported to be highly down-regulated in TMZ-resistant GBM cells. miR-370-3p suppresses *MGMT* expression in GBM cells and sensitive glioma cells to TMZ [51,65], inducing apoptosis of tumor cells [51,65]. Thus, miR-370-3p can have a potential therapeutic role in the treatment of recurring GBM if used to improve TMZ response [65].
 - f. miR-128 and miR-149 overexpression sensitize glioma cells to TMZ, especially in the case of non-stem GBM cells and, therefore, contribute to better prognosis [54].
 - g. miR-125b overexpression confers chemoresistance of GSCs to TMZ treatment. The combined inhibition of PI3K and miR-125b significantly enhances TMZ-induced inhibition of GSC proliferation and invasiveness [18]. miR-100 overexpression in glioma cells sensitized them to ionizing radiation by downregulating the ataxia telangiectasia mutated (*ATM*) gene [29].
 - h. miR-328 sensitizes GSC to TMZ by directly suppressing *ABCG2* expression [29]. miR-218 and miR-1268a are associated with enhanced TMZ response in GBM patients [18,29]. miR-1268a is downregulated in a patient with recurrent GBM, and its overexpression promotes TMZ sensitivity to GBM cells via inhibition of translation of the *ABCCL* gene [18].
 - i. miR-299-5p enhances TMZ sensitivity to GBM cells by inhibiting cell proliferation via regulation of the ERK signaling pathway [18].
 - j. Overexpression of miR-423-5p and miR-223 promotes GBM cell survival by decreasing TMZ response [18]. miR-223 expression suppresses TMZ, inducing the inhibition of cell proliferation as well as the miR-223/*PAX6* axis that further contributes to chemoresistance and decreases in TMZ response by regulating the PI3K/AKT signaling pathway.
 - k. miR-318, miR-381, and miR-20a overexpression also result in increased TMZ resistance [18]. Apart from the aforementioned miRNAs, new miRNAs are continuously being discovered that can be used as potential therapeutic tools in combination with established chemotherapy and radiation therapy.

By understanding the expression profiles of these dysregulated miRNAs in TMZ-resistant glioma cells, novel therapeutic targets can be determined, which can be further used in improving the outcome of conventional therapies.

Other than these, epigenetic therapies can be used in combination with traditional therapies to improve TMZ and other cytotoxic treatment responses. Epigenetic alterations that occur during GBM and confer chemoresistance can be targeted, and their effects can be reversed via epigenetic drug treatments. For example, GBM cells treated with 5-Aza-CR cause reversal of DNA methylation, thus sensitizing GBM cells to chemotherapy [57] and overcoming TMZ resistance.

Table 3. miRNA and epigenetic effect on TMZ response.

miRNA/Epigenetic Modulator	Expression	Effect on TMZ Response	Reference
<i>MGMT</i>	High	Induces TMZ resistance	[62]
miR-21	Up	Induces TMZ resistance	[18]
miR-181d	Up	Sensitizes glioma cells to TMZ	[18,63]

Table 3. Cont.

miRNA/Epigenetic Modulator	Expression	Effect on TMZ Response	Reference
miR-195 and miR-10a	Up	Confers TMZ resistance to glioma cells	[55]
miR-124, miR-134, and miR-128	Up	Promotes TMZ-induced cytotoxicity of glioma cells	[63]
miR-370-3p	Down	TMZ resistance	[51,65]
miR-125b	Up	Confers chemoresistance to GSCs against TMZ	[18]
miR-128 and miR-149	Up	Sensitizes non-stem glioma cells to TMZ	[54]
miR-328	Up	Enhances TMZ response to GBM by targeting ABCG2	[29]
miR-1268a and miR-218	Up	Inhibits translation of ABCCL and enhances TMZ sensitivity	[18]
miR-299-5p	Up	Inhibits cell proliferation and enhances TMZ sensitivity by regulating ERK signaling pathway	[18]
miR-423-5p and miR-223	Up	Decreases TMZ response and promotes GBM response	[18]
miR-318, miR-381, and miR-209	Up	Increases TMZ resistance	[18]

6. Diagnostic and Prognostic Molecular Tools in GBM: Do miRNAs Play a Role?

Biomarkers are chemical compounds that are used to monitor the biological state of disease and to measure risks associated with it [30]. They have a high diagnostic and prognostic value, which, when applied, helps in the early detection of a disease, e.g., GBM, and makes it possible to establish an appropriate time point to elicit maximum efficacy of the proposed treatment. All these aspects culminate in early recovery and prolonged survival of the patient. Thus, biomarkers play a critical role in early diagnosis and in the prediction of possible outcomes of the disease, which may help in reducing treatment costs and in extending median survival rates [63].

miRNAs are regulators of the pathways that play crucial roles in GBM invasion and progression. Their expression predicts the efficacy of conventional therapies that are routinely used in GBM treatment [30]. Most miRNAs have already been reported to be dysregulated in GBM so far. Therefore, miRNAs are currently being considered as potential diagnostic and prognostic biomarkers of gliomas [66]. Several studies have validated the potential roles of circulating miRNAs, particularly found in body fluids, such as CSF, plasma, and serum, in GBM diagnosis. We present the following list of promising miRNA biomarkers for high-grade glioma, i.e., GBM (Table 4):

- a. miR-21 is a potential biomarker of GBM with 90% sensitivity and 100% specificity [63]. It has been observed to have low expression in the post-operation serum of GBM patients, suggesting its potential as a serum-derived miRNA biomarker in GBM [38]. High levels of miR-21 have been reported in the plasma of GBM patients, and these levels get lower once the tumor is removed [21]. miR-21 might be used to discriminate between different WHO grades as well as to predict overall survival time in GBM patients [63].
- b. miR-26a and miR-21 are both circulatory miRNAs that are upregulated in GBM, and their serum expression levels have been observed to be reduced after surgery [38], suggesting their importance as candidate serum-based biomarkers in the diagnosis of GBM as well as in monitoring disease progression [38]. Additionally, reduced post-operative serum level of miR-26a also indicates the humoral origin of miR-26a.
- c. miR-10b is upregulated in GBM, and its overexpression promotes GBM progression and correlates with poor prognosis [63]. Its expression level positively correlates with WHO grades of gliomas as well as with tumor invasiveness [21]. Therefore, miR-10b might be used as a biomarker to evaluate glioma invasiveness and, subsequently, in the sub-classification of different tumor grades. Additionally, the combined assess-

- ment of miR-10b and miR-21 in the serum of GBM patients can aid in predicting the therapeutic effect of bevacizumab (BVZ) because miR-10b and 21 serum levels have been reported to be very high in GBM patients and associated with increased tumor diameter in BVZ treated patients.
- d. miR-328 is downregulated in GBM and acts as a tumor suppressor. The low expression level of miR-328 correlates with poor survival rate, thus it might be used as a candidate prognostic biomarker in GBM [52].
 - e. High plasma levels of miR-21 and low plasma levels of miR-128 and miR-342-3p act as candidate biomarkers in distinguishing GBM patients from healthy individuals with remarkably high sensitivity and specificity [67]. miR-342-3p expression is reduced in the plasma of glioma patients, and it is increased after surgery or chemotherapy. Therefore, miR-342-3p might be a candidate biomarker for the diagnosis and discrimination of glioma [67].
 - f. miR-320a is a tumor suppressor miRNA, and its suppression correlates with excessive cell proliferation, invasion, and tumor growth [31]. Therefore, it might be used as a prognostic biomarker [31]. miR-146b and miR-4492 can be useful as novel biomarkers in predicting and monitoring GBM progression [31]. miR-146b is an oncogenic miRNA, and its major target is TRAF6. Downregulation of miR-146b and upregulation of TRAF6 correlate with inhibition of cell proliferation as well as apoptosis of tumor cells due to a decrease in Ki-67 expression. Hence, miR-146b might be suggested as a candidate biomarker for understanding GBM prognosis as well as in discriminating different grades of glioma [31].
 - g. miR-29 plasma level serves as a potential biomarker to indicate malignancy and glioma progression from grades I-II to grades III-IV [68]. miR-454-3p serum expression levels have been found markedly increased in GBM patients, and its upregulation correlates with poor prognosis. Therefore, it can be used as a candidate prognostic biomarker [68].
 - h. Sometimes, single miRNA profiling is not sufficient enough to predict glioma outcomes. In such cases, profiles of several miRNAs are suggested. Seven miRNAs, including miR-15b, miR-23a, miR-133a, miR-150, miR-197, miR-497, and miR-548b-5p, are all downregulated in grades II-IV glioma patients, and the combined expression profiling of these miRNAs might be taken as a candidate biomarker in the prediction of GBM malignancy [68].
 - i. miR-181 is widely reported to be downregulated in GBM, especially in the early stages of this tumor [68]. Therefore, miR-181 might be used as a candidate biomarker for early prediction as well as in the identification of tumor grade. miR-181b and miR-181c act as predictive biomarkers of TMZ response in GBM [68] and may also help in choosing patients who are suitable for adjuvant therapy [30].
 - j. miR-221/222 is found to be significantly upregulated in plasma samples of glioma patients [30,69], and its overexpression contributes to poor prognosis and low survival rates [69]. The study conducted by Zhang R et al. has confirmed that miR-221 and miR-222 might be used as potential diagnostic and prognostic biomarkers [69].

Table 4. Dysregulated miRNA might be considered diagnostic or prognostic candidates in GBM.

Over-Expressed	Under-Expressed	Source Reference
miR-21		Serum [38] Plasma [63]
miR-26a and miR-21		Serum [38]
miR-21	miR-128 and miR-342-3p	Plasma [67]
miR-10b and miR-21		Serum [56]
miR-320a		
miR-146b		[31]

Table 4. Cont.

Over-Expressed	Under-Expressed	Source Reference
miR-454-3p		Serum [67]
miR-29		Plasma [67]
	miR-23a, miR-133a, miR-150, miR-197, miR-497, and miR-548b-5p	[67]
miR-221/222		Plasma [30,69]
	miR-181	[68]

7. GBM Therapy

As we have discussed in the previous section of this review, we can consider miRNAs as promising therapeutic targets on which potential GBM therapies can be developed. Recently, efforts have been made to characterize tumor-suppressing and oncogenic miRNAs involved in GBM that can be used as potential targets; some of them have even shown considerable efficacy [67]. The primary goal of miRNA-based therapies is to identify dysregulated miRNA and either inhibit those oncogenic miRNAs or replace the tumor suppressor miRNAs [67]. In addition to miRNA-based therapies, epigenetic therapies are also gaining lots of approval in the treatment of GBM. Many epigenetic drugs like azacytidine and decitabine have already been approved by the FDA for the treatment of different cancers. Apart from this, adjuvant therapies have also gained attention in recent years and have been reported to prolong overall survival [3]. Other than these therapies, molecular therapies based on alterations in miRNA genetic profiling has made a great advancement in recent years [70]. Studies have reported a significant efficacy of molecular targeted therapy in glioma treatment either in cases when they are applied alone or when applied in combination with cytotoxic chemotherapy [67]. Nevertheless, miRNA-based replacement therapy and oligonucleotide therapy are still candidate approaches but have not yet been used for therapy against GBM.

7.1. miRNA Based Glioma Therapy

Several oncogenic and tumor-suppressing miRNAs that have a deep impact on tumor progression and their aggressiveness have been identified, and these miRNA signatures have led to the development of miRNA-based therapies, such as miRNA replacement therapy (Figure 1), oligonucleotide therapy (Figure 2), etc. Amongst several oncogenic miRNAs, miR-21 and miR-10b [67] have been used as potential targets of oligonucleotide therapy, and several studies have demonstrated their pre-clinical efficacy. Apart from this, several tumor-suppressive miRNAs have also been identified as potential therapeutic targets, such as miR-34a, miR-128, and miR-182 [67]. Among them, miR-34 has received exceptional attention and has been reported to be entered into a phase-I trial, but it is reported to have inflammatory side effects. Despite that, it is still under trial [67].

7.1.1. miRNA-Based Replacement Therapy

The principle behind the miRNA-based replacement therapy (Figure 1) is to restore or increase the activity of tumor-suppressing miRNAs by delivering exogenous. miRNA mimics are chemically synthesized miRNAs of 17-26 nts that have the same sequence as endogenous miRNAs [55,71] and can be used against GBM cells in order to inhibit cell proliferation. Several miRNA mimics are under preclinical trials and have been reported to inhibit GBM growth:

miR-34a

It is a tumor-suppressing miRNA that is downregulated in GBM. miR-34a, via miR-34a mimic, restores miR-34a anti-tumor activity and leads to its overexpression, which induces cell death by targeting p53, BCL-2, KRAS, and MAPK [55,71].

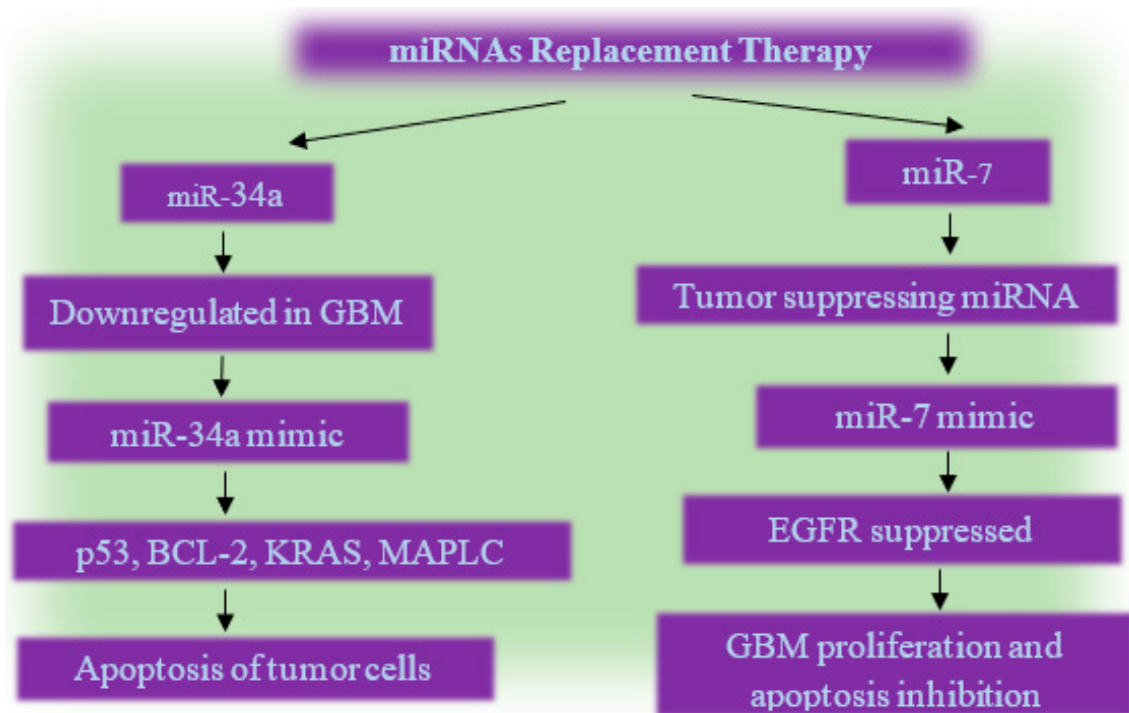


Figure 1. A flow chart of miRNAs replacement therapy, as a candidate experimental approach, but not yet used for therapy against GBM.

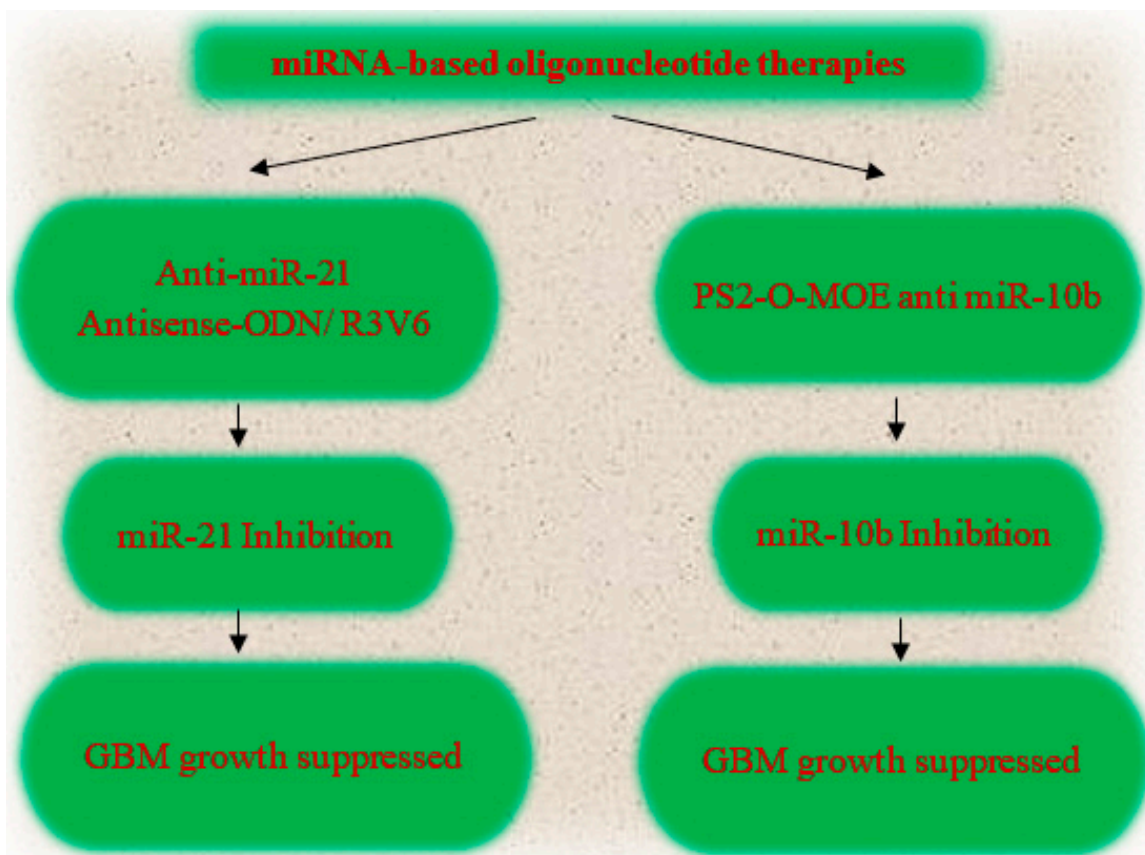


Figure 2. A flowchart of miRNA-based oligonucleotide therapy as a candidate experimental approach but not yet used for therapy against GBM.

miRNA-7

miRNA-7 is a tumor suppressor whose reduced expression level in GBM correlates with a high level of EGFR, which leads to uncontrolled cell proliferation. Thus, miR-7-based replacement therapy can be effective in controlling the recurrence of GBM. A study conducted on miR-7-based replacement therapy by Alamdari et al. [71] confirms that transfection of miR-7 mimic into human U373-MG GBM cell shows significant suppression in EGFR mRNA and protein level, as well as the inhibition of cell growth.

7.1.2. Oligonucleotide Therapy

This is one of the rapidly emerging anti-cancer drug therapies that have been approved by the FDA [72]. This therapy (Figure 2) is based on the Watson–Crick base pairing targeting mRNA resulting in gene silencing or alteration in the splicing pattern [72]. Oligonucleotide therapy includes ASOs, siRNA, miRNA, DNA enzymes, and aptamers, and it acts either via splicing modulation, gene correction, or translation termination [72]. Oligonucleotide therapy has been validated as a potential therapeutic approach because of its high specificity and sensitivity as well as its low toxicity [37]. Oligonucleotide therapy based on miRNA inhibition therapy can be proved as a potential therapy in the treatment of GBM. For example, miR-21, which is an oncogenic miRNA, can be inhibited via antagomiRs [37]. Injecting miR-21 antisense oligonucleotide in complex with amphiphilic R3V6 peptide in glioma cells causes inhibition of miR-21, resulting in suppression of tumor growth [37]. Another such example is miR-10b, which is also an oncogenic miRNA whose overexpression correlates with cell invasion and anti-apoptosis. miR-10b can be inhibited by PS2-O-MOE anti-miR-10b oligonucleotide, thus slowing down tumor growth [37]. These studies suggest that oligonucleotide therapy holds a promising future for GBM treatment.

7.2. Epigenetic Therapy

Epigenetics is one of the major mechanisms that contributes to and governs gliomagenesis. The epigenetic modulators that lead to epigenetic alterations can be potential therapeutic targets to try to reverse these epigenetic effects [73]. DNMT, enzymes, and genes, such as EZH2 and BMI1, are epigenetic modifiers [13]. The altered expression of enzymes has been identified as a pivotal epigenetic drug target for GBM treatment [73], and it is currently under preclinical and clinical trials [73].

7.2.1. DNMT Inhibitors

DNA methyltransferases are responsible for de novo DNA methylation at CpG islands and impart resistance of glioma cells to chemotherapeutic drugs, such as TMZ [73]. DNMTs are also considered epigenetic drug targets. Epigenetic drugs may inhibit DNMTs, which, then, would induce hypomethylation in gene promoter regions and expression of tumor-suppressing genes [13]. Some FDA-approved DNMT inhibitors are azacytidine and decitabine, but their effectiveness in the treatment of solid tumors still has to be approved [13]. A study conducted by Ghasemi et al. [8] demonstrated the effect of 5-aza-dc on methylation and expression levels of miR-219-1. They reported that 5-aza-dc on demethylated DNA resulted in increased expression of miR-219-1 by several folds, which, in turn, decreased cyclin A2 levels and thus prevented cell proliferation.

7.2.2. Histone Deacetylase Inhibitors (HDACIs)

HDACIs have shown tremendous potential as anti-cancerous drugs because they can activate genes that are silenced in GBM cells. Several research studies are under clinical trials [73]. HDAC inhibitors induce their anti-tumor effect by inducing cell cycle arrest in the G1 and G2 phases of the cycle [13,73], inhibiting angiogenesis and metastasis, as well as promoting apoptosis of glioma cells [13]. HDAC inhibitors that are reported to induce radio sensitization are valproic acid (VPA) and entinostat, thus making GBM more susceptible to radio therapy [73]. These studies suggest that thorough investigation should be carried out on these epigenetic drugs to elicit their maximum benefits as cancer therapeutic agents.

7.3. Molecular Target Therapy

Molecular-based therapies use small molecule inhibitors or monoclonal antibodies to inhibit growth factor pathways, angiogenesis pathways, and intracellular signaling pathways, such as PI3K/AKT/mTOR, which are involved in GBM progression [3,70]. The mechanism behind this therapy employs drugs to block signaling pathways that promote cell growth [70]. Monoclonal antibodies, such as imatinib, inhibit PDGF, a promoter of tumor growth [3], and other pathways, such as RTKs, unfortunately, lack efficacy [3]. Similarly, gefitinib and erlotinib, which are anti-EGFR drugs, are under clinical trials, but they have not shown any promising outcomes. Contrary to these drugs, bevacizumab, a monoclonal antibody that targets VEGF, has shown promising therapeutic efficacies and has been observed to be effective in promoting progression-free survival during clinical trials [3]. The combinational therapy of bevacizumab with radiotherapy and TMZ is currently under clinical trial [3]. Thus, overall molecular-based therapeutic agents are still in trial stages I/II, and they lack the desirable efficacy due to high toxicity [3].

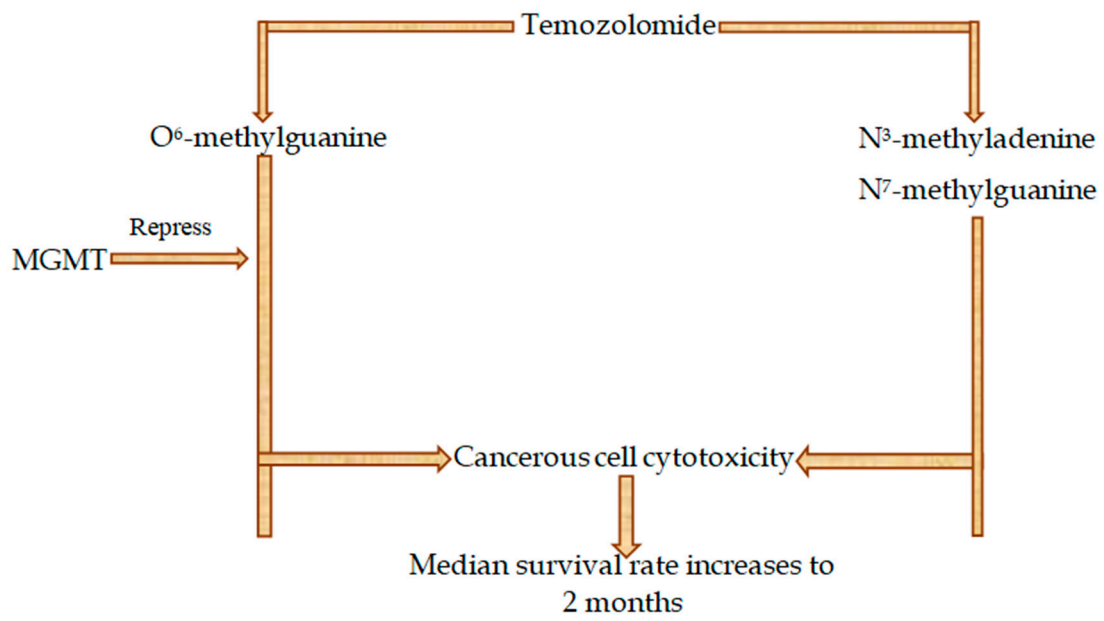
7.4. Adjuvant Therapy

Chemotherapies, such as TMZ and radiotherapy, are the conventional anti-cancer therapies that are integrally involved in the clinical management system of many cancers including GBM [74]. However, the combination of radiotherapy and TMZ after surgical resection has been shown to increase median survival time from 12.1 months to 14.6 months in a remarkable trial conducted in 2005 by Stupp et al. [74]. This study establishes adjuvant therapy to be a promising anti-cancer therapy for the treatment of GBM with high efficacy. However, the study fails to prove the efficacy of adjuvant therapy in p-GBM. Also, this therapy encounters tumor cell resistance to TMZ conferred by unmethylated *MGMT*, thereby decreasing the responsiveness of the therapy [3].

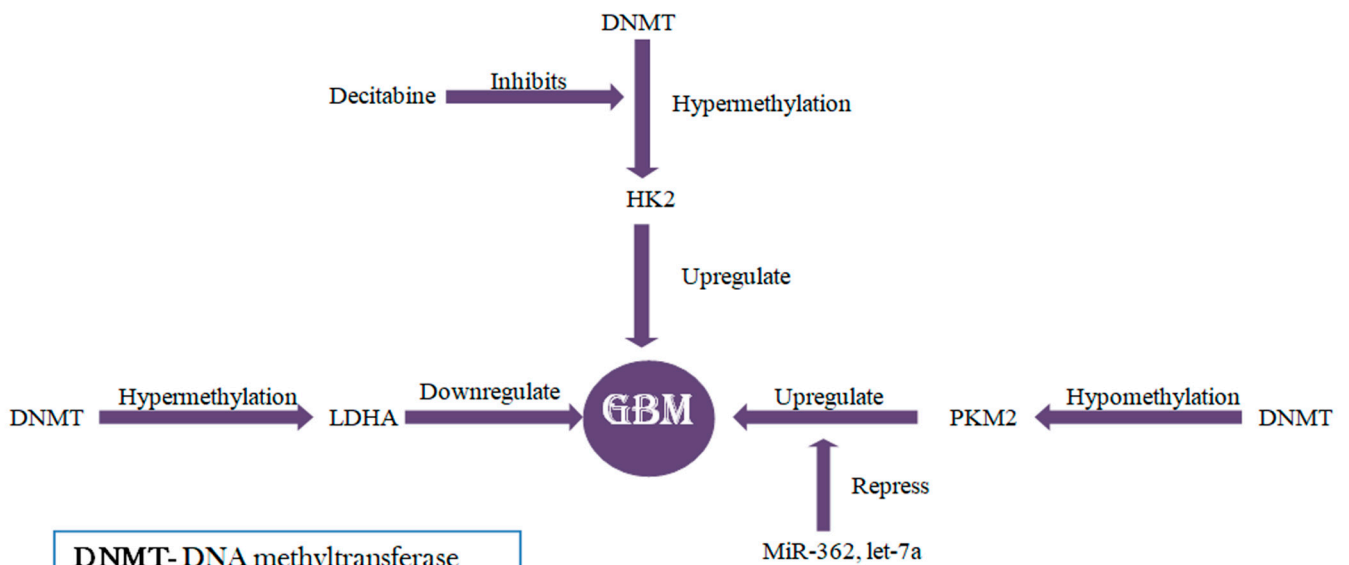
8. Challenges and Limitations

Despite the establishment and development of many anti-cancer therapies, such as chemotherapy, radiotherapy and adjuvant therapies, epigenetic therapies, and miRNA-based therapy, the prognosis of GBM is still poor. The main reason behind this is tumor heterogeneity, which contributes to drug resistance [70] and tumor cell infiltration, making surgical resection impossible. Other than high heterogeneity, the existence of biological barriers, such as the blood–brain barrier, makes it difficult to deliver miRNA across it [71]. Another challenge to miRNA delivery is the undesirable toxicities due to the activation of the innate immune system [71]. Besides this, there are other therapies, such as oligonucleotide therapies. They also face challenges, and their efficacy is limited by the presence of a blood–brain barrier as molar quantities of oligonucleotides are needed, which makes it difficult to penetrate the blood–brain barrier, thus reducing the therapeutic effect [37]. Molecularly targeted therapies are still under clinical trials and have not shown much desirable efficacy. Additionally, tumor heterogeneity confers chemoresistance to drugs associated with molecular targeted therapy, thus limiting its overall anti-cancer effect [70].

Our study is limited by the fact that no application to the clinic can be extracted from it. Rather, on the contrary, the impact of this work is on the line of the presentation and description of the important miRNAs and their epigenetic influence in GBM, linked to TMZ treatment and to *MGMT* expression, mainly (Figure 3). We consider this to be the first approach to the understanding of miRNA in GBM pathogenesis. A clinical approach would have required our knowledge of the clinical data and survival analyses in all articles reviewed, something that we assume to be very difficult or impossible to do. Our work concentrates much more on describing the importance of miRNA in GBM and their epigenetic effects without entering clinical aspects. From here, we can further jump, with different studies, to a clinically oriented approach in order to, e.g., also include the different epigenetic regulation pre- and post-therapy in GBM, with TMZ and/or any other treatment that might be subjected to testing.



(a)



DNMT- DNA methyltransferase
 LDHA- Lactate dehydrogenase
 PKM2- Pyruvate kinase iso-M2
 HK2- Hexokinase 2

(b)

Figure 3. Cont.

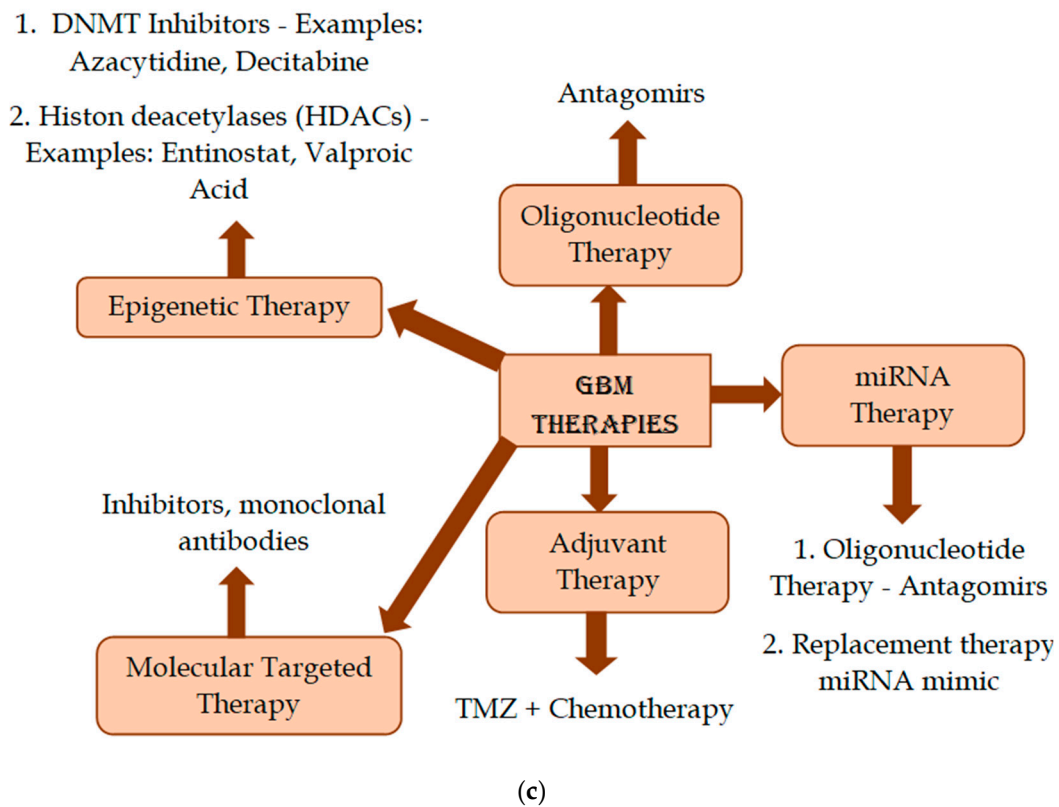


Figure 3. Overview of MGMT-TMZ relationship and possible experimental treatments against GBM: (a) Response to TMZ in GBM and role of epigenetic modifications: TMZ is a chemotherapeutic drug that kills tumor cells by methylating DNA at O6 and N7 position of guanine and at N3 position of adenine. However, TMZ efficacy is often limited by the DNA repair enzyme MGMT. Hypermethylation at the promoter region of *MGMT* can restore TMZ cytotoxic effect. (b) MiRNA and epigenetic regulation of glycolytic enzymes that are critical for GBM pathophysiology; PKM2, HK2, and LDHA are the glycolytic enzymes that are aberrantly expressed in glioma patients and strongly influenced by miRNA and epigenetic factors. HK2 hypermethylation exacerbates GBM progression, an effect that can be suppressed by inhibiting DNMT (DNA methyltransferases) with decitabine. On the other hand, hypermethylation of LDHA impedes GBM growth. PKM2 is regulated by both miRNAs as well as epigenetic factors. When hypomethylated by DNMT, PKM2 contributes to the growth and aggressiveness of GBM. Contrary to it, when PKM2 is targeted by miR-7, let-miR-7 and miR-326 repression of glioma is produced. (c) A possible interplay of non-clinical yet experimental possibilities of treatment against GBM.

9. Perspective and Conclusions

miRNAs and epigenetic alterations in gliomagenesis can provide an understanding of tumor progression, and thus, both can be used as potential diagnostic and prognostic tools and may help in taking clinical decisions. Circulating miRNAs can be used as potential biomarkers for early detection of GBM, which may result in increasing the overall life expectancy of glioma patients. Besides this, epigenetic modulators are gaining attention exceptionally, and they can be used as potential epigenetic drug targets to reverse epigenetic effects that contribute to tumorigenesis. Epigenetic-based therapies may also render the susceptibility of tumor cells to TMZ.

To improve the efficacies of various anti-tumor therapies, efforts should be made to identify prognostic markers for intra-tumor heterogeneity, which will aid in predicting and in the improvement of therapeutic results. To maximize the efficacy of oligonucleotide therapy, nanoparticles as a miRNA delivery system might be employed to test whether this strategy might constitute a promising therapy in the treatment of GBM.

Anyhow, we assume our work is just a small contribution to the understanding of miRNA participation in gliomagenesis, specifically performed at the level of describing the relevant participating miRNA, and the role they present in the TMZ treatment against GBM, principally influenced, to our knowledge, by MGMT promoter methylation. This work is an open door for others to test these molecular mechanisms in relation to clinical data and to various different experimental treatments in the following years.

Author Contributions: H.H., writing original draft; M.A. and M.H.S., concept, writing—reviewing and editing; J.S.C., writing—reviewing and editing. All authors have read and agreed to the published version of the manuscript.

Funding: This work was partially supported by a grant from the University of Navarra Foundation, Pamplona, Spain, to J.S.C.

Institutional Review Board Statement: Not applicable.

Informed Consent Statement: Not applicable.

Conflicts of Interest: The authors declare no conflict of interest.

References

- Louis, D.N.; Perry, A.; Wesseling, P.; Brat, D.J.; Cree, I.A.; Figarella-Branger, D.; Hawkins, C.; Ng, H.K.; Pfister, S.M.; Reifenberger, G.; et al. The 2021 WHO Classification of Tumors of the Central Nervous System: A summary. *Neuro Oncol.* **2021**, *23*, 1231–1251. [CrossRef] [PubMed]
- Sejda, A.; Grajkowska, W.; Trubicka, J.; Szutowicz, E.; Wojdacz, T.; Kloc, W.; Iżycka-Świeszewska, E. WHO CNS5 2021 classification of gliomas: A practical review and road signs for diagnosing pathologists and proper patho-clinical and neuro-oncological cooperation. *Folia Neuropathol.* **2022**, *60*, 137–152. [CrossRef]
- Wilson, T.A.; Karajannis, M.A.; Harter, D.H. Glioblastoma multiforme: State of the art and future therapeutics. *Surg. Neurol. Int.* **2014**, *5*, 64. [CrossRef] [PubMed]
- Lombardi, M.Y.; Assem, M. Glioblastoma Genomics: A Very Complicated Story. In *Glioblastoma*; De Vleeschouwer, S., Ed.; Codon Publications: Brisbane, Australia, 2017. [CrossRef]
- Mansouri, A.; Karamchandani, J.; Das, S. Molecular Genetics of Secondary Glioblastoma. In *Glioblastoma*; De Vleeschouwer, S., Ed.; Codon Publications: Brisbane, Australia, 2017. [CrossRef]
- Burgess, R.; Jenkins, R.; Zhang, Z. Epigenetic changes in gliomas. *Cancer Biol.* **2008**, *7*, 1326–1334. [CrossRef]
- Kreth, S.; Thon, N.; Kreth, F.W. Epigenetics in human gliomas. *Cancer Lett.* **2014**, *342*, 185–192. [CrossRef] [PubMed]
- Ghasemi, A.; Mohammadi, A.; Fallah, S. Epigenetic Modification of MicroRNA-219-1 and Its Association with Glioblastoma Multiforme. *Biochemistry* **2021**, *86*, 420–432. [CrossRef] [PubMed]
- Ayala-Ortega, E.; Arzate-Mejia, R.; Perez-Molina, R.; Gonzalez-Buendia, E.; Meier, K.; Guerrero, G.; Recillas-Targa, F. Epigenetic silencing of miR-181c by DNA methylation in glioblastoma cell lines. *BMC Cancer* **2016**, *16*, 226. [CrossRef]
- Marzese, D.M.; Hoon, D.S. Emerging technologies for studying DNA methylation for the molecular diagnosis of cancer. *Expert Rev. Mol. Diagn.* **2015**, *15*, 647–664. [CrossRef]
- Quintavalle, C.; Mangani, D.; Roscigno, G.; Romano, G.; Diaz-Lagares, A.; Iaboni, M.; Donnarumma, E.; Fiore, D.; De Marinis, P.; Soini, Y.; et al. MiR-221/222 target the DNA methyltransferase MGMT in glioma cells. *PLoS ONE* **2013**, *8*, e74466. [CrossRef]
- Kirstein, A.; Schmid, T.E.; Combs, S.E. The Role of miRNA for the Treatment of MGMT Unmethylated Glioblastoma Multiforme. *Cancers* **2020**, *12*, 1099. [CrossRef]
- Uddin, M.S.; Mamun, A.A.; Alghamdi, B.S.; Tewari, D.; Jeandet, P.; Sarwar, M.S.; Ashraf, G.M. Epigenetics of glioblastoma multiforme: From molecular mechanisms to therapeutic approaches. *Semin. Cancer Biol.* **2022**, *83*, 100–120. [CrossRef]
- Dong, Z.; Cui, H. Epigenetic modulation of metabolism in glioblastoma. *Semin. Cancer Biol.* **2019**, *57*, 45–51. [CrossRef]
- Chesnelong, C.; Chaumeil, M.M.; Blough, M.D.; Al-Najjar, M.; Stechishin, O.D.; Chan, J.A.; Pieper, R.O.; Ronen, S.M.; Weiss, S.; Luchman, H.A.; et al. Lactate dehydrogenase A silencing in IDH mutant gliomas. *Neuro Oncol.* **2014**, *16*, 686–695. [CrossRef]
- Di, H.; Zhang, X.; Guo, Y.; Shi, Y.; Fang, C.; Yuan, Y.; Wang, J.; Shang, C.; Guo, W.; Li, C. Silencing LDHA inhibits proliferation, induces apoptosis and increases chemosensitivity to temozolomide in glioma cells. *Oncol. Lett.* **2018**, *15*, 5131–5136. [CrossRef] [PubMed]
- Blakeway, D.; Karakoula, K.; Morris, M.; Rowther, F.; Eagles, L.; Darling, J.; Warr, T. Overexpression of Hexokinase 2 is epigenetically regulated by frequent hypomethylation in glioblastoma multiforme. *Neuro Oncol.* **2018**, *20*, i12. [CrossRef]
- Rezaei, O.; Honarmand, K.; Nateghinia, S.; Taheri, M.; Ghafouri-Fard, S. miRNA signature in glioblastoma: Potential biomarkers and therapeutic targets. *Exp. Mol. Pathol.* **2020**, *117*, 104550. [CrossRef] [PubMed]

19. Henriksen, M.; Johnsen, K.B.; Andersen, H.H.; Pilgaard, L.; Duroux, M. MicroRNA expression signatures determine prognosis and survival in glioblastoma multiforme—A systematic overview. *Mol. Neurobiol.* **2014**, *50*, 896–913. [CrossRef]
20. Balandeh, E.; Mohammadshafie, K.; Mahmoudi, Y.; Hossein Pourhanifeh, M.; Rajabi, A.; Bahabadi, Z.R.; Mohammadi, A.H.; Rahimian, N.; Hamblin, M.R.; Mirzaei, H. Roles of Non-coding RNAs and Angiogenesis in Glioblastoma. *Front. Cell Dev. Biol.* **2021**, *9*, 716462. [CrossRef]
21. Kalkan, R.; Atli, E.I. The Impacts of miRNAs in Glioblastoma Progression. *Crit. Rev. Eukaryot. Gene Expr.* **2016**, *26*, 137–142. [CrossRef]
22. Huang, D.; Qiu, S.; Ge, R.; He, L.; Li, M.; Li, Y.; Peng, Y. miR-340 suppresses glioblastoma multiforme. *Oncotarget* **2015**, *6*, 9257–9270. [CrossRef]
23. O'Brien, J.; Hayder, H.; Zayed, Y.; Peng, C. Overview of MicroRNA Biogenesis, Mechanisms of Actions, and Circulation. *Front. Endocrinol.* **2018**, *9*, 402. [CrossRef]
24. Marumoto, T.; Saya, H. Molecular biology of glioma. *Adv. Exp. Med. Biol.* **2012**, *746*, 2–11. [CrossRef] [PubMed]
25. Michlewski, G.; Caceres, J.F. Post-transcriptional control of miRNA biogenesis. *RNA* **2019**, *25*, 1–16. [CrossRef] [PubMed]
26. Wu, K.; He, J.; Pu, W.; Peng, Y. The Role of Exportin-5 in MicroRNA Biogenesis and Cancer. *Genom. Proteom. Bioinform.* **2018**, *16*, 120–126. [CrossRef]
27. Bovell, L.C.; Putcha, B.D.; Samuel, T.; Manne, U. Clinical implications of microRNAs in cancer. *Biotech. Histochem.* **2013**, *88*, 388–396. [CrossRef] [PubMed]
28. Alfardus, H.; McIntyre, A.; Smith, S. MicroRNA Regulation of Glycolytic Metabolism in Glioblastoma. *Biomed. Res. Int.* **2017**, *2017*, 9157370. [CrossRef]
29. Hassan, A.; Mosley, J.; Singh, S.; Zinn, P.O. A Comprehensive Review of Genomics and Noncoding RNA in Gliomas. *Top. Magn. Reson. Imaging* **2017**, *26*, 3–14. [CrossRef]
30. Barciszewska, A.M. MicroRNAs as efficient biomarkers in high-grade gliomas. *Folia Neuropathol.* **2016**, *54*, 369–374. [CrossRef]
31. de Menezes, M.R.; Acioli, M.E.A.; da Trindade, A.C.L.; da Silva, S.P.; de Lima, R.E.; da Silva Teixeira, V.G.; Vasconcelos, L.R.S. Potential role of microRNAs as biomarkers in human glioblastoma: A mini systematic review from 2015 to 2020. *Mol. Biol. Rep.* **2021**, *48*, 4647–4658. [CrossRef]
32. Junior, L.G.D.; Baroni, M.; Lira, R.C.P.; Teixeira, S.; Fedatto, P.F.; Silveira, V.S.; Suazo, V.K.; Veronez, L.C.; Panepucci, R.A.; Antonio, D.S.M.; et al. High-throughput microRNA profile in adult and pediatric primary glioblastomas: The role of miR-10b-5p and miR-630 in the tumor aggressiveness. *Mol. Biol. Rep.* **2020**, *47*, 6949–6959. [CrossRef]
33. Malhotra, M.; Sekar, T.V.; Ananta, J.S.; Devulapally, R.; Afjei, R.; Babikir, H.A.; Paulmurugan, R.; Massoud, T.F. Targeted nanoparticle delivery of therapeutic antisense microRNAs presensitizes glioblastoma cells to lower effective doses of temozolomide in vitro and in a mouse model. *Oncotarget* **2018**, *9*, 21478–21494. [CrossRef] [PubMed]
34. Sun, B.; Zhao, X.; Ming, J.; Liu, X.; Liu, D.; Jiang, C. Stepwise detection and evaluation reveal miR-10b and miR-222 as a remarkable prognostic pair for glioblastoma. *Oncogene* **2019**, *38*, 6142–6157. [CrossRef] [PubMed]
35. Coolen, M.; Katz, S.; Bally-Cuif, L. miR-9: A versatile regulator of neurogenesis. *Front. Cell. Neurosci.* **2013**, *7*, 220. [CrossRef]
36. Munoz, J.L.; Rodriguez-Cruz, V.; Rameshwar, P. High expression of miR-9 in CD133(+) glioblastoma cells in chemoresistance to temozolomide. *J. Cancer Stem Cell Res.* **2015**, *3*, e1003. [CrossRef]
37. Krichevsky, A.M.; Uhlmann, E.J. Oligonucleotide Therapeutics as a New Class of Drugs for Malignant Brain Tumors: Targeting mRNAs, Regulatory RNAs, Mutations, Combinations, and Beyond. *Neurotherapeutics* **2019**, *16*, 319–347. [CrossRef]
38. ParvizHamidi, M.; Haddad, G.; Ostadrahimi, S.; Ostadrahimi, N.; Sadeghi, S.; Fayaz, S.; Fard-Esfahani, P. Circulating miR-26a and miR-21 as biomarkers for glioblastoma multiform. *Biotechnol. Appl. Biochem.* **2019**, *66*, 261–265. [CrossRef]
39. Ernst, A.; Campos, B.; Meier, J.; Devens, F.; Liesenberg, F.; Wolter, M.; Reifenberger, G.; Herold-Mende, C.; Lichter, P.; Radlwimmer, B. De-repression of CTGF via the miR-17-92 cluster upon differentiation of human glioblastoma spheroid cultures. *Oncogene* **2010**, *29*, 3411–3422. [CrossRef]
40. Cai, Q.; Zhu, A.; Gong, L. Exosomes of glioma cells deliver miR-148a to promote proliferation and metastasis of glioblastoma via targeting CADM1. *Bull. Cancer* **2018**, *105*, 643–651. [CrossRef] [PubMed]
41. Che, S.; Sun, T.; Wang, J.; Jiao, Y.; Wang, C.; Meng, Q.; Qi, W.; Yan, Z. miR-30 overexpression promotes glioma stem cells by regulating Jak/STAT3 signaling pathway. *Tumour Biol.* **2015**, *36*, 6805–6811. [CrossRef]
42. Lai, N.S.; Wu, D.G.; Fang, X.G.; Lin, Y.C.; Chen, S.S.; Li, Z.B.; Xu, S.S. Serum microRNA-210 as a potential noninvasive biomarker for the diagnosis and prognosis of glioma. *Br. J. Cancer* **2015**, *112*, 1241–1246. [CrossRef]
43. Liu, X.; Kang, J.; Sun, S.; Luo, Y.; Ji, X.; Zeng, X.; Zhao, S. iASPP, a microRNA-124 target, is aberrantly expressed in astrocytoma and regulates malignant glioma cell migration and viability. *Mol. Med. Rep.* **2018**, *17*, 1970–1978. [CrossRef]
44. Bazzoni, R.; Bentivegna, A. Role of Notch Signaling Pathway in Glioblastoma Pathogenesis. *Cancers* **2019**, *11*, 292. [CrossRef]
45. Li, Y.; Guessous, F.; Zhang, Y.; Dipierro, C.; Kefas, B.; Johnson, E.; Marcinkiewicz, L.; Jiang, J.; Yang, Y.; Schmittgen, T.D.; et al. MicroRNA-34a inhibits glioblastoma growth by targeting multiple oncogenes. *Cancer Res.* **2009**, *69*, 7569–7576. [CrossRef] [PubMed]
46. Janaki Ramaiah, M.; Divyapriya, K.; Kartik Kumar, S.; Rajesh, Y. Drug-induced modifications and modulations of microRNAs and long non-coding RNAs for future therapy against Glioblastoma Multiforme. *Gene* **2020**, *723*, 144126. [CrossRef] [PubMed]

47. Yang, C.M.; Chiba, T.; Brill, B.; Delis, N.; von Manstein, V.; Vafaizadeh, V.; Oellerich, T.; Groner, B. Expression of the miR-302/367 cluster in glioblastoma cells suppresses tumorigenic gene expression patterns and abolishes transformation related phenotypes. *Int. J. Cancer* **2015**, *137*, 2296–2309. [CrossRef]
48. Allen, B.K.; Stathias, V.; Maloof, M.E.; Vidovic, D.; Winterbottom, E.F.; Capobianco, A.J.; Clarke, J.; Schurer, S.; Robbins, D.J.; Ayad, N.G. Epigenetic pathways and glioblastoma treatment: Insights from signaling cascades. *J. Cell. Biochem.* **2015**, *116*, 351–363. [CrossRef] [PubMed]
49. Ho, K.H.; Chen, P.H.; Hsi, E.; Shih, C.M.; Chang, W.C.; Cheng, C.H.; Lin, C.W.; Chen, K.C. Identification of IGF-1-enhanced cytokine expressions targeted by miR-181d in glioblastomas via an integrative miRNA/mRNA regulatory network analysis. *Sci. Rep.* **2017**, *7*, 732. [CrossRef] [PubMed]
50. Yang, C.H.; Wang, Y.; Sims, M.; Cai, C.; Pfeffer, L.M. MicroRNA-1 suppresses glioblastoma in preclinical models by targeting fibronectin. *Cancer Lett.* **2019**, *465*, 59–67. [CrossRef]
51. Nadaradjane, A.; Briand, J.; Bougras-Cartron, G.; Disdero, V.; Vallette, F.M.; Frenel, J.S.; Cartron, P.F. miR-370-3p Is a Therapeutic Tool in Anti-glioblastoma Therapy but Is Not an Intratumoral or Cell-free Circulating Biomarker. *Mol. Nucleic Acids* **2018**, *13*, 642–650. [CrossRef]
52. Wu, Z.; Sun, L.; Wang, H.; Yao, J.; Jiang, C.; Xu, W.; Yang, Z. MiR-328 expression is decreased in high-grade gliomas and is associated with worse survival in primary glioblastoma. *PLoS ONE* **2012**, *7*, e47270. [CrossRef]
53. Li, G.F.; Cheng, Y.Y.; Li, B.J.; Zhang, C.; Zhang, X.X.; Su, J.; Wang, C.; Chang, L.; Zhang, D.Z.; Tan, C.L.; et al. miR-375 inhibits the proliferation and invasion of glioblastoma by regulating Wnt5a. *Neoplasma* **2019**, *66*, 350–356. [CrossRef] [PubMed]
54. Cardoso, A.M.; Morais, C.M.; Pena, F.; Marante, T.; Cunha, P.P.; Jurado, A.S.; Pedroso de Lima, M.C. Differentiation of glioblastoma stem cells promoted by miR-128 or miR-302a overexpression enhances senescence-associated cytotoxicity of axitinib. *Hum. Mol. Genet.* **2021**, *30*, 160–171. [CrossRef] [PubMed]
55. Chen, M.; Medarova, Z.; Moore, A. Role of microRNAs in glioblastoma. *Oncotarget* **2021**, *12*, 1707–1723. [CrossRef] [PubMed]
56. Sasayama, T.; Tanaka, K.; Kohmura, E. The Roles of MicroRNAs in Glioblastoma Biology and Biomarker. In *Neurooncology: Newer Developments*; Agrawal, A., Ed.; IntechOpen: London, UK, 2016. [CrossRef]
57. Kelly, T.K.; De Carvalho, D.D.; Jones, P.A. Epigenetic modifications as therapeutic targets. *Nat. Biotechnol.* **2010**, *28*, 1069–1078. [CrossRef]
58. Banelli, B.; Forlani, A.; Allemanni, G.; Morabito, A.; Pistillo, M.P.; Romani, M. MicroRNA in glioblastoma: An overview. *Int. J. Genom.* **2017**, *2017*, 7639084. [CrossRef]
59. Morita, S.; Horii, T.; Kimura, M.; Ochiya, T.; Tajima, S.; Hatada, I. miR-29 represses the activities of DNA methyltransferases and DNA demethylases. *Int. J. Mol. Sci.* **2013**, *14*, 14647–14658. [CrossRef]
60. Bier, A.; Giladi, N.; Kronfeld, N.; Lee, H.K.; Cazacu, S.; Finniss, S.; Xiang, C.; Poisson, L.; deCarvalho, A.C.; Slavin, S.; et al. MicroRNA-137 is downregulated in glioblastoma and inhibits the stemness of glioma stem cells by targeting RTVP-1. *Oncotarget* **2013**, *4*, 665–676. [CrossRef]
61. Hiddingh, L.; Raktoe, R.S.; Jeuken, J.; Hulleman, E.; Noske, D.P.; Kaspers, G.J.; Vandertop, W.P.; Wesseling, P.; Wurdinger, T. Identification of temozolomide resistance factors in glioblastoma via integrative miRNA/mRNA regulatory network analysis. *Sci. Rep.* **2014**, *4*, 5260. [CrossRef]
62. Sun, J.; Ma, Q.; Li, B.; Wang, C.; Mo, L.; Zhang, X.; Tang, F.; Wang, Q.; Yan, X.; Yao, X.; et al. RPN2 is targeted by miR-181c and mediates glioma progression and temozolomide sensitivity via the wnt/ β -catenin signaling pathway. *Cell Death Dis.* **2020**, *11*, 890. [CrossRef]
63. Buruiana, A.; Florian, S.I.; Florian, A.I.; Timis, T.L.; Mihu, C.M.; Miclaus, M.; Osan, S.; Hrapasa, I.; Cataniciu, R.C.; Farcas, M.; et al. The Roles of miRNA in Glioblastoma Tumor Cell Communication: Diplomatic and Aggressive Negotiations. *Int. J. Mol. Sci.* **2020**, *21*, 1950. [CrossRef]
64. Gao, Y.T.; Chen, X.B.; Liu, H.L. Up-regulation of miR-370-3p restores glioblastoma multiforme sensitivity to temozolomide by influencing MGMT expression. *Sci. Rep.* **2016**, *6*, 32972. [CrossRef] [PubMed]
65. Areeb, Z.; Stylli, S.S.; Koldej, R.; Ritchie, D.S.; Siegal, T.; Morokoff, A.P.; Kaye, A.H.; Luwor, R.B. MicroRNA as potential biomarkers in Glioblastoma. *J. Neuro-Oncol.* **2015**, *125*, 237–248. [CrossRef]
66. Wang, Q.; Li, P.; Li, A.; Jiang, W.; Wang, H.; Wang, J.; Xie, K. Plasma specific miRNAs as predictive biomarkers for diagnosis and prognosis of glioma. *J. Exp. Clin. Cancer Res.* **2012**, *31*, 97. [CrossRef] [PubMed]
67. Zhang, Y.; Cruickshanks, N.; Pahuski, M.; Yuan, F.; Dutta, A.; Schiff, D.; Purow, B.; Abounader, R. Noncoding RNAs in Glioblastoma. In *Glioblastoma*; De Vleeschouwer, S., Ed.; Exon Publications: Brisbane, Australia, 2017. [CrossRef]
68. Yang, L.; Ma, Y.; Xin, Y.; Han, R.; Li, R.; Hao, X. Role of the microRNA 181 family in glioma development. *Mol. Med. Rep.* **2018**, *17*, 322–329. [CrossRef] [PubMed]
69. Zhang, R.; Pang, B.; Xin, T.; Guo, H.; Xing, Y.; Xu, S.; Feng, B.; Liu, B.; Pang, Q. Plasma miR-221/222 Family as Novel Descriptive and Prognostic Biomarkers for Glioma. *Mol. Neurobiol.* **2016**, *53*, 1452–1460. [CrossRef] [PubMed]
70. Mollaei, H.; Safaralizadeh, R.; Rostami, Z. MicroRNA replacement therapy in cancer. *J. Cell. Physiol.* **2019**, *234*, 12369–12384. [CrossRef] [PubMed]
71. Alamdari-Palangi, V.; Karami, Z.; Karami, H.; Baazm, M. MiRNA-7 Replacement Effect on Proliferation and Tarceva-Sensitivity in U373-MG Cell Line. *Asian Pac. J. Cancer Prev.* **2020**, *21*, 1747–1753. [CrossRef] [PubMed]

72. Xiong, H.; Veedu, R.N.; Diermeier, S.D. Recent Advances in Oligonucleotide Therapeutics in Oncology. *Int. J. Mol. Sci.* **2021**, *22*, 3295. [CrossRef] [PubMed]
73. Romani, M.; Pistillo, M.P.; Banelli, B. Epigenetic Targeting of Glioblastoma. *Front. Oncol.* **2018**, *8*, 448. [CrossRef]
74. Stupp, R.; Brada, M.; van den Bent, M.J.; Tonn, J.C.; Pentheroudakis, G. High-grade glioma: ESMO Clinical Practice Guidelines for diagnosis, treatment and follow-up. *Ann. Oncol.* **2014**, *25* (Suppl. S3), iii93–iii101. [CrossRef]

Disclaimer/Publisher's Note: The statements, opinions and data contained in all publications are solely those of the individual author(s) and contributor(s) and not of MDPI and/or the editor(s). MDPI and/or the editor(s) disclaim responsibility for any injury to people or property resulting from any ideas, methods, instructions or products referred to in the content.

Article

Insights into Gene Regulation under Temozolomide-Promoted Cellular Dormancy and Its Connection to Stemness in Human Glioblastoma

Carolin Kubelt ^{1,*}, Dana Hellmold ¹ , Daniela Esser ², Hajrullah Ahmeti ¹ , Michael Synowitz ¹ and Janka Held-Feindt ^{1,*}

¹ Department of Neurosurgery, University Medical Center Schleswig-Holstein UKSH, Campus Kiel, 24105 Kiel, Germany; dana.hellmold@uksh.de (D.H.); hajrullah.ahmeti@uksh.de (H.A.); michael.synowitz@uksh.de (M.S.)

² Institute of Clinical Chemistry, University Medical Center Schleswig-Holstein UKSH, Campus Kiel, 24105 Kiel, Germany; daniela.esser@uksh.de

* Correspondence: carolin.kubelt@uksh.de (C.K.); janka.held-feindt@uksh.de (J.H.-F.)

Abstract: The aggressive features of glioblastoma (GBM) are associated with dormancy. Our previous transcriptome analysis revealed that several genes were regulated during temozolomide (TMZ)-promoted dormancy in GBM. Focusing on genes involved in cancer progression, Chemokine (C-C motif) Receptor-Like (CCRL)1, Schlafen (SLFN)13, Sloan-Kettering Institute (SKI), Cdk5 and Abl Enzyme Substrate (Cables)1, and Dachshous Cadherin-Related (DCHS)1 were selected for further validation. All showed clear expression and individual regulatory patterns under TMZ-promoted dormancy in human GBM cell lines, patient-derived primary cultures, glioma stem-like cells (GSCs), and human GBM ex vivo samples. All genes exhibited complex co-staining patterns with different stemness markers and with each other, as examined by immunofluorescence staining and underscored by correlation analyses. Neurosphere formation assays revealed higher numbers of spheres during TMZ treatment, and gene set enrichment analysis of transcriptome data revealed significant regulation of several GO terms, including stemness-associated ones, indicating an association between stemness and dormancy with the involvement of SKI. Consistently, inhibition of SKI during TMZ treatment resulted in higher cytotoxicity, proliferation inhibition, and lower neurosphere formation capacity compared to TMZ alone. Overall, our study suggests the involvement of CCRL1, SLFN13, SKI, Cables1, and DCHS1 in TMZ-promoted dormancy and demonstrates their link to stemness, with SKI being particularly important.

Keywords: glioblastoma; temozolomide; dormancy; stemness; Chemokine (C-C motif) Receptor-Like (CCRL)1; Schlafen (SLFN)13; Sloan-Kettering Institute (SKI); Cdk5 and Abl Enzyme Substrate (Cables)1; Dachshous Cadherin-Related (DCHS)1



Citation: Kubelt, C.; Hellmold, D.; Esser, D.; Ahmeti, H.; Synowitz, M.; Held-Feindt, J. Insights into Gene Regulation under Temozolomide-Promoted Cellular Dormancy and Its Connection to Stemness in Human Glioblastoma. *Cells* **2023**, *12*, 1491. <https://doi.org/10.3390/cells12111491>

Academic Editors: Javier S. Castresana and Bárbara Meléndez

Received: 28 April 2023

Revised: 12 May 2023

Accepted: 24 May 2023

Published: 27 May 2023



Copyright: © 2023 by the authors. Licensee MDPI, Basel, Switzerland. This article is an open access article distributed under the terms and conditions of the Creative Commons Attribution (CC BY) license (<https://creativecommons.org/licenses/by/4.0/>).

1. Introduction

Glioblastoma (GBM) represents the most common and most malignant primary brain tumor in adults [1]. Besides its highly invasive nature, its resistance to chemo- and radiotherapy, the inevitable incidence of recurrences, and a vast intra- and intertumoral heterogeneity account for the up-to-now incurability of this tumor type. Intense research and technological advancements have allowed an increasing subclassification of the heterogeneous tumor entity [2], even though, to date, no breakthrough in therapy permitting a significant prolongation of life expectancy has been accomplished. Across subtypes, the aggressive properties of GBM were shown to be linked to distinct phenomena such as glioma stem-like cells (GSCs) and dormancy [3]. Since GSCs possess the capacity to self-renew and initiate a tumor, and play a decisive role in tumor progression and relapse, they represent an exciting starting point concerning new therapeutic approaches [4]. In the previous work

of our group, we were able to prove striking parallels between stemness and the concept of cellular dormancy in GBM [3]. As cellular dormancy depicts a reversible growth arrest of cells, dormant cells can escape conventional treatment strategies since they mainly affect fast-dividing cells. With time, the dormant state can be abandoned, leading to tumor recurrence following therapy. The entry into dormancy in GBM was shown to be characterized by the upregulation of a specific dormancy-associated gene set [5]. Interestingly, the agent temozolomide (TMZ) itself, used as standard chemotherapy in GBM, was shown to induce entry into a dormant stage [3]. Given this, in the framework of a previously performed microarray-based transcriptome analysis, our group investigated the influence of microenvironmental factors on GBM gene expression during TMZ-promoted cellular dormancy entry and exit. Altogether, 1512 genes were differentially regulated during TMZ-promoted cellular dormancy entry and 1381 during dormancy exit [6]. To narrow down the number of particularly interesting genes for this study, we only selected (1) known genes that (2) were regulated during TMZ-promoted cellular dormancy entry or exit in this specific setup with at least a $\log_2FC = 1.3$ value, (3) were expressed to clearly detectable extents after TMZ treatment, and (4) which could also be analyzed at the protein level. After this preselection, we focused on genes already described to be involved in tumor development, the progression or repression of malignancies, and to be connected to the phenomenon of stemness in the broadest sense. Following this procedure, we decided to exemplarily investigate five genes, namely Chemokine (C-C Motif) Receptor-Like (CCRL)1, Schlafen (SLFN)13, Sloan-Kettering Institute (SKI), Cdk5 and Abl Enzyme Substrate (Cables)1, and Dachsous Cadherin-Related (DCHS)1, to further evaluate their significance in GBM.

CCRL1 is an atypical chemokine receptor that was shown to predominantly exhibit tumor-restricting effects in different malignancies [7–9]. However, other studies found the promotion of epithelial-to-mesenchymal transition (EMT) by CCRL1 and hence postulated a tumor-promoting effect [10]. SLFN13 belongs to a family of genes that are involved in cell cycle regulation and mediate growth-inhibitory responses. Its function, especially in cancer, is still poorly understood. An analysis of “The Cancer Genome Atlas” database revealed the downregulation of SLFN13 in breast cancer, lung squamous carcinoma, prostate cancer, and rectal carcinoma, whereas the protein was upregulated in pancreatic- and renal-cell carcinoma [11]. SKI is a proto-oncogene overexpressed in tumor cells of various malignancies and hence involved in the growth, proliferation, invasion, metastasis, and tumor progression of cancer cells [12–14]. However, SKI was also shown to express the effect of a tumor suppressor gene in lung cancer [15]. Cables1 is a cyclin-dependent kinase-binding protein that was shown to be involved in the cell cycle, mitosis, cell death, development, and differentiation [16,17]. In multiple types of cancer, a very frequent loss of Cables1 has been observed which implies a potential suppressive effect on tumorigenesis [18]. However, a strong Cables1 expression was found in breast and pancreatic cancers [19]. DCHS1, also known as Cadherin (CDH)19, belongs to the cadherin superfamily and establishes and maintains intercellular connections [20]. It has been attributed to an important role in development, especially in the proliferation and differentiation of neural progenitor cells [20]. In different tumor types, DCHS1 seems to execute a tumor-suppressive effect [21–23].

To date, only limited-to-no data concerning the role of CCRL1, SLFN13, SKI, Cables1, and DCHS1 in GBM are available, and their relation to phenomena known to be associated with the high therapy resistance of the disease, such as dormancy and stemness, are still mainly uncharted. Hence, this study aimed to further validate the role of the markers in TMZ-promoted cellular dormancy, to examine whether CCRL1, SLFN13, SKI, Cables1, and DCHS1 inherit a potential connection to the phenomenon of stemness in GBM, and investigate whether targeting (any of) these markers can improve the antitumor potential of TMZ.

2. Materials and Methods

2.1. Human Specimens

Human tumor samples ($n = 20$) were obtained by surgical dissection at the Department of Neurosurgery (Kiel, Germany) with the approval of the ethics committee of the University of Kiel, Germany, after the written informed consent of donors (file reference: D471/15 and D524/17) and in accordance with the Helsinki Declaration of 1975, revised in 2013. Tumors were diagnosed and classified, according to World Health Organization (WHO) criteria, as GBMs CNS WHO Grade 4 by a pathologist (University Medical Center Hamburg-Eppendorf, UKE, Hamburg, Germany).

2.2. Human Glioblastoma (GBM) Cell Lines, Primary Culture Cells, and Stem-like Cells

The human glioblastoma cell lines LN229 (ATCC-CRL-2611), U251 (ECACC 89081403; formerly known as U373MG), U87MG (ECACC 89081402), and T98G (ECACC No. 92090213) were obtained from the European Collection of Authenticated Cell Cultures (ECACC, Salisbury, UK) or the American Type Culture Collection (ATCC, Manassas, VA, USA) and cultured as described previously [24]. Human primary GBM cultures ($n = 2$) were produced by dissociation and cultured according to established techniques as described before [24]. Human primary GBM stem-like cell cultures ($n = 8$) as well as GBM cell line-derived stem-like cells were established and intensively characterized by the formation of neurospheres, the ability to survive and proliferate under stem cell conditions, and the ability to differentiate into more mature cells as described before [3,25–27]. The purity of the GBM cells was ascertained by immunostaining with cell type-specific markers and by the absence of contamination with mycoplasmas. GBM cell line identity was verified by short tandem repeat profiling at the Department of Forensic Medicine (Kiel, Germany) using the Powerplex HS Genotyping Kit (Promega, Madison, WI, USA) and the 3500 Genetic Analyzer (Thermo Fisher Scientific, Waltham, MA, USA) as previously described [3].

2.3. Stimulation of Glioblastoma (GBM) Cells

As previously described in detail, 1.5×10^5 LN229, U251, primary culture (PC)a, or PCb cells, respectively, were stimulated for 10 days with TMZ (500 μ M, Sigma-Aldrich, St. Louis, MO, USA) dissolved in dimethyl sulfoxide (DMSO, Merck Millipore, Darmstadt, Germany) in Dulbecco's modified Eagle's medium (DMEM; Thermo Fisher Scientific) supplemented with 10% fetal bovine serum (FBS; Thermo Fisher Scientific). DMSO 0.5% (v/v) was used as a control. Hereafter, the medium was changed, and the cells were cultured for another 15 days without TMZ stimulation. Stem-like U251 and LN229 cells were stimulated under the same conditions and for the same periods, but in neurosphere medium [50% DMEM, 50% F12 medium (Thermo Fisher Scientific) containing the following supplements: 2 mM L-glutamine, 0.6% glucose (Roth, Karlsruhe, Germany), 9.5 ng/mL putrescine dihydrochloride (Sigma-Aldrich), 6.3 ng/mL progesterone (Sigma-Aldrich), 5.2 ng/mL sodium selenite (Sigma-Aldrich), 0.025 ng/mL insulin (Sigma-Aldrich), 2 μ g/mL heparin (Sigma-Aldrich), and 4 mg/mL bovine serum albumin (Thermo Fisher Scientific). The growth factors EGF (epidermal growth factor; PeproTech, Rocky Hill, NJ, USA) and bFGF (basic fibroblast growth factor; ImmunoTools, Friesoythe, Germany) were added at a concentration of 20 ng/mL as described before [27]. In addition, native LN229 cells were stimulated for 10 days with TMZ (500 μ M, Sigma-Aldrich) dissolved in DMSO (Merck Millipore) in DMEM (Thermo Fisher Scientific) supplemented with 10% FBS (Thermo Fisher Scientific) alone or in combination with Disitertide (P144; 100 μ g/mL; Tocris Bioscience, Bristol, UK) dissolved in 0.01 M phosphate-buffered saline (PBS), pH 7.4. DMSO 0.5% (v/v) and PBS were used as controls. Then, the medium was changed and the cells were used for different experiments or cultured for another 11 days without TMZ stimulation but with the continuous addition of Disitertide (100 μ g/mL) [6].

2.4. Reverse Transcription and Quantitative Real-Time PCR (qRT-PCR)

RNA of cells and tissue were isolated with the TRIzol[®] reagent (Invitrogen, Carlsbad, CA, USA) or with the ARCTURUS[®] PicoPure[®] RNA isolation kit (Applied Biosystems, Foster City, CA, USA) according to the manufacturer's instructions. DNase digestion, cDNA synthesis, and qRT-PCR were performed as previously described [28] using TaqMan primer probes (Applied Biosystems) listed in Supplementary Table S1. Cycles of threshold (C_T) were determined, and the ΔC_T values of each sample were calculated as $C_{T \text{ gene of interest}} - C_{T \text{ GAPDH}}$. Either ΔC_T values or linearized ΔC_T values ($2^{-\Delta C_T}$) are shown in the figures. The regulation of gene expression upon stimulation with Disitertide is displayed as n -fold expression changes = $2^{\Delta C_{T \text{ control}} - \Delta C_{T \text{ stimulus}}}$.

2.5. Immunofluorescence Staining

Cryostat sections of GBM ex vivo tissues were prepared as previously described [3]. Cells were incubated overnight with the primary antibodies at 4 °C, followed by the secondary antibodies for 1 h at 37 °C. The nuclei were counterstained with 4',6-diamidino-2-phenylindole (Thermo Fisher Scientific; 1:30,000, 30 min, room temperature) and the embedded slides were analyzed by fluorescence microscopy (AxioObserver.Z1; Carl Zeiss AG, Oberkochen, Germany) using the ZEN 3.5 (blue edition) software (Carl Zeiss AG). Used primary antibodies are listed in Supplementary Table S2. If primary antibodies were derived from the same species, non-specific binding was blocked by F(ab) fragments derived from that species (1:1000, from Jackson ImmunoResearch, West Grove, PA, USA). Primary antibodies were omitted for negative controls. Donkey anti-mouse or anti-rabbit IgGs labeled with Alexa Fluor 488 or Alexa Fluor 555 (1:1000; Thermo Fisher Scientific) served as secondary antibodies.

2.6. Gene Set Enrichment Analysis

Gene set enrichment analyses (GSEA) were performed with the tool gProfiler based on the gene ontology (GO) source 'biological process' [29]. p -values were adjusted using a Benjamini–Hochberg FDR correction.

2.7. Cytotoxicity Assay and Determination of Proliferation

The cytotoxic effects were determined using the CytoTox-FluorTM Cytotoxicity Assay (Promega) according to the manufacturer's instructions and as described before [27]. Supernatants of treated and control cells were collected at days 10 and 21 of stimulation, mixed with the bis-AAF-R110 substrate, and measured in a fluorescence microplate reader (Infinite M200Pro, TECAN, Zürich, Switzerland) at 485/535 nm. The numbers of dead cells were determined according to a prepared standard of digitonin-lysed (82.5 µg/mL; Merck Millipore) cell dilutions. Cell survival/proliferation was determined by counting viable cells with a hemocytometer at days 0, 10, and 21 of the treatment. The percentages [%] of dead cells were calculated as the n -fold number of viable cells as described in Equations (1) and (2) after 10 and 21 days of stimulation, respectively. Growth rates were calculated as an n -fold number of alive cells compared to day zero of the treatment.

$$\text{Dead cells (day 10) [\%]} = \frac{\text{number of dead cells [day 10]}}{\text{number of dead cells [day 10] + vital cells [day 10]}} \times 100 \quad (1)$$

$$\text{Dead cells (day 21) [\%]} = \frac{\text{number of dead cells [day 10 + day 21]}}{\text{number of dead cells [day 10 + day 21] + vital cells [day 21]}} \times 100 \quad (2)$$

2.8. Self-Renewal Capacity and Extreme Limiting Dilution Assay

The self-renewal capacity of 10- versus 3-day-TMZ-pretreated cells and 10 day-TMZ- or TMZ + Disitertide-pretreated cells were measured using an extreme limiting dilution analysis (ELDA) as described before [3]. Briefly, remaining cells after treatment were determined, and decreasing numbers (1600–800–400–200–100–75–50–25–10–5–1 cells per well) of cells were cultured in neurosphere medium (see above), plus 20 ng/mL of bFGF

and 20 ng/mL of EGF as described before [3]. Cultures were maintained until day 10 when the number of spheres per well and wells containing spheres for each cell plating density (number of positive cultures) were recorded and plotted using the online ELDA program25 (<http://bioinf.wehi.edu.au/software/elda>, accessed on 13 April 2023) [30].

2.9. Statistical and Correlation Analysis

Depending on the experimental setup, either a two-tailed Student's *t*-test or a one- or two-way analysis of variance (ANOVA) was performed using the GraphPad Prism 8 software (accessed on 13 April 2023; GraphPad Software, San Diego, CA, USA). The sample sizes and a description of the sample collection, including the number of biological/technical replicates, are described in the figure legends. In general, the data are presented as mean \pm standard deviation. Correlations were calculated with the Pearson correlation index. Statistical significance is marked with asterisks depending on the *p*-value: * $p < 0.05$, ** $p < 0.01$, and *** $p < 0.001$.

3. Results

3.1. Expression and Regulation of Selected Genes under Temozolomide (TMZ)-Promoted Cellular Dormancy in Glioblastoma (GBM) Cell Lines and Patient-Derived Primary Cultures

To evaluate the relevance of CCRL1, SLFN13, SKI, Cables1, and DCHS1 in GBM progression, we first examined their gene expression under TMZ-promoted dormancy entry and exit in different GBM cell lines (LN229 and U251) and primary cultures (PCa and PCb), respectively, using our previously established in vitro model with sole-TMZ stimulation.

Except for SLFN13, which was not found in PCb, all genes were expressed in the regarded cell lines and primary cultures at different levels. The highest gene expression level amongst all examined cell cultures was found for SKI, whereas CCRL1 and especially SLFN13 exhibited overall a rather low gene expression. The gene expression of DCHS1 and also, though to a lesser extent, Cables1, appeared heterogeneous among the different cell cultures.

Concerning gene regulation under TMZ-promoted cellular dormancy entry and exit, differences were observed amongst the regarded cells. Overall, a more homogeneous pattern of gene regulation was found, particularly within the primary culture group. Whereas most of the examined genes exhibited an upregulation in dormancy entry and exit in the primary cultures, the cell lines revealed a more complex profile of gene regulation (Figure 1). In detail, in LN229, CCRL1 showed downregulation, albeit only in tendency, both entering and leaving quiescence. Furthermore, a statistically significant upregulation of gene expression was observed for SLFN13 ($p = 0.017$), whereas Cables1 ($p = 0.028$) and DCHS1 ($p = 0.026$) revealed a downregulation in TMZ-promoted dormancy exit. Furthermore, Cables1 ($p = 0.008$) and DCHS1 ($p = 0.026$) showed a significantly higher gene expression after 15 days of stimulation with DMSO in comparison to 10 days of stimulation. Albeit not statistically significant, SKI was found to be slightly upregulated during the entry and downregulated during the exit of TMZ-promoted dormancy; however, high standard deviations were observed. U251 cells revealed the downregulation of CCRL1 ($p = 0.016$) after 15 days of stimulation with TMZ in comparison to 10 days. Contrary to this, SLFN13 ($p = 0.019$) was found to be upregulated after 15 days of stimulation with TMZ. In accordance with LN229, the expression of SKI tended to be downregulated during TMZ-promoted dormancy exit in U251 cells, and a significant downregulation was observed when comparing 10 and 15 days of TMZ stimulation ($p = 0.049$). Whereas Cables1 revealed a downregulation during TMZ-promoted dormancy entry ($p = 0.004$) and a trend of upregulation during exit, DCHS1 was downregulated in both scenarios (p entry = 0.011; p exit < 0.001). In addition, DCHS1 revealed an upregulation after 15 days of stimulation with DMSO versus 10 days ($p = 0.016$), and a downregulation after 15 days of stimulation with TMZ in comparison to after 10 days of treatment ($p = 0.005$). Concerning the primary cultures, tendencies or even statistically significant upregulations for CCRL1 (PCa: p entry = 0.021) and Cables1 (PCa: p entry = 0.003; p exit < 0.001; PCb: p exit < 0.001) during

TMZ-promoted dormancy entry and exit were observed. Whereas SLFN13 was found to be upregulated during the entry and exit of TMZ-promoted dormancy in PCa (p entry = 0.022; p exit < 0.001), no expression of the gene was observed in PCb. However, DCHS1 (p < 0.001), which was only detected in a low amount and not significantly regulated in PCa under TMZ-promoted dormancy, revealed an upregulation during dormancy exit in PCb. In PCa, SLFN13 (p = 0.007) and Cables1 (p < 0.001), and in PCb, Cables1 (p = 0.004) and DCHS1 (p < 0.001), exhibited upregulation after 15 days of TMZ stimulation in comparison to 10 days of stimulation. Data are presented in Figure 1.

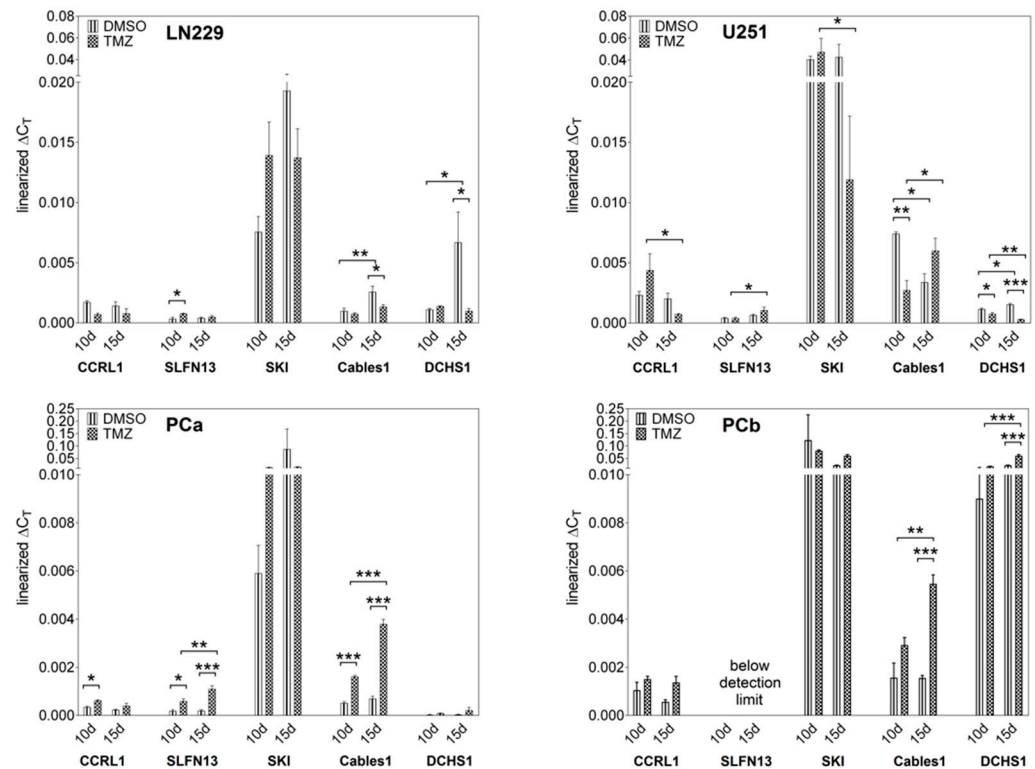


Figure 1. Gene regulation under TMZ-promoted cellular dormancy entry and exit. Gene expression under TMZ-promoted cellular dormancy entry and exit was analyzed by qRT-PCR (n = 3 biological replicates, n = 2 technical replicates each). After the treatment of cell lines (LN229, U251) and primary cultures (PCa, PCb) with 500 μ M TMZ or 0.5% (v/v) DMSO, respectively, for 10 days, followed by 15 days without TMZ stimulation, gene expression levels were detected after 10 days of stimulation (dormancy entry) and another 15 days without stimulation (dormancy exit). Gene regulation after TMZ stimulation was statistically analyzed by two-way ANOVA with Bonferroni's multiple-comparison post hoc test. * p < 0.05, ** p < 0.01, and *** p < 0.001. DMSO: Dimethyl sulfoxide; TMZ: Temozolomide; PCa/b: Primary culture a/b; CCRL1: Chemokine (C-C Motif) Receptor-Like 1; SLFN13: Schlafen 13; SKI: Sloan-Kettering Institute; Cables1: Cdk5 and Abl Enzyme Substrate 1; DCHS1: Dachsous Cadherin-Related 1; qRT-PCR: Reverse transcription and quantitative real-time polymerase chain reaction; ANOVA: analysis of variance.

3.2. Expression and Correlation of Selected Genes with Each Other in Patient-Derived Glioblastoma (GBM) Ex Vivo Samples

Next, we examined the basal gene expression of the selected genes in human GBM ex vivo samples to validate our previous findings. All of the selected genes were detected in the patient's material at different levels. The highest gene expression level was again found for SKI (average ΔC_T = 3.44), followed by DCHS1 (average ΔC_T = 4.23). SLFN13 (average ΔC_T = 6.87), CCRL1 (average ΔC_T = 7.19), and Cables1 (average ΔC_T = 7.22) altogether exhibited similar comparatively lower gene expression levels (see Figure 2A).

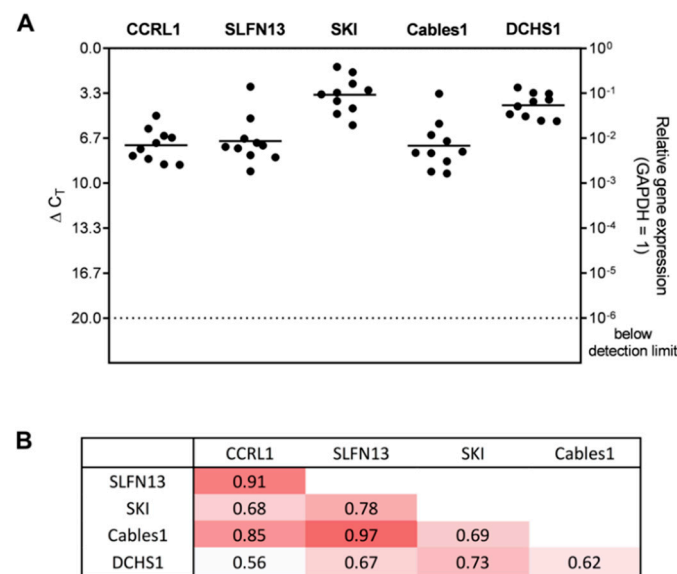


Figure 2. Gene expression of the selected genes in GBM ex vivo samples and their correlation with each other. **(A)** Basic gene expression levels were detected in human GBM ex vivo samples ($n = 10$; $n = 2$ technical replicates each) by qRT-PCR. Lines represent the mean gene expression for each gene ($\Delta C_T 3.3 = 10$ -fold expression difference). **(B)** The correlation of gene expression was analyzed by the Pearson correlation index. A darker shade of red corresponds to a higher correlation value. CCRL1: Chemokine (C-C Motif) Receptor-Like 1; SLFN13: Schlafen 13; SKI: Sloan-Kettering Institute; Cables1: Cdk5 and Abl Enzyme Substrate 1; DCHS1: Dachshous Cadherin-Related 1; GAPDH: Glyceraldehyde-3-phosphate dehydrogenase; GBM: Glioblastoma; qRT-PCR: Reverse transcription and quantitative real-time polymerase chain reaction.

To determine potential links between the selected genes, a correlation analysis was performed. All genes revealed positive correlations with each other. Particularly strong correlations were found for CCRL1 and SLFN13 (corr. = 0.91), SLFN13 and Cables1 (corr. = 0.97), and CCRL1 and Cables1 (corr. = 0.85). Medium correlations were detected for SKI and DCHS1 (corr. = 0.73), SKI and Cables1 (corr. = 0.69), SKI and CCRL1 (corr. = 0.68), Cables1 and DCHS1 (corr. = 0.62), and DCHS1 and CCRL1 (corr. = 0.56) (see Figure 2B).

3.3. Co-Staining Patterns of Selected Molecules with Each Other in Patient-Derived Glioblastoma (GBM) Ex Vivo Samples

Given the positive correlations found between the selected genes, immunofluorescence double staining of the respective molecules with each other was performed. Since this is a non-quantitative methodology and, in most cases, only individual or small groups of cells exhibit clear co-staining, a purely qualitative assessment of staining was performed here. Overall, staining for all five proteins was detected in the GBM samples. A co-staining of the molecules and solely positive cells was observed in all different staining combinations in varying amounts. Whereas most of the markers revealed either direct co-staining or solely positive cells, SLFN13 and Cables1 also often seemed to be stained in different structures of the same cell. Representative staining examples are shown in Figure 3.

3.4. Cellular Sources of Selected Molecules in Patient-Derived Glioblastoma (GBM) Ex Vivo Samples

To identify the cellular sources of the investigated genes, immunofluorescence double staining of the selected molecules with cell type-specific markers was carried out. Von Willebrand factor (vWF) served as a marker for endothelial cells, a cluster of differentiation molecule (CD)11b tagged microglia, and glial fibrillary acidic protein (GFAP) detected cells of astroglial origin. Furthermore, the stemness markers octamer binding transcription factor (OCT)4, sex-determining region Y-box (Sox)2, and krüppel-like factor (KLF)4 were used to detect a possible link of the markers to tumor stem-like cells.

CCRL1, SLFN13, SKI, Cables1, and DCHS1 were stained with or nearby vWF to different extents. Whereas SLFN13, SKI, and Cables1 mainly exhibited direct co-staining with vWF, respectively, DCHS1 and especially CCRL1 also seemed to be expressed in different structures of the same vWF-positive cell. Concerning the microglial marker, CD11b, CCRL1, SLFN13, SKI, and DCHS1 seemed to be expressed in different structures of the same CD11b-positive cell. In contrast, Cables1 revealed either a co-staining or was found to be stained separate from CD11b. All of the examined dormancy-associated markers were also found to be stained in GFAP-positive areas. In particular, SKI, Cables1, and DCHS1 revealed a co-staining with GFAP. Interestingly, all of the mentioned markers exhibited individual co-staining patterns with stemness markers. Since tumor stem-like cells are known to represent only a small subpopulation within the total tumor mass (ranging from ~2–20% depending on GBM and stem-like cell subtypes [31]), only single or small groups of double-positive cells have usually been found. Whereas CCRL1, SLFN13, and SKI most frequently appeared directly co-stained with the investigated stemness markers, Cables1 and DCHS1 also often seemed to be stained in different structures of the same cell. Single positive cells for all examined markers were detected. Representative staining examples are presented in Figure 4.

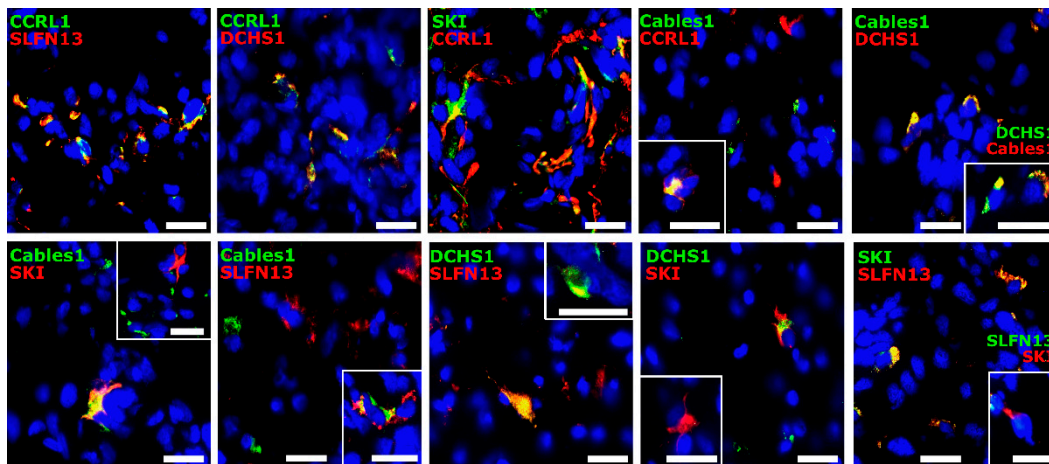


Figure 3. Immunofluorescence double-staining of the selected molecules. Human GBM ex vivo sections ($n = 5$, different patients; $n = 1$, technical replicate for each patient) were immunofluorescently stained regarding the presence of co-staining (yellow) for CCRL1, SLFN13, SKI, Cables1, and DCHS1 (green and red, respectively). Nuclei appear blue. Magnification $400\times$; white bar = $20\ \mu\text{m}$. CCRL1: Chemokine (C-C Motif) Receptor-Like 1; SLFN13: Schlafen 13; SKI: Sloan-Kettering Institute; Cables1: Cdk5 and Abl Enzyme Substrate 1; DCHS1: Dachshous Cadherin-Related 1; GBM: Glioblastoma.

3.5. Correlation Analysis of Dormancy-Associated Genes and Stemness Markers in Patient-Derived Glioblastoma (GBM) Ex Vivo Samples

Based on the previously described finding of a co-staining for CCRL1, SLFN13, SKI, Cables1, and DCHS1 with stemness markers, respectively, we examined the gene expressions of OCT4, Sox2, and KLF4 in human GBM ex vivo samples. All stemness markers were clearly detected in the samples to different extents (Figure 5). The highest gene expression was found for Sox2 (average $\Delta C_T = 4.37$), followed by KLF4 (average $\Delta C_T = 7.0$), and OCT4 (average $\Delta C_T = 7.14$). To validate the detected link between the genes regulated under TMZ-promoted dormancy and the stemness markers, we performed a correlation analysis. Positive correlations were found, especially for the stemness markers OCT4 and KLF4 with CCRL1, SLFN13, and SKI. In detail, medium correlations were found for OCT4 and SKI (corr. = 0.79), CCRL1 (corr. = 0.74), and SLFN13 (corr. = 0.68); and for KLF4 and CCRL1 (corr. = 0.75), SKI (corr. = 0.74), SLFN13 (corr. = 0.68), and Cables1 (corr. = 0.58). Sox2 exhibited medium correlations with DCHS1 (corr. = 0.65), and CCRL1 (corr. = 0.54).

Sox2 and Cables1 (corr. = 0.47), as well as Sox2 and SLFN13 (corr. = 0.45) only revealed weak correlations.

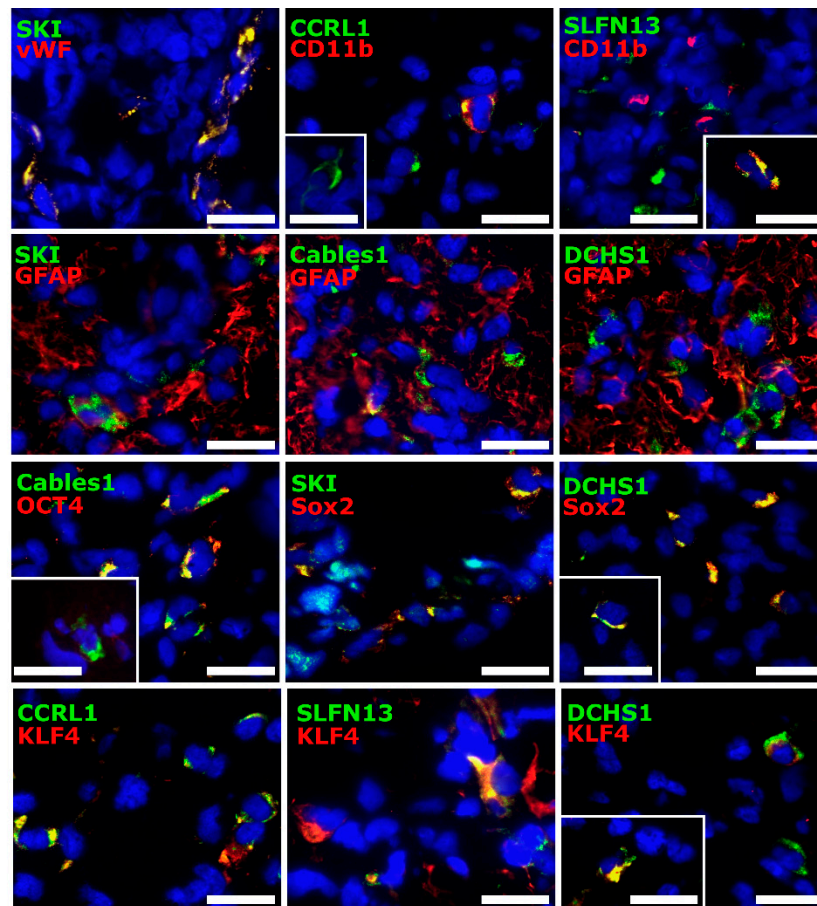


Figure 4. Source of molecules regulated under TMZ-promoted dormancy. Human GBM ex vivo sections ($n = 5$, different patients; $n = 1$, technical replicate for each patient) were immunofluorescently stained regarding the presence of a co-staining (yellow) for CCRL1, SLFN13, SKI, Cables1, and DCHS1 (green) with the cell type-specific markers vWF, CD11b, and GFAP and the stemness markers OCT4, Sox2, and KLF4 (red). Nuclei appear blue. Magnification $400\times$; white bar = $20\ \mu\text{m}$. CCRL1: Chemokine (C-C Motif) Receptor-Like 1; SLFN13: Schlafen 13; SKI: Sloan-Kettering Institute; Cables1: Cdk5 and Abl Enzyme Substrate 1; DCHS1: Dachshous Cadherin-Related 1; vWF: Von Willebrand factor; CD11b: Cluster of differentiation molecule 11b; GFAP: Glial fibrillary acidic protein; OCT4: Octamer binding transcription factor 4; Sox2: Sex determining region Y-box 2; KLF4: Krüppel-like factor 4; TMZ: Temozolomide; GBM: Glioblastoma.

3.6. Expression of Selected Genes in Stem-like Cells Generated from Glioblastoma (GBM) Cell Lines or Patient-Derived Primary Cultures

To further validate the link between CCRL1, SLFN13, SKI, Cables1, and DCHS1 with stemness properties, we examined their expression in stem-like cells of different GBM cell lines and patient-derived primary cultures.

In most cases, the markers were detectable in the stem-like cells generated from commercial cell lines to different extents. Overall, the highest gene expression in all stem-like cell lines was observed for SKI. The other markers revealed a rather heterogeneous pattern between the different stem-like cell lines, which was especially observed for SLFN13 and Cables1. In LN229, the gene expression of SKI (average $\Delta C_T = 7.65$) was followed by CCRL1 (average $\Delta C_T = 9.31$), DCHS1 (average $\Delta C_T = 10.96$), Cables1 (average $\Delta C_T = 12.02$), and SLFN13 (average $\Delta C_T = 13.89$). In U251, the gene expression of SKI (average $\Delta C_T = 6.05$) was followed by DCHS1 (average $\Delta C_T = 8.92$), Cables1 (average

$\Delta C_T = 10.66$), CCRL1 (average $\Delta C_T = 11.02$), and SLFN13 (average $\Delta C_T = 11.91$). In U87MG, the gene expression of SKI (average $\Delta C_T = 7.38$) was followed by CCRL1 (average $\Delta C_T = 10.47$), DCHS1 (average $\Delta C_T = 11.18$), SLFN13 (average $\Delta C_T = 14.06$), and Cables1 (average $\Delta C_T = 16.57$). Finally, in T98G, the gene expression of SKI (average $\Delta C_T = 7.45$) was followed by CCRL1 (average $\Delta C_T = 10.16$), Cables1 (average $\Delta C_T = 10.50$), DCHS1 (average $\Delta C_T = 13.14$), and SLFN13 (average $\Delta C_T = 15.77$). The data are displayed in Figure 6.

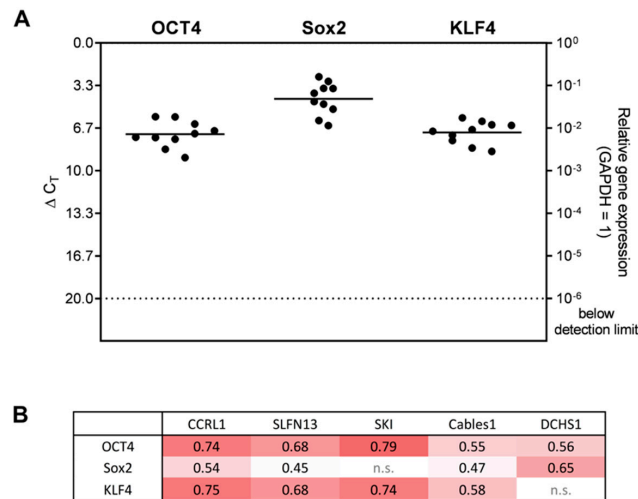


Figure 5. Gene expression of stemness markers in GBM ex vivo samples and their correlation with genes regulated under TMZ-promoted dormancy. **(A)** Basic gene expression levels were detected in human GBM ex vivo samples ($n = 10$; $n = 2$, technical replicates each) by qRT-PCR. Lines represent the mean gene expression for each gene ($\Delta C_T 3.3 = 10$ -fold expression difference). **(B)** The correlation of gene expression was analyzed by the Pearson correlation index. A darker shade of red corresponds to a higher correlation value. Non-statistically significant correlations are marked by n.s.. OCT4: Octamer binding transcription factor 4; Sox2: Sex determining region Y-box 2; KLF4: Krüppel-like factor 4; GAPDH: Glyceraldehyde-3-phosphate dehydrogenase; CCRL1: Chemokine (C-C Motif) Receptor-Like 1; SLFN13: Schlafen 13; SKI: Sloan-Kettering Institute; Cables1: Cdk5 and Abl Enzyme Substrate 1; DCHS1: Dachsaus Cadherin-Related 1; GBM: Glioblastoma; TMZ: Temozolomide; qRT-PCR: Reverse transcription and quantitative real-time polymerase chain reaction.

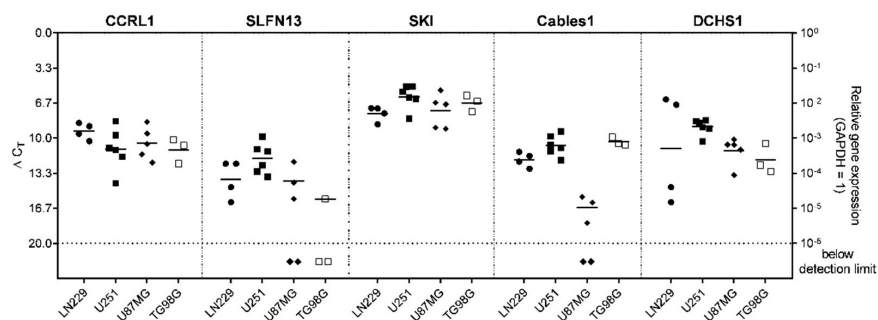


Figure 6. Expression of genes regulated under TMZ-promoted dormancy in stem-like cells generated from commercial cell lines. Basic gene expression levels were detected in stem-like cells from LN229, U251, U87MG, and T98G GBM cells ($n = 3-6$; $n = 2$, technical replicates each) by qRT-PCR. Lines represent the mean gene expression for each gene, the symbol tags the respective cell line ($\Delta C_T 3.3 = 10$ -fold expression difference). CCRL1: Chemokine (C-C Motif) Receptor-Like 1; SLFN13: Schlafen 13; SKI: Sloan-Kettering Institute; Cables1: Cdk5 and Abl Enzyme Substrate 1; DCHS1: Dachsaus Cadherin-Related 1; GAPDH: Glyceraldehyde-3-phosphate dehydrogenase; TMZ: Temozolomide; qRT-PCR: Reverse transcription and quantitative real-time polymerase chain reaction.

Except for SLFN13 ($\Delta C_T = 11.08$), the patient-derived GBM stem-like cells ($n = 8$) also mostly revealed an expression of the examined markers. DCHS1 (average $\Delta C_T = 7.26$) exhibited the highest gene expression among all markers, closely followed by SKI (average $\Delta C_T = 7.44$). The lowest gene expressions were observed for Cables1 (average $\Delta C_T = 11.15$), and CCRL1 (average $\Delta C_T = 12.00$). Data are shown in Figure 7.

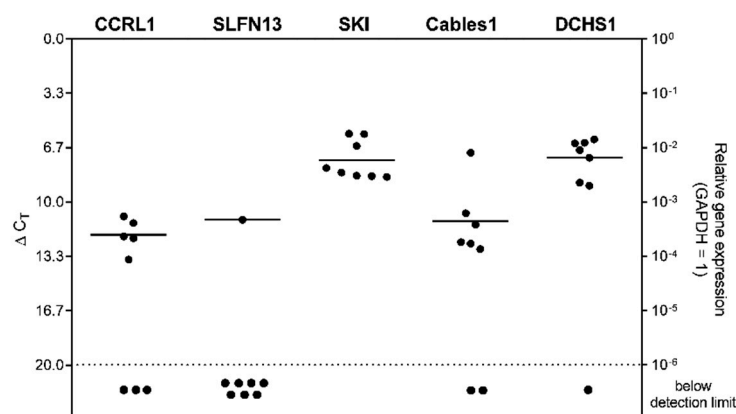


Figure 7. Expression of genes regulated under TMZ-promoted dormancy in patient-derived stem-like cells. Basic gene expression levels were detected in patient-derived GBM stem-like cells ($n = 8$; $n = 2$, technical replicates each) by qRT-PCR. Lines represent the mean gene expression for each gene (ΔC_T 3.3 = 10-fold expression difference). CCRL1: Chemokine (C-C Motif) Receptor-Like 1; SLFN13: Schlafen 13; SKI: Sloan-Kettering Institute; Cables1: Cdk5 and Abl Enzyme Substrate 1; DCHS1: Dachshous Cadherin-Related 1; GAPDH: Glyceraldehyde-3-phosphate dehydrogenase; TMZ: Temozolomide; qRT-PCR: Reverse transcription and quantitative real-time polymerase chain reaction.

3.7. Expression and Regulation of Selected Genes under Temozolomide-Promoted Cellular Dormancy in Stem-like Cells and Neurosphere Formation Assay

To further corroborate our findings, next, we examined the gene expression of CCRL1, SLFN13, SKI, Cables1, and DCHS1 under TMZ-promoted dormancy entry and exit in LN229 and U251 stem-like cells. The data are displayed in Figure 8.

Interestingly, the results in LN229 and U251 stem-like cells showed similar trends to those obtained for native LN229 and U251, although there were clear differences in some aspects (please compare to Figure 1). For example, in the LN229 and the U251 stem-like cells, similar to the respective native cells, SKI showed the highest expression in both dormancy entry and exit. Similar to the native cells, a statistically significant induction of SKI was observed for both stem-like cell types after 10 days of TMZ stimulation compared to the control (LN229: $p = 0.015$; U251: $p = 0.0216$), which was more pronounced in LN229 stem-like cells. When considering dormancy exit, SKI was slightly downregulated in LN229 stem-like cells, but further induced in U251 stem-like cells, and this was also in contrast to native U251 cells ($p < 0.0001$). CCRL1 and SLFN13 were rather lowly expressed in both stem-like cell types but showed partly significant induction of gene expression compared to the controls, respectively, after 10 days of TMZ stimulation and a further 15 days of recovery (CCRL1, LN229, entry: $p = 0.0170$; CCRL1, U251 entry and exit: $p = 0.0001$; SLFN13, U251, entry: $p = 0.0004$, and exit: $p < 0.0001$). The Cables1 expression level was at a rather low level in LN229 and U251 stem-like cells and was partially significantly induced in both cell types in dormancy entry and exit (U251 entry and exit: $p = 0.0005$). Interestingly, this aspect was not observed in native LN229 and U215 cells. Finally, a strong statistically significant reduction in DCHS1 expression in dormancy exit was observed, particularly in LN229 stem-like cells ($p < 0.0001$), which was consistent with the results observed in native LN229 cells. DCHS1 expression in U251 stem-like cells was more intermediate and was significantly induced in dormancy exit ($p < 0.0096$), whereas a reduction in gene expression was observed in native U251 cells in dormancy exit compared to the control.

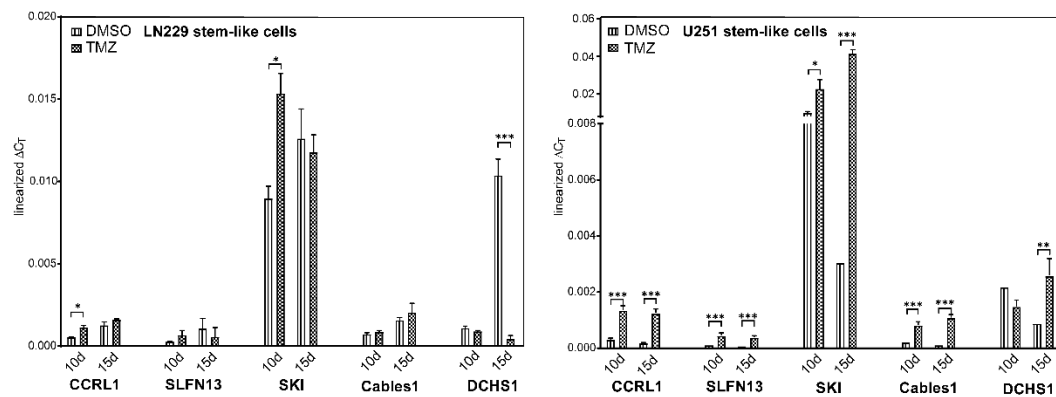


Figure 8. Gene regulation under TMZ-promoted cellular dormancy entry and exit in stem-like cells. Gene expression under TMZ-promoted cellular dormancy entry and exit was analyzed by qRT-PCR ($n = 3$, biological replicates; $n = 2$, technical replicates each). After the treatment of LN229 and U251 stem-like cells with 500 μ M TMZ or 0.5% (v/v) DMSO, respectively, for 10 days followed by 15 days without TMZ stimulation, gene expression levels were detected after 10 days of stimulation (dormancy entry) and another 15 days without stimulation (dormancy exit). Gene regulation after TMZ stimulation was statistically analyzed by two-way ANOVA with Bonferroni's multiple-comparison post hoc test. * $p < 0.05$, ** $p < 0.01$, and *** $p < 0.001$. DMSO: Dimethyl sulfoxide; TMZ: Temozolomide; CCRL1: Chemokine (C-C Motif) Receptor-Like 1; SLFN13: Schlafen 13; SKI: Sloan-Kettering Institute; Cables1: Cdk5 and Abl Enzyme Substrate 1; DCHS1: Dachshous Cadherin-Related 1; qRT-PCR: Reverse transcription and quantitative real-time polymerase chain reaction; ANOVA: analysis of variance.

To further support these results, we next performed neurosphere formation assays with extreme limiting dilution analysis (ELDA) to investigate sphere formation capacity after pretreatment with TMZ for 3 or 10 days. Here, previous work by our group using native LN229 as an example has shown that LN229 cells pretreated with TMZ for 10 days exhibited a higher self-renewal capacity compared to cells pretreated for a shorter time, yielding sphere formation even at high dilutions [3]. Since these studies were previously performed only with native LN229, we now performed ELDA analysis with patient-derived primary cells (native PCa cells). The data are displayed in Figure 9. Similar to the results observed for LN229 cells, 10 days of pretreatment with TMZ resulted in a higher neurosphere formation capacity of PCa cells in comparison to 3 days of pretreatment (Figure 9A). In accordance with this, induction of the stemness markers OCT4 and KLF4 was more pronounced after 10 days of TMZ pretreatment, whereas Sox2 expression remained unaffected (Figure 9B).

3.8. Gene Set Enrichment Analysis and Inhibition of Sloan-Kettering Institute (SKI)

As the relationship between the expression of CCRL1, SLFN13, SKI, Cables1, and DCHS1 and the stemness characteristics of GBM cells became increasingly clear based on our results, we next performed gene set enrichment analyses. We used the microarray-based transcriptome datasets previously published by our group, which analyzed the regulation of gene expression during TMZ-promoted entry and exit from cellular dormancy in GBM cells [6]. In detail, up- and downregulated genes comparing the groups of TMZ versus DMSO in both dormancy entry and exit were used for analysis.

Indeed, the stemness GO term GO:0019827 (stem cell population maintenance) yielded significant results ($p = 0.019$) for the comparison between TMZ versus DMSO in dormancy entry. Genes assigned to this GO term also included SKI. All data from the gene set enrichment analysis are given in Supplementary Tables S3 and S4, and the significantly regulated GO terms of the comparison of TMZ versus DMSO in dormancy entry and exit are visualized in a heatmap in Supplementary Figure S1.

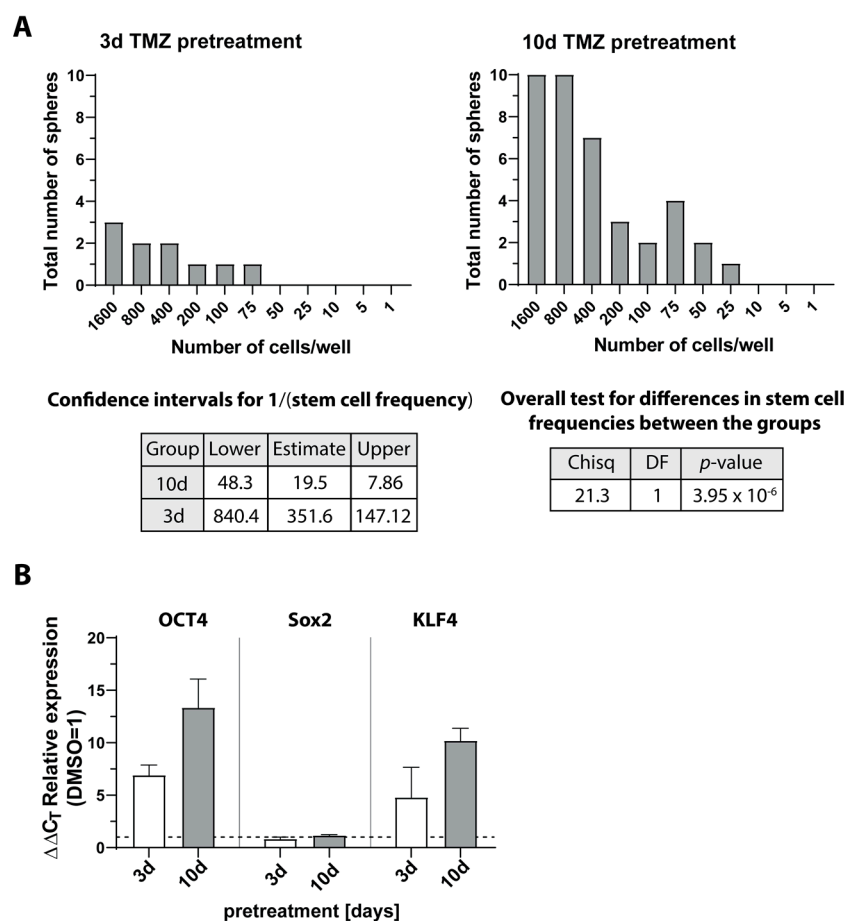


Figure 9. Self-renewal capacity, ELDA, and qRT-PCR analysis. Native primary culture (PCa) cells were stimulated with 500 μ M TMZ for 10 and 3 days, and (A) self-renewal capacity was determined under stem cell culture conditions with ELDA ($n = 2$). Briefly, cells were plated in decreasing numbers from 1600 cells/well to 1 cell/well. Cultures were maintained until day 10 when the number of spheres per well and wells containing spheres for each cell plating density (number of positive cultures) were recorded and plotted using online ELDA program²⁵; <http://bioinf.wehi.edu.au/software/elda>, accessed on 13 April 2023; (B) expression of stemness markers OCT4, Sox2, and KLF4 was determined by qRT-PCR. The induction of gene expression upon stimulation with TMZ was displayed as n-fold expression changes = $2^{\Delta\Delta C_T \text{ control} - \Delta C_T \text{ stimulus}}$. Error bars correspond to the standard deviation. TMZ: Temozolomide; DMSO: Dimethyl sulfoxide; OCT4: Octamer binding transcription factor 4; Sox2: Sex determining region Y-box 2; KLF4: Krüppel-like factor 4; ELDA: extreme limiting dilution analysis; qRT-PCR: Reverse transcription and quantitative real-time polymerase chain reaction.

Since SKI appeared to be particularly important in TMZ-promoted dormancy and its link to stemness, finally, we examined to what extent TMZ application with the simultaneous inhibition of SKI led to increased cytotoxicity and a decreased proliferation of GBM cells compared to TMZ treatment alone. Using our previously established in vitro model, native LN229 cells were stimulated with TMZ alone or in combination with Disitertide for 10 days, after which TMZ was omitted but Disitertide was added for an additional 11 days. Disitertide (also known as P144) itself is a TGF- β inhibitor, which also mediates its efficacy via the downregulation of SKI at both transcriptional and translational levels [32]. The number of dead cells was examined by cytotoxicity assay after 10 and 21 days of treatment, respectively, and the proliferation of cells was also analyzed over the course of treatment. In parallel, we determined the gene expression of SKI in the Disitertide-treated LN229 cells by qRT-PCR. The results are shown in Figure 10. After both 10 and 21 days of Disitertide

stimulation, the significant inhibition of SKI gene expression was observed compared to unstimulated controls (10 days: $p < 0.0002$; 21 days: $p < 0.0001$; Figure 10A). Similarly, a significantly increased cytotoxicity of the combination therapy of TMZ + Disitertide compared to TMZ stimulation alone was observed, especially after 21 days of treatment (Figure 10B; ~20% dead cells with TMZ alone, up to ~70% dead cells with TMZ + Disitertide; $p < 0.0011$). In line with this, treatment with TMZ + Disitertide significantly decreased the proliferation of LN229 to a higher extent in comparison to after the administration of TMZ alone (TMZ alone: $p < 0.0087$; TMZ + Disitertide: $p < 0.0083$, compared to control, respectively).

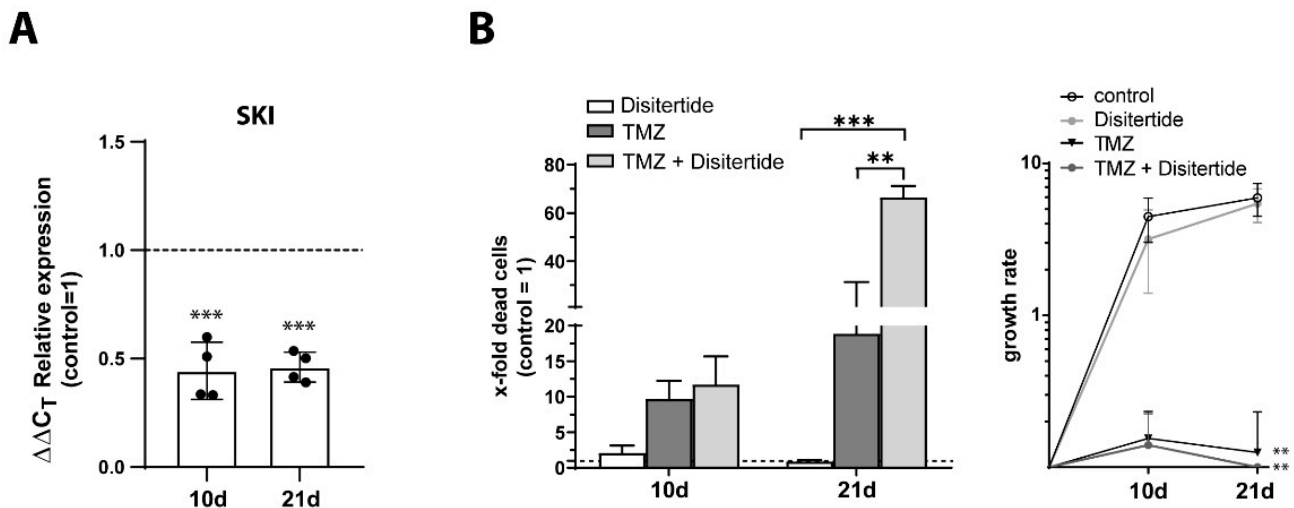


Figure 10. Cytotoxic and antiproliferative effect of TMZ application with simultaneous inhibition of SKI in GBM cells. LN229 cells were treated with TMZ + Disitertide (500 μ M TMZ, 100 μ g/mL Disitertide) for 10 days, followed by another 11 days without TMZ stimulation but with continuous addition of Disitertide (100 μ g/mL). (A) Gene expression of SKI was quantified by qRT-PCR at different time points of treatment. The induction of gene expression upon stimulation with Disitertide was displayed as n -fold expression changes = $2^{\Delta\Delta CT_{control} - \Delta CT_{stimulus}}$. (B) Death rates were obtained by performing a cytotoxicity assay after 10 and 21 days of stimulation, respectively. The cell survival/proliferation was determined by counting viable cells at days 0, 10, and 21 of the treatment. The percentages [%] of dead cells were calculated as the n -fold number of viable cells. $n = 2$, biological replicates, with $n = 2$, technical replicates each. The significances between different stimulations were determined using either a two-tailed Student's t -test (A) or a two-way ANOVA test followed by a Tukey's multiple-comparison test (B) (** $p < 0.01$; *** $p < 0.001$). Error bars correspond to the standard deviation. TMZ: Temozolomide; SKI: Sloan-Kettering Institute; GBM: Glioblastoma; qRT-PCR: Reverse transcription and quantitative real-time polymerase chain reaction; ANOVA: analysis of variance.

To further examine whether TMZ application with the simultaneous inhibition of SKI affected stemness properties, we performed neurosphere formation assays with ELDA to investigate the sphere formation capacity of native LN229 cells stimulated for 10 days with TMZ alone or with TMZ in combination with Disitertide. The results are shown in Figure 11. Indeed, compared with TMZ treatment alone, the surviving native LN229 cells of the TMZ + Disitertide stimulation showed a lower ability to form neurospheres, which indicated the inhibition of stemness capacity and further supported the higher efficiency of the combination therapy (Figure 11A). In agreement with this, a lower expression of KLF4 was also detected in cells treated for 10 days with TMZ + Disitertide (Figure 11B, $p = 0.006$).

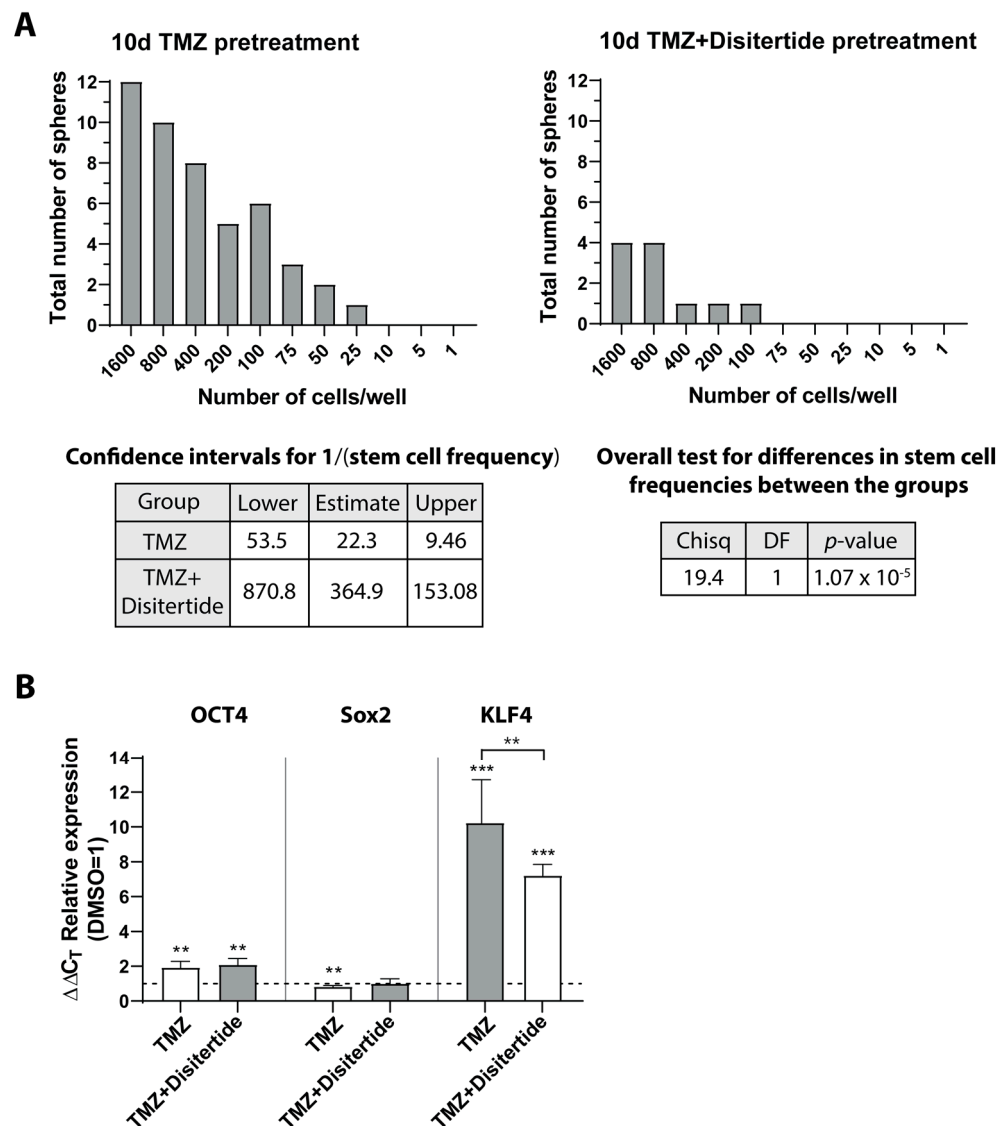


Figure 11. Self-renewal capacity, ELDA, and qRT-PCR analysis. Native LN229 cells were stimulated with 500 μ M TMZ or TMZ + Disitertide (500 μ M TMZ, 100 μ g/mL Disitertide) for 10 days, and (A) self-renewal capacity was determined under stem cell culture conditions with ELDA ($n = 2$). Briefly, cells were plated in decreasing numbers from 1600 cells/well to 1 cell/well. Cultures were maintained until day 10 when the number of spheres per well and wells containing spheres for each cell plating density (number of positive cultures) were recorded and plotted using online ELDA program25; <http://bioinf.wehi.edu.au/software/elda>, accessed on 13 April 2023; (B) expression of stemness markers OCT4, Sox2, and KLF4 was determined by qRT-PCR. The induction of gene expression upon stimulation was displayed as n-fold expression changes = $2^{\Delta\Delta C_T}$ control - ΔC_T stimulus. The significances between different stimulations were determined using either a two-tailed Student's *t*-test or a one-way ANOVA test followed by a Tukey's multiple-comparison test (** $p < 0.01$; *** $p < 0.001$). Error bars correspond to the standard deviation. TMZ: Temozolomide; DMSO: Dimethyl sulfoxide; OCT4: Octamer binding transcription factor 4; Sox2: Sex determining region Y-box 2; KLF4: Krüppel-like factor 4; ELDA: extreme limiting dilution analysis; qRT-PCR: Reverse transcription and quantitative real-time polymerase chain reaction; ANOVA: analysis of variance.

Overall, our study suggests the involvement of CCRL1, SLFN13, SKI, Cables1, and DCHS1 in TMZ-promoted dormancy and demonstrated their link to stemness with SKI being particularly important.

4. Discussion

GBM is the most aggressive primary brain tumor known and still an incurable disease with a medium life expectancy of 15 months despite surgery, and radio- and chemotherapy [1]. One of the reasons for this disastrous prognosis is the high therapy resistance, which has been shown to be linked to distinct phenomena such as, e.g., dormancy [3]. The currently used chemotherapeutic agent in GBM, TMZ, itself does promote dormancy. In the previous work of our group, we identified different genes which were regulated during drug-promoted dormancy entry and exit [6]. Focusing on genes already described to be involved in tumor development, progression, or repression of malignancies, and to be connected to the phenomenon of stemness in the broadest sense, we selected five promising genes associated with TMZ-promoted dormancy in GBM, namely CCRL1, SLFN13, SKI, Cables1, and DCHS1, for further validation.

We observed differences in the gene regulation patterns of chosen molecules under TMZ-promoted dormancy entry and exit between different GBM cell cultures. Whereas patient-derived GBM primary cultures revealed an upregulation of most of the markers during the entry and exit of dormancy, cell lines exhibited a more heterogeneous gene-regulation pattern.

GBM is known to exhibit a vast molecular intra- and inter-tumoral heterogeneity, which might account for the differences in the gene regulation observed. Intense research and technical advancements have yielded a subclassification of the tumor into either a classical, mesenchymal, and proneural subtype depending on the molecular signature [2]. Furthermore, the O⁶-methylguanine-DNA methyltransferase (MGMT) expression status does significantly affect TMZ response. Silencing of the DNA-repair enzyme MGMT by its promoter methylation abolishes its inhibitory effects against alkylating agents such as TMZ [33]. Additionally, more and more molecular markers are identified, which might affect gene regulation under TMZ-promoted dormancy entry and exit in a complex way [34–36], and hence contribute to the heterogeneous picture of gene regulation between the different GBM cells found. Concerning the investigated markers, to date, only CCRL1 was examined regarding its general gene expression in different molecular subtypes of GBM (isocitrate dehydrogenase mutant vs. wildtype, 1p19q codeletion vs. no codeletion). In this specific context, no clear expression changes were found [37].

Consistent with the upregulation of most of the markers during the entry into and exit from dormancy observed in the primary cultures, our study revealed a relationship between CCRL1, SLFN13, SKI, Cables1, and DCHS1 as indicated by co-staining and correlation analysis of their gene expressions. To date, no further studies focusing on a connection between these markers exist. Concerning the function of the respective markers, SLFN13, CCRL1, and SKI, especially, were shown to exert tumor-promoting effects in different malignancies. In accordance with the mainly observed upregulation of SLFN13 during TMZ-promoted dormancy exit in our study, previous investigations revealed an increase in the gene expression with progressive glioma grade and hence with incremental aggressive properties [38]. Concerning CCRL1, which was also mainly found to be upregulated during TMZ-promoted dormancy exit in the primary cultures in our study, previous studies documented a reduction in the adherence of cancer cells to each other and to extracellular matrix proteins, and the promotion of EMT by CCRL1 in breast cancer cells [10,39]. However, CCRL1 was also shown to execute opposite effects as an inhibitor of tumor cell proliferation, a reduction in EMT properties, and the tumor cell migration in breast-cancer, hepatocellular, and, nasopharyngeal carcinoma [7–9]. As mentioned above and in accordance with the correlations of SKI with CCRL1 and SLFN13 found in our study, SKI was mainly postulated to exert tumor-promoting effects [13–15]. Various mechanisms were identified to investigate its function as an influence on Wnt/beta-catenin, phosphatidylinositol 3-kinase/protein kinase B and transforming growth factor (TGF)- β signaling pathway [40–42]. Despite Chen et al. also postulating a tumor-suppressive function in lung cancer [12], in GBM, SKI was shown to negatively regulate the TGF- β signaling pathway, leading to the promotion of tumor progression [43]. Nevertheless, in the

specific setup of TMZ-promoted dormancy exit, SKI revealed a reduced gene expression in our study. In accordance with these contradictory findings, the downregulation of SKI by small interfering ribonucleic acid in pancreatic cancer cells resulted in decreased proliferation, whilst, at the same time also increasing EMT, and invasive and metastatic features were observed [43,44]. The mainly observed upregulation of Cables1 and DCHS1 during dormancy entry and exit in the primary cultures, and the correlations found with CCRL1, SLFN13, and SKI seem contradictory considering the tumor-restricting functions of Cables1 and DCHS1, both located on the same chromosome 18q [22,45], as postulated in the literature. Despite Wu et al. postulating an overexpression of Cables1 in breast and pancreatic cancers [19], most of the previous studies documented a very frequent loss of Cables1 in multiple types of cancer which promoted tumor progression [45]. DCHS1 was also proposed as a tumor suppressor gene candidate in gestational and non-gestational choriocarcinomas [22], and was found to be downregulated in colorectal tumors [23]. To date, no data regarding the expression of Cables1 in GBM are publicly available. In our study, Cables1 was clearly detectable in all cell lines, primary cultures, and GBM ex vivo samples. The interferences of all the genes can be documented concerning their molecular mechanisms of action. For instance, SKI, Cables1, and DCHS1 were all shown to be involved in the Wnt signaling pathway [40,45,46].

However, besides tumor cells, endothelial cells and tumor-associated microglia/macrophages were shown to account for the gene expression of the regarded markers. This finding might also contribute to the connection between the markers observed. Supporting our observations, atypical chemokine receptors, such as CCRL1, are known to be involved in adherence to endothelium and the extravasation from blood vessels [47]. Furthermore, CCRL1, SLFN13, SKI, Cables1, and DCHS1 were all found to be expressed in endothelial cells to different extents [48–51]. A particularly high expression was detected for SKI and DCHS1, whereas CCRL1 and SLFN13 only exhibited a low gene expression in endothelial cells [49]. Concerning the expression of the markers in tumor-associated microglia/macrophages and in accordance with our findings, an expression of SKI, Cables1, and DCHS1 was also described by previous studies [52–56]. Even though data concerning neither an expression of CCRL1 nor SLFN13 in tumor-associated microglia/macrophages are yet publicly available, both markers were previously described to be involved in immunological processes. Whereas CCRL1 controlled intratumor T cell accumulation and activation in a murine mammary cancer cell line [57], SLFN13 was described as an immune-related biomarker that might predict tumor recurrence in lung cancer after curative resection [58].

After performing co-staining and correlation analyses of the studied molecules with stemness-associated markers, and realizing expression studies in both stem-like cells generated from commercial GBM cell lines and patient-derived primary cultures, our results showed, in a first using this approach, an association between CCRL1, SLFN13, Cables1, DCHS1, and SKI, and stemness. Indeed, all the molecules studied were clearly expressed in GSCs and exhibited co-staining with OCT4, Sox2, and KLF4 to varying extents, underscoring the results of correlation analyses. Among them, CCRL1, SLFN13, and SKI particularly showed a correlation with the expression of OCT4 and KLF4. When we examined regulation during TMZ-promoted entry and exit from dormancy in GSCs, CCRL1, SLFN13, Cables1, DCHS1, and SKI were regulated in complex patterns, confirming our results from native GBM cell lines and patient-derived primary cultures. When neurosphere formation assays were performed from TMZ-treated native GBM cells, the ability to form neurospheres and the expression of stemness markers indeed increased during treatment. Finally, gene set enrichment analyses indicated the importance of SKI in the phenomenon of stemness in particular.

Consistent with our findings, Arslan et al. previously reported SLFN family members of SLFN13 to be expressed in GSCs [38]. Additionally, DCHS1 was postulated as a suitable marker and potential therapeutic target for minimally infiltrative GSCs, since it revealed a low expression in developing neuroectodermal tissue, specific upregulation in GSCs, and a potential angiogenic role in tumorigenesis [59]. Concerning SKI, a connection between SKI,

OCT4, and Sox2 was also previously described by Song et al. in pancreatic cancer. Here, enhanced SKI expression increased the expression of the pluripotency maintaining markers such as Sox2 and OCT4, and also components of the sonic-hedgehog pathway (Shh), indicating that SKI might be an important factor in maintaining the stemness of pancreatic cancer stem cells through modulating the Shh pathway [60]. Since SKI is involved in the TGF- β signaling pathway as previously mentioned [42], which in turn is known to support self-renewal of glioma-initiating stem cells [61], the TGF- β /SKI pathway appears to be of particular importance in GSCs. Indeed, when inhibiting SKI by Disitertide (P144) in our in vitro model of TMZ-promoted dormancy entry and exit, higher cytotoxicity, a stronger inhibition of GBM cell proliferation, and a reduced neurosphere formation capacity along with lower expression of stemness markers were observed. Disitertide is a TGF- β inhibitor peptide, which can decrease proliferation, migration, invasiveness, and tumorigenicity in GBM cells in vitro by a reduction in SMAD2 phosphorylation, the downregulation of SKI and the upregulation of SMAD7 [32]. Thus, in the context of TMZ-promoted entry and exit from dormancy, additional inhibition of transcriptional target genes of the TGF- β pathway, including SKI, appeared to result in a higher antitumor efficacy than TMZ treatment alone. However, because Disitertide, as a TGF- β inhibitor peptide, did not exclusively act on SKI expression, these effects cannot be attributed to the inhibition of SKI alone, although the observed effects underscore the role of this molecule in TMZ-promoted dormancy in GBMs.

Despite not being explored in GSCs yet, CCRL1 and Cables1 were shown to be connected to stemness. Whereas CCRL1 was found to label mesenchymal subpopulations in an alveolosphere model of mice [62], Cables1 was detected most robustly in embryonic neural tissues in zebrafish and hence postulated to be important for neural differentiation during embryogenesis [17]. In the setting of hematopoiesis, Cables1 was also found to be predominantly expressed in the progenitor cell compartment of bone marrow, hence suggested to be a stemness marker [45].

Although one limitation of our study is the limited amount of cell lines and primary cultures and the small sample sizes included, which prohibits the generalization of the results, our study points to an involvement of CCRL1, SLFN13, Cables1, DCHS1, and particularly SKI in TMZ-promoted dormancy and reveals their connection to the phenomenon of stemness. It seems that the roles of the markers in this disease are complex and also include the tumor microenvironment. However, our study provides basic descriptive research with initial insights into the functions of the selected genes during GBM progression. Further studies are needed to elucidate the detailed impact and function of the selected genes in GBM.

5. Conclusions

GBM still depicts an incurable disease due to phenomena such as dormancy—a reversible growth arrest even promoted by the standard-of-care TMZ itself—and stemness. These complex mechanisms, which contribute to the high therapy resistance of the disease, consist of a large number of downstream factors, whose activities partly overlap and are still not fully understood. In our study, CCRL1, SLFN13, SKI, Cables1, and DCHS1 were all shown to be regulated under TMZ-promoted dormancy and, besides tumor cells, to be expressed by endothelial cells and tumor-associated microglia/macrophages. Moreover, all of the markers, and of particular importance, SKI, were shown to be related to stemness, which highlights the connection between TMZ-promoted dormancy and this phenomenon. Future research is required to investigate the distinct function of CCRL1, SLFN13, SKI, Cables1, and DCHS1 in GBM. Only by understanding the mechanism involved will it be feasible to overcome the enormous therapy resistance and improve the disastrous outcome of GBM patients in the future.

Supplementary Materials: The following supporting information can be downloaded at: <https://www.mdpi.com/article/10.3390/cells12111491/s1>. Table S1: TaqMan primer probes (Applied Biosystems, Waltham, MA, USA) used; Table S2: Primary antibodies used for immunofluorescence staining.; Table S3: gene enrichment analysis, dormancy entry, TMZ versus DMSO, regulated, significant; Table S4: gene enrichment analysis, dormancy exit, TMZ versus DMSO, regulated, significant. Figure S1: Heatmap of the significantly regulated GO terms of the comparison TMZ versus DMSO in dormancy entry and exit.

Author Contributions: Conceptualization, J.H.-F.; methodology, C.K., D.H. and D.E.; software, C.K., D.H. and D.E.; validation, C.K., D.H. and D.E.; formal analysis, C.K., D.H. and D.E.; investigation, C.K. and D.H.; resources, M.S. and H.A.; data curation, C.K. and D.H.; writing—original draft preparation, C.K. and J.H.-F.; writing—review and editing, C.K., D.H., H.A., D.E., M.S. and J.H.-F.; visualization, C.K. and D.H.; supervision, J.H.-F.; project administration, J.H.-F.; funding acquisition, C.K. and J.H.-F. All authors have read and agreed to the published version of the manuscript.

Funding: This research was funded by the German Research Foundation (DFG) as part of the Research Training Group “Materials4Brain” (RTG2154; P8) and a sponsorship from the University Medical Center Schleswig-Holstein, UKSH (“Juniorförderung 2020”, given to CK).

Institutional Review Board Statement: The study was conducted in accordance with the Declaration of Helsinki, and approved by the Ethics Committee of the University of Kiel, Germany (file reference: D471/15 and D524/17).

Informed Consent Statement: Informed consent was obtained from all subjects involved in the study.

Data Availability Statement: Not applicable.

Acknowledgments: We thank Corinna Keller and Fereshteh Ebrahim for their expert technical assistance.

Conflicts of Interest: The authors declare no conflict of interest.

Abbreviations

GBM	Glioblastoma
TMZ	Temozolomide
CCRL1	Chemokine (C-C Motif) Receptor-Like 1
SLFN13	Schlafen 13
SKI	Sloan-Kettering Institute
Cables1	Like1Cdk5 and Abl Enzyme Substrate 1
DCHS1	Dachsous Cadherin-Related 1
qRT-PCR	Reverse transcription and quantitative real-time PCR
GSC	Glioma stem-like cells
EMT	Epithelial-to-mesenchymal transition
CDH19	Cadherin 19
WHO	World Health Organization
UKE	University Medical Center Hamburg-Eppendorf
ANOVA	Analysis of variance
PCa/b	Primary culture a/b
vWF	Von Willebrand factor
CD11b	Cluster of differentiation molecule 11b
GFAP	Glial fibrillary acidic protein
OCT4	Octamer binding transcription factor 4
Sox2	Sex determining region Y-box 2
KLF4	Krüppel-like factor 4
DMSO	Dimethyl sulfoxide
MGMT	O6-methylguanine-DNA methyltransferase
TGF- β	Transforming growth factor
Shh	Sonic hedgehog

References

- Amman, J.; Tamimi, A.F.; Juweid, M. Epidemiology and Outcome of Glioblastoma. In *Glioblastoma*; De Vleeschouwer, S., Ed.; Codon Publications: Brisbane, Australia, 2017; pp. 143–153. [CrossRef]
- Verhaak, R.G.W.; Hoadley, K.A.; Purdom, E.; Wang, V.; Wilkerson, M.D.; Miller, C.R.; Ding, L.; Golub, T.; Jill, P.; Alexe, G.; et al. Integrated genomic analysis identifies clinically relevant subtypes of glioblastoma characterized by abnormalities in PDGFRA, IDH1, EGFR, and NF1. *Cancer Cell* **2010**, *17*, 98–110. [CrossRef] [PubMed]
- Adamski, V.; Hempelmann, A.; Flüh, C.; Lucius, R.; Synowitz, M.; Hattermann, K.; Held-Feindt, J. Dormant glioblastoma cells acquire stem cell characteristics and are differentially affected by Temozolomide and AT101 treatment. *Oncotarget* **2017**, *8*, 108064–108078. [CrossRef] [PubMed]
- Chen, R.; Nishimura, M.C.; Bumbaca, S.M.; Kharbanda, S.; Forrest, W.F.; Kasman, I.M.; Greve, J.M.; Soriano, R.H.; Gilmour, L.L.; Rivers, C.S.; et al. A Hierarchy of Self-Renewing Tumor-Initiating Cell Types in Glioblastoma. *Cancer Cell* **2010**, *17*, 362–375. [CrossRef]
- Tong, L.; Yi, L.; Liu, P.; Abeysekera, I.R.; Hai, L.; Li, T.; Tao, Z.; Ma, H.; Xie, Y.; Huang, Y.; et al. Tumour cell dormancy as a contributor to the reduced survival of GBM patients who received standard therapy. *Oncol. Rep.* **2018**, *40*, 463–471. [CrossRef] [PubMed]
- Adamski, V.; Hattermann, K.; Kubelt, C.; Cohrs, G.; Lucius, R.; Synowitz, M.; Sebens, S.; Held-Feindt, J. Entry and exit of chemotherapeutically-promoted cellular dormancy in glioblastoma cells is differentially affected by the chemokines CXCL12, CXCL16, and CX3CL1. *Oncogene* **2020**, *39*, 4421–4435. [CrossRef] [PubMed]
- Shi, J.-Y.; Yang, L.-X.; Wang, Z.-C.; Wang, L.-Y.; Zhou, J.; Wang, X.-Y.; Shi, G.-M.; Ding, Z.-B.; Ke, A.-W.; Dai, Z.; et al. CC chemokine receptor-like 1 functions as a tumour suppressor by impairing CCR7-related chemotaxis in hepatocellular carcinoma. *J. Pathol.* **2015**, *235*, 546–558. [CrossRef] [PubMed]
- Feng, L.Y.; Ou, Z.L.; Wu, F.Y.; Shen, Z.Z.; Shao, Z.M. Involvement of a Novel Chemokine Decoy Receptor CCX-CKR in Breast Cancer Growth, Metastasis and Patient Survival. *Clin. Cancer Res.* **2009**, *15*, 2962–2970. [CrossRef] [PubMed]
- Ju, Y.; Sun, C.; Wang, X. Loss of atypical chemokine receptor 4 facilitates C-C motif chemokine ligand 21-mediated tumor growth and invasion in nasopharyngeal carcinoma. *Exp. Ther. Med.* **2019**, *17*, 613–620. [CrossRef]
- Harata-Lee, Y.; Turvey, M.E.; Brazzatti, J.A.; Gregor, C.E.; Brown, M.P.; Smyth, M.J.; Comerford, I.; McColl, S.R. The atypical chemokine receptor CCX-CKR regulates metastasis of mammary carcinoma via an effect on EMT. *Immunol. Cell Biol.* **2014**, *92*, 815–824. [CrossRef]
- Al-Marsoum, S.; Vomhof-DeKrey, E.E.; Basson, M.D. Schlafens: Emerging Proteins in Cancer Cell Biology. *Cells* **2021**, *10*, 2238. [CrossRef]
- Chen, W.; Lam, S.S.; Srinath, H.; Schiffer, C.A.; Royer, W.E.; Lin, K. Competition between Ski and CREB-binding protein for binding to Smad proteins in transforming growth factor-beta signaling. *J. Biol. Chem.* **2007**, *282*, 11365–11376. [CrossRef]
- Buess, M.; Terracciano, L.; Reuter, J.; Ballabeni, P.; Boulay, J.-L.; Laffer, U.; Metzger, U.; Herrmann, R.; Rochlitz, C.F. Amplification of SKI Is a Prognostic Marker in Early Colorectal Cancer. *Neoplasia* **2004**, *6*, 207–212. [CrossRef] [PubMed]
- Fukuchi, M.; Nakajima, M.; Fukai, Y.; Miyazaki, T.; Masuda, N.; Sohda, M.; Manda, R.; Tsukada, K.; Kato, H.; Kuwano, H. Increased expression of c-Ski as a co-repressor in transforming growth factor- β signaling correlates with progression of esophageal squamous cell carcinoma. *Int. J. Cancer* **2004**, *108*, 818–824. [CrossRef] [PubMed]
- Xie, M.; Wu, X.; Zhang, J.; Zhang, J.; Li, X. Ski regulates Smads and TAZ signaling to suppress lung cancer progression. *Mol. Carcinog.* **2017**, *56*, 2178–2189. [CrossRef]
- Kirley, S.D.; Rueda, B.R.; Chung, D.C.; Zukerberg, L.R. Increased growth rate, delayed senescence, and decreased serum dependence characterize CABLES-deficient cells. *Cancer Biol. Ther.* **2005**, *4*, 654–658. [CrossRef] [PubMed]
- Groeneweg, J.W.; White, Y.A.; Kokel, D.; Peterson, R.T.; Zukerberg, L.R.; Berin, I.; Rueda, B.R.; Wood, A.W. CABLES1 is required for embryonic neural development: Molecular, cellular, and behavioral evidence from the zebrafish. *Mol. Reprod. Dev.* **2011**, *78*, 22–32. [CrossRef] [PubMed]
- Dong, Q.; Kirley, S.; Rueda, B.; Zhao, C.; Zukerberg, L.; Oliva, E. Loss of CABLES, a novel gene on chromosome 18q, in ovarian cancer. *Mod. Pathol.* **2003**, *16*, 863–868. [CrossRef]
- Wu, C.L.; Kirley, S.D.; Xiao, H.; Chuang, Y.; Chung, D.C.; Zukerberg, L.R. CABLES enhances cdk2 tyrosine 15 phosphorylation by Wee1, inhibits cell growth, and is lost in many human colon and squamous cancers. *Cancer Res.* **2001**, *61*, 7325–7332.
- Cappello, S.; Gray, M.J.; Badouel, C.; Lange, S.; Einsiedler, M.; Srouf, M.; Chitayat, D.; Hamdan, F.F.; Jenkins, Z.A.; Morgan, T.R.; et al. Mutations in genes encoding the cadherin receptor-ligand pair DCHS1 and FAT4 disrupt cerebral cortical development. *Nat. Genet.* **2013**, *45*, 1300–1308. [CrossRef] [PubMed]
- Zhang, L.; Liu, Z.; Zhu, J. In silico screening using bulk and single-cell RNA-seq data identifies RIMS2 as a prognostic marker in basal-like breast cancer: A retrospective study. *Medicine* **2021**, *100*, e25414. [CrossRef]
- de Mello, J.B.H.; Cirilo, P.D.R.; Michelin, O.C.; Domingues, M.A.C.; Rudge, M.V.C.; Rogatto, S.R.; Maestá, I. Genomic profile in gestational and non-gestational choriocarcinomas. *Placenta* **2017**, *50*, 8–15. [CrossRef] [PubMed]
- Bujko, M.; Kober, P.; Mikula, M.; Ligaj, M.; Ostrowski, J.; Siedlecki, J.A. Expression changes of cell-cell adhesion-related genes in colorectal tumors. *Oncol. Lett.* **2015**, *9*, 2463–2470. [CrossRef]
- Hattermann, K.; Gebhardt, H.; Krossa, S.; Ludwig, A.; Lucius, R.; Held-Feindt, J.; Mentlein, R. Transmembrane chemokines act as receptors in a novel mechanism termed inverse signaling. *eLife* **2016**, *5*, e10820. [CrossRef]

25. Flüh, C.; Chitadze, G.; Adamski, V.; Hattermann, K.; Synowitz, M.; Kabelitz, D.; Held-Feindt, J. NKG2D ligands in glioma stem-like cells: Expression in situ and in vitro. *Histochem Cell Biol.* **2018**, *149*, 219–233. [CrossRef] [PubMed]
26. Hattermann, K.; Held-Feindt, J.; Lucius, R.; Mürköster, S.S.; Penfold, M.E.; Schall, T.J.; Mentlein, R. The chemokine receptor CXCR7 is highly expressed in human glioma cells and mediates antiapoptotic effects. *Cancer Res.* **2010**, *70*, 3299–3308. [CrossRef] [PubMed]
27. Caylioglu, D.; Meyer, R.J.; Hellmold, D.; Kubelt, C.; Synowitz, M.; Held-Feindt, J. Effects of the Anti-Tumorigenic Agent AT101 on Human Glioblastoma Cells in the Microenvironmental Glioma Stem Cell Niche. *Int. J. Mol. Sci.* **2021**, *22*, 3606. [CrossRef] [PubMed]
28. Kubelt, C.; Peters, S.; Ahmeti, H.; Huhndorf, M.; Huber, L.; Cohrs, G.; Hövener, J.-B.; Jansen, O.; Synowitz, M.; Held-Feindt, J. Intratumoral Distribution of Lactate and the Monocarboxylate Transporters 1 and 4 in Human Glioblastoma Multiforme and Their Relationships to Tumor Progression-Associated Markers. *Int. J. Mol. Sci.* **2020**, *21*, 6254. [CrossRef]
29. Raudvere, U.; Kolberg, L.; Kuzmin, I.; Arak, T.; Adler, P.; Peterson, H.; Vilo, J. g:Profiler: A web server for functional enrichment analysis and conversions of gene lists (2019 update). *Nucleic. Acids Res.* **2019**, *7*, W191–W198. [CrossRef]
30. Hu, Y.; Smyth, G.K. ELDA: Extreme limiting dilution analysis for comparing depleted and enriched populations in stem cell and other assays. *J. Immunol. Methods* **2009**, *347*, 70–78. [CrossRef]
31. Nikitin, P.V.; Musina, G.R.; Pekov, S.I.; Kuzin, A.A.; Popov, I.A.; Belyaev, A.Y.; Kobayakov, G.L.; Usachev, D.Y.; Nikolaev, V.N.; Mikhailov, V.P. Cell-Population Dynamics in Diffuse Gliomas during Gliomagenesis and Its Impact on Patient Survival. *Cancers* **2023**, *15*, 145. [CrossRef]
32. Gallo-Oller, G.; Vollmann-Zwerenz, A.; Meléndez, B.; Rey, J.A.; Hau, P.; Dotor, J.; Castresana, J.S. P144, a Transforming Growth Factor beta inhibitor peptide, generates antitumoral effects and modifies SMAD7 and SKI levels in human glioblastoma cell lines. *Cancer Lett.* **2016**, *381*, 67–75. [CrossRef]
33. Hegi, M.E.; Diserens, A.-C.; Gorlia, T.; Hamou, M.-F.; De Tribolet, N.; Weller, M.; Kros, J.M.; Hainfellner, J.A.; Mason, W.; Mariani, L.; et al. MGMT gene silencing and benefit from temozolomide in glioblastoma. *N. Engl. J. Med.* **2005**, *352*, 997–1003. [CrossRef] [PubMed]
34. Houillier, C.; Wang, X.; Kaloshi, G.; Mokhtari, K.; Guillemin, R.; Laffaire, J.; Paris, S.; Boisselier, B.; Idhah, A.; Laigle-Donadey, F.; et al. IDH1 or IDH2 mutations predict longer survival and response to temozolomide in low-grade gliomas. *Neurology* **2010**, *75*, 1560–1566. [CrossRef]
35. Han, B.; Meng, X.; Wu, P.; Li, Z.; Li, S.; Zhang, Y.; Zha, C.; Ye, Q.; Jiang, C.; Cai, J.; et al. ATRX/EZH2 complex epigenetically regulates FADD/PARP1 axis, contributing to TMZ resistance in glioma. *Theranostics* **2020**, *10*, 3351–3365. [CrossRef] [PubMed]
36. Amen, A.M.; Fellmann, C.; Soczek, K.M.; Ren, S.M.; Lew, R.J.; Knott, G.J.; Park, J.E.; McKinney, A.M.; Mancini, A.; Doudna, J.A.; et al. Cancer-specific loss of TERT activation sensitizes glioblastoma to DNA damage. *Proc. Natl. Acad. Sci. USA* **2021**, *118*, e2008772118. [CrossRef]
37. Isci, D.; D’uonno, G.; Wantz, M.; Rogister, B.; Lombard, A.; Chevigné, A.; Szpakowska, M.; Neirinckx, V. Patient-Oriented Perspective on Chemokine Receptor Expression and Function in Glioma. *Cancers* **2021**, *14*, 130. [CrossRef]
38. Arslan, A.D.; Sassano, A.; Saleiro, D.; Lisowski, P.; Kosciuczuk, E.M.; Fischietti, M.; Eckerdt, F.; Fish, E.N.; Plataniias, L.C. Human SLFN5 is a transcriptional co-repressor of STAT1-mediated interferon responses and promotes the malignant phenotype in glioblastoma. *Oncogene* **2017**, *36*, 6006–6019. [CrossRef]
39. Morein, D.; Erlichman, N.; Ben-Baruch, A. Beyond Cell Motility: The Expanding Roles of Chemokines and Their Receptors in Malignancy. *Front. Immunol.* **2020**, *11*, 952. [CrossRef] [PubMed]
40. Chen, D.; Xu, W.; Bales, E.; Colmenares, C.; Conacci-Sorrell, M.; Ishii, S.; Stavnezer, E.; Campisi, J.; E Fisher, D.; Ben-Ze’Ev, A.; et al. SKI activates Wnt/beta-catenin signaling in human melanoma. *Cancer Res.* **2003**, *63*, 6626–6634.
41. Zhao, X.; Fang, Y.; Wang, X.; Yang, Z.; Li, D.; Tian, M.; Kang, P. Knockdown of Ski decreases osteosarcoma cell proliferation and migration by suppressing the PI3K/Akt signaling pathway. *Int. J. Oncol.* **2020**, *56*, 206–218. [CrossRef]
42. Liu, P.; Wang, Q.-S.; Zhai, Y.; Xiong, R.-P.; Chen, X.; Peng, Y.; Zhao, Y.; Ning, Y.-L.; Yang, N.; Zhou, Y.-G. Ski mediates TGF- β 1-induced fibrosarcoma cell proliferation and promotes tumor growth. *J. Cancer* **2020**, *11*, 5929–5940. [CrossRef] [PubMed]
43. Jiang, H.; Jin, C.; Liu, J.; Hua, D.; Zhou, F.; Lou, X.; Zhao, N.; Lan, Q.; Huang, Q.; Yoon, J.-G.; et al. Next generation sequencing analysis of miRNAs: MiR-127-3p inhibits glioblastoma proliferation and activates TGF- β signaling by targeting SKI. *Omics J. Integr. Biol.* **2014**, *18*, 196–206. [CrossRef] [PubMed]
44. Maier, H.J.; Wirth, T.; Beug, H. Epithelial-Mesenchymal Transition in Pancreatic Carcinoma. *Cancers* **2010**, *2*, 2058–2083. [CrossRef] [PubMed]
45. Arnason, T.; Pino, M.S.; Yilmaz, O.; Kirley, S.D.; Rueda, B.R.; Chung, D.C.; Zukerberg, L.R. CABLES1 is a tumor suppressor gene that regulates intestinal tumor progression in Apc(Min) mice. *Cancer Biol. Ther.* **2013**, *14*, 672–678. [CrossRef]
46. Safran, M.; Rosen, N.; Twik, M.; BarShir, R.; Stein, T.I.; Dahary, D.; Fishilevich, S.; Lancet, D. The GeneCards Suite. In *Practical Guide to Life Science Databases*; Abugessaisa, I., Kasukawa, T., Eds.; Springer: Singapore, 2021; pp. 27–56. [CrossRef]
47. Sjöberg, E.; Meyrath, M.; Chevigné, A.; Östman, A.; Augsten, M.; Szpakowska, M. The diverse and complex roles of atypical chemokine receptors in cancer: From molecular biology to clinical relevance and therapy. *Adv. Cancer Res.* **2020**, *145*, 99–138. [CrossRef]

48. Lucas, B.; White, A.J.; Ulvmar, M.H.; Nibbs, R.J.B.; Sitnik, K.M.; Agace, W.W.; Jenkinson, W.E.; Anderson, G.; Rot, A. CCRL1/ACKR4 is expressed in key thymic microenvironments but is dispensable for T lymphopoiesis at steady state in adult mice. *Eur. J. Immunol.* **2015**, *45*, 574–583. [CrossRef] [PubMed]
49. Karlsson, M.; Zhang, C.; Méar, L.; Zhong, W.; Digre, A.; Katona, B.; Sjöstedt, E.; Butler, L.; Odeberg, J.; Dusart, P.; et al. A single-cell type transcriptomics map of human tissues. *Sci. Adv.* **2021**, *7*, eabh2169. [CrossRef]
50. Teresa, M.; Tan, M.; Tarango, M.; Fink, L.; Mihm, M.; Ma, Y.; Waner, M. Differential expression of SKI oncogene protein in hemangiomas. *Otolaryngol. Head Neck Surg.* **2009**, *141*, 213–218. [CrossRef] [PubMed]
51. He, L.; Beghi, F.; Baral, V.; Dépond, M.; Zhang, Y.; Joulin, V.; Rueda, B.R.; Gonin, P.; Foudi, A.; Wittner, M.; et al. CABLES1 Deficiency Impairs Quiescence and Stress Responses of Hematopoietic Stem Cells in Intrinsic and Extrinsic Manners. *Stem Cell Rep.* **2019**, *13*, 274–290. [CrossRef] [PubMed]
52. Spittau, B.; Wullkopf, L.; Zhou, X.; Rilka, J.; Pfeifer, D.; Kriegelstein, K. Endogenous transforming growth factor-beta promotes quiescence of primary microglia in vitro. *Glia* **2013**, *61*, 287–300. [CrossRef]
53. Zhai, Y.; Ye, S.-Y.; Wang, Q.-S.; Xiong, R.-P.; Fu, S.-Y.; Du, H.; Xu, Y.-W.; Peng, Y.; Huang, Z.-Z.; Yang, N.; et al. Overexpressed ski efficiently promotes neurorestoration, increases neuronal regeneration, and reduces astrogliosis after traumatic brain injury. *Gene Ther.* **2022**, *30*, 75–87. [CrossRef]
54. Abud, E.M.; Ramirez, R.N.; Martinez, E.S.; Healy, L.M.; Nguyen, C.H.H.; Newman, S.A.; Yeromin, A.V.; Scarfone, V.M.; Marsh, S.E.; Fimbres, C.; et al. iPSC-Derived Human Microglia-like Cells to Study Neurological Diseases. *Neuron* **2017**, *94*, 278–293e9. [CrossRef]
55. Dubbelaar, M.; Misriellal, C.; Bajramovic, J.; Burm, S.; Zuiderwijk-Sick, E.; Brouwer, N.; Grit, C.; Kooistra, S.; Shinjo, S.; Marie, S.; et al. Transcriptional profiling of macaque microglia reveals an evolutionary preserved gene expression program. *Brain Behav. Immun. Health* **2021**, *15*, 100265. [CrossRef]
56. Galatro, T.F.; Holtman, I.R.; Lerario, A.M.; Vainchtein, I.D.; Brouwer, N.; Sola, P.R.; Veras, M.M.; Pereira, T.F.; Leite, R.E.P.; Möller, T.; et al. Transcriptomic analysis of purified human cortical microglia reveals age-associated changes. *Nat. Neurosci.* **2017**, *20*, 1162–1171. [CrossRef]
57. Whyte, C.E.; Osman, M.; Kara, E.E.; Abbott, C.; Foeng, J.; McKenzie, D.R.; Fenix, K.A.; Harata-Lee, Y.; Foyle, K.; Boyle, S.T.; et al. ACKR4 restrains antitumor immunity by regulating CCL21. *J. Exp. Med.* **2020**, *217*, e20190634. [CrossRef] [PubMed]
58. Wang, Q.; Zhou, D.; Wu, F.; Liang, Q.; He, Q.; Peng, M.; Yao, T.; Hu, Y.; Qian, B.; Tang, J.; et al. Immune Microenvironment Signatures as Biomarkers to Predict Early Recurrence of Stage Ia-b Lung Cancer. *Front. Oncol.* **2021**, *11*, 680287. [CrossRef] [PubMed]
59. Zorniak, M.; Clark, P.A.; Kuo, J.S. Myelin-forming cell-specific cadherin-19 is a marker for minimally infiltrative glioblastoma stem-like cells. *J. Neurosurg.* **2015**, *122*, 69–77. [CrossRef] [PubMed]
60. Song, L.; Chen, X.; Gao, S.; Zhang, C.; Qu, C.; Wang, P.; Liu, L. Ski modulate the characteristics of pancreatic cancer stem cells via regulating sonic hedgehog signaling pathway. *Tumor Biol.* **2016**, *37*, 16115–16125. [CrossRef] [PubMed]
61. Kaminska, B.; Kocyk, M.; Kijewska, M. TGF beta signaling and its role in glioma pathogenesis. *Adv. Exp. Med. Biol.* **2013**, *986*, 171–187. [CrossRef]
62. Taghizadeh, S.; Heiner, M.; Vazquez-Armendariz, A.I.; Wilhelm, J.; Herold, S.; Chen, C.; Zhang, J.S.; Bellusci, S. Characterization in Mice of the Resident Mesenchymal Niche Maintaining At2 Stem Cell Proliferation in Homeostasis and Disease. *Stem Cells* **2021**, *39*, 1382–1394. [CrossRef]

Disclaimer/Publisher’s Note: The statements, opinions and data contained in all publications are solely those of the individual author(s) and contributor(s) and not of MDPI and/or the editor(s). MDPI and/or the editor(s) disclaim responsibility for any injury to people or property resulting from any ideas, methods, instructions or products referred to in the content.

Glycation Leads to Increased Invasion of Glioblastoma Cells

Paola Schildhauer¹, Philipp Selke², Christian Scheller¹ , Christian Strauss¹, Rüdiger Horstkorte², Sandra Leisz^{1,†}  and Maximilian Scheer^{1,*,†} 

¹ Department of Neurosurgery, Medical Faculty, Martin-Luther-University Halle-Wittenberg, Ernst-Grube-Str. 40, 06120 Halle (Saale), Germany

² Institute for Physiological Chemistry, Medical Faculty, Martin-Luther-University Halle-Wittenberg, 06114 Halle (Saale), Germany

* Correspondence: maximilian.scheer@uk-halle.de; Tel.: +49-0-345-557-1656

† These authors contributed equally to this work.

Abstract: Glioblastoma (GBM) is a highly aggressive and invasive brain tumor with a poor prognosis despite extensive treatment. The switch to aerobic glycolysis, known as the Warburg effect, in cancer cells leads to an increased production of methylglyoxal (MGO), a potent glycation agent with pro-tumorigenic characteristics. MGO non-enzymatically reacts with proteins, DNA, and lipids, leading to alterations in the signaling pathways, genomic instability, and cellular dysfunction. In this study, we investigated the impact of MGO on the LN229 and U251 (WHO grade IV, GBM) cell lines and the U343 (WHO grade III) glioma cell line, along with primary human astrocytes (hA). The results showed that increasing concentrations of MGO led to glycation, the accumulation of advanced glycation end-products, and decreasing cell viability in all cell lines. The invasiveness of the GBM cell lines increased under the influence of physiological MGO concentrations (0.3 mmol/L), resulting in a more aggressive phenotype, whereas glycation decreased the invasion potential of hA. In addition, glycation had differential effects on the ECM components that are involved in the invasion progress, upregulating TGF β , brevican, and tenascin C in the GBM cell lines LN229 and U251. These findings highlight the importance of further studies on the prevention of glycation through MGO scavengers or glyoxalase 1 activators as a potential therapeutic strategy against glioma and GBM.

Keywords: glycation; invasion; glioblastoma; glioma; astrocytes; methylglyoxal; advanced glycation end-products



Citation: Schildhauer, P.; Selke, P.; Scheller, C.; Strauss, C.; Horstkorte, R.; Leisz, S.; Scheer, M. Glycation Leads to Increased Invasion of Glioblastoma Cells. *Cells* **2023**, *12*, 1219. <https://doi.org/10.3390/cells12091219>

Academic Editors: Javier S. Castresana, Bárbara Meléndez and Pablo Martín-Vasallo

Received: 20 February 2023

Revised: 11 April 2023

Accepted: 20 April 2023

Published: 23 April 2023



Copyright: © 2023 by the authors. Licensee MDPI, Basel, Switzerland. This article is an open access article distributed under the terms and conditions of the Creative Commons Attribution (CC BY) license (<https://creativecommons.org/licenses/by/4.0/>).

1. Introduction

Glioblastoma (GBM, WHO grade IV glioma) is the most common and aggressive astrocytic brain tumor in adults with a high recurrence and mortality. Despite extensive treatment, including surgical resection, radiotherapy, and temozolomide chemotherapy, the median survival for patients diagnosed with GBM is 12–20 months [1]. The invasive nature of GBM leads to cells infiltrating diffusely into the brain parenchyma, making complete surgical resection difficult and promoting recurrence. For GBM cells to infiltrate and disseminate within a tumor, key changes in the energy metabolism, cell adhesion, and remodeling of the extracellular matrix (ECM) are required [2].

The ECM is a complex network of proteins and components, such as laminin, collagen, and proteoglycans, which provide anchorage of the cells and shape the consistency of the tissue [3]. Several ECM molecules involved in migration and invasion are proteoglycans (versican, brevican, cadherins) and glycoproteins (CD44, tenascin C, fibrinogen), which were found upregulated in higher grade gliomas [4]. GBM cells are known to secrete matrix metalloproteinase (MMP) to degrade the ECM, penetrating the surrounding parenchyma [5,6]. Moreover, GBM cells increase their invasiveness by upregulating tenascin C and brevican, thus creating a migration-promoting environment [7,8]. Through the upregulation of integrin receptors, GBM cells are able to bind other ECM molecules,

which facilitates migration [9]. Another mechanism that enhances migratory capacities is the epithelial-mesenchymal transition (EMT). GBM cells undergoing EMT lose epithelial characteristics and become more spindle-shaped and motile, with a downregulation of epithelial proteins such as E-cadherin and an upregulation of mesenchymal proteins such as N-cadherin and vimentin [10,11].

As is known for many cancer cells, GBM reprograms their metabolism to gain energy through aerobic glycolysis (Warburg effect) [12]. Due to the inefficient means of generating adenosine triphosphate (ATP) this way, the aerobic glycolysis occurs 10 to 100 times faster in cancer cells [13]. This produces an increased amount of by-products, which are favorable for tumor growth and progression [14]. During glycolysis, 0.1–0.4% of glucose are turned into methylglyoxal (MGO), a regular by-product, through the non-enzymatic elimination of the phosphate group of glyceraldehyde-3-phosphate [15].

MGO is a reactive dicarbonyl and one of the most potent glycation agents known to cause vascular complications of diabetes (neuropathy, retinopathy, nephropathy, and atherosclerosis) and central nervous system disorders [15]. Being 20,000 times more reactive than glucose, MGO reacts with the amino acids lysine, cysteine, and arginine to form advanced glycation end products (AGEs) [13]. This non-enzymatic reaction between the carbonyl groups of dicarbonyls (MGO or glyoxal) or sugars (glucose, fructose) with amino groups of proteins, lipids, and DNA is called glycation. The process of glycation affects all proteins and can cause protein crosslinking, which alters tertiary structures and protein functions [16,17]. In total, 90–99% of MGO is bound to macromolecules and the cellular concentration can reach up to 0.3 mmol/L [18]. Elevated MGO and AGE levels were found to be associated with Alzheimer's and cardiovascular disease and mortality in type 1 and 2 diabetes [19,20]. AGEs function through various transmembrane receptors inducing oxidative stress, inflammation, dysregulation of signaling pathways, and genomic instability, which can trigger the initiation and progression of cancer [21]. The activation of the receptor for AGEs (RAGE) can, for example, trigger the JNK/AP1 signaling pathway, which promotes cell survival, invasion, and metastasis [21]. In breast cancer tumors, an accumulation of MGO adducts have been found and studies have shown that MGO induces the remodeling of the ECM and the activation of migratory-signaling pathways, enhancing metastatic dissemination [22].

Our preliminary work showed that MGO led to glycation and increased invasion in benign meningioma cells [23]. Similar results were obtained after the glycation of neuroblastoma cells [24]. Here, an increase in cell migration and invasion associated with a reduction in adhesion was detected.

In this study, we analyzed the effect of MGO on the glioma (WHO grade III and IV) cell lines compared to normal human astrocytes (hAs). We focused on the effect of glycation on chemotaxis, adhesion, and invasion. Our results showed that glycation led to an increase in invasion in the GBM cell lines and a decrease in the hA. In addition, we analyzed the effect of glycation on ECM proteins and their potential role in the observed increased invasion.

2. Materials and Methods

2.1. Cell Lines and Cultivation

The human glioma cell lines U343, U251, and LN229 have been kindly provided by Jacqueline Kessler (Department of Radiotherapy, Martin Luther University Halle-Wittenberg, Halle (Saale), Germany). All three of the cell lines were cultured in RPMI 1640 (Gibco, Thermo Fisher Scientific, Waltham, MA, USA) supplemented with 1% Penicillin-Streptomycin (10,000 U/mL Penicillin/10,000 µg/mL Streptomycin) (Gibco, Thermo Fisher Scientific, Waltham, MA, USA) and 10% fetal bovine serum (FBS, Gibco, Thermo Fisher Scientific, Waltham, MA, USA) at 37 °C in a 5% CO₂ incubator. The hAs were obtained from ScienCell Research Laboratories (Carlsbad, CA, USA) and cultured with astrocyte media (ScienCell Research Laboratories, Carlsbad, CA, USA), as recommended by the manufacturer. All plates for hA were coated prior to use with a poly-L-Lysine solution (0.01%, EMD Millipore Corporation, Burlington, VT, USA).

2.2. MGO Treatment

The cell lines were seeded and incubated at 37 °C and 5% CO₂ in an incubator. After 4 h of attachment, the cells were treated with different concentrations of MGO (Merck, Sigma-Aldrich, St. Louis, MO, USA) (0.1, 0.3, 0.6, and 1.0 mmol/L), depending on the experiment. After the treatment, the cells were incubated again at 37 °C 5% CO₂ for 24–96 h. The untreated cells served as the control.

2.3. XTT Assay

The cellular metabolic activity of the glycosylated glioma cell lines LN229, U343, and U251, and the hAs were measured with a XTT assay (Roche, Sigma-Aldrich, St. Louis, MO, USA) as an indicator of cell vitality. In total, 5×10^4 cells were seeded in 96-well plates (Techno Plastic Products, TPP, Trasadingen, Switzerland) in 100 µL, incubated, and treated with MGO. As a control, a cell-free media without MGO was used. The XTT assay was performed after 24, 48, 72, and 96 h of MGO treatment. After each incubation period, 50 µL of the XTT labelling mixture was added to each well, according to the kit's instructions. The plate was incubated for 4 h in a humidified atmosphere, 37 °C, 5.0% CO₂ and then measured at a wavelength of 492 nm using the Tecan Infinite F200 Pro. (Tecan, Männedorf, Switzerland). The XTT assay was also performed using media with only 1% FBS.

2.4. Cell Microscopy

In total, 5×10^4 cells were seeded in 24-well plates (TPP) and treated with different MGO concentrations as described above. Microscope imaging was taken 24 and 48 h after treatment. The cells were stained with a propidium iodide solution (PI, 1.0 mg/mL, Sigma-Aldrich) and NucBlue Live Cell Stain ReadyProbes reagent (Thermo Fisher Scientific). The cells were washed with Dulbecco's phosphate-buffered saline (DPBS, Gibco, Thermo Fisher Scientific) and covered with FluoroBrite™ DMEM (Gibco, Thermo Fisher Scientific) and imaged with a Keyence BZ-800E microscope (Keyence, Neu-Isenburg, Germany). The quantification of PI and DAPI stained cells was performed using the IdentifyPrimaryObjects function of the software CellProfiler (Version 4.2.4, Broad Institute, Cambridge, MA, USA).

2.5. Glycation and Immunoblotting

The cells were seeded in 100 mm × 21 mm petri dishes (TPP) and treated with different concentrations of MGO accordingly. After 24 h, the cells were washed twice with ice cold PBS (Thermo Fisher Scientific) and harvested with PBS containing one diluted Pierce™ Protease Inhibitor Mini Tablet EDTA-free (Thermo Fisher Scientific). Benzonase Nuclease (Merck, Sigma Aldrich) was added to cleave the nucleic acid bonds. The proteins were extracted with 1× LDS sample buffer (Invitrogen, Thermo Fisher Scientific, Waltham, MA USA) and heated at 70 °C for 10 min. The protein concentration measurement was performed using the Pierce BCA Protein Assay Kit (Thermo Fisher Scientific) according to the manufacturer's instructions. Furthermore, 5% β-mercaptoethanol (Carl Roth, Karlsruhe, Germany) and 1× LDS sample buffer was added to the proteins and afterwards heated at 70 °C for 10 min.

The proteins were separated by sodium dodecyl sulphate polyacrylamide gel electrophoresis (SDS-PAGE) using the NuPAGE™ 4–12%, Bis-Tris, 1.5 mm, Mini-Protein-Gels and NuPAGE™ MES SDS Running Buffer (both Thermo Fisher Scientific). Blotting was performed using the iBlot 2 Dry Blotting System (Thermo Fisher Scientific) with iBlot™ 2 NC Regular Stacks (Thermo Fisher Scientific) followed by Ponceau S staining (0.1% Ponceau S, 3% trichloroacetic acid, and 3% sulfosalicylic acid).

The membranes were blocked with 5% skim milk powder (Carl Roth) in TRIS-buffered saline with 0.1% Tween (TBS-T, Sigma-Aldrich). The primary antibodies were added (Table 1) overnight at 4 °C and, after washing with TBS-T 5 times, the secondary antibodies were added for 60 min at room temperature. The protein level of glyceraldehyde 3-phosphate dehydrogenase (GAPDH) was used as the loading control.

Table 1. Antibodies used for immunofluorescence staining.

Antibody	Species	Dilution	Dilution Buffer	Manufacture
Anti-Carboxymethyl Lysine antibody (ab125145)	Mouse IgG	1:1000	5% MP in TBS-T	Abcam (Cambridge, UK)
Anti-E Cadherin antibody Intercellular Junction Marker (ab15148)	Rabbit IgG	1:1000	5% BSA in TBS-T	
Recombinant Anti-N Cadherin antibody (ab245117)	Rabbit IgG	1:1000	5% BSA in TBS-T	Cell Signaling Technology Inc. (Danvers, MA, USA)
GAPDH (14C10) (#2118)	Rabbit IgG	1:1000	5% BSA in TBS-T	
Anti-rabbit IgG, HRP-linked Antibody (#7074)	Goat	1:1000	2% MP in TBS-T	
Anti-mouse IgG, HRP-linked Antibody (#7076)	Horse	1:1000	2% MP in TBS-T	

Abbreviations: BSA, bovine serum albumin; IgG, immunoglobulin G; MP, milk powder.

The membranes were developed using the SuperSignal West Femto Chemiluminescent Substrate (Thermo Fisher Scientific) and signals were detected with a CCD camera (ImageQuant LAS4000, GE Healthcare, Freiburg, Germany). The quantification of the band intensity was performed using the ImageQuant TL software version 3.0 (GE Healthcare, Freiburg, Germany) and normalized to the corresponding GAPDH bands. All of the bands identified by the CML antibody, which indicate glycosylated protein, were included in the quantification process.

2.6. mRNA Isolation and qPCR

In total, 5×10^5 cells were seeded in 6-well plates (TPP) and treated with 0, 0.3, and 0.6 mmol/L MGO accordingly. After 24 h, the cells were washed twice with ice cold PBS. Afterwards, the cells were harvested in 300 μ L of lysis buffer LBP (MACHEREY-NAGEL, Düren, Germany) and the lysate was stored at -20°C . RNA was isolated using the NucleoSpin[®] RNA Plus Kit (MACHEREY-NAGEL, Düren, Germany), according to the manufacturer's instructions. Using the RevertAid First Strand cDNA Synthesis Kit (Thermo Fisher Scientific) 2 μ g of RNA was transcribed into cDNA.

Using the Platinum[®] SYBR[®] Green qPCR SuperMix-UDG (Invitrogen, Thermo Fisher Scientific), 0.5 μ L of the respective reverse and forward primers (Table 2) and 1 μ L of cDNA were prepared in a total volume of 20 μ L. qPCR was performed with the Rotor-Gene Q (Qiagen, Hilden, Germany).

Table 2. Primers used for real-time quantitative PCR.

Gene Name (Protein)	Oligo Sequence 5' to 3' (Forward, Reverse)	Annealing Temperature ($^\circ\text{C}$)	Product Length	Reference Sequence	Species
CD44	ACGCTTCAGCCTACTGCAAA GGTCCTGCTTTCCTTCGTGT	60	279	NM_000610.4	Homo sapiens
MMP2	ATGTCGCCCCAAAACGG CCGCATGGTCTCGATGGTAT	60	176	NM_004530.6	Homo sapiens
MMP9	TCTATGGTCTCGCCCTGAA CATCGTCCACCGGACTCAA	60	219	NM_004994.3	Homo sapiens
MMP14	GGAGAATTTGTGCTGCCCG TTGGTTATTCCTACCCGCC	60	247	NM_004995.4	Homo sapiens
Versican	GCAGAAACTGCATCACCCAG TCCCAGGGCTTCTTGGTACT	60	227	NM_004385.5	Homo sapiens
Brevican	ATGGTGGGACATGCTTGGAG GAACTCTGTCTCCTCGGGTG	60	233	NM_021948.5	Homo sapiens
Tensacin C	GAAACTGCAGAGACCAGCCT CAGGGGCTTGTTCAGTGGAT	60	244	NM_001410991.1	Homo sapiens
Fibronectin	GGTCCGGGACTCAATCCAAA GACAGAGTTGCCACCGTAA	60	279	NM_212482.4	Homo sapiens
Integrin β 1	AGCAACGGACAGATCTGCAA GCTGGGGTAAATTGTCCCGA	60	241	NM_002211.4	Homo sapiens
Integrin α 3	GGCCTGCCAAGCTAATGAGA GACTCACCCATCACTGTCCC	60	273	NM_002204.4	Homo sapiens
Integrin α 5	TCTCAGTGGAGTTTACCAGC CCGAGAGCCTTGTCTGCAA	60	173	NM_002205.5	Homo sapiens
Fibulin 3	TGTATGTGCCCCAGGGATA ATTGACTGGGGCAGTTCTCG	60	227	XM_005264205.5	Homo sapiens
Vimentin	GGAGTCCACTGAGTACCGGA AGGTGACGAGCCATTTCCTC	60	198	NM_003380.5	Homo sapiens
Snail (SNAI1)	CTCGAAAGGCCTTCAACTGC GACATTCGGGAGAAAGGTCCG	60	298	NM_005985.4	Homo sapiens
Slug (SNAI2)	TTTCAGACCCCAATGCCATT GAAAAAGGCTTCTCCCCCGT	60	292	NM_003068.5	Homo sapiens
Thrombospondin 1	ATCCTGGACTCGTGTAGGT AGAAAGGCCCGAGTATCCCT	60	209	NM_003246.4	Homo sapiens
GAPDH	TCGTGGAAGGACTCATGACC TTCCCGTTCAGCTCAGGGAT	60	172	NM_002046.7	Homo sapiens

2.7. Real-Time Cell Analysis

The chemotactic migration was measured using the Real-Time Cell Analyzer Dual Purpose (RTCA DP) Analyzer (ACEA Biosciences Inc., San Diego, CA, USA), along with the cell invasion and migration plate (CIM-plate 16, ACEA Biosciences Inc.).

In total, 160 μL of media with 20% FBS was added to the lower chamber and 50 μL of media containing 1% FBS was added to the upper chamber. The CIM-plates were assembled according to the manufacturer's instructions and incubated for 1 h at 37 °C, followed by background measurements. The cells were detached using Accutase (Capricorn Scientific GmbH, Ebsdorfergrund, Germany) and resuspended with 1% FBS media. In total, 2×10^4 cells in 100 μL were added to each well. After 30 min of incubation at room temperature, 0.3 mmol/L or 0.6 mmol/L MGO were added. The cell migration was measured with the RTCA DP Analyzer as a change in impedance every 15 min for 48 h and displayed with the RTCA program 2.0 (ACEA Biosciences Inc.). To analyze the invasion, the upper chamber of the CIM-plate was coated with 20 μL of Geltrex TM LDEV-FREE Reduced Growth Factor Basement Membrane Matrix (Thermo Fisher Scientific). The Geltrex Matrix solution gels were kept at 37 °C, forming a basement membrane and acting as a barrier through which the cells have to invade. The coated upper chambers were incubated for one hour at 37 °C for the Geltrex to polymerize. Afterwards, the CIM-plates were assembled and measured as described above.

For the adhesion assay, 96 \times E-plates (ACEA Biosciences Inc.) were coated with 10 $\mu\text{g}/\text{mL}$ of Fibronectin (EMD Millipore Corporation) or collagen IV (collagen from human placenta, Bornstein and Traub Type IV, Sigma Aldrich) and incubated for 1 h at 37 °C. Afterwards, the wells were washed with PBS and incubated with media for 20 min. To acquire the background measurements, 50 μL of media with 1% FBS was added to each well. Furthermore, 2×10^4 cells in 100 μL were added to each well. After 30 min of incubation at room temperature, 0.3 mmol/L or 0.6 mmol/L of MGO were added. Adhesion was measured every 15 min for 24 h with the RTCA.

2.8. Statistical Analysis

All analyses were performed using Excel Software (Microsoft Corporation, Redmond, WA, USA) and GraphPad Prism 4.9.1 (GraphPad Software Inc., San Diego, CA, USA). The half maximal inhibitory effect (IC50) was calculated using GraphPad Prisms nonlinear regression analysis and the dose-response inhibition equations.

An unpaired two-sided Student's *t*-test was performed for all cell lines compared to the untreated cells. The figures depict the mean and standard deviation (SD), respectively. At least three biological replicates were performed for each experiment.

3. Results

3.1. High MGO Concentrations Lead to Decreased Cell Vitality

The influence of MGO on the cell vitality of LN229, U343, U251, and hA after 24, 48, 72, and 96 h was investigated using an XTT assay (Supplementary Materials Figure S1). MGO showed concentration-dependent cytotoxic effects in all cell lines after 24 h (Figure 1). In LN229, the cell vitality decreased in a concentration-dependent manner, with a reduction in the cell vitality of $18.53 \pm 2.71\%$; $p < 0.001$ with 0.1 mmol/L, $34.15 \pm 15.07\%$; $p < 0.001$ with 0.3 mmol/L, $58.28 \pm 14.90\%$; $p < 0.001$ with 0.6 mmol/L; and the strongest effect with 1 mmol/L with a reduction of $64.53 \pm 10.11\%$; $p < 0.001$ (Figure 1A). Equivalent results were observed in the U251 and U343 cell lines (Figure 1B,C). The treatment with 0.1 mmol/L MGO did not affect the cell vitality of the U251 cells and 0.3 mmol/L MGO showed a $20.54 \pm 10.21\%$; $p = 0.047$ reduction in the cell vitality. The 0.6 mmol/L MGO decreased the cell vitality by $51.13 \pm 0.34\%$; $p < 0.001$ and 1 mmol/L by $57.69 \pm 4.00\%$; $p < 0.001$ (Figure 1B). In the U343 cells, 0.1 mmol/L reduced the cell vitality by $17.43 \pm 11.47\%$; $p = 0.018$, 0.3 mmol/L reduced it by $35.96 \pm 10.36\%$; $p < 0.001$, and 0.6 mmol/L MGO reduced it by $47.86 \pm 15.86\%$; $p < 0.001$. A $53.82 \pm 17.02\%$; $p < 0.001$ reduction in the cell vitality was observed at 1 mmol/L MGO (Figure 1C). In the hA cell line, the cell vitality was not

affected by treatment with 0.1 and 0.3 mmol/L MGO, but a $51.78 \pm 2.53\%$; $p < 0.001$ reduction in the cell vitality was observed at concentrations of 0.6 mmol/L and a $53.97 \pm 2.05\%$; $p < 0.001$ reduction was observed with 1 mmol/L MGO (Figure 1D). The IC₅₀ of MGO treatment measured 0.384 ± 0.040 mmol/L in the LN229 and 0.4379 ± 0.037 mmol/L in the U251 cells. For the U343 cells, the IC₅₀ was slightly lower at 0.368 ± 0.099 mmol/L and for the hA cells it was slightly lower at 0.333 ± 0.032 mmol/L MGO.

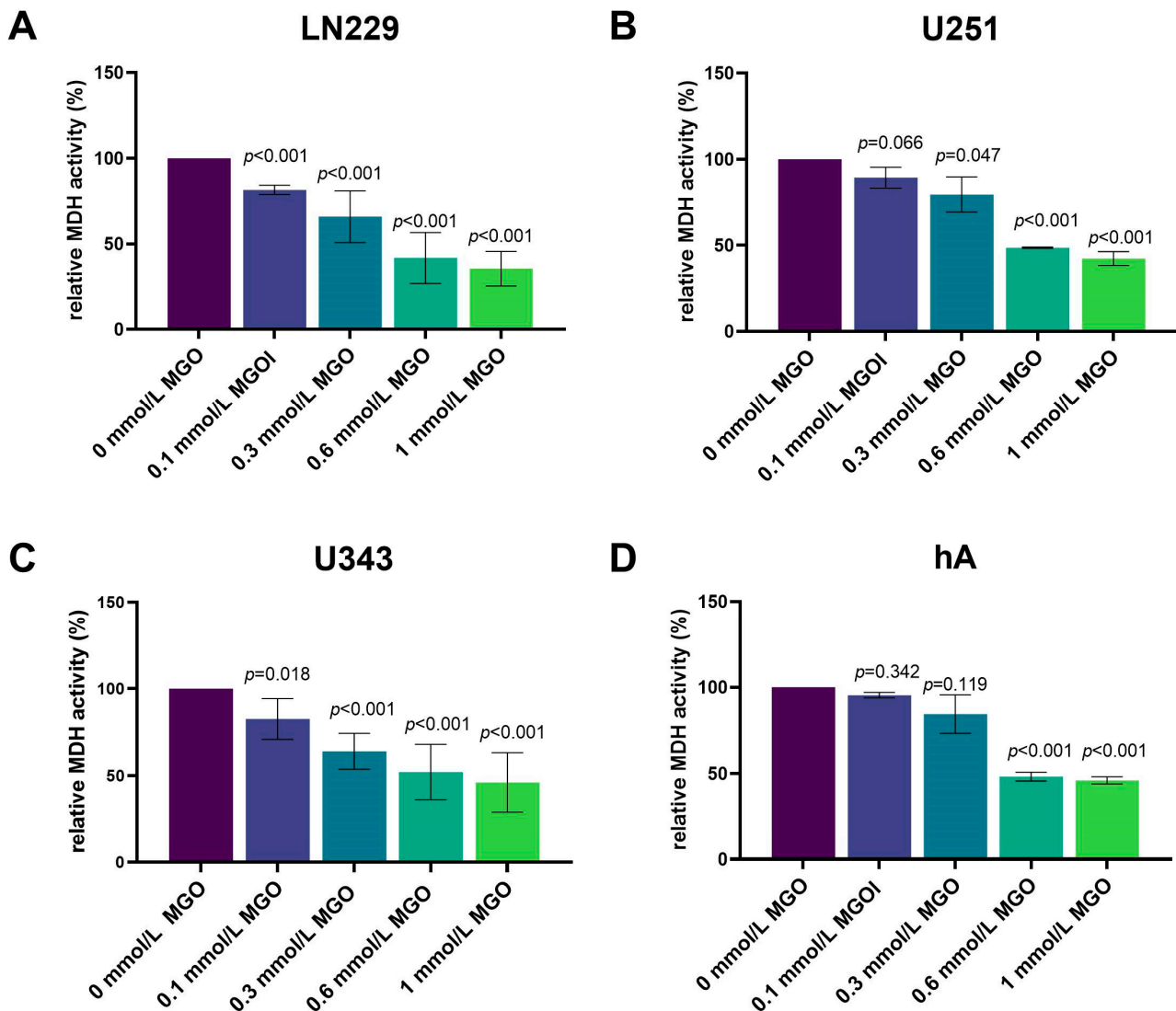


Figure 1. Cell vitality of glioma cell lines and hA after MGO treatment. The cell vitality of LN229 (A), U251 (B), U343 (C), and hA (D) cells was determined using an XTT assay after MGO treatment. Graphs show intracellular mitochondrial dehydrogenase (MDH) activity normalized to untreated cells after 24 h. Student's *t*-test was performed for statistical analysis. Graphs represent the means and SDs of three independent biological replicates.

3.2. High MGO Concentration Induce Altered Cell Morphology and Cell Death

In addition, we investigated the influence of MGO on the cell morphology. The cells were cultivated in the absence or in the presence of different concentrations of MGO (0.1–1 mmol/L) for 24 h (Figure 2) and 48 h (Supplementary Materials Figure S2). LN229 and U251 did not exhibit any changes in their morphology when cultured with MGO up to a concentration of 0.6 mmol/L. However, at 1 mmol/L MGO, there was a reduction in the cell amount and the cells became more spherical (Figure 2A,B). U343 and hA displayed a reduction in cell numbers already at 0.3 mmol/L MGO and changes in the morphology at

0.6 mmol/L MGO, appearing more granular and sporadic (Figure 2C,D). An increase in the number of dead cells, as indicated by PI staining, was observed at both 0.6 mmol/L and 1 mmol/L MGO for hA. The quantification of PI-stained cells showed a higher cell death with increasing concentrations of MGO (Supplementary Material Table S1).

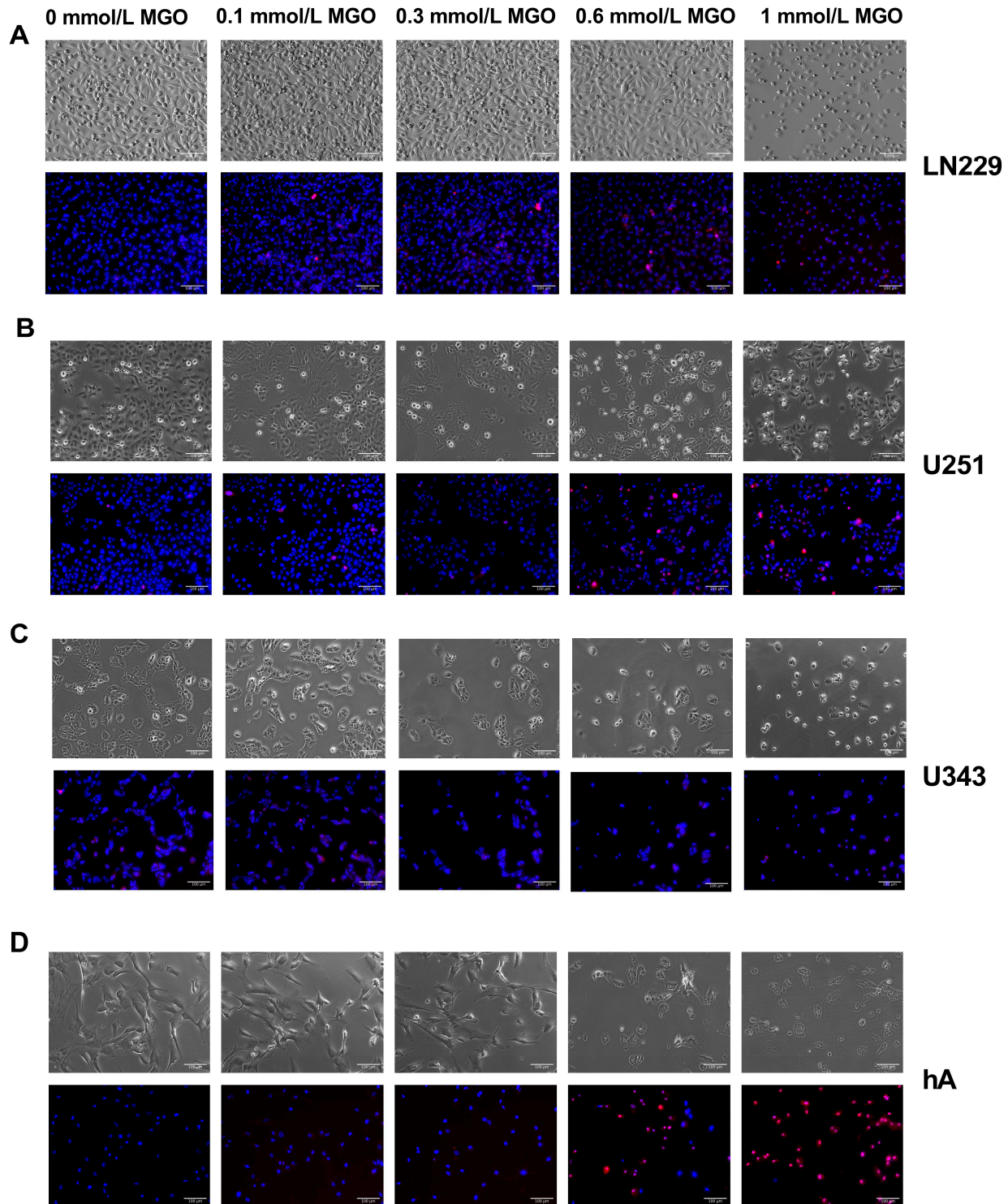


Figure 2. Microscope imaging of glioma cell lines and hA 24 h after MGO treatment. Bright field (above) and fluorescence (below) microscope imaging of LN229 (A), U251 (B), U343 (C), and hA (D) 24 h after MGO treatment. Cells were stained with DAPI (blue) and propidium iodide (red). Scale bar = 100 μ m.

In addition, for the LN229 and U251 cells a higher confluency compared to the U343 and hA cell lines was observed. This difference can be attributed to the higher proliferation rate of the GBM cell lines, such as LN229 and U251, in contrast to the grade III glioma cell line U343, and primary normal hA, which have slower growth rates. Additionally, the hA cells have a distinct morphology characterized by spindle-shaped cells with a larger cell body, which further contributes to their lower confluency.

3.3. MGO Treatment Increases Glycation in a Concentration-Dependent Manner

To evaluate the level of glycation with the increasing MGO concentration, immunoblotting was performed. The cells were treated with various concentrations of MGO (0.3, 0.6 and 1 mmol/L), and proteins were extracted and separated using SDS PAGE. Carboxymethyl Lysine antibody was used to verify glycation. An increase in glycation could be observed in all four cell lines in a concentration-dependent manner (Figure 3). In the LN229 cell line, protein glycation increased slightly after treatment with 0.3 and 0.6 mmol/L MGO and a $76.77 \pm 24.75\%$; $p = 0.011$ increase was observed with 1 mmol/L (Figure 3A). Similar results were detected in the U251, where 1 mmol/L led to an increase in glycation of $53.09 \pm 30.97\%$; $p = 0.072$ (Figure 3B). In the U343 cell line, 0.3 mmol/L MGO led to no increase in glycation but glycation increased with 0.6 mmol/L MGO by $34.06 \pm 14.85\%$; $p = 0.032$ and with 1 mmol/L by $63.43 \pm 33.89\%$; $p = 0.057$ (Figure 3C). The hA showed the strongest effect of glycation, with an increase of $72.30 \pm 62.41\%$; $p = 0.231$ with 0.3 mmol/L MGO, $93.80 \pm 77.57\%$; $p < 0.001$ with 0.6 mmol/L; and $152.21 \pm 81.69\%$; $p = 0.223$ with 1 mmol/L (Figure 3D). Interestingly, a distinct pattern of glycated proteins was observed in the cell lines.

3.4. Chemotactic Cell Migration after MGO Treatment

As chemotactic cell migration plays a crucial role in the dissemination and progression of tumors, we investigated the effect of MGO on chemotaxis. The LN229 cell line exhibited a decrease in cell migration in response to the MGO treatment in a dose-dependent manner, with a reduction of $26.66 \pm 10.92\%$; $p = 0.043$ observed after 48 h of treatment with 0.6 mmol/L MGO (Figure 4A). The treatment with MGO did not result in changes in the chemotactic migration of U251 cells after 24 and 48 h (Figure 4B). The U343 cell line showed a decrease in chemotactic migration activity after treatment with 0.3 mmol/L MGO for 24 and 48 h (Figure 4C). The hA cell line exhibited a reduction in chemotactic migration activity by $11.26 \pm 7.53\%$; $p = 0.041$ with 0.3 mmol/L after 24 h, but no other alterations in chemotactic migration were observed (Figure 4D). The effect of glycation on the cell motility was additionally analyzed using time-lapse microscopy. No significant changes were observed in the migration after MGO treatment compared to the untreated cells.

3.5. MGO Increases Invasion of GBM Cell Lines

Since invasiveness is one of the hallmarks of cancer cells, next we analyzed the influence of glycation on invasion. The invasion of the LN229 cells increased significantly with higher MGO concentrations, showing an increase of $23.06 \pm 14.46\%$; $p = 0.033$ after treatment with 0.3 mmol/L and $45.35 \pm 18.24\%$; $p = 0.025$ after treatment with 0.6 mmol/L MGO after 24 h (Figure 5A). Interestingly, the U251 cells only showed an increase in invasion after treatment with 0.3 mmol/L MGO. The enhancement of invasion with 0.6 mmol/L was not significant compared to the control cells (Figure 5B). The U343 cell line showed increased invasiveness with 0.6 mmol/L MGO. No difference was observed between the treatment with 0.3 mmol/L and the untreated cells (Figure 5C). The invasiveness of the hA decreased after MGO treatment in a concentration-dependent manner, showing a reduction of $21.02 \pm 8.37\%$; $p = 0.023$ with 0.3 mmol/L and $35.75 \pm 4.54\%$; $p < 0.001$ with 0.6 mmol/L MGO after 24 h (Figure 5D).

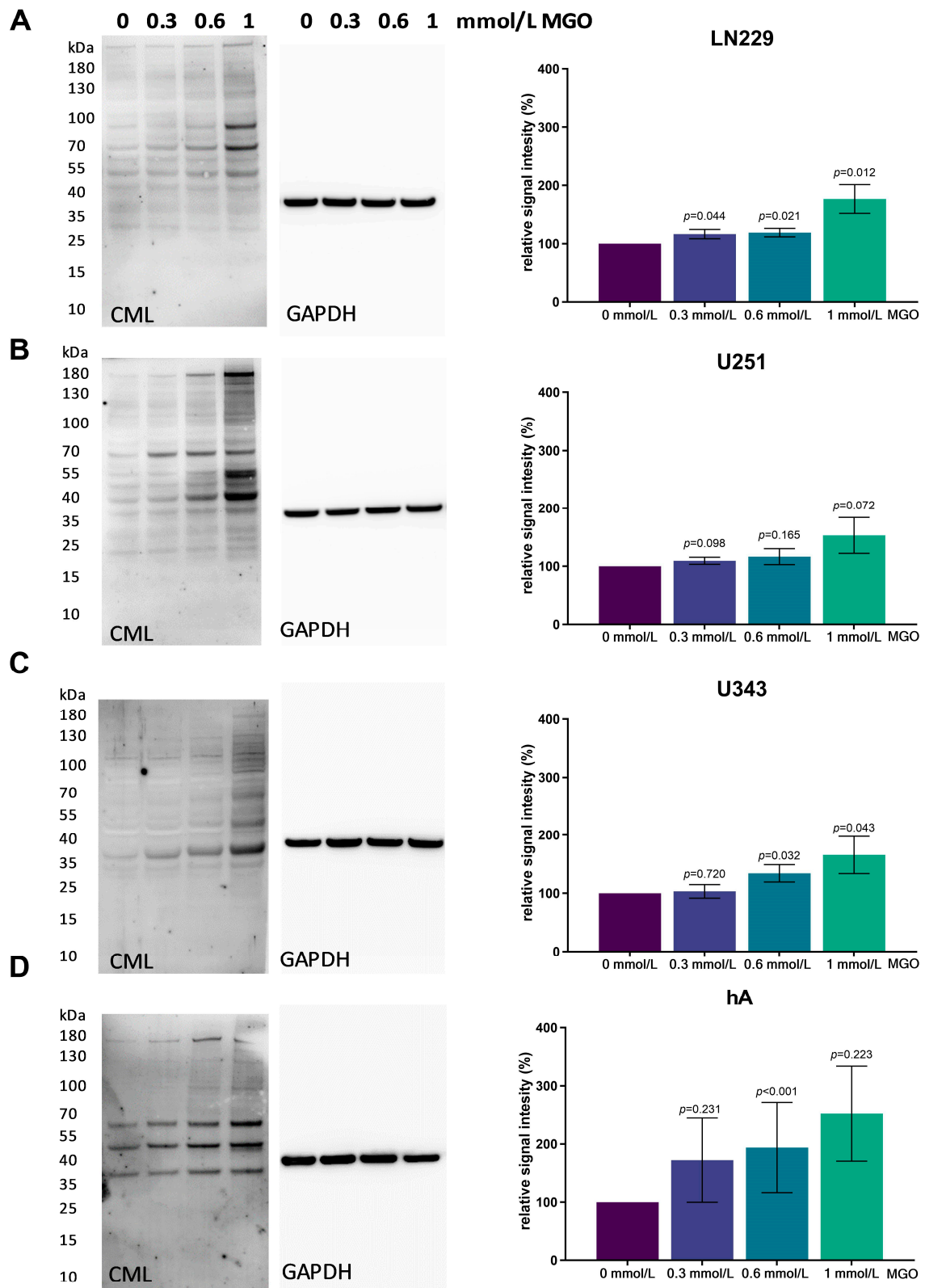


Figure 3. Glycation of glioma cell lines and hA. Immunoblot of LN229 (A), U251 (B), U343 (C), and hA (D) with different MGO concentrations (left). Antibody against carboxymethyl lysine (CML) was used to detect glycation. Graphs (right) show representative quantification of the blot, normalized to the untreated cells. GAPDH was used as loading control. Student’s *t*-test was performed for statistical analysis. Graphs represent the means and SDs of three independent biological replicates.

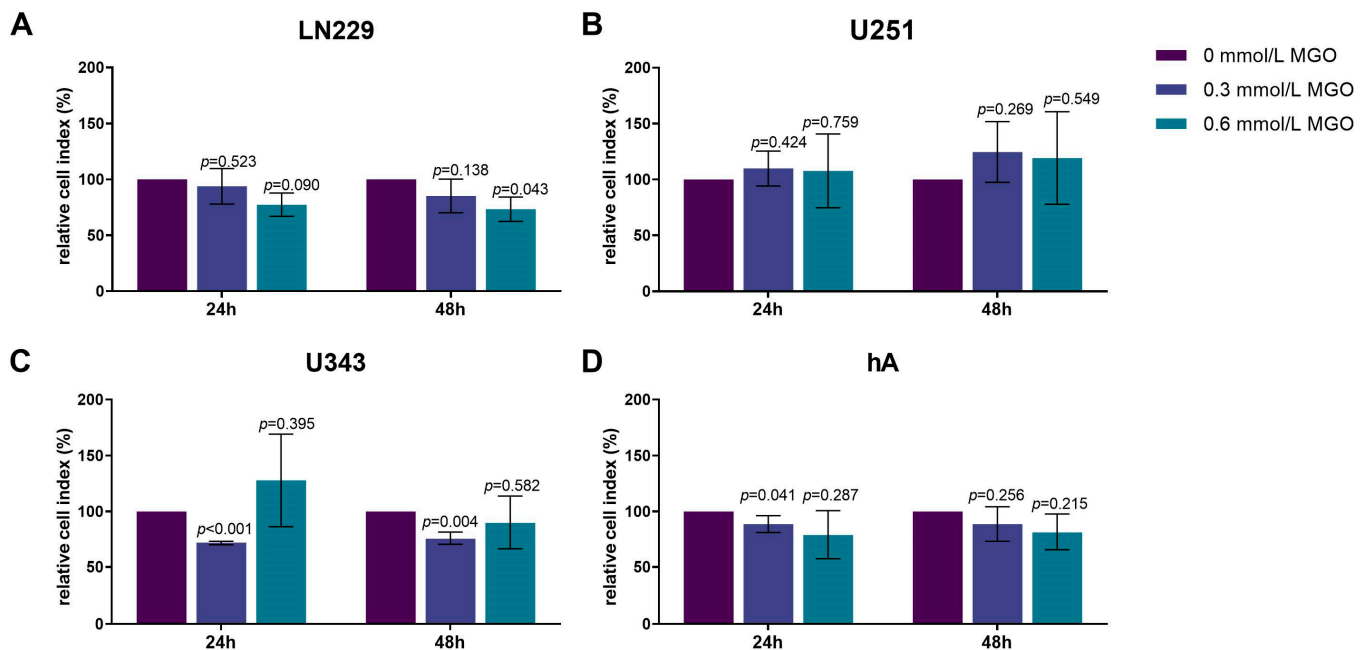


Figure 4. Chemotactic cell migration of glioma cell lines and hA after MGO treatment. Graphs display chemotaxis of LN229 (A), U251 (B), U343 (C), and hA (D) after 24 h and 48 h normalized to control cells, after treatment with 0.3 or 0.6 mmol/L MGO. Statistical analysis was performed using Student's *t*-test. Graphs represent the means and SDs of three independent biological replicates.

3.6. MGO Has No Effect on the Adhesion of Glioma Cell Lines or hA

Since the invasion was altered after glycation, we analyzed the effect of MGO on adhesion. The cells were seeded on different matrices (without coating, fibronectin, and collagen IV) and treated with MGO (0.3 or 0.6 mmol/L). No significant changes of adhesion were observed after glycation in any of the cell lines (Figure 6). However, differences in adhesion to the different matrices were observed. LN229, U343, and hA adhered best to fibronectin, followed by collagen IV and adhered least to the uncoated plates (Figure 6A,C,D). Surprisingly, U251 showed the least adhesion to collagen IV and no difference was measured between the uncoated plates and the fibronectin coating (Figure 6B).

3.7. Glycation Alters the Expression of ECM Components

Since cell-cell adhesion molecules, matrix-degrading enzymes, and various ECM components typically modulate invasion, we analyzed the effect of glycation on: versican, tenascin C, MMP 2, MMP 9, MMP 14, fibulin 3, thrombospondin, integrin β 1, integrin α 3, integrin α 5, brevican, fibronectin, vimentin, TGF- β , and transcription factors slug (SNAI2) and snail (SNAI1) (Figure 7).

The effect of glycation on various ECM components, cell-cell adhesion molecules, and matrix-degrading enzymes was analyzed in the LN229, U251, U343, and hA cell lines using qPCR. The mRNA expression levels of these components were found to be lower expressed in the malignant cell lines compared to hA, with the exception of CD44, SNAI1, and fibulin 3 (Figure 7B). The U251 showed a significantly higher expression of CD44 (3.612 ± 1.397 , $p = 0.041$) compared to the hA. SNAI1 and fibulin 3 were significantly higher expressed in LN229 (1.794 ± 0.488 , $p = 0.030$; 1.712 ± 0.379 , $p < 0.001$) (Figure 7B).

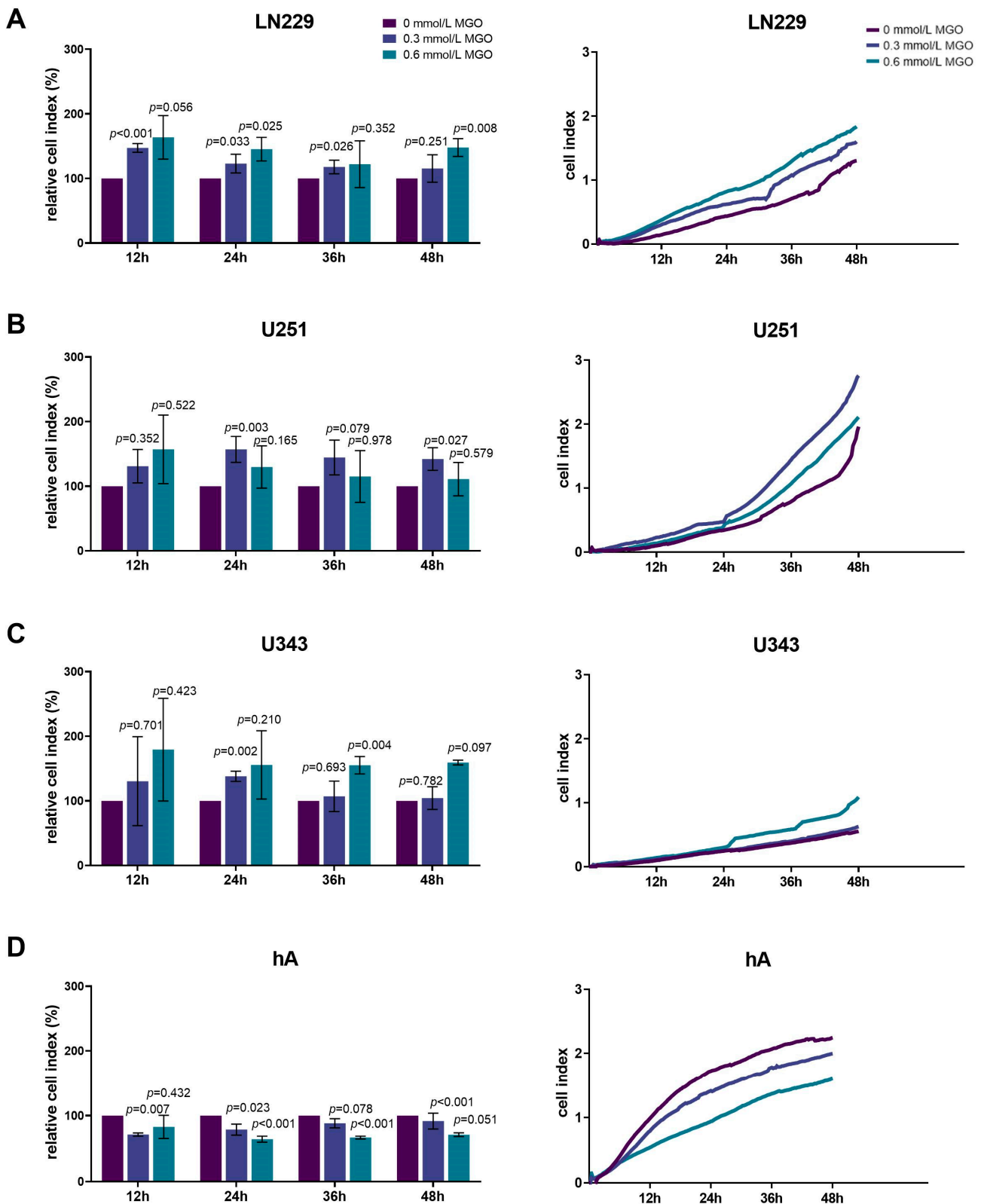


Figure 5. Invasion of glioma cell lines and hA after MGO treatment. LN229 (A), U251 (B), U343 (C), and hA (D) were cultivated in absence or presence of MGO (0.3 mmol/L or 0.6 mmol/L) on CIM-plates, coated with Geltrex to imitate basement membranes. Invasion was measured every 15 min for 48 h. Graphs (left column) show cell indices normalized to the untreated cells and graphs (right column) show measured cell indices for 12, 24, 36, and 48 h. Student's *t*-test was performed for statistical analysis. Graphs represent the means and SDs of three independent biological replicates.

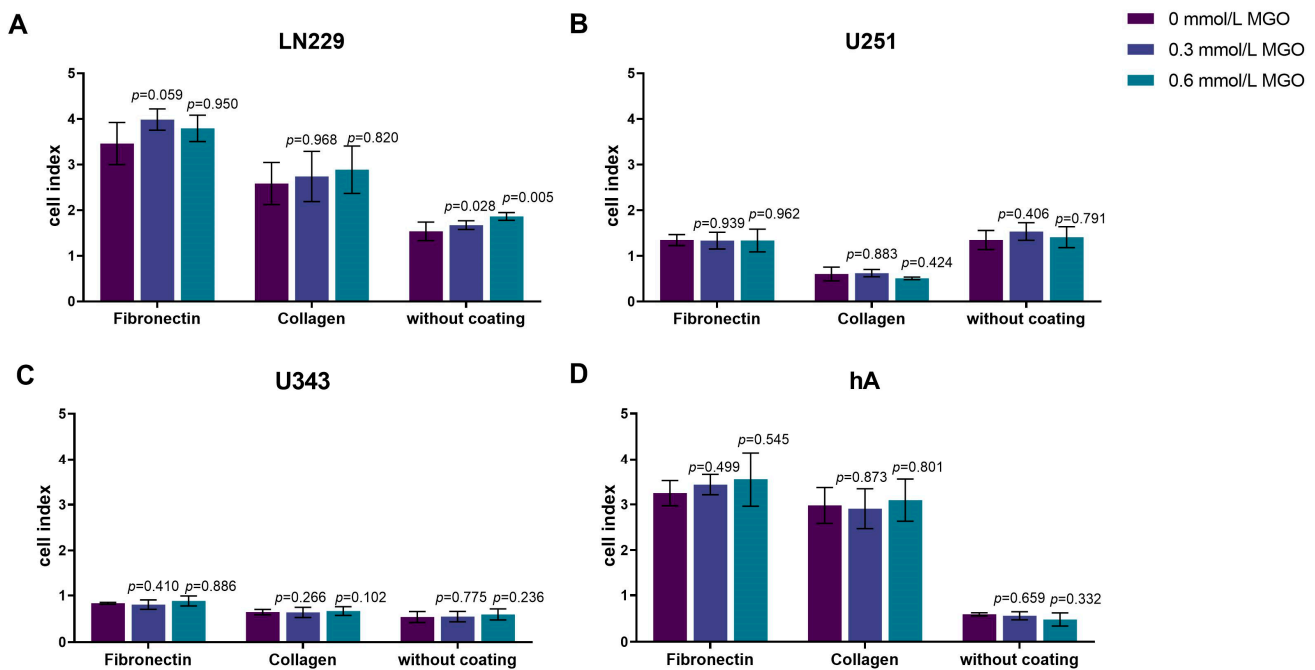


Figure 6. Adhesion of glioma cell lines and hA after MGO treatment. LN229 (A), U251 (B), U343 (C), and hA (D) were seeded at concentrations of 0.3 mmol/L and 0.6 mmol/L MGO on plates either coated with fibronectin, collagen, or left uncoated. Graphs display measured cell index after 4 h. Absolute cell index was used to show the different adherence to the different matrices and to illustrate the differences between the cells. Student's *t*-test was performed for statistical analysis. Graphs represent the means and SDs of three independent biological replicates.

The effect of glycation on the ECM components varied among the cell lines, with an overall upregulation in the LN229 cells. The strongest effect of glycation was observed on the expression of CD44, which was upregulated in the U251 (1.655 ± 0.259 , $p = 0.023$), U343 (1.548 ± 0.562 , $p = 0.240$), and hA (1.641 ± 0.657 , $p = 0.058$) cells, but remained unchanged in the LN229 cells (1.055 ± 0.145 , $p = 0.539$). Brevican expression was upregulated in the LN229 (1.498 ± 0.369 , $p = 0.057$) and U251 cells (1.303 ± 0.074 , $p = 0.004$) and downregulated in the U343 cells (0.725 ± 0.302 , $p = 0.166$). Similar results were observed with tenascin C, as the expression increased in the LN229 (1.203 ± 0.140 , $p = 0.046$) and U251 cells (1.655 ± 0.238 , $p = 0.018$). In the LN229 cells, versican and thrombospondin were upregulated (1.358 ± 0.174 , $p = 0.012$; 1.392 ± 0.151 , $p = 0.021$), as well as SNAI1 and SNAI2 (1.335 ± 0.160 , $p = 0.011$; 1.491 ± 0.294 , $p = 0.027$). The TGF- β expression increased in the LN229 and U251 cells (1.229 ± 0.099 , $p = 0.007$; 1.328 ± 0.596 , $p = 0.281$). The MMP2 expression decreased after glycation in the U251 cells (0.625 ± 0.094 , $p < 0.001$). On the contrary, the MMP2 expression increased in the LN229 and U343 cells after glycation (1.518 ± 0.294 , $p = 0.022$; 1.544 ± 0.466 , $p = 0.089$). No expression of MMP9 was detected in any of the analyzed cells. The remaining components were not differentially expressed by glycation.

In addition, we examined E- and N-cadherin, as they are involved in the epithelial mesenchymal transition (EMT). Therefore, the cells were treated with MGO and immunoblotting was performed using E- and N-cadherin antibodies (Figure 8).

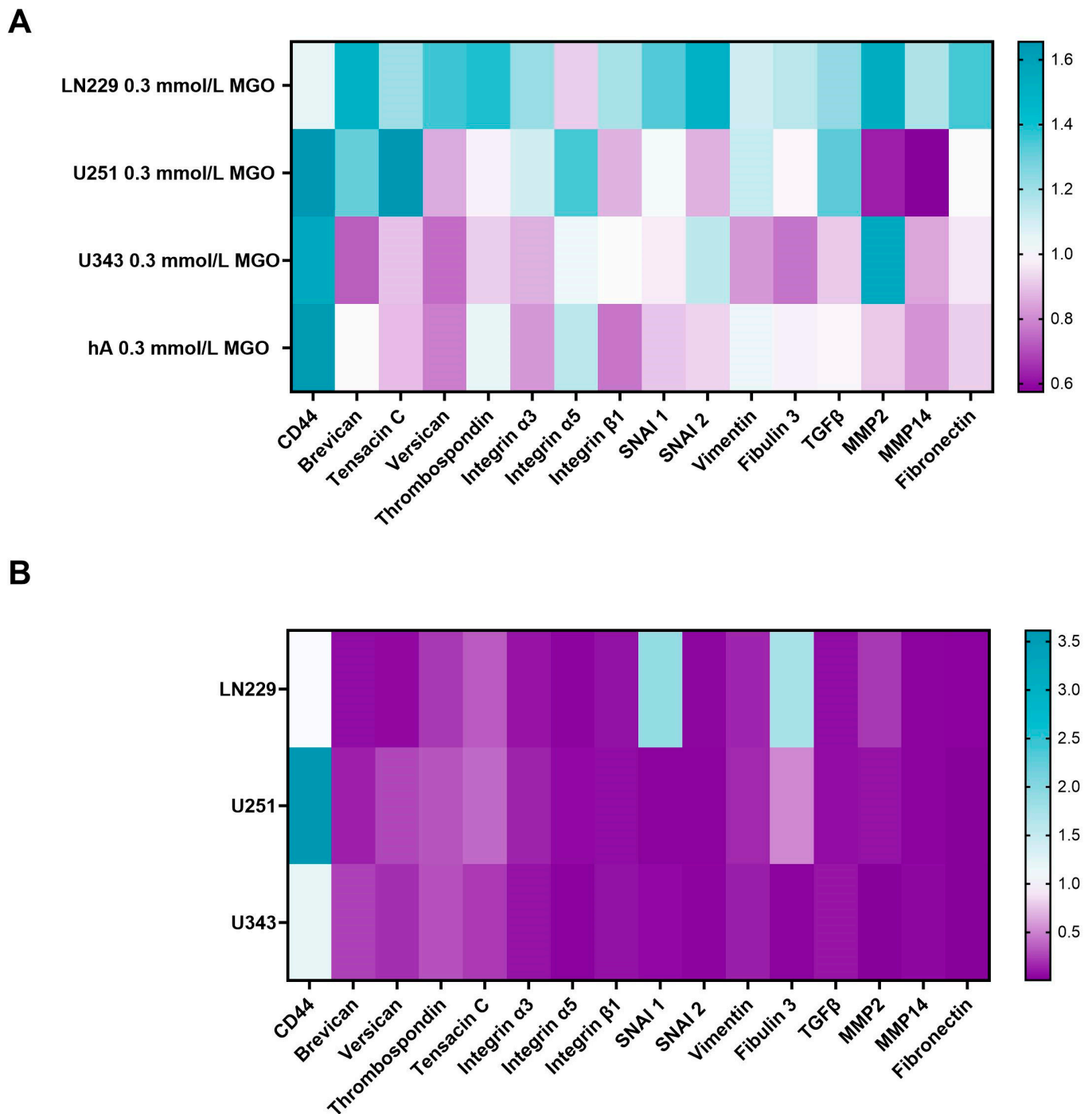


Figure 7. mRNA expression of invasion-associated ECM molecules and transcription factors. Heat map of mRNA expression of LN229, U251, U343, and hA after treatment with 0.3 mmol/L MGO normalized to untreated cells (A). Heatmap of mRNA expression of LN229, U251, and U343 cells normalized to the expression of hA (B). Three independent biological replicates of the mRNA were analyzed by qPCR.

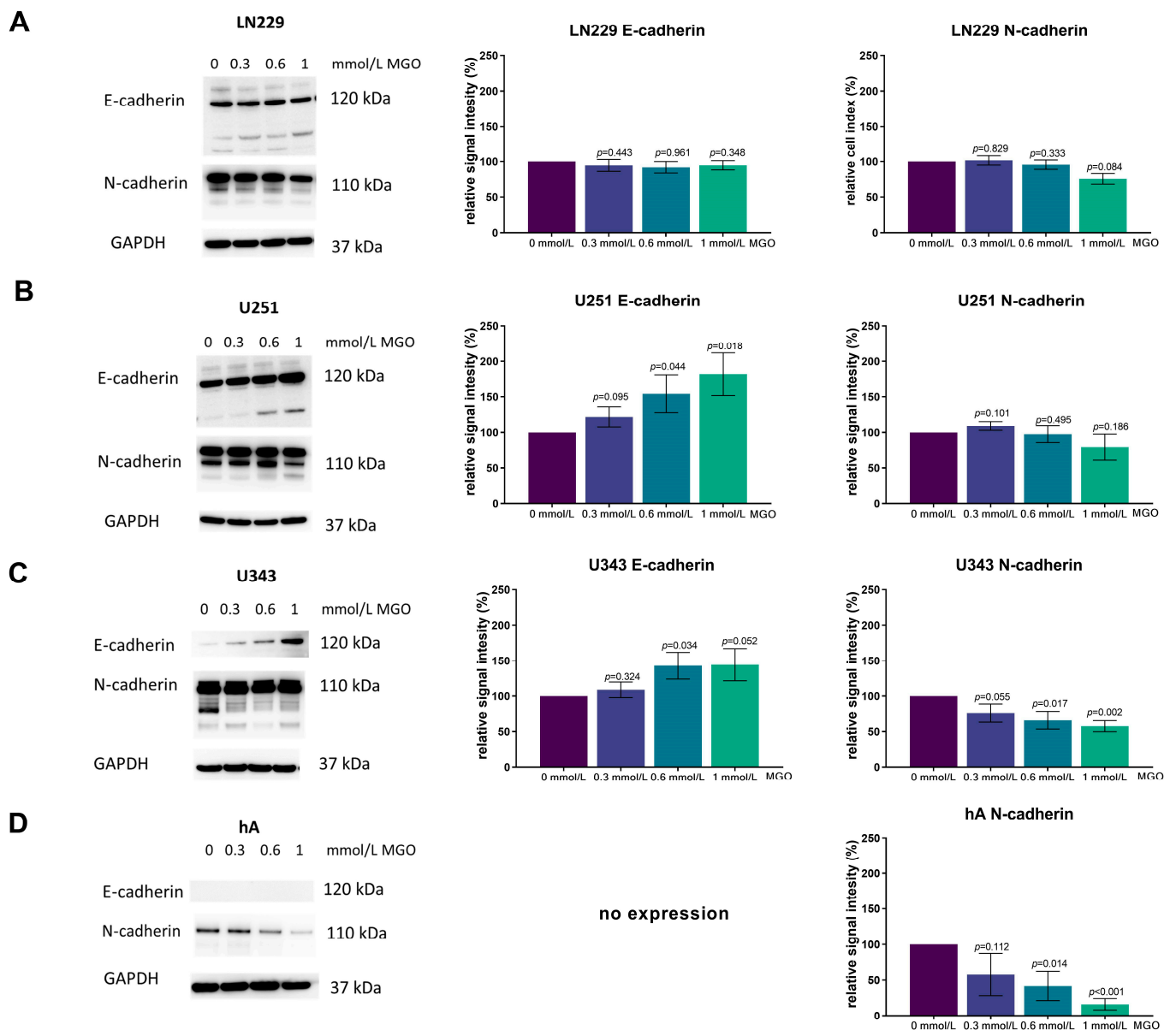


Figure 8. E- and N-cadherin expression after MGO treatment. Immunoblot of LN229 (A), U251 (B), U343 (C), and hA (D) cells with different MGO concentrations (0.3, 0.6, and 1 mmol/L) (left column) and antibody against E- and N-cadherin. GAPDH was used as loading control. Graphs show representative quantification of E-cadherin (middle column) and N-cadherin (right column) Western blots from three independent biological replicates, normalized to the untreated cells. Student’s *t*-test was performed for statistical analysis. Graphs represent the means and SDs.

In the LN229 cell line, the expression of both E- and N-cadherin remained unchanged after MGO treatment (Figure 8A). In the U251 cell line, the E-cadherin expression increased in a concentration-dependent manner, with an increase of $21.74 \pm 14.15\%$; $p = 0.095$, $54.26 \pm 26.53\%$; $p = 0.044$ and $81.86 \pm 30.09\%$; $p = 0.018$ observed with 0.3 mmol/L, 0.6 mmol/L, and 1 mmol/L MGO treatment, respectively. The N-cadherin expression was not affected by MGO treatment (Figure 8B). In the U343 cell line, both the E-cadherin and N-cadherin expressions were altered in a concentration-dependent manner, with E-cadherin increasing and N-cadherin decreasing. The E-cadherin expression increased by about $44.25 \pm 22.90\%$; $p = 0.052$ with 1 mmol/L MGO treatment and the N-cadherin expression decreased by about $42.36 \pm 7.79\%$; $p = 0.002$ with 1 mmol/L MGO treatment (Figure 8C). In the hA cell line, the E-cadherin expression was not detected and was not induced after

glycation. The N-cadherin expression was reduced in a concentration-dependent manner in the hA cells, with a reduction of $42.27 \pm 29.44\%$; $p = 0.112$ with 0.3 mmol/L , $58.27 \pm 20.45\%$; $p = 0.014$ with 0.6 mmol/L ; and $83.93 \pm 8.11\%$; $p < 0.001$ with 1 mmol/L MGO (Figure 8D).

4. Discussion

In earlier studies, MGO was initially thought to be toxic to cancer cells and, thus, considered as a therapeutic agent. However, recent studies have revealed that sub-toxic low doses of MGO can promote tumor development, as cancer cells acquire resistance to apoptosis and enhanced growth properties [25–32]. The glycolytic switch of cancer cells (Warburg effect) and increased glycation could positively impact signaling pathways, promoting tumor invasion and uncontrolled cell proliferation. In our study, we analyzed the effect of MGO on GBM and glioma cell behavior. High MGO concentrations (1 mmol/L) led to cytotoxic effects in all cell lines, but low doses increased invasion in the GBM and glioma cell lines, resulting in a more aggressive phenotype.

Similar outcomes were observed in human meningioma (BEN-MEN-1, WHO grade I) and neuroblastoma (Kelly) cells, where elevated levels of MGO inhibited cell growth and low levels boosted cell invasion [23,24]. Our findings are supported by Nokin et al. The authors implanted U87MG GBM cells on a chicken chorioallantoic membrane and exposed them to increasing MGO concentrations. Low doses of MGO (0.1 and 0.3 mmol/L) significantly increased the tumor volume compared to the untreated tumors, while higher doses (0.5 – 3 mmol/L) significantly reduced it [33]. According to Lee et al., high MGO doses reduce the crucial cell survival signaling pathway, gp130/STAT3, leading to an increased cytotoxicity in rat schwannoma RT4 cells, PC12 cells, and U87MG GBM cells. Lee did not observe significant harm to cell viability at a concentration of 0.5 mmol/L of MGO [34].

The pro-tumorigenic effect of MGO has been extensively studied previously [31]. One of the key mechanisms supporting cancer progression is the evasion of programmed cell death and the inhibition of tumor suppressors. This can occur as a result of the glycation of heat-shock proteins; for instance, MGO-modified heat-shock protein 27 prevents apoptosis of cancer cells in lung and gastrointestinal cancer [25,35]. In breast cancer, the MGO-altered heat shock protein 90 decreased the LATS1 expression, a kinase of the Hippo tumor suppressor pathway, enhancing growth and metastatic potential *in vivo* [27].

Sufficient evidence suggests that MGO increases invasion through various mechanisms. In anaplastic thyroid cancer, MGO promotes migration and EMT through modulation of the TGF- β 1/FAK signaling pathway [36]. Additionally, glycation has been linked to activating the RAGE/TLR4/MyD88 signaling pathway and upregulating MMP9 expression in breast cancer, thus increasing migration and invasion [37]. Moreover, MGO adduct accumulation, which is a consistent feature of high-stage colon carcinomas, has been linked to the promotion of proliferation, invasion, and EMT through the PI3K/AKT signaling pathway [38].

However, the regulations by glycation in cancer cells are described as differential. In hepatocellular carcinoma, glycation impaired migration and adhesion [39]. Interestingly, Selke et al. showed that glycation reduced the invasiveness of WHO grade III IOMM-Lee meningioma cells [23]. Our study also observed a decrease in the invasiveness of normal primary human astrocytes. This implies that the effects of glycation are cell-type specific. Furthermore, the effect of glycation on the ECM components can also be differential. While there is strong evidence for an EMT-like process in GBMs through well-described EMT-promoting pathways, such as ZEB1/ZEB2, SNAI1, SNAI2, TWIST, and the WNT-catenin pathway, we did not observe EMT to be the primary reason for increased invasion in our data [11]. Instead, we propose a reverse process of the mesenchymal-epithelial transition (MET) in the WHO grade III glioma cell line U343 (E-cadherin increase and N-cadherin decrease). Interestingly, Selke et al. also found an upregulation of E-cadherin and a downregulation of N-cadherin in meningioma cells (BEN-MEN-1, WHO grade I), in which increased invasion was observed, suggesting MET potentially having a role in the increased invasion [23]. According to Their et al., carcinoma cells sometimes undergo

MET after dissemination to distant tissue sites and ensuing extravasation in order to efficiently form metastases [40]. In the GBM cell line LN229, even though SNAI1 and SNAI2 was upregulated, E- and N-cadherin remained unaffected while also showing no EMT promoting expression pattern.

While E-cadherin expression is commonly described as non-abundant or absent in gliomas and GBM [41], our data showed E-cadherin expression in all three malignant cell lines (LN229, U251, U343) and an absence in the hA. Additionally, glycation even increased the E-cadherin expression in the U343 and U251 cell lines, where invasion was increased. The E-cadherin expression has been found in certain subtypes of glioblastoma with epithelial and pseudo-epithelial differentiation, where E-cadherin levels even correlated with a worse prognosis [42]. In a Xenograft mouse model by Lewis-Tuffin et al., the E-cadherin expression also correlated with the increased invasiveness of glioma cells. Additionally, endogenous E-cadherin expression promoted the growth and migration of the SF767 glioma cell line [42]. Together with these findings, our results could suggest a currently unknown role for E-cadherin in GBM.

Aberrant N-cadherin expression has been reported in many types of cancer, such as lung-, breast-, prostate-, and squamous cell cancer and has been linked to cell transformation, adhesion, apoptosis, angiogenesis, and invasion [43]. In some studies, N-cadherin expression was found to be upregulated in GBM and linked to the extracellular signal-regulated kinase (ERK) pathway, promoting cancer stem cell invasion [44]. Other researchers reported an inverse correlation between N-cadherin expression and invasion and that the downregulation of N-cadherin was linked to changes in cell polarization and abnormal motile behavior, resulting in increased tumor cell migration and invasiveness [45]. However, no consistent association between N-cadherin and invasiveness has been found in glioblastoma and glioma. We also did not find a correlation between invasiveness and N-cadherin expression.

Glycation also made cell line specific alterations on other ECM components. In our study, we found that glycation increased the expression of CD44 in the U343, U251, and hA cell lines. CD44 is a transmembrane glycoprotein which binds hyaluronic acid in the ECM and is recognized as a molecular marker for cancer stem cells. The binding of hyaluronic acid activates various signaling pathways, leading to cell proliferation, adhesion, migration, and invasion [46]. In GBM, CD44 has been linked to increasing tumor invasiveness, proliferation, and chemotherapy resistance [47]. However, in our study, CD44 upregulation was not associated with the increased invasion of the GBM cell lines.

Brevican and tenascin-C were upregulated in the LN229 and U251 cells, where the strongest increase in invasion was observed. Both brevicin and tenascin-C are glycoproteins in the human brain that are overexpressed in glioma cells and associated with a later tumor stage [48,49]. Brevican promotes glioma cell motility through the upregulation of integrins and proteolytic cleavage by ADAMTS4 [50]. According to Xia et al., tenascin-C increases the GBM invasion of MMP12 and ADAM9 and negatively regulates proliferation [51]. Although strong evidence suggests that versican and thrombospondin play a role in tumor invasion [4,8,52], our study found that they were only upregulated in the LN229 cells. For example, versican enhances locomotion and reduces cell adhesion of astrocytoma cells through the binding of its G1 domain to hyaluronan [53]. Interestingly, thrombospondin is upregulated upon TFG- β stimulation and enhances microtubule formation, which form important structural cell networks of GBM contributing to invasion and treatment resistance [54]. The upregulation of MMP2, which we observed in the LN229 and U343 cells, could increase invasion through remodeling and degradation of ECM.

Despite the differential gene expression of the ECM components, we did not observe any effects of glycation on chemotactic cell migration or adhesion at physiological concentrations. Notably, we only analyzed cell-matrix adhesion and not cell-cell adhesion. Invasion, however, is a fine balance between cell-cell and cell-extracellular matrix adhesions. We concluded that the GBM and glioma cell lined preferred fibronectin as substrate more than collagen IV. Fibronectin is a glycoprotein in the brain parenchyma and its expression is

increased in brain malignancies [55]. Collagen IV is less common in the brain and presence is usually restricted to the basement membrane of blood vessels or the glia limitans, which explains the poorer adherence [56].

In summary, our study found that high concentrations of MGO are cytotoxic to cells and sub-toxic levels lead to an increase in glycation, resulting in a more invasive phenotype of GBM cells (Figure 9). The underlying mechanism behind this correlation is not yet well understood and further analyses are necessary. Additionally, deglycation could present potential for novel therapeutic approaches, such as utilizing MGO scavengers or activating glyoxalase 1. In the case of colon cancer, the use of an MGO scavenger, carnosine, has shown promising results by enhancing the efficacy of cetuximab therapy in KRAS-mutated cancer cells [57].

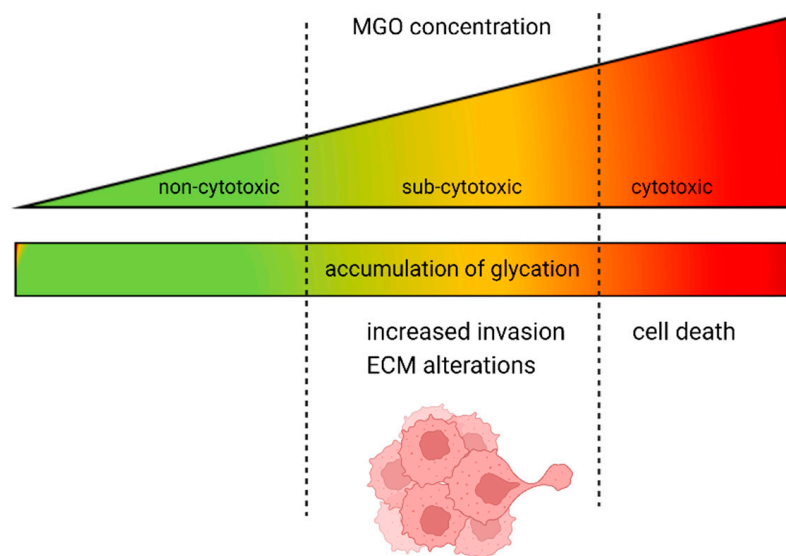


Figure 9. Dual role of MGO in GBM and glioma cells. The increase in glycation is proportional to the rising concentration of MGO. At high doses, MGO has a cytotoxic effect on GBM and glioma cells; however, when present at lower, physiological concentrations, it causes alterations in the ECM and increased invasion.

Limitations

Our study is limited by the fact that we used two glioblastoma cell lines and one glioma cell line. Different cell lines have unique genetic and epigenetic characteristics that affect their responses to glycation. The results may not necessarily apply to primary glioma cells and further analysis is needed to evaluate the effect of glycation in these contexts. Another limiting factor is that the invasion was only analyzed *in vitro*. The *in vitro* model does not accurately depict the complexity of the tumor microenvironment, including the impact of immune cell infiltration, physiological parameters (oxygen and pH), growth and angiogenic factors, and the unique composition and stiffness of the ECM.

5. Conclusions

In our study, we show that MGO leads to glycation in a concentration-dependent manner. While high concentrations of MGO were cytotoxic, lower concentrations increased the invasiveness of the GBM cell lines. In addition, glycation had differential effects on the ECM components that are involved in the invasion progress, upregulating TGF β , brevican, and tenascin C in the GBM cell lines.

Supplementary Materials: The following supporting information can be downloaded at: <https://www.mdpi.com/article/10.3390/cells12091219/s1>, Figure S1. Cell vitality of glioma cell lines and hA after MGO treatment; Figure S2. Microscope imaging of glioma cell lines and hA 48 h after MGO treatment; Table S1. Quantification of microscope imaging of glioma cell lines and hA after 24 h.

Author Contributions: Conceptualization, R.H. and M.S.; methodology, P.S. (Philipp Selke), R.H. and M.S.; formal analysis, P.S. (Paola Schildhauer) and S.L.; investigation, P.S. (Paola Schildhauer); resources, P.S. (Paola Schildhauer), C.S. (Christian Scheller), C.S. (Christian Strauss) and R.H.; data curation, P.S. (Paola Schildhauer), S.L. and M.S.; writing—original draft preparation, P.S. (Paola Schildhauer); writing—review and editing, P.S. (Philipp Selke), C.S. (Christian Scheller), R.H., S.L. and M.S.; supervision, C.S. (Christian Scheller), R.H., S.L. and M.S.; project administration, P.S. (Paola Schildhauer) and M.S.; funding acquisition, P.S. (Paola Schildhauer), C.S. (Christian Scheller), C.S. (Christian Strauss) and R.H. All authors have read and agreed to the published version of the manuscript for the term explanation.

Funding: P.S. (Paola Schildhauer) was funded by a fellowship from the Halle Doctoral College in Medicine (HaPKoM). M.S. was supported by the clinician scientist program of the Medical Faculty of Martin Luther University Halle-Wittenberg. R.H. and P.S. (Philipp Selke) received funding from the DFG (RTG 2155; ProMoAge and research consortium ProDGNE). We acknowledge the financial support within the funding programme Open Access Publishing by the German Research Foundation (DFG).

Institutional Review Board Statement: Not applicable.

Informed Consent Statement: Not applicable.

Data Availability Statement: The dataset is available from the corresponding author upon reasonable request.

Acknowledgments: We would like to thank Jacqueline Kessler (Department of Radiotherapy, Martin Luther University Halle-Wittenberg, Germany) for providing the glioma cell lines.

Conflicts of Interest: The authors declare no conflict of interest.

References

1. Stathis, A. *Treatment Overview. Handbook of Lymphoma*; Springer: Cham, Switzerland, 2016; Volume 20, pp. 33–44. [CrossRef]
2. Cuddapah, V.A.; Robel, S.; Watkins, S.; Sontheimer, H. REVIEWS A Neurocentric Perspective on Glioma Invasion. *Nat. Rev. Neurosci.* **2014**, *15*, 455–465. [CrossRef] [PubMed]
3. Yue, B. Biology of the Extracellular Matrix an Overview. *J. Glaucoma* **2014**, *23*, S20–S23. [CrossRef]
4. So, J.S.; Kim, H.; Han, K.S. Mechanisms of Invasion in Glioblastoma: Extracellular Matrix, Ca²⁺ Signaling, and Glutamate. *Front. Cell. Neurosci.* **2021**, *15*, 663092. [CrossRef] [PubMed]
5. Joester, A.; Faissner, A. The Structure and Function of Tenascins in the Nervous System. *Matrix Biol.* **2001**, *20*, 13–22. [CrossRef] [PubMed]
6. Demuth, T.; Berens, M.E. Molecular Mechanisms of Glioma Cell Migration and Invasion. *J. Neurooncol.* **2004**, *70*, 217–228. [CrossRef]
7. Zhang, H.; Kelly, G.; Zeritlo, C.; Jaworski, D.M.; Hockfield, S. Expression of a Cleaved Brain-Specific Extracellular Matrix Protein Mediates Glioma Cell Invasion in Vivo. *J. Neurosci.* **1998**, *18*, 2370–2376. [CrossRef]
8. Mentlein, R.; Hattermann, K.; Held-Feindt, J. Lost in Disruption: Role of Proteases in Glioma Invasion and Progression. *Biochim. Biophys. Acta* **2012**, *1825*, 178–185. [CrossRef]
9. Wolfenson, H.; Lavelin, I.; Geiger, B. Dynamic Regulation of the Structure and Functions of Integrin Adhesions. *Dev. Cell* **2013**, *24*, 447–458. [CrossRef]
10. Dongre, A.; Weinberg, R.A. New Insights into the Mechanisms of Epithelial–Mesenchymal Transition and Implications for Cancer. *Nat. Rev. Mol. Cell Biol.* **2019**, *20*, 69–84. [CrossRef]
11. Iwadate, Y. Epithelial–Mesenchymal Transition in Glioblastoma Progression. *Oncol. Lett.* **2016**, *11*, 1615–1620. [CrossRef]
12. Nguyen, T.T.T.; Shang, E.; Shu, C.; Kim, S.; Mela, A.; Humala, N.; Mahajan, A.; Yang, H.W.; Akman, H.O.; Quinzii, C.M.; et al. Aurora Kinase A Inhibition Reverses the Warburg Effect and Elicits Unique Metabolic Vulnerabilities in Glioblastoma. *Nat. Commun.* **2021**, *12*, 5203. [CrossRef] [PubMed]
13. Allaman, I.; Bélanger, M.; Magistretti, P.J. Methylglyoxal, the Dark Side of Glycolysis. *Front. Neurosci.* **2015**, *9*, 23. [CrossRef] [PubMed]
14. Manuscript, A. Spinothalamic Tract. *Encycl. Neurosci.* **2008**, *324*, 3828. [CrossRef]
15. Schalkwijk, C.G.; Stehouwer, C.D.A. Methylglyoxal, a Highly Reactive Dicarboxyl Compound, in Diabetes, Its Vascular Complications, and Other Age-Related Diseases. *Physiol. Rev.* **2020**, *100*, 407–461. [CrossRef]

16. Verzijl, N.; DeGroot, J. Crosslinking by Advanced Glycation End Products Increases the Stiffness of the Collagen Network in Human Articular Cartilage. *Arthritis Rheum.* **2002**, *46*, 114–123. [CrossRef] [PubMed]
17. Kass, D.A. Getting Better without Age: New Insights into the Diabetic Heart. *Circ. Res.* **2003**, *92*, 704–706. [CrossRef] [PubMed]
18. Chaplen, F.W.R. Incidence and Potential Implications of the Toxic Metabolite Methylglyoxal in Cell Culture: A Review. *Cytotechnology* **1998**, *26*, 173–183. [CrossRef]
19. Hanssen, N.M.J.; Westerink, J.; Scheijen, J.L.J.M.; Van Der Graaf, Y.; Stehouwer, C.D.A.; Schalkwijk, C.G. Higher Plasma Methylglyoxal Levels Are Associated with Incident Cardiovascular Disease and Mortality in Individuals with Type 2 Diabetes. *Diabetes Care* **2018**, *41*, 1689–1695. [CrossRef]
20. Dariya, B.; Nagaraju, G.P. Advanced Glycation End Products in Diabetes, Cancer and Phytochemical Therapy. *Drug Discov. Today* **2020**, *25*, 1614–1623. [CrossRef]
21. Muthyalaiyah, Y.S.; Jonnalagadda, B.; John, C.M.; Arockiasamy, S. Impact of Advanced Glycation End Products (AGEs) and Its Receptor (RAGE) on Cancer Metabolic Signaling Pathways and Its Progression. *Glycoconj. J.* **2021**, *38*, 717–734. [CrossRef]
22. Chiavarina, B.; Nokin, M.J.; Durieux, F.; Bianchi, E.; Turtoi, A.; Peulen, O.; Peixoto, P.; Irigaray, P.; Uchida, K.; Belpomme, D.; et al. Triple Negative Tumors Accumulate Significantly Less Methylglyoxal Specific Adducts than Other Human Breast Cancer Subtypes. *Oncotarget* **2014**, *5*, 5472–5482. [CrossRef] [PubMed]
23. Selke, P.; Rosenstock, P.; Bork, K.; Strauss, C.; Horstkorte, R.; Scheer, M. Glycation of Benign Meningioma Cells Leads to Increased Invasion. *Biol. Chem.* **2021**, *402*, 849–859. [CrossRef] [PubMed]
24. Scheer, M.; Bork, K.; Simon, F.; Nagasundaram, M.; Horstkorte, R.; Gnanapragassam, V.S. Glycation Leads to Increased Polysialylation and Promotes the Metastatic Potential of Neuroblastoma Cells. *Cells* **2020**, *9*, 868. [CrossRef]
25. van Heijst, J.W.J.; Niessen, H.W.M.; Musters, R.J.; van Hinsbergh, V.W.M.; Hoekman, K.; Schalkwijk, C.G. Argpyrimidine-Modified Heat Shock Protein 27 in Human Non-Small Cell Lung Cancer: A Possible Mechanism for Evasion of Apoptosis. *Cancer Lett.* **2006**, *241*, 309–319. [CrossRef] [PubMed]
26. Lin, J.A.; Wu, C.H.; Yen, G.C. Methylglyoxal Displays Colorectal Cancer-Promoting Properties in the Murine Models of Azoxymethane and CT26 Iso-grafts. *Free Radic. Biol. Med.* **2018**, *115*, 436–446. [CrossRef] [PubMed]
27. Nokin, M.J.; Durieux, F.; Peixoto, P.; Chiavarina, B.; Peulen, O.; Blomme, A.; Turtoi, A.; Costanza, B.; Smargiasso, N.; Baiwir, D.; et al. Methylglyoxal, a Glycolysis Side-Product, Induces Hsp90 Glycation and YAP-Mediated Tumor Growth and Metastasis. *Elife* **2016**, *5*, e19375. [CrossRef] [PubMed]
28. Chiavarina, B.; Nokin, M.J.; Bellier, J.; Durieux, F.; Bletard, N.; Sherer, F.; Lovinfosse, P.; Peulen, O.; Verset, L.; Dehon, R.; et al. Methylglyoxal-Mediated Stress Correlates with High Metabolic Activity and Promotes Tumor Growth in Colorectal Cancer. *Int. J. Mol. Sci.* **2017**, *18*, 213. [CrossRef]
29. Sharaf, H.; Matou-Nasri, S.; Wang, Q.; Rabhan, Z.; Al-Eidi, H.; Al Abdulrahman, A.; Ahmed, N. Advanced Glycation Endproducts Increase Proliferation, Migration and Invasion of the Breast Cancer Cell Line MDA-MB-231. *Biochim. Biophys. Acta-Mol. Basis Dis.* **2015**, *1852*, 429–441. [CrossRef]
30. Suh, Y.J.; Hall, M.S.; Huang, Y.L.; Moon, S.Y.; Song, W.; Ma, M.; Bonassar, L.J.; Segall, J.E.; Wu, M. Glycation of Collagen Matrices Promotes Breast Tumor Cell Invasion. *Integr. Biol.* **2019**, *11*, 109–117. [CrossRef]
31. Leone, A.; Nigro, C.; Nicolò, A.; Prevenzano, I.; Formisano, P.; Beguinot, F.; Miele, C. The Dual-Role of Methylglyoxal in Tumor Progression—Novel Therapeutic Approaches. *Front. Oncol.* **2021**, *11*, 645686. [CrossRef]
32. Bellahcène, A.; Nokin, M.J.; Castronovo, V.; Schalkwijk, C. Methylglyoxal-Derived Stress: An Emerging Biological Factor Involved in the Onset and Progression of Cancer. *Semin. Cancer Biol.* **2018**, *49*, 64–74. [CrossRef]
33. Nokin, M.; Durieux, F.; Bellier, J.; Peulen, O.; Uchida, K.; David, A.; Cochrane, J.R.; Hutton, C.A.; Castronovo, V.; Bellahcène, A. Hormetic Potential of Methylglyoxal, a Side-Product of Glycolysis, in Switching Tumours from Growth to Death. *Sci. Rep.* **2017**, *7*, 11722. [CrossRef]
34. Lee, H.K.; Seo, I.A.; Suh, D.J.; Lee, H.J.; Park, H.T. A Novel Mechanism of Methylglyoxal Cytotoxicity in Neuroglial Cells. *J. Neurochem.* **2009**, *108*, 273–284. [CrossRef]
35. Oya-Ito Tomoko, T.; Naito, Y.; Takagi, T.; Handa, O.; Matsui, H.; Yamada, M.; Shima, K.; Yoshikawa, T. Heat-Shock Protein 27 (Hsp27) as a Target of Methylglyoxal in Gastrointestinal Cancer. *Biochim. Biophys. Acta-Mol. Basis Dis.* **2011**, *1812*, 769–781. [CrossRef]
36. Antognelli, C.; Moretti, S.; Frosini, R.; Puxeddu, E.; Sidoni, A.; Talesa, V.N. Methylglyoxal Acts as a Tumor-Promoting Factor in Anaplastic Thyroid Cancer. *Cells* **2019**, *8*, 547. [CrossRef] [PubMed]
37. Pan, S.; Guan, Y.; Ma, Y.; Cui, Q.; Tang, Z.; Li, J.; Zu, C.; Zhang, Y.; Zhu, L.; Jiang, J.; et al. Advanced Glycation End Products Correlate with Breast Cancer Metastasis by Activating RAGE/TLR4 Signaling. *BMJ Open Diabetes Res. Care* **2022**, *10*, e002697. [CrossRef]
38. Liang, H. Advanced Glycation End Products Induce Proliferation, Invasion and Epithelial-Mesenchymal Transition of Human SW480 Colon Cancer Cells through the PI3K/AKT Signaling Pathway. *Oncol. Lett.* **2020**, *19*, 3215–3222. [CrossRef]
39. Loarca, L.; Sassi-gaha, S.; Artlett, C.M. Two α -Dicarbonyls Downregulate Migration, Invasion, and Adhesion of Liver Cancer Cells in a P53-Dependent Manner. *Dig. Liver Dis.* **2013**, *45*, 938–946. [CrossRef]
40. Their, J.P. Epithelial-Mesenchymal Transitions in Tumor Progression. *Nat. Rev. Cancer* **2002**, *2*, 442–454. [CrossRef]
41. Hwang, S.L.; Wu, C.H.; Cheng, T.S.; Sy, W.D.; Lin, P.C.K.; Wang, C.; Hong, Y.R. Differential Expression of Wnt Genes, β -Catenin and E-Cadherin in Human Brain Tumors. *Cancer Lett.* **2002**, *183*, 95–101. [CrossRef] [PubMed]

42. Lewis-Tuffin, L.J.; Rodriguez, F.; Giannini, C.; Scheithauer, B.; Necela, B.M.; Sarkaria, J.N.; Anastasiadis, P.Z. Misregulated E-Cadherin Expression Associated with an Aggressive Brain Tumor Phenotype. *PLoS ONE* **2010**, *5*, e13665. [CrossRef] [PubMed]
43. Cao, Z.Q.; Wang, Z.; Leng, P. Aberrant N-Cadherin Expression in Cancer. *Biomed. Pharmacother.* **2019**, *118*, 109320. [CrossRef]
44. Velpula, K.K.; Rehman, A.A.; Chelluboina, B.; Dasari, V.R.; Gondi, C.S.; Rao, J.S.; Veeravalli, K.K. Glioma Stem Cell Invasion through Regulation of the Interconnected ERK, Integrin A6 and N-Cadherin Signaling Pathway. *Cell. Signal.* **2012**, *24*, 2076–2084. [CrossRef]
45. Camand, E.; Peglion, F.; Osmani, N.; Sanson, M.; Etienne-Manneville, S. N-Cadherin Expression Level Modulates Integrin-Mediated Polarity and Strongly Impacts on the Speed and Directionality of Glial Cell Migration. *J. Cell Sci.* **2012**, *125*, 844–857. [CrossRef] [PubMed]
46. Senbanjo, L.T.; Chellaiah, M.A. CD44: A Multifunctional Cell Surface Adhesion Receptor Is a Regulator of Progression and Metastasis of Cancer Cells. *Front. Cell Dev. Biol.* **2017**, *5*, 18. [CrossRef]
47. Ivanova, E.L.; Costa, B.; Eisemann, T.; Lohr, S.; Boskovic, P.; Eichwald, V.; Meckler, J.; Jugold, M.; Orian-Rousseau, V.; Peterziel, H.; et al. CD44 Expressed by Myeloid Cells Promotes Glioma Invasion. *Front. Oncol.* **2022**, *12*, 3957. [CrossRef]
48. Lu, R.; Wu, C.; Guo, L.; Liu, Y.; Mo, W.; Wang, H.; Ding, J.; Wong, E.T.; Yu, M. The Role of Brevican in Glioma: Promoting Tumor Cell Motility in Vitro and in Vivo. *BMC Cancer* **2012**, *12*, 607. [CrossRef] [PubMed]
49. Xia, S.; Lal, B.; Tung, B.; Wang, S.; Goodwin, C.R.; Lattera, J. Tumor Microenvironment Tenascin-C Promotes Glioblastoma Invasion and Negatively Regulates Tumor Proliferation. *Neuro-Oncology* **2016**, *18*, 507–517. [CrossRef]
50. Viapiano, M.S.; Hockfield, S.; Matthews, R.T. BEHAB/Brevican Requires ADAMTS-Mediated Proteolytic Cleavage to Promote Glioma Invasion. *J. Neurooncol.* **2008**, *88*, 261–272. [CrossRef]
51. Sarkar, S.; Zemp, F.J.; Senger, D.; Robbins, S.M.; Yong, V.W. ADAM-9 is a novel mediator of tenascin-C-stimulated invasiveness of brain tumor-initiating cells. *Neuro-Oncology* **2015**, *17*, 1095–1105. [CrossRef] [PubMed]
52. Vollmann-Zwerenz, A.; Leidgens, V.; Feliciello, G.; Klein, C.A.; Hau, P. Tumor Cell Invasion in Glioblastoma. *Int. J. Mol. Sci.* **2020**, *21*, 1932. [CrossRef]
53. Ang, L.C.; Zhang, Y.; Cao, L.; Yang, B.L.; Young, B.; Kiani, C.; Lee, V.; Allan, K.; Yang, B.B. Versican Enhances Locomotion of Astrocytoma Cells and Reduces Cell Adhesion through Its G1 Domain. *J. Neuropathol. Exp. Neurol.* **1999**, *58*, 597–605. [CrossRef]
54. Joseph, J.V.; Magaut, C.R.; Storevik, S.; Geraldo, L.H.; Mathivet, T.; Latif, A.; Rudewicz, J.; Guyon, J.; Gambaretti, M.; Haukas, F.; et al. TGF- β promotes microtubule formation in glioblastoma through Thrombospondin 1. *Neuro-Oncology* **2022**, *24*, 541–553. [CrossRef] [PubMed]
55. Yu, Q.; Xue, Y.; Liu, J.; Xi, Z.; Li, Z.; Liu, Y.; Gregory, B.; Oliver, G. Fibronectin Promotes the Malignancy of Glioma Stem-Like Cells Via Modulation of Cell Adhesion, Differentiation, Proliferation and Chemoresistance. *Front. Mol. Neurosci.* **2018**, *11*, 130. [CrossRef] [PubMed]
56. Mohiuddin, E.; Wakimoto, H. Extracellular Matrix in Glioblastoma: Opportunities for Emerging Therapeutic Approaches. *Am. J. Cancer Res.* **2021**, *11*, 3742–3754. [PubMed]
57. Bellier, J.; Nokin, M.; Caprasse, M.; Peulen, O.; Bellier, J.; Nokin, M.; Caprasse, M.; Tiamiou, A.; Blomme, A.; Scheijen, J.L.; et al. Methylglyoxal Scavengers Resensitize KRAS-Mutated Colorectal Tumors to Cetuximab. *Cell Rep.* **2020**, *30*, 1400–1416. [CrossRef]

Disclaimer/Publisher’s Note: The statements, opinions and data contained in all publications are solely those of the individual author(s) and contributor(s) and not of MDPI and/or the editor(s). MDPI and/or the editor(s) disclaim responsibility for any injury to people or property resulting from any ideas, methods, instructions or products referred to in the content.

Review

Utility of the Cerebral Organoid Glioma ‘GLICO’ Model for Screening Applications

Freya R. Weth^{1,2}, Lifeng Peng², Erin Paterson¹, Swee T. Tan^{1,3,4}  and Clint Gray^{1,*}

- ¹ Gillies McIndoe Research Institute, 7 Hospital Road, Wellington 6021, New Zealand
² Centre for Biodiscovery and School of Biological Sciences, Victoria University of Wellington, Wellington 6021, New Zealand
³ Wellington Regional Plastic, Maxillofacial & Burns Unit, Hutt Hospital, Lower Hutt 5040, New Zealand
⁴ Department of Surgery, The Royal Melbourne Hospital, The University of Melbourne, Melbourne, VIC 3010, Australia
* Correspondence: clint.gray@gmri.org.nz

Abstract: Glioblastoma, a grade IV astrocytoma, is regarded as the most aggressive primary brain tumour with an overall median survival of 16.0 months following the standard treatment regimen of surgical resection, followed by radiotherapy and chemotherapy with temozolomide. Despite such intensive treatment, the tumour almost invariably recurs. This poor prognosis has most commonly been attributed to the initiation, propagation, and differentiation of cancer stem cells. Despite the unprecedented advances in biomedical research over the last decade, the current in vitro models are limited at preserving the inter- and intra-tumoural heterogeneity of primary tumours. The ability to understand and manipulate complex cancers such as glioblastoma requires disease models to be clinically and translationally relevant and encompass the cellular heterogeneity of such cancers. Therefore, brain cancer research models need to aim to recapitulate glioblastoma stem cell function, whilst remaining amenable for analysis. Fortunately, the recent development of 3D cultures has overcome some of these challenges, and cerebral organoids are emerging as cutting-edge tools in glioblastoma research. The opportunity to generate cerebral organoids via induced pluripotent stem cells, and to perform co-cultures with patient-derived cancer stem cells (GLICO model), has enabled the analysis of cancer development in a context that better mimics brain tissue architecture. In this article, we review the recent literature on the use of patient-derived glioblastoma organoid models and their applicability for drug screening, as well as provide a potential workflow for screening using the GLICO model. The proposed workflow is practical for use in most laboratories with accessible materials and equipment, a good first pass, and no animal work required. This workflow is also amenable for analysis, with separate measures of invasion, growth, and viability.

Keywords: glioblastoma; glioblastoma organoids; glioblastoma spheroids; cerebral organoids; glioblastoma stem cells; cancer stem cells; drug screening



Citation: Weth, F.R.; Peng, L.; Paterson, E.; Tan, S.T.; Gray, C. Utility of the Cerebral Organoid Glioma ‘GLICO’ Model for Screening Applications. *Cells* **2023**, *12*, 153. <https://doi.org/10.3390/cells12010153>

Academic Editors: Javier S. Castresana and Bárbara Meléndez

Received: 3 November 2022

Revised: 23 December 2022

Accepted: 27 December 2022

Published: 30 December 2022



Copyright: © 2022 by the authors. Licensee MDPI, Basel, Switzerland. This article is an open access article distributed under the terms and conditions of the Creative Commons Attribution (CC BY) license (<https://creativecommons.org/licenses/by/4.0/>).

1. Introduction

Glioblastoma is the most common and most aggressive primary brain tumour, characterised by high recurrence rates and exceptionally poor prognosis [1]. Standard treatment involves intensive multimodal therapy including tumour resection, tumour-treating fields (TTF) radiotherapy or standard radiotherapy, and chemotherapy with Temozolomide (TMZ). The overall median survival is only 16.0 months, with TTF-treated patients reaching an average of 20.9 months [2]. Despite such intensive treatment, less than 30% of patients survive more than 2 years [3]. The inability to effectively treat glioblastoma is due, in part, to the ability of a subpopulation of tumorigenic cells to infiltrate normal brain tissue, preventing complete surgical removal of cancer cells, leading to subsequent recurrence [4].

Improved treatments that target the source of chemotherapy resistance and tumour recurrence are urgently needed, as the overall median survival rates have remained relatively unchanged for 30 years [5].

For glioblastoma to establish beyond the primary site within the brain, this subpopulation of cells must be able to self-renew, generate differentiated tumour cells, and spawn a heterogeneous tumour [6]. Glioblastoma, like hematopoietic malignancies and other solid cancers, has been shown to comprise a small population of cancer stem cells (CSCs) known as glioma stem cells (GSCs) [7], which possess the capacity to recapitulate the heterogeneity of the parent tumour after serial dilution and intracranial implantation into immune-compromised mice [8]. Moreover, GSCs demonstrate particularly infiltrative properties and are thought to be primary contributors to chemotherapy and radiotherapy resistance and tumour recurrence [9]. Therefore, selectively targeting GSC proliferation and invasion in combination with current therapies is seen as a viable option to improve treatment outcomes for glioblastoma patients [10,11].

Proof-of-principle genetic studies have shown that blocking the self-renewal of GSCs leads to prolonged survival in GSC patient-derived mouse efficacy studies [12]. However, identifying optimal GSC-drug targets for clinical translation remains elusive [13]. Establishing disease models that recapitulate the function, heterogeneity, and behaviour of glioblastoma within the brain is therefore a high priority for the evaluation of new therapeutics. Past research into drug treatments for glioblastoma has often relied upon 2D cell culture methods—such as adherent cell culture, in which commonly established cell lines grow in a monolayer attached to a flat surface [14]. Such methods provided a foundation for basic research but have struggled to recapitulate essential features of glioblastoma cells within the brain, such as tumour heterogeneity. Fortunately, recent developments have allowed primary patient-derived tumour cells to be cultured in both 2D and 3D conditions (as both spheroids and organoids). These 3D models can better mimic tumour growth and reflect tumour cell contact within the *in vivo* tumour microenvironment, features which are not present in a traditional monolayer cell culture context [15]. Additionally, 3D cultures will mimic some of the physical barriers that therapeutic agents encounter when delivered *in vivo* that are not present in typical 2D cultures, such as hypoxia and impeded diffusion [14,15], ameliorating some of these limitations.

Recent studies have enabled drug screening using patient-derived glioblastoma 3D spheroid cultures [16,17]. Using a 1536-well format and an ultra-high throughput proliferation assay, Quereda et al. [18] demonstrate the applicability of this assay for large-scale high-throughput drug screening. Recent studies have also enabled the generation of a patient-derived glioblastoma-cerebral organoid model in which the resultant tumours phenocopy the patient's original glioblastoma tumour [19], allowing the study of glioblastoma biology in a human brain model. In this article, we review recent literature on the use of patient-derived glioblastoma organoid models and their applicability for drug screening, as well as providing a potential workflow for screening, using the GLICO model.

2. The Necessity of Human Cell-Based Models for Brain Tumour Research

A major challenge in glioblastoma research is to develop disease models that mirror the cellular complexity, aggressive nature and treatment resistance observed *in vivo*. Previous research models for drug testing and development have relied on an oversimplified approach which has resulted in many of the drugs investigated in traditional preclinical models (2D adherent culture, murine xenografts) yielding suboptimal results in clinical trials, culminating in an FDA approval rate as low as 3% for new oncologic therapies [20].

Established commercial cell lines grown *in vitro* in 2D adherent culture, offer only modest real-world disease relevance, due to the lack of spatial organisation, cellular heterogeneity, and interaction with non-cancer support cells [21]. Typical established cancer cell lines derived from patient tissues are inefficiently generated and involve extensive adaptation and clonal selection in 2D culture conditions [22]. Only rare clones can be expanded and maintained over many passages; those that can, may have been subject

to substantial genetic alterations, and may not recapitulate the genetic complexity of the parent tumour [22]. 2D adherent cultures are not able to accurately translate the function of a human brain and recapitulate the necessary hurdles drugs may encounter in the body—such as hypoxia and impeded diffusion, which calls into question their utility for drug development and testing.

Alternatively, transplantation of patient-derived tumour cells into the brains of immune-compromised mice (xenograft models) provides an *in vivo*-like model system to investigate the dynamic interplay between GSCs, which drive tumourigenesis, and the non-cancer microenvironment [23]. Unlike invertebrate model systems, tumour development in mice is accompanied by other complex biological processes such as angiogenesis, similar to those in a human cancer [24]. Although there are similarities in the overall cellular architecture between murine and human brains, mice have a much more primitive neocortex which is most highly evolved brain component in humans [25,26]. More importantly, despite similarities in cellular architecture, there are stark differences in gene expression patterns [27], especially of non-neuronal cells such as microglia [28]. Neurons in the human cortex arise from outer radial glia, which are not present (or are very sparse) in rodents [29]. This has important implications, as emerging genomic data from studies in human glioblastoma suggests an important role of non-neuronal cell types such as microglia in the evolution of glioblastoma [30,31]. Further, the genomic evolution of human tumour cells can be altered by the host; brain tumours are not cell autonomous, and they generate properties specific to the host [32]. This may dampen the translational relevance of some aspects of the mouse xenograft model system for drug screening and prediction of human responses in research. Immunodeficient animal husbandry is also a specialised and high-cost procedure with low throughput capabilities for drug screening due to the time taken to generate mice [24].

Recent advances in cell culture technology have led to the development of organoid models that mimic *in vivo* organ development, increasing our ability to study cellular diversity and complex tissue structures (Figure 1). The establishment of these systems involves either induced pluripotent stem cells (iPSCs) or adult stem cells (AdSC) isolated from a patient that, over extended periods of time, are exposed to various differentiation cues to mimic the developmental process [29]. Stem cells first aggregate to form organ buds and with further long-term culturing, can form organoids [33]. These 3D organoid models are used to study tumour initiation, progression, invasion, and response to drug treatments [34]. Recently, brain organoids developed from human iPSCs have been shown to recapitulate spatial organisation more accurately, cell–cell and cell-niche interactions found in the human brain [35].

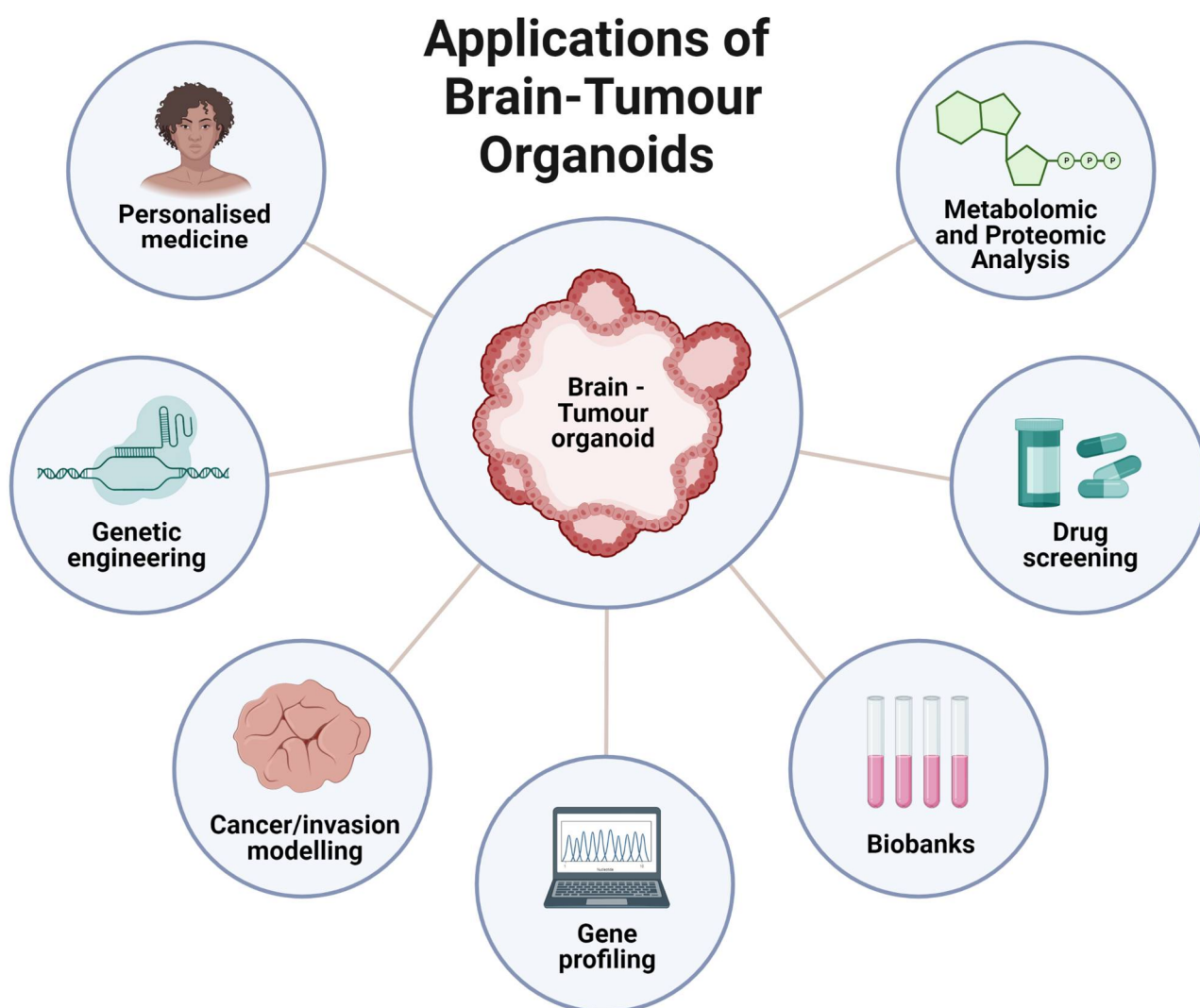


Figure 1. Applications of Brain-Tumour Organoids. Recent advances in cell culture technology have allowed the use of organoids as model systems for a myriad of applications such as personalised medicine, genetic engineering, cancer and invasion modelling, gene profiling, primary cell/tumour biobanks, drug screening, and metabolomic/ proteomic analyses. Created with Biorender.com accessed on 25 September 2022.

3. The Role of Glioma Stem Cells in Glioblastoma

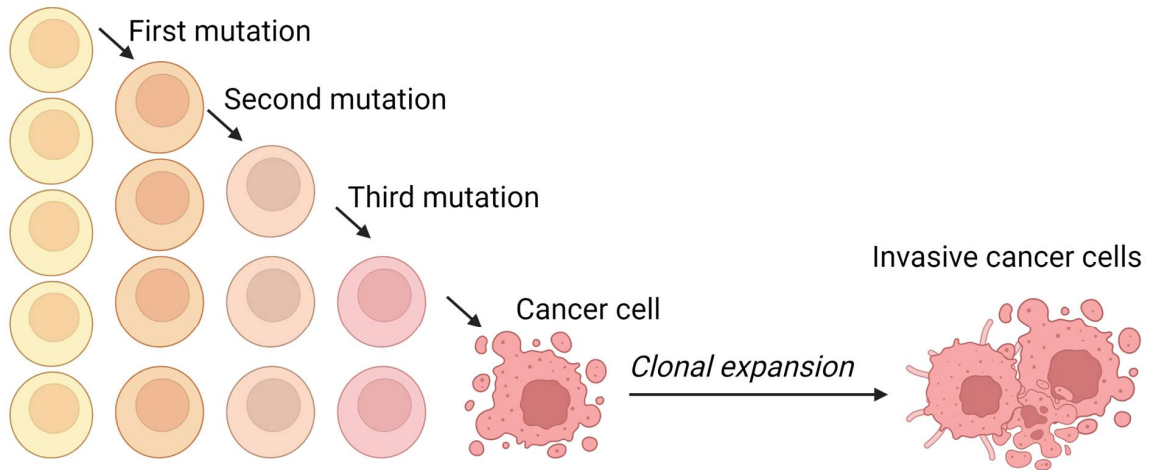
The cancer stem cell (CSC) concept of cancer, first proposed more than four decades ago, states that tumour growth is comparable to healthy tissue generation, i.e., it is fuelled by a small population of dedicated stem cells [12]. Decades of developmental and haematopoietic stem cell research [36] support this hypothesis; that cancer growth is maintained exclusively by a small subpopulation of cells with stem cell properties [12,37]. This explains clinical observations such as tumour dormancy, metastasis, and recurrence despite multimodal therapies [38] (Figure 2) and has provided an additional focus into how we should approach cancer treatment [37]. Instead of simply trying to minimise the size of tumours, focus needs to be placed on regulating CSCs—the controllers of long-term growth, tumour recurrence, and invasiveness [39].

In 2003, Singh et al. were the first to isolate CSCs from human brain tumours [40]. These cells exhibit stem cell properties *in vitro* and express CD133 (CD133+), a transmembrane cell-surface glycoprotein and stem cell biomarker. When transplanted into non-obese diabetic, severe combined immunodeficient mice, these cells are capable of both initiating tumour growth, and recapitulating the original parent tumour *in vivo* [40]. Glioblastoma

CSCs have since been coined GSCs which are quiescent-neoplastic cells [41,42], imbued with multipotency, and self-renewal properties.

A Stochastic Model of Cancer

Normal somatic cell



B Hierarchical Model of Cancer

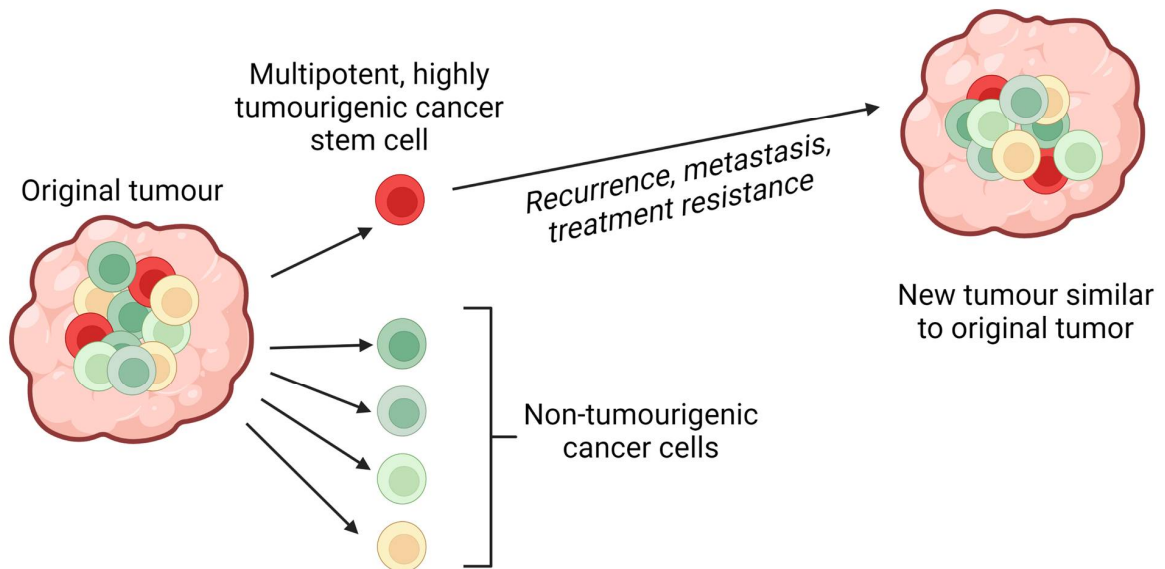


Figure 2. (A) The stochastic model of cancer proposes that a normal somatic cell accumulates oncogenic mutations in a stepwise manner and becomes a cancer cell that undergoes clonal expansion to form a tumour. (B) The hierarchical model of cancer proposes the presence of a highly tumourigenic cancer stem cell (CSC) sitting atop the tumour cellular hierarchy and divides asymmetrically to form non-tumourigenic cancer cells that form the bulk of the tumour, and identical CSCs that form new tumours like the original tumour. Created with Biorender.com accessed on 1 October 2022.

Through histological classification, glioblastoma has been traditionally classified as an astrocytoma, although the precise cell type from which the tumour originates is still a controversial issue. Some experts argue that the glioblastoma origin is a subpopulation of neural stem cells, while others propose that it is derived from differentiated astrocytes (Figure 2) [43]. It had long been thought to arise from differentiated glial cells of the central nervous system—hence the name glioblastoma [44]. The eventual isolation of CD133+ (GSC) cells [43] implies that a hierarchy may exist within the tumour cell population [9], because not all cells can maintain the tumour in culture [45]. Normal neural stem cells are also present in the CD133+ population of the foetal brain, suggesting that they may be the cell of origin for glioblastoma [46]. Recently, astrocyte-like neural stem cells in the subventricular zone have been proposed as the cell of origin for glioblastoma [47]. Further research into GSCs and further identification of neural stem cell surface markers may provide insight into this possibility. This could also clarify whether GSCs sit atop a lineage hierarchy or further down as lineage-restricted progenitor cells. Interestingly, emerging evidence suggests that GSCs in glioblastoma are highly heterogenous and rather than occupying an apex, are best described by their cellular state [8]. In support of this, Guilhamon et al. [48] show that chromatin accessibility in GSCs is a critical measure of their invasive property, which is linked to poor survival rates glioblastoma IDH-wild type cohort in the Cancer Genome Atlas, as well as when used in an orthotopic glioblastoma murine model.

GSCs are thought to be the initiators of tumour recurrence and the major contributor to the aggressive nature of glioblastoma [49]. They have been demonstrated to be inherently resistant to conventional therapies through multiple mechanisms, including increased transcription of anti-apoptotic genes and efflux transporters and increased capacity for DNA damage repair [13,24]. GSCs give rise to treatment-resistant clones that aggressively invade normal brain tissue, which is the primary cause of death [38]. Considerable evidence has been generated to support the concept that GSCs are the most biologically and phenotypically relevant cells to the parent tumour in glioblastoma patients [50]. GSCs have the innate capacity for self-renewal and multi-lineage differentiation. These cells are required for tumour initiation, maintenance, and invasion in vivo [51]. Furthermore, compared to other tumour cells, GSCs exhibit increased resistance to chemotherapy and radiotherapy, implicating them in glioblastoma treatment resistance [38] (Figure 3).

Given their vital role in glioblastoma, it seems logical to specifically target GSCs to achieve a durable treatment for glioblastoma. However, therapies aimed at intrinsic mechanisms of GSC proliferation have so far offered only limited success, partly due to the lack of suitable experimental model systems that recapitulate the complex invasive behaviour of GSCs in the human brain. The ability to understand and manipulate complex cancers such as glioblastoma—requires clinically relevant models which encompass the complexity of these tumours and can be used in drug development and testing [52]. Therefore, glioblastoma research models need to aim to recapitulate GSC function within the brain, whilst still being amenable for analysis.

Hallmarks of Glioma Stem Cells

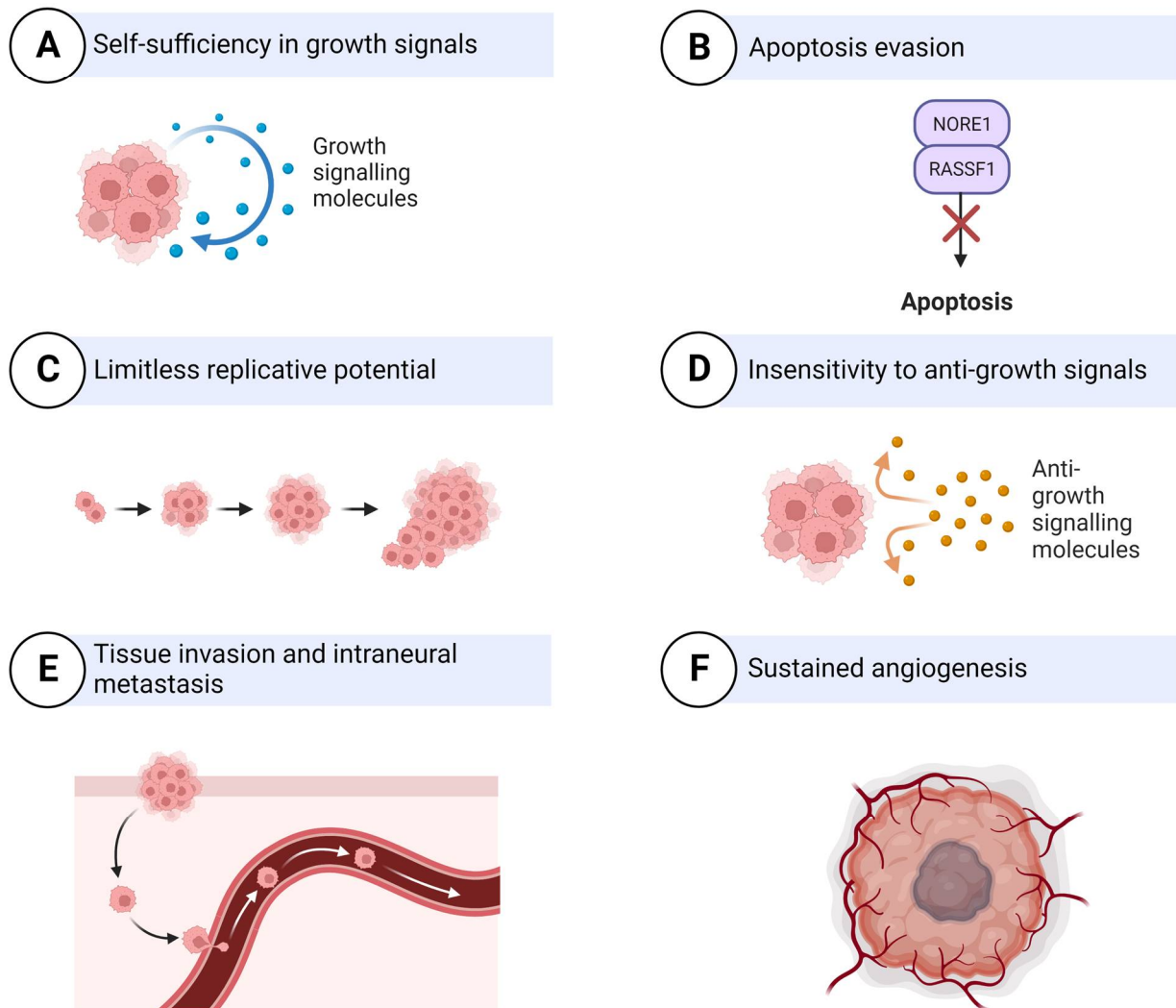


Figure 3. Hallmarks of Glioma Stem Cells (GSCs). GSCs are the primary contributors to the aggressive nature of glioblastoma. The features that make these cells particularly invasive are self-sustained growth signalling, evasion of programmed cell death, limitless replicative potential with minimal cell senescence, tissue invasion and intraneural metastasis and sustained angiogenesis/increased vascularisation. Adapted from Biorender.com accessed on 1 October 2022.

4. Patient-Derived Glioblastoma Organoids

Fortunately, the use of patient-derived tumour cells for the development of tumour spheroids and human cerebral organoids to both characterise and model glioblastoma has gone some way to fulfilling this need. Human cerebral organoids are powerful *in vitro* systems that recapitulate many aspects of human brain development and function [6].

The GSC subpopulation has often been associated with invasion as well as radiotherapy and chemotherapy resistance [38]. The interaction of GSCs with the tumour microenvironment and the ability for quiescence and regeneration is what seems to promote survival and makes these cells difficult to target with chemotherapeutics [32]. GSCs are present throughout the entire glioblastoma tumour. They are localised in both the dense core (hypoxic microenvironment) and at the proliferating edge (increased vascularisation) of the tumour [17,53], surrounded by immune cells such as microglia, which all influence survival and the stem-like state of GSCs [17,30,54].

GSCs isolated from tumour biopsies have been shown to recapitulate the heterogeneity of the patient's tumour when differentiated in culture or upon xenotransplantation into immune-deficient mice [16,55]. When commercialised glioblastoma cell lines are grown in adherent 2D monolayer cultures without specialised media containing relevant mitogens, they lack the intrinsic heterogeneity and 3D spatial organisation of the patient's parent tumour [22,56]. Treatment efficacy assays performed on 2D adherent cells often do not translate well to clinical use, with drugs that initially prove effective in the context of 2D cultured cell lines seldom yield equivalent results in a clinical trial setting [14,57,58]. More refined model systems that allow the recapitulation of complex cancer phenotypes and retain the ability to perform detailed analysis are urgently needed.

Patient-derived GSCs can be grown and sustained under specific culture conditions *in vitro*; with media supplemented with growth factors such as epidermal growth factor and fibroblast growth factor-2 [55]. These conditions can also be used for the expansion of neural stem cells, highlighting the close relationship between these two types of cells [7]. GSCs can be expanded in 2D adherent culture with supplemented media containing relevant GSC growth factors, or as 3D neurospheres [7,59]. Neurospheres, herein referred to as glioblastoma spheroids, can be considered the first "3D model" of glioblastoma, as cells maintain a certain degree of 7 polarisation and 3D spatial organisation [60]. Glioblastoma spheroids, however, have necrotic cores due to the absence of vasculature and can achieve a maximum size of ~300–400 μm before needing disruption and replating to survive [15,61]. On their own, glioblastoma spheroids are unable to form interactions with extracellular matrices or other healthy cells required to generate the specific tumour microenvironment, so are unlikely to completely replicate *in vivo* GSC behaviour [16].

Formation of human cerebral organoids involves stem cells, either iPSCs or AdSCs, which are sequentially exposed to specific and appropriate exogenous signals to stimulate the developmental process. These conditions allow stem cells to differentiate and aggregate to first form an organ bud/embryoid bodies, and over longer culture, form a cerebral organoid. Mature cerebral organoids can contain differentiated astrocytes, mature neuronal cell types, and even surprisingly microglia-like cells. Ramani et al., surprisingly observed microglial cells and astrocytes in their organoids [62]. Even though it is difficult to explain the development of non-ectodermal related cell types under controlled differentiation conditions, cerebral organoids appear to have some degree of plasticity depending on the differentiation cues.

Due to their potential utility for drug discovery and development, there are many organoid-glioblastoma models that have been developed recently. Hubert et al. [16] cultured minced pieces of resected glioblastoma from patients which successfully formed more complex organoid structures composed of multiple cell types. These organoids recapitulate key glioblastoma features, such as hypoxic gradients, cellular morphology, spacial distribution, and resistance to radiation, however, *in vivo* GSCs are not autonomous but are heavily influenced by tumour–host cell interactions and the tumour microenvironment [5], which this model does not particularly account for.

Along a similar vein are Bioprinted glioblastoma organoids, which are generated through patient-derived dissociated glioblastoma cells combined with a decellularised porcine brain 'bioink' composed of extracellular matrix proteins. On top of this, a layer of human umbilical vein endothelial cells is printed in the same bioink [63]. This model shows the invasion of the organoid into the surrounding endothelial cells and other key features of glioblastoma such as a hypoxic gradient and the presence of multiple cell types. However, there is still a lack of normal brain tissue for interaction as well as the requirement for costly specialised equipment.

Genetically modified cerebral organoids such as neoplastic cerebral organoids (neoCOR) have mutations introduced to induce the expression of oncogenes to cause tumorigenesis within developing iPSC-derived organoids [64,65]. NeoCORs are composed of both healthy and tumour tissue, allowing the study of tumour–brain interactions. However, their ability to recapitulate the heterogeneity of *in situ* glioblastoma remains to be seen, as they

are limited to known mutations of oncogenes that have been studied to date. Such tumour models are advantageous to model glioblastoma initiation, but they hardly recapitulate the genomic complexity of heterogeneous patient tumours, so their utility for drug screening remains limited.

A novel approach to overcome this disadvantage has been pioneered by the laboratories of Howard Fine and Amanda Linkous. This approach involves co-culture of patient-derived GSCs in the form of tumour spheroids, with iPSC-derived human cerebral organoids [66]. The authors co-cultured patient-derived GFP-tagged GSC cell lines with mature cerebral organoids and were able to show that GSCs proliferate, form microtubules, and integrate into the organoids. This model has been termed Glioma Cerebral Organoids (GLICO) [19,67]. The authors showed that different primary patient lines behaved in unique ways, with some showing diffuse invasion, others forming honeycomb-like structures, and some forming regional ‘nodes’ of proliferation [33]. The authors also found that co-cultured GSCs with the greatest invasiveness were more lethal when transplanted into mice [64], suggesting that the observed heterogeneity in growth and invasion in the GLICO model likely reflects certain intrinsic properties of patient-derived GSCs.

The behaviour of cancer cells in this system not only mimics the original tumour, but also maintains key genetic aberrations of the patient’s original tumour [19]. EGFR amplification was identified in two of their primary lines and was maintained in the GLICO model, but was lost in 2D adherent culture [19], indicating that this model may provide a more suitable tumour microenvironment to preserve the genetic characteristics of the tumour *in vivo*.

Unlike animal brains, human cerebral organoids provide a more species-specific microenvironment which is essential for GSCs to display their inherent characteristics [68]. These models are versatile to characterise various aspects of GSCs—invading, protruding, integrating, microtubule formation, and interaction with mature neurons of cerebral organoids [69,70]. However, current glioblastoma organoid models suffer from similar weaknesses of most other organoid models, in that they commonly lack vascularisation and innate immune cells [71]. This is important as GSC’s ability to resist many treatment modalities is due in part to interactions with microglial immune cells and increased vasculature within the tumour. Fortunately, methods to produce vascularised and immune-competent organoids are being generated [72,73], with some evidence suggesting microglia innately develop within cerebral organoids generated using the protocol developed by Linkous and Fine [5,74]. Vascularised organoids can be genetically engineered by induced expression of human ETS variant 2 [73]. This allows the cerebral organoids to form a complex vascular-like network. Alternatively, embedding human endothelial cells (hECs) into a Matrigel before cerebral organoids are incorporated allows the self-assembly of hECs into capillaries at the periphery of organoids, which invade the vascular network [75].

5. Prospective Drug Screening Using Patient-Derived Tumourspheres

When glioblastoma spheroids are cultured in basement membrane extracts such as Matrigel or Cultrex, tumour cell invasion can occur and is able to be measured [60]. Spheroid invasion assays are useful for rapid and reproducible assessment of the invasion of tumour cells into a semi-solid medium, making them particularly appropriate for *in vitro* drug screening for glioblastoma [76]. When supported, the cells can grow outward and invade the matrix in a 3D manner, forming a ‘micro-tumour’ [61]. Cell morphology in these tumourspheres and outgrowths are markedly different from the flat, adherent morphology that cells assume when growing on a solid substrate [77]. Invasion can be easily quantified using an imaging cytometer, an automated read out (Incucyte®), or a standard confocal microscope and imaging analysis software (such as TASI) [78]. The significance of this assay, compared to other standard invasion assays, is that tumour cells which invade into the surrounding matrix from the spheroid resemble a “micro-tumour” or a “micro-metastasis”. This, therefore, mimics particularly important aspects of the pathophysiology of a glioblastoma tumour mass, such as an interconnected network of tumour microtubules,

which aid in the invasion of normal host tissue [79]. Additionally, cells within glioblastoma spheroids may experience hypoxia and nutrient deprivation which, through changes in gene expression, can promote migration and invasion [80]. This is something that cannot be achieved with 2D assays.

Moreover, all of these techniques are starting to become more accessible, in high-throughput formats, using specific 96- and 384-well plates [18] and the latest imaging and bioinformatic technology [81,82], allowing more complex 3D assays to be used in drug screening. A limitation of the invasion assay method as for any such assays is the difficulty in distinguishing between invasion and proliferation, which the tumour cells are likely to undergo during the assay time frame [79]. For this reason, a parallel 3D growth assay may be performed to evaluate specific effects of any inhibitory or stimulatory agents [76]. If careful dose–response studies are performed, it may be possible to select concentrations of the desired drug/s that minimises the effects on proliferation to assess the effects of the drug on invasion only. For example, Vinci, Box and Eccles [79] have shown that the HSP90 inhibitor 17-AAG inhibits U-87 MG 3D tumour spheroid invasion at 24 h and at concentrations below the concentration inhibiting 3D growth by 50% (GI50). A prospective drug screen using patient-derived tumour spheres can be performed to ameliorate two of the main limitations relating to the generation of cerebral organoid models: time taken to culture and cost of materials.

6. Drug Screening Using a Patient-Derived Glioblastoma-Cerebral Organoid Model

Taking advantage of the GLICO model for higher-scale compound screening has not yet been achieved [83], likely due to the prohibitive costs and time taken to generate both human cerebral organoids, and a high-throughput drug screening system suitable for these 3D cultures. Still, progress has been made towards proving the useability of the GLICO model for these applications.

Utilising a genetically engineered luciferase-based assay to measure proliferation, Linkous et al. [19] were able to show that different GLICO models utilising different patient-derived tumours have differential sensitivities to chemotherapy (TMZ, BCNU) and radiotherapy. Interestingly, when the same patient samples were cultured in 2D, they showed equal susceptibility to TMZ and BCNU which was not the case for the GLICO model where differential sensitivity was seen [19]. The use of secreted luciferase as an indirect measure for determining viable glioblastoma cells within organoids offers simplicity, sensitivity, and scalability, making it amenable for high-throughput drug screening [84]. The limitation of the luciferase system, and other cell viability assays, is the inability to address key complex features of glioblastoma such as invasion and cell morphology [83]. Therefore, we propose live-cell immunofluorescent imaging of GSC invasion into GLICOs alongside viability measures (Figure 3). Our proposed workflow (Figure 4), for smaller scale screening using the GLICO model is particularly practical for use in most laboratories with accessible materials, accessible equipment, good for first pass, and no animal work required. This model is also amenable for analysis, with separate measures of invasion, growth, and viability. This workflow considers particularly important aspects of GSC function and how they may be altered upon therapeutic treatments. The reduction in cost and time taken to culture arises from the use of spheroids for preliminary screening prior to use of the GLICO model. The cost of generating and screening spheroids compared to organoids is significantly lower when using spheres which have specific and defined methods for quantification.

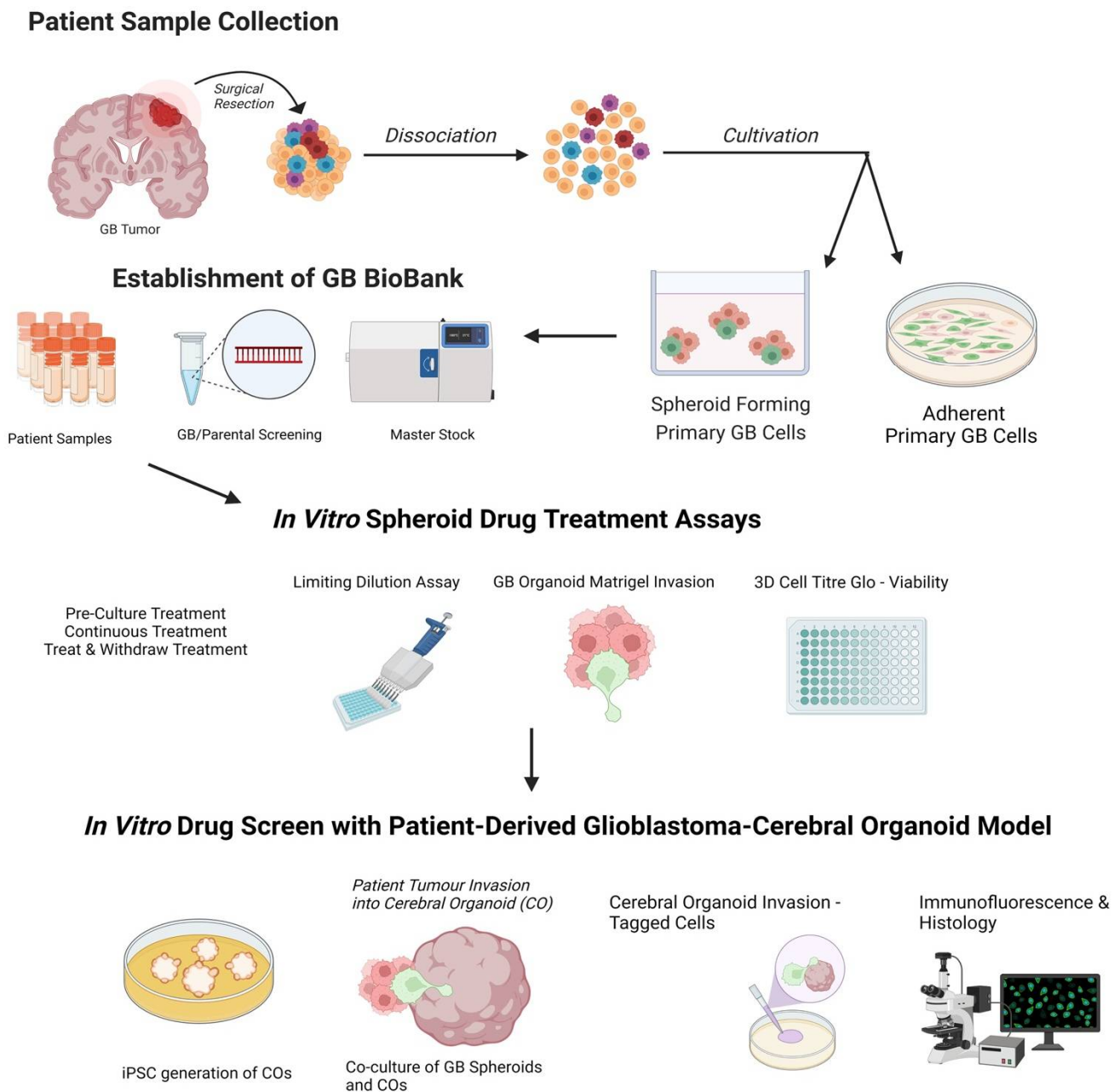


Figure 4. A potential workflow for drug screening using the GLICO model: 1. Generation of spheroid forming primary glioblastoma (GB) cells and biobanking of patient samples. 2. Prospective drug screen on glioblastoma spheroids. 3. Refined drug screen using patient-derived glioblastoma-cerebral organoid (GLICO) model. Created with Biorender.com accessed on 25 September 2022.

7. Conclusions and Perspectives

The ability to understand and manipulate cancers such as glioblastoma requires the disease models to be clinically and translationally relevant, replicating the cellular heterogeneity of such cancers. Therefore, brain cancer research models need to aim to recapitulate GSC function, whilst remaining amenable for analysis. Our proposed workflow of preliminary drug screening using glioblastoma spheroids as part of the GLICO model utilises patient-derived glioblastoma cells and cerebral organoids, providing the unique capability to investigate tumour–brain interactions. Despite their usefulness, the versatility and reliability of brain organoids in modelling glioblastoma remains to be standardised, with cost and time to culture being some of the greatest limitations. The GLICO model suffers from similar weaknesses as other organoid models, with the absence of vasculature and immune

cells, which are necessary for accurate recapitulation of the tumour microenvironment. However, recent research is making significant steps to ameliorate these limitations. Our proposed model for smaller-scale drug screening is particularly practical for use in most laboratories, or for those wanting to move into 3D cell culture/organoid research; with accessible materials, and accessible equipment, good for the first pass, and no animal work required.

Author Contributions: Conceptualisation, F.R.W. and C.G.; writing—original draft preparation, F.R.W. and C.G.; writing—review and editing, L.P., E.P. and S.T.T. All authors have read and agreed to the published version of the manuscript.

Funding: Freya Weth was supported by a Graham Langridge Scholarship and a Wellington Doctoral Scholarship.

Institutional Review Board Statement: Not applicable.

Informed Consent Statement: Not applicable.

Data Availability Statement: Not applicable.

Conflicts of Interest: The authors declare no conflict of interest.

References

- Huse, J.T.; Holland, E.; DeAngelis, L.M. Glioblastoma: Molecular Analysis and Clinical Implications. *Annu. Rev. Med.* **2013**, *64*, 59–70. [CrossRef] [PubMed]
- Stupp, R.; Taillibert, S.; Kanner, A.; Read, W.; Steinberg, D.M.; Lhermitte, B.; Toms, S.; Idbaih, A.; Ahluwalia, M.S.; Fink, K.; et al. Effect of Tumor-Treating Fields Plus Maintenance Temozolomide vs Maintenance Temozolomide Alone on Survival in Patients With Glioblastoma. *JAMA* **2017**, *318*, 2306–2316. [CrossRef] [PubMed]
- Stupp, R.; Mason, W.P.; van den Bent, M.J.; Weller, M.; Fisher, B.; Taphoorn, M.J.B.; Belanger, K.; Brandes, A.A.; Marosi, C.; Bogdahn, U.; et al. Radiotherapy plus Concomitant and Adjuvant Temozolomide for Glioblastoma. *New Engl. J. Med.* **2005**, *352*, 987–996. [CrossRef] [PubMed]
- Cloughesy, T.F.; Cavenee, W.K.; Mischel, P.S. Glioblastoma: From Molecular Pathology to Targeted Treatment. *Annu. Rev. Pathol. Mech. Dis.* **2014**, *9*, 1–25. [CrossRef]
- Linkous, A.; Fine, H.A. Generating Patient-Derived Gliomas within Cerebral Organoids. *STAR Protoc.* **2020**, *1*, 100008. [CrossRef] [PubMed]
- Andreatta, F.; Beccaceci, G.; Fortuna, N.; Celotti, M.; De Felice, D.; Lorenzoni, M.; Foletto, V.; Genovesi, S.; Rubert, J.; Alaimo, A. The Organoid Era Permits the Development of New Applications to Study Glioblastoma. *Cancers* **2020**, *12*, 3303. [CrossRef]
- Kim, S.-S.; Pirollo, K.F.; Chang, E.H. Isolation and Culturing of Glioma Cancer Stem Cells. *Curr. Protoc. Cell Biol.* **2015**, *67*, 23.10.1–23.10.10. [CrossRef]
- Rajcevic, U.; Petersen, K.; Knol, J.C.; Loos, M.; Bougnaud, S.; Klychnikov, O.; Li, K.W.; Pham, T.V.; Wang, J.; Miletic, H.; et al. iTRAQ-based Proteomics Profiling Reveals Increased Metabolic Activity and Cellular Cross-talk in Angiogenic Compared with Invasive Glioblastoma Phenotype. *Mol. Cell Proteom.* **2009**, *8*, 2595–2612. [CrossRef]
- Bradshaw, A.; Wickremsekera, A.; Tan, S.T.; Peng, L.; Davis, P.F.; Itinteang, T. Cancer Stem Cell Hierarchy in Glioblastoma Multiforme. *Front. Surg.* **2016**, *3*, 21. [CrossRef]
- Pearson, J.R.D.; Regad, T. Targeting cellular pathways in glioblastoma multiforme. *Signal. Transduct. Target.* **2017**, *2*, 17040. [CrossRef]
- Alves, A.L.V.; Gomes, I.N.F.; Carloni, A.C.; Rosa, M.N.; da Silva, L.S.; Evangelista, A.F.; Reis, R.M.; Silva, V.A.O. Role of glioblastoma stem cells in cancer therapeutic resistance: A perspective on antineoplastic agents from natural sources and chemical derivatives. *Stem Cell Res.* **2021**, *12*, 206. [CrossRef] [PubMed]
- Battle, E.; Clevers, H. Cancer stem cells revisited. *Nat. Med.* **2017**, *23*, 1124–1134. [CrossRef]
- Mao, H.; Lebrun, D.G.; Yang, J.; Zhu, V.F.; Li, M. Deregulated signaling pathways in glioblastoma multiforme: Molecular mechanisms and therapeutic targets. *Cancer Investig.* **2012**, *30*, 48–56. [CrossRef] [PubMed]
- Melissaridou, S.; Wiechec, E.; Magan, M.; Jain, M.V.; Chung, M.K.; Farnebo, L.; Roberg, K. The effect of 2D and 3D cell cultures on treatment response, EMT profile and stem cell features in head and neck cancer. *Cancer Cell Int.* **2019**, *19*, 16. [CrossRef]
- Gunti, S.; Hoke, A.T.K.; Vu, K.P.; London, N.R. Organoid and Spheroid Tumor Models: Techniques and Applications. *Cancers* **2021**, *13*, 874. [CrossRef]
- Hubert, C.G.; Rivera, M.; Spangler, L.C.; Wu, Q.; Mack, S.C.; Prager, B.C.; Couce, M.; McLendon, R.E.; Sloan, A.E.; Rich, J.N. A Three-Dimensional Organoid Culture System Derived from Human Glioblastomas Recapitulates the Hypoxic Gradients and Cancer Stem Cell Heterogeneity of Tumors Found In Vivo. *Cancer Res.* **2016**, *76*, 2465–2477. [CrossRef] [PubMed]
- Heddleston, J.M.; Li, Z.; McLendon, R.E.; Hjelmeland, A.B.; Rich, J.N. The hypoxic microenvironment maintains glioblastoma stem cells and promotes reprogramming towards a cancer stem cell phenotype. *Cell Cycle* **2009**, *8*, 3274–3284. [CrossRef] [PubMed]

18. Quereda, V.; Hou, S.; Madoux, F.; Scampavia, L.; Spicer, T.P.; Duckett, D. A Cytotoxic Three-Dimensional-Spheroid, High-Throughput Assay Using Patient-Derived Glioma Stem Cells. *Slas Discov. Adv. Sci. Drug Discov.* **2018**, *23*, 842–849. [CrossRef] [PubMed]
19. Linkous, A.; Balamatsias, D.; Snuderl, M.; Edwards, L.; Miyaguchi, K.; Milner, T.; Reich, B.; Cohen-Gould, L.; Storaska, A.; Nakayama, Y.; et al. Modeling Patient-Derived Glioblastoma with Cerebral Organoids. *Cell Rep.* **2019**, *26*, 3203–3211.e5. [CrossRef]
20. Wong, C.H.; Siah, K.W.; Lo, A.W. Estimation of clinical trial success rates and related parameters. *Biostatistics* **2019**, *20*, 273–286. [CrossRef]
21. Joseph, J.V.; Blaavand, M.S.; Daubon, T.; Kruyt, F.A.E.; Thomsen, M.K. Three-dimensional culture models to study glioblastoma—Current trends and future perspectives. *Curr. Opin. Pharmacol.* **2021**, *61*, 91–97. [CrossRef] [PubMed]
22. Azzarelli, R. Organoid Models of Glioblastoma to Study Brain Tumor Stem Cells. *Front. Cell Dev. Biol.* **2020**, *8*, 220. [CrossRef] [PubMed]
23. Da Hora, C.C.; Schweiger, M.W.; Wurdinger, T.; Tannous, B.A. Patient-Derived Glioma Models: From Patients to Dish to Animals. *Cells* **2019**, *8*, 1177. [CrossRef] [PubMed]
24. Mancuso, R.; Van Den Daele, J.; Fattorelli, N.; Wolfs, L.; Balusu, S.; Burton, O.; Liston, A.; Sierksma, A.; Fourne, Y.; Poovathingal, S.; et al. Stem-cell-derived human microglia transplanted in mouse brain to study human disease. *Nat. Neurosci.* **2019**, *22*, 2111–2116. [CrossRef]
25. Zhang, Q.; Zeng, Y.; Zhang, T.; Yang, T. Comparison Between Human and Rodent Neurons for Persistent Activity Performance: A Biologically Plausible Computational Investigation. *Front. Syst. Neurosci.* **2021**, *15*, 628839. [CrossRef]
26. Lui, J.H.; Hansen, D.V.; Kriegstein, A.R. Development and Evolution of the Human Neocortex. *Cell* **2011**, *146*, 18–36. [CrossRef]
27. Chen, J.; McKay, R.M.; Parada, L.F. Malignant Glioma: Lessons from Genomics, Mouse Models, and Stem Cells. *Cell* **2012**, *149*, 36–47. [CrossRef]
28. Fattorelli, N.; Martinez-Muriana, A.; Wolfs, L.; Geric, I.; De Strooper, B.; Mancuso, R. Stem-cell-derived human microglia transplanted into mouse brain to study human disease. *Nat. Protoc.* **2021**, *16*, 1013–1033. [CrossRef]
29. Kim, J.; Koo, B.-K.; Knoblich, J.A. Human organoids: Model systems for human biology and medicine. *Nat. Rev. Mol. Cell Biol.* **2020**, *21*, 571–584. [CrossRef]
30. Geribaldi-Doldán, N.; Fernández-Ponce, C.; Quiroz, R.N.; Sánchez-Gomar, I.; Escorcía, L.G.; Velásquez, E.P.; Quiroz, E.N. The Role of Microglia in Glioblastoma. *Front. Oncol.* **2021**, *10*, 603495. [CrossRef]
31. Maas, S.L.N.; Abels, E.R.; Van De Haar, L.L.; Zhang, X.; Morsett, L.; Sil, S.; Guedes, J.; Sen, P.; Prabhakar, S.; Hickman, S.E.; et al. Glioblastoma hijacks microglial gene expression to support tumor growth. *J. Neuroinflamm.* **2020**, *17*, 120. [CrossRef]
32. Ravi, V.M.; Will, P.; Kueckelhaus, J.; Sun, N.; Joseph, K.; Salié, H.; Vollmer, L.; Kuliesiute, U.; von Ehr, J.; Benotmane, J.K.; et al. Spatially resolved multi-omics deciphers bidirectional tumor-host interdependence in glioblastoma. *Cancer Cell* **2022**, *40*, 639–655.e13. [CrossRef] [PubMed]
33. Hicks, W.H.; Bird, C.E.; Gattie, L.C.; Shami, M.E.; Traylor, J.I.; Shi, D.D.; McBrayer, S.K.; Abdullah, K.G. Creation and Development of Patient-Derived Organoids for Therapeutic Screening in Solid Cancer. *Curr. Stem Cell Rep.* **2022**, *8*, 107–117. [CrossRef]
34. Agboola, O.S.; Hu, X.; Shan, Z.; Wu, Y.; Lei, L. Brain organoid: A 3D technology for investigating cellular composition and interactions in human neurological development and disease models in vitro. *Stem Cell Res. Ther.* **2021**, *12*, 430. [CrossRef] [PubMed]
35. Jacob, F.; Salinas, R.D.; Zhang, D.Y.; Nguyen, P.T.T.; Schnoll, J.G.; Wong, S.Z.H.; Thokala, R.; Sheikh, S.; Saxena, D.; Prokop, S.; et al. A Patient-Derived Glioblastoma Organoid Model and Biobank Recapitulates Inter- and Intra-tumoral Heterogeneity. *Cell* **2020**, *180*, 188–204.e22. [CrossRef] [PubMed]
36. Zhou, H.-M.; Zhang, J.-G.; Zhang, X.; Li, Q. Targeting cancer stem cells for reversing therapy resistance: Mechanism, signaling, and prospective agents. *Sig. Transduct. Target.* **2021**, *6*, 1–17. [CrossRef] [PubMed]
37. Mitchell, K.; Troike, K.; Silver, D.J.; Lathia, J.D. The evolution of the cancer stem cell state in glioblastoma: Emerging insights into the next generation of functional interactions. *Neuro-Oncol* **2021**, *23*, 199–213. [CrossRef]
38. Auffinger, B.; Spencer, D.; Pytel, P.; Ahmed, A.U.; Lesniak, M.S. The role of glioma stem cells in chemotherapy resistance and glioblastoma multiforme recurrence. *Expert Rev. Neurother.* **2015**, *15*, 741–752. [CrossRef]
39. Marzagalli, M.; Fontana, F.; Raimondi, M.; Limonta, P. Cancer Stem Cells—Key Players in Tumor Relapse. *Cancers* **2021**, *13*, 376. [CrossRef]
40. Singh, S.K.; Clarke, I.D.; Terasaki, M.; Bonn, V.E.; Hawkins, C.; Squire, J.; Dirks, P.B. Identification of a Cancer Stem Cell in Human Brain Tumors. *Cancer Res.* **2003**, *63*, 5821–5828.
41. Nik Nabil, W.N.; Xi, Z.; Song, Z.; Jin, L.; Zhang, X.D.; Zhou, H.; De Souza, P.; Dong, Q.; Xu, H. Towards a Framework for Better Understanding of Quiescent Cancer Cells. *Cells* **2021**, *10*, 562. [CrossRef] [PubMed]
42. Chen, W.; Dong, J.; Haiech, J.; Kilhoffer, M.-C.; Zeniou, M. Cancer Stem Cell Quiescence and Plasticity as Major Challenges in Cancer Therapy. *Stem Cells Int.* **2016**, *2016*, 1740936. [CrossRef] [PubMed]
43. Yuan, X.; Curtin, J.; Xiong, Y.; Liu, G.; Waschmann-Hogiu, S.; Farkas, D.L.; Black, K.L.; Yu, J.S. Isolation of cancer stem cells from adult glioblastoma multiforme. *Oncogene* **2004**, *23*, 9392–9400. [CrossRef] [PubMed]
44. Sundar, S.J.; Hsieh, J.K.; Manjila, S.; Lathia, J.D.; Sloan, A. The role of cancer stem cells in glioblastoma. *Neurosurg. Focus* **2014**, *37*, E6. [CrossRef] [PubMed]


45. Biserova, K.; Jakovlevs, A.; Uljanovs, R.; Strumfa, I. Cancer Stem Cells: Significance in Origin, Pathogenesis and Treatment of Glioblastoma. *Cells* **2021**, *10*, 621. [CrossRef]
46. Ahmed, S.I.; Javed, G.; Laghari, A.A.; Bareeqa, S.B.; Farrukh, S.; Zahid, S.; Samar, S.S.; Aziz, K. CD133 Expression in Glioblastoma Multiforme: A Literature Review. *Cureus* **2018**, *10*, e3439. [CrossRef]
47. Lee, J.H.; Lee, J.E.; Kahng, J.Y.; Kim, S.H.; Park, J.S.; Yoon, S.J.; Um, J.-Y.; Kim, W.K.; Lee, J.-K.; Park, J.; et al. Human glioblastoma arises from subventricular zone cells with low-level driver mutations. *Nature* **2018**, *560*, 243–247. [CrossRef]
48. Guilhamon, P.; Chesnelong, C.; Kushida, M.M.; Nikolic, A.; Singhal, D.; MacLeod, G.; Madani Tonekaboni, S.A.; Cavalli, F.M.; Arlidge, C.; Rajakulendran, N.; et al. Single-cell chromatin accessibility profiling of glioblastoma identifies an invasive cancer stem cell population associated with lower survival. *eLife* **2021**, *10*, e64090. [CrossRef]
49. Seymour, T.; Nowak, A.; Kakulas, F. Targeting aggressive cancer stem cells in glioblastoma. *Front. Oncol.* **2015**, *5*, 159. [CrossRef]
50. Di Tomaso, T.; Mazzoleni, S.; Wang, E.; Sovena, G.; Clavenna, D.; Franzin, A.; Mortini, P.; Ferrone, S.; Doglioni, C.; Marincola, F.M.; et al. Immunobiological Characterization of Cancer Stem Cells Isolated from Glioblastoma Patients. *Clin. Cancer Res.* **2010**, *16*, 800–813. [CrossRef]
51. Jorfi, M.; D'Avanzo, C.; Kim, D.Y.; Irimia, D. Three-Dimensional Models of the Human Brain Development and Diseases. *Adv. Healthc. Mater.* **2018**, *7*, 1700723. [CrossRef] [PubMed]
52. Shou, Y.; Liang, F.; Xu, S.; Li, X. The Application of Brain Organoids: From Neuronal Development to Neurological Diseases. *Front. Cell Dev. Biol.* **2020**, *8*, 579659. [CrossRef] [PubMed]
53. Kilmister, E.J.; Tan, S.T. The Role of the Renin–Angiotensin System in the Cancer Stem Cell Niche. *J Histochem. Cytochem.* **2021**, *69*, 835–847. [CrossRef] [PubMed]
54. Vinel, C.; Rosser, G.; Guglielmi, L.; Constantinou, M.; Pomella, N.; Zhang, X.; Boot, J.R.; Jones, T.A.; Millner, T.O.; Dumas, A.A.; et al. Comparative epigenetic analysis of tumour initiating cells and syngeneic EPSC-derived neural stem cells in glioblastoma. *Nat. Commun.* **2021**, *12*, 6130. [CrossRef]
55. Lee, J.; Kotliarova, S.; Kotliarov, Y.; Li, A.; Su, Q.; Donin, N.M.; Pastorino, S.; Purow, B.W.; Christopher, N.; Zhang, W.; et al. Tumor stem cells derived from glioblastomas cultured in bFGF and EGF more closely mirror the phenotype and genotype of primary tumors than do serum-cultured cell lines. *Cancer Cell* **2006**, *9*, 391–403. [CrossRef]
56. Ballav, S.; Deshmukh, A.J.; Siddiqui, S.; Aich, J.; Basu, S.; Ballav, S.; Deshmukh, A.J.; Siddiqui, S.; Aich, J.; Basu, S. *Two-Dimensional and Three-Dimensional Cell Culture and Their Applications*; IntechOpen: London, UK, 2021; ISBN 978-1-83969-446-2.
57. Paolillo, M.; Comincini, S.; Schinelli, S. In Vitro Glioblastoma Models: A Journey into the Third Dimension. *Cancers* **2021**, *13*, 2449. [CrossRef]
58. Edmondson, R.; Broglie, J.J.; Adcock, A.F.; Yang, L. Three-Dimensional Cell Culture Systems and Their Applications in Drug Discovery and Cell-Based Biosensors. *Assay Drug Dev. Technol.* **2014**, *12*, 207–218. [CrossRef]
59. Pollard, S.M.; Yoshikawa, K.; Clarke, I.D.; Danovi, D.; Stricker, S.; Russell, R.; Bayani, J.; Head, R.; Lee, M.; Bernstein, M.; et al. Glioma stem cell lines expanded in adherent culture have tumor-specific phenotypes and are suitable for chemical and genetic screens. *Cell Stem Cell* **2009**, *4*, 568–580. [CrossRef]
60. Białkowska, K.; Komorowski, P.; Bryszewska, M.; Miłowska, K. Spheroids as a Type of Three-Dimensional Cell Cultures—Examples of Methods of Preparation and the Most Important Application. *Int. J. Mol. Sci.* **2020**, *21*, 6225. [CrossRef]
61. Azari, H.; Millette, S.; Ansari, S.; Rahman, M.; Deleyrolle, L.P.; Reynolds, B.A. Isolation and expansion of human glioblastoma multiforme tumor cells using the neurosphere assay. *J. Vis. Exp.* **2011**, *30*, e3633. [CrossRef]
62. Ramani, A.; Müller, L.; Ostermann, P.N.; Gabriel, E.; Abida-Islam, P.; Müller-Schiffmann, A.; Mariappan, A.; Goureau, O.; Gruell, H.; Walker, A.; et al. SARS-CoV-2 targets neurons of 3D human brain organoids. *EMBO J.* **2020**, *39*, e106230. [CrossRef] [PubMed]
63. Yi, H.-G.; Jeong, Y.H.; Kim, Y.; Choi, Y.-J.; Moon, H.E.; Park, S.H.; Kang, K.S.; Bae, M.; Jang, J.; Youn, H.; et al. A bioprinted human-glioblastoma-on-a-chip for the identification of patient-specific responses to chemoradiotherapy. *Nat. Biomed. Eng.* **2019**, *3*, 509–519. [CrossRef] [PubMed]
64. Ogawa, J.; Pao, G.M.; Shokhirev, M.N.; Verma, I.M. Glioblastoma Model Using Human Cerebral Organoids. *Cell Rep.* **2018**, *23*, 1220–1229. [CrossRef] [PubMed]
65. Bian, S.; Repic, M.; Guo, Z.; Kavirayani, A.; Burkard, T.; Bagley, J.A.; Krauditsch, C.; Knoblich, J.A. Genetically engineered cerebral organoids model brain tumour formation. *Nat. Methods* **2018**, *15*, 631–639. [CrossRef]
66. Baskar, G.; Palaniyandi, T.; Viswanathan, S.; Rajendran, B.K.; Ravi, M.; Sivaji, A. Development of patient derived organoids for cancer drug screening applications. *Acta Histochem.* **2022**, *124*, 151895. [CrossRef]
67. Da Silva, B.; Mathew, R.K.; Polson, E.S.; Williams, J.; Wurdak, H. Spontaneous Glioblastoma Spheroid Infiltration of Early-Stage Cerebral Organoids Models Brain Tumor Invasion. *SLAS Discov.* **2018**, *23*, 862–868. [CrossRef]
68. Silvia, N.; Dai, G. Cerebral organoids as a model for glioblastoma multiforme. *Curr. Opin. Biomed. Eng.* **2020**, *13*, 152–159. [CrossRef]
69. Mariappan, A.; Goranci-Buzhala, G.; Ricci-Vitiani, L.; Pallini, R.; Gopalakrishnan, J. Trends and challenges in modeling glioma using 3D human brain organoids. *Cell Death Differ.* **2021**, *28*, 15–23. [CrossRef]
70. Goranci-Buzhala, G.; Mariappan, A.; Gabriel, E.; Ramani, A.; Ricci-Vitiani, L.; Buccarelli, M.; D'Alessandris, Q.G.; Pallini, R.; Gopalakrishnan, J. Rapid and Efficient Invasion Assay of Glioblastoma in Human Brain Organoids. *Cell Rep.* **2020**, *31*, 107738. [CrossRef]

71. Andrews, M.G.; Kriegstein, A.R. Challenges of Organoid Research. *Annu. Rev. Neurosci.* **2022**, *45*, 23–39. [CrossRef]
72. Zhang, W.; Jiang, J.; Xu, Z.; Yan, H.; Tang, B.; Liu, C.; Chen, C.; Meng, Q. Microglia-containing human brain organoids for the study of brain development and pathology. *Mol. Psychiatry* **2022**. [CrossRef] [PubMed]
73. Cakir, B.; Xiang, Y.; Tanaka, Y.; Kural, M.H.; Parent, M.; Kang, Y.-J.; Chapeton, K.; Patterson, B.; Yuan, Y.; He, C.-S.; et al. Engineering of human brain organoids with a functional vascular-like system. *Nat. Methods* **2019**, *16*, 1169–1175. [CrossRef] [PubMed]
74. Ormel, P.R.; Vieira de Sá, R.; van Bodegraven, E.J.; Karst, H.; Harschnitz, O.; Sneebouer, M.A.M.; Johansen, L.E.; van Dijk, R.E.; Scheefhals, N.; Berdenis van Berlekom, A.; et al. Microglia innately develop within cerebral organoids. *Nat. Commun.* **2018**, *9*, 4167. [CrossRef] [PubMed]
75. Pham, M.T.; Pollock, K.M.; Rose, M.D.; Cary, W.A.; Stewart, H.R.; Zhou, P.; Nolta, J.A.; Waldau, B. Generation of human vascularized brain organoids. *Neuroreport* **2018**, *29*, 588–593. [CrossRef] [PubMed]
76. Zaroni, M.; Piccinini, F.; Arienti, C.; Zamagni, A.; Santi, S.; Polico, R.; Bevilacqua, A.; Tesei, A. 3D tumor spheroid models for in vitro therapeutic screening: A systematic approach to enhance the biological relevance of data obtained. *Sci. Rep.* **2016**, *6*, 19103. [CrossRef]
77. Browning, A.P.; Sharp, J.A.; Murphy, R.J.; Gunasingh, G.; Lawson, B.; Burrage, K.; Haass, N.K.; Simpson, M. Quantitative analysis of tumour spheroid structure. *eLife* **2021**, *10*, e73020. [CrossRef]
78. Hou, Y.; Konen, J.; Brat, D.J.; Marcus, A.I.; Cooper, L.A.D. TASI: A software tool for spatial-temporal quantification of tumor spheroid dynamics. *Sci. Rep.* **2018**, *8*, 7248. [CrossRef]
79. Pinto, B.; Henriques, A.C.; Silva, P.M.A.; Bousbaa, H. Three-Dimensional Spheroids as In Vitro Preclinical Models for Cancer Research. *Pharmaceutics* **2020**, *12*, 186. [CrossRef]
80. Boyd, N.H.; Tran, A.N.; Bernstock, J.D.; Etminan, T.; Jones, A.B.; Gillespie, G.Y.; Friedman, G.K.; Hjelmeland, A.B. Glioma stem cells and their roles within the hypoxic tumor microenvironment. *Theranostics* **2021**, *11*, 665–683. [CrossRef]
81. Akay, M.; Hite, J.; Avci, N.G.; Fan, Y.; Akay, Y.; Lu, G.; Zhu, J.-J. Drug Screening of Human GBM Spheroids in Brain Cancer Chip. *Sci. Rep. (Nat. Publ. Group)* **2018**, *8*, 15423. [CrossRef]
82. Stein, A.M.; Demuth, T.; Mobley, D.; Berens, M.; Sander, L.M. A Mathematical Model of Glioblastoma Tumor Spheroid Invasion in a Three-Dimensional In Vitro Experiment. *Biophys J.* **2007**, *92*, 356–365. [CrossRef] [PubMed]
83. Rybin, M.J.; Ivan, M.E.; Ayad, N.G.; Zeier, Z. Organoid Models of Glioblastoma and Their Role in Drug Discovery. *Front. Cell. Neurosci.* **2021**, *15*, 605255. [CrossRef] [PubMed]
84. Coombe, D.R.; Nakhoul, A.M.; Stevenson, S.M.; Peroni, S.E.; Sanderson, C.J. Expressed luciferase viability assay (ELVA) for the measurement of cell growth and viability. *J. Immunol. Methods* **1998**, *215*, 145–150. [CrossRef] [PubMed]

Disclaimer/Publisher’s Note: The statements, opinions and data contained in all publications are solely those of the individual author(s) and contributor(s) and not of MDPI and/or the editor(s). MDPI and/or the editor(s) disclaim responsibility for any injury to people or property resulting from any ideas, methods, instructions or products referred to in the content.

Article

Elucidating the Anti-Tumorigenic Efficacy of Oltipraz, a Dithiolethione, in Glioblastoma

Upasana Kapoor-Narula * and Nibedita Lenka * 

National Centre for Cell Science, S.P. Pune University Campus, Ganeshkhind, Pune 411007, India

* Correspondence: upasanan@nccs.res.in (U.K.-N.); nibedita@nccs.res.in (N.L.)

Abstract: Glioblastoma multiforme (GBM), the most aggressive primary brain tumor, displays a highly infiltrative growth pattern and remains refractory to chemotherapy. Phytochemicals carrying specificity and low cytotoxicity may serve as potent and safer alternatives to conventional chemotherapy for treating GBM. We have evaluated the anticancer effects of Oltipraz (Olt), a synthetic dithiolethione found in many vegetables, including crucifers. While Olt exposure was non-toxic to the HEK-293 cell line, it impaired the cell growth in three GBM cell lines (LN18, LN229, and U-87 MG), arresting those at the G2/M phase. Olt-exposed GBM cells induced the generation of reactive oxygen species (ROS), mitochondrial depolarization, caspase 3/7-mediated apoptosis, nuclear condensation, and DNA fragmentation, and decreased glutathione, a natural ROS scavenger, as well as vimentin and β -catenin, the EMT-associated markers. Its effect on a subpopulation of GBM cells exhibiting glioblastoma stem cell (GSCs)-like characteristics revealed a reduced expression of Oct4, Sox2, CD133, CD44, and a decrease in ALDH⁺, Nestin⁺ and CD44⁺ cells. In contrast, there was an increase in the expression of GFAP and GFAP⁺ cells. The Olt also significantly suppressed the oncosphere-forming ability of cells. Its efficacy was further validated in vivo, wherein oral administration of Olt could suppress the ectopically established GBM tumor growth in SCID mice. However, there was no alteration in body weight, organ ratio, and biochemical parameters, reflecting the absence of any toxicity otherwise. Together, our findings could demonstrate the promising chemotherapeutic efficacy of Olt with potential implications in treating GBM.

Keywords: Oltipraz; glioblastoma; cancer stem cells; apoptosis; anticancer therapeutic



Citation: Kapoor-Narula, U.; Lenka, N. Elucidating the Anti-Tumorigenic Efficacy of Oltipraz, a Dithiolethione, in Glioblastoma. *Cells* **2022**, *11*, 3057. <https://doi.org/10.3390/cells11193057>

Academic Editors: Javier S. Castresana and Bárbara Meléndez

Received: 17 June 2022

Accepted: 21 July 2022

Published: 29 September 2022

Publisher's Note: MDPI stays neutral with regard to jurisdictional claims in published maps and institutional affiliations.



Copyright: © 2022 by the authors. Licensee MDPI, Basel, Switzerland. This article is an open access article distributed under the terms and conditions of the Creative Commons Attribution (CC BY) license (<https://creativecommons.org/licenses/by/4.0/>).

1. Introduction

Glioblastoma, also known as Glioblastoma multiforme (GBM) (World Health Organization grade IV glioma or astrocytoma), is the most prominent primary brain cancer associated with therapeutic resistance, high recurrence, and poor patient survival. Worldwide, an estimated 251,329 people have died from primary cancerous brain and CNS tumors in 2020 [1]. Similarly, as per the International Association of Cancer Registries, the mortality rate for GBM is ~86% every year for more than 28,000 cases reported annually in India [2]. GBM patients can have extremely poor prognoses with no current treatment modalities (for example, surgery, radiation, and chemotherapy) available that may facilitate extending median survival to a greater extent. Hence, it is considered the most aggressive and lethal multiforme. The GBM malignancy also increases by the presence of a sub-population of cancer cells, the cancer stem cells (CSCs), which are bestowed with profound tumorigenic potential. In the last decade, these cells have been identified in GBM and in a variety of cancers [3–5]. CSCs display the characteristics of self-renewal and multipotent differentiation potential similar to that seen in adult stem cells. Moreover, they are capable of generating new tumors with similar heterogeneity as that of the original ones. These cells are majorly responsible for aggressiveness and tumor relapse and contribute to chemo- and radio-resistance. In fact, CSCs are more resistant to conventional cancer therapies as compared to the non-CSC population, and thus are involved in the relapse

of tumors. Therefore, targeting CSCs in GBM can unveil an effective chemotherapeutic strategy, which may help overcome the issue pertaining to glioma recurrence.

The conventional GBM treatment involves surgical intervention followed by chemo- and radiotherapy. However, considering the aggressiveness of GBM that causes the degradation of the extracellular matrix (ECM) of brain tissues and leads to extensive metastasis, it poses a major hindrance to the surgical excision-based complete tumor removal [6]. Hence, it is the need of the hour to explore new therapeutic compounds that can precisely target cancer cells or tumors carrying lesser side effects than existing cytotoxic/cytostatic drugs [7]. Temozolomide (TMZ) is one of the preferred drugs for treating GBM. However, the development of resistance to TMZ over a period by GBM cells does restrict its long-term administration. Moreover, it has been reported that more than half of GBM patients do not respond to TMZ due to the overexpression of DNA repair enzymes such as APNG and MGMT [8]. Therefore, there is a pressing need to explore novel and potent therapeutic options that would act as an adjuvant to radio- or chemotherapy and enhance their efficacy [5,9].

The recent data suggest the use of alternative medicine by as much as 36% of cancer patients as an adjuvant to conventional therapy [10]. Therefore, exploring new candidates that can exert anticancer potential with lesser toxicity to normal cells but can contain GBM effectively becomes imperative. In this context, investigators are channelizing their search to retrieve phytochemicals from dietary and medicinal plants to use those as probable preventive and chemotherapeutic agents in treating cancer, more so because of their pro- and antioxidant activities based on the concentrations used. In normal cells, they serve as free radical scavengers when used at a lower concentration. Their antioxidant effects help maintain redox homeostasis, which is crucial for different cellular processes and disease-fighting efficacy. However, in cancer cells with very high levels of reactive oxygen species (ROS) than the normal cells, the phytochemicals at higher concentrations act as prooxidants and induce autophagy, apoptosis, and necroptosis via mTOR activation and PI3-Akt inhibition [11]. In recent years, the “integrative” oncology society has mandated advances from scientists to develop natural medicine [12]. Thus, they are considered to be a treasure house for developing novel drugs.

Oltipraz [5-(2-pyrazinyl)-4-methyl-1, 2-dithiol-3-thione] (Olt) is a synthetic dithiolethione found among the members of the Cruciferous family. The Olt and its oxidized metabolites carrying proven strong antioxidant effects have been studied in various diseases such as obesity, type 2 diabetes, heart failure, kidney injury, and renal and liver fibrosis in preclinical and clinical settings alike [13,14]. Jiang et al. [14] have demonstrated its role as an ROS scavenger that prevents glucose-induced oxidative stress generation and apoptosis in Schwann cells via Nrf2/NQO1 signaling. The preclinical evaluation of Olt has revealed its tumor-suppressive efficacy in breast, bladder, colon, stomach, liver, lymph nodes, lung, pancreas, and skin cancers induced by different carcinogens [15]. Phase I and II trials concerning the Olt in colon, breast, liver, and lung cancer patients have also revealed its anti-tumorigenic potential together with its minimal toxicity to normal cells [15]. However, its effect on human GBM cells or CSCs is yet to be explored.

In this study, we have used Olt to assess its efficacy in containing human GBM cell growth both in vitro and in vivo to gain new insights into the possible mechanism underlying the cytotoxicity activity of Olt in GBM cells. Here, we investigated the effects of Olt on cell viability, migration, invasion, and apoptotic-inducing properties in vitro and in a xenograft mouse model in vivo. We found that Olt leads to apoptosis in GBM cells and represses the expression of the vital genes associated with the CSC phenotype. Hence, it decreases the stemness properties of CSCs by directing them towards differentiation. Moreover, oral administration of Olt did not render systemic toxicity in mice. Thus, we propose that OLT may be a novel promising target for GBM therapy.

2. Material and Methods

2.1. Cell Culture and Treatments

Three glioblastoma cell lines (U-87 MG: ATCC Cat # HTB-14; LN-18: ATCC Cat # CRL2610; LN-229: ATCC Cat # CRL-2611) representing the grade IV GBM and HEK-293 (ATCC Cat # CRL-1573), the human embryonic kidney epithelial cells, were obtained from the cell repository of the National Centre for Cell Science (NCCS), Pune. We also considered the mesenchymal stem cells (MSCs) derived from gingival tissues, already available in the laboratory for comparative studies. MSC isolation was conducted prior to this study according to the guidelines of the Declaration of Helsinki (collected at AFMC, Pune, India with informed patient consent and Institutional Ethical Committee approval # NARI/RSP/12-13/). The HEK-293 and U-87 MG cells were maintained in culture using MEM- α with 10% FBS and 1 mM sodium pyruvate (all from Invitrogen) at 37 °C in an incubator with controlled humidity and a 5% CO₂-95% air atmosphere. For maintaining LN-18 and LN-229 in culture, MEM- α was substituted with DMEM. Similarly, MSCs were maintained in DMEM supplemented with 10% FBS, 2 mM L-glutamine, 1 \times non-essential amino acid, 100 IU/mL Penicillin:Streptomycin (all from Invitrogen, Carlsbad, CA, USA), and 100 μ M β -ME (Sigma–Aldrich, St. Louis, MO, USA). The propagation of cells was carried out at regular intervals after attaining 80–90% confluence. Various concentrations (20–60 μ M) of Olt (Sigma–Aldrich) were used to assess the dose–response on cell growth parameters.

2.2. Cell Viability Assay

Viability is a measure of the metabolic state of a cell population that indicates the growth potential. To examine the effects of Olt on control non-tumorigenic cells (HEK-293; MSC) and various GBM cells (LN-229, LN-18, U-87 MG) in culture, cell viability was measured by MTT assay, following the conventional protocol. HEK-293 cells with epithelial morphology similar to the stated GBM cells were used as control cells for comparison. Similarly, MSCs were considered as control cells since they give rise to myofibroblasts in the tumor microenvironment. Briefly, ~10,000 cells/well were seeded in a 96-well plate either with or without specified concentrations of Olt. After 24 and 48 h of incubation, we assessed the cell viability by incubating the cells with 10 μ L of MTT (5 mg/mL) (Sigma–Aldrich) for 4 h at 37 °C, followed by the addition of 100 μ L DMSO and further incubation for 1 h to dissolve the purple formazan crystals. The absorbance was taken at 570 nm using Spectramax 384 microplate reader (Molecular Devices, San Jose, CA, USA). The value of untreated cells (Ctrl) in each cell line was considered as 100%, and the comparative percent viability with Olt treatment was calculated accordingly.

2.3. Colony Formation and Cell Migration Assay

5000 cells/mL were taken in the treatment and control groups and incubated for 14 days with intermittent medium change. Colonies formed in all groups were stained with crystal violet (0.05%) and imaged. The migration assay was performed using the Transwell Boyden chamber (Corning) following the protocol [16]. Briefly, U-87 MG cells (1×10^5) pretreated with the Olt were placed in the upper chamber, while the lower chamber contained 10% FBS as a chemo-attractant. After 12 h of incubation at 37 °C in a CO₂ incubator, the cells that had migrated to the lower surface of the Transwell membrane were fixed with 4% paraformaldehyde (PFA) for 10 min. Further, the staining was carried out with 5% Crystal Violet (prepared in 25% methanol) for 10 min, followed by washing to remove the unbound stain. Migrated cells were photographed under an inverted microscope (TE2000-U, Nikon, Kawasaki, Japan).

2.4. Flow Cytometry Analysis

2.4.1. Cell Cycle Analysis

Cellular DNA content was studied to analyze the cell cycle progression by flow cytometry using propidium iodide (PI) as the DNA dye [17]. Briefly, the cells ($0.5\text{--}1 \times 10^6$) were fixed in ethanol, washed with PBS, and incubated for 30 min in the dark at room temperature with the staining solution containing RNase A (100 $\mu\text{g}/\text{mL}$) and PI (25 $\mu\text{g}/\text{mL}$). Flow cytometry (FACS Calibur, Beckton Dickinson, San Jose, CA, USA) was carried out to analyze the cell cycle, wherein PI fluorescence was measured through an FL-2 filter (585 nm).

2.4.2. Measurement of ROS

We have used the cell-permeable fluorescent dyes DCFDA (Thermo Fisher Scientific, Carlsbad, CA, USA) and DHE (Sigma–Aldrich, St. Louis, MO, USA), respectively, to quantify superoxide (O_2^-) and hydrogen peroxide (H_2O_2), the known subtypes of ROS [16]. Briefly, cells treated with phytochemicals for 48 h were trypsinized, washed, suspended in DHE (5 μM) or carboxy-DCFDA (5 μM), and incubated for 30 min in the dark at 37 °C. Subsequent to PBS wash, cells were resuspended in PBS, passed through a cell strainer, and quantified by flow cytometry (FACS Calibur, Beckton Dickinson, San Jose, CA, USA) using the CELL Quest PRO™ (v 5.2.1, Becton Dickinson, San Jose, CA, USA) software. Around 10,000 cells were examined for each sample. Unstained cells served as a negative control for background correction, and the untreated fluorophore-loaded cells could serve as a control (Ctrl).

2.4.3. Changes in Mitochondrial Membrane Potential (MMP: $\Delta\psi\text{m}$)

One of the major changes observed in apoptotic cells is the depolarization of the inner membrane of mitochondria. Hence, MMP was measured using Rhodamine 123 (Rh123) (Sigma–Aldrich), a fluorescent dye that binds to the inner mitochondrial membrane and is released upon membrane depolarization [18], to detect the Olt-induced apoptosis in U-87 MG cells. Briefly, U-87 MG cells (Ctrl and treated) were incubated in the dark with 5 $\mu\text{g}/\text{mL}$ of Rh123 for 30 min at room temperature. The signal was assessed by flow cytometry using FL-1 channel (590 nm band-pass filter) for detection.

2.4.4. GSH Estimation

Cell tracker green (CMFDA, Thermo Fischer Scientific, Carlsbad, CA, USA) was used to measure the total GSH, the major cellular thiol in cells, as described [19]. Briefly, the cells were incubated with the CMFDA (5 $\mu\text{g}/\text{mL}$) for 30 min in the dark at 37 °C. The treated cells were then acquired on the flow cytometer, and analysis was performed using the CELL Quest PRO™ software.

2.4.5. Assessment of Apoptosis Induction

(a) Annexin-PI assay: U-87 MG cells (ctrl and treated) were harvested after 48 h, and apoptosis was detected by staining with Annexin V-APC and PI [20]. Briefly, cells were trypsinized, washed with PBS, and then incubated with AnnexinV-APC (bd Biosciences) in the dark for 15 min. PI was added just before acquiring samples to differentiate between necrotic and live cells by flow cytometry. The data were analyzed using CELL Quest PRO™ software to determine the percentage of apoptotic cells present.

(b) Caspase 3/7 expression: Caspase 3/7 expression was assessed by flow cytometry using a commercially available CellEvent Caspase-3/7 Green Detection kit (Invitrogen) following the manufacturer's instructions. Briefly, cells were harvested, added to 500 nM solution of Caspase-3/7 Green Detection Reagent, and incubated at 37 °C for 25 min. Finally, 1 μM of SYTOX™ AADvanced™ stain solution was added to the reaction mix, incubated for 5 min, and quantified by flow cytometry.

(c) Hoechst 33242 staining and assessment of nuclear morphology: Hoechst 33342 (Thermo Fisher) that binds to DNA was used to identify any changes in the nuclear morphology [21]. Hoechst (5 mg/mL) was added to cells and incubated at 37 °C for 15 min. Cells were visualized under a Zeiss LSM510 META microscope (Carl Zeiss, Germany), and the image acquisition and analysis were carried out using LSM 5 Image Browser software (v AIM 4.2.0.121, Carl Zeiss, Oberkochen, Germany).

2.5. Analysis of Stem Cell Markers

2.5.1. ALDH Assay

ALDH⁺ cells were quantified using the ALDEFLUOR Kit from Stemcell Technologies, Vancouver, as per the manufacturer's protocol. Around 5×10^6 cells (U-87 MG) were considered for ALDH analysis and the sorting of the ALDH⁺ population using the FACS Aria III instrument (Becton Dickinson, Franklin Lakes, NJ, USA). Sorted ALDH⁺ cells were exposed to Olt (40- and 60 μ M) for 48 h and quantified further by flow cytometry to detect the influence of Olt on the ALDH⁺ population. The results were analyzed using FACS-Diva software (BD FACS-Diva v 6.1.3, Becton Dickinson, San Jose, CA, USA).

2.5.2. CD44 Estimation

U-87 MG cells were sorted based on the expression of CD44, the CSC marker, on their surface [22]. Cells were trypsinized and incubated with the primary antibody (Abcam; 1:1000 dilution) for 60 min at 4 °C, followed by thorough washing and binding with PE-conjugated secondary antibody (1:200 dilution) for another 30 min at 4 °C. Following thorough washing with PBS, the CD44⁺ and CD44⁻ cells were purified by FACS and seeded under maintenance conditions for 12 h for their adhesion and growth. The same were subjected to Olt (60 μ M) exposure for 48 h. Subsequently, the cells were trypsinized and quantified for CD44 expression by flow cytometry.

2.5.3. Flow Cytometry Quantification of Nestin⁺ and GFAP⁺ Cells

The Olt-treated cells were subjected to flow cytometry-based quantification of Nestin⁺ and GFAP⁺ cells following the protocol described [23]. Briefly, cells were trypsinized, fixed with 4% PFA for 20 min on ice, permeabilized using 0.05% saponin, and incubated at 4 °C with the appropriate primary antibody (1:200) in 1% blocking buffer for 60 min. Following thorough washing, the cells were incubated with PE-tagged secondary antibody (1:200) in 1% blocking buffer for 30 min at 4 °C. Cells were given PBS wash and acquired using FACS Calibur. The background fluorescence was subtracted using appropriate negative controls.

2.6. Immunocytochemistry

U-87 MG cells (Ctrl and Olt-treated) were seeded on cover-slips coated with gelatin. After 48 h of incubation, immunocytochemical analysis was performed following the standard protocol [24]. Antibodies used were against α -tubulin (Sigma–Aldrich; 1:1000), GFAP (Sigma–Aldrich; 1:500), γ H2AX (Abcam; 1:1000), CD44 (Abcam; 1:1000), CD133 (Abcam; 1:1000), Sox2 (Santacruz; 1:500), Oct-4 (Santacruz; 1:500), Nanog (Santacruz; 1:200), β -catenin (Santacruz; 1:200), Vimentin (Santacruz; 1:200), Nestin (Millipore; 1:200), and corresponding Cy3-conjugated secondary antibodies (Millipore; 1:500). Images were captured with a confocal laser scanning microscope (Zeiss LSM510, Germany) and analyzed.

2.7. Formation of Primary and Secondary Oncospheres

To assess the stemness and clonogenicity of plausible glioma stem cells (GSCs) present in U-87 MG cells and the influence of the Olt on them, an oncosphere formation assay was carried out using hanging drop method. Cells (control and treated) were considered for hanging drop preparation at a density of 500 cells/20 μ L in the maintenance medium [24]. After 48 h of incubation, the spheres designated as primary (1^o) oncospheres were collected and maintained in suspension culture for 3 days. Subsequently, they were enzymatically dispersed and subjected to secondary (2^o) sphere formation by the hanging drop method.

The number of (1°) and (2°) oncospheres generated were manually counted under the microscope, and the area of each was determined.

2.8. Ectopic GBM Model In Vivo

All animal experiments were carried out as per the institutional guidelines and following a protocol approved by the Institutional Animal Ethics Committee (IAEC), NCCS, Pune, India (Approval Code: EAF/2017/B-280 dated 13 March 2018). U-87 MG cells (0.5×10^6) suspended in 100 μ L sterile PBS were injected subcutaneously into the right flank of 4–5 wk old male SCID mice housed at the experimental animal facility (EAF) of NCCS. The mice with palpable tumors (~1 wk) were randomly divided into different groups with five animals each ($n = 5$) [Group (a): vehicle control; group (b and c): Olt (100 and 150 mg/kg body wt. respectively); and group (d): TMZ (50 mg/Kg body weight), as the positive control]. After completion of the experiment, blood was collected by retro-orbital route; the mice were sacrificed, and tumors and all vital organs were collected for hematoxylin and eosin (H&E) staining. We measured the tumor size in each using a Digital Vernier Caliper and calculated the respective tumor volume (mm^3) using the formula $A \times B^2 \times 0.52$ ($A = \text{length}$; $B = \text{width}$; all parameters in millimeters) [22]. Both blood and serum were used for hematological and biochemical analysis, respectively. The tissues were fixed using 4% PFA at 4 °C overnight, dehydrated with 20% sucrose, embedded in paraffin, and finally taken for sectioning. Around 5 μ M slices from each were mounted on glass slides for H&E staining.

2.9. Statistical Data

All data were presented as mean \pm SEM (standard error of the mean) with a minimum of 3 independent experiments, as mentioned in the figure legend; statistical significance was calculated using paired/unpaired Student's *t*-test (SigmaPlot v10.0, SysStat Software Inc., Palo Alto, CA, USA) compared to control. “*p*” values were calculated and are represented as follows: * $p \leq 0.05$; ** $p \leq 0.01$, *** $p \leq 0.001$.

3. Results

3.1. Olt Alters the Morphology and Growth of GBM Cells

To determine the effect of Olt on the cell growth characteristics, the MTT assay was carried out using the conventional chemotherapeutic drugs cisplatin (Cspln) and temozolomide (TMZ) as positive controls. The chemical structure of Olt is given in Figure 1a. As seen in Figure 1b, there was a significant impairment in cell viability in the case of GBM cells following their exposure to Cspln, TMZ, or the Olt. However, none of these impaired the cell viability in the case of HEK-293 cells and MSCs, indicating a lack of any adverse effects on normal cells. Interestingly, MSCs showed significantly higher viability with 20 μ M Olt exposure (129.42 ± 8.86) compared to the untreated control (Figure 1b). In contrast, the relative viability of treated GBM cells decreased significantly as the concentration of Olt increased. While ~65–75% of cells were viable with 20 μ M Olt exposure among various GBM cell lines studied, the same was 53–64% and 43–58% with 40- and 60 μ M Olt exposure, respectively. Strikingly, most of the cells from the GBM group got dislodged with 80 μ M Olt exposure by 48 h (Figure 1c). This prompted us to consider 40 and 60 μ M as the chosen doses of Olt for subsequent experiments using U-87 MG, one of the grade-IV GBM cell lines. Moreover, the inhibitory effect of Olt was maximum at 48 h. compared to 24 h (data not shown), and most cells were found necrotic by 72 h time point (Figure 1c). Hence, we chose the 48 h time point for all the subsequent experiments.

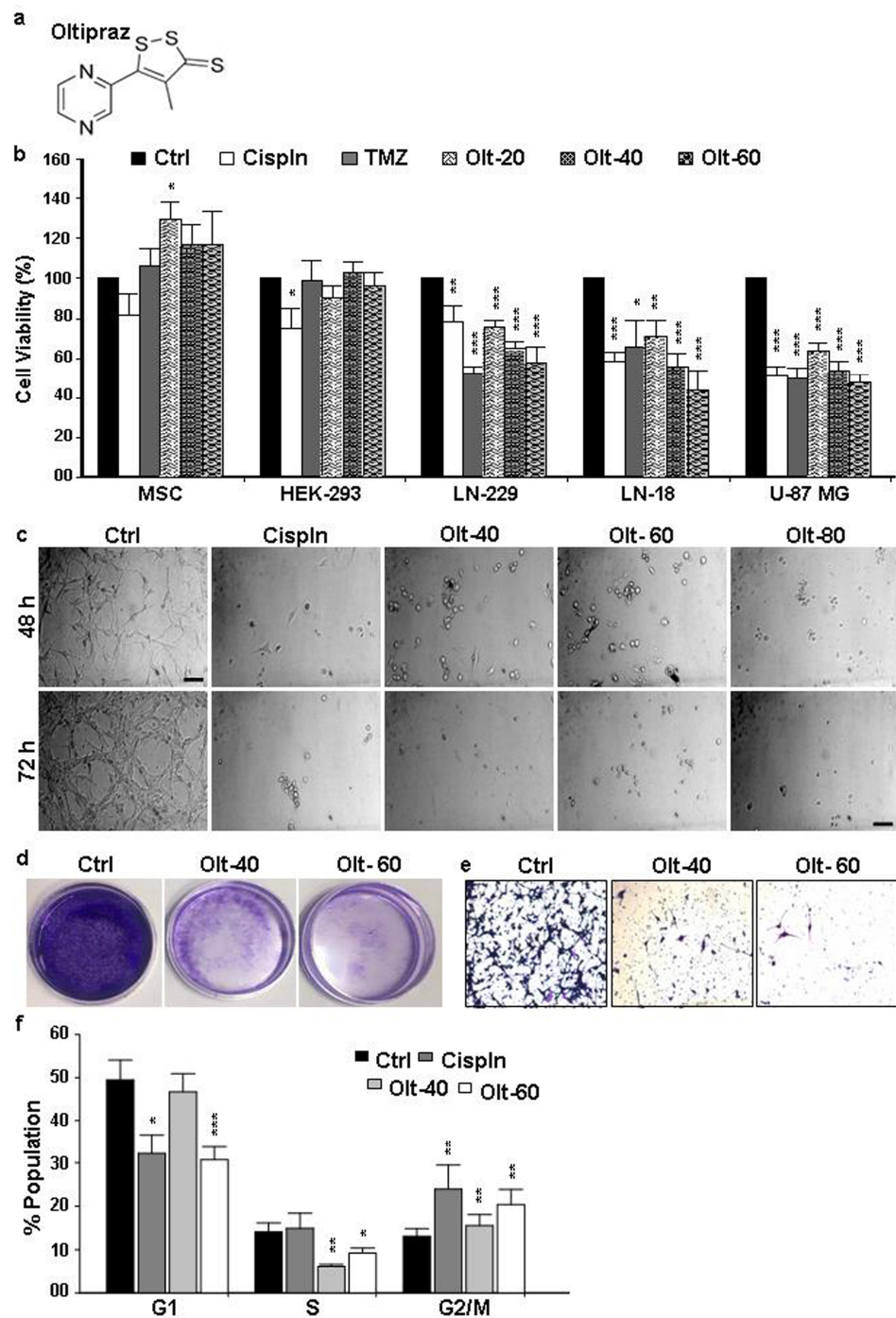


Figure 1. The inhibitory effect of Olt on GBM cell growth: (a) The chemical structure of Olt. (b) MTT assay depicting the % cell viability in normal (MSC), non-tumorigenic (HEK-293), and GBM (LN18, LN229, and U-87 MG) cell lines after 48 h of Olt treatment (20–60 μ M) compared to the untreated control (Ctrl) group in each (considered as 100% viable). The TMZ and Cispln exposure served as the positive controls for treatment groups in GBM cells. Values are represented as mean \pm SEM from independent experiments (n = 3–7). (c) Morphological changes in U-87 MG cells after treatment with Cispln and Olt (40-, 60- and 80 μ M) for 48- and 72 h (Scale bar 50 μ M). (d) Decrease in colony formation abilities of GBM cells after treatment of the Olt for 48 h. (e) Olt treatment (48 h) inhibited the migration of cells from the upper chamber to the lower chamber of the transwell plate. Scale bar: 100 μ M. (f) Flow cytometry analysis shows Olt-induced reduction in G1 and S phases and G2/M phase arrest in the cell cycle in U-87 MG cells. Data are presented as mean \pm SEM (n = 6). * $p \leq 0.05$; ** $p \leq 0.01$; *** $p \leq 0.001$ compared to the untreated Ctrl group.

To determine the effect of Olt on the morphology of U-87 MG cells, various concentrations (40- and 60 μM) of Olt exposure were given to cells, followed by monitoring of the morphological alterations under a microscope. As shown in Figure 1c, most of the untreated cells adhered to the tissue culture dish retaining an intact cytoskeleton. However, the cells treated with 40- and 60 μM Olt displayed a round and shrunken morphology similar to that with 30 μM Cispln. Moreover, the cells started dislodging from the dish and forming floating aggregates with 60 μM Olt after 48 h of exposure. A dramatic decrease in viable cell numbers with atypical apoptotic and necrotic morphology was detected among the remaining adherent ones.

3.2. Olt Impaired Migration and Colony Formation in GBM Cells

The treatment with the Olt at both the stated concentrations decreased the number of colonies and their size compared to Ctrl (Figure 1d). This finding suggested the efficacy of Olt in rendering anti-tumorigenicity. In fact, a negative correlation was noted between the increasing concentrations of Olt with that of the ability to form a colony in the soft-agar assay. Further, considering the highly aggressive and metastatic nature of GBM, the effect of Olt on cancer cell migration was studied using a trans-well migration assay. As seen in Figure 1e, Olt could attenuate the migration of U-87 MG cells.

3.3. The Mode of Action of Olt in Rendering Growth Inhibition in GBM Cells

To validate further the Olt responsive GBM cell growth impairment and the causative thereof, the cell cycle pattern was analyzed in U-87 MG cells treated with 40- and 60 μM Olt for 48 h. As seen in Figure 1f and Figure S1, the Olt exposure could arrest U-87 MG cells at the G2/M phase. While an increase in the G2/M population to $15.5 \pm 2.49\%$ could be seen with the 40 μM Olt, the same with 60 μM was $20.38 \pm 3.48\%$. On the contrary, the Olt exposure led to a decrease in the G1 and S phases of the cell cycle. This may reflect the association between G2/M phase cell cycle arrest and reduction in GBM cell viability.

Moreover, staining with annexin V-APC and PI followed by flow cytometry quantification revealed a significant increase in the apoptotic cell population in the Olt treated group (Figures 2a and S2). While there was a significant decrease in live population (Q1: Annexin V⁻/PI⁻) in the treatment group, the opposite was true for the early (Q4: Annexin V⁺/PI⁻) and late (Q3: Annexin V⁺/PI⁺) apoptotic population. However, a significant difference was not noted with respect to the necrotic population represented in Q2 (Annexin V⁻/PI⁺). Caspase 3/7 assay further validated this, showing increased Caspase 3/7⁺ cells with Olt exposure (Figure 2b). Collectively, our experimental evidence demonstrated that Olt might induce caspase-dependent apoptosis in human GBM cells.

Further verification of apoptosis was carried out using chromatin condensation and nuclear fragmentations assays, the hallmark characteristics of apoptotic cell nuclei by staining with Hoechst 33412 and phosphorylated H2A histone family member X (γH2AX -a marker of DNA double-strand break: DSB) (Figure 2c,d). The Olt exposed cells exhibited typical apoptotic features such as condensed chromatin, nuclear fragmentation, and membrane blebbing (Figure 2c). DSB was also evident by a notable increase in γH2Ax expression following exposure to the Olt. As seen in Figure 2d, there was a significant increase in punctate structures in the Olt-treated cells' nuclei. This was accompanied by a loss of cell integrity, as ascertained by monitoring microtubules disorganization through α -tubulin staining (Figure 2e). Olt exposure caused microtubule disruption in U-87 MG cells, as seen by compact and dense cellular microtubule bundles surrounding the nuclei compared with untreated Ctrl cells.

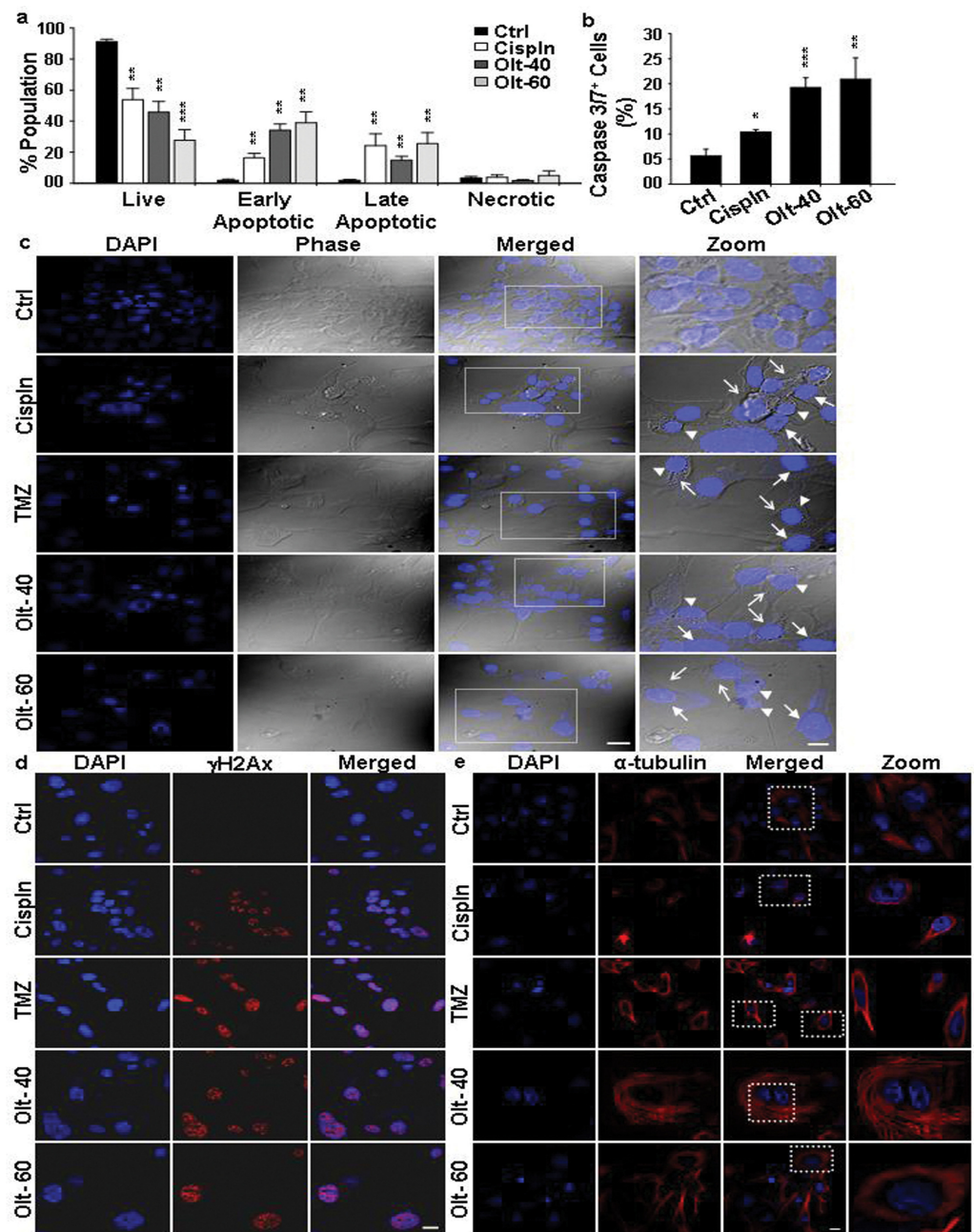


Figure 2. Pro-apoptotic influence of Olt on U-87 MG cells: (a,b) Flow cytometry quantification of (a) Annexin V/APC–PI and (b) Caspase 3/7 stained population indicates an increase in both early (Annexin V⁺/PI⁻) and late (Annexin V⁺/PI⁺) apoptotic cells and Caspase 3/7⁺ cells following Olt exposure of U-87 MG cells for 48 h. Cells treated with Cispln served as the positive control for the treatment group. Data are presented as mean ± SEM (n = 3–7). * $p \leq 0.05$; ** $p \leq 0.01$; *** $p \leq 0.001$ compared to the untreated Ctrl. (c) Hoechst 33342 staining reveals chromatin condensation (arrow-head), nuclear fragmentation (closed arrow), and membrane blebbing (open arrow) seen in U-87 MG cells treated with TMZ, Cispln (both positive controls), and Olt (40-, and 60 μM) for 48 h. Magnified views (Zoom) of the boxed regions are shown with contrast adjustment for better visualization. (d) γH2αX staining of U-87 MG cells displaying punctate nuclei in the treated groups reflects nuclear fragmentation upon exposure of Cispln, TMZ, and the Olt for 48 h. (e) Microtubules’ rearrangement was detected by α-tubulin staining in 48 h post-treated (Cispln, TMZ, Olt) U-87 MG cells. Magnified views (Zoom) of the boxed regions are shown for better visualization. Scale bar: 20 μM (c–e), 10 μM (zoomed images in c,e).

3.4. Olt Renders ROS-Dependent Apoptosis by Reducing Intracellular GSH Content and Disrupting Mitochondrial Membrane Potential

To ascertain if Olt-induced apoptosis was ROS-dependent, the levels of oxygen free radicals were determined by staining with DCHFDA and DHE. As seen in Figure 3a,b, there was ~3–5-fold increase in ROS in cells exposed to the Olt. In fact, the increase in the percentage of ROS-positive cells indicated a significant generation of free radicals/oxidative stress with the treatment of Olt, irrespective of the concentration used. There was also a loss of MMP, another hallmark of apoptosis (Figure 3c), along with a decrease (~3 folds) in GSH level (Figure 3d), compared to that of control. Taken together, these data demonstrated that Olt-induced apoptosis in GBM cells was manifested through mitochondrial dysfunction and ROS generation.

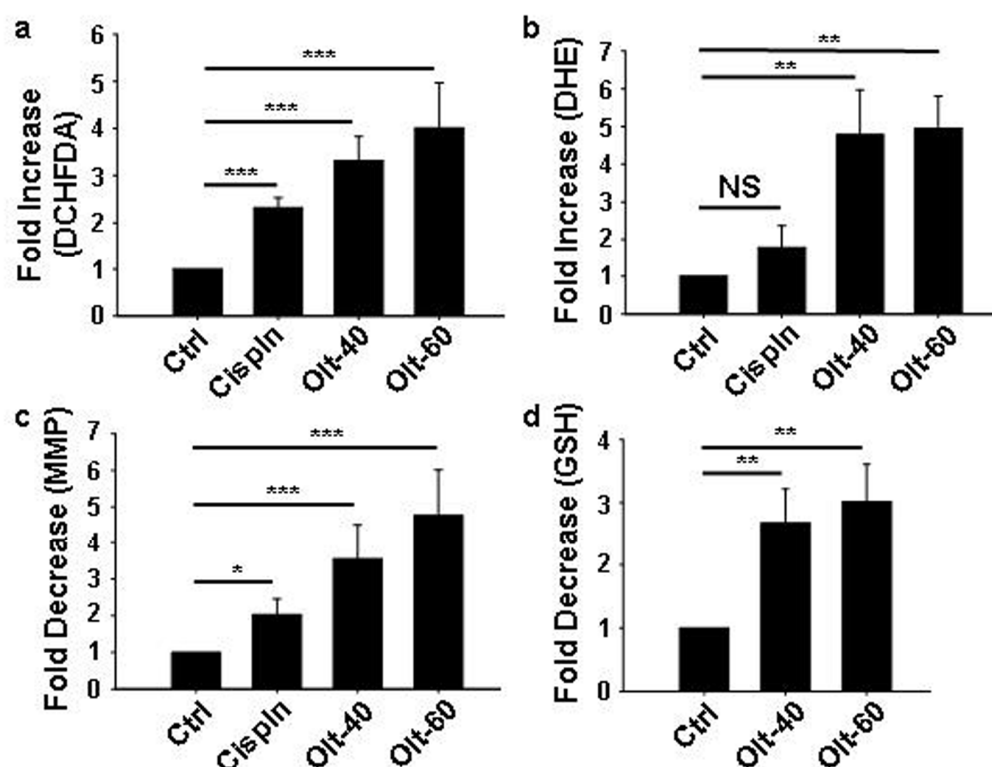


Figure 3. Influence of Olt on ROS and mitochondrial membrane potential: (a,b) Flow cytometry quantification of DCHFDA⁺ and DHE⁺ U-87 MG cells representing ROS-high state, following their exposure to Cispln and two different concentrations of Olt (40-, and 60 μ M). The data shows the fold increase in ROS in Cispln- and Olt-treated cells compared to untreated Ctrl. (c) Flow cytometry detection of loss of MMP by Rhodamine-123 staining. The data shown represent the fold difference in MMP loss in Cispln- and Olt-treated cells compared to untreated Ctrl. (d) Flow cytometry quantification of GSH reveals an Olt-mediated decrease in glutathione levels following Olt exposure of U-87 MG cells for 48 h. Data shown represents the fold decrease in glutathione levels in the Olt-treated cells compared to untreated Ctrl. Data are presented as mean \pm SEM (n = 4–8). * $p \leq 0.05$; ** $p \leq 0.01$; *** $p \leq 0.001$.

3.5. Olt Attenuates the Growth of GSCs and Induces Their Differentiation In Vitro

Glioma stem cells (GSCs) show a characteristic CD44⁺ phenotype and enhanced ALDH activity. To investigate the effect of Olt on these subpopulations of brain cancer cells, U-87 MG cells were stained with either CD44 or ALDH. Subsequently, the purification of both positive (ALDH⁺: ~55–75%; CD44⁺: ~75–90%) and negative populations was carried out in each by FACS. The sorted cells were further seeded both in the presence and absence of Olt and maintained in culture to assess the characteristics in each. Interestingly, ALDH⁺ cells post-seeding with Olt exposure exhibited a significant reduction in ALDH activity showing

around 47% and 45% ALDH⁺ cells with 40- and 60 μ M Olt, respectively (Figure 4a). There was also overall growth retardation with Olt exposure. The same was true in the case of CD44⁺ GSCs as well, which showed a reduction of around 20% CD44⁺ cells upon Olt exposure at 60 μ M concentration (Figure S3), suggesting the efficacy of the Olt in retarding CSCs growth. Intriguingly, CD44⁻ cells that were supposedly representing the non-CSCs regained CD44⁺ (43%) status post-seeding, albeit with a significant reduction in them upon Olt exposure (27%). This suggested the plausible occurrence of either dedifferentiation or the presence of primed GSCs in the CD44⁻ fraction. Together these data suggested the Olt to be effective in containing GSCs and non-GSCs alike.

One way to contain cancer would be to target the CSCs and induce them to differentiate. Hence, we analyzed the expression of CD44 in publicly available glioblastoma TCGA datasets using the ULCAN. CD44 expression was seen to be significantly enhanced in primary brain tumors as compared to normal brain tissues. In addition, patients with high CD44 expression had shorter overall survival when compared to patients with low CD44 expression (Figure S4). Accordingly, we compared the expression of various GSC and differentiation-specific markers in untreated control and the Olt-treated cells. While the number of nestin⁺ cells decreased with Olt treatment (Figure 4b), the reverse pattern was observed concerning GFAP, a differentiated astrocytic marker (Figure 4c). This was further validated by monitoring the expression of these markers by immunocytochemical analysis. We noticed a significant reduction in the expression of CD44, Sox2, Oct4, and Nanog in the Olt-exposed U-87 MG cells suggesting impairment in stemness characteristics (Figures 4d,e and S3). In contrast, an increased expression of GFAP in Olt exposed cells (Figure 4f) suggested that the Olt might have directed the GSCs to undergo differentiation, thereby curbing their self-renewal potential.

The ability to form oncospheres is used to assess the self-renewal capacity of CSCs. Considering that GSCs possess the capability to generate oncospheres in non-adherent culture, we developed the oncospheres by using the hanging drop method. Olt exposure could reduce the sphere-forming ability in U-87 MG cells, as ascertained by monitoring the number of oncospheres generated and their area. Treatment with the Olt significantly compromised the sphere-forming ability, as depicted by a significant decrease in the number of the primary (1^o) and secondary (2^o) oncospheres (Figure 4g,h). The same were further characterized by studying the expression of GSC markers, CD133 and CD44, in them. As seen in Figure 4i, a striking decrease in expression of CD133 and CD44 was seen in the Olt-treated (1^o) oncospheres as compared to Ctrl.

3.6. Olt Attenuates the Epithelial to Mesenchymal Transition

Because EMT is another hallmark of cancer metastasis, we investigated the effect of Olt on EMT markers, i.e., β -catenin and vimentin, after treatment with the Olt. There was a significant reduction in the expression of β -catenin and vimentin in Olt-treated cells compared to control (Figure 5a–d). These results suggest a plausible role of Olt in modulating EMT via β -catenin and vimentin expressions. Further work in this context would indicate the underlying EMT mechanism.

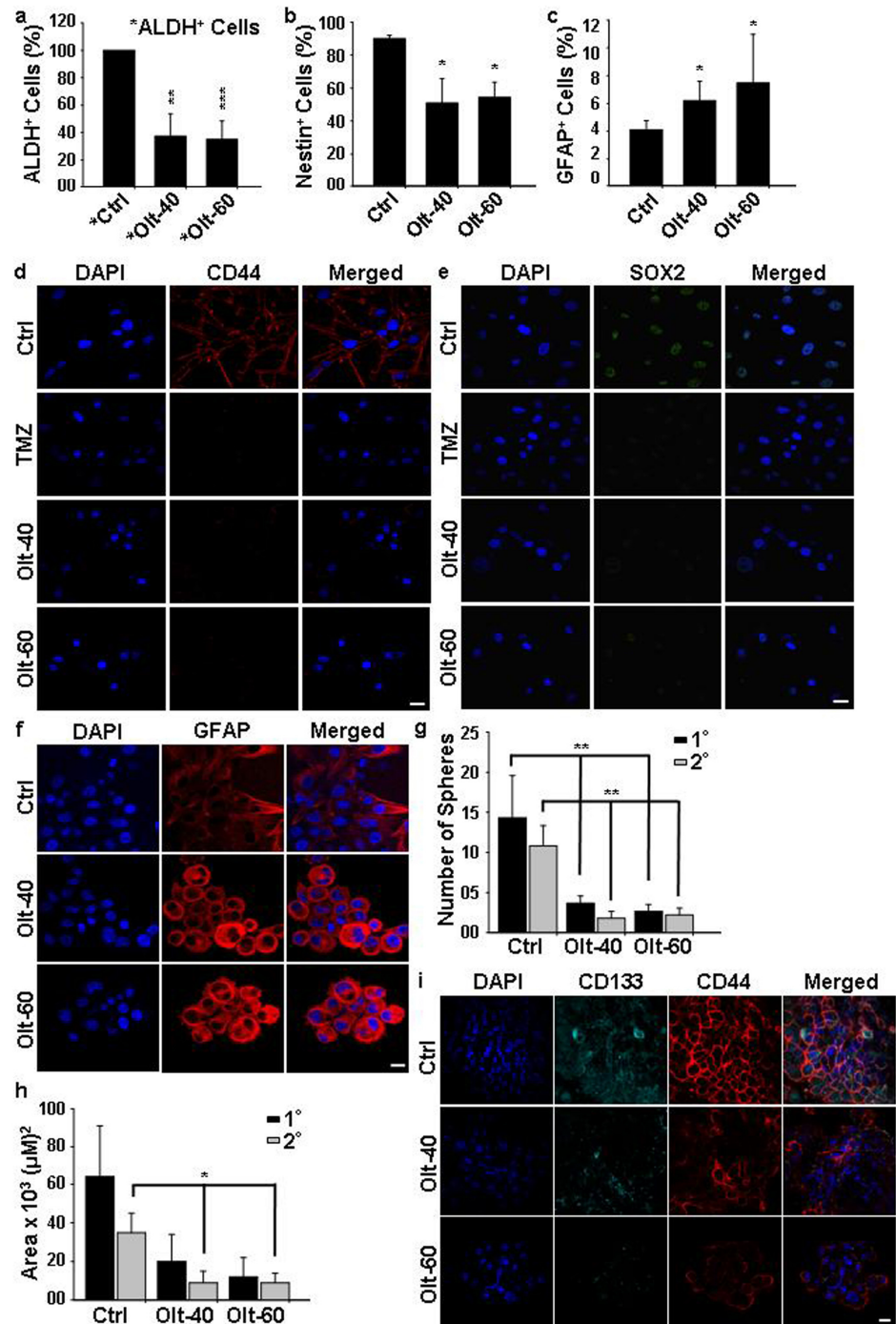


Figure 4. Influence of Olt on GSC population in vitro: (a) The ALDH⁺ cells representing the GSCs pool from U-87 MG cells, following their purification by FACS and reseeded, displayed a significant reduction in ALDH⁺ cells upon their exposure to the Olt for 48 h. (b,c) Olt exposure of U-87 MG cells for 48 h in culture decreased the number of Nestin⁺ cells (b) but increased the GFAP⁺ cells (c). (d,e) The immunostained pattern also revealed a reduction in U-87 MG cells exhibiting stem cell markers such as CD44 (d) and SOX2 (e) expression upon Olt exposure. (f) Olt exposure of U-87 MG cells led to an increase in GFAP, a mature astroglial marker, expression in them compared to untreated Ctrl. (g,h) Decrease in the number (g) and size (h) of primary (1°) and secondary (2°) oncospheres in U-87 MG cells post-treatment of the Olt for 48 h. (i) Immunostaining of CD44 and CD133 in oncospheres developed showed a decrease in the expression of the CD133 and CD44 populations in the Olt-treated U-87 MG cells. Scale bar: 20 μM. Data are presented as mean ± SEM (n = 4 in a–c, and 3 in g,h). * *p* ≤ 0.05, ** *p* ≤ 0.01, *** *p* ≤ 0.001 compared to the untreated Ctrl.

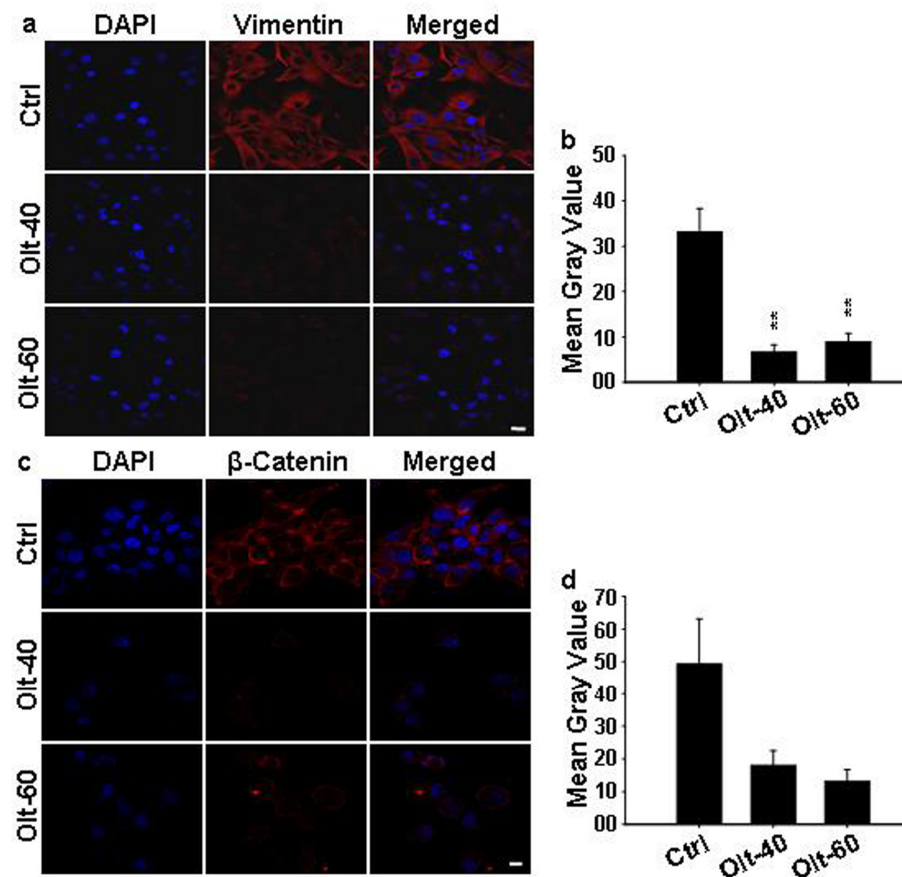


Figure 5. Influence of Olt on EMT reversal: (a,c) Immunofluorescence examination of EMT marker vimentin (a) and β -catenin (c) expression in U-87 MG cells revealed a reduction in the same following their exposure to Olt. Scale bar: 20 μ M. (b,d) Respective intensity quantification from (a) and (c) (from 3 different fields). Data are presented as mean \pm SEM (n = 3–4). ** $p \leq 0.01$.

3.7. The Effect of Olt Administration on the Ectopic GBM Mouse Model

Since our data suggested the anti-tumorigenic potential of Olt in U-87 MG cells *in vitro*, we were interested in assessing its efficacy *in vivo* as well by establishing an ectopic GBM model. The schematic for *in vivo* experiment is given in Figure 6a. Palpable tumors were detected in SCID mice after 1 wk of injection of U-87 MG cells in them. There was a significant reduction of more than 40% in tumor volume and weight in the Olt administration group compared to the Ctrl (Figure 6b–d). The TMZ was used as a positive control in these experiments. However, there was no change in the body weight in the Olt- and TMZ-treated groups compared to the vehicle control group (Table 1). Similarly, no significant difference was noted between the organ body weight ratio of different vital organs such as brain, liver, kidney, lungs, and spleen in treatment as well as Ctrl groups, suggesting no induction of systemic toxicity, if any, with the administration of Olt (Table 2). In contrast, there was a significant increase in spleen weight in disease control compared to healthy control (Table 2). Furthermore, concerning the biochemical (SGOT, SGPT, ALP, Albumin, Creatinine, blood urea nitrogen) and hematological parameters, no striking difference was noticed in any of the groups tested (Table 3). Similarly, the H&E staining of respective tissue sections revealed no evident histopathological abnormalities in any of the vital organs (brain, heart, liver, kidney, and lungs) tested (Figure 6e). However, extensive necrosis with occasional nuclear debris could be seen in tumor slices of Olt- and TMZ-treated groups compared to the disease control group. Together, our data suggested the efficacy of Olt in containing GBM similar to that of TMZ.

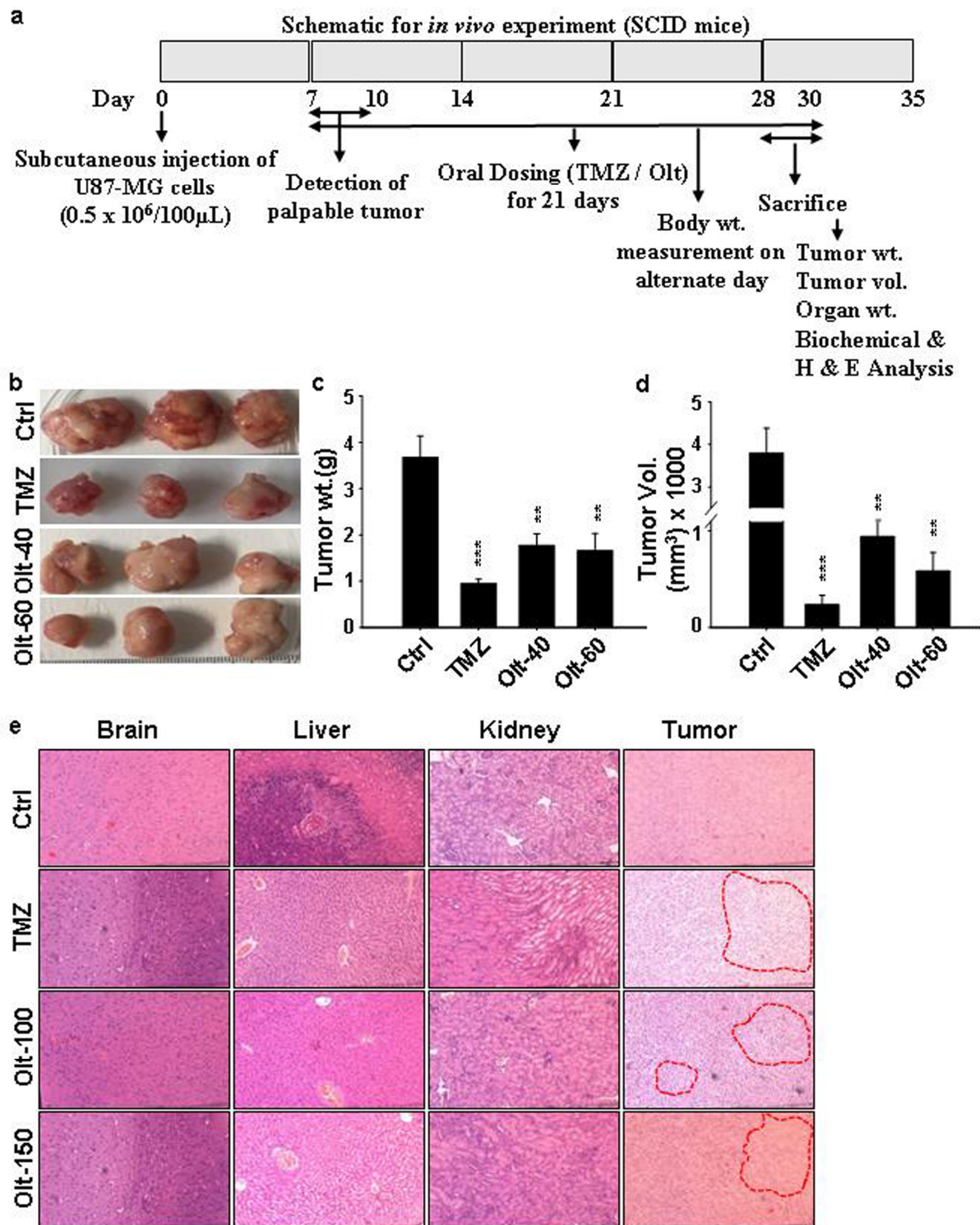


Figure 6. Anti-tumorigenic efficacy of Olt *in vivo*. TMZ (positive control) and Olt administration for 3 w, at the stated doses, led to reduced tumor progression in the U-87 MG cell-induced GBM xenograft mouse model. (a) The schematic for *in vivo* experiment. (b) Representative images of tumors excised from different groups (n = 5/group). (c,d) Measurement of tumor weight (c) and volume (d) in each group post-sacrifice. Data are presented as mean ± SEM ** p ≤ 0.01, *** p ≤ 0.001 compared to the disease control (Ctrl) group. (e) Representative images of H&E-stained tissue sections taken from tumor and stated vital organs from disease control (Ctrl) and U-87 MG cell-induced GBM tumor-bearing mice.

Table 1. Body Weight of tumor-bearing mice after oral administration of Olt for 21 days.

Groups	Initial/Day 0	Week-I	Week-II	Week-III
Ctrl	21.5 ± 1.73	21.9 ± 1.21	21.3 ± 1.24	22.5 ± 1.58
TMZ-50 *	21.5 ± 1.96	21.9 ± 1.36	20.5 ± 1.41	21.8 ± 1.09
Olt-100 *	21.3 ± 2.31	20.0 ± 1.02	20.3 ± 0.74	20.5 ± 0.86
Olt-150 *	20.4 ± 1.56	20.8 ± 1.07	20.9 ± 0.82	21.1 ± 1.40

* Drugs in mg.

Table 2. Relative organ weight (g%) of tumor-bearing mice administered with the Olt for 21 days post-sacrifice.

Organs	Ctrl	TMZ-50 *	Olt-100 *	Olt-150 *
Brain	1.52 ± 0.30	1.89 ± 0.11	2.16 ± 0.14	2.06 ± 0.22
Liver	4.27 ± 0.93	5.78 ± 0.54	5.38 ± 0.40	5.86 ± 1.54
Kidney	1.15 ± 0.27	1.39 ± 0.13	1.35 ± 0.07	1.34 ± 0.20
Heart	0.44 ± 0.10	0.68 ± 0.09	0.57 ± 0.09	0.52 ± 0.07
Lungs	0.93 ± 0.24	0.95 ± 0.16	1.28 ± 0.19	1.17 ± 0.19
Spleen	0.80 ± 0.24	0.45 ± 0.03 *	0.76 ± 0.12	0.56 ± 0.21

* Drugs in mg.

Table 3. Assessment of serum biochemical parameters in tumor-bearing mice administered with the Olt for 21 days post-sacrifice.

Biochemical Parameters	Ctrl	TMZ-50 *	Olt-100 *	Olt-150 *
Total Bilirubin (mg/dL)	0.42 ± 0.04	0.47 ± 0.05	0.60 ± 0.20	0.57 ± 0.08
Bilirubin Direct (mg/dL)	0.25 ± 0.03	0.28 ± 0.04	0.30 ± 0.05	0.26 ± 0.03
Bilirubin Indirect (mg/dL)	0.17 ± 0.02	0.15 ± 0.02	0.30 ± 0.10	0.23 ± 0.03
SGPT (IU/L)	34.67 ± 17.33	43.08 ± 5.84	55.63 ± 6.71	44.66 ± 8.17
SGOT (IU/L)	108.32 ± 15.2	122.28 ± 22.91	93.00 ± 21.0	131 ± 77.7
Blood Urea (mg/dL)	39.77 ± 6.14	44.87 ± 3.48	38.33 ± 4.40	38.5 ± 3.06
Blood Urea nitrogen (mg/dL)	18.58 ± 2.87	20.96 ± 1.62	17.91 ± 2.06	17.99 ± 1.43
Uric Acid (mg/dL)	1.3 ± 0.33	1.75 ± 0.09	1.60 ± 0.20	1.60 ± 0.34

* Drugs in mg.

4. Discussion

GBM, usually found in the cerebral hemispheres, is considered as one of the most aggressive tumors of the brain. It consists of poorly differentiated astrocytes having an extremely proliferative and invasive nature. Considering the survival time for GBM patients is very low, and that ~95% of patients die during the early months of diagnosis, identifying the prognostic factors related to GBM becomes difficult. The widely used chemotherapeutic drug, namely TMZ, has also been found to be associated with chemo-resistance against GBM treatment. This is primarily due to the domineering effect of the DNA repair enzyme O6-methylguanine-DNA methyltransferase (MGMT), which negates the TMZ-induced DNA alkylation [25]. Undoubtedly, the emerging drug resistance leads to higher mortality. Hence, the need of the hour is to develop suitable anticancer drugs for the treatment of GBM that should have fewer side effects, and that can act as adjuvant drugs to improve the efficacy of surgery and chemotherapy along with potency to avert tumor relapse [26,27].

One of the plausible strategic modalities for new drug screening would involve inhibition of proliferation, migration, and invasion of GBM cells. Accordingly, in the present work, we have evaluated the GBM tumor-specific anti-proliferative and cytotoxic activities of the dithiolethione Olt and its anti-tumorigenic efficacy both in vitro and in vivo. Several studies have shown that dithiolethione can decrease cell viability in lung and breast cancers [28,29]. In human metastatic breast cancer cells, Olt was shown to inhibit growth, induce the formation of apoptotic bodies, and increase DNA fragmentation and

laddering [30]. Moreover, in various carcinogenesis models, Olt was seen rendering protection from the induction of cancers in the skin, breast, bladder, lung, colon, pancreas, stomach, and liver [15]. Our results did suggest a differential response of Olt in normal and different grades of GBM cell lines. While a significant reduction in the viability of GBM cell lines accompanied by G2/M arrest was apparent following Olt exposure (40- and 60 μ M), the same in MSCs and the HEK293 cell line remained unaltered compared to the untreated control. Indeed, the higher viability of MSCs at a lower concentration (20 μ M) of Olt reflected its antioxidant effect in normal cells in contrast to the prooxidant effect in GBM cells. Natural compounds such as withaferin and gastrodin have also been shown to decrease the cell viability of GBM cells by arresting cells at the G2/M phase [31,32]. Similar results were reported with dioscin, a natural compound isolated from *Polygonatum sibiricum*, which led to the cell cycle arrest of HepG2 cells at the G2/M phase [33]. Moreover, a hybrid of Olt has also been shown to cause G2/M cell cycle arrest and induce apoptosis in human leukemia HL-60 cells [17]. Hence, Olt might be exerting its tumor-specific cell viability influence via G2/M arrest.

Since cell migration is a key process to the underlying immune response, wound healing, invasion, and metastasis, microtubules play a crucial role in mitosis and cell division, and these factors have emerged as important targets in cancer therapy [34]. In our study, we found that Olt significantly attenuated the ability of GBM cell migration. Moreover, a noticeable disarrangement of microtubules suggested that Olt decreased the metastatic potential of GBM cells. Similar results were obtained by Hirtz et al. [35], showing GPER agonist G1 promoting cell death and a decrease in cell viability in LN-229 and U-251 cells via the modulation of microtubule dynamics.

Several key parameters, such as increased ROS, decreased MMP, and glutathione level, activate intrinsic apoptosis and, thus, direct cell death [35]. GSH is the most critical thiol-containing molecule and functions against oxidative stress. Indeed, the balance between intracellular ROS and GSH levels controls cell death in cancer cells [36]. Excessive buildup of ROS leads to change in mitochondrial functions and activates a series of mitochondria-associated events corresponding to apoptosis [36]. Moreover, ROS accumulation can cause depolarization of the mitochondrial membrane and thereby promote apoptosis [27,37]. It has also been proposed that ROS generation plays an essential role in the apoptotic cell death induced by cytotoxic drugs [38]. In agreement with these concepts, our findings demonstrate that Olt induces apoptosis in GBM cells through the disturbance of MMP and enhanced ROS production with a concomitant reduction in GSH level. Moreover, the detection of punctate nuclei via γ H2 α X staining could also validate nuclear condensation and fragmentation, the characteristic apoptotic features, in Olt exposed cells. Similar results were obtained by Liang et al. [32], who showed gastrodin-induced ROS-mediated cell death and apoptosis in GBM cells. Moreover, a significant increase in executioner caspase 3/7 activity in Olt-treated cells as compared to Ctrl suggested that the Olt-induced apoptosis was executed through caspase 3/7 activation, which is in line with similar studies conducted using gingerol, silymarin, and CHBC—an indole derivative [20,39]

The GBM malignancy is also augmented by the presence of a niche population of cells called CSCs that possess an enormously high potential for tumorigenicity. The presence of CSCs has been verified in many cancers, including GBM. They possess self-renewal, multi-potent differentiation properties, and the capacity to generate new tumors [4]. CSCs have been attributed to aggressiveness, relapse, and resistance to chemotherapy in GBM [40]. CD44 is widely used as a marker for the identification of CSCs in various cancers, including that of the brain [4,41–45]. In fact, its expression level is negatively correlated with GBM patients' survival [45]. Similarly, Aldehyde dehydrogenases (ALDH), a group of enzymes that are involved in detoxifying aldehydic products produced by ROS and that, hence, contribute to cell survival, have been ascribed to the CSC phenotype [7,46–48]. Moreover, ALDH enzyme activity is important for eliciting its response in chemo-resistance, cell proliferation, and differentiation. In fact, several studies have indicated a decrease in ALDH⁺ cells in response to various curative and preventive treatments [47,48]. In the human

prostate cancer cell line, LNcaP, PC-3luc, and the inhibition of ALDH1 were reported to induce differentiation *in vitro* and impair clonogenicity [47]. Our findings with the Olt exposure of GBM showing a significant reduction in the expression of CD44, ALDH, and other stem cell markers, such as Oct4 and Nanog, reflected a decrease in the stemness of CSCs and a directive towards differentiation. Moreover, the repressor effect of Olt exposure on both CD44⁺ and CD44⁻ populations suggested that the Olt was effective in containing GSCs as well as non-GSCs.

One way to contain cancer would be to target the CSCs and induce them to differentiate. Lately, many studies have focused on targeting CSCs to remove cancer cells by regulating stem cells with a therapeutic strategy called differentiation therapy [49–51]. Hence, a significant reduction in the CSC population marked by a decrease in the expression of stem cell markers, reduced sphere-forming ability characterized by a decline in the number of spheres as well as a reduction of sphere area also validated the antagonistic effect of Olt on CSCs. Similar results have been reported in many other studies where chemotherapeutic drugs and natural compounds have caused differentiation of CSCs by inducing apoptosis [5,42,43,48]. The natural compound curcumin was also found to decrease the malignant characteristics of GSCs and glioma-initiating cells via the induction of ROS and autophagy [52,53]. Nestin is one of the intermediate filament proteins detected abundantly in neuroepithelial stem/progenitor cells in the growing central nervous system [23]. Hence, the loss of Nestin expression and enhanced GFAP expression accompanied by increased GFAP⁺ cells seen following Olt treatment in our experiment was indicative of cellular differentiation.

In the case of solid tumors such as GBM, the process of EMT is commonly linked with aggressiveness, relapse, and the metastasis of cancer. Moreover, its induction in cancer causes the acquisition of the CSC-like phenotype. Having detected the efficacy of Olt *in vitro* and *in vivo*, we further wanted to study the effect of Olt on EMT markers β -catenin and vimentin. β -catenin is known to interact with the members of the LEF/TCF family of transcription factors and mediates the trans-activation of genes involved in metastasis and invasion. A study has shown the presence of TCF/LEF-1-binding motifs in the Vimentin promoter [54]. Hence, canonical Wnt activation mediated β -catenin nuclear translocation and binding to these motifs might activate Vimentin expression and, therefore, EMT induction [55]. This may support the role of β -catenin and Vimentin in EMT and malignant transformation. Accordingly, the Olt-mediated reduction in β -catenin and Vimentin expression seen in our study might facilitate reversing the process of EMT.

In many recent articles, it has been reported that CD44 is a downstream target of Wnt signalling and is widely proven to maintain the stemness of GSCs [22,56]. In gastric cancer, CD44 was shown to modulate Wnt/ β -catenin signaling, which is primarily involved in tumor metastasis and progression [57]. The authors have suggested that CD44 downregulation reduces its interaction with N-WASP and ErbB2. This eventually affects the phosphorylation of β -catenin and inhibits actin polymerization to reduce cancer cell migration. Hence, downregulation of CD44 in cancer cells would inhibit migration and the invasion of cells through the impairment of β -catenin expression. Thus, we speculated that a decrease in the expression of CD44 in GBM cells would reduce migration and the invasion of cancer cells by modulating β -catenin. Further investigation of the modulation of Wnt signaling by Olt would address this.

In line with our *in vitro* findings, the ectopic model for GBM using SCID mice *in vivo* also validated the efficacy of Olt in containing GBM. The Olt-administered group showed a significant reduction in tumor growth within the monitored time regimen and without rendering any systemic toxicity in any of the vital organs tested. This was ascertained by monitoring no significant changes in biochemical and hematological parameters as well as in tissue architecture, hence suggesting its suitability for patient usage without any adverse effects on other organs. These findings corroborated well with our *in vitro* cell viability assay performed with HEK293 cells and MSCs, where the Olt did not adversely impact cell growth and viability. Similar results have also been reported by several other natural

compounds such as curcumin, epoxyazadiradione, Magnolol, Kukoamine A, AECHL-1, etc. [7,26,52,58,59]. Collectively, our data suggested the potential anti-tumorigenic propensity of Olt that can serve as a plausible adjuvant therapeutic for containing GBM.

5. Conclusions

The lingering bottleneck in oncotherapy pertains to chemo-resistance and toxicity to normal cells. Although a majority of chemotherapeutics are targeted to induce apoptosis within a tumor, non-specific effects on normal cells as well as bi-allelic inactivation in cancer cells pose a major hindrance to the same. Hence, strategies to curb cancer cell proliferation induce autophagy in parallel to differentiation induction may serve as plausible alternatives. Our investigation using the Olt demonstrated the potential of Olt to induce apoptosis in GBM cells by modulating tubulin arrangements and arresting the cell cycle, whereas it remained non-toxic to normal cells. In fact, its anti-cancerous effect *in vitro* was either akin to or superior to the standard drug Cispln. Undoubtedly, the encouraging results obtained with the Olt from both *in vitro* and *in vivo* studies have formed a strong basis for its further exploration and usage as an advanced anticancer adjuvant drug candidate for the possible prevention and treatment of GBM and other cancers using patient samples and patient-derived xenograft models. Notwithstanding, an advanced study on the mechanistic action of the Olt and its clinical efficacy may render its bedside translation.

Supplementary Materials: The following supporting information can be downloaded at: <https://www.mdpi.com/article/10.3390/cells11193057/s1>, Figure S1: Representative image showing cell cycle pattern of U-87 MG cells following exposure to Cispln and Olt (40 and 60 μ M) for 48 h; Figure S2: Representative image showing annexin-PI pattern of U-87 MG cells following exposure to Cispln (30 μ M) and Olt (40 and 60 μ M) for 48 h; Figure S3: (a) Decrease in CD44⁺ population in post-sorted CD44⁺ cells exposed to Olt 60 μ M for 48 h, (b,c): Immunostaining for detection of Oct4 and Nanog in U-87 MG cells after treatment of Olt for 48 h; Figure S4: (a) *In silico* analysis with the data from TCGA for the relative CD44 expression in normal and primary tumor samples using the ULCAN web, (b) The survival rates of patients with GBM, as estimated by Kaplan-Meier method.

Author Contributions: Conceptualization, U.K.-N. and N.L.; Data curation, U.K.-N. and N.L.; Formal analysis, U.K.-N. and N.L.; Funding acquisition, N.L.; Investigation, U.K.-N.; Resources, N.L.; Supervision, N.L.; Writing—original draft, U.K.-N.; Writing—review and editing, N.L. All authors have read and agreed to the published version of the manuscript.

Funding: This research was partially supported by funding from DBT (project # BT/PR16655/NER/95/132/2015) and intramural support from NCCS to NL. The APC was funded by NCCS intramural support.

Institutional Review Board Statement: The animal study protocol was approved by the Institutional Animal Ethics Committee of NCCS, Pune, India (Approval code: EAF/2017/b-280 dated 13/03/2018).

Informed Consent Statement: Not Applicable.

Data Availability Statement: Not Applicable.

Acknowledgments: Authors acknowledge the help rendered by Prachi Bhagat in analyzing H&E stained tissue sections and B.K. Deshmukh for assisting in animal experiments. N.L. acknowledges the funding received from NCCS intramural funding and DBT (project # BT/PR16655/NER/95/132/2015). UK-N is supported by the N-PDF programme from DST and RA from ICMR.

Conflicts of Interest: The authors declare no conflict of interest.

References

1. Miller, K.D.; Ostrom, Q.T.; Kruchko, C.; Patil, N.; Tihan, T.; Cioffi, G.; Fuchs, H.E.; Waite, K.A.; Jemal, A.; Siegel, R.L.; et al. Brain and other central nervous system tumor statistics, 2021. *CA Cancer J. Clin.* **2021**, *71*, 381–406. [CrossRef] [PubMed]
2. Mathur, P.; Sathishkumar, K.; Chaturvedi, M.; Das, P.; Sudarshan, K.L.; Santhappan, S.; Nallasamy, V.; John, A.; Narasimhan, S.; Roselind, F.S.; et al. Cancer statistics, 2020: Report from national cancer registry programme, India. *JCO Glob. Oncol.* **2020**, *6*, 1063–1075. [CrossRef] [PubMed]

3. Mondal, S.; Bhattacharya, K.; Mandal, C. Nutritional stress reprograms dedifferentiation in glioblastoma multiforme driven by PTEN/Wnt/Hedgehog axis: A stochastic model of cancer stem cells. *Cell Death Discov.* **2018**, *4*, 110. [CrossRef] [PubMed]
4. Giacomelli, C.; Daniele, S.; Natali, L.; Iofrida, C.; Flamini, G.; Braca, A.; Trincavelli, M.L.; Martini, C. Carnosol controls the human glioblastoma stemness features through the epithelial-mesenchymal transition modulation and the induction of cancer stem cell apoptosis. *Sci. Rep.* **2017**, *7*, 15174. [CrossRef]
5. Zhou, H.M.; Zhang, J.G.; Zhang, X.; Li, Q. Targeting cancer stem cells for reversing therapy resistance: Mechanism, signaling, and prospective agents. *Signal Transduct. Target Ther.* **2021**, *6*, 62. [CrossRef]
6. Qazi, M.A.; Vora, P.; Venugopal, C.; Sidhu, S.S.; Moffat, J.; Swanton, C.; Singh, S.K. Intratumoral heterogeneity: Pathways to treatment resistance and relapse in human glioblastoma. *Ann. Oncol.* **2017**, *28*, 1448–1456. [CrossRef]
7. Sawant, M.A.; Dasgupta, A.; Lavhale, M.S.; Sitasawad, S.L. Novel triterpenoid AECHL-1 induces apoptosis in breast cancer cells by perturbing the mitochondria–endoplasmic reticulum interactions and targeting diverse apoptotic pathways. *Biochim. Biophys. Acta.* **2016**, *1860*, 1056–1070. [CrossRef]
8. Sorribes, I.C.; Handelman, S.K.; Jain, H.V. Mitigating temozolomide resistance in glioblastoma via DNA damage-repair inhibition. *J. R. Soc. Interface* **2020**, *17*, 20190722. [CrossRef]
9. Lan, F.; Pan, Q.; Yu, H.; Yue, X. Sulforaphane enhances temozolomide-induced apoptosis because of down-regulation of miR-21 via Wnt/ β -catenin signaling in glioblastoma. *J. Neurochem.* **2015**, *134*, 811–818. [CrossRef]
10. Moskwa, J.; Naliwajko, S.K.; Markiewicz-Żukowskam, R.; Gromkowska-Kępką, K.J.; Nowakowski, P.; Strawa, J.W.; Borawska, M.H.; Tomczyk, M.; Socha, K. Chemical composition of Polish propolis and its antiproliferative effect in combination with *Bacopa monnieri* on glioblastoma cell lines. *Sci. Rep.* **2020**, *10*, 21127. [CrossRef]
11. Fernando, W.; Rupasinghe, H.P.V.; Hoskin, D.W. Dietary phytochemicals with antioxidant and prooxidant activities: A double-edged sword in relation to adjuvant chemotherapy and radiotherapy? *Cancer Lett.* **2019**, *452*, 168–177. [CrossRef] [PubMed]
12. Ammendola, M.; Haponska, M.; Balik, K.; Modrakowska, P.; Matulewicz, K.; Kazmierski, L.; Lis, A.; Kozłowska, J.; Garcia-Valls, R.; Giamberini, M.; et al. Stability and anti-proliferative properties of biologically active compounds extracted from *Cistus L.* after sterilization treatments. *Sci. Rep.* **2020**, *10*, 6521. [CrossRef] [PubMed]
13. Díaz, A.F.; Polo, S.; Gallardo, N.; Leáñez, S.; Pol, O. Analgesic and antidepressant effects of oltipraz on neuropathic pain in mice by modulating microglial activation. *J. Clin. Med.* **2019**, *8*, 890. [CrossRef] [PubMed]
14. Jiang, Z.; Bian, M.; Wu, J.; Li, D.; Ding, L.; Zeng, Q. Oltipraz prevents high glucose-induced oxidative stress and apoptosis in RSC96 cells through the Nrf2/NQO1 signaling pathway. *BioMed Res. Int.* **2020**, *23*, 2020.
15. Yagishita, Y.; Gathonton-Schwager, T.N.; McCallum, M.L.; Kensler, T.W. Current Landscape of NRF2 Biomarkers in Clinical Trials. *Antioxidants* **2020**, *9*, 716. [CrossRef] [PubMed]
16. Kapoor, R.; Sirohi, V.K.; Gupta, K.; Dwivedi, A. Naringenin ameliorates progression of endometriosis by modulating Nrf2/Keap1/HO1 axis and inducing apoptosis in rats. *J. Nutri. Biochem.* **2019**, *70*, 215–226. [CrossRef] [PubMed]
17. Lin, J.; Zhang, L.; Wang, Z.; Guan, Q.; Bao, K.; Wu, L. G2/M cell cycle arrest and apoptosis induced by COH-203 in human promyelocytic leukemia HL-60 cells. *Oncol. Lett.* **2021**, *22*, 815. [CrossRef] [PubMed]
18. Galluzzi, L.; Zamzami, N.; de La Motte Rouge, T.; Lemaire, C.; Brenner, C.; Kroemer, G. Methods for the assessment of mitochondrial membrane permeabilization in apoptosis. *Apoptosis* **2007**, *12*, 803–813. [CrossRef] [PubMed]
19. Singh, B.K.; Tripathi, M.; Chaudhari, B.P.; Pandey, P.K.; Kakkar, P. Natural terpenes prevent mitochondrial dysfunction, oxidative stress and release of apoptotic proteins during nimesulide-hepatotoxicity in rats. *PLoS ONE* **2012**, *7*, e34200. [CrossRef]
20. Nguyen, P.; Doan, P.; Murugesan, A.; Ramesh, T.; Rimpilainen, T.; Candeias, N.R.; Yli-Harja, O.; Kandhavelu, M. GPR17 signaling activation by CHBC agonist induced cell death via modulation of MAPK pathway in glioblastoma. *Life Sci.* **2022**, *291*, 120307. [CrossRef]
21. Lee, D.; Lee, Y.H.; Lee, K.H.; Lee, B.S.; Alishir, A.; Ko, Y.J.; Kang, K.S.; Kim, K.H. Aviculin isolated from *Lespedeza cuneata* induce apoptosis in breast cancer cells through mitochondria-mediated caspase activation pathway. *Molecules* **2020**, *25*, 1708. [CrossRef]
22. Liu, Q.; Guan, Y.; Li, Z.; Wang, Y.; Liu, Y.; Cui, R.; Wang, Y. miR-504 suppresses mesenchymal phenotype of glioblastoma by directly targeting the FZD7-mediated Wnt– β -catenin pathway. *J. Exp. Clin. Cancer Res.* **2019**, *38*, 358. [CrossRef] [PubMed]
23. Ramasamy, S.K.; Lenka, N. Notch exhibits ligand bias and maneuvers stage-specific steering of neural differentiation in embryonic stem cells. *Mol. Cell. Biol.* **2010**, *30*, 1946–1957. [CrossRef] [PubMed]
24. Verma, M.K.; Lenka, N. Temporal and contextual orchestration of cardiac fate by WNT-BMP synergy and threshold. *J. Cell. Mol. Med.* **2010**, *8*, 2094–2108. [CrossRef]
25. Ranjan, A.; Kaushik, I.; Srivastava, S.K. Pimozide suppresses the growth of brain tumors by targeting STAT3-mediated autophagy. *Cells* **2020**, *9*, 2141. [CrossRef]
26. Cheng, Y.C.; Hueng, D.Y.; Huang, H.Y.; Chen, J.Y.; Chen, Y. Magnolol and honokiol exert a synergistic anti-tumor effect through autophagy and apoptosis in human glioblastomas. *Oncotarget* **2016**, *7*, 29116–29130. [CrossRef]
27. Yang, H.L.; Tsai, C.H.; Shrestha, S.; Lee, C.C.; Liao, J.W.; Hseu, Y.C. Coenzyme Q0, a novel quinone derivative of *Antrodia camphorata*, induces ROS-mediated cytotoxic autophagy and apoptosis against human glioblastoma cells in vitro and in vivo. *Food Chem. Toxicol.* **2021**, *155*, 112384. [CrossRef]
28. Moody, T.W.; Switzer, C.; Santana-Flores, W.; Ridnour, L.A.; Berna, M.; Thill, M.; Jensen, R.T.; Sparatore, A.; DelSoldato, P.; Yeh, G.C.; et al. Dithiolethione modified valproate and diclofenac increase E-cadherin expression and decrease proliferation of non-small cell lung cancer cells. *Lung Cancer* **2010**, *68*, 154–160. [CrossRef] [PubMed]

29. Switzer, C.H.; Cheng, R.Y.; Ridnour, L.A.; Murray, M.C.; Tazzari, V.; Sparatore, A.; Del Soldato, P.; Hines, H.B.; Glynn, S.A.; Ambs, S.; et al. Dithiolethiones inhibit NF- κ B activity via covalent modification in human estrogen receptor-negative breast cancer. *Cancer Res.* **2012**, *72*, 2394–2404.
30. Nho, C.W.; O'Dwyer, P.J. NF- κ B activation by the chemopreventive dithiolethione oltipraz is exerted through stimulation of MEKK3 signaling. *J. Biol. Chem.* **2004**, *279*, 26019–26027. [CrossRef]
31. Tang, Q.; Ren, L.; Liu, J.; Li, W.; Zheng, X.; Wang, J.; Du, G. Withaferin A triggers G2/M arrest and intrinsic apoptosis in glioblastoma cells via ATF4-ATF3-CHOP axis. *Cell Prolif.* **2020**, *53*, e12706. [CrossRef] [PubMed]
32. Liang, W.Z.; Jan, C.R.; Hsu, S.S. Cytotoxic effects of gastrodin extracted from the rhizome of *Gastrodia elata* Blume in glioblastoma cells, but not in normal astrocytes, via the induction of oxidative stress-associated apoptosis that involved cell cycle arrest and p53 activation. *Food Chem. Toxicol.* **2017**, *107*, 280–292. [CrossRef] [PubMed]
33. Zhang, Y.S.; Ma, Y.L.; Thakur, K.; Hussain, S.S.; Wang, J.; Zhang, Q.; Zhang, J.G.; Wei, Z.J. Molecular mechanism and inhibitory targets of dioscin in HepG2 cells. *Food Chem. Toxicol.* **2018**, *120*, 143–154. [CrossRef]
34. Sahai, E. Mechanisms of cancer cell invasion. *Curr. Opin. Gen. Dev.* **2005**, *15*, 87–96. [CrossRef]
35. Hirtz, A.; Lebourdais, N.; Rech, F.; Bailly, Y.; Vaginay, A.; Smail-Tabbone, M.; Dubois-Pot-Schneider, H.; Dumond, H. GPER agonist G-1 disrupts tubulin dynamics and potentiates temozolomide to impair glioblastoma cell proliferation. *Cells* **2021**, *10*, 3438. [CrossRef] [PubMed]
36. Pathak, N.; Khandelwal, S. Role of oxidative stress and apoptosis in cadmium induced thymic atrophy and splenomegaly in mice. *Toxicol. Lett.* **2007**, *169*, 95–108. [CrossRef]
37. Hseu, Y.C.; Tsai, T.J.; Korivi, M.; Liu, J.Y.; Chen, H.J.; Lin, C.M.; Shen, Y.C.; Yang, H.L. Antitumor properties of Coenzyme Q0 against human ovarian carcinoma cells via induction of ROS-mediated apoptosis and cytoprotective autophagy. *Sci. Rep.* **2017**, *7*, 8062. [CrossRef]
38. Queiroz, R.M.; Takiya, C.M.; Guimarães, L.P.; Rocha, G.D.; Alviano, D.S.; Blank, A.F.; Alviano, C.S.; Gattass, C.R. Apoptosis-inducing effects of *Melissa officinalis* L. essential oil in glioblastoma multiforme cells. *Cancer Investig.* **2014**, *32*, 226–235. [CrossRef]
39. Czarnik-Kwaśniak, J.; Kwaśniak, K.; Kwasek, P.; Świerzowska, E.; Strojewska, A.; Tabarkiewicz, J. The influence of lycopene, [6]-gingerol, and silymarin on the apoptosis on U-118MG glioblastoma cells in vitro model. *Nutrients* **2019**, *12*, 96. [CrossRef]
40. Suzuka, J.; Tsuda, M.; Wang, L.; Kohsaka, S.; Kishida, K.; Semba, S.; Sugino, H.; Aburatani, S.; Frauenlob, M.; Kurokawa, T.; et al. Rapid reprogramming of tumour cells into cancer stem cells on double-network hydrogels. *Nat. Biomed. Eng.* **2021**, *5*, 914–925. [CrossRef]
41. Brescia, P.; Richichi, C.; Pelicci, G. Current strategies for identification of glioma stem cells: Adequate or unsatisfactory? *J. Oncol.* **2012**, *2012*, 376894. [CrossRef] [PubMed]
42. Colapietro, A.; Mancini, A.; Vitale, F.; Martellucci, S.; Angelucci, A.; Llorens, S.; Mattei, V.; Gravina, G.L.; Alonso, G.L.; Festuccia, C. Crocetin extracted from saffron shows antitumor effects in models of human glioblastoma. *Int. J. Mol. Sci.* **2020**, *21*, 423. [CrossRef] [PubMed]
43. Shen, S.; Xu, X.; Lin, S.; Zhang, Y.; Liu, H.; Zhang, C.; Mo, R. A nanotherapeutic strategy to overcome chemotherapeutic resistance of cancer stem-like cells. *Nat. Nanotech.* **2021**, *16*, 104–113. [CrossRef] [PubMed]
44. Yeh, M.; Wang, Y.Y.; Yoo, J.Y.; Oh, C.; Otani, Y.; Kang, J.M.; Park, E.S.; Kim, E.; Chung, S.; Jeon, Y.J.; et al. MicroRNA-138 suppresses glioblastoma proliferation through downregulation of CD44. *Sci. Rep.* **2021**, *11*, 9219. [CrossRef] [PubMed]
45. Nishikawa, M.; Inoue, A.; Ohnishi, T.; Yano, H.; Ozaki, S.; Kanemura, Y.; Suehiro, S.; Ohtsuka, Y.; Kohno, S.; Ohue, S.; et al. Hypoxia-induced phenotypic transition from highly invasive to less invasive tumors in glioma stem-like cells: Significance of CD44 and osteopontin as therapeutic targets in glioblastoma. *Transl. Oncol.* **2021**, *14*, 101137. [CrossRef]
46. Rasper, M.; Schäfer, A.; Piontek, G.; Teufel, J.; Brockhoff, G.; Ringel, F.; Heindl, S.; Zimmer, C.; Schlegel, J. Aldehyde dehydrogenase 1 positive glioblastoma cells show brain tumor stem cell capacity. *Neuro. Oncol.* **2010**, *12*, 1024–1033. [CrossRef]
47. van den Hoogen, C.; vander Horst, G.; Cheung, H.; Buijs, J.T.; Lippitt, J.M.; Guzmán-Ramírez, N.; Hamdy, F.C.; Eaton, C.L.; Thalmann, G.N.; Cecchini, M.G.; et al. High aldehyde dehydrogenase activity identifies tumor-initiating and metastasis-initiating cells in human prostate cancer. *Cancer Res.* **2010**, *70*, 5163–5173. [CrossRef]
48. MacDonagh, L.; Santiago, R.M.; Gray, S.G.; Breen, E.; Cuffe, S.; Finn, S.P.; O'Byrne, K.J.; Barr, M.P. Exploitation of the vitamin A/retinoic acid axis depletes ALDH1-positive cancer stem cells and re-sensitises resistant non-small cell lung cancer cells to cisplatin. *Transl. Oncol.* **2021**, *14*, 101025. [CrossRef]
49. de Thé, H. Differentiation therapy revisited. *Nat. Rev. Cancer* **2018**, *18*, 117–127. [CrossRef]
50. Enane, F.O.; Sauntharajah, Y.; Korc, M. Differentiation therapy and the mechanisms that terminate cancer cell proliferation without harming normal cells. *Cell Death Dis.* **2018**, *9*, 912. [CrossRef]
51. Friedman, M.D.; Jeevan, D.S.; Tobias, M.; Murali, R.; Jhanwar-Uniyal, M. Targeting cancer stem cells in glioblastoma multiforme using mTOR inhibitors and the differentiating agent all-trans retinoic acid. *Oncol. Rep.* **2013**, *30*, 1645–1650. [CrossRef] [PubMed]
52. Gersey, Z.C.; Rodriguez, G.A.; Barbarite, E.; Sanchez, A.; Walters, W.M.; Ohaeto, K.C.; Komotar, R.J.; Graham, R.M. Curcumin decreases malignant characteristics of glioblastoma stem cells via induction of reactive oxygen species. *BMC Cancer* **2017**, *17*, 99. [CrossRef] [PubMed]
53. Zhuang, W.; Long, L.; Zheng, B.; Ji, W.; Yang, N.; Zhang, Q.; Liang, Z. Curcumin promotes differentiation of glioma-initiating cells by inducing autophagy. *Cancer Sci.* **2012**, *103*, 684–690. [CrossRef] [PubMed]
54. Gilles, C.; Polette, M.; Mestdagt, M.; Nawrocki-Raby, B.; Ruggeri, P.; Birembaut, P.; Foidart, J.M. Transactivation of vimentin by β -catenin in human breast cancer cells. *Cancer Res.* **2003**, *63*, 2658–2664. [CrossRef]

55. Wu, B.; Zhu, J.; Dai, X.; Ye, L.; Wang, B.; Cheng, H.; Wang, W. Raddeanin A inhibited epithelial-mesenchymal transition (EMT) and angiogenesis in glioblastoma by downregulating β -catenin expression. *Int. J. Med. Sci.* **2021**, *18*, 1609. [CrossRef]
56. Schmitt, M.; Metzger, M.; Gradl, D.; Davidson, G.; Orian-Rousseau, V. CD44 functions in Wnt signaling by regulating LRP6 localization and activation. *Cell Death Differ.* **2015**, *22*, 677–689. [CrossRef]
57. Baek, S.; Lee, W.R. Down-regulation of CD44 inhibits Wnt/ β -catenin mediated cancer cell migration and invasion in gastric cancer. *J. Emerg. Investig.* **2021**, *4*, 1–6.
58. Zanotto-Filho, A.; Braganhol, E.; Klafke, K.; Figueiro, F.; Terra, S.R.; Paludo, F.J.; Morrone, M.; Bristot, I.J.; Battastini, A.M.; Forcelini, C.M.; et al. Autophagy inhibition improves the efficacy of curcumin/temozolomide combination therapy in glioblastomas. *Cancer Lett.* **2015**, *358*, 220–231. [CrossRef]
59. Ghosh, S.; Dutta, N.; Banerjee, P.; Gajbhiye, R.L.; Sareng, H.R.; Kapse, P.; Pal, S.; Burdelya, L.; Mandal, N.C.; Ravichandiran, V.; et al. Induction of monoamine oxidase A-mediated oxidative stress and impairment of NRF2-antioxidant defence response by polyphenol-rich fraction of *Bergenia ligulata* sensitizes prostate cancer cells in vitro and in vivo. *Free Radic. Biol. Med.* **2021**, *172*, 136–151. [CrossRef]

Review

Current Opportunities for Targeting Dysregulated Neurodevelopmental Signaling Pathways in Glioblastoma

Danijela Drakulic ^{1,*}, Marija Schwirtlich ¹, Isidora Petrovic ¹, Marija Mojsin ¹, Milena Milivojevic ¹,
Natasa Kovacevic-Grujicic ¹ and Milena Stevanovic ^{1,2,3}

¹ Laboratory for Human Molecular Genetics, Institute of Molecular Genetics and Genetic Engineering, University of Belgrade, 11042 Belgrade, Serbia

² Faculty of Biology, University of Belgrade, 11158 Belgrade, Serbia

³ Serbian Academy of Sciences and Arts, 11000 Belgrade, Serbia

* Correspondence: danijeladrakulic@imgge.bg.ac.rs

Abstract: Glioblastoma (GBM) is the most common and highly lethal type of brain tumor, with poor survival despite advances in understanding its complexity. After current standard therapeutic treatment, including tumor resection, radiotherapy and concomitant chemotherapy with temozolomide, the median overall survival of patients with this type of tumor is less than 15 months. Thus, there is an urgent need for new insights into GBM molecular characteristics and progress in targeted therapy in order to improve clinical outcomes. The literature data revealed that a number of different signaling pathways are dysregulated in GBM. In this review, we intended to summarize and discuss current literature data and therapeutic modalities focused on targeting dysregulated signaling pathways in GBM. A better understanding of opportunities for targeting signaling pathways that influences malignant behavior of GBM cells might open the way for the development of novel GBM-targeted therapies.

Keywords: glioblastoma; GBM subtypes; SHH signaling; Wnt/ β -catenin signaling; Notch signaling; TGF β signaling; BMP signaling; Hippo signaling; RA signaling



Citation: Drakulic, D.; Schwirtlich, M.; Petrovic, I.; Mojsin, M.; Milivojevic, M.; Kovacevic-Grujicic, N.; Stevanovic, M. Current Opportunities for Targeting Dysregulated Neurodevelopmental Signaling Pathways in Glioblastoma. *Cells* **2022**, *11*, 2530. <https://doi.org/10.3390/cells11162530>

Academic Editors: Javier S. Castresana and Bárbara Meléndez

Received: 7 June 2022

Accepted: 9 August 2022

Published: 15 August 2022

Publisher's Note: MDPI stays neutral with regard to jurisdictional claims in published maps and institutional affiliations.



Copyright: © 2022 by the authors. Licensee MDPI, Basel, Switzerland. This article is an open access article distributed under the terms and conditions of the Creative Commons Attribution (CC BY) license (<https://creativecommons.org/licenses/by/4.0/>).

1. Glioblastoma

Glioblastoma (GBM), a grade IV glioma [1], represents the most aggressive and the deadliest malignant brain tumor, characterized by fast spreading, infiltrative growth and high level of molecular/cytological heterogeneity [2–5]. Despite decades of research, patients have poor clinical prognosis, with less than 5% surviving 5 years after diagnosis and a median survival time of less than 15 months [6]. The standard treatment for these tumors is radical surgical resection followed by radiotherapy and chemotherapy using temozolomide (TMZ) as currently the main chemotherapeutic agent [7–9]. Unfortunately, rapid recurrence after therapy is detected in virtually all patients, which worsens the prognosis (reviewed in [10]). Major contributors of the aggressive course of the disease include the highly mutated genome of GBM and dysregulated signaling pathways involved in cell proliferation, growth, and survival (reviewed in [11–13]).

GBM consists of heterogeneous populations of cells in different phases of differentiation (reviewed in [4,5,14,15]). At the apex of GBM cellular hierarchy is a population of undifferentiated, self-renewing, and highly proliferative stem cells named glioblastoma stem cells (GSCs) (reviewed in [16]). These cells are characterized by high plasticity and the ability to give rise to heterogeneous cancer cells within the GBM (reviewed in [17,18]). Multiple studies demonstrated that, besides heterogeneity, GSCs play an indispensable role in the formation, growth, and progression as well as in therapeutic resistance and recurrence of GBM [19–21], indicating that these cells could be a crucial target for treatment (reviewed in [18,22]).

Our knowledge of the molecular biology of GBM has increased in recent decades. There are several cellular events during gliomagenesis. They include genetic instability, loss of cell cycle control, overexpression of growth factors and their receptors, angiogenesis, migration, invasion, and aberrant apoptosis (reviewed in [23]). All these processes are regulated by various signaling pathways, and accordingly, targeting key molecules in signaling pathways holds promise for developing novel therapeutic approaches. Targeting of key signaling pathways found deregulated in GBM, such as EGFR, PDGFR, PI3K–PTEN–Akt–mTOR, cell cycle-associated pathways (CDK4/6, CDKN2A/B), P53, pRB, RAS/MAPK, and STAT3, has been previously described in detail (reviewed in [11,24–26]).

Strong evidence in the last decade has suggested that GBMs may actually arise from neural stem cells (NSCs) residing in the lining of lateral ventricles that undergo malignant transformation (reviewed in [27,28]). Furthermore, the same studies underscored the parallels between neural development and gliomagenesis [27,28]. A comparison of the lineage hierarchy of the developing human brain to the transcriptome of GBM cells and GSCs derived from IDH-mutant astrocytoma, WHO grade 4, revealed that this type of brain tumor develops along neurodevelopmental gene programs encompassing a rapidly dividing progenitor population [29]. IDH-mutant astrocytoma, WHO grade 4, is hierarchically organized into three cell lineages that correspond to three normal neural lineages, astrocytic, neuronal, and oligodendrocytic, with progenitor cancer cells at its apex [29]. The results of genetic studies from more than 500 GBMs indicated that during tumor growth and invasion, these cells employ the same signaling networks as NSCs during neurogenesis and/or gliogenesis (reviewed in [13]). Signaling pathways involved in the regulation of nervous system development are dysregulated in CNS malignancies including GBM. Having in mind the aforementioned, in the present review, we focus on current strategies for targeting major neurodevelopmental signaling pathways that have been described to promote GBM growth and invasion (reviewed in [13,30]). These signaling pathways include Sonic Hedgehog (SHH), Bone Morphogenetic Protein (BMPs), Transforming Growth Factor β (TGF β), Wnt, Notch, Hippo and retinoic acid (RA) pathway (reviewed in [30]). Further, these signaling pathways are active in GSCs, a subpopulation of cells within the tumor responsible for increased resistance to chemotherapy and radiotherapy [31,32]. In GSCs, these signaling pathways are mainly responsible for regulation of self-renewal or differentiation [31–35]. In addition to their role in the maintenance of GSCs, they play important roles in the regulation of proliferative, migratory and invasive abilities of GBM cells, contributing to the growth and progression of GBM.

Having in mind the inter- and intra-heterogeneity of GBMs (reviewed in [14]), stratifications of GBMs into molecular subtypes, including profiling of signaling pathway status, is important for clinical management of patients with GBMs.

2. Molecular GBM Subtypes

Many different classifications of GBM into subtypes have emerged over the years. Through these classifications, different GBM subtypes are characterized by different features and gene alterations, and they should be considered for different targeted treatments for fighting GBM (Figure 1).

One of the first molecular stratifications of GBM is based on the presence/absence of mutations in isocitrate dehydrogenase 1 (*IDH1*) or 2 (*IDH2*) genes (Figure 1, Supplementary Table S1). Based on this, GBM is subdivided into two subtypes: *IDH* wild-type GBM and *IDH* mutant GBM (reviewed in [36]). *IDH* wild-type GBM is found in more than 90% of all patients (mostly in elderly patients), and the vast majority of *IDH* wild-type GBM are primary GBM that develop de novo (reviewed in [36]). *IDH* mutant GBM is detected in less than 10% of patients with GBM (almost all in young adults) and the vast majority of *IDH* mutant GBM represent secondary GBM, developed from diffuse or anaplastic astrocytoma (reviewed in [36]). Based on the progress in the diagnosis and management of gliomas from 2016, the term *IDH*-mutant GBM is discontinued and replaced with *IDH*-mutant astrocytoma, WHO grade 4 (Figure 1, Supplementary Table S1) [37].

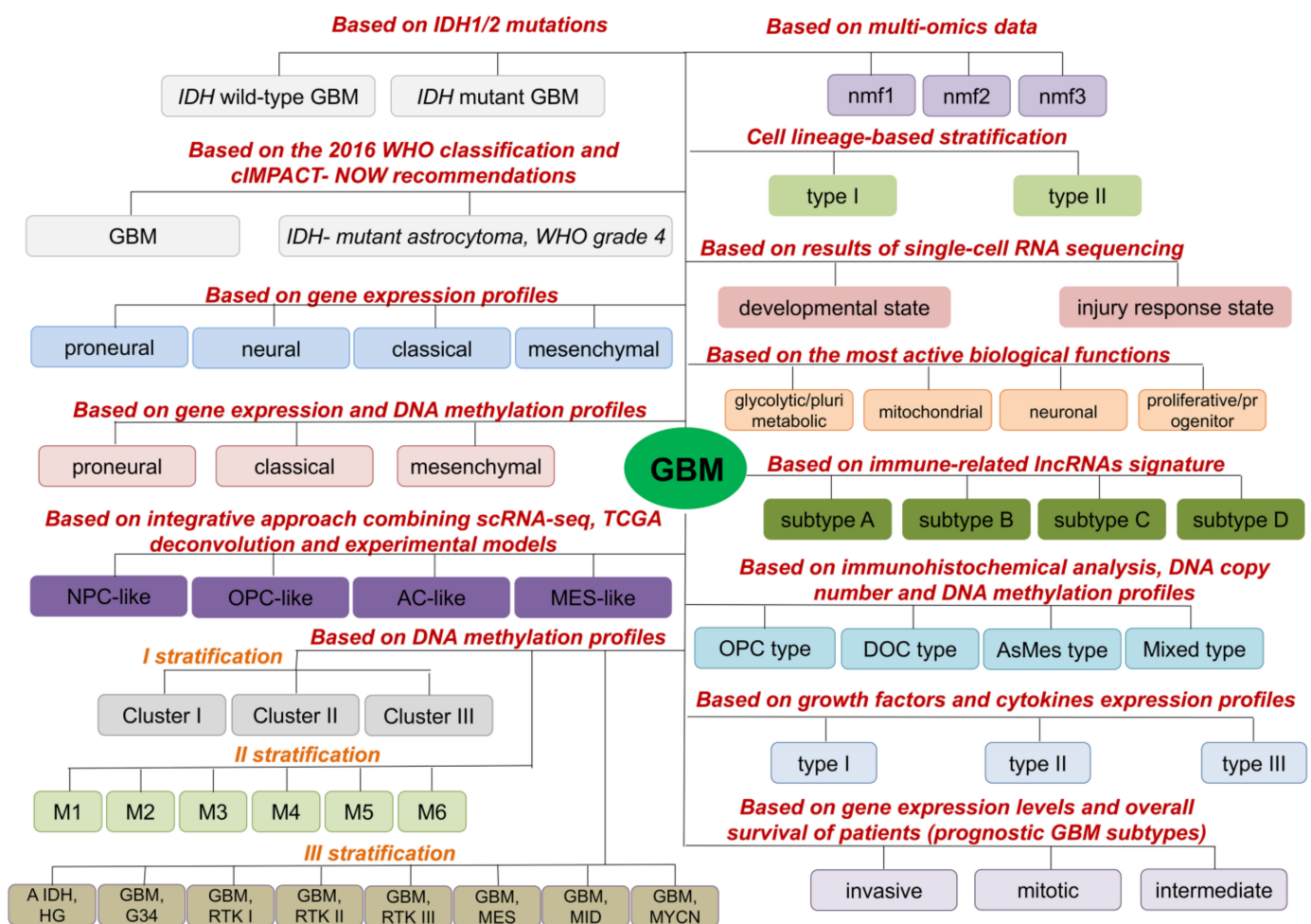


Figure 1. Stratification of GBM into subtypes. This summary is based on the previously reported publications listed in the main text and in Supplementary Table S1.

Based on gene expression profile, Verhaak and co-workers classified GBM into four subtypes: proneural, neural, classical, and mesenchymal [38] (Figure 1, Supplementary Table S1). These subtypes differ in mutations, genes expression, as well as responses to chemo- and radiotherapy (reviewed in [39]). Results obtained by Wang and co-workers, analyzing *IDH* wild-type GBMs, indicated neural subtype as normal neural lineage contamination [40]. Previously, neural subtype has been related to the margin of the tumor where normal neural tissue is likely to be detected [41,42]. The mesenchymal subtype is associated with poor overall survival and poor response to radiotherapy, while the proneural is related to a more favorable outcome [43–46]. Furthermore, it was detected that a GBM tumor from one patient can harbor cells having characteristics of different GBM molecular subtypes [47]. Additionally, switching from one GBM subtype to another within one GBM tumor has been demonstrated (reviewed in [39]).

Ensenyat-Mendez and co-workers constructed the iGlioSub classifier using machine learning, computational biology algorithms and prioritization of highly informative transcriptomic and epigenomic features which, based on gene expression and DNA methylation profiles, classified GBMs into classical, mesenchymal and proneural subtypes (Figure 1, Supplementary Table S1). This classifier showed better performance in stratifying patients compared to stratification based on gene expression profiles only [48].

An integrative approach applied by Neftel and co-workers revealed that tumor cells in GBM exist in four cellular states that recapitulate neural progenitor-like (NPC-like), oligodendrocyte-progenitor-like (OPC-like), astrocyte-like (AC-like) and mesenchymal-like (MES-like) states (Figure 1, Supplementary Table S1). MES-like cells are further divided

into hypoxia-independent (MES1) and hypoxia-dependent (MES2) sub-groups, while NPC-like cells are divided into NPC1 and NPC2 sub-groups that were distinguished by inclusion of OPC-related genes in NPC1 and neuronal lineage genes in NPC2 (Figure 1, Supplementary Table S1) [49].

Three stratifications of GBM into subtypes are proposed based on DNA methylation profiles (Figure 1). In stratification I, Ma and co-workers identified three different GBM prognosis subgroups (Cluster 1–3) with Cluster 3 associated with poor prognosis and relatively lower sample methylation level, and Cluster 2 associated with the best prognosis [50]. On the other side, Brennan and co-workers stratified GBM patients into six methylation classes (M1, M2, M3, M4, M5 (G-CIMP), M6) [51]. Based on DNA methylation in CNS tumors, Capper and co-workers grouped most of the IDH-mutant astrocytoma, WHO grade 4, into methylation subclass “A IDH, HG”, while IDH wild-type GBM were stratified into seven methylation classes (“GBM, G34”, “GBM, RTK I”, “GBM, RTK II”, “GBM, RTK III”, “GBM, MES”, “GBM, MID”, “GBM, MYCN”) [52].

Based on multi-omics data (CNVs, gene expression, protein and phosphoprotein abundances), Wang and co-workers defined three clusters in IDH wild-type GBMs-nmf1 (proneural-like), nmf2 (mesenchymal-like) and nmf3 (classical-like) (Figure 1) enriched in neuron activity-related pathways, immune response pathways and cell cycle pathways, respectively [53]. Furthermore, classification of GBM into lineage-specific subtypes which possess diverse functional properties and therapeutic vulnerabilities was described (Figure 1, Supplementary Table S1) [54]. Based on the results of single-cell RNA sequencing (scRNA-seq) of GSCs and malignant cells from primary GBM tumors, Richards and co-workers stratified cells along a transcriptional gradient from a ‘Developmental’ state to an ‘Injury Response’ state [55,56]. On the other hand, Garofano and co-workers identified four tumor cell states in GBM (proliferative/progenitor, neuronal, mitochondrial and glycolytic/plurimetabolic) converging on two biological axes-neurodevelopmental and metabolic (Figure 1) [57].

Since long noncoding RNAs (lncRNAs) have important roles in development and progression of GBM, and tumor-associated immune processes, Yu and co-workers used immune-related lncRNAs signature for classification of GBM into four subtypes (A–D) (Figure 1), with GBM subtype A showing the most favorable prognosis [58]. Additionally, based on immunohistochemical results in combination with DNA copy number and DNA methylation profiles, Motomura and co-workers stratified GBM into four subtypes: oligodendrocyte precursor type (OPC), differentiated oligodendrocyte type (DOC), astrocytic mesenchymal type (AsMes) and mixed type (Figure 1, Supplementary Table S1) with OPC type showing the most favorable outcome [59]. Based on growth factors and cytokines expression profiles of GBM patients, Hu and co-workers identified three GBM subtypes (type I–III) (Figure 1, Supplementary Table S1) [60]. Prognosis is poorer for patients with GBM Type III compared to patients with Types I and II [60].

According to gene expression levels and overall survival of patients, three prognostic GBM subtypes were identified: invasive (poor), mitotic (favorable), and intermediate (Figure 1) [61].

Results of microarray analysis revealed the presence of two subtypes of GSCs, proneural and mesenchymal [43,62]. These two subtypes are phenotypically different; mesenchymal GSCs are more invasive, angiogenic and more resistant to radiotherapy compared to the proneural subtype [43,62]. Furthermore, a proneural subtype of GSCs might be switched to the mesenchymal upon certain conditions, such as radiation treatment [62], anti-angiogenic therapy [63], increased intracellular levels of reactive oxygen [64], upregulation of transglutaminase 2 (TGM2) [65], upregulation of N-Myc downstream regulated gene 1 (NDRG1) [66], activation of NFE2L2 transcriptional network [64], upregulation of TAZ expression [67], and activation of nuclear factor kappa B (NF- κ B) [43].

Stratification of GBMs into different molecular subtypes enables the identification of markers significant for diagnosis, prognosis, and more effective treatment. Precise

identification of GBM molecular subtypes is important for improving clinical management of GBM and might lead to targeted molecular therapy for GBM patients.

Molecular GBM stratification revealed that multiple signaling pathways are dysregulated in GBM. Thus, the development of therapies that are focused on targeting dysregulated signaling pathways in GBM provides a new avenue for improving the clinical management of GBM patients. Among others, dysregulated signaling pathways in GBM include SHH, Wnt/ β -catenin, Notch, BMP, TGF β , Hippo and RA signaling pathways. In this review, we have summarized the current data concerning the approaches for targeting these signaling pathways in GBM.

3. Targeting Sonic Hedgehog Signaling Pathway in GBM

The Hedgehog (HH) signaling is a well-conserved pathway in animals that plays a pivotal role during embryonic development, tissue homeostasis, maintenance of adult stem cells and regeneration [68–70]. Its role is critical for the development of brain and spinal cord including midbrain and ventral forebrain neuronal differentiation and proliferation [71–73]. There are three mammalian HH ligand proteins, Sonic Hedgehog (SHH), Indian Hedgehog (IHH), and Desert Hedgehog (DHH). Canonical HH signaling occurs by binding HH ligand protein to a transmembrane receptor protein patched (PTCH) [74]. In the absence of HH ligands, PTCH functions as an inhibitor of another transmembrane protein smoothed (SMO). Binding of HH ligands to PTCH receptor relieves the suppression of SMO, resulting in downstream activation of final effectors, GLI transcription factors (GLI1, GLI2, and GLI3) responsible for the transmission of HH signaling to downstream target genes (Figure 2) [75,76].

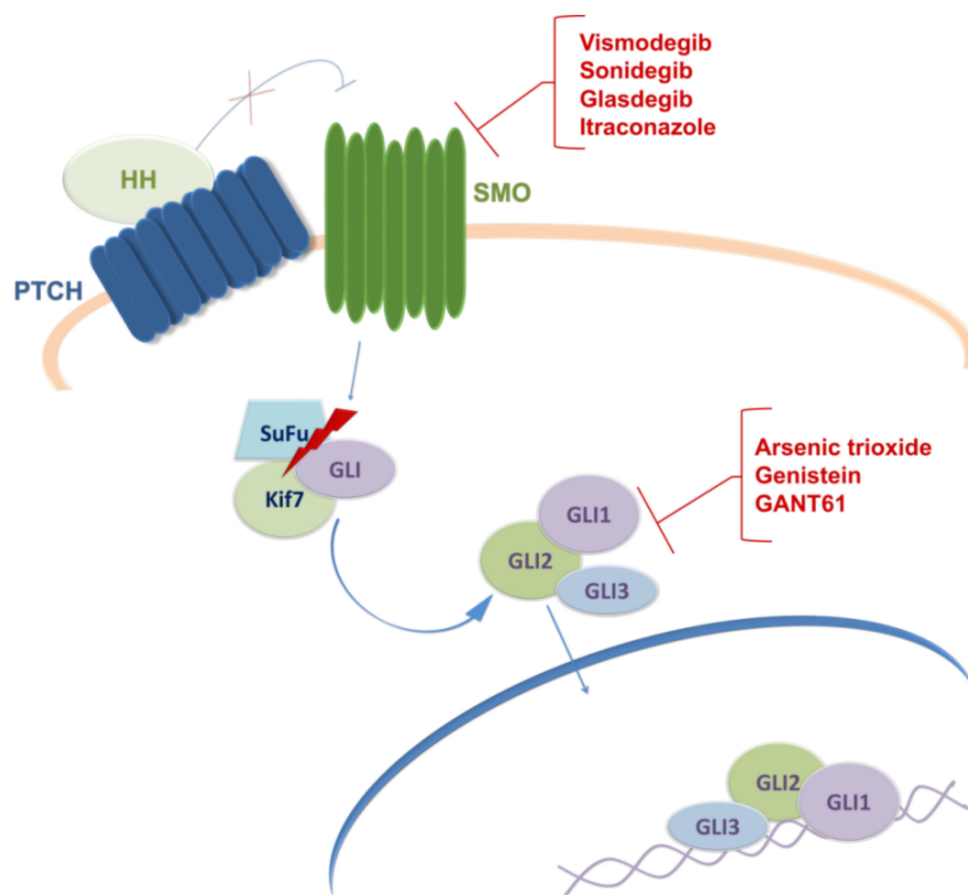


Figure 2. The canonical activation of HH pathway and its pharmaceutical inhibitors. The activation of pathway occurs when HH ligand binds to PTCH at the cell membrane. In response to this binding, PTCH no longer inhibits SMO and initiates the downstream signaling, causing rapid dissociation of

the SuFu–GLI complex and thus allowing GLI to enter the nucleus and regulate transcription of target genes. Proven pharmacological inhibitors that target SHH signaling components (SMO receptor or GLI transcription factors) are presented in red. References are included in the main text.

Accumulating evidence suggests that aberrant activation of the HH signaling pathway by deregulation of any of its components may be involved in the development and progression of cancers and diseases. Accordingly, dysregulation of SHH signaling has been implicated in the initiation and/or maintenance of different tumor types including GBM [77,78]. The transcriptomics data on 149 clinical cases of The Cancer Genome Atlas–Glioblastoma database showed a strong correlation between *PTCH1* and *GLI1* upregulated expression in GBM indicating that activation of the canonical SHH pathway might be associated with this malignancy [79]. Furthermore, it was demonstrated that the endothelial cells within the tumor microenvironment (TME) provide the SHH ligand that activates the HH signaling pathway in GBM cells and promotes the appearance of GSCs, as demonstrated by increases in tumorigenicity and expression of stemness genes [80]. It has been revealed that GSCs highly express SHH and that targeting this signaling pathway may overcome chemoresistance and provide a novel therapeutic strategy [22,80,81].

Currently, there are two approaches to inhibiting SHH signaling: ligand-dependent approach, by antagonizing the SMO receptor, and ligand-independent approach, by inhibiting its final effectors, GLI transcription factors [77]. In preclinical studies, various SMO inhibitors exerted antiproliferative effect against tumor cells including those originating from GBM. Cyclopamine, isolated from *Veratrum californicum* plant, is a natural inhibitor of SMO that consequently blocks the SHH signaling pathway [77,82]. Carballo and co-workers presented data showing that SHH pathway inhibition with cyclopamine interferes with GBM cell viability and also suggested that cyclopamine inhibition of the SHH pathway prior to TMZ treatment could reduce the aggressiveness of the tumor cells by sensitizing the GSCs to TMZ [83]. Among SMO inhibitors, there are two inhibitors, vismodegib, and sonidegib, approved by the FDA for the treatment of locally advanced and metastatic basocellular carcinoma [84]. Bureta and co-workers presented data on the antiproliferative effect of vismodegib on GBM cell lines alone or in combination with arsenic trioxide (ATO) and TMZ [85].

Presently, there are several ongoing clinical trials evaluating SMO inhibitors for the treatment of different types of brain tumors. Initially, SMO was the principal target for the development of SHH inhibitors, and the first clinical trial performed using an SMO inhibitor to treat a brain tumor was conducted in 2008 in a male patient with metastatic medulloblastoma who was treated with a novel HH pathway inhibitor, GDC-0449 (vismodegib) [86]. Treatment led to rapid regression of the tumor and reduction in symptoms, but only transiently [86]. It was observed that the HH pathway inhibition resulted in an incomplete response that led to tumor re-growth, and unfortunately, the patient died after five months of treatment [86]. Vismodegib was evaluated in clinical trials against GBM, but so far, it has not demonstrated clinical benefit as a single agent. Patients with recurrent GBM, in a phase 2 trial, were randomized to a pre-operative and post-operative vismodegib group (group I) versus only the post-operative vismodegib group (group II), with the idea that HH pathway inhibitors selectively target GSCs. Although a significant decrease in the number of CD133+ neurospheres was observed in group I, vismodegib was not efficacious as a single agent in recurrent GBM [87]. It is important to highlight that the efficiency of vismodegib is still being evaluated in one clinical trial for medulloblastoma (NCT01878617) and one for GBM (NCT03158389). Another FDA-approved SMO inhibitor sonidegib was also evaluated in relapsed medulloblastoma in a phase 1/2 trial, with both adult and pediatric patients. Fifty percent of the patients with activated HH pathway in their tumor had a response to sonidegib, which was translated to longer disease-free survival [88]. Currently, two additional SMO inhibitors are under evaluation in clinical trials for the treatment of GBM, and they both belong to drugs approved for other diseases (NCT03466450; NCT02770378). The first is glasdegib, a small molecule inhibitor of SMO and FDA-approved medication for acute myeloid leukemia [89]. The other one is itracona-

zole, an antifungal drug used for the treatment of fungal infections, which is currently in phase I clinical trial in combination with TMZ (CUSP9v3 Treatment Protocol) for recurrent GBM. Previously, itraconazole has been explored as an anticancer agent for patients with basal cell carcinoma, non-small cell lung cancer, and prostate cancer [90–93].

Most HH inhibitors that have entered clinical trials targeted SMO, although several mechanisms of resistance to SMO inhibitors have been identified. This is why alternative SHH antagonists that act directly on GLI transcription factors are already being tested in the brain and central nervous system tumors as co-adjuvant therapy with TMZ (reviewed in [77]). ATO is a drug that is being tested for gliomas in phase I and II clinical trials. ATO is an FDA-approved drug which was first used for the treatment of patients with acute promyelocytic leukemia. It has been shown that ATO inhibits GLI-dependent growth in a medulloblastoma mouse model [94]. A recent study demonstrated that treatment of patients in combination with ATO, TMZ, and radiation apparently does not improve the overall outcome in GBM patients [95]. Genistein is an isoflavone found in legumes which is able to inhibit GLI1, and there was a clinical study of its potential against brain malignancies (NCT02624388); unfortunately, the study was terminated due to poor enrolment. However, clinical trials of genistein in cancer therapy have been conducted for other malignancies, including breast, bladder, and prostate cancer. Currently, its clinical applications are still limited due to its poor solubility and bioavailability [96]. Honorato and co-workers reported that selective ligand-independent inhibition of SHH by GANT-61 through targeting GLI1 increased the oxidative stress damage potentiating TMZ effect and inducing cell death in GBM cell lines [97]. Another preclinical study also showed that GANT61 sensitizes glioma cells to TMZ treatment [98]. However, currently, there are no data regarding its clinical evaluation.

Nowadays, the SMO receptor is the primary target used for the development of SHH pathway inhibitors, and there are several ongoing clinical trials for different types of brain tumors. On the other hand, several reports demonstrated that SHH could signal through a noncanonical route, and while it is still unclear how the cells select between canonical and non-canonical routes, it is understood that efficient targeting of downstream effectors (GLIs) could lead to promising results in clinical trials. In conclusion, it is considered that the best way to control the tumor recurrence is to evaluate and establish novel protocols combining SHH signaling inhibition with conventional therapies.

4. Targeting Canonical Wnt/ β -Catenin Signaling Pathway in GBM

Wnt/ β -catenin signaling pathway plays essential roles in embryonic development and the maintenance of homeostasis and regeneration of adult tissues [99,100]. Canonical Wnt/ β -catenin signaling pathway is the most studied part of the complex and evolutionarily conserved Wnt signaling [101].

β -catenin is a central player in the canonical Wnt signaling pathway [102,103]. When Wnt signaling is inactive, the level of β -catenin is kept low due to the activity of the destruction complex in the cytoplasm [104]. The complex is consisting of APC (adenomatous polyposis coli), AXIN1/2 (axis inhibition proteins 1/2), CK1 (casein kinase 1), and GSK3 β (glycogen synthase kinase 3 β) [104]. Two scaffold proteins, APC and AXIN, bring β -catenin in the position for CK1/GSK3 β -mediated phosphorylation which prime it for subsequent ubiquitination and proteasomal degradation [104,105]. Decreased concentration of β -catenin in a cytoplasm prevents its nuclear translocation. In the absence of β -catenin, members of TCF/LEF (T-cell factor/lymphoid enhancer-binding factor) families of transcription factors remain in complexes with corepressors, the Groucho and TLE (transducin-like enhancer), bound to Wnt responsive elements thus repressing transcription of Wnt target genes [106].

Activation of canonical Wnt signaling starts by binding of WNT ligands (family of 19 secreted glycoproteins in mammals) to the Fzd seven-transmembrane receptor (Frizzled) and LRP5/6 (co-receptor low-density lipoprotein receptor-related protein 5, 6) [107,108]. Upon activation, Fzd interacts with Dsh (Disheveled) cytoplasmic protein. Dsh also inter-

acts with Axin, and LRP5/6, via Axin interactions with the coreceptor. These interactions inactivate β -catenin destruction complex [107,108]. Increased concentration of stabilized β -catenin in cytoplasm leads to its nuclear translocation. In the nucleus, β -catenin forms complexes with the members of the TCF/LEF family of transcription factors and co-activators, e.g., CBP (CREB-binding protein) and p300, and enhances transcription of Wnt target genes [106].

Aberrant activity of Wnt/ β -catenin signaling is associated with diverse human diseases including cancer [99,100]. Aberrant activation of the Wnt/ β -catenin signaling pathway is involved in GBM pathogenesis and progression, maintaining of GSC stemness and acquisition of radio- and chemotherapy resistance [15,109–111].

Mutations in key components of Wnt signaling e.g., APC, β -catenin, and AXIN are not hallmarks of GBM, although several studies linked mutations in Wnt signaling proteins to gliomagenesis. In a study on seven patients, Tang and co-workers showed that APC gene mutations occurred in 13% of cases, with a mutation frequency of 14.5% [112]. A study by Morris correlated homozygous deletion in tumor suppressor *FAT1* (atypical cadherin 1), negative regulator of the Wnt pathway, with the activation of Wnt signaling. Homozygous deletion of *FAT1* occurred in 57% of GBM and was associated with a prolonged survival [113,114]. A study by Sareddy and co-workers showed overexpression of PELP1 (proline-, glutamic acid-, and leucine-rich protein 1) in 100% of the GBM samples. PELP1 is co-regulator of several nuclear receptors, and a potent activator of β -catenin and Wnt signaling [115]. MicroRNA and lncRNA profiling of GBM versus the normal brain revealed the role of epigenetic mechanisms in the activation of Wnt signaling in GBM [116,117].

In search of anticancer therapeutics, numerous natural and synthetic antagonists and agonists were isolated or designed to target major cascades in Wnt/ β -catenin signaling pathway, i.e., inhibitors targeting Wnt ligand/FZD receptor complex, inhibitors and agonists targeting the β -catenin-destruction complex and inhibitors targeting β -catenin/TCF complex [108]. Although the Wnt pathway is a validated target in cancer, and drugs targeting this pathway in various cancer types have entered the clinical trials, there are still no FDA-approved drugs targeting this pathway [118]. Unfortunately, only a few candidates have reached early phase clinical trials as therapies targeting GBM [24,119].

Extensive search and chemical screening for Wnt inhibitors identified numerous small molecules and biologics that targeted the Wnt signaling cascade [120]. Small molecules that act as Wnt agonists or antagonists, modulation of Wnt signaling activity induced by these molecules, and their effects on the properties of GBM cells and GSCs are listed in Table 1, Section A [121–129]. A schematic representation of their action on the Wnt signaling cascade is given in Figure 3.

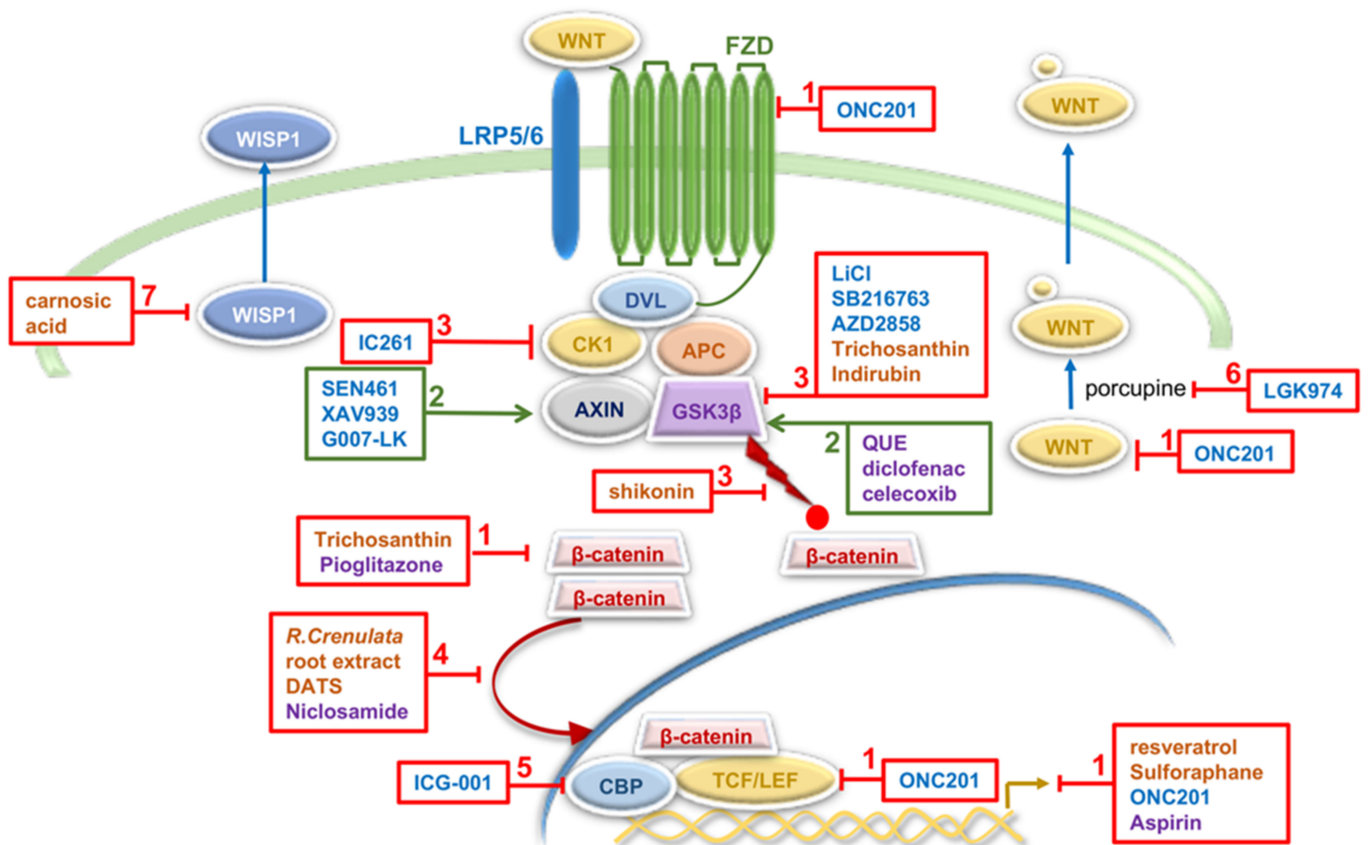


Figure 3. Overview of the Wnt/ β -catenin signaling cascade, targets for potential therapeutic intervention in GBM and molecules investigated in preclinical and clinical studies (based on the data listed in Table 1). Mechanisms of modulation of Wnt/ β -catenin activity in GBM (described in detail in Table 1) include (1) down-regulation of expression of Wnt components and Wnt targets, (2) promotion of β -catenin degradation, (3) increasing β -catenin stability, (4) inhibition of β -catenin nuclear translocation, (5) inhibition of β -catenin/CBP transcription complex, (6) down-regulation of WNT secretion and (7) inhibition of Wnt/ β -catenin-WISP1 signaling. Small molecules are presented in blue letters, natural agents in orange and repurposed drugs in purple. Molecules in red boxes inhibit expression and activity of denoted Wnt component or processes within the Wnt cascade. Molecules in green increase activity of denoted components. Red circle represents phosphate group; yellow circle represents palmitoyl groups. Based on [120,130] and references included in the main text and the Table 1.

Table 1. Molecules targeting Wnt/ β -catenin cascade, mechanisms of action and effects on GBM cells and GSCs: A: Small molecules; B: Natural agents; and C: Repurposed drugs.

Molecule	Modulation of Wnt Signaling Activity	Effects on GBM Cells and GSCs Properties	Reference
A: Small molecules			
ONC201	inhibits expression of components of Wnt pathway and Wnt targets	induces apoptosis in GBM cells induces cytotoxicity in chemo- and radiation-resistant GBM patient samples inhibits the growth of GSCs in 3D neurospheres established from human GBM tumors inhibits tumor growth in GBM mouse models	[121,127]
SEN461	induces AXIN stabilization	inhibits anchorage-independent growth of human GBM cell lines and patient-derived primary tumor cells reduces tumor growth in a mouse GBM xenograft model	[122]

Table 1. Cont.

Molecule	Modulation of Wnt Signaling Activity	Effects on GBM Cells and GSCs Properties	Reference
XAV939	antagonist of tankyrase-enzymes involved in the degradation of AXIN	decreases the survival and clonogenicity of GBM cells reduces GSC population increases radiosensitization in in vivo radiation model derived from a single human GBM specimen	[125]
LiCl SB216763	inhibits GSK3 β	induces the expression of differentiation markers in GBM cells depletes GSCs population reduces colony formation and induces cell death in GBM cell-lines	[126]
G007-LK	inhibitor of tankyrase-enzymes involved in the degradation of AXIN	decreases in vitro proliferation and sphere formation in primary GSC cultures reduction in GSC sphere formation in cotreatment with TMZ	[124]
IC261	inhibitor of CK1	inhibits growth of GBM cells and GSCs in vitro and induces growth inhibition of human GBM xenografts in mice	[129]
LGK974	inhibitor of porcupine proteins that modulate Wnt ligands	acts synergistically with TMZ to inhibit growth of GBM cells	[128]
ICG-001	CBP antagonist	reduces proliferation and survival of GBM cells	[123]
AZD2858	inhibits GSK-3 β	reduces proliferation and survival of GBM cells inhibits the invasion and migration of GBM cells	[123]
B: Natural agents			
shikonin	inhibits β -catenin phosphorylation	inhibits proliferation, migration and invasion of GBM cells	[131]
Trichosanthin	inhibits expression of Wnt components	inhibits proliferation, invasion and migration and induces apoptosis of GBM cells	[132]
<i>R. crenulata</i> root extract	decreases nuclear localization of β -catenin	inhibits proliferation and tumorsphere formation and promotes differentiation of GBM cells	[133]
resveratrol	decreases expression of Wnt signaling components and Wnt targets	inhibits proliferation, motility and invasion of GSCs	[134]
carnosic acid	decreases expression of WISP1	reduces GSC viability suppresses GSC tumorsphere formation inhibits the growth of GSC-derived xenografts	[135]
Indirubin	inhibitor of GSK-3 β	reduces invasion of GBM and GSC-enriched neurospheres both in vitro and in vivo improves survival of intracranial glioma-bearing mice	[136]
DATS	decreases nuclear β -catenin level	inhibits cell growth, induces apoptosis and decreases migration and invasion in GBM cells	[137]
Sulforaphane	inhibits Wnt/ β -catenin signaling	enhances TMZ-induced apoptosis	[138]
C: Repurposed drugs			
NSAIDs diclofenac celecoxib	reduces phosphorylation of GSK3 β	inhibits proliferation, colony formation and migration of GBM cells	[139]
aspirin	inhibits expression of Wnt targets	inhibits proliferation and invasion and induces apoptosis of GBM cells	[140]

Table 1. Cont.

Molecule	Modulation of Wnt Signaling Activity	Effects on GBM Cells and GSCs Properties	Reference
Niclosamide	decreases concentration of β -catenin in the nucleus	decreases cell viability, exerts antimigratory effects and inhibits the malignant potential of primary GBMs	[141]
		combined treatment with TMZ inhibits viability, stemness, and invasive properties of human GBM tumorspheres and decreases tumor growth in mouse xenograft models	[142]
QUE	decreases phosphorylation of GSK3 β	suppresses GSCs-initiated tumor growth in mouse models of gliomas acts synergistically with TMZ to suppress growth of TMZ-resistant tumors originated from GSCs	[143]
Pioglitazone	inhibits β -catenin expression	reduces cell viability, suppresses invasion and induces apoptosis of GBM cells	[144]
		induces decrease in cell viability and proliferation of GSC lines isolated from GBM patients	[145]

LiCl, lithium chloride; DATS, garlic-derived diallyl trisulfide; NSAID, nonsteroidal anti-inflammatory drugs; QUE, Quetiapine.

The most promising agent is ONC201, a member of the imipridone class of small molecules. This dopamine receptor D2 antagonist is a widely studied inhibitor of GSC markers expression and suppressor of signaling pathways associated with GSC self-renewal, glioma-initiation and progression, and therapy resistance including Wnt ligands, receptors, and effectors (WNT16, FZD2, FZD4, TCF7L2) [127,146,147]. Additionally, ONC201 showed promising results in phase II clinical trial in patients with recurrent GBM [148]. ONC201 is currently in phase II clinical trial for patients with recurrent GBM and distinct subtypes of glial tumors H3 K27M mutant and Midline Glioma (NCT02525692).

Several biologics targeting Wnt signaling were investigated in various cancer types [120]. Fusion protein Ipafricept (OMP54F28; IPA), which competes with WNT ligands for binding to FZD8 receptor [149–151], and Vantictumab (OMP-18R5), a monoclonal antibody targeting FZD1, FZD2, FZD5, FZD7, and FZD8 receptors [150,151], act as Wnt/FZD antagonists and reached clinical I/II phase for breast, pancreatic, hepatocellular and ovarian cancer [120]. However, there are no available data about ongoing clinical trials or plans for further investigations of these biologics in GBM treatments.

Numerous natural products act as inhibitors of the canonical Wnt signaling and show significant therapeutic relevance in various cancer model systems [130]. They mainly act via β -catenin by regulating different steps involved in its stability and transcriptional activity, i.e., expression of β -catenin and its phosphorylation, degradation and nuclear translocation [130]. It is important to point out that about 33% of FDA-approved anticancer drugs are natural products and their derivatives [152] and that natural products represent a major source for drug discovery and development [153,154]. Natural agents acting through Wnt signaling in GBM are presented in Table 1, Section B [131–138]. They affect different processes in the Wnt cascade: β -catenin phosphorylation (shikonin), expression of key proteins in the Wnt/ β -catenin signaling pathway (trichosanthin), nuclear translocation of β -catenin (*R. crenulata* root extract, DATS), expression of Wnt signaling components and Wnt targets (resveratrol, sulforaphane), activity of GSK-3 β (indirubin), and Wnt/ β -catenin-WISP1 signaling (carnosic acid) (Table 1, Section B and Figure 3) [131–138]. WISP1 (Wnt-induced signaling protein 1) is secreted by GSCs to facilitate a pro-tumor microenvironment and promote survival of both GSCs and tumor-associated macrophages [135].

One of the promising strategies to develop Wnt-targeting anti-GBM therapies is drug repurposing. Several studies revealed tumor-suppressive effects of various drug types: nonsteroidal anti-inflammatory drugs (NSAIDs); niclosamide, an anthelmintic drug for treating intestinal parasite infections; quetiapine (QUE), an atypical antipsychotic drug and pioglitazone, an anti-diabetic drug used to treat type 2 diabetes (Table 1, Section C and

Figure 3) [139–145]. The most promising repurposed drug targeting Wnt signaling in GBM is celecoxib. This NSAID was tested in GBM patients in several phase I and II clinical trials in combination with other drugs. Some trials are still ongoing but preliminary results are not encouraging [24,155]. Tested in phase II trial in newly diagnosed GBMs, celecoxib had no survival benefit when combined with TMZ (NCT00112502) [24].

Several studies point to the translational potential of therapeutic approaches that combined Wnt pathway inhibitors and chemotherapy. For example, Huang and co-workers discovered that canonical Wnt signaling plays a crucial role in stemness activation and chemoresistance in GBM-associated vascular endothelial cells through the HGF/c-Met/ β -catenin axis [156]. In endothelial cells under glioma conditions, HGF (hepatocyte growth factor) induces direct β -catenin phosphorylation at Ser675 by HGF receptor kinase c-Met, leading to the β -catenin nuclear translocation and LEF1-mediated activation of Wnt target genes [156]. RNA seq data revealed activation of genes associated with stemness that govern endothelial cells transformation into mesenchymal stem cell-like cells. In addition, they detected increased expression of ABCC1 (multidrug resistance-associated protein 1 (MRP-1)), which is responsible for drug efflux and chemoresistance of these cells. In further investigation of the potential therapeutic relevance of these findings, the authors examined the effects of treatment with Wnt inhibitor XAV939 and TMZ. The combined treatment of XAV939 and TMZ extended mouse survival and inhibited tumor growth, suggesting that Wnt inhibition with XAV939 sensitizes GBM to TMZ chemotherapy [156]. The authors also revealed that Wnt-mediated chemoresistance is potentially endothelial cells-selective mechanism in GBM [156].

In addition, canonical Wnt signaling is involved in one of the molecular pathways of the GBM cells vessel co-option [157], a mechanism of the tumor cells movement towards and along the pre-existing vasculature [158]. Griveau and co-workers described Olig2-Wnt7 signaling axis responsible for single-cell vessel co-option and consequent increased infiltration of patient-derived oligodendrocyte precursors-like cells with preservation of the blood–brain barrier (BBB) [159]. In contrast, Olig2- and Wnt7-negative astrocyte-like GBM cells show collective clusters vessel co-option, which leads to the destruction of the BBB and consequent inflammation [159,160]. It has been also shown that vessel co-option is invasion strategy for orthotopically implanted mouse, rat and human glioma cells and GSCs [161].

In vivo and ex vivo inhibition of Wnt signaling with porcupine inhibitor LGK974 reduced vessel co-option and improved survival in combination with TMZ treatment [159]. Additionally, in patient-derived proneural cell lines, LGK974 treatment down-regulated OLIG2 and WNT7A expression and up-regulated VEGFA, while treatment with VEGF inhibitor B20 increased expression of OLIG2. In vivo, LGK974 treatment increased VEGF expression, whereas B20 treatment increased Wnt activity [159]. In addition, up-regulation of both Wnt7a and Wnt7b were observed in U87 GBM cells resistant to bevacizumab compared to bevacizumab-sensitive U87 cells [159]. This is in concordance with the clinical studies that showed that vessel co-option occurs in some GBM subtypes intrinsically resistant to anti-angiogenic treatment, but it is also a mechanism of resistance to anti-angiogenic treatments (bevacizumab) in the innately angiogenic tumors [158,162]. The ability of GBM cells to switch between co-opting and angiogenic phenotype has great therapeutic relevance. Computational modeling of the inhibition of both mechanisms suggests that sequential inhibition (vessel co-option inhibition followed by anti-angiogenesis therapy) is more efficient than simultaneous blockage [163]. These findings also highlight the importance of classification of the GBM patients based on vessel co-option occurrence.

Inhibition of Wnt in GBM is also challenging due to the essential roles of this pathway in CNS vascularization and BBB integrity [100]. During CNS development, neural progenitors-derived Wnt7a and Wnt7b ligands activate canonical Wnt signaling in vascular endothelium, thus promoting vascularization of CNS and formation of BBB [164]. The same mechanism maintains integrity of BBB in adult brain. In brain endothelial cells, Wnt7 binds to the co-receptor complex RECK-GPR124, consisting of RECK (reversion-inducing

cysteine-rich protein with Kazal motifs) and GPR124 (G protein-coupled receptor 124), to activate canonical Wnt signaling through Fz receptor [165,166]. Martin and co-workers took advantage of the selective binding of linker domain of Wnt7a to Fz receptor only in the presence of RECK-GPR124 complex to restrict Wnt activation to the endothelial cells of CNS and avoid their pleiotropic Fz signaling [167]. The authors engineered the Wnt7a mutant ligand, a Gpr124/Reck agonist that showed no off-target activity in the brain [167]. Delivered in the circulation of mouse model of brain tumor, by adeno-associated virus injection, the Gpr124/Reck agonist restored Wnt signaling in endothelial cells, normalized BBB function and reduced GBM expansion [167].

This approach also showed improved BBB function in cerebral artery occlusion model of stroke [167], which is in concordance with previous studies that highlighted the role of Wnt signaling activation in CNS vascularization during development and in hypoxic brain injury. Chavali and co-workers revealed that crosstalk between oligodendrocyte precursor cells (OPCs) and endothelial cells regulates vascular development in neonatal white matter in a Wnt-dependent manner [168]. The authors showed that in hypoxic brain injury, OPCs expressed the Wnt7A ligand, which resulted in paracrine activation of the canonical Wnt signaling in endothelial cells in their proximity and expression of Wnt targets *Apcc1* and *Axin2* [168]. They also showed that loss of Wnt ligand production led to the decreased proliferation of endothelial cells and disrupted angiogenic sprouting [168]. The authors concluded that Wnt activity is essential for the maintenance of white matter integrity and that expression of Wnt7 in OPCs is an indicator of the white matter susceptibility to a hypoxic injury [168].

Other Wnt ligands also control brain vasculature in pathological conditions. Reis and co-workers showed that forced activation of canonical Wnt signaling in GBM endothelia, up-regulated by glioma-derived Wnt1, increased *Dll4* (Delta-like 4) expression and induced Notch signaling, leading to an angiogenic blockage and quiescence of endothelial cells [169]. Additionally, transcriptional activity of β -catenin induced expression of PDGF-B (platelet derived growth factor B) and consequent recruitment of mural cells [169]. Both cascades led to the vessel stabilization and normalization of BBB function [169].

Although selective targeting of Wnt cascade in neuroendothelia seemed unachievable due to its pleiotropic mode of action, a study by Martin and co-workers provides a promising strategy for BBB-focused therapy approach in GBM [167].

5. Targeting Canonical Notch Signaling Pathway in GBM

Notch signaling is an ancient and evolutionarily conserved signaling pathway that plays a critical role in multiple cellular processes throughout life, including stem cell maintenance, cell fate decisions, cell proliferation and differentiation (reviewed in [170,171]). Accordingly, it was shown to be essential for neural stem cell maintenance and proper control of neurogenesis in both embryonic and adult central nervous system (CNS) [172]. Activation of Notch signaling can inhibit neurogenesis, maintain neural progenitor identity and, in certain settings, promote gliogenesis and drive binary fate choices, leading to various neuronal cell types (reviewed in [173]).

The canonical Notch signaling pathway involves activation of Notch receptor through series of proteolytic cleavages, resulting in translocation of Notch intracellular domain (NICD) to the nucleus, where it activates transcription of target genes through association with DNA-binding proteins and transcriptional co-activators (reviewed in [174,175]). Activation of Notch signaling is accomplished through physical interactions between the Notch receptor of the signal-receiving cell and the membrane-bound ligands of its neighbor, a signal-sending cell. There are four mammalian Notch receptor paralogs (Notch1, Notch2, Notch3 and Notch4), representing large single-pass type I transmembrane proteins that display redundant as well as unique functions [176,177]. Notch receptors in mammals are activated by five type I transmembrane, three Delta-like (*Dll1*, *Dll3* and *Dll4*) and two Serrate/Jagged (*Jag1* and *Jag2*) [175] ligands. After translation, Notch polypeptide undergoes a series of glycosylations in the endoplasmic reticulum (ER) [178,179] and then

translocates into the Golgi apparatus, where it is cleaved by furin-like convertase (S1 cleavage) into a heterodimer in which Notch extracellular domain (NECD) and Notch transmembrane and intracellular domain are non-covalently bonded and transported to the cell membrane (Figure 4) [180,181]. Ligand binding triggers conformational change in the Notch receptor facilitating a second NECD cleavage (S2 cleavage) by ADAM (a disintegrin and metalloprotease) proteases [182,183]. This process detaches NECD from the cell surface leaving the membrane-bound Notch extracellular truncation (NEXT) fragment, which is then cleaved by γ -secretase complex to release the Notch intracellular domain (NICD) (Figure 4) [184,185]. NICD translocates to the nucleus, where it interacts with the DNA-binding protein CSL [186–188] and Mastermind-like transcriptional coactivators (MAML) [189]. The stable ternary complex that is formed [190–192] further recruits coactivators, such as histone acetyltransferases (CBP/p300) and chromatin remodeling complexes [193,194] to activate transcription of Notch target genes. On the other hand, when NICD is not present, CSL associates with ubiquitous corepressor (Co-R) proteins and histone deacetylases (HDACs) to repress transcription of Notch target genes. The first Notch target genes to be discovered included *Hairy/Enhancer of split (HES)* and *HES-related repressor protein (HERP)* gene families (also known as *HES-related with YRPW motif- HEY*) that encode basic helix–loop–helix transcriptional repressors that play important roles in lineage-commitment decisions [195,196].

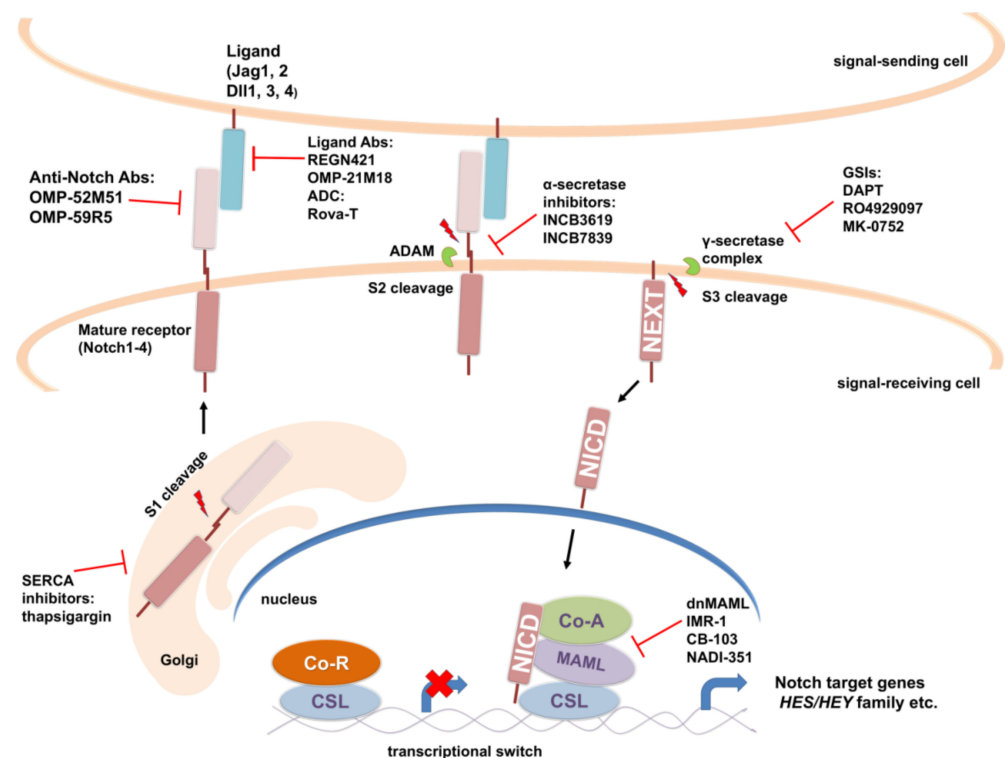


Figure 4. Scheme of a canonical Notch signaling pathway and therapeutic targets. During transport through endoplasmic reticulum and Golgi apparatus, Notch precursor is glycosylated, cleaved into a heterodimer (S1 cleavage) and transported to the cell membrane. Binding with Notch ligand induces second cleavage (S2 cleavage) by a member of ADAM family of proteases, leaving membrane-bound Notch extracellular truncation (NEXT) fragment. NEXT is subsequently cleaved by γ -secretase complex (S3 cleavage) releasing the active form of the Notch receptor, Notch intracellular domain (NICD), which can translocate to the nucleus, where it activates transcription of Notch target genes by forming transcriptional complex with DNA-binding protein CSL (also known as CBF1/in mammals, Suppressor of Hairless in *Drosophila*, and LAG-1 in *C. elegans*) and MAML, which further recruits other transcriptional coactivators (Co-A). Classes of inhibitors and antibodies (Abs, ADC) that target Notch pathway components are indicated. References are included in the main text.

Notch signaling pathway is often deregulated in different cancers including gliomas. Various studies have demonstrated increased expression of distinct components of Notch signaling pathway (such as Notch1, Notch2, Dll1, Dll4 and Jag1) and Notch target genes (*Hey1*, *Hey2*, *Hes1*) in glioma cell lines or primary human glioma samples including GBM [197–199].

Depending on the context, Notch signaling pathway may exhibit oncogenic or tumor-suppressive functions in glioma (reviewed in [200]). It has been reported that increased Notch activity is correlated with improved patient survival in defined subsets of glioma [201]. Numerous studies support oncogenic function of Notch signaling in brain tumors. Down-regulation of Notch1 receptor or its ligands through RNA interference inhibited proliferation and induced apoptosis of a variety of glioma cell lines and prolonged survival in a mouse orthotopic brain tumor model [198]. Activation of the Notch signaling pathway in GBM-derived neurosphere lines having stem cell-like properties is crucial for their growth in vitro and in vivo [202]. Hu and co-workers have shown that, as in the case with neural stem cells, Notch signaling plays a critical role in the maintenance of the patient-derived glioma stem cells by promoting their self-renewal and inhibiting their differentiation [33]. Endothelial cells in GBM actively participate in this process by providing Notch ligands to Notch receptors expressed in GBM cancer stem-like cells, thereby generating a stem cell niche that enables their self-renewal [203]. Notch signaling also plays a critical role in promoting radioresistance of GSCs via activation of the PI3K/Akt pathway [204] as well as in chemoprotection and repopulation of TMZ-treated gliomas [205].

To date, several approaches for targeting Notch signaling in vitro and in vivo have been developed, with two major classes of Notch inhibitors emerging as promising for the clinical development (Figure 4). In the treatment of cancer, the most utilized are γ -secretase inhibitors (GSIs), which block S3 cleavage and the release of the active form of Notch receptor (NICD) by the γ -secretase complex. The other major approach is usage of monoclonal antibodies (mAbs) against specific Notch ligands or receptors to interfere with their interaction or activation. GSIs were originally developed for the treatment of Alzheimer's disease because they inhibit cleavage of the amyloid precursor protein that leads to generation of neurotoxic amyloid β -protein. Numerous reports provide evidence of the effectiveness of GSIs against GBM alone or in combination with other therapeutic approaches [206]. One of the most widely used GSIs—DAPT (also known as GSI-IX)—augmented the effect of radiation and reduced proliferation and self-renewal of tumor cells as well as proliferation of endothelial cells, thereby hampering the perivascular niche in GBM explants [207]. Other studies have also shown that Notch blockage by GSIs (DAPT and GSI-I) enhance radiosensitivity of CD133+ GSCs [204,208]. One of the important findings was that the subset of GBM-derived tumor-initiating cells sensitive to three structurally distinct GSIs (DAPT, RO4929097 and BMS-708163) are characterized by a signature enriched in proneural genes and high Notch activity [209]. Notch inhibition by GSIs led to reduced proliferation and self-renewal of these responder GBM-derived tumor-initiating cells and their neuronal and astrocytic differentiation. However, clinical application of these findings is not straightforward because of the intratumoral heterogeneity of GBM. Namely, only about 50% of proneural GBMs also have Notch pathway signature [209].

Although numerous in vitro and in vivo preclinical studies of anticancer effect of GSIs in GBM have shown promising results, to date, only two GSIs, RO4929097 and MK-0752, have been tested in clinical trials in that respect. Phase 0/I trial was conducted to evaluate the effect of chemo-radiotherapy in combination with RO4929097 in patients with newly diagnosed GBM or anaplastic astrocytoma [210] (NCT01119599). The combination of RO4929097 with TMZ and radiotherapy was well tolerated, and no dose-limiting toxicities were observed. A substantial reduction in proliferation and NICD expression by tumor cells and blood vessels was detected. Treatment with RO4929097 resulted in specific reduction in the CD133+ cancer-initiating cells population in patient-derived tumor explant cultures. There was a modulation of glioma vasculature during RO4929097 treatment. However, in about one-third of the patients, there was tumor recurrence, which might be the result

of tumors switching to a Notch-independent angiogenic profile, underscoring the need of targeting multiple signaling pathways simultaneously in gliomas. Another phase I clinical trial has addressed the issue of angiogenesis, where combined effect of RO4929097 and bevacizumab (Vascular endothelial growth factor inhibitor) in patients with recurrent malignant glioma was evaluated [211] (NCT01189240). The combination of RO4929097 and bevacizumab was well tolerated, but definitive conclusions regarding clinical activity of the drug combination could not be made because of the small number of patients enrolled in the study. A phase II trial of RO4929097 for patients with recurrent and progressive GBM (NCT01122901) demonstrated the lack of activity of RO4929097 against recurrent GBM with minimal inhibition of neurosphere formation in fresh tissue samples [212]. Poor clinical activity of RO4929097 could be explained by autoinduction of RO4929097 metabolism, since it increases CYP3A4 activity in vivo, which might result in a decrease in steady-state drug levels [213]. Another selective GSI, MK-0752, has undergone a phase I trial in children with refractory or recurrent CNS malignancies including GBM [214] (NCT00572182). MK-0752 was well tolerated; however, most patients experienced progression of their disease except for two patients: one patient with ependymoma and one patient with GBM that experienced prolonged stable disease. A phase I pharmacologic and pharmacodynamic study of the GSI MK-0752 in adult patients with advanced solid tumors did not show any clinical activity of MK-0752 in extracranial solid tumors, but a modest level of activity of this drug was observed in patients with various types of glioma [215] (NCT00106145). One patient with an anaplastic astrocytoma had a complete response, and ten patients with various gliomas including GBM had prolonged stable disease.

GSIs cause severe intestinal toxicity on account of inhibiting overall Notch pathway [216,217]. Besides processing Notch receptors, γ -secretase complex cleaves a multitude of other membrane proteins affecting other signaling pathways and likely contributing to the GSIs toxicity [218,219]. In order to inhibit Notch signaling pathway more specifically than GSIs, the researchers have been developing antibodies specifically targeting different receptors and ligands of the Notch signaling pathway (Figure 4). There are two classes of antibodies against Notch receptors: (i) antibodies that target Notch negative regulatory region (NRR) preventing the S2 cleavage by ADAMs necessary for activation of receptor; (ii) antibodies that block interactions between Notch receptor and ligand by targeting epidermal growth factor (EGF)-like repeats of the receptor necessary for ligand binding [220,221]. Antibodies targeting Notch1 (Brontictuzumab, OMP-52M51; NCT01778439), Notch2/Notch3 (Tarextumab, OMP-59R5; NCT01277146) and DLL4 (Enoticumab, REGN421, NCT00187159; Demcizumab, OMP-21M18, NCT00744563) have been tested in phase I trials in patients with solid tumors; however, no GBM patients were included.

Antibodies directed at two or three targets/pathways at the same time (bi- or trispecific IgG-like molecules) have been an attractive and promising strategy in anticancer therapy. In preclinical studies, dual-variable domain immunoglobulin targeting simultaneously DLL4 and VEGF (ABT-165, dilpacimab), significantly inhibited tumor growth and decreased functional tumor angiogenesis in U87-MG human GBM xenograft model [222]. Additionally, in combination with TMZ, ABT-165 substantially increased tumor growth delay compared with either monotherapy alone.

Another approach for more specific targeting of Notch in cancer cells involves usage of antibody–drug conjugates (ADC) that target specific antigens (Notch receptor or ligand) highly expressed in tumor cells to deliver a cytotoxic drug (known as the “payload”) to them [223]. In that context, Notch ligand DLL3 represents an attractive therapeutic target, since it is highly and homogeneously expressed in *IDH* mutant gliomas and rarely detected in non-tumor brain tissue [224]. In vitro studies have shown that patient-derived *IDH* mutant glioma tumorspheres could be effectively targeted by the anti-DLL3-ADC, rovalpituzumab tesirine (Rova-T) [224]. This first-in-class anti-DLL3-ADC showed promising results in a phase I study of antitumor activity in patients with recurrent small-cell lung carcinoma (SCLC) that exhibit high DLL3 expression (NCT01901653) [225]. However, further work on Rova-T was terminated because later phase III studies showed a lack of survival benefit

for patients with SCLC [226,227]. Nevertheless, DLL3 remains an attractive target for the development of new, improved antibody-based biologics.

Another strategy for inhibiting Notch signaling pathway that has emerged over the years is to block the Notch transcriptional complex using dominant-negative form of the MAML coactivator, stapled peptides or small molecules that interfere with protein–protein interactions between the components of the NICD-CSL-MAML transcriptional complex (Figure 4). The lentivirally expressed dominant negative form of Notch coactivator MAML1 (dnMAML1) has been shown to significantly inhibit Notch signaling and reduce GBM cell growth in vitro and in vivo through induction of G0/G1 cell cycle arrest and apoptosis in GBM cell lines [228]. Opačak-Bernardi and co-workers have developed conjugate of dnMAML peptide, thermo-responsive elastin-like polypeptide (for targeted delivery to tumor cells) and cell penetrating peptide (for enhanced cellular uptake and BBB penetration) which was efficiently delivered to GBM cells, causing cell cycle arrest, apoptosis and downregulation of Notch target genes *Hes-1* and *Hey-L* [229].

Small-molecule inhibitors of the Notch transcriptional complex, such as IMR-1 (prevents MAML1 recruitment to the transcription complex), CB-103 (interferes with assembly of the Notch transcription complex), and NADI-351 (first specific inhibitor of Notch1 transcriptional complex) have exhibited antitumor activity in different xenograft models [230–232]. Additionally, antitumor activity of recently discovered small organic molecules (JI051 and JI130) that impair the ability of Hes1 to repress transcription have been demonstrated [233]. These molecules represent an attractive avenue to pursue in the treatment of GBM.

Attempts have been made to inhibit ADAMs, a family of α -secretases that cleave Notch extracellular domain upon ligand binding (Figure 4). Floyd and co-workers reported that an α -secretase inhibitor, INCB3619, decreased proliferation of GBM cell lines as well as GBM stem cell lines mainly through Notch inhibition [234]. Moreover, INCB3619 inhibited tumor growth and prolonged the survival in a human GBM stem cell xenograft model in mice. There is an ongoing phase I trial of INCB7839 (aderbasib), inhibitor of the ADAM 10 and 17 proteases, for children with recurrent or progressive high-grade gliomas (NCT04295759). A group of natural compounds (e.g., thapsigargin) that inhibit sarco-endoplasmic reticulum Ca^{2+} -ATPase (SERCA) and affect intracellular trafficking of the Notch receptor causing accumulation of unprocessed Notch1 in the ER/Golgi compartment have emerged as potential therapeutics in cancers associated with *NOTCH1* mutations [235]. In a phase II trial of mipsagargin (a thapsigargin prodrug) in patients with recurrent or progressive GBM (NCT02067156), drug treatment led to disease stabilization in 22% of patients [236].

A number of FDA-approved drugs used to treat other diseases/cancers are able to modulate Notch signaling in different cancer cell lines and could potentially be considered for treatment of GBM. These encompass histone deacetylase (HDAC) inhibitors (e.g., vorinostat) [237], enhancer of zeste homolog 2 (EZH2) inhibitors (which now include FDA-approved drug tazemetostat) [238], a thalidomide derivative lenalidomide [239], and antibiotic quinomycin A [240], most of which have been shown to have an antitumor effect on GBM cell lines in vitro or in vivo [241–243]. In addition to blockage of the SHH signaling pathway, ATO downregulates Notch signaling by decreasing the levels of Notch1 and Hes1 proteins having an inhibitory effect on GBM cancer stem-like cells in vitro and in vivo [244]. The other study showed that ATO depletes cancer stem-like cells in GBM and inhibits neurosphere recovery and secondary neurosphere formation by inhibition of the phosphorylation and activation of Akt and STAT3 through blockade of Notch signaling [245]. N-acetylcysteine (NAC) is a sulfhydryl-containing compound, with antioxidant, anti-inflammatory and mucolytic properties, initially used for treating cystic fibrosis, acetaminophen overdose and chronic obstructive lung disease [246]. Recently, Deng and co-workers revealed that NAC could efficiently inhibit Notch2 and its downstream signaling by facilitating Notch 2 degradation through lysosome pathway in GBM cell lines [247]. Moreover, NAC was able to reduce proliferation and induce apoptosis in vitro, and to suppress tumor growth of GBM cells in vivo.

Over the years, a great amount of data regarding the ability of different natural products and their derivatives to modulate Notch signaling and to alter the malignant properties of various cancer cells types have been accumulated (reviewed in [248,249]). They include compounds such as quercetin [250], curcumin [251], butein and its derivative chalcone 8 [252], honokiol [253], resveratrol [254], xanthohumol [255], ginsenoside [256], DATS [257], artemisinin [258], luteolin [259] juglone [260], withaferin A [261] and cucurbitacin B [262]. Most of them display antitumor effect on GBM cells in vitro or in vivo through various mechanisms and by affecting multiple signaling pathways, thereby representing promising alternative or adjuvant therapeutics that need to be further explored to improve outcomes of GBM patients.

The list of developed Notch-targeting approaches for combatting cancer is quite remarkable and is constantly expanding. However, a lot of challenges have to be overcome for successful translation of preclinical results into the clinical setting, including a reduction in drug toxicity associated with Notch inhibition, identification of reliable biomarkers of Notch activity for stratification of patients that would benefit from Notch-targeting therapy, and use of Notch therapies in combination with other agents or conventional chemotherapy or radiotherapy to affect multiple targets and cancer-associated processes simultaneously.

6. Targeting TGF β Signaling Pathway in GBM

TGF β (Transforming growth factor) is a multifunctional cytokine that plays important roles in the regulation of development and differentiation as well as adult tissue homeostasis (reviewed in [263,264]). In particular, TGF β is crucial for every step of neural development and is expressed in neurons, astrocytes, and microglia (reviewed in [265]). It is shown that TGF β and WNT signaling crosstalk controls the growth and size of the developing brain by regulating neural stem cell maintenance and differentiation [266].

The TGF β family comprises proteins divided into the following: (I) the TGF β subfamily, which contains TGF β , activin beta chains, and the protein Nodal, and (II) the bone morphogenetic protein (BMP) subfamily that comprises BMPs, growth differentiation factors (GDFs), and mullerian inhibitory factor (MIF) (reviewed in [267]). In mammals, there are three isoforms of TGF β (TGF β 1, 2 and 3) [268–270]. After activation, TGF β ligands bind to TGF β receptor II (TGF β RII), which is a constitutive active kinase that phosphorylates TGF β receptor I (TGF β RI), thus enabling the transduction of extracellular signal into the cell (Figure 5). In the canonical (Smad-dependent) pathway, TGF β RI activates receptor-regulated (R-) Smad proteins (Smad 2/3), which form transcription regulatory complexes with the Co-Smad (Smad 4) and translocate into the nucleus where they bind to target DNA sequences to regulate the transcription of numerous genes (reviewed in [264,271]). Smad proteins which have an inhibitory function (I-Smads- Smad 6 and 7) suppress phosphorylation and nuclear translocation of Smad 2/3, thus regulating TGF β through negative feedback mechanism [272] (Figure 5). In addition to the canonical pathway, TGF β has the ability to activate various signaling pathways. In the non-canonical (Smad-independent) pathway, TGF β triggers mitogen-activated protein kinases (MAPK) pathways, such as ERK1/ERK2, Jun-N terminal kinase (JNK) and p38 and PI3K kinases (reviewed in [273]).

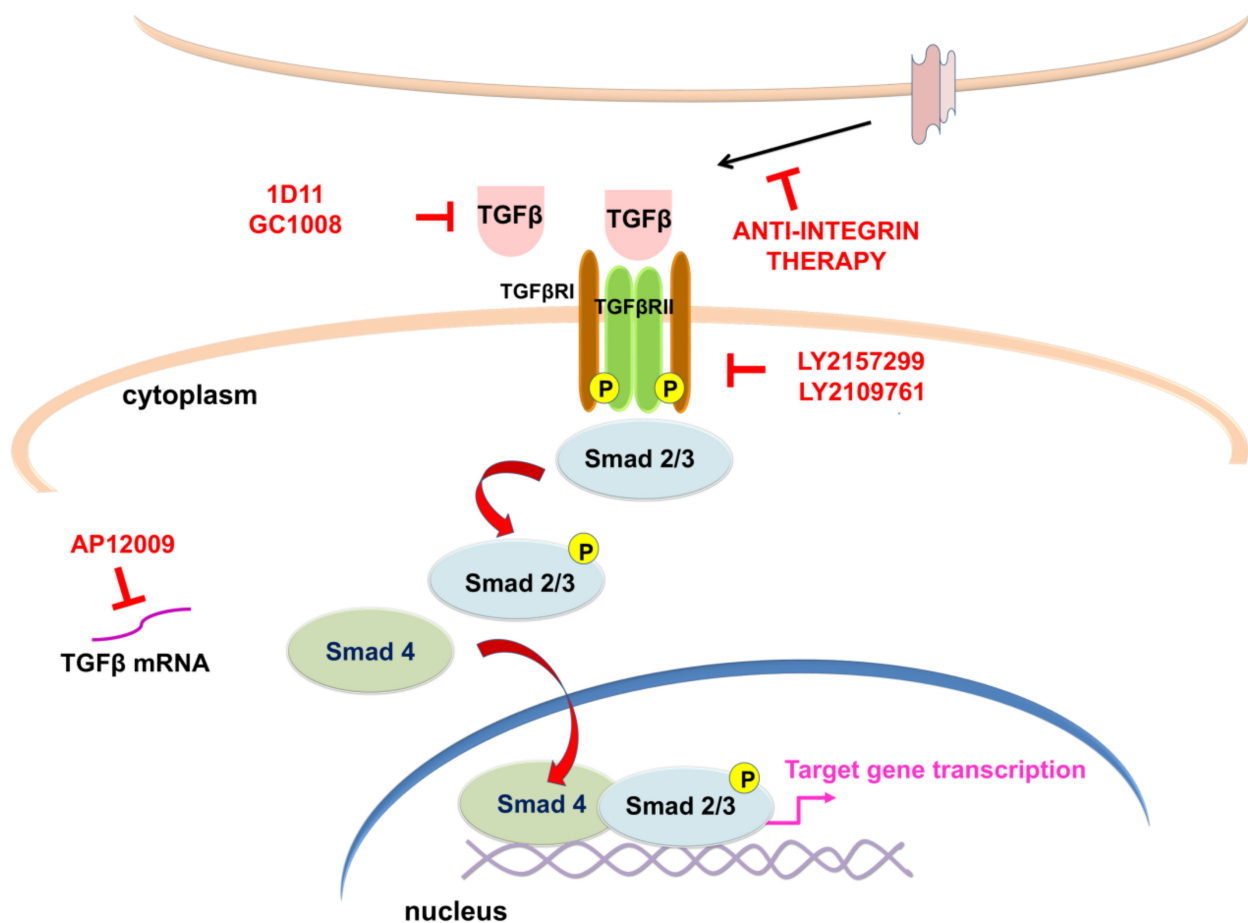


Figure 5. Schematic representation of the canonical (Smad-dependent) TGF β pathway and TGF β signaling therapies which have undergone clinical trials in GBM. TGF β binding to TGF β receptors II (TGF β RII) results in phosphorylation and activation of TGF β receptors I (TGF β RI), phosphorylation of Smad 2/3, which interact with Smad 4 and form a complex that translocates into the nucleus to activate target genes. Antisense oligonucleotides (AP12009), anti-integrins, kinase inhibitors (LY2157299, LY2109761) or neutralizing antibodies (1D11, GC1008) used for targeting TGF β signaling pathway are presented in red. Based on [274] and references included in the main text.

Under pathological conditions such as neurodegenerative diseases, injury, and cancer, a significant increase in the expression of TGF β was noticed (reviewed in [275–277]). Increased mRNA levels of the TGF β isoforms were detected in GBM, which correlated with the degree of malignancy and prognosis [278]. TGF β promotes proliferation of gliomas [279,280], invasion [281], angiogenesis (reviewed in [282]), and maintenance of stemness of patient-derived GSCs via the TGF β -Sox4-Sox2 pathway [34]. Depending on the stage of malignancy, TGF β has a dual function. At an early stage of the tumor, TGF β reduces cell proliferation, promotes cell cycle arrest, induces apoptosis, and induces DNA damage in malignant cells acting as a tumor suppressor (reviewed in [277,283,284]). Later, in an advanced stage of malignancy, TGF β acts as a tumor promoter directly inducing epithelial–mesenchymal transition (EMT), invasion, and metastasis of malignant cells, or indirectly, by promoting angiogenesis (reviewed in [277,285,286]). TGF β -Smad activity is elevated in aggressive, highly proliferative gliomas and is related to poor patient prognosis [279].

Recently, many studies highlighted the significance of TGF β in actively shaping and developing the glioma TME. The TME consists of different cells and extracellular materials surrounding the tumor which are responsible for promoting tumorigenesis through processes such as invasion, metastasis, and resistance to therapy. Studies revealed

that various cell types, non-immune and immune cells, are associated with TGF β activation and secretion during cancer progression. Accumulating evidence support the fact TGF β has a dual role in glioma (reviewed in [287]). TGF β secreted by glioma cells maintains tumor growth through inducing immune cells to become immunosuppressive, leading to the lack of an effective immune response against gliomas and formation of a permissive microenvironment. On the other hand, TGF β produced by immune cells upregulates TGF β RI and TGF β RII on glioma cells and supports tumor progression (reviewed in [288]). Further, TGF β controls differentiation, angiogenesis, and metabolic reprogramming of stromal cells of the TME during tumorigenesis (reviewed in [289]).

Growing evidence suggests that inhibition of TGF β signaling could provide novel therapeutic options for treating GBM. Knock-down of TGF β or TGF β receptors has been shown to limit migration, invasion, and tumorigenicity of glioma cells [281,290]. Numerous different strategies to target TGF β signaling pathway in GBM have been established and tested in clinical trials including antisense oligonucleotides, neutralizing antibodies, and kinase inhibitors. One of the approaches tested in clinical trials is usage of antisense oligonucleotides (ASOs). ASOs are specifically designed to bind TGF β mRNA and inhibit its translation thus decreasing its expression. AP 12009 (Trabedersen) is a synthetic phosphorothioate oligodeoxynucleotide that targets one of the TGF β isoforms, TGF β 2 mRNA (reviewed in [291,292]). Hau and co-workers performed in vitro experiments that demonstrated the specificity and efficacy of AP 12009 in patient-derived malignant glioma cells [293]. They also showed that AP 12009 treatment reversed the immunosuppressive effects of tumor-derived TGF β . In an autologous cytotoxicity assay, where peripheral blood mononuclear cells isolated from glioma patients were activated by IL-2 and co-incubated with the glioma cells from the same patient, treatment with AP 12009 restored their cytotoxic activity against glioma cells. Additionally, three phase I/II studies confirmed that AP 12009 achieved safety and tolerability in patients with recurrent or refractory malignant (high-grade) glioma, anaplastic astrocytoma (WHO grade III) or GBM. Most importantly, in two patients, complete tumor remission was detected, showing promising efficacy of AP 12009 [293]. Lastly, the phase III clinical trial (NCT00761280) using AP 12009 in the treatment of recurrent or refractory anaplastic astrocytoma or secondary GBM, has been terminated due to insufficient recruitment of patients.

Anti-integrin therapy is considered a promising strategy for inhibition of processes involved in the GBM progression [294]. Roth and co-workers demonstrated that cilengitide, a selective integrin inhibitor, reduced phosphorylation of Smad 2 in vivo, confirming that integrins control TGF β pathway in GBM [294]. A phase III clinical trial CENTRIC (NCT00689221) was conducted to determine overall survival as well as efficacy and safety of cilengitide in combination with standard chemoradiotherapy, compared to standard treatment alone, in newly diagnosed GBM patients with methylated O6-methylguanine-DNA-methyltransferase (*MGMT*) gene promoter. Unfortunately, the clinical trial revealed no improvement in overall survival or progression-free survival of patients [295].

Kinase inhibitors reduce TGF β kinase activity, thus modulating downstream signaling transduction. In various tumors, including GBM, it is well documented that kinase inhibitors can decrease tumor growth and metastasis, and prevent recurrence and angiogenesis in mouse models [296–299]. In particular, LY2109761, a TGF β RI kinase inhibitor, reduced the survival of U87 and T98 glioma cell lines, and inhibited migration and angiogenesis. Furthermore, LY2109761 delayed tumor growth in vivo alone or in combination with radiation and TMZ [299]. Galunisertib (LY2157299), a small-molecule inhibitor, reduces a kinase activity of TGF β RI in Smad 2/3 phosphorylation. In a preclinical study, Yingling and co-workers confirmed anti-tumor activity of galunisertib in vitro and in vivo [300]. However, a phase I/II clinical trial showed that galunisertib treatment with TMZ-based chemoradiation had no clinical benefit compared to standard TMZ-based chemoradiation [301]. Further, in another phase II study, treatment by galunisertib in combination with lomustine in patients with recurrent glioma did not improve overall survival relative to placebo with lomustine [302]. Spender and co-workers reported preclinical study regarding antitumor

effect of two TGF β RI inhibitors, AZ12601011 and AZ12799734. They demonstrated that AZ12601011 and AZ12799734 were more effective in inhibiting TGF β RI-induced transcription and migration than galunisertib. Additionally, the authors confirmed inhibition of tumor growth and metastasis *in vivo* using a murine model of breast cancer [303].

Preventing TGF β signaling transduction is possible by administration of antibodies against ligand or its receptors. To accomplish this objective, several antibodies against TGF β are developed. Literature data revealed that inhibition of TGF β signaling by applying TGF β -neutralizing monoclonal antibody 1D11 increased glioma-associated antigen peptide vaccines efficiency in mice [304]. Further, Hulper and co-workers have demonstrated that 1D11 TGF β neutralizing antibody can be detected in subcutaneous and intracranial gliomas after intravenous injection [305]. Nevertheless, 1D11 treatment of gliomas had diverse effects on the gliomas in immunocompetent and immunodeficient mice. 1D11 treatment of immunocompetent mice bearing subcutaneous glioma resulted in tumor remission, while the same treatment in immunodeficient mice increased tumor size. Additionally, 1D11 treatment of intracranially implanted gliomas impaired glioma cell invasion in normal brain tissue but did not reduce tumor size [305]. One of the important aspects of treating glioma is the permeability of BBB that often prevents the drugs to reach the target site. Radiolabeled human IgG4 monoclonal antibody that recognizes and neutralize TGF β , 89Zr-GC1008, showed excellent uptake in patients with recurrent high-grade gliomas with no observed toxicity (NCT01472731). However, 89Zr-GC1008 did not demonstrate an antitumor effect [306].

GSCs, which cause GBM tumor recurrences, are able to inhibit natural killer (NK) cell activity via releasing and activation of TGF β , thus evading immune attack. It was shown that genetic disruption of TGF β R2 in NK cells results in antitumor activity *in vivo* [307]. There is an ongoing phase I trial (NCT04991870) conducted to evaluate the best dose, possible benefits and side effects of engineered NK cells, with deleted TGF β RII and glucocorticoid receptor NR3C1, for the treatment of recurrent GBM (reviewed in [308]). Additionally, the trial is aimed to determine overall survival, duration of clinical response, progression-free survival and time to progression.

Using bioactive compounds in combination therapy could be a promising strategy for targeting TGF β signaling pathways. It was shown that resveratrol, a polyphenolic compound obtained from plants, modulates TGF β signaling (reviewed in [309]) and exhibits the antitumor effect in various tumors [310,311]. In particular, resveratrol suppresses EMT, migration, invasion, and EMT-generated stem cell-like properties in GBM *in vitro* via canonical TGF β signaling, and also inhibits the EMT process *in vivo* [312].

Taken together, clinical trials data presented above display no sufficient benefit of targeting TGF β signaling in patients with GBM. The complexity of TGF β signaling itself as well as interactions with various signaling pathways could explain the discouraging results of clinical studies regarding inhibition of TGF β signaling in GBM.

7. Targeting BMP Signaling Pathway in GBM

The bone morphogenetic proteins (BMPs), the largest part of the TGF β family, are important regulators of a multitude of processes during embryonic development and homeostasis (reviewed in [313–317]). The body of literature indicates that in the CNS, these proteins have a pleiotropic role during neural stem cell (NSC) proliferation, apoptosis, cell fate decisions and maturation. Furthermore, in the adult neurogenic niches, subventricular and subgranular zones, BMPs are critical for proliferation, maintenance, and survival of NSCs as well as terminal differentiation of newborn neurons (reviewed in [314,315,318,319]), thus profoundly affecting the homeostasis in the adult brain. Interestingly, in contrast to early development, NSCs derived from older animals undergo astrocytic differentiation in response to BMPs (reviewed in [320]).

BMP ligands exert their activities in the cells through both canonical and non-canonical pathways (Figure 6) (reviewed in [317,321]). In the canonical signaling pathway, BMP ligands bind to the cell surface receptors to form a heterotetrameric complex, comprising

two dimers of type I and type II serine/threonine kinase receptors. There are three “type I” receptors, type 1A BMP (BMPR-1A or ALK3), type 1B BMP (BMPR-1B or ALK6), and type 1A activin receptor (ActR-1A or ALK2) and three “type II” receptors, type 2 BMP (BMPR-2), type 2 activin (ActR-2A), and type 2B activin receptor (ActR-2B). Following the formation of a heterotetrameric complex, the constitutively active type II receptor trans-phosphorylates the type I receptor and allows phosphorylation of the immediately downstream substrate proteins known as the receptor-regulated Smads (R-Smads): Smad 1, 5, and 8 (Figure 6). R-Smads then associate with the Smad 4, and this complex translocates to the nucleus, where it functions as a transcription factor with coactivators and corepressors to regulate gene expression, as already mentioned in the previous section. In addition, non-canonical (Smad-independent) pathways for BMPs can also lead to regulation of gene expression [321]. It has been found to affect different components including TAK-1, a serine–threonine kinase of the MAPK family, PI3K/Akt, P/kc, Rho-GTPases.

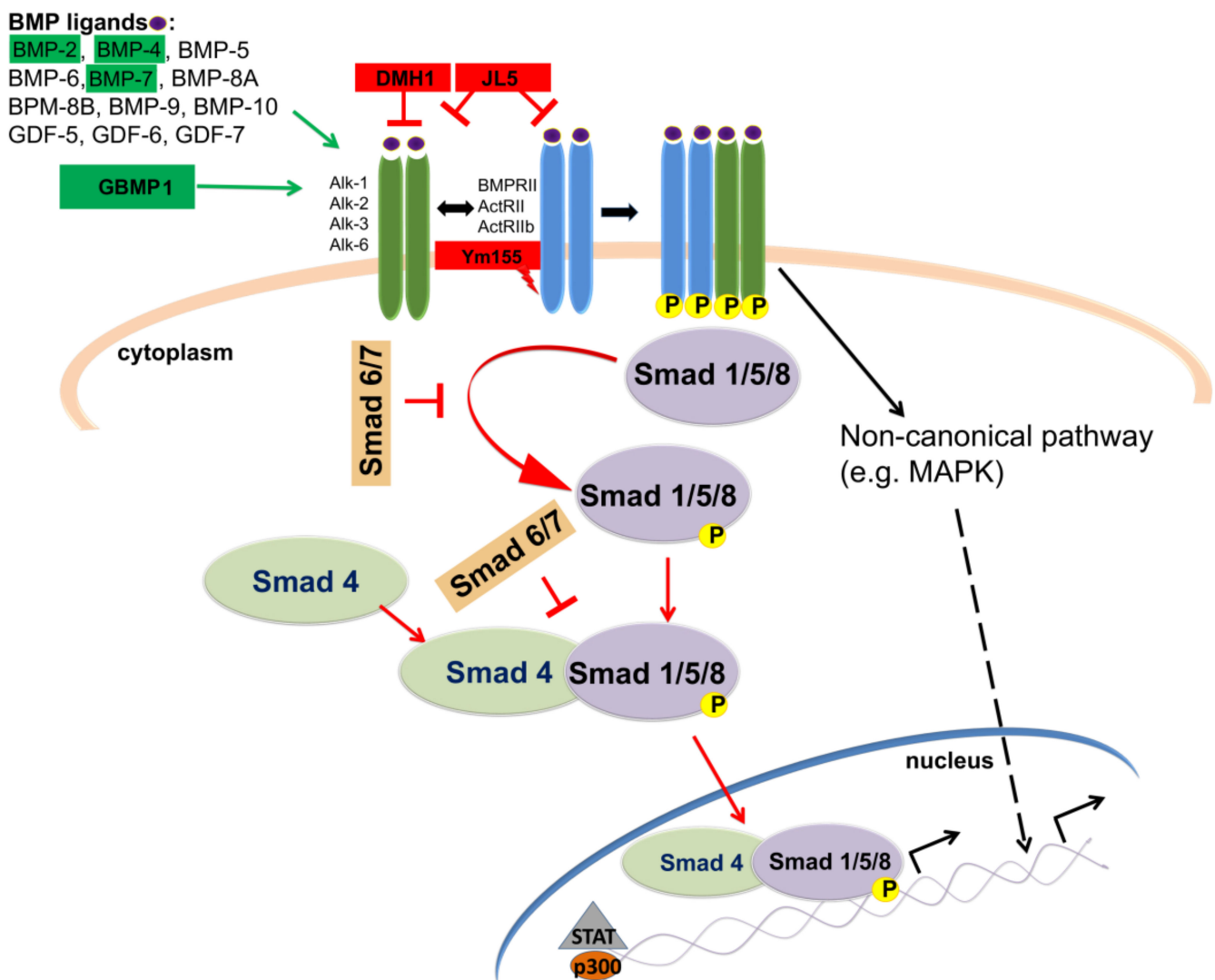


Figure 6. Overview of the canonical BMP cell signaling pathway and molecules investigated for potential therapeutic intervention in GBM. In canonical pathway, various BMP ligands binds to two receptor types (type I and type II) to form a heterotetrameric complex, which then binds to and phosphorylates the receptor-activated Smad 1, Smad 5 and Smad 8. Extracellular inhibitors of BMPs including Noggin, Chordin, and Gremlin inhibit activity of this signaling pathway. Activated Smads (Smad 1, 5, and 8) form complexes with Smad 4, enter the cell nucleus and in combination with co-binding partners, such as p300 or STAT, act as transcription factors and activate multiple gene

expression. BMP ligands that activate BMP signaling in the GBM and GSCs are in the green boxes. Receptor inhibitors that suppress BMP signaling in the GBM and GSCs are in the red boxes. DMH1 targets BMP type 1 receptors, JL5 inhibits both the type 1 and type 2 BMP receptors. Ym155 does not bind to the BMP receptors but induces the degradation of BMPR2. References are included in the main text.

Growing data demonstrate that some BMPs are implicated in different pathologies, including processes related to carcinogenesis, such as angiogenesis and EMT, and driving cancer stem cell resistance to treatments (reviewed in [322–326]). Functional studies revealed that depending on the type of cell, TME, epigenetic background of the patient, or stage of tumor growth, some BMPs can be linked to tumor progression, while others can serve as tumor suppressors (reviewed in [325,327,328]). In glioma, expression analysis of molecular components of the BMP pathway revealed significant differences in the level of expression in tumor tissues that were associated with tumor grade and prognosis pointing to them as novel biomarker with potential important therapeutic implications [329–331].

Results of previous *in vitro* and *in vivo* studies indicate that BMPs are among the most potent therapeutics in preventing the growth and recurrence of GBM. Exposure of stem-like brain tumor cells to neurosphere-derived BMP7 induced differentiation, reduced stem-like marker expression, self-renewal, and the ability for tumor initiation in mice [332]. Similarly, the BMP7 variant decreased proliferation and induced differentiation of GBM stem-like cells and inhibited angiogenic endothelial cord formation [333]. In the same study, the mouse models with subcutaneously or orthotopically implanted GBM stem-like cells reflected *in vitro* results [333]. In the study where BMP7 was encapsulated in microspheres in the form which provided an effective release for several weeks, primary tumors showed a growth delay. This effect was correlated with the activation of the BMP canonical pathway [334]. BMP4 is another cytokine whose expression is significantly lower in glioma tumor tissue compared to adjacent normal tissue [330]. Previous studies also showed that BMP4 inhibited cell proliferation and induced apoptosis in GSCs [335] and GBM [336] and initiated GBM-derived stem cell astrocyte differentiation [35]. Liu and co-workers detected decreased expression of BMP4 in the multi-drug resistant (MDR) U251 cell line (U251/TMZ) compared to the parental U251 cells. In line with this result, the overexpression of BMP4 in U251/TMZ cells abolished the MDR both *in vitro* and *in vivo* through modulation of Bcl-2 and GDNF [337]. BMP2 also makes GSCs more susceptible to TMZ treatment through destabilization of HIF-1 [338], further suggesting BMPs are promising candidates for GSC-targeting GBM therapy. However, the main obstacle could be that glioma stem cells have mechanisms to avoid BMP-induced differentiation as they express a BMP antagonist Gremlin1 [339].

A recent study on patient-derived GSCs showed that treatment with BMP4 caused downregulation of stem cell marker CD133 expression, induced asymmetric cell division and suppressed self-renewal ability of cells [340]. An extensive study using 40 different human GBM-initiating cell cultures demonstrated an extensive diversity in the inhibitory effect of BMP4 on the tumor growth between cell lines [341]. Responsiveness to BMP4 was correlated with a level of SOX2 and proneural mRNA expression in cells [341].

In the contrast to the aforementioned therapeutic strategy to induce BMP signaling to initiate differentiation of GSCs, most recently, Kaye and co-workers showed that inhibition of BMP signaling could also have potential therapeutic relevance for fighting GBM [342]. In this study, BMP receptor inhibitors, DMH1, JL5, and Ym155 significantly decreased the expression of the inhibitor of differentiation protein 1 (ID1) in GBM cell lines [342]. The members of the ID family of protein, are co-expressed in diverse cell populations of GBM and conditional deletion of *ID1*, *ID2* and *ID3* alleles suppressed the GBM tumor growth and diminished the population of GSCs (reviewed in [343]). Furthermore, Kaye and co-workers demonstrated that spheres formed from GBM cell lines after BMP4 treatment were smaller in size and number. However, treatment with JL5 completely prevented the formation of spheres, suggesting that inhibition of BMP signaling suppressed self-renewal more than its activation [342].

In addition to activation of direct effectors of BMP signaling, such as BMP4 and BMP7, simulation of the BMP pathway is performed using mimic effectors. Recently, the BMP2 protein mimicking peptide GBMP1 has been synthesized by Rampazzo and co-workers and demonstrated to enhance osteogenic differentiation of mesenchymal stem cells and astroglial differentiation of GSCs in vitro [344]. However, further studies are necessary to prove the usage of this drug in clinical studies.

To this day, numerous strategies that enable modulation of the BMP pathway in vivo (starting from upstream of receptors to effector activity) in different cancer and non-cancer-related pathologies have been described in the literature (reviewed in [24,326,345]). However, to the best of our knowledge, there is only one active phase I clinical trial for the treatment of adults with progressive and/or multiple recurrent GBM, in which human recombinant BMP4 is being administered through intratumoral and interstitial convection-enhanced delivery (CED) (NCT02869243) (reviewed in [24]). The reasons for a low number of clinical trials may come from the fact that these tumors are highly heterogeneous, and that BMP signaling regulates a large network of genes and pathways, and only a small portion of those directly relates to the disease pathology or may even have the opposite effect on the clinical outcome.

8. Targeting Hippo Signaling Pathway in GBM

The Hippo pathway is an evolutionarily well-conserved signaling pathway involved in tissue development and regeneration that controls organ size by regulating cell proliferation and apoptosis [346]. In physiological conditions, the Hippo pathway suppresses growth, mediates stress-induced apoptosis or regulates cell fate decisions [347]. The Hippo pathway consists of a complex cascade of serine/threonine-protein kinases and its core kinases MST1/2 (Mammalian STE-like protein kinase 1/2) and LATS1/2 (Large tumor suppressor 1/2) [348]. Their roles are to inhibit the transcription cofactors YAP (Yes-Associated Protein 1) and its ortholog TAZ (Transcriptional co-activator with PDZ-binding motif). When the pathway is initiated by activation of MST1/2 associated with SAV1 (Salvatore) they further phosphorylate LATS1/2 and its cofactor MOB1, which in turn phosphorylates the transcription cofactors YAP/TAZ, leading to inhibition of their nuclear translocation [349] (Figure 7).

Phosphorylated YAP/TAZ is sequestered in the cytoplasm or degraded by the proteasome [350]. When the Hippo pathway is inactivated, the unphosphorylated YAP/TAZ complex is translocated to the nucleus, where it binds the TEAD (TEA domain) transcription factor family. Indeed, YAP/TAZ association with TEAD transcription factors is essential to the control of several targeted genes, such as *MYC* (MYC proto-oncogene bHLH transcription factor), *BIRC5* (baculoviral IAP repeat containing 5), *AXL* (AXL receptor tyrosine kinase), *CTGF* (Connective Tissue Growth Factor) and *CYR61* (Cysteine Rich Angiogenic Inducer 61) involved in cell proliferation and survival [351]. This pathway is regulated by cell–cell contact, cell polarity, and actin cytoskeleton, as well as a wide range of signals, including stress signals, cellular energy status, and mechanical and hormonal signals that act through G-protein-coupled receptors (GPCR) [352].

Since MST1/2 and LATS1/2 core constitute a regulatory part of the Hippo signaling associated with a tumor suppressor effect, the transcriptional cofactors YAP/TAZ associated with TEAD transcription factors represent the terminal effectors of this pathway and play a pro-oncogenic role. YAP/TAZ activation is involved in cell proliferation, mesenchymal transition, invasion, and metastasis, as well as in cancer stem cell maintenance and chemoresistance [353]. Elevated levels and nuclear localization of YAP and in some cases TAZ have been reported in a majority of solid cancers, suggesting widespread deregulation of Hippo signaling in human neoplasia [354]. High levels of nuclear YAP1 immunoreactivity were detected in GBM tissues, and it was shown that silencing of YAP1 in glioma cell lines led to a significant reduction in cell growth [355]. In line with this, a comparison of single-cell RNA-seq datasets from patients with GBM revealed that YAP and TAZ drive a regulatory network associated with the GSC state [356]. It has been shown that YAP/TAZ are

required to establish GSC properties in primary cells and required for tumor initiation and maintenance *in vivo* in different mouse and human GBM models [356]. Further, Bhat and co-workers showed elevated expression of TAZ in GBM tissues and associated TAZ expression with mesenchymal gene signature showing a direct role of TAZ and TEAD in driving the mesenchymal differentiation in malignant glioma [67]. Various studies have also found that hyperactivation of YAP/TAZ is associated with resistance to canonical chemotherapies, radiotherapies, and targeted therapies [357,358]. Current evidence suggests that multiple mechanisms contribute to the deregulation of YAP and TAZ in human cancers, including promoter hypermethylation, mutation, and amplification [354]. Reasonably, YAP/TAZ represents one of the most attractive targets in anticancer therapy as final effectors of the Hippo signaling pathway.

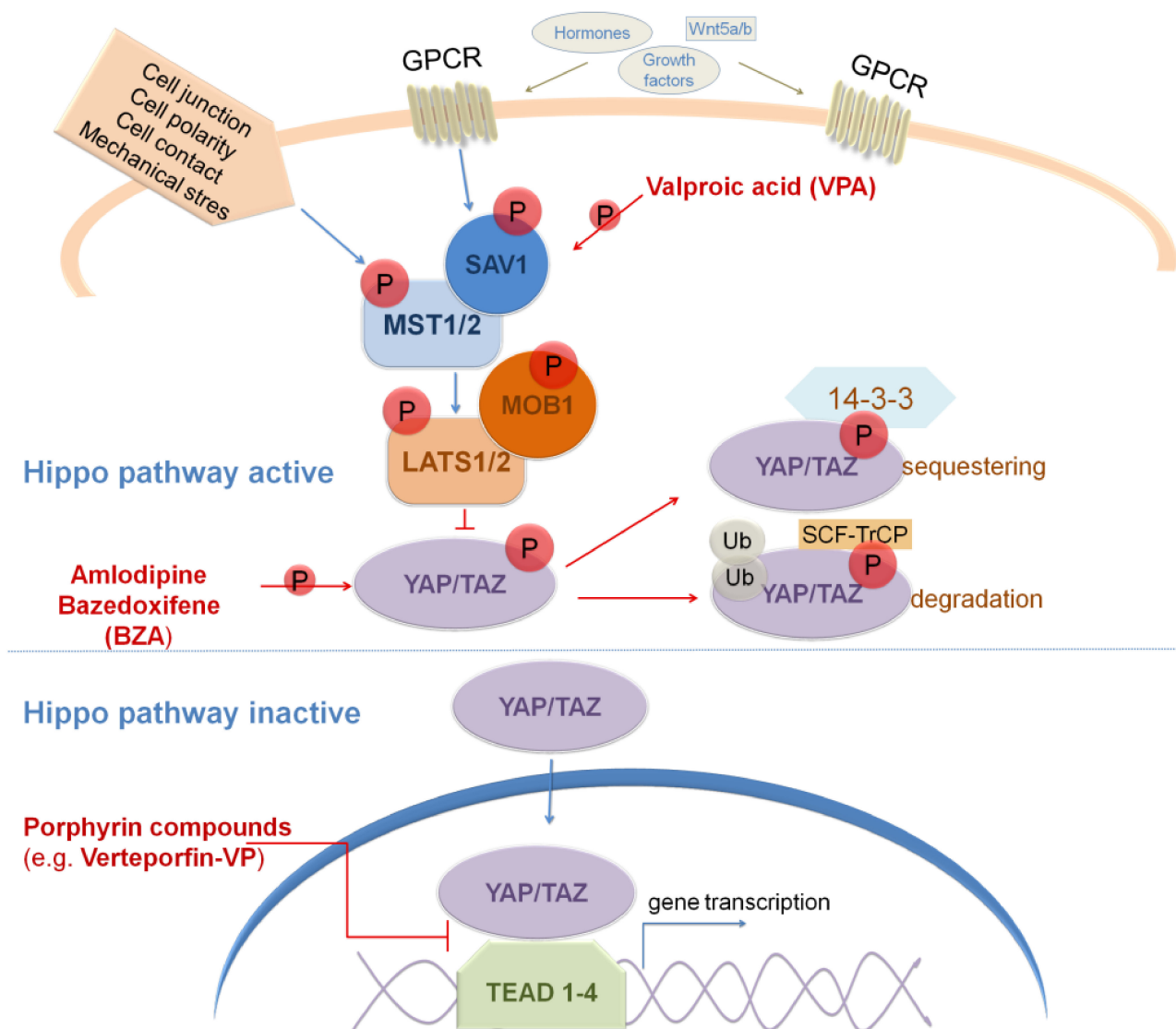


Figure 7. The canonical Hippo pathway and its pharmaceutical inhibitors. Various extracellular signals including mechanical stress, cellular contact, hormones and growth factors activates Hippo signaling cascades that through serial phosphorylations involving block of kinases inhibits nuclear translocation of transcriptional co-activator YAP/TAZ and consequently their involvement in the regulation of gene transcription. When Hippo pathway is inactive, YAP/TAZ translocates to the nucleus, associates with TEAD family of transcription factors and participates in the regulation of target genes expression. Inhibitors that target important pathway components are indicated in red. References are included in the main text.

High-throughput screening of approximately 3300 FDA-approved drugs for inhibitors of the transcriptional activity of YAP identified 71 hits including several porphyrin compounds, protoporphyrin IX (PPIX), hematoporphyrin (HP), and verteporfin (VP), which stood out among the top candidates [359]. These compounds disrupt physical interactions between YAP and TEAD, thereby inhibiting YAP transcriptional activity, but more importantly, they are able to cross BBB and accumulate in the brain [360]. Vigneswaran and co-workers showed that VP acts as an inducer of apoptosis of patient-derived GBM cells that successfully suppressed expression of YAP/TAZ transcriptional target genes, and had significant survival benefit in an orthotopic xenograft GBM model [361]. Further, a phase 0 clinical trial reported that liposomal VP was effectively absorbed by GBM cells in patients' tumor tissue, and VP-treated participants preliminarily showed lower YAP/TAZ protein levels compared with a representative untreated control patient [361]. Further studies are needed to elucidate their efficiency in therapeutic protocols, alone or more likely in combination with established treatment regimens.

Another approved drug that emerged as an interesting therapeutic in GBM is valproic acid (VPA). It has been demonstrated that VPA inhibited glioma cell proliferation, migration, and invasion [362]. Experiments on human GBM cell lines have shown that VPA had a strong antiproliferative effect and also led to a reduction in CD44 expression (a cancer stem cell marker) [363]. Further, it has been shown that CD44 is upregulated in GBM tissue samples and that its depletion blocked glioma cells growth in vitro and in vivo and sensitized GBM cells to cytotoxic drugs in vivo [364]. CD44 functions upstream of the mammalian Hippo signaling pathway, and when CD44 is silenced, it is followed by sustained phosphorylation of MST1/2 and LATS1/2 and, consequently, phosphorylation/inactivation of YAP [364]. There have been several trials of VPA in combination with TMZ and radiation for the treatment of brain tumors. Results of a single-group study where newly diagnosed GBM patients started VPA treatment following maximal safe resection (all of them were treated with chemoradiation and TMZ) demonstrated no significant treatment-related toxicity; younger patients (age \leq 45 years) showed a significantly better overall survival (25 months) versus older patients (8 months) [365]. Limitations of this study include the small sample size, no randomization, and the lack of information regarding other potential prognostic factors. Yuan and co-workers performed a meta-analysis using EMBASE, MEDLINE, ClinicalTrials.gov, and Cochrane Central Register of the Controlled Trials databases to assess the effects of VPA on survival times and GBM recurrence [366]. A total of 1634 patients with a confirmed GBM diagnosis were examined in this meta-analysis, and the authors concluded that GBM patients using VPA showed a relatively better outcome when compared to patients using no antiepileptic drugs or other-antiepileptic drugs [366]. This and similar retrospective studies can be useful as a guide in planning other clinical trials investigating the impact of co-medication with VPA in GBM patients.

Amlodipine, a calcium channel blocker medication used to treat high blood pressure and coronary artery disease, has been shown to provoke actin cytoskeleton remodeling and new assembly of F-actin that, in turn, starts kinase cascade and phosphorylates YAP, leading to its degradation [367]. The authors showed that amlodipine inhibits the survival of GBM cell line LN229 by suppressing YAP/TAZ activities and preventing their accumulation in the cell nucleus [367]. Amlodipine, along with several other antihypertensives, has demonstrated promising preclinical results, but unfortunately, it has not gone into clinical trial yet.

Bazedoxifene (BZA) is a small molecule inhibitor currently used in the clinic as a third-generation selective estrogen receptor modulator to treat postmenopausal osteoporosis [368]. BZA preferentially disrupts the gp130-IL6 receptor complex [369], and a recent study displayed that BZA treatment also accelerated YAP phosphorylation, hypothesizing that there is a cross-talk between IL-6-gp130 and YAP [370]. Wightman and co-workers identified BZA as a candidate therapeutic for GBM, showing its ability to penetrate the BBB and increase the time of survival in an orthotopic syngeneic mouse model [371]. Addi-

tionally, as presented by Fu and co-workers, BZA combined with paclitaxel had a stronger ability to suppress YAP signaling and inhibit GBM tumor growth in the orthotopic GBM mouse model [370].

It has been already reported that statins impair the viability of GBM cell lines through TGF β inhibition [372]. Importantly there is evidence that statins, in particular fluvastatin, could inhibit nuclear localization of YAP and TAZ and, consequently, YAP/TAZ-TEAD-dependent reporter activity [373]. A meta-analysis performed by Xie and co-workers included a total of 2519 patients with GBM, including 430 statin users and 2089 nonstatin users [374]. Analyzed data regarding progression-free survival and overall survival revealed that the use of statins was not associated with prolonged survival of patients with GBM [374]. However, a subgroup analysis showed that the use of statins before diagnosis favors the overall survival of GBM patients, while statin usage after diagnosis might be harmful [374]. Currently, there are two clinical trials evaluating the use of statins: a phase I trial evaluating the safety of fluvastatin and celecoxib (Celebrex) association in gliomas (NCT02115074), and a phase II study assessing the efficacy and safety of atorvastatin in combination with radiotherapy and TMZ in GBM (NCT02029573).

In summary, there are many approved drugs that are considered for repurposed use in GBM, and novel randomized trials are needed for proving their therapeutic efficacy. The general opinion is that repurposed agents are more likely to be combined with current standard regimens, suggesting that they should be considered when planning future trials.

9. Targeting Retinoic Acid Signaling Pathway in GBM

Retinoic acid signaling has key roles in vertebrate development [375]. Functions of retinoic acid (RA), a morphogen synthesized from vitamin A [376], in the regulation of different processes, such as fate specification, differentiation, proliferation, apoptosis, immune response, homeostasis, regeneration and maintenance of circadian rhythms have been reported (reviewed in [377–379]).

Postnatally, retinoids are derived from carotenoids and retinyl esters. Following ingestion, carotenoids are cleaved into retinal and then reduced to retinol, while retinyl esters are hydrolyzed to retinol. Upon entering into the bloodstream, retinol is bound to retinol-binding protein 4 (RBP4) and this complex enters cells via stimulated-by-retinoic-acid 6 (STRA6) (reviewed in [380]) or by membrane diffusion [381] (Figure 8). Intracellularly retinol is metabolized to RA through a series of oxidation steps (reviewed in [377]). Namely, within cells, retinol is converted to retinaldehyde by cytosolic alcohol dehydrogenases (ADHs) and microsomal retinol dehydrogenases (RDHs). After that, retinaldehyde is oxidized to RA by three aldehyde dehydrogenases ALDH1A1–A3 (reviewed in [380,382]). There are three naturally occurring RA stereoisomers: all-trans retinoic acid (ATRA), 13-cis retinoic acid (13-cis RA) and 9-cis retinoic acid (9-cis RA) (reviewed in [383]). Acting on the producing (autocrine signaling) or the receiving (paracrine signaling) cells, RA enters the nucleus via cellular RA-binding protein 2 (CRABP2) (reviewed in [384]) and interacts with retinoic acid receptor (RAR-RAR α , RAR β , RAR γ)/retinoid X receptor (RXR-RXR α , RXR β , RXR γ) heterodimer. Subsequently, this complex interacts with RA-response element (RARE) in the promoter region of RA target genes influencing the transcription of over 500 genes (reviewed in [377]). RA is inactivated by cytochrome P450 family 26 (CYP26) oxidase (reviewed in [382]).

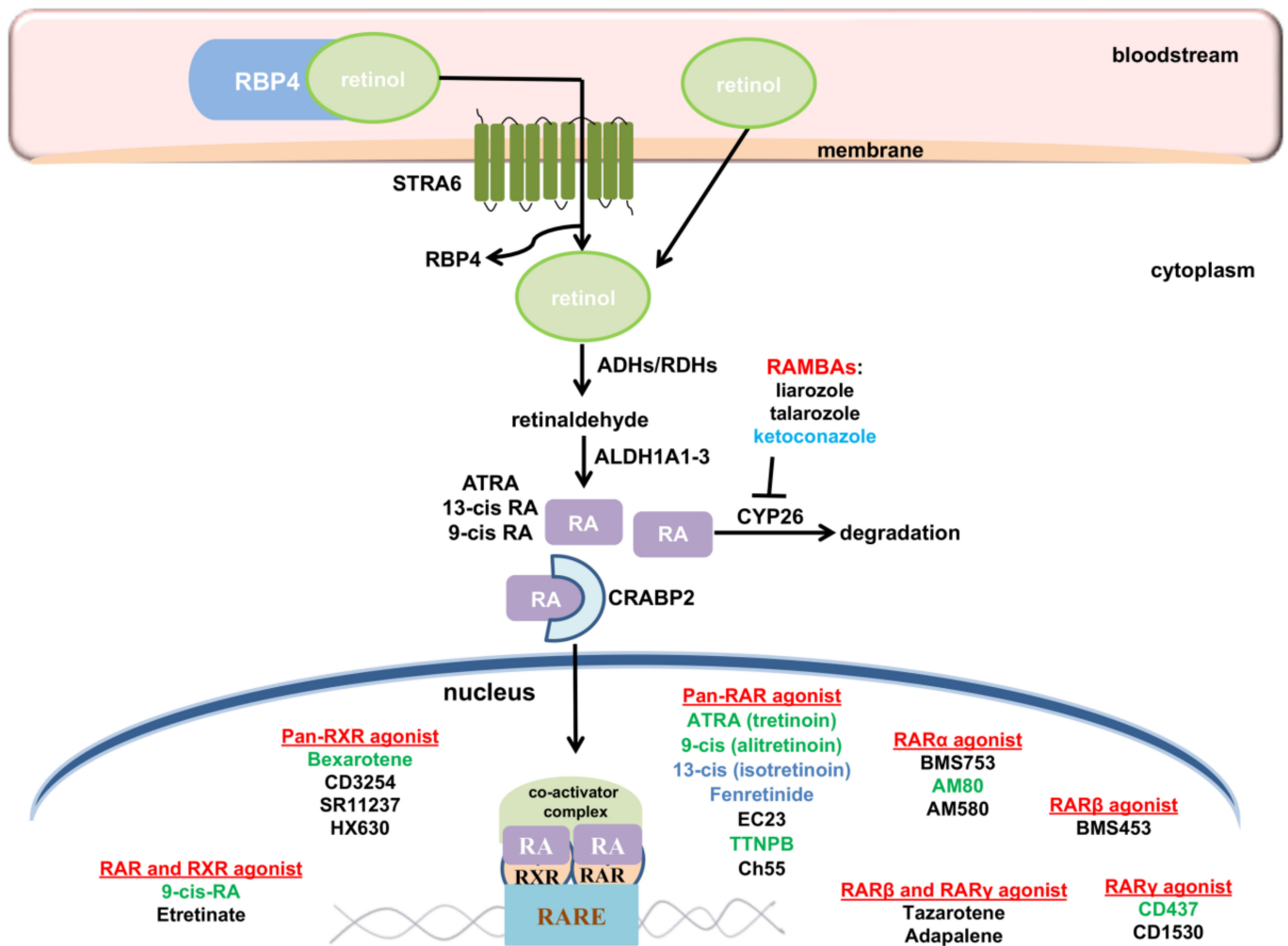


Figure 8. Overview of RA signaling pathway and RAR/RXR agonists and RAMBAs. In the bloodstream, retinol forms complex with RBP4 and enters the cells via STRA6 or by membrane diffusion. Within cells, retinol is converted to retinaldehyde by ADHs and RDHs and subsequently oxidized to RA by ALDH1A1-3. Three naturally occurring RA stereoisomers are ATRA, 13-cis RA and 9-cis RA. RA enters the nucleus via CRABP2, where it interacts with RAR/RXR heterodimer forming a complex that binds to RARE in the promoter regions of RA target genes. RA is inactivated by CYP26 oxidase (modified based on [380]). Summary of inhibitors of the CYP26A1 enzyme (RAMBAs) and RARs/RXRs agonists is made based on [383] and <https://resources.tocris.com/pdfs/literature/reviews/retinoid-receptors-review-2019-web.pdf> (accessed on 23 May 2022), respectively. RAR and RXR agonists and RAMBAs used for treatment of GBM cells in vitro or in vivo are presented in green letters, and RAR and RXR agonists and RAMBAs used in clinical trials for GBMs are presented in blue letters, while RAR and RXR agonists and RAMBAs not yet used in treatment of GBM are presented in black letters (based on results of previously reported publications included in the main text and results obtained by [385–390]).

Dysregulation of the RA signaling pathway underlies the etiology of different malignancies, such as leukemias, neuroblastoma, lung, skin, breast, ovarian, prostate, head/neck, pancreatic, liver and bladder cancers, renal cell carcinoma and GBM (reviewed in [391]). On the other hand, RA and its derivatives are used for the treatment of cancers. ATRA is a very effective and curative therapy for patients with acute promyelocytic leukemia and a potential therapeutic agent against oral squamous cell carcinoma and oral dysplasia (reviewed in [383]). Preclinical studies demonstrated the usefulness of 9-cis RA in the prevention of prostate and breast cancers and randomized trial of 13-cis RA showed promising results

in the treatment of children with high-risk neuroblastoma (reviewed in [383]). It has been reported that RA inhibits the proliferation of tumor cells, promotes their differentiation, induces apoptosis, and inhibits angiogenesis and metastasis [392].

A series of alterations in the RA signaling pathway was reported in GBMs. Methylation in the *RBP1* gene was identified in *IDH1* and *IDH2* mutant tumors. GBM patients with *RBP1*-unmethylated tumors had decreased median overall survival compared with the patients with *RBP1*-methylated GBMs [393]. Additionally, *CRABP2* was suppressed in GBM through epigenetic silencing [394]. Sanders and co-workers demonstrated increased expression of *ALDH1A2* in GBM compared to the expression detected in low-grade gliomas and upregulation of *ALDH1A2* expression upon GBM recurrence [395]. Campos and co-workers revealed that the expression of *ALDH1A1-3* was decreased in GBMs compared to expression detected in non-tumorous brain tissue [396]. Additionally, *CRABP2* expression was reduced in high-grade gliomas [394] and when comparing primary GBM tissues of short-term and long-term survivors Barbus and co-workers detected that *RBP1* and *CRABP2* expression was higher in GBMs of short-term survivors [397]. Methylation of RAR β was detected in about 70% of GBMs [398]. Literature data showed that glioma cell lines express RAR γ [399], while primary cultures of biopsy material from human GBMs expressed RAR γ and RXR α [399]. Furthermore, stem-like glioma cells, isolated from primary GBM, expressed RAR α . ATRA induced differentiation of these cells, causing antitumorigenic, anti-invasive, antimigratory, antiangiogenic, growth-inhibiting and proapoptotic effects [400]. A block in the retinoid receptor proteasomal degradation pathway and accumulation of sumoylated and high-molecular-weight forms of retinoid receptors that lack transcriptional activity were revealed in glioma stem-like cells [401].

The literature data demonstrated that retinoids might affect the malignant behavior of glioma cells. Bouterfa and co-workers treated glioma cell lines and primary cultures of GBMs with different retinoids (ATRA, 9-cis-RA, 13-cis-RA) and demonstrated that glioma cell lines are generally unresponsive to retinoids, while treatment of primary cultures of GBMs reduced the proliferation and migration of these cells [399]. It has been shown that RA increases the proliferation of GL-15 GBM cells at low concentrations and inhibits proliferation of these cells at high concentration [402]. Additionally, the proliferation of GL-15 GBM cells was inhibited by two structurally related RAR γ agonists, CD-437 and CD-2325 [402]. In vitro experiments using GBM cell lines demonstrated that ATRA might induce morphological changes, differentiation, apoptosis, change in the mode of cell migration and reduction in growth, proliferation, invasiveness and adhesion of these cells [403–406]. Additionally, ATRA increased the asymmetric cell division of GSCs isolated from the U87 GBM cell line [407], induced differentiation and decreased proliferation and invasiveness of U87 cancer stem-like cells [408], induced morphology changes, growth arrest and differentiation of GBM stem-like cells [409] and induced differentiation and apoptosis and reduced proliferation and self-renewal of neurospheres of GBM therapy-resistant cancer stem cells [410]. On the other hand, ATRA treatment of brain tumor stem cells, isolated from the fresh GBM specimen, promoted proliferation and induced differentiation of these cells [411]. Additionally, ATRA has a pro-proliferative and pro-survival effect on stem-like glioma cells mediated by RAR α and RAR γ [412]. It has been demonstrated that cis-RA treatment of glioma cells may inhibit proliferation and invasiveness and induce differentiation of these cells [399,413,414], while treatment of GSCs with 9-cis RA and 13-cis RA inhibited proliferation and induced their differentiation into neurons, astrocytes and oligodendrocytes [409,415,416]. 13-cis RA showed a significant inhibitory effect on proliferation and clonogenicity of U343 GBM cells [417]. Bexarotene, a RXR agonist, induced morphological changes and differentiation of cultured primary GBM cells and inhibited their neurospheroidal colony formation and migration [418]. Bexarotene or ATRA, alone, reduced tumor size; on the other hand, when treatment was discontinued, the tumor size started to increase [418].

There are literature data about the combined effects of retinoids and other drugs/compounds on the malignant behavior of GBM cells and GSCs. Namely, ATRA in combination with

TMZ enhanced TMZ effects on malignant behavior of GBM cells [419], in combination with interferon-gamma (IFN- γ), it induced apoptosis of GBM cell lines [404], and in combination with taxol, paclitaxel or IFN- γ , it induced differentiation, apoptosis and reduction in tumor volume of xenografts of GBM cell lines [420–422]. Combined treatment of metformin and 9-cis RA reduced the proliferation rate and increased apoptosis in C6 glioma stem-like cells [423], while 13-cis RA combined with thalidomide delayed the growth of GBM xenografts [424]. Reduced proliferation, invasion and migration of U87 cells, decreased number of colonies of these cells, increased number of apoptotic cells and reduced tumor volumes have been found upon treatment of cells with 6-OH-11-O-hydroxyfenantrene (IIF), an RXR agonist, and pioglitazone, a synthetic PPAR γ agonist [425]. Systemic administration of TMZ combined with convection-enhanced delivery (direct intracranial drug infusion technique) of polymeric micellar Am80, a synthetic agonist with high affinity to nuclear RAR, provided longer survival of rats with GBM xenografts compared to controls [390].

The therapeutic benefit of retinoids for therapy of GBM is largely contradictory. Results obtained by Pitz and co-workers demonstrated that there are no significant differences between the survival of GBM patients who were treated with TMZ and cis RA for up to 24 months after surgery and radiation therapy and GBM patients treated for 6 months with TMZ [426]. Additionally, the results of a phase II clinical trial demonstrated that a retinoid combined with TMZ did not increase progression-free survival of GBM patients [155]. Additionally, a phase II trial was conducted to evaluate the effect of concurrent treatment with TMZ and 13-cis RA in combination with conventional radiation therapy in adults with supratentorial GBM, which did not show a survival advantage compared with studies using radiation therapy with TMZ [427]. Furthermore, the phase II trial of fenretinide (4-hydroxyphenyl-retinamide) (NSC 374551), a synthetic derivative of ATRA, in adults with recurrent GBM did not demonstrate clinical efficacy [428]. On the other hand, the combination of 13-cis RA (Accutane) and celecoxib, a COX-2 inhibitor, demonstrated a modest effect on progression-free survival of patients with progressive GBM, but this combination was not more effective than 13-cis RA alone [429]. A phase II evaluation of TMZ and 13-cis RA (NABTC 98–03) revealed a 6-month progression-free survival rate of 32% for patients with GBM [430].

On ClinicalTrial.gov, six studies were found by searching with keywords “retinoid” and “GBM”. Among them, the only one active is focused on evaluating the effects of combined therapy of vorinostat, isotretinoin and TMZ in patients with GBM (NCT00555399). The results of the study NCT00112502 indicated that adding isotretinoin to dose-dense TMZ may be detrimental [155]. Furthermore, there are two on-going studies analyzing the effects of ketoconazole, an inhibitor of the CYP26A1 enzyme. The first study (NCT04869449) analyzes if ketoconazole can enter brain tumors (GBM) at a high enough amount to stop the tumor cells from dividing, while the second (NCT03796273) studies the side effects and how well ketoconazole works before surgery in treating patients with glioma that has come back.

The main limitations of pharmacological applications of RA include poor solubility in aqueous solutions, photosensitivity, rapid metabolism of RA upon intravenous administration, which reduces its efficiency, and side effects after systemic delivery (reviewed in [431]). The results obtained by using ATRA-encapsulated polymeric micelles of a chitosan graft copolymer indicated that encapsulated ATRA is more effective at inhibiting U87 cell migration than free ATRA [432]. Additionally, to stabilize ATRA, Jones and co-workers used a porous poly(1,8-octanediol-co-citrate; POC) wafer which enabled slow release of ATRA leading to differentiation, apoptosis, and inhibition of proliferation of U87 GBM cells [433]. Generally, several strategies for the delivery of RA were used, and the most common strategy used is liposomal or polymeric nanoparticles formed by polyesters, polyimines, polysaccharides and proteins (reviewed in [431]). In conclusions, the use of drug delivery systems that enhance RA solubility, prolong its presence in circulation, and decreased its toxicity might improve its efficiency in cancer treatment, including GBM (reviewed in [431]).

10. Conclusions and Future Perspectives

Common genetic alterations in GBM include the loss of the chromosome arm 10q, alterations in tumor suppressor TP53 and tumor suppressor retinoblastoma RB, amplifications of EGFR and PDGFR, and aberrations in RTK/Ras/PI3K signaling pathways, all of which are major known drivers of GBM pathology (reviewed in [11]). Other frequent mutations include alterations in NF1, PTEN, and MDM2 [38,434]. On the other hand, multiple signaling pathways dysregulated in GBM are involved in the promotion of malignant behavior of GBM cells [12]. Their altered activities in GBM are mostly due to changes in the expression rather than mutations in key pathway components. Mutations in components of signaling pathways presented in this paper are not hallmarks of GBM, although some studies linked several mutations to gliomagenesis. In particular, one study detected mutation in *APC* gene, a WNT signaling component, in GBM patient samples [112]. Further, mutations in TGF β receptor that inactivate the receptor are detected in early stages of malignant glioma tumorigenesis [435]. Additionally, studies have reported mutations of Notch pathway genes in grade II and III gliomas [436]. Unlike low-grade gliomas, Notch mutations in GBM are very scarce. Since no other driver mutations in signaling pathways have been identified so far in GBM, evidently, regulation of these pathways activity depends of other mechanisms, including epigenetic alterations. Sakthikumar and co-workers provided results of whole genome sequencing showing evidence for enrichment of non-coding constraint mutations in GBM-associated genes, as well as in more than 1776 other genes that have not been previously linked to GBM, but may have a functional impact on the disease [437]. This could offer an explanation for differences in the regulation of gene expression and, consequently, changes in signaling pathways activity. Importantly, GBMs frequently evolve and, within a single patient, could display numerous subtypes, various gene expression profiles, transcriptome patterns, and methylation statuses, all features that favor subclonal selection and direct response to therapy. There is always a risk that some important players are not identified, but with the current knowledge, it becomes obvious that the combination of inhibitors of multiple pathways and other therapies should be considered as a future direction for GBM treatment. Here, we summarized recent findings of the progress made in targeting these signaling pathways in GBM. Although numerous studies of the anti-GBM effects of modulators of various signaling pathways gave promising results in *in vitro* and *in vivo* models, only a small fraction of them reached the first phases of clinical trials. Additionally, most of the agents that entered clinical trials as monotherapy or in combination with chemo- and radiotherapy displayed poor clinical activity or lack of survival benefit for patients.

Several reasons may explain these disappointing results. One of the reasons lies in the fact that adequate patients' molecular stratifications are often lacking. It has been demonstrated that individual prognostic factors of each patient, including *MGMT* methylation status, presence of mutant epidermal growth factor variant III (EGFRvIII), the status of signaling pathways activities, baseline performance status, tumor location, and age could influence the success of the trial and final results [438]. The identification of subtype-specific alternations in genes and their expression and related signaling pathways is a crucial step in the discovery and development of new prognostic and therapeutic strategies to target GBM. For example, in search of the subtype-specific prognostic core genes, Park and co-workers showed that in the mesenchymal subtype of GBM, genes were enriched with Wnt/ β -catenin-related genes, suggesting that targeting Wnt signaling would be more effective in this subtype of GBM [439]. El-Sehemy and co-workers showed that Norrin, a Wnt ligand that binds FZD4 and activates canonical Wnt/ β -catenin signaling, in GSCs with low expression of proneural factor *ASCL1* (Achaete-scute homolog 1), exerts tumor-suppressive effects via Wnt signaling, while in GSCs with high *ASCL1* expression, Norrin acts as an oncogene by promoting Notch signaling in Wnt-independent manner [440]. These results suggest that Wnt should be considered as a therapeutic target exclusively in GBM with low expression of *ASCL1*, while in the GBM subtype with high expression of *ASCL1*, the inhibition of Notch could be a strategy of choice for therapy of GBM. Thus, stratifications

of patients based on molecular profiling of their GBMs, including the activity of signaling pathways, would enable the identification of the most relevant targets for each patient.

Several issues need to be addressed for achieving desirable results in GBM therapy, including GBM heterogeneity and plasticity, as well as TME, which contributes to the tumorigenesis and progression of GBM. Today it is accepted that due to the GBM complexity, it is not likely that a single molecular agent could provide a final therapeutic strategy, and combination therapy approaches are likely to perform better in designing novel clinical trials. Based on this, agents that simultaneously target multiple dysregulated pathways might be involved in the development of future therapeutic strategies for GBM. A number of studies have been aimed to identify or develop small-molecule compounds, natural or synthetic, that are able to target multiple signaling pathways simultaneously to combat cancer. Natural compounds with such properties include resveratrol (affects Wnt/ β -catenin, Notch and Smad-dependent TGF β signaling) [134,254,312], DATS (decreases Wnt/ β -catenin and Notch) [137,257], honokiol (downregulates Notch and PI3K/Akt/mTOR) [253,441] and garlic-derived Z-ajoene (affects Notch, Wnt and HH) [442]. In our previous work, we found that extracts from *Phlomis fruticosa* L., *Ononis spinosa* L. and *Anthriscus cerefolium* L. plants and bis-Bibenzyls from the Liverwort *Pellia endiviifolia* have anti-GBM activity in vitro [443–446], and future research of these extracts and compounds should decipher whether the mechanism underlying their antitumor effect involves targeting dysregulated signaling pathways in GBM. It is important to point out that targeting the same signaling pathway in GSCs and GBM tumor cells can affect diverse sets of target genes and, consequently, different cellular processes. Kaye and co-workers recently demonstrated that both activation and suppression of the BMP signaling pathway had a negative effect on tumor sphere growth by affecting different targets [342]. Thus, there is a constant requirement for further laboratory and clinical research to investigate the mechanisms of receptor signaling downstream pathways in GSCs and GBM tumor cells.

In recent years, 3D and 4D model systems for investigation of different aspects of GBM biology have emerged, holding great potential for the assessment of therapeutic responses and personalized drug screening (reviewed in [447]). They include 3D human brain organoids grafted with patient-derived GSCs or GSC spheres [448] and a 4D platform of GBM patient-derived organoids that self-transforms from 3D cell-culture inserts into histological cassettes [449]. Additionally, different in vitro models of the BBB have been developed (reviewed in [450]). These models can be employed to test the antitumor effect of the inhibitors/modulators of signaling pathways and their ability to cross BBB before considering their inclusion in in vivo or clinical studies. Additionally, significant progress has been made in the development of systems for drug delivery, selective disruption of the BBB using high intensity focused ultrasound, and different systems for intratumoral drug delivery in order to achieve therapeutic drug concentration at the site of the tumor (reviewed in [451]). Having in mind that signaling pathways have key roles in the regulation of cell activity, it is important to develop controlled release systems for targeting signaling pathways in tumor cells in order to avoid targeting normal cells and prevent undesirable toxicity. By controlled release systems, fluctuation of drug concentration might be decreased and side effects might be minimized (reviewed in [452]). It has been shown that hydrogels of natural and synthetic polymers enable controlled release of drugs and targeting, as well as protection of drugs from degradation and metabolism, thereby enhancing treatment efficacy and decreasing toxic effects on normal cells (reviewed in [453]). Nanotechnology enables the delivery of agents into tumor tissues, and the development of stimuli-responsive nanocarriers represents a promising strategy for the delivery of agents that target signaling pathways. Researchers have developed stimuli-responsive nanocarriers that can release drugs into tumor tissue in response to different stimuli, such as temperature, pH, and redox [454,455].

Despite successful outcomes of treatment of other aggressive cancers [456,457]), immunotherapy in GBM faced challenges due to the numerous mechanisms of resistance, including the location of the tumor within the brain and the nature of the BBB, as well as

the tumor heterogeneity and its immunosuppressive microenvironment (reviewed in [458]). Numerous immunotherapy strategies for GBM treatment have been employed, including antibodies that reeducate tumor macrophages, vaccinations that introduce tumor-specific dendritic cells (DCs), checkpoint molecule inhibition, and modified T-cells and proteins that help T-cells engage directly with tumor cells (reviewed in [459–461]). Even though these strategies applied as monotherapy had only limited benefits for patient survival, preclinical studies showed encouraging results. Strategies that might deliver the real medical benefit for GBM patients include concurrent stimulation of the immune response and inhibition of immunosuppressive components or a combination of immune checkpoint blockade (ICB) with chemotherapy, radiotherapy inducing immunogenic cell death or vaccines (reviewed in [459–461]). Currently, there are ongoing clinical trials studying combinations of multiple ICBs and combination of ICBs with radiotherapy or vaccination (reviewed in [460]).

Over the years, single-cell RNA sequencing (scRNA-seq) along with other single-cell profiling techniques have become a powerful tool for examining glioma tumors at a resolution of individual cells, providing a comprehensive insight into the glioma biology, intratumoral genetic heterogeneity, cellular lineages, cancer stem cell programs, TME composition, glioma classification, and response to therapies (reviewed in [462,463]). Unraveling the multiple layers of complexity that characterize GBM will ultimately lead to the identification of novel, more efficient targeted therapies. For example, pathway-based classification by using multiple datasets from GBM scRNA-seq and bulk tumors identified four tumor cell states and GBM subtypes, of which the mitochondrial GBM subtype exhibited significant sensitivity to inhibitors of oxidative phosphorylation, suggesting that GBM patients with this subtype could benefit from targeted metabolic therapy [57]. scRNA-seq profiling of individual GBMs by Neftel and co-workers uncovered that four different malignant cellular states, NPC-like, OPC-like, AC-like, and MES-like, are shared across the GBM subtypes, and that each GBM subtype displays an abundance of distinct cellular states [49,464]. All four GBM cellular states display a proliferation signature, and three of them are able to propagate tumors, with the AC-like state showing decreased potential for tumor initiation. GSCs that may exhibit multiple cellular states, which may also interconvert, pose a great challenge for targeted eradication of GSCs [464]. Suva and Tirosh proposed induction of an AC-like state as a potentially relevant approach in differentiation therapy of IDH-mutant and H3K27M gliomas [464].

In conclusion, although myriad agents targeting signaling pathways dysregulated in cancer have been identified, there is always a need for finding novel drugs or improving the existing drugs in terms of their efficacy and safety in anticancer therapy. Investigating novel or better predictive biomarkers, improving patient stratification, developing of computational methods to accurately predict the response of different parts of the tumor to a given therapy, and decreasing drug toxicities by designing more selective drugs and combinatory regimens that affect multiple targets and processes including proliferation, tumor angiogenesis, and invasiveness, are required to overcome the challenges of signaling pathways-targeting therapies in cancer and in GBM in particular. In the light of current knowledge, the optimal approach to target GBM and control tumor recurrence might be to combine modulators of dysregulated signaling pathways with conventional therapies and immunotherapies.

Supplementary Materials: The following supporting information can be downloaded at: <https://www.mdpi.com/article/10.3390/cells11162530/s1>, Table S1: Stratification of GBM into molecular subtypes and characteristics of subtypes.

Author Contributions: Conceptualization, D.D. and M.S. (Milena Stevanovic); literature analyses, all authors; writing—original draft preparation, D.D., M.S. (Marija Schwirtlich), I.P., M.M. (Marija Mojsin), M.M. (Milena Milivojevic), N.K.-G. and M.S. (Milena Stevanovic); writing—review and editing, D.D., M.S. (Marija Schwirtlich), I.P., M.M. (Marija Mojsin), M.M. (Milena Milivojevic), N.K.-G. and M.S. (Milena Stevanovic); designing the figures, D.D., M.S. (Marija Schwirtlich), I.P., M.M. (Marija Mojsin), M.M. (Milena Milivojevic), N.K.-G. and M.S. (Milena Stevanovic); supervision, D.D.; funding

acquisition, M.S. (Milena Stevanovic). All authors have read and agreed to the published version of the manuscript.

Funding: This research was funded by the Ministry of Education, Science and Technological Development of the Republic of Serbia (Agreement no. 451-03-68/2022-14/200042) and the Serbian Academy of Sciences and Arts (Grant number F24).

Institutional Review Board Statement: Not applicable.

Informed Consent Statement: Not applicable.

Data Availability Statement: Not applicable.

Conflicts of Interest: The authors declare no conflict of interest.

References

- Louis, D.N.; Ohgaki, H.; Wiestler, O.D.; Cavenee, W.K.; Burger, P.C.; Jouvet, A.; Scheithauer, B.W.; Kleihues, P. The 2007 WHO classification of tumours of the central nervous system. *Acta Neuropathol.* **2007**, *114*, 97–109. [CrossRef] [PubMed]
- Parker, N.R.; Khong, P.; Parkinson, J.F.; Howell, V.M.; Wheeler, H.R. Molecular heterogeneity in glioblastoma: Potential clinical implications. *Front. Oncol.* **2015**, *5*, 55. [CrossRef] [PubMed]
- Wick, W.; Platten, M. Understanding and Treating Glioblastoma. *Neurol. Clin.* **2018**, *36*, 485–499. [CrossRef] [PubMed]
- Soeda, A.; Hara, A.; Kunisada, T.; Yoshimura, S.; Iwama, T.; Park, D.M. The evidence of glioblastoma heterogeneity. *Sci. Rep.* **2015**, *5*, 7979. [CrossRef]
- Becker, A.P.; Sells, B.E.; Haque, S.J.; Chakravarti, A. Tumor Heterogeneity in Glioblastomas: From Light Microscopy to Molecular Pathology. *Cancers* **2021**, *13*, 761. [CrossRef]
- Ostrom, Q.T.; Gittleman, H.; Fulop, J.; Liu, M.; Blanda, R.; Kromer, C.; Wolinsky, Y.; Kruchko, C.; Barnholtz-Sloan, J.S. CBTRUS Statistical Report: Primary Brain and Central Nervous System Tumors Diagnosed in the United States in 2008–2012. *Neuro-Oncology* **2015**, *17* (Suppl. 4), iv1–iv62. [CrossRef]
- Stupp, R.; Mason, W.P.; van den Bent, M.J.; Weller, M.; Fisher, B.; Taphoorn, M.J.; Belanger, K.; Brandes, A.A.; Marosi, C.; Bogdahn, U.; et al. Radiotherapy plus concomitant and adjuvant temozolomide for glioblastoma. *N. Engl. J. Med.* **2005**, *352*, 987–996. [CrossRef]
- Johnson, B.E.; Mazar, T.; Hong, C.; Barnes, M.; Aihara, K.; McLean, C.Y.; Fouse, S.D.; Yamamoto, S.; Ueda, H.; Tatsuno, K.; et al. Mutational analysis reveals the origin and therapy-driven evolution of recurrent glioma. *Science* **2014**, *343*, 189–193. [CrossRef]
- Oronsky, B.; Reid, T.R.; Oronsky, A.; Sandhu, N.; Knox, S.J. A Review of Newly Diagnosed Glioblastoma. *Front. Oncol.* **2020**, *10*, 574012. [CrossRef]
- Birzu, C.; French, P.; Caccese, M.; Cerretti, G.; Idbaih, A.; Zagonel, V.; Lombardi, G. Recurrent Glioblastoma: From Molecular Landscape to New Treatment Perspectives. *Cancers* **2020**, *13*, 47. [CrossRef]
- Mao, H.; Lebrun, D.G.; Yang, J.; Zhu, V.F.; Li, M. Deregulated signaling pathways in glioblastoma multiforme: Molecular mechanisms and therapeutic targets. *Cancer Invest.* **2012**, *30*, 48–56. [CrossRef]
- Khabibov, M.; Garifullin, A.; Boumber, Y.; Khaddour, K.; Fernandez, M.; Khamitov, F.; Khalikova, L.; Kuznetsova, N.; Kit, O.; Kharin, L. Signaling pathways and therapeutic approaches in glioblastoma multiforme (Review). *Int. J. Oncol.* **2022**, *60*, 69. [CrossRef]
- Mehta, S.; Lo Cascio, C. Developmentally regulated signaling pathways in glioma invasion. *Cell. Mol. Life Sci.* **2018**, *75*, 385–402. [CrossRef]
- Lauko, A.; Lo, A.; Ahluwalia, M.S.; Lathia, J.D. Cancer cell heterogeneity & plasticity in glioblastoma and brain tumors. *Semin Cancer Biol.* **2022**, *82*, 162–175. [CrossRef]
- Ryskalin, L.; Gaglione, A.; Limanaqi, F.; Biagioni, F.; Familiari, P.; Frati, A.; Esposito, V.; Fornai, F. The Autophagy Status of Cancer Stem Cells in Glioblastoma Multiforme: From Cancer Promotion to Therapeutic Strategies. *Int. J. Mol. Sci.* **2019**, *20*, 3824. [CrossRef]
- Lathia, J.D.; Mack, S.C.; Mulkearns-Hubert, E.E.; Valentim, C.L.; Rich, J.N. Cancer stem cells in glioblastoma. *Genes Dev.* **2015**, *29*, 1203–1217. [CrossRef]
- Stevanovic, M.; Kovacevic-Grujicic, N.; Mojsin, M.; Milivojevic, M.; Drakulic, D. SOX transcription factors and glioma stem cells: Choosing between stemness and differentiation. *World J. Stem Cells* **2021**, *13*, 1417–1445. [CrossRef]
- Prager, B.C.; Bhargava, S.; Mahadev, V.; Hubert, C.G.; Rich, J.N. Glioblastoma Stem Cells: Driving Resilience through Chaos. *Trends Cancer* **2020**, *6*, 223–235. [CrossRef]
- Cheng, L.; Wu, Q.; Guryanova, O.A.; Huang, Z.; Huang, Q.; Rich, J.N.; Bao, S. Elevated invasive potential of glioblastoma stem cells. *Biochem. Biophys. Res. Commun.* **2011**, *406*, 643–648. [CrossRef]
- Chen, J.; Li, Y.; Yu, T.S.; McKay, R.M.; Burns, D.K.; Kernie, S.G.; Parada, L.F. A restricted cell population propagates glioblastoma growth after chemotherapy. *Nature* **2012**, *488*, 522–526. [CrossRef]
- Satterlee, A.B.; Dunn, D.E.; Lo, D.C.; Khagi, S.; Hingtgen, S. Tumoricidal stem cell therapy enables killing in novel hybrid models of heterogeneous glioblastoma. *Neuro-Oncology* **2019**, *21*, 1552–1564. [CrossRef]

22. Tang, X.; Zuo, C.; Fang, P.; Liu, G.; Qiu, Y.; Huang, Y.; Tang, R. Targeting Glioblastoma Stem Cells: A Review on Biomarkers, Signal Pathways and Targeted Therapy. *Front. Oncol.* **2021**, *11*, 701291. [CrossRef]
23. Nakada, M.; Kita, D.; Watanabe, T.; Hayashi, Y.; Teng, L.; Pyko, I.V.; Hamada, J. Aberrant signaling pathways in glioma. *Cancers* **2011**, *3*, 3242–3278. [CrossRef]
24. Cruz Da Silva, E.; Mercier, M.C.; Etienne-Selloum, N.; Dontenwill, M.; Choulier, L. A Systematic Review of Glioblastoma-Targeted Therapies in Phases II, III, IV Clinical Trials. *Cancers* **2021**, *13*, 1795. [CrossRef]
25. Fabro, F.; Lamfers, M.L.M.; Leenstra, S. Advancements, Challenges, and Future Directions in Tackling Glioblastoma Resistance to Small Kinase Inhibitors. *Cancers* **2022**, *14*, 600. [CrossRef]
26. Liu, H.; Qiu, W.; Sun, T.; Wang, L.; Du, C.; Hu, Y.; Liu, W.; Feng, F.; Chen, Y.; Sun, H. Therapeutic strategies of glioblastoma (GBM): The current advances in the molecular targets and bioactive small molecule compounds. *Acta Pharm. Sin. B* **2022**, *12*, 1781–1804. [CrossRef]
27. Zhang, G.L.; Wang, C.F.; Qian, C.; Ji, Y.X.; Wang, Y.Z. Role and mechanism of neural stem cells of the subventricular zone in glioblastoma. *World J. Stem Cells* **2021**, *13*, 877–893. [CrossRef]
28. Matarredona, E.R.; Pastor, A.M. Neural Stem Cells of the Subventricular Zone as the Origin of Human Glioblastoma Stem Cells. Therapeutic Implications. *Front. Oncol.* **2019**, *9*, 779. [CrossRef]
29. Couturier, C.P.; Ayyadhury, S.; Le, P.U.; Nadaf, J.; Monlong, J.; Riva, G.; Allache, R.; Baig, S.; Yan, X.; Bourgey, M.; et al. Single-cell RNA-seq reveals that glioblastoma recapitulates a normal neurodevelopmental hierarchy. *Nat. Commun.* **2020**, *11*, 3406. [CrossRef]
30. Curry, R.N.; Glasgow, S.M. The Role of Neurodevelopmental Pathways in Brain Tumors. *Front. Cell Dev. Biol.* **2021**, *9*, 659055. [CrossRef]
31. Bar, E.E.; Chaudhry, A.; Lin, A.; Fan, X.; Schreck, K.; Matsui, W.; Piccirillo, S.; Vescovi, A.L.; DiMeco, F.; Olivi, A.; et al. Cyclopamine-mediated hedgehog pathway inhibition depletes stem-like cancer cells in glioblastoma. *Stem Cells* **2007**, *25*, 2524–2533. [CrossRef] [PubMed]
32. Clement, V.; Sanchez, P.; de Tribolet, N.; Radovanovic, I.; Ruiz i Altaba, A. HEDGEHOG-GLI1 signaling regulates human glioma growth, cancer stem cell self-renewal, and tumorigenicity. *Curr. Biol.* **2007**, *17*, 165–172. [CrossRef] [PubMed]
33. Hu, Y.Y.; Zheng, M.H.; Cheng, G.; Li, L.; Liang, L.; Gao, F.; Wei, Y.N.; Fu, L.A.; Han, H. Notch signaling contributes to the maintenance of both normal neural stem cells and patient-derived glioma stem cells. *BMC Cancer* **2011**, *11*, 82. [CrossRef] [PubMed]
34. Ikushima, H.; Todo, T.; Ino, Y.; Takahashi, M.; Miyazawa, K.; Miyazono, K. Autocrine TGF-beta signaling maintains tumorigenicity of glioma-initiating cells through Sry-related HMG-box factors. *Cell Stem Cell* **2009**, *5*, 504–514. [CrossRef]
35. Piccirillo, S.G.; Reynolds, B.A.; Zanetti, N.; Lamorte, G.; Binda, E.; Broggi, G.; Brem, H.; Olivi, A.; Dimeco, F.; Vescovi, A.L. Bone morphogenetic proteins inhibit the tumorigenic potential of human brain tumour-initiating cells. *Nature* **2006**, *444*, 761–765. [CrossRef]
36. Masui, K.; Mischel, P.S.; Reifenberger, G. Molecular classification of gliomas. *Handb. Clin. Neurol.* **2016**, *134*, 97–120. [CrossRef]
37. Weller, M.; van den Bent, M.; Preusser, M.; Le Rhun, E.; Tonn, J.C.; Minniti, G.; Bendszus, M.; Balana, C.; Chinot, O.; Dirven, L.; et al. EANO guidelines on the diagnosis and treatment of diffuse gliomas of adulthood. *Nat. Rev. Clin. Oncol.* **2021**, *18*, 170–186. [CrossRef]
38. Verhaak, R.G.; Hoadley, K.A.; Purdom, E.; Wang, V.; Qi, Y.; Wilkerson, M.D.; Miller, C.R.; Ding, L.; Golub, T.; Mesirov, J.P.; et al. Integrated genomic analysis identifies clinically relevant subtypes of glioblastoma characterized by abnormalities in PDGFRA, IDH1, EGFR, and NF1. *Cancer Cell* **2010**, *17*, 98–110. [CrossRef]
39. Agnihotri, S.; Aldape, K.D.; Zadeh, G. Isocitrate dehydrogenase status and molecular subclasses of glioma and glioblastoma. *Neurosurg. Focus* **2014**, *37*, E13. [CrossRef]
40. Wang, Q.; Hu, B.; Hu, X.; Kim, H.; Squatrito, M.; Scarpacci, L.; de Carvalho, A.C.; Lyu, S.; Li, P.; Li, Y.; et al. Tumor Evolution of Glioma-Intrinsic Gene Expression Subtypes Associates with Immunological Changes in the Microenvironment. *Cancer Cell* **2017**, *32*, 42–56.e46. [CrossRef]
41. Gill, B.J.; Pisapia, D.J.; Malone, H.R.; Goldstein, H.; Lei, L.; Sonabend, A.; Yun, J.; Samanamud, J.; Sims, J.S.; Banu, M.; et al. MRI-localized biopsies reveal subtype-specific differences in molecular and cellular composition at the margins of glioblastoma. *Proc. Natl. Acad. Sci. USA* **2014**, *111*, 12550–12555. [CrossRef]
42. Sturm, D.; Witt, H.; Hovestadt, V.; Khuong-Quang, D.A.; Jones, D.T.; Konermann, C.; Pfaff, E.; Tonjes, M.; Sill, M.; Bender, S.; et al. Hotspot mutations in H3F3A and IDH1 define distinct epigenetic and biological subgroups of glioblastoma. *Cancer Cell* **2012**, *22*, 425–437. [CrossRef]
43. Bhat, K.P.L.; Balasubramanian, V.; Vaillant, B.; Ezhilarasan, R.; Hummelink, K.; Hollingsworth, F.; Wani, K.; Heathcock, L.; James, J.D.; Goodman, L.D.; et al. Mesenchymal differentiation mediated by NF-kappaB promotes radiation resistance in glioblastoma. *Cancer Cell* **2013**, *24*, 331–346. [CrossRef]
44. Huse, J.T.; Phillips, H.S.; Brennan, C.W. Molecular subclassification of diffuse gliomas: Seeing order in the chaos. *Glia* **2011**, *59*, 1190–1199. [CrossRef]
45. Phillips, H.S.; Kharbanda, S.; Chen, R.; Forrest, W.F.; Soriano, R.H.; Wu, T.D.; Misra, A.; Nigro, J.M.; Colman, H.; Soroceanu, L.; et al. Molecular subclasses of high-grade glioma predict prognosis, delineate a pattern of disease progression, and resemble stages in neurogenesis. *Cancer Cell* **2006**, *9*, 157–173. [CrossRef]
46. Zheng, S.; Chheda, M.G.; Verhaak, R.G. Studying a complex tumor: Potential and pitfalls. *Cancer J.* **2012**, *18*, 107–114. [CrossRef]

47. Sottoriva, A.; Spiteri, I.; Piccirillo, S.G.; Touloumis, A.; Collins, V.P.; Marioni, J.C.; Curtis, C.; Watts, C.; Tavare, S. Intratumor heterogeneity in human glioblastoma reflects cancer evolutionary dynamics. *Proc. Natl. Acad. Sci. USA* **2013**, *110*, 4009–4014. [CrossRef]
48. Ensenyat-Mendez, M.; Iniguez-Munoz, S.; Sese, B.; Marzese, D.M. iGlioSub: An integrative transcriptomic and epigenomic classifier for glioblastoma molecular subtypes. *BioData Min.* **2021**, *14*, 42. [CrossRef]
49. Neftel, C.; Laffy, J.; Filbin, M.G.; Hara, T.; Shore, M.E.; Rahme, G.J.; Richman, A.R.; Silverbush, D.; Shaw, M.L.; Hebert, C.M.; et al. An Integrative Model of Cellular States, Plasticity, and Genetics for Glioblastoma. *Cell* **2019**, *178*, 835–849.e821. [CrossRef]
50. Ma, H.; Zhao, C.; Zhao, Z.; Hu, L.; Ye, F.; Wang, H.; Fang, Z.; Wu, Y.; Chen, X. Specific glioblastoma multiforme prognostic-subtype distinctions based on DNA methylation patterns. *Cancer Gene* **2020**, *27*, 702–714. [CrossRef]
51. Brennan, C.W.; Verhaak, R.G.; McKenna, A.; Campos, B.; Nounshmehr, H.; Salama, S.R.; Zheng, S.; Chakravarty, D.; Sanborn, J.Z.; Berman, S.H.; et al. The somatic genomic landscape of glioblastoma. *Cell* **2013**, *155*, 462–477. [CrossRef]
52. Capper, D.; Stichel, D.; Sahm, F.; Jones, D.T.W.; Schrimpf, D.; Sill, M.; Schmid, S.; Hovestadt, V.; Reuss, D.E.; Koelsche, C.; et al. Practical implementation of DNA methylation and copy-number-based CNS tumor diagnostics: The Heidelberg experience. *Acta Neuropathol.* **2018**, *136*, 181–210. [CrossRef]
53. Wang, L.B.; Karpova, A.; Gritsenko, M.A.; Kyle, J.E.; Cao, S.; Li, Y.; Rykunov, D.; Colaprico, A.; Rothstein, J.H.; Hong, R.; et al. Proteogenomic and metabolomic characterization of human glioblastoma. *Cancer Cell* **2021**, *39*, 509–528.e520. [CrossRef]
54. Wang, Z.; Sun, D.; Chen, Y.J.; Xie, X.; Shi, Y.; Tabar, V.; Brennan, C.W.; Bale, T.A.; Jayewickreme, C.D.; Laks, D.R.; et al. Cell Lineage-Based Stratification for Glioblastoma. *Cancer Cell* **2020**, *38*, 366–379. [CrossRef]
55. Hubert, C.G.; Lathia, J.D. Seeing the GBM diversity spectrum. *Nat. Cancer* **2021**, *2*, 135–137. [CrossRef]
56. Richards, L.M.; Whitley, O.K.N.; MacLeod, G.; Cavalli, F.M.G.; Coutinho, F.J.; Jaramillo, J.E.; Svergun, N.; Riverin, M.; Croucher, D.C.; Kushida, M.; et al. Gradient of Developmental and Injury Response transcriptional states defines functional vulnerabilities underpinning glioblastoma heterogeneity. *Nat. Cancer* **2021**, *2*, 157–173. [CrossRef]
57. Garofano, L.; Migliozzi, S.; Oh, Y.T.; D’Angelo, F.; Najac, R.D.; Ko, A.; Frangaj, B.; Caruso, F.P.; Yu, K.; Yuan, J.; et al. Pathway-based classification of glioblastoma uncovers a mitochondrial subtype with therapeutic vulnerabilities. *Nat. Cancer* **2021**, *2*, 141–156. [CrossRef]
58. Yu, W.; Ma, Y.; Hou, W.; Wang, F.; Cheng, W.; Qiu, F.; Wu, P.; Zhang, G. Identification of Immune-Related lncRNA Prognostic Signature and Molecular Subtypes for Glioblastoma. *Front. Immunol.* **2021**, *12*, 706936. [CrossRef]
59. Motomura, K.; Natsume, A.; Watanabe, R.; Ito, I.; Kato, Y.; Momota, H.; Nishikawa, R.; Mishima, K.; Nakasu, Y.; Abe, T.; et al. Immunohistochemical analysis-based proteomic subclassification of newly diagnosed glioblastomas. *Cancer Sci.* **2012**, *103*, 1871–1879. [CrossRef]
60. Hu, B.; Ruan, Y.; Wei, F.; Qin, G.; Mo, X.; Wang, X.; Zou, D. Identification of three glioblastoma subtypes and a six-gene prognostic risk index based on the expression of growth factors and cytokines. *Am. J. Transl. Res.* **2020**, *12*, 4669–4682.
61. Park, J.; Shim, J.K.; Yoon, S.J.; Kim, S.H.; Chang, J.H.; Kang, S.G. Transcriptome profiling-based identification of prognostic subtypes and multi-omics signatures of glioblastoma. *Sci. Rep.* **2019**, *9*, 10555. [CrossRef] [PubMed]
62. Mao, P.; Joshi, K.; Li, J.; Kim, S.H.; Li, P.; Santana-Santos, L.; Luthra, S.; Chandran, U.R.; Benos, P.V.; Smith, L.; et al. Mesenchymal glioma stem cells are maintained by activated glycolytic metabolism involving aldehyde dehydrogenase 1A3. *Proc. Natl. Acad. Sci. USA* **2013**, *110*, 8644–8649. [CrossRef] [PubMed]
63. Piao, Y.; Liang, J.; Holmes, L.; Henry, V.; Sulman, E.; de Groot, J.F. Acquired resistance to anti-VEGF therapy in glioblastoma is associated with a mesenchymal transition. *Clin. Cancer Res.* **2013**, *19*, 4392–4403. [CrossRef] [PubMed]
64. Singer, E.; Judkins, J.; Salomonis, N.; Matlaf, L.; Soteropoulos, P.; McAllister, S.; Soroceanu, L. Reactive oxygen species-mediated therapeutic response and resistance in glioblastoma. *Cell Death Dis.* **2015**, *6*, e1601. [CrossRef]
65. Yin, J.; Oh, Y.T.; Kim, J.Y.; Kim, S.S.; Choi, E.; Kim, T.H.; Hong, J.H.; Chang, N.; Cho, H.J.; Sa, J.K.; et al. Transglutaminase 2 Inhibition Reverses Mesenchymal Transdifferentiation of Glioma Stem Cells by Regulating C/EBPbeta Signaling. *Cancer Res.* **2017**, *77*, 4973–4984. [CrossRef]
66. Narayanan, A.; Gagliardi, F.; Gallotti, A.L.; Mazzoleni, S.; Cominelli, M.; Fagnocchi, L.; Pala, M.; Piras, I.S.; Zordan, P.; Moretta, N.; et al. The proneural gene ASCL1 governs the transcriptional subgroup affiliation in glioblastoma stem cells by directly repressing the mesenchymal gene NDRG1. *Cell Death Differ.* **2019**, *26*, 1813–1831. [CrossRef]
67. Bhat, K.P.; Salazar, K.L.; Balasubramanian, V.; Wani, K.; Heathcock, L.; Hollingsworth, F.; James, J.D.; Gumin, J.; Diefes, K.L.; Kim, S.H.; et al. The transcriptional coactivator TAZ regulates mesenchymal differentiation in malignant glioma. *Genes Dev.* **2011**, *25*, 2594–2609. [CrossRef]
68. Beachy, P.A.; Karhadkar, S.S.; Berman, D.M. Tissue repair and stem cell renewal in carcinogenesis. *Nature* **2004**, *432*, 324–331. [CrossRef]
69. Huangfu, D.; Anderson, K.V. Signaling from Smo to Ci/Gli: Conservation and divergence of Hedgehog pathways from Drosophila to vertebrates. *Development* **2006**, *133*, 3–14. [CrossRef]
70. Ingham, P.W.; McMahon, A.P. Hedgehog signaling in animal development: Paradigms and principles. *Genes Dev.* **2001**, *15*, 3059–3087. [CrossRef]
71. Ericson, J.; Morton, S.; Kawakami, A.; Roelink, H.; Jessell, T.M. Two critical periods of Sonic Hedgehog signaling required for the specification of motor neuron identity. *Cell* **1996**, *87*, 661–673. [CrossRef]
72. Ruiz i Altaba, A. Gli proteins and Hedgehog signaling: Development and cancer. *Trends Genet.* **1999**, *15*, 418–425. [CrossRef]

73. Wechsler-Reya, R.J.; Scott, M.P. Control of neuronal precursor proliferation in the cerebellum by Sonic Hedgehog. *Neuron* **1999**, *22*, 103–114. [CrossRef]
74. Stone, D.M.; Hynes, M.; Armanini, M.; Swanson, T.A.; Gu, Q.; Johnson, R.L.; Scott, M.P.; Pennica, D.; Goddard, A.; Phillips, H.; et al. The tumour-suppressor gene patched encodes a candidate receptor for Sonic hedgehog. *Nature* **1996**, *384*, 129–134. [CrossRef]
75. Hooper, J.E.; Scott, M.P. Communicating with Hedgehogs. *Nat. Rev. Mol. Cell Biol.* **2005**, *6*, 306–317. [CrossRef]
76. Villavicencio, E.H.; Walterhouse, D.O.; Iannaccone, P.M. The sonic hedgehog-patched-gli pathway in human development and disease. *Am. J. Hum. Genet.* **2000**, *67*, 1047–1054. [CrossRef]
77. Carballo, G.B.; Honorato, J.R.; de Lopes, G.P.F.; Spohr, T. A highlight on Sonic hedgehog pathway. *Cell Commun. Signal.* **2018**, *16*, 11. [CrossRef]
78. Gupta, S.; Takebe, N.; Lorusso, P. Targeting the Hedgehog pathway in cancer. *Adv. Med. Oncol.* **2010**, *2*, 237–250. [CrossRef]
79. Chandra, V.; Das, T.; Gulati, P.; Biswas, N.K.; Rote, S.; Chatterjee, U.; Ghosh, S.N.; Deb, S.; Saha, S.K.; Chowdhury, A.K.; et al. Hedgehog signaling pathway is active in GBM with GLI1 mRNA expression showing a single continuous distribution rather than discrete high/low clusters. *PLoS ONE* **2015**, *10*, e0116390. [CrossRef]
80. Yan, G.N.; Yang, L.; Lv, Y.F.; Shi, Y.; Shen, L.L.; Yao, X.H.; Guo, Q.N.; Zhang, P.; Cui, Y.H.; Zhang, X.; et al. Endothelial cells promote stem-like phenotype of glioma cells through activating the Hedgehog pathway. *J. Pathol.* **2014**, *234*, 11–22. [CrossRef]
81. Hung, H.C.; Liu, C.C.; Chuang, J.Y.; Su, C.L.; Gean, P.W. Inhibition of Sonic Hedgehog Signaling Suppresses Glioma Stem-Like Cells Likely Through Inducing Autophagic Cell Death. *Front. Oncol.* **2020**, *10*, 1233. [CrossRef]
82. Lee, S.T.; Welch, K.D.; Panter, K.E.; Gardner, D.R.; Garrossian, M.; Chang, C.W. Cyclopamine: From cyclops lambs to cancer treatment. *J. Agric. Food Chem.* **2014**, *62*, 7355–7362. [CrossRef]
83. Carballo, G.B.; Matias, D.; Ribeiro, J.H.; Pessoa, L.S.; Arrais-Neto, A.M.; Spohr, T. Cyclopamine sensitizes glioblastoma cells to temozolomide treatment through Sonic hedgehog pathway. *Life Sci.* **2020**, *257*, 118027. [CrossRef]
84. Xie, H.; Paradise, B.D.; Ma, W.W.; Fernandez-Zapico, M.E. Recent Advances in the Clinical Targeting of Hedgehog/GLI Signaling in Cancer. *Cells* **2019**, *8*, 394. [CrossRef]
85. Bureta, C.; Saitoh, Y.; Tokumoto, H.; Sasaki, H.; Maeda, S.; Nagano, S.; Komiya, S.; Taniguchi, N.; Setoguchi, T. Synergistic effect of arsenic trioxide, vismodegib and temozolomide on glioblastoma. *Oncol. Rep.* **2019**, *41*, 3404–3412. [CrossRef]
86. Rudin, C.M.; Hann, C.L.; Laterra, J.; Yauch, R.L.; Callahan, C.A.; Fu, L.; Holcomb, T.; Stinson, J.; Gould, S.E.; Coleman, B.; et al. Treatment of medulloblastoma with hedgehog pathway inhibitor GDC-0449. *N. Engl. J. Med.* **2009**, *361*, 1173–1178. [CrossRef]
87. Sloan, A.E.; Nock, C.J.; Kerstetter, A.; Supko, J.; Ye, X.; Barnholtz-Sloan, J.S.; Miller, R.; Rich, J.; Takebe, N.; Prados, M.; et al. Targeting glioma stem cells (GSC): A biomarker and phase ii study of gdc-0449 in patients with recurrent glioblastoma multiforme (GBM). *Neuro-Oncology* **2012**, *14*, vi101–vi105. [CrossRef]
88. Kieran, M.W.; Chisholm, J.; Casanova, M.; Brandes, A.A.; Aerts, I.; Bouffet, E.; Bailey, S.; Leary, S.; MacDonald, T.J.; Mechinaud, F.; et al. Phase I study of oral sonidegib (LDE225) in pediatric brain and solid tumors and a phase II study in children and adults with relapsed medulloblastoma. *Neuro-Oncology* **2017**, *19*, 1542–1552. [CrossRef]
89. Thomas, X.; Heiblig, M. An evaluation of glasdegib for the treatment of acute myelogenous leukemia. *Expert Opin. Pharm.* **2020**, *21*, 523–530. [CrossRef] [PubMed]
90. Aftab, B.T.; Dobromilskaya, I.; Liu, J.O.; Rudin, C.M. Itraconazole inhibits angiogenesis and tumor growth in non-small cell lung cancer. *Cancer Res.* **2011**, *71*, 6764–6772. [CrossRef]
91. Antonarakis, E.S.; Heath, E.L.; Smith, D.C.; Rathkopf, D.; Blackford, A.L.; Danila, D.C.; King, S.; Frost, A.; Ajiboye, A.S.; Zhao, M.; et al. Repurposing itraconazole as a treatment for advanced prostate cancer: A noncomparative randomized phase II trial in men with metastatic castration-resistant prostate cancer. *Oncologist* **2013**, *18*, 163–173. [CrossRef] [PubMed]
92. Ip, K.H.; McKerrow, K. Itraconazole in the treatment of basal cell carcinoma: A case-based review of the literature. *Australas J. Derm.* **2021**, *62*, 394–397. [CrossRef] [PubMed]
93. Rudin, C.M.; Brahmer, J.R.; Juergens, R.A.; Hann, C.L.; Ettinger, D.S.; Sebree, R.; Smith, R.; Aftab, B.T.; Huang, P.; Liu, J.O. Phase 2 study of pemetrexed and itraconazole as second-line therapy for metastatic nonsquamous non-small-cell lung cancer. *J. Thorac. Oncol.* **2013**, *8*, 619–623. [CrossRef]
94. Beauchamp, E.M.; Ringer, L.; Bulut, G.; Sajwan, K.P.; Hall, M.D.; Lee, Y.C.; Peaceman, D.; Ozdemirli, M.; Rodriguez, O.; Macdonald, T.J.; et al. Arsenic trioxide inhibits human cancer cell growth and tumor development in mice by blocking Hedgehog/GLI pathway. *J. Clin. Investig.* **2011**, *121*, 148–160. [CrossRef]
95. Kumthekar, P.; Grimm, S.; Chandler, J.; Mehta, M.; Marymont, M.; Levy, R.; Muro, K.; Helenowski, I.; McCarthy, K.; Fountas, L.; et al. A phase II trial of arsenic trioxide and temozolomide in combination with radiation therapy for patients with malignant gliomas. *J. Neurooncol.* **2017**, *133*, 589–594. [CrossRef]
96. Shen, H.; He, D.; Wang, S.; Ding, P.; Wang, J.; Ju, J. Preparation, characterization, and pharmacokinetics study of a novel genistein-loaded mixed micelles system. *Drug Dev. Ind. Pharm.* **2018**, *44*, 1536–1542. [CrossRef]
97. Honorato, J.R.; Hauser-Davis, R.A.; Saggiaro, E.M.; Correia, F.V.; Sales-Junior, S.F.; Soares, L.O.S.; Lima, L.D.R.; Moura-Neto, V.; Lopes, G.P.F.; Spohr, T. Role of Sonic hedgehog signaling in cell cycle, oxidative stress, and autophagy of temozolomide resistant glioblastoma. *J. Cell Physiol.* **2020**, *235*, 3798–3814. [CrossRef]
98. Li, J.; Cai, J.; Zhao, S.; Yao, K.; Sun, Y.; Li, Y.; Chen, L.; Li, R.; Zhai, X.; Zhang, J.; et al. GANT61, a GLI inhibitor, sensitizes glioma cells to the temozolomide treatment. *J. Exp. Clin. Cancer Res.* **2016**, *35*, 184. [CrossRef]

99. Krishnamurthy, N.; Kurzrock, R. Targeting the Wnt/beta-catenin pathway in cancer: Update on effectors and inhibitors. *Cancer Treat. Rev.* **2018**, *62*, 50–60. [CrossRef]
100. Nusse, R.; Clevers, H. Wnt/beta-Catenin Signaling, Disease, and Emerging Therapeutic Modalities. *Cell* **2017**, *169*, 985–999. [CrossRef]
101. Croce, J.C.; McClay, D.R. Evolution of the Wnt pathways. *Methods Mol. Biol.* **2008**, *469*, 3–18. [CrossRef]
102. Gordon, M.D.; Nusse, R. Wnt signaling: Multiple pathways, multiple receptors, and multiple transcription factors. *J. Biol. Chem.* **2006**, *281*, 22429–22433. [CrossRef]
103. Logan, C.Y.; Nusse, R. The Wnt signaling pathway in development and disease. *Annu. Rev. Cell Dev. Biol.* **2004**, *20*, 781–810. [CrossRef]
104. Bilic, J.; Huang, Y.L.; Davidson, G.; Zimmermann, T.; Cruciat, C.M.; Bienz, M.; Niehrs, C. Wnt induces LRP6 signalosomes and promotes dishevelled-dependent LRP6 phosphorylation. *Science* **2007**, *316*, 1619–1622. [CrossRef]
105. He, X.; Semenov, M.; Tamai, K.; Zeng, X. LDL receptor-related proteins 5 and 6 in Wnt/beta-catenin signaling: Arrows point the way. *Development* **2004**, *131*, 1663–1677. [CrossRef] [PubMed]
106. MacDonald, B.T.; Tamai, K.; He, X. Wnt/beta-catenin signaling: Components, mechanisms, and diseases. *Dev. Cell* **2009**, *17*, 9–26. [CrossRef]
107. Cheng, X.; Xu, X.; Chen, D.; Zhao, F.; Wang, W. Therapeutic potential of targeting the Wnt/beta-catenin signaling pathway in colorectal cancer. *Biomed. Pharm.* **2019**, *110*, 473–481. [CrossRef]
108. Zhang, X.; Wang, L.; Qu, Y. Targeting the beta-catenin signaling for cancer therapy. *Pharm. Res.* **2020**, *160*, 104794. [CrossRef]
109. Latour, M.; Her, N.G.; Kesari, S.; Nurmemmedov, E. WNT Signaling as a Therapeutic Target for Glioblastoma. *Int. J. Mol. Sci.* **2021**, *22*, 8428. [CrossRef]
110. Patel, A.P.; Tirosch, I.; Trombetta, J.J.; Shalek, A.K.; Gillespie, S.M.; Wakimoto, H.; Cahill, D.P.; Nahed, B.V.; Curry, W.T.; Martuza, R.L.; et al. Single-cell RNA-seq highlights intratumoral heterogeneity in primary glioblastoma. *Science* **2014**, *344*, 1396–1401. [CrossRef]
111. Pulvirenti, T.; Van Der Heijden, M.; Droms, L.A.; Huse, J.T.; Tabar, V.; Hall, A. Dishevelled 2 signaling promotes self-renewal and tumorigenicity in human gliomas. *Cancer Res.* **2011**, *71*, 7280–7290. [CrossRef]
112. Tang, C.; Guo, J.; Chen, H.; Yao, C.J.; Zhuang, D.X.; Wang, Y.; Tang, W.J.; Ren, G.; Yao, Y.; Wu, J.S.; et al. Gene mutation profiling of primary glioblastoma through multiple tumor biopsy guided by 1H-magnetic resonance spectroscopy. *Int. J. Clin. Exp. Pathol.* **2015**, *8*, 5327–5335. [PubMed]
113. Lorzadeh, S.; Kohan, L.; Ghavami, S.; Azarpira, N. Autophagy and the Wnt signaling pathway: A focus on Wnt/beta-catenin signaling. *Biochim. Biophys. Acta Mol. Cell Res.* **2021**, *1868*, 118926. [CrossRef] [PubMed]
114. Morris, L.G.; Kaufman, A.M.; Gong, Y.; Ramaswami, D.; Walsh, L.A.; Turcan, S.; Eng, S.; Kannan, K.; Zou, Y.; Peng, L.; et al. Recurrent somatic mutation of FAT1 in multiple human cancers leads to aberrant Wnt activation. *Nat. Genet.* **2013**, *45*, 253–261. [CrossRef] [PubMed]
115. Sareddy, G.R.; Pratap, U.P.; Viswanadhappalli, S.; Venkata, P.P.; Nair, B.C.; Krishnan, S.R.; Zheng, S.; Gilbert, A.R.; Brenner, A.J.; Brann, D.W.; et al. PELP1 promotes glioblastoma progression by enhancing Wnt/beta-catenin signaling. *Neurooncol. Adv.* **2019**, *1*, vdz042. [CrossRef]
116. Shaji, S.K.; Sunilkumar, D.; Mahalakshmi, N.V.; Kumar, G.B.; Nair, B.G. Analysis of microarray data for identification of key microRNA signatures in glioblastoma multiforme. *Oncol. Lett.* **2019**, *18*, 1938–1948. [CrossRef]
117. Vecera, M.; Sana, J.; Lipina, R.; Smrcka, M.; Slaby, O. Long Non-Coding RNAs in Gliomas: From Molecular Pathology to Diagnostic Biomarkers and Therapeutic Targets. *Int. J. Mol. Sci.* **2018**, *19*, 2754. [CrossRef]
118. Wang, Y.N.; Chen, W.Q.; Shi, Y.X.; Yan, C.R.; Kong, Z.R.; Wang, Y.K.; Wang, Y.; Ma, W.B. Imposing Phase II and Phase III Clinical Trials of Targeted Drugs for Glioblastoma: Current Status and Progress. *Front. Oncol.* **2021**, *11*, 3611. [CrossRef]
119. He, L.; Zhou, H.; Zeng, Z.; Yao, H.; Jiang, W.; Qu, H. Wnt/beta-catenin signaling cascade: A promising target for glioma therapy. *J. Cell Physiol.* **2019**, *234*, 2217–2228. [CrossRef]
120. Zhang, Y.; Wang, X. Targeting the Wnt/beta-catenin signaling pathway in cancer. *J. Hematol. Oncol.* **2020**, *13*, 165. [CrossRef]
121. Allen, J.E.; Krigsfeld, G.; Mayes, P.A.; Patel, L.; Dicker, D.T.; Patel, A.S.; Dolloff, N.G.; Messaris, E.; Scata, K.A.; Wang, W.; et al. Dual inactivation of Akt and ERK by TIC10 signals Foxo3a nuclear translocation, TRAIL gene induction, and potent antitumor effects. *Sci. Transl. Med.* **2013**, *5*, 171ra117. [CrossRef]
122. De Robertis, A.; Valensin, S.; Rossi, M.; Tunici, P.; Verani, M.; De Rosa, A.; Giordano, C.; Varrone, M.; Nencini, A.; Pratelli, C.; et al. Identification and characterization of a small-molecule inhibitor of Wnt signaling in glioblastoma cells. *Mol. Cancer Ther.* **2013**, *12*, 1180–1189. [CrossRef]
123. Gao, L.; Chen, B.; Li, J.; Yang, F.; Cen, X.; Liao, Z.; Long, X. Wnt/beta-catenin signaling pathway inhibits the proliferation and apoptosis of U87 glioma cells via different mechanisms. *PLoS ONE* **2017**, *12*, e0181346. [CrossRef]
124. Kierulf-Vieira, K.S.; Sandberg, C.J.; Waaler, J.; Lund, K.; Skaga, E.; Saberniak, B.M.; Panagopoulos, I.; Brandal, P.; Krauss, S.; Langmoen, I.A.; et al. A Small-Molecule Tankyrase Inhibitor Reduces Glioma Stem Cell Proliferation and Sphere Formation. *Cancers* **2020**, *12*, 1630. [CrossRef]
125. Kim, Y.; Kim, K.H.; Lee, J.; Lee, Y.A.; Kim, M.; Lee, S.J.; Park, K.; Yang, H.; Jin, J.; Joo, K.M.; et al. Wnt activation is implicated in glioblastoma radioresistance. *Lab. Investig.* **2012**, *92*, 466–473. [CrossRef]

126. Korur, S.; Huber, R.M.; Sivasankaran, B.; Petrich, M.; Morin, P., Jr.; Hemmings, B.A.; Merlo, A.; Lino, M.M. GSK3beta regulates differentiation and growth arrest in glioblastoma. *PLoS ONE* **2009**, *4*, e7443. [CrossRef]
127. Prabhu, V.V.; Lulla, A.R.; Madhukar, N.S.; Ralff, M.D.; Zhao, D.; Kline, C.L.B.; Van den Heuvel, A.P.J.; Lev, A.; Garnett, M.J.; McDermott, U.; et al. Cancer stem cell-related gene expression as a potential biomarker of response for first-in-class imipridone ONC201 in solid tumors. *PLoS ONE* **2017**, *12*, e0180541. [CrossRef]
128. Suwala, A.K.; Koch, K.; Rios, D.H.; Aretz, P.; Uhlmann, C.; Ogorek, I.; Felsberg, J.; Reifenberger, G.; Kohrer, K.; Deenen, R.; et al. Inhibition of Wnt/beta-catenin signaling downregulates expression of aldehyde dehydrogenase isoform 3A1 (ALDH3A1) to reduce resistance against temozolomide in glioblastoma in vitro. *Oncotarget* **2018**, *9*, 22703–22716. [CrossRef]
129. Varghese, R.T.; Young, S.; Pham, L.; Liang, Y.; Pridham, K.J.; Guo, S.; Murphy, S.; Kelly, D.F.; Sheng, Z. Casein Kinase 1 Epsilon Regulates Glioblastoma Cell Survival. *Sci. Rep.* **2018**, *8*, 13621. [CrossRef]
130. Yu, W.K.; Xu, Z.Y.; Yuan, L.; Mo, S.; Xu, B.; Cheng, X.D.; Qin, J.J. Targeting beta-Catenin Signaling by Natural Products for Cancer Prevention and Therapy. *Front. Pharm.* **2020**, *11*, 984. [CrossRef]
131. Zhang, F.Y.; Hu, Y.; Que, Z.Y.; Wang, P.; Liu, Y.H.; Wang, Z.H.; Xue, Y.X. Shikonin Inhibits the Migration and Invasion of Human Glioblastoma Cells by Targeting Phosphorylated beta-Catenin and Phosphorylated PI3K/Akt: A Potential Mechanism for the Anti-Glioma Efficacy of a Traditional Chinese Herbal Medicine. *Int. J. Mol. Sci.* **2015**, *16*, 23823–23848. [CrossRef]
132. Miao, J.; Jiang, Y.; Wang, D.; Zhou, J.; Fan, C.; Jiao, F.; Liu, B.; Zhang, J.; Wang, Y.; Zhang, Q. Trichosanthin suppresses the proliferation of glioma cells by inhibiting LGR5 expression and the Wnt/beta-catenin signaling pathway. *Oncol. Rep.* **2015**, *34*, 2845–2852. [CrossRef]
133. Mora, M.C.; Bassa, L.M.; Wong, K.E.; Tirabassi, M.V.; Arenas, R.B.; Schneider, S.S. Rhodiola crenulata inhibits Wnt/beta-catenin signaling in glioblastoma. *J. Surg. Res.* **2015**, *197*, 247–255. [CrossRef]
134. Cilibrasi, C.; Riva, G.; Romano, G.; Cadamuro, M.; Bazzoni, R.; Butta, V.; Paoletta, L.; Dalpra, L.; Strazzabosco, M.; Lavitrano, M.; et al. Resveratrol Impairs Glioma Stem Cells Proliferation and Motility by Modulating the Wnt Signaling Pathway. *PLoS ONE* **2017**, *12*, e0169854. [CrossRef]
135. Tao, W.; Chu, C.; Zhou, W.; Huang, Z.; Zhai, K.; Fang, X.; Huang, Q.; Zhang, A.; Wang, X.; Yu, X.; et al. Dual Role of WISP1 in maintaining glioma stem cells and tumor-supportive macrophages in glioblastoma. *Nat. Commun.* **2020**, *11*, 3015. [CrossRef]
136. Williams, S.P.; Nowicki, M.O.; Liu, F.; Press, R.; Godlewski, J.; Abdel-Rasoul, M.; Kaur, B.; Fernandez, S.A.; Chiocca, E.A.; Lawler, S.E. Indirubins decrease glioma invasion by blocking migratory phenotypes in both the tumor and stromal endothelial cell compartments. *Cancer Res.* **2011**, *71*, 5374–5380. [CrossRef] [PubMed]
137. Tao, Q.; Wu, C.; Xu, R.; Niu, L.; Qin, J.; Liu, N.; Zhang, P.; Wang, C. Diallyl trisulfide inhibits proliferation, invasion and angiogenesis of glioma cells by inactivating Wnt/beta-catenin signaling. *Cell Tissue Res.* **2017**, *370*, 379–390. [CrossRef] [PubMed]
138. Lan, F.; Pan, Q.; Yu, H.; Yue, X. Sulforaphane enhances temozolomide-induced apoptosis because of down-regulation of miR-21 via Wnt/beta-catenin signaling in glioblastoma. *J. Neurochem.* **2015**, *134*, 811–818. [CrossRef] [PubMed]
139. Sareddy, G.R.; Kesanakurti, D.; Kirti, P.B.; Babu, P.P. Nonsteroidal anti-inflammatory drugs diclofenac and celecoxib attenuates Wnt/beta-catenin/Tcf signaling pathway in human glioblastoma cells. *Neurochem. Res.* **2013**, *38*, 2313–2322. [CrossRef] [PubMed]
140. Lan, F.; Yue, X.; Han, L.; Yuan, X.; Shi, Z.; Huang, K.; Yang, Y.; Zou, J.; Zhang, J.; Jiang, T.; et al. Antitumor effect of aspirin in glioblastoma cells by modulation of beta-catenin/T-cell factor-mediated transcriptional activity. *J. Neurosurg.* **2011**, *115*, 780–788. [CrossRef]
141. Wieland, A.; Trageser, D.; Gogolak, S.; Reinartz, R.; Hofer, H.; Keller, M.; Leinhaas, A.; Schelle, R.; Normann, S.; Klaas, L.; et al. Anticancer effects of niclosamide in human glioblastoma. *Clin. Cancer Res.* **2013**, *19*, 4124–4136. [CrossRef]
142. Oh, H.C.; Shim, J.K.; Park, J.; Lee, J.H.; Choi, R.J.; Kim, N.H.; Kim, H.S.; Moon, J.H.; Kim, E.H.; Chang, J.H.; et al. Combined effects of niclosamide and temozolomide against human glioblastoma tumorspheres. *J. Cancer Res. Clin. Oncol.* **2020**, *146*, 2817–2828. [CrossRef]
143. Wang, Y.; Huang, N.; Li, H.; Liu, S.; Chen, X.; Yu, S.; Wu, N.; Bian, X.W.; Shen, H.Y.; Li, C.; et al. Promoting oligodendroglial-oriented differentiation of glioma stem cell: A repurposing of quetiapine for the treatment of malignant glioma. *Oncotarget* **2017**, *8*, 37511–37524. [CrossRef]
144. Wan, Z.; Shi, W.; Shao, B.; Shi, J.; Shen, A.; Ma, Y.; Chen, J.; Lan, Q. Peroxisome proliferator-activated receptor gamma agonist pioglitazone inhibits beta-catenin-mediated glioma cell growth and invasion. *Mol. Cell Biochem* **2011**, *349*, 1–10. [CrossRef]
145. Cilibrasi, C.; Butta, V.; Riva, G.; Bentivegna, A. Pioglitazone Effect on Glioma Stem Cell Lines: Really a Promising Drug Therapy for Glioblastoma? *PPAR Res.* **2016**, *2016*, 7175067. [CrossRef]
146. Jin, X.; Jeon, H.Y.; Joo, K.M.; Kim, J.K.; Jin, J.; Kim, S.H.; Kang, B.G.; Beck, S.; Lee, S.J.; Kim, J.K.; et al. Frizzled 4 regulates stemness and invasiveness of migrating glioma cells established by serial intracranial transplantation. *Cancer Res.* **2011**, *71*, 3066–3075. [CrossRef]
147. Zeppernick, F.; Ahmadi, R.; Campos, B.; Dictus, C.; Helmke, B.M.; Becker, N.; Lichter, P.; Unterberg, A.; Radlwimmer, B.; Herold-Mende, C.C. Stem cell marker CD133 affects clinical outcome in glioma patients. *Clin. Cancer Res.* **2008**, *14*, 123–129. [CrossRef]
148. Arrillaga-Romany, I.; Kurz, S.; Tarapore, R.S.; Sumrall, A.; Butowski, N.; Harrison, R.; de Groot, J.; Chi, A.; Shonka, N.; Umemura, Y.; et al. Efficacy of Onc201 in Patients with Onc201 for Recurrent H3 K27m-Mutant Diffuse Midline Glioma. *Neuro-Oncology* **2020**, *22*, 50–51. [CrossRef]

149. Le, P.N.; McDermott, J.D.; Jimeno, A. Targeting the Wnt pathway in human cancers: Therapeutic targeting with a focus on OMP-54F28. *Pharmacol. Ther.* **2015**, *146*, 1–11. [CrossRef]
150. Gurney, A.; Axelrod, F.; Bond, C.J.; Cain, J.; Chartier, C.; Donigan, L.; Fischer, M.; Chaudhari, A.; Ji, M.; Kapoun, A.M.; et al. Wnt pathway inhibition via the targeting of Frizzled receptors results in decreased growth and tumorigenicity of human tumors. *Proc. Natl. Acad. Sci. USA* **2012**, *109*, 11717–11722. [CrossRef]
151. Pavlovic, Z.; Adams, J.J.; Blazer, L.L.; Gakhal, A.K.; Jarvik, N.; Steinhart, Z.; Robitaille, M.; Mascall, K.; Pan, J.; Angers, S.; et al. A synthetic anti-Frizzled antibody engineered for broadened specificity exhibits enhanced anti-tumor properties. *Mabs* **2018**, *10*, 1157–1167. [CrossRef]
152. Newman, D.J.; Cragg, G.M. Natural Products as Sources of New Drugs over the Nearly Four Decades from 01/1981 to 09/2019. *J. Nat. Prod.* **2020**, *83*, 770–803. [CrossRef]
153. Qian, B.; Nag, S.A.; Su, Y.; Voruganti, S.; Qin, J.J.; Zhang, R.; Cho, W.C. miRNAs in cancer prevention and treatment and as molecular targets for natural product anticancer agents. *Curr. Cancer Drug Targets* **2013**, *13*, 519–541. [CrossRef]
154. Qin, J.; Wang, W.; Zhang, R. Novel natural product therapeutics targeting both inflammation and cancer. *Chin. J. Nat. Med.* **2017**, *15*, 401–416. [CrossRef]
155. Penas-Prado, M.; Hess, K.R.; Fisch, M.J.; Lagrone, L.W.; Groves, M.D.; Levin, V.A.; De Groot, J.F.; Puduvali, V.K.; Colman, H.; Volas-Redd, G.; et al. Randomized phase II adjuvant factorial study of dose-dense temozolomide alone and in combination with isotretinoin, celecoxib, and/or thalidomide for glioblastoma. *Neuro-Oncology* **2015**, *17*, 266–273. [CrossRef]
156. Huang, M.; Zhang, D.; Wu, J.Y.; Xing, K.; Yeo, E.; Li, C.; Zhang, L.; Holland, E.; Yao, L.; Qin, L.; et al. Wnt-mediated endothelial transformation into mesenchymal stem cell-like cells induces chemoresistance in glioblastoma. *Sci. Transl. Med.* **2020**, *12*, eaay7522. [CrossRef]
157. Seano, G.; Jain, R.K. Vessel co-option in glioblastoma: Emerging insights and opportunities. *Angiogenesis* **2020**, *23*, 9–16. [CrossRef]
158. Jain, R.K. Antiangiogenesis strategies revisited: From starving tumors to alleviating hypoxia. *Cancer Cell* **2014**, *26*, 605–622. [CrossRef]
159. Griveau, A.; Seano, G.; Shelton, S.J.; Kupp, R.; Jahangiri, A.; Obernier, K.; Krishnan, S.; Lindberg, O.R.; Yuen, T.J.; Tien, A.C.; et al. A Glial Signature and Wnt7 Signaling Regulate Glioma-Vascular Interactions and Tumor Microenvironment. *Cancer Cell* **2018**, *33*, 874–889.e877. [CrossRef]
160. Watkins, S.; Robel, S.; Kimbrough, I.F.; Robert, S.M.; Ellis-Davies, G.; Sontheimer, H. Disruption of astrocyte-vascular coupling and the blood-brain barrier by invading glioma cells. *Nat. Commun.* **2014**, *5*, 4196. [CrossRef]
161. Baker, G.J.; Yadav, V.N.; Motsch, S.; Koschmann, C.; Calinescu, A.A.; Mineharu, Y.; Camelo-Piragua, S.I.; Orringer, D.; Bannykh, S.; Nichols, W.S.; et al. Mechanisms of glioma formation: Iterative perivascular glioma growth and invasion leads to tumor progression, VEGF-independent vascularization, and resistance to antiangiogenic therapy. *Neoplasia* **2014**, *16*, 543–561. [CrossRef] [PubMed]
162. Di Tomaso, E.; Snuderl, M.; Kamoun, W.S.; Duda, D.G.; Auluck, P.K.; Fazlollahi, L.; Andronesi, O.C.; Frosch, M.P.; Wen, P.Y.; Plotkin, S.R.; et al. Glioblastoma recurrence after cediranib therapy in patients: Lack of “rebound” revascularization as mode of escape. *Cancer Res.* **2011**, *71*, 19–28. [CrossRef] [PubMed]
163. Voutouri, C.; Kirkpatrick, N.D.; Chung, E.; Mpekris, F.; Baish, J.W.; Munn, L.L.; Fukumura, D.; Stylianopoulos, T.; Jain, R.K. Experimental and computational analyses reveal dynamics of tumor vessel cooption and optimal treatment strategies. *Proc. Natl. Acad. Sci. USA* **2019**, *116*, 2662–2671. [CrossRef] [PubMed]
164. Whelan, R.; Hargaden, G.C.; Knox, A.J.S. Modulating the Blood-Brain Barrier: A Comprehensive Review. *Pharmaceutics* **2021**, *13*, 1980. [CrossRef]
165. Cho, C.; Smallwood, P.M.; Nathans, J. Reck and Gpr124 Are Essential Receptor Cofactors for Wnt7a/Wnt7b-Specific Signaling in Mammalian CNS Angiogenesis and Blood-Brain Barrier Regulation. *Neuron* **2017**, *95*, 1056–1073.e1055. [CrossRef]
166. Vanhollebeke, B.; Stone, O.A.; Bostaille, N.; Cho, C.; Zhou, Y.; Maquet, E.; Gauquier, A.; Cabochette, P.; Fukuhara, S.; Mochizuki, N.; et al. Tip cell-specific requirement for an atypical Gpr124- and Reck-dependent Wnt/beta-catenin pathway during brain angiogenesis. *eLife* **2015**, *4*, e06489. [CrossRef]
167. Martin, M.; Vermeiren, S.; Bostaille, N.; Eubelen, M.; Spitzer, D.; Vermeersch, M.; Profaci, C.P.; Pozuelo, E.; Toussay, X.; Raman-Nair, J.; et al. Engineered Wnt ligands enable blood-brain barrier repair in neurological disorders. *Science* **2022**, *375*, eabm4459. [CrossRef]
168. Chavali, M.; Ulloa-Navas, M.J.; Perez-Borreda, P.; Garcia-Verdugo, J.M.; McQuillen, P.S.; Huang, E.J.; Rowitch, D.H. Wnt-Dependent Oligodendroglial-Endothelial Interactions Regulate White Matter Vascularization and Attenuate Injury. *Neuron* **2020**, *108*, 1130–1145.e1135. [CrossRef]
169. Reis, M.; Czupalla, C.J.; Ziegler, N.; Devraj, K.; Zinke, J.; Seidel, S.; Heck, R.; Thom, S.; Macas, J.; Bockamp, E.; et al. Endothelial Wnt/beta-catenin signaling inhibits glioma angiogenesis and normalizes tumor blood vessels by inducing PDGF-B expression. *J. Exp. Med.* **2012**, *209*, 1611–1627. [CrossRef]
170. Andersson, E.R.; Sandberg, R.; Lendahl, U. Notch signaling: Simplicity in design, versatility in function. *Development* **2011**, *138*, 3593–3612. [CrossRef]
171. Liu, J.; Sato, C.; Cerletti, M.; Wagers, A. Notch signaling in the regulation of stem cell self-renewal and differentiation. *Curr. Top. Dev. Biol.* **2010**, *92*, 367–409. [CrossRef]

172. Imayoshi, I.; Sakamoto, M.; Yamaguchi, M.; Mori, K.; Kageyama, R. Essential roles of Notch signaling in maintenance of neural stem cells in developing and adult brains. *J. Neurosci.* **2010**, *30*, 3489–3498. [CrossRef]
173. Pierfelice, T.; Alberi, L.; Gaiano, N. Notch in the vertebrate nervous system: An old dog with new tricks. *Neuron* **2011**, *69*, 840–855. [CrossRef]
174. Bray, S.J. Notch signalling: A simple pathway becomes complex. *Nat. Rev. Mol. Cell Biol.* **2006**, *7*, 678–689. [CrossRef]
175. Kopan, R.; Ilagan, M.X. The canonical Notch signaling pathway: Unfolding the activation mechanism. *Cell* **2009**, *137*, 216–233. [CrossRef]
176. Cheng, H.T.; Kim, M.; Valerius, M.T.; Surendran, K.; Schuster-Gossler, K.; Gossler, A.; McMahon, A.P.; Kopan, R. Notch2, but not Notch1, is required for proximal fate acquisition in the mammalian nephron. *Development* **2007**, *134*, 801–811. [CrossRef]
177. Krebs, L.T.; Iwai, N.; Nonaka, S.; Welsh, I.C.; Lan, Y.; Jiang, R.; Saijoh, Y.; O'Brien, T.P.; Hamada, H.; Gridley, T. Notch signaling regulates left-right asymmetry determination by inducing Nodal expression. *Genes Dev.* **2003**, *17*, 1207–1212. [CrossRef]
178. Matsuura, A.; Ito, M.; Sakaidani, Y.; Kondo, T.; Murakami, K.; Furukawa, K.; Nadano, D.; Matsuda, T.; Okajima, T. O-linked N-acetylglucosamine is present on the extracellular domain of notch receptors. *J. Biol. Chem.* **2008**, *283*, 35486–35495. [CrossRef]
179. Moloney, D.J.; Shair, L.H.; Lu, F.M.; Xia, J.; Locke, R.; Matta, K.L.; Haltiwanger, R.S. Mammalian Notch1 is modified with two unusual forms of O-linked glycosylation found on epidermal growth factor-like modules. *J. Biol. Chem.* **2000**, *275*, 9604–9611. [CrossRef]
180. Blaumueller, C.M.; Qi, H.; Zagouras, P.; Artavanis-Tsakonas, S. Intracellular cleavage of Notch leads to a heterodimeric receptor on the plasma membrane. *Cell* **1997**, *90*, 281–291. [CrossRef]
181. Sanchez-Irizarry, C.; Carpenter, A.C.; Weng, A.P.; Pear, W.S.; Aster, J.C.; Blacklow, S.C. Notch subunit heterodimerization and prevention of ligand-independent proteolytic activation depend, respectively, on a novel domain and the LNR repeats. *Mol. Cell Biol.* **2004**, *24*, 9265–9273. [CrossRef] [PubMed]
182. Brou, C.; Logeat, F.; Gupta, N.; Bessia, C.; LeBail, O.; Doedens, J.R.; Cumano, A.; Roux, P.; Black, R.A.; Israel, A. A novel proteolytic cleavage involved in Notch signaling: The role of the disintegrin-metalloprotease TACE. *Mol. Cell* **2000**, *5*, 207–216. [CrossRef]
183. Van Tetering, G.; van Diest, P.; Verlaan, I.; van der Wall, E.; Kopan, R.; Vooijs, M. Metalloprotease ADAM10 is required for Notch1 site 2 cleavage. *J. Biol. Chem.* **2009**, *284*, 31018–31027. [CrossRef] [PubMed]
184. De Strooper, B.; Annaert, W.; Cupers, P.; Saftig, P.; Craessaerts, K.; Mumm, J.S.; Schroeter, E.H.; Schrijvers, V.; Wolfe, M.S.; Ray, W.J.; et al. A presenilin-1-dependent gamma-secretase-like protease mediates release of Notch intracellular domain. *Nature* **1999**, *398*, 518–522. [CrossRef]
185. Mumm, J.S.; Schroeter, E.H.; Saxena, M.T.; Griesemer, A.; Tian, X.; Pan, D.J.; Ray, W.J.; Kopan, R. A ligand-induced extracellular cleavage regulates gamma-secretase-like proteolytic activation of Notch1. *Mol. Cell* **2000**, *5*, 197–206. [CrossRef]
186. Christensen, S.; Kodoyianni, V.; Bosenberg, M.; Friedman, L.; Kimble, J. lag-1, a gene required for lin-12 and glp-1 signaling in *Caenorhabditis elegans*, is homologous to human CBF1 and *Drosophila* Su(H). *Development* **1996**, *122*, 1373–1383. [CrossRef]
187. Fortini, M.E.; Artavanis-Tsakonas, S. The suppressor of hairless protein participates in notch receptor signaling. *Cell* **1994**, *79*, 273–282. [CrossRef]
188. Tamura, K.; Taniguchi, Y.; Minoguchi, S.; Sakai, T.; Tun, T.; Furukawa, T.; Honjo, T. Physical interaction between a novel domain of the receptor Notch and the transcription factor RBP-J kappa/Su(H). *Curr. Biol.* **1995**, *5*, 1416–1423. [CrossRef]
189. Wu, L.; Sun, T.; Kobayashi, K.; Gao, P.; Griffin, J.D. Identification of a family of mastermind-like transcriptional coactivators for mammalian notch receptors. *Mol. Cell Biol.* **2002**, *22*, 7688–7700. [CrossRef]
190. Kovall, R.A. More complicated than it looks: Assembly of Notch pathway transcription complexes. *Oncogene* **2008**, *27*, 5099–5109. [CrossRef]
191. Nam, Y.; Sliz, P.; Song, L.; Aster, J.C.; Blacklow, S.C. Structural basis for cooperativity in recruitment of MAML coactivators to Notch transcription complexes. *Cell* **2006**, *124*, 973–983. [CrossRef]
192. Wilson, J.J.; Kovall, R.A. Crystal structure of the CSL-Notch-Mastermind ternary complex bound to DNA. *Cell* **2006**, *124*, 985–996. [CrossRef]
193. Kadam, S.; Emerson, B.M. Transcriptional specificity of human SWI/SNF BRG1 and BRM chromatin remodeling complexes. *Mol. Cell* **2003**, *11*, 377–389. [CrossRef]
194. Wallberg, A.E.; Pedersen, K.; Lendahl, U.; Roeder, R.G. p300 and PCAF act cooperatively to mediate transcriptional activation from chromatin templates by notch intracellular domains in vitro. *Mol. Cell Biol.* **2002**, *22*, 7812–7819. [CrossRef]
195. Iso, T.; Sartorelli, V.; Chung, G.; Shichinohe, T.; Kedes, L.; Hamamori, Y. HERP, a new primary target of Notch regulated by ligand binding. *Mol. Cell Biol.* **2001**, *21*, 6071–6079. [CrossRef]
196. Jarriault, S.; Brou, C.; Logeat, F.; Schroeter, E.H.; Kopan, R.; Israel, A. Signalling downstream of activated mammalian Notch. *Nature* **1995**, *377*, 355–358. [CrossRef]
197. El Hindy, N.; Keyvani, K.; Pagenstecher, A.; Dammann, P.; Sandalcioglu, I.E.; Sure, U.; Zhu, Y. Implications of Dll4-Notch signaling activation in primary glioblastoma multiforme. *Neuro-Oncology* **2013**, *15*, 1366–1378. [CrossRef]
198. Purow, B.W.; Haque, R.M.; Noel, M.W.; Su, Q.; Burdick, M.J.; Lee, J.; Sundaresan, T.; Pastorino, S.; Park, J.K.; Mikolaenko, I.; et al. Expression of Notch-1 and its ligands, Delta-like-1 and Jagged-1, is critical for glioma cell survival and proliferation. *Cancer Res.* **2005**, *65*, 2353–2363. [CrossRef]
199. Shih, A.H.; Holland, E.C. Notch signaling enhances nestin expression in gliomas. *Neoplasia* **2006**, *8*, 1072–1082. [CrossRef]

200. Parmigiani, E.; Taylor, V.; Giachino, C. Oncogenic and Tumor-Suppressive Functions of NOTCH Signaling in Glioma. *Cells* **2020**, *9*, 2304. [CrossRef]
201. Giachino, C.; Boulay, J.L.; Ivanek, R.; Alvarado, A.; Tostado, C.; Lugert, S.; Tchorz, J.; Coban, M.; Mariani, L.; Bettler, B.; et al. A Tumor Suppressor Function for Notch Signaling in Forebrain Tumor Subtypes. *Cancer Cell* **2015**, *28*, 730–742. [CrossRef]
202. Fan, X.; Khaki, L.; Zhu, T.S.; Soules, M.E.; Talsma, C.E.; Gul, N.; Koh, C.; Zhang, J.; Li, Y.M.; Maciaczyk, J.; et al. NOTCH pathway blockade depletes CD133-positive glioblastoma cells and inhibits growth of tumor neurospheres and xenografts. *Stem Cells* **2010**, *28*, 5–16. [CrossRef]
203. Zhu, T.S.; Costello, M.A.; Talsma, C.E.; Flack, C.G.; Crowley, J.G.; Hamm, L.L.; He, X.; Hervey-Jumper, S.L.; Heth, J.A.; Muraszko, K.M.; et al. Endothelial cells create a stem cell niche in glioblastoma by providing NOTCH ligands that nurture self-renewal of cancer stem-like cells. *Cancer Res.* **2011**, *71*, 6061–6072. [CrossRef]
204. Wang, J.; Wakeman, T.P.; Lathia, J.D.; Hjelmeland, A.B.; Wang, X.F.; White, R.R.; Rich, J.N.; Sullenger, B.A. Notch promotes radioresistance of glioma stem cells. *Stem Cells* **2010**, *28*, 17–28. [CrossRef]
205. Gilbert, C.A.; Daou, M.C.; Moser, R.P.; Ross, A.H. Gamma-secretase inhibitors enhance temozolomide treatment of human gliomas by inhibiting neurosphere repopulation and xenograft recurrence. *Cancer Res.* **2010**, *70*, 6870–6879. [CrossRef]
206. Bazzoni, R.; Bentivegna, A. Role of Notch Signaling Pathway in Glioblastoma Pathogenesis. *Cancers* **2019**, *11*, 292. [CrossRef]
207. Hovinga, K.E.; Shimizu, F.; Wang, R.; Panagiotakos, G.; Van Der Heijden, M.; Moayedpardazi, H.; Correia, A.S.; Soulet, D.; Major, T.; Menon, J.; et al. Inhibition of notch signaling in glioblastoma targets cancer stem cells via an endothelial cell intermediate. *Stem Cells* **2010**, *28*, 1019–1029. [CrossRef]
208. Lin, J.; Zhang, X.M.; Yang, J.C.; Ye, Y.B.; Luo, S.Q. gamma-secretase inhibitor-I enhances radiosensitivity of glioblastoma cell lines by depleting CD133+ tumor cells. *Arch. Med. Res.* **2010**, *41*, 519–529. [CrossRef]
209. Saito, N.; Fu, J.; Zheng, S.; Yao, J.; Wang, S.; Liu, D.D.; Yuan, Y.; Sulman, E.P.; Lang, F.F.; Colman, H.; et al. A high Notch pathway activation predicts response to gamma secretase inhibitors in proneural subtype of glioma tumor-initiating cells. *Stem Cells* **2014**, *32*, 301–312. [CrossRef]
210. Xu, R.; Shimizu, F.; Hovinga, K.; Beal, K.; Karimi, S.; Droms, L.; Peck, K.K.; Gutin, P.; Iorgulescu, J.B.; Kaley, T.; et al. Molecular and Clinical Effects of Notch Inhibition in Glioma Patients: A Phase 0/I Trial. *Clin. Cancer Res.* **2016**, *22*, 4786–4796. [CrossRef]
211. Pan, E.; Supko, J.G.; Kaley, T.J.; Butowski, N.A.; Cloughesy, T.; Jung, J.; Desideri, S.; Grossman, S.; Ye, X.; Park, D.M. Phase I study of RO4929097 with bevacizumab in patients with recurrent malignant glioma. *J. Neurooncol.* **2016**, *130*, 571–579. [CrossRef] [PubMed]
212. Peereboom, D.M.; Ye, X.; Mikkelsen, T.; Lesser, G.J.; Lieberman, F.S.; Robins, H.I.; Ahluwalia, M.S.; Sloan, A.E.; Grossman, S.A. A Phase II and Pharmacodynamic Trial of RO4929097 for Patients With Recurrent/Progressive Glioblastoma. *Neurosurgery* **2021**, *88*, 246–251. [CrossRef] [PubMed]
213. Tolcher, A.W.; Messersmith, W.A.; Mikulski, S.M.; Papadopoulos, K.P.; Kwak, E.L.; Gibbon, D.G.; Patnaik, A.; Falchook, G.S.; Dasari, A.; Shapiro, G.I.; et al. Phase I study of RO4929097, a gamma secretase inhibitor of Notch signaling, in patients with refractory metastatic or locally advanced solid tumors. *J. Clin. Oncol.* **2012**, *30*, 2348–2353. [CrossRef] [PubMed]
214. Fouladi, M.; Stewart, C.F.; Olson, J.; Wagner, L.M.; Onar-Thomas, A.; Kocak, M.; Packer, R.J.; Goldman, S.; Gururangan, S.; Gajjar, A.; et al. Phase I trial of MK-0752 in children with refractory CNS malignancies: A pediatric brain tumor consortium study. *J. Clin. Oncol.* **2011**, *29*, 3529–3534. [CrossRef] [PubMed]
215. Krop, I.; Demuth, T.; Guthrie, T.; Wen, P.Y.; Mason, W.P.; Chinnaiyan, P.; Butowski, N.; Groves, M.D.; Kesari, S.; Freedman, S.J.; et al. Phase I pharmacologic and pharmacodynamic study of the gamma secretase (Notch) inhibitor MK-0752 in adult patients with advanced solid tumors. *J. Clin. Oncol.* **2012**, *30*, 2307–2313. [CrossRef]
216. Milano, J.; McKay, J.; Dagenais, C.; Foster-Brown, L.; Pognan, F.; Gadiant, R.; Jacobs, R.T.; Zacco, A.; Greenberg, B.; Ciaccio, P.J. Modulation of notch processing by gamma-secretase inhibitors causes intestinal goblet cell metaplasia and induction of genes known to specify gut secretory lineage differentiation. *Toxicol. Sci.* **2004**, *82*, 341–358. [CrossRef]
217. Riccio, O.; van Gijn, M.E.; Bezdek, A.C.; Pellegrinet, L.; van Es, J.H.; Zimmer-Strobl, U.; Strobl, L.J.; Honjo, T.; Clevers, H.; Radtke, F. Loss of intestinal crypt progenitor cells owing to inactivation of both Notch1 and Notch2 is accompanied by derepression of CDK inhibitors p27Kip1 and p57Kip2. *EMBO Rep.* **2008**, *9*, 377–383. [CrossRef]
218. Beal, A.J.; Sanders, C.R. Substrate specificity of gamma-secretase and other intramembrane proteases. *Cell Mol. Life Sci.* **2008**, *65*, 1311–1334. [CrossRef]
219. Hemming, M.L.; Elias, J.E.; Gygi, S.P.; Selkoe, D.J. Proteomic profiling of gamma-secretase substrates and mapping of substrate requirements. *PLoS Biol.* **2008**, *6*, e257. [CrossRef]
220. Aste-Amezaga, M.; Zhang, N.; Lineberger, J.E.; Arnold, B.A.; Toner, T.J.; Gu, M.; Huang, L.; Vitelli, S.; Vo, K.T.; Haytko, P.; et al. Characterization of Notch1 antibodies that inhibit signaling of both normal and mutated Notch1 receptors. *PLoS ONE* **2010**, *5*, e9094. [CrossRef]
221. Wu, Y.; Cain-Hom, C.; Choy, L.; Hagenbeek, T.J.; de Leon, G.P.; Chen, Y.; Finkle, D.; Venook, R.; Wu, X.; Ridgway, J.; et al. Therapeutic antibody targeting of individual Notch receptors. *Nature* **2010**, *464*, 1052–1057. [CrossRef]
222. Li, Y.; Hickson, J.A.; Ambrosi, D.J.; Haasch, D.L.; Foster-Duke, K.D.; Eaton, L.J.; DiGiammarino, E.L.; Panchal, S.C.; Jiang, F.; Mudd, S.R.; et al. ABT-165, a Dual Variable Domain Immunoglobulin (DVD-Ig) Targeting DLL4 and VEGF, Demonstrates Superior Efficacy and Favorable Safety Profiles in Preclinical Models. *Mol. Cancer* **2018**, *17*, 1039–1050. [CrossRef]

223. Parakh, S.; Nicolazzo, J.; Scott, A.M.; Gan, H.K. Antibody Drug Conjugates in Glioblastoma—Is There a Future for Them? *Front. Oncol.* **2021**, *11*, 718590. [CrossRef]
224. Spino, M.; Kurz, S.C.; Chiriboga, L.; Serrano, J.; Zeck, B.; Sen, N.; Patel, S.; Shen, G.; Vasudevaraja, V.; Tsirigos, A.; et al. Cell Surface Notch Ligand DLL3 is a Therapeutic Target in Isocitrate Dehydrogenase-mutant Glioma. *Clin. Cancer Res.* **2019**, *25*, 1261–1271. [CrossRef]
225. Rudin, C.M.; Pietanza, M.C.; Bauer, T.M.; Ready, N.; Morgensztern, D.; Glisson, B.S.; Byers, L.A.; Johnson, M.L.; Burris, H.A., 3rd; Robert, F.; et al. Rovalpituzumab tesirine, a DLL3-targeted antibody-drug conjugate, in recurrent small-cell lung cancer: A first-in-human, first-in-class, open-label, phase 1 study. *Lancet Oncol.* **2017**, *18*, 42–51. [CrossRef]
226. Blackhall, F.; Jao, K.; Greillier, L.; Cho, B.C.; Penkov, K.; Reguart, N.; Majem, M.; Nackaerts, K.; Syrigos, K.; Hansen, K.; et al. Efficacy and Safety of Rovalpituzumab Tesirine Compared With Topotecan as Second-Line Therapy in DLL3-High SCLC: Results From the Phase 3 TAHOE Study. *J. Thorac. Oncol.* **2021**, *16*, 1547–1558. [CrossRef]
227. Johnson, M.L.; Zvirbule, Z.; Laktionov, K.; Helland, A.; Cho, B.C.; Gutierrez, V.; Colinet, B.; Lena, H.; Wolf, M.; Gottfried, M.; et al. Rovalpituzumab Tesirine as a Maintenance Therapy After First-Line Platinum-Based Chemotherapy in Patients With Extensive-Stage-SCLC: Results From the Phase 3 MERU Study. *J. Thorac. Oncol.* **2021**, *16*, 1570–1581. [CrossRef]
228. Chen, J.; Kesari, S.; Rooney, C.; Strack, P.R.; Chen, J.; Shen, H.; Wu, L.; Griffin, J.D. Inhibition of notch signaling blocks growth of glioblastoma cell lines and tumor neurospheres. *Genes Cancer* **2010**, *1*, 822–835. [CrossRef]
229. Opacak-Bernardi, T.; Ryu, J.S.; Raucher, D. Effects of cell penetrating Notch inhibitory peptide conjugated to elastin-like polypeptide on glioblastoma cells. *J. Drug Target.* **2017**, *25*, 523–531. [CrossRef]
230. Alvarez-Trotta, A.; Guerrant, W.; Astudillo, L.; Lahiry, M.; Diluvio, G.; Shersher, E.; Kaneku, H.; Robbins, D.J.; Orton, D.; Capobianco, A.J. Pharmacological Disruption of the Notch1 Transcriptional Complex Inhibits Tumor Growth by Selectively Targeting Cancer Stem Cells. *Cancer Res.* **2021**, *81*, 3347–3357. [CrossRef]
231. Astudillo, L.; Da Silva, T.G.; Wang, Z.; Han, X.; Jin, K.; VanWye, J.; Zhu, X.; Weaver, K.; Oashi, T.; Lopes, P.E.; et al. The Small Molecule IMR-1 Inhibits the Notch Transcriptional Activation Complex to Suppress Tumorigenesis. *Cancer Res.* **2016**, *76*, 3593–3603. [CrossRef]
232. Lehal, R.; Zaric, J.; Vigolo, M.; Urech, C.; Frisimantas, V.; Zangger, N.; Cao, L.; Berger, A.; Chicote, I.; Loubery, S.; et al. Pharmacological disruption of the Notch transcription factor complex. *Proc. Natl. Acad. Sci. USA* **2020**, *117*, 16292–16301. [CrossRef]
233. Perron, A.; Nishikawa, Y.; Iwata, J.; Shimojo, H.; Takaya, J.; Kobayashi, K.; Imayoshi, I.; Mbenza, N.M.; Takenoya, M.; Kageyama, R.; et al. Small-molecule screening yields a compound that inhibits the cancer-associated transcription factor Hes1 via the PHB2 chaperone. *J. Biol. Chem.* **2018**, *293*, 8285–8294. [CrossRef]
234. Floyd, D.H.; Kefas, B.; Seleverstov, O.; Mykhaylyk, O.; Dominguez, C.; Comeau, L.; Plank, C.; Purow, B. Alpha-secretase inhibition reduces human glioblastoma stem cell growth in vitro and in vivo by inhibiting Notch. *Neuro-Oncology* **2012**, *14*, 1215–1226. [CrossRef]
235. Roti, G.; Carlton, A.; Ross, K.N.; Markstein, M.; Pajcini, K.; Su, A.H.; Perrimon, N.; Pear, W.S.; Kung, A.L.; Blacklow, S.C.; et al. Complementary genomic screens identify SERCA as a therapeutic target in NOTCH1 mutated cancer. *Cancer Cell* **2013**, *23*, 390–405. [CrossRef]
236. Piccioni, D.; Juarez, T.; Brown, B.; Rose, L.; Allgood, V.; Kesari, S. Atct-18phase Ii Study of Mipsagargin (G-202), a PsmA-Activated Prodrug Targeting the Tumor Endothelium, in Adult Patients with Recurrent or Progressive Glioblastoma. *Neuro-Oncology* **2015**, *17*, v5. [CrossRef]
237. Zhang, H.; Liu, L.; Liu, C.; Pan, J.; Lu, G.; Zhou, Z.; Chen, Z.; Qian, C. Notch3 overexpression enhances progression and chemoresistance of urothelial carcinoma. *Oncotarget* **2017**, *8*, 34362–34373. [CrossRef]
238. Granit, R.Z.; Masury, H.; Condiotti, R.; Fixler, Y.; Gabai, Y.; Glikman, T.; Dalin, S.; Winter, E.; Nevo, Y.; Carmon, E.; et al. Regulation of Cellular Heterogeneity and Rates of Symmetric and Asymmetric Divisions in Triple-Negative Breast Cancer. *Cell Rep.* **2018**, *24*, 3237–3250. [CrossRef]
239. Ding, W.; Zeng, T.; Tao, W.; Ge, W.; Deng, J.; Lei, H.; Xiao, Y.; Liao, F. Effect of lenalidomide on the human gastric cancer cell line SGC7901/vincristine Notch signaling. *J. Cancer Res.* **2018**, *14*, S237–S242. [CrossRef]
240. Ponnurangam, S.; Dandawate, P.R.; Dhar, A.; Tawfik, O.W.; Parab, R.R.; Mishra, P.D.; Ranadive, P.; Sharma, R.; Mahajan, G.; Umar, S.; et al. Quinomycin A targets Notch signaling pathway in pancreatic cancer stem cells. *Oncotarget* **2016**, *7*, 3217–3232. [CrossRef]
241. Hanashima, Y.; Sano, E.; Sumi, K.; Ozawa, Y.; Yagi, C.; Tatsuoka, J.; Yoshimura, S.; Yamamuro, S.; Ueda, T.; Nakayama, T.; et al. Antitumor effect of lenalidomide in malignant glioma cell lines. *Oncol. Rep.* **2020**, *43*, 1580–1590. [CrossRef] [PubMed]
242. Kader, B.A.; Distefano, R.; West, K.L.; West, A.G. EZH2 inhibition in glioblastoma stem cells increases the expression of neuronal genes and the neuronal developmental regulators ZIC2, ZNF423 and MAFB. *bioRxiv* **2021**, 20211122469535. [CrossRef]
243. Yin, D.; Ong, J.M.; Hu, J.; Desmond, J.C.; Kawamata, N.; Konda, B.M.; Black, K.L.; Koeffler, H.P. Suberoylanilide hydroxamic acid, a histone deacetylase inhibitor: Effects on gene expression and growth of glioma cells in vitro and in vivo. *Clin. Cancer Res.* **2007**, *13*, 1045–1052. [CrossRef] [PubMed]
244. Zhen, Y.; Zhao, S.; Li, Q.; Li, Y.; Kawamoto, K. Arsenic trioxide-mediated Notch pathway inhibition depletes the cancer stem-like cell population in gliomas. *Cancer Lett.* **2010**, *292*, 64–72. [CrossRef]

245. Wu, J.; Ji, Z.; Liu, H.; Liu, Y.; Han, D.; Shi, C.; Shi, C.; Wang, C.; Yang, G.; Chen, X.; et al. Arsenic trioxide depletes cancer stem-like cells and inhibits repopulation of neurosphere derived from glioblastoma by downregulation of Notch pathway. *Toxicol. Lett.* **2013**, *220*, 61–69. [CrossRef]
246. Schwalfenberg, G.K. N-Acetylcysteine: A Review of Clinical Usefulness (an Old Drug with New Tricks). *J. Nutr. Metab.* **2021**, *2021*, 9949453. [CrossRef]
247. Deng, J.; Liu, A.D.; Hou, G.Q.; Zhang, X.; Ren, K.; Chen, X.Z.; Li, S.S.C.; Wu, Y.S.; Cao, X. N-acetylcysteine decreases malignant characteristics of glioblastoma cells by inhibiting Notch2 signaling. *J. Exp. Clin. Cancer Res.* **2019**, *38*, 2. [CrossRef]
248. Majumder, S.; Crabtree, J.S.; Golde, T.E.; Minter, L.M.; Osborne, B.A.; Miele, L. Targeting Notch in oncology: The path forward. *Nat. Rev. Drug Discov.* **2021**, *20*, 125–144. [CrossRef]
249. Zhdanovskaya, N.; Firrincieli, M.; Lazzari, S.; Pace, E.; Scribani Rossi, P.; Felli, M.P.; Talora, C.; Screpanti, I.; Palermo, R. Targeting Notch to Maximize Chemotherapeutic Benefits: Rationale, Advanced Strategies, and Future Perspectives. *Cancers* **2021**, *13*, 5106. [CrossRef]
250. Li, Y.; Wang, Z.; Jin, J.; Zhu, S.X.; He, G.Q.; Li, S.H.; Wang, J.; Cai, Y. Quercetin pretreatment enhances the radiosensitivity of colon cancer cells by targeting Notch-1 pathway. *Biochem. Biophys. Res. Commun.* **2020**, *523*, 947–953. [CrossRef]
251. Li, Y.; Zhang, J.; Ma, D.; Zhang, L.; Si, M.; Yin, H.; Li, J. Curcumin inhibits proliferation and invasion of osteosarcoma cells through inactivation of Notch-1 signaling. *FEBS J.* **2012**, *279*, 2247–2259. [CrossRef]
252. Mori, M.; Tottone, L.; Quaglio, D.; Zhdanovskaya, N.; Ingallina, C.; Fusto, M.; Ghirga, F.; Peruzzi, G.; Crestoni, M.E.; Simeoni, F.; et al. Identification of a novel chalcone derivative that inhibits Notch signaling in T-cell acute lymphoblastic leukemia. *Sci. Rep.* **2017**, *7*, 2213. [CrossRef]
253. Lai, I.C.; Shih, P.H.; Yao, C.J.; Yeh, C.T.; Wang-Peng, J.; Lui, T.N.; Chuang, S.E.; Hu, T.S.; Lai, T.Y.; Lai, G.M. Elimination of cancer stem-like cells and potentiation of temozolomide sensitivity by Honokiol in glioblastoma multiforme cells. *PLoS ONE* **2015**, *10*, e0114830. [CrossRef]
254. Lubecka, K.; Kurzava, L.; Flower, K.; Buvala, H.; Zhang, H.; Teegarden, D.; Camarillo, I.; Suderman, M.; Kuang, S.; Andrisani, O.; et al. Stilbenoids remodel the DNA methylation patterns in breast cancer cells and inhibit oncogenic NOTCH signaling through epigenetic regulation of MAML2 transcriptional activity. *Carcinogenesis* **2016**, *37*, 656–668. [CrossRef]
255. Sun, Z.; Zhou, C.; Liu, F.; Zhang, W.; Chen, J.; Pan, Y.; Ma, L.; Liu, Q.; Du, Y.; Yang, J.; et al. Inhibition of breast cancer cell survival by Xanthohumol via modulation of the Notch signaling pathway in vivo and in vitro. *Oncol. Lett.* **2018**, *15*, 908–916. [CrossRef]
256. Kang, M.S.; Baek, S.H.; Chun, Y.S.; Moore, A.Z.; Landman, N.; Berman, D.; Yang, H.O.; Morishima-Kawashima, M.; Osawa, S.; Funamoto, S.; et al. Modulation of lipid kinase PI4KIIalpha activity and lipid raft association of presenilin 1 underlies gamma-secretase inhibition by ginsenoside (20S)-Rg3. *J. Biol. Chem.* **2013**, *288*, 20868–20882. [CrossRef]
257. Kiesel, V.A.; Stan, S.D. Diallyl trisulfide, a chemopreventive agent from Allium vegetables, inhibits alpha-secretases in breast cancer cells. *Biochem. Biophys. Res. Commun.* **2017**, *484*, 833–838. [CrossRef]
258. Ohtaka, M.; Itoh, M.; Tohda, S. BMI1 Inhibitors Down-regulate NOTCH Signaling and Suppress Proliferation of Acute Leukemia Cells. *Anticancer Res.* **2017**, *37*, 6047–6053. [CrossRef]
259. Sun, D.W.; Zhang, H.D.; Mao, L.; Mao, C.F.; Chen, W.; Cui, M.; Ma, R.; Cao, H.X.; Jing, C.W.; Wang, Z.; et al. Luteolin Inhibits Breast Cancer Development and Progression In Vitro and In Vivo by Suppressing Notch Signaling and Regulating MiRNAs. *Cell Physiol. Biochem.* **2015**, *37*, 1693–1711. [CrossRef]
260. Giuli, M.V.; Diluvio, G.; Giuliani, E.; Franciosa, G.; Di Magno, L.; Pignataro, M.G.; Tottone, L.; Nicoletti, C.; Besharat, Z.M.; Peruzzi, G.; et al. Notch3 contributes to T-cell leukemia growth via regulation of the unfolded protein response. *Oncogenesis* **2020**, *9*, 93. [CrossRef]
261. Koduru, S.; Kumar, R.; Srinivasan, S.; Evers, M.B.; Damodaran, C. Notch-1 inhibition by Withaferin-A: A therapeutic target against colon carcinogenesis. *Mol. Cancer* **2010**, *9*, 202–210. [CrossRef]
262. Dandawate, P.; Subramaniam, D.; Panovich, P.; Standing, D.; Krishnamachary, B.; Kaushik, G.; Thomas, S.M.; Dhar, A.; Weir, S.J.; Jensen, R.A.; et al. Cucurbitacin B and I inhibits colon cancer growth by targeting the Notch signaling pathway. *Sci. Rep.* **2020**, *10*, 1290. [CrossRef]
263. Kubiczikova, L.; Sedlarikova, L.; Hajek, R.; Sevcikova, S. TGF-beta—An excellent servant but a bad master. *J. Transl. Med.* **2012**, *10*, 183. [CrossRef]
264. Xu, X.; Zheng, L.; Yuan, Q.; Zhen, G.; Crane, J.L.; Zhou, X.; Cao, X. Transforming growth factor-beta in stem cells and tissue homeostasis. *Bone Res.* **2018**, *6*, 2. [CrossRef] [PubMed]
265. Meyers, E.A.; Kessler, J.A. TGF-beta Family Signaling in Neural and Neuronal Differentiation, Development, and Function. *Cold Spring Harb. Perspect. Biol.* **2017**, *9*, a022244. [CrossRef]
266. Falk, S.; Wurdak, H.; Ittner, L.M.; Ille, F.; Sumara, G.; Schmid, M.T.; Draganova, K.; Lang, K.S.; Paratore, C.; Leveen, P.; et al. Brain area-specific effect of TGF-beta signaling on Wnt-dependent neural stem cell expansion. *Cell Stem Cell* **2008**, *2*, 472–483. [CrossRef] [PubMed]
267. Baba, A.B.; Rah, B.; Bhat, G.R.; Mushtaq, I.; Parveen, S.; Hassan, R.; Hameed Zargar, M.; Afroze, D. Transforming Growth Factor-Beta (TGF-beta) Signaling in Cancer-A Betrayal Within. *Front. Pharm.* **2022**, *13*, 791272. [CrossRef]
268. Proetzl, G.; Pawlowski, S.A.; Wiles, M.V.; Yin, M.; Boivin, G.P.; Howles, P.N.; Ding, J.; Ferguson, M.W.; Doetschman, T. Transforming growth factor-beta 3 is required for secondary palate fusion. *Nat. Genet.* **1995**, *11*, 409–414. [CrossRef] [PubMed]

269. Letterio, J.J.; Roberts, A.B. Transforming growth factor-beta1-deficient mice: Identification of isoform-specific activities in vivo. *J. Leukoc. Biol.* **1996**, *59*, 769–774. [CrossRef] [PubMed]
270. Sanford, L.P.; Ormsby, I.; Gittenberger-de Groot, A.C.; Sariola, H.; Friedman, R.; Boivin, G.P.; Cardell, E.L.; Doetschman, T. TGFbeta2 knockout mice have multiple developmental defects that are non-overlapping with other TGFbeta knockout phenotypes. *Development* **1997**, *124*, 2659–2670. [CrossRef] [PubMed]
271. Han, J.; Alvarez-Breckenridge, C.A.; Wang, Q.E.; Yu, J. TGF-beta signaling and its targeting for glioma treatment. *Am. J. Cancer Res.* **2015**, *5*, 945–955.
272. Nakao, A.; Afrakhte, M.; Moren, A.; Nakayama, T.; Christian, J.L.; Heuchel, R.; Itoh, S.; Kawabata, M.; Heldin, N.E.; Heldin, C.H.; et al. Identification of Smad7, a TGFbeta-inducible antagonist of TGF-beta signalling. *Nature* **1997**, *389*, 631–635. [CrossRef]
273. Moustakas, A.; Heldin, C.H. Non-Smad TGF-beta signals. *J. Cell Sci.* **2005**, *118*, 3573–3584. [CrossRef]
274. Teixeira, A.F.; Ten Dijke, P.; Zhu, H.J. On-Target Anti-TGF-beta Therapies Are Not Succeeding in Clinical Cancer Treatments: What Are Remaining Challenges? *Front. Cell Dev. Biol.* **2020**, *8*, 605. [CrossRef]
275. Dugger, B.N.; Dickson, D.W. Pathology of Neurodegenerative Diseases. *Cold Spring Harb. Perspect. Biol.* **2017**, *9*, a028035. [CrossRef]
276. Lindholm, D.; Castren, E.; Kiefer, R.; Zafra, F.; Thoenen, H. Transforming growth factor-beta 1 in the rat brain: Increase after injury and inhibition of astrocyte proliferation. *J. Cell Biol.* **1992**, *117*, 395–400. [CrossRef]
277. Lebrun, J.J. The Dual Role of TGFbeta in Human Cancer: From Tumor Suppression to Cancer Metastasis. *ISRN Mol. Biol.* **2012**, *2012*, 381428. [CrossRef]
278. Kjellman, C.; Olofsson, S.P.; Hansson, O.; Von Schantz, T.; Lindvall, M.; Nilsson, I.; Salford, L.G.; Sjogren, H.O.; Widegren, B. Expression of TGF-beta isoforms, TGF-beta receptors, and SMAD molecules at different stages of human glioma. *Int. J. Cancer* **2000**, *89*, 251–258. [CrossRef]
279. Bruna, A.; Darken, R.S.; Rojo, F.; Ocana, A.; Penuelas, S.; Arias, A.; Paris, R.; Tortosa, A.; Mora, J.; Baselga, J.; et al. High TGFbeta-Smad activity confers poor prognosis in glioma patients and promotes cell proliferation depending on the methylation of the PDGF-B gene. *Cancer Cell* **2007**, *11*, 147–160. [CrossRef]
280. Alexandrow, M.G.; Moses, H.L. Transforming growth factor beta and cell cycle regulation. *Cancer Res.* **1995**, *55*, 1452–1457.
281. Wesolowska, A.; Kwiatkowska, A.; Slomnicki, L.; Dembinski, M.; Master, A.; Sliwa, M.; Franciszkiwicz, K.; Chouaib, S.; Kaminska, B. Microglia-derived TGF-beta as an important regulator of glioblastoma invasion—an inhibition of TGF-beta-dependent effects by shRNA against human TGF-beta type II receptor. *Oncogene* **2008**, *27*, 918–930. [CrossRef] [PubMed]
282. Nana, A.W.; Yang, P.M.; Lin, H.Y. Overview of Transforming Growth Factor beta Superfamily Involvement in Glioblastoma Initiation and Progression. *Asian Pac. J. Cancer Prev.* **2015**, *16*, 6813–6823. [CrossRef] [PubMed]
283. Katz, L.H.; Li, Y.; Chen, J.S.; Munoz, N.M.; Majumdar, A.; Chen, J.; Mishra, L. Targeting TGF-beta signaling in cancer. *Expert Opin Targets* **2013**, *17*, 743–760. [CrossRef] [PubMed]
284. Zhang, Y.; Alexander, P.B.; Wang, X.F. TGF-beta Family Signaling in the Control of Cell Proliferation and Survival. *Cold Spring Harb. Perspect. Biol.* **2017**, *9*, a022145. [CrossRef]
285. Battle, E.; Massague, J. Transforming Growth Factor-beta Signaling in Immunity and Cancer. *Immunity* **2019**, *50*, 924–940. [CrossRef]
286. Gu, S.; Feng, X.H. TGF-beta signaling in cancer. *Acta Biochim. Biophys. Sin.* **2018**, *50*, 941–949. [CrossRef]
287. Gieryng, A.; Pszczolkowska, D.; Walentynowicz, K.A.; Rajan, W.D.; Kaminska, B. Immune microenvironment of gliomas. *Lab. Invest.* **2017**, *97*, 498–518. [CrossRef]
288. Li, W.; Graeber, M.B. The molecular profile of microglia under the influence of glioma. *Neuro-Oncology* **2012**, *14*, 958–978. [CrossRef]
289. Xue, V.W.; Chung, J.Y.; Cordoba, C.A.G.; Cheung, A.H.; Kang, W.; Lam, E.W.; Leung, K.T.; To, K.F.; Lan, H.Y.; Tang, P.M. Transforming Growth Factor-beta: A Multifunctional Regulator of Cancer Immunity. *Cancers* **2020**, *12*, 3099. [CrossRef]
290. Friese, M.A.; Wischhusen, J.; Wick, W.; Weiler, M.; Eisele, G.; Steinle, A.; Weller, M. RNA interference targeting transforming growth factor-beta enhances NKG2D-mediated antiglioma immune response, inhibits glioma cell migration and invasiveness, and abrogates tumorigenicity in vivo. *Cancer Res.* **2004**, *64*, 7596–7603. [CrossRef]
291. Schlingensiepen, K.H.; Schlingensiepen, R.; Steinbrecher, A.; Hau, P.; Bogdahn, U.; Fischer-Blass, B.; Jachimczak, P. Targeted tumor therapy with the TGF-beta 2 antisense compound AP 12009. *Cytokine Growth Factor Rev.* **2006**, *17*, 129–139. [CrossRef]
292. Jaschinski, F.; Rothhammer, T.; Jachimczak, P.; Seitz, C.; Schneider, A.; Schlingensiepen, K.H. The antisense oligonucleotide trabedersen (AP 12009) for the targeted inhibition of TGF-beta2. *Curr. Pharm. Biotechnol.* **2011**, *12*, 2203–2213. [CrossRef]
293. Hau, P.; Jachimczak, P.; Schlingensiepen, R.; Schulmeyer, F.; Jauch, T.; Steinbrecher, A.; Brawanski, A.; Proescholdt, M.; Schlaier, J.; Buchroithner, J.; et al. Inhibition of TGF-beta2 with AP 12009 in recurrent malignant gliomas: From preclinical to phase I/II studies. *Oligonucleotides* **2007**, *17*, 201–212. [CrossRef]
294. Roth, P.; Silginer, M.; Goodman, S.L.; Hasenbach, K.; Thies, S.; Maurer, G.; Schraml, P.; Tabatabai, G.; Moch, H.; Tritschler, I.; et al. Integrin control of the transforming growth factor-beta pathway in glioblastoma. *Brain* **2013**, *136*, 564–576. [CrossRef]
295. Stupp, R.; Hegi, M.E.; Gorlia, T.; Erridge, S.C.; Perry, J.; Hong, Y.-K.; Aldape, K.D.; Lhermitte, B.; Pietsch, T.; Grujicic, D.; et al. Cilengitide combined with standard treatment for patients with newly diagnosed glioblastoma with methylated MGMT promoter (CENTRIC EORTC 26071-22072 study): A multicentre, randomised, open-label, phase 3 trial. *Lancet Oncol.* **2014**, *15*, 1100–1108. [CrossRef]

296. Suzuki, E.; Kim, S.; Cheung, H.K.; Corbley, M.J.; Zhang, X.; Sun, L.; Shan, F.; Singh, J.; Lee, W.C.; Albelda, S.M.; et al. A novel small-molecule inhibitor of transforming growth factor beta type I receptor kinase (SM16) inhibits murine mesothelioma tumor growth in vivo and prevents tumor recurrence after surgical resection. *Cancer Res.* **2007**, *67*, 2351–2359. [CrossRef]
297. Rausch, M.P.; Hahn, T.; Ramanathapuram, L.; Bradley-Dunlop, D.; Mahadevan, D.; Mercado-Pimentel, M.E.; Runyan, R.B.; Besselsen, D.G.; Zhang, X.; Cheung, H.K.; et al. An orally active small molecule TGF-beta receptor I antagonist inhibits the growth of metastatic murine breast cancer. *Anticancer Res.* **2009**, *29*, 2099–2109.
298. Zhang, M.; Kleber, S.; Rohrich, M.; Timke, C.; Han, N.; Tuettenberg, J.; Martin-Villalba, A.; Debus, J.; Peschke, P.; Wirkner, U.; et al. Blockade of TGF-beta signaling by the TGFbetaR-I kinase inhibitor LY2109761 enhances radiation response and prolongs survival in glioblastoma. *Cancer Res.* **2011**, *71*, 7155–7167. [CrossRef]
299. Zhang, M.; Herion, T.W.; Timke, C.; Han, N.; Hauser, K.; Weber, K.J.; Peschke, P.; Wirkner, U.; Lahn, M.; Huber, P.E. Trimodal glioblastoma treatment consisting of concurrent radiotherapy, temozolomide, and the novel TGF-beta receptor I kinase inhibitor LY2109761. *Neoplasia* **2011**, *13*, 537–549. [CrossRef]
300. Yingling, J.M.; McMillen, W.T.; Yan, L.; Huang, H.; Sawyer, J.S.; Graff, J.; Clawson, D.K.; Britt, K.S.; Anderson, B.D.; Beight, D.W.; et al. Preclinical assessment of galunisertib (LY2157299 monohydrate), a first-in-class transforming growth factor-beta receptor type I inhibitor. *Oncotarget* **2018**, *9*, 6659–6677. [CrossRef]
301. Wick, A.; Desjardins, A.; Suarez, C.; Forsyth, P.; Gueorguieva, I.; Burkholder, T.; Cleverly, A.L.; Estrem, S.T.; Wang, S.; Lahn, M.M.; et al. Phase 1b/2a study of galunisertib, a small molecule inhibitor of transforming growth factor-beta receptor I, in combination with standard temozolomide-based radiochemotherapy in patients with newly diagnosed malignant glioma. *Investig. New Drugs* **2020**, *38*, 1570–1579. [CrossRef]
302. Brandes, A.A.; Carpentier, A.F.; Kesari, S.; Sepulveda-Sanchez, J.M.; Wheeler, H.R.; Chinot, O.; Cher, L.; Steinbach, J.P.; Capper, D.; Specenier, P.; et al. A Phase II randomized study of galunisertib monotherapy or galunisertib plus lomustine compared with lomustine monotherapy in patients with recurrent glioblastoma. *Neuro-Oncology* **2016**, *18*, 1146–1156. [CrossRef]
303. Spender, L.C.; Ferguson, G.J.; Hughes, G.D.; Davies, B.R.; Goldberg, F.W.; Herrera, B.; Taylor, R.G.; Strathearn, L.S.; Sansom, O.J.; Barry, S.T.; et al. Preclinical Evaluation of AZ12601011 and AZ12799734, Inhibitors of Transforming Growth Factor beta Superfamily Type 1 Receptors. *Mol. Pharm.* **2019**, *95*, 222–234. [CrossRef]
304. Ueda, R.; Fujita, M.; Zhu, X.; Sasaki, K.; Kastenhuber, E.R.; Kohanbash, G.; McDonald, H.A.; Harper, J.; Lonning, S.; Okada, H. Systemic inhibition of transforming growth factor-beta in glioma-bearing mice improves the therapeutic efficacy of glioma-associated antigen peptide vaccines. *Clin. Cancer Res.* **2009**, *15*, 6551–6559. [CrossRef]
305. Hulper, P.; Schulz-Schaeffer, W.; Dullin, C.; Hoffmann, P.; Harper, J.; Kurtzberg, L.; Lonning, S.; Kugler, W.; Lakomek, M.; Erdlenbruch, B. Tumor localization of an anti-TGF-beta antibody and its effects on gliomas. *Int. J. Oncol.* **2011**, *38*, 51–59.
306. Den Hollander, M.W.; Bensch, F.; Glaudemans, A.W.; Oude Munnink, T.H.; Enting, R.H.; den Dunnen, W.F.; Heesters, M.A.; Kruijff, F.A.; Lub-de Hooge, M.N.; Cees de Groot, J.; et al. TGF-beta Antibody Uptake in Recurrent High-Grade Glioma Imaged with ⁸⁹Zr-Fresolimumab PET. *J. Nucl. Med.* **2015**, *56*, 1310–1314. [CrossRef]
307. Shaim, H.; Shanley, M.; Basar, R.; Daher, M.; Gumin, J.; Zamlar, D.B.; Uprety, N.; Wang, F.; Huang, Y.; Gabrusiewicz, K.; et al. Targeting the alpha v integrin/TGF-beta axis improves natural killer cell function against glioblastoma stem cells. *J. Clin. Investig.* **2021**, *131*, e142116. [CrossRef]
308. Niedbala, M.; Malarz, K.; Sharma, G.; Kramer-Marek, G.; Kaspera, W. Glioblastoma: Pitfalls and Opportunities of Immunotherapeutic Combinations. *OncoTargets Ther.* **2022**, *15*, 437–468. [CrossRef]
309. Ashrafizadeh, M.; Najafi, M.; Orouei, S.; Zabolian, A.; Saleki, H.; Azami, N.; Sharifi, N.; Hushmandi, K.; Zarrabi, A.; Ahn, K.S. Resveratrol Modulates Transforming Growth Factor-Beta (TGF-beta) Signaling Pathway for Disease Therapy: A New Insight into Its Pharmacological Activities. *Biomedicines* **2020**, *8*, 261. [CrossRef]
310. Kabel, A.M.; Atef, A.; Estfanous, R.S. Ameliorative potential of sitagliptin and/or resveratrol on experimentally-induced clear cell renal cell carcinoma. *Biomed. Pharm.* **2018**, *97*, 667–674. [CrossRef] [PubMed]
311. Zhang, Y.; Yang, S.; Yang, Y.; Liu, T. Resveratrol induces immunogenic cell death of human and murine ovarian carcinoma cells. *Infect. Agent Cancer* **2019**, *14*, 27. [CrossRef] [PubMed]
312. Song, Y.; Chen, Y.; Li, Y.; Lyu, X.; Cui, J.; Cheng, Y.; Zheng, T.; Zhao, L.; Zhao, G. Resveratrol Suppresses Epithelial-Mesenchymal Transition in GBM by Regulating Smad-Dependent Signaling. *Biomed. Res. Int.* **2019**, *2019*, 1321973. [CrossRef] [PubMed]
313. Nie, X.; Luukko, K.; Kettunen, P. BMP signalling in craniofacial development. *Int. J. Dev. Biol.* **2006**, *50*, 511–521. [CrossRef] [PubMed]
314. Bond, A.M.; Bhalala, O.G.; Kessler, J.A. The dynamic role of bone morphogenetic proteins in neural stem cell fate and maturation. *Dev. Neurobiol.* **2012**, *72*, 1068–1084. [CrossRef]
315. Chen, H.L.; Panchision, D.M. Concise review: Bone morphogenetic protein pleiotropism in neural stem cells and their derivatives—alternative pathways, convergent signals. *Stem Cells* **2007**, *25*, 63–68. [CrossRef]
316. Gamez, B.; Rodriguez-Carballo, E.; Ventura, F. BMP signaling in telencephalic neural cell specification and maturation. *Front. Cell Neurosci.* **2013**, *7*, 87. [CrossRef]
317. Katagiri, T.; Watabe, T. Bone Morphogenetic Proteins. *Cold Spring Harb. Perspect. Biol.* **2016**, *8*, a021899. [CrossRef]
318. Bond, A.M.; Peng, C.Y.; Meyers, E.A.; McGuire, T.; Ewaleifoh, O.; Kessler, J.A. BMP signaling regulates the tempo of adult hippocampal progenitor maturation at multiple stages of the lineage. *Stem Cells* **2014**, *32*, 2201–2214. [CrossRef]

319. Choe, Y.; Pleasure, S.J.; Mira, H. Control of Adult Neurogenesis by Short-Range Morphogenic-Signaling Molecules. *Cold Spring Harb. Perspect. Biol.* **2015**, *8*, a018887. [CrossRef]
320. Panchision, D.M.; McKay, R.D. The control of neural stem cells by morphogenic signals. *Curr. Opin. Genet. Dev.* **2002**, *12*, 478–487. [CrossRef]
321. Wang, R.N.; Green, J.; Wang, Z.; Deng, Y.; Qiao, M.; Peabody, M.; Zhang, Q.; Ye, J.; Yan, Z.; Denduluri, S.; et al. Bone Morphogenetic Protein (BMP) signaling in development and human diseases. *Genes Dis* **2014**, *1*, 87–105. [CrossRef]
322. Choi, S.; Yu, J.; Park, A.; Dubon, M.J.; Do, J.; Kim, Y.; Nam, D.; Noh, J.; Park, K.S. BMP-4 enhances epithelial mesenchymal transition and cancer stem cell properties of breast cancer cells via Notch signaling. *Sci. Rep.* **2019**, *9*, 11724. [CrossRef]
323. Ye, L.; Jiang, W.G. Bone morphogenetic proteins in tumour associated angiogenesis and implication in cancer therapies. *Cancer Lett* **2016**, *380*, 586–597. [CrossRef]
324. Guyot, B.; Lefort, S.; Voeltzel, T.; Pecheur, E.I.; Maguer-Satta, V. Altered BMP2/4 Signaling in Stem Cells and Their Niche: Different Cancers but Similar Mechanisms, the Example of Myeloid Leukemia and Breast Cancer. *Front. Cell Dev. Biol.* **2021**, *9*, 787989. [CrossRef]
325. Kallioniemi, A. Bone morphogenetic protein 4-a fascinating regulator of cancer cell behavior. *Cancer Genet.* **2012**, *205*, 267–277. [CrossRef]
326. Lowery, J.W.; Brookshire, B.; Rosen, V. A Survey of Strategies to Modulate the Bone Morphogenetic Protein Signaling Pathway: Current and Future Perspectives. *Stem Cells Int.* **2016**, *2016*, 7290686. [CrossRef]
327. Bach, D.H.; Park, H.J.; Lee, S.K. The Dual Role of Bone Morphogenetic Proteins in Cancer. *Mol. Oncolytics* **2018**, *8*, 1–13. [CrossRef]
328. Zhang, L.; Ye, Y.; Long, X.; Xiao, P.; Ren, X.; Yu, J. BMP signaling and its paradoxical effects in tumorigenesis and dissemination. *Oncotarget* **2016**, *7*, 78206–78218. [CrossRef]
329. Bao, Z.; Zhang, C.; Yan, W.; Liu, Y.; Li, M.; Zhang, W.; Jiang, T. BMP4, a strong better prognosis predictor, has a subtype preference and cell development association in gliomas. *J. Transl. Med.* **2013**, *11*, 100. [CrossRef]
330. Wu, Q.; Yao, J. BMP4, a new prognostic factor for glioma. *World J. Surg. Oncol.* **2013**, *11*, 264. [CrossRef]
331. Liu, C.; Tian, G.; Tu, Y.; Fu, J.; Lan, C.; Wu, N. Expression pattern and clinical prognostic relevance of bone morphogenetic protein-2 in human gliomas. *Jpn J. Clin. Oncol.* **2009**, *39*, 625–631. [CrossRef]
332. Chirasani, S.R.; Sternjak, A.; Wend, P.; Momma, S.; Campos, B.; Herrmann, I.M.; Graf, D.; Mitsiadis, T.; Herold-Mende, C.; Besser, D.; et al. Bone morphogenetic protein-7 release from endogenous neural precursor cells suppresses the tumorigenicity of stem-like glioblastoma cells. *Brain* **2010**, *133*, 1961–1972. [CrossRef]
333. Tate, C.M.; Pallini, R.; Ricci-Vitiani, L.; Dowless, M.M.; Shiyanova, T.; D'Alessandris, G.Q.; Morgante, L.; Giannetti, S.; Larocca, L.M.; di Martino, S.; et al. A BMP7 variant inhibits the tumorigenic potential of glioblastoma stem-like cells. *Cell Death Differ.* **2012**, *19*, 1644–1654. [CrossRef]
334. Gonzalez-Gomez, P.; Crecente-Campo, J.; Zahonero, C.; de la Fuente, M.; Hernandez-Lain, A.; Mira, H.; Sanchez-Gomez, P.; Garcia-Fuentes, M. Controlled release microspheres loaded with BMP7 suppress primary tumors from human glioblastoma. *Oncotarget* **2015**, *6*, 10950–10963. [CrossRef]
335. Zhou, Z.; Sun, L.; Wang, Y.; Wu, Z.; Geng, J.; Miu, W.; Pu, Y.; You, Y.; Yang, Z.; Liu, N. Bone morphogenetic protein 4 inhibits cell proliferation and induces apoptosis in glioma stem cells. *Cancer Biother. Radiopharm.* **2011**, *26*, 77–83. [CrossRef]
336. Liu, B.; Tian, D.; Yi, W.; Wu, L.; Cai, Q.; Dong, H.; Shen, H.; Ji, B.; Wang, L.; Zhang, S.; et al. Effect of bone morphogenetic protein 4 in the human brain glioma cell line U251. *Cell Biochem. Biophys.* **2010**, *58*, 91–96. [CrossRef]
337. Liu, B.; Chen, Q.; Tian, D.; Wu, L.; Dong, H.; Wang, J.; Ji, B.; Zhu, X.; Cai, Q.; Wang, L.; et al. BMP4 reverses multidrug resistance through modulation of BCL-2 and GDNF in glioblastoma. *Brain Res.* **2013**, *1507*, 115–124. [CrossRef]
338. Persano, L.; Pistollato, F.; Rampazzo, E.; Della Puppa, A.; Abbadi, S.; Frasson, C.; Volpin, F.; Indraccolo, S.; Scienza, R.; Basso, G. BMP2 sensitizes glioblastoma stem-like cells to Temozolomide by affecting HIF-1alpha stability and MGMT expression. *Cell Death Dis.* **2012**, *3*, e412. [CrossRef]
339. Yan, K.; Wu, Q.; Yan, D.H.; Lee, C.H.; Rahim, N.; Tritschler, I.; DeVecchio, J.; Kalady, M.F.; Hjelmeland, A.B.; Rich, J.N. Glioma cancer stem cells secrete Gremlin1 to promote their maintenance within the tumor hierarchy. *Genes Dev.* **2014**, *28*, 1085–1100. [CrossRef]
340. Koguchi, M.; Nakahara, Y.; Ito, H.; Wakamiya, T.; Yoshioka, F.; Ogata, A.; Inoue, K.; Masuoka, J.; Izumi, H.; Abe, T. BMP4 induces asymmetric cell division in human glioma stem-like cells. *Oncol. Lett.* **2020**, *19*, 1247–1254. [CrossRef] [PubMed]
341. Dalmo, E.; Johansson, P.; Niklasson, M.; Gustavsson, I.; Nelander, S.; Westermark, B. Growth-Inhibitory Activity of Bone Morphogenetic Protein 4 in Human Glioblastoma Cell Lines Is Heterogeneous and Dependent on Reduced SOX2 Expression. *Mol. Cancer Res.* **2020**, *18*, 981–991. [CrossRef] [PubMed]
342. Kaye, J.; Mondal, A.; Foty, R.; Jia, D.; Langenfeld, J. Bone morphogenetic protein receptor inhibitors suppress the growth of glioblastoma cells. *Mol. Cell Biochem.* **2022**, *477*, 1583–1595. [CrossRef] [PubMed]
343. Lasorella, A.; Benezra, R.; Iavarone, A. The ID proteins: Master regulators of cancer stem cells and tumour aggressiveness. *Nat. Rev. Cancer* **2014**, *14*, 77–91. [CrossRef] [PubMed]
344. Rampazzo, E.; Dettin, M.; Maule, F.; Scabello, A.; Calvanese, L.; D'Auria, G.; Falcigno, L.; Porcu, E.; Zamuner, A.; Della Puppa, A.; et al. A synthetic BMP-2 mimicking peptide induces glioblastoma stem cell differentiation. *Biochim. Biophys. Acta Gen. Subj.* **2017**, *1861*, 2282–2292. [CrossRef]

345. Lowery, J.W.; Rosen, V. Bone Morphogenetic Protein-Based Therapeutic Approaches. *Cold Spring Harb. Perspect. Biol.* **2018**, *10*, a022327. [CrossRef]
346. Huang, J.; Wu, S.; Barrera, J.; Matthews, K.; Pan, D. The Hippo signaling pathway coordinately regulates cell proliferation and apoptosis by inactivating Yorkie, the Drosophila Homolog of YAP. *Cell* **2005**, *122*, 421–434. [CrossRef]
347. Halder, G.; Johnson, R.L. Hippo signaling: Growth control and beyond. *Development* **2011**, *138*, 9–22. [CrossRef]
348. Bae, S.J.; Luo, X. Activation mechanisms of the Hippo kinase signaling cascade. *Biosci. Rep.* **2018**, *38*, BSR20171469. [CrossRef]
349. Nishio, M.; Goto, H.; Suzuki, M.; Fujimoto, A.; Mimori, K.; Suzuki, A. The Hippo Signaling Pathway: A Candidate New Drug Target for Malignant Tumors. In *Innovative Medicine*; Nakao, K., Minato, N., Uemoto, S., Eds.; Springer: Tokyo, Japan, 2015.
350. Zhao, B.; Wei, X.; Li, W.; Udan, R.S.; Yang, Q.; Kim, J.; Xie, J.; Ikenoue, T.; Yu, J.; Li, L.; et al. Inactivation of YAP oncoprotein by the Hippo pathway is involved in cell contact inhibition and tissue growth control. *Genes Dev.* **2007**, *21*, 2747–2761. [CrossRef]
351. Pobbati, A.V.; Hong, W. Emerging roles of TEAD transcription factors and its coactivators in cancers. *Cancer Biol.* **2013**, *14*, 390–398. [CrossRef]
352. Meng, Z.; Moroishi, T.; Guan, K.L. Mechanisms of Hippo pathway regulation. *Genes Dev.* **2016**, *30*, 1–17. [CrossRef]
353. Zanconato, F.; Cordenonsi, M.; Piccolo, S. YAP/TAZ at the Roots of Cancer. *Cancer Cell* **2016**, *29*, 783–803. [CrossRef]
354. Johnson, R.; Halder, G. The two faces of Hippo: Targeting the Hippo pathway for regenerative medicine and cancer treatment. *Nat. Rev. Drug Discov.* **2014**, *13*, 63–79. [CrossRef]
355. Orr, B.A.; Bai, H.; Ochia, Y.; Jain, D.; Anders, R.A.; Eberhart, C.G. Yes-associated protein 1 is widely expressed in human brain tumors and promotes glioblastoma growth. *J. Neuropathol. Exp. Neurol.* **2011**, *70*, 568–577. [CrossRef]
356. Castellan, M.; Guarnieri, A.; Fujimura, A.; Zanconato, F.; Battilana, G.; Panciera, T.; Sladitschek, H.L.; Contessotto, P.; Citron, A.; Grilli, A.; et al. Single-cell analyses reveal YAP/TAZ as regulators of stemness and cell plasticity in Glioblastoma. *Nat. Cancer* **2021**, *2*, 174–188. [CrossRef]
357. Fernandez, L.A.; Squatrito, M.; Northcott, P.; Awan, A.; Holland, E.C.; Taylor, M.D.; Nahle, Z.; Kenney, A.M. Oncogenic YAP promotes radioresistance and genomic instability in medulloblastoma through IGF2-mediated Akt activation. *Oncogene* **2012**, *31*, 1923–1937. [CrossRef]
358. Tian, T.; Li, A.; Lu, H.; Luo, R.; Zhang, M.; Li, Z. TAZ promotes temozolomide resistance by upregulating MCL-1 in human glioma cells. *Biochem. Biophys. Res. Commun.* **2015**, *463*, 638–643. [CrossRef]
359. Liu-Chittenden, Y.; Huang, B.; Shim, J.S.; Chen, Q.; Lee, S.J.; Anders, R.A.; Liu, J.O.; Pan, D. Genetic and pharmacological disruption of the TEAD-YAP complex suppresses the oncogenic activity of YAP. *Genes Dev.* **2012**, *26*, 1300–1305. [CrossRef]
360. Hill, J.S.; Kaye, A.H.; Sawyer, W.H.; Morstyn, G.; Megison, P.D.; Stylli, S.S. Selective uptake of hematoporphyrin derivative into human cerebral glioma. *Neurosurgery* **1990**, *26*, 248–254. [CrossRef]
361. Vigneswaran, K.; Boyd, N.H.; Oh, S.Y.; Lallani, S.; Boucher, A.; Neill, S.G.; Olson, J.J.; Read, R.D. YAP/TAZ Transcriptional Coactivators Create Therapeutic Vulnerability to Verteporfin in EGFR-mutant Glioblastoma. *Clin. Cancer Res.* **2021**, *27*, 1553–1569. [CrossRef]
362. Han, W.; Guan, W. Valproic Acid: A Promising Therapeutic Agent in Glioma Treatment. *Front. Oncol.* **2021**, *11*, 687362. [CrossRef]
363. Knupfer, M.M.; Hernaiz-Driever, P.; Poppenborg, H.; Wolff, J.E.; Cinatl, J. Valproic acid inhibits proliferation and changes expression of CD44 and CD56 of malignant glioma cells in vitro. *Anticancer Res.* **1998**, *18*, 3585–3589.
364. Xu, Y.; Stamenkovic, I.; Yu, Q. CD44 attenuates activation of the hippo signaling pathway and is a prime therapeutic target for glioblastoma. *Cancer Res.* **2010**, *70*, 2455–2464. [CrossRef]
365. Valiyaveetil, D.; Malik, M.; Joseph, D.M.; Ahmed, S.F.; Kothwal, S.A.; Vijayasaradhi, M. Effect of valproic acid on survival in glioblastoma: A prospective single-arm study. *South. Asian J. Cancer* **2018**, *7*, 159–162. [CrossRef]
366. Yuan, Y.; Xiang, W.; Qing, M.; Yanhui, L.; Jiewen, L.; Yunhe, M. Survival analysis for valproic acid use in adult glioblastoma multiforme: A meta-analysis of individual patient data and a systematic review. *Seizure* **2014**, *23*, 830–835. [CrossRef]
367. Liu, Z.; Wei, Y.; Zhang, L.; Yee, P.P.; Johnson, M.; Zhang, X.; Gulley, M.; Atkinson, J.M.; Trebak, M.; Wang, H.G.; et al. Induction of store-operated calcium entry (SOCE) suppresses glioblastoma growth by inhibiting the Hippo pathway transcriptional coactivators YAP/TAZ. *Oncogene* **2019**, *38*, 120–139. [CrossRef]
368. Miller, P.D.; Chines, A.A.; Christiansen, C.; Hoeck, H.C.; Kendler, D.L.; Lewiecki, E.M.; Woodson, G.; Levine, A.B.; Constantine, G.; Delmas, P.D. Effects of bazedoxifene on BMD and bone turnover in postmenopausal women: 2-yr results of a randomized, double-blind, placebo-, and active-controlled study. *J. Bone Min. Res.* **2008**, *23*, 525–535. [CrossRef]
369. Wu, X.; Cao, Y.; Xiao, H.; Li, C.; Lin, J. Bazedoxifene as a Novel GP130 Inhibitor for Pancreatic Cancer Therapy. *Mol. Cancer* **2016**, *15*, 2609–2619. [CrossRef] [PubMed]
370. Fu, W.; Zhao, P.; Li, H.; Fu, H.; Liu, X.; Liu, Y.; Wu, J.; Fu, W. Bazedoxifene enhances paclitaxel efficacy to suppress glioblastoma via altering Hippo/YAP pathway. *J. Cancer* **2020**, *11*, 657–667. [CrossRef] [PubMed]
371. Wightman, S.M.; Alban, T.J.; Chen, X.; Lathia, J.D.; Wang, Y.; Stark, G.R. Bazedoxifene inhibits sustained STAT3 activation and increases survival in GBM. *Transl. Oncol.* **2021**, *14*, 101192. [CrossRef] [PubMed]
372. Xiao, A.; Brenneman, B.; Floyd, D.; Comeau, L.; Spurio, K.; Olmez, I.; Lee, J.; Nakano, I.; Godlewski, J.; Bronisz, A.; et al. Statins affect human glioblastoma and other cancers through TGF-beta inhibition. *Oncotarget* **2019**, *10*, 1716–1728. [CrossRef]
373. Oku, Y.; Nishiya, N.; Shito, T.; Yamamoto, R.; Yamamoto, Y.; Oyama, C.; Uehara, Y. Small molecules inhibiting the nuclear localization of YAP/TAZ for chemotherapeutics and chemosensitizers against breast cancers. *FEBS Open Bio* **2015**, *5*, 542–549. [CrossRef]

374. Xie, Y.; Lu, Q.; Lenahan, C.; Yang, S.; Zhou, D.; Qi, X. Whether statin use improves the survival of patients with glioblastoma?: A meta-analysis. *Medicine* **2020**, *99*, e18997. [CrossRef]
375. Cunningham, T.J.; Duester, G. Mechanisms of retinoic acid signalling and its roles in organ and limb development. *Nat. Rev. Mol. Cell Biol.* **2015**, *16*, 110–123. [CrossRef]
376. Wiesinger, A.; Boink, G.J.J.; Christoffels, V.M.; Devalla, H.D. Retinoic acid signaling in heart development: Application in the differentiation of cardiovascular lineages from human pluripotent stem cells. *Stem Cell Rep.* **2021**, *16*, 2589–2606. [CrossRef]
377. Dubey, A.; Rose, R.E.; Jones, D.R.; Saint-Jeannet, J.P. Generating retinoic acid gradients by local degradation during craniofacial development: One cell's cue is another cell's poison. *Genesis* **2018**, *56*, e23091. [CrossRef]
378. Ni, X.; Hu, G.; Cai, X. The success and the challenge of all-trans retinoic acid in the treatment of cancer. *Crit. Rev. Food Sci. Nutr.* **2019**, *59*, S71–S80. [CrossRef]
379. Ozgun, G.; Senturk, S.; Erkek-Ozhan, S. Retinoic acid signaling and bladder cancer: Epigenetic deregulation, therapy and beyond. *Int. J. Cancer* **2020**, *148*, 2364–2374. [CrossRef]
380. Thompson, B.; Katsanis, N.; Apostolopoulos, N.; Thompson, D.C.; Nebert, D.W.; Vasilioi, V. Genetics and functions of the retinoic acid pathway, with special emphasis on the eye. *Hum. Genom.* **2019**, *13*, 61. [CrossRef]
381. Fex, G.; Johannesson, G. Retinol transfer across and between phospholipid bilayer membranes. *Biochim. Biophys. Acta* **1988**, *944*, 249–255. [CrossRef]
382. Luo, T.; Wagner, E.; Drager, U.C. Integrating retinoic acid signaling with brain function. *Dev. Psychol.* **2009**, *45*, 139–150. [CrossRef]
383. Hunsu, V.O.; Facey, C.O.B.; Fields, J.Z.; Boman, B.M. Retinoids as Chemo-Preventive and Molecular-Targeted Anti-Cancer Therapies. *Int. J. Mol. Sci.* **2021**, *22*, 7731. [CrossRef] [PubMed]
384. Al Tanoury, Z.; Piskunov, A.; Rochette-Egly, C. Vitamin A and retinoid signaling: Genomic and nongenomic effects. *J. Lipid Res.* **2013**, *54*, 1761–1775. [CrossRef] [PubMed]
385. Agnihotri, S.; Mansouri, S.; Burrell, K.; Li, M.; Mamatjan, Y.; Liu, J.; Nejad, R.; Kumar, S.; Jalali, S.; Singh, S.K.; et al. Ketoconazole and Posaconazole Selectively Target HK2-expressing Glioblastoma Cells. *Clin. Cancer Res.* **2019**, *25*, 844–855. [CrossRef] [PubMed]
386. Chattopadhyay, N.; Butters, R.R.; Brown, E.M. Agonists of the retinoic acid- and retinoid X-receptors inhibit hepatocyte growth factor secretion and expression in U87 human astrocytoma cells. *Brain Res. Mol. Brain Res.* **2001**, *87*, 100–108. [CrossRef]
387. Costa, S.L.; Paillaud, E.; Fages, C.; Rochette-Egly, C.; Plassat, J.L.; Jouault, H.; Perzelova, A.; Tardy, M. Effects of a novel synthetic retinoid on malignant glioma in vitro: Inhibition of cell proliferation, induction of apoptosis and differentiation. *Eur. J. Cancer* **2001**, *37*, 520–530. [CrossRef]
388. Hacioglu, C.; Kar, F.; Kacar, S.; Sahinturk, V.; Kanbak, G. Bexarotene inhibits cell proliferation by inducing oxidative stress, DNA damage and apoptosis via PPARgamma/NF-kappaB signaling pathway in C6 glioma cells. *Med. Oncol.* **2021**, *38*, 31. [CrossRef] [PubMed]
389. Lena, A.; Rechichi, M.; Salvetti, A.; Bartoli, B.; Vecchio, D.; Scarcelli, V.; Amoroso, R.; Benvenuti, L.; Gagliardi, R.; Gremigni, V.; et al. Drugs targeting the mitochondrial pore act as cytotoxic and cytostatic agents in temozolomide-resistant glioma cells. *J. Transl. Med.* **2009**, *7*, 13. [CrossRef]
390. Yokosawa, M.; Sonoda, Y.; Sugiyama, S.; Saito, R.; Yamashita, Y.; Nishihara, M.; Satoh, T.; Kumabe, T.; Yokoyama, M.; Tominaga, T. Convection-enhanced delivery of a synthetic retinoid Am80, loaded into polymeric micelles, prolongs the survival of rats bearing intracranial glioblastoma xenografts. *Tohoku J. Exp. Med.* **2010**, *221*, 257–264. [CrossRef]
391. Di Masi, A.; Leboffe, L.; De Marinis, E.; Pagano, F.; Cicconi, L.; Rochette-Egly, C.; Lo-Coco, F.; Ascenzi, P.; Nervi, C. Retinoic acid receptors: From molecular mechanisms to cancer therapy. *Mol. Asp. Med.* **2015**, *41*, 1–115. [CrossRef]
392. Li, M.; Sun, Y.; Guan, X.; Shu, X.; Li, C. Advanced progress on the relationship between RA and its receptors and malignant tumors. *Crit. Rev. Oncol. Hematol.* **2014**, *91*, 271–282. [CrossRef]
393. Chou, A.P.; Chowdhury, R.; Li, S.; Chen, W.; Kim, A.J.; Piccioni, D.E.; Selfridge, J.M.; Mody, R.R.; Chang, S.; Lalezari, S.; et al. Identification of retinol binding protein 1 promoter hypermethylation in isocitrate dehydrogenase 1 and 2 mutant gliomas. *J. Natl. Cancer Inst.* **2012**, *104*, 1458–1469. [CrossRef]
394. Campos, B.; Warta, R.; Chaisaingmongkol, J.; Geiselhart, L.; Popanda, O.; Hartmann, C.; von Deimling, A.; Unterberg, A.; Plass, C.; Schmezer, P.; et al. Epigenetically mediated downregulation of the differentiation-promoting chaperon protein CRABP2 in astrocytic gliomas. *Int. J. Cancer* **2012**, *131*, 1963–1968. [CrossRef]
395. Sanders, S.; Herpai, D.M.; Rodriguez, A.; Huang, Y.; Chou, J.; Hsu, F.C.; Seals, D.; Mott, R.; Miller, L.D.; Debinski, W. The Presence and Potential Role of ALDH1A2 in the Glioblastoma Microenvironment. *Cells* **2021**, *10*, 2485. [CrossRef]
396. Campos, B.; Weisang, S.; Osswald, F.; Ali, R.; Sedlmeier, G.; Bageritz, J.; Mallm, J.P.; Hartmann, C.; von Deimling, A.; Popanda, O.; et al. Retinoid resistance and multifaceted impairment of retinoic acid synthesis in glioblastoma. *Glia* **2015**, *63*, 1850–1859. [CrossRef]
397. Barbus, S.; Tews, B.; Karra, D.; Hahn, M.; Radlwimmer, B.; Delhomme, N.; Hartmann, C.; Felsberg, J.; Krex, D.; Schackert, G.; et al. Differential retinoic acid signaling in tumors of long- and short-term glioblastoma survivors. *J. Natl. Cancer Inst.* **2011**, *103*, 598–606. [CrossRef]
398. Piperi, C.; Themistocleous, M.S.; Papavassiliou, G.A.; Farmaki, E.; Levidou, G.; Korkolopoulou, P.; Adamopoulos, C.; Papavassiliou, A.G. High incidence of MGMT and RARbeta promoter methylation in primary glioblastomas: Association with histopathological characteristics, inflammatory mediators and clinical outcome. *Mol. Med.* **2010**, *16*, 1–9. [CrossRef]

399. Bouterfa, H.; Picht, T.; Kess, D.; Herbold, C.; Noll, E.; Black, P.M.; Roosen, K.; Tonn, J.C. Retinoids inhibit human glioma cell proliferation and migration in primary cell cultures but not in established cell lines. *Neurosurgery* **2000**, *46*, 419–430. [CrossRef]
400. Campos, B.; Wan, F.; Farhadi, M.; Ernst, A.; Zeppernick, F.; Tagscherer, K.E.; Ahmadi, R.; Lohr, J.; Dictus, C.; Gdynia, G.; et al. Differentiation therapy exerts antitumor effects on stem-like glioma cells. *Clin. Cancer Res.* **2010**, *16*, 2715–2728. [CrossRef]
401. Rodriguez, V.; Bailey, R.; Larion, M.; Gilbert, M.R. Retinoid receptor turnover mediated by sumoylation, ubiquitination and the valosin-containing protein is disrupted in glioblastoma. *Sci. Rep.* **2019**, *9*, 16250. [CrossRef]
402. Paillaud, E.; Costa, S.; Fages, C.; Plassat, J.L.; Rochette-Egly, C.; Monville, C.; Tardy, M. Retinoic acid increases proliferation rate of GL-15 glioma cells, involving activation of STAT-3 transcription factor. *J. Neurosci. Res.* **2002**, *67*, 670–679. [CrossRef] [PubMed]
403. Chen, P.H.; Shih, C.M.; Chang, W.C.; Cheng, C.H.; Lin, C.W.; Ho, K.H.; Su, P.C.; Chen, K.C. MicroRNA-302b-inhibited E2F3 transcription factor is related to all trans retinoic acid-induced glioma cell apoptosis. *J. Neurochem.* **2014**, *131*, 731–742. [CrossRef] [PubMed]
404. Haque, A.; Das, A.; Hajiaghamohseni, L.M.; Younger, A.; Banik, N.L.; Ray, S.K. Induction of apoptosis and immune response by all-trans retinoic acid plus interferon-gamma in human malignant glioblastoma T98G and U87MG cells. *Cancer Immunol. Immunother.* **2007**, *56*, 615–625. [CrossRef] [PubMed]
405. Marjanović Vičentić, J.; Schwirtlich, M.; Kovačević-Grujičić, N.; Stevanović, M.; Drakulić, D. All-trans retinoic acid influences viability, migration and adhesion of U251 glioblastoma cells. *Arch. Biol. Sci.* **2017**, *69*, 699–706. [CrossRef]
406. Zeng, Y.; Yang, Z.; Xu, J.G.; Yang, M.S.; Zeng, Z.X.; You, C. Differentially expressed genes from the glioblastoma cell line SHG-44 treated with all-trans retinoic acid in vitro. *J. Clin. Neurosci.* **2009**, *16*, 285–294. [CrossRef] [PubMed]
407. Wang, R.; Liu, C. All-trans retinoic acid therapy induces asymmetric division of glioma stem cells from the U87MG cell line. *Oncol. Lett.* **2019**, *18*, 3646–3654. [CrossRef] [PubMed]
408. Ling, G.Q.; Liu, Y.J.; Ke, Y.Q.; Chen, L.; Jiang, X.D.; Jiang, C.L.; Ye, W. All-trans retinoic acid impairs the vasculogenic mimicry formation ability of U87 stem-like cells through promoting differentiation. *Mol. Med. Rep.* **2015**, *12*, 165–172. [CrossRef]
409. Ying, M.; Wang, S.; Sang, Y.; Sun, P.; Lal, B.; Goodwin, C.R.; Guerrero-Cazares, H.; Quinones-Hinojosa, A.; Lathera, J.; Xia, S. Regulation of glioblastoma stem cells by retinoic acid: Role for Notch pathway inhibition. *Oncogene* **2011**, *30*, 3454–3467. [CrossRef]
410. Karsy, M.; Albert, L.; Tobias, M.E.; Murali, R.; Jhanwar-Uniyal, M. All-trans retinoic acid modulates cancer stem cells of glioblastoma multiforme in an MAPK-dependent manner. *Anticancer Res.* **2010**, *30*, 4915–4920.
411. Niu, C.S.; Li, M.W.; Ni, Y.F.; Chen, J.M.; Mei, J.M.; Li, J.; Fu, X.M. Effect of all-trans retinoic acid on the proliferation and differentiation of brain tumor stem cells. *J. Exp. Clin. Cancer Res.* **2010**, *29*, 113. [CrossRef]
412. Choschzick, I.; Hirseland, E.; Cramer, H.; Schultz, S.; Leppert, J.; Tronnier, V.; Zechel, C. Responsiveness of stem-like human glioma cells to all-trans retinoic acid and requirement of retinoic acid receptor isotypes alpha, beta and gamma. *Neuroscience* **2014**, *279*, 44–64. [CrossRef]
413. Reboul, P.; George, P.; Louisot, P.; Broquet, P. Study of retinoic acid effect upon retinoic acid receptors beta (RAR-beta) in C6 cultured glioma cells. *Biochem. Mol. Biol. Int.* **1995**, *36*, 1097–1105.
414. Rodts, G.E., Jr.; Black, K.L. Trans retinoic acid inhibits in vivo tumour growth of C6 glioma in rats: Effect negatively influenced by nerve growth factor. *Neurol. Res.* **1994**, *16*, 184–186. [CrossRef]
415. See, S.J.; Levin, V.A.; Yung, W.K.; Hess, K.R.; Groves, M.D. 13-cis-retinoic acid in the treatment of recurrent glioblastoma multiforme. *Neuro-Oncology* **2004**, *6*, 253–258. [CrossRef]
416. Tang, K.; Cao, L.; Fan, S.Q.; Wu, M.H.; Huang, H.; Zhou, Y.H.; Zhou, M.; Tang, Y.L.; Wang, R.; Zeng, F.; et al. Effect of all-trans-retinoic acid on C6 glioma cell proliferation and differentiation. *Zhong Nan Da Xue Xue Bao Yi Xue Ban* **2008**, *33*, 892–897.
417. Milanovic, D.; Maier, P.; Lohr, F.; Wenz, F.; Herskind, C. Inhibition of 13-cis retinoic acid-induced gene expression of homeobox B7 by thalidomide. *Int. J. Cancer* **2007**, *121*, 1205–1211. [CrossRef]
418. Heo, J.C.; Jung, T.H.; Lee, S.; Kim, H.Y.; Choi, G.; Jung, M.; Jung, D.; Lee, H.K.; Lee, J.O.; Park, J.H.; et al. Effect of bexarotene on differentiation of glioblastoma multiforme compared with ATRA. *Clin. Exp. Metastasis* **2016**, *33*, 417–429. [CrossRef]
419. Shi, L.; Li, H.; Zhan, Y. All-trans retinoic acid enhances temozolomide-induced autophagy in human glioma cells U251 via targeting Keap1/Nrf2/ARE signaling pathway. *Oncol. Lett.* **2017**, *14*, 2709–2714. [CrossRef]
420. Karmakar, S.; Banik, N.L.; Patel, S.J.; Ray, S.K. Combination of all-trans retinoic acid and taxol regressed glioblastoma T98G xenografts in nude mice. *Apoptosis* **2007**, *12*, 2077–2087. [CrossRef]
421. Karmakar, S.; Banik, N.L.; Ray, S.K. Combination of all-trans retinoic acid and paclitaxel-induced differentiation and apoptosis in human glioblastoma U87MG xenografts in nude mice. *Cancer* **2008**, *112*, 596–607. [CrossRef]
422. Karmakar, S.; Choudhury, S.R.; Banik, N.L.; Ray, S.K. Activation of Multiple Molecular Mechanisms for Increasing Apoptosis in Human Glioblastoma T98G Xenograft. *J. Cancer Sci.* **2010**, *2*, 107–113. [CrossRef]
423. Songthaveesin, C.; Sa-Nongdej, W.; Limboonreung, T.; Chongthammakun, S. Combination of metformin and 9-cis retinoic acid increases apoptosis in C6 glioma stem-like cells. *Heliyon* **2018**, *4*, e00638. [CrossRef]
424. Milanovic, D.; Sticht, C.; Rohrich, M.; Maier, P.; Grosu, A.L.; Herskind, C. Inhibition of 13-cis retinoic acid-induced gene expression of reactive-resistance genes by thalidomide in glioblastoma tumours in vivo. *Oncotarget* **2015**, *6*, 28938–28948. [CrossRef]
425. Papi, A.; Tatenhorst, L.; Terwel, D.; Hermes, M.; Kummer, M.P.; Orlandi, M.; Heneka, M.T. PPARgamma and RXRgamma ligands act synergistically as potent antineoplastic agents in vitro and in vivo glioma models. *J. Neurochem.* **2009**, *109*, 1779–1790. [CrossRef] [PubMed]

426. Pitz, M.W.; Lipson, M.; Hosseini, B.; Lambert, P.; Guilbert, K.; Lister, D.; Schroeder, G.; Jones, K.; Mihalicioiu, C.; Eisenstat, D.D. Extended adjuvant temozolomide with cis-retinoic acid for adult glioblastoma. *Curr. Oncol.* **2012**, *19*, 308–314. [CrossRef] [PubMed]
427. Butowski, N.; Prados, M.D.; Lamborn, K.R.; Larson, D.A.; Sneed, P.K.; Wara, W.M.; Malec, M.; Rabbitt, J.; Page, M.; Chang, S.M. A phase II study of concurrent temozolomide and cis-retinoic acid with radiation for adult patients with newly diagnosed supratentorial glioblastoma. *Int. J. Radiat. Oncol. Biol. Phys.* **2005**, *61*, 1454–1459. [CrossRef] [PubMed]
428. Puduvalli, V.K.; Yung, W.K.; Hess, K.R.; Kuhn, J.G.; Groves, M.D.; Levin, V.A.; Zwiebel, J.; Chang, S.M.; Cloughesy, T.F.; Junck, L.; et al. Phase II study of fenretinide (NSC 374551) in adults with recurrent malignant gliomas: A North American Brain Tumor Consortium study. *J. Clin. Oncol.* **2004**, *22*, 4282–4289. [CrossRef]
429. Levin, V.A.; Giglio, P.; Puduvalli, V.K.; Jochec, J.; Groves, M.D.; Yung, W.K.; Hess, K. Combination chemotherapy with 13-cis-retinoic acid and celecoxib in the treatment of glioblastoma multiforme. *J. Neurooncol.* **2006**, *78*, 85–90. [CrossRef]
430. Jaecle, K.A.; Hess, K.R.; Yung, W.K.; Greenberg, H.; Fine, H.; Schiff, D.; Pollack, I.F.; Kuhn, J.; Fink, K.; Mehta, M.; et al. Phase II evaluation of temozolomide and 13-cis-retinoic acid for the treatment of recurrent and progressive malignant glioma: A North American Brain Tumor Consortium study. *J. Clin. Oncol.* **2003**, *21*, 2305–2311. [CrossRef]
431. Ferreira, R.; Napoli, J.; Enver, T.; Bernardino, L.; Ferreira, L. Advances and challenges in retinoid delivery systems in regenerative and therapeutic medicine. *Nat. Commun.* **2020**, *11*, 4265. [CrossRef]
432. Jeong, Y.I.; Kim, S.H.; Jung, T.Y.; Kim, I.Y.; Kang, S.S.; Jin, Y.H.; Ryu, H.H.; Sun, H.S.; Jin, S.; Kim, K.K.; et al. Polyion complex micelles composed of all-trans retinoic acid and poly (ethylene glycol)-grafted-chitosan. *J. Pharm. Sci.* **2006**, *95*, 2348–2360. [CrossRef]
433. Jones, T.; Zhang, B.; Major, S.; Webb, A. All-trans retinoic acid eluting poly(diols citrate) wafers for treatment of glioblastoma. *J. Biomed. Mater. Res. B Appl. Biomater.* **2020**, *108*, 619–628. [CrossRef]
434. Reifenberger, G.; Liu, L.; Ichimura, K.; Schmidt, E.E.; Collins, V.P. Amplification and overexpression of the MDM2 gene in a subset of human malignant gliomas without p53 mutations. *Cancer Res.* **1993**, *53*, 2736–2739.
435. Izumoto, S.; Arita, N.; Ohnishi, T.; Hiraga, S.; Taki, T.; Tomita, N.; Ohue, M.; Hayakawa, T. Microsatellite instability and mutated type II transforming growth factor-beta receptor gene in gliomas. *Cancer Lett.* **1997**, *112*, 251–256. [CrossRef]
436. Suzuki, H.; Aoki, K.; Chiba, K.; Sato, Y.; Shiozawa, Y.; Shiraishi, Y.; Shimamura, T.; Niida, A.; Motomura, K.; Ohka, F.; et al. Mutational landscape and clonal architecture in grade II and III gliomas. *Nat. Genet.* **2015**, *47*, 458–468. [CrossRef]
437. Sakthikumar, S.; Roy, A.; Haseeb, L.; Pettersson, M.E.; Sundstrom, E.; Marinescu, V.D.; Lindblad-Toh, K.; Forsberg-Nilsson, K. Whole-genome sequencing of glioblastoma reveals enrichment of non-coding constraint mutations in known and novel genes. *Genome Biol.* **2020**, *21*, 127. [CrossRef]
438. Madsen, H.; Hellwinkel, J.E.; Graner, M.W. Clinical Trials in Glioblastoma—Designs and Challenges. In *Molecular Considerations and Evolving Surgical Management Issues in the Treatment of Patients with a Brain Tumor*; Lichtor, T., Ed.; IntechOpen: Rijeka, Croatia, 2015. [CrossRef]
439. Park, A.K.; Kim, P.; Ballester, L.Y.; Esquenazi, Y.; Zhao, Z. Subtype-specific signaling pathways and genomic aberrations associated with prognosis of glioblastoma. *Neuro-Oncology* **2019**, *21*, 59–70. [CrossRef]
440. El-Sehemy, A.; Selvadurai, H.; Ortin-Martinez, A.; Pokrajac, N.; Mamatjan, Y.; Tachibana, N.; Rowland, K.; Lee, L.; Park, N.; Aldape, K.; et al. Notch mediates tumor-promoting and -suppressive effects in glioblastoma via Notch and Wnt. *J. Clin. Investig.* **2020**, *130*, 3069–3086. [CrossRef]
441. Lin, C.J.; Chen, T.L.; Tseng, Y.Y.; Wu, G.J.; Hsieh, M.H.; Lin, Y.W.; Chen, R.M. Honokiol induces autophagic cell death in malignant glioma through reactive oxygen species-mediated regulation of the p53/PI3K/Akt/mTOR signaling pathway. *Toxicol. Appl. Pharm.* **2016**, *304*, 59–69. [CrossRef]
442. Jung, Y.; Park, H.; Zhao, H.Y.; Jeon, R.; Ryu, J.H.; Kim, W.Y. Systemic approaches identify a garlic-derived chemical, Z-ajoene, as a glioblastoma multiforme cancer stem cell-specific targeting agent. *Mol. Cells* **2014**, *37*, 547–553. [CrossRef]
443. Ivkovic, I.; Novakovic, M.; Veljic, M.; Mojsin, M.; Stevanovic, M.; Marin, P.D.; Bukvicki, D. Bis-Bibenzyls from the Liverwort *Pellia endiviifolia* and Their Biological Activity. *Plants* **2021**, *10*, 1063. [CrossRef]
444. Stojkovic, D.; Drakulic, D.; Dias, M.I.; Zengin, G.; Barros, L.; Ivanov, M.; Gasic, U.; Rajcevic, N.; Stevanovic, M.; Ferreira, I.; et al. *Phlomis fruticosa* L. exerts in vitro antineurodegenerative and antioxidant activities and induces prooxidant effect in glioblastoma cell line. *EXCLI J.* **2022**, *21*, 387–399. [CrossRef]
445. Stojkovic, D.; Drakulic, D.; Gasic, U.; Zengin, G.; Stevanovic, M.; Rajcevic, N.; Sokovic, M. *Ononis spinosa* L., an edible and medicinal plant: UHPLC-LTQ-Orbitrap/MS chemical profiling and biological activities of the herbal extract. *Food Funct.* **2020**, *11*, 7138–7151. [CrossRef]
446. Stojkovic, D.; Drakulic, D.; Schwirtlich, M.; Rajcevic, N.; Stevanovic, M.; Sokovic, M.D.; Gasic, U. Extract of *Herba Anthrisci cerefolii*: Chemical Profiling and Insights into Its Anti-Glioblastoma and Antimicrobial Mechanism of Actions. *Pharmaceuticals* **2021**, *14*, 55. [CrossRef]
447. Mariappan, A.; Goranci-Buzhala, G.; Ricci-Vitiani, L.; Pallini, R.; Gopalakrishnan, J. Trends and challenges in modeling glioma using 3D human brain organoids. *Cell Death Differ.* **2021**, *28*, 15–23. [CrossRef]
448. Goranci-Buzhala, G.; Mariappan, A.; Gabriel, E.; Ramani, A.; Ricci-Vitiani, L.; Buccarelli, M.; D’Alessandris, Q.G.; Pallini, R.; Gopalakrishnan, J. Rapid and Efficient Invasion Assay of Glioblastoma in Human Brain Organoids. *Cell Rep.* **2020**, *31*, 107738. [CrossRef]

449. Chadwick, M.; Yang, C.; Liu, L.; Gamboa, C.M.; Jara, K.; Lee, H.; Sabaawy, H.E. Rapid Processing and Drug Evaluation in Glioblastoma Patient-Derived Organoid Models with 4D Bioprinted Arrays. *iScience* **2020**, *23*, 101365. [CrossRef]
450. Stankovic, T.; Randelovic, T.; Dragoj, M.; Stojkovic Buric, S.; Fernandez, L.; Ochoa, I.; Perez-Garcia, V.M.; Pestic, M. In vitro biomimetic models for glioblastoma—a promising tool for drug response studies. *Drug Resist. Updat.* **2021**, *55*, 100753. [CrossRef]
451. Alomari, S.; Zhang, I.; Hernandez, A.; Kraft, C.Y.; Raj, D.; Kedda, J.; Tyler, B. Drug Repurposing for Glioblastoma and Current Advances in Drug Delivery—A Comprehensive Review of the Literature. *Biomolecules* **2021**, *11*, 1870. [CrossRef]
452. Aghabegi Moghanjoughi, A.; Khoshnevis, D.; Zarrabi, A. A concise review on smart polymers for controlled drug release. *Drug Deliv. Transl. Res.* **2016**, *6*, 333–340. [CrossRef]
453. Nouri, Z.; Fakhri, S.; Nouri, K.; Wallace, C.E.; Farzaei, M.H.; Bishayee, A. Targeting Multiple Signaling Pathways in Cancer: The Rutin Therapeutic Approach. *Cancers* **2020**, *12*, 2276. [CrossRef] [PubMed]
454. Fathi, M.; Sahandi Zangabad, P.; Majidi, S.; Barar, J.; Erfan-Niya, H.; Omid, Y. Stimuli-responsive chitosan-based nanocarriers for cancer therapy. *Bioimpacts* **2017**, *7*, 269–277. [CrossRef] [PubMed]
455. Liu, M.; Du, H.; Zhang, W.; Zhai, G. Internal stimuli-responsive nanocarriers for drug delivery: Design strategies and applications. *Mater. Sci. Eng. C Mater. Biol. Appl.* **2017**, *71*, 1267–1280. [CrossRef] [PubMed]
456. Hodi, F.S.; O’Day, S.J.; McDermott, D.F.; Weber, R.W.; Sosman, J.A.; Haanen, J.B.; Gonzalez, R.; Robert, C.; Schadendorf, D.; Hassel, J.C.; et al. Improved survival with ipilimumab in patients with metastatic melanoma. *N. Engl. J. Med.* **2010**, *363*, 711–723. [CrossRef]
457. Kazandjian, D.; Suzman, D.L.; Blumenthal, G.; Mushti, S.; He, K.; Libeg, M.; Keegan, P.; Pazdur, R. FDA Approval Summary: Nivolumab for the Treatment of Metastatic Non-Small Cell Lung Cancer with Progression on or after Platinum-Based Chemotherapy. *Oncologist* **2016**, *21*, 634–642. [CrossRef]
458. Yu, M.W.; Quail, D.F. Immunotherapy for Glioblastoma: Current Progress and Challenges. *Front. Immunol.* **2021**, *12*, 676301. [CrossRef]
459. Bausart, M.; Preat, V.; Malfanti, A. Immunotherapy for glioblastoma: The promise of combination strategies. *J. Exp. Clin. Cancer Res.* **2022**, *41*, 35. [CrossRef]
460. Chan, H.Y.; Choi, J.; Jackson, C.; Lim, M. Combination immunotherapy strategies for glioblastoma. *J. Neurooncol.* **2021**, *151*, 375–391. [CrossRef]
461. Yuan, B.; Wang, G.; Tang, X.; Tong, A.; Zhou, L. Immunotherapy of glioblastoma: Recent advances and future prospects. *Hum. Vaccines Immunother.* **2022**, *18*, 2055417. [CrossRef]
462. Gonzalez Castro, L.N.; Tirosh, I.; Suva, M.L. Decoding Cancer Biology One Cell at a Time. *Cancer Discov.* **2021**, *11*, 960–970. [CrossRef]
463. Tirosh, I.; Suva, M.L. Dissecting human gliomas by single-cell RNA sequencing. *Neuro-Oncology* **2018**, *20*, 37–43. [CrossRef]
464. Suva, M.L.; Tirosh, I. The Glioma Stem Cell Model in the Era of Single-Cell Genomics. *Cancer Cell* **2020**, *37*, 630–636. [CrossRef]

Review

Ribosomes and Ribosomal Proteins Promote Plasticity and Stemness Induction in Glioma Cells via Reprogramming

Takuichiro Hide *, Ichiyo Shibahara , Madoka Inukai, Ryota Shigeeda and Toshihiro Kumabe

Department of Neurosurgery, Kitasato University School of Medicine, 1-15-1 Kitasato, Minami-ku, Sagami-hara 252-0374, Japan; ichiyoo@hotmail.com (I.S.); madoca@mtg.biglobe.ne.jp (M.I.); geshi.rugby.no2@gmail.com (R.S.); kuma@kitasato-u.ac.jp (T.K.)

* Correspondence: thide@med.kitasato-u.ac.jp; Tel.: +81-42-778-9337

Abstract: Glioblastoma multiforme (GBM) is a lethal tumor that develops in the adult brain. Despite advances in therapeutic strategies related to surgical resection and chemo-radiotherapy, the overall survival of patients with GBM remains unsatisfactory. Genetic research on mutation, amplification, and deletion in GBM cells is important for understanding the biological aggressiveness, diagnosis, and prognosis of GBM. However, the efficacy of drugs targeting the genetic abnormalities in GBM cells is limited. Investigating special microenvironments that induce chemo-radioresistance in GBM cells is critical to improving the survival and quality of life of patients with GBM. GBM cells acquire and maintain stem-cell-like characteristics via their intrinsic potential and extrinsic factors from their special microenvironments. The acquisition of stem-cell-like phenotypes and aggressiveness may be referred to as a reprogramming of GBM cells. In addition to protein synthesis, deregulation of ribosome biogenesis is linked to several diseases including cancer. Ribosomal proteins possess both tumor-promotive and -suppressive functions as extra-ribosomal functions. Incorporation of ribosomes and overexpression of ribosomal protein S6 reprogram and induce stem-cell-like phenotypes in GBM cells. Herein, we review recent literature and our published data on the acquisition of aggressiveness by GBM and discuss therapeutic options through reprogramming.

Keywords: ribosomal protein; reprogramming; glioblastoma; extra-ribosomal function; microenvironment; glioma stem cell; ribosomal protein S6; ribosome biogenesis; transdifferentiation; plasticity



Citation: Hide, T.; Shibahara, I.; Inukai, M.; Shigeeda, R.; Kumabe, T. Ribosomes and Ribosomal Proteins Promote Plasticity and Stemness Induction in Glioma Cells via Reprogramming. *Cells* **2022**, *11*, 2142. <https://doi.org/10.3390/cells11142142>

Academic Editors: Javier S. Castresana and Bárbara Meléndez

Received: 27 May 2022

Accepted: 5 July 2022

Published: 7 July 2022

Publisher's Note: MDPI stays neutral with regard to jurisdictional claims in published maps and institutional affiliations.



Copyright: © 2022 by the authors. Licensee MDPI, Basel, Switzerland. This article is an open access article distributed under the terms and conditions of the Creative Commons Attribution (CC BY) license (<https://creativecommons.org/licenses/by/4.0/>).

1. Introduction

The chemo-radioresistant characteristics and high recurrence potential of glioblastoma multiforme (GBM) pose major clinical problems in its treatment. Thus, the mean survival time of patients with GBM is approximately 1 year, and the 5-year overall survival rate is only 9.8% [1,2]. To improve the prognosis of patients with GBM, innovation in both the surgical tumor resection and chemo-radiotherapy is critical. GBM was classified into GBM, IDH-wildtype (primary GBM) and GBM, IDH-mutant (secondary GBM) in the fourth edition of the World Health Organization (WHO) classification of tumors of the central nervous system published in 2016 [3]. In the fifth edition published in 2021, GBM was only mentioned as GBM, IDH-wildtype; conversely, GBM, IDH-mutant was classified into astrocytoma, IDH-mutant [4].

GBM contains a small population of characteristic cells possessing stem-cell-like features, such as self-renewal, multilineage differentiation, and tumor initiation [5]. This population of cells, referred to as glioma stem cells (GSCs), is considered to be the cause of resistance to chemo-radiotherapy and the consequent recurrence. Investigations on the GSCs derived from GBM tissue, several types of induced GSC-like cells, genetically engineered mouse GBM models, and GBM organoid models have been performed to elucidate the mechanisms of the development, progression, therapeutic resistance, and recurrence of GBM [6–10].

A comprehensive analysis using microarrays revealed intratumoral, intertumoral, and spatiotemporal heterogeneities in GBM [11–15]. Moreover, a single-cell RNA-sequencing analysis provided deep insights into the heterogeneity of GBM cells through dynamic alterations in the gene expression patterns [16,17]. Thus, the diversity and plasticity of GBM cells are the causes of therapeutic resistance and recurrence, which are fundamental issues that need to be elucidated [11,18].

In the dynamic phenotypical alteration of glioma cells, the tumor microenvironment through secreted molecules (growth factors, cytokines, chemokines, and extracellular vesicles [EVs]), cell–cell adhesion, cell–extracellular matrix contact, and exposure to physiological conditions (hypoxia, hypothermia, and starvation) plays important roles [19–25]. To acquire aggressiveness, GBM cells also exploit stimuli from other GBM cells and non-GBM cells such as neurons, astrocytes, oligodendrocytes, macrophages or microglia, immune cells, and endothelial cells [20,21,26–28]. Thus, various kinds of stimuli in the tumor microenvironment of GBM can modulate the phenotypes of GBM cells. A clinical challenge in GBM is the high plasticity or reprogramming potential of GBM cells.

Interestingly, Ito et al. reported that incorporating ribosomes isolated from prokaryotes and eukaryotes into human dermal fibroblasts (HDFs) induces cell cluster formation and transdifferentiation into three germ-layer cells, which is similar to the phenomenon of iPS cell induction through Yamanaka’s factors [29–31]. The 80S ribosome is assembled from the 40S and 60S subunits, both of which are composed of ribosomal RNAs (rRNAs) and ribosomal proteins (RPs) [32]. The RPs participate in numerous biological phenomena, including not only protein synthesis, but also tumorigenesis, immune signaling, and development, as extra-ribosomal functions [33,34]. The relationships between the deregulation of RPs and cancers, including colon, prostate, breast, liver, gastric, lung, and brain cancers, have been reported [35,36].

From the point of the extra-ribosomal function and cancer, we hypothesized that RPs are molecules that may potentially induce stem-cell-like characteristics in GBM cells. Ribosomal protein S6 (RPS6) has been reported to be associated with cancers, such as leukemia [37], pancreatic cancer [38], and non-small cell lung cancer [39]. Therefore, we focused on RPS6 to investigate the therapeutic resistance of GBM via the induction of stem-cell-like characteristics in GBM cells [36]. In this line of studies, we found that the expression of RPS6 is correlated with the grade of glioma. In RPS6-knockdown experiments, stem-cell-like phenotypes were downregulated; in contrast, these phenotypes were upregulated in the RPS6 overexpression experiments. RPS6 is overexpressed in GSC niches [36]. Moreover, GBM cells form sphere-like structures by incorporating extrinsic ribosomes, wherein cells transdifferentiate into adipocytes and osteocytes [40]. The acquisition of stem-cell-like features and the transdifferentiation potential are regarded to be a result of GBM cell reprogramming.

Here, we focus on and discuss the reprogramming potential and extra-ribosomal function in GBM cells as potential therapeutic targets from the perspectives of plasticity and transdifferentiation potentials.

2. Microenvironments Induce Heterogeneity and Therapeutic Resistance in GBM

GBM is a lethal tumor commonly developing in the adult brain parenchyma, and GBM cells invade the contralateral hemisphere, even in the early stage of tumor progression [41]. Even with complete resection of the enhanced tumor mass lesion in gadolinium-enhanced T1-weighted (Gd-T1WI) magnetic resonance imaging (MRI) followed by chemoradiotherapies, GBM generally recurs locally [20].

To examine the site of GBM recurrence, we retrospectively analyzed Gd-T1WI MRI. The resection rate in 89 consecutive cases of primary GBM was analyzed using Gd-T1WI obtained within 72 h of resection. Complete resection of the enhanced mass lesion was attained in 43 cases (48%); recurrence was observed in 30 of these cases (70%) on the monthly MRI within the follow-up period of 1.5–4.5 years. Local recurrence in the white matter around the tumor removal cavity was observed in 26 cases (87%), while in the gray

matter it was observed in 0 cases; distal recurrence was detected in four cases (13%) [20]. Characteristically, oligodendrocyte precursor cells (OPCs) increase at the tumor border and secrete FGF1 and EGF from OPCs to induce stem-cell-like characteristics in glioma cells [20]. These data suggest that some GBM cells dynamically acquire suitable phenotypes to survive and recur in the unique microenvironment of the white matter around the tumor removal cavity.

Clinically, the reactivity of individual patients with GBM to chemo-radiotherapies is different, and different parts of the tumor in the same patients can have varying degrees of sensitivity. Even if the tumor mass can be reduced for some time with chemo-radiotherapy, resistant GBM cells survive and reconstruct the mass lesion later. Many genetic and epigenetic alterations that cause heterogenic phenotypes in GBM have been identified. Several types of heterogeneity in GBM have been reported: (1) intertumoral heterogeneity among tumors of different patients; (2) intratumoral heterogeneity, i.e., different genetic and epigenetic patterns can be detected depending on the site in the same tumor; (3) spatiotemporal heterogeneity between primary and recurrent tumors, depending on the site and time of recurrence [12–15,42–44]. This phenotypical heterogeneity in GBM depends on the high plastic potential.

Recently, data from a single-cell RNA-sequencing analysis showed that human GBM cells can be classified into four subtypes according to the set of gene expression patterns—neural-progenitor-like (NPC-like), oligodendrocyte-progenitor-like (OPC-like), astrocyte-like (AC-like), and mesenchymal-like (MES-like). A single GBM cell can produce all four types of descendants in a xenografted mouse brain [17]. Thus, the dynamic alteration of cell phenotypes in GBM tissue occurs through various kinds of stimuli. GBM cells are affected by the tumor microenvironment constructed with other GBM cells, neural cells, immune cells, vascular cells, extracellular matrix, and physical conditions, and subsequently acquire intercellular heterogeneity (Figure 1). These results explain the limited efficacy of drugs targeting a single pathway in GBM [17].

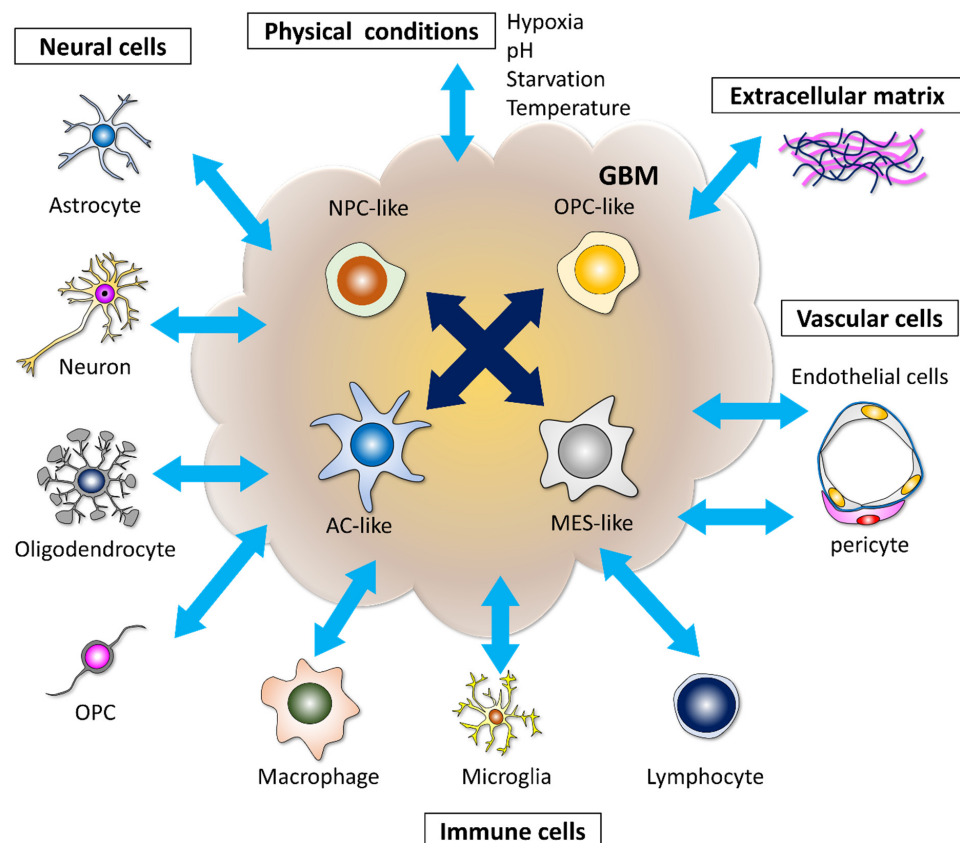


Figure 1. Plasticity and heterogeneity in GBM cells. GBM cells are classified into four subtypes—

neural-progenitor-like (NPC-like), oligodendrocyte-progenitor-like (OPC-like), astrocyte-like (AC-like), and mesenchymal-like (MES-like). A single GBM cell can produce all four types of descendants in the xenografted mouse brain under the influence of stimuli from the microenvironment. GBM cells are affected by physical conditions, the extracellular matrix, other GBM cells, and non-GBM cells, including neural cells, immune cells, and vascular cells. The reprogramming of GBM cells is modulated by multidimensional communication in microenvironments.

The higher plastic ability of GBM cells leads to intratumoral heterogeneity and therapeutic resistance in GBM. Simultaneously, this higher plastic ability of GBM cells transiting into other subtypes can be termed “reprogramming”.

3. Reprogramming Potential of Glioma Cells

3.1. Indirect Reprogramming and Direct Reprogramming of Non-Cancer Cells

Takahashi and Yamanaka demonstrated the possibility of developing induced pluripotent stem cells (iPSCs) by reprogramming fibroblasts transfected with four transcription factors—octamer-binding transcription factor 3/4 (*Oct3/4*), sex-determining region Y-box 2 (*Sox2*), Kruppel-like factor 4 (*Klf4*), and *c-Myc*—and then iPSCs can differentiate into all three germ layers cells in chimeric mice (Figure 2A) [30,31]. This discovery has had a major effect on the biology and medical fields.

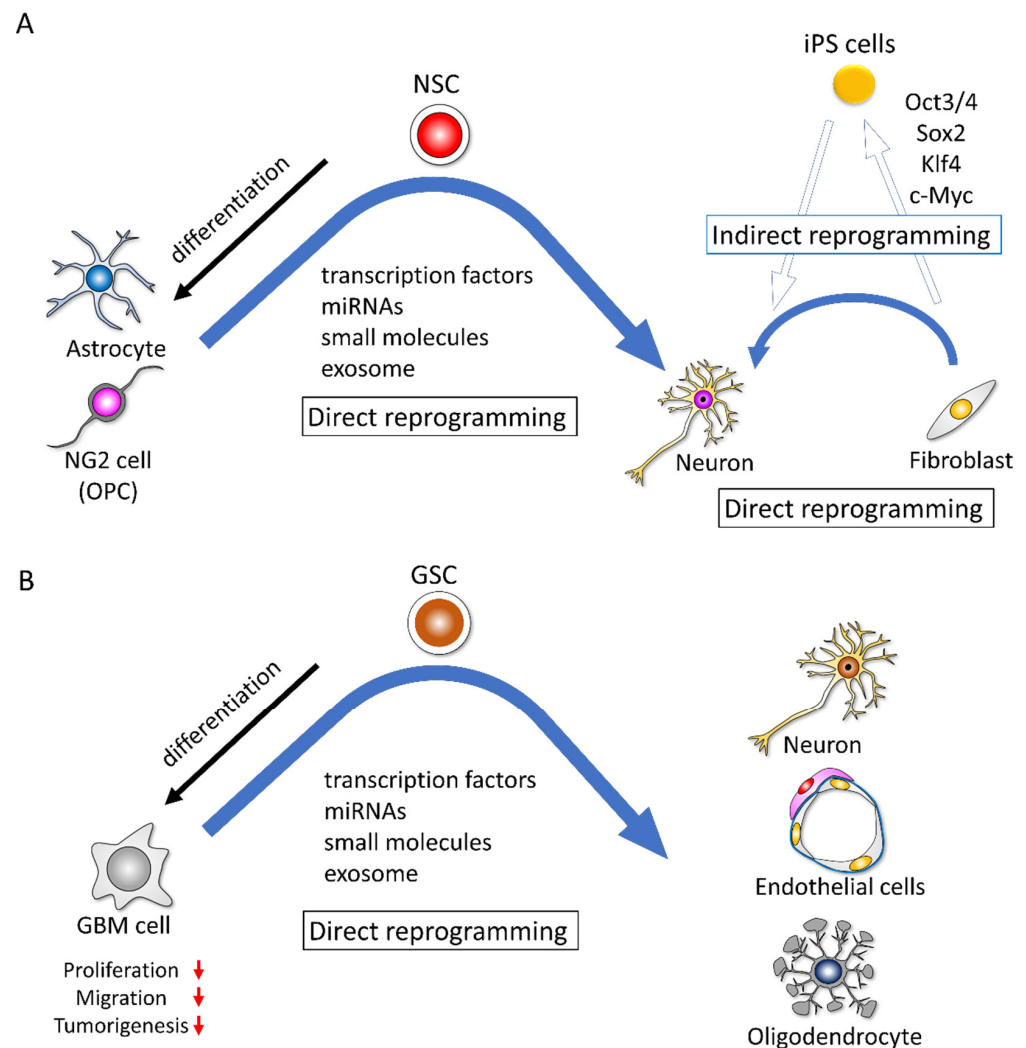


Figure 2. Indirect reprogramming and direct reprogramming in normal cells and GBM cells. (A) In

indirect reprogramming, pluripotency is induced in fibroblasts by Yamanaka's factor (Oct3/4, Sox2, Klf4, c-Myc). These iPSC cells are then differentiated into three germ layer cells under suitable differentiation culture conditions. In direct reprogramming, fibroblasts, astrocytes, and neuron-glia antigen 2 (NG2) cells (oligodendrocyte progenitor cells (OPCs)) can be directly converted into neurons by transcription factors, microRNAs (miRNAs), small molecules, or exosomes. (B) The functions of proliferation, migration, and tumorigenesis are downregulated in the differentiated GBM cells. GBM cells can be directly converted into neurons, oligodendrocytes, and endothelial-like cells.

Reprogramming can be either "indirect" or "direct" (Figure 2A). Generally, indirect reprogramming means that differentiated somatic cells acquire different cellular phenotypes accompanied by the methylation of DNA and modifications of histones and gene expression profiles [45]. In indirect reprogramming, the cells transit into an iPSC stage and then differentiate into the desired lineage of cells under specific differentiation conditions. In direct reprogramming, the cells convert directly to another cell type with epigenetic or metabolic alterations, bypassing the iPSC stage (Figure 2A) [45–48].

3.2. Glioma Cells Possess Potential for Reprogramming and Transdifferentiation

In immunohistochemical analyses, there are cases in which some GBM cells are stained with the neuronal marker MAP2. GBM contains a small population of GSCs that possess the potential to differentiate and express other neural lineage marker genes [5]. The induction of the terminal differentiation of GSCs into neural lineage cells and other lineage cell types is an interesting challenge and should be a potential therapeutic option [49–51].

A screening study of a kinase inhibitor library revealed that the mechanistic target of rapamycin (mTOR) and Rho-associated coiled-coil-containing protein kinase (ROCK) inhibitors are sufficient to reprogram GBM cells into neurons, which express neuronal markers and generate action potentials and neurotransmitter-receptor-mediated currents [52]. Another study showed that a small-molecule cocktail consisting of forskolin, ISX9, CHIR99021 I-BET 151, and DAPT could turn human GBM cells into terminally differentiated neurons over 13 days. The reprogrammed cells displayed morphological and immunocytochemical characteristics associated with neuronal phenotypes. This chemical cocktail upregulates the expression of neuronal marker genes [53]. Similarly, Gao et al. reported that by using three small molecules (Fasudil (F), a Rho kinase inhibitor; Tranilast (T), a transforming growth factor- β (TGF- β) inhibitor; and TMZ (T)), they (FTT) reprogrammed patient-derived GBM cells to acquire neuronal phenotypes (Figure 2B) [54].

Zinc finger protein 117 (ZNF117) was identified from a combination of image-based genome-wide RNAi screening and single-cell RNA-sequencing as a regulator of GSC differentiation. The downregulation of ZNF117 promotes the differentiation of GSCs toward the oligodendrocyte lineage, and the decreased tumorigenic potential influences the JAG2 signaling and regulated NOTCH signaling (Figure 2B) [51].

Unexpectedly, several studies have reported that GSCs can differentiate into endothelial-like cells [55–57]. In these studies, the orthotopic injection of patient-derived GSCs into mice produced tumor xenografts with a vasculature composed of human endothelial-like cells. The tumor-derived endothelial-like cells originated from tumor-initiating cells and did not result from cell fusion. Generally, the hypoxia-inducible factor-vascular endothelial growth factor (HIF-VEGF) pathway is important for tumor cell survival and angiogenesis under hypoxic conditions. However, the differentiation of GBM cells into endothelial-like cells is independent of VEGF (Figure 2B) [56].

To adapt to hypoxia, GBM cells communicate with their surrounding microenvironment through secreted molecules and vesicles. Under hypoxic conditions, exosomes secreted by GBM cells control the hypoxia-dependent intercellular signaling, where abundant hypoxia-regulated messenger RNAs (mRNAs) and proteins exist [58]. Endothelial cells are reprogrammed by GBM cell-derived hypoxia exosomes in order to secrete several potent growth factors and cytokines and to stimulate pericyte PI3K/AKT signaling, activation, and migration (Figure 2B) [58]. Lucero et al. reported that GBM-derived microRNA

(miRNA)-containing EVs induce angiogenesis by reprogramming brain endothelial cells to resemble tumor endothelial cells [59]. These results suggest that GBM cells possess the ability for reprogramming and transdifferentiation into other lineage cells, and exosomes from GBM cells under hypoxic conditions make normal endothelial cells reprogram into GBM tumor endothelial cells. Therefore, GBM cells alter their microenvironment spontaneously and dynamically to survive and multiply.

3.3. GBM Cells Acquire an Aggressive Phenotype by Reprogramming through Intercellular Communication

GBM cells acquire an aggressive phenotype to multiply and survive by reprogramming themselves. Genetic and epigenetic alterations are important events for GBM cells. Moreover, GBM cells communicate with other GBM cells and the tumor microenvironment constantly and dynamically.

Under physiological stress conditions, such as hypoxia and starvation, non-GSC GBM cells acquire GSC-like characteristics and survive through metabolic reprogramming from aerobic to anaerobic glycolysis [60]. Hypoxic conditions promote stem cell marker expression and induce a quiescence state and GSC-like phenotypes related to chemo-radioresistance [61–63]. A comparison of RNA expression levels in U87MG cells cultured under hypoxia and those under normoxia showed that genes in the ribosome biogenesis pathway and TNF signaling pathway were enriched [64]. Irradiation itself induces dedifferentiation and increased tumorigenicity in GBM cells [65].

GBM cells communicate with neighboring and distant cells through direct contact and several types of intervention, including some molecules and EVs in the extracellular space (Figure 3).

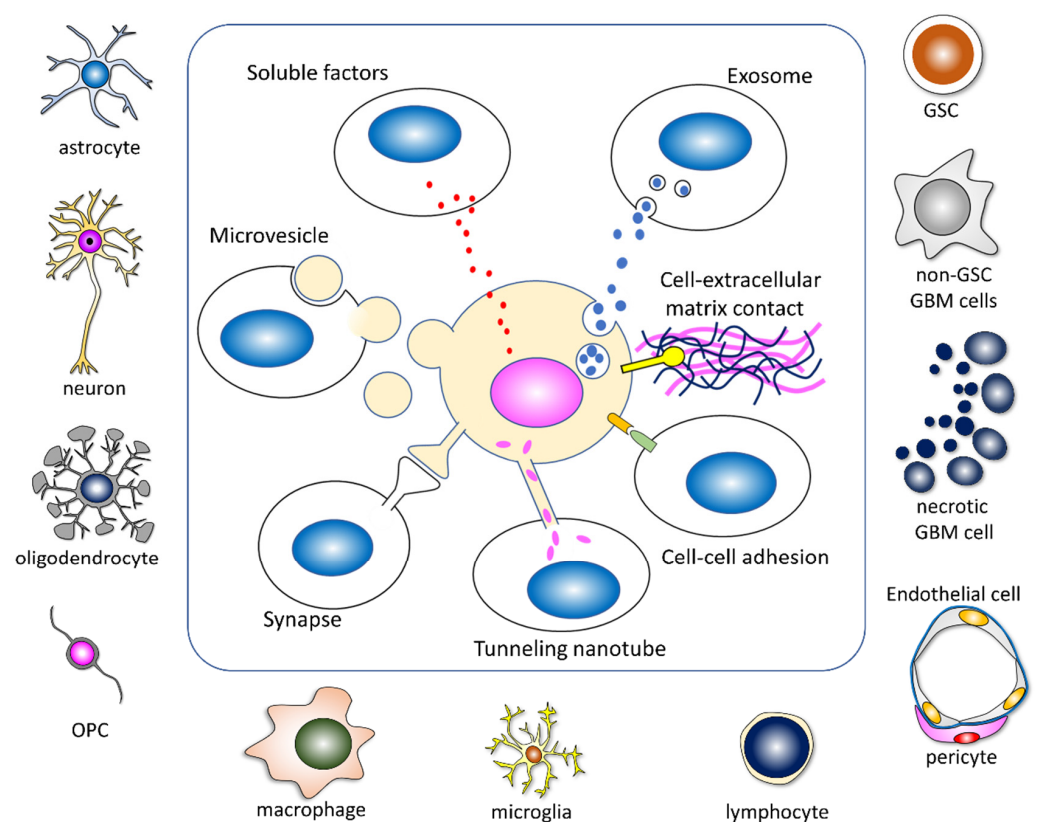


Figure 3. Multidimensional intercellular communication. GBM cells are affected by tumor microenvironments through direct contact and several interventions from GBM cells and non-GBM cells. Some extracellular vesicles contain informative molecules containing proteins, RNAs, DNAs, and surface receptors.

Direct cell–cell adhesion, cell–extracellular contact, tumor microtubes, and synapses between GBM cells or non-GBM cells play important roles in reprogramming (Figure 3). The formation of electrochemical networks through synapse-like structures with neurons [26,66], astrocytes [67–69], and OPCs [70–72] enhances tumor growth. Furthermore, their communication through tumor microtubes confers GBM cells with the advantages of invasion, proliferation, and resistance to radiotherapy [73,74]. The enrichment of synaptic gene expression is mainly found in OPC-like GBM cells [26]. An analysis of the shape of the GBM extension on Gd-T1WI MRI revealed that GBMs extend along the neuronal fibers, such as association and commissural fibers, rather than the capillary network [75]. As oligodendrocytes support neuronal activity and proliferated OPC secret growth factors and cytokines at the tumor border, communication with neurons and oligodendrocytes appears to promote an aggressive phenotype in GBM cells [20,26,66,75]. Astrocytes actively influence the proliferation, migration, invasion, anti-apoptotic ability, chemoprotection, and immunoprotection of GBM cells [76]. Tumor-associated reactive astrocytes interact with GBM cells through ion channels and ion transporters and facilitate tumor progression, aggression, and survival by releasing various cytokines [77].

Several kinds of soluble factors such as growth factors and cytokines are secreted from GBM cells and non-GBM cells via exocytosis. Epidermal growth factor (EGF) and fibroblast growth factor (FGF) are reported as key molecules for neural stem cell and GSC cultures and expand stem cell populations [5,78]. The autocrine function of EGF and FGF sustains the self-renewal of GSCs [79]. As for cytokines, CCL2, referred to as monocyte chemoattractant protein-1 (MCP-1), is an important cytokine characterized as a glioma-cell-derived monocyte chemotactic factor [80]. The CCL2–CCR2 axis is highly expressed in GBM and related to the immune escape, angiogenesis, and proliferation of GBM cells; conversely, reduced CCL2 levels are associated with GSC growth inhibition [81,82]. CCL2 is secreted from GBM, immune cells, and oligodendrocytes, which interact mutually [83,84]. Regrettably, we omitted many other important growth factors, including cytokines and chemokines [84–88].

EVs including microvesicles, exosomes, apoptotic bodies, and oncosomes transfer some informative molecules containing proteins, RNAs, DNAs, and surface receptors to target cells, and this promotes the reprogramming of GBM cells and therapeutic resistance [19–21,89–93]. GBM-derived EVs induce the tumor-promoting phenotype in NSCs [94]. Several key genes, including *S100B*, *CXCL14*, *EFEMP1*, *SCRG1*, *GLIPR1*, and *CD44*, and dysregulated signaling are linked to the transformation of NSCs [94]. Exosomes derived from GSCs can reprogram non-GSC into GSCs [95]. The ability for proliferation, sphere-formation, invasive capacities, and tumorigenicity in non-GSC GBM cells is upregulated substantially after GSC exosome treatment [95]. Gao et al. reported that the transfer of genetic material is achieved mainly through EVs, although cell fusion also plays a minor role, and individual GBM cells communicate with distinct sets of non-GBM cells [96].

Moreover, EVs released by GBM cells stimulate normal astrocytes to acquire a tumor-supportive phenotype that promotes migration and invasion, enhances cytokine production, and activates tumor cell growth [97,98]. Moreover, in a soft agar assay, EVs derived from GBM cells showed a transformative effect on normal human astrocytes [98]. GBM-derived EVs promote the neoplastic growth of pre-transformed astrocytes but not normal human or mouse astrocytes through metabolic reprogramming. GBM EV-mediated reprogramming is partially associated with the transfer of full-length mRNAs encoding RPs, oxidative phosphorylation, and glycolytic factors [99]. Thus, through reprogramming, various types of stimuli promote aggressive phenotypes in GBM cells and modulate tumor-supportive phenotypes in non-GBM cells to reconstruct beneficial microenvironments as GSC niches.

4. Deregulation of Ribosome Biogenesis in Cancer

Human ribosomal biogenesis includes several steps, such as the transcription of ribosomal DNA (rDNA), processing and modification of ribosomal RNA (rRNA), and assembly and maturation of the 40S and 60S subunits. The small 40S subunit is constructed with 18S

rRNA and 33 RPs, and the large 60S subunit is formed with three rRNAs (28S, 5.8S, and 5S) and 48 RPs, then finally small and large subunits are assembled. Consequently, mature 80S ribosomes are constructed, which function in protein synthesis (Figure 4) [100–102]. Therefore, RPs are essential molecules for constructing ribosomal subunits and mature ribosomes. In ribosome biogenesis, TP53, PTEN, and Rb function as potent ribosome biogenesis suppressors [103,104]; conversely, PI3K-Akt-mTOR, c-MYC, RAS-MAPK, and NF- κ B function as activators [105–109].

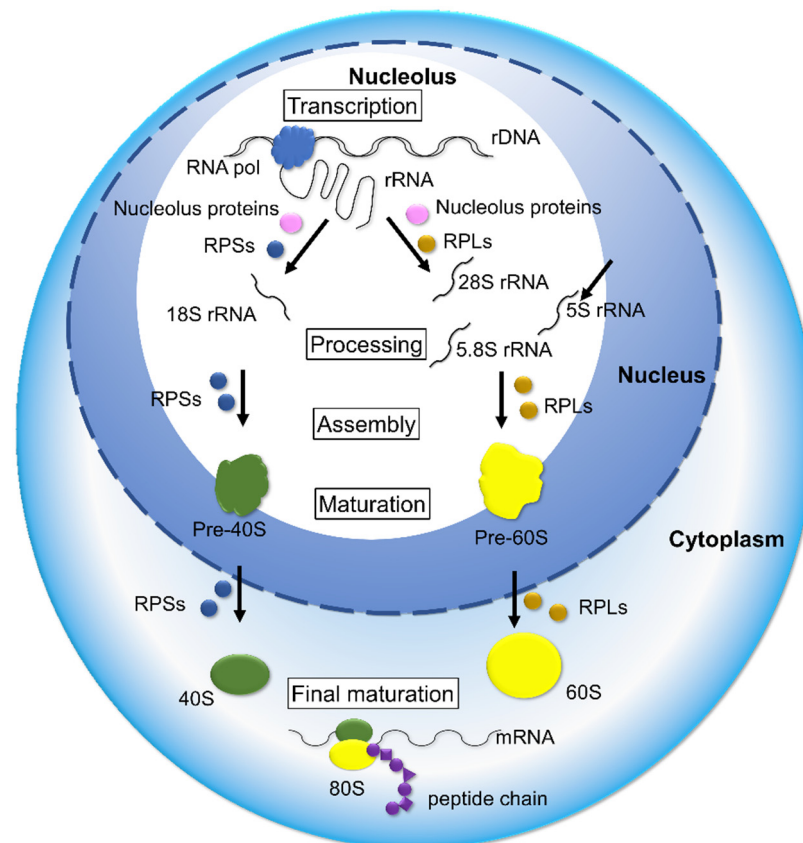


Figure 4. In ribosome biogenesis, many molecules participate in multiple steps, including rDNA transcription, rRNA processing, nucleolus protein assembly, ribosomal proteins, rRNAs, the maturation of large and small ribosomal subunits, and finally the maturation of 80S ribosome. The deregulation of ribosome biogenesis causes an abundance or shortage of ribosomal proteins, which induce tumor-promotive or -suppressive effects in cancer.

Interestingly, the deregulation of ribosome biogenesis exhibits a paradoxical function from a hypo-proliferative cellular response to a hyper-proliferative oncogenic phenotype, which was referred to as Dameshek's riddle [110]. Ribosome insufficiency leads to ribosome misassembly, the dysregulation of protein synthesis, and oncogenic protein expression; moreover, some RPs regulate major cancer proteins [101,111].

Ribosome-free RPs are known to have several functions. RPs are related to a variety of aspects of carcinogenesis; the positive effects in cancer progression are the upregulation of the proliferation and migration potential and the induction of stemness. Conversely, the negative effects are induced cell cycle arrest, apoptosis, and cellular senescence as extra-ribosomal functions [33–36,40,101,112–115] (Figure 5).

The tumor-suppressive effects of extra-ribosomal functions involve nucleolar stress, which activates the RP-MDM2-p53 pathway with the consequent sustained p53 stabilization, which induces cell cycle arrest, apoptosis, and cell death [33,114,116,117]. Impaired ribosome biogenesis through the deregulation of polymerase I transcription, rRNA process-

ing, ribosome assembly, and transport promote tumor-suppressive functions, including cell cycle arrest, apoptosis, senescence, dormancy, differentiation, and cell death (Figure 5).

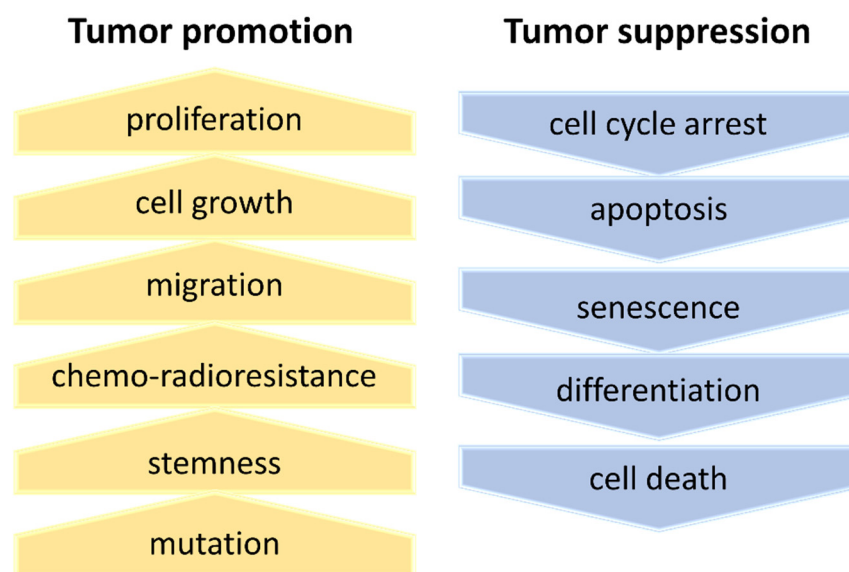


Figure 5. Extra-ribosomal function in cancer. The deregulation of ribosome biogenesis induces tumor-promotive and -suppressive functions.

In addition, the p53-independent pathway has been reported, and it is involved in c-MYC inhibition by RPL5, RPL11, and RPS14, while other tumor-suppressive functions are regulated by nucleolar proteins such as nucleophosmin (NPM) and ARF [101,118–121].

In contrast, the tumor-promotive functions upregulate cell proliferation, growth, migration, chemo-radioresistance, and stemness (Figure 5). Moreover, the nucleolar stress conditions through the deregulation of ribosome biogenesis also promote metabolic reprogramming and secondary mutation [111].

Ribosomopathies are rare inherited diseases, wherein genetic mutations in ribosome biogenesis reduce the ribosome levels [122]. Patients with ribosomopathies have a higher risk of developing cancer [111]. Ribosomopathies are divided into two major classes based on their predispositions to cancer [122–124]. Patients with inherited bone marrow failure, including Diamond–Blackfan anemia, Shwachman–Diamond syndrome, and dyskeratosis congenita, show a high predisposition to cancer, but those with Treacher–Collins syndrome do not [122–124].

5. Ribosome Incorporation Induces Reprogramming in Somatic Cells

Tumor-suppressive and -promotive functions of RPs in cancer have been discussed as extra-ribosomal functions. Additionally, Ito et al. reported that incorporating ribosomes into adult HDFs promotes reprogramming and multipotency, which is a novel and interesting finding regarding ribosome function [29]. Originally, Ohta had reported that adult HDF incorporation of lactic acid bacteria (LAB) resulted in the formation of embryoid-body-like cell clusters similar to embryoid bodies derived from ES cells and expressed a set of pluripotent markers, including Nanog, Sox2, Oct3/4 and TdGF1. These cells differentiated into all three germ layer cells [125]. An investigation of factors in LAB that induce multipotency showed that ribosome incorporation into HDFs promotes dedifferentiation and transdifferentiation potentials [29]. Through ribosome incorporation, HDFs form ribosome-induced cell clusters (RICs), wherein cells express pluripotency marker genes. Moreover, dedifferentiated cells in RICs can differentiate into the three germ-layer cells, such as ectodermal neurons, mesodermal cardiomyocytes, endodermal hepatocytes, adipocytes, and chondrocytes [29]. Ribosomes from various prokaryotes (Gram-positive and -negative bacteria) and eukaryotes (yeast, mouse, and human) promote

RIC formation [29]. These ribosome-mediated reprogramming potentials were not related to the translational activity of the incorporated extrinsic ribosomes [29,126]. Based on these interesting results, we hypothesized that incorporating ribosomes promotes plasticity and reprogramming in GBM cells, through which GBM cells acquire GSC-like properties and therapeutic resistance.

6. Incorporation of Ribosomal Proteins S6 Induces Reprogramming in Glioma Cells

To clarify whether the incorporation of ribosomes promotes stem cell properties and therapeutic resistance in glioma cells, investigations focusing on RPS6 were performed because the overexpression and phosphorylation of RPS6 have been reported in various types of cancers, including acute myeloid leukemia [37,127], non-Hodgkin lymphoma [128], oral squamous cell carcinoma [129], non-small cell lung cancer [39], breast cancer [130], gastric cancer [131], pancreatic cancer [38], renal cell carcinoma [132], ovarian cancer [133], melanoma [134], and others [112]. RPS6 processes 30S pre-rRNA into 18S rRNA, which is used to form the small 40S subunit. Thereafter, the small 40S and large 60S subunits assemble and form mature 80S ribosomes [135].

The immunohistochemical analysis showed significant upregulation of RPS6 expression in high-grade glioma compared with that in low-grade gliomas [36]. The sphere-forming ability and expression of the stem cell marker genes *Nestin* and *Sox2* were down-regulated by the knockdown of RPS6, whereas the sphere-forming ability increased in overexpression experiments in U251MG and U87MG glioma cell lines [36], both of which were classified as GBM, IDH-wildtype. RPS6-specific siRNA reduced the sphere-forming ability and expression of *Nestin* and *Sox2* and phosphorylated STAT3 (pSTAT3). The Janus kinase/signal transducers and activators of transcription (JAK/STAT) inhibitor (AG490) suppress the sphere-forming ability. Moreover, an immunohistochemical analysis showed that the RPS6 expression was predominant in the perivascular, perinecrotic, and border niches of GBM tissues [36]. To confirm these data, we used the Ivy Glioblastoma Atlas Project database, which provided gene expression data via the microdissection of several areas regarded as GSC-dominant [136]. The expression of RPS6 is significantly higher in GSC-dominant areas, such as the site of microvascular proliferation, pseudopalisading cells around necrosis, infiltrating tumors, and the leading edge [36]. RPS6 is predominantly present in sites containing GSC niches. Similar to RPS6 expression, many other ribosomal proteins show higher expression in the GSC-dominant sites. Thus, the intrinsic RPS6 can induce stem-cell-like properties in glioma cells (Figure 6) [36].

Moreover, to investigate the effects of extrinsic ribosomes on phenotype alterations in glioma cells, we harvested ribosomes derived from prokaryotes and U251MG using ultracentrifugation. Ribosomes derived from prokaryotes were added to the culture dish where U251MG cells were plated in DMEM/F12 (serum-free and growth-factor-free). These GBM cells formed ribosome-induced cancer cell spheroids (RICCS) and showed increased expression of the stemness genes *Nestin* and *Sox2*. In the differentiation analysis, these cells in RICCS could be transdifferentiated into adipocytes and chondrocytes via culturing in a differentiation-specific medium of each cell type [40]. These effects were modulated through intrinsic RPS6 phosphorylation. These effects were interrupted by an inhibitor of RPS6 signaling (PF4708671, ribosomal S6 kinase inhibitor). The extrinsic ribosomes derived from GBM cells induce the formation of RICCS and the expression of RPS6, phosphorylated RPS6, and the stemness genes *Nestin* and *Sox2*. These effects of the ribosome incorporation were interrupted by an inhibitor of RPS6 signaling (PF4708671, ribosomal S6 kinase inhibitor) [40]. These results demonstrated that intrinsic and extrinsic RPS6 can promote the induction of stem-cell-like characteristics in GBM cells [113]. This ability for stemness induction is a novel extra-ribosomal function of RPS6 (Figure 6) [36,40,113].

Taken together, GBM cells that are cultured for long periods with serum could be reprogrammed and could acquire transdifferentiation potential via ribosome incorporation, resembling the phenotypes of RICs derived from HDFs. Thus, the reprogramming ability caused by ribosome incorporation appears to be conserved in normal cells and cancer cells.

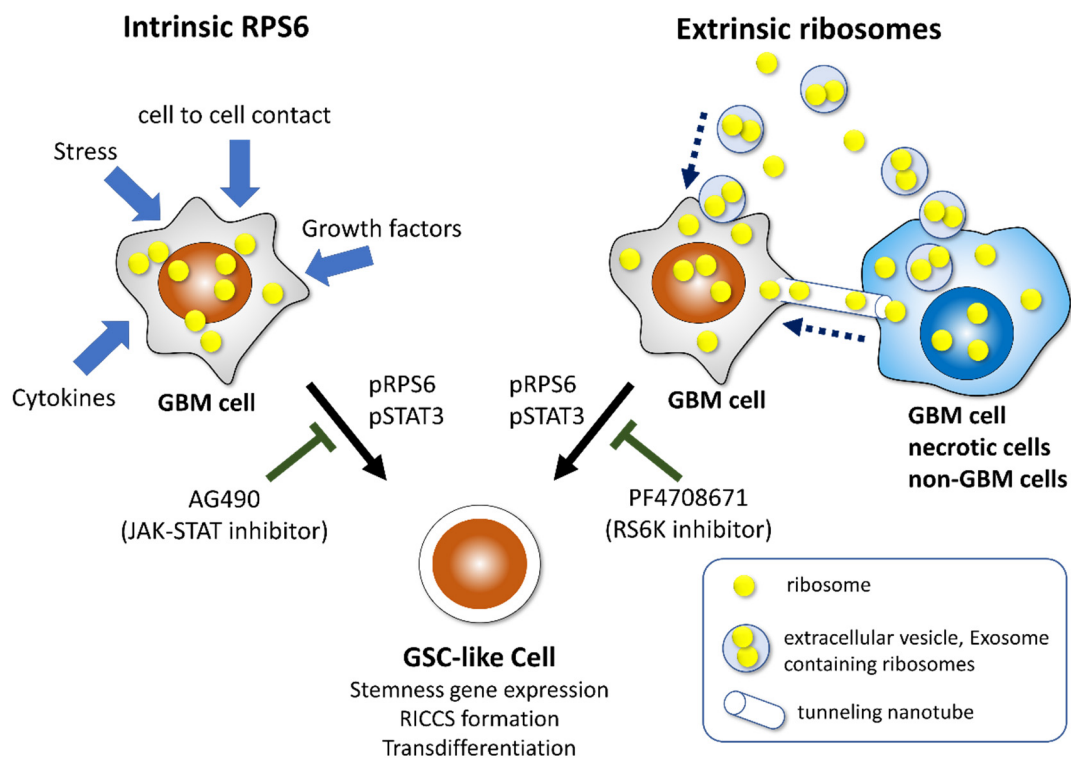


Figure 6. Intrinsic RPS6 and extrinsic ribosomes induce GSC-like phenotypes in GBM cells. Multiple stimuli in the tumor microenvironment induce ribosome biogenesis. The overexpression of RPS6 increases stemness gene expression and RICCS formation, which is suppressed by AG490 (JAK-STAT inhibitor). GBM cells communicate with other GBM cells, necrotic cells, and non-GBM cells through extracellular vesicles, including exosomes and tumor nanotubes. Ribosome incorporation promotes stemness gene expression and RICCS formation, which is suppressed by PF4708671 (RPS6K inhibitor). Cells in RICCS acquire transdifferentiation potentials.

7. Deregulation of Ribosome Biogenesis Modulates Aggressiveness in GBM

The expression levels of several ribosomal proteins in GBM have been reported (Table 1). RPS27, also called metalloproteinase-1, is a component of the 40S subunit of ribosomes, which is highly expressed in the various types of tissues, including malignancies in the colon [137], prostate [138], breast [139], and stomach [140]. An increased RPS27 level in the serum has been identified; this is a useful marker for the early detection of various types of cancer [141]. As for brain tumors, in a previous study, the mRNA of RPS27 was 6.2- and 8.8-fold (mean) enhanced in gliomas of WHO grades II and III with ($p < 0.01$) and without IDH mutation ($p = 0.01$), respectively, compared with that in the normal healthy brain. Additionally, GBM displayed a 4.6-fold increased mean expression ($p = 0.02$). However, the expression of RPS27 was not related to the WHO grade in gliomas [142]. In the findings of an analysis using the IVY GAP database, the expression of RPS27 was dominantly detected in the area of microvascular proliferation and in pseudopalisading cells around necrosis, but not in the infiltrating area of tumor cells. The levels of RPS27 were not related to the progression-free survival or the overall survival of patients with GBM [142]. Moreover, how RPS27 functions in gliomagenesis remains unclear.

RPS15A is overexpressed in GBM tissues. The knockdown of RPS15A inhibits cell proliferation and colony formation and induces apoptosis in U251 cells [143]. Correspondingly, the knockdown of RPS15A suppressed tumorigenesis in xenograft models via the Akt pathway [144].

RPL34 is a component of the pre-ribosome 60S subunit [145]. The expression of RPL34 is significantly higher in GBM than in low-grade gliomas and the normal brain and is related to poor survival and the proliferation of GBM cells [145].

Table 1. Ribosomal protein in glioblastomas.

Ribosomal Protein	Function	Induced Phenotypes	Reference
RPS6	Oncogenic	Sphere-forming ability Stemness gene expression (<i>Nestin, Sox2</i>) Higher expression in GBM Higher expression at GSC-dominant area	[34,38]
RPS27	Oncogenic	High expression in gliomas Higher expression at GSC-dominant area No relation to survival time	[136]
RPS15A	Oncogenic	Higher expression in GBM Proliferation Colony formation Anti-apoptosis Tumorigenesis Poor survival	[137,138]
RPL34	Oncogenic	Higher expression in GBM Proliferation Anti-apoptosis Poor survival	[139]
RPL5	Tumor-suppressive	Mutation 2.5%, deletion 8.4% in GBM Poor survival time in low RPL5 expression	[140]
RPS11 RPS16 RPS18	Tumor-suppressive	High expression levels mean high susceptibility to topoisomerase II inhibitors (etoposide and doxorubicin)	[141]

Conversely, some ribosomal proteins play a role in suppressing tumorigenesis by activating some tumor suppressors and inactivating oncoproteins [33]. Heterozygous deletion or mutation of RPL5 was found in 11% of GBM [146]. Clinically, patients expressing low levels of RPL5 have been shown to have shorter 5-year overall survival and mean survival times (13.8 months, $n = 414$) than those expressing high levels of RPL5 (14.7 months, $n = 442$) [146]. Thus, RPL5 has a tumor-suppressive function in GBM.

RPS11, RPS16, and RPS18 influence the susceptibility of GBM cells to topoisomerase II inhibitor (etoposide) treatment, and a loss of RPS11 leads to resistance to etoposide [147]. Under cellular stress conditions, intrinsic ribosome biogenesis is increased, and ribosome-free RPs promote GSC-like phenotypes and aggressiveness in GBM cells as extra-ribosomal functions.

Meanwhile, the mechanisms of incorporating extrinsic RPs into GBM cells have not yet been revealed. Thus, some questions remain regarding how RPs are secreted and incorporated into GBM cells in the tumor microenvironment.

In RPS6, approximately 5% of endogenous RPS6 is detected in ribosome-free subcellular fractions [148]. Regarding the secretion of RPs, Kim et al. reported that protein secretion is a general phenomenon by which cells communicate with the extracellular environment, and RPS3 is secreted in several cancer cell lines such as HT1080 (human fibrosarcoma) and MPC11 (mouse plasmacytoma). The secreted RPS3 level increased in doxorubicin-resistant MPC11 cells compared with that in original MPC11 cells [149].

EVs transfer some informative molecules containing proteins, RNAs, DNAs, and surface receptors to target cells. GBM EVs contain full-length mRNAs encoding RPs, are involved in oxidative phosphorylation, and act as glycolytic factors [99]. Exosomes containing RPs from Schwann cells are transferred to axons [150,151]. EVs, including exosomes, appear to be important vehicles for the intercellular communication of ribosomes. Tunneling nanotubes, which are thin, membranous, open-ended tubes, are another candidate because they directly transfer cellular materials, including mitochondria, to GBM cells [152].

8. Incorporation of Ribosome Induces Reprogramming and Transdifferentiation Potential in Cancer Cells

The overexpression of intrinsic RPS6 induces GSC-like phenotypes. Moreover, extrinsic ribosome incorporation promotes GSC-like phenotypes and the reprogramming and transdifferentiation potentials in GBM cells linked to pRPS6 and pSTAT3 [36,40]. Similarly, extrinsic ribosome incorporation induces reprogramming and transdifferentiation potentials in several types of cancers.

When extrinsic ribosomes purified from *Escherichia coli* strain JE28 were transferred into human breast cancer cell line MCF7, the cell proliferation potential decreased and the population in the G0 phase increased, while cyclinD1 expression disappeared in RICCS on day 20 in culture, but those in control cells remained. These data suggest that cell cycle arrest was induced by ribosome incorporation. During RICCS formation, the expression of TGF- β and *Snail*, which is a marker gene in epithelial–mesenchymal transition, was upregulated from 1 h to day 1 and then downregulated, although the expression of E-cadherin was similar to that in the control, resulting in incomplete EMT inhibition. The autophagy pathway is activated by ribosome incorporation. These results demonstrated that ribosomal incorporation induces cell cycle arrest and reprogramming, which alters the phenotypes of MCF7 [153].

Through extrinsic ribosome incorporation, the non-small cell lung cancer cell line, A549, and gastric tubular adenocarcinoma cell line, H-111-TC, also formed RICCS within 2–3 days, and both cells showed transdifferentiation potentials into adipocytes and osteoblasts in the specific induction medium. Ribosome incorporation in the A549 cell line gradually upregulated cell proliferation marker Ki67, but the expression of *EGFR* and *cyclicD1* peaked on day 7 and then decreased on day 14; however, that of *CXCR4* increased until day 14 [154].

Ribosomes derived from eukaryotic, prokaryotic, and GBM cells promote RICCS formation in glioma cells, breast cancer cells, lung cancer cells, and gastric cancer cells, and these RICCS cells acquire transdifferentiation potentials [40,153,154]. During the senescence-like state, RICCS are reprogrammed and the state is reversed under the stimuli of the differentiation induction medium, resulting in temporal proliferation and transdifferentiation [126]. Therefore, reprogramming by ribosome incorporation is conserved in several types of cancer (Table 2).

Table 2. Ribosome incorporation into cancer cells.

Cell Line	Ribosome	Alteration of Phenotypes	Reference
Glioblastoma U251MG	Prokaryote	RICCS formation Stemness gene expression (<i>Nestin</i> , <i>Sox2</i>) pRPS6, RPS6 expression pSTAT3 expression Transdifferentiation (adipocyte, osteocyte)	[38,107]
	Eukaryote (U252MG)	RICCS formation Stemness gene expression (<i>Nestin</i> , <i>Sox2</i>) pRPS6, RPS6 expression pRPS6 co-expressed <i>Nestin</i> RPS6K inhibitor (PF4708671) suppresses RICCS formation RPS6K inhibitor (PF4708671) suppresses the expression of <i>Nestin</i> and <i>Sox2</i>	[38,107]
Breast cancer MCF7	Prokaryote	RICCS formation Increased G0 and early G1 phase cells EMT-like phenomenon Autophagy pathway activation p53-mediated stress response	[120,147]

Table 2. Cont.

Cell Line	Ribosome	Alteration of Phenotypes	Reference
Non-small cell lung cancer A549	Prokaryote	RICCS formation Transdifferentiation (adipocyte, osteoblast) EGFR expression was increased on day 7, then decreased on day 14 CXCR4 expression was increased on day 14 Ki67-positive cells increased gradually on day 14 cyclinD1 expression increased by day 7, then decreased by day 14 In the tumor-forming assay, direct injection of ribosomes into the tumor mass No significant difference in tumor size and volume between control and ribosome-incorporated tumor	[120,148]
Gastric tubular adenocarcinoma H-111-TC	Prokaryote	RICCS formation Transdifferentiation (adipocyte, osteoblast)	[120,148]

9. Ribosome Biogenesis as the Therapeutic Target for GBM

Generally, increased ribosome biogenesis and protein synthesis are observed during the growth of normal tissues as a result of the expansion of the size and number of cells. However, the deregulation of ribosome biogenesis in cancer is observed, increasing oncogenic and decreasing tumor-suppressive ribosomes.

The functions of ribosomal proteins are still intricate; however, the potential to induce aggressive phenotypes and transdifferentiation ability by reprogramming in GBM cells is considered a novel therapeutic target.

Investigations focusing on ribosome biogenesis as the therapeutic target in GBM have been conducted. Ribosome-inactivating proteins (RIPs) form a large family and are found in several plants, which inactivate the 60S ribosomal subunits and are used in chemotherapeutic agents for cancers [155]. Combination therapy with quinoic acid, a type 1 RIP from quinoa seeds, and temozolomide has shown synergistic cytotoxic effects in GBM cells [156].

Pescadillo ribosomal biogenesis factor 1 (Pes1), block of proliferation 1 (BOP1), and WD repeat domain 12 (WDR12) play crucial roles in the ribosome biogenesis pathway. The Pes1-BOP1-WDR12 complex modulates pre-rRNA processing for the maturation of 28S and 5.8S rRNAs [157–159]. Pes1 is related to tumor cell proliferation, invasion, and metastasis in various types of cancers [159]. WDR12 is an essential factor for processing the 32S pre-rRNA. WDR12 is required for ribosome biogenesis in GSCs, and higher expression of WDR12 has been observed in GSCs than in non-GSCs and normal brain cells [160]. The increased expression of WDR12 is related to the progression of GBM and shorter overall survival [160]. Silencing WDR12 via small hairpin RNA induces the degradation of the PeBoW complex and suppresses the maturation of 28S rRNA [158]. A lack of WDR12 inhibits GSC proliferation and tumor growth and prolongs the survival time of mice-injected GSCs [160,161].

Similarly, the inhibition of the purine guanosine monophosphate biosynthesis decreases the production of rRNA and GBM cell growth [162]. Purine metabolism is an important key mediator of DNA repair and radiation resistance in GBM [163]. GBM cells depend on the de novo biosynthesis of pyrimidines to support the rDNA transcription and cell growth. However, the effects of the inhibition of pyrimidine biosynthesis in normal cells are not sufficient for pyrimidine synthesis, rRNA production, and proliferation [164]. To generate rRNA, GBM cells strongly depend on the de novo pyrimidine biosynthesis pathway; therefore, the specific inhibitor of this pathway is an expected therapeutic target of GBM [164]. The effects of brequinar (dihydroorotate dehydrogenase (DHODH) inhibitor) are specific to GBM cells, and it may be a safe drug with minimal adverse effects [164].

ErbB3 expression correlates with an increased expression of the 47S ribosome precursor and cell proliferation [165]. ErbB3/C23 (nucleolin) interferes with RNA polymerase I activity and 47S rRNA synthesis. Actinomycin D binds to ErbB3/C23 (nucleolin) and induces nuclear accumulation of ErbB3/C23, which inhibits rRNA transcription [165]. Actinomycin D induces nucleolar stress and is a new treatment strategy for GBM [165].

STAT6 is downregulated in human GBM specimens. Under hypoxic conditions, the expression of STAT6 is downregulated, and HIF-1 α protein synthesis is increased through the activation of the mTOR/S6K (RPS6 kinase)/S6 (RPS6) signaling pathway, which promotes cell survival and maintains GSC phenotypes [166]. The expression of p-mTOR and p-RPS6 is substantially suppressed by the Jinlong capsule, and the inhibition of mTOR reduces cell migration and the invasion ability in GBM cells [167].

Alpha Thalassemia/X-linked mental retardation syndrome (ATRX) mutation is one of the important genes for diagnosing gliomas. ATRX maintains rDNA heterochromatin formation and stability, and ATRX loss of function contributes to tumorigenesis through the rDNA instability [168].

Many chemotherapeutic drugs target the process of ribosome biogenesis, and each drug inhibits ribosomal RNA synthesis at the stage of (i) rRNA transcription (e.g., oxaliplatin, doxorubicin, mitoxantrone, methotrexate), (ii) early rRNA processing (e.g., camptothecin, flavopiridol, roscovitine), or (iii) late rRNA processing (e.g., 5-fluorouracil, MG-132, homoharringtonine) [169].

Several compounds, including CX-3543 [170], CX-5461 [171], and BMH-21 [172], inhibiting pol I have been developed. A clinical trial for CX-5461 showed that p53 wild-type leukemia cells are more sensitive, while p53 mutant cells can also be responsive [173–175].

10. Conclusions and Future Directions

The elucidation of the mechanisms underlying the acquisition of stemness in GBM cells is a fundamental clinical issue for improving the prognosis of patients with GBM. In this review, we described the possibility of increasing intrinsic ribosomes by deregulating ribosome biogenesis and incorporating extrinsic ribosomes that promote reprogramming in GBM cells, which induces aggressiveness, chemo-radioresistance, and transdifferentiation potential in GBM cells. However, we could realize and develop new therapeutic approaches. Regulating ribosome biogenesis in GBM cells induces (i) nucleolar stress and hypo-proliferative tumor-suppressive phenotypes and (ii) induces a terminally differentiated phenotype and converts malignancy to benignity with epigenetic modifications [45]. Indeed, some chemotherapeutic drugs targeting ribosome biogenesis have been studied [101,143,176]. Notably, reprogramming GBM cells differentiated into neurons using ROCK-mTOR inhibitors or three small molecules (FTT) significantly suppressed the tumor growth and prolonged the survival time in xenografted mice [52,54]. The downregulation of ZNF117 promoted the differentiation of GSC toward the oligodendrocyte lineage and decreased the tumorigenic potential [51]. There is a possibility that small molecules regulate the GSC differentiation into desired lineage cells in the future.

The dynamic phenotype alteration of GBM cells complicates chemoradiotherapies, which also demonstrates a possibility that different subtypes of GBM cells acquire distinct phenotypes through the reprogramming process. There are several hurdles that need to be overcome before clinical trials of cancer cell reprogramming therapy, such as clarifying the mechanism, efficacy, safety, and delivery methods for such agents. However, the transdifferentiation of GBM cells into other neural lineage cells or benign cells or hypo-proliferative states, including senescence, apoptosis, and cell death, may be a feasible challenge for future studies.

Therefore, through further knowledge on reprogramming in GBM cells, the residual GBM cells might be differentiated into non-proliferating functional cells. Moreover, if neurons derived from GBM cells can reconstruct neural networks, an improvement of neurological deficits might be expected (Figure 7). The transdifferentiation of GBM cells

into non-malignant cells through cancer cell reprogramming therapy might contribute to future GBM treatments.

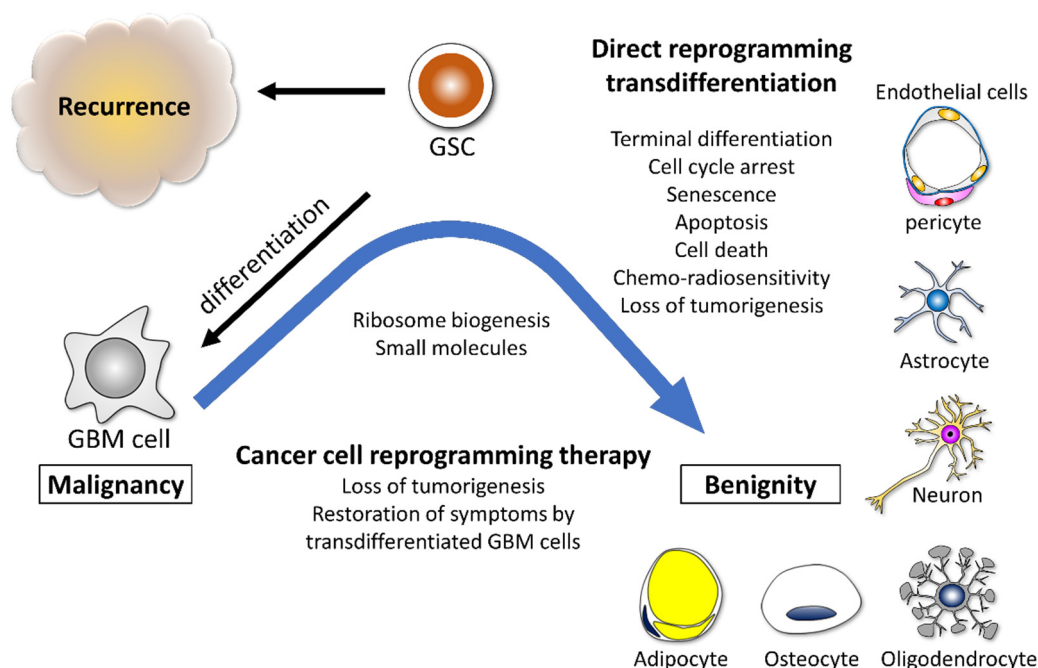


Figure 7. Cancer cell reprogramming therapy might convert malignancy to benignity. In reprogramming processes, malignant phenotypes convert to benign phenotypes. By inducing terminal differentiation, a hypo-proliferation state, chemo-radiosensitivity, and tumorigenicity loss, GBM cells are eliminated or they exist as non-proliferating cells in the brain. Ideally, if terminally differentiated GBM cells possess normal neuronal functions and are integrated into a normal brain, tumor deletion and regenerative medicine to improve neurological deficits could coexist.

Author Contributions: Conceptualization, T.H., I.S. and T.K.; formal analysis, T.H., I.S. and T.K.; writing—original draft preparation, T.H., I.S. and T.K.; writing—review and editing, R.S. and M.I.; supervision, M.I. and T.K. All authors have read and agreed to the published version of the manuscript.

Funding: This research was supported by Grants-in-Aid for Scientific Research (C) under Grant Number JP20K09374 (to Takuichiro Hide) from the Ministry of Education, Culture, Sports, Science and Technology.

Institutional Review Board Statement: Not applicable.

Informed Consent Statement: Not applicable.

Data Availability Statement: Not applicable.

Conflicts of Interest: The authors declare no conflict of interest.

References

1. Stupp, R.; Hegi, M.E.; Mason, W.P.; van den Bent, M.J.; Taphoorn, M.J.; Janzer, R.C.; Ludwin, S.K.; Allgeier, A.; Fisher, B.; Belanger, K.; et al. Effects of radiotherapy with concomitant and adjuvant temozolomide versus radiotherapy alone on survival in glioblastoma in a randomised phase III study: 5-year analysis of the EORTC-NCIC trial. *Lancet Oncol.* **2009**, *10*, 459–466. [CrossRef]
2. Stupp, R.; Mason, W.P.; van den Bent, M.J.; Weller, M.; Fisher, B.; Taphoorn, M.J.; Belanger, K.; Brandes, A.A.; Marosi, C.; Bogdahn, U.; et al. Radiotherapy plus concomitant and adjuvant temozolomide for glioblastoma. *N. Engl. J. Med.* **2005**, *352*, 987–996. [CrossRef] [PubMed]
3. Louis, D.N.; Perry, A.; Reifenberger, G.; von Deimling, A.; Figarella-Branger, D.; Cavenee, W.K.; Ohgaki, H.; Wiestler, O.D.; Kleihues, P.; Ellison, D.W. The 2016 World Health Organization Classification of Tumors of the Central Nervous System: A summary. *Acta Neuropathol.* **2016**, *131*, 803–820. [CrossRef] [PubMed]

4. Louis, D.N.; Perry, A.; Wesseling, P.; Brat, D.J.; Cree, I.A.; Figarella-Branger, D.; Hawkins, C.; Ng, H.K.; Pfister, S.M.; Reifenberger, G.; et al. The 2021 WHO Classification of Tumors of the Central Nervous System: A summary. *Neuro. Oncol.* **2021**, *23*, 1231–1251. [CrossRef]
5. Singh, S.K.; Hawkins, C.; Clarke, I.D.; Squire, J.A.; Bayani, J.; Hide, T.; Henkelman, R.M.; Cusimano, M.D.; Dirks, P.B. Identification of human brain tumour initiating cells. *Nature* **2004**, *432*, 396–401. [CrossRef]
6. Hide, T.; Takezaki, T.; Nakatani, Y.; Nakamura, H.; Kuratsu, J.; Kondo, T. Sox11 prevents tumorigenesis of glioma-initiating cells by inducing neuronal differentiation. *Cancer Res.* **2009**, *69*, 7953–7959. [CrossRef] [PubMed]
7. Hide, T.; Takezaki, T.; Nakatani, Y.; Nakamura, H.; Kuratsu, J.; Kondo, T. Combination of a p53 inhibitor and an epidermal growth factor receptor-signaling inhibitor prevents tumorigenesis of oligodendrocyte lineage-derived glioma-initiating cells. *Stem Cells* **2011**, *29*, 590–599. [CrossRef]
8. Agnihotri, S.; Burrell, K.E.; Wolf, A.; Jalali, S.; Hawkins, C.; Rutka, J.T.; Zadeh, G. Glioblastoma, a brief review of history, molecular genetics, animal models and novel therapeutic strategies. *Arch. Immunol. Ther. Exp.* **2013**, *61*, 25–41. [CrossRef]
9. Miyai, M.; Tomita, H.; Soeda, A.; Yano, H.; Iwama, T.; Hara, A. Current trends in mouse models of glioblastoma. *J. Neurooncol.* **2017**, *135*, 423–432. [CrossRef]
10. Jacob, F.; Salinas, R.D.; Zhang, D.Y.; Nguyen, P.T.T.; Schnoll, J.G.; Wong, S.Z.H.; Thokala, R.; Sheikh, S.; Saxena, D.; Prokop, S.; et al. A Patient-Derived Glioblastoma Organoid Model and Biobank Recapitulates Inter- and Intra-tumoral Heterogeneity. *Cell* **2020**, *180*, 188–204.e122. [CrossRef]
11. Bernstock, J.D.; Mooney, J.H.; Ilyas, A.; Chagoya, G.; Estevez-Ordonez, D.; Ibrahim, A.; Nakano, I. Molecular and cellular intratumoral heterogeneity in primary glioblastoma: Clinical and translational implications. *J. Neurosurg.* **2019**, *133*, 655–663. [CrossRef] [PubMed]
12. Kim, J.; Lee, I.H.; Cho, H.J.; Park, C.K.; Jung, Y.S.; Kim, Y.; Nam, S.H.; Kim, B.S.; Johnson, M.D.; Kong, D.S.; et al. Spatiotemporal Evolution of the Primary Glioblastoma Genome. *Cancer Cell* **2015**, *28*, 318–328. [CrossRef] [PubMed]
13. Lee, J.K.; Wang, J.; Sa, J.K.; Ladewig, E.; Lee, H.O.; Lee, I.H.; Kang, H.J.; Rosenbloom, D.S.; Camara, P.G.; Liu, Z.; et al. Spatiotemporal genomic architecture informs precision oncology in glioblastoma. *Nat. Genet.* **2017**, *49*, 594–599. [CrossRef]
14. Suzuki, H.; Aoki, K.; Chiba, K.; Sato, Y.; Shiozawa, Y.; Shiraishi, Y.; Shimamura, T.; Niida, A.; Motomura, K.; Ohka, F.; et al. Mutational landscape and clonal architecture in grade II and III gliomas. *Nat. Genet.* **2015**, *47*, 458–468. [CrossRef] [PubMed]
15. Sottoriva, A.; Spiteri, I.; Piccirillo, S.G.; Touloumis, A.; Collins, V.P.; Marioni, J.C.; Curtis, C.; Watts, C.; Tavare, S. Intratumor heterogeneity in human glioblastoma reflects cancer evolutionary dynamics. *Proc. Natl. Acad. Sci. USA* **2013**, *110*, 4009–4014. [CrossRef] [PubMed]
16. Patel, A.P.; Tirosh, I.; Trombetta, J.J.; Shalek, A.K.; Gillespie, S.M.; Wakimoto, H.; Cahill, D.P.; Nahed, B.V.; Curry, W.T.; Martuza, R.L.; et al. Single-cell RNA-seq highlights intratumoral heterogeneity in primary glioblastoma. *Science* **2014**, *344*, 1396–1401. [CrossRef] [PubMed]
17. Neftel, C.; Laffy, J.; Filbin, M.G.; Hara, T.; Shore, M.E.; Rahme, G.J.; Richman, A.R.; Silverbush, D.; Shaw, M.L.; Hebert, C.M.; et al. An Integrative Model of Cellular States, Plasticity, and Genetics for Glioblastoma. *Cell* **2019**, *178*, 835–849.e821. [CrossRef]
18. Chuang, D.F.; Lin, X. Targeted Therapies for the Treatment of Glioblastoma in Adults. *Curr. Oncol. Rep.* **2019**, *21*, 61. [CrossRef]
19. Yekula, A.; Yekula, A.; Muralidharan, K.; Kang, K.; Carter, B.S.; Balaj, L. Extracellular Vesicles in Glioblastoma Tumor Microenvironment. *Front. Immunol.* **2019**, *10*, 3137. [CrossRef]
20. Hide, T.; Komohara, Y.; Miyasato, Y.; Nakamura, H.; Makino, K.; Takeya, M.; Kuratsu, J.I.; Mukasa, A.; Yano, S. Oligodendrocyte Progenitor Cells and Macrophages/Microglia Produce Glioma Stem Cell Niches at the Tumor Border. *EBioMedicine* **2018**, *30*, 94–104. [CrossRef]
21. Broekman, M.L.; Maas, S.L.N.; Abels, E.R.; Mempel, T.R.; Krichevsky, A.M.; Breakefield, X.O. Multidimensional communication in the microenvirons of glioblastoma. *Nat. Rev. Neurol.* **2018**, *14*, 482–495. [CrossRef] [PubMed]
22. Papale, M.; Buccarelli, M.; Mollinari, C.; Russo, M.A.; Pallini, R.; Ricci-Vitiani, L.; Tafani, M. Hypoxia, Inflammation and Necrosis as Determinants of Glioblastoma Cancer Stem Cells Progression. *Int. J. Mol. Sci.* **2020**, *21*, 2660. [CrossRef] [PubMed]
23. Colwell, N.; Larion, M.; Giles, A.J.; Seldomridge, A.N.; Sizzdahkhani, S.; Gilbert, M.R.; Park, D.M. Hypoxia in the glioblastoma microenvironment: Shaping the phenotype of cancer stem-like cells. *Neuro Oncol.* **2017**, *19*, 887–896. [CrossRef] [PubMed]
24. Wang, L.; Shang, Z.; Zhou, Y.; Hu, X.; Chen, Y.; Fan, Y.; Wei, X.; Wu, L.; Liang, Q.; Zhang, J.; et al. Autophagy mediates glucose starvation-induced glioblastoma cell quiescence and chemoresistance through coordinating cell metabolism, cell cycle, and survival. *Cell Death Dis.* **2018**, *9*, 213. [CrossRef]
25. Shi, L.; Fei, X.; Sun, G.; Wang, Z.; Wan, Y.; Zeng, Y.; Guo, J. Hypothermia stimulates glioma stem spheres to spontaneously dedifferentiate adjacent non-stem glioma cells. *Cell Mol. Neurobiol.* **2015**, *35*, 217–230. [CrossRef]
26. Venkatesh, H.S.; Morishita, W.; Geraghty, A.C.; Silverbush, D.; Gillespie, S.M.; Arzt, M.; Tam, L.T.; Espenel, C.; Ponnuswami, A.; Ni, L.; et al. Electrical and synaptic integration of glioma into neural circuits. *Nature* **2019**, *573*, 539–545. [CrossRef]
27. Azambuja, J.H.; Ludwig, N.; Yerneni, S.S.; Braganhol, E.; Whiteside, T.L. Arginase-1+ Exosomes from Reprogrammed Macrophages Promote Glioblastoma Progression. *Int. J. Mol. Sci.* **2020**, *21*, 3990. [CrossRef]
28. Mega, A.; Hartmark Nilsen, M.; Leiss, L.W.; Tobin, N.P.; Miletic, H.; Sleire, L.; Strell, C.; Nelander, S.; Krona, C.; Hagerstrand, D.; et al. Astrocytes enhance glioblastoma growth. *Glia* **2020**, *68*, 316–327. [CrossRef]
29. Ito, N.; Katoh, K.; Kushige, H.; Saito, Y.; Umamoto, T.; Matsuzaki, Y.; Kiyonari, H.; Kobayashi, D.; Soga, M.; Era, T.; et al. Ribosome Incorporation into Somatic Cells Promotes Lineage Transdifferentiation towards Multipotency. *Sci. Rep.* **2018**, *8*, 1634. [CrossRef]

30. Takahashi, K.; Tanabe, K.; Ohnuki, M.; Narita, M.; Ichisaka, T.; Tomoda, K.; Yamanaka, S. Induction of pluripotent stem cells from adult human fibroblasts by defined factors. *Cell* **2007**, *131*, 861–872. [CrossRef]
31. Takahashi, K.; Yamanaka, S. Induction of pluripotent stem cells from mouse embryonic and adult fibroblast cultures by defined factors. *Cell* **2006**, *126*, 663–676. [CrossRef] [PubMed]
32. Kressler, D.; Hurt, E.; Bassler, J. Driving ribosome assembly. *Biochim. Biophys. Acta* **2010**, *1803*, 673–683. [CrossRef] [PubMed]
33. Zhou, X.; Liao, W.J.; Liao, J.M.; Liao, P.; Lu, H. Ribosomal proteins: Functions beyond the ribosome. *J. Mol. Cell Biol.* **2015**, *7*, 92–104. [CrossRef] [PubMed]
34. Warner, J.R.; McIntosh, K.B. How common are extraribosomal functions of ribosomal proteins? *Mol. Cell* **2009**, *34*, 3–11. [CrossRef] [PubMed]
35. El Khoury, W.; Nasr, Z. Deregulation of ribosomal proteins in human cancers. *Biosci. Rep.* **2021**, *41*, BSR20211577. [CrossRef] [PubMed]
36. Shirakawa, Y.; Hide, T.; Yamaoka, M.; Ito, Y.; Ito, N.; Ohta, K.; Shinojima, N.; Mukasa, A.; Saito, H.; Jono, H. Ribosomal protein S6 promotes stem-like characters in glioma cells. *Cancer Sci.* **2020**, *111*, 2041–2051. [CrossRef]
37. Chow, S.; Minden, M.D.; Hedley, D.W. Constitutive phosphorylation of the S6 ribosomal protein via mTOR and ERK signaling in the peripheral blasts of acute leukemia patients. *Exp. Hematol.* **2006**, *34*, 1183–1191. [CrossRef]
38. Khalailah, A.; Dreazen, A.; Khatib, A.; Apel, R.; Swisa, A.; Kidess-Bassir, N.; Maitra, A.; Meyuhas, O.; Dor, Y.; Zamir, G. Phosphorylation of ribosomal protein S6 attenuates DNA damage and tumor suppression during development of pancreatic cancer. *Cancer Res.* **2013**, *73*, 1811–1820. [CrossRef]
39. Chen, B.; Tan, Z.; Gao, J.; Wu, W.; Liu, L.; Jin, W.; Cao, Y.; Zhao, S.; Zhang, W.; Qiu, Z.; et al. Hyperphosphorylation of ribosomal protein S6 predicts unfavorable clinical survival in non-small cell lung cancer. *J. Exp. Clin. Cancer Res.* **2015**, *34*, 126. [CrossRef]
40. Shirakawa, Y.; Ohta, K.; Miyake, S.; Kanemaru, A.; Kuwano, A.; Yonemaru, K.; Uchino, S.; Yamaoka, M.; Ito, Y.; Ito, N.; et al. Glioma Cells Acquire Stem-like Characters by Extrinsic Ribosome Stimuli. *Cells* **2021**, *10*, 2970. [CrossRef]
41. Wilson, C.B. Glioblastoma: The past, the present, and the future. *Clin. Neurosurg.* **1992**, *38*, 32–48. [PubMed]
42. Sturm, D.; Witt, H.; Hovestadt, V.; Khuong-Quang, D.A.; Jones, D.T.; Konermann, C.; Pfaff, E.; Tonjes, M.; Sill, M.; Bender, S.; et al. Hotspot mutations in H3F3A and IDH1 define distinct epigenetic and biological subgroups of glioblastoma. *Cancer Cell* **2012**, *22*, 425–437. [CrossRef] [PubMed]
43. Snuderl, M.; Fazlollahi, L.; Le, L.P.; Nitta, M.; Zhelyazkova, B.H.; Davidson, C.J.; Akhavanfard, S.; Cahill, D.P.; Aldape, K.D.; Betensky, R.A.; et al. Mosaic amplification of multiple receptor tyrosine kinase genes in glioblastoma. *Cancer Cell* **2011**, *20*, 810–817. [CrossRef] [PubMed]
44. Verhaak, R.G.; Hoadley, K.A.; Purdom, E.; Wang, V.; Qi, Y.; Wilkerson, M.D.; Miller, C.R.; Ding, L.; Golub, T.; Mesirov, J.P.; et al. Integrated genomic analysis identifies clinically relevant subtypes of glioblastoma characterized by abnormalities in PDGFRA, IDH1, EGFR, and NF1. *Cancer Cell* **2010**, *17*, 98–110. [CrossRef] [PubMed]
45. Gong, L.; Yan, Q.; Zhang, Y.; Fang, X.; Liu, B.; Guan, X. Cancer cell reprogramming: A promising therapy converting malignancy to benignity. *Cancer Commun.* **2019**, *39*, 48. [CrossRef]
46. Reik, W.; Dean, W.; Walter, J. Epigenetic reprogramming in mammalian development. *Science* **2001**, *293*, 1089–1093. [CrossRef]
47. Faubert, B.; Solmonson, A.; DeBerardinis, R.J. Metabolic reprogramming and cancer progression. *Science* **2020**, *368*, eaaw5473. [CrossRef]
48. Grath, A.; Dai, G. Direct cell reprogramming for tissue engineering and regenerative medicine. *J. Biol. Eng.* **2019**, *13*, 14. [CrossRef]
49. Sell, S. Cancer stem cells and differentiation therapy. *Tumour Biol.* **2006**, *27*, 59–70. [CrossRef]
50. Massard, C.; Deutsch, E.; Soria, J.C. Tumour stem cell-targeted treatment: Elimination or differentiation. *Ann. Oncol.* **2006**, *17*, 1620–1624. [CrossRef]
51. Liu, J.; Wang, X.; Chen, A.T.; Gao, X.; Himes, B.T.; Zhang, H.; Chen, Z.; Wang, J.; Sheu, W.C.; Deng, G.; et al. ZNF117 regulates glioblastoma stem cell differentiation towards oligodendroglial lineage. *Nat. Commun.* **2022**, *13*, 2196. [CrossRef] [PubMed]
52. Yuan, J.; Zhang, F.; Hallahan, D.; Zhang, Z.; He, L.; Wu, L.G.; You, M.; Yang, Q. Reprogramming glioblastoma multiforme cells into neurons by protein kinase inhibitors. *J. Exp. Clin. Cancer Res.* **2018**, *37*, 181. [CrossRef] [PubMed]
53. Lee, C.; Robinson, M.; Willerth, S.M. Direct Reprogramming of Glioblastoma Cells into Neurons Using Small Molecules. *ACS Chem. Neurosci.* **2018**, *9*, 3175–3185. [CrossRef] [PubMed]
54. Gao, L.; Huang, S.; Zhang, H.; Hua, W.; Xin, S.; Cheng, L.; Guan, W.; Yu, Y.; Mao, Y.; Pei, G. Suppression of glioblastoma by a drug cocktail reprogramming tumor cells into neuronal like cells. *Sci. Rep.* **2019**, *9*, 3462. [CrossRef] [PubMed]
55. Ricci-Vitiani, L.; Pallini, R.; Biffoni, M.; Todaro, M.; Invernici, G.; Cenci, T.; Maira, G.; Parati, E.A.; Stassi, G.; Larocca, L.M.; et al. Tumour vascularization via endothelial differentiation of glioblastoma stem-like cells. *Nature* **2010**, *468*, 824–828. [CrossRef]
56. Soda, Y.; Marumoto, T.; Friedmann-Morvinski, D.; Soda, M.; Liu, F.; Michiue, H.; Pastorino, S.; Yang, M.; Hoffman, R.M.; Kesari, S.; et al. Transdifferentiation of glioblastoma cells into vascular endothelial cells. *Proc. Natl. Acad. Sci. USA* **2011**, *108*, 4274–4280. [CrossRef]
57. Wang, R.; Chadalavada, K.; Wilshire, J.; Kowalik, U.; Hovinga, K.E.; Geber, A.; Fligelman, B.; Leversha, M.; Brennan, C.; Tabar, V. Glioblastoma stem-like cells give rise to tumour endothelium. *Nature* **2010**, *468*, 829–833. [CrossRef]
58. Kucharczyk, P.; Christianson, H.C.; Welch, J.E.; Svensson, K.J.; Fredlund, E.; Ringner, M.; Morgelin, M.; Bourseau-Guilmain, E.; Bengzon, J.; Belting, M. Exosomes reflect the hypoxic status of glioma cells and mediate hypoxia-dependent activation of vascular cells during tumor development. *Proc. Natl. Acad. Sci. USA* **2013**, *110*, 7312–7317. [CrossRef]

59. Lucero, R.; Zappulli, V.; Sammarco, A.; Murillo, O.D.; Cheah, P.S.; Srinivasan, S.; Tai, E.; Ting, D.T.; Wei, Z.; Roth, M.E.; et al. Glioma-Derived miRNA-Containing Extracellular Vesicles Induce Angiogenesis by Reprogramming Brain Endothelial Cells. *Cell Rep.* **2020**, *30*, 2065–2074.e4. [CrossRef]
60. Domenech, M.; Hernandez, A.; Plaja, A.; Martinez-Balibrea, E.; Balana, C. Hypoxia: The Cornerstone of Glioblastoma. *Int. J. Mol. Sci.* **2021**, *22*, 12608. [CrossRef]
61. Chedeville, A.L.; Madureira, P.A. The Role of Hypoxia in Glioblastoma Radiotherapy Resistance. *Cancers* **2021**, *13*, 542. [CrossRef] [PubMed]
62. Kolenda, J.; Jensen, S.S.; Aaberg-Jessen, C.; Christensen, K.; Andersen, C.; Brunner, N.; Kristensen, B.W. Effects of hypoxia on expression of a panel of stem cell and chemoresistance markers in glioblastoma-derived spheroids. *J. Neurooncol.* **2011**, *103*, 43–58. [CrossRef] [PubMed]
63. Fidoamore, A.; Cristiano, L.; Antonosante, A.; d'Angelo, M.; Di Giacomo, E.; Astarita, C.; Giordano, A.; Ippoliti, R.; Benedetti, E.; Cimini, A. Glioblastoma Stem Cells Microenvironment: The Paracrine Roles of the Niche in Drug and Radioresistance. *Stem Cells Int.* **2016**, *2016*, 6809105. [CrossRef]
64. Bhushan, A.; Kumari, R.; Srivastava, T. Scouting for common genes in the heterogenous hypoxic tumor microenvironment and their validation in glioblastoma. *3 Biotech* **2021**, *11*, 451. [CrossRef] [PubMed]
65. Dahan, P.; Martinez Gala, J.; Delmas, C.; Monferran, S.; Malric, L.; Zentkowski, D.; Lubrano, V.; Toulas, C.; Cohen-Jonathan Moyal, E.; Lemarie, A. Ionizing radiations sustain glioblastoma cell dedifferentiation to a stem-like phenotype through survivin: Possible involvement in radioresistance. *Cell Death Dis.* **2014**, *5*, e1543. [CrossRef]
66. Venkataramani, V.; Tanev, D.I.; Strahle, C.; Studier-Fischer, A.; Fankhauser, L.; Kessler, T.; Korber, C.; Kardorff, M.; Ratliff, M.; Xie, R.; et al. Glutamatergic synaptic input to glioma cells drives brain tumour progression. *Nature* **2019**, *573*, 532–538. [CrossRef] [PubMed]
67. Allen, N.J.; Eroglu, C. Cell Biology of Astrocyte-Synapse Interactions. *Neuron* **2017**, *96*, 697–708. [CrossRef]
68. Araque, A.; Carmignoto, G.; Haydon, P.G.; Oliet, S.H.; Robitaille, R.; Volterra, A. Gliotransmitters travel in time and space. *Neuron* **2014**, *81*, 728–739.
69. Allen, N.J.; Lyons, D.A. Glia as architects of central nervous system formation and function. *Science* **2018**, *362*, 181–185. [CrossRef]
70. Bergles, D.E.; Roberts, J.D.; Somogyi, P.; Jahr, C.E. Glutamatergic synapses on oligodendrocyte precursor cells in the hippocampus. *Nature* **2000**, *405*, 187–191. [CrossRef]
71. Habermacher, C.; Angulo, M.C.; Benamer, N. Glutamate versus GABA in neuron-oligodendroglia communication. *Glia* **2019**, *67*, 2092–2106. [CrossRef] [PubMed]
72. Kula, B.; Chen, T.J.; Kukley, M. Glutamatergic signaling between neurons and oligodendrocyte lineage cells: Is it synaptic or non-synaptic? *Glia* **2019**, *67*, 2071–2091. [CrossRef] [PubMed]
73. Osswald, M.; Jung, E.; Sahm, F.; Solecki, G.; Venkataramani, V.; Blaes, J.; Weil, S.; Horstmann, H.; Wiestler, B.; Syed, M.; et al. Brain tumour cells interconnect to a functional and resistant network. *Nature* **2015**, *528*, 93–98. [CrossRef] [PubMed]
74. Weil, S.; Osswald, M.; Solecki, G.; Grosch, J.; Jung, E.; Lemke, D.; Ratliff, M.; Hanggi, D.; Wick, W.; Winkler, F. Tumor microtubules convey resistance to surgical lesions and chemotherapy in gliomas. *Neuro Oncol.* **2017**, *19*, 1316–1326. [CrossRef]
75. Hide, T.; Shibahara, I.; Kumabe, T. Novel concept of the border niche: Glioblastoma cells use oligodendrocytes progenitor cells (GAOs) and microglia to acquire stem cell-like features. *Brain Tumor Pathol.* **2019**, *36*, 63–73. [CrossRef]
76. Brandao, M.; Simon, T.; Critchley, G.; Giamas, G. Astrocytes, the rising stars of the glioblastoma microenvironment. *Glia* **2019**, *67*, 779–790. [CrossRef]
77. Guan, X.; Hasan, M.N.; Maniar, S.; Jia, W.; Sun, D. Reactive Astrocytes in Glioblastoma Multiforme. *Mol. Neurobiol.* **2018**, *55*, 6927–6938. [CrossRef]
78. Lois, C.; Alvarez-Buylla, A. Proliferating subventricular zone cells in the adult mammalian forebrain can differentiate into neurons and glia. *Proc. Natl. Acad. Sci. USA* **1993**, *90*, 2074–2077. [CrossRef]
79. Li, G.; Chen, Z.; Hu, Y.D.; Wei, H.; Li, D.; Ji, H.; Wang, D.L. Autocrine factors sustain glioblastoma stem cell self-renewal. *Oncol. Rep.* **2009**, *21*, 419–424.
80. Kuratsu, J.; Leonard, E.J.; Yoshimura, T. Production and characterization of human glioma cell-derived monocyte chemotactic factor. *J. Natl. Cancer Inst.* **1989**, *81*, 347–351. [CrossRef]
81. Chang, A.L.; Miska, J.; Wainwright, D.A.; Dey, M.; Rivetta, C.V.; Yu, D.; Kanojia, D.; Pituch, K.C.; Qiao, J.; Pytel, P.; et al. CCL2 Produced by the Glioma Microenvironment Is Essential for the Recruitment of Regulatory T Cells and Myeloid-Derived Suppressor Cells. *Cancer Res.* **2016**, *76*, 5671–5682. [CrossRef] [PubMed]
82. Shono, K.; Yamaguchi, I.; Mizobuchi, Y.; Kagusa, H.; Sumi, A.; Fujihara, T.; Nakajima, K.; Kitazato, K.T.; Matsuzaki, K.; Saya, H.; et al. Downregulation of the CCL2/CCR2 and CXCL10/CXCR3 axes contributes to antitumor effects in a mouse model of malignant glioma. *Sci. Rep.* **2020**, *10*, 15286. [CrossRef] [PubMed]
83. Zeis, T.; Enz, L.; Schaeren-Wiemers, N. The immunomodulatory oligodendrocyte. *Brain Res.* **2016**, *1641*, 139–148. [CrossRef] [PubMed]
84. Urbantat, R.M.; Vajkoczy, P.; Brandenburg, S. Advances in Chemokine Signaling Pathways as Therapeutic Targets in Glioblastoma. *Cancers* **2021**, *13*, 2983. [CrossRef] [PubMed]
85. Yeo, E.C.F.; Brown, M.P.; Gargett, T.; Ebert, L.M. The Role of Cytokines and Chemokines in Shaping the Immune Microenvironment of Glioblastoma: Implications for Immunotherapy. *Cells* **2021**, *10*, 607. [CrossRef]

86. Sil, S.; Periyasamy, P.; Thangaraj, A.; Chivero, E.T.; Buch, S. PDGF/PDGFR axis in the neural systems. *Mol. Aspects Med.* **2018**, *62*, 63–74. [CrossRef]
87. Almiron Bonnin, D.A.; Havrda, M.C.; Lee, M.C.; Liu, H.; Zhang, Z.; Nguyen, L.N.; Harrington, L.X.; Hassanpour, S.; Cheng, C.; Israel, M.A. Secretion-mediated STAT3 activation promotes self-renewal of glioma stem-like cells during hypoxia. *Oncogene* **2018**, *37*, 1107–1118. [CrossRef]
88. Rodriguez, S.M.B.; Staicu, G.A.; Sevastre, A.S.; Baloi, C.; Ciubotaru, V.; Dricu, A.; Tataranu, L.G. Glioblastoma Stem Cells-Useful Tools in the Battle against Cancer. *Int. J. Mol. Sci.* **2022**, *23*, 4602. [CrossRef]
89. Quezada, C.; Torres, A.; Niechi, I.; Uribe, D.; Contreras-Duarte, S.; Toledo, F.; San Martin, R.; Gutierrez, J.; Sobrevia, L. Role of extracellular vesicles in glioma progression. *Mol. Aspects Med.* **2018**, *60*, 38–51. [CrossRef]
90. Matarredona, E.R.; Pastor, A.M. Extracellular Vesicle-Mediated Communication between the Glioblastoma and Its Microenvironment. *Cells* **2019**, *9*, 96. [CrossRef]
91. Simon, T.; Jackson, E.; Giamas, G. Breaking through the glioblastoma micro-environment via extracellular vesicles. *Oncogene* **2020**, *39*, 4477–4490. [CrossRef] [PubMed]
92. Maas, S.L.N.; Breakefield, X.O.; Weaver, A.M. Extracellular Vesicles: Unique Intercellular Delivery Vehicles. *Trends Cell Biol.* **2017**, *27*, 172–188. [CrossRef] [PubMed]
93. Skog, J.; Wurdinger, T.; van Rijn, S.; Meijer, D.H.; Gainche, L.; Sena-Estevés, M.; Curry, W.T., Jr.; Carter, B.S.; Krichevsky, A.M.; Breakefield, X.O. Glioblastoma microvesicles transport RNA and proteins that promote tumour growth and provide diagnostic biomarkers. *Nat. Cell Biol.* **2008**, *10*, 1470–1476. [CrossRef] [PubMed]
94. Wang, J.; Liu, J.; Sun, G.; Meng, H.; Wang, J.; Guan, Y.; Yin, Y.; Zhao, Z.; Dong, X.; Yin, S.; et al. Glioblastoma extracellular vesicles induce the tumour-promoting transformation of neural stem cells. *Cancer Lett.* **2019**, *466*, 1–12. [CrossRef]
95. Sun, Z.; Wang, L.; Zhou, Y.; Dong, L.; Ma, W.; Lv, L.; Zhang, J.; Wang, X. Glioblastoma Stem Cell-Derived Exosomes Enhance Stemness and Tumorigenicity of Glioma Cells by Transferring Notch1 Protein. *Cell Mol. Neurobiol.* **2020**, *40*, 767–784. [CrossRef]
96. Gao, X.; Zhang, Z.; Mashimo, T.; Shen, B.; Nyagilo, J.; Wang, H.; Wang, Y.; Liu, Z.; Mulgaonkar, A.; Hu, X.L.; et al. Gliomas Interact with Non-glioma Brain Cells via Extracellular Vesicles. *Cell Rep.* **2020**, *30*, 2489–2500.e5. [CrossRef]
97. Hallal, S.; Mallawaarachy, D.M.; Wei, H.; Ebrahimkhani, S.; Stringer, B.W.; Day, B.W.; Boyd, A.W.; Guillemin, G.J.; Buckland, M.E.; Kaufman, K.L. Extracellular Vesicles Released by Glioblastoma Cells Stimulate Normal Astrocytes to Acquire a Tumor-Supportive Phenotype Via p53 and MYC Signaling Pathways. *Mol. Neurobiol.* **2019**, *56*, 4566–4581. [CrossRef]
98. Oushy, S.; Hellwinkel, J.E.; Wang, M.; Nguyen, G.J.; Gunaydin, D.; Harland, T.A.; Anchordoquy, T.J.; Graner, M.W. Glioblastoma multiforme-derived extracellular vesicles drive normal astrocytes towards a tumour-enhancing phenotype. *Philos. Trans. R Soc. Lond B Biol. Sci.* **2018**, *373*, 20160477. [CrossRef]
99. Zeng, A.; Wei, Z.; Rabinovsky, R.; Jun, H.J.; El Fatimy, R.; Deforz, E.; Arora, R.; Yao, Y.; Yao, S.; Yan, W.; et al. Glioblastoma-Derived Extracellular Vesicles Facilitate Transformation of Astrocytes via Reprogramming Oncogenic Metabolism. *iScience* **2020**, *23*, 101420. [CrossRef]
100. Piazzini, M.; Bavelloni, A.; Gallo, A.; Faenza, I.; Blalock, W.L. Signal Transduction in Ribosome Biogenesis: A Recipe to Avoid Disaster. *Int. J. Mol. Sci.* **2019**, *20*, 2718. [CrossRef]
101. Kang, J.; Brajanovski, N.; Chan, K.T.; Xuan, J.; Pearson, R.B.; Sanij, E. Ribosomal proteins and human diseases: Molecular mechanisms and targeted therapy. *Signal Transduct. Target. Ther.* **2021**, *6*, 323. [CrossRef] [PubMed]
102. Nakao, A.; Yoshihama, M.; Kenmochi, N. RPG: The Ribosomal Protein Gene database. *Nucleic Acids Res.* **2004**, *32*, D168–D170. [CrossRef] [PubMed]
103. Gaviraghi, M.; Vivori, C.; Tonon, G. How Cancer Exploits Ribosomal RNA Biogenesis: A Journey beyond the Boundaries of rRNA Transcription. *Cells* **2019**, *8*, 1098. [CrossRef] [PubMed]
104. Drygin, D.; Rice, W.G.; Grummt, I. The RNA polymerase I transcription machinery: An emerging target for the treatment of cancer. *Annu. Rev. Pharmacol. Toxicol.* **2010**, *50*, 131–156. [CrossRef]
105. Stefanovsky, V.Y.; Pelletier, G.; Hannan, R.; Gagnon-Kugler, T.; Rothblum, L.I.; Moss, T. An immediate response of ribosomal transcription to growth factor stimulation in mammals is mediated by ERK phosphorylation of UBF. *Mol. Cell* **2001**, *8*, 1063–1073. [CrossRef]
106. Franke, T.F. PI3K/Akt: Getting it right matters. *Oncogene* **2008**, *27*, 6473–6488. [CrossRef]
107. Grandori, C.; Gomez-Roman, N.; Felton-Edkins, Z.A.; Ngouenet, C.; Galloway, D.A.; Eisenman, R.N.; White, R.J. c-Myc binds to human ribosomal DNA and stimulates transcription of rRNA genes by RNA polymerase I. *Nat. Cell Biol.* **2005**, *7*, 311–318. [CrossRef]
108. Arabi, A.; Wu, S.; Ridderstrale, K.; Bierhoff, H.; Shiue, C.; Fatyol, K.; Fahlen, S.; Hydbring, P.; Soderberg, O.; Grummt, I.; et al. c-Myc associates with ribosomal DNA and activates RNA polymerase I transcription. *Nat. Cell Biol.* **2005**, *7*, 303–310. [CrossRef]
109. Thoms, H.C.; Stark, L.A. The NF-kappaB Nucleolar Stress Response Pathway. *Biomedicines* **2021**, *9*, 1082. [CrossRef]
110. Dameshek, W. Riddle: What do aplastic anemia, paroxysmal nocturnal hemoglobinuria (PNH) and hypoplastic leukemia have in common? *Blood* **1967**, *30*, 251–254. [CrossRef]
111. Kampen, K.R.; Sulima, S.O.; Vereecke, S.; De Keersmaecker, K. Hallmarks of ribosomopathies. *Nucleic Acids Res.* **2020**, *48*, 1013–1028. [CrossRef] [PubMed]
112. Yi, Y.W.; You, K.S.; Park, J.S.; Lee, S.G.; Seong, Y.S. Ribosomal Protein S6: A Potential Therapeutic Target against Cancer? *Int. J. Mol. Sci.* **2021**, *23*, 48. [CrossRef] [PubMed]

113. Hide, T.; Shibahara, I.; Inukai, M.; Shigeeda, R.; Shirakawa, Y.; Jono, H.; Shinojima, N.; Mukasa, A.; Kumabe, T. Ribosomal proteins induce stem cell-like characteristics in glioma cells as an extra-ribosomal function. *Brain Tumor Pathol.* **2022**, *39*, 51–56. [CrossRef] [PubMed]
114. Penzo, M.; Montanaro, L.; Trere, D.; Derenzini, M. The Ribosome Biogenesis-Cancer Connection. *Cells* **2019**, *8*, 55. [CrossRef] [PubMed]
115. Pecoraro, A.; Pagano, M.; Russo, G.; Russo, A. Ribosome Biogenesis and Cancer: Overview on Ribosomal Proteins. *Int. J. Mol. Sci.* **2021**, *22*, 5496. [CrossRef]
116. Pestov, D.G.; Strezoska, Z.; Lau, L.F. Evidence of p53-dependent cross-talk between ribosome biogenesis and the cell cycle: Effects of nucleolar protein Bop1 on G(1)/S transition. *Mol. Cell Biol.* **2001**, *21*, 4246–4255. [CrossRef]
117. Liu, Y.; Deisenroth, C.; Zhang, Y. RP-MDM2-p53 Pathway: Linking Ribosomal Biogenesis and Tumor Surveillance. *Trends Cancer* **2016**, *2*, 191–204. [CrossRef]
118. Lo, S.J.; Fan, L.C.; Tsai, Y.F.; Lin, K.Y.; Huang, H.L.; Wang, T.H.; Liu, H.; Chen, T.C.; Huang, S.F.; Chang, C.J.; et al. A novel interaction of nucleophosmin with BCL2-associated X protein regulating death evasion and drug sensitivity in human hepatoma cells. *Hepatology* **2013**, *57*, 1893–1905. [CrossRef]
119. Eymin, B.; Claverie, P.; Salon, C.; Leduc, C.; Col, E.; Brambilla, E.; Khochbin, S.; Gazzeri, S. p14ARF activates a Tip60-dependent and p53-independent ATM/ATR/CHK pathway in response to genotoxic stress. *Mol. Cell Biol.* **2006**, *26*, 4339–4350. [CrossRef]
120. James, A.; Wang, Y.; Raje, H.; Rosby, R.; DiMario, P. Nucleolar stress with and without p53. *Nucleus* **2014**, *5*, 402–426. [CrossRef]
121. Russo, A.; Russo, G. Ribosomal Proteins Control or Bypass p53 during Nucleolar Stress. *Int. J. Mol. Sci.* **2017**, *18*, 140. [CrossRef] [PubMed]
122. Correll, C.C.; Bartek, J.; Dunder, M. The Nucleolus: A Multiphase Condensate Balancing Ribosome Synthesis and Translational Capacity in Health, Aging and Ribosomopathies. *Cells* **2019**, *8*, 869. [CrossRef] [PubMed]
123. Aspesi, A.; Ellis, S.R. Rare ribosomopathies: Insights into mechanisms of cancer. *Nat. Rev. Cancer* **2019**, *19*, 228–238. [CrossRef] [PubMed]
124. Orgebin, E.; Lamoureux, F.; Isidor, B.; Charrier, C.; Ory, B.; Lezot, F.; Baud'huin, M. Ribosomopathies: New Therapeutic Perspectives. *Cells* **2020**, *9*, 2080.
125. Ohta, K.; Kawano, R.; Ito, N. Lactic acid bacteria convert human fibroblasts to multipotent cells. *PLoS ONE* **2012**, *7*, e51866. [CrossRef]
126. Istiaq, A.; Ohta, K. Ribosome-Induced Cellular Multipotency, an Emerging Avenue in Cell Fate Reversal. *Cells* **2021**, *10*, 2276. [CrossRef]
127. Grundy, M.; Jones, T.; Elmi, L.; Hall, M.; Graham, A.; Russell, N.; Pallis, M. Early changes in rpS6 phosphorylation and BH3 profiling predict response to chemotherapy in AML cells. *PLoS ONE* **2018**, *13*, e0196805.
128. Hagner, P.R.; Mazan-Mamczarz, K.; Dai, B.; Balzer, E.M.; Corl, S.; Martin, S.S.; Zhao, X.F.; Gartenhaus, R.B. Ribosomal protein S6 is highly expressed in non-Hodgkin lymphoma and associates with mRNA containing a 5' terminal oligopyrimidine tract. *Oncogene* **2011**, *30*, 1531–1541. [CrossRef]
129. Chaisuparat, R.; Rojanawatsirivej, S.; Yodsanga, S. Ribosomal protein S6 phosphorylation is associated with epithelial dysplasia and squamous cell carcinoma of the oral cavity. *Pathol. Oncol. Res.* **2013**, *19*, 189–193. [CrossRef]
130. Yanai, A.; Inoue, N.; Yagi, T.; Nishimukai, A.; Miyagawa, Y.; Murase, K.; Imamura, M.; Enomoto, Y.; Takatsuka, Y.; Watanabe, T.; et al. Activation of mTOR/S6K But Not MAPK Pathways Might Be Associated with High Ki-67, ER(+), and HER2(−) Breast Cancer. *Clin. Breast Cancer* **2015**, *15*, 197–203. [CrossRef]
131. Zheng, Z.; Zheng, Y.; Zhang, M.; Wang, J.; Yu, G.; Fang, W. Reciprocal expression of p-AMPKα and p-S6 is strongly associated with the prognosis of gastric cancer. *Tumour Biol.* **2016**, *37*, 4803–4811. [CrossRef] [PubMed]
132. Knoll, M.; Macher-Goeppinger, S.; Kopitz, J.; Duensing, S.; Pahernik, S.; Hohenfellner, M.; Schirmacher, P.; Roth, W. The ribosomal protein S6 in renal cell carcinoma: Functional relevance and potential as biomarker. *Oncotarget* **2016**, *7*, 418–432. [CrossRef] [PubMed]
133. Liu, Z.; Yun, R.; Yu, X.; Hu, H.; Huang, G.; Tan, B.; Chen, T. Overexpression of Notch3 and pS6 Is Associated with Poor Prognosis in Human Ovarian Epithelial Cancer. *Mediators Inflamm.* **2016**, *2016*, 5953498. [CrossRef]
134. Corcoran, R.B.; Rothenberg, S.M.; Hata, A.N.; Faber, A.C.; Piris, A.; Nazarian, R.M.; Brown, R.D.; Godfrey, J.T.; Winokur, D.; Walsh, J.; et al. TORC1 suppression predicts responsiveness to RAF and MEK inhibition in BRAF-mutant melanoma. *Sci. Transl. Med.* **2013**, *5*, 196ra198. [CrossRef] [PubMed]
135. Zhang, D.; Chen, H.P.; Duan, H.F.; Gao, L.H.; Shao, Y.; Chen, K.Y.; Wang, Y.L.; Lan, F.H.; Hu, X.W. Aggregation of Ribosomal Protein S6 at Nucleolus Is Cell Cycle-Controlled and Its Function in Pre-rRNA Processing Is Phosphorylation Dependent. *J. Cell Biochem.* **2016**, *117*, 1649–1657. [CrossRef]
136. Puchalski, R.B.; Shah, N.; Miller, J.; Dalley, R.; Nomura, S.R.; Yoon, J.G.; Smith, K.A.; Lankerovich, M.; Bertagnolli, D.; Bickley, K.; et al. An anatomic transcriptional atlas of human glioblastoma. *Science* **2018**, *360*, 660–663. [CrossRef]
137. Ganger, D.R.; Hamilton, P.D.; Fletcher, J.W.; Fernandez-Pol, J.A. Metallopanstimulin is overexpressed in a patient with colonic carcinoma. *Anticancer Res.* **1997**, *17*, 1993–1999.
138. Fernandez-Pol, J.A.; Fletcher, J.W.; Hamilton, P.D.; Klos, D.J. Expression of metallopanstimulin and oncogenesis in human prostatic carcinoma. *Anticancer Res.* **1997**, *17*, 1519–1530.

139. Atsuta, Y.; Aoki, N.; Sato, K.; Oikawa, K.; Nochi, H.; Miyokawa, N.; Hirata, S.; Kimura, S.; Sasajima, T.; Katagiri, M. Identification of metalloproteinase-1 as a member of a tumor associated antigen in patients with breast cancer. *Cancer Lett.* **2002**, *182*, 101–107. [CrossRef]
140. Wang, Y.W.; Qu, Y.; Li, J.F.; Chen, X.H.; Liu, B.Y.; Gu, Q.L.; Zhu, Z.G. In vitro and in vivo evidence of metalloproteinase-1 in gastric cancer progression and tumorigenicity. *Clin. Cancer Res.* **2006**, *12*, 4965–4973. [CrossRef]
141. Fernandez-Pol, J.A. Increased serum level of RPS27/S27 protein in patients with various types of cancer is useful for the early detection, prevention and therapy. *Cancer Genom. Proteom.* **2012**, *9*, 203–256.
142. Feldheim, J.; Kessler, A.F.; Schmitt, D.; Salvador, E.; Monoranu, C.M.; Feldheim, J.J.; Ernestus, R.I.; Lohr, M.; Hagemann, C. Ribosomal Protein S27/Metalloproteinase-1 (RPS27) in Glioma-A New Disease Biomarker? *Cancers* **2020**, *12*, 1085. [CrossRef] [PubMed]
143. Zhang, C.; Fu, J.; Xue, F.; Ryu, B.; Zhang, T.; Zhang, S.; Sun, J.; Xu, X.; Shen, Z.; Zheng, L.; et al. Knockdown of ribosomal protein S15A induces human glioblastoma cell apoptosis. *World J. Surg. Oncol.* **2016**, *14*, 129. [CrossRef]
144. Yao, Y.; Liu, Y.; Lv, X.; Dong, B.; Wang, F.; Li, J.; Zhang, Q.; Xu, R.; Xu, Y. Down-regulation of ribosomal protein S15A inhibits proliferation of human glioblastoma cells in vivo and in vitro via AKT pathway. *Tumour Biol.* **2016**, *37*, 4979–4990. [CrossRef] [PubMed]
145. Nissan, T.A.; Bassler, J.; Petfalski, E.; Tollervey, D.; Hurt, E. 60S pre-ribosome formation viewed from assembly in the nucleolus until export to the cytoplasm. *EMBO J.* **2002**, *21*, 5539–5547. [CrossRef] [PubMed]
146. Fancellò, L.; Kampen, K.R.; Hofman, I.J.; Verbeeck, J.; De Keersmaecker, K. The ribosomal protein gene RPL5 is a haploinsufficient tumor suppressor in multiple cancer types. *Oncotarget* **2017**, *8*, 14462–14478. [CrossRef] [PubMed]
147. Awah, C.U.; Chen, L.; Bansal, M.; Mahajan, A.; Winter, J.; Lad, M.; Warnke, L.; Gonzalez-Buendia, E.; Park, C.; Zhang, D.; et al. Ribosomal protein S11 influences glioma response to TOP2 poisons. *Oncogene* **2020**, *39*, 5068–5081. [CrossRef]
148. Jeon, Y.J.; Kim, I.K.; Hong, S.H.; Nan, H.; Kim, H.J.; Lee, H.J.; Masuda, E.S.; Meyuhas, O.; Oh, B.H.; Jung, Y.K. Ribosomal protein S6 is a selective mediator of TRAIL-apoptotic signaling. *Oncogene* **2008**, *27*, 4344–4352. [CrossRef]
149. Kim, Y.; Kim, H.D.; Youn, B.; Park, Y.G.; Kim, J. Ribosomal protein S3 is secreted as a homodimer in cancer cells. *Biochem. Biophys. Res. Commun.* **2013**, *441*, 805–808. [CrossRef]
150. Court, F.A.; Hendriks, W.T.; MacGillavry, H.D.; Alvarez, J.; van Minnen, J. Schwann cell to axon transfer of ribosomes: Toward a novel understanding of the role of glia in the nervous system. *J. Neurosci.* **2008**, *28*, 11024–11029. [CrossRef]
151. Lopez-Leal, R.; Alvarez, J.; Court, F.A. Origin of axonal proteins: Is the axon-schwann cell unit a functional syncytium? *Cytoskeleton* **2016**, *73*, 629–639. [CrossRef] [PubMed]
152. Pinto, G.; Saenz-de-Santa-Maria, I.; Chastagner, P.; Perthame, E.; Delmas, C.; Toulas, C.; Moyal-Jonathan-Cohen, E.; Brou, C.; Zurzolo, C. Patient-derived glioblastoma stem cells transfer mitochondria through tunneling nanotubes in tumor organoids. *Biochem. J.* **2021**, *478*, 21–39. [CrossRef] [PubMed]
153. Kudo, M.; Anam, M.B.; Istiaq, A.; Ahmad, S.A.I.; Ito, N.; Ohta, K. Ribosome Incorporation Induces EMT-like Phenomenon with Cell Cycle Arrest in Human Breast Cancer Cell. *Cells Tissues Organs* **2022**, *211*, 212–221. [CrossRef] [PubMed]
154. Anam, M.B.; Istiaq, A.; Kariya, R.; Kudo, M.; Ishtiyahq Ahmad, S.A.; Ito, N.; Okada, S.; Ohta, K. Ribosome induces transdifferentiation of A549 and H-111-TC cancer cell lines. *Biochem. Biophys. Rep.* **2021**, *26*, 100946. [CrossRef] [PubMed]
155. Setayesh-Mehr, Z.; Poorsargol, M. Toxic proteins application in cancer therapy. *Mol. Biol. Rep.* **2021**, *48*, 3827–3840. [CrossRef]
156. Rotondo, R.; Ragucci, S.; Castaldo, S.; Oliva, M.A.; Landi, N.; Pedone, P.V.; Arcella, A.; Di Maro, A. Cytotoxicity Effect of Quinoin, Type 1 Ribosome-Inactivating Protein from Quinoa Seeds, on Glioblastoma Cells. *Toxins* **2021**, *13*, 684. [CrossRef]
157. Lapik, Y.R.; Fernandes, C.J.; Lau, L.F.; Pestov, D.G. Physical and functional interaction between Pes1 and Bop1 in mammalian ribosome biogenesis. *Mol. Cell* **2004**, *15*, 17–29. [CrossRef]
158. Holzel, M.; Rohrmoser, M.; Schlee, M.; Grimm, T.; Harasim, T.; Malamoussi, A.; Gruber-Eber, A.; Kremmer, E.; Hiddemann, W.; Bornkamm, G.W.; et al. Mammalian WDR12 is a novel member of the Pes1-Bop1 complex and is required for ribosome biogenesis and cell proliferation. *J. Cell Biol.* **2005**, *170*, 367–378. [CrossRef]
159. Li, Y.Z.; Zhang, C.; Pei, J.P.; Zhang, W.C.; Zhang, C.D.; Dai, D.Q. The functional role of Pescadillo ribosomal biogenesis factor 1 in cancer. *J. Cancer* **2022**, *13*, 268–277. [CrossRef]
160. Mi, L.; Qi, Q.; Ran, H.; Chen, L.; Li, D.; Xiao, D.; Wu, J.; Cai, Y.; Zhang, S.; Li, Y.; et al. Suppression of Ribosome Biogenesis by Targeting WD Repeat Domain 12 (WDR12) Inhibits Glioma Stem-Like Cell Growth. *Front. Oncol.* **2021**, *11*, 751792. [CrossRef]
161. Li, J.L.; Chen, C.; Chen, W.; Zhao, L.F.; Xu, X.K.; Li, Y.; Yuan, H.Y.; Lin, J.R.; Pan, J.P.; Jin, B.L.; et al. Integrative genomic analyses identify WDR12 as a novel oncogene involved in glioblastoma. *J. Cell Physiol.* **2020**, *235*, 7344–7355. [CrossRef] [PubMed]
162. Kofuji, S.; Hirayama, A.; Eberhardt, A.O.; Kawaguchi, R.; Sugiura, Y.; Sampetean, O.; Ikeda, Y.; Warren, M.; Sakamoto, N.; Kitahara, S.; et al. IMP dehydrogenase-2 drives aberrant nucleolar activity and promotes tumorigenesis in glioblastoma. *Nat. Cell Biol.* **2019**, *21*, 1003–1014. [CrossRef] [PubMed]
163. Zhou, W.; Yao, Y.; Scott, A.J.; Wilder-Romans, K.; Dresser, J.J.; Werner, C.K.; Sun, H.; Pratt, D.; Sajjakulnukit, P.; Zhao, S.G.; et al. Purine metabolism regulates DNA repair and therapy resistance in glioblastoma. *Nat. Commun.* **2020**, *11*, 3811. [CrossRef] [PubMed]
164. Lafita-Navarro, M.C.; Venkateswaran, N.; Kilgore, J.A.; Kanji, S.; Han, J.; Barnes, S.; Williams, N.S.; Buszczak, M.; Burma, S.; Conacci-Sorrell, M. Inhibition of the de novo pyrimidine biosynthesis pathway limits ribosomal RNA transcription causing nucleolar stress in glioblastoma cells. *PLoS Genet.* **2020**, *16*, e1009117. [CrossRef]

165. Tagliaferro, M.; Rosa, P.; Bellenchi, G.C.; Bastianelli, D.; Trotta, R.; Tito, C.; Fazi, F.; Calogero, A.; Ponti, D. Nucleolar localization of the ErbB3 receptor as a new target in glioblastoma. *BMC Mol. Cell Biol.* **2022**, *23*, 13. [CrossRef]
166. Park, S.J.; Kim, H.; Kim, S.H.; Joe, E.H.; Jou, I. Epigenetic downregulation of STAT6 increases HIF-1alpha expression via mTOR/S6K/S6, leading to enhanced hypoxic viability of glioma cells. *Acta Neuropathol. Commun.* **2019**, *7*, 149. [CrossRef]
167. Shi, J.; Zhang, W.; He, L.; Kong, F.; Pan, M.; Guo, J.; Xu, X.; Guo, J.; Wang, H.; Wang, Y. Jinlong capsule inhibits migration and invasion in human glioblastoma cells via the modulation of mTOR/S6 signaling pathway. *Drug Des. Devel. Ther.* **2019**, *13*, 1023–1032. [CrossRef]
168. Udugama, M.; Sanij, E.; Voon, H.P.J.; Son, J.; Hii, L.; Henson, J.D.; Chan, F.L.; Chang, F.T.M.; Liu, Y.; Pearson, R.B.; et al. Ribosomal DNA copy loss and repeat instability in ATRX-mutated cancers. *Proc. Natl. Acad. Sci. USA* **2018**, *115*, 4737–4742. [CrossRef]
169. Burger, K.; Muhl, B.; Harasim, T.; Rohrmoser, M.; Malamoussi, A.; Orban, M.; Kellner, M.; Gruber-Eber, A.; Kremmer, E.; Holzel, M.; et al. Chemotherapeutic drugs inhibit ribosome biogenesis at various levels. *J. Biol. Chem.* **2010**, *285*, 12416–12425. [CrossRef]
170. Drygin, D.; Siddiqui-Jain, A.; O'Brien, S.; Schwaebe, M.; Lin, A.; Bliesath, J.; Ho, C.B.; Proffitt, C.; Trent, K.; Whitten, J.P.; et al. Anticancer activity of CX-3543: A direct inhibitor of rRNA biogenesis. *Cancer Res.* **2009**, *69*, 7653–7661. [CrossRef]
171. Drygin, D.; Lin, A.; Bliesath, J.; Ho, C.B.; O'Brien, S.E.; Proffitt, C.; Omori, M.; Haddach, M.; Schwaebe, M.K.; Siddiqui-Jain, A.; et al. Targeting RNA polymerase I with an oral small molecule CX-5461 inhibits ribosomal RNA synthesis and solid tumor growth. *Cancer Res.* **2011**, *71*, 1418–1430. [CrossRef] [PubMed]
172. Peltonen, K.; Colis, L.; Liu, H.; Trivedi, R.; Moubarek, M.S.; Moore, H.M.; Bai, B.; Rudek, M.A.; Bieberich, C.J.; Laiho, M. A targeting modality for destruction of RNA polymerase I that possesses anticancer activity. *Cancer Cell* **2014**, *25*, 77–90. [CrossRef] [PubMed]
173. Ferreira, R.; Schneekloth, J.S., Jr.; Panov, K.I.; Hannan, K.M.; Hannan, R.D. Targeting the RNA Polymerase I Transcription for Cancer Therapy Comes of Age. *Cells* **2020**, *9*, 266. [CrossRef] [PubMed]
174. Negi, S.S.; Brown, P. rRNA synthesis inhibitor, CX-5461, activates ATM/ATR pathway in acute lymphoblastic leukemia, arrests cells in G2 phase and induces apoptosis. *Oncotarget* **2015**, *6*, 18094–18104. [CrossRef] [PubMed]
175. Taylor, J.S.; Zeki, J.; Ornell, K.; Coburn, J.; Shimada, H.; Ikegaki, N.; Chiu, B. Down-regulation of MYCN protein by CX-5461 leads to neuroblastoma tumor growth suppression. *J. Pediatr. Surg.* **2019**, *54*, 1192–1197. [CrossRef]
176. Figueiredo, V.C.; McCarthy, J.J. Targeting cancer via ribosome biogenesis: The cachexia perspective. *Cell Mol. Life Sci.* **2021**, *78*, 5775–5787. [CrossRef]

Article

The Glycoprotein M6a Is Associated with Invasiveness and Radioresistance of Glioblastoma Stem Cells

Marie Geraldine Lacore ¹, Caroline Delmas ^{1,2}, Yvan Nicaise ¹, Aline Kowalski-Chauvel ¹, Elizabeth Cohen-Jonathan-Moyal ^{1,2} and Catherine Seva ^{1,*}

¹ INSERM UMR 1037 Cancer Research Center of Toulouse (CRCT), University Paul Sabatier Toulouse III, Avenue Hubert Curien, 31100 Toulouse, France; mglacore@gmail.com (M.G.L.); delmas.caroline@iuct-oncopole.fr (C.D.); yvan.nicaise@inserm.fr (Y.N.); a.chauvel@free.fr (A.K.-C.); moyal.elizabeth@iuct-oncopole.fr (E.C.-J.-M.)

² IUCT-Oncopole, Avenue Hubert Curien, 31100 Toulouse, France

* Correspondence: cathy.seva@inserm.fr; Tel.: +33-(5)82741604

Abstract: Systematic recurrence of glioblastoma (GB) despite surgery and chemo-radiotherapy is due to GB stem cells (GBSC), which are particularly invasive and radioresistant. Therefore, there is a need to identify new factors that might be targeted to decrease GBSC invasive capabilities as well as radioresistance. Patient-derived GBSC were used in this study to demonstrate a higher expression of the glycoprotein M6a (GPM6A) in invasive GBSC compared to non-invasive cells. In 3D invasion assays performed on primary neurospheres of GBSC, we showed that blocking GPM6A expression by siRNA significantly reduced cell invasion. We also demonstrated a high correlation of GPM6A with the oncogenic protein tyrosine phosphatase, PTPRZ1, which regulates GPM6A expression and cell invasion. The results of our study also show that GPM6A and PTPRZ1 are crucial for GBSC sphere formation. Finally, we demonstrated that targeting GPM6A or PTPRZ1 in GBSC increases the radiosensitivity of GBSC. Our results suggest that blocking GPM6A or PTPRZ1 could represent an interesting approach in the treatment of glioblastoma since it would simultaneously target proliferation, invasion, and radioresistance.

Keywords: glioblastomas; invasion; radioresistance; cancer stem cells; GPM6A; PTPRZ1



Citation: Lacore, M.G.; Delmas, C.; Nicaise, Y.; Kowalski-Chauvel, A.; Cohen-Jonathan-Moyal, E.; Seva, C. The Glycoprotein M6a Is Associated with Invasiveness and Radioresistance of Glioblastoma Stem Cells. *Cells* **2022**, *11*, 2128. <https://doi.org/10.3390/cells11142128>

Academic Editors: Javier S. Castresana and Bárbara Meléndez

Received: 30 May 2022

Accepted: 4 July 2022

Published: 6 July 2022

Publisher's Note: MDPI stays neutral with regard to jurisdictional claims in published maps and institutional affiliations.



Copyright: © 2022 by the authors. Licensee MDPI, Basel, Switzerland. This article is an open access article distributed under the terms and conditions of the Creative Commons Attribution (CC BY) license (<https://creativecommons.org/licenses/by/4.0/>).

1. Introduction

Glioblastoma (GB) is an aggressive and infiltrating tumor of the central nervous system (CNS) with a median overall survival of less than two years [1]. The invasive phenotype makes surgical resection difficult and incomplete. The recurrence of glioblastoma is systematic despite surgery and chemo-radiotherapy. Certain clinical characteristics, including the localization and difficult surgical access, can favor this high recurrence. In particular, tumors in contact with the periventricular zone are more aggressive and have a decreased overall survival (OS) rate when compared to cortical tumors [2,3]. Patients with multiple lesion glioblastoma also have a poor prognosis and present a shorter progression-free survival and OS [4]. Based on genetic characteristics, GB have been classified into different subtypes including the classical, proneural, and mesenchymal subtype, the latter being the most aggressive and resistant to radio-chemotherapy. GB stem cells (GBSC), which have the capacity for self-renewal and contribute to tumor initiation, are particularly resistant to therapies and have also been involved in recurrence [5,6]. GBSC are characterized by a high invasive potential, but the mechanisms that regulate their invasive capacity are not fully understood. Currently, there is no clinical therapy that targets GBSC. Therefore, deciphering the molecular mechanisms responsible for the resistance and invasiveness of GBSC is critically needed to develop new effective therapies for GB.

In the present paper, we focused on the glycoprotein M6a (GPM6A), a four trans-membrane protein that belongs to the proteolipid protein (PLP) family. GPM6A is highly

expressed in the CNS, and transcriptomic datasets per cell type, publicly available in the Human Protein Atlas Database, have shown that GPM6A is particularly well-expressed in astrocytes, oligodendrocyte precursor cells, and microglia. In normal neuronal cells, GPM6A accumulates in lipid raft domains and acts as a transducer for extracellular signals such as laminin [7]. It plays an important role in neurite outgrowth, filopodia formation, and neuronal migration. GPM6A overexpression in neuronal and non-neuronal cells induces extensive formation of filopodia-like protrusions, presumably through the activation of the small GTPase Rac1 and kinases such as PAK1, Src, and MAPK. GPM6A has also been shown to be involved in the proliferation of neuronal stem cells and non-neuronal cells [7–11]. The role of GPM6A in cancer cells has not been extensively studied. In lymphoid leukemias, GPM6A and GPM6B are overexpressed and act as oncogenes in the development of these malignancies [12]. In sporadic non-functioning pituitary adenomas, Falch et al. reported a higher expression of GPM6A in fast-growing compared to slow-growing adenomas [13]. In colorectal cancer, the up-regulation of GPM6A was closely related to a poorer overall survival. In addition, a higher expression of GPM6A was observed in the poorly differentiated compared to the highly differentiated colorectal carcinoma tissues [14,15].

In the Human Protein Atlas Database, the RNA expression overview from The Cancer Genome Atlas shows an enrichment of GPM6A and GPM6B RNA in glioma. However, the role of these proteins in glioblastoma has never been studied. Only one publication has reported that the high expression of GPM6B in patient samples allowed discrimination between glioblastoma and meningioma cases [16].

In this study, we report that GPM6A is overexpressed in highly invasive GBSC. We also demonstrate that targeting GPM6A represses cell invasion, decreases neurosphere formation, and increases the radiosensitivity of GBSC.

2. Materials and Methods

2.1. GB Patient-Derived Cells

GB biopsies were performed in the Neurosurgery Department at Toulouse University Hospital under an approved clinical protocol (ethical code 12TETE01, ID-RCB number 2012-A00585-38, date of approval: 7 May 2012). Written informed consents were obtained for all the patients. WHO was used to classify the tumors as GB. The GBSC were isolated from GB specimens and cultured as described by Avril et al. [17] in DMEM-F12 (GIBCO, Waltham, MA, USA) including N2 and B27 (LifeTechnologies, Carlsbad, CA, USA), and EGF and FGF2 (PeproTech, East Windsor, NJ, USA) at 37 °C in a CO₂ incubator (5%). The GBSC used in the study (3 mesenchymal: GSC08, GSC10, and GSC14 and 11 proneural: GSC01, GSC02, GSC03, GSC04, GSC05, GSC06, GSC07, GSC09, GSC11, GSC12, and GSC13) have been characterized by the overexpression of stem cell markers (SOX2, OLIG2), their ability to differentiate into neural lineages, self-renewal, and their tumorigenic potential in vivo (Table S1). Neurospheres are cultured for fewer than 12 passages to keep stem characteristics.

2.2. Three-Dimensional Invasion Assays

Three-dimensional invasion assays have been previously described by Vinci M. et al. [18]. Briefly, the cells were seeded into ultra-low attachment 96-well round-bottom plates, which allowed for the formation of a single spheroid/well. When the spheroid was formed (48–72 h), Matrigel was added and solidified for 1 h at 37 °C. Images of each spheroid were taken with a microscope (Nikon software NIS Elements) at T0 and T24 h. The Image J software was used to measure the spheres' area at T0 and the area covered by the invading cells at T24 h. The results represent the ratio T24 h/T0 for each primary culture. When indicated, the spheroids were transfected, with specific siRNA or a scramble control with Lipofectamine RNAi Max (Invitrogen, Waltham, MA, USA). 24 h after transfection, 3D invasion assays were performed as described above.

2.3. Western Blot Analysis

Western blots were performed, as previously described [19], using the indicated antibodies: Actin (Millipore, Burlington, MA, USA) and GPM6A (BioLegend, San Diego, CA, USA).

2.4. Immunofluorescence Staining and Microscopy

Invasive neurospheres seeded in Lab-Tek chamber slides coated with Matrigel were fixed with 4% PFA for 15 min at RT. Quenching and permeabilization steps were performed using PBS solution containing 5% BSA (Sigma–Aldrich, Burlington, MA, USA) and 0.3% Triton-X100. The primary antibody, anti-GPM6A (Genetex, Irvine, CA, USA), was incubated in PBS 5% BSA and 0.3% Triton-X100 solution for 2 h. The secondary antibody, Donkey anti-Rabbit Alexa Fluor™ 488 (Invitrogen), or Phalloidin–iFluor 594 conjugate (AATBioquest, Sunnyvale, CA, USA) were incubated for 1 h in PBS 5% BSA and 0.3% Triton-X100. Mounting was performed with VECTASHIELD Vibrance® Antifade Mounting Medium with DAPI (Vector Laboratories, Newark, CA, USA). Immunofluorescence stains were analyzed on a Nikon Eclipse Ti with the Nikon software NIS Element AR and on a LSM 880 Fast Airyscan-Zeiss inverted confocal microscope with the Zeiss software Zen 2.

2.5. Transfection, RNA Extraction, Reverse Transcription and Real-Time PCR

The scramble control or the specific siRNA against GPM6A, PTPRZ1, or ZEB1 were purchased from Qiagen. Lipofectamine RNAi Max was used for the transfections (Invitrogen). The purification of total RNA was performed with the RNeasy RNA Isolation Kit (Qiagen, Germantown, MD, USA). Reverse transcription was performed using the Prime Script RT Reagent Kit (TAKARA). The ABI-Stepone+ was used for Real-time PCR (Applied Biosystems, Waltham, MA, USA). Normalization was completed with GAPDH.

2.6. Genes Correlations

The correlations between GPM6A expression and PTPRZ1 or ZEB1 were performed in Gliovis [20] using the TCGA database and the Pearson correlation coefficients with their associated *p*-values.

2.7. 3D Spheroid Formation

GBSC, transfected with specific siRNA or a scramble control, were seeded (500 cells/well) in 96 wells flat bottom plates (6 wells/condition). The number of spheres/well was counted under the microscope after 8–10 days.

2.8. 3D Survival Assay under Radiation

GBSC expressing the siRNA (si-GPM6A, si-PTPRZ1, si-Scr) were seeded in 96-well flat-bottom plates (500 cells/wells, 12 wells per condition). Cells were irradiated after 24 h with different doses of X-rays (0 to 6 Gy) using the SmART+ irradiator (Precision X-ray Inc., Madison, WI, USA). The number of spheres/well were counted 8–10 days post-IR. The calculation of the surviving fraction takes into account the plating efficiency (PE) in the non-irradiated condition ($PE = \text{spheres number} / \text{seeded cells number} \times 100$).

3. Results

3.1. Blocking GPM6A Expression Represses Invasion of GBSC

In the first part of this study, we analyzed the invasive capacities of primary cultures of GBSC isolated from 14 patient samples. We performed 3D invasion assays, as described in the Methods. The area covered by the invading cells was measured 24 h after the inclusion in Matrigel. As shown in Figure 1A, we observed high heterogeneity in the invasive capacities of the primary neurospheres derived from the different GB samples. Figure 1B shows some examples of invasion profiles obtained in the 3D invasion assays.

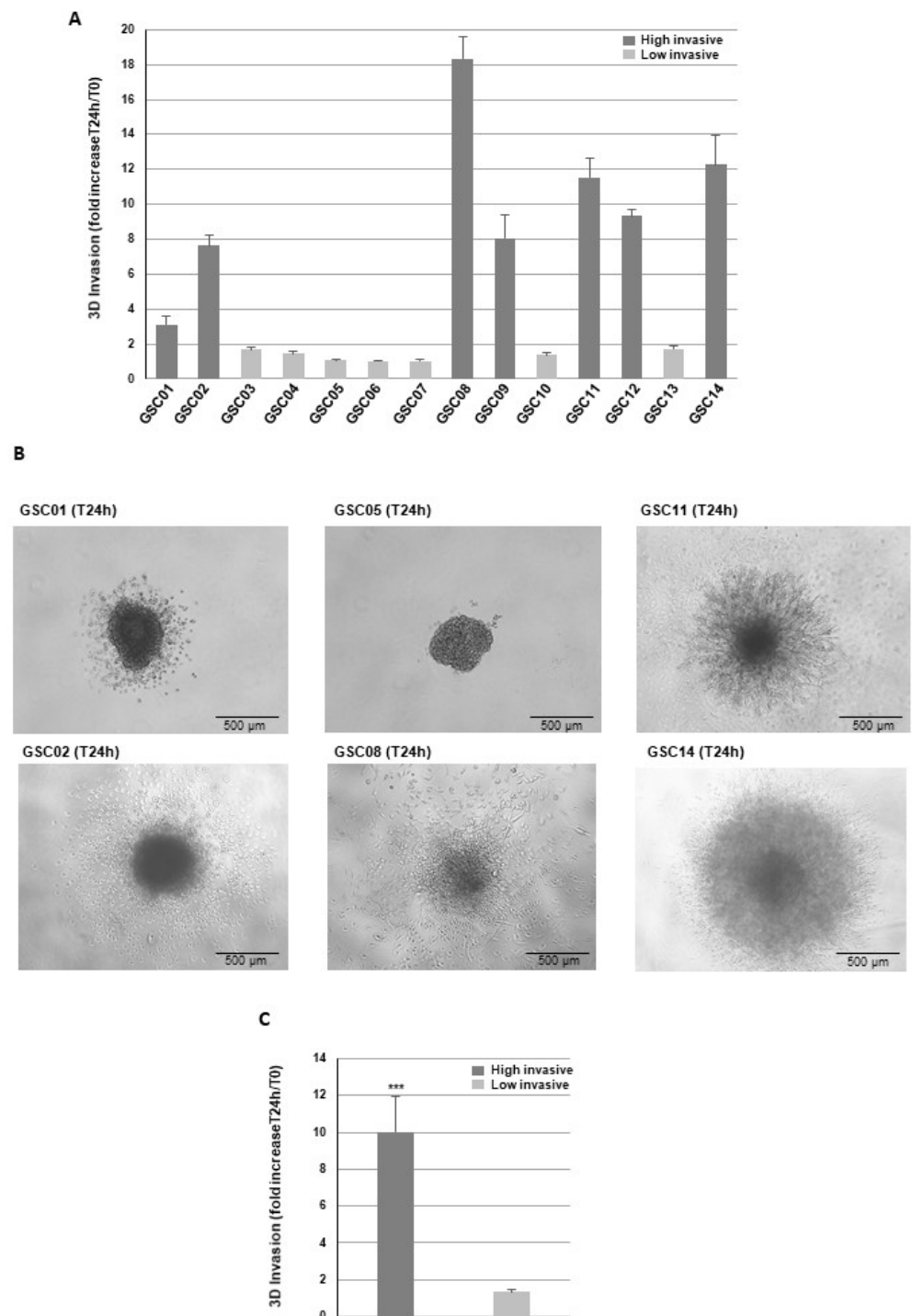


Figure 1. Invasive capacities of GBSC. Primary cultures of GBSC isolated from 14 patient samples were analyzed in 3D invasion assays. (A,C) Quantification of tumor cells invasion was performed, 24 h after embedding, on 3 independent experiments as described in “Methods”. Cells were classified into two groups, highly invasive and low invasive, based on a ratio invading cells area/sphere area greater than 2. (B) Representative micrographs of Matrigel-embedded GB spheroids taken 24 h after invasion into the Matrigel. (B) Results are presented as means ± SD. *** $p < 0.001$.

Cells were classified into two groups, highly invasive and low invasive, based on a ratio invading cells area/sphere area greater than 2. Figure 1C shows the significant difference in the invasive capacity between the two groups.

Then, using quantitative PCR, we analyzed the expression of GPM6A and GPM6B in the 14 primary neurospheres and compared the expression levels between the highly and low invasive groups. We observed a significantly higher level of GPM6A in the group of highly invasive GBSC (Figure 2A and Figure S1). On the contrary, GPM6B expression level was not different between the two groups (Figure 2B). Differential expression of GPM6A between highly and low invasive cells was also confirmed at the protein level by Western blot analysis on a panel of highly invasive and low invasive neurospheres (Figure 2C).

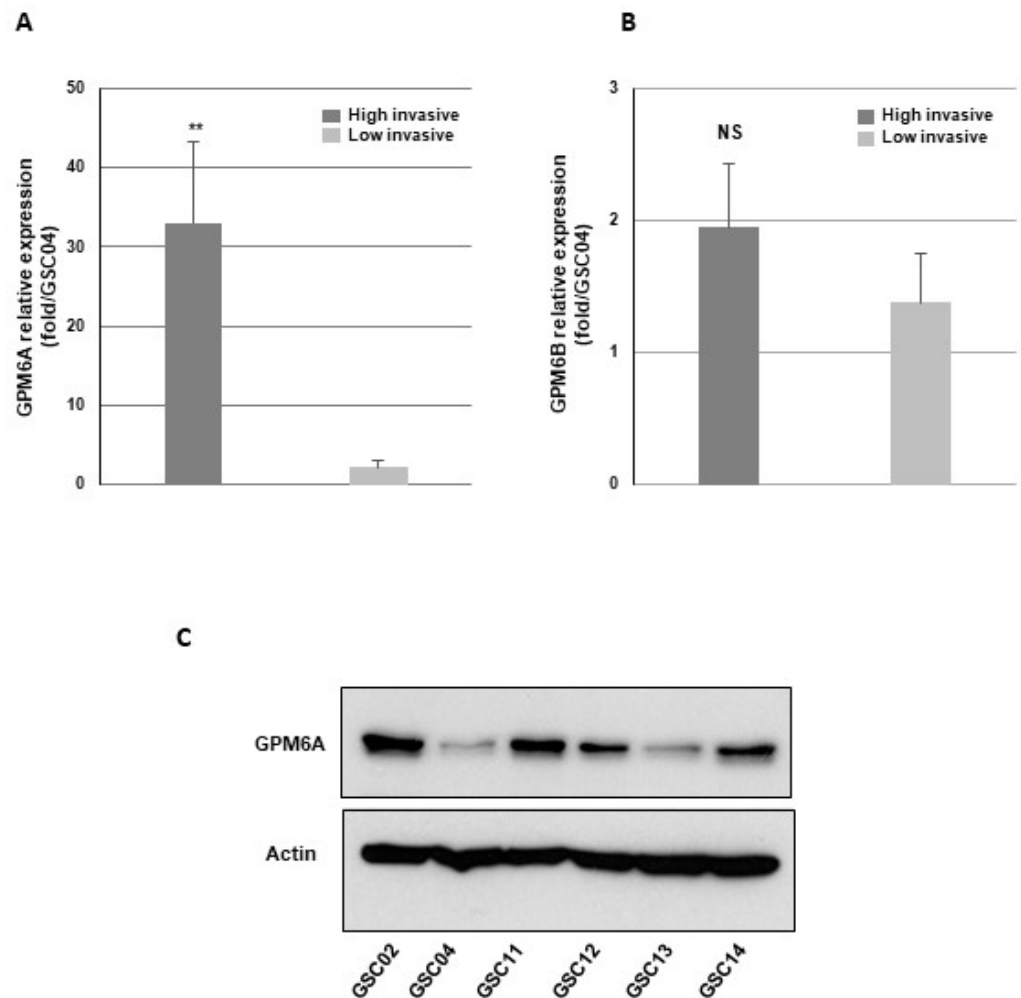


Figure 2. GPM6A is overexpressed in the highly invasive GBSC. mRNA expression of (A) GPM6A and (B) GPM6B was analyzed by real-time PCR in the 14 primary neurospheres. GAPDH was used for normalization. Results are presented as fold compared to GSC04 expression (which presents the lowest expression). Quantifications between the two groups, highly invasive and low invasive, are presented as means \pm SD. ** $0.001 < p < 0.01$; NS, non-significant. (C) GPM6A protein expression was analyzed by Western blot analysis in a panel of highly invasive and low invasive neurospheres.

We also analyzed the localization of GPM6A in the invasive cells by immunofluorescence. Invasive neurospheres were analyzed 24 h after seeding. We observed a high staining of GPM6A in the neurospheres as well as in the invasive cells (Figure 3A,B). Confocal microscopy analyses showed a punctated staining in lamellipodia/pseudopodia-like structures (Figure 3C,D,E), suggesting a potential role in cell migration.

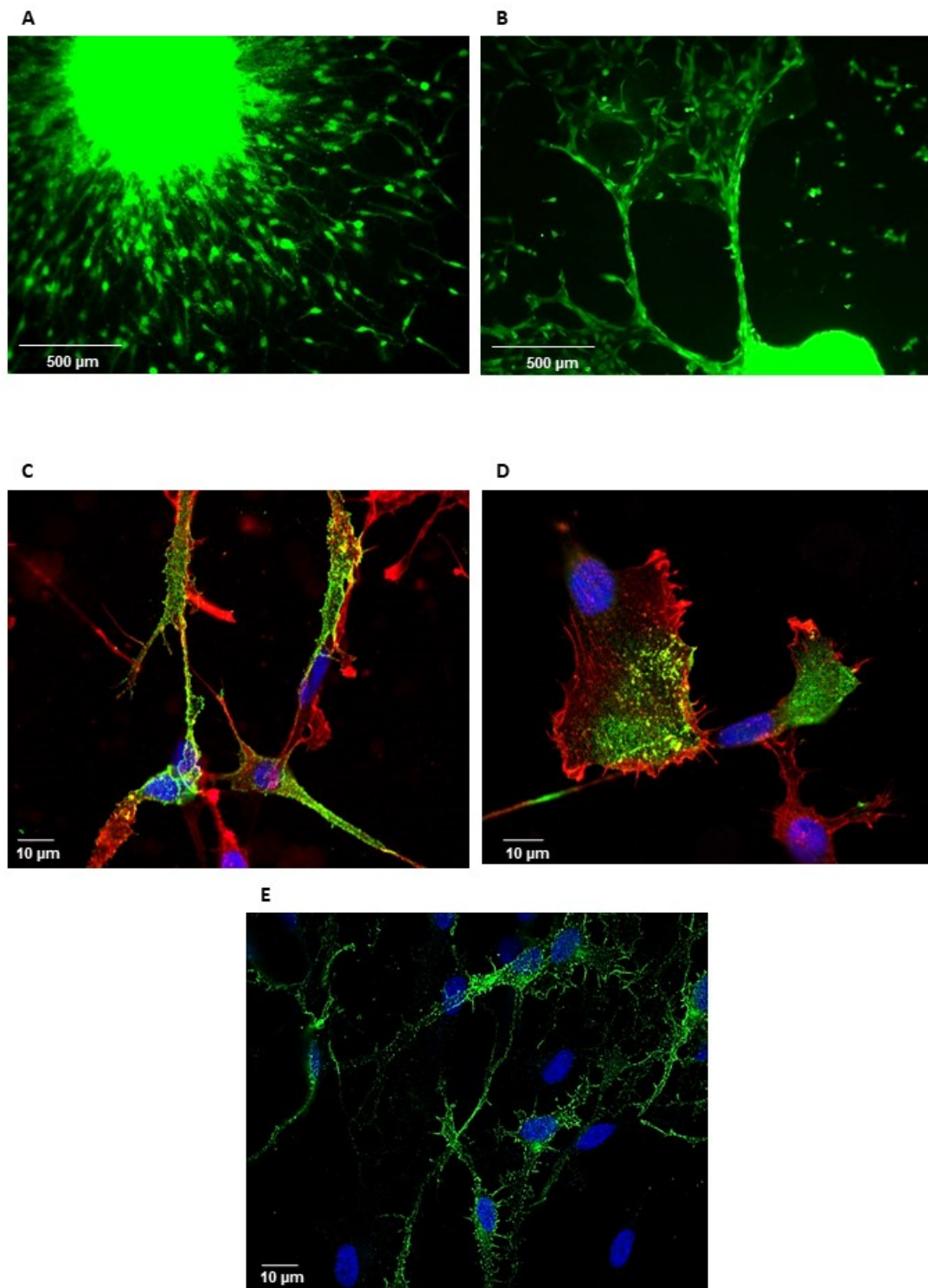


Figure 3. Immunofluorescent staining of GPM6A in invasive GBSC. Invasive neurospheres seeded in Lab-Tek chamber slides coated with Matrigel were immuno-stained with anti-GPM6A antibodies (green) and incubated with phalloidin (red) or Dapi (blue) as described in “Methods”. (A,B) Immunofluorescence stainings were analyzed on a Nikon Eclipse Ti with the Nikon software NIS Element AR (original magnification 10×). (C–E) Immunofluorescence stainings were analyzed and on a LSM 880 Fast Airyscan-Zeiss inverted confocal microscope with the Zeiss software Zen 2 (original magnification 60×).

To our knowledge, the role of GPM6A in GB cells' invasion has never been published. To investigate if GPM6A could be involved in this process, we performed 3D invasion assays, using invasive primary neurospheres derived from three GB biopsy specimens in which GPM6A was knocked down using a specific siRNA validated for its efficiency to inhibit GPM6A expression in the GB neurospheres compared to a scramble control (Figure 4A,B). As shown in Figure 4C,D, GB spheroids deficient for GPM6A exhibited a significant inhibition of invasion capability relative to control spheroids, confirming the role of this glycoprotein in GBSC invasion.

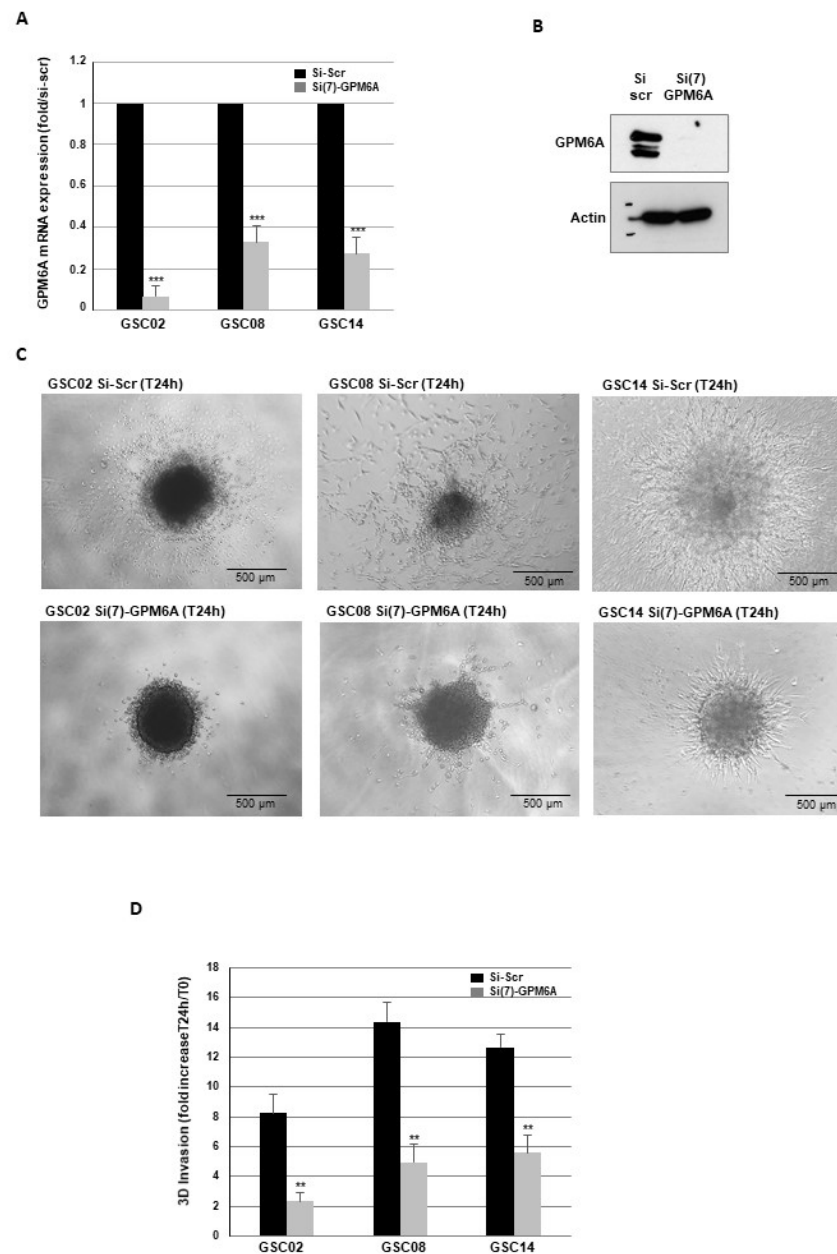


Figure 4. Blocking GPM6A gene expression represses invasion of GBSC. Primary neurospheres from different invasive GB biopsy specimens (GSC02, GSC08, GSC14) were transfected with a specific GPM6A siRNA (si(7)-GPM6A) or a scramble control (si-Scr). GPM6A expression was analyzed by real-time PCR (A) or Western blot (B). (C,D) Three-dimensional invasion assays were performed as described in the Methods. Images are representative of three independent experiments. Quantification of 3 experiments are presented as means \pm SD. *** $p < 0.001$; ** $0.001 < p < 0.01$.

To assess a potential off-target effect of the GPM6A siRNA, we used a second siRNA and showed in GB neurospheres, a high inhibition of GPM6A expression as well as similar results in 3D invasion assays (Figure S2).

3.2. Targeting PTPRZ1 Inhibits GPM6A Expression and GBSC Invasion

We then analyzed, in the glioblastoma database of the Cancer Genome Atlas (TCGA), the correlations between the expression GPM6A and other genes potentially involved in GB cells invasion. One of the strongest correlation observed in the database was with PTPRZ1, an oncogenic protein tyrosine phosphatase highly expressed in GB that has been involved in cell invasion [21]. As shown in Figure 5A, a significant positive correlation was observed, at the mRNA level, between the expression of GPM6A and PTPRZ1 in GB. GPM6A was also positively correlated with the transcription factor ZEB1, which is known for its role in cell invasion, including in GB (Figure 5B). On the contrary, we did not find any positive correlation between GPM6A and the other main transcription factors involved in invasion such as TWIST1, Snail, Slug, or YAP1, whose involvement in the migration of GBSC was previously shown [22,23]. In the GBSC used in this study, we showed that PTPRZ1 and ZEB1 mRNAs, such as those of GPM6A, were preferentially expressed in the group of highly invasive GBSC (Figure 5C,D).

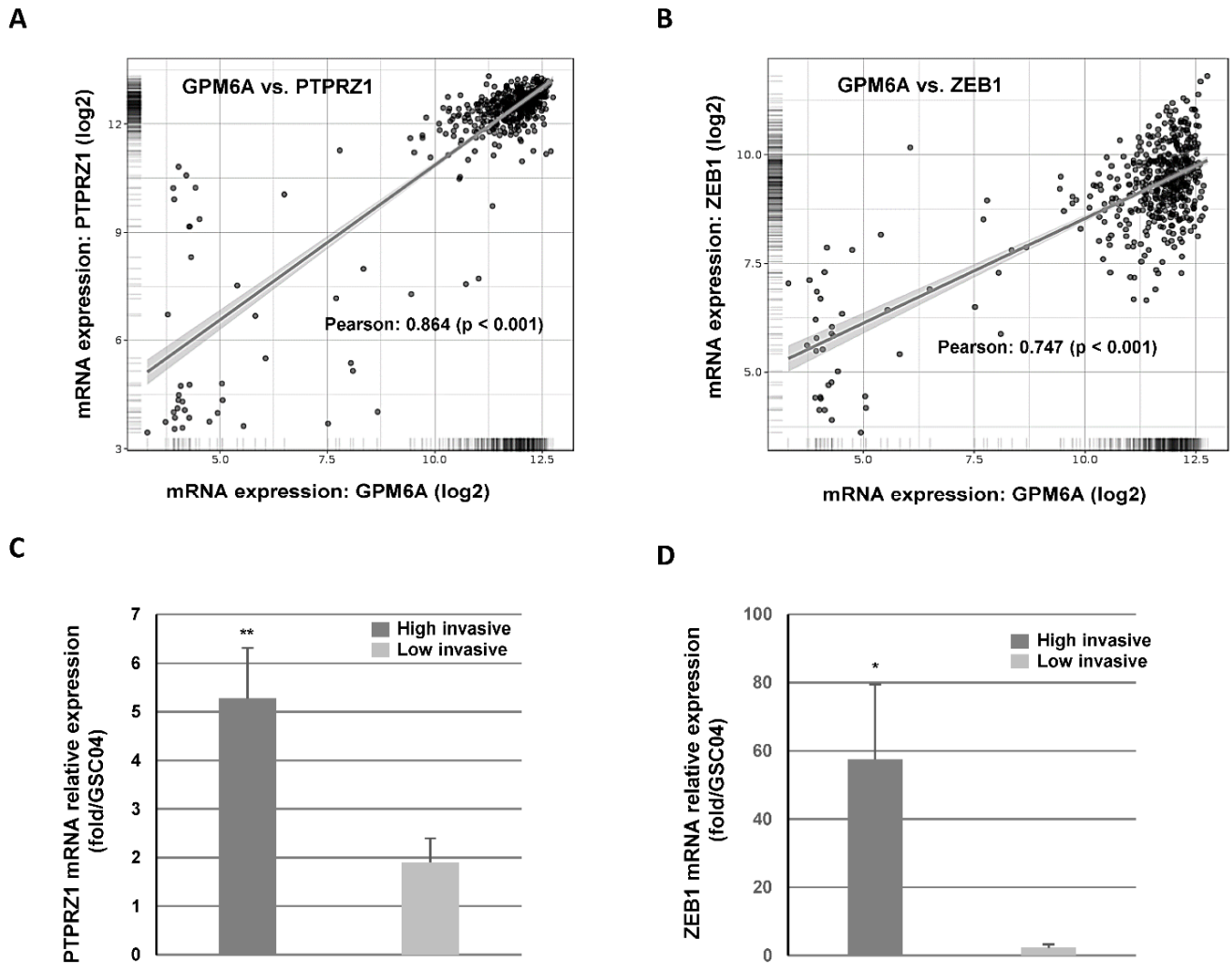


Figure 5. Cont.

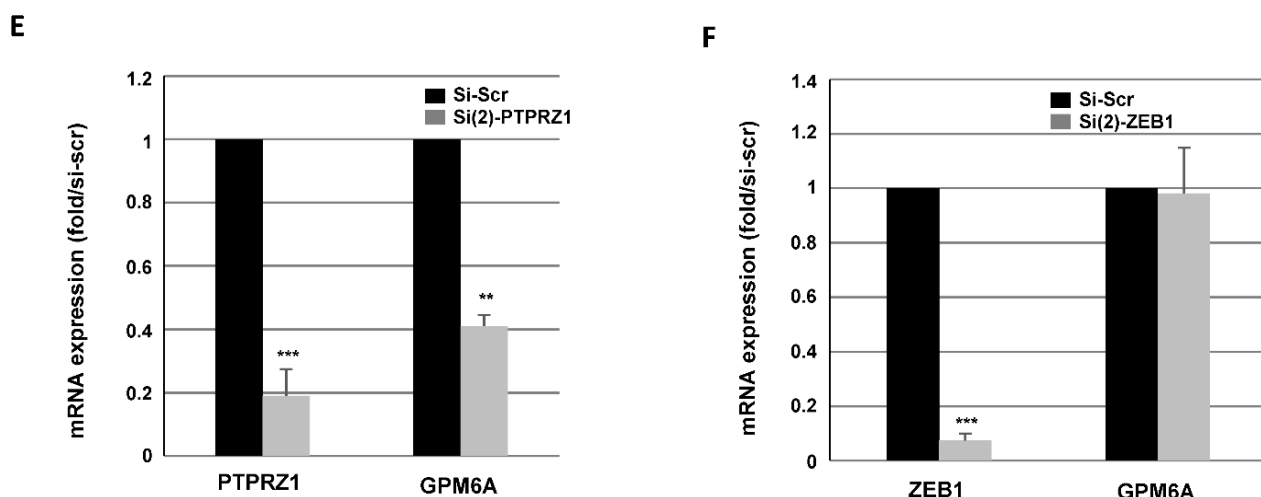


Figure 5. GPM6A and PTPRZ1 expression are correlated in GB. (A,B) The correlations between GPM6A mRNA expression and PTPRZ1 or ZEB1 were obtained by the co-expression analysis in Gliovis [20] using the TCGA database. Values correspond to the Pearson correlation coefficient and its associated p -value. (C,D) mRNA expression of (C) PTPRZ1 and (D) ZEB1 was analyzed by real-time PCR in each of the 14 primary cultures of GBSC isolated from 14 patient samples. GAPDH was used for normalization. Results are presented as means of the relative expression (compared to GSC04 which has the lowest expression) for each group (highly or low invasive). Quantifications between the two groups are presented as means \pm SD. *** $p < 0.001$; ** $0.001 < p < 0.01$; * $0.01 < p < 0.05$. (E,F) Primary neurospheres were transfected with a specific PTPRZ1 siRNA (si(2)-PTPRZ1), a specific ZEB1 siRNA (si(2)-ZEB1), or a scramble control (si-Scr). PTPRZ1, GPM6A, and ZEB1 mRNA expression was analyzed by real-time PCR. GAPDH was used for normalization. Quantifications of 3 experiments are presented as means \pm SD. *** $p < 0.001$; ** $0.001 < p < 0.01$; * $0.01 < p < 0.05$.

Based on the correlations observed between GPM6A and PTPRZ1 or ZEB1, we tested if the down-regulation of PTPRZ1 or ZEB1 could affect the expression of GPM6A. We observed a decrease in GPM6A mRNA expression in cells transfected with a PTPRZ1 siRNA, which confirmed the direct correlation between the two genes in GB (Figure 5E). In contrast, blocking ZEB1 expression with previously characterized siRNA did not affect GPM6A expression, suggesting a more indirect correlation between ZEB1 and GPM6A (Figure 5F).

In addition, in the primary neurospheres transfected with specific PTPRZ1 siRNAs, validated for their ability to block PTPRZ1 expression, we observed a significant reduction in the invasive capacity of GBSC (Figure 6A).

3.3. Down-Regulation of GPM6A or PTPRZ1 Gene Expression Decreases Sphere-Forming Ability of GBSC

Since PTPRZ1 has been previously shown to regulate the proliferation and sphere-forming ability of GB cells [21,24,25], we also analyzed the role of GPM6A in these two processes. The proliferation of GBSC, measured by cell counting, was weakly but significantly decreased after 48 h when the expression of GPM6A was blocked by specific siRNA (Figure 6B). As expected, we also observed an inhibition of GBSC proliferation in cells transfected with PTPRZ1 siRNAs (Figure 6B). The formation of neurospheres was examined in GBSC transfected with GPM6A, PTPRZ1 siRNAs, or a scramble control. Under these conditions, we observed a significant decrease in the number of spheres when GPM6A or PTPRZ1 were blocked with their respective, specific siRNA (Figure 6C,D).

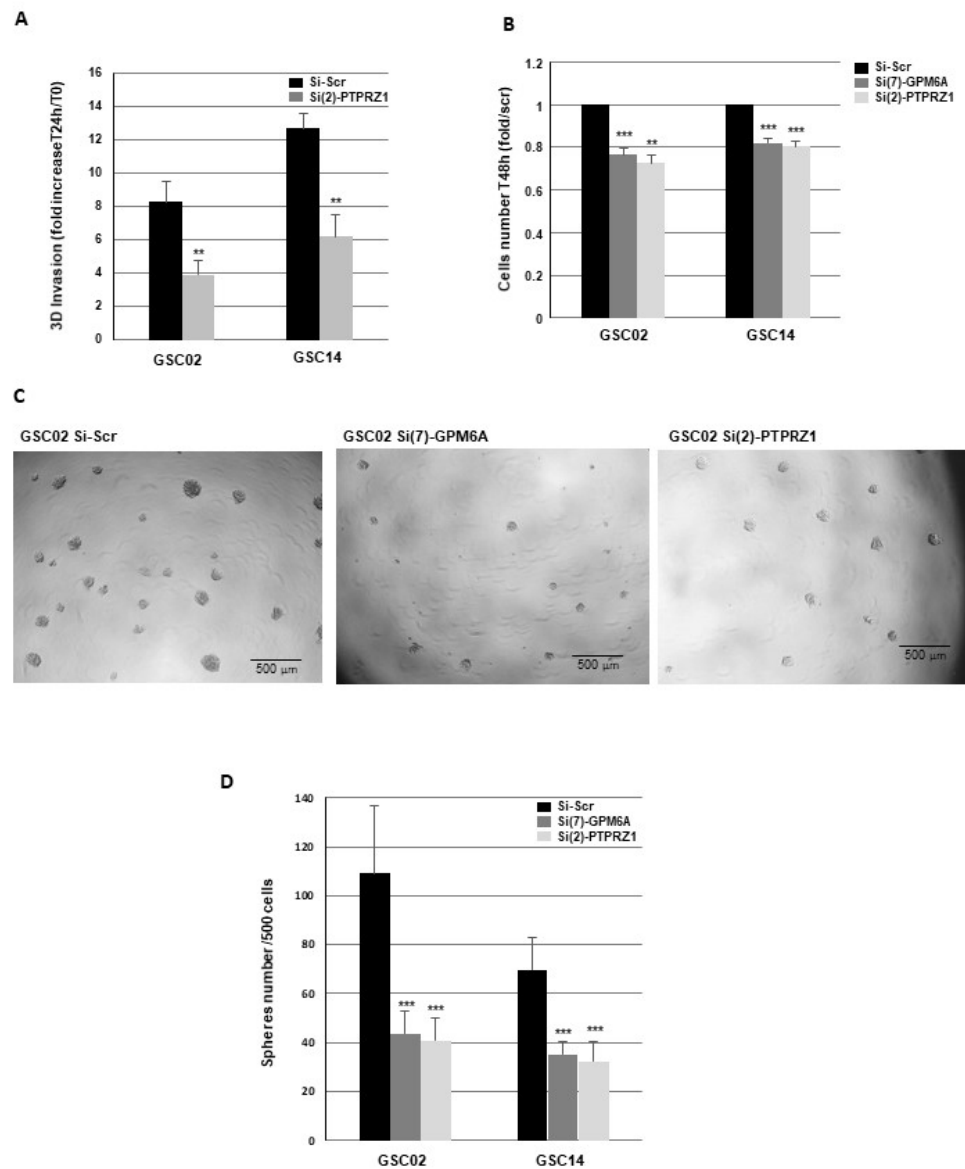


Figure 6. Targeting GPM6A or PTPRZ1 expression decreases invasion and sphere-forming ability of GBSC. (A–D) GBSC from different GB biopsy specimens (GSC02, GSC14) were transfected with specific PTPRZ1 siRNA (si(2)-PTPRZ1), specific GPM6A siRNA (si(7)-GPM6A), or a scramble control (si-Scr). (A) Following transfection, 3D invasion assays were performed as described in the Methods. (B) The number of cells was measured by using the cell counter Countess II FL. (C,D) Following the transfection, cells were seeded in 96-well plates (500 cells/well). After 8–10 days, the number of neurospheres/well was counted under the microscope. (C) Micrographs from representative fields were taken ($\times 20$). (A,B,D) Quantifications of 3 experiments are presented as means \pm SD. *** $p < 0.001$; ** $0.001 < p < 0.01$.

3.4. Blocking GPM6A or PTPRZ1 Radiosensitizes GBSC

Radiotherapy is the reference treatment for GB, but the local recurrence, which occurs in almost all cases, highlights the strong radioresistance of GB and GBSC in particular.

To determine whether GPM6A or PTPRZ1 affects radiation sensitivity, we performed 3D survival assays with increasing doses of IR in neurospheres expressing high levels of GPM6A and PTPRZ1. The survival fractions after IR were significantly decreased in GBSC transfected with the specific GPM6A or PTPRZ1 siRNAs compared to the control siRNA,

indicating that the down-regulation of their expression radiosensitizes GBSC (Figure 7A,B).

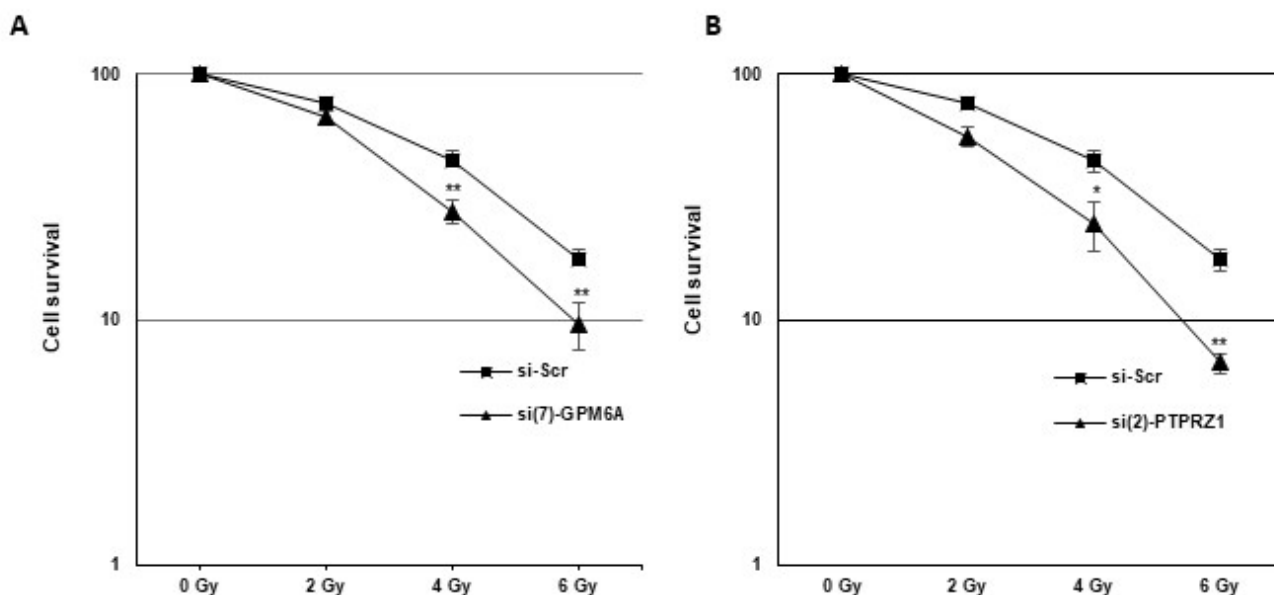


Figure 7. Down-regulation of GPM6A or PTPRZ1 gene expression radiosensitizes GBSC. Primary neurospheres (GSC02) expressing specific siRNAs (A) si(7)-GPM6A or (B) si(2)-PTPRZ1 or a scramble control (si-Scr) were used in a 3D survival assays with increasing doses of IR (2 to 6 Gy) as described in the Methods. Quantifications of 3 experiments are presented as means \pm SD. ** $0.001 < p < 0.01$; * $0.01 < p < 0.05$.

4. Discussion

GB is one of the most aggressive brain tumors, being particularly invasive and resistant to radiotherapy. This aggressiveness is essentially due to the presence of tumor stem cells for which there is as yet no targeted clinical therapy [5,6]. Therefore, it is important to understand the mechanisms of invasion and radioresistance of these cells.

In the present study, we demonstrate for the first time the important role of a membrane glycoprotein, GPM6A, in these two processes. Very few data are available on the involvement of GPM6A in cancers. While GPM6A has been identified as a potential oncogene in lymphoid leukemia [12], and contributes to the poor prognosis of colorectal cancer [14,15], its role in GB has never been reported. First, we showed that GPM6A is overexpressed in the invasive GBSC compared to non-invasive cells and localized in lamellipodia/pseudopodia-like structures, suggesting a role in cell migration/invasion. In addition, we demonstrated that blocking its expression in GBSC spheroids with specific siRNA drastically reduces their invasive capacity. Our results are the first to demonstrate the involvement of GPM6A in human tumor cell invasion. Previously, its role in the migration and formation of filopodia had only been demonstrated in primary cultures of neurons expressing endogenous GPM6A, or non-neuronal cells, such as COS-7 or NIH/3T3, transfected with GPM6A [7–11].

The results of our study also show that GPM6A expression is crucial for the formation of spheres by GBSC since the knockdown of GPM6A significantly decreases the number of neurospheres formed by GBSC derived from GB biopsy specimens. These results and those obtained for invasion, support a potential role of GPM6A in the tumorigenicity and aggressiveness of GB.

In a non-tumor context, GPM6A is highly expressed in the CNS and its functions could be dependent on its interaction with laminin [26]. It is interesting to note that GB cells can secrete different forms of laminins, which contribute to tumor progression by playing a role in the invasion and resistance to therapies [27–30]. Although laminins are known

to interact mainly with integrins and mediate their effects, they might also play a role in GPM6A functions in GB.

We also analyzed the potential molecular mechanism regulating the expression of GPM6A in invasive GBSC. In the TCGA database, we showed a very strong correlation between GPM6A expression and a transmembrane tyrosine phosphatase, PTPRZ1. We confirmed the correlation between these two genes in the highly invasive group of GBSC. First, we observed a higher expression level of PTPRZ1 in the invasive cells compared to the non-invasive cells, and secondly, GBSC spheroids deficient for PTPRZ1 exhibited a significantly reduced expression of GPM6A. Similar to GPM6A, PTPRZ1 is highly expressed in the glial cells of the CNS, including astrocytes, oligodendrocyte precursor cells, and oligodendrocytes [31]. PTPRZ1 is also strongly expressed in GB and has been associated with tumorigenicity. This pro-oncogenic phosphatase regulates the proliferation and migration of GB cells and promotes tumor formation. It is also recognized as a stemness marker, which regulates stem-cell-like features and spheres formation [20,23,32,33]. Its high correlation with GPM6A in GB and its involvement in the regulation of GPM6A expression reinforce the hypothesis of a pro-tumoral role of GPM6A in this cancer.

Radiation therapy is one of the standard treatments for GB. However, the intrinsic radioresistance of cancer cells, or the resistance acquired during treatment by adaptation mechanisms, leads to systematic therapeutic failure. Understanding the mechanisms of this resistance could help to identify new therapeutic targets, the inhibition of which could allow radiosensitization.

The role of GPM6A or PTPRZ1 in the radioresistance of GB or other cancer types has never been reported. To our knowledge, this study is the first one demonstrating that GPM6A or PTPRZ1 are involved in the resistance to radiotherapy of GBSC. We showed that targeting GPM6A or PTPRZ1 in GBSC neurospheres, which express high levels of these markers, sensitize cells to radiations.

All of our results suggest that blocking GPM6A or PTPRZ1 could represent an interesting approach in the treatment of glioblastoma, since it would simultaneously target proliferation, invasion, and radioresistance. At present, there is no pharmacological inhibitor capable of blocking GPM6A functions. On the contrary, several laboratories have developed small molecules or monoclonal antibodies targeting PTPRZ1 that are able to suppress GB cell proliferation and migration [24,25,34]. These molecules might also present the possibility to radiosensitize GBSC.

5. Conclusions

In summary, our study highlights the overexpression of GPM6A and PTPRZ1 in invasive GBSC and their role in regulating invasiveness, as well as radioresistance. Since there is currently no therapy against GBSC, which are particularly radioresistant and invasive, our study opens perspectives on the potential interest of these biomarkers as therapeutic targets. Their expression may be used to target GBSC invasion, optimize radiotherapy treatments, or to predict the response to radiotherapy.

Supplementary Materials: The following supporting information can be downloaded at: <https://www.mdpi.com/article/10.3390/cells11142128/s1>, Table S1: GBSC characterization. Figure S1: GPM6A is overexpressed in the highly invasive GBSC. Figure S2: Checking of a potential off-target effect with GPM6A siRNA.

Author Contributions: Conceptualization, C.S.; Formal analysis, M.G.L., C.D., Y.N., A.K.-C. and C.S.; Funding acquisition, E.C.-J.-M. and C.S.; Methodology, M.G.L., C.D., Y.N., A.K.-C. and C.S.; Supervision, C.S.; Validation, E.C.-J.-M. and C.S.; Writing—original draft, C.S.; Writing—review and editing, E.C.-J.-M., C.D. and Y.N. All authors have read and agreed to the published version of the manuscript.

Funding: This work was supported by INSERM (“Institut National de la Santé et de la Recherche Médicale” grant 2021–2022), La Ligue contre le Cancer (LNCC31 R21026BB 2021–2022), l’Association pour la Recherche sur les Tumeurs Cérébrales (ARTC 2021).

Institutional Review Board Statement: GB biopsies were obtained in the Neurosurgery Department at Toulouse University Hospital as part of the clinical protocol (PI Pr. E. Cohen-Jonathan-Moyal) approved by the Human Research Ethics Committee (ethical code 12TETE01, ID-RCB number 2012-A00585-38, date of approval: 7 May 2012).

Informed Consent Statement: Informed consent was obtained from all subjects involved in the study. Written informed consent has been obtained from the patients to publish this paper.

Data Availability Statement: Not applicable.

Acknowledgments: We thank Vincent Lubrano from the Neurosurgery Department at Toulouse University Hospital, Purpan, for the human GBM specimens. We thank Laetitia Ligat from the «Pôle Technologique du CRCT for the confocal microscopy acquisition.


Conflicts of Interest: The authors declare no conflict of interest.

References

- Weller, M.; Butowski, N.; Tran, D.D.; Recht, L.D.; Lim, M.; Hirte, H.; Ashby, L.; Mechtler, L.; Goldlust, S.A.; Iwamoto, F.; et al. Rindopepimut with temozolomide for patients with newly diagnosed, EGFRvIII-expressing glioblastoma (ACT IV): A randomised, double-blind, international phase 3 trial. *Lancet Oncol.* **2017**, *18*, 1373–1385. [CrossRef]
- Khalifa, J.; Tensaouti, F.; Lusque, A.; Plas, B.; Lotterie, J.A.; Benouaich-Amiel, A.; Uro-Coste, E.; Lubrano, V.; Cohen-Jonathan Moyal, E. Subventricular zones: New key targets for glioblastoma treatment. *Radiat. Oncol.* **2017**, *12*, 67. [CrossRef] [PubMed]
- Armocida, D.; Pesce, A.; Palmieri, M.; D’Andrea, G.; Salvati, M.; Santoro, A.; Frati, A. Periventricular zone involvement as a predictor of survival in glioblastoma patients: A single centre cohort-comparison investigation concerning a distinct clinical entity. *Interdiscip. Neurosurg.* **2021**, *25*, 101185. [CrossRef]
- Armocida, D.; Pesce, A.; Di Giammarco, F.; Frati, A.; Salvati, M.; Santoro, A. Histological, molecular, clinical and outcomes characteristics of multiple lesion glioblastoma. A retrospective monocentric study and review of literature. *Neurocirurgia* **2021**, *32*, 114–123. [CrossRef] [PubMed]
- Bao, S.; Wu, Q.; McLendon, R.E.; Hao, Y.; Shi, Q.; Hjelmeland, A.B.; Dewhirst, M.W.; Bigner, D.D.; Rich, J.N. Glioma stem cells promote radioresistance by preferential activation of the DNA damage response. *Nature* **2006**, *444*, 756–760. [CrossRef]
- Ortensi, B.; Setti, M.; Osti, D.; Pelicci, G. Cancer stem cell contribution to glioblastoma invasiveness. *Stem. Cell Res. Ther.* **2013**, *4*, 18. [CrossRef]
- Ito, Y.; Honda, A.; Igarashi, M. Glycoprotein M6a as a signaling transducer in neuronal lipid rafts. *Neurosci. Res.* **2018**, *128*, 19–24. [CrossRef]
- Alvarez Julia, A.; Frasnich, A.C.; Fuchsova, B. Neuronal filopodium formation induced by the membrane glycoprotein M6a (Gpm6a) is facilitated by coronin-1a, Rac1, and p21-activated kinase 1 (Pak1). *J. Neurochem.* **2016**, *137*, 46–61. [CrossRef]
- Scorticati, C.; Formoso, K.; Frasnich, A.C. Neuronal glycoprotein M6a induces filopodia formation via association with cholesterol-rich lipid rafts. *J. Neurochem.* **2011**, *119*, 521–531. [CrossRef]
- Alfonso, J.; Fernandez, M.E.; Cooper, B.; Flugge, G.; Frasnich, A.C. The stress-regulated protein M6a is a key modulator for neurite outgrowth and filopodium/spine formation. *Proc. Natl. Acad. Sci. USA* **2005**, *102*, 17196–17201. [CrossRef]
- Michibata, H.; Okuno, T.; Konishi, N.; Wakimoto, K.; Kyono, K.; Aoki, K.; Kondo, Y.; Takata, K.; Kitamura, Y.; Taniguchi, T. Inhibition of mouse GPM6A expression leads to decreased differentiation of neurons derived from mouse embryonic stem cells. *Stem Cells Dev.* **2008**, *17*, 641–651. [CrossRef] [PubMed]
- Charfi, C.; Edouard, E.; Rassart, E. Identification of GPM6A and GPM6B as potential new human lymphoid leukemia-associated oncogenes. *Cell Oncol.* **2014**, *37*, 179–191. [CrossRef] [PubMed]
- Falch, C.M.; Sundaram, A.Y.M.; Oystese, K.A.; Normann, K.R.; Lekva, T.; Silamikelis, I.; Eieland, A.K.; Andersen, M.; Bollerslev, J.; Olarescu, N.C. Gene expression profiling of fast- and slow-growing non-functioning gonadotroph pituitary adenomas. *Eur. J. Endocrinol.* **2018**, *178*, 295–307. [CrossRef] [PubMed]
- Lv, J.; Wang, J.; Shang, X.; Liu, F.; Guo, S. Survival prediction in patients with colon adenocarcinoma via multi-omics data integration using a deep learning algorithm. *Biosci. Rep.* **2020**, *40*, BSR20201482. [CrossRef]
- Ye, Z.; Li, Y.; Xie, J.; Feng, Z.; Yang, X.; Wu, Y.; Pu, Y.; Gao, J.; Xu, X.; Zhu, Z.; et al. Integrated bioinformatics identifies the dysregulation induced by aberrant gene methylation in colorectal carcinoma. *Genes Dis.* **2021**, *8*, 521–530. [CrossRef]
- Castells, X.; Acebes, J.J.; Boluda, S.; Moreno-Torres, A.; Pujol, J.; Julia-Sape, M.; Candiota, A.P.; Arino, J.; Barcelo, A.; Arus, C. Development of a predictor for human brain tumors based on gene expression values obtained from two types of microarray technologies. *OMICS* **2010**, *14*, 157–164. [CrossRef]
- Avril, T.; Vauleon, E.; Hamlat, A.; Saikali, S.; Etcheverry, A.; Delmas, C.; Diabira, S.; Mosser, J.; Quillien, V. Human glioblastoma stem-like cells are more sensitive to allogeneic NK and T cell-mediated killing compared with serum-cultured glioblastoma cells. *Brain Pathol.* **2012**, *22*, 159–174. [CrossRef]
- Vinci, M.; Box, C.; Eccles, S.A. Three-dimensional (3D) tumor spheroid invasion assay. *J. Vis. Exp.* **2015**, *99*, e52686. [CrossRef]

19. Kowalski-Chauvel, A.; Gouaze-Andersson, V.; Baricault, L.; Martin, E.; Delmas, C.; Toulas, C.; Cohen-Jonathan-Moyal, E.; Seva, C. Alpha6-integrin regulates FGFR1 expression through the ZEB1/YAP1 transcription complex in glioblastoma stem cells resulting in enhanced proliferation and stemness. *Cancers* **2019**, *11*, 406. [CrossRef]
20. Data Visualization Tools for Brain Tumor Datasets. Available online: <http://gliovis.bioinfo.cnio.es/> (accessed on 25 May 2022).
21. Nagai, K.; Fujii, M.; Kitazume, S. Protein tyrosine phosphatase receptor type z in central nervous system disease. *Int. J. Mol. Sci.* **2022**, *23*, 4414. [CrossRef]
22. Majc, B.; Sever, T.; Zaric, M.; Breznik, B.; Turk, B.; Lah, T.T. Epithelial-to-mesenchymal transition as the driver of changing carcinoma and glioblastoma microenvironment. *Biochim. Biophys. Acta Mol. Cell Res.* **2020**, *1867*, 118782. [CrossRef] [PubMed]
23. Kowalski-Chauvel, A.; Lacore, M.G.; Arnauduc, F.; Delmas, C.; Toulas, C.; Cohen-Jonathan-Moyal, E.; Seva, C. The m6A RNA demethylase ALKBH5 promotes radioresistance and invasion capability of glioma stem cells. *Cancers* **2020**, *13*, 40. [CrossRef] [PubMed]
24. Fujikawa, A.; Sugawara, H.; Tanaka, T.; Matsumoto, M.; Kuboyama, K.; Suzuki, R.; Tanga, N.; Ogata, A.; Masumura, M.; Noda, M. Targeting PTPRZ inhibits stem cell-like properties and tumorigenicity in glioblastoma cells. *Sci. Rep.* **2017**, *7*, 5609. [CrossRef] [PubMed]
25. Fujikawa, A.; Nagahira, A.; Sugawara, H.; Ishii, K.; Imajo, S.; Matsumoto, M.; Kuboyama, K.; Suzuki, R.; Tanga, N.; Noda, M.; et al. Small-molecule inhibition of PTPRZ reduces tumor growth in a rat model of glioblastoma. *Sci. Rep.* **2016**, *6*, 20473. [CrossRef] [PubMed]
26. Honda, A.; Ito, Y.; Takahashi-Niki, K.; Matsushita, N.; Nozumi, M.; Tabata, H.; Takeuchi, K.; Igarashi, M. Extracellular signals induce glycoprotein M6a clustering of lipid rafts and associated signaling molecules. *J. Neurosci.* **2017**, *37*, 4046–4064. [CrossRef]
27. Lathia, J.D.; Li, M.; Hall, P.E.; Gallagher, J.; Hale, J.S.; Wu, Q.; Venere, M.; Levy, E.; Rani, M.R.; Huang, P.; et al. Laminin alpha 2 enables glioblastoma stem cell growth. *Ann. Neurol.* **2012**, *72*, 766–778. [CrossRef]
28. Liu, J.; Liu, D.; Yang, Z.; Yang, Z. High LAMC1 expression in glioma is associated with poor prognosis. *Onco Targets Ther.* **2019**, *12*, 4253–4260. [CrossRef]
29. Sun, T.; Patil, R.; Galstyan, A.; Klymyshyn, D.; Ding, H.; Chesnokova, A.; Cavenee, W.K.; Furnari, F.B.; Ljubimov, V.A.; Shatalova, E.S.; et al. Blockade of a laminin-411-notch axis with CRISPR/Cas9 or a nanobioconjugate inhibits glioblastoma growth through tumor-microenvironment cross-talk. *Cancer Res.* **2019**, *79*, 1239–1251. [CrossRef]
30. Yu, Q.; Xiao, W.; Sun, S.; Sohrabi, A.; Liang, J.; Seidlits, S.K. Extracellular matrix proteins confer cell adhesion-mediated drug resistance through integrin alpha v in glioblastoma cells. *Front. Cell Dev. Biol.* **2021**, *9*, 616580. [CrossRef]
31. Maeda, N.; Hamanaka, H.; Shintani, T.; Nishiwaki, T.; Noda, M. Multiple receptor-like protein tyrosine phosphatases in the form of chondroitin sulfate proteoglycan. *FEBS Lett.* **1994**, *354*, 67–70. [CrossRef]
32. Muller, S.; Kunkel, P.; Lamszus, K.; Ulbricht, U.; Lorente, G.A.; Nelson, A.M.; von Schack, D.; Chin, D.J.; Lohr, S.C.; Westphal, M.; et al. A role for receptor tyrosine phosphatase zeta in glioma cell migration. *Oncogene* **2003**, *22*, 6661–6668. [CrossRef] [PubMed]
33. Ulbricht, U.; Brockmann, M.A.; Aigner, A.; Eckerich, C.; Muller, S.; Fillbrandt, R.; Westphal, M.; Lamszus, K. Expression and function of the receptor protein tyrosine phosphatase zeta and its ligand pleiotrophin in human astrocytomas. *J. Neuropathol. Exp. Neurol.* **2003**, *62*, 1265–1275. [CrossRef] [PubMed]
34. Foehr, E.D.; Lorente, G.; Kuo, J.; Ram, R.; Nikolich, K.; Urfer, R. Targeting of the receptor protein tyrosine phosphatase beta with a monoclonal antibody delays tumor growth in a glioblastoma model. *Cancer Res.* **2006**, *66*, 2271–2278. [CrossRef] [PubMed]

Role of Circular RNA in Brain Tumor Development

Swalih P. Ahmed ¹, Javier S. Castresana ² and Mehdi H. Shahi ^{1,*}

¹ Interdisciplinary Brain Research Centre, Faculty of Medicine, J. N. Medical College, Aligarh Muslim University, Aligarh 202002, India; swalihpahmed@gmail.com

² Department of Biochemistry and Genetics, University of Navarra School of Sciences, 31008 Pamplona, Spain; jscastresana@unav.es

* Correspondence: mehdihayat.md@amu.ac.in

Abstract: Central nervous system tumors are a leading cause of cancer-related death in children and adults, with medulloblastoma (MB) and glioblastoma (GBM) being the most prevalent malignant brain tumors, respectively. Despite tremendous breakthroughs in neurosurgery, radiation, and chemotherapeutic techniques, cell heterogeneity and various genetic mutations impacting cell cycle control, cell proliferation, apoptosis, and cell invasion result in unwanted resistance to treatment approaches, with a 5-year survival rate of 70–80% for medulloblastoma, and the median survival time for patients with glioblastoma is only 15 months. Developing new medicines and utilizing combination medications may be viewed as excellent techniques for battling MB and GBM. Circular RNAs (circRNAs) can affect cancer-developing processes such as cell proliferation, cell apoptosis, invasion, and chemoresistance in this regard. As a result, several compounds have been introduced as prospective therapeutic targets in the fight against MB and GBM. The current study aims to elucidate the fundamental molecular and cellular mechanisms underlying the pathogenesis of GBM in conjunction with circRNAs. Several mechanisms were examined in detail, including PI3K/Akt/mTOR signaling, Wnt/-catenin signaling, angiogenic processes, and metastatic pathways, in order to provide a comprehensive knowledge of the involvement of circRNAs in the pathophysiology of MB and GBM.



Citation: Ahmed, S.P.; Castresana, J.S.; Shahi, M.H. Role of Circular RNA in Brain Tumor Development. *Cells* **2022**, *11*, 2130. <https://doi.org/10.3390/cells11142130>

Academic Editor: Steven G. Gray

Received: 11 June 2022

Accepted: 4 July 2022

Published: 6 July 2022

Publisher's Note: MDPI stays neutral with regard to jurisdictional claims in published maps and institutional affiliations.



Copyright: © 2022 by the authors. Licensee MDPI, Basel, Switzerland. This article is an open access article distributed under the terms and conditions of the Creative Commons Attribution (CC BY) license (<https://creativecommons.org/licenses/by/4.0/>).

Keywords: circular RNA; miRNA; brain tumor; medulloblastoma; glioblastoma; pituitary adenoma; ependymoma; signaling pathway; diagnosis; treatment

1. Introduction

While central nervous system tumors account for a modest proportion of cancer diagnoses, they account for a significant proportion of cancer-related fatalities. Annually, almost 13,000 people die in the United States of America due to primary malignant brain and central nervous system tumors [1]. Medulloblastoma (MB) and glioblastoma (GBM) are the most prevalent CNS tumors in children and adults, respectively [2]. The WHO schemes are known for grading individual tumor classes (I, II, III, and IV) so that they can predict how they will behave. If there is no treatment, higher grade cancer (grades III and IV) is likely to be more aggressive than its lower grade counterpart in terms of how it looks and how quickly it gets better (grades I and II) [2]. A patient with the most common type of glioma, glioblastoma, can expect to live for only 15 months on average. As a result, radiation and chemotherapy have been more effective in treating childhood medulloblastoma, but the long-term side effects of these treatments can be very bad. The 5-year survival rate for this type of tumor has now reached 70% to 80% [3,4].

The most frequent pediatric brain tumor, medulloblastoma, has a 5-year survival rate of 71.9 percent. Medulloblastomas are the most common type of tumor on the cerebellum in childhood [5]. They are neuroepithelial tumors that account for 20% of all intracranial tumors in children, and for 40% of all childhood tumors in the fourth ventricle. Medulloblastoma is most common at 8 years old, but 30% of medulloblastomas happen in adults [6].

Medulloblastoma emerges from primitive neuroectoderm remnants in the fourth ventricle roof. It fills the ventricle and commonly invades the brainstem through the ependyma in the ventricle's floor. Rarely, the tumor occurs in the cerebellar hemispheres [7]. The current standard of care for patients with an average risk is surgical resection followed by radiation and chemotherapy for medulloblastomas. However, radiation is frequently avoided in patients younger than three years of age due to the highly harmful effects on the developing brain [8]. High-risk patients with medulloblastoma are different from standard-risk patients because they are less than 3 years old, have metastases, or show residual tumor after surgery. They should receive more rigorous treatment than standard-risk patients [5].

The 5-year survival rate for the most common adult brain tumor, glioblastoma multiforme (GBM), is only 5.1% [9]. Glioblastoma is the most prevalent type of adult brain tumor [10]. But children are diagnosed with 8–9 percent of the illnesses [11]. Due to the tumor's invasive, aggressive, and diffuse nature, treatment often consists of surgical excision followed by radiation and chemotherapy [12]. Malignant gliomas and medulloblastomas continue to provide significant treatment problems, many of which stem from the genetic and cellular heterogeneity of these tumor types. They include innate and acquired resistance, as well as the blood–brain barrier's impediment to effective drug administration [2]. The difficulty of treating malignant tumors, along with the highly harmful effects of radiation on the developing brains of young children, makes alternate therapy extremely desirable.

Circular RNAs (circRNAs) are important among the non-coding RNA family members. They are single-stranded closed circRNA molecules that lack a 5'-end cap or a 3'-end poly(A) tail; and are formed through covalent bonding [13]. CircRNAs are abundant; they are stable structures; and they are extensively dispersed across a variety of tissues, cell types, and biological fluids, making them easily identifiable [14,15]. Numerous studies have established that circRNAs are differentially expressed in many types of tumor cells [16,17]. Additionally, researchers have discovered a substantial association between circRNA expression and several types of cancer, implying that circRNAs may operate as tumor inhibiting or tumor-promoting agents [18]. Numerous studies have been conducted to determine the function of various circRNAs in MB and GBM cell proliferation, migration, invasion, and apoptosis, and thus these molecules have been identified as viable therapeutic targets in the fight against MB and GBM [19–23]. Hence, a comprehensive understanding of circRNAs and their roles in the signaling and molecular mechanisms underlying MB and GBM may result in identifying more potent therapy methods. As a result, this review will focus on the underlying processes and signaling pathways impacted by circRNAs throughout the evolution of MB and GBM. The study's findings may be useful for MB and GBM early diagnosis, pathological grading, targeted therapy, and prognostic evaluation.

2. Challenges, Perspective, and Clinical Significance

Medulloblastoma (MB), a type of primitive neuroectodermal tumor (PNET), is both the most prevalent malignant brain tumor in kids and the most common cause of cancer-related death in children [24,25]. The typical age of diagnosis for MB is six, with the majority diagnosed before the age of seventeen [24,26]. In the United States, there are about 500 cases of pediatric medulloblastoma every year [27,28]. These tumors make up 40% of all tumors in the posterior fossa. They can grow quickly and invade important structures, causing cerebellar dysfunction and causing cerebrospinal fluid to flow backwards. This pattern of growth can show up in the way people look and how they feel. Cerebellar signs are often seen in children, and they may have problems with coordination and walking. They may also experience headaches in the early morning, nausea, vomiting, papilledema, and double vision (hydrocephalus). The usual duration between symptom development and diagnosis is less than two to three months, but it can be even shorter [29].

Glioblastoma is the most prevalent malignant primary brain tumor, accounting for roughly 57% of all gliomas and 48% of all malignant primary central nervous system (CNS) tumors. Based on data from 2011 to 2015, the average yearly incidence of glioblastoma

in the United States is 3.21 per 100,000 individuals [29]. The incidence varies according to age and sex. The median age of diagnosis is 65 years, with the highest incidence occurring in the 75–84 year age group. Males are 1.58 times more likely than females to acquire glioblastoma, with an annual age-adjusted incidence of 4.00 versus 2.53 per 100,000 population, respectively [30]. Glioblastoma prognosis remains poor. Advanced age, poor performance status, and insufficient resection extent are all well-established risk factors for poor outcomes. The median survival time for elderly individuals receiving only the best supportive care is four months [31,32]. The relative 1-year survival rate for patients diagnosed in the United States between 2000 and 2014 was 41.4 percent, up from 34.4 percent between 2000 and 2004, and 44.6 percent between 2005 and 2014. Despite these gradual increases in short-term survival rates over time, the 5-year survival rate has remained largely stable, at 5.8% five years after diagnosis [9,29,30].

The diagnosis of brain tumor necessitates the use of time-consuming diagnostic methods such as histological and molecular characterization, magnetic resonance imaging (MRI), and cytological examination of cerebrospinal fluid (CSF). As a result of the variability of clinical manifestations, which are typically characterized by easily ignored symptoms, it might take weeks or even months to confirm a diagnosis [33]. As a result, tumors are frequently rather big, and 20–30% of patients present with metastasis at diagnosis [34]. Treatment options for children with medulloblastomas remain uncertain. Over the last three decades, survival rates for children with medulloblastoma have increased, due to a variety of variables, including improved surgery, increased use of preoperative craniospinal radiation therapy, and, more recently, the addition of chemotherapy [35,36]. At the moment, conventional therapy for brain tumors is limited and consists of surgical excision of the tumor followed by radiation and adjuvant chemotherapy [37].

3. Circular RNA

Circular RNAs have been found to play critical roles in various biological processes, including cell proliferation, epithelial-mesenchymal transition, and tumor growth [38]. CircRNAs were discovered in eukaryotes more than two decades ago [39–41]. A vast group of mostly non-coding circular RNAs has important roles in tumorigenesis. Disease stage, outcome, age, and gender were associated with circRNA patterns [42]. CircRNAs are a type of noncoding RNAs (ncRNAs) that have a continuous closed loop rather than 5' caps and 3' tails [21,43]. Numerous traits are conferred by the described features, including very high stability, which explains why they are so prevalent in the cytoplasm. CircRNAs are synthesized via back-splicing from pre-messenger RNA [21]. Certain circular transcripts may also be formed via direct RNA ligation, circularization of emancipated introns, or splicing of intermediates. Additionally, two different types of circular transcripts have been introduced: exon-skipping events, which happen in a small number of genes and involve internal splicing of skipped exons, and intron pairing-driven circularization, which happens when intronic motifs like Alu repeats cause the molecule to close by bringing the splice sites together [21,44]. CircRNAs were numerous and even substantially produced in mammalian cells compared to the host gene's linear RNA isoforms [21]. CircRNAs have emerged as a diverse class of endogenous RNAs with primarily non-coding functions essential for development and illness [42]. However, increased interest in circRNA has emerged in recent years as a result of their increasing operations in human biology [45–48]. They have tissue-specific expression patterns and account for a sizable portion of cellular RNA, particularly in the brain [42]. CircRNAs have been implicated in miRNA response elements and gene expression regulation [21]. Circular RNAs have been involved in various biochemical processes (Figure 1).

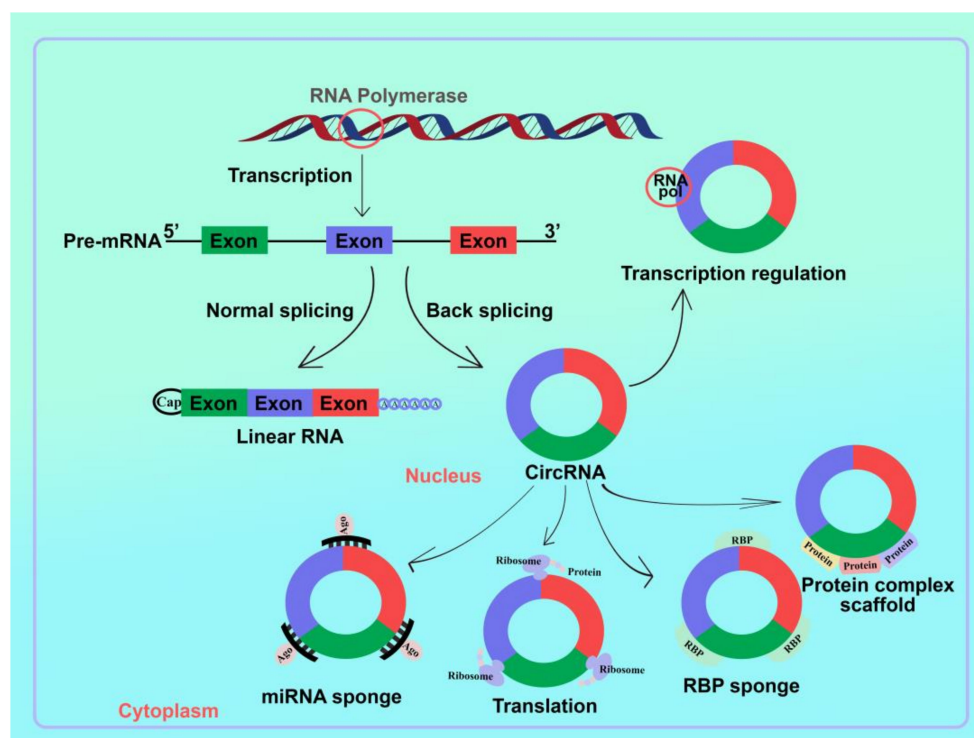


Figure 1. The function of circRNAs; miRNA molecular sponging: circRNAs with miRNA binding sites can prevent miRNA from attaching to its target mRNA and hence prevent miRNA from inhibiting the target protein. Regulation of translation: circRNAs to bind to the ribosome in order to regulate translation. RBP sponging: circRNAs with an RBP binding site can regulate protein activity. Protein complex scaffold: circRNAs may serve as protein scaffolds.

4. Role of circRNAs in Medulloblastoma

Medulloblastoma (MB), a primitive neuroectodermal tumor (PNET), is the most prevalent malignant brain tumor in children and the major cause of childhood cancer-related mortality [9,27–29,49], it is a prevalent malignant pediatric brain cancer and is the second leading cause of child death after leukemia [50]. MB is frequently found in the cerebellum; the primary symptoms and signs are produced by intracranial hypertension and hydrocephaly [51]. MB is currently treated mostly through surgery, radiation, and chemotherapy. While MB is radiation and chemotherapy sensitive, infection, peripheral neuropathy, ototoxicity, and myelosuppression are common secondary side effects of excessive treatment in children who are often in the formative stage [51]. Patients at average risk (defined as children older than three years of age who have had their tumor nearly completely removed and are free of metastatic illness) have an estimated 5-year overall survival rate of 85% [52–54]. Patients with high-risk malignancies (tumors that develop in children younger than three years of age with less than complete resection and metastatic disease at presentation) have a survival rate of closer to 60–70 percent [54,55]. CircRNAs have been shown to modulate cancer-related processes including tumorigenesis, tumor development, and apoptosis [16,17].

Additionally, researchers have discovered a substantial association between circRNA expression and several types of cancer, implying that circRNAs may operate as tumor-inhibiting or tumor-promoting agents [18]. Numerous studies have been conducted in this context to determine the role of various circRNAs in MB cell proliferation, migration, invasion, and apoptosis. Therefore, these compounds have been presented as feasible therapeutic targets in the fight against MB. Thus, a better understanding of circRNAs and their roles in the signaling and molecular pathways underlying MB may result in the identification of more effective therapy methods. Most circRNAs were downregulated in MB tissues, consistent with prior findings in breast cancer, hepatocellular carcinoma, laryn-

geal cancer, colorectal cancer, gastric cancer, and prostate adenocarcinoma [21]. However, the role of circRNAs in medulloblastoma (MB) remains uncertain [21]. The purpose of this work was to determine the expression profiles of circRNAs that regulate tumor cell proliferation and growth in MB.

The levels of expression of eight distinct circ-DTL (hsa-circ-0000179), circRNAs [circ-SKA3 (hsa-circ-0029696), circ-CRTAM, circ-RIMS1-1 (hsa-circ-0132250), circ-MAP3K5 (hsa-circ-0006856), circ-RIMS1-2 (hsa-circ-0076967)] circ-SKA3, and circ-DTL were tested. Circ-SKA3 and circ-DTL using short interfering RNAs and overexpressed their host genes to study their function in the pathogenesis of MB. 33 circRNAs showed differential expression in MB tissues, three of which were upregulated and thirty of which were downregulated; six of these circRNAs were successfully experimentally confirmed. By modulating the expression of host genes, upregulated circ-SKA3 and circ-DTL enhanced proliferation, migration, and invasion in vitro. This innovative work used circRNA profiling to indicate that circ-SKA3 and circ-DTL were critical in the carcinogenesis and progression of MB and may be viewed as novel and prospective biomarkers for diagnosis and new targets for treatments [21]. This study shows that circ-SKA3, circ-DTL, and circ-CASC15 are upregulated MB. Circular RNAs circ-UNC13C, circ-BRWD3, circ-CNTN6, circ-CRTAM, circ-MCU, circ-RIMS1-1, circ-FLT31, circ-DGKH, circ-FLT3-2, circ-SPHKAP, circ-GRM1, circ-GABRB2, circ-RIMS1-2, circ-ICA1, circ-GRIK2, circ-ATP8A2, circ-EPHX2, circ-WAC, circ-TENM1, circ-SNORD109A, circ-UNC13C, circ-GRIK2, circ-MAP3K5, circ-CAMKK2, circ-SVEP1, circ-CADPS2, circ-CAMK4-1, and circ-CAMK4-2 inhibited medulloblastoma growth [21] (Figure 2 and Table 1).

Table 1. List of circRNAs responsible for the down-regulation and up-regulation of medulloblastoma.

Sl. No.	CircRNA	Function	Expression	Reference
1	Circ-SKA3	Sponging miR-383-5p/miR-326	Upregulated	[19,20]
2	Circ-CASC15		Upregulated	[21]
3	Circ-DTL		Upregulated	[21]
4	Circ-UNC13C		Downregulated	[21]
5	Circ-BRWD3		Downregulated	[21]
6	Circ-CNTN6		Downregulated	[21]
7	Circ-CRTAM		Downregulated	[21]
8	Circ-MCU		Downregulated	[21]
9	Circ-RIMS1-1		Downregulated	[21]
10	Circ-FLT31		Downregulated	[21]
11	Circ-DGKH		Downregulated	[21]
12	Circ-FLT3-2		Downregulated	[21]
13	Circ-SPHKAP		Downregulated	[21]
14	Circ-GRM1		Downregulated	[21]
15	Circ-GABRB2		Downregulated	[21]
16	Circ-RIMS1-2		Downregulated	[21]
17	Circ-ICA1		Downregulated	[21]
18	Circ-GRIK2		Downregulated	[21]
19	Circ-ATP8A2		Downregulated	[21]
20	Circ-EPHX2		Downregulated	[21]
21	Circ-WAC		Downregulated	[21]
22	Circ-TENM1		Downregulated	[21]

Table 1. *Cont.*

Sl. No.	CircRNA	Function	Expression	Reference
23	Circ-SNORD109A		Downregulated	[21]
24	Circ-UNC13C		Downregulated	[21]
25	Circ-GRIK2		Downregulated	[21]
26	Circ-MAP3K5		Downregulated	[21]
27	Circ-CAMKK2		Downregulated	[21]
28	Circ-SVEP1		Downregulated	[21]
29	Circ-CADPS2		Downregulated	[21]
30	Circ-CAMK4-1		Downregulated	[21]
31	Circ-CAMK4-2		Downregulated	[21]

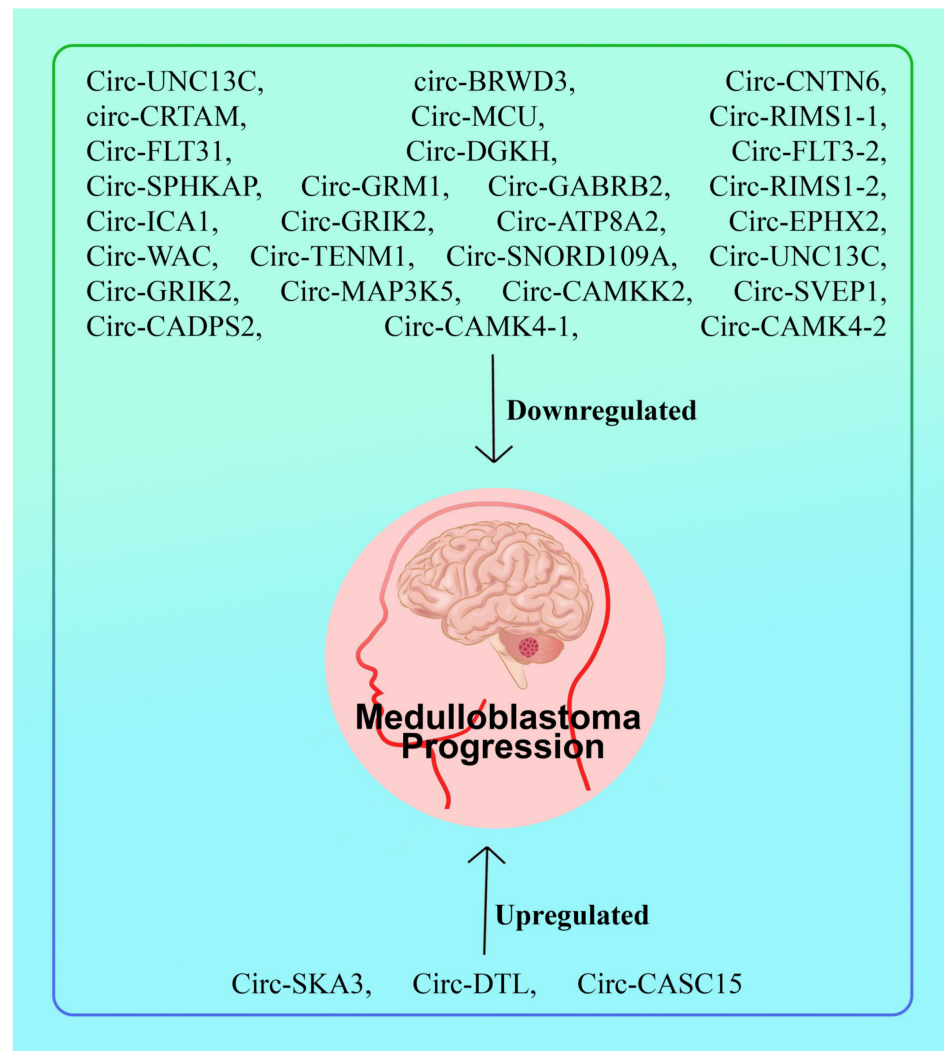


Figure 2. CircRNA regulation on medulloblastoma: various circRNAs including circ-UNC13C, circ-BRWD3, circ-CNTN6, circ-CRTAM, circ-MCU, circ-RIMS1-1, circ-FLT31, circ-DGKH, circ-FLT3-2, circ-SPHKAP, circ-GRM1, circ-GABRB2, circ-RIMS1-2, circ-ICA1, circ-GRIK2, circ-ATP8A2, circ-EPHX2, circ-WAC, circ-TENM1, circ-SNORD109A, circ-UNC13C, circ-GRIK2, circ-MAP3K5, circ-CAMKK2, circ-SVEP1, circ-CADPS2, circ-CAMK4-1, and circ-CAMK4-2 are responsible for the downregulation of medulloblastoma growth. Although, various circRNAs including circ-SKA3, circ-DTL, and circ-CASC15 are responsible for the up-regulation of medulloblastoma growth.

Circ-SKA3 and FOXM1 levels were raised, whereas miR-383-5p levels were decreased in MB tissues. Circ-SKA3 was shown to sponge miR-383-5p, which targets FOXM1. In vitro, suppressing circ-SKA3 slowed cell proliferation, migration, and invasion while inhibiting xenograft tumor growth in vivo. miR-383-5p reduced MB cell proliferation, migration, and invasion while increasing apoptosis via FOXM1. Circ-SKA3 [15] was substantially expressed in MB, and circ-SKA3 was found to be involved in regulating cell proliferation, migration, and invasion in MB [17]. With respect to circ-SKA3 expression in MB specimens and cells, functional investigations demonstrated that knocking down circ-SKA3 decreased not only MB cell proliferation, migration, and invasion in vitro, but also tumor initiation and growth in vivo, it identified miR-326 as a target of circ-SKA3 and demonstrated that it might also interact with ID3. Circ-SKA3 increased the development of MB in vitro and in vivo by boosting ID3 expression via miR-326 targeting, which may be another technique for treating MB in future [20] (Figure 2 and Table 1).

5. Role of circRNAs in Glioblastoma

Glioblastoma multiforme (GBM) is still considered a lethal form of brain cancer, accounting for around half of all initial brain tumors [56]. It is an astrocytoma of WHO grade IV that accounts for around 30% of all brain cancers [57]. This is an extremely vascularized and infiltrating tumor [58]. GBM has remained as an incurable cancer with an average survival time of approximately 12–15 months [56,59]. It is a glial cell tumor with a poor prognosis and a high mortality rate in adults [60]. GBM is resistant to apoptosis induction and overexpresses anti-apoptotic proteins [61]. The propensity to proliferate rapidly has been identified as a characteristic of GB, resulting in therapies followed by a poor clinical evolution [62]. The WHO's current international standard for naming and diagnosing glioma classifies these tumors into four subtypes. More broadly, gliomas are classified as low-grade gliomas (LGG, WHO I, and II) or high-grade gliomas (HGG, WHO III, and IV). Grade I gliomas are benign lesions with little proliferative potential to be healed surgically. Still, grades II to IV gliomas are highly infiltrative tumors and constitute the most frequent and malignant glioma grades [63]. Numerous studies have been conducted in this context to determine the function of various circRNAs in GBM cell proliferation, migration, invasion, and apoptosis. Therefore these molecules have been introduced as viable therapeutic targets in the fight against GBM [64–66]. It has emerged that circRNAs are key oncogenic drivers and tumor suppressors in glioblastoma and glioma of adults [42]. There may be better ways to treat GBM if we know more about how circRNAs work and how they affect GBM-related signaling and molecular mechanisms. So, this study will look into how circRNAs affect the basic mechanisms and signaling pathways that happen during the growth and spread of GBM.

5.1. CircRNAs Responsible for the Up-Regulation of Glioblastoma

Hsa-circ-0046701 was highly elevated in glioma tissues and cell lines, and knockdown of hsa-circ-0046701 decreased cell proliferation and invasion in glioma tissues and cell lines. Luciferase reporter experiments revealed that hsa-circ-0046701 acts as a sponge for miR-142-3p and is involved in regulating ITGB8 transcriptional activity. Silencing of hsa-circ-0046701 could result in an increase in miR-142-3p expression, which in turn resulted in a decrease in ITGB8 expression. hsa-circ-0046701/miR-142-3p/ITGB8 axis may play essential regulatory functions in the pathogenesis and progression of glioma [67] (Figure 3 and Table 2).

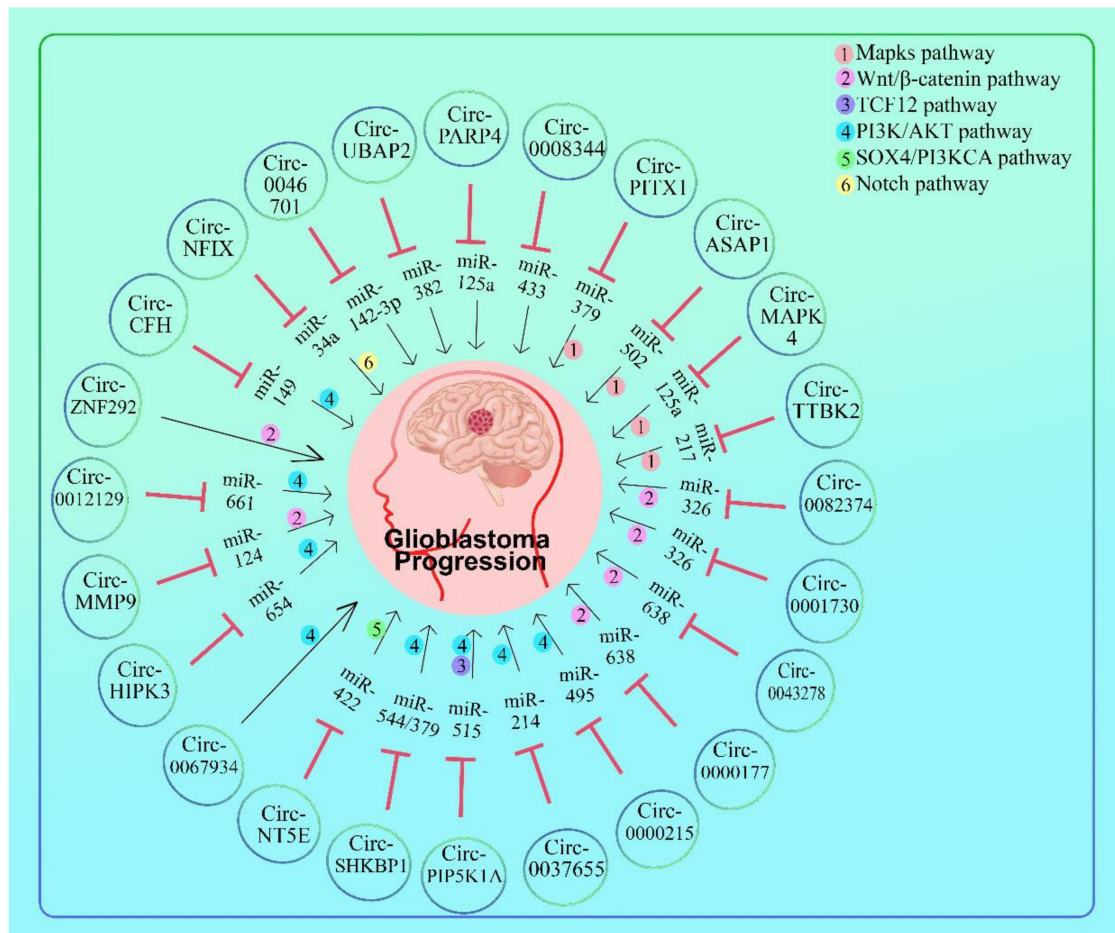


Figure 3. CircRNAs responsible for upregulation of glioblastoma growth: A schematic representation of the circRNAs involved in the regulation of glioma cell proliferation, migration, and invasion, among other functions. Numerous known circRNAs operate as miRNA sponges, subsequently increasing the amount of expression of the appropriate target genes. These target genes or proteins further influence downstream factors involved in cancer signaling pathways by functioning as transcription factors or regulatory proteins, as well as through other mechanisms. CircRNAs such as hsa-circ-0046701, circ-UBAP2, circ-PARP4, Hsa-circ-0008344, circ-PITX1, circ-ASAP1, circ-MAPK4, circ-TTBK2, circ-0082374, circ-0001730, circ-0043278, circ-0000177, circ-0000215, circ-0037655, circ-PIP5K1A, circ-SHKBP1, circ-NT5E, hsa-circ-0067934, circ-HIPK3, circ-MMP9, hsa-circ-0012129, circ-ZNF292, circ-CFH, and circ-NFIX are responsible for the up-regulation of glioblastoma growth through different pathways including those of the Mapks, Wnt/ β -catenin, TCF12, PI3K/AKT, SOX4/PI3KCA, and Notch. For example, circ-TTBK2 activates the Mapks signaling pathway through miR-217.

The expression of circBAP2 was increased in glioblastoma. In vitro, circ-UBAP2 upregulates cell proliferation, migration, and invasion while decreasing apoptosis and regulating tumor development in vivo. Circ-UBAP2 was found to be directly linked to miR-1205 and miR-382. miR-1205 and miR-382 were found to be involved in the regulation of circ-UBAP2 silencing on glioma cell behavior. Additionally, miR-1205 and miR-382 were functional targets of GPRC5A in modulating glioma cell activities. Moreover, circBAP2 induced GPRC5A expression in glioma cells via miR-1205 or miR-382. Circ-UBAP2 knockdown inhibited malignant glioma development in part by downregulating GPRC5A via miR-1205 and miR-382. UBAP2 specifically targeted miR-1205 and miR-382, which had been identified as tumor suppressors in glioma [68] (Figure 3 and Table 2).

Circ-PARP4 up-regulates glioma cell proliferation, migration, invasion, and epithelial-mesenchymal transformation. In vivo and in vitro investigations indicated that circ-PARP4, as a miRNA sponge, directly interacted with miR-125a-5p, which then controlled FUT4

to produce the oncogenic influence on glioma behavior. These findings highlight the activities of circ-PARP4 in influencing glioma progression through the miR-125a-5p/FUT4 pathway. miR-125a-5p has been reported to inhibit glioma cell proliferation and to promote cell differentiation by targeting TAZ. Suppression of miR-125a-5p can restore malignant phenotypes after inhibiting oncogene BCYRN1 in glioma. Down-regulated miR-125a-3p has been seen in CD133+ stem-like GBM cells compared with the CD133+ cells, and it can induce the differentiation of stem-like GBM cells, suggesting its involvement in the regulation of glioma stem cells. miR-125a-3p is considered as a tumor suppressor underlying the regulation of oncogenic circ-PARP4, which provides a novel and potential target for glioma therapy [69] (Figure 3 and Table 2).

Hsa-circ-0008344 silencing showed inhibited glioblastoma cell growth, colony formation, migration, and invasion but enhanced cell apoptosis in *in vitro* experiments. Bioinformatics predicts that hsa-circ-0008344 may interact with numerous miRNAs, including miR-433-3p and miR-450b-3p, whereas miR-433-3p has been shown to decrease cell proliferation and boost chemosensitivity in glioblastoma by targeting CREB, it is hypothesized that hsa-circ-0008344 can sponge tumor suppressor miRNAs, resulting in the disinhibition of the expression of particular targeted oncogenic genes, which leads to the progression of glioblastoma. Hsa-circ-0008344 expressions are increased in glioblastoma and may have a role in the progression of this cancer [65] (Figure 3 and Table 2).

Hsa-circ-0012129 expression was dramatically enhanced in cell lines and glioma tissues; knockdown of hsa-circ-0012129 greatly inhibited the proliferation, migration, and invasion capacities of cells U373 and SHG44. A dual-luciferase reporter assay revealed that hsa-circ-0012129 shared a complementary binding site and that its expression had a negative effect on miR-661. MiR-661 rescue studies demonstrated that it could reverse the effects of hsa-circ-0012129 on glioma cell survival, migration, and invasion *in vitro*. This study's findings suggested that circRNA hsa-circ-0012129 may operate as a natural miR-661 sponge in human glioma cells and that miR-661 may have inhibitory effects on circ-0012129 expression. Hsa-circ-0012129 has the potential to serve as a diagnostic or predictive biomarker for human glioma, as well as a therapeutic target [70] (Figure 3 and Table 2).

Circ-CDC45 and CSF-1 expression was increased in GBM tissues and cells; however, miR-485-5p expression was decreased. *In vivo*, silencing circ-CDC45 or CSF-1 inhibited GBM cell proliferation, invasion, migration, and tumor development. Circ-CDC45 favorably regulated CSF-1 expression by targeting miR-485-5p. miR-485-5p inhibition reduced the biological effects of circ-CDC45 deregulation in GBM cells [71] (Figure 4 and Table 2).

Circ-0029426 overexpression was associated with a poor prognosis in GBM, and circ-0029426 restorations increased GBM cell proliferation while inhibiting cell apoptosis. The expression of Circ-0029426 is highly associated with the clinical severity and prognosis of patients. Circ-0029426 significantly increased cell proliferation, migration, and invasion while inhibiting cell death. Circ-0029426 was predicted and confirmed to sponge miR-197. More critically, circ-0029426's carcinogenic properties are partially related to its inhibition of miR-197. Although the chemical mechanism by which circ-0029426 works has not been extensively investigated, circ-0029426 can still be considered a possible treatment target for GBM [72] (Figure 4 and Table 2).

Five circRNAs that are overexpressed are found, including circ-ENTPD7 (hsa-circ-0019421), hsa-circ-0040705, hsa-circ-0003026, hsa-circ-0040719, and hsa-circ-0040708. Five more circRNAs were discovered as underexpressed, including hsa-circ-0000722, hsa-circ-0040723, hsa-circ-0040733, hsa-circ-0040738, and hsa-circ-0007361 [73] (Figure 4 and Table 2).

In glioblastoma tissues, circ-ENTPD7 (hsa-circ-0019421) expression was increased. When circ-ENTPD7 expression levels were elevated in glioblastoma patients, Kaplan–Meier analysis revealed a low overall survival. Circ-ENTPD7 silencing decreased glioblastoma cell motility and growth. Additionally, circ-ENTPD7 worked as a sponge for miR-101-3p, regulating ROS1 expression and promoting glioblastoma cell proliferation and motility [73] (Figure 4 and Table 2).

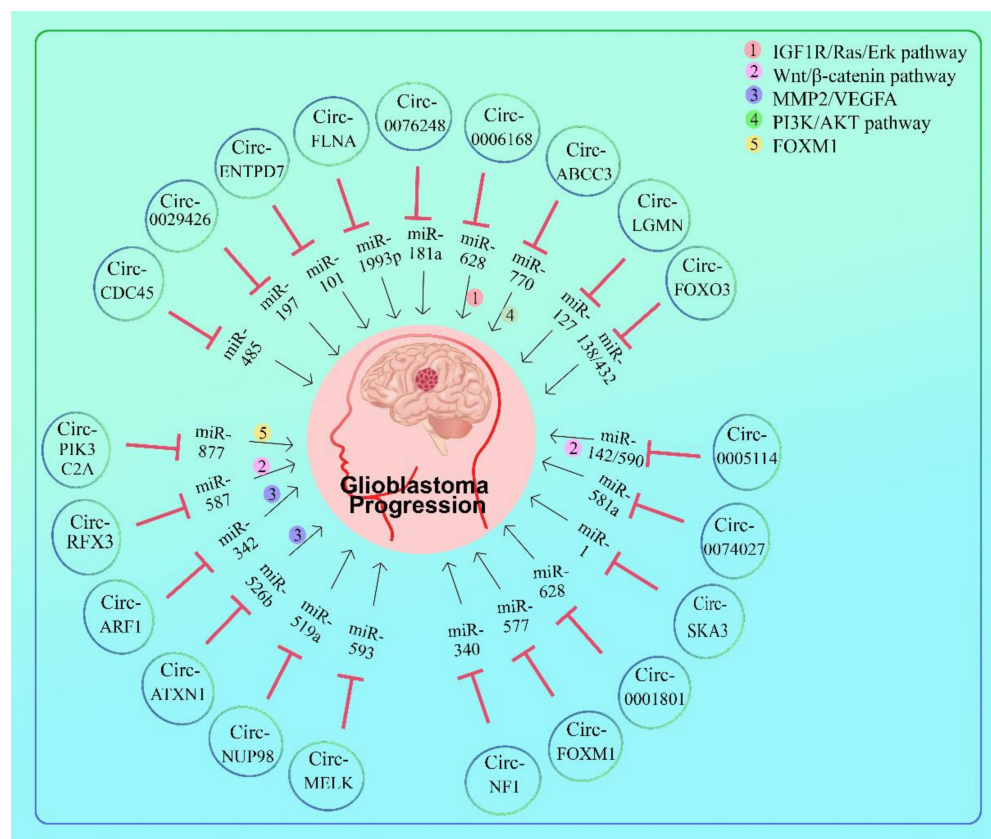


Figure 4. CircRNAs responsible for upregulation of glioblastoma growth: A schematic representation of the circRNAs involved in the regulation of glioma cell proliferation, migration, and invasion, among other functions. Numerous known circRNAs operate as miRNA sponges, subsequently increasing the amount of expression of the appropriate target gene. These target genes or proteins further influence downstream factors involved in cancer signaling pathways by functioning as transcription factors or regulatory proteins, as well as through other mechanisms. CircRNAs such as circ-CDC45, circ-0029426, circ-ENTPD7, circ-FLNA, hsa-circ-0076248, circ-0006168, circ-ABCC3, circ-LGMN, circ-FOXO3, hsa-circ-0005114, circ-0074027, circ-SKA3, circ-0001801, Circ-FOXM1, circ-NF1, circ-MELK, circ-NUP98, circ-ATXN1, circ-ARF1, circ-RFX3, and circ-PIK3C2A are responsible for the up-regulation of glioblastoma growth through different pathways including those of the IGF1R/Ras/Erk, Wnt/ β -catenin, MMP2/VEGFA, PI3K/AKT, and FOXM1. For example, circ-RFX3 activates the Wnt/ β -catenin pathway through miR-587.

High levels of circ-FLNA expression were linked to a poor outcome in GBM. miR-1993p later suggested to be a circ-FLNA target. Following circ-FLNA knockdown, the inhibition of cell growth and invasion by miR-1993p was partially reversed. Finally, the current study's findings discovered unexpected roles for circ-FLNA in GBM and suggested that the circ-FLNA/miR-1993p signaling axis may play a crucial role in GBM progression. As a result, circ-FLNA could be a unique target for the diagnosis and treatment of GBM [38] (Figure 4 and Table 2).

In vitro and in vivo hsa-circ-0076248 downregulation or miR-181a upregulation could inhibit glioma growth and invasion and significantly increase temozolomide chemotherapy sensitivity. Downregulating hsa-circ-0076248 or upregulating miR-181a could boost p53 and SIRT1 expression. The downregulation of SIRT1 expression appears to be the mechanism by which hsa-circ-0076248 governs glioma development and invasion. This implies that hsa-circ-0076248, miR-181a, and SIRT1 may be viable therapeutic feasible targets for glioma [74] (Figure 4 and Table 2).

The most prevalent circRNA generated from LGMN was hsa-circ-0033009 (circ-LGMN). Circ-LGMN expression was elevated in high-grade glioma (HGG), and it was associated

with a worse outcome in patients with glioma. Circ-LGMN overexpression boosted the proliferation and invasion of GBM cells. Circ-LGMN acts as a sponge for miR-127-3p, preventing the degradation of LGMN mRNA by miR-127-3p, resulting in enhanced LGMN protein expression. Treatment of GBM cells overexpressing circ-LGMN with a miR-127-3p mimic inhibited proliferation and reduced invasion. Furthermore, overexpression of circ-LGMN enhanced GBM malignancy *in vivo*, whereas overexpression of miR-127-3p reversed this effect. Taken together, circ-LGMN is a new tumor-promoting circRNA that promotes LGMN expression by sponging miR-127-3p. Thus, targeting the circ-LGMN/miR-127-3p/LGMN axis for GBM treatment may be a potential therapeutic option [75] (Figure 4 and Table 2).

Circ-FOXO3 expression was considerably increased in GBM tissues compared to normal tissue. Proliferation and invasion of GBM cells were decreased when circ-FOXO3 was knocked down and increased when circ-FOXO3 was overexpressed. Further biochemical investigation revealed that circ-FOXO3 acted as a competitive endogenous RNA (ceRNA) to promote nuclear factor of activated T cells 5 (NFAT5) production by sponging both miR-138-5p and miR-432-5p. Notably, miR-138-5p/miR-432-5p inhibitors were able to reverse tumor inhibition caused by circ-FOXO3 downregulation in GBM cells. Additionally, GBM cells that expressed less circ-FOXO3 generated less aggressive tumors *in vivo*. Circ-FOXO3 can act as a regulator in GBM, and microRNA sequestration caused by ceRNA may be a therapeutic option for GBM [76] (Figure 4 and Table 2).

Circ-0074027 contributes to the development of GBM through modulating miR-518a-5p/IL17RD signaling. NEAT1 promotes colorectal cancer carcinogenesis by sponging miR-193a-3p, hence increasing IL17RD expression. The current study established that elevated expression of IL17RD may accelerate cell progression in GBM. Additionally, circ-0074027 acts as a miR-518a-5p sponge, increasing IL17RD expression and conferring carcinogenic characteristics. Thus, the circ-0074027/miR-518a-5p/IL17RD network enables a novel element of GBM treatment [66] (Figure 4 and Table 2).

Circ-SKA3 expression is increased in GBM and associates with poor prognosis. Circ-SKA3 may inhibit miR-1 expression by methylation, hence promoting GBM cell growth. Circ-SKA3 expression was increased in GBM tissues and was inversely linked with miR-1. High levels of circ-SKA3 and low levels of miR-1 were shown to be substantially associated with poor survival in GBM patients. In GBM cells, overexpression of circ-SKA3 boosted miR-1 gene methylation and decreased miR-1 expression. The CCK-8 experiment demonstrated that overexpression of circ-SKA3 decreased miR-1's inhibitory effect on cell growth. Thus, circ-SKA3 may suppress miR-1 expression in GBM via methylation, thereby promoting cancer cell growth [77] (Figure 4 and Table 2).

Circ-0001801 helped GBM cells grow, move, invade, and become more like other cells by interacting with miR-628-5p. Circ-0001801 knockdown inhibited cell proliferation, migration, invasion, and epithelial-mesenchymal transition (EMT). Then, using the Dual-Luciferase reporter assay, the interaction between miR-628-5p and circ-0001801 or HMGB3 was confirmed. Reduced miR-628-5p expression in GBM tumors and cells established miR-628-inhibitory 5p's activity. Additionally, inhibition of miR-628-5p may be able to reverse the suppressive effect of circ-0001801 silencing on GBM cell growth and EMT. Increased expression of HMGB3 may compensate for the inhibitory effect of circ-0001801 silencing on GBM cell growth. Circ-0001801 promoted cell survival, migration, invasion, and EMT in GBM via absorbing miR-628-5p. This study identifies novel biomarkers for the diagnosis and treatment of GBM [78] (Figure 4 and Table 2).

Silencing circ-FOXM1 inhibited the growth of GBM cells, as well as the growth of the tumor. miR-577 may be sponged by circ-FOXM1, and inhibiting it may reverse the inhibitory effect of circ-FOXM1 deregulation on GBM progression. E2F5 was a miR-577 target, and its silencing had the same effect on GBM development as circ-FOXM1 silencing. Circ-FOXM1 controlled E2F5 expression positively, whereas miR-577 regulated E2F5 expression negatively. In conclusion, this research established that might act as a sponge, thereby accelerating the progression of GBM by targeting E2F5, implying that circ-FOXM1 could be used as a biomarker for GBM treatment [79] (Figure 4 and Table 2).

Circ-NF1 expression was found to be increased in GBM and was found to be associated with patient survival. Circ-NF1 siRNA knockdown increased mature miR-340 expression in GBM cells, but not the precursor miR-340. Cell proliferation assays revealed that suppressing circ-NF1 siRNA and overexpression of miR-340 inhibited GBM cell proliferation. Additionally, the miR-340a inhibitor inhibited the proliferation-promoting effect of circ-NF1 siRNA silencing. In GBM cells, circ-NF1 inhibited miR-340 maturation and lowered its expression level. These data show that circ-NF1 may be a good candidate for GBM therapy [80] (Figure 4 and Table 2).

Circ-MELK is a sponge for the tumor-suppressing miR-593, specifically targeting the oncogenic gene Eph receptor B2 (EphB2). To assess the interactions between miR-593 and circ-MELK or EphB2, dual-luciferase reporter assays were used. Circ-MELK expression was increased in GBM, acting as an oncogene and regulating GBM mesenchymal transition and GSC maintenance through miR-593 sponging. Additionally, it discovered that EphB2 was implicated in GBM carcinogenesis produced by the circ-MELK/miR-593 axis. This function creates a window of opportunity to make a potential therapeutic target for gliomas [81] (Figure 4 and Table 2).

Circ-NUP98 and pre-mature miR-519a-3p expression were increased in GB; however, mature miR-519a-3p expression was decreased. Circ-NUP98 was negatively connected with mature miR-519a-3p but favorably correlated with pre-mature miR-519a-3p across cancer tissues. Circ-NUP98 was found in both the nucleus and cytoplasm of GBM cells and interacted with pre-mature miR-519a-3p. Circ-NUP98 boosted the expression of pre-mature miR-519a-3p in GBM cells while decreasing the expression of mature miR-519a-3p. BrdU and cholecystokinin octapeptide (CCK-8) tests demonstrated that overexpression of circ-NUP98 inhibited miR-519a-3p-mediated cell proliferation inhibition. Circ-NUP98 increased tumor size, which resulted in dramatically decreased mouse survival. Circ-NUP98 inhibits miR-519a-3p maturation, hence promoting GBM cell proliferation [82] (Figure 4 and Table 2).

5.1.1. Mapks Pathway

Circ-PITX1 could act as a molecular sponge to make miR-379-5p less effective. miR-379-5p also targeted MAP3K2 as an upstream target. Moreover, miR-379-5p, MAP3K2, and circ-PITX1 were present in the RISC complex simultaneously. In addition, miR-379-5p could enhance the expression of MAP3K2 through circ-PITX1. Thus, circular RNA PITX1 acts as a ceRNA to regulate the miR-379-5p/MAP3K2 axis and promotes glioblastoma growth. Circ-PITX1 may be a novel research focus in GBM [83] (Figure 3; Table 2).

Circ-PITX1 expression was substantially higher in GBM tissues compared to control tissues. Additionally, this research established that circ-PITX1 aided in the formation of GBM by acting as a competitive endogenous RNA that absorbed miR-584-5p, thereby regulating KPNB1 expression. The roles of circ-PITX1 proposed a mechanism for circ-PITX1 involvement in the progression of GBM. In GBM tissues, circ-PITX1 expression was elevated and was inversely linked with miR-584-5p expression. Additionally, it was established that circ-PITX1 induced cancer in GBM through targeting the miR-584-5p/KPNB1 axis, implying that circ-PITX1/miR-584-5p/KPNB1 could be used as a diagnostic marker for GBM patients [84] (Figure 3 and Table 2).

Circ-ASAP1 expression was shown to be considerably higher in recurrent GBM tissues and TMZ-resistant cell lines. Circ-ASAP1 overexpression increased GBM cell proliferation and TMZ resistance, in which circ-ASAP1 knockdown reduced. Further research demonstrated that circ-ASAP1 boosted NRAS expression by sponging miR-502-5p. Furthermore, circ-ASAP1 depletion restored the sensitivity of TMZ-resistant xenografts [85] (Figure 3 and Table 2).

Circ-ASAP1 expression was very high in recurrent GBM tissues and TMZ-resistant cell lines. Circ-ASAP1 overexpression led to more GBM cell growth and resistance to TMZ, which could be reduced by knocking down circ-ASAP1. Further tests showed that circ-ASAP1 made NRAS more active by sponging miR-502-5p. In addition, circ-

ASAP1 depletion restored the sensitivity of TMZ-resistant xenografts to TMZ treatment in the clinic. Circ-ASAP1 has then regulatory roles in GBM, and competing endogenous RNA (ceRNA)-mediated microRNA sequestration might be a good way to treat GBM [85] (Figure 3 and Table 2).

Circ-MAPK4 served as an oncogene in gliomas, was inversely regulated, and was associated with the clinico-pathological stage of gliomas ($p < 0.05$). Following that, circ-MAPK4 increased glioma cell survival and prevented apoptosis in vitro and in vivo. Additionally, circ-MAPK4 regulated the p38/MAPK pathway, which influenced the development and apoptosis of gliomas. miR-125a-3p, exhibited tumor-suppressive action by modulating the p38/MAPK pathway, which was elevated when circ-MAPK4 was inhibited and could be brought down by circ-MAPK4. Inhibition of miR-125a-3p partially compensates for the increased phosphorylation of p38/MAPK and the increased quantity of apoptosis-inducing protein caused by circ-MAPK4 knockdown. Circ-MAPK4 has a vital role in glioma cell survival and apoptosis by modulation of miR-125a-3p, which may provide a novel therapeutic target for the treatment of gliomas [86] (Figure 3 and Table 2).

Circular TTBK2 expression was increased in glioma tissues and cell lines, whereas linear TTBK2 expression was not altered in glioma tissues or cells. Increased circ-TTBK2 expression facilitated cell proliferation, migration, and invasion while inhibiting apoptosis. miR-217 expression levels were decreased in glioma tissues and cell lines. Additionally, It discovered that circ-TTBK2, but not linear TTBK2, behaved as a sequence-specific miR-217 sponge. Furthermore, increased circ-TTBK2 expression lowered miR-217 expression, resulting in a reciprocal negative feedback loop in an Argonaute2-dependent manner. Additionally, restoration of miR-217 dramatically reversed the stimulation of glioma growth by circ-TTBK2. HNF1 was a direct miR-217 target and acted as an oncogene in glioma cells. Surprisingly, the combination of circ-TTBK2 silencing and miR-217 overexpression resulted in tumor regression in vivo. Inhibition of the circ-TTBK2/miR-217/HNF1/Derlin-1 axis may be a viable target for human gliomas [87] (Figure 3 and Table 2).

5.1.2. PI3K/AKT Pathway

Circ-0000215 and CXCR2 expression were significantly increased in glioma cells and tissues. Circ-0000215 overexpression boosted proliferation, invasion, and EMT while prevented apoptosis in glioma cells, whereas circ-0000215 knockdown had the opposite impact. Additionally, miR-495-3p, a sponge RNA derived from circ-0000215, suppressed glioma cell proliferation, invasion, and EMT. CXCR2 was a particular target of miR-495-3p, which negatively affected the CXCR2/PI3K/Akt pathway. However, the effects of miR-495-3p were all diminished when circ-0000215 was overexpressed. Circ-0000215 acts as a competitive endogenous RNA by sponging miR-495-3p, increasing glioma growth via the CXCR2 axis. By targeting the miR-495-3p/CXCR2/PI3K/Akt axis, overexpression of circ-0000215 can increase glioma growth. It is beneficial for the early detection and treatment of glioma, as well as for assessing its stage and prognosis [88] (Figure 3 and Table 2).

Circ-0037655 was more common in glioma tissues and cell lines (U251 and SHG-44) than in normal tissues and cell lines. Inhibiting circ-0037655 could make glioma cells less able to live and spread. Circ-0037655 is a sponge for miR-214, and when miR-214 is blocked, si-circ-0037655 can make cells less able to live and invade. Over-producing miR-214 could make p-Akt less likely to be found in the body (PI3K pathway indicator). This study looked at the expression of circRNAs in gliomas. It found that circ-0037655 could help glioma growth by controlling miR-214/PI3K signaling, which could be a new way to treat gliomas [89] (Figure 3 and Table 2).

Circ-PIP5K1A expression was increased in glioma tissues (compared to normal surrounding tissues), and overexpression was associated with glioma volume and histopathological grade. In vivo and in vitro overexpression of circ-PIP5K1A significantly increased glioma cell proliferation, invasion, and EMT while inhibiting apoptosis. Additionally, circ-PIP5K1A increased TCF12 expression and PI3K/AKT activation. Bioinformatics investigation established that circ-PIP5K1A and TCF12 shared a target, miR-515-5p, while the dual-

Luciferase reporter assay and RNA immunoprecipitation (RIP) experiment demonstrated that circ-PIP5K1A specifically targeted miR-515-5p, which bound the 3'-untranslated region (UTR) of TCF12. Circ-PIP5K1A is a possible prognostic marker for glioma and affects glioma evolution via the miR-515-5p-mediated TCF12/PI3K/AKT axis [90] (Figure 3 and Table 2).

Circ-SHKBP1 regulates the angiogenesis of endothelial cells exposed to U87 glioma (GECs). Circ-SHKBP1 expression, but not linear SHKBP1, was considerably increased in GECs compared to endothelial cells exposed to astrocytes (AECs). The absence of circ-SHKBP1 significantly reduced the viability, migration, and tube formation of GECs. In GECs, expression of miR-379/miR-544a was suppressed, and circ-SHKBP1 targeted miR-544a/miR-379 via the RNA-induced silencing complex (RISC). A dual-luciferase reporter assay revealed that miR-544a/miR-379 targeted forkhead box P1/P2 (FOXP1/FOXP2). FOXP1/FOXP2 expression was increased in GECs, and inhibiting FOXP1/FOXP2 decreased GEC viability, migration, and tube formation. At the transcriptional level, FOXP1/FOXP2 enhanced angiogenic factor with G patch and FHA domains 1 (AGGF1) expression. Additionally, through the PI3K/AKT and extracellular signal-regulated kinase (ERK1/2) pathways, knocking down AGGF1 decreased GECs' survival, migration, and tube formation. Circ-SHKBP1 regulated the angiogenesis of GECs via the miR-544a/FOXP1 and miR-379/FOXP2 pathways, and these findings suggest that circ-SHKBP1 may be a useful target and method for combination therapy of gliomas [91] (Figure 3 and Table 2).

Circ-0067934 was a lot more common in GBM tissues and cancer cells than in normal tissues and cells. Kaplan–Meier survival curves revealed that patients with more hsa-circ-0067934 had better overall survival and a better chance of being disease-free. The functional tests showed that the knockdown of hsa-circ-0067934 slowed GBM cell growth, metastasis, and EMT and encouraged apoptosis. Furthermore, the mechanical analysis showed that the down-regulation of hsa-circ-0067934 had a big impact on the activation of the PI3K-AKT pathway. Circ-0067934 is overexpressed in GBM and plays a role in cancer cell growth and metastasis by upregulating the PI3K-AKT pathway. This means that hsa-circ-0067934 is likely to be an effective treatment for GBM [92] (Figure 3 and Table 2).

Circ-HIPK3 expression was increased in glioma tissues. Elevated circ-HIPK3 levels have been associated with a poor prognosis. Circ-HIPK3 enhances glioma cell proliferation and invasion, as well as tumor propagation in vivo, according to functional analysis. Additionally, circ-HIPK3 was discovered as a target of miR-654, whereas miR-654 was identified as a target of IGF2BP3. Circ-HIPK3 may enhance IGF2BP3 expression in glioma cells by interacting with miR-654. Finally, CCK8 and transwell experiments demonstrated that overexpression of IGF2BP3 could reverse the consequences of IGF2BP3 deficiency. Overall, these data indicate that circ-HIPK3 promotes glioma progression by targeting miR-654 from IGF2BP3, implying that circ-HIPK3 may be a therapeutic target for glioma [93] (Figure 3 and Table 2).

Circ-CFH expression was found to be greatly increased in glioma tissue and was found to be associated with tumor grade. Circ-CFH expression was also significantly increased in U251 and U373 glioma cell lines. Circ-CFH deficiency impairs cell proliferation and colony formation. Circ-CFH acts as a sponge for miR-149 and suppresses its action in U251 and U373 cells, as determined by luciferase experiments. AKT1 has since been determined as a direct target of the circ-CFH/miR-149 axis. Circ-CFH promotes glioma growth via miR-149 sponging and AKT1 signaling pathway regulation. The circ-CFH/miR-149/AKT1 axis has the potential to be a therapeutic target for glioblastoma [94] (Figure 3 and Table 2).

Circ-ABCC3 and SOX2 expression were significantly increased in glioblastoma tissues and cells; however, miR-770-5p expression was substantially decreased compared to control groups. Circ-ABCC3 expression was significantly increased in stage III glioblastoma tissues compared to stage I + II glioblastoma tissues, strongly linked to the tumor-node-metastasis (TNM) stage. Circ-ABCC3 deficiency decreased cell proliferation, migration, invasion, tube formation, and PI3K/AKT pathway activation in glioblastoma but promoted cell death. Additionally, circ-ABCC3 functioned as a sponge for miR-770-5p, directed against SOX2. Inhibitors of miR-770-5p attenuated the effects of circ-ABCC3 silencing

on glioblastoma development, angiogenesis, and the PI3K/AKT pathway. Additionally, circ-ABCC3 silencing inhibited tumor growth *in vivo*. Circ-ABCC3 influenced the growth of glioblastoma via the miR-770-5p/SOX2 axis and the PI3K/AKT pathway. This discovery establishes a theoretical foundation for further investigation of circRNA-directed treatment for glioblastoma [95] (Figure 4 and Table 2).

5.1.3. SOX4/PI3KCA Pathway

Circ-NT5E is controlled by ADARB2 binding to sites around circRNA-forming introns. Circ-NT5E may act as a sponge against miR-422a in developing glioblastoma tumors. Multiple pathogenic processes were regulated by circ-NT5E, including cell proliferation, migration, and invasion. Circ-NT5E interacted directly with miR-422a and reduced its activity. Additionally, it was revealed that circ-NT5E sponges other miRNAs, demonstrating tumor suppressor-like properties in glioblastoma. Taken together, these findings suggest that circRNA has a unique carcinogenic role in glioblastoma [96] (Figure 3 and Table 2).

5.1.4. Notch Pathway

Circ-NFIX was the only circRNA overexpressed in glioma using five different experimental approaches. Additionally, when paired normal brain tissues were compared to tumor tissues, the Notch signaling system was significantly elevated. Circ-NFIX was found to behave like a sponge for miR-34a-5p, a miRNA that targeted NOTCH1. Both circ-NFIX downregulation and miR-34a-5p overexpression decreased cell proliferation and migration. Additionally, a miR-34a-5p inhibitor abolished si-suppressive circ-NFIX's impact on glioma cells. Circ-NFIX and miR-34a-5p mimics induced apoptosis in cells. Additionally, circ-NFIX was shown *in vivo* to inhibit glioma growth via the regulation of miR-34a-5p and NOTCH1. Circ-NFIX expression was significantly increased in glioma cells. Circ-NFIX may enhance glioma growth via the Notch signaling pathway by sponging miR-34a-5p. This finding gave new information on the role of circ-NFIX in the progression of human glioma malignancy [97] (Figure 3 and Table 2).

5.1.5. Wnt/ β -catenin Pathway

The expression of circ-0082374 was higher in glioma tissues and cells. Circ-0082374 silencing inhibited glioma cell survival, migration, invasion, and glycolysis. miR-326 was a target of circ-0082374, and miR-326 silencing diminished circ-0082374's inhibitory effect on glioma progression. SIRT1 was a miR-326 target, and circ-0082374 acted as a miR-326 sponge, promoting SIRT1 production. SIRT1 inhibition inhibited circ-0082374's prognostic glioma-promoting action. *In vivo*, miR-326/SIRT1 knockdown decreased xenograft tumor development. Collectively, silencing circ-0082374 inhibited viability, migration, invasion, and glycolysis in glioma cells via a ceRNA mechanism involving miR-326 and SIRT1, thereby elucidating a novel pathogenic mechanism for glioma [98] (Figure 3 and Table 2).

Circ-0001730 knockdown inhibited glioblastoma cell motility and proliferation. SP1 binds to the promoter of the circ-0001730 host gene EPHB4, therefore boosting circ-0001730 expression. Circ-0001730 stimulated the Wnt/ β -catenin signaling pathway via the miR-326/Wnt7B axis. Circ-0001730 knockdown inhibited glioblastoma cell invasion. In glioblastoma cells, silencing circ-0001730 reversed the EMT phenotype. Circ-0001730 expression increased with increasing clinical stage in the clinical data analysis. In high-grade glioma samples, increased circ-0001730 expression associated with a lower overall survival and DFS rate. Through the miR-326/Wnt7B axis, circ-000173 increased proliferation and invasion in glioblastoma cells. Circ-0001730 deficiency inhibited glioblastoma cell growth by inducing cell cycle arrest at the G1/S transition [99] (Figure 3 and Table 2).

Circ-0043278 directly sponged miR-638 to increase HOXA9 expression in GBM, which can stimulate Wnt/ β -catenin signaling. Additionally, miR-638 directly targets the HOXA9 3'UTR, suppresses HOXA9 expression, and inhibits the two Wnt signaling effectors c-Myc and Cyclin D1, whereas overexpression of HOXA9 can partially counteract the effects of miR-638 in glioma. In both, U87 and U251 cells, silencing circ-0043278 decreases HOXA9

protein expression. miR-638 inhibition corrected the impairment of malignant tumor behavior caused by circ-0043278 silencing. The circ-0043278/miRNA-638/Homeobox A9 (HOXA9) axis had a critical role in the progression of GBM [100] (Figure 3 and Table 2).

Hsa-circ-0000177 was more common in glioma tissues and cell lines than in normal tissues and cell lines. Moreover, high levels of hsa-circ-0000177 were linked to a poor prognosis in glioma patients. In functional experiments, hsa-circ-0000177 knockdown dramatically slowed the growth and spread of glioma cells in the lab. Consistently, knocking down hsa-circ-0000177 had a big impact on glioma growth in the clinic. Hsa-circ-0000177 functions as a miRNA sponge for miR-638, which targets the FZD7 gene. Through the inhibition of miR-638, it was found that hsa-circ-0000177 enhanced FZD7 expression and activation of the Wnt signaling pathway, ultimately leading to progression of glioma growth. This study showed that hsa circ 0000177 stimulates glioma cell proliferation and invasion in vitro, while also increasing the rate of tumor progression in mice. This result also revealed that hsa-circ-0000177 may be a prognostic biomarker for glioma patients [101] (Figure 3 and Table 2).

Circ-MMP9 served as an oncogene, increased GBM, and facilitated GBM cell proliferation, motility, and invasion. Following that, circ-MMP9 acted as a sponge for miR-124, increasing GBM cell proliferation, motility, and invasion via miR-124 targeting. Additionally, cyclin-dependent kinase 4 (CDK4) and aurora kinase A (AURKA) were implicated in the GBM carcinogenesis produced by the circ-MMP9/miR-124 axis. Finally, the MMP9 mRNA transcript-binding eukaryotic initiation factor 4A3 (eIF4A3) increased circ-MMP9 cyclization and expression in GBM [102] (Figure 3 and Table 2).

In human glioma cell lines, circ-ZNF292 silencing decreased tube development. The circ-ZNF292 is involved in the development of human glioma tubes. cZNF292 is a significant circular oncogenic RNA required for tube formation to progress. It is discovered that silencing cZNF292 inhibits tube formation in glioma cells by reducing proliferation and cell cycle progression. The Wnt/-catenin signaling pathway and associated genes such as PRR11, Cyclin A, p-CDK2, VEGFR-1/2, p-VEGFR-1/2, and EGFR were used to arrest cell cycle progression in human glioma U87MG and U251 cells at the S/G2/M phase. The data indicate that suppressing cZNF292 is required for tube development and may be used as a therapeutic target and biomarker in glioma. Circ-ZNF292 is required for the proliferation and tube development of gliomas. Circ-ZNF292 action may be mediated by controlling the cell cycle and associated genes. However, more mechanistic investigations are required to elucidate the mechanism of action of circ-ZNF292 [103] (Figure 3 and Table 2).

Hsa-circ-0005114 was shown to interact with both hsa- miR-142-3p and hsa-miR-590-5p, which may play a role in glioma. Hsa-circ-0005114 was shown to be involved in insulin secretion, while APC was found to be linked to Wnt signaling. Hsa-circ-0005114-miR-142-3p/miR-590-5p-APC ceRNA axis could be involved in the formation and progression of gliomas. miR-142/3p/miR-590/5p and APC ceRNA axis may be viable targets for the therapy of GBM [104] (Figure 4 and Table 2).

Circ-RFX3 expression was significantly enhanced in both GBM cell lines and tumors. Circ-RFX3 was found to enhance the proliferation, invasion, and migration of GBM cells in several overexpression and knockdown tests. Circ-RFX3 demonstrated to function as a sponge for miR-587, and its function as a competitive endogenous RNA (ceRNA) in the formation of GBM is evaluated using dual-luciferase reporter gene and RNA pull-down tests. Additionally, PDIA3 has been shown to be a miR-587 downstream target and modulate the Wnt/-catenin pathway. Circ-RFX3 may function as a pro-cancer circRNA by encouraging the development of GBM and modulating the miR-587/PDIA3/-catenin axis. This work may identify a potential molecular target for GBM therapy [105] (Figure 4 and Table 2).

5.1.6. IGF1R/Ras/Erk Pathway

Hsa-circ-0006168 and IGF1R were increased in human GBM cells and tissues, while miR-628-5p was downregulated in the same cells and tissues; blocking hsa-circ-0006168 and increasing miR-628-5p made A172 and LN229 cells less likely to grow and move, as well as

less likely to form colonies and become apoptotic. In A172 and LN229 cells, inhibiting hsa-circ-0006168 and increasing miR-628-5p expression inhibited cell proliferation, migration, invasion, and expression of vimentin and Snail (mesenchymal markers), decreased colony formation, and increased E-cadherin (epithelial marker) and apoptosis rate. miR-628-5p silencing reversed the suppressive effect of hsa-circ-0006168 deficit, restored IGF1R function and inhibited miR-628-5p-mediated inhibition. Moreover, silencing hsa-circ-0006168 suppresses the formation of xenograft tumors in vivo and decreases the levels of Ras and phosphorylated Erk1/2 both in vitro and in vivo. IGF1R was a novel target of miR-628-5p that was mechanically targeted and sponged by Hsa-circ-0006168. Inhibiting miR-628-5p may abolish the in vitro function of hsa-circ-0006168 silencing. By competing with miR-628-5p and regulating the IGF1R/Ras/Erk pathway, silencing hsa-circ-0006168 may inhibit the growth and motility of GBM cells [68] (Figure 4 and Table 2).

5.1.7. MMP2/VEGFA

Circ-ATXN1 and SRSF10 expression levels were substantially higher in GECs than astrocyte-associated endothelial cells (AECs). SRSF10 or circ-ATXN1 knockdown dramatically decreased the viability, migration, and tube formation of GECs, whereas SRSF10 knockdown functioned by blocking the production of circ-ATXN1. Additionally, when SRSF10 and circ-ATXN1 were knocked down simultaneously, the inhibitory effects on cell survival, migration, and tube formation in GECs were dramatically amplified compared to when SRSF10 and circ-ATXN1 were knocked down separately. miR-526b-3p expression was decreased in GECs. Circ-ATXN1 functionally targeted miR-526b-3p in an RNA-induced silencing complex. Increased miR-526b-3p expression decreased the viability, migration, and tube formation of GECs. Additionally, miR-526b-3p influenced the angiogenesis of GECs by suppressing the production of MMP2/VEGFA. The SRSF10/circ-ATXN1/miR-526b-3p axis was critical in regulating GEC angiogenesis. The discoveries above identified novel anti-angiogenic targets in glioma [106] (Figure 4 and Table 2).

Circ-ARF1 was found to have an oncogenic impact. ISL2 was overexpressed in gliomas and was associated with a bad prognosis. ISL2 regulated VEGFA expression in GSCs and increased the proliferation, invasion, and angiogenesis of hBMECs via ERK signaling mediated by VEGFA. Circ-ARF1 increased ISL2 expression in GSCs via miR-342-3p sponging. Additionally, U2AF2 coupled to and enhanced the stability and expression of cytoplasmic ARF1, whereas ISL2 encouraged U2AF2 expression, forming a feedback loop in GSCs. Both U2AF2 and circ-ARF1 were carcinogenic, overexpressed in glioma, and associated with a poor prognosis. In GSCs, a new feedback loop between U2AF2, Circ-ARF1, miR-342-3p, and ISL2 was discovered. This feedback loop boosted tumor angiogenesis and may be exploited as a biomarker for glioma diagnosis and prognosis, as well as for targeted therapy [107] (Figure 4 and Table 2).

5.1.8. FOXM1

Circ-PIK3C2A expression increased the proliferation, invasion, and creation of tumor cells; deletion of circ-PIK3C2A function had the exact opposite effect on the tumor cells' growth and development. The establishment of a subcutaneous xenograft tumor model in nude mice demonstrated that the loss of function of circ-PIK3C2A efficiently reduced tumor load in vivo and prolonged the survival duration of tumor-bearing animals. The interaction between circ-PIK3C2A/miR-877-5p and FOXM1 was validated using a luciferase reporter experiment. Circ-PIK3C2A acts as an endogenous competitive RNA by sponging miR-877-5p through specific binding sites, thereby altering FOXM1 expression. These findings collectively show that circ-PIK3C2A acts as a ceRNA via modulating the miR-877-5p/FOXM1 axis, opening up a unique avenue for future clinical intervention with glioblastoma [108] (Figure 4 and Table 2).

Table 2. List of circRNAs responsible for the up-regulation of glioblastoma.

Sl. No.	CircRNA	Function	Signaling Pathway	Expression	Reference
1	Hsa-circ-0046701	Sponging miR-142-3p		Upregulated	[67]
2	Circ-UBAP2	Sponging miR-1205 and miR-382		Upregulated	[68]
3	Circ-PARP4	Sponging miR-125a-5p		Upregulated	[69]
4	Hsa-circ-0008344	miR-433-3p		Upregulated	[65]
5	Hsa-circ-0012129	Sponging miR-661		Upregulated	[70]
6	Circ-CDC45	Sponging miR-485-5p		Upregulated	[71]
7	Circ-0029426	Sponging miR-197		Upregulated	[72]
8	Circ-ENTPD7	Sponging miR-101-3p		Upregulated	[73]
9	Circ-FLNA	Sponging miR-1993p		Upregulated	[38]
10	Hsa-circ-0076248	Sponging miR-181a		Upregulated	[74]
11	Circ-LGMN	Sponging miR-127-3p		Upregulated	[75]
12	Circ-FOXO3	Sponging miR-138-5p/miR-432-5p		Upregulated	[76]
13	Circ-0074027	Sponging miR-518a-5p		Upregulated	[66]
14	Circ-SKA3	Sponging miR-1		Upregulated	[77]
15	Circ-0001801	Sponging miR-628-5p		Upregulated	[78]
16	Circ-FOXM1	Sponging miR-577		Upregulated	[79]
17	Circ-NF1	Sponging miR-340		Upregulated	[80]
18	Circ-MELK	Sponging miR-593		Upregulated	[81]
19	Circ-NUP98	Sponging miR-519a-3p		Upregulated	[82]
20	Circ-PITX1	Sponging miR-379-5p	Mapks pathway	Upregulated	[83,84]
21	Circ-ASAP1	Sponging miR-502-5p	Mapks pathway	Upregulated	[85]
22	Circ-MAPK4	Sponging miR-125a-3p	Mapks pathway	Upregulated	[86]
23	Circ-TTBK2	Sponging miR-217	Mapks pathway	Upregulated	[87]
24	Circ-0000215	Sponging miR-495-3p	CXCR2/PI3K/AKT pathway	Upregulated	[88]
25	Circ-0037655	Sponging miR-214	PI3K pathway	Upregulated	[89]
26	Circ-PIP5K1A	Sponging miR-515-5p	TCF12 and PI3K/AKT pathway	Upregulated	[90]
27	Circ-SHKBP1	Sponging miR-544a/miR-379	PI3K/AKT pathway	Upregulated	[91]
28	Hsa-circ-0067934		PI3K/AKT pathway	Upregulated	[92]
29	Circ-HIPK3	Sponging miR-654	IGF2/PI3K/AKT pathway	Upregulated	[93]
30	Circ-CFH	Sponging miR-149	PI3K/AKT pathway	Upregulated	[94]
31	Circ-ABCC3	Sponging miR-770-5p	PI3K/AKT pathway	Upregulated	[95]
32	Circ-NT5E	Sponging miR-422a	SOX4/PI3KCA pathway	Upregulated	[96]
33	Circ-NFIX	Sponging miR-34a-5p	Notch pathway	Upregulated	[97]
34	Circ-0082374	Sponging miR-326	Wnt/ β -catenin pathway	Upregulated	[98]
35	Circ-0001730	Sponged miR-326	Wnt/ β -catenin pathway	Upregulated	[99]
36	Circ-0043278	Sponged miR-638	Wnt/ β -catenin pathway	Upregulated	[100]
37	Circ-0000177	Sponging miR-638	Wnt/ β -catenin pathway	Upregulated	[101]

Table 2. Cont.

Sl. No.	CircRNA	Function	Signaling Pathway	Expression	Reference
38	Circ-MMP9	Sponging miR-124	Wnt/ β -catenin pathway	Upregulated	[102]
39	Circ-ZNF292		Wnt/ β -catenin pathway	Upregulated	[103]
40	Hsa-circ-0005114	Sponging miR-142-3p/miR-590-5p	Wnt/ β -catenin pathway	Upregulated	[104]
41	Circ-RFX3	Sponging miR-587	Wnt/ β -catenin pathway	Upregulated	[105]
42	Circ-0006168	Sponging miR-628-5p	IGF1R/Ras/Erk pathway	Upregulated	[68]
43	Circ-ATXN1	Sponging miR-526b-3p	MMP2/VEGFA	Upregulated	[106]
44	Circ-ARF1	Sponging miR-342-3p	MMP2/VEGFA	Upregulated	[107]
45	Circ-PIK3C2A	Sponging miR-877-5p	FOXM1	Upregulated	[108]

5.2. Circ-RNAs Responsible for the Down-Regulation of Glioblastoma

Circ-SHPRH generates a “UGA” stop codon by overlapping genetic codes, resulting in the translation of the 17 kDa SHPRH-146aa. In normal human brains, both circ-SHPRH and SHPRH-146aa are abundantly expressed, however in glioblastoma they are suppressed. Overexpression of SHPRH-146aa lowers the malignant behavior and tumorigenicity of U251 and U373 glioblastoma cells in vitro and in vivo. SHPRH-146aa functions by preventing full-length SHPRH from being degraded by the ubiquitin-proteasome. As an E3 ligase, SHPRH stabilizes sequentially ubiquitinates proliferating cell nuclear antigen (PCNA), inhibiting cell proliferation and tumorigenesis. SHPRH-146aa, derived from circ-overlapping SHPRH’s genetic codes, functions as a tumor suppressor in human glioblastoma [109] (Figure 5 and Table 3).

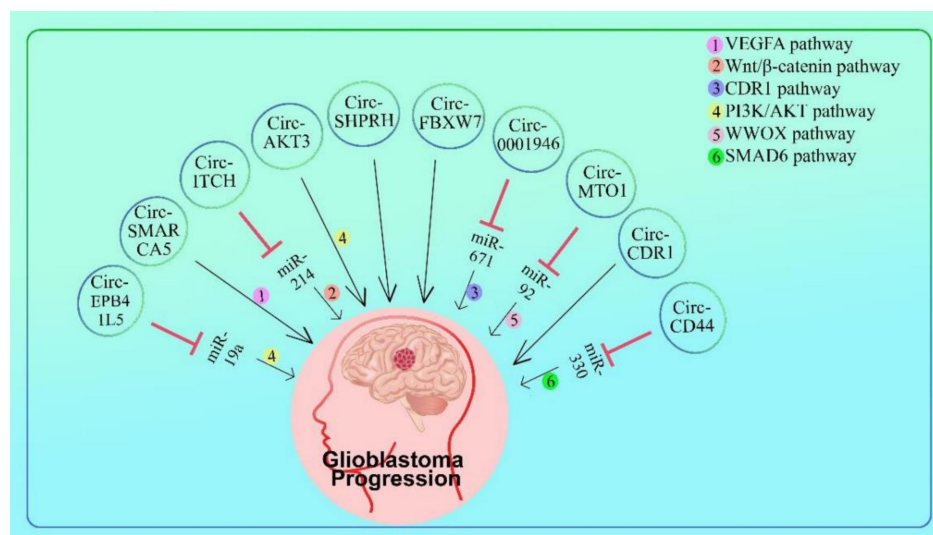


Figure 5. CircRNAs that downregulate glioblastoma growth: A schematic representation of the circRNAs involved in the regulation of glioma cell proliferation, migration, and invasion, among other functions. Numerous discovered circRNAs operate as miRNA sponges, therefore downregulating the amount of expression of the relevant target gene. These target genes or proteins further influence downstream factors involved in cancer signaling pathways by functioning as transcription factors, regulatory proteins. CircRNAs such as circ-CDC45, circ-0029426, circ-ENTPD7, circ-FLNA, hsa-circ-0076248, circ-0006168, circ-ABCC3, circ-LGMN, Circ-FOXO3, Hsa-circ-0005114, Circ-0074027, Circ-SKA3, Circ-0001801, Circ-FOXM1, Circ-NF1, Circ-MELK, Circ-NUP98, circ-ATXN1, circ-ARF1, circ-RFX3, and circ-PIK3C2A are responsible for the down-regulation of glioblastoma growth through different pathways including those of the VEGFA, Wnt/ β -catenin, CDR1, PI3K/AKT, WWOX, and SMAD6 pathways. For example, circ-ITCH promotes the Wnt/ β -catenin signaling pathway via miR-214.

In cancer cells, overexpression of FBXW7-185aa reduced proliferation and cell cycle acceleration, whereas knockdown increased aggressive phenotypes *in vitro* and *in vivo*. FBXW7-185aa decreased the half-life of c-Myc by inhibiting the stabilization of c-Myc produced by USP28. In glioblastoma clinical samples, circ-FBXW7 and FBXW7-185aa levels were significant than in paired tumor-adjacent tissues. Circ-FBXW7 expression was linked considerably with overall survival in glioblastoma patients. Endogenous circRNA encodes a functional protein in human cells, and circ-FBXW7 and FBXW7-185aa may be predictive of brain cancer prognosis [110] (Figure 5 and Table 3).

Circ-CDR1as has been found to bind to the p53 protein, which is made by the body's cells. With each glioma grade, the amount of CDR1as in the brain decreases, and it is a good predictor of overall survival in glioma, especially in GBM. CDR1as does not act as a miRNA sponge, but it does keep p53 proteins stable by stopping them from being ubiquitinated. CDR1as directly interacts with the p53 DBD domain, which is important for MDM2 binding. This stops the p53/MDM2 complex from forming. In the case of DNA damage, CDR1as may keep p53 working and protect cells from DNA damage. Significantly, CDR1as slows down tumor growth in both the lab and in the clinic, but it does not work in cells where p53 is missing or mutated. Because CDR1as depletion may play a big role in promoting tumorigenesis by lowering p53 expression in glioma, this may be the case. These findings help us better understand the roles and mechanisms of action of circular RNAs in general and CDR1as in particular, and they could lead to new ways for the treatment of glioma [111] (Figure 5 and Table 3).

5.2.1. PI3K/AKT Pathway

Circ-EPB41L5 expression levels were significantly decreased in glioblastoma tissues and cell lines relative to normal brain tissues and cell lines. Low circ-EPB41L5 expression was associated with a poor prognosis in glioblastoma patients, although overexpression suppressed glioma cell proliferation, clone formation, migration, and invasion abilities, whereas suppression had the opposite impact. RNA-seq analysis revealed that the host gene was circ-EPB41L5, which acted as a sponge against miR-19a, inhibiting miR-19a activity from upregulating EPB41L5 expression. Through EPB41L5, circ-EPB41L5 regulated RhoC expression and AKT phosphorylation. The study demonstrates that circ-EPB41L5/miR-19a/EPB41L5/p-AKT regulatory axis plays a significant role in glioblastoma progression, providing a fresh insight into the mechanisms underlying glioblastoma [112] (Figure 5 and Table 3).

Circ-AKT3 expression is reduced in GBM tissues compared to paired neighboring normal brain regions. By exploiting overlapping start-stop codons, circ-AKT3 encodes a 174 amino acid (aa) new protein called AKT3-174aa. Overexpression of AKT3-174aa inhibited cell proliferation, radiation resistance, and *in vivo* tumorigenicity in GBM cells, whereas circ-AKT3 knockdown improved the malignant characteristics of astrocytoma cells. AKT3-174aa interacts competitively with phosphorylated PDK1, inhibits AKT-thr308 phosphorylation, and acts as a negative regulator of the PI3K/AKT signaling intensity. Circular RNA expression of the AKT3 gene leads to the development of GBM tumors, and this data support the concept that restoring AKT3-174aa while reducing active AKT may give additional benefits for select GBM patients [113] (Figure 5 and Table 3).

5.2.2. Wnt/ β -catenin Pathway

In glioma tissues and cell lines, circ-ITCH expression was decreased. According to the receiver operating curve analysis, circ-ITCH has a pretty high diagnosis accuracy. The Kaplan–Meier analysis demonstrated that a decreasing circ-ITCH level was related to a decreased survival rate in patients with glioma. Circ-ITCH dramatically enhanced glioma cell proliferation, migration, and invasion. Following identification of the linear isomer of circ-ITCH, the ITCH gene was identified as the downstream target. Following that, RNA immunoprecipitation demonstrated unequivocally that circ-ITCH sponged miR-214, hence promoting ITCH expression. The gain and loss of function experiments revealed that

circ-ITCH exerts anti-oncogenic activity through sponging miR-214 and modulating the ITCH-Wnt/-catenin pathway. These findings indicate that circ-ITCH functions as a tumor suppressor gene in glioma and may serve as a promising predictive biomarker for patients with glioma. Thus, re-expression of circ-ITCH may be a potential direction for developing a unique therapy technique [114] (Figure 5 and Table 3).

5.2.3. VEGFA Pathway

Numerous differentially expressed circRNAs were identified, with circ-SMARCA5 and circ-FBXW7 being the most downregulated. Both are recognized as tumor suppressors in adult glioma and glioblastoma. Furthermore, in unsupervised hierarchical cluster analysis, patients with a poor prognosis were clustered independently from those with a favorable prognosis [42] (Figure 5 and Table 3).

In glioblastoma multiforme, circ-SMARCA5 functions as a sponge for the splicing factor serine and arginine rich splicing factor 1 (SRSF1) (GBM). After establishing physical contact between SRSF1 and circ-SMARCA5, the expression of total, pro-angiogenic (Iso8a), and anti-angiogenic (Iso8b) mRNA isoforms of vascular endothelial growth factor A (VEGFA), a known SRSF1 splicing target, was examined. The Iso8a to Iso8b ratio increased significantly in GBM biopsies compared to parenchyma controls, was negatively correlated with circ-SMARCA5 expression, and decreased significantly in U87-MG overexpressing circ-SMARCA5 compared to the negative control. Blood vascular microvessel density was negatively correlated with circ-SMARCA5 expression but favorably associated with SRSF1 expression. Kaplan–Meier survival analysis revealed that patients with GBM who had low circ-SMARCA5 expression had worse overall and progression-free survival rates than those with high circ-SMARCA5 expression. This data strongly imply that circ-SMARCA5 is an upstream regulator of the ratio of pro- to anti-angiogenic VEGFA isoforms in GBM cells and a highly potential prognostic and anti-angiogenic molecule in GBM [115] (Figure 5 and Table 3).

The glioblastoma cell line U87MG, overexpressing circ-SMARCA5, expressed a higher level of the serine and arginine-rich splicing factor 3 (SRSF3) RNA isoform including exon 4, which is ordinarily skipped in an SRSF1-dependent manner, resulting in non-productive nonsense-mediated decay (NMD) substrate. SRSF3 has been shown to interact with two additional splicing factors, polypyrimidine tract binding protein 1 (PTBP1), and polypyrimidine tract binding protein 2 (PTBP2), which promote glioma cell motility. Circ-SMARCA5 is highly downregulated in GBM, and it may work by influencing the activity of SRSF1, hence affecting the splicing and expression of SRSF3 and PTBP1. An in-depth examination of the relationship between circ-SMARCA5 and SRSF1 and its downstream network in GBM cells was carried out, with the goal of bolstering the case for circ-SMARCA5 as a GBM biomarker [116] (Figure 5 and Table 3).

5.2.4. CDR1 Pathway

Circ-0001946 and CDR1 expressions were low in GBM cells, although miR-671p expression was high. Circ-0001946 inhibited the expression of miR-671p, hence increasing the expression of CDR1 in the miR-671p target gene. Circ-0001946 and CDR1 inhibited proliferation, migration, and invasion of GBM cells while increasing apoptosis, but miR-671p had the reverse impact. Circ-0001946 decreased GBM growth and Ki67 expression in GBM cells, as demonstrated by the xenograft mouse model and immunohistochemistry data [117] (Figure 5 and Table 3).

5.2.5. WWOX Signaling Pathway

Circ-MTO1 expression was significantly decreased in glioblastoma tumors compared to neighboring normal tissues. In glioblastoma, a lower circ-MTO1 level was substantially related to shorter overall survival. circ-MTO1 decreased U251 cell proliferation. CircumMTO1 induces the expression of WWOX in U251 cells, and WWOX is involved in the circ-MTO1-induced reduction of U251 cell proliferation. miR-92 inhibits WWOX

production by specifically targeting its mRNA 3' UTR. More crucially, circ-MTO1 interacts directly with miR-92 and acts as a miRNA sponge, increasing WWOX expression. Circ-MTO1 suppresses glioblastoma cell growth via the miR-92/WWOX signaling pathway [64] (Figure 5 and Table 3).

5.2.6. SMAD6 Signaling Pathway

Circ-CD44 expression was decreased in glioblastoma multiforme (GBM) tissues and primary GBM cells. LRRC4 interacts with SAM68. By blocking the interaction of SAM68 and CD44 pre-mRNA, LRRC4 enhanced the production of circ-CD44. In vivo, re-expression of circ-CD44 dramatically inhibited GBM cell proliferation, colony formation, and invasion, as well as tumor growth. Circ-CD44 acts as a ceRNA for miR-326 and miR-330-5p in GBM growth, enhancing SMAD6 expression and regulating the TGF- β signaling pathway. Thus, the LRRC4/Sam68/circ-CD44/miR-326/miR-330-5p/SMAD6 signaling axis may provide a therapeutic target for GBM [118] (Figure 5 and Table 3).

Table 3. List of circRNAs responsible for the down-regulation of glioblastoma.

Sl. No.	CircRNA	Function	Signaling Pathway	Expression	Reference
1	Circ-SHPRH			Downregulated	[109]
2	Circ-FBXW7			Downregulated	[110]
3	Circ- CDR1			Downregulated	[111]
4	Circ-EPB41L5	Sponging miR -19a	PI3K/ AKT pathway	Downregulated	[112]
5	Circ-AKT3		PI3K/ AKT pathway	Downregulated	[113]
6	Circ-ITCH	Sponging miR -214	Wnt pathway	Downregulated	[114]
7	Circ-SMARCA5		VEGFA pathway	Downregulated	[115,116]
8	Circ- 0001946	Sponging miR-671-5p	CDR1 pathway	Downregulated	[117]
9	Circ-MTO1	Sponging miR-92	WWOX signaling pathway	Downregulated	[64]
10	Circ-CD44	Sponging miR-326/miR-330-5p	SMAD6 signaling pathway	Downregulated	[118]

6. Role of circRNAs in Other Brain Tumors

6.1. Pituitary Adenoma

Circ-VPS13C was shown to be considerably higher in non-functioning pituitary adenoma (NFPA) samples and cell line studies. In vitro and in vivo experiments including gain- and loss-of-function mutations revealed that silencing circ-VPS13C decreases the growth of pituitary tumor cells in vitro and in vivo. Silencing circ-VPS13C enhanced the expression of IFITM1 and activated its downstream genes involved in the MAPK- and apoptosis-associated signaling pathways. VPS13C reduced IFITM1 expression, detected by a new method, primarily by competitively interacting with RRBP1, an endoplasmic reticulum membrane ribosome-binding protein, and thereby decreasing the stability of IFITM1 mRNA. By controlling mRNA stability by interacting with ribosome-binding proteins on the endoplasmic reticulum membrane, circ-VPS13C has been demonstrated to be a key regulator in the proliferation and development of NFPA [119].

Circ-NFIX was significantly expressed in invasive pituitary adenomas. Circ-NFIX regulated the expression of miR-34a-5p and CCNB1 during the in vivo and in vitro development and progression of pituitary adenomas. However, miR-34a-5p expression was nearly the opposite. Circ-NFIX silencing or miR-34a-5p overexpression decreased invasion, migration, and proliferation of pituitary adenoma tumors by regulating CCNB1 [120].

Overexpression of circ-OMA1 (hsa circRNA 0002316) was shown to sponge miR-145-5p, whose inhibition on NFPA cells was abolished. miR-145-5p was dramatically lowered in NFPA samples and linked adversely with NFPA invasiveness. miR-145-5p

overexpression decreased NFPA cell growth and invasiveness and induced apoptosis. Translationally controlled tumor protein (TPT1) was identified as a target of miR-145-5p and as a mediator of miR-145-5p. TPT1 and its downstream components Mcl-1 and Bcl-xL were downregulated, and Bax was increased by miR-145-5p. Circ-OMA1 promotes NFPA growth by functioning as the sponge of tumor suppressor miR-145-5p to regulate the TPT1 signaling pathway, indicating a therapeutic target in suppressing the tumorigenesis of NFPA [121].

6.2. Ependymoma

CircRNAs exhibits diverse expression patterns in ependymomas in comparison to controls and between patients who survived and those who had a poor prognosis, which suggests that circRNAs might be utilized as a diagnostic and prognostic biomarker in the future. CircRNAs such as circ-VCAN, circ-RMST, circ-LRBA, circ-WDR78, circ-DRC1, and circ-BBS9 were specifically upregulated in ependymomas. CircRNAs such as circ-SMARCA5, circ-FBXW7, circ-RIMS1, circ-RIMS2, and circ-EPB41L5 showed to be significantly downregulated in ependymomas [42].

7. Future Prospective of Circular RNAs in Brain Tumors

In this review paper, we have tried to talk about different miRNAs that are either directly or indirectly controlling the growth of glioblastoma. CircRNAs have a lot of power in the field of clinical prognosis and diagnosis because they sponge the different miRNAs and control more than one molecular pathway. The expression or function of circRNAs could be used as a possible treatment for brain tumors. This could lead to better survival rates and allow for more research into the treatment of brain tumors. There is a lot of work that needs to be done to find out how these things work, and more research needs to be done on how circRNAs work. This study, on the other hand, could help improve future molecular therapies for medulloblastoma and glioblastoma. When it comes to brain tumors biomarkers, circRNAs could be very useful in the future. Because some circRNAs are oncogenes and others are tumor suppressors, they could be used for treatment and act as brain tumors biomarkers in the future.

8. Conclusions

While circRNAs are gaining prominence in the research community, medulloblastoma and glioblastoma are the most prevalent CNS tumors in children and adults, respectively. As a result, the relationship between circRNAs in medulloblastoma and glioblastoma clinical features is complex and mostly unknown, and the processes causing glioma and medulloblastoma-specific circRNA expression patterns warrant additional exploration. CircRNA knockout has remained a challenge thus far. As the bulk of circRNAs are produced from genes with the ability to code, silencing or downregulating the corresponding circRNAs will definitely influence the host genes. Additionally, ubiquitous low levels of circRNA expression may inhibit their protein translation in MB, GBM, and other human disorders.

These RNA molecules might influence various biological processes associated with the spread of GBM, including cell proliferation, apoptosis, invasion, and treatment resistance. These effects are accomplished through the activation of important molecular processes and signaling pathways. Certain circRNAs have been shown to positively influence critical pathways such as the PI3K/Akt/mTOR signaling, the Wnt/catenin pathway, and the MAPK cascade, while others have been shown to negatively affect them. The advancement of recently discovered circRNA-identification methods is enhancing the diagnostic and treatment approaches for MB and GBM based on circRNAs, which will be an important moment in eradicating these life-threatening tumors. In the future, critical phases of glioma development must be researched further to identify particular circRNAs, create a comprehensive gene–protein interaction network, and clarify their role and fundamental mechanism of action by a combination of in vitro and in vivo and clinical studies. CircRNAs are predicted to become a focal point of research in the field of non-coding RNAs in the near

future. Additional research will be required to confirm that circRNAs play a critical role in medulloblastoma, glioblastoma, and other disorders, hence opening up new avenues for early detection, pathological grading, targeted therapy, and prognosis of these diseases.

Author Contributions: S.P.A. writing original draft. M.H.S. Concept, writing—reviewing and editing; J.S.C. writing—reviewing and editing. All authors have read and agreed to the published version of the manuscript.

Funding: This work was supported by a grant from the Indian Council of Medical Research, from Government of India to M.H.S. (Project No. 2019-3331-CMB/Adhoc/BMS), and by a grant from University of Navarra Foundation, Pamplona, Spain, to J.S.C.

Institutional Review Board Statement: Not applicable.

Informed Consent Statement: Not applicable.

Conflicts of Interest: The authors declare no conflict of interest.

References

- Dolecek, T.A.; Propp, J.M.; Stroup, N.E.; Kruchko, C. CBTRUS Statistical Report: Primary Brain and Central Nervous System Tumors Diagnosed in the United States in 2005–2009. *Neuro. Oncol.* **2012**, *14*, v1–v49. [CrossRef] [PubMed]
- Huse, J.T.; Holland, E.C. Targeting Brain Cancer: Advances in the Molecular Pathology of Malignant Glioma and Medulloblastoma. *Nat. Rev. Cancer* **2010**, *10*, 319–331. [CrossRef] [PubMed]
- Stupp, R.; Mason, W.P.; van den Bent, M.J.; Weller, M.; Fisher, B.; Taphoorn, M.J.B.; Belanger, K.; Brandes, A.A.; Marosi, C.; Bogdahn, U.; et al. Radiotherapy plus Concomitant and Adjuvant Temozolomide for Glioblastoma. *N. Engl. J. Med.* **2005**, *352*, 987–996. [CrossRef] [PubMed]
- Wen, P.Y.; Kesari, S. Malignant Gliomas in Adults. *N. Engl. J. Med.* **2008**, *359*, 492–507. [CrossRef]
- Gilbertson, R.J. Medulloblastoma: Signalling a Change in Treatment. *Lancet. Oncol.* **2004**, *5*, 209–218. [CrossRef]
- Cervoni, L.; Maleci, A.; Salvati, M.; Delfini, R.; Cantore, G. Medulloblastoma in Late Adults: Report of Two Cases and Critical Review of the Literature. *J. Neurooncol.* **1994**, *19*, 169–173. [CrossRef]
- Raffel, C. Medulloblastoma: Molecular Genetics and Animal Models. *Neoplasia* **2004**, *6*, 310–322. [CrossRef]
- Mueller, S.; Chang, S. Pediatric Brain Tumors: Current Treatment Strategies and Future Therapeutic Approaches. *Neurother. J. Am. Soc. Exp. Neurother.* **2009**, *6*, 570–586. [CrossRef]
- Ostrom, Q.T.; Gittleman, H.; Farah, P.; Ondracek, A.; Chen, Y.; Wolinsky, Y.; Stroup, N.E.; Kruchko, C.; Barnholtz-Sloan, J.S. CBTRUS Statistical Report: Primary Brain and Central Nervous System Tumors Diagnosed in the United States in 2006–2010. *Neuro. Oncol.* **2013**, *15*, ii1–ii56. [CrossRef]
- Collins, V.P. Gliomas. *Cancer Surv.* **1998**, *32*, 37–51.
- Dohrmann, G.J.; Farwell, J.R.; Flannery, J.T. Glioblastoma Multiforme in Children. *J. Neurosurg.* **1976**, *44*, 442–448. [CrossRef] [PubMed]
- Nicholas, M.K. Glioblastoma Multiforme: Evidence-Based Approach to Therapy. *Expert Rev. Anticancer. Ther.* **2007**, *7*, S23–S27. [CrossRef] [PubMed]
- Chen, L.-L.; Yang, L. Regulation of CircRNA Biogenesis. *RNA Biol.* **2015**, *12*, 381–388. [CrossRef] [PubMed]
- Li, P.; Chen, S.; Chen, H.; Mo, X.; Li, T.; Shao, Y.; Xiao, B.; Guo, J. Using Circular RNA as a Novel Type of Biomarker in the Screening of Gastric Cancer. *Clin. Chim. Acta* **2015**, *444*, 132–136. [CrossRef]
- Wang, S.; Zhang, K.; Tan, S.; Xin, J.; Yuan, Q.; Xu, H.; Xu, X.; Liang, Q.; Christiani, D.C.; Wang, M.; et al. Circular RNAs in Body Fluids as Cancer Biomarkers: The New Frontier of Liquid Biopsies. *Mol. Cancer* **2021**, *20*, 13. [CrossRef]
- Arnaiz, E.; Sole, C.; Manterola, L.; Iparraguirre, L.; Otaegui, D.; Lawrie, C.H. CircRNAs and Cancer: Biomarkers and Master Regulators. *Semin. Cancer Biol.* **2019**, *58*, 90–99. [CrossRef]
- Patop, I.L.; Kadener, S. CircRNAs in Cancer. *Curr. Opin. Genet. Dev.* **2018**, *48*, 121–127. [CrossRef]
- Wang, F.; Nazarali, A.J.; Ji, S. Circular RNAs as Potential Biomarkers for Cancer Diagnosis and Therapy. *Am. J. Cancer Res.* **2016**, *6*, 1167–1176.
- Wang, X.; Xu, D.; Pei, X.; Zhang, Y.; Zhang, Y.; Gu, Y.; Li, Y. Circska3 Modulates Foxm1 to Facilitate Cell Proliferation, Migration, and Invasion While Confine Apoptosis in Medulloblastoma via Mir-383-5p. *Cancer Manag. Res.* **2020**, *12*, 13415–13426. [CrossRef]
- Zhao, X.; Guan, J.; Luo, M. Circ-SKA3 Upregulates ID3 Expression by Decoying MiR-326 to Accelerate the Development of Medulloblastoma. *J. Clin. Neurosci.* **2021**, *86*, 87–96. [CrossRef]
- Lv, T.; Miao, Y.F.; Jin, K.; Han, S.; Xu, T.Q.; Qiu, Z.L.; Zhang, X.H. Dysregulated Circular RNAs in Medulloblastoma Regulate Proliferation and Growth of Tumor Cells via Host Genes. *Cancer Med.* **2018**, *7*, 6147–6157. [CrossRef] [PubMed]
- Salami, R.; Salami, M.; Mafi, A.; Vakili, O.; Asemi, Z. Circular RNAs and Glioblastoma Multiforme: Focus on Molecular Mechanisms. *Cell Commun. Signal.* **2022**, *20*, 13. [CrossRef] [PubMed]
- Zhang, Y.; Lin, X.; Geng, X.; Shi, L.; Li, Q.; Liu, F.; Fang, C.; Wang, H. Advances in Circular RNAs and Their Role in Glioma (Review). *Int. J. Oncol.* **2020**, *57*, 67–79. [CrossRef] [PubMed]

24. Taylor, M.D.; Northcott, P.A.; Korshunov, A.; Remke, M.; Cho, Y.-J.; Clifford, S.C.; Eberhart, C.G.; Parsons, D.W.; Rutkowski, S.; Gajjar, A.; et al. Molecular Subgroups of Medulloblastoma: The Current Consensus. *Acta Neuropathol.* **2012**, *123*, 465–472. [CrossRef]
25. Smoll, N.R.; Drummond, K.J. The Incidence of Medulloblastomas and Primitive Neuroectodermal Tumours in Adults and Children. *J. Clin. Neurosci. Off. J. Neurosurg. Soc. Australas.* **2012**, *19*, 1541–1544. [CrossRef] [PubMed]
26. Van Ommeren, R.; Garzia, L.; Holgado, B.L.; Ramaswamy, V.; Taylor, M.D. The Molecular Biology of Medulloblastoma Metastasis. *Brain Pathol.* **2020**, *30*, 691–702. [CrossRef]
27. Phoenix, T.N.; Patmore, D.M.; Boop, S.; Boulos, N.; Jacus, M.O.; Patel, Y.T.; Roussel, M.F.; Finkelstein, D.; Goumnerova, L.; Perreault, S.; et al. Medulloblastoma Genotype Dictates Blood Brain Barrier Phenotype. *Cancer Cell* **2016**, *29*, 508–522. [CrossRef]
28. Massimino, M.; Biassoni, V.; Gandola, L.; Garrè, M.L.; Gatta, G.; Giangaspero, F.; Poggi, G.; Rutkowski, S. Childhood Medulloblastoma. *Crit. Rev. Oncol. Hematol.* **2016**, *105*, 35–51. [CrossRef]
29. Ostrom, Q.T.; Gittleman, H.; Truitt, G.; Boscia, A.; Kruchko, C.; Barnholtz-Sloan, J.S. CBTRUS Statistical Report: Primary Brain and Other Central Nervous System Tumors Diagnosed in the United States in 2011–2015. *Neuro. Oncol.* **2018**, *20*, iv1–iv86. [CrossRef]
30. Ostrom, Q.T.; Cote, D.J.; Ascha, M.; Kruchko, C.; Barnholtz-Sloan, J.S. Adult Glioma Incidence and Survival by Race or Ethnicity in the United States from 2000 to 2014. *JAMA Oncol.* **2018**, *4*, 1254–1262. [CrossRef]
31. Lacroix, M.; Abi-Said, D.; Fourney, D.R.; Gokaslan, Z.L.; Shi, W.; DeMonte, F.; Lang, F.F.; McCutcheon, I.E.; Hassenbusch, S.J.; Holland, E.; et al. A Multivariate Analysis of 416 Patients with Glioblastoma Multiforme: Prognosis, Extent of Resection, and Survival. *J. Neurosurg.* **2001**, *95*, 190–198. [CrossRef] [PubMed]
32. Lamborn, K.R.; Chang, S.M.; Prados, M.D. Prognostic Factors for Survival of Patients with Glioblastoma: Recursive Partitioning Analysis. *Neuro. Oncol.* **2004**, *6*, 227–235. [CrossRef] [PubMed]
33. Vinchon, M.; Leblond, P. Medulloblastoma: Clinical Presentation. *Neurochirurgie* **2021**, *67*, 23–27. [CrossRef] [PubMed]
34. Zapotocky, M.; Mata-Mbemba, D.; Sumerauer, D.; Liby, P.; Lassaletta, A.; Zamecnik, J.; Krskova, L.; Kyncl, M.; Stary, J.; Laughlin, S.; et al. Differential Patterns of Metastatic Dissemination across Medulloblastoma Subgroups. *J. Neurosurg. Pediatr.* **2018**, *21*, 145–152. [CrossRef]
35. Packer, R.J.; Sutton, L.N.; D’Angio, G.; Evans, A.E.; Schut, L. Management of Children with Primitive Neuroectodermal Tumors of the Posterior Fossa/Medulloblastoma. *Pediatr. Neurosci.* **1986**, *12*, 272–282. [CrossRef]
36. Packer, R.J.; Sutton, L.N.; Elterman, R.; Lange, B.; Goldwein, J.; Nicholson, H.S.; Mulne, L.; Boyett, J.; D’Angio, G.; Wechsler-Jentsch, K. Outcome for Children with Medulloblastoma Treated with Radiation and Cisplatin, CCNU, and Vincristine Chemotherapy. *J. Neurosurg.* **1994**, *81*, 690–698. [CrossRef]
37. Udaka, Y.T.; Packer, R.J. Pediatric Brain Tumors. *Neurol. Clin.* **2018**, *36*, 533–556. [CrossRef]
38. Sun, Y.; Ma, G.; Xiang, H.; Wang, X.; Wang, H.; Zhang, Y.; Qie, F.; Li, C. CircFLNA Promotes Glioblastoma Proliferation and Invasion by Negatively Regulating MiR-199-3p Expression. *Mol. Med. Rep.* **2021**, *24*, 786. [CrossRef]
39. Cocquerelle, C.; Mascrez, B.; Héтуin, D.; Bailleul, B. Mis-Splicing Yields Circular RNA. *FASEB J.* **1993**, *7*, 155–160. [CrossRef]
40. Nigro, J.M.; Cho, K.R.; Fearon, E.R.; Kern, S.E.; Ruppert, J.M.; Oliner, J.D.; Kinzler, K.W.; Vogelstein, B. Scrambled Exons. *Cell* **1991**, *64*, 607–613. [CrossRef]
41. Zaphiropoulos, P.G. Circular RNAs from Transcripts of the Rat Cytochrome P450 2C24 Gene: Correlation with Exon Skipping Gene:Correlation with Exon Skipping. *Proc. Natl. Acad. Sci. USA* **1996**, *93*, 6536–6541. [CrossRef] [PubMed]
42. Ahmadov, U.; Bendikas, M.M.; Ebbesen, K.K.; Sehested, A.M.; Kjems, J.; Broholm, H.; Kristensen, L.S. Distinct Circular RNA Expression Profiles in Pediatric Ependymomas. *Brain Pathol.* **2021**, *31*, 387–392. [CrossRef] [PubMed]
43. Zhang, X.O.; Wang, H.B.; Zhang, Y.; Lu, X.; Chen, L.L.; Yang, L. Complementary Sequence-Mediated Exon Circularization. *Cell* **2014**, *159*, 134–147. [CrossRef] [PubMed]
44. Okholm, T.L.H.; Nielsen, M.M.; Hamilton, M.P.; Christensen, L.L.; Vang, S.; Hedegaard, J.; Hansen, T.B.; Kjems, J.; Dyrskjot, L.; Pedersen, J.S. Circular RNA Expression Is Abundant and Correlated to Aggressiveness in Early-Stage Bladder Cancer. *NPJ Genom. Med.* **2017**, *2*, 36. [CrossRef]
45. Rybak-Wolf, A.; Stottmeister, C.; Glažar, P.; Jens, M.; Pino, N.; Giusti, S.; Hanan, M.; Behm, M.; Bartok, O.; Ashwal-Fluss, R.; et al. Circular RNAs in the Mammalian Brain Are Highly Abundant, Conserved, and Dynamically Expressed. *Mol. Cell* **2015**, *58*, 870–885. [CrossRef]
46. Piwecka, M.; Glažar, P.; Hernandez-Miranda, L.R.; Memczak, S.; Wolf, S.A.; Rybak-Wolf, A.; Filipchyk, A.; Klironomos, F.; Jara, C.A.C.; Fenske, P.; et al. Loss of a Mammalian Circular RNA Locus Causes MiRNA Dereglulation and Affects Brain Function. *Science* **2017**, *357*, eaam8526. [CrossRef]
47. Salzman, J.; Gawad, C.; Wang, P.L.; Lacayo, N.; Brown, P.O. Circular RNAs Are the Predominant Transcript Isoform from Hundreds of Human Genes in Diverse Cell Types. *PLoS ONE* **2012**, *7*, e30733. [CrossRef]
48. Memczak, S.; Jens, M.; Elefsinioti, A.; Torti, F.; Krueger, J.; Rybak, A.; Maier, L.; Mackowiak, S.D.; Gregersen, L.H.; Munschauer, M.; et al. Circular RNAs Are a Large Class of Animal RNAs with Regulatory Potency. *Nature* **2013**, *495*, 333–338. [CrossRef]
49. Rossi, A.; Caracciolo, V.; Russo, G.; Reiss, K.; Giordano, A. Medulloblastoma: From Molecular Pathology to Therapy. *Clin. Cancer Res. Off. J. Am. Assoc. Cancer Res.* **2008**, *14*, 971–976. [CrossRef]
50. Rutka, J.T.; Hoffman, H.J. Medulloblastoma: A Historical Perspective and Overview. *J. Neurooncol.* **1996**, *29*, 1–7. [CrossRef]



51. Pollack, I.F.; Jakacki, R.I. Childhood Brain Tumors: Epidemiology, Current Management and Future Directions. *Nat. Rev. Neurol.* **2011**, *7*, 495–506. [CrossRef] [PubMed]
52. Packer, R.J.; Gajjar, A.; Vezina, G.; Rorke-Adams, L.; Burger, P.C.; Robertson, P.L.; Bayer, L.; LaFond, D.; Donahue, B.R.; Marymont, M.H.; et al. Phase III Study of Craniospinal Radiation Therapy Followed by Adjuvant Chemotherapy for Newly Diagnosed Average-Risk Medulloblastoma. *J. Clin. Oncol. Off. J. Am. Soc. Clin. Oncol.* **2006**, *24*, 4202–4208. [CrossRef] [PubMed]
53. Strother, D.; Lafay-Cousin, L. Adjuvant Therapy for High-Risk Medulloblastoma: More Is Better? *Neuro. Oncol.* **2021**, *23*, 1048–1049. [CrossRef] [PubMed]
54. Gajjar, A.; Chintagumpala, M.; Ashley, D.; Kellie, S.; Kun, L.E.; Merchant, T.E.; Woo, S.; Wheeler, G.; Ahern, V.; Krasin, M.J.; et al. Risk-Adapted Craniospinal Radiotherapy Followed by High-Dose Chemotherapy and Stem-Cell Rescue in Children with Newly Diagnosed Medulloblastoma (St Jude Medulloblastoma-96): Long-Term Results from a Prospective, Multicentre Trial. *Lancet Oncol.* **2006**, *7*, 813–820. [CrossRef]
55. Ray, S.; Chaturvedi, N.K.; Bhakat, K.K.; Rizzino, A.; Mahapatra, S. Subgroup-Specific Diagnostic, Prognostic, and Predictive Markers Influencing Pediatric Medulloblastoma Treatment. *Diagnostics* **2022**, *12*, 61. [CrossRef]
56. Thakkar, J.P.; Dolecek, T.A.; Horbinski, C.; Ostrom, Q.T.; Lightner, D.D.; Barnholtz-Sloan, J.S.; Villano, J.L. Epidemiologic and Molecular Prognostic Review of Glioblastoma. *Cancer Epidemiol. Biomark. Prev.* **2014**, *23*, 1985–1996. [CrossRef]
57. Tielking, K.; Fischer, S.; Preissner, K.T.; Vajkoczy, P.; Xu, R. Extracellular RNA in Central Nervous System Pathologies. *Front. Mol. Neurosci.* **2019**, *12*, 254. [CrossRef]
58. Fareh, M.; Turchi, L.; Virolle, V.; Debruyne, D.; Almairac, F.; De-La-Forest, D.S.; Paquis, P.; Preynat-Seauve, O.; Krause, K.-H.; Chneiweiss, H.; et al. The MiR 302-367 Cluster Drastically Affects Self-Renewal and Infiltration Properties of Glioma-Initiating Cells through CXCR4 Repression and Consequent Disruption of the SHH-GLI-NANOG Network. *Cell Death Differ.* **2012**, *19*, 232–244. [CrossRef] [PubMed]
59. Glaser, T.; Han, I.; Wu, L.; Zeng, X. Targeted Nanotechnology in Glioblastoma Multiforme. *Front. Pharmacol.* **2017**, *8*, 166. [CrossRef]
60. Id, K.C.; Chen, P.; Ho, K.; Shih, C. IGF-1-Enhanced MiR-513a-5p Signaling Desensitizes Glioma Cells to Temozolomide by Targeting the NEDD4L-Inhibited Wnt/ β -Catenin Pathway. *PLoS ONE* **2019**, *14*, e0225913. [CrossRef]
61. Skarkova, V.; Krupova, M.; Vitovcova, B.; Skarka, A.; Kasparova, P.; Krupa, P.; Kralova, V.; Rudolf, E. The Evaluation of Glioblastoma Cell Dissociation and Its Influence on Its Behavior. *Int. J. Mol. Sci.* **2019**, *20*, 4630. [CrossRef] [PubMed]
62. Luo, H.; Xu, R.; Chen, B.; Dong, S.; Zhou, F.; Yu, T.; Xu, G.; Zhang, J.; Wang, Y.; You, Y. MicroRNA-940 Inhibits Glioma Cells Proliferation and Cell Cycle Progression by Targeting CKS1. *Am. J. Transl. Res.* **2019**, *11*, 4851–4865. [PubMed]
63. Swalih, A.P.; Javier, S. Glioblastoma and MiRNAs. *Cancers* **2021**, *13*, 1581. [CrossRef]
64. Zhang, X.; Zhong, B.; Zhang, W.; Wu, J. Circular RNA CircMTO1 Inhibits Proliferation of Glioblastoma Cells via MiR-92/WWOX Signaling Pathway. *Med. Sci. Monit.* **2019**, *25*, 6454–6461. [CrossRef]
65. Zhou, J.; Wang, H.; Chu, J.; Huang, Q.; Li, G.; Yan, Y.; Xu, T.; Chen, J.; Wang, Y. Circular RNA Hsa_circ_0008344 Regulates Glioblastoma Cell Proliferation, Migration, Invasion, and Apoptosis. *J. Clin. Lab. Anal.* **2018**, *32*, e22454. [CrossRef]
66. Qian, L.; Guan, J.; Wu, Y.; Wang, Q. Upregulated Circular RNA Circ_0074027 Promotes Glioblastoma Cell Growth and Invasion by Regulating MiR-518a-5p/IL17RD Signaling Pathway. *Biochem. Biophys. Res. Commun.* **2019**, *510*, 515–519. [CrossRef]
67. Li, G.; Yang, H.; Han, K.; Zhu, D.; Lun, P.; Zhao, Y. A Novel Circular RNA, Hsa_circ_0046701, Promotes Carcinogenesis by Increasing the Expression of MiR-142-3p Target ITGB8 in Glioma. *Biochem. Biophys. Res. Commun.* **2018**, *498*, 254–261. [CrossRef]
68. Wang, T.; Mao, P.; Feng, Y.; Cui, B.; Zhang, B.; Chen, C.; Xu, M.; Gao, K. Blocking Hsa_circ_0006168 Suppresses Cell Proliferation and Motility of Human Glioblastoma Cells by Regulating Hsa_circ_0006168/MiR-628-5p/IGF1R CeRNA Axis. *Cell Cycle* **2021**, *20*, 1181–1194. [CrossRef]
69. Zhou, J.; Wang, H.; Hong, F.; Hu, S.; Su, X.; Chen, J.; Chu, J. CircularRNA CircPARP4 Promotes Glioblastoma Progression through Sponging MiR-125a-5p and Regulating FUT4. *Am. J. Cancer Res.* **2021**, *11*, 138–156.
70. Xie, G. Circular RNA Hsa-Circ-0012129 Promotes Cell Proliferation and Invasion in 30 Cases of Human Glioma and Human Glioma Cell Lines U373, A172, and SHG44, by Targeting MicroRNA-661 (MiR-661). *Med. Sci. Monit.* **2018**, *24*, 2497–2507. [CrossRef]
71. Liu, R.; Dai, W.; Wu, A.; Li, Y. CircCDC45 Promotes the Malignant Progression of Glioblastoma by Modulating the MiR-485-5p/CSF-1 Axis. *BMC Cancer* **2021**, *21*, 1090. [CrossRef] [PubMed]
72. Zhang, G.; Sun, W.; Zhu, L.; Feng, Y.; Wu, L.; Li, T. Overexpressed Circ_0029426 in Glioblastoma Forecasts Unfavorable Prognosis and Promotes Cell Progression by Sponging MiR-197. *J. Cell. Biochem.* **2019**, *120*, 10295–10302. [CrossRef]
73. Zhu, F.; Cheng, C.; Qin, H.; Wang, H.; Yu, H. A Novel Circular RNA CircENTPD7 Contributes to Glioblastoma Progression by Targeting ROS1. *Cancer Cell Int.* **2020**, *20*, 118. [CrossRef]
74. Lei, B.; Huang, Y.; Zhou, Z.; Zhao, Y.; Thapa, A.J.; Li, W.; Cai, W.; Deng, Y. Circular RNA Hsa_circ_0076248 Promotes Oncogenesis of Glioma by Sponging MiR-181a to Modulate SIRT1 Expression. *J. Cell. Biochem.* **2019**, *120*, 6698–6708. [CrossRef] [PubMed]
75. Chen, B.; Wang, M.; Huang, R.; Liao, K.; Wang, T.; Yang, R.; Zhang, W.; Shi, Z.; Ren, L.; Lv, Q.; et al. Circular RNA CircLGMN Facilitates Glioblastoma Progression by Targeting MiR-127-3p/LGMN Axis. *Cancer Lett.* **2021**, *522*, 225–237. [CrossRef] [PubMed]
76. Zhang, S.; Liao, K.; Miao, Z.; Wang, Q.; Miao, Y.; Guo, Z.; Qiu, Y.; Chen, B.; Ren, L.; Wei, Z.; et al. CircFOXO3 Promotes Glioblastoma Progression by Acting as a Competing Endogenous RNA for NFAT5. *Neuro. Oncol.* **2019**, *21*, 1284–1296. [CrossRef] [PubMed]

77. Zhou, M.; Li, H.; Chen, K.; Ding, W.; Yang, C.; Wang, X. Circska3 Downregulates Mir-1 through Methylation in Glioblastoma to Promote Cancer Cell Proliferation. *Cancer Manag. Res.* **2021**, *13*, 509–514. [CrossRef]
78. Chen, W.L.; Jiang, L.; Wang, J.S.; Liao, C.X. Circ-0001801 Contributes to Cell Proliferation, Migration, Invasion and Epithelial to Mesenchymal Transition (EMT) in Glioblastoma by Regulating MiR-628-5p/HMGB3 Axis. *Eur. Rev. Med. Pharmacol. Sci.* **2019**, *23*, 10874–10885. [CrossRef]
79. Fan, X.; Liu, M.; Fei, L.; Huang, Z.; Yan, Y. CircFOXO1 Promotes the Proliferation, Migration, Invasion, and Glutaminolysis of Glioblastoma by Regulating the MiR-577/E2F5 Axis. *Bosn. J. Basic Med. Sci.* **2021**, *8601*, 205. [CrossRef]
80. Liu, L.; Jia, L.; Shao, J.; Liu, H.; Wu, Q.; Wu, X. Circular RNA CircNF1 SiRNA Silencing Inhibits Glioblastoma Cell Proliferation by Promoting the Maturation of MiR-340. *Front. Neurol.* **2021**, *12*, 658076. [CrossRef]
81. Zhou, F.; Wang, B.; Wang, H.; Hu, L.; Zhang, J.; Yu, T.; Xu, X.; Tian, W.; Zhao, C.; Zhu, H.; et al. CircMELK Promotes Glioblastoma Multiforme Cell Tumorigenesis through the MiR-593/EphB2 Axis. *Mol. Ther. Nucleic Acids* **2021**, *25*, 25–36. [CrossRef] [PubMed]
82. Lu, J.; Lou, G.; Jiang, L.; Liu, X.; Jiang, J.; Wang, X. CircNUP98 Suppresses the Maturation of MiR-519a-3p in Glioblastoma. *Front. Neurol.* **2021**, *12*, 2039. [CrossRef] [PubMed]
83. Lv, X.; Wang, M.; Qiang, J.; Guo, S. Circular RNA Circ-PITX1 Promotes the Progression of Glioblastoma by Acting as a Competing Endogenous RNA to Regulate MiR-379-5p/MAP3K2 Axis. *Eur. J. Pharmacol.* **2019**, *863*, 172643. [CrossRef] [PubMed]
84. Cao, Y.; Wang, F.; Chen, Y.; Wang, Y.; Song, H.; Long, J. CircPITX1 Regulates Proliferation, Angiogenesis, Migration, Invasion, and Cell Cycle of Human Glioblastoma Cells by Targeting MiR-584-5p/KPNB1 Axis. *J. Mol. Neurosci.* **2021**, *71*, 1683–1695. [CrossRef]
85. Wei, Y.; Lu, C.; Zhou, P.; Zhao, L.; Lyu, X.; Yin, J.; Shi, Z.M.; You, Y. EIF4A3-Induced Circular RNA ASAP1 Promotes Tumorigenesis and Temozolomide Resistance of Glioblastoma via NRAS/MEK1/ERK1-2 Signaling. *Neuro. Oncol.* **2021**, *23*, 611–624. [CrossRef]
86. He, J.; Huang, Z.; He, M.; Liao, J.; Zhang, Q.; Wang, S.; Xie, L.; Ouyang, L.; Koeffler, H.P.; Yin, D.; et al. Circular RNA MAPK4 (Circ-MAPK4) Inhibits Cell Apoptosis via MAPK Signaling Pathway by Sponging MiR-125a-3p in Gliomas. *Mol. Cancer* **2020**, *19*, 17. [CrossRef]
87. Zheng, J.; Liu, X.; Xue, Y.; Gong, W.; Ma, J.; Xi, Z.; Que, Z.; Liu, Y. TTBK2 Circular RNA Promotes Glioma Malignancy by Regulating MiR-217/HNF1 β /Derlin-1 Pathway. *J. Hematol. Oncol.* **2017**, *10*, 52. [CrossRef]
88. Mutalifu, N.; Du, P.; Zhang, J.; Akbar, H.; Yan, B.; Alimu, S.; Tong, L.; Luan, X. Circ_0000215 Increases the Expression of CXCR2 and Promoted the Progression of Glioma Cells by Sponging MiR-495-3p. *Technol. Cancer Res. Treat.* **2020**, *19*, 1533033820957026. [CrossRef]
89. Qiao, J.; Liu, M.; Tian, Q.; Liu, X. Microarray Analysis of CircRNAs Expression Profile in Gliomas Reveals That Circ_0037655 Could Promote Glioma Progression by Regulating MiR-214/PI3K Signaling. *Life Sci.* **2020**, *245*, 117363. [CrossRef]
90. Zheng, K.; Xie, H.; Wu, W.; Wen, X.; Zeng, Z.; Shi, Y. CircRNA PIP5K1A Promotes the Progression of Glioma through Upregulation of the TCF12/PI3K/AKT Pathway by Sponging MiR-515-5p. *Cancer Cell Int.* **2021**, *21*, 27. [CrossRef]
91. He, Q.; Zhao, L.; Liu, Y.; Liu, X.; Zheng, J.; Yu, H.; Cai, H.; Ma, J.; Liu, L.; Wang, P.; et al. Circ-SHKBP1 Regulates the Angiogenesis of U87 Glioma-Exposed Endothelial Cells through MiR-544a/FOXP1 and MiR-379/FOXP2 Pathways. *Mol. Ther. Nucleic Acids* **2018**, *10*, 331–348. [CrossRef] [PubMed]
92. Xin, J.; Zhang, X.Y.; Sun, D.K.; Tian, L.Q.; Xu, P. Up-Regulated Circular RNA Hsa_circ_0067934 Contributes to Glioblastoma Progression through Activating PI3K-AKT Pathway. *Eur. Rev. Med. Pharmacol. Sci.* **2019**, *23*, 3447–3454. [CrossRef] [PubMed]
93. Jin, P.; Huang, Y.; Zhu, P.; Zou, Y.; Shao, T.; Wang, O. CircRNA CircHIPK3 Serves as a Prognostic Marker to Promote Glioma Progression by Regulating MiR-654/IGF2BP3 Signaling. *Biochem. Biophys. Res. Commun.* **2018**, *503*, 1570–1574. [CrossRef] [PubMed]
94. Bian, A.; Wang, Y.; Liu, J.; Wang, X.; Liu, D.; Jiang, J.; Ding, L.; Hui, X. Circular RNA Complement Factor H (CFH) Promotes Glioma Progression by Sponging MIR-149 and Regulating AKT1. *Med. Sci. Monit.* **2018**, *24*, 5704–5712. [CrossRef]
95. Zhang, H.; Xu, W. CircABCC3 Knockdown Inhibits Glioblastoma Cell Malignancy by Regulating MiR-770-5p/SOX2 Axis through PI3K/AKT Signaling Pathway. *Brain Res.* **2021**, *1764*, 147465. [CrossRef]
96. Wang, R.; Zhang, S.; Chen, X.; Li, N.; Li, J.; Jia, R.; Pan, Y.; Liang, H. CircNT5E Acts as a Sponge of MiR-422a to Promote Glioblastoma Tumorigenesis. *Cancer Res.* **2018**, *78*, 4812–4825. [CrossRef]
97. Xu, H.; Zhang, Y.; Qi, L.; Ding, L.; Jiang, H.; Yu, H. NFIX Circular RNA Promotes Glioma Progression by Regulating MiR-34a-5p via Notch Signaling Pathway. *Front. Mol. Neurosci.* **2018**, *11*, 225. [CrossRef]
98. Wang, B.; Li, B.; Si, T. Knockdown of Circ0082374 Inhibits Cell Viability, Migration, Invasion and Glycolysis in Glioma Cells by MiR-326/SIRT1. *Brain Res.* **2020**, *1748*, 147108. [CrossRef]
99. Lu, Y.; Deng, X.; Xiao, G.; Zheng, X.; Ma, L.; Huang, W. Circ0001730 Promotes Proliferation and Invasion via the MIR-326/Wnt7B Axis in Glioma Cells. *Epigenomics* **2019**, *11*, 1335–1352. [CrossRef]
100. Wu, Z.; Zheng, M.; Zhang, Y.; Xie, M.; Tian, S.; Ding, T.; Li, L.; Guan, Q. Hsa_circ_0043278 Functions as Competitive Endogenous RNA to Enhance Glioblastoma Multiforme Progression by Sponging MiR-638. *Aging* **2020**, *12*, 21114–21128. [CrossRef]
101. Chen, Z.; Duan, X. Hsa-Circ-0000177-MiR-638-FZD7-Wnt Signaling Cascade Contributes to the Malignant Behaviors in Glioma. *DNA Cell Biol.* **2018**, *37*, 791–797. [CrossRef] [PubMed]
102. Wang, R.; Zhang, S.; Chen, X.; Li, N.; Li, J.; Jia, R.; Pan, Y.; Liang, H. Correction to: EIF4A3-Induced Circular RNA MMP9 (CircMMP9) Acts as a Sponge of MiR-124 and Promotes Glioblastoma Multiforme Cell Tumorigenesis. *Mol. Cancer* **2018**, *17*, 166. [CrossRef] [PubMed]

103. Yang, P.; Qiu, Z.; Jiang, Y.; Dong, L.; Yang, W.; Gu, C.; Li, G.; Zhu, Y. Silencing of CZN292 Circular RNA Suppresses Human Glioma Tube Formation via the Wnt/ β -Catenin Signaling Pathway. *Oncotarget* **2016**, *7*, 63449–63455. [CrossRef] [PubMed]
104. Wei, B.; Wang, L.; Zhao, J. Circular RNA Hsa_circ_0005114-MiR-142-3p/MiR-590-5p-Adenomatous Polyposis Coli Protein Axis as a Potential Target for Treatment of Glioma. *Oncol. Lett.* **2021**, *21*, 58. [CrossRef]
105. Li, T.; Xu, J.; Liu, Y. A Novel Circular RNA CircRFX3 Serves as a Sponge for MicroRNA-587 in Promoting Glioblastoma Progression via Regulating PDIA3. *Front. Cell Dev. Biol.* **2021**, *9*, 3167. [CrossRef]
106. Liu, X.; Shen, S.; Zhu, L.; Su, R.; Zheng, J.; Ruan, X.; Shao, L.; Wang, D.; Yang, C.; Liu, Y. SRSF10 Inhibits Biogenesis of Circ-ATXN1 to Regulate Glioma Angiogenesis via MiR-526b-3p/MMP2 Pathway. *J. Exp. Clin. Cancer Res.* **2020**, *39*, 121. [CrossRef]
107. Jiang, Y.; Zhou, J.; Zhao, J.; Zhang, H.; Li, L.; Li, H.; Chen, L.; Hu, J.; Zheng, W.; Jing, Z. The U2AF2/CircRNA ARF1/MiR-342-3p/ISL2 Feedback Loop Regulates Angiogenesis in Glioma Stem Cells. *J. Exp. Clin. Cancer Res.* **2020**, *39*, 182. [CrossRef]
108. Yang, J.; Tian, S.; Wang, B.; Wang, J.; Cao, L.; Wang, Q.; Xie, W.; Liang, Z.; Zhao, H.; Zhao, Y.; et al. CircPIK3C2A Facilitates the Progression of Glioblastoma via Targeting MiR-877-5p/FOXO1 Axis. *Front. Oncol.* **2021**, *11*, 801776. [CrossRef]
109. Zhang, M.; Huang, N.; Yang, X.; Luo, J.; Yan, S.; Xiao, F.; Chen, W.; Gao, X.; Zhao, K.; Zhou, H.; et al. A Novel Protein Encoded by the Circular Form of the SHPRH Gene Suppresses Glioma Tumorigenesis. *Oncogene* **2018**, *37*, 1805–1814. [CrossRef]
110. Yang, Y.; Gao, X.; Zhang, M.; Yan, S.; Sun, C.; Xiao, F.; Huang, N.; Yang, X.; Zhao, K.; Zhou, H.; et al. Novel Role of FBXW7 Circular RNA in Repressing Glioma Tumorigenesis. *J. Natl. Cancer Inst.* **2018**, *110*, 304–315. [CrossRef]
111. Lou, J.; Hao, Y.; Lin, K.; Lyu, Y.; Chen, M.; Wang, H.; Zou, D.; Jiang, X.; Wang, R.; Jin, D.; et al. Circular RNA CDR1as Disrupts the P53/MDM2 Complex to Inhibit Gliomagenesis. *Mol. Cancer* **2020**, *19*, 138. [CrossRef] [PubMed]
112. Lv, T.; Miao, Y.; Xu, T.; Sun, W.; Sang, Y.; Jia, F.; Zhang, X. Circ-EPB41L5 Regulates the Host Gene EPB41L5 via Sponging MiR-19a to Repress Glioblastoma Tumorigenesis. *Aging* **2020**, *12*, 318–339. [CrossRef] [PubMed]
113. Xia, X.; Li, X.; Li, F.; Wu, X.; Zhang, M.; Zhou, H.; Huang, N.; Yang, X.; Xiao, F.; Liu, D.; et al. A Novel Tumor Suppressor Protein Encoded by Circular AKT3 RNA Inhibits Glioblastoma Tumorigenicity by Competing with Active Phosphoinositide-Dependent Kinase-1. *Mol. Cancer* **2019**, *18*, 131. [CrossRef] [PubMed]
114. Li, F.; Ma, K.; Sun, M.; Shi, S. Identification of the Tumor-Suppressive Function of Circular RNA ITCH in Glioma Cells through Sponging MiR-214 and Promoting Linear ITCH Expression. *Am. J. Transl. Res.* **2018**, *10*, 1373–1386; Erratum in *Am. J. Transl. Res.* **2021**, *13*, 14239.
115. Barbagallo, D.; Caponnetto, A.; Brex, D.; Mirabella, F.; Barbagallo, C.; Lauretta, G.; Morrone, A.; Certo, F.; Broggi, G.; Caltabiano, R.; et al. CircSMARCA5 Regulates VEGFA mRNA Splicing and Angiogenesis in Glioblastoma Multiforme through the Binding of SRSF1. *Cancers* **2019**, *11*, 194. [CrossRef]
116. Barbagallo, D.; Caponnetto, A.; Ciriigliaro, M.; Brex, D.; Barbagallo, C.; D'Angeli, F.; Morrone, A.; Caltabiano, R.; Barbagallo, G.M.; Ragusa, M.; et al. CircSMARCA5 Inhibits Migration of Glioblastoma Multiforme Cells by Regulating a Molecular Axis Involving Splicing Factors SRSF1/SRSF3/PTB. *Int. J. Mol. Sci.* **2018**, *19*, 480. [CrossRef] [PubMed]
117. Li, X.; Diao, H. Circular RNA Circ_0001946 Acts as a Competing Endogenous RNA to Inhibit Glioblastoma Progression by Modulating MiR-671-5p and CDR1. *J. Cell. Physiol.* **2019**, *234*, 13807–13819. [CrossRef]
118. Feng, J.; Ren, X.; Fu, H.; Li, D.; Chen, X.; Zu, X.; Liu, Q.; Wu, M. LRRC4 Mediates the Formation of Circular RNA CD44 to Inhibit GBM Cell Proliferation. *Mol. Ther. Nucleic Acids* **2021**, *26*, 473–487. [CrossRef]
119. Zhang, W.; Chen, S.; Du, Q.; Bian, P.; Chen, Y.; Liu, Z.; Zheng, J.; Sai, K.; Mou, Y.; Chen, Z.; et al. CircVPS13C Promotes Pituitary Adenoma Growth by Decreasing the Stability of IFITM1 mRNA via Interacting with RRBP1. *Oncogene* **2022**, *41*, 1550–1562. [CrossRef]
120. Cheng, J.; Nie, D.; Li, B.; Gui, S.B.; Li, C.Z.; Zhang, Y.Z.; Zhao, P. CircNFIX Promotes Progression of Pituitary Adenoma via CCNB1 by Sponging MiR-34a -5p. *Mol. Cell. Endocrinol.* **2021**, *525*, 111140. [CrossRef]
121. Du, Q.; Hu, B.; Feng, Y.; Wang, Z.; Wang, X.; Zhu, D.; Zhu, Y.; Jiang, X.; Wang, H. Circoma1-Mediated MiR-145-5p Suppresses Tumor Growth of Nonfunctioning Pituitary Adenomas by Targeting TPT1. *J. Clin. Endocrinol. Metab.* **2019**, *104*, 2419–2434. [CrossRef] [PubMed]

Article

XRN2 Is Required for Cell Motility and Invasion in Glioblastomas

Tuyen T. Dang ¹, Megan Lerner ², Debra Saunders ³, Nataliya Smith ³, Rafal Gulej ³, Michelle Zalles ³, Rheal A. Towner ³ and Julio C. Morales ^{1,*}

¹ Department of Neurosurgery, Sttephenson Cancer Center University of Oklahoma Health Science Center, Oklahoma City, OK 73104, USA; tuyen-dang@ouhsc.edu

² Department of Surgery, University of Oklahoma Health Science Center, Oklahoma City, OK 73104, USA; megan-lerner@ouhsc.edu

³ Department of Pathology, University of Oklahoma Health Science Center, Advanced Magnetic Resonance Center, Oklahoma Medical Research Foundation, Oklahoma City, OK 73104, USA; debra-saunders@omrf.org (D.S.); nataliya-smith@ouhsc.edu (N.S.); rafal-gulej@ouhsc.edu (R.G.); mzalles@mdanderson.org (M.Z.); rheal-towner@omrf.org (R.A.T.)

* Correspondence: julio-morales@ouhsc.edu

Abstract: One of the major obstacles in treating brain cancers, particularly glioblastoma multiforme, is the occurrence of secondary tumor lesions that arise in areas of the brain and are inoperable while obtaining resistance to current therapeutic agents. Thus, gaining a better understanding of the cellular factors that regulate glioblastoma multiforme cellular movement is imperative. In our study, we demonstrate that the 5'-3' exoribonuclease XRN2 is important to the invasive nature of glioblastoma. A loss of XRN2 decreases cellular speed, displacement, and movement through a matrix of established glioblastoma multiforme cell lines. Additionally, a loss of XRN2 abolishes tumor formation in orthotopic mouse xenograft implanted with G55 glioblastoma multiforme cells. One reason for these observations is that loss of XRN2 disrupts the expression profile of several cellular factors that are important for tumor invasion in glioblastoma multiforme cells. Importantly, XRN2 mRNA and protein levels are elevated in glioblastoma multiforme patient samples. Elevation in XRN2 mRNA also correlates with poor overall patient survival. These data demonstrate that XRN2 is an important cellular factor regulating one of the major obstacles in treating glioblastomas and is a potential molecular target that can greatly enhance patient survival.

Keywords: XRN2; cell motility; invasion; tumor progression



Citation: Dang, T.T.; Lerner, M.; Saunders, D.; Smith, N.; Gulej, R.; Zalles, M.; Towner, R.A.; Morales, J.C. XRN2 Is Required for Cell Motility and Invasion in Glioblastomas. *Cells* **2022**, *11*, 1481. <https://doi.org/10.3390/cells11091481>

Academic Editors: Javier S. Castresana and Bárbara Meléndez

Received: 21 February 2022

Accepted: 26 April 2022

Published: 28 April 2022

Publisher's Note: MDPI stays neutral with regard to jurisdictional claims in published maps and institutional affiliations.



Copyright: © 2022 by the authors. Licensee MDPI, Basel, Switzerland. This article is an open access article distributed under the terms and conditions of the Creative Commons Attribution (CC BY) license (<https://creativecommons.org/licenses/by/4.0/>).

1. Introduction

Glioblastoma multiforme tumors (GBMs) are lethal brain tumors, as they are highly aggressive in both growth rate and invasiveness. The five-year survival rate for GBM patients is <5% [1], with a median survival rate of 16 months [2]. GBMs are primarily treated with tumor resection, followed by radio- and chemo-therapies [3]. One of the major obstacles in treating GBMs is their highly invasive nature, exhibiting itself in extensive tumor infiltration into the surrounding parenchyma [4]. This invasive nature of GBMs results in tumor recurrence, with limited surgical treatment options, and acquisition of radio- and chemo-resistance in nearly 100% of patients [5].

The first step in GBM progression is the movement of a few tumor cells away from the primary tumor (dissemination), followed by the colonization and formation of a tumor in a secondary site within the brain [6]. GBM dissemination into the surrounding brain regions is a complex multi-step process [7] that depends on two characteristics: (1) the inherent movement of tumor cells (cell motility) and (2) the ability of tumor cells to migrate through a matrix (cell invasion). Thus, gaining a better understanding of the means driving cell motility and invasion is important for understanding the mechanisms behind GBM

secondary site formation. Our current study demonstrates that XRN2 is a regulator of GBM aggressiveness.

XRN2 is a 5'-3' exoribonuclease that participates in several cellular processes. Classically, XRN2, the human homolog of the yeast protein RAT1, plays a role in transcription termination [8]. Moreover, XRN2 participates in transcription elongation by mediating premature termination [9]. In addition to having a function in transcription, XRN2 is also required for maintaining genomic stability, double-strand break repair, and RNA:DNA hybrid (R-loop) resolution [10,11]. Furthermore, XRN2 may affect additional cellular processes indirectly through an extended role in gene regulation by mediating R-loop resolution [12] and miRNA formation [13]. In fact, it has been shown that XRN2 can mediate the epithelial–mesenchymal transition (EMT) in lung cancer by regulating the maturation of miR-10a [13].

In this study, we demonstrate a role for XRN2 in mediating cell motility and migration through a matrix in GBM cells. We found that a loss of XRN2 can lead to decreased speed and displacement of U87 and U251 GBM cells. Along with this, we found that loss of XRN2 impaired the ability of GBM cells to migrate through a solid matrix. Strikingly, a loss of XRN2 resulted in a ~90% reduction in tumor volume when G55 cells were injected into mouse brains. Lastly, we demonstrate that XRN2 alters the transcriptional profile of GBM cells, suggesting that XRN2 can mediate the expression of cellular factors for cell motility and invasion in GBMs similar to the observations in lung cancer [13].

2. Materials and Methods

2.1. G55 Xenograft Model and Treatment

All animal studies were conducted with the approval of the Oklahoma Medical Research Foundation and University of Oklahoma Health Sciences Center Institutional Animal Care Use Committee policies, which follow NIH guidelines. Human G55 xenograft cells (modified and unmodified) were injected intracerebrally in two-month-old male mice (Hsd: Athymic Nude-Foxn1nu mice; Harlan Inc., Indianapolis, IN, USA), as previously described [14]. All mice were euthanized when tumors reached ~150 mm³, or up to 27 days post-implantation of G55 cells.

2.2. Magnetic Resonance Imaging

Mice were anesthetized and positioned in a cradle that was inserted into a 30 cm horizontal bore Bruker Biospin magnet operating at 7 Tesla (Bruker BioSpin GmbH, Karlsruhe, Germany). All MRI experiments were carried out using the Bruker BA6 gradient set and mouse head coil, as previously described [14]. All animals were imaged every 3–4 days until the end of the study starting at 10 days post-G55 implantation surgery.

2.3. Patient Gene Expression

XRN2 mRNA expression in normal and glioblastoma patient samples and patient survivorship were generated using R2: Genomics Analysis and Visualization Platform using default program settings. The following databases were used: Berchtold [15], Pfister [16], Loeffler [17], Hegi [18], Kawaguchi [19], French [20], and Sun [21]. These data were accessed from 2018 to 2021. XRN2 mRNA expression across brain tumors was generated using OncoPrint with the Sun database [21] accessed in September 2016.

2.4. Cell Culture

Cells were maintained in a humidified 37 °C environment supplemented with 5% CO₂. Growth media for each of the cell lines were as follows: 10% fetal bovine serum (FBS) in DMEM for G55 cells, 10% FBS in MEM supplemented with 2 mM L-glutamine and 1 mM sodium pyruvate for U251 and U87 cells, and 5% FBS in DMEM for LN229. All growth media were supplemented with 1X penicillin–streptomycin.

2.5. H2B-GFP Labeling and shRNA Knockdown of Cells

Over-expression of histone 2B GFP fusion protein was achieved through transduction of cells with virus produced from transfection of pCLNR-H2BG (plasmid #17735, Addgene) in 293GP with respective virial packaging plasmids [22]. Shluciferase, shXRN2-3640, and shXRN2-3639 cells were generated through transduction with virus produced from transfection of the listed below plasmids from Sigma Aldrich into 293T with respective virial packaging plasmids [22].

2.6. VCL siRNA

VCL #1: GCAUUCAGGCCUCAGUGAA
 VCL #2: GCAUAGAGGAAGCUUUA
 VCL #3: CAAGAUGAUUGACGAGAGA

2.7. Shluciferase (sku #SHC007): Proprietary Sequence

shXRN2-3640 (TRCN0000293640): CCGGGTGTATTCTAGATCATCTAAGCTCGAGC
 TTAGATGATCTAGAATACTTTTTG
 shXRN2-3639 (TRCN0000293639): CCGGTACATAGCTGATCGTTTAAATCTCGA-
 GATTAAACGATCAGCTATGTATTTTTG

2.8. Western Blot

Cells were lysed in RIPA buffer supplemented with a protease inhibitor cocktail. Samples were denatured in Laemmli buffer, ran on a 10% SDS-PAGE gel, and transferred on a PVDF membrane. Membranes were probed with XRN2 antibody (cat no. A301-103A, Bethyl, Montgomery, TX, USA) and GAPDH (cat no. ab181602, Abcam, Boston, MA, USA). Alexa-488 or Alexa-680 secondary antibodies were used to visualize expression on the Chemidoc MP (BioRad, Herules, CA, USA).

2.9. siRNA Transfection/RT-PCR

Cells were reverse transfected with 50 nM of siRNAs (listed in ref) using MISSION siRNA transfection reagent (cat no. S1452-1ML, Sigma Aldrich, St. Louis, MO, USA). Then, 72 h after transfection, the total RNA was harvested using a miRNeasy Micro kit (cat no. 217084, Qiagen, Germantown, MD, USA) following manufacturer's protocol. Real-time PCR (RT-PCR) was used to verify knockdown. Briefly, 500 ng of total RNA was converted into cDNA using iScriptTM cDNA Synthesis Kit (cat no. 1708890, BioRad) following manufacturer's protocol. BioRad CFX 96 Real-Time System, iTaqTM Universal SYBR[®] Green Supermix (cat no. 1725125), and XRN2 and GAPDH primers (sequences listed below) were used for RT-PCR. Expression change was determined with GAPDH used as a loading control and fold change in ΔCt .

XRN2 forward primer: CAGCAACTGATTACACCAG
 XRN2 reverse primer: ACTGTCAATTTTTCCACCC
 GAPDH forward primer: CTTTTGCGTCGCCAG
 GAPDH reverse primer: TTGATGGCAATATCCAC

2.10. RNA-Seq

Total RNA was submitted to the core facility OUHSC Laboratory for Molecular Biology and Cytometry Research for library build, RNA sequencing, genome alignment, and quality analysis. RNAseq libraries were constructed using the Illumina TruSeq RNA LT v2 kit and established protocols. The library construction was carried out using total RNA isolated from human GBM cell lines (1 ug). RNA quality for each prep was analyzed prior to construction using the Agilent Bioanalyzer 2100 and nano total RNA chips. Each library was indexed during library construction in order to multiplex for sequencing on the Illumina MiSeq platform. Samples were normalized and sequenced in batches of 3 libraries per 2×150 bp for paired-end sequencing run on the Illumina MiSeq. On average, 44 million reads (7 Gb) of sequencing data were collected per run. Raw data for each sample were

analyzed using CLC Genomics Workbench version 10.0.1 software from Qiagen (formerly CLCBio). Raw sequence reads were mapped to the Homo sapiens genome to identify genes expressed under each condition. A pairwise comparison of the expression results were performed using the total mapping results which specified experimental groups. Differential gene lists were created with 1.3-fold expression cutoff and significant p values of ≤ 0.05 to identify genes that were up- or down-regulated under each condition.

2.11. Live Cell Imaging

Cells were reverse transfected for 48 to 72 h. Cells were fed with fresh 1% FBS growth media supplemented with 100 ng/mL epidermal growth factor before imaging. Imaging was conducted on the LSM710 (Zeiss) from the Oklahoma Research Medical Foundation Imaging core. The microscope was stored in a humidified, temperature- and CO₂-controlled chamber. Images were taken with a 10× objective taken at 30 min intervals for at least 6 h. TrackMate [23] was used to track the movement of cells overtime.

2.12. Inverted Vertical Invasion Assay (Up-Invasion)

Cells were either reverse-transfected with siRNAs or transduced with shRNAs, and were plated in a 96-well plate at a density where the wells were ~100% confluent by 48 h. A mixture of 50:50 collagen I–Matrigel were plated at a volume of 50 μ L per well on top of the monolayer. After the matrix had solidified (~1 h), 150 μ L of growth media was overlaid. Cells were allowed to invade for 48 h before fixation with 2% formaldehyde diluted in 1X PBS for 20–40 min. Wells were then washed and stored in 1X PBS. Cultures were imaged on the LSM710 confocal using a 10× objective. Z-stacks were obtained by imaging 50 micron below and 100 micron above the monolayer with 5 micron slices. Invading cells were cells that had invaded 50+ micron above the monolayer. The extent of invasion was normalized to control conditions [24].

2.13. Immunohistochemistry/H&E

Human patient samples were taken from a commercial tissue microarray (cat no. BS17017b, US Biomax, Rockville, MD, USA). Patient samples were stained with 1:2000 dilution of XRN2 antibody (A301-103A, Bethyl Laboratories, Montgomery, TX, USA). Briefly, samples were baked at 60 °C for 30 min follow by xylene and alcohol washes. Subsequently, pH 6 citrate antigen retrieval was carried out for 20 min, peroxidase block was carried out at room temperature for 10 min, blocking was carried out for 20 min with 2.5% horse serum, and incubation with primary antibodies was carried out for 60 min at room temperature. The Impress Excel-Amplified Polymer Stain Anti-Rabbit Peroxidase kit (MP7601, Vector Labs, San Francisco, CA, USA) and Nova Red, as the chromogen, were used to visualize XRN2 staining, as per manufacturer’s instructions. Tumors from xenografts were fixed in formalin and then embedded in paraffin. Afterwards, tumors were sliced 5 microns thick for hematoxylin and eosin staining (H&E). Briefly, samples were washed in xylene and alcohol washes; incubated in Harris hematoxylin, acidic alcohol, and water washes for 15 min; and subjected to eosin staining, followed by alcohol and xylene washes. Images were captured on the Cytation 5 imaging system (BioTek, Winooski, VT, USA).

2.14. XRN2 Immunohistochemistry Staining Quantification

To quantify XRN2 expression, stained tissue sections were scanned on the Aperio Scanscope CS System (Aperio Technologies, Inc., Vista, CA, USA) and analyzed using the Aperio ImageScope program specifically the Positive Pixel Count 2004-08-11 algorithm. Positive XRN2 pixel staining was determined by a medium to strong pixel intensity. Positivity was determined by the number of positive pixels divided by total pixels and then multiplied by 100. A value of 2 positivity was considered as positive XRN2 staining. Normal brain tissues had positivity values between 0.31 and 1.37.

3. Results

3.1. *XRN2 Display Elevated Expression in Gliomas*

In recent years, XRN2 has emerged as a regulator of cancer cell migration in lung cancer and oral carcinoma [13,25]. To determine if XRN2 may also contribute to the progression of GBMs, we examined the Pfister, Loeffler, and Hegi glioma gene expression datasets for XRN2 expression, using the R2: Genomic Analysis and Visualization Platform (<http://r2.amc.nl>, accessed 1 March 2019). We found that XRN2 mRNA levels were elevated in glioma samples as compared to normal brain samples (Berchtold) (Figure 1A). This mRNA elevation of XRN2 suggests that XRN2 may play a role in GBM disease and may also be a potential biomarker for the disease.

To determine if XRN2 has a functional role in GBMs, we examined XRN2 protein expression in patient samples. Using a glioma tissue microarray (product number GL803c) purchased from US Biomax, we examined XRN2 protein expression levels through immunohistochemistry (IHC). The microarray contained 30 GBM, 28 astrocytoma, 9 oligodendroglioma, 4 oligoastrocytoma, and 4 normal brain tissue samples. Consistent with the elevation of XRN2 mRNA, we found increased XRN2 protein expression in GBM patient samples as compared to normal brain tissues (Figure 1B and Supplemental Figure S1A). Using the Aperio ImageScope (Leica Biosystems), we quantified a XRN2 IHC 2% or greater positivity staining in 22 of the 30 GBM samples, while no normal brain sample displayed 2% positivity staining (Figure 1C). Interestingly, we found that XRN2 mRNA and protein levels were elevated in GBMs, as compared to astrocytoma and oligodendrogliomas (Supplemental Figure S1B,C). Lastly, using the Kawaguchi data, we found that increased XRN2 mRNA levels correlated with poor overall patient survival, as compared to patients with lower XRN2 expression (Figure 1D). The poor survivorship suggests that XRN2 may not only play a role in GBM tumors, but also in the progression of the disease.

3.2. *XRN2 Mediates GBM Cell Motility*

As XRN2 has been shown to mediate epithelial-derived tumor migration, we wanted to know if XRN2 may also drive the motility of non-epithelial cancers, such as GBMs. We examined how XRN2 loss affected the migration of glioma cells. To examine this, we employed U87 glioma cell lines modified to express histone 2B fused with green fluorescent protein (U87-GFP) (Figure 2A). We exposed U87-GFP cells to control and XRN2 siRNAs (Supplemental Figure S2A,B). Using live-cell imaging, we monitored single-cell movement in U87 cells with and without XRN2 (Figure 2A,B; Supplemental Movie S1). We found that loss of XRN2 resulted in a ~25% decrease in speed and displacement in U87 cells (Figure 2C), as compared to control cells. Yet, this decrease was not the same as the ~50% decrease found in cells exposed to cytochalasin D (cytoD) (Figure 2C). We found a similar ~25% decrease in speed and displacement in U251 GBM cells (Supplemental Figure S2C). Based on these results, XRN2 is required for the intrinsic motility of GBM cells.

3.3. *Loss of XRN2 Impairs GBM Invasiveness*

Even though cell motility is a required step in metastasis, it is not sufficient to induce invasion. Thus, to determine if XRN2 is required for invasion, we examined if XRN2 mediates glioma cell invasion through a matrix. We utilized the inverted vertical invasion assay to measure invasiveness through a matrix [26]. To perform this inverted vertical invasion assay, we plated previously described control and XRN2-deficient G55 GBM cell lines [10] in a 96-well plate. After 48 h, we layered a collagen I–Matrigel matrix over the cells. After the matrix was solidified, we overlaid media and allowed the cells to grow and invade for another 48 h (Figure 3A). We then fixed the cells and used the LSM710 confocal microscope for image invasion of control and XRN2-deficient G55 cells (Figure 3B). We found that the loss of XRN2 resulted in a ~50% decrease in the relative invasion of two different XRN2-deficient cell lines (shXRN2-3640 and shXRN2-3639), as compared to control (shluc) cells (Figure 3C). Relative invasion was determined by dividing the number of cells that traveled $\geq 50 \mu\text{m}$ above the monolayer in XRN2-deficient cell lines by the

number of cells that traveled > 50 μm above the monolayer in control samples [24]. The requirement of XRN2 in invasion was repeated when we used siRNAs to down-regulate XRN2 expression (Supplemental Figure S3A,B).

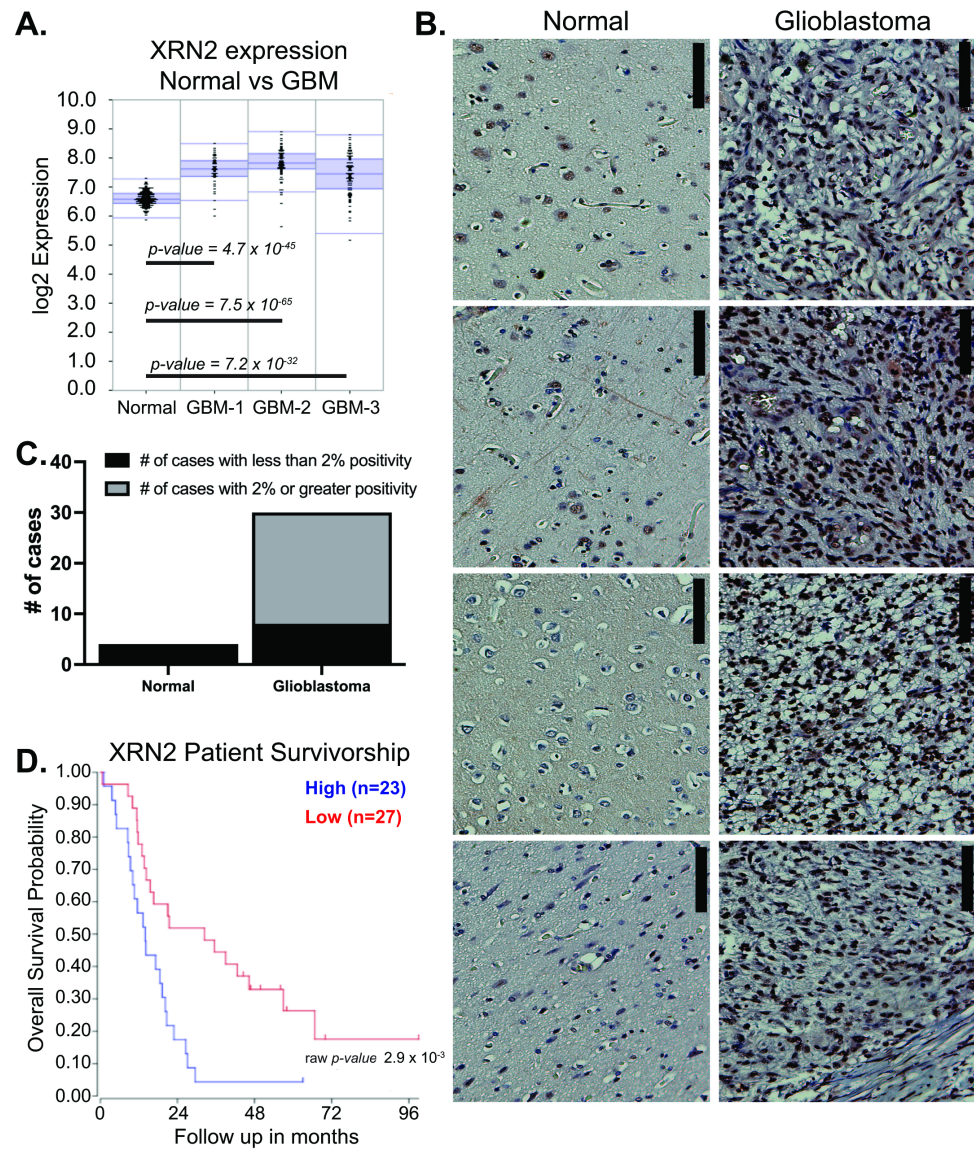


Figure 1. XRN2 expression confers with glioblastoma disease and poor patient survival. (A) Log₂ XRN2 mRNA expression levels in normal (Berchtold, 172 samples), GBM-1 (Pfister, 46 samples), GBM-2 (Loeffler, 70 samples), and GBM-3 (Hegi, 84 samples) databases. Graph generated from R2: Genomics Analysis and Visualization Platform. (B) Representative XRN2 immunohistochemistry staining of normal and glioblastoma patient samples. Brown signal is XRN2. Blue signal is hematoxylin (nuclei). Scale bar is 100 microns. (C) Quantification of XRN2 signal from immunohistochemistry staining of normal and GBM patient samples. A signal of less than 2% is considered negative, while a signal of 2% or greater is considered positive. (D) Glioma patient survival outlook based on XRN2 mRNA levels (Kawaguchi, 50 patients). Blue line denotes patients with high expression of XRN2. Red line denotes patients with low expression of XRN2. Graph generated from R2: Genomics Analysis and Visualization Platform. Statistical analysis was performed using the default setting provided by platform.

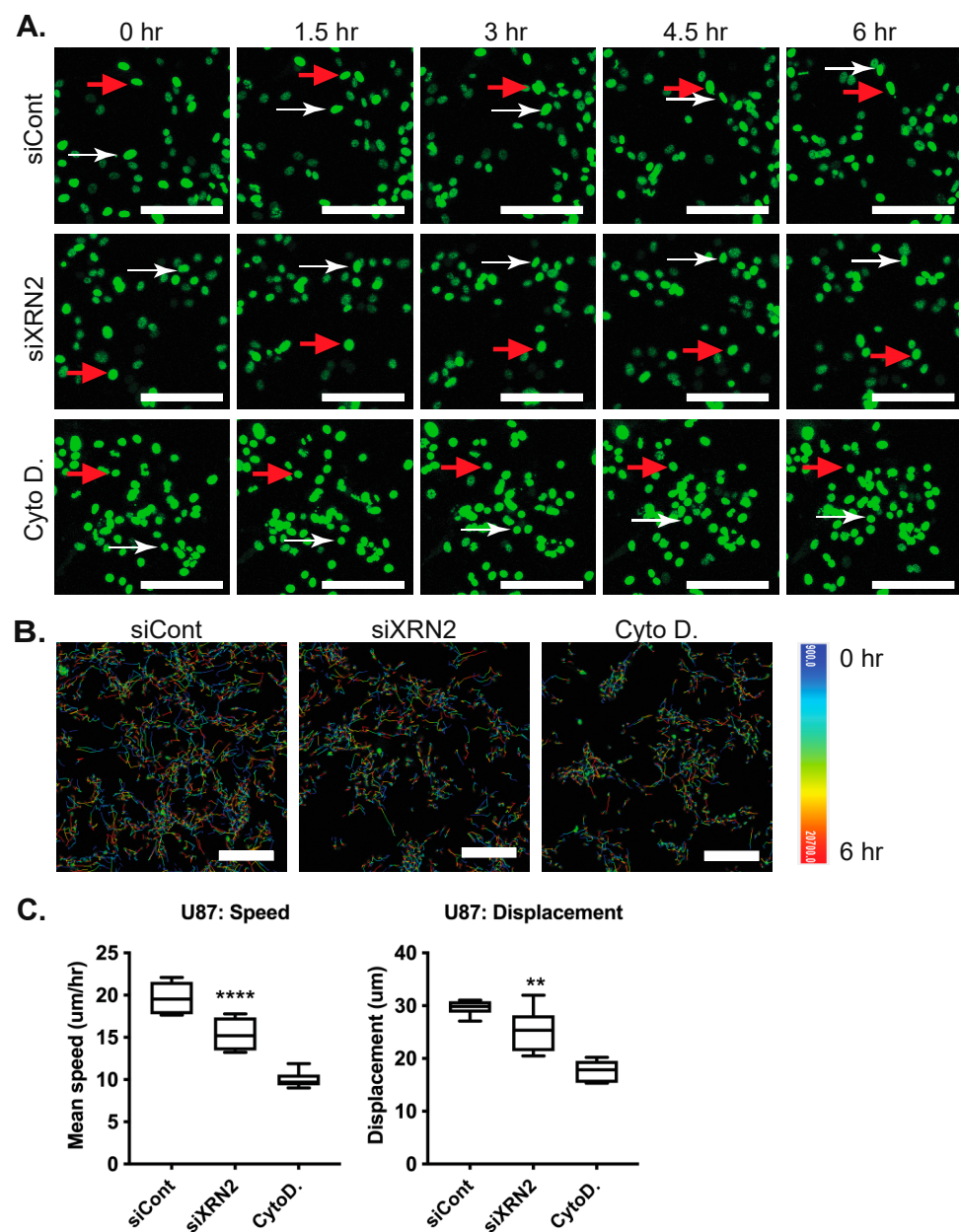


Figure 2. XRN2 is required for GBM cell motility. (A) Image stills from live-cell imaging of U87-GFP cells. Arrows track the movement of two representative cells over time. Tracking was over 6 h with images taken at 30-min intervals. (B) Positional tracks of U87 H2B-GFP cells during the 6 h live-cell imaging. White marks the position of the cells at the beginning of time to red, the position of the cells at the end of imaging. (C) Quantification of U87-GFP tracking. Changes in speed and displacement upon XRN2 knockdown by siRNA are shown. Scale bar is 100 micron. ** p -value ≤ 0.01 , **** p -value ≤ 0.0001 . The Students t -test was used for statistical analysis.

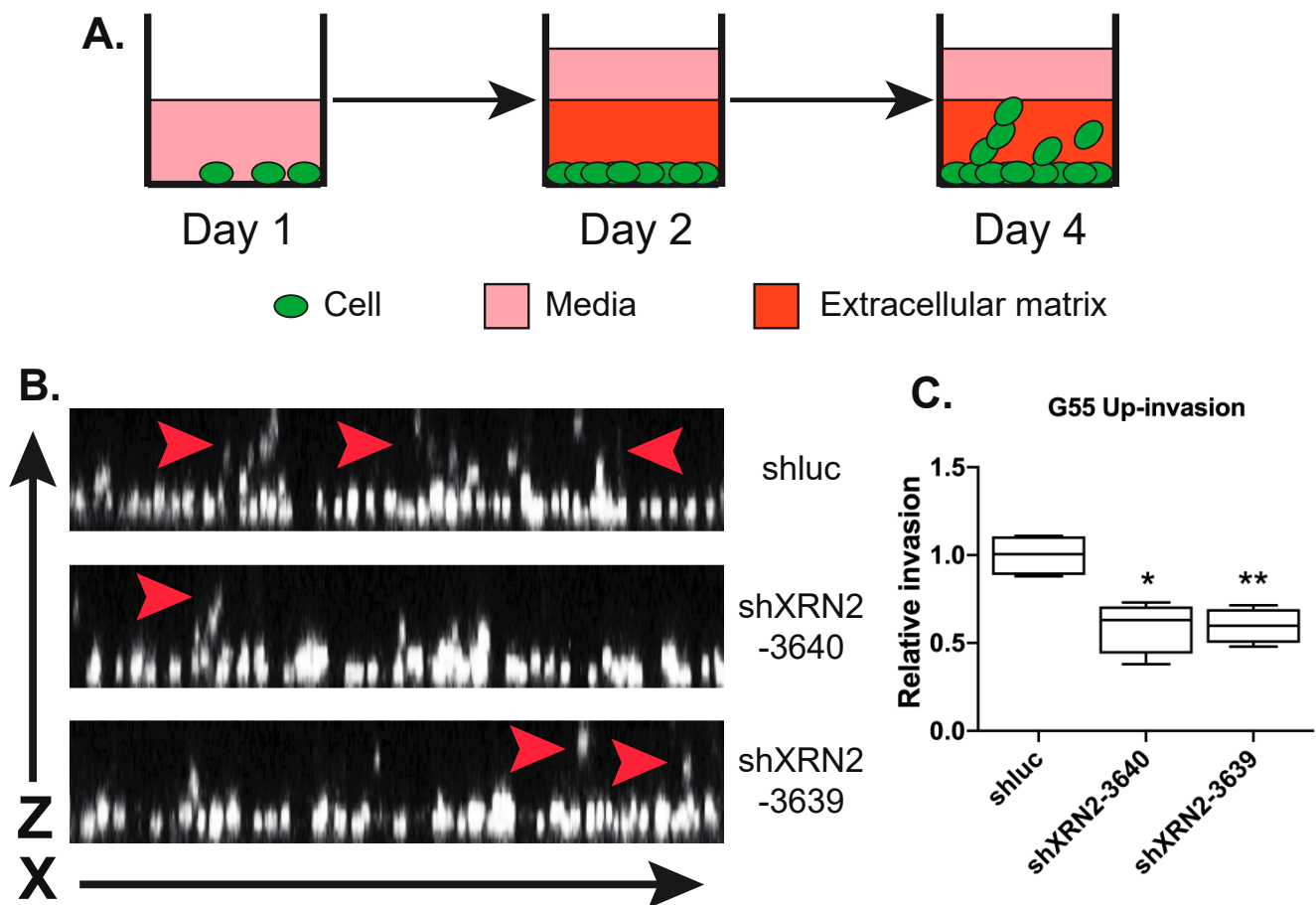


Figure 3. XRN2 is required for invasion through a matrix. (A) Diagram of inverted vertical invasion. Day 1—cells are plated at near confluent levels. Day 2—extracellular matrix is applied to the confluent cells. Day 4—cultures are fixed, stained, and imaged for invasion analysis. (B) Representative ZX image of invading G55 cells (white). Red arrows denote invading cells. (C) Quantification of up-invasion of G55 cells with the listed shRNAs. * = p -value ≤ 0.05 , ** = p -value ≤ 0.01 . The Students t -test was used for statistical analysis.

3.4. Loss of XRN2 Diminishes GBM Growth In Vivo

To extend the observations made in vitro, G55 cells with or without XRN2 [10] were orthotopically injected into mouse brains for tumor xenograft studies. We used G55 GBM cells, as they are highly aggressive and readily form tumors in vivo when injected into mouse brains [14,27]. We injected six mice with control G55 cells, seven mice with G55-shXRN2, and four mice with G44-shXRN2 #2 cell. Using histological examination, we found that a loss of XRN2 reduced the tumor size visualized through the cross-sectioning of mouse brains (Supplemental Figure S4). Consistent with histological data, using magnetic resonance imaging, we found that the tumor volume of two unique XRN2-deficient G55 cells was 5.85 and 2.85 mm³ (G55-shXRN2 (shXRN2-3640) and G55-shXRN2 #2 (shXRN2-3639), respectively), as compared to the 98.8 mm³ volume observed with control cells (Figure 4). We also found that a loss of XRN2 decreased the relative invasion in XRN2 LN229-deficient cells as compared to the control cells (Supplemental Figure S5). Importantly, we have shown that a loss of XRN2 does not affect proliferation or elicit cell-cycle changes in G55 cells [10], consistent with other published reports [28,29]. Based on these results, XRN2 seems to play a vital role in tumor development.

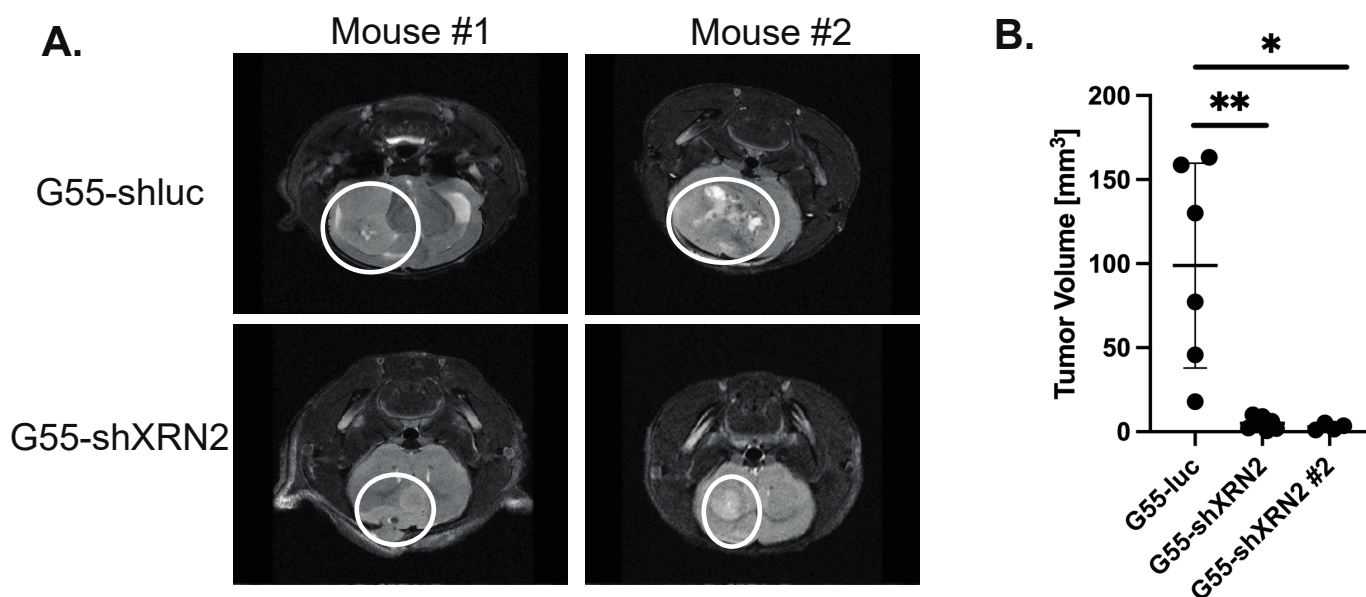


Figure 4. Loss of XRN2 results in decreased tumor volume in vivo. (A) Magnetic resonance imaging was used to detect control (G55-shluc) and XRN2-deficient (G55-shXRN2) tumors in mouse brains. (B) Quantitation of tumor volumes obtained from control (G55-shluc) and two unique XRN2-deficient (G55-shXRN2 and G55-shXRN2 #2) G55 cell lines. * = p -value ≤ 0.05 , ** = p -value ≤ 0.01 . The Students t -test was used for statistical analysis.

3.5. Loss of XRN2 Alters the Transcriptional Profile of Glioma Cells

Previous studies found that XRN2 plays a role in regulating miRNA maturation [13] and RNA:DNA hybrid formation [10,11]. As RNA:DNA hybrids and miRNAs can act to modulate gene expression, we chose to examine how a loss of XRN2 can influence the global transcriptional profile of gliomas. We exposed LN229 and U251 GBM cells to control and XRN2 siRNAs. Transfection of XRN2 siRNA resulted in a ~80% decrease in XRN2 expression in both LN229 and U251 cells lines (Figure 5A). Using RNA sequencing, we found substantial gene expression loss and gains after XRN2 loss (Figure 5B), with 194 of these genes demonstrating similar expression changes in both U251 and LN229 cell lines (Figure 5C). Using ingenuity pathway analysis, we found five biological pathways (cell cycle, cellular assembly and organization, cellular movement, DNA replication, recombination, and repair and cellular development) most affected by XRN2 loss (Figure 5D). These pathways are commonly used by tumor cells in the process of metastasis.

Interestingly, one of the genes identified as having a positive correlation with XRN2 was vinculin (VCL). VCL has been shown to promote tumor progression in GBMs and prostate cancer [30,31]. Thus, we examined how a loss of VCL affected the speed and displacement of GBMs. We treated U251 cells with control, VCL, or XRN2 siRNA, along with CytoD. We found that cells treated with either VCL or XRN2 siRNAs displayed a ~30% decrease in speed (Figure 6A) and a ~40% decrease in displacement (Figure 6B), as compared to cells exposed to control siRNA. There was no significant difference in the speed or displacement in cells transfected with XRN2 or VCL siRNA. Additionally, the decrease in speed or displacement in VCL or XRN2 siRNA was not the same as the decrease seen in cells treated with CytoD (Figure 6A,B). Interestingly, these observations were made even though XRN2 siRNAs led to a ~50% reduction in VCL expression, while VCL directed siRNAs resulted in a ~90% reduction (Supplemental Figure S6). These data suggest that XRN2 plays a role in cell motility and invasion in order to mediate the expression of genes in these processes.

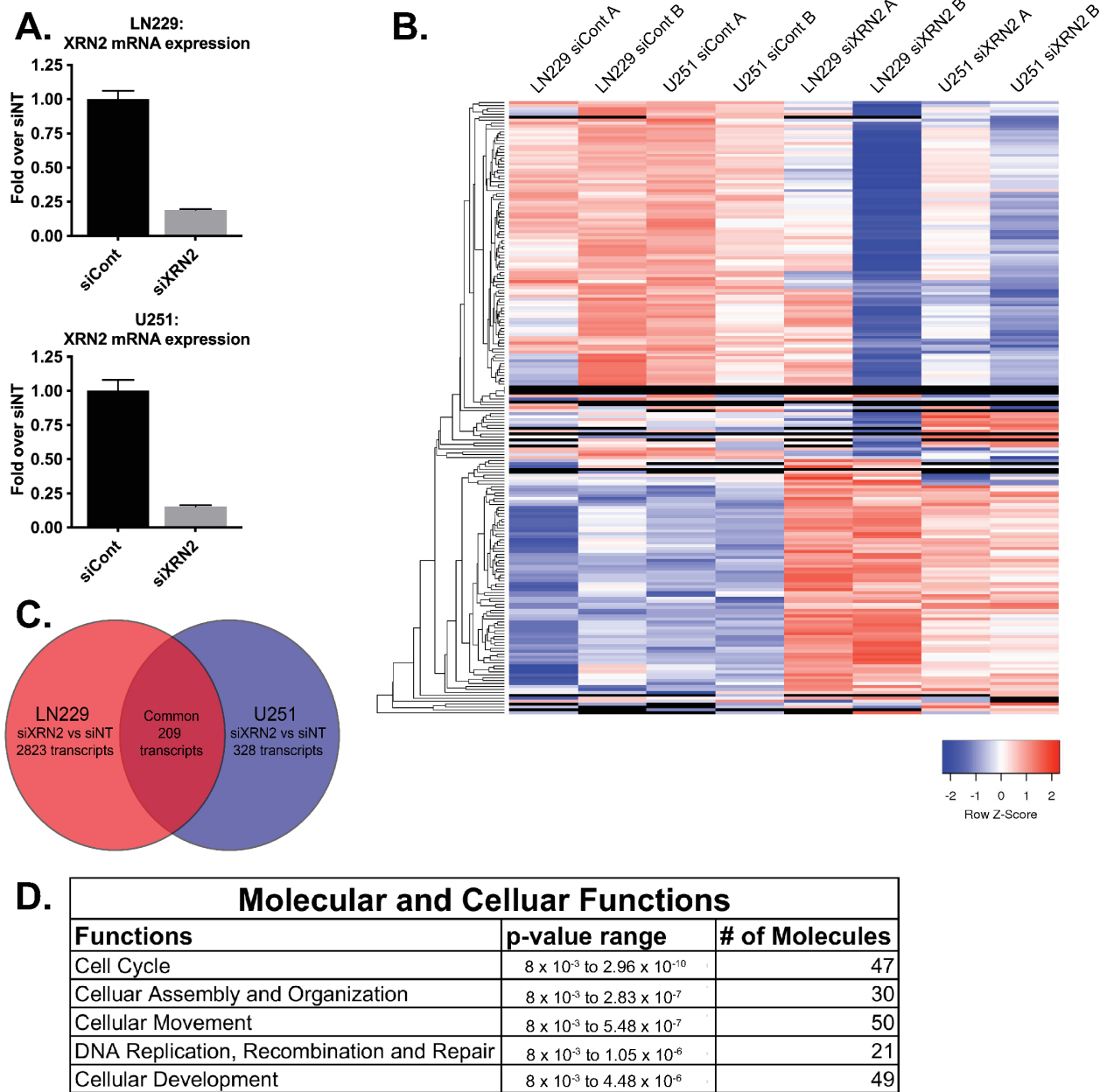


Figure 5. XRN2-mediated transcriptome landscape. (A) qPCR of XRN2 expression of samples used in the RNA-Seq in B. (B) RNA-Seq heat map of LN229 and U251 transfected with siCont or siXRN2. Heat map generated from transcripts with a log 1.3 or greater change and a *p*-value of 0.05 or better. (C) Venn diagram of overlapping transcripts from B. (D) Ingenuity pathway analysis of the overlapping transcripts in C.

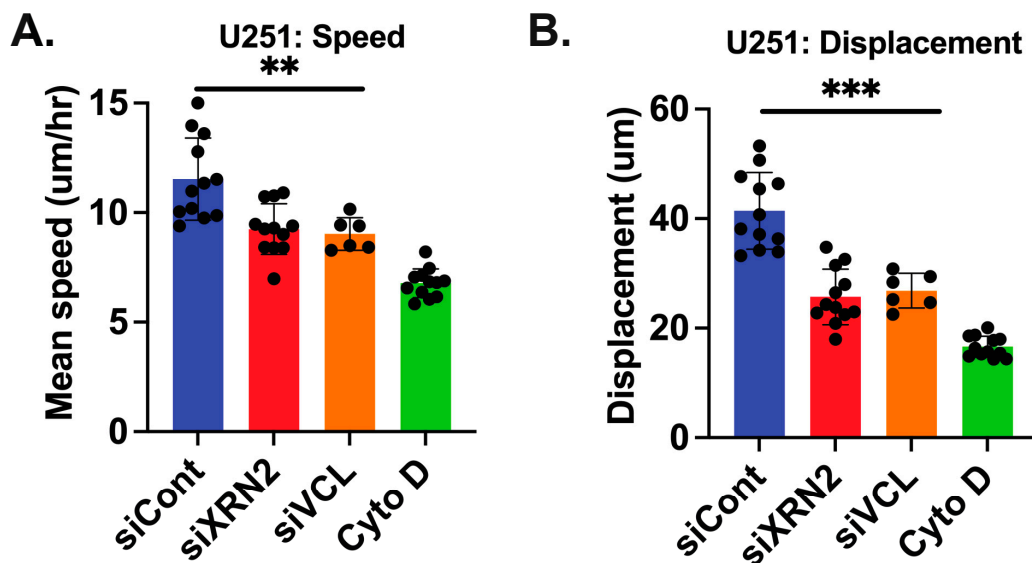


Figure 6. Loss of VCL or XRN2 results in a similar decrease in the speed or displacement in GBM cells. Quantification of U251-GFP tracking. Changes in (A) speed and (B) displacement upon control, VCL or XRN2 knockdown by siRNA are shown. ** p -value ≤ 0.01 , *** p -value ≤ 0.001 . The Students t -test was used for statistical analysis.

4. Discussion

One of the major obstacles in treating GBMs is the dissemination of tumor cells from the primary site to the secondary site within the brain [4]. In addition, secondary site formation of recurrent glioblastomas often occurs in areas of the brain which are inaccessible to surgical resection [5]. As these recurrent GBMs also acquire resistance to radio- and chemo-therapies, a second major obstacle [5] is that treatment options are limited for these patients. Thus, understanding the mechanisms that mediate the dissemination of glioblastoma tumor cells from the primary site to secondary sites can help improve overall patient survival.

4.1. Role of XRN2 in Glioblastoma Progression

Dissemination of tumors cells from a primary site to a secondary site is a multiple-step process that depends on several cellular characteristics, including (1) the cell's inherent ability to move away from the primary tumor site (cell motility) and (2) the cell's ability to migrate through a solid matrix and confined spaces (invasion) [32].

In our current study, we found that a loss of XRN2 reduces cell motility by ~25% in glioblastoma cells when compared to control cells. While not essential for cell motility, XRN2 is required for efficient glioblastoma cellular movement. In addition, we found that XRN2 loss also reduces migration through a matrix by ~50% as compared to the control cells. These results are consistent with observations made in lung cancer, i.e., that XRN2 is required for tumor cell invasion [13].

As we have found that XRN2 mediates dissemination of glioblastomas, XRN2's mechanistic role in this process remains unclear. In lung cancer, it has been suggested that XRN2 regulation of miR-10a is responsible for the migration process [13]. We found that a loss of XRN2 alters the transcriptional profile of U251 and LN229 glioblastoma cells. Yet, we did not find changes in miR-10a in glioblastoma cells. One possibility for this may be that the next-generation sequencing we performed was not sensitive enough to distinguish changes in miRNAs.

One intriguing reason for the change in the glioblastoma transcriptome is the formation of RNA:DNA hybrids or R-loops. R-loops can mediate the expression of genes through a variety of different mechanisms, such as regulating the methylation status of CpG island in the promoter region of genes [33]. We have found that a loss of XRN2 results in increased

R-loop formation in glioblastoma cells [10]. A loss of XRN2 has also been shown to lead to changes in the expression of genes through an R-loop-dependent manner [12]. These data suggest that R-loop regulation plays a role in mediating cell motility and invasion.

4.2. XRN2 as a Potential Target for Glioblastoma Therapy

We provide evidence that XRN2 is important for glioblastoma maintenance *in vivo*. XRN2 expression is increased in glioblastoma patient samples as compared to normal brain. This increase in XRN2 expression also correlates with poor overall patient survival. In addition, XRN- deficient G55 cells also fail to form tumors when injected into mouse brains. Our current study demonstrates that XRN2 is required for the efficient dissemination of glioblastoma cells. Interestingly, we have previously shown that XRN2 also plays a role in the DNA damage response [10,11]. A loss of XRN2 impairs the two major double-strand break repair pathways: non-homologous end-joining and homologous recombination [10,11]. XRN2 deficiency also results in increased sensitivity to several different types of genotoxic stress, such as ionizing radiation and PARP1 inhibitors [10,11]. Our data suggest that measuring XRN2 levels in GBMs can help to determine how a patient will respond to radiation or chemotherapy. This is especially important considering that we found the highest XRN2 levels in GBMs, even when compared to other brain malignancies. Thus, XRN2 may be an important biomarker in the treatment of patients suffering from GBMs.

As previously mentioned, there are two major obstacles in treating GBM patients: (1) the recurrence of GBMs at a secondary/un-operatable area of the brain and (2) the acquisition of therapeutic resistance in the recurrent GBMs. Targeting XRN2 can impair both of the major obstacles. First, our current study demonstrates that targeting XRN2 can impair GBM cell motility and invasion, which can then limit the potential for secondary site formation. Second, targeting XRN2 can also enhance anti-GBM therapies, especially radiation, which is a first-line anti-GBM therapy [5], as well as PARP1 inhibitors, which are currently used in clinical trials for GBM therapy [34].

Supplementary Materials: The following are available online at <https://www.mdpi.com/article/10.3390/cells11091481/s1>, Figure S1: XRN2 expression is elevated in glioblastoma, Figure S2: XRN2 is required for cell motility, Figure S3: Loss of XRN2 reduces G55 cell's ability to invade into matrix, Figure S4: Loss of XRN2 reduces LN229 cell's ability to invade into matrix, Figure S5: XRN2 deficient G55 cells form tumors with reduced tumor volumes, Figure S6: Loss of XRN2 results in loss of VCL expression, Video S1: Loss of XRN2 decreases cell speed and motility in U87 GBM cells.

Author Contributions: T.T.D. and J.C.M. conceptualized the study. J.C.M. and T.T.D. analyzed the data. J.C.M. wrote the original draft and T.T.D. edited the manuscript. T.T.D., D.S., N.S., M.L., R.G. and M.Z. performed the experiments. J.C.M. and R.A.T. obtained funding for the study. All authors have read and agreed to the published version of the manuscript.

Funding: This research was funded by the NIH (P20GM103639), the College of Medicine Alumni Association (C5112501), the Oklahoma Center for Adult Stem Cell Research (221006) to J.C.M. and NIH (1S10OD023508-01), and the Oklahoma Medical Research Foundation to R.A.T.

Institutional Review Board Statement: All animal studies were performed with the approval (protocol 17-48) of the Oklahoma Medical Research Foundation Institutional Animal Care Use Committee policies, which follow NIH guidelines.

Informed Consent Statement: Not applicable.

Data Availability Statement: Links to public data sources and RNA-seq data are listed in methods.

Acknowledgments: We would like to acknowledge the imaging Core at the Oklahoma Medical Research Foundation (OMRF) for use of the LSM710 confocal microscope used to perform the imaging presented in this manuscript. We also thank the Laboratory for Molecular Biology and Cytometry Research at OUHSC for the use of the Core Facility which provided an RNA sequencing service. Research reported in this publication was partly supported by the National Cancer Institute Cancer Center Support Grant P30CA225520, awarded to the Sttphenson Cancer Center and used by

the Molecular Biology shared resource, as well as the Oklahoma Tobacco Settlement Endowment Trust, awarded to the Sttephenson Cancer Center.

Conflicts of Interest: The authors declare no conflict of interest. The funders had no role in the design of the study; in the collection, analyses, or interpretation of data; in the writing of the manuscript; or in the decision to publish the results.

References

- Delgado-López, P.D.; Corrales-García, E.M. Survival in glioblastoma: A review on the impact of treatment modalities. *Clin. Transl. Oncol.* **2016**, *18*, 1062–1071. [CrossRef] [PubMed]
- Koshy, M.; Villano, J.L.; Dolecek, T.A.; Howard, A.; Mahmood, U.; Chmura, S.J.; Weichselbaum, R.R.; McCarthy, B.J. Improved survival time trends for glioblastoma using the SEER 17 population-based registries. *J. Neurooncol.* **2012**, *107*, 207–212. [CrossRef] [PubMed]
- Minniti, G.; Muni, R.; Lanzetta, G.; Marchetti, P.; Enrici, R.M. Chemotherapy for Glioblastoma: Current Treatment and Future Perspectives for Cytotoxic and Targeted Agents. *Anticancer. Res.* **2009**, *29*, 5171–5184. [PubMed]
- Li, C.; Wang, S.; Yan, J.L.; Torheim, T.; Boonzaier, N.R.; Sinha, R.; Matys, T.; Markowitz, F.; Price, S.J. Characterizing tumor invasiveness of glioblastoma using multiparametric magnetic resonance imaging. *J. Neurosurg.* **2019**, *132*, 1465–1472. [CrossRef] [PubMed]
- Filley, A.C.; Henriquez, M.; Dey, M. Recurrent glioma clinical trial, CheckMate-143: The game is not over yet. *Oncotarget* **2017**, *8*, 91779–91794. [CrossRef]
- Mehlen, P.; Puisieux, A. Metastasis: A question of life or death. *Nat. Rev. Cancer* **2006**, *6*, 449–458. [CrossRef]
- Liu, C.-A.; Chang, C.-Y.; Hsueh, K.-W.; Su, H.-L.; Chiou, T.-W.; Lin, S.-Z.; Harn, H.-J. Migration/Invasion of Malignant Gliomas and Implications for Therapeutic Treatment. *Int. J. Mol. Sci.* **2018**, *19*, 1115. [CrossRef]
- West, S.; Gromak, N.; Proudfoot, N.J. Human 5' → 3' exonuclease Xrn2 promotes transcription termination at co-transcriptional cleavage sites. *Nature* **2004**, *432*, 522–525. [CrossRef]
- Wagschal, A.; Rousset, E.; Basavarajaiah, P.; Contreras, X.; Harwig, A.; Laurent-Chabalier, S.; Nakamura, M.; Chen, X.; Zhang, K.; Meziane, O.; et al. Microprocessor, Setx, Xrn2, and Rrp6 Co-operate to Induce Premature Termination of Transcription by RNAPII. *Cell* **2012**, *150*, 1147–1157. [CrossRef]
- Dang, T.T.; Morales, J.C. XRN2 Links RNA:DNA Hybrid Resolution to Double Strand Break Repair Pathway Choice. *Cancers* **2020**, *12*, 1821. [CrossRef]
- Morales, J.C.; Richard, P.; Patidar, P.L.; Motea, E.A.; Dang, T.T.; Manley, J.L.; Boothman, D.A. XRN2 Links Transcription Termination to DNA Damage and Replication Stress. *PLoS Genet.* **2016**, *12*, e1006107. [CrossRef] [PubMed]
- Villarreal, O.D.; Mersaoui, S.Y.; Yu, Z.; Masson, J.Y.; Richard, S. Genome-wide R-loop analysis defines unique roles for DDX5, XRN2, and PRMT5 in DNA/RNA hybrid resolution. *Life Sci. Alliance* **2020**, *3*, e202000762. [CrossRef] [PubMed]
- Zhang, H.; Lu, Y.; Chen, E.; Li, X.; Lv, B.; Vikis, H.G.; Liu, P. XRN2 promotes EMT and metastasis through regulating maturation of miR-10a. *Oncogene* **2017**, *36*, 3925–3933. [CrossRef]
- Zalles, M.; Smith, N.; Saunders, D.; Saran, T.; Thomas, L.; Gulej, R.; Lerner, M.; Fung, K.-M.; Chung, J.; Hwang, K.; et al. Assessment of an scFv Antibody Fragment against ELTD1 in a G55 Glioblastoma Xenograft Model. *Transl. Oncol.* **2020**, *13*, 100737. [CrossRef] [PubMed]
- Berchtold, N.C.; Cribbs, D.H.; Coleman, P.D.; Rogers, J.; Head, E.; Kim, R.; Beach, T.; Miller, C.; Troncoso, J.; Trojanowski, J.Q.; et al. Gene expression changes in the course of normal brain aging are sexually dimorphic. *Proc. Natl. Acad. Sci. USA* **2008**, *105*, 15605–15610. [CrossRef] [PubMed]
- Sturm, D.; Witt, H.; Hovestadt, V.; Khuong-Quang, D.A.; Jones, D.T.; Konermann, C.; Pfaff, E.; Tönjes, M.; Sill, M.; Bender, S.; et al. Hotspot mutations in H3F3A and IDH1 define distinct epigenetic and biological subgroups of glioblastoma. *Cancer Cell* **2012**, *22*, 425–437. [CrossRef]
- Reifenberger, G.; Weber, R.G.; Riehm, V.; Kaulich, K.; Willscher, E.; Wirth, H.; Gietzelt, J.; Hentschel, B.; Westphal, M.; Simon, M.; et al. Molecular characterization of long-term survivors of glioblastoma using genome- and transcriptome-wide profiling. *Int. J. Cancer* **2014**, *135*, 1822–1831. [CrossRef]
- Murat, A.; Migliavacca, E.; Goria, T.; Lambiv, W.L.; Shay, T.; Hamou, M.F.; De Tribolet, N.; Regli, L.; Wick, W.; Kouwenhoven, M.; et al. Stem cell-related “self-renewal” signature and high epidermal growth factor receptor expression associated with resistance to concomitant chemoradiotherapy in glioblastoma. *J. Clin. Oncol.* **2008**, *26*, 3015–3024. [CrossRef]
- Kawaguchi, A.; Yajima, N.; Tsuchiya, N.; Homma, J.; Sano, M.; Natsumeda, M.; Takahashi, H.; Fujii, Y.; Kakuma, T.; Yamanaka, R. Gene expression signature-based prognostic risk score in patients with glioblastoma. *Cancer Sci.* **2013**, *104*, 1205–1210. [CrossRef]
- Gravendeel, L.A.; Kouwenhoven, M.C.; Gevaert, O.; de Rooij, J.J.; Stubbs, A.P.; Duijm, J.E.; Daemen, A.; Bleeker, F.E.; Bralten, L.B.C.; Kloosterhof, N.K.; et al. Intrinsic gene expression profiles of gliomas are a better predictor of survival than histology. *Cancer Res.* **2009**, *69*, 9065–9072. [CrossRef]
- Sun, L.; Hui, A.-M.; Su, Q.; Vortmeyer, A.; Kotliarov, Y.; Pastorino, S.; Passaniti, A.; Menon, J.; Walling, J.; Bailey, R.; et al. Neuronal and glioma-derived stem cell factor induces angiogenesis within the brain. *Cancer Cell* **2006**, *9*, 287–300. [CrossRef] [PubMed]

22. Dang, T.T.; Prechtel, A.M.; Pearson, G.W. Breast Cancer Subtype-Specific Interactions with the Microenvironment Dictate Mechanisms of Invasion. *Cancer Res.* **2011**, *71*, 6857. [CrossRef] [PubMed]
23. Tinevez, J.-Y.; Perry, N.; Schindelin, J.; Hoopes, G.M.; Reynolds, G.D.; Laplantine, E.; Bednarek, S.Y.; Shorte, S.L.; Eliceiri, K.W. TrackMate: An open and extensible platform for single-particle tracking. *Methods* **2017**, *115*, 80–90. [CrossRef] [PubMed]
24. Westcott, J.M.; Prechtel, A.M.; Maine, E.A.; Dang, T.T.; Esparza, M.A.; Sun, H.; Zhou, Y.; Xie, Y.; Pearson, G.W. An epigenetically distinct breast cancer cell subpopulation promotes collective invasion. *J. Clin. Investig.* **2015**, *125*, 1927–1943. [CrossRef]
25. Liu, J.-C.; Gao, L.; Li, S.-M.; Zheng, J.-J.; Li, D.-G.; Zhi, K.-Q.; Ren, W.-H. Upregulation of XRN2 acts as an oncogene in oral squamous cell carcinoma and correlates with poor prognosis. *Pathol.-Res. Pract.* **2021**, *219*, 153355. [CrossRef]
26. McArdle, T.J.; Ogle, B.M.; Noubissi, F.K. An In Vitro Inverted Vertical Invasion Assay to Avoid Manipulation of Rare or Sensitive Cell Types. *J. Cancer* **2016**, *7*, 2333–2340. [CrossRef]
27. Zalles, M.; Smith, N.; Ziegler, J.; Saunders, D.; Remerowski, S.; Thomas, L.; Gulej, R.; Mamedova, N.; Lerner, M.; Fung, K.; et al. Optimized monoclonal antibody treatment against ELTD1 for GBM in a G55 xenograft mouse model. *J. Cell. Mol. Med.* **2020**, *24*, 1738–1749. [CrossRef]
28. Patidar, P.L.; Viera, T.; Morales, J.C.; Singh, N.; Motea, E.A.; Khandelwal, M.; Fattah, F.J. XRN2 interactome reveals its synthetic lethal relationship with PARP1 inhibition. *Sci. Rep.* **2020**, *10*, 14253. [CrossRef]
29. Chakraborty, P.; Huang, J.T.J.; Hiom, K. DHX9 helicase promotes R-loop formation in cells with impaired RNA splicing. *Nat. Commun.* **2018**, *9*, 4346. [CrossRef]
30. Zheng, X.; Xu, H.; Gong, L.; Cao, D.; Jin, T.; Wang, Y.; Pi, J.; Yang, Y.; Yi, X.; Liao, D.; et al. Vinculin orchestrates prostate cancer progression by regulating tumor cell invasion, migration, and proliferation. *Prostate* **2021**, *81*, 347–356. [CrossRef]
31. de Semir, D.; Bezrookove, V.; Nosrati, M.; Scanlon, K.R.; Singer, E.; Judkins, J.; Rieken, C.; Wu, C.; Shen, J.; Schmudermayer, C.; et al. PHIP drives glioblastoma motility and invasion by regulating the focal adhesion complex. *Proc. Natl. Acad. Sci. USA* **2020**, *117*, 9064–9073. [CrossRef] [PubMed]
32. Stuelten, C.H.; Parent, C.A.; Montell, D.J. Cell motility in cancer invasion and metastasis: Insights from simple model organisms. *Nat. Rev. Cancer* **2018**, *18*, 296–312. [CrossRef]
33. Santos-Pereira, J.M.; Aguilera, A. R loops: New modulators of genome dynamics and function. *Nat. Rev. Genet.* **2015**, *16*, 583–597. [CrossRef] [PubMed]
34. Blakeley, J.O.; Grossman, S.A.; Chi, A.S.; Mikkelsen, T.; Rosenfeld, M.R.; Ahluwalia, M.S.; Nabors, L.B.; Eichler, A.; Ribas, I.G.; Desideri, S.; et al. Phase II Study of Iniparib with Concurrent Chemoradiation in Patients with Newly Diagnosed Glioblastoma. *Clin. Cancer Res.* **2019**, *25*, 73–79. [CrossRef] [PubMed]

Article

Transcriptomic Profiling of DNA Damage Response in Patient-Derived Glioblastoma Cells before and after Radiation and Temozolomide Treatment

Mathew Lozinski ^{1,2,3} , Nikola A. Bowden ^{2,3,4} , Moira C. Graves ^{2,3,4}, Michael Fay ^{2,3,4,5}, Bryan W. Day ⁶, Brett W. Stringer ⁷  and Paul A. Tooney ^{1,2,3,*} 

- ¹ School of Biomedical Sciences and Pharmacy, College of Health, Medicine and Wellbeing, University of Newcastle, Newcastle, NSW 2308, Australia; mathew.lozinski@uon.edu.au
- ² Centre for Drug Repurposing and Medicines Research, University of Newcastle, Newcastle, NSW 2308, Australia; nikola.bowden@newcastle.edu.au (N.A.B.); moira.graves@newcastle.edu.au (M.C.G.); mike@advancell.com.au (M.F.)
- ³ Hunter Medical Research Institute, New Lambton Heights, NSW 2305, Australia
- ⁴ School of Medicine and Public Health, College of Health, Medicine and Wellbeing, University of Newcastle, Newcastle, NSW 2308, Australia
- ⁵ GenesisCare, Newcastle, NSW 2290, Australia
- ⁶ QIMR Berghofer Medical Research Institute, Brisbane, QLD 4006, Australia; bryan.day@qimrberghofer.edu.au
- ⁷ College of Medicine and Public Health, Flinders University, Adelaide, SA 5042, Australia; brett.stringer@flinders.edu.au
- * Correspondence: paul.tooney@newcastle.edu.au; Tel.: +61-2-4921-8691



Citation: Lozinski, M.; Bowden, N.A.; Graves, M.C.; Fay, M.; Day, B.W.; Stringer, B.W.; Tooney, P.A. Transcriptomic Profiling of DNA Damage Response in Patient-Derived Glioblastoma Cells before and after Radiation and Temozolomide Treatment. *Cells* **2022**, *11*, 1215. <https://doi.org/10.3390/cells11071215>

Academic Editors: Javier S. Castresana and Bárbara Meléndez

Received: 9 March 2022

Accepted: 1 April 2022

Published: 4 April 2022

Publisher's Note: MDPI stays neutral with regard to jurisdictional claims in published maps and institutional affiliations.



Copyright: © 2022 by the authors. Licensee MDPI, Basel, Switzerland. This article is an open access article distributed under the terms and conditions of the Creative Commons Attribution (CC BY) license (<https://creativecommons.org/licenses/by/4.0/>).

Abstract: Glioblastoma is a highly aggressive, invasive and treatment-resistant tumour. The DNA damage response (DDR) provides tumour cells with enhanced ability to activate cell cycle arrest and repair treatment-induced DNA damage. We studied the expression of DDR, its relationship with standard treatment response and patient survival, and its activation after treatment. The transcriptomic profile of DDR pathways was characterised within a cohort of isocitrate dehydrogenase (IDH) wild-type glioblastoma from The Cancer Genome Atlas (TCGA) and 12 patient-derived glioblastoma cell lines. The relationship between DDR expression and patient survival and cell line response to temozolomide (TMZ) or radiation therapy (RT) was assessed. Finally, the expression of 84 DDR genes was examined in glioblastoma cells treated with TMZ and/or RT. Although distinct DDR cluster groups were apparent in the TCGA cohort and cell lines, no significant differences in OS and treatment response were observed. At the gene level, the high expression of *ATP23*, *RAD51C* and *RPA3* independently associated with poor prognosis in glioblastoma patients. Finally, we observed a substantial upregulation of DDR genes after treatment with TMZ and/or RT, particularly in RT-treated glioblastoma cells, peaking within 24 h after treatment. Our results confirm the potential influence of DDR genes in patient outcome. The observation of DDR genes in response to TMZ and RT gives insight into the global response of DDR pathways after adjuvant treatment in glioblastoma, which may have utility in determining DDR targets for inhibition.

Keywords: glioblastoma; DNA damage response; treatment resistance; temozolomide; radiation

1. Introduction

Glioblastoma is the most common and aggressive type of primary malignant brain tumour in adults. The diagnosis of glioblastoma, updated in the WHO Classification of Tumors of the Central Nervous System 2021, involves a combination of histological (microvascular proliferation or necrosis) and molecular characteristics, including the criteria of having the isocitrate dehydrogenase (IDH) wild-type gene [1]. Standard treatment involves safe maximal surgical resection of the tumour; however, since glioblastoma has an indistinct tumour border, complete resection is not usually possible. Consequently,

patients undergo intensive radiation therapy (RT) and temozolomide (TMZ) chemotherapy to treat residual tumour cells. These treatments cause single-stranded breaks (SSBs) or double-stranded breaks (DSBs) in the DNA of glioblastoma cells that may lead to cell cycle arrest and activation of cell death pathways [2]. Despite intense treatment, resistance frequently develops, causing a rapid recurrence at the primary tumour site, leaving patients with few treatment options, a poor prognosis and a median survival time of 15 months [3].

Evidence suggests that DNA damage response (DDR) pathways respond to treatment-induced damage and aid in tumour survival, leading to treatment resistance in glioblastoma [4]. The base excision repair (BER) pathway repairs SSBs caused by RT and methylated lesions caused by TMZ, whilst homologous recombination (HR), non-homologous end joining (NHEJ), and the Fanconi anemia (FA) pathway collectively respond to the potentially cytotoxic DSBs and stalled replication forks caused by both treatment approaches. Furthermore, DDR is constitutively active as a consequence of oncogenic-induced replication stress in glioblastoma [5,6], with increased expression in a number of DDR pathways shown to facilitate treatment resistance [7,8]. Recent studies have profiled DNA repair pathways in glioblastoma to gain targetable insights in efforts to sensitise tumour cells to DNA-damaging agents [9,10].

We investigated the transcriptomic expression of DDR genes and pathways in a TCGA cohort of IDH wild-type glioblastoma patients and its relation to overall patient survival. We identified DDR profiles of 12 patient-derived glioblastoma cell lines and compared TMZ and RT sensitivity of cells stratified on the degree of DDR pathway expression. Lastly, these cell lines were exposed to a clinically relevant dose of RT and/or TMZ to investigate the extent and timing of DDR genes and pathways responding to treatment-induced damage.

2. Materials and Methods

2.1. Ethics

This study was approved by the Human Research Ethics Committee of the University of Newcastle (H-2020-0389).

2.2. TCGA Glioblastoma Cohort

To study the baseline DDR profile in glioblastoma, fragments per kilobase million (FPKM) values were collated from 140 IDH wild-type glioblastoma patients within the TCGA database [11]. FPKM values were converted to transcript per kilobase million (TPM) values [12] and single-sample gene set enrichment analysis (ssGSEA) was performed on the TCGA data in R. Gene sets were assigned corresponding to the major DDR pathways including BER, NER, mismatch repair (MMR), HR and NHEJ (Table S1). Enrichment scores for each pathway were converted to log-transformed z-scores for data visualisation. RNAseq by expected maximisation (RSEM) data were collated for 84 DDR genes (Table S2). Patient groups were stratified into “high” and “low” expression based on a median split of RSEM expression values per gene. The log-rank test was used to find potential differences in overall survival (OS) between groups. Multiple Cox regression was implemented on genes with significant difference in OS from the log-rank test ($p < 0.05$), using clinical covariables that were determined to be significant through univariate Cox regression (Table S3).

2.3. Cell Lines and Reagents

Twelve patient-derived glioblastoma cell lines were kindly provided by the QIMR Berghofer Medical Research Institute (Brisbane, Australia). The cell lines are fully characterised with publicly available molecular and patient data, published by Stringer et al. [13]. Cells were grown as adherent monolayers in Matrigel[®] (Corning[®], Corning, NY, USA)-coated tissue culture flasks in StemPro[®] NSC SFM (Gibco[™], Waltham, MA, USA) containing 100 I.U./mL penicillin and 100 µg/mL streptomycin (Gibco[™], Waltham, MA, USA), and incubated at 37 °C in 5% CO₂/95% humidified air. Cells were passaged using StemPro[®] Accutase[®] solution (Gibco[™], Waltham, MA, USA) for detachment of adherent cells. TMZ was purchased from Sigma-Aldrich (Burlington, MA, USA), aliquoted in dimethyl sulfox-

ide (DMSO) (100 mM) and stored between 2 and 8 °C. RT was delivered using a medical linear accelerator (LINAC) at GenesisCare, Gateshead NSW (Australia) or RS-2000 Small Animal Irradiator (Rad Source, Buford, GA, USA).

2.4. RNA Sequencing Analysis

RNA sequencing data from all 12 glioblastoma cell lines were obtained from the publicly available QMIR database (<https://www.qimrberghofer.edu.au/commercial-collaborations/partner-with-us/q-cell/> accessed on 10 May 2021). RNA extraction methods and RNA sequencing analysis from the cell lines are described in Stringer et al. [13]. ssGSEA was performed on TPM values for each cell line, using the same gene sets as used in the TCGA cohort (Table S1).

2.5. Cell Viability Assay

To assess cell viability, 96-well plates were coated with Matrigel under ice-cold conditions prior to plating with cells. Adherent glioblastoma cell lines were passaged and seeded at 4000 Cells/well in 96-well plates overnight, before treatment with a clinically relevant dose of TMZ (35 µM) [14] or RT (2 Gy). After 7 days, 50 µL of a 2 mg/mL solution of MTT Formazan (Sigma-Aldrich, USA) and Dulbecco's Phosphate Buffer Saline (DPBS, without magnesium chloride and calcium chloride Gibco™, Waltham, MA, USA) was added to each well and incubated for 3 h. The medium/MTT solution was aspirated and DMSO (120 µL) added into each well. Each plate was shaken using an IKA® MS 3 basic shaker (Sigma Aldrich, Saint Louis, MO, USA) at 600 rpm for 2 min. Absorbance was read at 570 nM using the SPECTROstar®Nano microplate reader (BMG LABTECH, Ortenberg, Germany).

2.6. Comparison of Cell Line DDR Profile and Treatment Response

Glioblastoma cell lines were stratified into two cluster groups (C1 and C2) based on hierarchical clustering of ssGSEA scores in each DDR pathway. Cell lines were also assigned into “high” or “low” expression groups according to each DDR pathway based on a median split of ssGSEA scores. Differences in TMZ or RT cell viability between cluster groups or “high” vs. “low” DDR expression groups was assessed through an unpaired student's *t*-test.

2.7. Time Course and Quantitative PCR

Four glioblastoma cell lines (HW1, FPW1, SB2b and MN1) were seeded at 300,000 cells/well in 6-well Matrigel-coated plates overnight and treated with a clinically relevant dose of RT (2Gy), followed by TMZ (35 µM) one hour later. Cells were harvested at 2, 24 and 48 h after TMZ treatment and extracted for RNA using the AllPrep DNA/RNA/Protein Mini Kit (Qiagen, Germantown, MD, USA). RNA was converted to cDNA using the High-Capacity cDNA Reverse Transcription Kit (ThermoFisher Scientific, Waltham, MA, USA). In accordance with supplier instructions, gene expression of 84 DDR genes (Table S2) was examined using a TaqMan™® Gene Expression Custom Array Card (ThermoFisher Scientific, Waltham, MA, USA). Samples were run as biological triplicates using the QuantStudio™ 7 Pro Real-Time PCR System (ThermoFisher Scientific, Waltham, MA, USA). The geometric means of housekeeping genes (Table S2) were used to determine the absolute expression and fold changes of target genes for each cell line using the Δ Ct and $\Delta\Delta$ Ct method. Differentially expressed genes (DEGs) were identified within each cell line as significantly expressed genes for a particular treatment and time point when compared to the untreated control, using Dunnett's multiple comparison test of absolute expression values [15].

2.8. Statistical Analysis

The statistical analyses including the Mann–Whitney test, the Kruskal–Wallis test and Dunnett's multiple comparison test were conducted in GraphPad Prism 7. Unsupervised

hierarchical clustering (Ward's method) of ssGSEA scores was performed in R using the 'stats' package and visualised using the 'ComplexHeatmap' package. Survival analyses using the log-rank test and Cox regression were performed in R using the 'survival' package. p -values < 0.05 were considered significant.

3. Results

3.1. Expression of DDR Genes and Association with Patient Survival

First, we analysed RNA sequencing data from 140 IDH wild-type glioblastoma patient samples in the TCGA to determine distinct DDR profiles using ssGSEA. This method calculates enrichment scores of gene sets within a single sample and thus represents the degree to which such gene sets are up- or downregulated within a sample [16]. Five gene sets were used in this study, representing the five canonical DDR pathways (BER, MMR, NER, HR and NHEJ) [17]. Hierarchical clustering of ssGSEA scores from each DDR pathway identified three distinct clusters (TC1–TC3), wherein TC3 had the highest gene expression of each DDR pathway, followed by TC2, and lastly TC1, which had the lowest gene expression in each DDR pathway (Figure 1A). There was a trend of small increases in the proportion of *MGMT* methylated patients when comparing cluster C1 through to C3 (C1 = 34.2% (13/48), C2 = 41.5% (17/41), C3 = 53.3% (16/30)). A similar trend occurred for the proportion of *TP53* alterations (C1 = 13% (7/54), C2 = 20.8% (11/53), C3 = 33.3% (11/33)). Although distinct DDR gene profiles were apparent, no survival difference was found across clusters (Figure 1B).

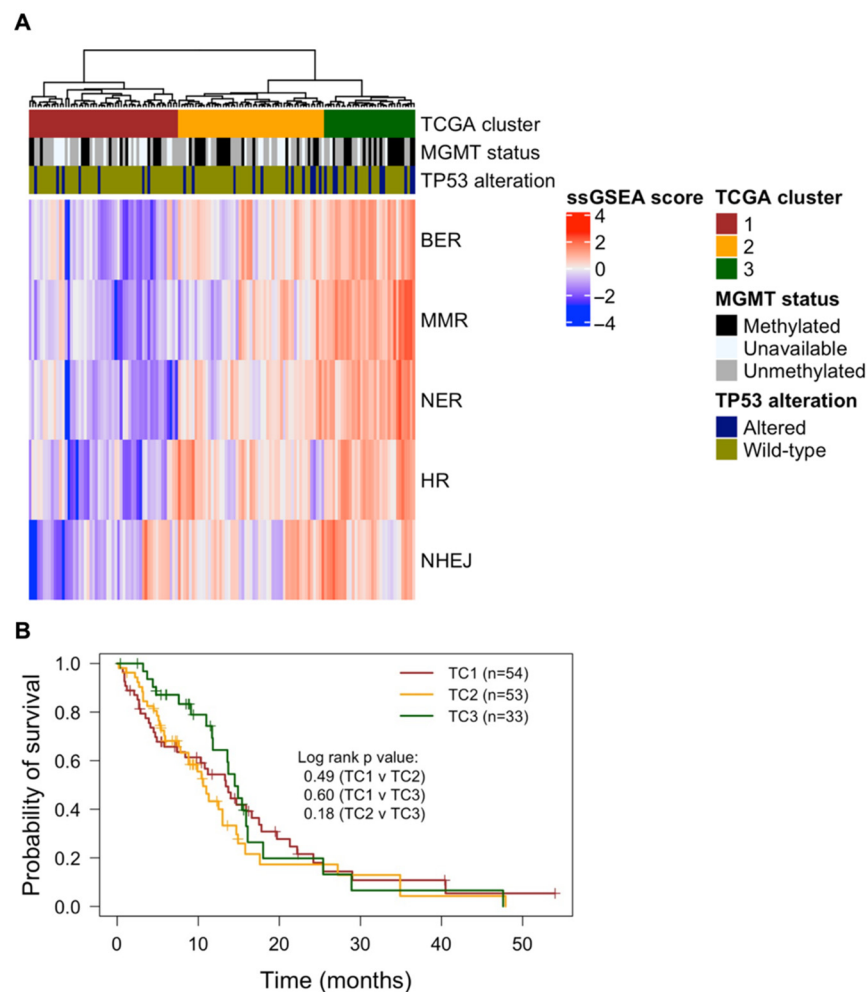


Figure 1. Transcriptomic profile of DDR pathways of glioblastoma patients in the TCGA cohort ($n = 140$). (A) Log-transformed ssGSEA scores are represented for each DDR pathway; and after hierarchical clustering (Ward's method), three distinct TCGA clusters were identified (TC1, TC2, and

TC3). The Kruskal–Wallis test was used to compare ssGSEA scores of each pathway between clusters, with the same trend followed across all DDR pathways: TC1 < TC2 < TC3 ($p < 0.01$). *MGMT* methylation status and *TP53* alterations (SNVs or homozygous deletions) are also depicted for respective patient samples. (B) Kaplan–Meier plots of OS are shown for patients within DDR clusters (TC1—red; TC2—yellow; TC3—green). The log-rank test was performed between each combination of clusters, revealing no significant OS differences between clusters. Statistical significance was determined with a p -value < 0.05.

Next, using the same TCGA patient cohort, we asked whether the expression of individual DDR genes could predict OS outcomes of glioblastoma patients. “High” and “low” expression groups were determined for DDR genes and Kaplan–Meier survival analysis was performed. After accounting for covariates using Cox regression (Table S3), high expression of DDR genes *ATP23*, *RAD51C* and *RPA3* was independently associated with poorer overall patient survival (Figure 2).

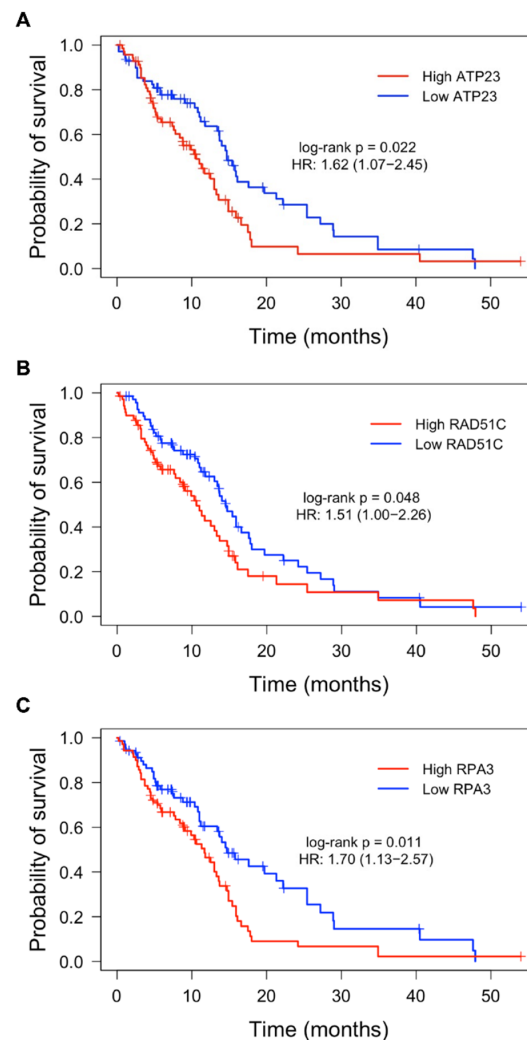


Figure 2. Kaplan–Meier plots of OS for high and low expression of *ATP23*, *RAD51C* and *RPA3* in the TCGA glioblastoma cohort. Patients were stratified into “high” (red) and “low” (blue) expression groups based on a median split of RNA expression for each respective DDR gene. Across all samples ($n = 140$), high expression of *ATP23* (A), *RAD51C* (B) and *RPA3* (C) was significantly associated with lower OS. Log-rank p -values and hazard ratio prior to multiple Cox regression are shown. Significance was established in genes with p -value < 0.05 after both a log-rank test and multiple Cox regression of significant clinical features (i.e., therapy).

3.2. Expression of DDR Pathways Influence Treatment Response in Glioblastoma Cell Lines

Next, we examined the baseline gene expression profiles of DDR pathways in 12 patient-derived glioblastoma cell lines (Table S4) using ssGSEA. Hierarchical cluster analysis identified two distinct clusters, C1 and C2 (Figure 3A). C1 had high expression of BER and NER genes, while C2 was significantly upregulated in MMR and HR ($p = 0.004$) genes (Figure 3A). NHEJ, although appearing upregulated in C1 (Figure 3A), was not significantly altered between C1 and C2 ($p = 0.154$). To determine whether cell line DDR gene expression clusters had similarities to the TCGA gene expression clusters, hierarchical clustering was performed on combined ssGSEA scores of TCGA samples and cell lines. All cell lines from C1 clustered within a combined cluster resembling TC1, while all cell lines belonging to C2 did not associate with any TCGA DDR cluster (Figure S1).

To investigate the extent at which baseline gene expression in DDR pathways contributes to differential treatment response, cell viability of glioblastoma cells treated with clinically relevant doses of TMZ (35 μ M) and/or RT (2Gy) was assessed (Figure 4). Across the cell lines, there was a differential response to TMZ, while most cell lines had similar sensitivity to single-dose RT (Figure 4). *MGMT* methylation status is a clinical biomarker of TMZ sensitivity [18]. As expected, *MGMT* methylated cell lines had a significantly reduced cell viability than *MGMT* unmethylated cell lines ($p = 0.004$) in response to TMZ (Figure S2). Three cell lines (HW1, FPW1 and SJH1) were identified as *TP53* mutants; however, their sensitivity to TMZ or RT was not significantly different compared to *TP53* wild-type cell lines ($p = 0.39$ and 0.86 , respectively). Whilst distinct differences in DDR gene expression were observed between clusters C1 and C2, no significant differences in cell viability were observed in response to TMZ ($p = 0.32$) or RT ($p = 0.097$) (Figure 3B,C).

When stratified into “high” and “low” DDR expression groups, treatment response varied in certain pathways (Figure 3D,E). High gene expression of the NER pathway was associated with more TMZ resistance ($p = 0.032$), while cells with high MMR gene expression were more sensitive to TMZ ($p = 0.0039$) (Figure 3D). Interestingly, TMZ response did not significantly differ between high and low expression of BER, HR and NHEJ genes. When comparing RT response, high HR gene expression was associated with increased resistance to RT ($p = 0.0038$) whilst there was no significant difference in other DDR pathways (Figure 3E). Collectively, these results suggests that transcriptomic expression of NER and MMR pathways may influence TMZ sensitivity, while gene expression of the HR pathway may influence RT response.

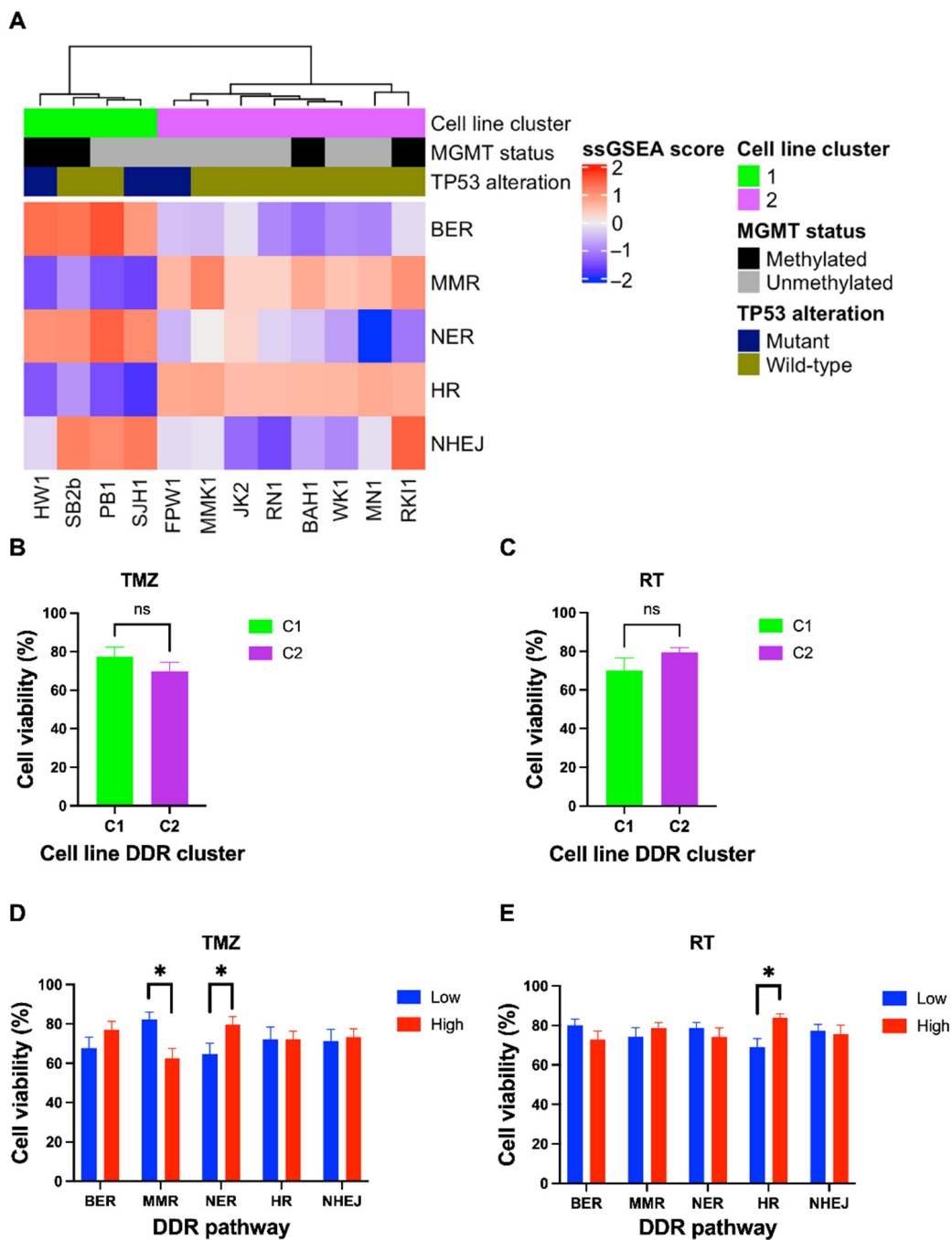


Figure 3. Transcriptomic profiling of DDR pathways in 12 patient-derived glioblastoma cell lines and response to standard treatment. (A) Log-transformed ssGSEA z-scores are shown corresponding to relevant DDR pathways, including *MGMT* methylation status and *TP53* mutation of glioblastoma cell lines. Two distinct clusters were identified (C1 and C2), in which C1 had a significant upregulation of BER and NER pathways ($p = 0.004$), while MMR and HR were upregulated in C2 ($p = 0.004$). Cell lines were treated with a clinically relevant dose of TMZ (35 μ M) or RT (2 Gy) for 7 days, cell viability assessed using MTT assay. Cell lines were grouped and compared using a student's *t*-test to assess differences in TMZ and RT response based on DDR cluster (B,C) as well as “high” and “low” expression of DDR pathways (D,E). There was no significant difference in cell viability between the C1 or C2 cell line clusters after TMZ or RT treatment (B,C). TMZ sensitivity was associated with high MMR gene expression, while TMZ resistance was associated with high NER gene expression (D). RT resistance was associated with high HR gene expression (E). p -values < 0.05 were considered significant (* $p < 0.05$) (ns = non-significant).

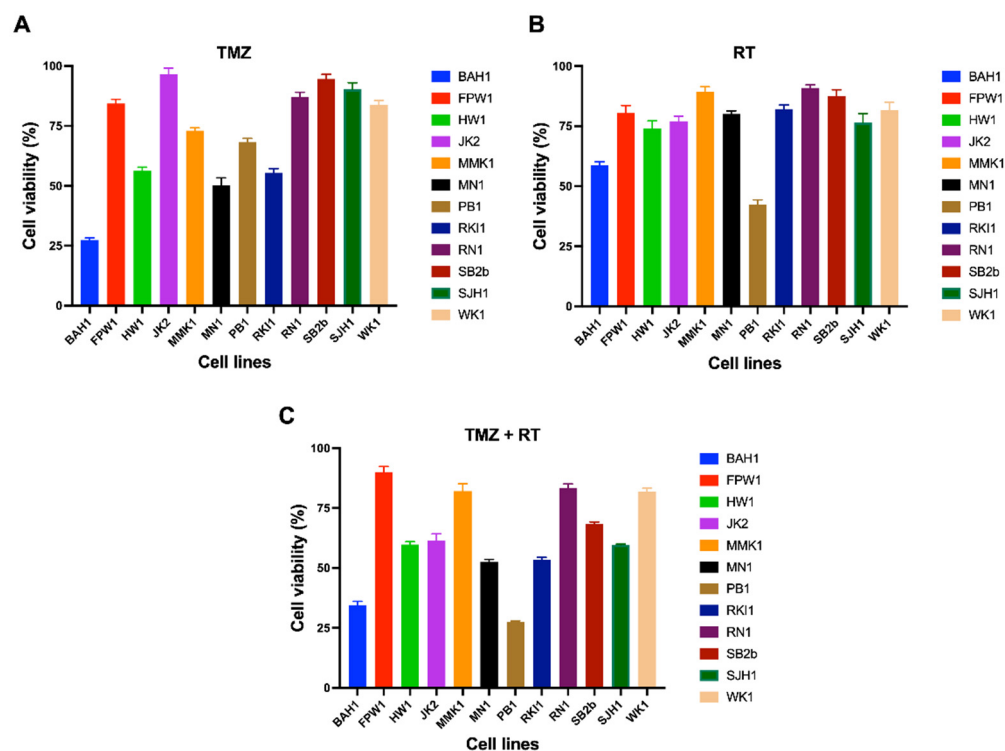


Figure 4. Cell viability of 12 patient-derived glioblastoma cell lines treated with TMZ (A), RT (B) or TMZ + RT (C). Cell lines were treated with a clinically relevant dose of TMZ (35 μ M) and/or RT (2 Gy), grown as adherent cultures for 7 days before being assessed for cell viability with an MTT assay. Data points represent the mean and SEM of three biological replicates over three independent experiments.

3.3. Upregulation of DDR Genes after Standard Treatment in Glioblastoma Cell Lines

Few studies have specifically examined the expression of multiple DDR pathways in glioblastoma cells treated with TMZ or RT to determine the timing of treatment-induced DDR pathway activation and the extent at which they repair DNA. Here, we used qPCR to determine the expression of 84 DDR genes in glioblastoma cell lines (SB2b, FPW1, MN1 and HW1) treated with a clinically relevant dose of TMZ and/or RT at 2, 24 and 48 h post-treatment. These cell lines represented to various degrees different cluster groups, *MGMT* statuses, and responses to TMZ or RT treatment (Figures 3 and 4). Within the context of this study, DEGs were identified as significantly up- or downregulated genes in treated cells compared to the untreated control at each specific time point.

When observing the frequency and distribution of DEGs across all cell lines, several trends appeared. Figure 5 summarises the accumulated degree of DDR upregulation and downregulation in all four cell lines treated with TMZ, RT, or TMZ + RT (Figure 5A), as well as the proportion of DEGs belonging to DDR pathways for the average cell line (Figure 5B–G). Furthermore, Figure 6 depicts the 16 most frequently significantly up- or downregulated genes across all cell lines, treatments, and time points. Notably, the majority of DEGs across all four cell lines were upregulated (88%). There appeared to be variability between cell lines and treatments (Figure S3); however, an overall trend across cell lines was the predominant upregulation of genes within 24 h after treatment, especially in RT- and TMZ + RT-treated cells (Figure 5A).

Differences in the frequency of DEGs were apparent between treatments across time points. On average, TMZ induced the lowest frequency of DEGs, whereas RT induced the most robust response causing the highest frequency of DEGs across each time point (Figure 5B,C). The combination treatment induced more DEGs than TMZ alone, but surprisingly less DEGs than RT alone (Figure 5D). This suggests that the addition of TMZ to RT-treated cells disrupts the dynamics of DDR in this context.

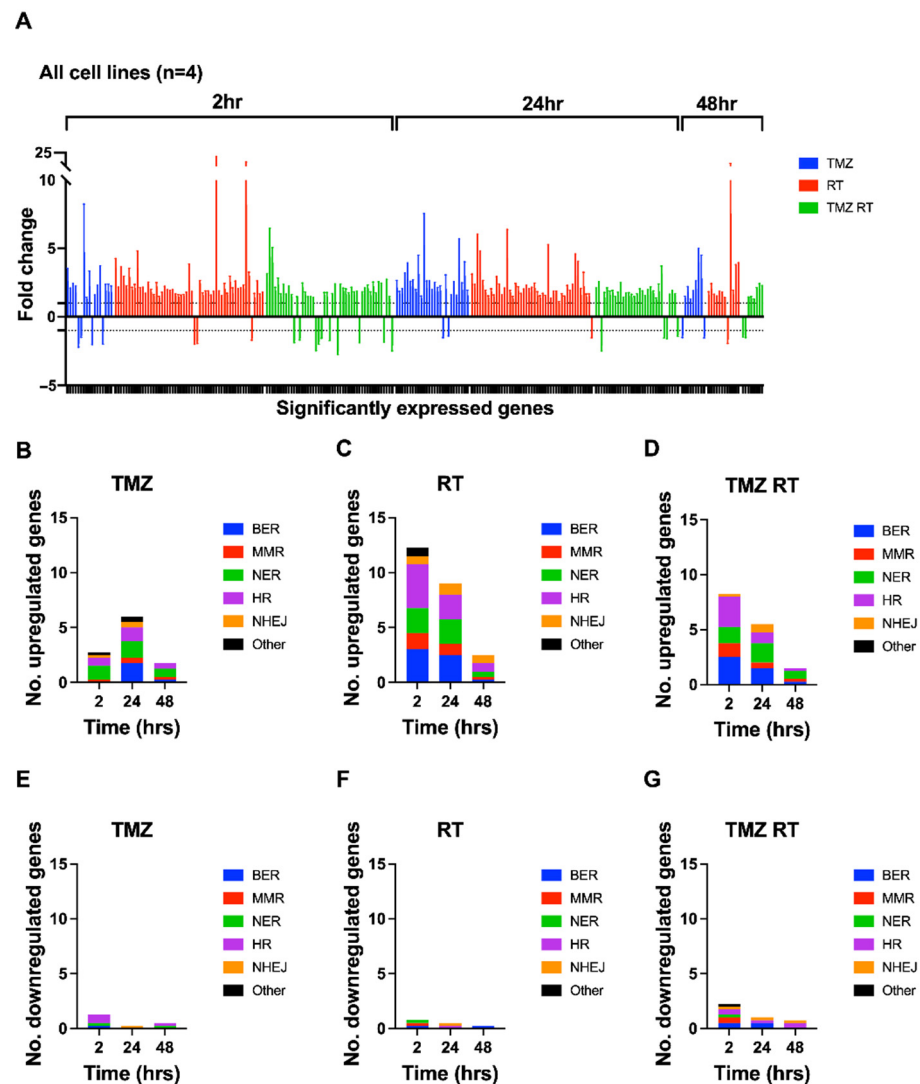


Figure 5. Accumulated frequency and distribution of DEGs across four patient-derived glioblastoma cell lines (FPW1, HW1, SB2b and MN1) in response to treatment. Cell lines were treated with RT (2Gy) and/or TMZ (35 μ M) before being harvested for RNA extraction at 2, 24 and 48 h after treatment. Quantitative PCR using a Custom TaqMan array card was undertaken to assess mRNA expression of 84 DDR genes. (A) Fold changes (\pm SEM) represent the sum total of DEGs across all cell lines, treatments (TMZ—blue; RT—red; TMZ + RT—green), and time points. Positive fold-changes (>1) represent upregulated genes and negative fold-changes (<-1) represent downregulated genes, while the area between 1 and -1 represents baseline expression. To view genes and their fold-changes in order of (A), see Table S5. (B–G) The average numbers of upregulated or downregulated genes across all cell lines for TMZ- (B,E), RT- (C,F) and TMZ + RT- (D,G) treated cells are graphically shown and represent the proportion of pathways that the DDR genes belong to at given time points after treatment. DDR pathways for each gene are depicted in Table S2. BER—blue; MMR—red; NER—green; HR—purple; NHEJ—orange; other—black.

The frequency of DEGs belonging to specific DDR pathways was also distinct for each treatment between time points. Although variability in response was observed between cell lines (Figure S4), trends appeared when considering the average expression across all four cell lines. On average, cells treated with TMZ at 2 h had an upregulation of NER genes while several genes involved in BER, HR, NHEJ and MMR were upregulated 24 h after treatment (Figure 5B). Cells treated with RT had upregulation in all DDR pathways and remained consistent for the 2 and 24 h time points before a reduction in expression

at 48 h (Figure 5C). For TMZ + RT-treated cells at 2 h, the BER, MMR, NER and HR pathways were upregulated, while NHEJ and NER genes increased in expression at 24 h post TMZ + RT treatment (Figure 5D). Then, at 48 h post TMZ + RT treatment, most genes returned to baseline levels where fewer genes were upregulated with NER expression the most prominent.

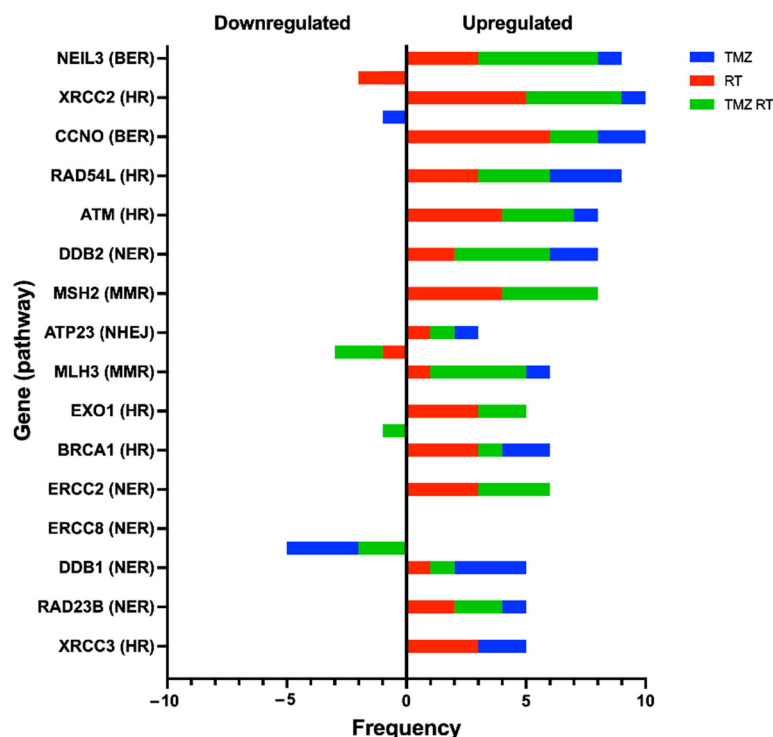


Figure 6. Top 16 most frequently up- or downregulated genes across all four glioblastoma cell lines (FPW1, HW1, SB2b and MN1). Data include the accumulated frequency across all variables for each respective gene, including the number of upregulated (positive values) or downregulated (negative values) occurrences, and the occurrence of this change in each specific treatment (TMZ = blue, RT = red, TMZ RT = green).

When considering the frequency of specific genes across all time points and treatments, genes from several pathways were represented, in particular HR and BER genes. *NEIL3* and *CCNO* (BER), *XRCC2*, *RAD54L* and *ATM* (HR), *DDB2* (NER), and *MSH2* (MMR) were among the most differentially expressed and upregulated (Figure 6). The NER gene, *ERCC8*, was the most frequently downregulated ($n = 5$) and appeared in cells treated with TMZ or TMZ + RT (Figure 6), suggesting that TMZ may influence its expression. From the three prognostically significant genes identified from the TCGA cohort, *RPA3* and *RAD51C* were upregulated only once across all cell lines while *ATP23* appeared to be upregulated in FPW1 cells and downregulated in the HW1 cell line (Table S5). Overall, these results emphasise the broad response of DDR genes and pathways after DNA-damaging treatment.

4. Discussion

Glioblastoma is an extremely aggressive and treatment-resistant disease, often prone to recurrence and poor patient survival due to the failure of standard treatment. The activation of DDR pathways is a significant factor in reducing treatment efficacy, enabling efficient repair of treatment-induced DNA damage, and increasing the likelihood of tumour cell survival [5,6]. We investigated DDR through a transcriptional lens to identify whether DDR is a significant feature in glioblastoma survival and response to standard treatment.

Firstly, we identified three distinct clusters (TC1–3) of TCGA glioblastoma patients based on the overall expression of DDR pathway genes using ssGSEA. Despite the clusters

displaying low, moderate, and high DDR gene expression, respectively, no significant OS differences were observed between clusters. A study by Meng et al. [19] found low DDR gene expression to indicate favourable prognosis in a combined cohort of low-grade glioma (LGG) and glioblastoma patients; however, consistent with our findings here, no survival difference was apparent in glioblastoma patients alone. Interestingly, a trend appeared, whereby the proportion of *TP53* alterations increased from TC1 to TC3 and thus aligned with the extent of DDR expression across each cluster. This may be the case as *TP53* alterations can enhance genomic stress within rapidly dividing cells and thus induce an increased activation of DDR to counteract such stresses [20]. Furthermore, a similar trend occurred for *MGMT* methylation, where the proportion of *MGMT* methylated patients increased from TC1 to TC3. Given that *MGMT* methylation plays a significant prognostic role in determining a longer overall survival in glioblastoma patients [18], its higher proportion within TC3, together with low sample sizes, may play a factor as to why no significant survival was observed even though higher DDR expression was evident. Despite this, we investigated individual DDR gene expression and their influence on OS outcomes. From the 84 DDR genes assessed, the high expression of *ATP23*, *RAD51C* and *RPA3* was independently associated with poor OS outcomes in the TCGA IDH wild-type glioblastoma cohort. All three genes play roles in the repair of DSBs and may enhance treatment resistance. For instance, *ATP23*, a commonly amplified gene within glioblastoma, is involved in NHEJ and is upregulated in response to RT [21]. *RAD51C* plays an important role as a stabiliser of complexes involved in HR [22], while *RPA3* is part of the three-subunit replication protein A (RPA) complex involved in HR and DSB repair and has been implicated in glioblastoma OS outcome [23]. These data suggest that DDR gene expression influences patient outcome and warrants further investigation on the role DDR plays in glioblastoma treatment resistance.

Stringer et al. [13] described efforts to fully characterise the 12 patient-derived glioblastoma cell lines, including use in a xenograft model to show they are morphologically representative of the patient's original tumour. This would suggest that the cell lines used in the current study are a good representation of the original tumour. We investigated the DDR baseline gene expression in these cell lines and found two distinct clusters (C1 and C2) with differential pathway expression. When compared to the glioblastoma TCGA cohort, four cell lines in the C1 cluster aligned with TC1 cluster of the TCGA cohort with respect to baseline DDR gene expression. The TCGA cohort was a significantly larger sample size at 140 cases, and thus it was surprising that 8 of the cell lines did not align with a TCGA cluster in baseline DDR gene expression. Furthermore, the C1 and C2 cell line clusters do not appear to have any relationship to known characteristics of glioblastoma such as *MGMT* methylation status. In regard to these discrepancies between the TCGA data and the baseline data from the 12 patient-derived glioblastoma cell lines, Stringer et al. showed in their original publication of the cell line data that 7 of the 12 cell lines maintained a molecular signature equivalent to that from the original tumour tissue [13]. As such, we cannot exclude the possibility that the cell culture conditions affected the baseline gene expression signatures [24]. However, with respect to the cell lines treated with TMZ and/or RT, our analysis used a non-treated control which will negate the effect of factors such as cell culture conditions, as the only change between groups is the treatments. With respect to the aim of investigating DDR gene expression and effects on treatment response, there was no difference in response to either RT or TMZ between the two cell line clusters, suggesting that the cell lines were responding in a similar manner to the treatment despite a difference in baseline DDR gene expression. Further investigation of the characteristics of the glioblastoma cell lines may help to explain the differences in the C1 and C2 DDR clusters.

When examining individual pathway expression in the cell lines, we showed that genes in DDR pathways are associated with response to TMZ or RT. Cells with a higher expression of NER genes were more resistant to TMZ, while high expression of MMR genes conferred TMZ sensitivity. Previous studies have suggested similar trends with

respect to NER components [8,25], while alterations in MMR genes such as MSH6 have been associated with TMZ resistance and recurrent glioblastoma tumours [26]. Our data also showed that gene expression of the HR pathway was inversely associated with RT response. The inhibition of HR components has enhanced radiosensitivity in glioblastoma cells [27,28], hence cells with a higher expression of HR genes may be more likely to survive than tumours which have a lower baseline expression [4,6,17,29]. Further investigation is needed to explore these results in more depth.

A limitation to this analysis is the bulk transcriptomic lens of tumours prior to any treatment, which does not adequately reflect changes in DDR expression from standard treatment. Thus, studying DDR across a pre- and post-treatment time course may reveal greater insight. In this regard, one of the important aspects of the work presented here is the time course analysis of DDR gene expression response, showing that several genes and pathways are upregulated in response to standard treatment, especially RT. These data may inform the feasibility of targeting DDR components to enhance treatment response in glioblastoma patients. One such approach is being explored through the development of small-molecule inhibitors of DDR proteins including poly (ADP-ribose) polymerase (PARP), Wee1, checkpoint kinase 1 and 2 (Chk1 and Chk2), ataxia-telangiectasia mutated (ATM), ataxia-telangiectasia and rad3-related (ATR), and DNA-dependent protein kinase (DNA-PK) [4,30]. Across all treatments, DDR gene expression changes occurred within a 24 h period after treatment. RT had the greatest response, with numerous pathways showing gene upregulation, suggesting activation at 2 and 24 h after treatment. TMZ on the other hand had a lower level of DDR gene upregulation. The composition of genes was also different to RT, with a predominance of NER genes expressed at 2 h before a sharp increase in BER gene upregulation, as well as upregulation in HR, MMR and NHEJ genes at 24 h. These observations agree with the understanding that O⁶-meG adducts caused by TMZ form DNA breaks only after several replication cycles have occurred [31,32], in contrast to RT, which results in immediate DNA damage formation [29]. The combination of TMZ and RT resulted in a comparative decrease in the number of differentially expressed DDR genes compared to RT alone across all time points, and the up- or downregulation of DDR genes from either RT or TMZ alone was not always observed in the cells treated with TMZ + RT. This may have occurred as the two treatments alone produce varying degrees of DDR activation across different time points and pathways.

Across the four cell lines, several DDR genes were frequently observed as differentially expressed. The most notable and frequent included *NEIL3*, *XRCC2*, *CCNO*, *RAD54L*, *ATM*, *DDB2*, and *MSH2*, all of which have been linked to treatment resistance in glioma or solid tumours such as colorectal cancer [10,26,33–38]. Interestingly, the expression of *RPA3* and *RAD51C* rarely changed although being associated with OS outcomes in the TCGA cohort, while *ATP23*, was either upregulated or downregulated depending on the cell line. This suggests that baseline expression and associated patient outcome may not entirely capture the direct role such genes play in DDR when examined across time, and further investigation is needed. This study also shows the upregulation of several NER genes in response to TMZ and RT, which is an underreported DDR pathway in glioblastoma. ATR, a global sensor of DNA damage, has been implicated in NER activation [39] and is thus a potential therapeutic target. The transcriptional lens of this study, however, cannot conclusively answer this and an in-depth analysis is required to elucidate the exact function that NER and its components play in response to the standard treatment of glioblastoma, which may reveal druggable targets for its inhibition. Furthermore, our study of DDR expression has focused on characteristic DDR genes with less emphasis on DNA polymerases and ligases that play overlapping functions across pathways [40–42]. Thus, future work will seek to include these genes with overlapping functions to gain greater insight into the response of DDR pathways and their influence on treatment resistance.

Overall, this study reveals an influence of DDR genes and subsequent pathways in glioblastoma cellular responses to treatment. Specific clusters of DDR expression failed to show significant differences in patient survival outcome or cell line response to TMZ

or RT. However, our analysis revealed that the high expression of three DDR genes associated with poorer overall patient survival, while expression of MMR, NER and HR influenced sensitivity to TMZ or RT in glioblastoma cell lines. Our results suggest that the DDR is primarily upregulated within a 24 h period after treatment of TMZ and/or RT, with distinct trends of DDR activation apparent between treatments. Such data give insight into the changes in DDR gene expression in response to standard treatment and the potential for targeting commonly upregulated DDR components to produce radio- or chemo-sensitising agents.

Supplementary Materials: The following supporting information can be downloaded at: <https://www.mdpi.com/article/10.3390/cells11071215/s1>, Figure S1: Combined hierarchical cluster of glioblastoma cell lines and TCGA patients; Figure S2: Cell viability of *MGMT* methylated and unmethylated glioblastoma cell lines treated with TMZ; Figure S3: Distribution of DEGs across time points and treatments; Figure S4: Frequency of DEGs per cell line; Table S1: Gene list of DDR pathways for ssGSEA analysis title; Table S2: List of DDR genes and housekeeping genes; Table S3: Overall survival cox regression analysis of clinical features in glioblastoma TCGA patients ($n = 140$); Table S4: Molecular characteristics and DDR gene expression profiles of patient-derived glioblastoma cell lines; Table S5: Differentially expressed genes (DEGs) across each cell line, time point and treatment.

Author Contributions: M.L. and P.A.T. developed the scope of this study. M.L. performed the experiments, data analysis, developed figures and wrote the manuscript with feedback from P.A.T. and N.A.B. gave input into experimental design and interpretation of results. M.F. gave clinical input on glioblastoma and its treatment. B.W.D. and B.W.S. provided the patient-derived glioblastoma cell lines and associated data for this study. P.A.T., N.A.B., M.C.G., M.F., B.W.D. and B.W.S. gave feedback to M.L. and edited and approved the final manuscript. All authors have read and agreed to the published version of the manuscript.

Funding: This work was supported by a Hunter Medical Research Institute (HMRI) grant (G2100196), a Mark Hughes Foundation Innovation Grant (G1901583) and a Tour de Cure Pioneering Research Grant (G1901173). ML is supported by a University of Newcastle Postgraduate Research Scholarship (UNRS Central), a Tour de Cure PhD Support Scholarship (G1901174) and the HMRI MM Sawyer and Greaves Family PhD Stipend Award in Cancer Research (G2100427).

Institutional Review Board Statement: This study was approved by the Human Research Ethics Committee of the University of Newcastle (H-2020-0389).

Informed Consent Statement: Not applicable.

Data Availability Statement: Research data are stored in an institutional repository and will be shared upon request to the corresponding author.

Acknowledgments: Special thanks to Troy Sykes, Jaclyn Matthews and Kristie Harrison from Genesis-Care, Newcastle NSW for allowing access to their radiation facilities for the irradiation of glioblastoma cell lines.

Conflicts of Interest: The authors declare no conflict of interest.

References

1. Louis, D.N.; Perry, A.; Wesseling, P.; Brat, D.J.; Cree, I.A.; Figarella-Branger, D.; Hawkins, C.; Ng, H.K.; Pfister, S.M.; Reifenberger, G.; et al. The 2021 WHO Classification of Tumors of the Central Nervous System: A summary. *Neuro-Oncology* **2021**, *23*, 1231–1251. [CrossRef] [PubMed]
2. Rubner, Y.; Muth, C.; Strnad, A.; Derer, A.; Sieber, R.; Buslei, R.; Frey, B.; Fietkau, R.; Gaipl, U.S. Fractionated radiotherapy is the main stimulus for the induction of cell death and of Hsp70 release of p53 mutated glioblastoma cell lines. *Radiat. Oncol.* **2014**, *9*, 89. [CrossRef] [PubMed]
3. Poon, M.T.C.; Sudlow, C.L.M.; Figueroa, J.D.; Brennan, P.M. Longer-term (≥ 2 years) survival in patients with glioblastoma in population-based studies pre- and post-2005: A systematic review and meta-analysis. *Sci. Rep.* **2020**, *10*, 11622. [CrossRef] [PubMed]
4. Lozinski, M.; Bowden, N.A.; Graves, M.C.; Fay, M.; Tooney, P.A. DNA damage repair in glioblastoma: Current perspectives on its role in tumour progression, treatment resistance and PIKking potential therapeutic targets. *Cell. Oncol.* **2021**, *44*, 961–981. [CrossRef] [PubMed]

5. Bartkova, J.; Hamerlik, P.; Stockhausen, M.-T.; Ehrmann, J.; Hlobilkova, A.; Laursen, H.; Kalita, O.; Kolar, Z.; Poulsen, H.S.; Broholm, H.; et al. Replication stress and oxidative damage contribute to aberrant constitutive activation of DNA damage signalling in human gliomas. *Oncogene* **2010**, *29*, 5095–5102. [CrossRef] [PubMed]
6. Carruthers, R.D.; Ahmed, S.U.; Ramachandran, S.; Strathdee, K.; Kurian, K.M.; Hedley, A.; Gomez-Roman, N.; Kalna, G.; Neilson, M.P.; Gilmour, L.; et al. Replication Stress Drives Constitutive Activation of the DNA Damage Response and Radioresistance in Glioblastoma Stem-like Cells. *Cancer Res.* **2018**, *78*, 5060–5071. [CrossRef]
7. Yoshimoto, K.; Mizoguchi, M.; Hata, N.; Murata, H.; Hatae, R.; Amano, T.; Nakamizo, A.; Sasaki, T. Complex DNA repair pathways as possible therapeutic targets to overcome temozolomide resistance in glioblastoma. *Front. Oncol.* **2012**, *2*, 186. [CrossRef]
8. Nagel, Z.D.; Kitange, G.J.; Gupta, S.K.; Joughin, B.; Chaim, I.A.; Mazzucato, P.; Lauffenburger, D.A.; Sarkaria, J.N.; Samson, L.D. DNA Repair Capacity in Multiple Pathways Predicts Chemoresistance in Glioblastoma Multiforme. *Cancer Res.* **2017**, *77*, 198–206. [CrossRef]
9. Gobin, M.; Nazarov, P.V.; Warta, R.; Timmer, M.; Reifenberger, G.; Felsberg, J.; Vallar, L.; Chalmers, A.J.; Herold-Mende, C.C.; Goldbrunner, R.; et al. A DNA Repair and Cell-Cycle Gene Expression Signature in Primary and Recurrent Glioblastoma: Prognostic Value and Clinical Implications. *Cancer Res.* **2019**, *79*, 1226–1238. [CrossRef]
10. de Sousa, J.F.; Torrieri, R.; Serafim, R.B.; Di Cristofaro, L.F.M.; Escanfella, F.D.; Ribeiro, R.; Zanette, D.L.; Paçó-Larson, M.L.; da Silva, W.A., Jr.; Tirapelli, D.P.D.C.; et al. Expression signatures of DNA repair genes correlate with survival prognosis of astrocytoma patients. *Tumor Biol.* **2017**, *39*. [CrossRef]
11. Brennan, C.W.; Verhaak, R.G.W.; McKenna, A.; Campos, B.; Nounshmehr, H.; Salama, S.R.; Zheng, S.; Chakravarty, D.; Sanborn, J.Z.; Berman, S.H.; et al. The Somatic Genomic Landscape of Glioblastoma. *Cell* **2013**, *155*, 462–477. [CrossRef] [PubMed]
12. Zhao, S.; Ye, Z.; Stanton, R. Misuse of RPKM or TPM normalization when comparing across samples and sequencing protocols. *RNA* **2020**, *26*, 903–909. [CrossRef] [PubMed]
13. Stringer, B.W.; Day, B.W.; D’Souza, R.; Jamieson, P.R.; Ensbey, K.S.; Bruce, Z.C.; Lim, Y.C.; Goasdoué, K.; Offenhäuser, C.; Akgul, S.; et al. A reference collection of patient-derived cell line and xenograft models of proneural, classical and mesenchymal glioblastoma. *Sci. Rep.* **2019**, *9*, 4902. [CrossRef] [PubMed]
14. Liston, D.R.; Davis, M. Clinically Relevant Concentrations of Anticancer Drugs: A Guide for Nonclinical Studies. *Clin. Cancer Res.* **2017**, *23*, 3489–3498. [CrossRef]
15. Remans, T.; Keunen, E.; Bex, G.J.; Smeets, K.; Vangronsveld, J.; Cuypers, A. Reliable Gene Expression Analysis by Reverse Transcription-Quantitative PCR: Reporting and Minimizing the Uncertainty in Data Accuracy. *Plant Cell* **2014**, *26*, 3829–3837. [CrossRef]
16. Barbie, D.A.; Tamayo, P.; Boehm, J.S.; Kim, S.Y.; Moody, S.E.; Dunn, I.F.; Schinzel, A.C.; Sandy, P.; Meylan, E.; Scholl, C.; et al. Systematic RNA interference reveals that oncogenic KRAS-driven cancers require TBK1. *Nature* **2009**, *462*, 108–112. [CrossRef]
17. Maréchal, A.; Zou, L. DNA Damage Sensing by the ATM and ATR Kinases. *Cold Spring Harb. Perspect. Biol.* **2013**, *5*, a012716. [CrossRef]
18. Stupp, R.; Mason, W.P.; van den Bent, M.J.; Weller, M.; Fisher, B.; Taphoorn, M.J.B.; Belanger, K.; Brandes, A.A.; Marosi, C.; Bogdahn, U.; et al. Radiotherapy plus Concomitant and Adjuvant Temozolomide for Glioblastoma. *N. Engl. J. Med.* **2005**, *352*, 987–996. [CrossRef]
19. Meng, X.; Duan, C.; Pang, H.; Chen, Q.; Han, B.; Zha, C.; Dinislam, M.; Wu, P.; Li, Z.; Zhao, S.; et al. DNA damage repair alterations modulate M2 polarization of microglia to remodel the tumor microenvironment via the p53-mediated MDK expression in glioma. *EBioMedicine* **2019**, *41*, 185–199. [CrossRef]
20. Reaper, P.M.; Griffiths, M.R.; Long, J.M.; Charrier, J.-D.; MacCormick, S.; Charlton, P.A.; Golec, J.M.C.; Pollard, J.R. Selective killing of ATM- or p53-deficient cancer cells through inhibition of ATR. *Nat. Chem. Biol.* **2011**, *7*, 428–430. [CrossRef]
21. Fischer, U.; Rheinheimer, S.; Krempler, A.; Löbrich, M.; Meese, E. Glioma-amplified sequence KUB3 influences double-strand break repair after ionizing radiation. *Int. J. Oncol.* **2013**, *43*, 50–56. [CrossRef] [PubMed]
22. Miller, K.A.; Sawicka, D.; Barsky, D.; Albala, J.S. Domain mapping of the Rad51 paralog protein complexes. *Nucleic Acids Res.* **2004**, *32*, 169–178. [CrossRef] [PubMed]
23. Du, J.; Yan, X.; Mi, S.; Li, Y.; Ji, H.; Hou, K.; Ma, S.; Ba, Y.; Zhou, P.; Chen, L.; et al. Identification of Prognostic Model and Biomarkers for Cancer Stem Cell Characteristics in Glioblastoma by Network Analysis of Multi-Omics Data and Stemness Indices. *Front. Cell Dev. Biol.* **2020**, *8*, 558961. [CrossRef] [PubMed]
24. Ryu, A.H.; Eckalbar, W.L.; Kreimer, A.; Yosef, N.; Ahituv, N. Use antibiotics in cell culture with caution: Genome-wide identification of antibiotic-induced changes in gene expression and regulation. *Sci. Rep.* **2017**, *7*, 7533. [CrossRef] [PubMed]
25. Boccard, S.G.; Marand, S.V.; Geraci, S.; Pycroft, L.; Berger, F.R.; Pelletier, L.A. Inhibition of DNA-repair genes Ercc1 and Mgmt enhances temozolomide efficacy in gliomas treatment: A pre-clinical study. *Oncotarget* **2015**, *6*, 29456–29468. [CrossRef] [PubMed]
26. Felsberg, J.; Thon, N.; Eigenbrod, S.; Hentschel, B.; Sabel, M.C.; Westphal, M.; Schackert, G.; Kreth, F.W.; Pietsch, T.; Löffler, M.; et al. Promoter methylation and expression of MGMT and the DNA mismatch repair genes MLH1, MSH2, MSH6 and PMS2 in paired primary and recurrent glioblastomas. *Int. J. Cancer* **2011**, *129*, 659–670. [CrossRef] [PubMed]
27. King, H.O.; Brend, T.; Payne, H.L.; Wright, A.; Ward, T.; Patel, K.; Egnuni, T.; Stead, L.F.; Patel, A.; Wurdak, H.; et al. RAD51 Is a Selective DNA Repair Target to Radiosensitize Glioma Stem Cells. *Stem Cell Rep.* **2017**, *8*, 125–139. [CrossRef]

28. Kim, N.; Kim, S.H.; Kang, S.-G.; Moon, J.H.; Cho, J.; Suh, C.-O.; Yoon, H.I.; Chang, J.H. ATM mutations improve radio-sensitivity in wild-type isocitrate dehydrogenase-associated high-grade glioma: Retrospective analysis using next-generation sequencing data. *Radiat. Oncol.* **2020**, *15*, 184. [CrossRef]
29. Huang, R.-X.; Zhou, P.-K. DNA damage response signaling pathways and targets for radiotherapy sensitization in cancer. *Signal Transduct. Target. Ther.* **2020**, *5*, 60. [CrossRef]
30. Ferri, A.; Stagni, V.; Barilà, D. Targeting the DNA Damage Response to Overcome Cancer Drug Resistance in Glioblastoma. *Int. J. Mol. Sci.* **2020**, *21*, 4910. [CrossRef]
31. Noonan, E.M.; Shah, D.; Yaffe, M.B.; Lauffenburger, D.A.; Samson, L.D. O6-Methylguanine DNA lesions induce an intra-S-phase arrest from which cells exit into apoptosis governed by early and late multi-pathway signaling network activation. *Integr. Biol.* **2012**, *4*, 1237–1255. [CrossRef] [PubMed]
32. Quiros, S.; Roos, W.; Kaina, B. Processing of O6-methylguanine into DNA double-strand breaks requires two rounds of replication whereas apoptosis is also induced in subsequent cell cycles. *Cell Cycle* **2010**, *9*, 168–178. [CrossRef] [PubMed]
33. Klattenhoff, A.W.; Thakur, M.; Chu, C.S.; Ray, D.; Habib, S.L.; Kidane, D. Loss of *NEIL3* DNA glycosylase markedly increases replication associated double strand breaks and enhances sensitivity to ATR inhibitor in glioblastoma cells. *Oncotarget* **2017**, *8*, 112942–112958. [CrossRef] [PubMed]
34. Struve, N.; Binder, Z.A.; Stead, L.F.; Brend, T.; Bagley, S.J.; Faulkner, C.; Ott, L.; Müller-Goebel, J.; Weik, A.-S.; Hoffer, K.; et al. EGFRvIII upregulates DNA mismatch repair resulting in increased temozolomide sensitivity of *MGMT* promoter methylated glioblastoma. *Oncogene* **2020**, *39*, 3041–3055. [CrossRef] [PubMed]
35. Li, L.; Cao, Y.; Zhou, H.; Li, Y.; He, B.; Zhou, X.; Nie, Z.; Liang, L.; Liu, Y.; Ye, L. Knockdown of *CCNO* decreases the tumorigenicity of gastric cancer by inducing apoptosis. *Oncotargets Ther.* **2018**, *11*, 7471–7481. [CrossRef] [PubMed]
36. Tang, L.; Deng, L.; Bai, H.X.; Sun, J.; Neale, N.; Wu, J.; Wang, Y.; Chang, K.; Huang, R.Y.; Zhang, P.J.; et al. Reduced expression of DNA repair genes and chemosensitivity in 1p19q codeleted lower-grade gliomas. *J. Neuro-Oncol.* **2018**, *139*, 563–571. [CrossRef] [PubMed]
37. Liu, Z.; Zhang, W.; Cheng, X.; Wang, H.; Bian, L.; Wang, J.; Han, Z.; Wang, Y.; Lian, X.; Liu, B.; et al. Overexpressed *XRCC2* as an independent risk factor for poor prognosis in glioma patients. *Mol. Med.* **2021**, *27*, 52. [CrossRef] [PubMed]
38. Qin, C.-J.; Song, X.-M.; Chen, Z.-H.; Ren, X.-Q.; Xu, K.-W.; Jing, H.; He, Y.-L. *XRCC2* as a predictive biomarker for radioresistance in locally advanced rectal cancer patients undergoing preoperative radiotherapy. *Oncotarget* **2015**, *6*, 32193–32204. [CrossRef]
39. Auclair, Y.; Rouget, R.; Affar, E.B.; Drobetsky, E.A. ATR kinase is required for global genomic nucleotide excision repair exclusively during S phase in human cells. *Proc. Natl. Acad. Sci. USA* **2008**, *105*, 17896–17901. [CrossRef]
40. Kurosawa, A.; Saito, S.; So, S.; Hashimoto, M.; Iwabuchi, K.; Watabe, H.; Adachi, N. DNA Ligase IV and Artemis Act Cooperatively to Suppress Homologous Recombination in Human Cells: Implications for DNA Double-Strand Break Repair. *PLoS ONE* **2013**, *8*, e72253. [CrossRef]
41. Hegde, M.L.; Hazra, T.K.; Mitra, S. Early steps in the DNA base excision/single-strand interruption repair pathway in mammalian cells. *Cell Res.* **2008**, *18*, 27–47. [CrossRef] [PubMed]
42. Masani, S.; Han, L.; Meek, K.; Yu, K. Redundant function of DNA ligase 1 and 3 in alternative end-joining during immunoglobulin class switch recombination. *Proc. Natl. Acad. Sci. USA* **2016**, *113*, 1261–1266. [CrossRef] [PubMed]

Article

Single-Cell Molecular Characterization to Partition the Human Glioblastoma Tumor Microenvironment Genetic Background

Francesca Lessi ^{1,*}, Sara Franceschi ¹, Mariangela Morelli ¹, Michele Menicagli ¹, Francesco Pasqualetti ^{2,3}, Orazio Santonocito ⁴, Carlo Gambacciani ⁴, Francesco Pieri ⁴, Filippo Aquila ⁴, Paolo Aretini ¹, and Chiara Maria Mazzanti ¹

- ¹ Section of Genomics and Transcriptomics, Fondazione Pisana per la Scienza, San Giuliano Terme, 56017 Pisa, Italy; s.franceschi@fpscience.it (S.F.); m.morelli@fpscience.it (M.M.); m.menicagli@fpscience.it (M.M.); p.aretini@fpscience.it (P.A.); c.mazzanti@fpscience.it (C.M.M.)
- ² Department of Radiation Oncology, Azienda Ospedaliera Universitaria Pisana, University of Pisa, 56126 Pisa, Italy; francep24@hotmail.com
- ³ Department of Oncology, University of Oxford, Oxford OX1 2JD, UK
- ⁴ Division of Neurosurgery, Spedali Riuniti di Livorno—USL Toscana Nord-Ovest, 57124 Livorno, Italy; orazio.santonocito@uslnordovest.toscana.it (O.S.); carlo.gambacciani@uslnordovest.toscana.it (C.G.); francesco.pieri@uslnordovest.toscana.it (F.P.); filippo.aquila@uslnordovest.toscana.it (F.A.)
- * Correspondence: f.lessi@fpscience.it; Tel.: +39-050-8753545



Citation: Lessi, F.; Franceschi, S.; Morelli, M.; Menicagli, M.; Pasqualetti, F.; Santonocito, O.; Gambacciani, C.; Pieri, F.; Aquila, F.; Aretini, P.; et al. Single-Cell Molecular Characterization to Partition the Human Glioblastoma Tumor Microenvironment Genetic Background. *Cells* **2022**, *11*, 1127. <https://doi.org/10.3390/cells11071127>

Academic Editors: Javier S. Castresana and Bárbara Meléndez

Received: 4 March 2022

Accepted: 24 March 2022

Published: 26 March 2022

Publisher's Note: MDPI stays neutral with regard to jurisdictional claims in published maps and institutional affiliations.



Copyright: © 2022 by the authors. Licensee MDPI, Basel, Switzerland. This article is an open access article distributed under the terms and conditions of the Creative Commons Attribution (CC BY) license (<https://creativecommons.org/licenses/by/4.0/>).

Abstract: Background: Glioblastoma (GB) is a devastating primary brain malignancy. The recurrence of GB is inevitable despite the standard treatment of surgery, chemotherapy, and radiation, and the median survival is limited to around 15 months. The barriers to treatment include the complex interactions among the different cellular components inhabiting the tumor microenvironment. The complex heterogeneous nature of GB cells is helped by the local inflammatory tumor microenvironment, which mostly induces tumor aggressiveness and drug resistance. Methods: By using fluorescent multiple labeling and a DEPArray cell separator, we recovered several single cells or groups of single cells from populations of different origins from IDH-WT GB samples. From each GB sample, we collected astrocytes-like (GFAP+), microglia-like (IBA1+), stem-like cells (CD133+), and endothelial-like cells (CD105+) and performed Copy Number Aberration (CNA) analysis with a low sequencing depth. The same tumors were subjected to a bulk CNA analysis. Results: The tumor partition in its single components allowed single-cell molecular subtyping which revealed new aspects of the GB altered genetic background. Conclusions: Nowadays, single-cell approaches are leading to a new understanding of GB physiology and disease. Moreover, single-cell CNAs resource will permit new insights into genome heterogeneity, mutational processes, and clonal evolution in malignant tissues.

Keywords: single-cell; glioblastoma; tumor microenvironment; copy number aberrations; DEPArray

1. Introduction

Glioblastoma (GB) is the most aggressive and deadly primary tumor of the central nervous system in adults with an overall survival of fewer than 15 months [1]. The extremely poor prognosis of GB, despite the development in recent decades of new and innovative therapies, is enhanced by the resistance developed towards radio and chemotherapy [2]. In this tumor, as well as in other cancer types, the tumor microenvironment (TME) plays a pivotal role in treatment resistance [2]. The GB microenvironment is composed of a massive number of different cells, and besides malignant astrocytes and cancer stem cells, stromal cells, endothelial cells, pericytes, and a huge number of immune cells are present [3]. Moreover, intratumoral heterogeneity (ITH), which is one of the major features of GB tumors, is also hugely involved in anticancer treatment resistance [4,5] and is critical to promote tumoral growth and aggressiveness [6]. In support of this last remark, it has recently been

demonstrated in GB that different sub-clones co-exist within the same tumor that respond differently to differing therapies [7]. These sub-populations of cells show distinct genomic profiles that reveal an individual behavior peculiar to the whole cell population [8]. Currently, the single-cell approach in GB is becoming increasingly popular. Reaching single-cell resolution enables avoiding the averaging of bulk analysis and capturing the heterogeneity of cells. Copy number aberration (CNA) is one of the most important somatic alterations in cancer [9,10], defined as somatic changes to the chromosome structure such as the gain and/or deletion of a particular DNA segment (>1 kb) [11]. The most common CNAs in GB include the loss, or partial loss, of chromosomes 9 and 10; the gain of chromosomes 7, 19, and 20; the focal deletion of the CDKN2A/B locus (9p21.3); and the focal high-level amplification of the EGFR locus (7p11.2) [12,13]. In particular, it is well known that CNAs targeting chromosomes 7 and 10 are some of the earliest events in GB tumor evolution [14]. The analysis of these aberrations is interesting because CNAs are detected with much greater accuracy than individual mutations and are associated with ITH in most cancers [15]. Moreover, the aggregation of cells sharing the same CNA profiles allows improving the phylogenetic analysis at the single nucleotide level [16].

In this work, we collected three human GB tumors and after dissociation, a certain number of single and groups of single cells were isolated through DEPArray technology, paying particular attention to four cell populations: astrocytes-like, microglia-like cells, endothelial-like cells, and stem-like cells. Afterwards, we investigated the genomic aberrations (CNA analysis) in these different types of tumor cells, thus performing a single-cell CNA analysis. The whole parental tumors were subjected to a bulk CNA analysis as well, to compare their molecular profiles with the single-cell results. The tumor partition in its single components allowed single-cell molecular profiling which revealed new aspects of the GB altered genetic background. Our work demonstrates that the single-cell approach is more representative and detailed than the bulk analysis, which contributes to a deeper insight into the basic molecular mechanisms of GB. Moreover, we presented an innovative approach to isolate and characterize different tumor populations of cells at the single-cell level.

2. Materials and Methods

2.1. Human Glioblastoma Tissue Collection

The study has been performed according to the Declaration of Helsinki and the samples' collection protocol was approved by the Ethics Committee of the University Hospital of Pisa (787/2015). Tumor tissues were obtained from patients who underwent surgical resection of histologically confirmed GB after informed consent. Samples were obtained from the Unit of Neurosurgery of Livorno Civil Hospital. Three patient cases (GB01, GB02, and GB03) were included in the present study, the clinical and demographic data and the pathological and therapeutical information are summarized in Table 1. All cases had a diagnosis of GB with no previous history of any brain neoplasia and were not carrying R132 IDH1 or R172 IDH2 mutations. Surgically resected tumors were collected and stored in MACS tissue storage solution (Miltenyi Biotec, Bergisch Gladbach, Germany) at 4 °C for 2–4 h. Each tumor sample was washed with Dulbecco's phosphate-buffered saline (DPBS) in a sterile dish and portioned with a scalpel into about 0.5–2 cm² pieces under a biological hood. Afterward, they were vital frozen at –140 °C in 90% fetal bovine serum (FBS) and 1% dimethyl sulfoxide (DMSO) for further analyses.

Table 1. Patient clinical, demographic, pathological, and therapeutical data.

Cases	Age	Sex	Primary or Recurrence	Brain Location	IDH1/IDH2	Pathology Report	Therapy Administered
GB01	30	M	Primary	parietal lobe	WT	Glioblastoma (Grade IV WHO) (GFAP+, MKI67-20%)	Levetiracetam, Soldesam, Lansoprazole
GB02	47	M	Primary	right temporal lobe	WT	Glioblastoma (Grade IV WHO) (GFAP+, MKI67-30%)	Levetiracetam, Dexamethasone, Omeprazole
GB03	65	M	Primary	right frontal lobe	WT	Glioblastoma (Grade IV WHO) (GFAP+, MKI67-20%)	Levetiracetam, Lansoprazole, Dexamethasone (Mannitol pre-op)

2.2. Tumor Dissociation to Single-Cell Suspensions

Frozen GB tissues were defrosted in a water bath at 37 °C, washed with DPBS in a sterile dish and cut with a scalpel into small pieces. We used 0.11 gr, 0.16 gr, and 0.14 gr of GB01, GB02, and GB03 respectively. These finely minced tumor chunks were transferred in a C-tube (Miltenyi Biotec, Bergisch Gladbach, Germany) with the appropriate volume of buffer X following the protocol (Brain Tumor Dissociation Kit, Miltenyi Biotec, Bergisch Gladbach, Germany) for tumor dissociation with the gentleMACs Dissociator (Miltenyi Biotec, Bergisch Gladbach, Germany).

2.3. Immunofluorescence of Single-Cell Suspensions

The cell suspensions obtained were transferred to 1.5 mL LoBind tubes and washed three times with DPBS. After centrifugation at 300 × g for 10 min at room temperature, the supernatant was removed, and the cells were resuspended in 400 µL of running buffer composed of MACS BSA stock solution (Miltenyi Biotec, Bergisch Gladbach, Germany) 1:20 with autoMACS Rinsing Solution (Miltenyi Biotec, Bergisch Gladbach, Germany). The cells were fixed by adding 400 µL of paraformaldehyde 4%; cells were incubated with fixation solution for 20 min at room temperature. To stop the reaction, the sample tubes were filled with DPBS and centrifuged at 400 × g for 5 min at room temperature. Afterward, we performed two washes with DPBS to the sample tubes and then we incubated the pellet with blocking solution for 10 min at room temperature (BSA 3% in DPBS). The blocking reaction was stopped by filling the tube with DPBS, before centrifugation at 400 × g for 5 min at room temperature. The cells were resuspended in running buffer and counted with a Luna Automated Cell Counter (Logos Biosystems, Anyang-si, Gyeonggi-do, Korea). For the immunofluorescence, a maximum of 100,000 fixed cells was used for the staining. The antibodies chosen for the staining were: anti-GFAP APC (130-124-040, Miltenyi Biotec, Bergisch Gladbach, Germany) for astrocytes, anti-IBA1 PE (ab209942, Abcam, Cambridge, UK) for microglia/macrophages cells, anti-CD105 PerCP/Cy5.5 (ab234265, Abcam, Cambridge, UK) for endothelial cells, anti-CD133 FITC (11-1339-42, eBioscience, San Diego, CA, USA) for stem cells, and Hoechst 33342 (62249, Thermofisher Scientific, Waltham, MA, USA) for nuclei. A total of 20 µL of anti-CD105 and 25 µL of anti-CD133 were added to the cell suspensions and mixed by gently pipetting. The samples were incubated for 15 min in the dark at 4 °C. The reaction was stopped by adding 1 mL of running buffer and mixed by gently pipetting. Then, the sample tubes were centrifuged at 400 × g for 10 min at room temperature, the supernatant was removed, and the cells were resuspended with 100 µL of Inside Perm Buffer (Inside Stain Kit, Miltenyi Biotec, Bergisch Gladbach, Germany). A total of 8 µL of anti-GFAP and 2.5 µL of anti-IBA1 were added to the cell suspensions and mixed by gently pipetting. The samples were incubated for 20 min in the dark at room temperature. The reaction was stopped by adding 1 mL of Inside Perm Buffer, and mixed by gently pipetting. Then, the sample tubes were centrifuged at 400 × g for 10 min at room temperature, the supernatant was removed, and the cells were resuspended

with 1 mL of running buffer. Then, 1 μ L of Hoechst (1 mg/mL) was added to the sample tubes and mixed by gently pipetting. The samples were incubated for 5 min in the dark at room temperature. Then, the sample tubes were centrifuged at $400\times g$ for 10 min at room temperature and resuspended in 200 μ L of running buffer.

2.4. Single-Cell Isolation by DEPArrayTM NxT

Single cells were isolated and sorted with DEPArray NxT (Menarini, Silicon Biosystems, Bologna, Italy). After the immunofluorescence of the single cell suspensions was measured, the cells were counted; we used a maximum of 24,000 cells to load the DEPArray NxT Cartridge. The samples were washed two times with 1 mL of SB115 Buffer (Menarini, Silicon Biosystems, Bologna, Italy) and the cells were loaded onto the DEPArray NxT cartridge following the protocol instructions. CellBrowserTM (Menarini, Silicon Biosystems, Bologna, Italy) analysis software, integrated into the DEPArrayTM system, allows the user to view and select cells from the particle database according to multiple criteria, based on qualitative and quantitative marker evaluation and cell morphology. This software enables the user to create populations and sub-populations of cells using analysis tools such as scatter plots, histograms, and image panels. Cells become un-routable based on their positions; when these are out of the cage, it is no longer possible to move them and therefore complete the recovery. First of all, we excluded clusters of two or three cells, clumps, and spurious events and focused only on single cells with the desired fluorescence, analyzing only the “centered” DAPI cells in the cage. The single cells were selected manually based on fluorescence labeling and morphology. About 20 different single cells were recovered for each tumor patient and volume reduction was performed with a VRNxT-Volume Reduction Instrument (Menarini, Silicon Biosystems, Bologna, Italy) according to the instruction manual. The isolated cells were stored at $-20\text{ }^{\circ}\text{C}$ until later downstream analysis.

2.5. Immunofluorescence of GB Tissues

Formalin-fixed, paraffin-embedded (FFPE) tissue blocks, obtained from our GB samples, were cut into 2–4 μ m thick sections. Antigen unmasking was achieved with Epitote Retrieval Solution (pH = 8) (Leica Microsystems, Wetzlar, Germany) in a microwave. GFAP monoclonal (ASTRO6) (MA5-12023, Thermofisher Scientific, Waltham, MA, USA) and IBA1 polyclonal (091-19741, Wako Chemicals, Neuss, Germany) primary antibodies were then applied at dilutions of 1:100 and 1:1000, respectively, overnight at $4\text{ }^{\circ}\text{C}$. The goat anti-rabbit Alexa Fluor 488 (Thermofisher Scientific, Waltham, MA, USA) and goat anti-mouse Alexa Fluor 568 (Thermofisher Scientific, Waltham, MA, USA) were diluted 1:500 and incubated for 1 h. Cells were counterstained with DAPI (Sigma Aldrich, St. Louis, MO, USA) and visualized using an Olympus Fluoview 3000 confocal microscope at a magnification of $60\times$.

2.6. DNA Extraction from Fresh Tissues

Genomic DNA was extracted directly from up to 50 mg of fresh tissue of GB01, GB02, and GB03 using the Maxwell[®] 16 Instrument with the Maxwell[®] 16 Tissue DNA Purification Kit (Promega, Madison, WI, USA). DNA concentration was determined using the Qubit Fluorometer (Life Technologies, Carlsbad, CA, USA) and the quality was assessed using the Agilent 2200 TapeStation (Agilent Technologies, Santa Clara, CA, USA) system.

2.7. Ampli1TM Whole Genome Amplification and Low Pass Analysis

Whole-genome amplification on all recovered single cells was performed using the Ampli1TM WGA Kit version 02 (Menarini, Silicon Biosystems, Bologna, Italy) following the manufacturer’s instructions. The same procedure was adjusted for the DNA obtained from fresh tissues starting from 1 μ L of 1 ng/ μ L. Afterward, the WGA product was cleaned up with SPRIselect Beads (Beckman Coulter, Brea, CA, USA) and sequencing-ready libraries were prepared with an AmpliTM LowPass Kit (Menarini, Silicon Biosystems, Bologna, Italy) to detect chromosomal aneuploidies and copy number aberrations (CNAs) with a low sequencing depth. To sequence our libraries, we used an Ion 520/530-OT2 kit (Ion

Torrent, Life Technologies, Grand Island, NY, USA) with the Ion 530 Chip (Ion Torrent, Life Technologies, Grand Island, NY, USA). The runs were conducted on the Ion S5 system (Ion Torrent, Life Technologies, Grand Island, NY, USA).

2.8. CNA Calling

The data obtained from low-pass whole genome sequencing were processed with the IchorCNA tool [17]. The CNA segmented number profiles obtained from IchorCNA were processed with the CNApp tool [18] with default cutoffs.

3. Results

3.1. Isolation of Single-Cells from GB Fresh Tissues with DEPArray™ NxT

Three GB fresh tissues obtained from the Unit of Neurosurgery of Livorno Civil Hospital were analyzed with DEPArray™ NxT, the overview of the procedure is shown in Figure 1 in which H&E images for each tumor tissue are also present. After DEPArray NxT Cartridge loading, we selected the routable cells using the CellBrowser™ analysis software. In detail, for GB01, 2880 routable cells, for GB02, 17,378 routable cells, and for GB03, 4788 routable cells, were observed. After that, we performed the exclusion of cell clusters obtaining single and routable cells: 2654, 9535, and 4278 cells respectively for GB01, GB02, and GB03.

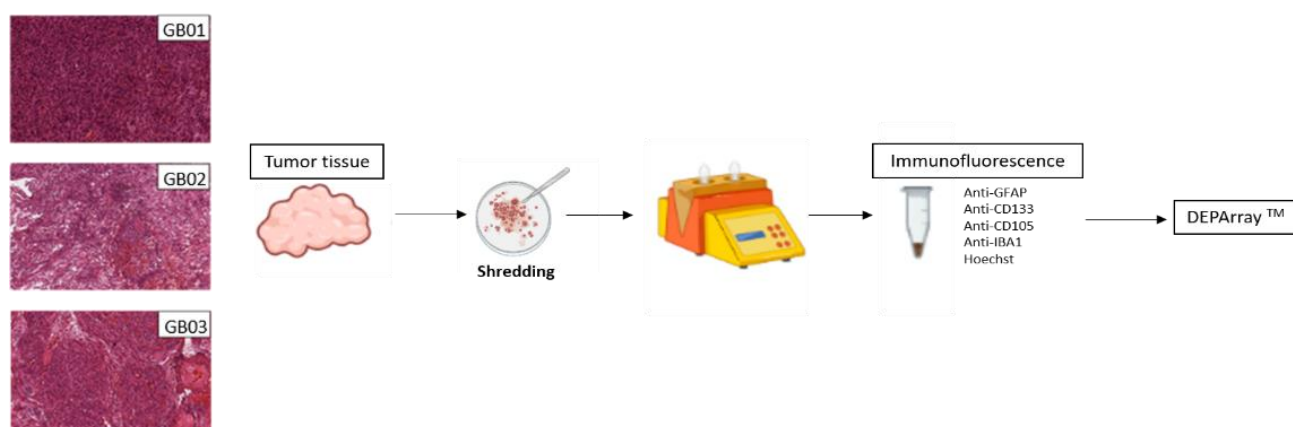


Figure 1. Histological images of GB01, GB02, and GB03. Experimental design starting from tumor shredding to DEPArray analysis.

Cell Populations in GB01, GB02, and GB03

We chose four different conventional markers to identify the four most representative subpopulations of GB (astrocytes, microglia, endothelial cells, and stem cells): GFAP, IBA1, CD105, and CD133. We decided to call them: astrocyte-like, microglia-like, endothelial-like, and stem-like cells because of their similarity to these particular cells. Moreover, we found some cells with double fluorescence staining.

An example of the main populations is shown in Figure 2. In Figure 3, percentages of the main populations found in the three samples are summarized, while in the Supplementary Materials (Figure S1), double fluorescence stained cells and unlabeled cells are shown. We recovered both single cells and groups of a maximum of five single cells with the same characteristics. The recovered cells for the three samples are summarized in Figure 4. In particular, for GB01 we selected 20 cells: 3 single astrocytes-like, 3 groups of astrocytes-like, 4 microglia-like single cells, 2 groups of microglia-like cells, 1 group of endothelial-like cells, 1 single stem-like cell, 2 single astrocytes/microglia-like cells (positive for both GFAP and IBA1), and 3 single cells and 1 group of single cells without labeling (positive to Hoechst 33342 only). For GB02, 26 cells were recovered: 6 single astrocytes-like, 5 microglia-like single cells, 5 single endothelial-like cells, 3 groups of endothelial-like cells, 5 single stem/endothelial-like cells (positive both for CD133 and CD105), 1 group of

stem/endothelial-like cells (positive both for CD133 and CD105), and 1 single cell without labeling (Hoechst 33342 signal only). Finally, for GB03, 17 cells were selected: 6 single astrocytes-like, 5 single microglia-like cells, and 6 single endothelial-like cells.

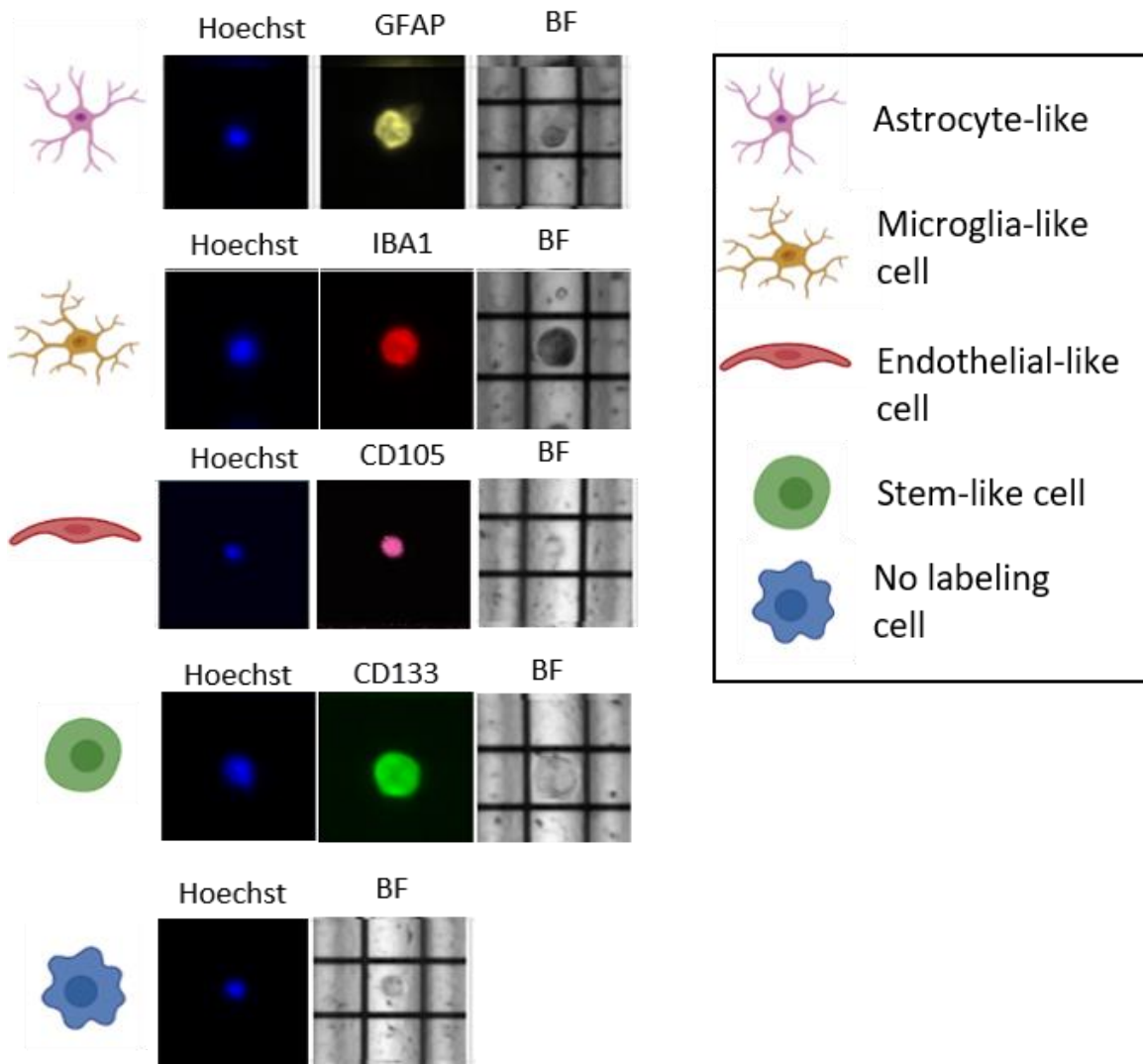


Figure 2. Example of DEPAArray images of single cells belonging to the main GB populations, stained in yellow with GFAP (astrocytes-like), in red with IBA1 (microglia-like), in purple with CD105 (endothelial-like cells), in green with CD133 (stem-like cells) and in blue with Hoechst. BF: Brightfield.

3.2. Copy Number Aberrations (CNAs) Analysis

3.2.1. GB Bulk Tissues

Cellular genomic profiling was performed on the selected cells using the Ampli1™ LowPass kit to identify genome-wide CNAs at the single-cell level and to obtain information on ITH. The same analysis was also carried out on the DNA obtained from fresh tumor tissues (GB01, GB02, and GB03), to compare the bulk molecular profile to the one derived from single cells. In Figure 5, the CNA pattern of the fresh GB tissues is shown: as expected, each sample has a different CNA configuration due to GB ITH. However, all three samples presented chromosome 10q deletion, and GB01 and GB02 also presented chromosome 7 amplification, which represent typical GB alterations. Consequently, for each sample, tumors in bulk and single-cell CNAs were compared.

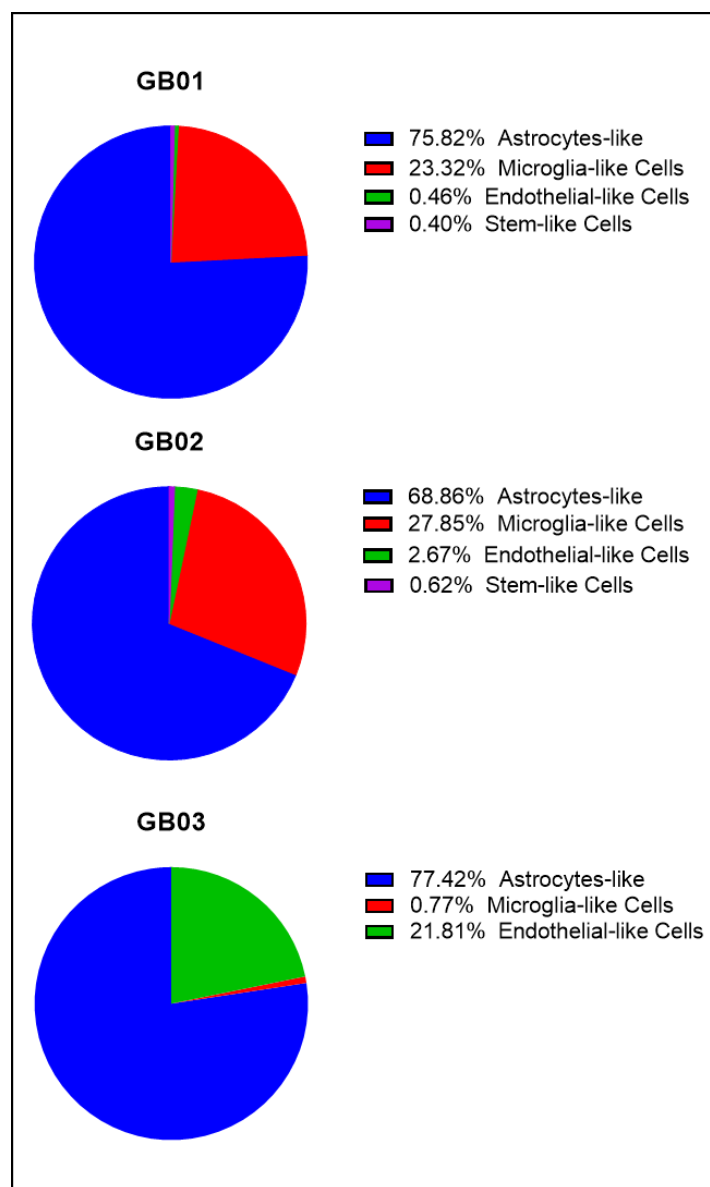


Figure 3. Pie charts of the percentages of the main cell type populations found in GB01, GB02, and GB03.

3.2.2. GB Single Cells

The summarized results obtained from CNA analysis on single cells are described in Tables 2–4. In GB01, we found a group of wild type endothelial-like cells; of these, there were six microglia-like cells (four single cells and two groups of cells), two were wild type (one single cell and one group of cells), one cell showed a chr 19 deletion only, and the other cells showed different alterations, sharing a chr 10 deletion, and chr 7, 9q, and 17q amplifications; six astrocytes-like (three single cells and three groups of cells) were altered, sharing a chr 10 deletion, and chr 7, 9q, and 17q amplifications; one stem-like cell with a chr 1p and 10 deletion and chr 7, 9, 17q, and 19q amplifications. In GB01, moreover, two cells with double staining (GFAP and IBA1) were found with the same alterations, chr 1p and 10 deletions and chr 7, 9, 17q, and 19q amplifications. Finally, three out of four unstained cells (three single and one group of cells) were wild type and one exhibited chr 1p, 10, and 17p deletion and chr 7, 9q, 17q, and 19q amplifications. In GB02, we found eight endothelial-like cells (five single and three groups of cells), two were wild type and the others carried a chr 19 deletion except for only one having chr 9p, 10, 13q, 14q, and 22q deletions. Then, of six single astrocytes-like cells, one was wild type, one had a chr

19 deletion, and the others shared chr 9p, 10, 13q, 14q, and 22q deletions. Indeed, of five single microglia-like cells, two were wild type and three had a chr 19 deletion. In GB02, we selected six double staining cells (CD133 and CD105 positive), of these, four were wild type and the others shared chr 10, 13q, 14q, and 22q deletions. Finally, one unstained cell was wild type. GB03 counted six single endothelial-like cells, four of which were wild type and the other two presented different alterations sharing in particular chr 9p, 10, and 22q deletion and chr 7, 9q, and 20 amplifications. Five single microglia-like cells were all wild type. Finally, six single astrocytes-like were selected, one was wild type while the other cells showed all the same alterations: chr 9p, 10, and 22q deletions and chr 7, 9q, and 20 amplifications.




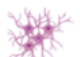















GB01	GB02	GB03
 3 Single GFAP+ cells	 6 Single GFAP+ cells	 6 Single GFAP+ cells
 3 Group of GFAP+ cells	 5 Single IBA1+ cells	 5 Single IBA1+ cells
 4 Single IBA1+ cells	 5 Single CD105+ cells	 6 Single CD105+ cells
 2 Group of IBA1+ cells	 3 Group of CD105+ cells	
 2 Single GFAP+/IBA1+ cells	 5 Single CD133+/CD105+ cells	
 1 Group of CD105+ cells	 1 Group of CD133+/CD105+ cells	
 1 Single CD133+ cell	 1 Single not stained cell	
 1 Group of not stained cells		
 3 Single not stained cells		

Figure 4. Summary of all the recovered cells after DEPArray analysis from GB01, GB02, and GB03. Astrocytes-like, microglia-like, endothelial-like, and stem-like cells were collected. Double staining cells and only Hoechst positive cells are shown.

3.2.3. Comparison between Bulk Tissues and Single Cells

In Figure 6, the comparison between bulk fresh tumor CNAs and single cell CNAs obtained with the CNApp tool is shown. Cells with CNAs have similar alterations to those found in the bulk tissues and also show additional alterations. The molecular alteration profiles in single cells are more strongly highlighted, as in bulk tumors many alterations may be hidden since many cells are analyzed at the same time.

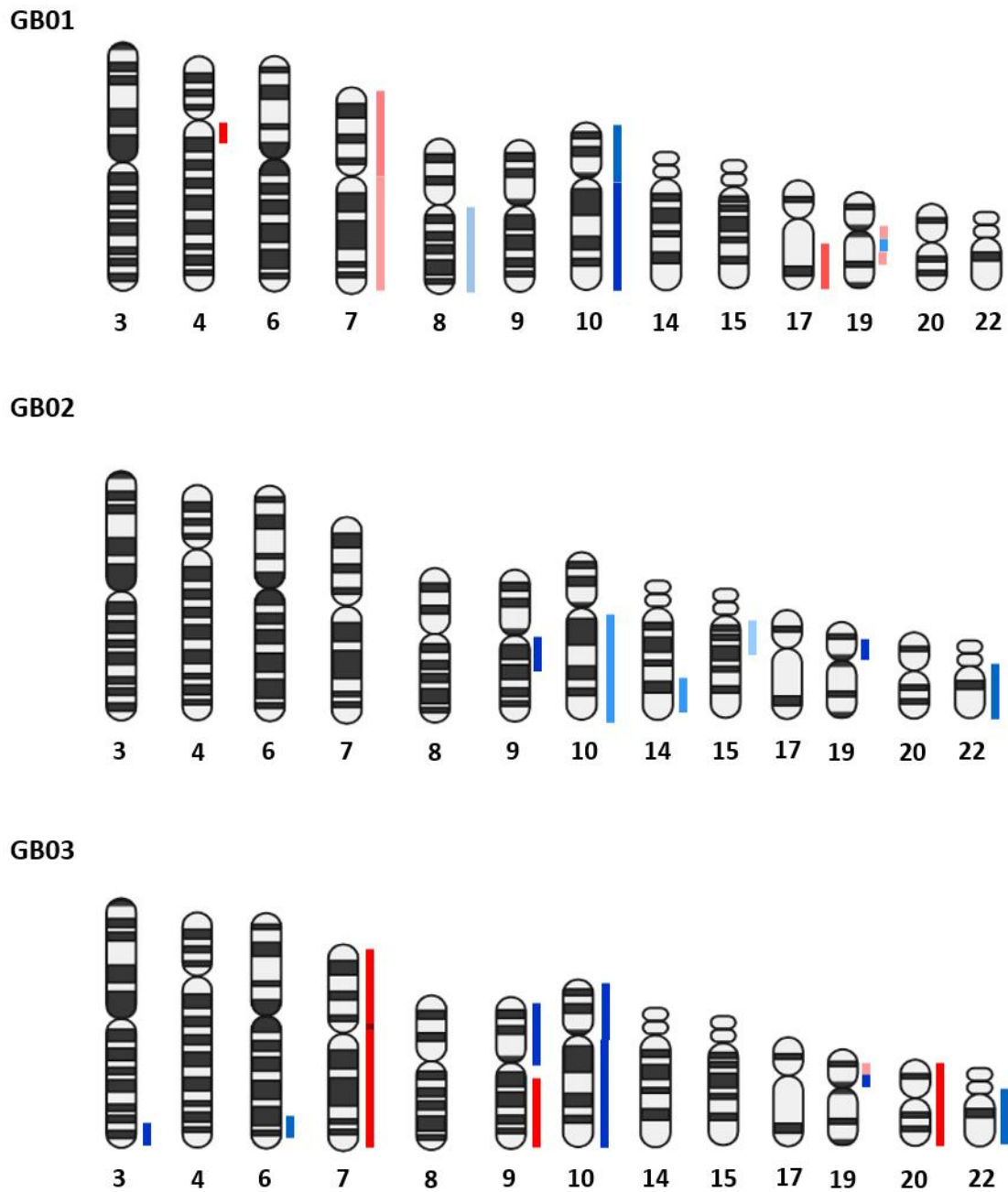


Figure 5. CNA pattern of the fresh GB tissues in bulk. The chromosomal amplifications are shown in red, and in blue the deletions. The intensity of the red and blue color components correlates with the gain and loss values based on the results obtained from the CNApp tool.

3.3. Double Staining Cells Immunofluorescence

To confirm the presence of double staining cells in our tissues, we performed immunofluorescence with anti-GFAP (red) and anti-IBA1 (green) on our tissues' slides. We observed some cells with these characteristics in GB01 tissue slides, as shown in Figure 7.

Table 2. CNAs results obtained after CNApp processing for single cells and groups of single cells collected in the GB01 sample.

GB01	
Single Cells Collected	CNA
Group of endothelial-like cells	WT
Microglia-like cell	19-
Microglia-like cell	WT
Microglia-like cell	1p-, 7+, 9q+, 10-, 17q+, 19+
Microglia-like cell	1q+, 2-, 5+, 7+, 9p-, 9q+, 10-, 17q+, 19+
Group of microglia-like cells	WT
Group of microglia-like cells	7+, 9q+, 10-, 17q+
Astrocyte-like	1p-, 7+, 9q+, 10-, 17q+, 19+
Astrocyte-like	1p-, 7+, 9q+, 10-, 17q+, 19+
Astrocyte-like	1q+, 5+, 7+, 9p-, 9q+, 10-, 17p-, 17q+, 19q+
Group of astrocytes-like	1p-, 7+, 9q+, 10-, 17p-, 17q+, 19+
Group of astrocytes-like	1p-, 7+, 9+, 10-, 17p-, 17q+, 19+
Group of astrocytes-like	1p-, 7+, 9q+, 10-, 17q+
Stem-like cell	1p-, 7+, 9+, 10-, 17q+, 19q+
Astrocyte/microglia-like cell	1p-, 7+, 9+, 10-, 17q+, 19q+
Astrocyte/microglia-like cell	1p-, 7+, 9+, 10-, 17q+, 19+
Not stained cell	WT
Not stained cell	WT
Not stained cell	1p-, 7+, 9q+, 10-, 17p-, 17q+, 19q+
Group of not stained cells	WT

Table 3. CNAs results obtained after CNApp processing for single cells and groups of single cells collected in the GB02 sample.

GB02	
Single Cells Collected	CNA
Endothelial-like cell	WT
Endothelial-like cell	19-
Endothelial-like cell	19-
Endothelial-like cell	19-
Endothelial-like cell	9p-, 10-, 13q-, 14q-, 22q-
Group of endothelial-like cells	WT
Group of endothelial-like cells	19-
Group of endothelial-like cells	19-
Astrocyte-like	WT

Table 3. *Cont.*

GB02	
Single Cells Collected	CNA
Astrocyte-like	19-
Astrocyte-like	9p-, 10-, 13q-, 14q-, 22q-
Astrocyte-like	9p-, 10-, 11- 13q-, 14q-, 19p-, 22q-
Astrocyte-like	9p-, 10-, 11- 13q-, 14q-, 20+, 22q-
Astrocyte-like	9p-, 10-, 13q-, 14q-, 19p-, 20+ 22q-
Microglia-like cell	WT
Microglia-like cell	WT
Microglia-like cell	19-
Microglia-like cell	19-
Microglia-like cell	19-
Endothelial/stem-like cell	WT
Endothelial/stem-like cell	WT
Endothelial/stem-like cell	WT
Endothelial/stem-like cell	9p-, 10-, 13q-, 14q-, 22q-
Endothelial/stem-like cell	10-, 11-, 13q-, 14q-, 16+, 22q-
Group of endothelial/stem-like cells	WT
Not stained cell	9p-, 10-, 13q-, 14q-, 22q-

Table 4. CNAs results obtained after CNApp processing for single cells and groups of single cells collected in the GB03 sample.

GB03	
Single Cells Collected	CNA
Endothelial-like cell	WT
Endothelial-like cell	WT
Endothelial-like cell	WT
Endothelial-like cell	WT
Endothelial-like cell	7+, 9p-, 9q+, 10-, 20+, 22q-
Endothelial-like cell	3q-, 7+, 9p-, 9q+, 10-, 20+, 22q-
Microglia-like cell	WT
Microglia-like cell	WT
Microglia-like cell	WT
Microglia-like cell	WT
Microglia-like cell	WT
Astrocyte-like	WT
Astrocyte-like	7+, 9p-, 9q+, 10-, 20+, 22q-
Astrocyte-like	7+, 9p-, 9q+, 10-, 20+, 22q-
Astrocyte-like	7+, 9p-, 9q+, 10-, 20+, 22q-
Astrocyte-like	7+, 9p-, 9q+, 10-, 20+, 22q-
Astrocyte-like	7+, 9p-, 9q+, 10-, 20+, 22q-

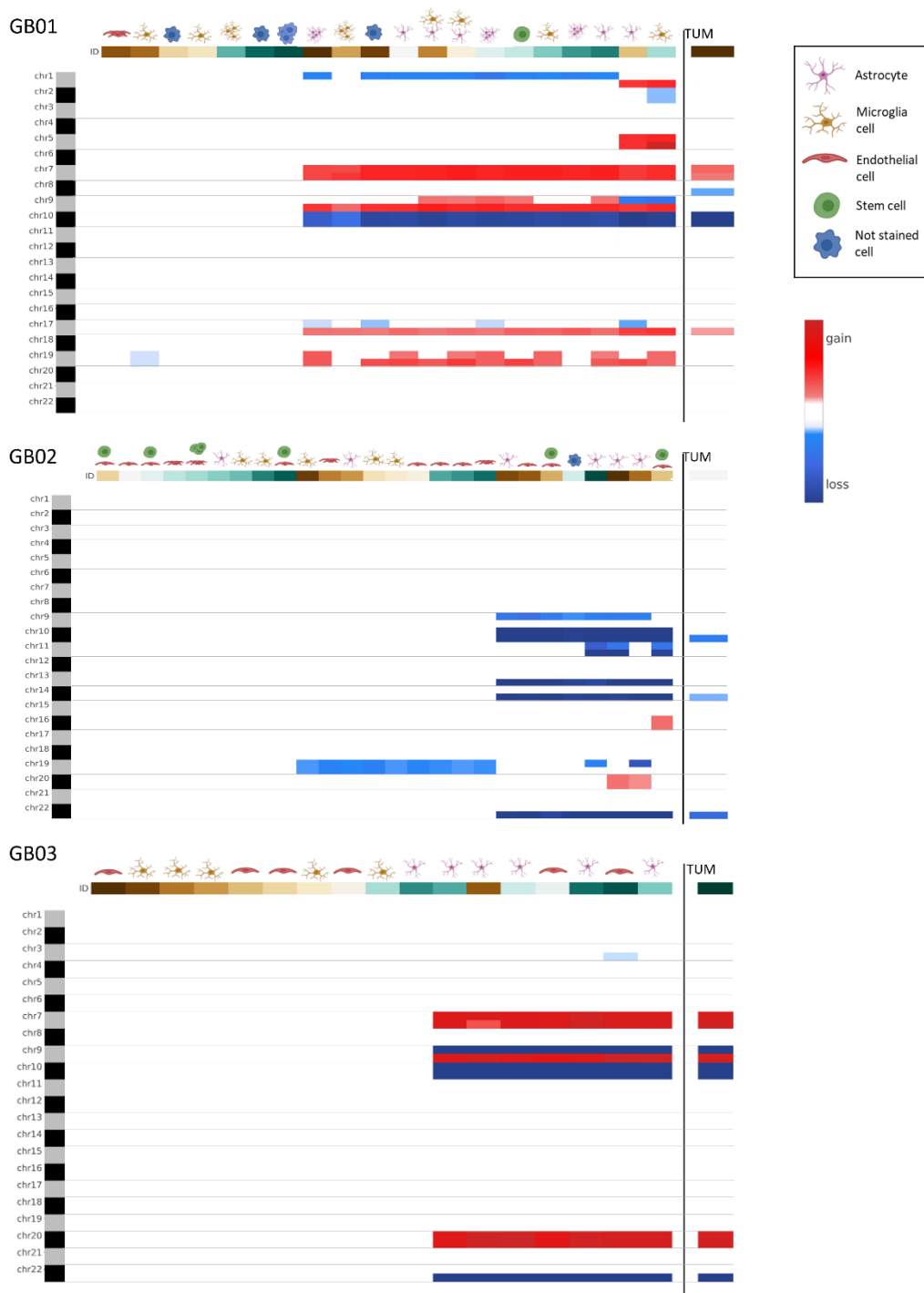


Figure 6. Genome-wide chromosome arm CNA profile heatmap for GB01, GB02, and GB03. For each sample, the CNA profile of the single cells collected is shown and on the right the CNA profile of the tumor tissue in bulk.

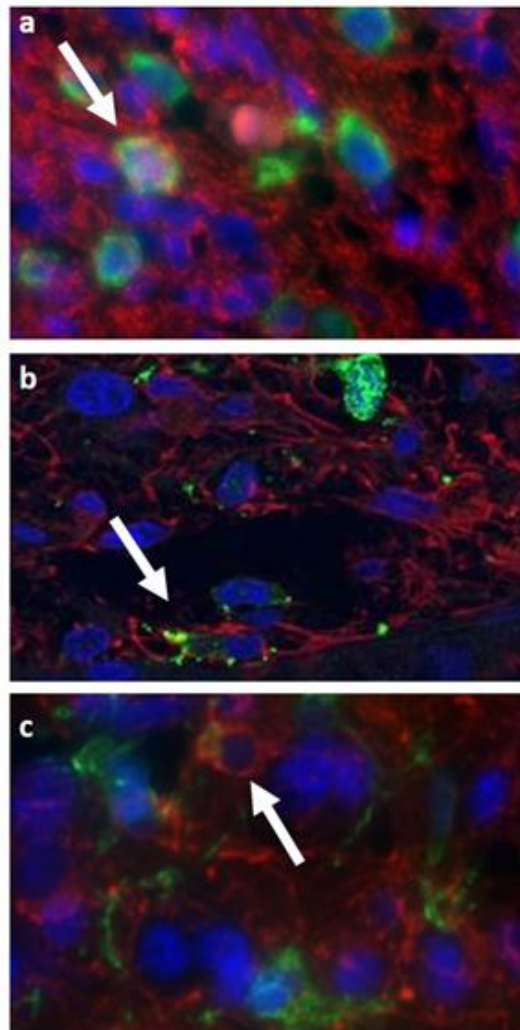


Figure 7. Immunofluorescence assays of GB01 tissue: (a–c) three different portions of GB01 tissue with GFAP (red) and IBA1 (green) markers shown. Arrows indicate cells with the double-positive signal.

4. Discussion

Despite the new therapies developed in the last few years, GB still remains an incurable and devastating disease [19]. The adjective “*multiforme*”, often used to define GB, was coined in 1926 by Percival Bailey and Harvey Cushing [20] to describe the various appearances of necrosis, cysts, and hemorrhage. As a matter of fact, this definition also fits from a molecular point of view to explain the high degree of heterogeneity in GB. The poor prognosis of GB patients is mainly associated with ITH, which represents the presence in the tumor mass of multiple sub-clones, each characterized by different molecular and genomic alterations [21]. The sub-clones’ alterations are certainly masked during bulk tumor analysis [22]. There are several approaches to assess the degree of ITH, such as flow cytometry or more innovative methods such as single-cell sequencing and DEPARray analysis. These are certainly three technologies used to decipher ITH, but none can replace the others; rather, they aim to be complementary. Recently, in some single-cell sequencing studies, to investigate the ITH, CNAs investigations were conducted instead of the identification of individual mutations with a gain in sensitivity and accuracy [4,15,23]. Regarding these different techniques, single-cell RNA seq is mainly a discovery analysis: recent single-cell transcriptome studies in GB have made it possible to identify tumor cell populations and to highlight tumor plasticity and hierarchy [24,25]. DEPARray analysis, instead, allows us to select, isolate, and analyze specific cells or groups of cells providing

a higher level of precision and accuracy in cell selection than traditional flow cytometry, with a high transfer efficiency and unprecedented purity for molecular analysis. In this work, we decided to focus our attention on some of the most representative GB populations: astrocytes, microglia, stem cells, and endothelial cells. We have assumed that we have isolated the above-mentioned cells, based on the positivity of the chosen markers. However, as only one marker is used *per* cell, we cannot be sure that we have exactly the hypothesized cell, so we use the suffix “-like” to describe the cells isolated. Through selection and isolation with DEPArray, we investigated the molecular alterations of the isolated cells by comparing them with whole tumor tissue, in terms of CNAs. Astrocytes are star-shaped cells of the brain with different active roles in both healthy people and in brain pathological conditions [26]. For example, they regulate neural signaling and give support in blood-brain barrier (BBB) formation [26]. Regarding GB tumorigenesis, a much-debated topic concerns the cell-of-origin in the cancer stem cell (CSC) or hierarchical hypothesis: GB stem cells (GSCs) or glioma initiating cells seem to be responsible for tumor formation [3]. They are a small population of stem cells characterized by self-renewal and differentiation properties [27]. GSCs are involved in tumor growth, invasion, and recurrence development [28]. Based on this theory, GSCs can arise from neural stem cells [29] but also from already differentiated astrocytes transformed through genetic and epigenetic mutations [30,31]. Therefore, based on this hypothesis, the cell population initiating GB is composed of a mixture of cells including astrocytes and stem cells. In our work, most of the astrocytes-like cells in all three tumors, were altered with a CNA pattern identical to the bulk tumor. In some cells, more alterations were observed than in the bulk, in support of the concept of the higher sensitivity and accuracy of the single-cell analysis approach. Indeed, the only stem-like cell collected in GB02 showed a CNA pattern typical of a transformed tumor cell. This suggests that the cumulative acquisition of mutations in the stem cells can be responsible for invasive cancer generation.

In the brain, microglial cells, a specialized population of macrophage-like cells, represent resident innate immune cells and are involved in many crucial physiological processes [32]. Microglia have been ignored for a long time but by now it is common knowledge that these cells are an integral part of the tumor, constituting approximately 30% of tumor mass [33] and participating in tumor progression and anti-cancer treatment resistance [34]. Indeed, microglial cells have a key role in many brain diseases [35]. From our results, we observed some microglia-like cells with normal chromosomes sets, as we expected, but we also found some cells presenting CNAs, indicating that within the tumor there are also microglia cells with potential tumoral behavior. From a transcriptional point of view, some alterations have been described in GB microglia [36]. In 2020, Maas and colleagues defined a particular type of transformed microglial cells. In this context, tumoral GB cells hijack microglial gene expression to enhance tumor proliferation, suppressing the immune response [37].

Endothelial cells (ECs) represent the principal components of the BBB [38]. Different brain pathologies, including GB, show molecular alterations of ECs [39]. In GB, vessels are necessary for cancer cell spreading and it has been demonstrated that ECs regulate tumor invasion through crosstalk with GB cells [40]. Our results illustrate the presence of wild type endothelial-like cells also carrying CNAs, confirming that the tumor mass can contain tumor-ECs (also defined tumor-associated ECs) as has been highlighted in some recent publications [41–43]. In these papers, the tumor-associated ECs showed different phenotypic and functional characteristics concerning normal ECs. Moreover, the relationship between ECs and GB tumor cells was demonstrated in two recent studies, in particular it was observed that tumor-derived ECs and GB stem cells shared the same genomic mutations and that CD144 and VEGFR2 genes are expressed by the emerging endothelium [44,45].

Moreover, in our study, we observed and then recovered some cells with a double signal of labeling: astrocytes/microglia-like cells in GB01 and stem/endothelial-like cells in GB02. Indeed, in the literature, the detection of dual positive cells has been reported in

experiments using our same technology, especially in the circulating tumor cell studies [46]. The presence of these double stained cells, in particular GFAP+/IBA1+, was also confirmed by immunofluorescence experiments (Figure S2) to strengthen our findings. Fais et al. in 2007 introduced the concept of cannibalism as an exclusive property of malignant tumor cells [47]. Moreover, Coopman et al. assumed that phagocytosis is the mechanism used by invasive tumor cells to allow migration into the surrounding tissues [48]. In this regard, in malignant gliomas, phagocytic tumor cells were detected, particularly in GB [49,50]. A different hypothesis could be the cell fusion formation, for example, Huysentruyt et al. observed fusion between macrophages and tumor cells [51].

A further aspect that emerged from our results is the detection both in GB01 and in GB02 of some unstained cells with CNAs. We observed, in fact, that not all the astrocytes are positive for GFAP and it has also been demonstrated in the literature that GFAP is not an astrocytes-exclusive marker, as GFAP expression in GB varies significantly [52].

The use of CNAs as a method of evaluating tumor cells is more popular lately. The CNA burden is assessed in different tumors, such as in prostate cancer [53], meaning as the analysis of the variable amounts of amplifications or deletions in different patients. In particular, Hieronymus et al. [53] observed that patients with a high CNA burden showed a greater risk of relapse after treatment. For this reason, CNA analysis can also be considered as a useful marker. Therefore, the tumor CNA burden, rather than individual CNAs, can be associated with cancer outcomes. Recently, CNA analysis has been evaluated as more advantageous than mutational analysis for diagnostic reasons in particular in association with survival [54]: CNAs and miRNA analysis had a better performance than mutational data for poorly predicted survival. In addition, in melanoma, Roh et al. demonstrated that the association of CNAs and the mutational burden can be very useful for prognosis and the response to therapy [55].

To the best of our knowledge, this is the first time that our approach is used to partition a GB tumor tissue into its cellular components and provide its molecular profile. Single-cell CNA analysis has the potential to yield new insights into the molecular dynamics of cellular populations. Measuring single-cell genome alterations in tissues and cell populations will greatly advance the clonal decomposition of malignant tissues, resolving rare cell population genotypes and identifying DNA amplification and the deletion states of individual cells, which are difficult to establish when cellular information is destroyed in bulk sequencing. A novel feature of our approach is also the capture, by brightfield and immunofluorescence imaging, of the morphologic features of cells, permitting analytical integration with genomic properties.

5. Conclusions

In conclusion, in this work, we were able to isolate single cells from fresh GB tissues based on markers that assigned them to the four cell subpopulations: astrocytes, microglia, endothelial cells, and stem cells. CNA analysis allows us to distinguish the tumor cells inside the tumor microenvironment. This is a preliminary work based on an innovative technique, single-cell CNA analysis with DEPArray, to select single tumor cells and study their molecular alterations in depth. This new type of experimental approach is proposed as a complementary procedure to conventional methodologies and provides a baseline for further analyses that aim to explore in depth the different subpopulations in the GB microenvironment. Moreover, the single-cell approach allows a very sensitive analysis rather than bulk analysis, obtaining molecular profiles more accurately. In such an aggressive and lethal tumor, any kind of information is crucial and can be useful to better understand the mechanisms underlying the development of the tumor and its propagation.

Supplementary Materials: The following supporting information can be downloaded at: <https://www.mdpi.com/article/10.3390/cells11071127/s1>, Figure S1: Pie charts of the double-stained cells; Figure 7: Immunofluorescence assay.

Author Contributions: Conceptualization, C.M.M. and F.L.; methodology, F.L.; software, P.A.; validation, M.M. (Michele Menicagli), M.M. (Mariangela Morelli) and S.F.; investigation, F.L.; resources, O.S., C.G., F.P. (Francesco Pieri), and F.A.; data curation, F.P. (Francesco Pasqualetti); writing—original draft preparation, F.L.; writing—review and editing, F.L. and S.F.; visualization, M.M. (Mariangela Morelli); supervision, C.M.M.; project administration, F.P. (Francesco Pasqualetti). All authors have read and agreed to the published version of the manuscript.

Funding: This research received no external funding.

Institutional Review Board Statement: This study was conducted in accordance with the Declaration of Helsinki, and approved by the Ethics Committee of the University Hospital of Pisa (787/2015).

Informed Consent Statement: Informed consent was obtained from all subjects involved in this study.

Conflicts of Interest: The authors declare no conflict of interest.

References



1. Stupp, R.; Hegi, M.E.; Mason, W.P.; van den Bent, M.J.; Taphoorn, M.J.; Janzer, R.C.; Ludwin, S.K.; Allgeier, A.; Fisher, B.; Belanger, K.; et al. Effects of radiotherapy with concomitant and adjuvant temozolomide versus radiotherapy alone on survival in glioblastoma in a randomised phase III study: 5-year analysis of the EORTC-NCIC trial. *Lancet Oncol.* **2009**, *10*, 459–466. [CrossRef]
2. Zhang, X.; Ding, K.; Wang, J.; Li, X.; Zhao, P. Chemoresistance caused by the microenvironment of glioblastoma and the corresponding solutions. *Biomed. Pharmacother.* **2019**, *109*, 39–46. [CrossRef] [PubMed]
3. Hambardzumyan, D.; Bergers, G. Glioblastoma: Defining Tumor Niches. *Trends Cancer* **2015**, *1*, 252. [CrossRef] [PubMed]
4. Patel, A.P.; Tirosh, I.; Trombetta, J.J.; Shalek, A.K.; Gillespie, S.M.; Wakimoto, H.; Cahill, D.P.; Nahed, B.V.; Curry, W.T.; Martuza, R.L.; et al. Single-cell RNA-seq highlights intratumoral heterogeneity in primary glioblastoma. *Science* **2014**, *344*, 1396–1401. [CrossRef] [PubMed]
5. Zhu, Y.; Parada, L.F. The molecular and genetic basis of neurological tumours. *Nat. Rev. Cancer* **2002**, *2*, 616–626. [CrossRef]
6. Yap, T.A.; Gerlinger, M.; Futreal, P.A.; Pusztai, L.; Swanton, C. Intratumor Heterogeneity: Seeing the Wood for the Trees. *Sci. Transl. Med.* **2012**, *4*, 127ps10. [CrossRef]
7. Meyer, M.; Reimand, J.; Lan, X.; Head, R.; Zhu, X.; Kushida, M.; Bayani, J.; Pressey, J.C.; Lionel, A.C.; Clarke, I.D.; et al. Single cell-derived clonal analysis of human glioblastoma links functional and genomic heterogeneity. *Proc. Natl. Acad. Sci. USA* **2015**, *112*, 851–856. [CrossRef]
8. Shlush, L.I.; Hershkovitz, D. Clonal evolution models of tumor heterogeneity. *Am. Soc. Clin. Oncol. Educ. Book. Am. Soc. Clin. Oncol. Annu. Meet.* **2015**, *35*, e662–e665. [CrossRef]
9. Albertson, D.G.; Collins, C.; McCormick, F.; Gray, J.W. Chromosome aberrations in solid tumors. *Nat. Genet.* **2003**, *34*, 369–376. [CrossRef]
10. Shlien, A.; Malkin, D. Copy number variations and cancer. *Genome Med.* **2009**, *1*, 1–9. [CrossRef]
11. Stratton, M.R.; Campbell, P.J.; Futreal, P.A. The cancer genome. *Nature* **2009**, *458*, 719–724. [CrossRef] [PubMed]
12. McLendon, R.; Friedman, A.; Bigner, D.; Van Meir, E.G.; Brat, D.J.; Mastrogiannis, G.M.; Olson, J.J.; Mikkelsen, T.; Lehman, N.; Aldape, K.; et al. Comprehensive genomic characterization defines human glioblastoma genes and core pathways. *Nature* **2008**, *455*, 1061–1068. [CrossRef]
13. Assem, M.; Sibenaller, Z.; Agarwal, S.; Al-Keilani, M.S.; Alqudah, M.A.Y.; Ryken, T.C. Enhancing Diagnosis, Prognosis, and Therapeutic Outcome Prediction of Gliomas Using Genomics. *Omics A J. Integr. Biol.* **2012**, *16*, 113–122. [CrossRef] [PubMed]
14. Stichel, D.; Ebrahimi, A.; Reuss, D.; Schrimpf, D.; Ono, T.; Shirahata, M.; Reifenberger, G.; Weller, M.; Hänggi, D.; Wick, W.; et al. Distribution of EGFR amplification, combined chromosome 7 gain and chromosome 10 loss, and TERT promoter mutation in brain tumors and their potential for the reclassification of IDHwt astrocytoma to glioblastoma. *Acta Neuropathol.* **2018**, *136*, 793–803. [CrossRef] [PubMed]
15. Taylor, A.M.; Shih, J.; Ha, G.; Gao, G.F.; Zhang, X.; Berger, A.C.; Schumacher, S.E.; Wang, C.; Hu, H.; Liu, J.; et al. Genomic and Functional Approaches to Understanding Cancer Aneuploidy. *Cancer Cell* **2018**, *33*, 676. [CrossRef]
16. Laks, E.; McPherson, A.; Zahn, H.; Lai, D.; Steif, A.; Brimhall, J.; Biele, J.; Wang, B.; Masud, T.; Ting, J.; et al. Clonal Decomposition and DNA Replication States Defined by Scaled Single-Cell Genome Sequencing. *Cell* **2019**, *179*, 1207. [CrossRef]
17. Adalsteinsson, V.A.; Ha, G.; Freeman, S.S.; Choudhury, A.D.; Stover, D.G.; Parsons, H.A.; Gydush, G.; Reed, S.C.; Rotem, D.; Rhoades, J.; et al. Scalable whole-exome sequencing of cell-free DNA reveals high concordance with metastatic tumors. *Nat. Commun.* **2017**, *8*, 1–13. [CrossRef]
18. Franch-Expósito, S.; Bassaganyas, L.; Vila-Casadesús, M.; Hernández-Illán, E.; Esteban-Fabro, R.; Díaz-Gay, M.; Lozano, J.J.; Castells, A.; Llovet, J.M.; Castellví-Bel, S.; et al. CNApp, a tool for the quantification of copy number alterations and integrative analysis revealing clinical implications. *Elife* **2020**, *9*, e50267. [CrossRef]
19. Fan, F.; Zhang, H.; Dai, Z.; Zhang, Y.; Xia, Z.; Cao, H.; Yang, K.; Hu, S.; Guo, Y.; Ding, F.; et al. A comprehensive prognostic signature for glioblastoma patients based on transcriptomics and single cell sequencing. *Cell. Oncol. (Dordr)* **2021**, *44*, 917–935. [CrossRef]

20. Bailey, P.; Cushing, H. A Classification of the Tumors of the Glioma Group on a Histogenetic Basis with a Correlated Study of Prognosis. *J. Am. Med. Assoc.* **1926**, *87*, 268. [CrossRef]
21. Burrell, R.A.; McGranahan, N.; Bartek, J.; Swanton, C. The causes and consequences of genetic heterogeneity in cancer evolution. *Nature* **2013**, *501*, 338–345. [CrossRef] [PubMed]
22. Castro, L.N.G.; Tirosh, I.; Suvà, M.L. Decoding Cancer Biology One Cell at a Time. *Cancer Discov.* **2021**, *11*, 960. [CrossRef] [PubMed]
23. Tirosh, I.; Izar, B.; Prakadan, S.M.; Wadsworth, M.H.; Treacy, D.; Trombetta, J.J.; Rotem, A.; Rodman, C.; Lian, C.; Murphy, G.; et al. Dissecting the multicellular ecosystem of metastatic melanoma by single-cell RNA-seq. *Science* **2016**, *352*, 189–196. [CrossRef] [PubMed]
24. Couturier, C.P.; Ayyadhury, S.; Le, P.U.; Nadaf, J.; Monlong, J.; Riva, G.; Allache, R.; Baig, S.; Yan, X.; Bourgey, M.; et al. Single-cell RNA-seq reveals that glioblastoma recapitulates a normal neurodevelopmental hierarchy. *Nat. Commun.* **2020**, *11*, 1–19. [CrossRef] [PubMed]
25. Neftel, C.; Laffy, J.; Filbin, M.G.; Hara, T.; Shore, M.E.; Rahme, G.J.; Richman, A.R.; Silverbush, D.; Shaw, M.L.; Hebert, C.M.; et al. An integrative model of cellular states, plasticity and genetics for glioblastoma. *Cell* **2019**, *178*, 835. [CrossRef] [PubMed]
26. Reemst, K.; Noctor, S.C.; Lucassen, P.J.; Hol, E.M. The Indispensable Roles of Microglia and Astrocytes during Brain Development. *Front. Hum. Neurosci.* **2016**, *10*, 566. [CrossRef]
27. Singh, S.K.; Clarke, I.D.; Terasaki, M.; Bonn, V.E.; Hawkins, C.; Squire, J.; Dirks, P.B. Identification of a Cancer Stem Cell in Human Brain Tumors. *Cancer Res.* **2003**, *63*, 5821–5828.
28. Bao, S.; Wu, Q.; McLendon, R.E.; Hao, Y.; Shi, Q.; Hjelmeland, A.B.; Dewhirst, M.W.; Bigner, D.D.; Rich, J.N. Glioma stem cells promote radioresistance by preferential activation of the DNA damage response. *Nature* **2006**, *444*, 756–760. [CrossRef]
29. Lee, J.H.; Lee, J.E.; Kahng, J.Y.; Kim, S.H.; Park, J.S.; Yoon, S.J.; Um, J.Y.; Kim, W.K.; Lee, J.K.; Park, J.; et al. Human glioblastoma arises from subventricular zone cells with low-level driver mutations. *Nature* **2018**, *560*, 243–247. [CrossRef]
30. Matias, D.; Balça-Silva, J.; da Graça, G.C.; Wanjiru, C.M.; Macharia, L.W.; Nascimento, C.P.; Roque, N.R.; Coelho-Aguiar, J.M.; Pereira, C.M.; Dos Santos, M.F.; et al. Microglia/astrocytes–glioblastoma crosstalk: Crucial molecular mechanisms and microenvironmental factors. *Front. Cell. Neurosci.* **2018**, *12*, 235. [CrossRef]
31. Gimple, R.C.; Bhargava, S.; Dixit, D.; Rich, J.N. Glioblastoma stem cells: Lessons from the tumor hierarchy in a lethal cancer. *Genes Dev.* **2019**, *33*, 591–609. [CrossRef] [PubMed]
32. Keane, L.; Cheray, M.; Blomgren, K.; Joseph, B. Multifaceted microglia-key players in primary brain tumour heterogeneity. *Nat. Rev. Neurol.* **2021**, *17*, 243–259. [CrossRef] [PubMed]
33. Graeber, M.B.; Scheithauer, B.W.; Kreutzberg, G.W. Microglia in brain tumors. *Glia* **2002**, *40*, 252–259. [CrossRef] [PubMed]
34. Leite, D.M.; Zvar Baskovic, B.; Civita, P.; Neto, C.; Gumbleton, M.; Pilkington, G.J. A human co-culture cell model incorporating microglia supports glioblastoma growth and migration, and confers resistance to cytotoxics. *FASEB J.* **2020**, *34*, 1710–1727. [CrossRef] [PubMed]
35. Wolf, S.A.; Boddeke, H.W.G.M.; Kettenmann, H. Microglia in Physiology and Disease. *Annu. Rev. Physiol.* **2017**, *79*, 619–643. [CrossRef] [PubMed]
36. Bowman, R.L.; Klemm, F.; Akkari, L.; Pyonteck, S.M.; Sevenich, L.; Quail, D.F.; Dhara, S.; Simpson, K.; Gardner, E.E.; Iacobuzio-Donahue, C.A.; et al. Macrophage Ontogeny Underlies Differences in Tumor-Specific Education in Brain Malignancies. *Cell Rep.* **2016**, *17*, 2445–2459. [CrossRef]
37. Maas, S.L.N.; Abels, E.R.; Van De Haar, L.L.; Zhang, X.; Morsett, L.; Sil, S.; Guedes, J.; Sen, P.; Prabhakar, S.; Hickman, S.E.; et al. Glioblastoma hijacks microglial gene expression to support tumor growth. *J. Neuroinflamm.* **2020**, *17*, 1–18. [CrossRef] [PubMed]
38. Daneman, R.; Prat, A. The blood–brain barrier. *Cold Spring Harb. Perspect. Biol.* **2015**, *7*, a020412. [CrossRef]
39. Xie, Y.; He, L.; Lugano, R.; Zhang, Y.; Cao, H.; He, Q.; Chao, M.; Liu, B.; Cao, Q.; Wang, J.; et al. Key molecular alterations in endothelial cells in human glioblastoma uncovered through single-cell RNA sequencing. *JCI Insight* **2021**, *6*, e150861. [CrossRef]
40. Chouleur, T.; Tremblay, M.L.; Bikfalvi, A. Mechanisms of invasion in glioblastoma. *Curr. Opin. Oncol.* **2020**, *32*, 631–639. [CrossRef]
41. Charalambous, C.; Hofman, F.M.; Chen, T.C. Functional and phenotypic differences between glioblastoma multiforme-derived and normal human brain endothelial cells. *J. Neurosurg.* **2005**, *102*, 699–705. [CrossRef] [PubMed]
42. Miebach, S.; Grau, S.; Hummel, V.; Rieckmann, P.; Tonn, J.C.; Goldbrunner, R.H. Isolation and culture of microvascular endothelial cells from gliomas of different WHO grades. *J. Neurooncol.* **2006**, *76*, 39–48. [CrossRef] [PubMed]
43. Luissint, A.C.; Artus, C.; Glacial, F.; Ganeshamoorthy, K.; Couraud, P.O. Tight junctions at the blood brain barrier: Physiological architecture and disease-associated dysregulation. *Fluids Barriers CNS* **2012**, *9*, 1–12. [CrossRef] [PubMed]
44. Wang, R.; Chadalavada, K.; Wilshire, J.; Kowalik, U.; Hovinga, K.E.; Geber, A.; Fligelman, B.; Leversha, M.; Brennan, C.; Tabar, V. Glioblastoma stem-like cells give rise to tumour endothelium. *Nature* **2010**, *468*, 829–835. [CrossRef] [PubMed]
45. Ricci-Vitiani, L.; Pallini, R.; Biffoni, M.; Todaro, M.; Invernici, G.; Cenci, T.; Maira, G.; Parati, E.A.; Stassi, G.; Larocca, L.M.; et al. Tumour vascularization via endothelial differentiation of glioblastoma stem-like cells. *Nature* **2010**, *468*, 824–830. [CrossRef] [PubMed]
46. Reduzzi, C.; Vismara, M.; Gerratana, L.; Silvestri, M.; De Braud, F.; Raspagliesi, F.; Verzoni, E.; Di Cosimo, S.; Locati, L.D.; Cristofanilli, M.; et al. The curious phenomenon of dual-positive circulating cells: Longtime overlooked tumor cells. *Semin. Cancer Biol.* **2020**, *60*, 344–350. [CrossRef]
47. Fais, S. Cannibalism: A way to feed on metastatic tumors. *Cancer Lett.* **2007**, *258*, 155–164. [CrossRef]

48. Coopman, P.J.; Do, M.T.; Thompson, E.W.; Mueller, S.C. Phagocytosis of cross-linked gelatin matrix by human breast carcinoma cells correlates with their invasive capacity. *Clin. Cancer Res.* **1998**, *4*, 507–515.
49. Persson, A.; Englund, E. The glioma cell edge—Winning by engulfing the enemy? *Med. Hypotheses* **2009**, *73*, 336–337. [CrossRef]
50. Chang, G.H.F.; Barbaro, N.M.; Pieper, R.O. Phosphatidylserine-dependent phagocytosis of apoptotic glioma cells by normal human microglia, astrocytes, and glioma cells. *Neuro Oncol.* **2000**, *2*, 174–183. [CrossRef]
51. Huysentruyt, L.C.; Seyfried, T.N. Perspectives on the mesenchymal origin of metastatic cancer. *Cancer Metastasis Rev.* **2010**, *29*, 695–707. [CrossRef] [PubMed]
52. Wilhelmsson, U.; Eliasson, C.; Bjerkvig, R.; Pekny, M. Loss of GFAP expression in high-grade astrocytomas does not contribute to tumor development or progression. *Oncogene* **2003**, *22*, 3407–3411. [CrossRef] [PubMed]
53. Hieronymus, H.; Murali, R.; Tin, A.; Yadav, K.; Abida, W.; Moller, H.; Berney, D.; Scher, H.; Carver, B.; Scardino, P.; et al. Tumor copy number alteration burden is a pan-cancer prognostic factor associated with recurrence and death. *Elife* **2018**, *7*, e37294. [CrossRef] [PubMed]
54. Gómez-Rueda, H.; Martínez-Ledesma, E.; Martínez-Torteya, A.; Palacios-Corona, R.; Trevino, V. Integration and comparison of different genomic data for outcome prediction in cancer. *BioData Min.* **2015**, *8*, 1–12. [CrossRef]
55. Roh, W.; Chen, P.L.; Reuben, A.; Spencer, C.N.; Prieto, P.A.; Miller, J.P.; Gopalakrishnan, V.; Wang, F.; Cooper, Z.A.; Reddy, S.M.; et al. Integrated molecular analysis of tumor biopsies on sequential CTLA-4 and PD-1 blockade reveals markers of response and resistance. *Sci. Transl. Med.* **2017**, *9*, eaah3560. [CrossRef]

Article

Combining HDAC and MEK Inhibitors with Radiation against Glioblastoma-Derived Spheres

Eno I. Essien ^{1,2}, Thomas P. Hofer ³, Michael J. Atkinson ⁴ and Nataša Anastasov ^{1,2,*}

- ¹ Institute of Biological and Medical Imaging, Helmholtz Center Munich, German Research Center for Environmental Health, 85764 Neuherberg, Germany; eno.essien@helmholtz-muenchen.de
- ² Institute of Radiation Biology, Helmholtz Center Munich, German Research Center for Environmental Health, 85764 Neuherberg, Germany
- ³ Immunoanalytics Research Group Tissue Control of Immunocytes & Core Facility, German Research Center for Environmental Health, 81377 Munich, Germany; hofer@helmholtz-muenchen.de
- ⁴ Chair of Radiation Biology, Technical University of Munich, 80333 Munich, Germany; m.j.atkinson@tum.de
- * Correspondence: natasa.anastasov@helmholtz-muenchen.de; Tel.: +49-893-187-3798; Fax: +49-893-187-3378

Abstract: Glioblastoma stem-like cells (GSLCs) in glioblastoma limit effective treatment and promote therapeutic resistance and tumor recurrence. Using a combined radiation and drug-screening platform, we tested the combination of a histone deacetylase inhibitor (HDACi) and MAPK/ERK kinase inhibitor (MEKi) with radiation to predict the efficacy against GSLCs. To mimic a stem-like phenotype, glioblastoma-derived spheres were used and treated with a combination of HDACi (MS-275) and MEKi (TAK-733 or trametinib) with 4 Gy irradiation. The sphere-forming ability after the combined radiochemotherapy was investigated using a sphere formation assay, while the expression levels of the GSLC markers (CD44, Nestin and SOX2) after treatment were analyzed using Western blotting and flow cytometry. The combined radiochemotherapy treatment inhibited the sphere formation in both glioblastoma-derived spheres, decreased the expression of the GSLC markers in a cell-line dependent manner and increased the dead cell population. Finally, we showed that the combined treatment with radiation was more effective at reducing the GSLC markers compared to the standard treatment of temozolomide and radiation. These results suggest that combining HDAC and MEK inhibition with radiation may offer a new strategy to improve the treatment of glioblastoma.

Keywords: glioblastoma; glioblastoma-derived spheres; HDAC inhibitor; MEK inhibitor; radiation; combination therapy



Citation: Essien, E.I.; Hofer, T.P.; Atkinson, M.J.; Anastasov, N. Combining HDAC and MEK Inhibitors with Radiation against Glioblastoma-Derived Spheres. *Cells* **2022**, *11*, 775. <https://doi.org/10.3390/cells11050775>

Academic Editors: Javier S. Castresana and Bárbara Meléndez

Received: 31 January 2022

Accepted: 18 February 2022

Published: 23 February 2022

Publisher's Note: MDPI stays neutral with regard to jurisdictional claims in published maps and institutional affiliations.



Copyright: © 2022 by the authors. Licensee MDPI, Basel, Switzerland. This article is an open access article distributed under the terms and conditions of the Creative Commons Attribution (CC BY) license (<https://creativecommons.org/licenses/by/4.0/>).

1. Introduction

Glioblastoma (GB), a grade IV astrocytoma, is one of the most aggressive primary brain tumors. Despite the adoption of a standard therapy combining surgical resection, radiotherapy and chemotherapy with temozolomide (TMZ), the poor prognoses of patients with GB have failed to improve, with a median survival of only 14.6 months [1]. One factor that limits the success of GB therapy is the presence of a sub-population of glioblastoma stem-like cells (GSLCs) within the tumor [2]. These GSLCs possess characteristics of tissue stem cells, including the ability to self-renew and to generate further malignant progeny [3]. GSLCs are considered to be drug and radiation resistant, as well as promote tumor angiogenesis and tumor recurrence, all of which hinder the effective treatment of GB [2,4,5]. A therapeutic strategy that improves the control of GSLCs offers an opportunity to improve treatment outcomes for GB.

One approach against GB may be to inhibit the MAPK/ERK kinase (MEK), situated downstream of the *RAS-RAF-MEK-MAPK* pathway, stimulating the proliferation and

survival of GSLCs [6,7]. The MAPK pathway is activated by a series of phosphorylation events that can be targeted through MEK, the downstream activator of MAPK. Trametinib and TAK-733 are small-molecule-selective MEK inhibitors with antitumor activity in cancers, such as gliomas, multiple myeloma, melanoma and triple-negative breast cancer [8–12]. Trametinib has recently been applied in clinical studies of brain tumors, suggesting that it has the ability to cross the blood–brain barrier (BBB) [13,14]. Although these MEK inhibitors (MEKi) were found to have good safety profiles in clinical trials, they only exhibited limited antitumor activity as single agents due to resistance [10,11,15]. Therefore, MEKi in combination with other anti-cancer agents may lead to more effective therapies. For instance, we recently showed that the effect of TAK-733 on reducing the migratory potential of breast cancer cells was enhanced by 4 Gy irradiation [12].

Various studies reported enhanced antitumor activity when combining MEK and histone deacetylases inhibitors (HDACis) [16–19]. HDACs are enzymes that decrease acetylation and are epigenetic regulators of gene expression that contribute to the pathogenesis of cancers, such as GB. Therefore, HDACis are considered promising therapeutics for cancer treatment [20,21]. For example, it was shown that the HDACis Entinostat (MS-275) and trichostatin A (TSA) inhibited the formation of GB-derived neurospheres and reduced GB xenograft growth [22]. It is also noteworthy that MS-275 demonstrated the ability to cross the BBB in vivo via increased acetylation of histone H3 in brain tissue of syngeneic rats after intratumoral injection [23]. Several other HDACis showed promising results in preclinical studies but few made it to clinical trials due to limited efficacy for GB therapy as a single treatment [24]. However, the combined effect of HDACis with other anticancer agents seems more promising and is being investigated in preclinical and clinical combination studies [24–26].

The combination of an HDACi and a MEKi showed promising results in other cancers [16,27,28] but, to date, has not been explored regarding GB. Clinical studies of GB revealed that monotherapy with newly discovered therapeutics failed to improve survival [29]. In addition, tumor heterogeneity, as well as multiple dysregulated pathways, characterizes GB; therefore, a combination treatment strategy was proposed as the most effective approach to improve therapy [30]. Thus, the aim of our study was to investigate the potential effects of combining the HDACi MS-275 and the MEKi TAK-733 or trametinib with radiation using human GB-derived spheres that mimic a stem-like phenotype. A panel of markers (ALDH1A1, CD133, CD44, Nestin and SOX2) that is associated with stemness to drive tumorigenesis was used to measure and predict the effect of this radiochemotherapy approach against GSLCs. The results demonstrated that this multimodal therapeutic strategy is promising and could offer an opportunity to improve the treatment and survival of GB patients.

2. Materials and Methods

2.1. Growth and Maintenance of Cell Lines

The human GB cell lines U87 and U251 were obtained from Sirion Biotech GmbH (Martinsried, Germany). Both GB cell lines were cultured in high-glucose Dulbecco's Modified Eagle Medium (DMEM) with GlutaMAX™-I, 4.5 g/L glucose, pyruvate and 10% FCS. The cell lines were maintained under standard incubator conditions at 37 °C in a humidified atmosphere containing 5% CO₂. In addition, the U87 and U251 cell lines were cultured as spheres (U87-sph and U251-sph) in a serum-free DMEM/F12 high-glucose medium with GlutaMAX™-I, 4.5 g/L glucose and pyruvate to induce a stem-like phenotype. The stem cell supplements were 1× B27 supplement (Gibco Life Technologies, Darmstadt, Germany), 1× N2 supplement (Gibco Life Technologies, Darmstadt, Germany), 1× Penicillin-Streptomycin (Sigma-Aldrich, Steinheim, Germany), 1× D-(+)-Glucose Solution 45% in H₂O (Sigma-Aldrich, Steinheim, Germany), 20 ng/mL Epidermal Growth Factor (EGF) Human+ (Sigma-Aldrich, Steinheim, Germany), and

20 ng/mL Fibroblast Growth Factor (FGF) Basic Human+ (Sigma-Aldrich, Steinheim, Germany). The glioblastoma-derived spheres were cultured for at least eight passages and the expressions of stem cell markers were analyzed before they were used for experiments. The cell lines were checked for mycoplasma contamination using the MycoAlert Detection Kit (Lonza Group Ltd., Basel, Switzerland), while the cell line authentication was done via genetic profiling using the PowerPlex[®] 21 System (Eurofins, Ebersberg, Germany).

2.2. Web Database Analysis of GB

The GEPIA web server (<http://gepia.cancer-pku.cn>, accessed on 19 January 2021) [31] was used to obtain the GB stem cell marker expression. Box plots were downloaded to compare the CD44, Nestin and SOX2 expression levels between non-cancerous (207 samples) and GB tumor samples (163 samples) from the TCGA and GTEx databases.

2.3. Immunofluorescence Assay

The assay was performed by seeding 4×10^5 cells (U87, U87-sph, U251 and U251-sph) on microscopic slides placed in 4-well chambered plates and left overnight. The cells were fixed the next day in 4% paraformaldehyde (PFA) for 15 min at room temperature, followed by 3 washes with PBS. Permeabilization was done with 0.2% Triton X-100 for 5 min (only for the intracellular staining of ALDH1A1, SOX2 and Nestin). The cells were washed 2 times in PBS and blocked in 1% BSA and 0.15% glycine in PBS for 1 h at room temperature. After blocking, incubation was done overnight at 4 °C with the following antibodies; ALDH1A1 (36671, 1:100; Cell Signalling Technology, Danvers, MA, USA), CD133 (Ab16518, 1:100; Abcam, Cambridge, UK), CD44 (3570s, 1:1000; Cell Signaling Technology, Danvers, MA, USA), SOX2 (3579s, 1:500; Cell Signaling Technology, Danvers, MA, USA) and Nestin (MA1-110, 1:500; Thermo Fisher Scientific, Darmstadt, Germany). The next day, the cells were washed with PBS and incubated with the secondary antibody mix for 1 h at room temperature. The secondary antibodies were Cy3-Goat Anti-Rabbit (A10520, Red, 1:300) and Alexa Flour 488-Goat Anti-Mouse (A11029, Green, 1:200, Life Technologies, Eugene, OR, USA). The cells were washed 3 times with PBS and cell nuclei were stained with DAPI. Imaging of cells was performed at a magnification of 40× using a Keyence BZ 9000 fluorescence microscope (Keyence, Frankfurt, Germany).

2.4. Treatment with HDACi, MEKi and Radiation

The GB-derived spheres were treated according to previously published protocols [26,32]. Briefly, the following conditions were applied: (1) 1 μM of the HDACi MS-275 (S1053; purchased from Selleck Chemicals), (2) 1 μM of the MEKi TAK-733 (S2617; purchased from Selleck Chemicals), (3) 1 μM trametinib (S2673; purchased from Selleck Chemicals), (4) a combination of 1 μM MS-275 plus 1 μM TAK-733 or (5) a combination of 1 μM MS-275 plus 1 μM trametinib. Where specified, the GB-derived spheres were treated with the standard compound TMZ at 50 μM (SC-203292; purchased from Santa Cruz Biotechnology, Dallas, TX, USA) for comparison. All compounds were diluted to give a final concentration of 1% *v/v* DMSO and the controls were treated with 1% *v/v* DMSO. The GB-derived spheres were treated 72 h after seeding the cells to allow time for sphere formation. After 24 h of compound treatment, the spheres were irradiated at room temperature with X-rays using an X-Strahl RS225 radiation device (X-Strahl LTD, Camberlay, UK). The 4 Gy irradiation dose was delivered at a rate of 0.824 Gy/min using a 3 mm aluminum filter. The sham irradiated controls were handled under the same conditions but were not exposed to radiation.

2.5. Cell Viability Assay

Cell viability was tested using CellTiter-Glo[®] Luminescent Cell Viability Assays (Cat.Nr. G75751) according to the manufacturer's instructions (Promega, Madison, WI, USA) and previously published data [12]. U87-sph and U251-sph cells were seeded at 3×10^5 cells per well in 12-well ultra-low-attachment (ULA) plates (Corning, NY, USA). Since the spheres were dissociated into single cells for seeding, the spheroid formation was allowed for 72 h. This was followed by treatment with increasing concentrations of MS-275, TAK-733, trametinib and TMZ at 1 μ M, 10 μ M and 50 μ M. Irradiation was done 24 h after treatment at 4 Gy and incubated for an additional 72 h to have a final time point for analysis of 96 h. After this period, the spheres were dissociated with Accutase and counted to re-seed them at 1×10^4 in 96-well ULA plates. The cell CellTiter-Glo[®] reagent was added after 72 h under cell culture conditions. Incubation was done for 10 min at room temperature before recording the luminescence at 560 nm emission using an infinite M200 plate reader (TECAN, Maennedorf, Switzerland). The measurements were performed in quadruplicates for three independent experiments.

2.6. Sphere Formation Assay

After 72 h of treatment (described in Section 2.4) with both compounds and radiation, the GB-derived spheres were harvested and reseeded in triplicates at 200 cells per well in 96-well ULA plates (Corning Inc., Corning, NY, USA) and cultured for at least 2 weeks. The images of spheres in each well were taken using an Operetta imaging system (PerkinElmer, Waltham, MA, USA). The images were taken using the brightfield channel and 10 \times magnification, while the sphere number per well was counted manually. The sphere formation rate was determined by the number of spheres formed divided by the total number of starting cells.

2.7. Western Blot Analysis

Cell pellets were collected after 72 h of compound and radiation treatment (described in Section 2.4). Lysing, protein extraction and immunoblotting were performed as previously described [12]. The target proteins of the GSLC markers were detected with the same antibodies used for immunofluorescence staining listed in Section 2.3, including Acetyl-Histone H3 (9677) and Histone H3 (4499, 1:1000; Cell Signaling, Danvers, MA, USA), MAPK (9101) and phospho-MAPK (9102, Cell Signaling, Danvers, MA, USA), with β -Actin (A5441, 1:20,000; Sigma Aldrich, Steinheim, Germany) as the loading control. The secondary antibodies were horseradish peroxidase-conjugated anti-mouse (A16066, 1:20,000) and anti-rabbit (A16096, 1:10,000; Invitrogen, Carlsbad, CA, USA). The bands of the secondary bound antibodies were detected using enhanced chemiluminescence (ECL) (Amersham, England) reagents. The luminescent signal was detected and captured using an Alpha Innotech ChemiImager system (Biozym, Hessisch Oldendorf, Germany). The GSLC markers ALDH1A1 and CD133 were not detected well using Western blotting and, therefore, excluded from further analysis.

In the case of reprobing, the membranes were stripped with Restore PLUS Western Blot Stripping Buffer (Thermo Scientific, Rockford, IL, USA) for 15 min at room temperature. For the quantification of the band intensities, the Image-J image analysis software [33] was used.

2.8. Flow Cytometry Analysis

The cells were harvested 72 h after treatment (described in Section 2.4) and washed once with PBS. Afterward, the cells were blocked in Anti-Hu Fc Receptor Binding Inhibitor (14916173, 1:10 in PBS, Invitrogen, Carlsbad, CA, USA) for 10 min at 4 $^{\circ}$ C and then washed with PBS. Live–dead staining of cells was done via incubation with a Zombie Aqua[™] Fixable Viability Kit (423101, 1:100 in PBS, BioLegend, San Diego, CA, USA) for 30 min at room temperature. After washing in FACS buffer (0.5% BSA in PBS), the cells were stained with BV-785-conjugated CD44 (103041, 1:100; Biole-

gend, San Diego, CA, USA) diluted in FACS buffer and incubated for 30 min at 4 °C. Next, the cells were fixed in 1× fixation buffer for 30 min at room temperature and washed with 1× permeabilization buffer using the Foxp3/Transcription Factor Staining Buffer Set (5523, Invitrogen, Carlsbad, CA, USA). This was followed by incubation with an antibody mix of APC-Conjugated Nestin (MA5-23650, 1:100; Thermo Fisher Scientific, Darmstadt, Germany) and PerCP-Cy5.5-Conjugated SOX2 (561506, 1:50; BD Biosciences, San Diego CA, USA) in 1× permeabilization buffer for 1 h at room temperature. Additionally, staining with PerCP-CyTM5.5 Mouse IgG1 κ Isotype Control (550795, 1:50; BD Biosciences, San Diego CA, USA) was applied. The cells were washed twice in 1× permeabilization buffer, resuspended in PBS and passed through a 40 µm mesh filter into FACS tubes to remove clumped cells and obtain a single-cell suspension.

The cells were analyzed via flow cytometry using a CytoFLEX LX Flow Cytometer and CytExpert software (Beckman Coulter, Krefeld, Germany). The CytoFLEX LX instrument has a capacity for 21 fluorescence detections and is equipped with a 355 nm (UV) laser, 405 nm (violet) laser, 488 nm (blue) laser, 561 nm (yellow-green) laser, 638 nm (red) laser and 808 nm (infrared) laser. Fluorescence and side scatter light of the CytoFLEX LX were delivered via fiber optics to avalanche photodiode detector arrays, while the emission profiles were collected using reflective optics and single-transmission band-pass filters. Unstained cells were used to set the voltages, while compensation beads (BD Biosciences, San Diego, CA, USA) were used for compensation to correct for spectral overlap across the fluorescent channels. The gating strategy to set a cut-off for negative and positive populations was done using two gating controls. First, unstained cells were used to set negative and positive gates, while the fluorescence minus one (FMO) control was used to address any spillover-induced background [34]. Additionally, an isotype control for SOX2 was included to set gates against non-specific antibody binding. The gating region on the controls was set to contain less than 1% of the cells for both single- and double-positive populations (Figures S4, S5 and S7).

2.9. Statistical Analysis

All experiments consisted of three biological replicates unless otherwise indicated and the data represent the mean ± standard error of the mean (SEM). The differences in mean values between two groups (control and treated) were compared using Student's t-tests and statistical significance defined with *p*-values as follows: * *p* ≤ 0.05, ** *p* ≤ 0.01 and *** *p* ≤ 0.001.

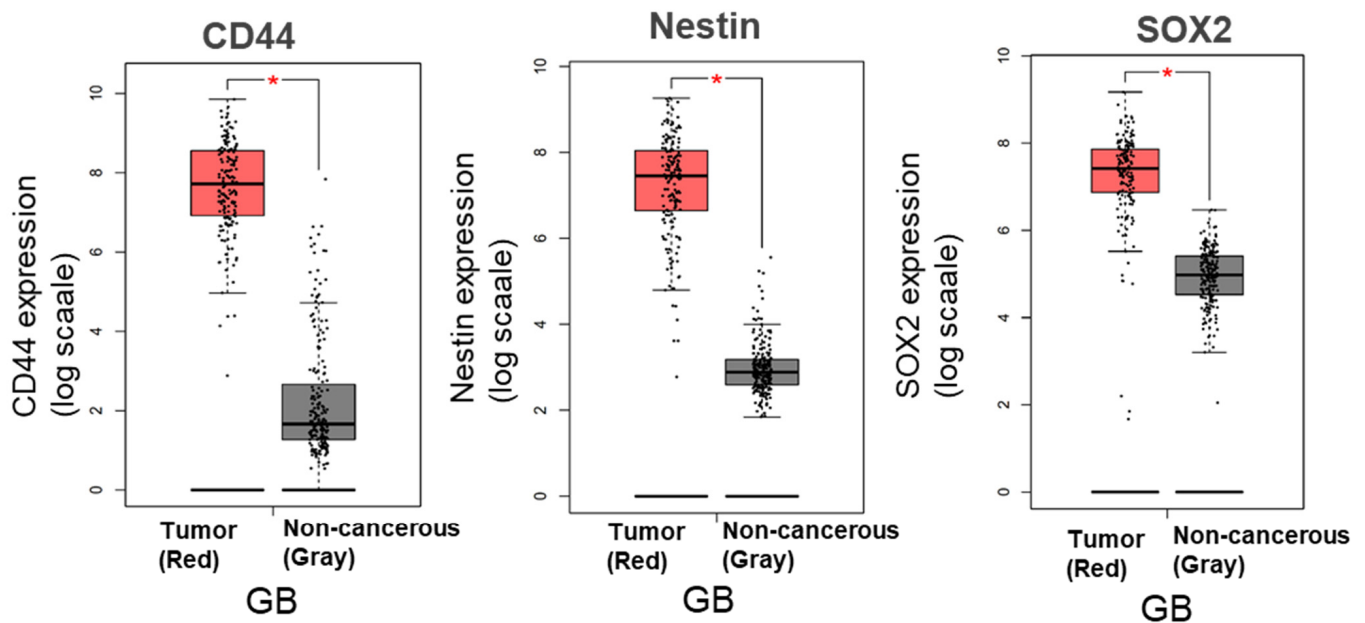
3. Results

3.1. Influence of Radiation Alone on Specific GSLC Marker Expression

The expression of CD44, Nestin and SOX2 in the GB samples and adjacent non-cancerous brain tissue were examined using the GEPIA webserver to interrogate publicly available gene expression databases from the TCGA and GTEx projects. Within the matched TCGA normal and GTEx data, 163 GB tumor samples and 207 non-cancerous samples were analyzed. The gene expression of CD44, Nestin and SOX2 were all significantly higher in GB tumor samples than in the non-cancerous tissue samples (Figure 1a).

The protein expressions of CD44, Nestin and SOX2 were further detected in the U87 and U251 human GB cell lines. All three markers could be detected in both cell lines, except for SOX2 not detected in U87. Additionally, the effect of radiation alone was investigated and it was observed that there was no beneficial effect on the expression of the GSLC markers 72 h after 4 Gy radiation in vitro (Figure 2b). Since Nestin, CD44 and SOX2 are associated with stemness in GB, their elevated levels in the GB tumor samples suggested that these markers may drive the progression and radioresistance of GB.

(a) Glioblastoma stem cell marker expression in GB (TCGA and GTEx database)



(b)

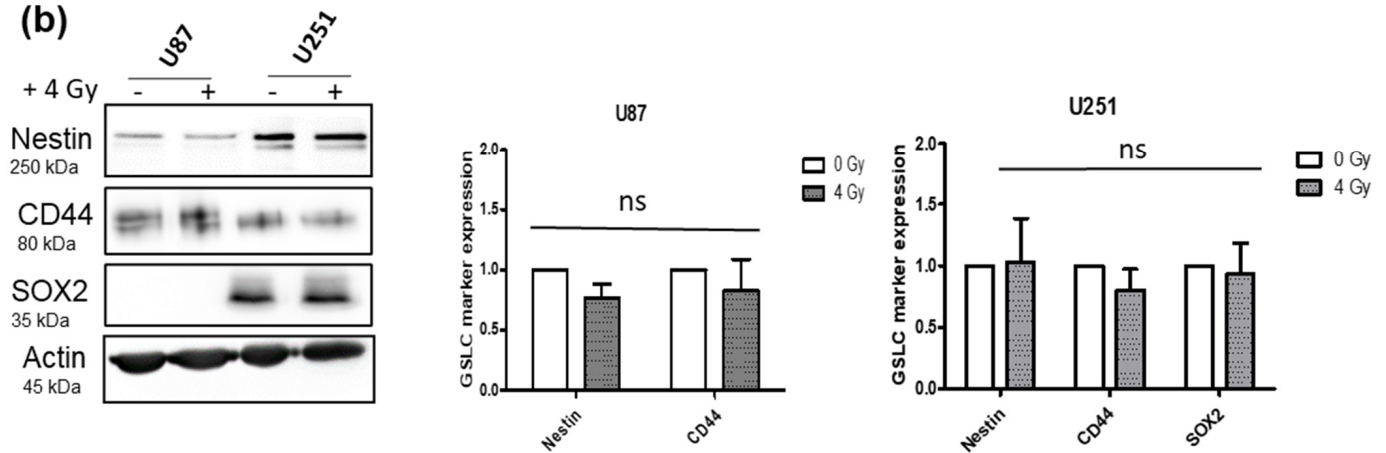


Figure 1. Glioblastoma stem cell marker expression in GB (from TCGA and GTEx database) and GB cell lines: **(a)** TCGA database comparison of GB stem cell marker (CD44, Nestin and SOX2) expression between GB (red; 163 samples) and non-cancerous tissue (gray; 207 samples). Box plots derived from matching TCGA normal and GTEx data downloaded via the GEPIA webserver (* p -value < 0.05). **(b)** Protein expression of CD44, Nestin and SOX2 in U87 and U251 GB cell lines and the effect of 4 Gy irradiation. Data represent mean values of three replicates and the error bars \pm SEM ($n = 3$; ns—nonsignificant).

3.2. Induced GSLC Marker Expression by GB-Derived Spheroid Culture in Serum-Free Medium

To determine whether a stem-like phenotype was induced by the spheroid culture in the serum-free medium in vitro, co-immunofluorescence staining of GSLC markers was performed. After eight passages in the serum-free medium, the GB-derived spheres and their parental cell lines were immunostained to compare the GSLC marker levels in both the serum-free and serum-containing culture conditions. The results showed an increased co-expression of CD133 and CD44, ALDH1A1 and Nestin or SOX2 and Nestin in U87-sph cells (grown in serum-free medium) compared to U87 cells (grown in medium containing

10% FCS) (Figure 2b). Most of the U251-sph cells expressed CD133, CD44, Nestin and SOX2, while fewer U251 cells expressed these stem cell markers. However, ALDH1A1 was not detected in both. Similar results were observed in the U87 parental cells and U87-sph cells. More cells expressed all GSLC markers in U87-sph compared to U87 cells (Figure 2d). These results implied that the culture of the GB cell lines in the serum-free medium could enrich GSLC marker expression.

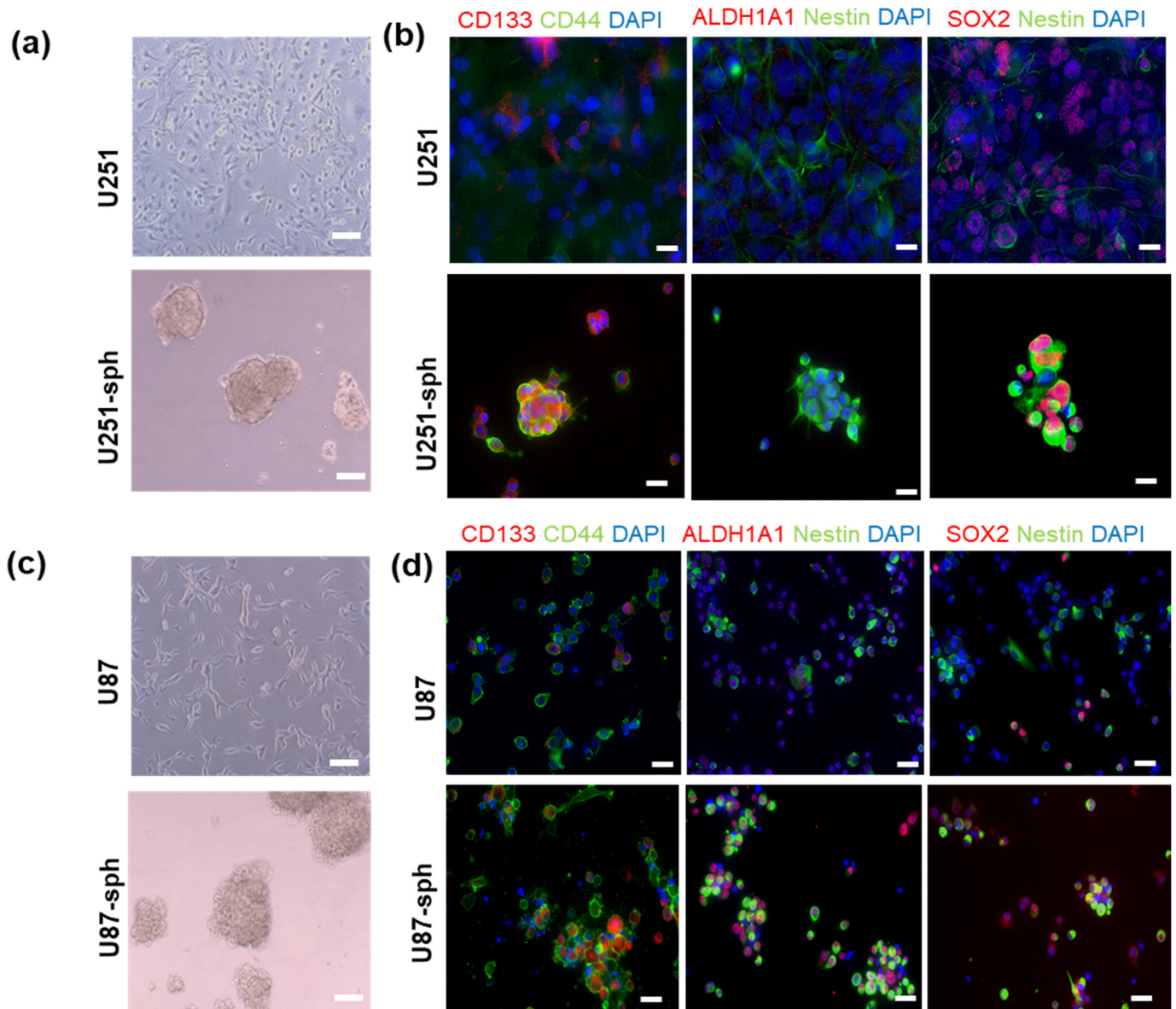


Figure 2. Induction of the stem-like phenotype in U251 and U87 cell lines by a spheroid culture. (a) Representative images of the morphology of U251 (cultured in the medium containing 10% FCS) and U251-sph (cultured in the serum-free medium; scale bar: 100 μm). (b) Representative images of co-immunofluorescence staining of U251 and U251-sph. The U251-sph cells showed an increased dual expression of the GSLC markers CD133 (red), CD44 (green), Nestin (green) and SOX2 (red) compared to the U251 cells. Nuclei were stained with DAPI (blue). Scale bar: 100 μm. (c) Representative images of the morphology of U87 (cultured in the medium containing 10% FCS) and U87-sph (cultured in the serum-free medium; scale bar: 100 μm). (d) Representative images of immunofluorescence staining of U87 and U87-sph. The U87-sph cells showed an increased co-expression of the GSLC markers CD133 (red), CD44 (green), ALDH1A1 (red), Nestin (green) and SOX2 (red) compared to the U87 cells. Nuclei were stained with DAPI (blue). Scale bar: 100 μm.

3.3. HDAC and MEK Inhibitors with 4 Gy Radiation Decreased Cell Viability and Sphere Formation

To identify the most potent concentration of the inhibitors in combination with 4 Gy radiation, U87-sph and U251-sph were treated in an increasing concentration range of 1, 10 and 50 μM and the cell viability was determined 72 h after radiation exposure. For both U251-sph and U87-sph, the viability was significantly decreased by the HDACi (MS-275) or the MEKi (TAK-733 or trametinib) alone and with 4 Gy irradiation in a concentration-dependent manner (Figure S2a–f). Interestingly, the viability of the U251-sph cells was significantly increased by treatment with the standard compound TMZ, even at 50 μM ; when combined with radiation, no change was observed in comparison to the 4 Gy irradiation alone (Figure S2d–f). This suggested that the HDAC and MEK inhibitors were more potent at lower concentrations (1 μM) compared to the standard compound TMZ (50 μM) used for radiochemotherapy of GB.

The activities of the inhibitors were additionally validated in both GB-derived spheres. Treatment with MS-275 at 1 and 10 μM increased the amount of acetylated histone H3, indicating that HDACs were inhibited (Figure S1a). The inhibitory effects of TAK-733 and trametinib at 1 and 10 μM were confirmed by low amounts of activated MAPK (pMAPK) compared to MAPK (Figure S1b).

To further investigate the effect of combining the inhibitors with radiation compared to either alone, the sphere-forming ability of U87-sph and U251-sph were also tested after treatment. Radiation alone (4 Gy) reduced the number of spheres formed in U87-sph, but not significantly in U251-sph, while the HDACi and MEKi alone at 1 μM significantly reduced the number of spheres formed in both (Figure 3a,b and Figure S3). The effect of the inhibitors alone was significantly enhanced in U87-sph when combined with radiation, but not significantly in U251-sph. Additionally, the combination of the HDACi and MEKi (MS-275 and TAK-733 or MS-275 and trametinib) alone at 1 μM further significantly reduced the number of spheres formed in both U251-sph and U87-sph compared to the control ($p \leq 0.001$) (Figure 3a,b). Upon the addition of 4 Gy radiation, the combined inhibitory effect was more enhanced in U87-sph ($p \leq 0.01$) compared to U251-sph ($p \leq 0.05$) (Figure 3a,b). Treatment with the standard compound TMZ (at 50 μM) alone or with radiation was more effective in reducing sphere formation in the U87-sph cells compared to the U251-sph cells (Figure 3a,b). Since sphere formation measures the self-renewal of stem-like cells [35–37], these results suggest that the combined treatment of the HDACi and MEKi with radiation could potentially decrease the self-renewal ability of GSLCs.

3.4. Differential Responses of GSLC Marker Protein Levels to the Combination of HDACi and MEKi with Radiation

In order to determine whether the combination of the HDAC and MEK inhibitors with radiation was effective against the GSLC marker (Nestin, CD44 and SOX2) protein levels, Western blot quantification was performed 72 h after the combined treatment.

In U251-sph, radiation alone did not change the protein level of all markers; however, treatment with the HDACi or MEKi alone and with radiation reduced Nestin (Figure 4a). A decrease in SOX2 via treatment with the HDACi MS-275 alone or with radiation was detected, while CD44 was not changed by the compounds alone or with radiation (Figure 4b). Subsequently, the combination of the HDACi and MEKi (MS-275 and TAK-733 or MS-275 and trametinib) alone or with radiation significantly eradicated Nestin ($p \leq 0.001$) and SOX2 ($p \leq 0.05$, $p \leq 0.001$) and significantly reduced CD44 ($p \leq 0.05$, $p \leq 0.01$) (Figure 4a–d).

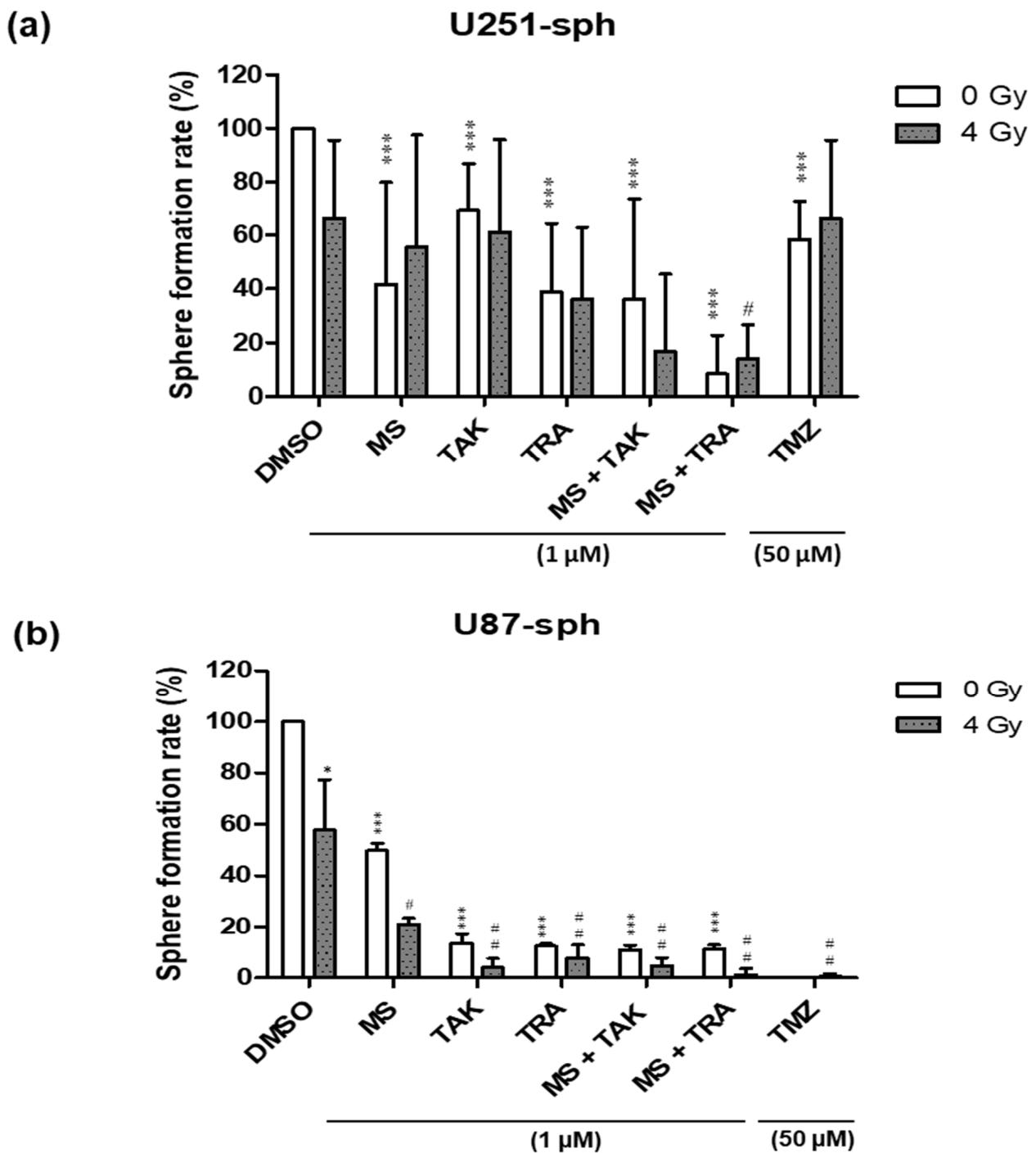


Figure 3. Treatment of HDAC and MEK inhibitors with radiation-inhibited sphere formation of GB-derived spheres. (a) Quantification of sphere formation rate (%) after the treatment of U251-sph and (b) U87-sph with HDCAi (1 μ M MS-275 (MS)), MEKi (1 μ M TAK-733 (TAK) or 1 μ M trametinib (TRA)), a combination of both (1 μ M MS-275 + 1 μ M TAK-733 or 1 μ M MS-275 + 1 μ M trametinib) and 50 μ M TMZ alone or with 4 Gy radiation. The sphere formation rate was normalized to the DMSO-treated cells as the control, which were set to 100%. Data represent the mean of 3 independent experiments performed in triplicates ($n = 3; \pm$ SEM). Asterisks indicate significant differences between 0 Gy DMSO and treated samples using Student's *t*-test: * $p \leq 0.05$ and *** $p \leq 0.001$, while hash symbols indicate significant differences between 4 Gy DMSO and 4 Gy treated samples using Student's *t*-test: # $p \leq 0.05$ and ## $p \leq 0.01$.

Comparable results were detected in U87-sph, where treatments with either HDACi or MEKi alone and with radiation significantly reduced the protein level of Nestin and SOX2 (Figure 4e,g). Upon combination of both HDACi and MEKi with radiation, the protein level of SOX2 was significantly eradicated ($p \leq 0.01$), while Nestin remained significantly decreased ($p \leq 0.001$) (Figure 4e,g,h). Contrary to U251-sph, the CD44 protein level was increased in U87-sph by all the different treatment conditions (Figure 4f). Furthermore, the treatment with the standard compound TMZ alone or with radiation in both cell lines was less effective against the GSLC marker protein levels compared to the combination treatments (Figure 4a–h). Overall, these results suggested that, while combining the HDACi and MEKi with radiation has great potential to reduce the protein levels of GSLC markers, there may be differential effectiveness against CD44 levels.

3.5. Single and Double Expression of GSLC Markers Reduced by the Combination of HDACi and MEKi with Radiation

The effects of the combined inhibitor and radiation treatment were subsequently evaluated using flow cytometry analysis of the GSLC markers. Similar to the protein analysis results, only the combination of the HDACi and MEKi (MS-275 and TAK-733 or MS-275 and trametinib) could significantly reduce the Nestin+, CD44+ and SOX2+ populations in U251-sph (Figure 5a,b). However, these decreases in the positive GSLC marker populations were significantly more pronounced when combined with 4 Gy irradiation ($p \leq 0.001$) (Figure 5a,b and Figure S5). For example, the Nestin+ population in U251-sph decreased from $97 \pm 3\%$ with 4 Gy irradiation alone to $42 \pm 12\%$ when treated with MS-275 and TAK-733 alone and a further reduction to $12 \pm 1\%$ by adding 4 Gy irradiation to the combination (Figure 5a,b). A similar effect of radiation was also observed with the combination of MS-275 and trametinib in U251-sph (Figure 5a,b).

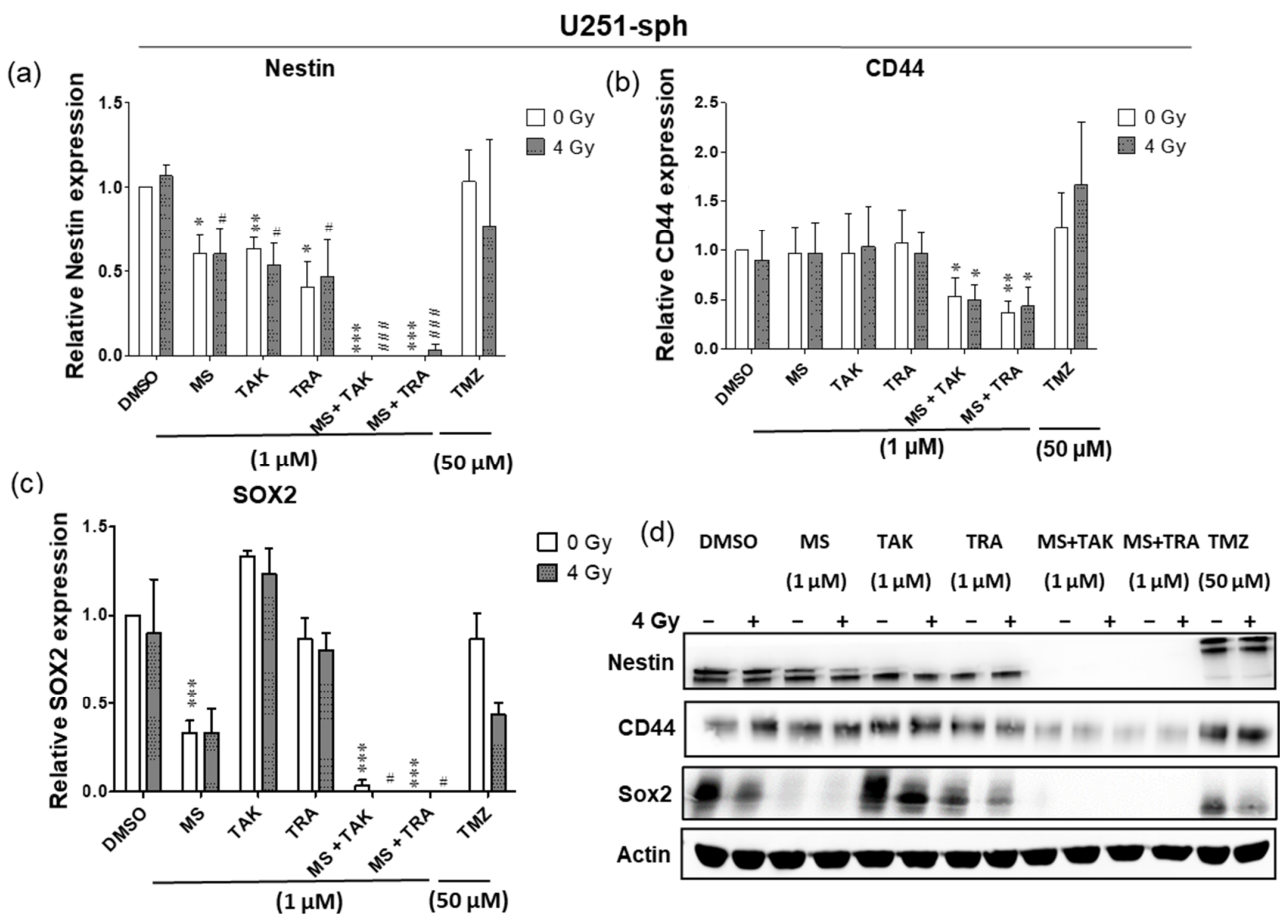


Figure 4. Cont.

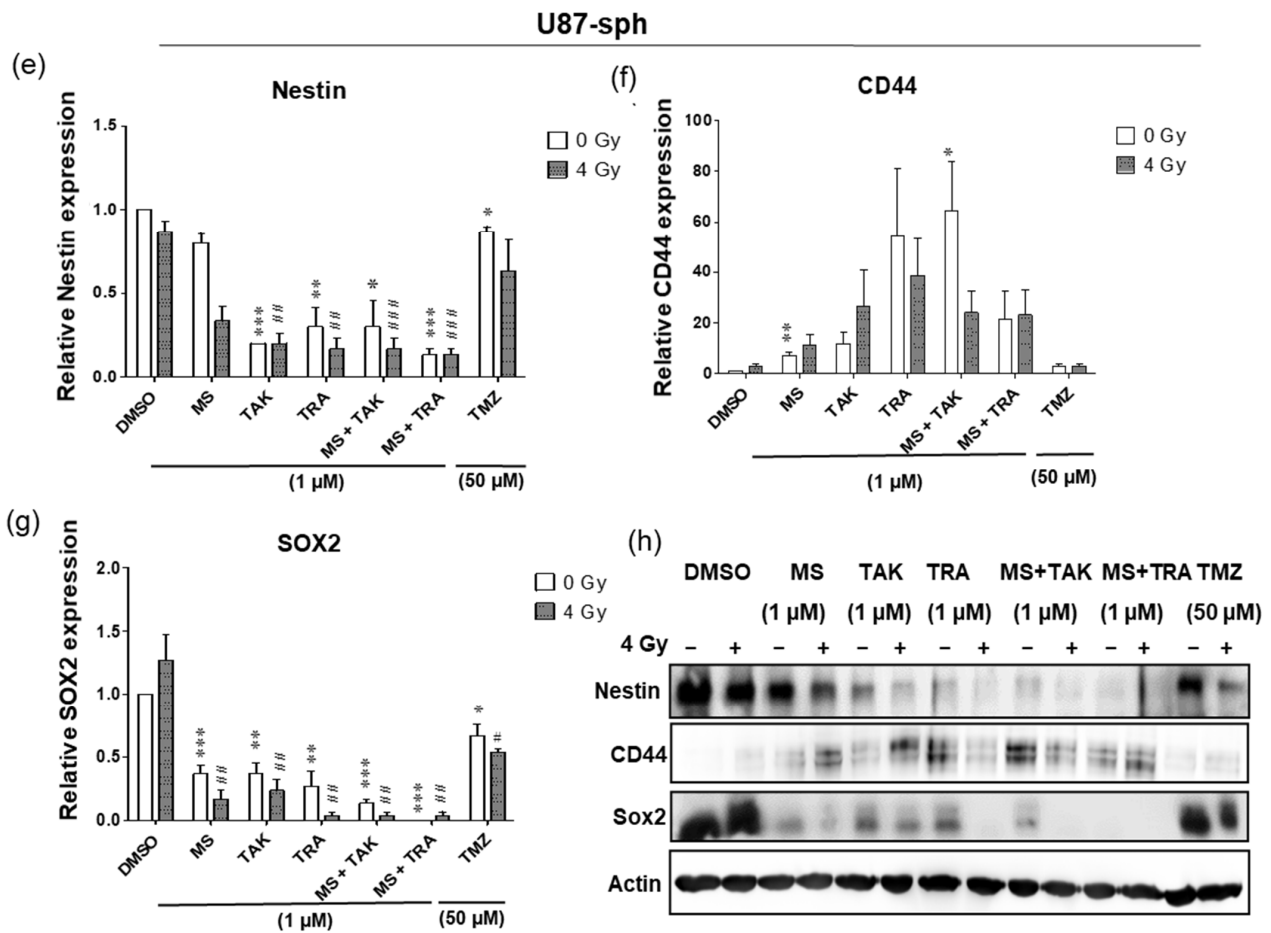


Figure 4. Differential responses of GB-derived spheres to the combination of HDAC and MEK inhibition with radiation. (a) U251-sph protein levels of Nestin, (b) CD44 and (c) SOX2 72 h after the spheres were treated with HDCAi (1 μM MS-275), MEKi (1 μM TAK-733 or 1 μM trametinib), a combination of both (1 μM MS-275 + 1 μM TAK-733 or 1 μM MS-275 + 1 μM trametinib) and 50 μM TMZ alone or with 4 Gy radiation. (d) Representative Western blots of GSLC marker protein levels in U251-sph. (e) U87-sph protein levels of Nestin. (f) CD44 and (g) SOX2 after the GSLCs were treated with HDCAi (1 μM MS-275), MEKi (1 μM TAK-733 or 1 μM trametinib), a combination of both (1 μM MS-275 + 1 μM TAK-733 or 1 μM MS-275 + 1 μM trametinib) and 50 μM TMZ alone or with 4 Gy radiation. (h) Representative Western blots of GSLC marker protein levels in U87-sph. Relative GSLC marker expressions were first normalized to Actin and then to the sham irradiated control cells treated with DMSO. *n* = 3; ± SEM. Asterisks indicate significant differences between 0 Gy DMSO and treated samples using Student’s *t*-test: * *p* ≤ 0.05, ** *p* ≤ 0.01 and *** *p* ≤ 0.001, while hash symbols indicate significant differences between 4 Gy DMSO and 4 Gy treated samples using Student’s *t*-test: # *p* ≤ 0.05, ## *p* ≤ 0.01 and ### *p* ≤ 0.001.

In U87-sph, the Nestin+ and SOX2+ populations were significantly decreased by the MEK inhibitors (TAK-733 and trametinib) alone and with 4 Gy irradiation (Figure 5c). Upon the combination of the MEK inhibitors with the HDCAi MS-275 and 4 Gy irradiation, a significantly stronger decrease was detected (*p* ≤ 0.001) (Figures 5c and S7b,c). However, CD44 expression was not affected by all treatment conditions in U87-sph (Figures 5c and S7a).

It is now widely accepted that the GSLC population is more accurately identified by the expression of more than one GSLC marker. Since a multicolor approach was used, we further analyzed the co-expression changes of the GSLC markers (CD44+Nestin+, Nestin+SOX2+ and CD44+SOX2+) after the combined treatment with radiation. All three

double-positive populations of cells were significantly reduced by the MEK inhibitors (TAK-733 and trametinib) alone or in combination with 4 Gy radiation in U87-sph, but not in U251-sph (Figure 6b,c).

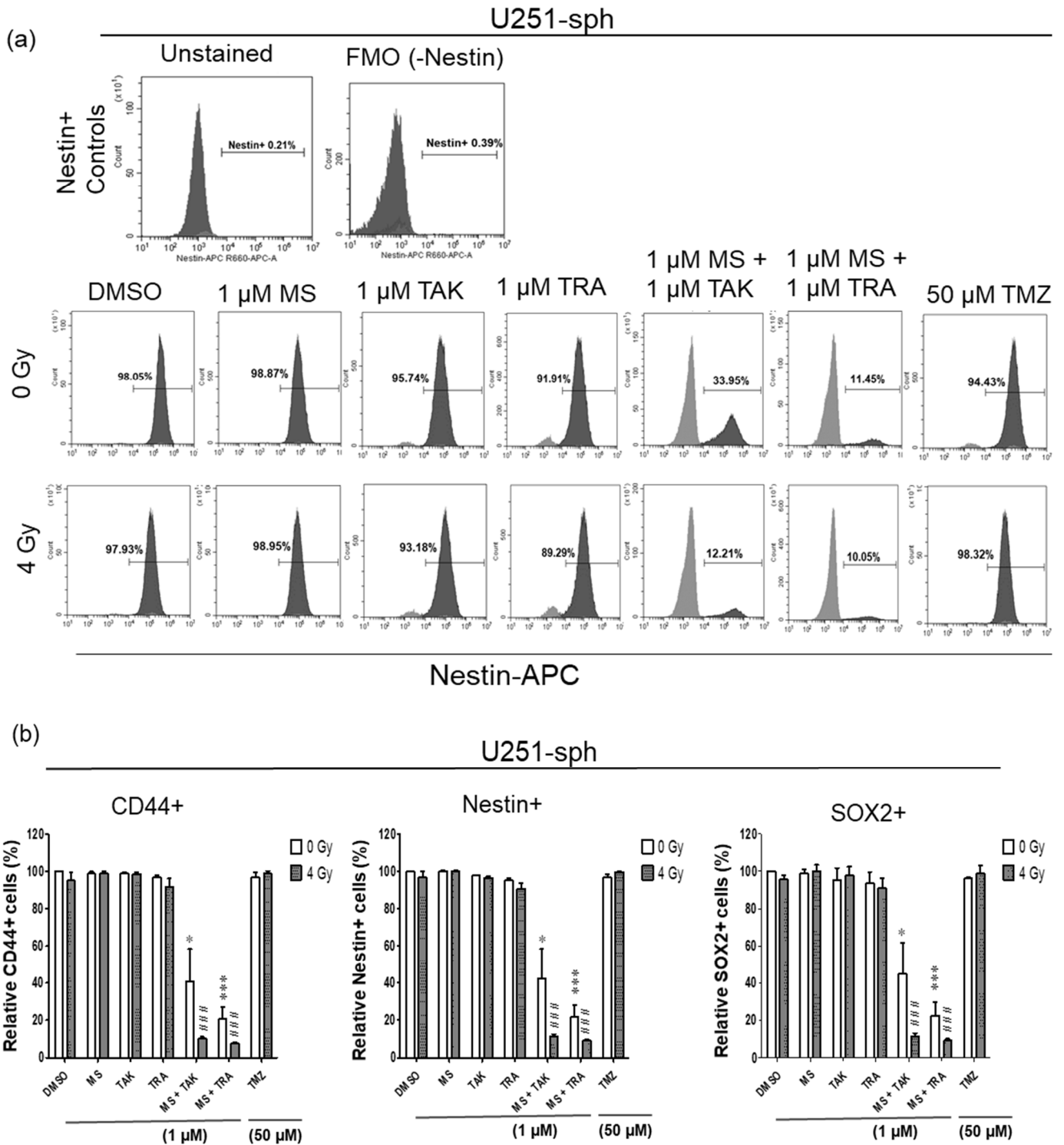


Figure 5. Cont.

(c)

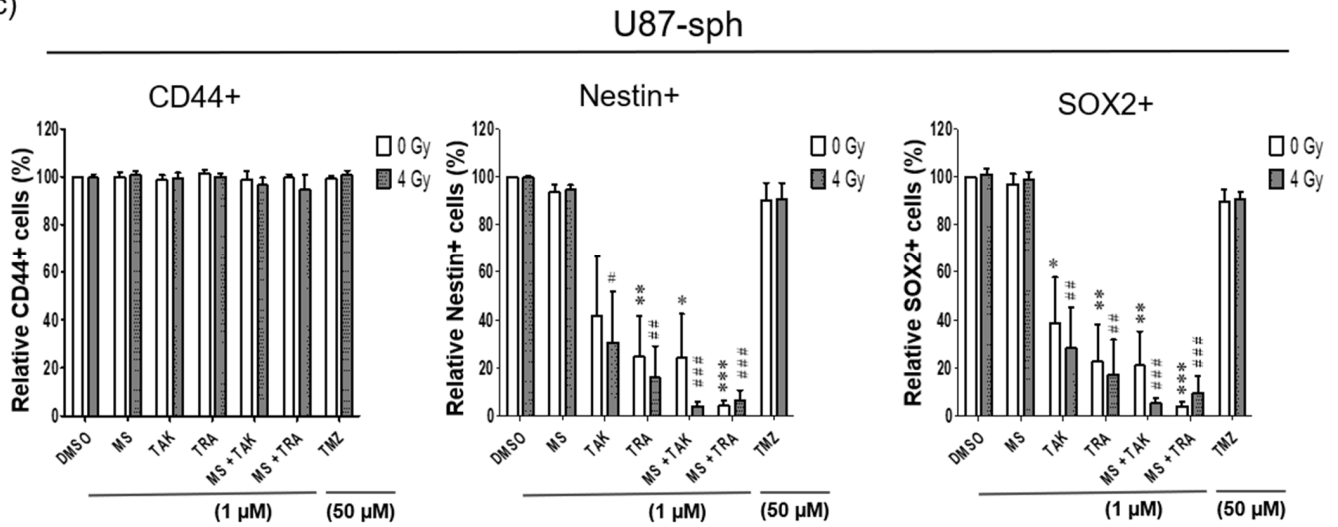


Figure 5. Single expression of GSLC markers reduced by the combination of HDAC and MEK inhibitor with radiation. (a) Representative example of flow cytometric histograms of Nestin in U251-sph 72 h after the spheres were treated with HDCAi (1 μ M MS-275), MEKi (1 μ M TAK-733 or 1 μ M trametinib), a combination of both (1 μ M MS-275 + 1 μ M TAK-733 or 1 μ M MS-275 + 1 μ M trametinib) and 50 μ M TMZ alone or with 4 Gy radiation. Upper histograms represent the unstained sample and fluorescence minus one (FMO) control for the gating percentage of Nestin-positive cells (Nestin+). Lower histograms show the percentage of Nestin-positive cells after the indicated treatment conditions and 4 Gy irradiation. Values inside each histogram represent the percentage of positive single cells from a total of approximately 2×10^4 cells acquired. (b) Quantification of CD44+, Nestin+ and SOX2+ relative to sham irradiated control cells (DMSO) set to 100% in U251-sph and (c) U87-sph. Data represent means \pm SEM ($n = 3$). Asterisks indicate significant differences between 0 Gy DMSO and treated samples using Student's t -test: * $p \leq 0.05$, ** $p \leq 0.01$ and *** $p \leq 0.001$, while hash symbols indicate significant differences between 4 Gy DMSO and 4 Gy treated samples using Student's t -test: # $p \leq 0.05$, ## $p \leq 0.01$ and ### $p \leq 0.001$.

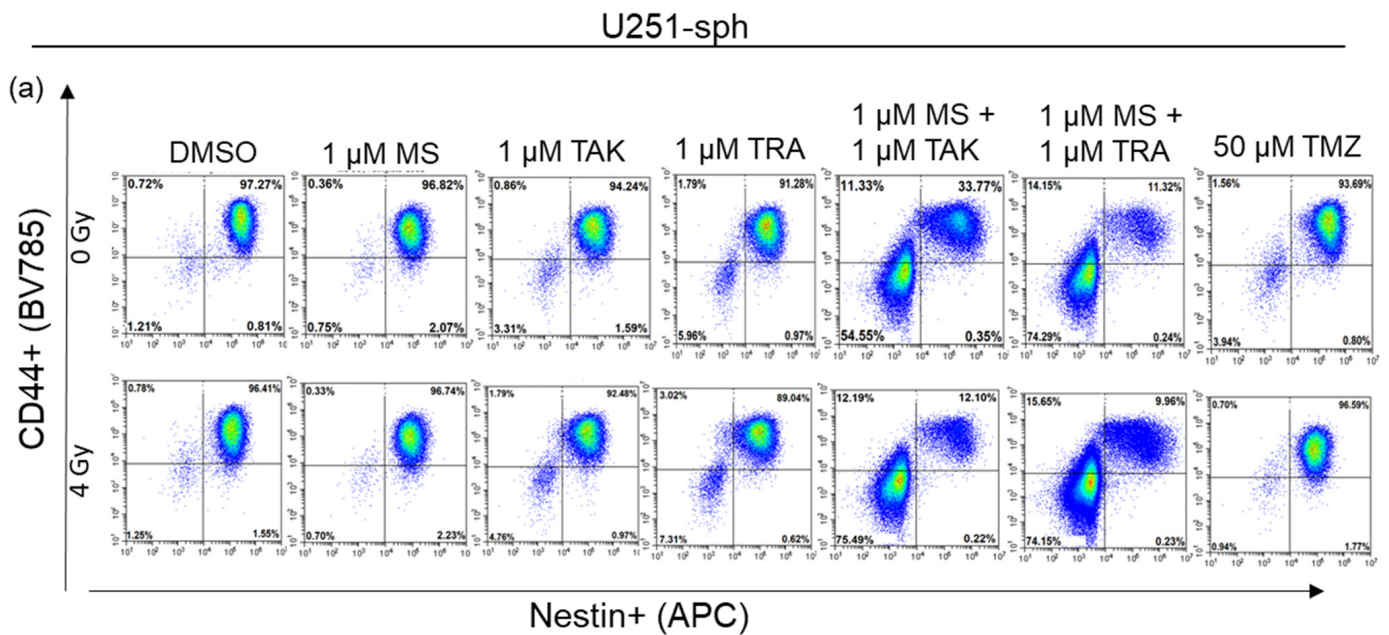


Figure 6. Cont.

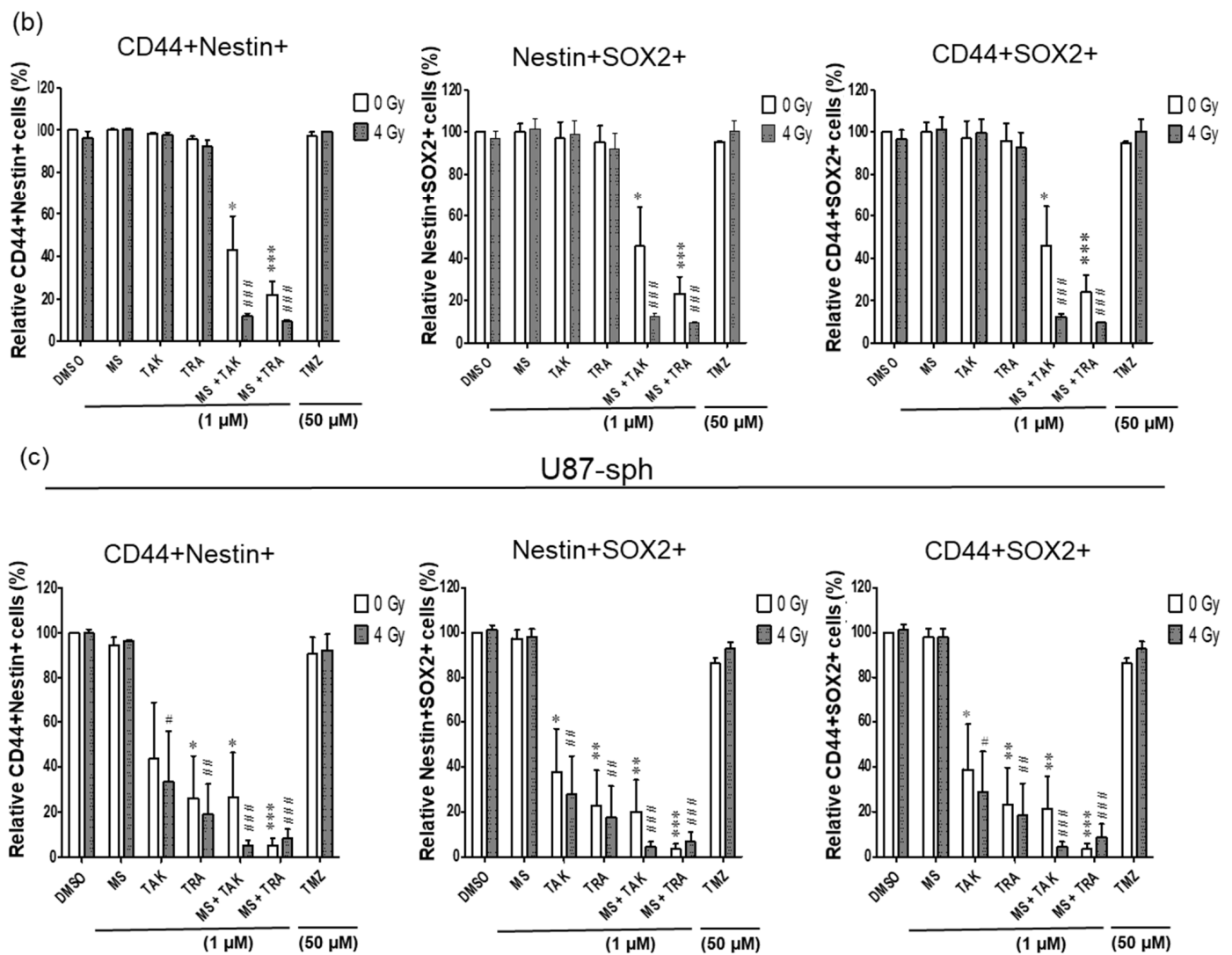


Figure 6. Double expression of GSLC markers reduced by the combination of HDAC and MEK inhibitors with radiation. (a) Representative example of flow cytometric plots in U251-sph 72 h after the spheres were treated with HDCAi (1 μ M MS-275), MEKi (1 μ M TAK-733 or 1 μ M trametinib), a combination of both (1 μ M MS-275 + 1 μ M TAK-733 or 1 M MS-275 + 1 μ M trametinib) and 50 μ M TMZ alone or with 4 Gy radiation. Percentages of double-positive cells for CD44 and Nestin (CD44+Nestin+; upper-right quadrant) after the indicated treatment conditions are shown. Values inside each plot represent the percentage of single cells from a total of approximately 2×10^4 cells acquired. (b) Quantification of CD44+Nestin+, Nestin+SOX2+ and CD44+SOX2+ relative to sham-irradiated control cells (DMSO) set to 100% in U251-sph and (c) U87-sph. Data represent means \pm SEM ($n = 3$). Asterisks indicate significant differences between 0 Gy DMSO and treated samples using Student’s *t*-test: * $p \leq 0.05$, ** $p \leq 0.01$ and *** $p \leq 0.001$, while hash symbols indicate significant differences between 4 Gy DMSO and 4 Gy treated samples using Student’s *t*-test: # $p \leq 0.05$, ## $p \leq 0.01$ and ### $p \leq 0.001$.

Additionally, combining HDACi and MEKi significantly reduced all double-positive populations in both U251-sph and U87-sph (Figures 6, S6 and S8). However, further exposing the combined inhibitors to 4 Gy radiation significantly enhanced the reduction of all three double-positive populations in both GB-derived spheres ($p \leq 0.001$) (Figures 6, S6 and S8). This enhanced effect of radiation was more evident in U251-sph than in U87-sph (Figure 6b,c). Again, the standard compound TMZ alone or with 4 Gy radiation was less effective against the single or double expression of the GSLCs markers

(Figures 5 and 6). Taken together, these results suggested that the combination of HDACi and MEKi with radiation could reduce the GSLC marker expression more efficiently than the standard treatment of TMZ and radiation.

3.6. Population of Dead Cells Increased by the Combination of HDACi and MEKi with Radiation

Live–dead staining was performed during flow cytometry antibody staining using a Zombie Aqua dye that is permeant to dead cells due to compromised membranes and non-permeant to live cells. Therefore, it was possible to access the live versus dead status of the cells after the different treatment conditions.

In U251-sph, the dead cell population was not significantly affected by the single treatments of HDACi or MEKi alone and with radiation (Figure 7a). Upon combination, a significant increase in the percentage of dead cells was detected. The dead cells increased from $8 \pm 5\%$ with only 4 Gy radiation to $58 \pm 16\%$ with MS-275 and TAK-733 alone and further to $88 \pm 1\%$ by adding radiation to the combination. Similarly, the percentage of dead cells was $78 \pm 6\%$ with MS-275 and trametinib alone and further increased to $90 \pm 1\%$ by including radiation.

Likewise, in U87-sph, the dead cell population was unchanged by single treatments of HDACi and radiation (Figure 7b). Although the MEKi alone and with radiation increased the dead cell population, the highest increase was detected upon the combined treatment of the MEKi and HDACi with radiation.

In contrast, the standard treatment of TMZ and radiation did not significantly affect the dead cell population in both U251-sph and U87-sph.

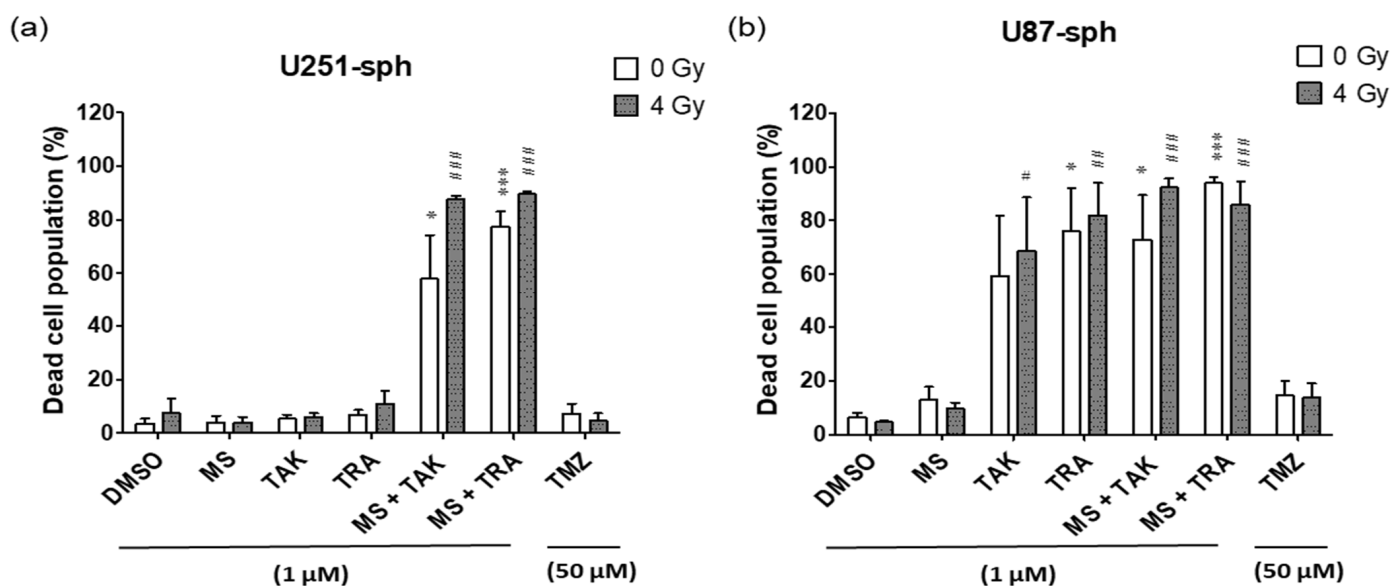


Figure 7. High population of dead cells in GB-derived spheres after treatment with HDACi or MEKi as single or combined compounds with radiation. Quantification data showing the percentage of dead cells in (a) U251-sph and (b) U87-sph after the different treatment conditions. Data represent mean values \pm SEM ($n = 3$). Asterisks indicate significant differences between 0 Gy DMSO and treated samples using Student's *t*-test: * $p \leq 0.05$ and *** $p \leq 0.001$, while hash symbols indicate significant differences between 4 Gy DMSO and 4 Gy treated samples using Student's *t*-test: # $p \leq 0.05$, ## $p \leq 0.01$ and ### $p \leq 0.001$.

4. Discussion

Radiation plus TMZ remains the most effective non-surgical therapy for GB, although this is mostly palliative due to the radioresistance of GSLCs present within the tumor [2]. Furthermore, GB patients often develop resistance to the DNA-alkylating agent TMZ, along with severe side effects [38]. HDAC and MEK inhibitors have shown promising results as anticancer agents in GB and other tissues [9,12,39]. However, they are considered more

potent when combined with other anticancer agents [40,41]. The combination of HDAC and MEK inhibitors as a chemotherapeutic strategy in tumors was first proposed in a study that showed MEK inhibitors sensitized colon, lung and prostate cancer cells to HDACi-induced cell death [42]. Another study reported that the MEK inhibitors PD184352 or AZD6244 in human colon and lung tumor xenograft models enhanced the efficacy of the HDACi MS-275 and suggested this combination as a promising chemotherapeutic strategy [43]. Subsequently, a Phase 1 study was conducted combining the HDACi MS-275 and the MAPK pathway inhibitor sorafenib to treat patients with solid tumors or acute myeloid leukemia (AML) [44]. This combination increased apoptosis in various cancer cell lines and was well tolerated [44]. As a result, combining HDAC and MEK inhibitors was further investigated in other studies [16,18,27,28,42,45].

MEK inhibition alone in pre-clinical studies of GB displayed antitumor effects, but neither enhanced the efficacy of the standard treatment (radiation or TMZ) nor blocked their effectiveness [46]. HDACis, on the other hand, were proposed as promising anticancer compounds capable of targeting GSLCs in single or combination treatments [47]. The current study, therefore, examined the efficacy of combining an HDACi (MS-275) with MEK inhibitors (TAK-733 or trametinib) via a new approach that includes ionizing radiation as an additional strategy against GB. We employed the spheroid culture method for in vitro enrichment of GSLC markers to induce a stem-like phenotype [48,49] and predict the efficacy of the combined treatment against GSLCs.

The Genomics of Drug Sensitivity in Cancer (GDSC) database revealed that the half-maximal inhibitory concentration (IC_{50}) of the compounds in GB treatment range from 0.9–51.5 μ M for HDACi and 0.1–48.1 μ M for MEKi [50]. However, the HDACi and MEKi concentrations were chosen based on the potency of the compounds to reduce the cell viability of the GB-derived spheres at 1 μ M alone or in combination with 4 Gy radiation. TMZ, on the other hand, was less effective against the viability of the cells at low concentrations. This was consistent with a study that reported GSLCs to be less sensitive to TMZ treatment via cell viability quantification [51]. Therefore, we decided to use 1 μ M HDACi and MEKi, while TMZ was used at a higher concentration of 50 μ M.

The combination of the HDAC and MEK inhibitors (MS-275 and TAK-733 or MS-275 and trametinib), both at a low concentration of 1 μ M, with 4 Gy radiation decreased the sphere formation rate of the GB-derived spheres. Nevertheless, a higher concentration of TMZ (50 μ M) with radiation achieved a similar effect. Overall, given that combination therapy is applied to enhance effectiveness, lower doses of the single compounds involved are often desired to lower the risk of drug toxicity to healthy cells [52]. Hence, the efficacy of the HDAC and MEK inhibitors at very low concentrations suggests an improved safety profile and tolerance level for GB therapy as opposed to TMZ [53].

The expressions of GSLC markers CD44, Nestin and SOX2 required for the maintenance of the GSLC population in GB [3] were used to further measure the effect of the combined therapy. All three GSLC markers are reportedly highly expressed in GB compared to normal brain tissues, indicating that they may be responsible for the progression of the tumor and low patient survival rates [54–56]. These GSLC markers were also implicated in GB tumorigenesis and aggressiveness [57]. Therefore, a therapy aimed at downregulating the GSLC markers could be more effective at preventing progression and improving GB treatment [2].

Indeed, we found that combining the HDAC and MEK inhibitors (both at 1 μ M) with 4 Gy radiation completely eradicated Nestin and SOX2 protein levels in U251-sph and significantly reduced CD44 protein levels. Similarly, the protein levels of Nestin and SOX2 in U87-sph were also significantly decreased. However, in contrast to U251-sph, the CD44 protein levels were surprisingly upregulated in U87-sph after the combined treatment. This may imply that the sensitivity of CD44 protein levels to the combined HDAC and MEK inhibitor treatment with radiation could be cell line dependent. Similar to our findings, differential responses of protein levels to treatment in the U87-sph and U251-sph were reported [49].

Subsequently, the HDAC and MEK inhibitor treatment with radiation strongly reduced the single positive (CD44+, Nestin+ and SOX2+) populations in both cell lines, except for CD44 expression, which remained unchanged in U87-sph. The differential response of CD44 to the combined treatment in both GB-derived spheres could have also been due to the different genetic alterations present in both cell lines.

Since there has been a dispute regarding whether a single GSLC marker expression accurately identifies the GSLC population [57,58], we further evaluated the double expressions of the GSLC markers after the combined treatment. Again, we found that all three double-positive populations (CD44+Nestin+, Nestin+SOX2+ and CD44+SOX2+) were significantly reduced in both GB-derived spheres by the combined HDAC and MEK inhibitor treatment with radiation. Live–dead staining also revealed that the percentage of the dead cell population in both GB-derived spheres was greatly increased upon the combined treatment with radiation. This finding suggested that the mechanism behind the reduced GSLC marker expression after the combined treatment may be due to the killing of the U251-sph and U87-sph cells. While others have shown that the combination of HDACi and MEKi can enhance tumor cell killing compared to either alone [59], our new approach of including radiation shows a further enhancement of this anti-tumor effect in GB. Although more investigations are required, these data suggested that the combined radiochemotherapy may have great potential against the highly resistant GB cells.

Interestingly, the current standard drug TMZ at a higher concentration (50 μ M), alone or with radiation, either did not have any effect or increased the expression of GSLC markers. In addition, the population of dead cells was not significantly changed compared to the sham irradiated control cells. Some studies have reported TMZ chemoresistance of glioma stem cells and GB [60,61]. Another study reported an increase in the CD44+ population in patient-derived GSLCs in response to TMZ and radiation [51]. An explanation for the chemoresistance to TMZ could be an increased expression of a DNA repair enzyme known as MGMT (*O*-6-methylguanine-DNA methyltransferase) [62]. MGMT efficiently repairs the DNA damage caused by TMZ, hence only GB cells with an epigenetically silenced expression of the enzyme can benefit from TMZ treatment [63]. Our data has shown that TMZ alone or with radiation was less effective, whereas the combination of the HDAC and MEK inhibitors with radiation efficiently reduced the GSLC markers.

Some reported anti-tumor mechanisms behind the HDAC and MEK inhibitor combination in other cancer studies include enhanced production of ROS (reactive oxygen species) [42], activation of cell-cycle inhibitors [45], increased apoptosis and deregulated survival pathways [59]. In addition to this, we showed that by including the cytotoxic effects of radiation as a novelty, the combined radiochemotherapy treatment could be more effective in the killing of GB tumor cells.

A limitation to our study was that the GB-derived spheres did not fully represent the GSLC population due to the artificial culture conditions, nor did our work establish the combination index of the HDAC and MEK inhibitors. To better elucidate the efficacy of the combined therapy with radiation, further research is necessary using experimental models that involve purely isolated GSLC populations. This can be achieved through fluorescence-activated cell sorting (FACS) to isolate side populations expressing GSLC markers [64] or low-passage patient-derived primary GSLCs [65]. In addition, *in vivo* validations are required since the *in vitro* cultures fail to either address the heterogeneity of the original tumor or recapitulate the hierarchy of GSLCs [3,66].

5. Conclusions

In conclusion, our findings support the proposition that a combination therapy approach against GB may be an effective way to improve outcomes [40]. The efficacy of this approach was demonstrated by a reduction in the ability of the GB-derived spheres to form spheroids after the combined HDAC and MEK inhibitor (MS-275 and TAK-733 or MS-275 and trametinib) treatment with radiation. The combined treatment with radiation further decreased the expression of the GSLC markers Nestin and SOX2, while the effect on CD44

was cell line dependent. Moreover, the combined treatment was more efficient compared to the standard treatment of TMZ and radiation. Although more research is needed to validate the efficacy of this combination strategy, the results suggested that this may be a promising multimodal therapy against the highly resistant GB that can inhibit recurrence and increase the survival of patients.

Supplementary Materials: The following are available online at <https://www.mdpi.com/article/10.3390/cells11050775/s1>. Figure S1: Activities of the HDACi MS-275 (MS) and the MEKi TAK-733 (TAK) or trametinib (TRA) in GSLC lines. (a) Western blots showing the increased acetylation effect of MS-275 on histone H3 in whole-cell lysates from U87-sph and U251-sph cells ($n = 2$). (b) Western blots showing the inhibitory effects of TAK-733 and trametinib on phosphorylated MAPK (pMAPK) in U87-sph and U251-sph cells. Figure S2: Cell viability decreased with increasing concentration of compounds (MS-275, TAK-733, trametinib and TMZ), with and without 4 Gy radiation. (a) Cell viability of U87-sph after the 1 μ M, (b) 10 μ M and (c) 50 μ M compound and radiation treatments. (d) Cell viability of U251-sph after the 1 μ M, (e) 10 μ M and (f) 50 μ M compound and radiation treatment. Values were normalized to control samples (DMSO) set to 1. Bars not visible represent values less than or equal to 0. Data represent the mean \pm SEM of three independent experiments performed in quadruplicates (t -test, *** $p \geq 0.0001$). Figure S3: Treatment of HDAC and MEK inhibitors with radiation-inhibited sphere formation of GSLC lines. (a) Representative images of spheres formed 14 days after treatment with compounds and radiation in U87-sph cells and (b) U251-sph cells (scale bar: 100 μ m). Figure S4: Gating strategy and FMO controls for the flow cytometry results shown in Figures 5 and 6. (a) Cells were gated based on size and granularity using side scatter area (SSC-A) vs. forward scatter area (FSC-A) to remove debris and clumped cells. From this cell gate, single cells (singlets) were sub-gated using forward scatter height (FSC-H) vs. FSC-A to remove doublets. From the singlets gates, the control and treated samples were sub-gated to obtain the negative and positive single or double populations. (b) Fluorescence minus one (FMO) controls used to gate the double-positive populations for Figure 6 are shown. The gating region on the FMO controls was set to contain less than 1% of the cells for double-positive populations. FMO control minus (–) of each indicated antibody is shown. Figure S5: Representative pictures for the single positive populations of (a) CD44+ and (b) SOX2+ in U251-sph for Figure 5b. Unstained, FMO and isotype control (SOX2) for gating positive population are shown. Figure S6: Representative pictures for the double-positive populations of (a) Nestin+SOX2+ and (b) CD44+SOX2+ in U251-sph for Figure 6b. Figure S7: Representative pictures for the single positive populations of (a) CD44+, (b) SOX2+ and (c) Nestin+ in U87-sph for Figure 5c. Unstained, FMO and isotype control (SOX2) for gating positive populations are shown. Values inside each flow cytometric plot represent the percentage of single positive cells from a total of approximately 2×10^4 cells acquired. Figure S8: Representative pictures for the double-positive populations of (a) CD44+Nestin+, (b) Nestin+SOX2+ and (c) CD44+SOX2+ in U87-sph for Figure 6c.

Author Contributions: Conceptualization, M.J.A. and N.A.; methodology, E.I.E., T.P.H., M.J.A. and N.A.; validation, E.I.E., T.P.H., M.J.A. and N.A.; formal analysis, E.I.E., T.P.H., M.J.A. and N.A.; investigation, E.I.E.; resources, E.I.E., T.P.H., M.J.A. and N.A.; data curation, E.I.E. and N.A.; writing—original draft preparation, E.I.E.; writing—review and editing, E.I.E., T.P.H., M.J.A. and N.A.; visualization, E.I.E. and N.A.; supervision, M.J.A. and N.A.; project administration, M.J.A. and N.A.; funding acquisition, M.J.A. and N.A. All authors have read and agreed to the published version of the manuscript.

Funding: This research received no external funding.

Institutional Review Board Statement: Not applicable.

Informed Consent Statement: Not applicable.

Data Availability Statement: Data is contained within the article or supplementary material.

Acknowledgments: The authors thank Kamyar Hadian and Kenji Schorpp for the Operetta Imaging System maintenance and the HMGU Immunoanalytics-Core Facility for support with the flow cytometry experiments. We also thank Michael Rosemann for his advice on the statistical data.

Conflicts of Interest: The authors declare no conflict of interest.

References

1. Stupp, R.; Mason, W.P.; van den Bent, M.J.; Weller, M.; Fisher, B.; Taphoorn, M.J.; Belanger, K.; Brandes, A.A.; Marosi, C.; Bogdahn, U.; et al. Radiotherapy plus concomitant and adjuvant temozolomide for glioblastoma. *N. Engl. J. Med.* **2005**, *352*, 987–996. [CrossRef] [PubMed]
2. Huang, Z.; Cheng, L.; Guryanova, O.A.; Wu, Q.; Bao, S. Cancer stem cells in glioblastoma—molecular signaling and therapeutic targeting. *Protein Cell* **2010**, *1*, 638–655. [CrossRef] [PubMed]
3. Lathia, J.D.; Mack, S.C.; Mulkearns-Hubert, E.E.; Valentim, C.L.L.; Rich, J.N. Cancer stem cells in glioblastoma. *Genes Dev.* **2015**, *29*, 1203–1217. [CrossRef] [PubMed]
4. Bao, S.; Wu, Q.; McLendon, R.E.; Hao, Y.; Shi, Q.; Hjelmeland, A.B.; Dewhirst, M.W.; Bigner, D.D.; Rich, J.N. Glioma stem cells promote radioresistance by preferential activation of the DNA damage response. *Nature* **2006**, *444*, 756–760. [CrossRef]
5. Yi, Y.; Hsieh, I.-Y.; Huang, X.; Li, J.; Zhao, W. Glioblastoma Stem-Like Cells: Characteristics, Microenvironment, and Therapy. *Front. Pharmacol.* **2016**, *7*. [CrossRef]
6. Fremin, C.; Meloche, S. From basic research to clinical development of MEK1/2 inhibitors for cancer therapy. *J. Hematol. Oncol.* **2010**, *3*, 8. [CrossRef]
7. Bayin, N.S.; Modrek, A.S.; Placantonakis, D.G. Glioblastoma stem cells: Molecular characteristics and therapeutic implications. *World J. Stem Cells* **2014**, *6*, 230–238. [CrossRef]
8. Akinleye, A.; Furqan, M.; Mukhi, N.; Ravella, P.; Liu, D. MEK and the inhibitors: From bench to bedside. *J. Hematol. Oncol.* **2013**, *6*, 27. [CrossRef]
9. Perreault, S.; Larouche, V.; Tabori, U.; Hawkin, C.; Lippé, S.; Ellezam, B.; Décarie, J.-C.; Théoret, Y.; Métras, M.-É.; Sultan, S.; et al. A phase 2 study of trametinib for patients with pediatric glioma or plexiform neurofibroma with refractory tumor and activation of the MAPK/ERK pathway: TRAM-01. *BMC Cancer* **2019**, *19*, 1250. [CrossRef]
10. de la Puente, P.; Muz, B.; Jin, A.; Azab, F.; Luderer, M.; Salama, N.N.; Azab, A.K. MEK inhibitor, TAK-733 reduces proliferation, affects cell cycle and apoptosis, and synergizes with other targeted therapies in multiple myeloma. *Blood Cancer J.* **2016**, *6*, e399. [CrossRef]
11. Cheng, Y.; Tian, H. Current Development Status of MEK Inhibitors. *Molecules* **2017**, *22*, 1551. [CrossRef] [PubMed]
12. Anastasov, N.; Hirmer, E.; Klenner, M.; Ott, J.; Falkenberg, N.; Bao, X.; Mutschelknaus, L.; Moertl, S.; Combs, S.; Atkinson, M.J.; et al. MEK1 Inhibitor Combined with Irradiation Reduces Migration of Breast Cancer Cells Including miR-221 and ZEB1 EMT Marker Expression. *Cancers* **2020**, *12*, 3760. [CrossRef] [PubMed]
13. Manoharan, N.; Choi, J.; Chordas, C.; Zimmerman, M.A.; Scully, J.; Clymer, J.; Filbin, M.; Ullrich, N.J.; Bandopadhyay, P.; Chi, S.N.; et al. Trametinib for the treatment of recurrent/progressive pediatric low-grade glioma. *J. Neuro-Oncol.* **2020**, *149*, 253–262. [CrossRef] [PubMed]
14. Paul, M.R.; Pehlivan, K.C.; Milburn, M.; Yeh-Nayre, L.; Elster, J.; Crawford, J.R. Trametinib-based Treatment of Pediatric CNS Tumors: A Single Institutional Experience. *J. Pediatric Hematol. Oncol.* **2020**, *42*, e730–e737. [CrossRef]
15. Adjei, A.A.; LoRusso, P.; Ribas, A.; Sosman, J.A.; Pavlick, A.; Dy, G.K.; Zhou, X.; Gangolli, E.; Kneissl, M.; Faucette, S.; et al. A phase I dose-escalation study of TAK-733, an investigational oral MEK inhibitor, in patients with advanced solid tumors. *Invest New Drugs* **2017**, *35*, 47–58. [CrossRef]
16. Carson, R.; Celtikci, B.; Fenning, C.; Javadi, A.; Crawford, N.; Carbonell, L.P.; Lawler, M.; Longley, D.B.; Johnston, P.G.; Van Schaeybroeck, S. HDAC Inhibition Overcomes Acute Resistance to MEK Inhibition in BRAF-Mutant Colorectal Cancer by Downregulation of c-FLIPL. *Clin. Cancer Res. Off. J. Am. Assoc. Cancer Res.* **2015**, *21*, 3230–3240. [CrossRef]
17. Thurn, K.T.; Thomas, S.; Moore, A.; Munster, P.N. Rational therapeutic combinations with histone deacetylase inhibitors for the treatment of cancer. *Future Oncol* **2011**, *7*, 263–283. [CrossRef]
18. Chao, M.-W.; Chang, L.-H.; Tu, H.-J.; Chang, C.-D.; Lai, M.-J.; Chen, Y.-Y.; Liou, J.-P.; Teng, C.-M.; Pan, S.-L. Combination treatment strategy for pancreatic cancer involving the novel HDAC inhibitor MPT0E028 with a MEK inhibitor beyond K-Ras status. *Clin. Epigenetics* **2019**, *11*, 85. [CrossRef]
19. Zhang, G.; Park, M.A.; Mitchell, C.; Hamed, H.; Rahmani, M.; Martin, A.P.; Curiel, D.T.; Yacoub, A.; Graf, M.; Lee, R.; et al. Vorinostat and Sorafenib Synergistically Kill Tumor Cells via FLIP Suppression and CD95 Activation. *Clin. Cancer Res.* **2008**, *14*, 5385. [CrossRef]
20. Nagarajan, R.P.; Costello, J.F. Epigenetic mechanisms in glioblastoma multiforme. *Semin. Cancer Biol.* **2009**, *19*, 188–197. [CrossRef]
21. Mottamal, M.; Zheng, S.; Huang, T.L.; Wang, G. Histone Deacetylase Inhibitors in Clinical Studies as Templates for New Anticancer Agents. *Molecules* **2015**, *20*, 3898–3941. [CrossRef] [PubMed]
22. Sun, P.; Xia, S.; Lal, B.; Eberhart, C.G.; Quinones-Hinojosa, A.; Maciaczyk, J.; Matsui, W.; Dimeco, F.; Piccirillo, S.M.; Vescovi, A.L.; et al. DNER, an epigenetically modulated gene, regulates glioblastoma-derived neurosphere cell differentiation and tumor propagation. *Stem Cells* **2009**, *27*, 1473–1486. [CrossRef] [PubMed]
23. Eyupoglu, I.Y.; Hahnen, E.; Trankle, C.; Savaskan, N.E.; Siebzehrubl, F.A.; Buslei, R.; Lemke, D.; Wick, W.; Fahlbusch, R.; Blumcke, I. Experimental therapy of malignant gliomas using the inhibitor of histone deacetylase MS-275. *Mol. Cancer Ther.* **2006**, *5*, 1248–1255. [CrossRef] [PubMed]
24. Chen, R.; Zhang, M.; Zhou, Y.; Guo, W.; Yi, M.; Zhang, Z.; Ding, Y.; Wang, Y. The application of histone deacetylases inhibitors in glioblastoma. *J. Exp. Clin. Cancer Res.* **2020**, *39*, 138. [CrossRef]

25. Bezecny, P. Histone deacetylase inhibitors in glioblastoma: Pre-clinical and clinical experience. *Med. Oncol.* **2014**, *31*, 985. [CrossRef]
26. Moertl, S.; Payer, S.; Kell, R.; Winkler, K.; Anastasov, N.; Atkinson, M.J. Comparison of Radiosensitization by HDAC Inhibitors CUDC-101 and SAHA in Pancreatic Cancer Cells. *Int. J. Mol. Sci.* **2019**, *20*, 3259. [CrossRef]
27. Nishioka, C.; Ikezoe, T.; Yang, J.; Koeffler, H.P.; Yokoyama, A. Inhibition of MEK/ERK signaling synergistically potentiates histone deacetylase inhibitor-induced growth arrest, apoptosis and acetylation of histone H3 on p21waf1 promoter in acute myelogenous leukemia cell. *Leukemia* **2008**, *22*, 1449–1452. [CrossRef]
28. Torres-Adorno, A.M.; Lee, J.; Kogawa, T.; Ordentlich, P.; Tripathy, D.; Lim, B.; Ueno, N.T. Histone Deacetylase Inhibitor Enhances the Efficacy of MEK Inhibitor through NOXA-Mediated MCL1 Degradation in Triple-Negative and Inflammatory Breast Cancer. *Clin. Cancer Res. Off. J. Am. Assoc. Cancer Res.* **2017**, *23*, 4780–4792. [CrossRef]
29. Polivka, J.; Polivka, J.; Holubec, L.; Kubikova, T.; Pribran, V.; Hes, O.; Pivovarcikova, K.; Treskova, I. Advances in Experimental Targeted Therapy and Immunotherapy for Patients with Glioblastoma Multiforme. *Anticancer Res.* **2017**, *37*, 21–33. [CrossRef]
30. Burster, T.; Traut, R.; Yermekkyzy, Z.; Mayer, K.; Westhoff, M.-A.; Bischof, J.; Knippschild, U. Critical View of Novel Treatment Strategies for Glioblastoma: Failure and Success of Resistance Mechanisms by Glioblastoma Cells. *Front. Cell Dev. Biol.* **2021**, *9*. [CrossRef]
31. Tang, Z.; Li, C.; Kang, B.; Gao, G.; Li, C.; Zhang, Z. GEPIA: A web server for cancer and normal gene expression profiling and interactive analyses. *Nucleic Acids Res.* **2017**, *45*, W98–W102. [CrossRef]
32. Anastasov, N.; Höfig, I.; Radulović, V.; Ströbel, S.; Salomon, M.; Lichtenberg, J.; Rothenaigner, I.; Hadian, K.; Kelm, J.M.; Thirion, C.; et al. A 3D-microtissue-based phenotypic screening of radiation resistant tumor cells with synchronized chemotherapeutic treatment. *BMC Cancer* **2015**, *15*, 466. [CrossRef] [PubMed]
33. Schneider, C.A.; Rasband, W.S.; Eliceiri, K.W. NIH Image to ImageJ: 25 years of image analysis. *Nat. Methods* **2012**, *9*, 671–675. [CrossRef]
34. Maecker, H.T.; Trotter, J. Flow cytometry controls, instrument setup, and the determination of positivity. *Cytometry. Part A J. Int. Soc. Anal. Cytol.* **2006**, *69*, 1037–1042. [CrossRef] [PubMed]
35. Kanabur, P.; Guo, S.; Simonds, G.R.; Kelly, D.F.; Gourdie, R.G.; Verbridge, S.S.; Sheng, Z. Patient-derived glioblastoma stem cells respond differentially to targeted therapies. *Oncotarget* **2016**, *7*, 86406–86419. [CrossRef] [PubMed]
36. Yuan, X.; Curtin, J.; Xiong, Y.; Liu, G.; Waschmann-Hogiu, S.; Farkas, D.L.; Black, K.L.; Yu, J.S. Isolation of cancer stem cells from adult glioblastoma multiforme. *Oncogene* **2004**, *23*, 9392–9400. [CrossRef]
37. Fukaya, R.; Ohta, S.; Yamaguchi, M.; Fujii, H.; Kawakami, Y.; Kawase, T.; Toda, M. Isolation of cancer stem-like cells from a side population of a human glioblastoma cell line, SK-MG-1. *Cancer Lett.* **2010**, *291*, 150–157. [CrossRef]
38. Trinh, V.A.; Patel, S.P.; Hwu, W.-J. The safety of temozolomide in the treatment of malignancies. *Expert Opin. Drug Saf.* **2009**, *8*, 493–499. [CrossRef]
39. Camphausen, K.; Scott, T.; Sproull, M.; Tofilon, P.J. Enhancement of Xenograft Tumor Radiosensitivity by the Histone Deacetylase Inhibitor MS-275 and Correlation with Histone Hyperacetylation. *Clin. Cancer Res.* **2004**, *10*, 6066. [CrossRef]
40. Ghosh, D.; Nandi, S.; Bhattacharjee, S. Combination therapy to checkmate Glioblastoma: Clinical challenges and advances. *Clin. Transl. Med.* **2018**, *7*, 33. [CrossRef]
41. Suraweera, A.; O'Byrne, K.J.; Richard, D.J. Combination Therapy with Histone Deacetylase Inhibitors (HDACi) for the Treatment of Cancer: Achieving the Full Therapeutic Potential of HDACi. *Front. Oncol.* **2018**, *8*, 92. [CrossRef] [PubMed]
42. Ozaki, K.; Minoda, A.; Kishikawa, F.; Kohno, M. Blockade of the ERK pathway markedly sensitizes tumor cells to HDAC inhibitor-induced cell death. *Biochem. Biophys. Res. Commun.* **2006**, *339*, 1171–1177. [CrossRef] [PubMed]
43. Sakamoto, T.; Ozaki, K.-i.; Fujio, K.; Kajikawa, S.-h.; Uesato, S.-i.; Watanabe, K.; Tanimura, S.; Koji, T.; Kohno, M. Blockade of the ERK pathway enhances the therapeutic efficacy of the histone deacetylase inhibitor MS-275 in human tumor xenograft models. *Biochem. Biophys. Res. Commun.* **2013**, *433*, 456–462. [CrossRef] [PubMed]
44. Ngamphaiboon, N.; Dy, G.; Ma, W.W.; Zhao, Y.; Reungwetwattana, T.; DePaolo, D.; Ding, Y.; Brady, W.; Fetterly, G.; Adjei, A. A phase I study of the histone deacetylase (HDAC) inhibitor entinostat, in combination with sorafenib in patients with advanced solid tumors. *Investig. New Drugs* **2014**, *33*, 225–232. [CrossRef] [PubMed]
45. Yamada, T.; Amann, J.M.; Tanimoto, A.; Taniguchi, H.; Shukuya, T.; Timmers, C.; Yano, S.; Shilo, K.; Carbone, D.P. Histone Deacetylase Inhibition Enhances the Antitumor Activity of a MEK Inhibitor in Lung Cancer Cells Harboring RAS Mutations. *Mol. Cancer Ther.* **2018**, *17*, 17–25. [CrossRef]
46. Selvasaravanan, K.D.; Wiederspohn, N.; Hadzalic, A.; Strobel, H.; Payer, C.; Schuster, A.; Karpel-Massler, G.; Siegelin, M.D.; Halatsch, M.-E.; Debatin, K.-M.; et al. The limitations of targeting MEK signalling in Glioblastoma therapy. *Sci. Rep.* **2020**, *10*, 7401. [CrossRef]
47. Reddy, R.G.; Bhat, U.A.; Chakravarty, S.; Kumar, A. Advances in histone deacetylase inhibitors in targeting glioblastoma stem cells. *Cancer Chemother. Pharmacol.* **2020**, *86*, 165–179. [CrossRef]
48. Zhang, S.; Xie, R.; Wan, F.; Ye, F.; Guo, D.; Lei, T. Identification of U251 glioma stem cells and their heterogeneous stem-like phenotypes. *Oncol. Lett.* **2013**, *6*, 1649–1655. [CrossRef]
49. Liu, J.; Liu, Y.; Xie, T.; Luo, L.; Xu, C.; Gao, Q.; Shen, L.; Wan, F.; Lei, T.; Ye, F. Radiation-induced G2/M arrest rarely occurred in glioblastoma stem-like cells. *Int. J. Radiat. Biol.* **2018**, *94*, 394–402. [CrossRef]

50. Yang, W.; Soares, J.; Greninger, P.; Edelman, E.J.; Lightfoot, H.; Forbes, S.; Bindal, N.; Beare, D.; Smith, J.A.; Thompson, I.R.; et al. Genomics of Drug Sensitivity in Cancer (GDSC): A resource for therapeutic biomarker discovery in cancer cells. *Nucleic Acids Res.* **2012**, *41*, D955–D961. [CrossRef]
51. Brown, D.V.; Filiz, G.; Daniel, P.M.; Hollande, F.; Dworkin, S.; Amiridis, S.; Kountouri, N.; Ng, W.; Morokoff, A.P.; Mantamadiotis, T. Expression of CD133 and CD44 in glioblastoma stem cells correlates with cell proliferation, phenotype stability and intra-tumor heterogeneity. *PLoS ONE* **2017**, *12*, e0172791. [CrossRef] [PubMed]
52. Bayat Mokhtari, R.; Homayouni, T.S.; Baluch, N.; Morgatskaya, E.; Kumar, S.; Das, B.; Yeager, H. Combination therapy in combating cancer. *Oncotarget* **2017**, *8*, 38022–38043. [CrossRef]
53. Chamberlain, M.C. Temozolomide: Therapeutic limitations in the treatment of adult high-grade gliomas. *Expert Rev. Neurother.* **2010**, *10*, 1537–1544. [CrossRef] [PubMed]
54. Kaaijk, P.; Troost, D.; Morsink, F.; Keehnen, R.M.; Leenstra, S.; Bosch, D.A.; Pals, S.T. Expression of CD44 splice variants in human primary brain tumors. *J. Neuro-Oncol.* **1995**, *26*, 185–190. [CrossRef]
55. Schmitz, M.; Temme, A.; Senner, V.; Ebner, R.; Schwind, S.; Stevanovic, S.; Wehner, R.; Schackert, G.; Schackert, H.K.; Fussel, M.; et al. Identification of SOX2 as a novel glioma-associated antigen and potential target for T cell-based immunotherapy. *Br. J. Cancer* **2007**, *96*, 1293–1301. [CrossRef]
56. Zhang, M.; Song, T.; Yang, L.; Chen, L.; Wu, L.; Yang, Z.; Fang, J. Nestin and CD133: Valuable stem cell-specific markers for determining clinical outcome of glioma patients. *J. Exp. Clin. Cancer Res.* **2008**, *27*, 85. [CrossRef] [PubMed]
57. Bradshaw, A.; Wickremsekera, A.; Tan, S.T.; Peng, L.; Davis, P.F.; Itinteang, T. Cancer Stem Cell Hierarchy in Glioblastoma Multiforme. *Front. Surg.* **2016**, *3*, 21. [CrossRef]
58. Lee, G.; Auffinger, B.; Guo, D.; Hasan, T.; Deheeger, M.; Tobias, A.L.; Kim, J.Y.; Atashi, F.; Zhang, L.; Lesniak, M.S.; et al. Dedifferentiation of Glioma Cells to Glioma Stem-like Cells By Therapeutic Stress-induced HIF Signaling in the Recurrent GBM Model. *Mol. Cancer Ther.* **2016**, *15*, 3064. [CrossRef] [PubMed]
59. Corno, C.; Arrighetti, N.; Ciusani, E.; Corna, E.; Carenini, N.; Zaffaroni, N.; Gatti, L.; Perego, P. Synergistic Interaction of Histone Deacetylase 6- and MEK-Inhibitors in Castration-Resistant Prostate Cancer Cells. *Front. Cell Dev. Biol.* **2020**, *8*. [CrossRef]
60. Yamada, R.; Nakano, I. Glioma stem cells: Their role in chemoresistance. *World Neurosurg.* **2012**, *77*, 237–240. [CrossRef]
61. Hombach-Klonisch, S.; Mehrpour, M.; Shojaei, S.; Harlos, C.; Pitz, M.; Hamai, A.; Siemianowicz, K.; Likus, W.; Wiechec, E.; Toyota, B.D.; et al. Glioblastoma and chemoresistance to alkylating agents: Involvement of apoptosis, autophagy, and unfolded protein response. *Pharmacol. Ther.* **2018**, *184*, 13–41. [CrossRef]
62. Liu, G.; Yuan, X.; Zeng, Z.; Tunici, P.; Ng, H.; Abdulkadir, I.R.; Lu, L.; Irvin, D.; Black, K.L.; Yu, J.S. Analysis of gene expression and chemoresistance of CD133+ cancer stem cells in glioblastoma. *Mol. Cancer* **2006**, *5*, 67. [CrossRef] [PubMed]
63. Wick, W.; Weller, M.; van den Bent, M.; Sanson, M.; Weiler, M.; von Deimling, A.; Plass, C.; Hegi, M.; Platten, M.; Reifenberger, G. MGMT testing—the challenges for biomarker-based glioma treatment. *Nat. Rev. Neurol.* **2014**, *10*, 372–385. [CrossRef] [PubMed]
64. Inocencio, J.; Frenster, J.D.; Placantonakis, D.G. Isolation of Glioblastoma Stem Cells with Flow Cytometry. In *Glioblastoma: Methods and Protocols*; Placantonakis, D.G., Ed.; Springer: New York, NY, USA, 2018; pp. 71–79.
65. Dundar, T.T.; Hatiboglu, M.A.; Ergul, Z.; Seyithanoglu, M.H.; Sozen, E.; Tuzgen, S.; Kaynar, M.Y.; Karaoz, E. Glioblastoma Stem Cells and Comparison of Isolation Methods. *J. Clin. Med. Res.* **2019**, *11*, 415–421. [CrossRef] [PubMed]
66. Pastrana, E.; Silva-Vargas, V.; Doetsch, F. Eyes wide open: A critical review of sphere-formation as an assay for stem cells. *Cell Stem Cell* **2011**, *8*, 486–498. [CrossRef]

Article

Interaction of Glia Cells with Glioblastoma and Melanoma Cells under the Influence of Phytocannabinoids

Urszula Hohmann ^{1,†} , Christoph Walsleben ^{1,†}, Chalid Ghadban ¹, Frank Kirchhoff ² , Faramarz Dehghani ¹ 
and Tim Hohmann ^{1,*} 

¹ Department of Anatomy and Cell Biology, Medical Faculty, Martin Luther University Halle-Wittenberg, Grosse Steinstrasse 52, 06108 Halle (Saale), Germany; urszula.hohmann@medizin.uni-halle.de (U.H.); cwalsleben@t-online.de (C.W.); chalid.ghadban@medizin.uni-halle.de (C.G.); faramarz.dehghani@medizin.uni-halle.de (F.D.)

² CIPMM, Department of Physiology, Faculty of Medicine, Saarland University, Building 48, 66421 Homburg, Germany; frank.kirchhoff@uks.eu

* Correspondence: tim.hohmann@medizin.uni-halle.de; Tel.: +49-3455571316

† These authors contributed equally to this work.

Abstract: Brain tumor heterogeneity and progression are subject to complex interactions between tumor cells and their microenvironment. Glioblastoma and brain metastasis can contain 30–40% of tumor-associated macrophages, microglia, and astrocytes, affecting migration, proliferation, and apoptosis. Here, we analyzed interactions between glial cells and LN229 glioblastoma or A375 melanoma cells in the context of motility and cell–cell interactions in a 3D model. Furthermore, the effects of phytocannabinoids, cannabidiol (CBD), tetrahydrocannabinol (THC), or their co-application were analyzed. Co-culture of tumor cells with glial cells had little effect on 3D spheroid formation, while treatment with cannabinoids led to significantly larger spheroids. The addition of astrocytes blocked cannabinoid-induced effects. None of the interventions affected cell death. Furthermore, glial cell-conditioned media led to a significant slowdown in collective, but not single-cell migration speed. Taken together, glial cells in glioblastoma and brain metastasis micromilieu impact the tumor spheroid formation, cell spreading, and motility. Since the size of spheroid remained unaffected in glial cell tumor co-cultures, phytocannabinoids increased the size of spheroids without any effects on migration. This aspect might be of relevance since phytocannabinoids are frequently used in tumor therapy for side effects.

Keywords: THC; CBD; microglia; astrocytes; glioblastoma; melanoma; brain metastasis



Citation: Hohmann, U.; Walsleben, C.; Ghadban, C.; Kirchhoff, F.; Dehghani, F.; Hohmann, T. Interaction of Glia Cells with Glioblastoma and Melanoma Cells under the Influence of Phytocannabinoids. *Cells* **2022**, *11*, 147. <https://doi.org/10.3390/cells11010147>

Academic Editors: Javier S. Castresana, Bárbara Meléndez and Pablo Martín-Vasallo

Received: 16 November 2021

Accepted: 31 December 2021

Published: 3 January 2022

Publisher's Note: MDPI stays neutral with regard to jurisdictional claims in published maps and institutional affiliations.



Copyright: © 2022 by the authors. Licensee MDPI, Basel, Switzerland. This article is an open access article distributed under the terms and conditions of the Creative Commons Attribution (CC BY) license (<https://creativecommons.org/licenses/by/4.0/>).

1. Introduction

Controlling the microenvironment and immune system seem to be promising strategies to treat brain tumors. For both glioblastoma (GBM) and brain metastases, the effect of total neurosurgical resection and other therapy options are limited and survival rates remain very poor. The standard treatment consists of surgery, followed by adjuvant radio- and chemotherapy. Therefore, new effective treatment strategies and targets for GBM and brain metastasis are needed, including therapies targeting the tumor micromilieu. The cellular components of the micromilieu in brain tumors include mainly tumor-associated microglia, macrophages and astrocytes, and cells of the perivascular niche and additional peripheral immune cells [1,2]. The composition of immune cells and activation types within the tumor is dynamic and stage dependent [3].

In GBM, the most malignant form of primary brain tumors, up to 30% of the tumor mass can be comprised of tumor-associated microglia and macrophages (TAM) [4,5]. Interestingly, the amount of TAM negatively correlates with clinical outcome and positively with the staging of glioma [6]. In response to endogenous or exogenous stimuli microglia appear in many distinct stages of activation with different motility, expression of molecules

and cytokines. The tumor-associated microglia display an amoeboid morphology similar to activated microglia observed in other pathologies [3]. Untreated primary murine microglia were shown to promote the migration of GL261 mouse glioma cells in Boyden chamber assays. Furthermore, the invasion of GBM cells was significantly reduced in absence of microglia [7,8]. Most effects of microglia on tumor cell migration and motility were associated with secreted soluble factors, such as transforming growth factor-beta (TGF)- β , epidermal growth factor receptor (EGFR) ligands, diverse interleukins, and matrix metalloproteinases (MMP) [9–13]. In addition, untreated microglia reduced sphere formation of brain tumor-initiating cells in culture [14]. Despite microglia, also other cells of glial origin, including astrocytes, interact with and are found within brain tumors. Immunohistochemistry revealed that reactive astrocytes surrounded and infiltrated glioma in human biopsies and murine samples [15–17]. Astrocytes had not only glioma-protective effects against chemotherapy but also enhanced tumor invasion into the brain [16,18–23]. Furthermore, reactive astrocytes were described as a key component of a tumor-supportive post-surgery microenvironment [24]. Notably, astrocytes were activated by brain metastasis, such as melanoma, facilitating tumor cell invasion into the brain [25,26]. Astrocytes appeared to mediate their effects on the one hand via secreted factors such as TGF- β , interleukins, growth factors, etc. [21,27–32], and, on the other hand, via direct connections to tumor cells via gap junctions [20,33,34].

In past studies, cannabinoids that target the cannabinoid receptors CB₁ and/or CB₂ were shown to exert anti-tumoral effects in both GBM and melanoma. The two phytocannabinoids tetrahydrocannabinol (THC) and cannabidiol (CBD) reduced the tumor size in glioma xenograft models when applied alone or combined [35–43]. Similarly, in melanoma xenografts THC reduced tumor size and proliferation in a CB-dependent manner [44,45]. Despite that, cannabinoid receptor targeting could be associated with altered motility and cell elasticity in GBM cells and others [46,47], thus potentially affecting collective migration as well. Interestingly, both melanoma [48] and GBM [49] possess CB₁ and CB₂, while astrocytes express mostly CB₁ and microglia mainly CB₂ upon activation [50]. Paired with the anti-tumoral effects of cannabinoids these observations make CBs a potential substance class for targeting tumor cells and interfering with the tumor-stroma-cell cross talk. Currently, the question is not addressed if and how cannabinoids affect tumor-stroma cell cross-talk in the central nervous system.

In this study, the effects of the two phytocannabinoids, namely THC and CBD were evaluated on melanoma or GBM spheroid formation, as well as collective and single-cell migration. Furthermore, the impact of astrocytes or microglia on spheroid formation was analyzed, and the impact of cannabinoids on interactions between tumor and astrocytes or tumor and microglia was investigated.

2. Materials and Methods

All experiments involving animal material were performed in accordance with the directive 2010/63/EU of the European Parliament and the Council of the European Union (22 September 2010) and approved by local authorities of the State of Saxony-Anhalt (permission number: I11M18) protecting animals and regulating tissue collection used for scientific purposes.

2.1. Cell Culture

Primary microglia and astrocytes were isolated and cultured from C57BL/6J and CX3CR1^{GFP/wt} [51,52] mice as described before [53,54]. After 10–14 days microglial cells were isolated from astrocytic monolayer and used for further experiments. A375 [55] (gifted by Simon Jasinski-Bergner, University Halle-Wittenberg, Halle (Saale), Germany), BV2 microglia [56] (obtained from Ullrich, University of Zürich, Zürich, Switzerland) and primary glial cells were cultured in DMEM (Invitrogen, Carlsbad, CA, USA) supplemented with 10% FBS (Invitrogen) and 1% penicillin/streptomycin (Invitrogen). LN229 [57] were cultured in RPMI medium (Lonza, Basel, Switzerland) with 10% FBS and 1% penicillin/streptomycin.

After two days, the medium was collected from confluent astrocytes or BV2 microglia, filtered (Sarstedt, Nümbrecht, Germany), and applied on the tumor cells in a 1:1 ratio with the respective culture medium. This medium was added 3 h before starting the imaging for both single cell and collective migration experiments.

For cannabinoid treatment cannabidiol (5 μ M, Tocris Bioscience, Bristol, UK) [39,58,59], tetrahydrocannabinol (5 μ M, Tocris) [42] or a combination of both was applied 3 h before the start of the experiments. THC and CBD were both dissolved in DMSO.

2.2. Single Cell Migration

For time-lapse microscopy, 4000 cells were seeded in a 12-well plate (Greiner, Kremsmünster, Austria) 24 h prior to the start of the experiments. On the day of experiment, cells were treated with cannabinoids and/or BV2 (BV2CM) or astrocyte conditioned (ACM) media and 3 h later the measurements were performed. Images were obtained every 10 min with a microscope (Leica DMI8, Leica, Wetzlar, Germany) equipped with CO₂ (5% *v/v*) and temperature (37 °C) regulation. The experiments were conducted as described previously [46] and the mean speed of each cell was calculated. Briefly, using the Sobel operator and morphological opening and closing cells were segmented and tracked over time.

2.3. Collective Migration

Cells (250,000 A375 or 400,000 LN229) were placed in a 12-well plate to obtain a dense monolayer. On the next day, the treatment with THC and/or CBD and/or BV2 or astrocyte conditioned medium was performed. Three hours later, measurements were started capturing a single image every 3 min.

Velocity fields were calculated using particle image velocimetry [60–62], with a cross-correlation window size of 32 \times 32 pixels (pixel size: 0.48 μ m).

The 4-point susceptibility χ was calculated for quantifying size and lifetime of collectively moving cells:

$$\chi = N[\langle Q(\Delta t)^2 \rangle - \langle Q(\Delta t) \rangle^2]$$

The peak of χ is proportional to the number of collectively moving cells in a dense layer, and the peak position corresponds to the pack life time [63,64]. Q is the self-overlap or order parameter given as:

$$Q(\Delta t) = \frac{1}{N} \sum_{i=1}^N w_i \text{ with } w = \begin{cases} 1; & \text{if } \Delta r > 0.2d \\ 0; & \text{else} \end{cases}$$

where N is the cell number and Δr is the cell's distance to its initial position and d is its diameter. Q gives the relative number of cells that moved away more than 20% of their cell size from their initial position.

2.4. 3D Spheroid Co-Culture Assay

Three-dimensional (3D) tumor aggregates were generated by using the liquid-overlay method as described before [65]. Cells (20,000) were placed in 96-wells coated with 4% (*w/v*) agarose (Peglabs, Erlangen, Germany) and imaged for 72 h, every 15 min. Image analysis was performed with self-developed software as described before [65]. Notably, imaging of spheroids started 6 h after cell seeding, because cells were needed to settle down and form an initially loose cell cluster corresponding to the final position of the aggregate inside the well.

Co-culture spheroids were generated with 5%, 10%, 15%, and 30% of astrocytes or CX3CR1 Δ /^{wt} microglia and tumor cells adding up to a total of 20,000 cells, and the optimal proportion of glia cells was determined. It must be noted that glia and tumor cells were added as a suspension together at the same time to the well plate for the formation of the spheroid. For further experiments, 30% of astrocytes were used since astrocytes made up to 30% of the tumor mass and this percentage showed the largest effects. For

microglia, a 10% ratio was chosen since it had the strongest effects, without fully disturbing spheroid formation.

For image analysis of spheroids, a custom-written software written in MatLab (The MathWorks, Natick, MA, USA) was used as described earlier [65]. Briefly, spheroids were segmented using a level set function for tracking each spheroid over time. To determine the size of the spheroid, the amount of its comprising pixels was assessed. After analysis, the spheroid size was normalized to the initial size (0 h) of the control of the respective cell line. For further analysis of growth characteristics, an exponential regime in the area oversize plot was identified manually in the log-log plot and fitted using the following equation:

$$A = A_0 \times e^{-t/t_0} + A_1$$

where A denotes the projected area of the spheroid and t the time. The ratio A_0/t_0 can be understood as a characteristic shrinkage rate.

2.5. Analysis of Proliferation in 3D Spheroids

Spheroids were removed from culture medium 72 h after seeding on agarose and fixed with 4% PFA. For staining, spheroids were incubated after fixation with succhrose (Carl Roth, Karlsruhe, Germany) and cut on a cryostat (Leica, Wetzlar, Germany) in 12 μ m thick slices.

First, normal goat serum was applied for 30 min before incubation with primary antibody overnight (anti-Ki67 antibody for proliferation assessment, DSC innovative Diagnostic System, Hamburg, German). On the next day, washing steps were performed, before application of secondary antibodies (anti-rabbit Alexa Fluor 488, Thermo Fisher Scientific, Waltham, MA, USA) followed by incubation with DAPI (Sigma-Aldrich). Finally, sections were washed and covered with DAKO mounting medium.

After labeling, slices were imaged with a laser scanning microscope (Leica DMI8), using a 63 \times objective. For proliferation analysis, DAPI and Ki67 images were first denoised using the BM3D filter [66] and subsequently thresholded to obtain binary images of both the DAPI and Ki67 channel. A proliferative index was calculated as the ratio of the number of Ki67 positive pixels that were also DAPI positive relative to the number of DAPI positive pixels.

2.6. Flow Cytometry Measurements and Gating Strategies

Spheroids from at least three independent experiments were dissociated with trypsin/EDTA (Thermo Fisher Scientific, Waltham, MA, USA) and propidium iodide (1 μ L/mL, Miltenyi Biotec GmbH, Bergisch Gladbach, Germany) was added to identify dead cells. All samples were measured (30–80,000 events per panel) by using the flow cytometry analyzer MACS Quant 10 (Miltenyi Biotec GmbH).

The gating strategy is depicted in Supplementary Figure S5. Data are presented as the percentage of dead cells relative to the overall number of cells measured. Co-expression analyses of GFP and PI were performed in one flow cytometric multi-color panel to prove the presence of dead microglia.

2.7. Statistics

Data are presented as the mean standard error of the mean (SEM) of at least three independent experiments. The SEM is depicted either as error bars or shaded areas. Precise sample sizes are given in the Supplementary Materials—Table S1. Data were analyzed with a one-way ANOVA test with Tukey post test. Differences were considered significant at $p \leq 0.05$.

3. Results

3.1. Cannabinoid Induced Slowdown of Spheroid Formation Is Abrogated by Glia Cells

For co-culture experiments evaluating the effect of astrocytes and microglia on spheroid formation, an optimal glial to tumor cell ratio was established with microglia or astrocyte proportions from 5 to 30%. The strongest deviations from control conditions were

observed for 10% microglia and 30% astrocytes (Supplementary Figures S1 and S2), and these concentrations were used for further experiments. Notably, the sample size (Supplementary Table S1) for these initial tests was lower and after the addition of 30% microglia to A375 cells the spheroid formation was significantly distorted.

Interestingly, both CBD and THC alone inhibited spheroid aggregation in terms of spheroid size in pure A375 melanoma and LN229 GBM cell cultures (Figures 1a–c and 2a–c).

Adding CX3CR1^{GFP/wt} microglia [51] cells alone led to an initial inhibition of the aggregation process, but did not influence the state of equilibrium for spheroid aggregation after 70 h for both tumor cell types (Figures 1e–g and 2e–g). For A375 cells, the addition of both cannabinoids to the microglia-A375 co-culture did not affect initial aggregation speed and only led to larger spheroids in equilibrium after 70 h for all cannabinoid combinations when compared to the microglia-A375 co-cultures (Figure 1e–g). For LN229 cells, adding THC, CBD, or a combination of both to the LN229-microglia co-cultures led to an initial acceleration of spheroid aggregation that could not be observed anymore in equilibrium. CBD or THC alone did not cause an initially increased aggregation and led to an inhibition of aggregation in equilibrium after 70 h compared to the LN229-microglia co-cultures (Figure 1e–g).

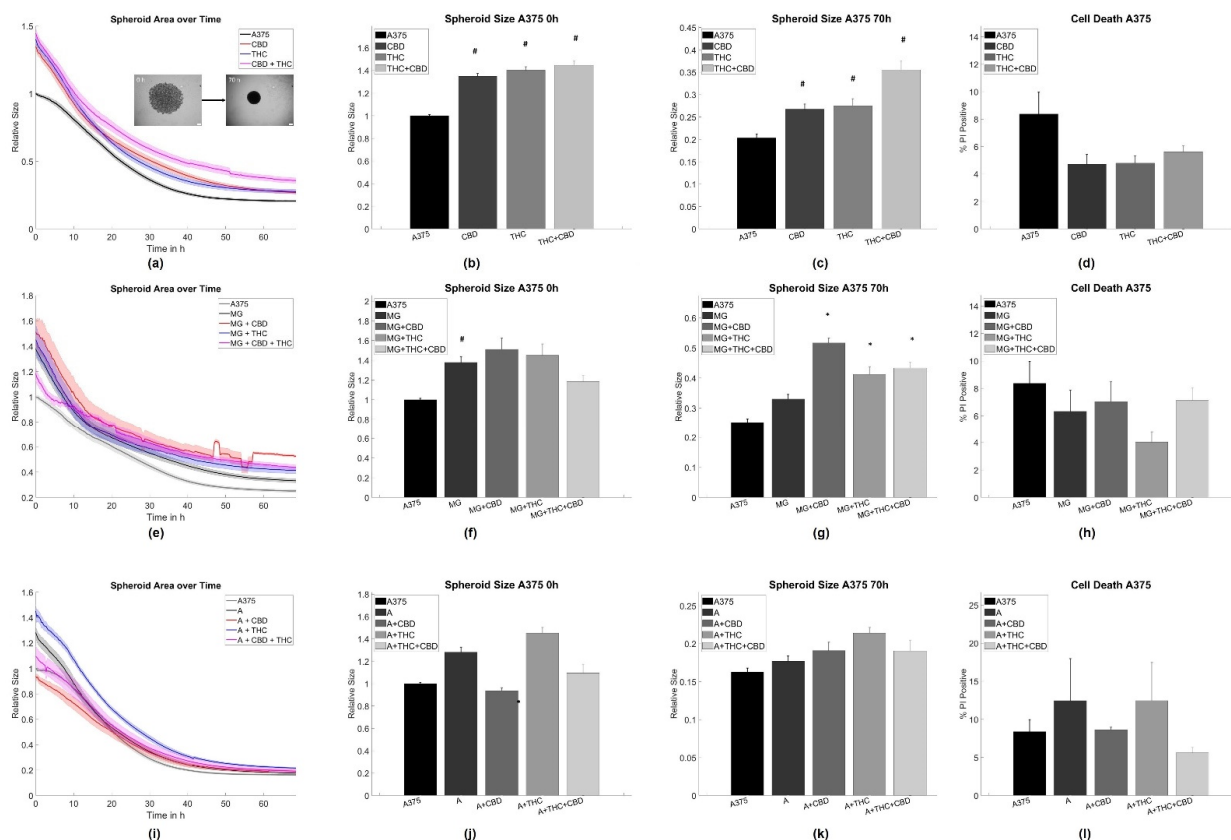


Figure 1. Aggregation results for A375 melanoma cells. (a–c) Average time evolutions of spheroid sizes for A375 cells treated with cannabinoids. The inset depicts a typical spheroid aggregation. (d,h,l) Ratio of cell death in A375 spheroids treated with cannabinoids. (e–g) Time evolution of tumor-microglia (MG) spheroid sizes and cell death for co-cultures with and without cannabinoid treatment. (i–k) Time evolution of tumor-astrocyte (A) spheroid sizes and cell death for treatment co-cultures with and without cannabinoid treatment. Relative size: Values are normalized to the respective untreated control cell line at time point 0 h referring to the start of the measurement. Stars (*) depict significant results against the spheroids mixed with astrocytes or microglia, respectively. Hashes (#) depict significant results against the untreated control. Error bars and shaded areas depict the standard error of the mean. Abbreviations: CTL: control, CBD: cannabidiol, THC: tetrahydrocannabinol, A: astrocytes, MG: microglia.

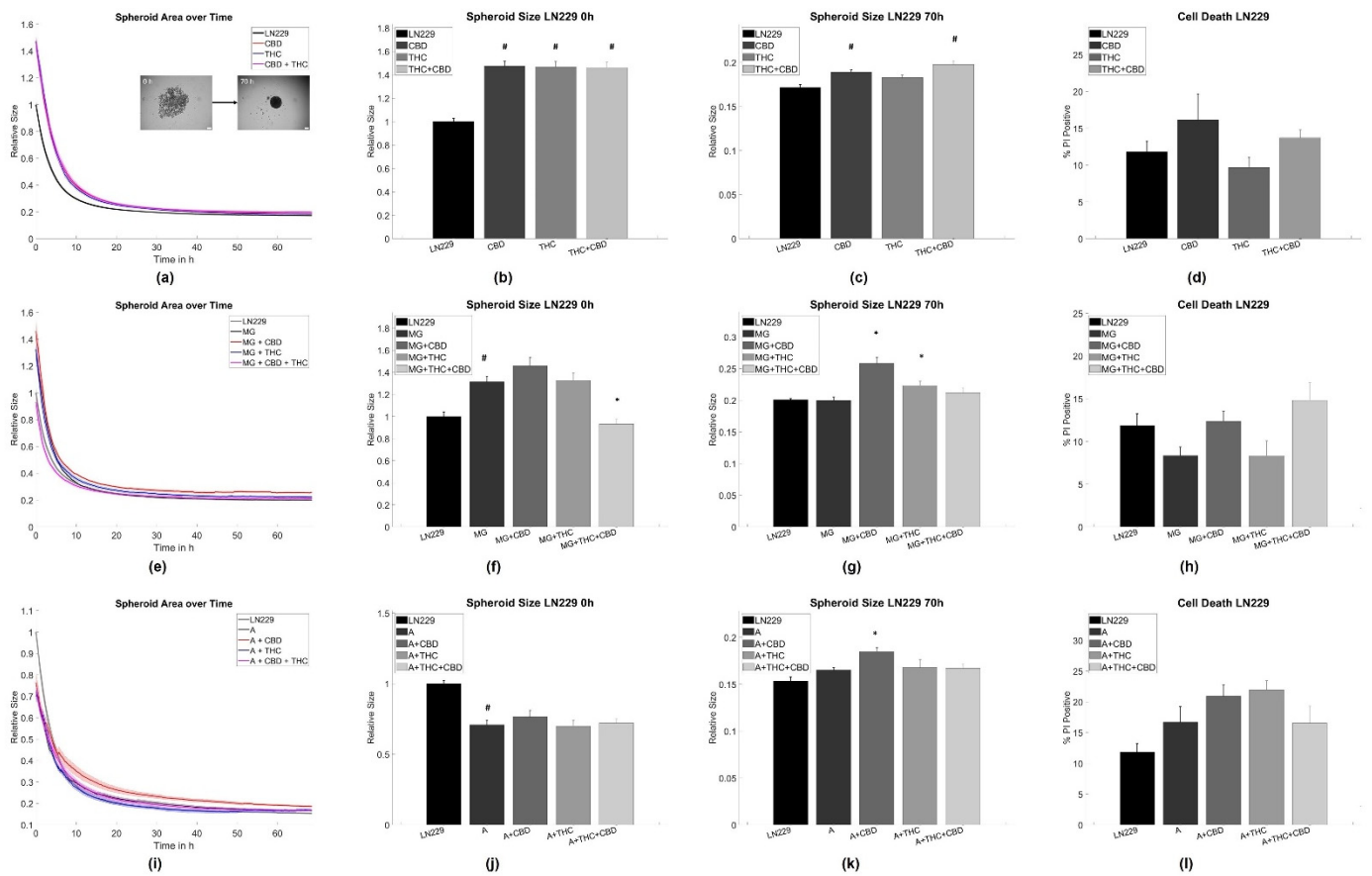


Figure 2. Aggregation results for LN229 GBM cells. (a–c) Average time evolutions of spheroid sizes for LN229 cells treated with cannabinoids. The inset depicts a typical spheroid aggregation. (d,h,l) Ratio of cell death in LN229 spheroids treated with cannabinoids. (e–g) Time evolution of tumor-microglia (MG) spheroid sizes and cell death for co-cultures with and without cannabinoid treatment. (i–k) Time evolution of tumor-astrocytes (A) spheroid sizes and cell death for co-cultures with and without cannabinoid treatment. Relative size: Values are normalized to the respective untreated control cell line at time point 0 h referring to the start of the measurement. Stars (*) depict significant results against the spheroids mixed with astrocytes or microglia, respectively. Hashes (#) depict significant results against the untreated control. Error bars and shaded areas depict the standard error of the mean. Abbreviations: CTL: control, CBD: cannabidiol, THC: tetrahydrocannabinol, A: astrocytes, MG: microglia.

Creating astrocyte-tumor co-cultures had no significant effect on spheroid formation in A375 cells but led to an initial acceleration of the aggregation process in LN229 that was not found after 70 h anymore. The addition of astrocytes to both tumor cell types inhibited most of the cannabinoid-induced effects. Significant differences were found in the initial aggregation behavior for astrocyte-A375 co-cultures when treated with CBD and in the equilibrium conditions for astrocyte-LN229 co-cultures treated with CBD, when compared to the untreated co-cultures (Figures 1i–k and 2i–k).

For further analysis of the aggregation dynamics beyond the starting and end point, the aggregation speed was investigated in an exponential shrinkage phase (Supplementary Figure S3), corresponding to the interval of 2–20 h for LN229 and 15–45 h for A375 cells. Notably, most of the shrinkage of the spheroids occurred in the mentioned time intervals. In LN229 spheroids, both cannabinoids induced faster aggregation when applied alone or in combination, while the addition of astrocytes slowed down spheroid aggregation and blocked the cannabinoid effects in the exponential phase. Furthermore, the addition of microglia cells reduced the spheroid aggregation speed of LN229 cells, but to a lesser

extent than astrocytes. Microglia cells also abolished cannabinoid-associated effects on aggregation speed for THC, CBD, and the combined treatment. For the THC+CBD treatment aggregation was—in contrast to the control conditions—slowed down.

For A375, the characteristic aggregation speeds were not influenced by cannabinoids, astrocytes, or cannabinoids + astrocytes. Only microglia slowed down the aggregation speed in A375 cells and this effect was not affected by cannabinoid treatment (Supplementary Table S2).

As cannabinoids are known to induce cell death, it was evaluated if any of the chosen treatments caused changes in cell viability, as this may alter spheroid formation. For both cell types and all treatments, we did not find significant changes in cell viability, and cell death rates were between 10–20% for A375 cells and 4–12% for LN229 cells, depending on the exact treatment (Figure 1d,h,k and Figure 2d,h,k). Similarly, cannabinoid treatment is associated with changes in proliferation. Thus, the relative number of cells not being in the G0 phase using Ki67 labeling in spheroid sections was analyzed. The analysis revealed that the overall amount of proliferative cells was very low (<5%), independent of the chosen treatment, and no statistically significant differences were found (supplementary Table S3, Supplementary Figure S4). Consequently, proliferation is considered to be—at most—of minor importance in this specific model.

As spheroid aggregation, especially in the initial phase, largely depends on the formation of cell–cell contacts and tension, it was next evaluated if cannabinoids and/or supernatants of astrocytes or microglia affect single cell or collective migration.

3.2. BV2 and Astrocyte Supernatants Inhibit Collective But Not Single Cell Migration

To assess single tumor cell motility, the application of both CBD and/or THC alone or in combination with BV2 and astrocyte supernatants was performed, corresponding to the same groups as for the spheroid formation assay. Thereby, no statistically significant difference for A375 melanoma and LN229 GBM cells was found Figures 3a,d,g and 4a,d,g. Next, the collective migration speed of both cell types was analyzed in a dense monolayer under the same conditions. Again, cannabinoids alone did not influence the mean layer migration speed Figures 3b,c and 4b,c, but the supernatants of both BV2 cells and astrocytes reduced layer speed to 55–65% of the control levels for both tumor types. Notably, this effect was not significantly altered after the addition of both cannabinoids Figures 3e,f,h,i and 4e,f,h,i.

To further evaluate the origin of changes in migratory behavior, the order parameter and the four-point susceptibility were evaluated. Again no effects of cannabinoids were seen on the order parameter for both cell lines (Figure 5a,c). The application of supernatant resulted in a delayed drop of the order parameter for both cell types (Figure 5e,g,i,k). Such behavior implies that cells stay significantly longer near their initial location and the monolayer shows less reorganization, agreeing with the reduced layer migration speed. From the order parameter, the four-point susceptibility was calculated to analyze the time cells move together as packs (position of the peak) and how many cells move as a pack together (Figure 5b,d,f,h,j,l). After determination of the peak heights, A375 cells were found to move in packs of 3.3 ± 3 cells and all treatments resulted in pack sizes from 2.7 to 6.1 cells, with similar standard deviations. For LN229, the pack size was around 4.1 ± 3 cells and all treatments altered pack size to values from 2.4 to 7 cells, with similar standard deviations. Thus, none of the interventions had a significant impact on the number of collectively moving cells for both tumor entities. Analyzing the peak position cannabinoids showed no significant effect on the time cells move together in a pack for both A375 cells (from 135 min to 123 to 165 min) and LN229 (from 156 min to 147 to 170 min). Supernatants of astrocytes and BV2 cells increased the time A375 cells move together as a pack from 135 min to 225 min or 183 min, respectively. For LN229 cells, a qualitatively similar behavior was found, with both supernatants increased pack life time from 156 min to 291 min or 255 min, respectively (Figure 5b,d,f,h,j,l). Consequently, this analysis supports the results obtained from the layer migration speed and order parameter and shows that A375 and LN229 cells treated with supernatants display statistically less layer reorganization and thus migration.

Cannabinoids did not significantly change the effects of supernatants on both tumor cell types. Thus, this data indicates, that both cannabinoids do not influence single-cell or collective migration, while supernatants of BV2 microglia or primary astrocytes inhibit collective but not single-cell migration.

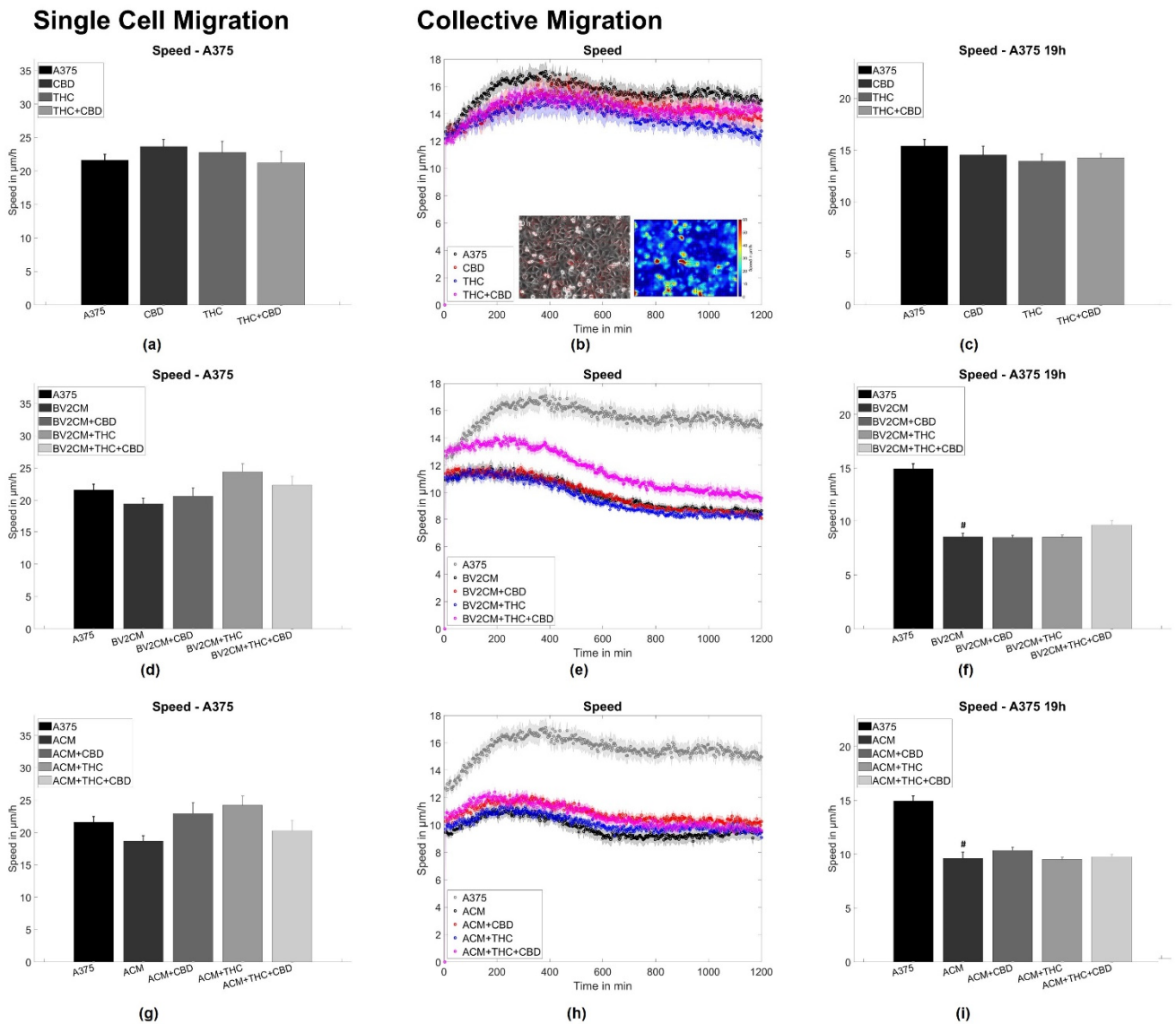


Figure 3. Single cell and collective motion of A375 melanoma cells. (a) Single-cell motility of A375 cells treated with cannabinoids. (b) Collective migration speed for A375 cells treated with cannabinoids. The inlet shows a typical phase contrast image, overlaid with the associated velocity vectors and a heat map of the local speed overlaid with the velocity vectors. (c) Shows the averaged collective migration speeds from 18–20 h of A375 cells treated with cannabinoids. (d–f) Same measurements as shown in (a–c) but for A375 cells treated with microglia conditioned media and cannabinoids. (g–i) Same measurements as shown in (a–c) but for A375 cells treated with microglia conditioned media and cannabinoids. Hashes (#) depict significant results against the untreated control. Error bars and shaded areas depict the standard error of the mean. Abbreviations: CTL: control, CBD: cannabidiol, THC: tetrahydrocannabinol, ACM: astrocyte conditioned media, BV2CM: BV2 cell-conditioned media.

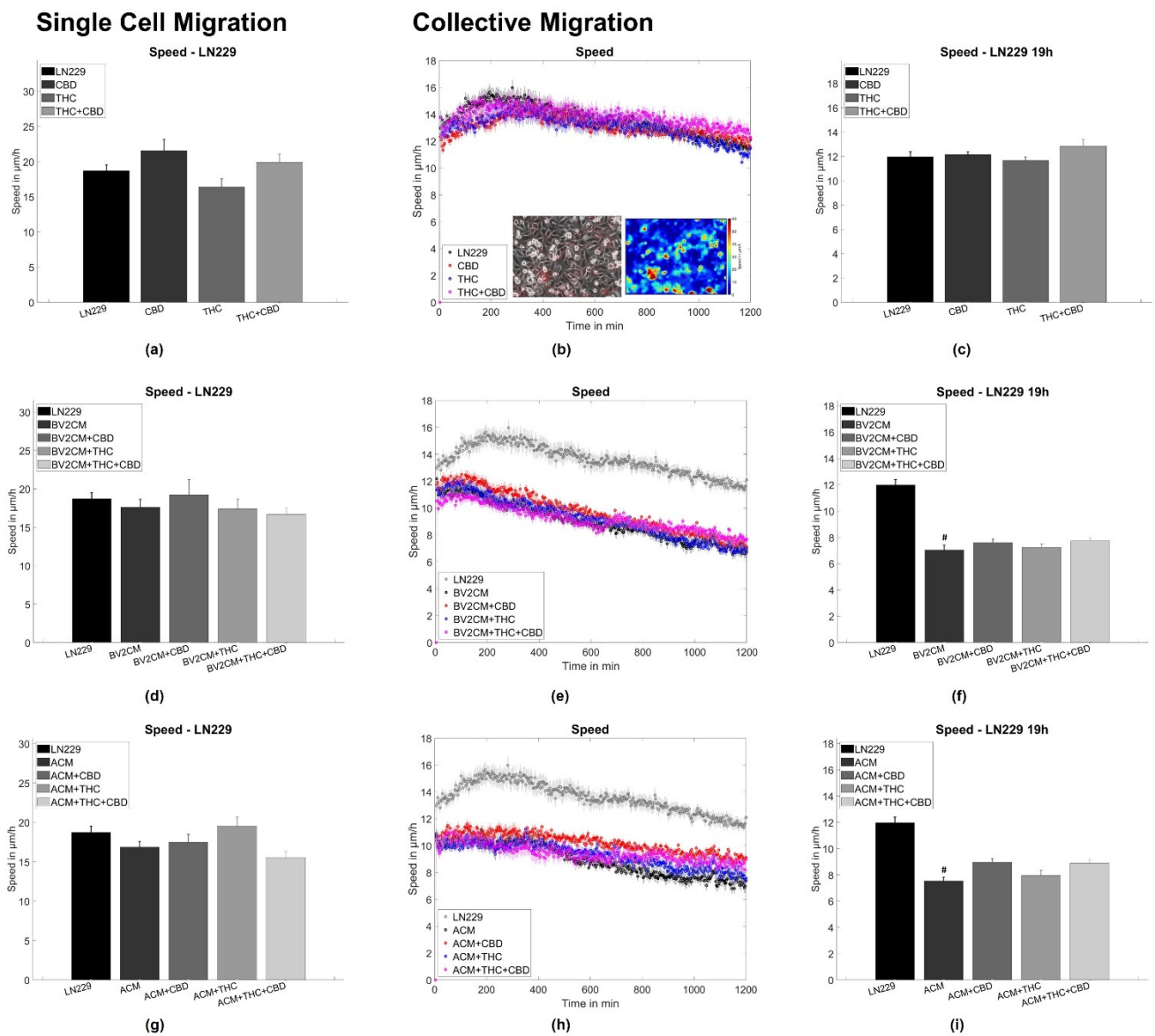


Figure 4. Single cell and collective motion of LN229 GBM cells. (a) Single-cell motility of LN229 cells treated with cannabinoids. (b) Collective migration speed for LN229 cells treated with cannabinoids. The inlet shows a typical phase contrast image, overlaid with the associated velocity vectors and a heat map of the local speed overlaid with the velocity vectors. (c) Shows the averaged collective migration speeds from 18–20 h of LN229 cells treated with cannabinoids. (d–f) Same measurements as shown in (a–c) but for LN229 cells treated with microglia conditioned media and cannabinoids. (g–i) Same measurements as shown in (a–c) but for LN229 cells treated with microglia conditioned media and cannabinoids.. Hashes (#) depict significant results against the untreated control. Error bars and shaded areas depict the standard error of the mean. Abbreviations: CTL: control, CBD: cannabidiol, THC: tetrahydrocannabinol, ACM: astrocyte conditioned media, BV2CM: BV2 cell-conditioned media.

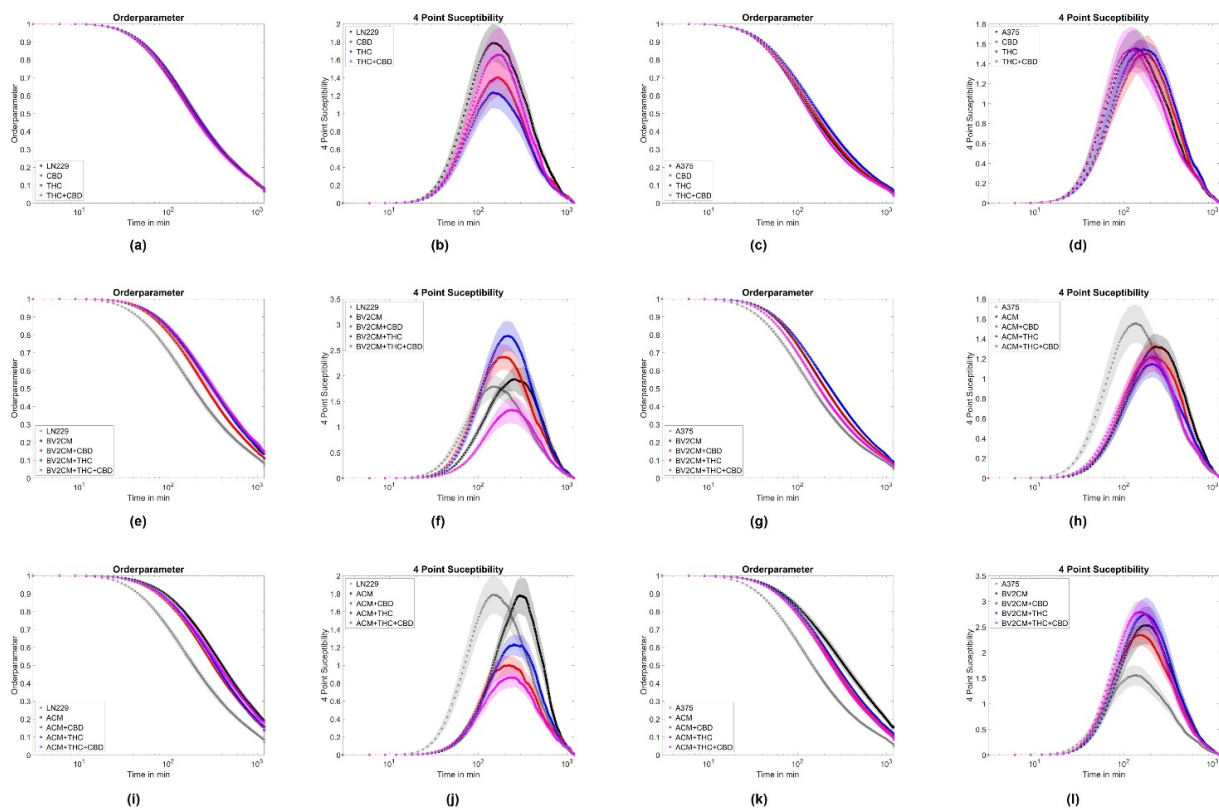


Figure 5. Collective motion parameters for LN229 and A375 cells. (a,e,i) represent the average order parameter Q for LN229 cells, when treated with cannabinoids, astrocyte supernatants and cannabinoids or microglia supernatants and cannabinoids. (b,f,j) show the associated four-point susceptibility for LN229 cells. (c,g,k) represent the average order parameter Q for A375 cells, when treated with cannabinoids, astrocyte supernatants, and cannabinoids or microglia supernatants and cannabinoids. (d,h,l) show the associated four-point susceptibility for A375 cells. Shaded areas depict the standard error of the mean. Abbreviations: CTL: control, CBD: cannabidiol, THC: tetrahydrocannabinol, ACM: astrocyte conditioned media, BV2CM: BV2 cell-conditioned media.

4. Discussion

In this study, the functional role of tumor–stroma cell interactions was examined, and the influence of CBD and THC on these interactions was explored. The tumor stroma, the non-neoplastic part of the tumor microenvironment is composed of extracellular matrix and non-neoplastic cells [67]. Here, we focused on interactions between tumor cells and glial cells, especially astrocytes and microglia cells. For both astrocytes and microglia, it is known that they have complementary functions in homeostasis [68]. Furthermore, the glial cells without contact with tumor cells behave differently and have anti-tumorous properties in contrast to tumor-associated cells [69]. Here, microglia and astrocytes affected the initial formation dynamics of 3D aggregates but not the equilibrium conditions (70 h), while cannabinoids tended to hamper aggregate formation. Furthermore, astrocyte and microglia supernatants inhibited collective but not single-cell migration. In addition, cannabinoids did not affect cell migration.

4.1. Astrocytes and Microglia Inhibit Initial Spheroid Formation

Both astrocytes and microglia reduced spheroid formation speed in LN229 cells, whereas in A375 co-cultures microglia but not astrocytes reduced the speed of spheroid formation. All treatments did not affect spheroid size at 70 h. During the formation of 3D aggregates, the size and shape of spheroids have been shown to be primarily determined by cell–cell and cell–matrix adhesion and generated tension [70–72]. Consequently, the addition of astrocytes or microglia in the current study likely affects the formation of

adhesion sites and/or the buildup of tension. As a significant part of the tumor spheroid in co-cultures consisted of stroma cells, it cannot be excluded that the here observed effects are—at least partly—mediated by a physical blockade or different affinities of tumor cell–tumor cell and tumor cell–glial cell adhesions. Following this argument, a linear or bimodal relation between the stroma-to-tumor cell ratio and the spheroid size was expected. Yet, no dependence of aggregate size on glial cell number was observed here. Thus, the hindered spheroid aggregation was likely not only caused by physical/space constraints. A further potential explanation might be altered signaling pathways causing changes in tension and/or adhesion. TAM and tumor-associated astrocytes were demonstrated to secrete increased amounts of growth factors, such as EGFR ligands, TGF- β , interleukins, and others [9–13,21,27–32]. These molecules were previously demonstrated to induce changes in cytoskeletal organization and expression of adhesion molecules, such as N-cadherin, actin, or vimentin [73–79]. Despite secreted molecules, direct contacts via gap junctions were found to be a major contributor to astrocyte–tumor interactions. Noteworthy is connexin 43, which interacts with F-actin, β -tubulin, N-cadherin, myosin II, and the actin-binding proteins drebrin und cortactin [80–83]. Via such signaling, it seems plausible that astrocytes and microglia affected adhesion and tension and thus spheroid formation in this study. Yet, the exact mechanisms need to be elucidated. Our data additionally suggest that the astrocyte/microglia-induced changes affect mostly the adhesion/tension dynamics of spheroid formation, as the effects were only present at the beginning of the measurement and did not persist in equilibrium. Notably, the effects of astrocytes and microglia on spheroid formation and speed were very similar for both, pointing to a more general mechanism although the signaling might be strongly different between melanoma and GBM cells [84,85]. In spheroid-based models, multiple cell types can be cultured together to generate multicellular heterotypic spheroids, accurately recapitulating tumor features including cellular heterogeneity, molecular mechanism, cell–cell/cell–matrix interactions, similar to those under *in vivo* conditions [67]. In this study, tumor cells and one specific glia cell type were co-cultured to analyze the impact of glia cells on interactions between tumor cells and glia. The model used herein qualifies as an important step in understanding tumor–stroma interactions. Indeed, in more complex organotypic models and tumor slice cultures, additional interactions will potentially yield a more complex behavior as a sum of effects will be detected caused by differential extracellular matrix composition and further cell types, such as e.g., infiltrating immune cells, endothelial cells, etc. However, this complexity will prevent the investigation of the impact of a single cell type.

4.2. THC and CBD Inhibit Spheroid Aggregation

The effect of cannabinoids on the final aggregates of melanoma and GBM cells was qualitatively the same, as the treatment with CBD and THC led to larger aggregates. In terms of dynamics cannabinoids induced faster aggregation in LN229 cells, but not in A375, while the addition of glial cells tended to reduce the aggregation speeds in both cell lines. GBM and melanoma cells express both cannabinoid receptors [46,49,86]. Both cannabinoids appeared to change the ratio of tension to adhesion in favor of tension. A previous study demonstrated changes in cell-elastic modulus and reduction in adhesion in GBM cells after targeting CB₁ or CB₂ [46]. Both effects might explain the observed larger spheroid sizes and altered dynamics. Furthermore, cannabinoids—including THC—were found to affect signaling cascades relevant for cytoskeletal organization and adhesion formation, such as decreased FAK phosphorylation in mammary carcinoma cells [87,88] or increased FAK phosphorylation in lung carcinoma cells [89]. Moreover, in PC12, Chinese hamster ovarian and neuroblastoma cells THC and CBD reduced the levels of β -tubulin and β -actin and/or induced changes in cytoskeletal organization [90–92]. Additionally, the CB₁/CB₂ agonist HU210 induced significant reorganization of the actin and microtubule cytoskeleton and reduced expression of β -tubulin and β -actin in PC12 cells [93]. These observations are in agreement with our previous results demonstrating cell-type and receptor-dependent changes in actin cytoskeleton organization after targeting CB₁ or CB₂ [94]. All mentioned

signaling routes may affect tension and adhesion formation and thus be potential candidates explaining the observed effects of cannabinoids on spheroid formation.

Another issue causing an increase in spheroid size may be increased proliferation. Nevertheless, past studies reported anti-proliferative effects of both THC and CBD, often for significantly higher doses [48,95,96]. In our model system, we did not see significant proliferative activity in spheroids with on average less than 5% of cells not being in the G0 phase, independent of the used treatment. Consequently, effects associated with proliferation or apoptosis appear unlikely as cause for changes in spheroid aggregation.

The effects of phytocannabinoids are dependent on their preparation, concentration, the treated cell type, and the abundance of receptor targets. In GBM, both THC and CBD have been shown to activate in part similar targets and include several cellular pathways which are possibly involved in the regulation of spheroid size [95] as observed here. CBD modulated the activation of pAKT, mTOR, pERK, β -catenin, PLCG1, and p38 MAPK, and pSTAT3 [43,97]. THC, CBD, or a combination of both reduced the activation of pAKT [98]. Administration of THC inhibited MMP-2 expression in an in vivo model of glioma [35,99,100]. Furthermore, THC induced phosphorylation of eukaryotic translation initiation factor 2 α (eIF2 α) followed by activation of an ER stress response that promoted autophagy via tribbles homolog 3-dependent (TRB3-dependent) and inhibited Akt/mammalian target of rapamycin complex 1 (mTORC1) axis [42].

Little is known about the effects of THC or CBD on signaling cascades in melanoma cells. Akt was involved in the inhibition of melanoma cell proliferation after THC treatment, while ERK, JNK, and p38 MAPK were not significantly affected [48]. THC-induced autophagy was not prevented by knockdown of Beclin-1, suggesting that in contrast to glioma, noncanonical autophagy-mediated apoptosis in response to THC in melanoma [42,45,100]. In the current study, a highly complex system was used containing GBM or melanoma cells in co-culture with glial cells treated with up to two cannabinoids. This complex model makes the comparison with other in vitro models very difficult and needs a systematic analysis of intracellular pathways in order to better understand the tumor microenvironment and effects of cannabinoids.

Interestingly, when cannabinoids were applied to tumor-astrocyte co-cultures most cannabinoid-associated effects were abolished, while for tumor-microglia co-cultures most effects persisted. Recent studies demonstrated the formation of gap junctions between astrocytes and melanoma and GBM cells mediating chemo-protective effects in a potentially calcium-dependent manner [32,101]. Moreover, astrocytes were demonstrated to actively rescue GBM cells from apoptosis [102]. Comparable mechanisms might be responsible for the absence of effects in the astrocyte co-cultures treated with cannabinoids. Opposing effects of TAM have been reported in different tumor types. They have been shown to be partly responsible for resistance to classical anti-tumor treatments, but also to improve treatment efficacy [103,104].

4.3. Supernatants of Astrocytes and Microglia But Not THC or CBD Inhibit Collective Migration

As the results from spheroid aggregation experiments hint towards changes in adhesion and/or tension dynamics we evaluated the effects of astrocyte or microglia supernatants on single cell and collective migration. Interestingly, for both cell types, supernatants of microglia and astrocytes did not influence single-cell motility but reduced the collective migration speed, implying effects on cell–cell interactions. Furthermore, supernatants triggered both melanoma and GBM cells to move a prolonged time together, indicating that the type of motion inside the layer became slower but more persistent. Responsible molecular processes might be similar to those discussed for the spheroid aggregation experiments, involving growth factors, such as EGFR-ligands, TGF- β , interleukins, and others [9–13,21,27–32]. Interestingly, the reduction in collective migration after incubation with microglia or astrocytes supernatant seems to contradict previously published results, demonstrating that both astrocytes and microglia favor tumor migration and infiltration [7,8,24]. These differences might arise from the differences in the used

models. In studies citing the Boyden chamber, scratch assays or brain slice cultures were used. While Boyden chambers are mainly chemotaxis driven, scratch assays are strongly affected by proliferation and (single) cell migration. The model used here does not contain large-scale spatial or chemical inhomogeneity, and thus is not affected by chemotaxis and less impacted by proliferation. The last part is noteworthy, as both astrocytes and microglia increased the proliferation of tumor cells [101,105]. Contrary to these effects, we did not observe any effects of THC or CBD on collective cellular motion independent of the presence of astrocyte or microglia supernatants. Thus, from a functional perspective, these cannabinoids only appear to affect tumor cohesiveness.

5. Conclusions

In this study, we demonstrated astrocytes and microglia cells to slow down the initial 3D aggregate formation of melanoma and GBM cells, as well as inhibiting collective cellular migration speed. Yet, supernatants of astrocytes and microglia led to a more directed collective motion with cells moving for a prolonged time together. Furthermore, THC and CBD were shown to slow down the spheroid formation of melanoma or GBM cells but these effects were absent when astrocytes were co-cultured. THC and CBD did not affect collective migration of both cell types. Thus, our results imply on the one hand that astrocyte or microglia secreted factors impact tumor cell migration. On the other hand, astrocytes seem to hamper the effects of cannabinoids.

Taken together, the current study provides an important and necessary basis for further molecular analysis of the interactions of glioblastoma/melanoma cells and the brain micromilieu, as well as the influence of cannabinoids in this system. Described effects should be evaluated in further model systems, such as organoids, patient-derived cells, and slices. Furthermore, the presented results largely rule out signaling cascades associated with proliferation or cell death in here investigated models, as no effects on these parameters were observed.

Supplementary Materials: The following supporting information can be downloaded at: <https://www.mdpi.com/article/10.3390/cells11010147/s1>, Figure S1: Establishment of astrocyte and microglia concentration for co-culture with A375 cells; Figure S2: Establishment of astrocyte and microglia concentration for co-culture with LN229 cells; Figure S3: Spheroid aggregation dynamics; Figure S4: Representative labelings of sectioned spheroids for analysis of proliferation; Figure S5: Gating strategy; Table S1. Sample size; Table S2: Characteristic spheroid size, aggregation time and aggregation speed; Table S3: Proliferation index of cells inside of spheroids.

Author Contributions: Conceptualization, U.H., F.D. and T.H.; methodology, U.H., T.H. and F.K.; software, T.H.; validation, U.H., T.H. and C.G.; formal analysis, T.H.; investigation, C.W., C.G. and U.H.; resources, F.D. and F.K.; data curation, C.W.; writing—original draft preparation, T.H. and U.H.; writing—review and editing, C.W., F.D., U.H., T.H. and F.K.; visualization, T.H.; supervision, F.D. and T.H.; project administration, T.H. All authors have read and agreed to the published version of the manuscript.

Funding: This research received no external funding.

Institutional Review Board Statement: All experiments involving animal material were performed in accordance with the Declaration of Helsinki and directive 2010/63/EU of the European Parliament and the Council of the European Union (22 November 2010) and approved by local authorities of the State of Saxony-Anhalt (permission number: I11M18) protecting animals and regulating tissue collection used for scientific purposes.

Informed Consent Statement: Not applicable.

Data Availability Statement: All datasets generated for this study are included in the article/supplementary material.

Acknowledgments: The authors would like to appreciate technical assistance of Liudmila Litvak.

Conflicts of Interest: The authors declare no conflict of interest.

References

1. Antunes, A.R.P.; Scheyltjens, I.; Duerinck, J.; Neyns, B.; Movahedi, K.; Van Ginderachter, J.A. Understanding the glioblastoma immune microenvironment as basis for the development of new immunotherapeutic strategies. *Elife* **2020**, *9*, 1–16. [CrossRef]
2. Mega, A.; Hartmark Nilsen, M.; Leiss, L.W.; Tobin, N.P.; Miletic, H.; Sleire, L.; Strell, C.; Nelander, S.; Krona, C.; Hägerstrand, D.; et al. Astrocytes enhance glioblastoma growth. *Glia* **2020**, *68*, 316–327. [CrossRef]
3. Charles, N.A.; Holland, E.C.; Gilbertson, R.; Glass, R.; Kettenmann, H. The brain tumor microenvironment. *Glia* **2012**, *60*, 502–514. [CrossRef] [PubMed]
4. Chen, Z.; Feng, X.; Herting, C.J.; Garcia, V.A.; Nie, K.; Pong, W.W.; Rasmussen, R.; Dwivedi, B.; Seby, S.; Wolf, S.A.; et al. Cellular and molecular identity of tumor-associated macrophages in glioblastoma. *Cancer Res.* **2017**, *77*, 2266–2278. [CrossRef]
5. Watters, J.J.; Schartner, J.M.; Badie, B. Microglia function in brain tumors. *J. Neurosci. Res.* **2005**, *81*, 447–455. [CrossRef] [PubMed]
6. Yi, L.; Xiao, H.; Xu, M.; Ye, X.; Hu, J.; Li, F.; Li, M.; Luo, C.; Yu, S.; Bian, X.; et al. Glioma-initiating cells: A predominant role in microglia/macrophages tropism to glioma. *J. Neuroimmunol.* **2011**, *232*, 75–82. [CrossRef]
7. Markovic, D.S.; Glass, R.; Synowitz, M.; Van Rooijen, N.; Kettenmann, H. Microglia stimulate the invasiveness of glioma cells by increasing the activity of metalloprotease-2. *J. Neuropathol. Exp. Neurol.* **2005**, *64*, 754–762. [CrossRef] [PubMed]
8. Bettinger, I.; Thanos, S.; Paulus, W. Microglia promote glioma migration. *Acta Neuropathol.* **2002**, *103*, 351–355. [CrossRef]
9. Matias, D.; Balça-Silva, J.; da Graça, G.C.; Wanjiru, C.M.; Macharia, L.W.; Nascimento, C.P.; Roque, N.R.; Coelho-Aguiar, J.M.; Pereira, C.M.; Dos Santos, M.F.; et al. Microglia/astrocytes–glioblastoma crosstalk: Crucial molecular mechanisms and microenvironmental factors. *Front. Cell. Neurosci.* **2018**, *12*, 1–22. [CrossRef]
10. Coniglio, S.J.; Eugenin, E.; Dobrenis, K.; Stanley, E.R.; West, B.L.; Symons, M.H.; Segall, J.E. Microglial stimulation of glioblastoma invasion involves epidermal growth factor receptor (EGFR) and colony stimulating factor 1 receptor (CSF-1R) signaling. *Mol. Med.* **2012**, *18*, 519–527. [CrossRef]
11. Wagner, S.; Czub, S.; Greif, M.; Vince, G.H.; Süss, N.; Kerkau, S.; Rieckmann, P.; Roggendorf, W.; Roosen, K.; Tonn, J.C. Microglial/macrophage expression of interleukin 10 in human glioblastomas. *Int. J. Cancer* **1999**, *82*, 12–16. [CrossRef]
12. Ye, X.; Xu, S.; Xin, Y.; Yu, S.; Ping, Y.; Chen, L.; Xiao, H.; Wang, B.; Yi, L.; Wang, Q.; et al. Tumor-Associated Microglia/Macrophages Enhance the Invasion of Glioma Stem-like Cells via TGF- β 1 Signaling Pathway. *J. Immunol.* **2012**, *189*, 444–453. [CrossRef]
13. Da Fonseca, A.C.C.; Romão, L.; Amaral, R.F.; Assad Kahn, S.; Lobo, D.; Martins, S.; Marcondes de Souza, J.; Moura-Neto, V.; Lima, F.R.S. Microglial stress inducible protein 1 promotes proliferation and migration in human glioblastoma cells. *Neuroscience* **2012**, *200*, 130–141. [CrossRef]
14. Sarkar, S.; Döring, A.; Zemp, F.J.; Silva, C.; Lun, X.; Wang, X.; Kelly, J.; Hader, W.; Hamilton, M.; Mercier, P.; et al. Therapeutic activation of macrophages and microglia to suppress brain tumor-initiating cells. *Nat. Neurosci.* **2014**, *17*, 46–55. [CrossRef]
15. O'Brien, E.; Howarth, C.; Sibson, N.R. The role of astrocytes in CNS tumours: Pre-clinical models and novel imaging approaches. *Front. Cell. Neurosci.* **2013**, *7*, 1–13. [CrossRef]
16. Lin, Q.; Liu, Z.; Ling, F.; Xu, G. Astrocytes protect glioma cells from chemotherapy and upregulate survival genes via gap junctional communication. *Mol. Med. Rep.* **2016**, *13*, 1329–1335. [CrossRef]
17. Nagashima, G.; Suzuki, R.; Asai, J.I.; Fujimoto, T. Immunohistochemical analysis of reactive astrocytes around glioblastoma: An immunohistochemical study of postmortem glioblastoma cases. *Clin. Neurol. Neurosurg.* **2002**, *104*, 125–131. [CrossRef]
18. Le, D.M.; Besson, A.; Fogg, D.K.; Choi, K.S.; Waisman, D.M.; Goodyer, C.G.; Rewcastle, B.; Yong, V.W. Exploitation of astrocytes by glioma cells to facilitate invasiveness: A mechanism involving matrix metalloproteinase-2 and the urokinase-type plasminogen activator-plasmin cascade. *J. Neurosci.* **2003**, *23*, 4034–4043. [CrossRef]
19. Shabtay-Orbach, A.; Amit, M.; Binenbaum, Y.; Na'Ara, S.; Gil, Z. Paracrine regulation of glioma cells invasion by astrocytes is mediated by glial-derived neurotrophic factor. *Int. J. Cancer* **2015**, *137*, 1012–1020. [CrossRef] [PubMed]
20. Sin, W.C.; Aftab, Q.; Bechberger, J.F.; Leung, J.H.; Chen, H.; Naus, C.C. Astrocytes promote glioma invasion via the gap junction protein connexin43. *Oncogene* **2016**, *35*, 1504–1516. [CrossRef] [PubMed]
21. Chen, W.; Xia, T.; Wang, D.; Huang, B.; Zhao, P.; Wang, J.; Qu, X.; Li, X. Human astrocytes secrete IL-6 to promote glioma migration and invasion through upregulation of cytomembrane MMP14. *Oncotarget* **2016**, *7*, 62425–62438. [CrossRef]
22. Chen, W.; Wang, D.; Du, X.; He, Y.; Chen, S.; Shao, Q.; Ma, C.; Huang, B.; Chen, A.; Zhao, P.; et al. Glioma cells escaped from cytotoxicity of temozolomide and vincristine by communicating with human astrocytes. *Med. Oncol.* **2015**, *32*, 43. [CrossRef] [PubMed]
23. Yang, N.; Yan, T.; Zhu, H.; Liang, X.; Leiss, L.; Sakariassen, P.Ø.; Skaftnesmo, K.O.; Huang, B.; Costea, D.E.; Enger, P.Ø.; et al. A co-culture model with brain tumor-specific bioluminescence demonstrates astrocyte-induced drug resistance in glioblastoma. *J. Transl. Med.* **2014**, *12*, 1–9. [CrossRef] [PubMed]
24. Okolie, O.; Bago, J.R.; Schmid, R.S.; Irvin, D.M.; Bash, R.E.; Miller, C.R.; Hingtgen, S.D. Reactive astrocytes potentiate tumor aggressiveness in a murine glioma resection and recurrence model. *Neuro. Oncol.* **2016**, *18*, 1622–1633. [CrossRef]
25. Klein, A.; Schwartz, H.; Sagi-Assif, O.; Meshel, T.; Izraely, S.; Ben Menachem, S.; Bengaiev, R.; Ben-Shmuel, A.; Nahmias, C.; Couraud, P.O.; et al. Astrocytes facilitate melanoma brain metastasis via secretion of IL-23. *J. Pathol.* **2015**, *236*, 116–127. [CrossRef] [PubMed]
26. Izraely, S.; Sagi-Assif, O.; Klein, A.; Meshel, T.; Tsarfaty, G.; Pasmanik-Chor, M.; Nahmias, C.; Couraud, P.O.; Ateh, E.; Bryant, J.L.; et al. The metastatic microenvironment: Brain-residing melanoma metastasis and dormant micrometastasis. *Int. J. Cancer* **2012**, *131*, 1071–1082. [CrossRef]

27. Kim, J.K.; Jin, X.; Sohn, Y.W.; Jin, X.; Jeon, H.Y.; Kim, E.J.; Ham, S.W.; Jeon, H.M.; Chang, S.Y.; Oh, S.Y.; et al. Tumoral RANKL activates astrocytes that promote glioma cell invasion through cytokine signaling. *Cancer Lett.* **2014**, *353*, 194–200. [CrossRef] [PubMed]
28. Katz, A.M.; Amankulor, N.M.; Pitter, K.; Helmy, K.; Squatrito, M.; Holland, E.C. Astrocyte-specific expression patterns associated with the PDGF-induced glioma microenvironment. *PLoS ONE* **2012**, *7*, e32453. [CrossRef] [PubMed]
29. Rath, B.H.; Fair, J.M.; Jamal, M.; Camphausen, K.; Tofilon, P.J. Astrocytes Enhance the Invasion Potential of Glioblastoma Stem-Like Cells. *PLoS ONE* **2013**, *8*, e54752. [CrossRef]
30. Rath, B.H.; Wahba, A.; Camphausen, K.; Tofilon, P.J. Coculture with astrocytes reduces the radiosensitivity of glioblastoma stem-like cells and identifies additional targets for radiosensitization. *Cancer Med.* **2015**, *4*, 1705–1716. [CrossRef]
31. Guan, X.; Hasan, M.N.; Maniar, S.; Jia, W.; Sun, D. Reactive Astrocytes in Glioblastoma Multiforme. *Mol. Neurobiol.* **2018**, *55*, 6927–6938. [CrossRef]
32. Placone, A.L.; Quiñones-Hinojosa, A.; Searson, P.C. The role of astrocytes in the progression of brain cancer: Complicating the picture of the tumor microenvironment. *Tumor Biol.* **2016**, *37*, 61–69. [CrossRef]
33. Hong, X.; Sin, W.C.; Harris, A.L.; Naus, C.C. Gap junctions modulate glioma invasion by direct transfer of microRNA. *Oncotarget* **2015**, *6*, 15566–15577. [CrossRef]
34. Sin, W.C.; Crespín, S.; Mesnil, M. Opposing roles of connexin43 in glioma progression. *Biochim. Biophys. Acta—Biomembr.* **2012**, *1818*, 2058–2067. [CrossRef] [PubMed]
35. Blázquez, C.; Salazar, M.; Carracedo, A.; Lorente, M.; Egia, A.; Gonzalez-Feria, L.; Haro, A.; Velasco, G.; Guzmán, M. Cannabinoids Inhibit Glioma Cell Invasion by Down-regulating Matrix Metalloproteinase-2 Expression. *Cancer Res.* **2008**, *68*, 1945–1952. [CrossRef]
36. Blázquez, C.; Carracedo, A.; Salazar, M.; Lorente, M.; Egia, A.; González-Feria, L.; Haro, A.; Velasco, G.; Guzmán, M. Down-regulation of tissue inhibitor of metalloproteinases-1 in gliomas: A new marker of cannabinoid antitumoral activity? *Neuropharmacology* **2008**, *54*, 235–243. [CrossRef]
37. Galve-Roperh, I.; Sánchez, C.; Cortés, M.L.; del Pulgar, T.G.; Izquierdo, M.; Guzmán, M. Anti-tumoral action of cannabinoids: Involvement of sustained ceramide accumulation and extracellular signal-regulated kinase activation. *Nat. Med.* **2000**, *6*, 313–319. [CrossRef] [PubMed]
38. Sánchez, C.; Gómez del Pulgar, T.; Rueda, D.; Velasco, G.; Galve-Roperh, I.; Guzmán, M.; De Ceballos, M.L.; Corbacho, C.; Ramón y Cajal, S.; Huffman, J.W. Inhibition of glioma growth in vivo by selective activation of the CB2 cannabinoid receptor. *Cancer Res.* **2001**, *61*, 5784–5789. [PubMed]
39. Massi, P.; Vaccani, A.; Ceruti, S.; Colombo, A.; Abbracchio, M.P.; Parolaro, D. Antitumor Effects of Cannabidiol, a Nonpsychoactive Cannabinoid, on Human Glioma Cell Lines. *J. Pharmacol. Exp. Ther.* **2004**, *308*, 838–845. [CrossRef] [PubMed]
40. Aguado, T.; Carracedo, A.; Julien, B.; Velasco, G.; Milman, G.; Mechoulam, R.; Alvarez, L.; Guzmán, M.; Galve-Roperh, I. Cannabinoids induce glioma stem-like cell differentiation and inhibit gliomagenesis. *J. Biol. Chem.* **2007**, *282*, 6854–6862. [CrossRef]
41. Torres, S.; Lorente, M.; Rodríguez-Fornés, F.; Hernández-Tiedra, S.; Salazar, M.; García-Taboada, E.; Barcia, J.; Guzmán, M.; Velasco, G. A combined preclinical therapy of cannabinoids and temozolomide against glioma. *Mol. Cancer Ther.* **2011**, *10*, 90–103. [CrossRef] [PubMed]
42. Salazar, M.; Carracedo, A.; Salanueva, Í.J.; Hernández-tiedra, S.; Lorente, M.; Egia, A.; Vázquez, P.; Blázquez, C.; Torres, S.; García, S.; et al. Cannabinoid action induces autophagy-mediated cell death through stimulation of ER stress in human glioma cells. *J. Clin. Investig.* **2009**, *119*, 1359–1372. [CrossRef]
43. Singer, E.; Judkins, J.; Salomonis, N.; Matlaf, L.; Soteropoulos, P.; McAllister, S.; Soroceanu, L. Reactive oxygen species-mediated therapeutic response and resistance in glioblastoma. *Cell Death Dis.* **2015**, *6*, e1601-11. [CrossRef] [PubMed]
44. Glodde, N.; Jakobs, M.; Bald, T.; Tüting, T.; Gaffal, E. Differential role of cannabinoids in the pathogenesis of skin cancer. *Life Sci.* **2015**, *138*, 35–40. [CrossRef]
45. Armstrong, J.L.; Hill, D.S.; McKee, C.S.; Hernandez-Tiedra, S.; Lorente, M.; Lopez-Valero, I.; Anagnostou, M.E.; Babatunde, F.; Corazzari, M.; Redfern, C.P.F.; et al. Exploiting cannabinoid-induced cytotoxic autophagy to drive melanoma cell death. *J. Investig. Dermatol.* **2015**, *135*, 1629–1637. [CrossRef]
46. Hohmann, T.; Grabiec, U.; Ghadban, C.; Feese, K.; Dehghani, F. The Influence of Biomechanical Properties and Cannabinoids on Tumor Invasion. *Cell Adh. Migr.* **2017**, *11*, 54–67. [CrossRef] [PubMed]
47. Gentilini, D.; Besana, A.; Vigano, P.; Dalino, P.; Vignali, M.; Melandri, M.; Busacca, M.; Di Blasio, A.M. Endocannabinoid system regulates migration of endometrial stromal cells via cannabinoid receptor 1 through the activation of PI3K and ERK1/2 pathways. *Fertil. Steril.* **2010**, *93*, 2588–2593. [CrossRef]
48. Blázquez, C.; Carracedo, A.; Barrado, L.; Real, P.J.; Fernández-Luna, J.L.; Velasco, G.; Malumbres, M.; Guzmán, M. Cannabinoid receptors as novel targets for the treatment of melanoma. *FASEB J.* **2006**, *20*, 2633–2635. [CrossRef]
49. Dumitru, C.A.; Sandalcioğlu, I.E.; Karsak, M. Cannabinoids in Glioblastoma Therapy: New Applications for Old Drugs. *Front. Mol. Neurosci.* **2018**, *11*, 159. [CrossRef]
50. Stella, N. Cannabinoid and cannabinoid-like receptors in microglia, astrocytes, and astrocytomas. *Glia* **2010**, *58*, 1017–1030. [CrossRef]

51. Jung, S.; Aliberti, J.; Graemmel, P.; Sunshine, M.J.; Kreutzberg, G.W.; Sher, A.; Littman, D.R. Analysis of Fractalkine Receptor CX3CR1 Function by Targeted Deletion and Green Fluorescent Protein Reporter Gene Insertion. *Mol. Cell. Biol.* **2000**, *20*, 4106–4114. [CrossRef]
52. Nimmerjahn, A.; Kirchhoff, F.; Helmchen, F. Resting microglial cells are highly dynamic surveillants of brain parenchyma in vivo. *Neuroforum* **2005**, *11*, 95–96. [CrossRef]
53. Hohmann, U.; Pelzer, M.; Kleine, J.; Hohmann, T.; Ghadban, C.; Dehghani, F. Opposite Effects of Neuroprotective Cannabinoids, Palmitoylethanolamide, and 2-Arachidonoylglycerol on Function and Morphology of Microglia. *Front. Neurosci.* **2019**, *13*. [CrossRef] [PubMed]
54. Grabiec, U.; Hohmann, T.; Ghadban, C.; Rothgänger, C.; Wong, D.; Antonietti, A.; Groth, T.; Mackie, K.; Dehghani, F. Protective effect of N-arachidonoyl glycine-GPR18 signaling after excitotoxic lesion in murine organotypic hippocampal slice cultures. *Int. J. Mol. Sci.* **2019**, *20*, 1266. [CrossRef] [PubMed]
55. Giard, D.J.; Aaronson, S.A.; Todaro, G.J.; Arnstein, P.; Kersey, J.H.; Parks, W.P. In vitro cultivation of human tumors: Establishment of cell lines derived from a series of solid tumors. *J. Natl. Cancer Inst.* **1973**, *51*, 1417–1423. [CrossRef] [PubMed]
56. Blasi, E.; Barluzzi, R.; Bocchini, V.; Mazzolla, R.; Bistoni, F. Immortalization of murine microglial cells by a v-raf / v-myc carrying retrovirus. *J. Neuroimmunol.* **1990**, *27*, 229–237. [CrossRef]
57. Diserens, A.C.; de Tribolet, N.; Martin-Achard, A.; Gaide, A.C.; Schnegg, J.F.; Carrel, S. Characterization of an established human malignant glioma cell line: LN-18. *Acta Neuropathol.* **1981**, *53*, 21–28. [CrossRef]
58. Nabissi, M.; Morelli, M.B.; Santoni, M.; Santoni, G. Triggering of the TRPV2 channel by cannabidiol sensitizes glioblastoma cells to cytotoxic chemotherapeutic agents. *Carcinogenesis* **2013**, *34*, 48–57. [CrossRef]
59. Alharris, E.; Singh, N.P.; Nagarkatti, P.S.; Nagarkatti, M. Role of miRNA in the regulation of cannabidiol-mediated apoptosis in neuroblastoma cells. *Oncotarget* **2019**, *10*, 45–59. [CrossRef]
60. Angelini, T.E.; Hannezo, E.; Trepac, X.; Marquez, M.; Fredberg, J.J.; Weitz, D.A. Glass-like dynamics of collective cell migration. *Proc. Natl. Acad. Sci. USA* **2011**, *108*, 4714–4719. [CrossRef] [PubMed]
61. Park, J.A.; Kim, J.H.; Bi, D.; Mitchel, J.A.; Qazvini, N.T.; Tantisira, K.; Park, C.Y.; McGill, M.; Kim, S.H.; Gweon, B.; et al. Unjamming and cell shape in the asthmatic airway epithelium. *Nat. Mater.* **2015**, *14*, 1040–1048. [CrossRef]
62. Garcia, S.; Hannezo, E.; Elgeti, J.; Joanny, J.F.; Silberzan, P.; Gov, N.S. Physics of active jamming during collective cellular motion in a monolayer. *Proc. Natl. Acad. Sci. USA* **2015**, *112*, 15314–15319. [CrossRef] [PubMed]
63. Abate, A.R.; Durian, D.J. Topological persistence and dynamical heterogeneities near jamming. *Phys. Rev. E -Stat. Nonlinear Soft Matter Phys.* **2007**, *76*, 1–9. [CrossRef]
64. Tambe, D.T.; Corey Hardin, C.; Angelini, T.E.; Rajendran, K.; Park, C.Y.; Serra-Picamal, X.; Zhou, E.H.; Zaman, M.H.; Butler, J.P.; Weitz, D.A.; et al. Collective cell guidance by cooperative intercellular forces. *Nat. Mater.* **2011**, *10*, 469–475. [CrossRef]
65. Hohmann, T.; Hohmann, U.; Kolbe, M.R.; Dahlmann, M.; Kobelt, D.; Stein, U. MACC1 driven alterations in cellular biomechanics facilitate cell motility in glioblastoma. *Cell Commun. Signal.* **2020**, *18*, 1–13. [CrossRef]
66. Dabov, K.; Foi, A.; Katkovnik, V.; Egiazarian, K. Image Denoising by Sparse 3-D Transform-Domain Collaborative Filtering. *IEEE Trans. Image Process.* **2007**, *16*, 2080–2095. [CrossRef]
67. Rodrigues, J.; Heinrich, M.A.; Teixeira, L.M.; Prakash, J. 3D In Vitro Model (R)evolution: Unveiling Tumor–Stroma Interactions. *Trends Cancer* **2021**, *7*, 249–264. [CrossRef]
68. Vainchtein, I.D.; Molofsky, A.V. Astrocytes and Microglia: In Sickness and in Health. *Trends Neurosci.* **2020**, *43*, 144–154. [CrossRef] [PubMed]
69. Henrik Heiland, D.; Ravi, V.M.; Behringer, S.P.; Frenking, J.H.; Wurm, J.; Joseph, K.; Garrelfs, N.W.C.; Strähle, J.; Heynckes, S.; Grauvogel, J.; et al. Tumor-associated reactive astrocytes aid the evolution of immunosuppressive environment in glioblastoma. *Nat. Commun.* **2019**, *10*, 2541. [CrossRef]
70. Frasca, G.; Du, V.; Bacri, J.-C.; Gazeau, F.; Gay, C.; Wilhelm, C. Magnetically shaped cell aggregates: From granular to contractile materials. *Soft Matter* **2014**, *10*, 5045. [CrossRef] [PubMed]
71. Shawky, J.H.; Davidson, L.A. Tissue mechanics and adhesion during embryo development. *Dev. Biol.* **2015**, *401*, 152–164. [CrossRef] [PubMed]
72. Saias, L.; Gomes, A.; Cazales, M.; Ducommun, B.; Lobjois, V. Cell-cell adhesion and cytoskeleton tension oppose each other in regulating tumor cell aggregation. *Cancer Res.* **2015**, *75*, 2426–2433. [CrossRef] [PubMed]
73. Azuaje, F.; Tiemann, K.; Niclou, S.P. Therapeutic control and resistance of the EGFR-driven signaling network in glioblastoma. *Cell Commun. Signal.* **2015**, *13*, 1–13. [CrossRef]
74. Hohmann, T.; Dehghani, F. The Cytoskeleton—A Complex Interacting Meshwork. *Cells* **2019**, *8*, 362. [CrossRef]
75. Kim, H.-D.; Guo, T.W.; Wu, A.P.; Wells, A.; Gertler, F.B.; Lauffenburger, D.A. Epidermal Growth Factor-induced Enhancement of Glioblastoma Cell Migration in 3D Arises from an Intrinsic Increase in Speed But an Extrinsic Matrix- and Proteolysis-dependent Increase in Persistence. *Mol. Biol. Cell* **2008**, *19*, 4249–4259. [CrossRef] [PubMed]
76. Platten, M.; Wick, W.; Wild-Bode, C.; Aulwurm, S.; Dichgans, J.; Weller, M. Transforming Growth Factors β 1 (TGF- β 1) and TGF- β 2 Promote Glioma Cell Migration via Up-Regulation of α V β 3 Integrin Expression. *Biochem. Biophys. Res. Commun.* **2000**, *268*, 607–611. [CrossRef] [PubMed]

77. Paulus, W.; Baur, I.; Huettner, C.; Schmaußer, B.; Roggendorf, W.; Schlingensiepen, K.H.; Brysch, W. Effects of Transforming Growth Factor-B1 on Collagen Synthesis, Integrin Expression, Adhesion and Invasion of Glioma Cells. *J. Neuropathol. Exp. Neurol.* **1995**, *54*, 236–244. [CrossRef] [PubMed]
78. Tabatabaei, P.; Visse, E.; Bergström, P.; Brännström, T.; Siesjö, P.; Bergenheim, A.T. Radiotherapy induces an immediate inflammatory reaction in malignant glioma: A clinical microdialysis study. *J. Neurooncol.* **2017**, *131*, 83–92. [CrossRef] [PubMed]
79. Zhang, B.; Shi, L.; Lu, S.; Sun, X.; Liu, Y.; Li, H.; Wang, X.; Zhao, C.; Zhang, H.; Wang, Y. Autocrine IL-8 promotes F-actin polymerization and mediate mesenchymal transition via ELMO1-NF- κ B-Snail signaling in glioma. *Cancer Biol. Ther.* **2015**, *16*, 898–911. [CrossRef]
80. Hervé, J.C.; Bourmeyster, N.; Sarrouilhe, D. Diversity in protein-protein interactions of connexins: Emerging roles. *Biochim. Biophys. Acta—Biomembr.* **2004**, *1662*, 22–41. [CrossRef]
81. Wei, C.J.; Francis, R.; Xu, X.; Lo, C.W. Connexin43 associated with an N-cadherin-containing multiprotein complex is required for gap junction formation in NIH3T3 cells. *J. Biol. Chem.* **2005**, *280*, 19925–19936. [CrossRef]
82. Olk, S.; Zoidl, G.; Dermietzel, R. Connexins, cell motility, and the cytoskeleton. *Cell Motil. Cytoskeleton* **2009**, *66*, 1000–1016. [CrossRef] [PubMed]
83. Kardami, E.; Dang, X.; Iacobas, D.A.; Nickel, B.E.; Jeyaraman, M.; Srisakuldee, W.; Makazan, J.; Tanguy, S.; Spray, D.C. The role of connexins in controlling cell growth and gene expression. *Prog. Biophys. Mol. Biol.* **2007**, *94*, 245–264. [CrossRef] [PubMed]
84. Mao, H.; Lebrun, D.G.; Yang, J.; Zhu, V.F.; Li, M. Deregulated signaling pathways in glioblastoma multiforme: Molecular mechanisms and therapeutic targets. *Cancer Investig.* **2012**, *30*, 48–56. [CrossRef]
85. Kunz, M.; Vera, J. Modelling of protein kinase signaling pathways in melanoma and other cancers. *Cancers (Basel)* **2019**, *11*, 465. [CrossRef]
86. Ladin, D.A.; Soliman, E.; Griffin, L.T.; Van Dross, R. Preclinical and clinical assessment of cannabinoids as anti-cancer agents. *Front. Pharmacol.* **2016**, *7*, 1–18. [CrossRef]
87. Grimaldi, C.; Pisanti, S.; Laezza, C.; Malfitano, A.M.; Santoro, A.; Vitale, M.; Caruso, M.G.; Notarnicola, M.; Iacuzzo, I.; Portella, G.; et al. Anandamide inhibits adhesion and migration of breast cancer cells. *Exp. Cell Res.* **2006**, *312*, 363–373. [CrossRef]
88. Laezza, C.; Pisanti, S.; Malfitano, A.M.; Bifulco, M. The anandamide analog, Met-F-AEA, controls human breast cancer cell migration via the RHOA/RHO kinase signaling pathway. *Endocr. Relat. Cancer* **2008**, *15*, 965–974. [CrossRef]
89. Preet, A.; Ganju, R.K.; Groopman, J.E. Delta9-Tetrahydrocannabinol inhibits epithelial growth factor-induced lung cancer cell migration in vitro as well as its growth and metastasis in vivo. *Oncogene* **2008**, *27*, 339–346. [CrossRef] [PubMed]
90. Cabral, G.A.; McNERney, P.J.; Mishkin, E.M. Interaction of delta-9-tetrahydrocannabinol with rat B103 neuroblastoma cells. *Arch. Toxicol.* **1987**, *60*, 438–449. [CrossRef]
91. Tahir, S.K.; Zimmerman, A.M. Influence of marijuana on cellular structures and biochemical activities. *Pharmacol. Biochem. Behav.* **1991**, *40*, 617–623. [CrossRef]
92. Tahir, S.K.; Trogadis, J.E.; Stevens, J.K.; Zimmerman, A.M. Cytoskeletal organization following cannabinoid treatment in undifferentiated and differentiated PC12 cells. *Biochem. Cell Biol.* **1992**, *70*, 1159–1173. [CrossRef] [PubMed]
93. Wilson, R.G.; Tahir, S.K.; Mechoulam, R.; Zimmerman, S.; Zimmerman, A.M. Cannabinoid enantiomer action on the cytoarchitecture. *Cell Biol. Int.* **1996**, *20*, 147–157. [CrossRef]
94. Hohmann, T.; Feese, K.; Ghadban, C.; Dehghani, F.; Grabiec, U. On the influence of cannabinoids on cell morphology and motility of glioblastoma cells. *PLoS ONE* **2019**, *14*, e0212037. [CrossRef]
95. McAllister, S.D.; Soroceanu, L.; Desprez, P.Y. The Antitumor Activity of Plant-Derived Non-Psychoactive Cannabinoids. *J. Neuroimmune Pharmacol.* **2015**, *10*, 255–267. [CrossRef] [PubMed]
96. Seltzer, E.S.; Watters, A.K.; MacKenzie, D.; Granat, L.M.; Zhang, D. Cannabidiol (CBD) as a Promising Anti-Cancer Drug. *Cancers* **2020**, *12*, 3203. [CrossRef]
97. Soroceanu, L.; Murase, R.; Limbad, C.; Singer, E.; Allison, J.; Adrados, I.; Kawamura, R.; Pakdel, A.; Fukuyo, Y.; Nguyen, D.; et al. Id-1 is a key transcriptional regulator of glioblastoma aggressiveness and a novel therapeutic target. *Cancer Res.* **2013**, *73*, 1559–1569. [CrossRef] [PubMed]
98. Scott, K.A.; Dagleish, A.G.; Liu, W.M. The combination of cannabidiol and Delta9-tetrahydrocannabinol enhances the anticancer effects of radiation in an orthotopic murine glioma model. *Mol. Cancer Ther.* **2014**, *13*, 2955–2967. [CrossRef]
99. Blázquez, C.; Casanova, M.L.; Planas, A.; del Pulgar, T.; Villanueva, C.; Fernandez-Acenero, M.; Aragonés, J.; Huffman, J.; Jorcano, J.; Guzman, M. Inhibition of tumor angiogenesis by cannabinoids. *FASEB J.* **2003**, *17*, 529–531. [CrossRef]
100. Carracedo, A.; Lorente, M.; Egia, A.; Blázquez, C.; García, S.; Giroux, V.; Malicet, C.; Villuendas, R.; Gironella, M.; González-Feria, L.; et al. The stress-regulated protein p8 mediates cannabinoid-induced apoptosis of tumor cells. *Cancer Cell* **2006**, *9*, 301–312. [CrossRef]
101. Zhang, H.; Zhou, Y.; Cui, B.; Liu, Z.; Shen, H. Novel insights into astrocyte-mediated signaling of proliferation, invasion and tumor immune microenvironment in glioblastoma. *Biomed. Pharmacother.* **2020**, *126*, 110086. [CrossRef] [PubMed]
102. Civita, P.; Leite, D.M.; Pilkington, G.J. Pre-clinical drug testing in 2d and 3d human in vitro models of glioblastoma incorporating non-neoplastic astrocytes: Tunneling nano tubules and mitochondrial transfer modulates cell behavior and therapeutic responses. *Int. J. Mol. Sci.* **2019**, *20*, 6017. [CrossRef] [PubMed]
103. Mantovani, A.; Allavena, P. The interaction of anticancer therapies with tumor-associated macrophages. *J. Exp. Med.* **2015**, *212*, 435–445. [CrossRef] [PubMed]

104. Anfray, C.; Ummarino, A.; Andon, F.T.; Allavena, P. Current Strategies to Target Tumor-Associated-Macrophages to Improve Anti-Tumor Immune Responses. *Cells* **2019**, *9*, 46. [CrossRef] [PubMed]
105. Gutmann, D.H.; Kettenmann, H. Microglia/Brain Macrophages as Central Drivers of Brain Tumor Pathobiology. *Neuron* **2019**, *104*, 442–449. [CrossRef]

Article

Corosolic Acid Attenuates the Invasiveness of Glioblastoma Cells by Promoting CHIP-Mediated AXL Degradation and Inhibiting GAS6/AXL/JAK Axis

Li-Wei Sun ^{1,2,†}, Shao-Hsuan Kao ^{1,3,†}, Shun-Fa Yang ^{1,3}, Shang-Wun Jhang ^{2,4}, Yi-Chen Lin ¹, Chien-Min Chen ^{2,5,6,*} and Yi-Hsien Hsieh ^{1,3,*}

¹ Institute of Medicine, Chung Shan Medical University, Taichung 40201, Taiwan; medicaldragon007@gmail.com (L.-W.S.); kaosh@csmu.edu.tw (S.-H.K.); ysf@csmu.edu.tw (S.-F.Y.); mo915915@gmail.com (Y.-C.L.)

² Division of Neurosurgery, Department of Surgery, Changhua Christian Hospital, Changhua 50006, Taiwan; 133393@cch.org.tw

³ Department of Medical Research, Chung Shan Medical University Hospital, Taichung 40201, Taiwan

⁴ Department of Veterinary Medicine, National Chung Hsing University, Taichung 40201, Taiwan

⁵ School of Medicine, Kaohsiung Medical University, Kaohsiung 80708, Taiwan

⁶ College of Nursing and Health Sciences, Dayeh University, Changhua 51591, Taiwan

* Correspondence: 96015@cch.org.tw (C.-M.C.); hyhsien@csmu.edu.tw (Y.-H.H.)

† These authors contributed equally to this work.



Citation: Sun, L.-W.; Kao, S.-H.; Yang, S.-F.; Jhang, S.-W.; Lin, Y.-C.; Chen, C.-M.; Hsieh, Y.-H. Corosolic Acid Attenuates the Invasiveness of Glioblastoma Cells by Promoting CHIP-Mediated AXL Degradation and Inhibiting GAS6/AXL/JAK Axis. *Cells* **2021**, *10*, 2919. <https://doi.org/10.3390/cells10112919>

Academic Editors: Javier S. Castresana, Bárbara Meléndez and Pablo Martín-Vasallo

Received: 11 September 2021

Accepted: 26 October 2021

Published: 28 October 2021

Publisher's Note: MDPI stays neutral with regard to jurisdictional claims in published maps and institutional affiliations.



Copyright: © 2021 by the authors. Licensee MDPI, Basel, Switzerland. This article is an open access article distributed under the terms and conditions of the Creative Commons Attribution (CC BY) license (<https://creativecommons.org/licenses/by/4.0/>).

Abstract: Corosolic acid (CA), a bioactive compound obtained from *Actinidia chinensis*, has potential anti-cancer activities. Glioblastoma (GBM) is a malignant brain tumor and whether CA exerts anti-cancer activity on GBM remains unclear. This study was aimed to explore the anticancer activity and its underlying mechanism of CA in GBM cells. Our findings showed that CA $\leq 20 \mu\text{M}$ did not affect cell viability and cell proliferative rate of normal astrocyte and four GBM cells. Notably, 10 or 20 μM CA significantly inhibited cell migration and invasion of three GBM cells, decreased the protein level of F-actin and disrupted F-actin polymerization in these GBM cells. Further investigation revealed that CA decreased AXL level by promoting ubiquitin-mediated proteasome degradation and upregulating the carboxyl terminus of Hsc70-interacting protein (CHIP), an inducer of AXL polyubiquitination. CHIP knock-down restored the CA-reduced AXL and invasiveness of GBM cells. Additionally, we observed that CA-reduced Growth arrest-specific protein 6 (GAS6) and inhibited JAK2/MEK/ERK activation, and GAS6 pre-treatment restored attenuated JAK2/MEK/ERK activation and invasiveness of GBM cells. Furthermore, molecular docking analysis revealed that CA might bind to GAS6 and AXL. These findings collectively indicate that CA attenuates the invasiveness of GBM cells, attributing to CHIP upregulation and binding to GAS6 and AXL and subsequently promoting AXL degradation and downregulating GAS6-mediated JAK2/MEK/ERK cascade. Conclusively, this suggests that CA has potential anti-metastatic activity on GBM cells by targeting the CHIP/GAS6/AXL axis.

Keywords: corosolic acid; glioblastoma cell; invasiveness; AXL; CHIP; GAS6; JAK2

1. Introduction

Glioma is the most common form of brain tumor, and glioblastoma (GBM) is the most malignant glioma, accounting for 3–4% of all cancer-associated deaths [1]. The five-year survival rate for patients with GBM is approximately 4–5%, indicating that the prognosis of GBM is poor [2]. The standard treatment for GBM includes resection with concurrent radiotherapy and chemotherapy. However, the current standard treatment did not significantly increase the survival rate of patients with GBM compared with those with glioma and other subtypes [3]. Due to the introduction of alkylating agents, such as temozolomide and adjuvant therapy combined with radiotherapy and temozolomide, the

median survival time of patients with GBM increased from 12.1 months to 14.6 months. [4,5]. However, the inherent or induced resistance to temozolomide leads to unsatisfactory clinical efficacy of GBM. Therefore, new therapies for this deadly tumor still need a more comprehensive understanding of its progress, drug resistance mechanisms and novel therapeutic targets.

Abnormal activation of receptor tyrosine kinase (RTK) is highly correlated with tumorigenesis, leading to uncontrolled proliferation, inhibition of apoptosis, and promotion of metastasis. Among RTK family, the TAM (Tyro-3, AXL, Mer) kinases have been implicated in the development of a serial of cancers [6,7]. TAM kinases are overexpressed in numerous cancers, including myeloid and lymphoblastic leukaemia, breast, lung, colon, liver, gastric, kidney and brain cancers [8–10]; particularly, both overexpression of AXL and its ligand growth arrest specific 6 (Gas6) have been reported as poor prognosis markers in GBM patients [11]. Downstream signaling of AXL and Mer results in a serial oncogenic mechanism including cell growth and survival, metastasis, angiogenesis, and chemoresistance in solid tumors [12]. In addition, AXL also plays an important role in regulation of glioblastoma stem-like cells [13]. Therefore, it is suggested that inhibition of AXL and GAS6 could be a promising target for GBM treatment [14].

Corosolic acid (CA) is a pentacyclic triterpene compound that can be extracted from the leaves of *Eriobotrya japonica* [15], the fruit of *Cratoegus pinnatifida* var. *psilosa* [16], and the root of *Actinidia chinensis* [17]. Recently, the anti-tumor activity of CA has attracted more attention [18,19]. CA possesses cytotoxic activity to cervical cancer [20], hepatocellular carcinoma [17], and lung cancer [19]. Fujiwara et al. also reported that CA could inhibit proliferation of glioblastoma cell and M2 polarization of tumor-associated macrophages (TAMs) [18]; however, whether CA has anti-metastatic activity on GBM cells is incompletely studied. Therefore, in this study, anti-metastatic potential of CA on GBM cells is first explored with emphasis on AXL and its associated signal components.

2. Materials and Methods

2.1. Reagents and Antibodies

Chemicals and reagents were obtained from Sigma-Aldrich (St. Louis, MO, USA) or as indicated. Corosolic acid (CA; Purity \geq 98%) was purchased from ChemFaces company (Wuhan, Hubei, China). The antibodies source and dilution factor were: F-actin (200 μ g/mL; dilution factor: 1:1000), AXL (200 μ g/mL; dilution factor: 1:1000), Ubiquitin (200 μ g/mL; dilution factor: 1:1000), CHIP (200 μ g/mL; dilution factor: 1:1000), GAS6 (200 μ g/mL; dilution factor: 1:1000), phospho(p)-JAK2 (200 μ g/mL; dilution factor: 1:1000), pan-JAK (200 μ g/mL; dilution factor: 1:1000), p-MEK-1/2 (Ser 218/Ser222; 200 μ g/mL; dilution factor: 1:1000), pan-ERK (200 μ g/mL; dilution factor: 1:1000), p-MEK (200 μ g/mL; dilution factor: 1:1000), pan-MEK (200 μ g/mL; dilution factor: 1:1000), GAPDH (200 μ g/mL; dilution factor: 1:5000), and peroxidase-conjugated antibodies against mouse IgG (200 μ g/mL; dilution factor: 1:5000) or rabbit IgG (200 μ g/mL; dilution factor: 1:5000) were obtained from Santa Cruz Biotechnology (Santa Cruz, CA, USA). The phospho(p)-ERK1/2(Thr202/Tyr204), (dilution factor: 1:1000), GAS6 (dilution factor: 1:1000), Phospho-JAK2 (Tyr1007/1008), (dilution factor: 1:1000) were purchased from Cell Signaling Technology (Beverly, MA, USA). MG132 and Cycloheximide were purchased from Selleck Chemicals (Houston, TX, USA). Recombinant Human GAS6 Protein (Rh-GAS6) was purchased from R&D Systems, Inc (Minneapolis, MN, USA)

2.2. CA Treatment

The stock concentration of CA is 50 mM and dissolved in dimethyl sulfoxide (DMSO) at -20°C and diluted using the culture medium with a final DMSO concentration of 0.1%. MTT assay were detected cell viability and cytotoxicity by using the CA concentration at 10, 15, 20, 25 and 30 μ M for 24 and 48 h. The CA concentrations used in colony formation, cell cycle, apoptosis, in vitro migration/invasion assay and western blotting at 10, 15 and

20 μM for 24 h. Control were treated with same amount of DMSO as corresponding group in this study.

2.3. Cell Culture

Rat astrocyte CTX-TNA2 cells was established from primary cultures of astrocytes in old rats (brain frontal cortex tissue) and kindly provided from Dr. Nu-Man Tsai (School of Medical Laboratory and Biotechnology, Chung Shan Medical University, Taichung, Taiwan). The U251-MG cell lines were a gift from Professor Dah-Yu Lu of China Medical University (Taichung, Taiwan). The astrocyte CTX-TNA2 cells was maintained in Dulbecco's Modified Eagle's Medium (DMEM) with 4.5 g/L glucose and 10% (*v/v*) fetal bovine serum (FBS). GBM8401, M059K and U-87MG were acquired from BCRC (Bioresources Collection and Research Center, Hsinchu, Taiwan). Additionally, cells were grown in Dulbecco's modified Eagle's medium (DMEM) supplemented with 10% (*v/v*) FBS and 1% penicillin/streptomycin at 37 °C in a humidified CO₂ (5%)-controlled incubators. Finally, subculture was performed when cells reached 80% confluency.

2.4. Cell Viability Assay

Cell viability was determined using Thiazolyl Blue Tetrazolium Bromide (MTT) assay as previously described [21]. Briefly, 2×10^4 cells were seeded into a 24-well plate and treated with CA at 10, 15, 20, 25, and 30 μM for 24 or 48 h (h), and then incubated with the MTT solution. After adding isopropanol to solubilize the formed formazan, the absorbance of the solution at 563 nm was measured using a spectrophotometer. The percentage of viable cells was estimated by comparing with control.

2.5. Colony Formation Assay

Cells (4×10^5) were seeded onto 6-well culture plates and then incubated with treated with CA at 10, 15 and 20 μM and then incubated at 37 °C for 7 days. At the end of incubation, the cell colonies were fixed with methanol, stained with crystal violet (1:20), then photographed using a light microscopy. The colonies were counted for quantitation by ImageJ software.

2.6. Migration and Invasion Ability by Boyden Chamber Assay

First, cells were incubated in serum-free DMEM containing CA at 10, 15 and 20 μM and then seeded on 24-well cell culture inserts using 8 μm GVS PCTE Filter Membranes (GVS Life Sciences, Zola Predosa, Bologna, Italy). Next, 20% FBS was added to the lower chamber and used as the chemoattractant. After 24 h of incubation, cells that migrated to the lower surface of the insert were fixed with 10% neutral-buffered formalin and stained with Giemsa reagent (Millipore). Then, the stained cells were photographed, and the total cell number from five random fields was counted by light microscopy. For the invasion assay, 100- μL Matrigel (20 \times dilution in PBS) was added to the culture inserts and then air-dried before cell seeding (as described above).

2.7. Immunofluorescence Staining

Cells were fixed by 4% ice-cold formaldehyde, reacted with blocking buffer containing 5% bovine serum albumin (BSA) and 0.5% Triton X-100 in PBS solution for 1 h at 25 °C, and incubated with primary antibodies for 16 h at 4 °C. Next, the cells were washed with PBS, and the bound primary antibodies were detected using F-Actin Labeling Kit; Red Fluorescence (AAT Bioquest, Inc., Sunnyvale, CA, USA) was used to detect polymerized F-actin microfilaments. Finally, fluorescence images were acquired using a laser scanning confocal microscope (Zeiss 510-Meta, Zeiss, Oberkochen, Germany).

2.8. Western Blot

Western blot was conducted as previously described [22]. Briefly, cells were lysed in Tris lysis buffer containing protease and phosphatase inhibitor cocktail (Sigma-Aldrich). Then,

the resulting crude proteins were separated by sodium dodecyl sulphate-polyacrylamide gel electrophoresis (SDS-PAGE), transferred to Immobilon-P polyvinylidene difluoride (PVDF) membrane (Merck, Kenilworth, NJ, USA) and then reacted with primary antibodies followed by secondary antibodies. The bound antibodies were detected using Immobilon Western Chemiluminescent HRP Substrate (Merck, Darmstadt, Germany) and an image analysis system by LAS-4000 mini (GE Healthcare Bio-Sciences, Piscataway, NJ, USA). Densitometric analysis was performed for semi-quantitation of chemiluminescence signals.

2.9. Quantitative Real-Time Polymerase Chain Reaction (qPCR)

After treatment, cells were harvested and then lysed for total RNA extraction using Isol-RNA-Lysis Reagent (Gaithersburg, MD, USA). The complementary DNA (cDNA) was acquired by reverse transcription of total RNA using the ReverTra Ace qPCR RT Master Mix kit (TOYOBO, Osaka, Japan). Then, qPCR was conducted using a StepOne Real-Time PCR System (Applied Biosystems, Foster City, CA, USA). The primers used for human gene expression by qPCR included AXL, (F) 5'-GTT TGG AGC TGT GAT GGA AGG C-3', (R) 5'-CGC TTC ACT CAG GAA ATC CTC C-3' (NM_021913, OriGene, Mission Biotech, Taipei, Taiwan). Finally, relative gene expression quantitation was normalized with endogenous GAPDH using the $2^{-\Delta\Delta C_t}$ method.

2.10. Knockdown of CHIP by Small Inhibitory RNAs

CHIP expression knockdown was conducted using specific small inhibitory RNAs (siRNAs) according to the manufacturer's protocol. Briefly, GBM8401 cells were transfected with CHIP siRNA into a pool of three siRNA duplexes (si-CHIP; sc-43555A, sc-43555B and sc-43555C) and a scrambled control siRNA (Santa Cruz Biotechnology, CA, USA). The siRNA transfection reagent used was Lipofectamine RNAiMAX (Thermo Fisher Scientific Inc., Waltham, MA, USA) at 37 °C and 5% CO₂ for 72 h.

2.11. Molecular Docking Approach

Binding mode and selectivity of AXL kinase and GAS6 with CA were studied using AutoDock Vina [23], which required the ligand (GAS6: 1H30) and receptor (AXL: 5U6B) in RCSB protein database bank (PDB, <http://www.rcsb.org>; GAS6: accessed on 30 January 2003; AXL: accessed on 26 July 2017). Additionally, CAs structure was downloaded from NCBI PubChem (CID: 6918774). Molecular docking score was calculated using mcule with Autodock vina. The program PyMOL (<http://www.pymol.org/>; GAS6: accessed on 15 December 2009; AXL: accessed on 15 December 2009) was analyzed for visualizing 3D structures.

2.12. Statistical Analysis

The data from three independent experiments were presented as the mean \pm standard deviation (SD) except indicated. Student's *t*-test and one-way analysis of variance (ANOVA) followed by Dunnett's post hoc test were used to analyze significant differences, and results with $p < 0.05$ or $p < 0.01$ were considered statistically significant.

3. Results

3.1. Effects of CA on the Cell Viability and Colony Formation Potential of Normal Astrocyte and GBM Cells

CA's structure is shown in Figure 1A, and its effects on cell viability of normal astrocytes, CTX-TNA2 and human GBM cell lines, GBM8401, M059K, U251-MG, and U87-MG, were first explored. After 24- or 48-h treatments, cell viability was remarkably reduced by CA at 25 and 30 μ M ($p < 0.05$), but unaffected by CA at 10, 15 and 20 μ M compared with the control (Figure 1B,C). Notably, an exception showed that 20 μ M CA treatment for 48 h could decrease the cell viability of CTX-TNA2 cells to $84.7\% \pm 5.3\%$ of control ($p < 0.05$) were detected by MTT assay. Then, we evaluated the effects of low-dose CA (10, 15 and 20 μ M) on the colony formation potential of GBM cells. Our results showed that

low-dose CA treatment did not influence the colony formation potential of GBM8401 cells (Figure 1D). Therefore, CA at 10, 15 and 20 μM were used for further cell experiments.

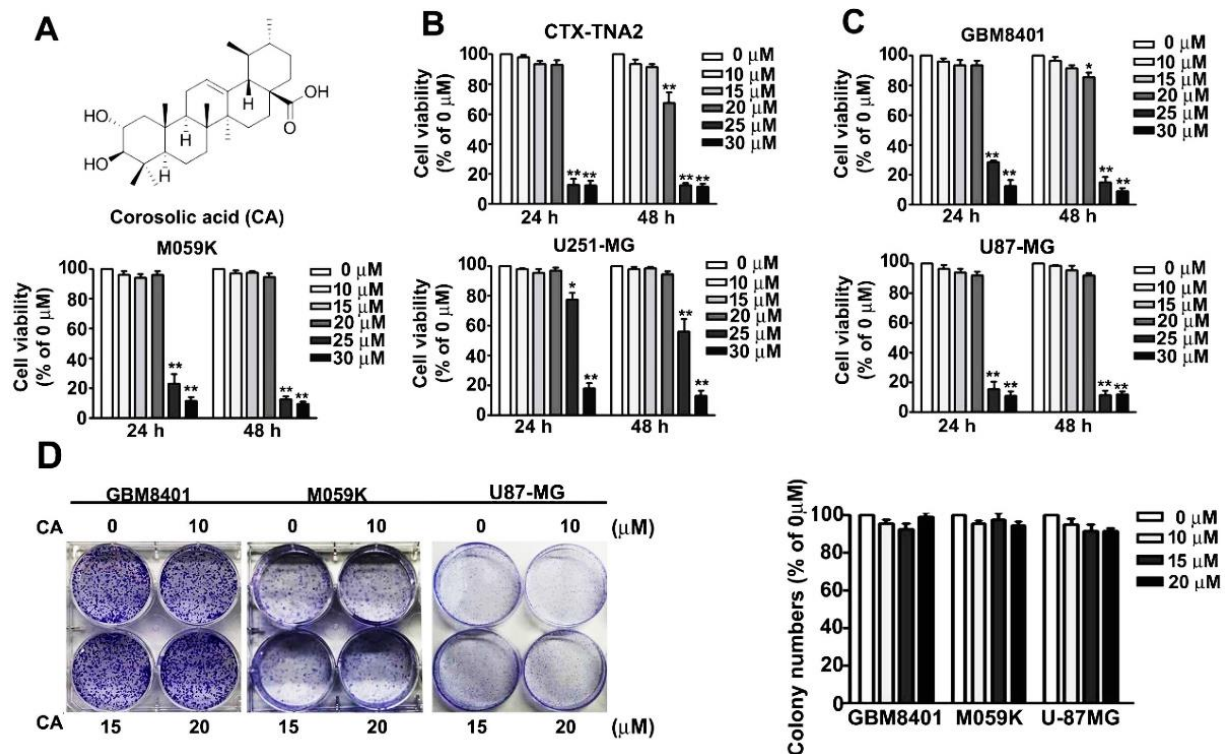


Figure 1. Effect of CA on cell viability and colony formation of GBM cells. (A) Structure of CA. (B,C) Normal astrocyte, CTX-TNA2 and GBM cell lines, GBM8401, M059K, U251-MG and U87-MG, were treated with CA at the indicated concentrations for 24 or 48 h. Then, cell viability was assessed by MTT assay and presented as a percentage of control. (D) GBM8401, M059K and U87-MG were seeded onto cell culture dishes containing without or with CA at 10, 15 and 20 μM for 7 days, and then cell colonies were stained with Giemsa and counted using a light micro-scope. Three independent experiments were performed for statistical analysis. * $p < 0.05$; ** $p < 0.01$ compared with control (DMSO-treated cells).

3.2. Effects of CA on the Cell Cycle and Cell Death of Three GBM Cells

Low-dose CA treatments do not affect the cell viability and proliferation ability of GBM cells. To determine which cell cycle arrest or cell death on GBM8401, M059K and U-87MG cells was influenced by CA. Our results showed that no effect on cell cycle distribution (G0/G1, S or G2/M phase) in CA-treated GBM8401, M059K and U87-MG cells, which was shown by PI (propidium iodide) staining using a flow cytometer (Figure 2A). However, we also observed that CA does not affect cell death of GBM8401, M059K and U87-MG by Annexin V/PI staining assay (Figure 2B). These pieces of evidence suggest that low-dose CA treatment is independent on cell viability and death.

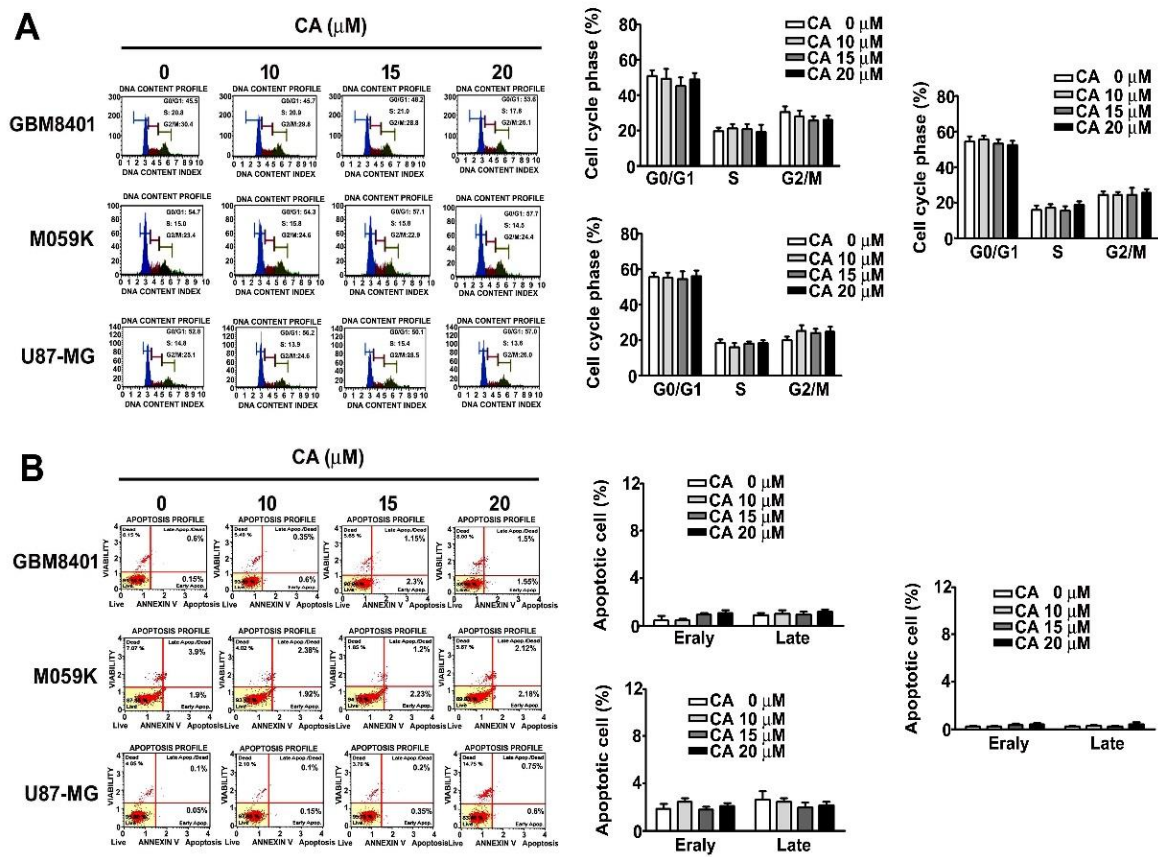


Figure 2. Effect of CA on cell cycle and death of GBM cells. (A) GBM cell lines, GBM8401, M059K, U251-MG and U87-MG, were treated with CA at the indicated concentrations for 24 h, and then the cell cycle was detected with PI staining assay by flow cytometry. (B) Cell death was measured by Annexin V/PI staining using a flow cytometer and presented as a percentage of the control.

3.3. CA Attenuates the Invasiveness of Human GBM Cells and Reduces F-Actin Expression

Since low-dose CA treatment insignificantly affected cell viability and colony formation capability of GBM cells, whether low-dose CA exhibited anti-metastatic activity on GBM cells was further evaluated. CA treatments dose-dependently and significantly attenuated the migratory and invasive potentials of GBM8401 and M059K cells up to $17.5\% \pm 2.4\%$ and $11.6\% \pm 1.7\%$ of control, respectively (for 20 μM CA, $p < 0.01$ compared with control at 0 μM; Figure 3A). Furthermore, aberrant regulation of the actin cytoskeleton is highly associated with the invasiveness of tumor cells [24]. Thus, whether CA altered F-actin expression in GBM cells, important cytoskeletal actin involved in tumor metastasis [25], was examined. Our observation showed that 20 μM CA decreased the protein level of F-actin by 0.15- and 0.28-fold of the control in GBM8401 and M059K cells, respectively (Figure 3B). Additionally, 20 μM CA disrupted the F-actin cytoskeletal organization in the three GBM cells (Figure 3C). Collectively, these findings reveal that CA inhibits the invasiveness of GBM cells, downregulates F-actin expression and disrupts the cytoskeletal organization.

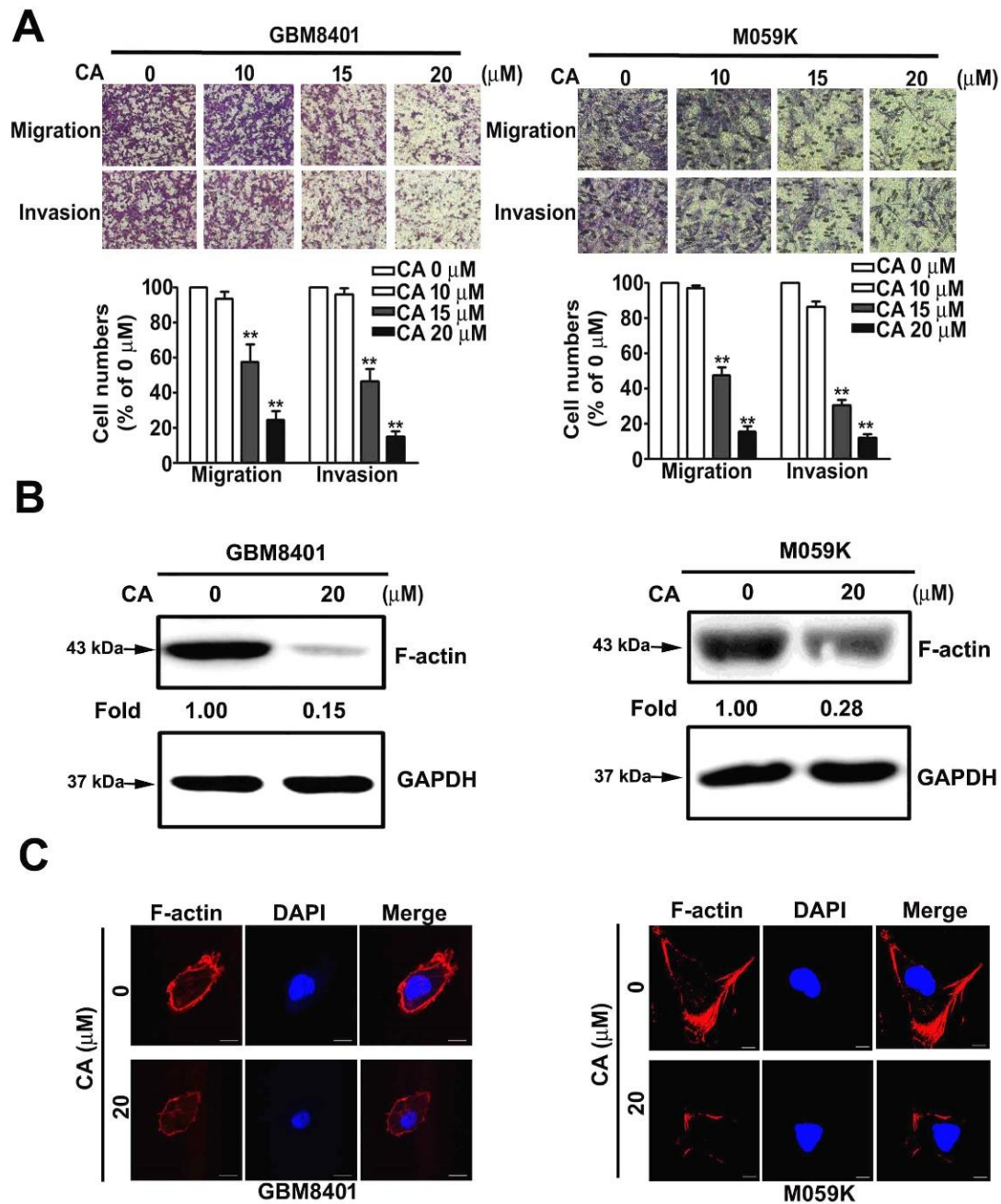


Figure 3. CA attenuated the migration and invasion of GBM cells and reduced expression and organization of cytoskeletal F-actin in GBM cells. (A) GBM8401 and M059K cells were treated with CA at indicated concentrations, and then cell migration and invasion were assessed and quantitated as a percentage of the control. ** $p < 0.01$ compared with the control. (B) GBM8401 and M059K cells were treated with CA (20 μM) and then lysed for immunodetection of F-actin by Western blotting. GAPDH was used as an internal control. (C) GBM8401 and M059K cells were treated with CA (20 μM) and then stained with phalloidin for F-actin (red) and DAPI for the nucleus (blue). Images were acquired using a confocal microscope at 200× magnification. ** $p < 0.01$ compared with the control (DMSO-treated cells). Scale bar = 50 μm.

3.4. CA Reduces the Protein Level of AXL by Promoting Ubiquitin-Mediated Proteasome Degradation

Next, the mechanism by which CA disrupted the F-actin cytoskeletal organization was investigated. Among the essential cytoskeleton regulators, AXL overexpression, a receptor, tyrosine, has been observed in different cancers and associated with an aggressive phenotype, invasiveness and progression [8,26]. Thus, CA influence on AXL was assessed.

In addition, CA treatment decreased the protein level of AXL in GBM8401 and M059K (Figure 4A). Interestingly, CA treatment did not alter the mRNA expression of AXL in both cells (Figure 4B, $p > 0.05$). As a result, whether CA affected the protein stability of AXL was then examined. Compared with inhibition of protein synthesis by cycloheximide (CHX) alone, CA combined with CHX treatments showed an insignificant effect on the stability of AXL protein in GBM8401 cells (Figure 4C). Notably, compared with CA treatment alone, pre-treatment with the proteasome inhibitor, MG132, with CA treatments significantly restored AXL protein levels in GBM8401 and M059K cells (Figure 4D). Moreover, combining MG132 pre-treatment and CA treatment also increased the level of polyubiquitinated proteins in both cells compared with CA treatment alone (Figure 4E). Collectively, these observations indicate that CA downregulates AXL protein levels by promoting ubiquitin-mediated proteasome degradation.

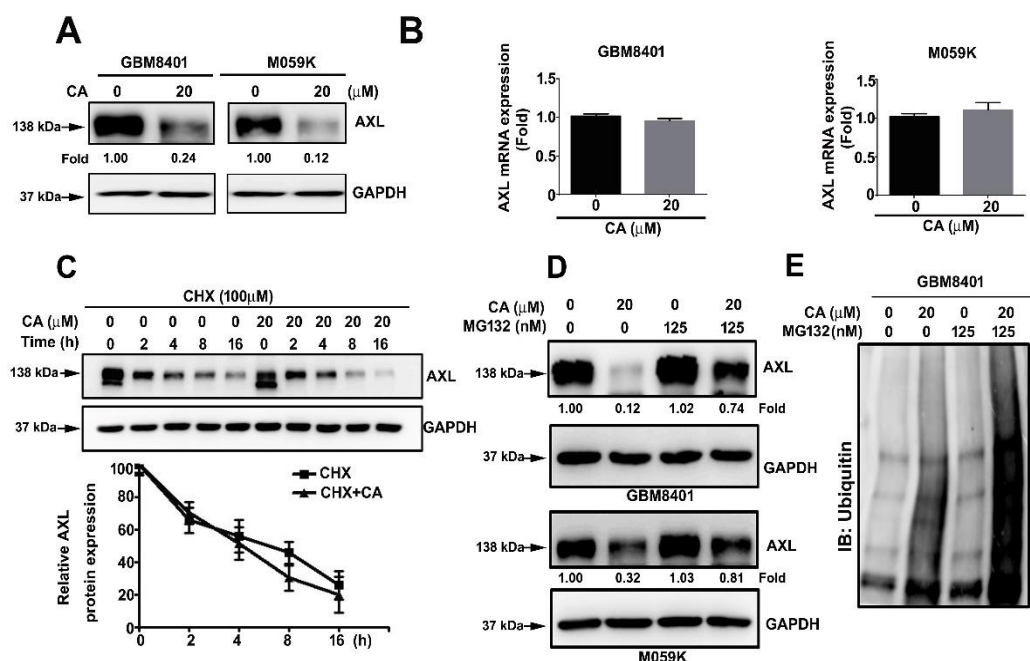


Figure 4. CA decreased AXL protein level by promoting ubiquitin-mediated proteasome degradation in GBM8401 cells (A,B) GBM8401 and M059K cells were treated with CA at 20 μM for 24 or 6 h, and then lysed for AXL immunodetection by Western blotting (A) or for mRNA expression assessment of AXL by RT-qPCR (B). (C) GBM801 cells were treated with cycloheximide (CHX) alone or with CHX and CA for the indicated times and then lysed for AXL immunodetection by Western blotting. Chemiluminescence signal was semi-quantitated by densitometric analysis, and GAPDH was used as an internal control. (D,E) GBM8401 and M059K cells were treated with CA, MG132 or CA and MG132 for 24 h and lysed for AXL immunodetection (D) or ubiquitin (E) by Western blotting.

3.5. Involvement of CHIP in CA-Reduced AXL and F-Actin and CA-Attenuated Invasiveness of GBM8401 Cell

Previous studies indicate that ubiquitin E3 ligase carboxyl terminus of HSC70-interacting protein (CHIP) plays a vital role in AXL degradation [27]. Thus, CHIP involvement in AXL and F-actin downregulation in response to CA was explored. First, CA treatment increased the CHIP protein level in GBM8401 cells (Figure 5A). Then, a specific siRNA against CHIP (si-CHIP) was designed to silence the gene expression of CHIP; results showed that CHIP silencing markedly decreased CHIP protein levels and increased AXL protein levels in GBM8401 cells (Figure 5B). Additionally, CHIP treatment decreased AXL and F-actin levels and increased CHIP levels in GBM8401 cells; CHIP and CA co-treatment further decreased AXL and F-actin levels compared with CHIP and CA alone (Figure 5C). Next, using si-CHIP, we observed that the CA-downregulated AXL and F-actin protein levels

were markedly reversed in GBM8401 cells (Figure 5D). Thus, consistent with CHIP changes, CHIP treatment synergistically promoted the inhibitory effects of CA on the migration and invasion of GBM8401 cells (Figure 5E); and silencing CHIP reversed the inhibitory effects of CA on the migration and invasion of GBM8401 cells (Figure 5F). Altogether, these findings reveal that CHIP is involved in AXL and F-actin downregulation induced by CA and the suppression of GBM8401 cell migration and invasion by CA treatment.

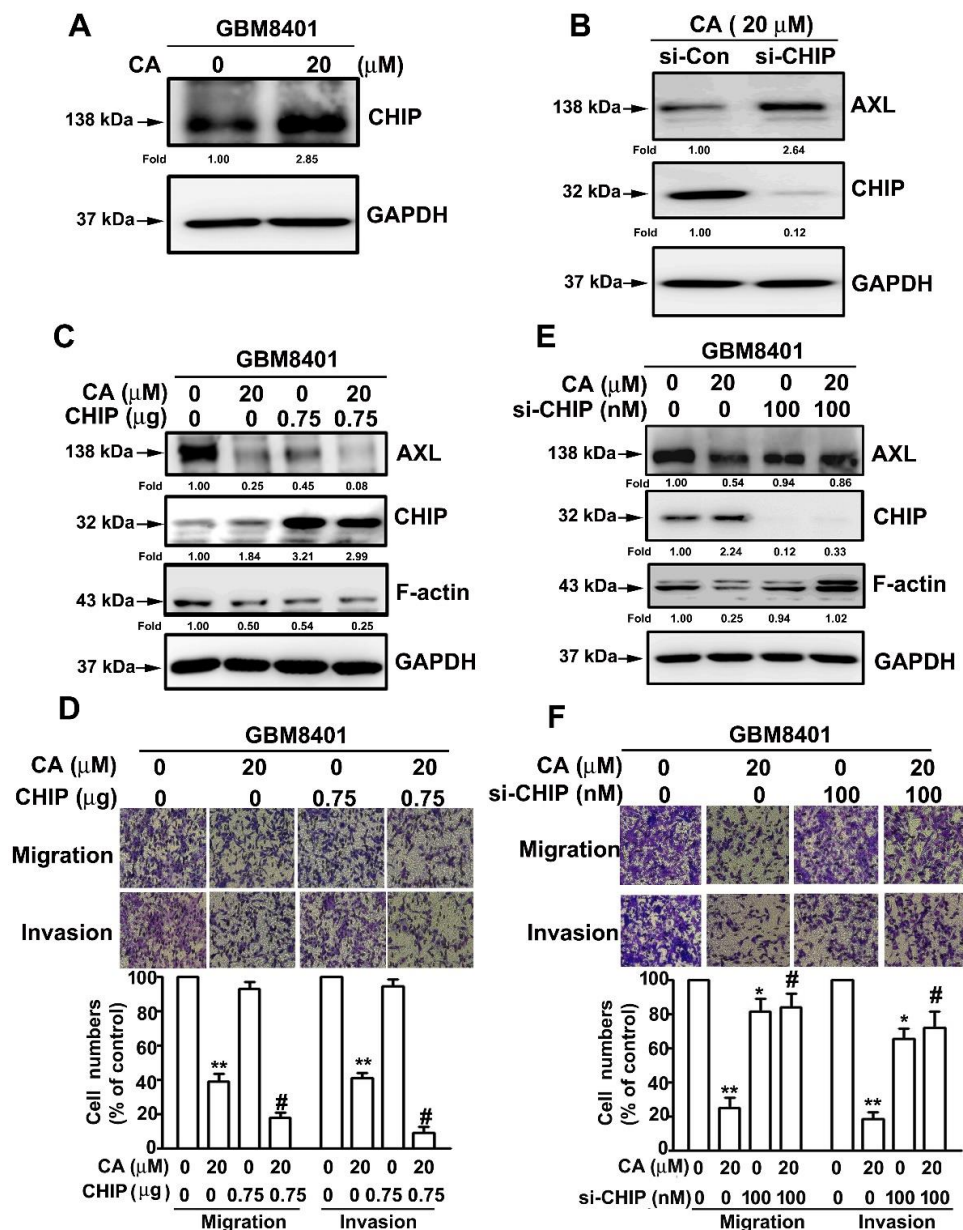


Figure 5. CHIP involvement in CA-inhibited migration and invasion of GBM8401 cells. (A,B) Cells were treated with CA (20 μM) (A) or siRNA against CHIP (si-CHIP) (B) and then lysed for CHIP and AXL immunodetection by Western blotting. (C,D) Cells were treated with CA (20 μM), CHIP (0.75 μg) or CA and CHIP, and then lysed for AXL, CHIP and F-actin immunodetection by Western blotting (C) or subjected to migration and invasion assay (D). (E,F) Cells were treated with CA (20 μM), si-CHIP (100 nM) or CA and si-CHIP, and then lysed for AXL, CHIP and F-actin immunodetection by Western blotting (E) or subjected to migration and invasion assay (F) Chemiluminescence signal was semi-quantitated by densitometric analysis, and GAPDH was used as an internal control. * and ** $p < 0.05$ and 0.01 , respectively, compared with the control (DMSO-treated cells). # $p < 0.05$ compared with CA alone. Images were acquired by light microscopy at $200\times$ magnification.

3.6. Involvement of GAS6 in CA-Attenuated Invasiveness of GBM Cells

AXL is also activated by GAS6 (growth arrest-specific 6), a member of vitamin K-dependent proteins [8]. As a result, whether CA affected GAS6 and its associated signaling was then investigated. CA (20 μ M) reduced AXL and GAS6 levels in GBM8401 and M059K cells and inhibited JAK2, MEK and ERK phosphorylation in both cells (Figure 6A). With exposure to GAS6, JAK2 and ERK phosphorylation and GAS6 level were increased in M059K cells compared with the control (Figure 6B), and CA diminished the GAS6-induced phosphorylation of JAK2 and ERK and GAS6 level in M059K cells (Figure 6B). Moreover, CA also decreased GAS6-induced F-actin level in M059K cells compared with the GAS6 treatment alone (Figure 6C). By migration and invasion assays, GAS6 treatments promoted the migration and invasion of M059K cells compared with the control (Figure 6D, $p < 0.05$). Notably, CA significantly lowered the migration and invasion of M059K cells exposed to GAS6 than those exposed to GAS6 alone (Figure 6D, $p < 0.05$). Thus, these findings reveal that CA downregulates GAS6 expression level and inhibits GAS6-associated signaling, consequently suppressing the migration and invasion of GBM cells

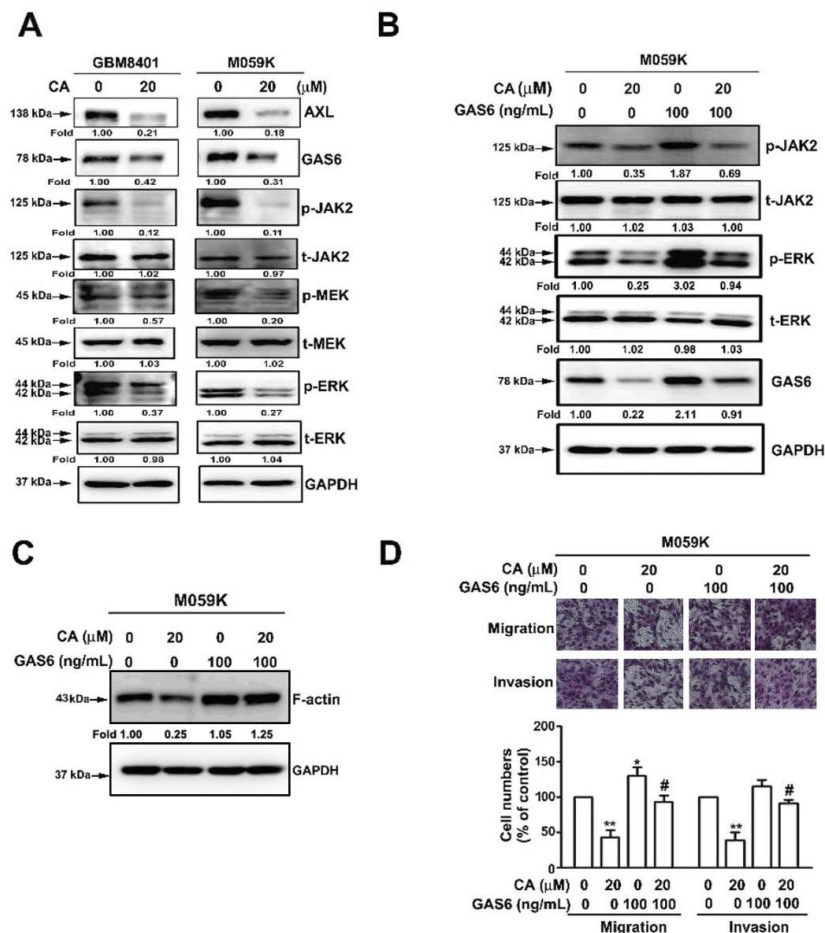


Figure 6. Involvement of GAS6-associated cascade in CA-inhibited migration and invasion of GBM cells. (A) Cells were treated with CA (20 μ M) and then lysed for immunodetection of the indicated targets by Western blotting. (B,C) Cells were treated with CA (20 μ M), GAS6 (100 ng/mL), or a combination of CA and GAS6, and then lysed for immunodetection of the indicated targets (B) or F-actin (C) by Western blotting. (D) Cells were treated with CA (20 μ M), GAS6 (100 ng/mL) or a combination of CA and GAS6, then subjected to migration and invasion assay. Chemiluminescence signal was semi-quantitated by densitometric analysis, and GAPDH was used as an internal control. * and ** $p < 0.05$ and 0.01 , respectively, compared with the control (DMSO-treated cells). # $p < 0.05$ compared with CA alone. Images were acquired using a light microscope at 200 \times magnification.

3.7. Docking Study of CA with AXL and GAS6

Based on the inhibitory effects of CA on GAS6 and AXL, the possible interaction between CA and GAS6 was investigated by molecular docking. Docking analysis revealed hydro-gen bonds between the Phe328 and His668 of GAS6 and the 10-hydroxy groups of CA and between the Gly477 of GAS6 and 11-hydroxy groups of CA (Figure 7A). Additionally, docking analysis showed hydrogen bonding networks between the Leu542 of AXL and the 10-hydroxy groups of CA and between the Asn677, Arg676 and Asp672 of AXL and the 4a-carboxylic group of CA (Figure 7B). These observations showed that CA exhibited strong binding to GAS6 and AXL, mainly by hydrogen bonding and hydrophobic interactions, which may result in increased CHIP and decreased GAS6, and the consequent promotion of AXL degradation and inhibition of JAK2/MEK/ERK cascade (Figure 7C).

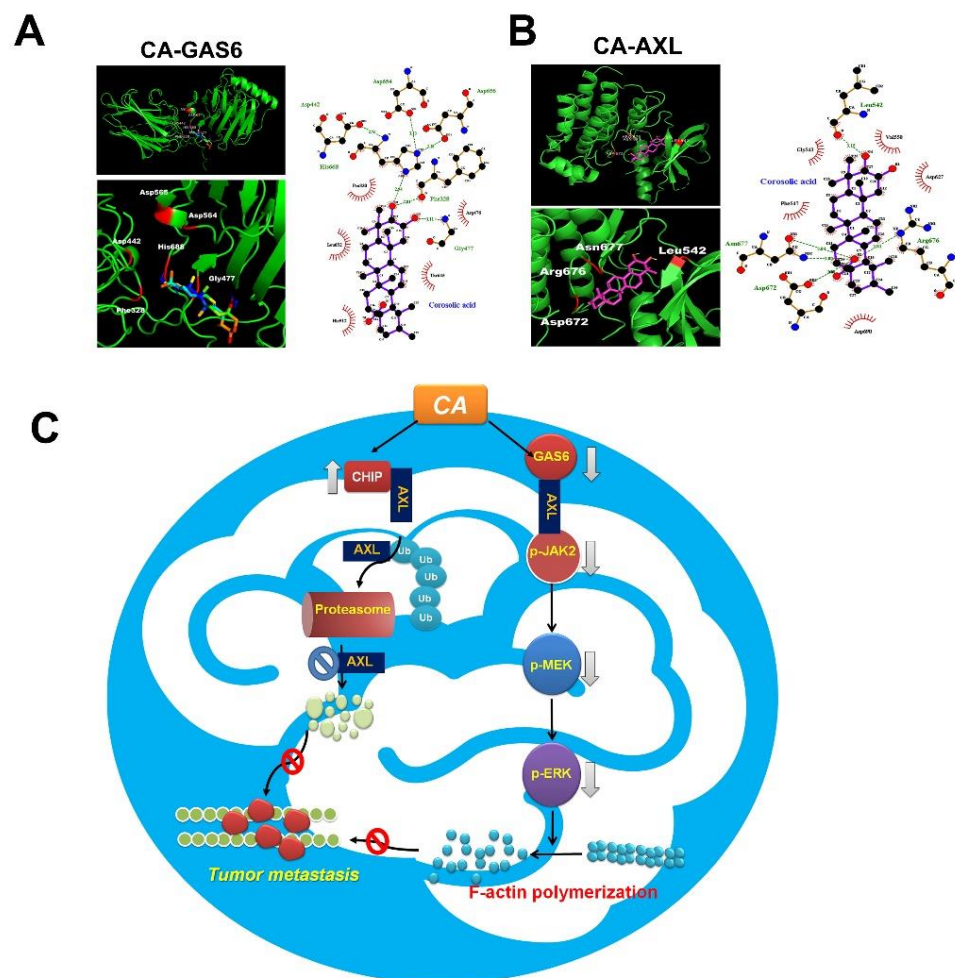


Figure 7. Molecular docking analysis and proposed mechanism for CA-inhibited invasiveness of GBM cells. **(A)** Superposition of GAS6 (green) and template CA (cyan), hydro-gen bonding interactions with GAS6 and CA. Binding affinity: -7.6 kcal/mol. **(B)** Superposition of AXL (green) and template CA (cyan), hydrogen bonding interactions with AXL and CA. Binding affinity: -5.6 kcal/mol. Interacting amino acid residues: Asn677, Arg676, Leu542 and Asp672. **(C)** Proposed mechanism for CA-inhibited invasiveness of GBM cells.

4. Discussion

Recently, inhibition of AXL tyrosine kinases has become an important method for cancer treatment. However, most small molecules with an inhibitory activity on AXL kinase are not primarily synthesized for AXL; therefore, the inhibitory activity against

AXL is not as robust as the inhibitory activity against other kinases [28,29]. Our findings reveal that CA induces the polyubiquitination of AXL, thereby reducing AXL levels by promoting its proteasomal degradation. However, AXL may not simultaneously inhibit other kinases with similar catalytic domains (such as c-MET and MERTK kinases) as competitive ATP-binding inhibitors.

From our results of MTT assay showed that the proliferation of rat astrocyte CTX-TNA2 was moderately decreased to $84.7\% \pm 5.3\%$ of control in response to 48 h-CA treatment at 20 μM . Our flow cytometry analysis indicated that the cell cycle distribution of the astrocyte was not altered by the same treatment (data not shown). In addition, previous studies also report that CA has several protective effects, including that CA can protect cardiomyocytes from doxorubin-induced cytotoxicity [30], prevent oxidative stress and reduce inflammation [31], and ameliorate non-alcoholic steatohepatitis [32] and diabetes [33]. Therefore, we suggest that CA may not have a cytotoxic effect on astrocytes or at least, only have slight cytotoxicity to astrocytes. Accordingly, we suggest that CA could be a potential treatment for human brain tumors.

AXL and its ligand, GAS6, have been implicated in metastasis and tumorigenesis of various cancers. Recently, GAS6/AXL-triggered actin remodeling has been demonstrated to play an important role in driving the invasion and macropinocytosis of glioblastoma cells in a PI3K-dependent manner [34]. In addition to the PI3K/Akt cascade, GAS6-induced AXL activation and triggers kinase signaling, including ERK and PEAK1, which contribute to the high invasiveness of breast cancer cells [35]. Furthermore, JAK2-activating mutation has been observed in chronic myeloproliferative neoplasms (MPNs), such as chronic myeloid leukemia (CML), polycythemia vera and myelofibrosis [36,37]. However, JAK2 inhibitors have limited clinical success in treating MPNs. It has been demonstrated that AXL is associated with CML resistance, and its inhibitory effect has therapeutic potential in BCR/ABL-resistant CML [38]. Moreover, Pearson et al. reported that inhibiting AXL may be a new therapeutic target for JAK2-induced MPNs [39]. CA induced the glioblastoma cell apoptosis through inhibition of STAT3 and NF- κ B activation and induction of apoptotic-related caspases pathways. In addition, CA also reduced tumor proliferation by inhibition of M2 macrophage polarization [18]. However, our results show that GAS6 treatment promotes the p-JAK2, p-ERK and F-actin expression in M059K cells by CA-treated M059K cells. This indicates that GAS6 induces AXL activation and the downstream signaling JAK2/MEK/ERK-dependent F-actin expression. Notably, the GAS6-evoked JAK2/ERK signaling and consequent F-actin polymerization can be diminished by CA, which may result from the downregulation of GAS6 and AXL in response to the direct interaction of CA/GAS6 and CA/AXL as proposed by molecular docking analysis (Figure 7).

Glioma stem cells (GSC) are one of the first types of cancer stem cells isolated from solid tumors, and only 100 GSCs could produce tumors that recapitulate the parental tumors when transplanted into xenograft immunodeficient mice [40]. Two subtypes of GSCs, namely mesenchymal and proneural GSC, have been identified basing on transcriptomic signatures [41]. Notably, AXL is demonstrated as a key regulator for mesenchymal GSC, and knockdown of AXL significantly diminishes the *in vitro* self-renewal of mesenchymal GSCs and suppresses the *in vivo* growth of glioblastoma in xenograft mice [13]. In addition to GAS6, it is shown that tumor-associated microglia produce protein S which subsequently interacts with and activates AXL in mesenchymal GSCs and promotes growth of GBM cells, and inhibition of AXL suppresses the promoted growth of GBM cells [42]. Our findings reveal that CA downregulates AXL expression and inhibits AXL-driven signaling, suggesting that CA may have inhibitory effect on mesenchymal GSCs and mesenchymal GSC-promoting GBM growth. However, further investigation is needed. Therefore, our findings indicate that CA can inhibit the migration and invasion of GBM cells and reduce F-actin expression and its polymerization. Additionally, the CA-inhibited invasiveness of GBM cells is attributed to the upregulation of CHIP and subsequent down-regulation of AXL by ubiquitin-mediated proteasome degradation, downregulation of GAS6 and subsequent inhibition of the JAK2/MEK/ERK axis.

5. Conclusions

Thus, these findings reveal that CA has potent anti-metastatic potential against GBM cells and highlight the potential of targeting the AXL/CHIP/GAS6 axis for GBM treatment.

Author Contributions: Conceptualization, L.-W.S., S.-H.K. and Y.-H.H.; methodology, Y.-C.L., C.-M.C. and Y.-H.H.; software, Y.-H.H. and S.-F.Y.; validation, L.-W.S., S.-F.Y. and C.-M.C.; formal analysis, S.-W.J., S.-H.K. and S.-F.Y.; investigation, S.-W.J., Y.-C.L. and Y.-H.H.; resources, S.-F.Y. and Y.-C.L.; data curation, Y.-C.L. and Y.-H.H.; writing—original draft preparation, L.-W.S. and S.-H.K.; writing—review and editing, C.-M.C. and Y.-H.H.; visualization, S.-F.Y. and Y.-H.H.; supervision, S.-F.Y., S.-H.K. and Y.-H.H.; project administration, L.-W.S., S.-H.K. and Y.-H.H.; funding acquisition, C.-M.C. and Y.-H.H. All authors have read and agreed to the published version of the manuscript.

Funding: This research was funded and supported by grants from Changhua Christian Hospital, Changhua, Taiwan (109-CCH-IRP-016) and Ministry of Science and Technology (MOST 108-2320-B-040-007-MY3 and MOST 110-2320-B-040-005-MY3).

Institutional Review Board Statement: Not applicable.

Informed Consent Statement: Not applicable.

Data Availability Statement: All experiment data generated or analyzed during in this published article.

Conflicts of Interest: The authors declare no conflict of interest.

References

- Louis, D.N.; Ohgaki, H.; Wiestler, O.D.; Cavenee, W.K.; Burger, P.C.; Jouvet, A.; Scheithauer, B.W.; Kleihues, P. The 2007 WHO classification of tumours of the central nervous system. *Acta Neuropathol.* **2007**, *114*, 97–109. [CrossRef]
- McLendon, R.E.; Halperin, E.C. Is the long-term survival of patients with intracranial glioblastoma multiforme overstated? *Cancer* **2003**, *98*, 1745–1748. [CrossRef]
- Stewart, L.A. Chemotherapy in adult high-grade glioma: A systematic review and meta-analysis of individual patient data from 12 randomised trials. *Lancet* **2002**, *359*, 1011–1018. [CrossRef]
- Sung, H.; Ferlay, J.; Siegel, R.L.; Laversanne, M.; Soerjomataram, I.; Jemal, A.; Bray, F. Global Cancer Statistics 2020: GLOBOCAN Estimates of Incidence and Mortality Worldwide for 36 Cancers in 185 Countries. *CA Cancer J. Clin.* **2021**, *71*, 209–249. [CrossRef] [PubMed]
- Phillips, R.E.; Soshnev, A.A.; Allis, C.D. Epigenomic Reprogramming as a Driver of Malignant Glioma. *Cancer Cell* **2020**, *38*, 647–660. [CrossRef] [PubMed]
- Linger, R.M.; Keating, A.K.; Earp, H.S.; Graham, D.K. TAM receptor tyrosine kinases: Biologic functions, signaling, and potential therapeutic targeting in human cancer. *Adv. Cancer Res.* **2008**, *100*, 35–83. [CrossRef] [PubMed]
- Graham, D.K.; DeRyckere, D.; Davies, K.D.; Earp, H.S. The TAM family: Phosphatidyserine sensing receptor tyrosine kinases gone awry in cancer. *Nat. Rev. Cancer* **2014**, *14*, 769–785. [CrossRef] [PubMed]
- Tanaka, M.; Siemann, D.W. Gas6/Axl Signaling Pathway in the Tumor Immune Microenvironment. *Cancers* **2020**, *12*, 1850. [CrossRef]
- Wium, M.; PACEZ, J.D.; Zerbini, L.F. The Dual Role of TAM Receptors in Autoimmune Diseases and Cancer: An Overview. *Cells* **2018**, *7*, 166. [CrossRef]
- Nakada, M.; Kita, D.; Teng, L.; Pyko, I.V.; Watanabe, T.; Hayashi, Y.; Hamada, J.I. Receptor Tyrosine Kinases: Principles and Functions in Glioma Invasion. *Adv. Exp. Med. Biol.* **2020**, *1202*, 151–178. [CrossRef]
- Hutterer, M.; Knyazev, P.; Abate, A.; Reschke, M.; Maier, H.; Stefanova, N.; Knyazeva, T.; Barbieri, V.; Reindl, M.; Muigg, A.; et al. Axl and growth arrest-specific gene 6 are frequently overexpressed in human gliomas and predict poor prognosis in patients with glioblastoma multiforme. *Clin. Cancer Res.* **2008**, *14*, 130–138. [CrossRef]
- Linger, R.M.; Keating, A.K.; Earp, H.S.; Graham, D.K. Taking aim at Mer and Axl receptor tyrosine kinases as novel therapeutic targets in solid tumors. *Expert Opin. Ther. Targets* **2010**, *14*, 1073–1090. [CrossRef] [PubMed]
- Cheng, P.; Phillips, E.; Kim, S.H.; Taylor, D.; Hielscher, T.; Puccio, L.; Hjelmeland, A.B.; Lichter, P.; Nakano, I.; Goidts, V. Kinome-wide shRNA screen identifies the receptor tyrosine kinase AXL as a key regulator for mesenchymal glioblastoma stem-like cells. *Stem Cell Rep.* **2015**, *4*, 899–913. [CrossRef]
- Dong, M.; Xiao, Q.; Hu, J.; Cheng, F.; Zhang, P.; Zong, W.; Tang, Q.; Li, X.; Mao, F.; He, Y.; et al. Targeting LRIG2 overcomes resistance to EGFR inhibitor in glioblastoma by modulating GAS6/AXL/SRC signaling. *Cancer Gene Ther.* **2020**, *27*, 878–897. [CrossRef]
- Wang, Q.; Sun, Q.; Ma, X.; Rao, Z.; Li, H. Probing the binding interaction of human serum albumin with three bioactive constituents of *Eriobotrya japonica* leaves: Spectroscopic and molecular modeling approaches. *J. Photochem. Photobiol. B* **2015**, *148*, 268–276. [CrossRef] [PubMed]

16. Ahn, K.S.; Hahm, M.S.; Park, E.J.; Lee, H.K.; Kim, I.H. Corosolic acid isolated from the fruit of *Crataegus pinnatifida* var. *psilosa* is a protein kinase C inhibitor as well as a cytotoxic agent. *Planta Med.* **1998**, *64*, 468–470. [CrossRef]
17. Ku, C.Y.; Wang, Y.R.; Lin, H.Y.; Lu, S.C.; Lin, J.Y. Corosolic Acid Inhibits Hepatocellular Carcinoma Cell Migration by Targeting the VEGFR2/Src/FAK Pathway. *PLoS ONE* **2015**, *10*, e0126725. [CrossRef]
18. Fujiwara, Y.; Komohara, Y.; Ikeda, T.; Takeya, M. Corosolic acid inhibits glioblastoma cell proliferation by suppressing the activation of signal transducer and activator of transcription-3 and nuclear factor-kappa B in tumor cells and tumor-associated macrophages. *Cancer Sci.* **2011**, *102*, 206–211. [CrossRef]
19. Nho, K.J.; Chun, J.M.; Kim, H.K. Corosolic acid induces apoptotic cell death in human lung adenocarcinoma A549 cells in vitro. *Food Chem. Toxicol.* **2013**, *56*, 8–17. [CrossRef] [PubMed]
20. Xu, Y.; Ge, R.; Du, J.; Xin, H.; Yi, T.; Sheng, J.; Wang, Y.; Ling, C. Corosolic acid induces apoptosis through mitochondrial pathway and caspase activation in human cervix adenocarcinoma HeLa cells. *Cancer Lett.* **2009**, *284*, 229–237. [CrossRef]
21. Lin, C.S.; Lin, C.L.; Ying, T.H.; Chiou, H.L.; Hung, C.H.; Liao, W.S.; Hsieh, Y.H.; Kao, S.H. Beta-Mangostin inhibits the metastatic power of cervical cancer cells attributing to suppression of JNK2/AP-1/Snail cascade. *J. Cell. Physiol.* **2020**, *235*, 8446–8460. [CrossRef] [PubMed]
22. Lin, R.C.; Yang, S.F.; Chiou, H.L.; Hsieh, S.C.; Wen, S.H.; Lu, K.H.; Hsieh, Y.H. Licochalcone A-Induced Apoptosis Through the Activation of p38MAPK Pathway Mediated Mitochondrial Pathways of Apoptosis in Human Osteosarcoma Cells In Vitro and In Vivo. *Cells* **2019**, *8*, 1441. [CrossRef]
23. Trott, O.; Olson, A.J. AutoDock Vina: Improving the speed and accuracy of docking with a new scoring function, efficient optimization, and multithreading. *J. Comput. Chem.* **2010**, *31*, 455–461. [CrossRef] [PubMed]
24. Yamaguchi, H.; Condeelis, J. Regulation of the actin cytoskeleton in cancer cell migration and invasion. *Biochim. Biophys. Acta* **2007**, *1773*, 642–652. [CrossRef]
25. Izdebska, M.; Zielinska, W.; Grzanka, D.; Gagat, M. The Role of Actin Dynamics and Actin-Binding Proteins Expression in Epithelial-to-Mesenchymal Transition and Its Association with Cancer Progression and Evaluation of Possible Therapeutic Targets. *BioMed Res. Int.* **2018**, *2018*, 4578373. [CrossRef]
26. Wium, M.; Ajayi-Smith, A.F.; Paccetz, J.D.; Zerbini, L.F. The Role of the Receptor Tyrosine Kinase Axl in Carcinogenesis and Development of Therapeutic Resistance: An Overview of Molecular Mechanisms and Future Applications. *Cancers* **2021**, *13*, 1521. [CrossRef] [PubMed]
27. Krishnamoorthy, G.P.; Guida, T.; Alfano, L.; Avilla, E.; Santoro, M.; Carlomagno, F.; Melillo, R.M. Molecular mechanism of 17-allylamino-17-demethoxygeldanamycin (17-AAG)-induced AXL receptor tyrosine kinase degradation. *J. Biol. Chem.* **2013**, *288*, 17481–17494. [CrossRef] [PubMed]
28. Holland, S.J.; Pan, A.; Franci, C.; Hu, Y.; Chang, B.; Li, W.; Duan, M.; Torneros, A.; Yu, J.; Heckrodt, T.J.; et al. R428, a selective small molecule inhibitor of Axl kinase, blocks tumor spread and prolongs survival in models of metastatic breast cancer. *Cancer Res.* **2010**, *70*, 1544–1554. [CrossRef] [PubMed]
29. Qi, W.; Cooke, L.S.; Stejskal, A.; Riley, C.; Croce, K.D.; Saldanha, J.W.; Bearss, D.; Mahadevan, D. MP470, a novel receptor tyrosine kinase inhibitor, in combination with Erlotinib inhibits the HER family/PI3K/Akt pathway and tumor growth in prostate cancer. *BMC Cancer* **2009**, *9*, 142. [CrossRef]
30. Che, Y.; Wang, Z.; Yuan, Y.; Zhou, H.; Wu, H.; Wang, S.; Tang, Q. By restoring autophagic flux and improving mitochondrial function, corosolic acid protects against Dox-induced cardiotoxicity. *Cell Biol. Toxicol.* **2021**. [CrossRef]
31. Yamaguchi, Y.; Yamada, K.; Yoshikawa, N.; Nakamura, K.; Haginaka, J.; Kunitomo, M. Corosolic acid prevents oxidative stress, inflammation and hypertension in SHR/NDmcr-cp rats, a model of metabolic syndrome. *Life Sci.* **2006**, *79*, 2474–2479. [CrossRef] [PubMed]
32. Liu, G.; Cui, Z.; Gao, X.; Liu, H.; Wang, L.; Gong, J.; Wang, A.; Zhang, J.; Ma, Q.; Huang, Y.; et al. Corosolic acid ameliorates non-alcoholic steatohepatitis induced by high-fat diet and carbon tetrachloride by regulating TGF-beta1/Smad2, NF-kappaB, and AMPK signaling pathways. *Phytother. Res.* **2021**, *35*, 5214–5226. [CrossRef] [PubMed]
33. Sivakumar, G.; Vail, D.R.; Nair, V.; Medina-Bolivar, F.; Lay, J.O., Jr. Plant-based corosolic acid: Future anti-diabetic drug? *Biotechnol. J.* **2009**, *4*, 1704–1711. [CrossRef] [PubMed]
34. Zdzalik-Bielecka, D.; Poswiata, A.; Kozik, K.; Jastrzebski, K.; Schink, K.O.; Brewinska-Olchowik, M.; Piwocka, K.; Stenmark, H.; Miaczynska, M. The GAS6-AXL signaling pathway triggers actin remodeling that drives membrane ruffling, macropinocytosis, and cancer-cell invasion. *Proc. Natl. Acad. Sci. USA* **2021**, *118*. [CrossRef] [PubMed]
35. Abu-Thuraia, A.; Goyette, M.A.; Boulais, J.; Dellioux, C.; Apcher, C.; Schott, C.; Chidiac, R.; Bagci, H.; Thibault, M.P.; Davidson, D.; et al. AXL confers cell migration and invasion by hijacking a PEAK1-regulated focal adhesion protein network. *Nat. Commun.* **2020**, *11*, 3586. [CrossRef] [PubMed]
36. Baxter, E.J.; Scott, L.M.; Campbell, P.J.; East, C.; Fourouclas, N.; Swanton, S.; Vassiliou, G.S.; Bench, A.J.; Boyd, E.M.; Curtin, N.; et al. Acquired mutation of the tyrosine kinase JAK2 in human myeloproliferative disorders. *Lancet* **2005**, *365*, 1054–1061. [CrossRef]
37. Kralovics, R.; Passamonti, F.; Buser, A.S.; Teo, S.S.; Tiedt, R.; Passweg, J.R.; Tichelli, A.; Cazzola, M.; Skoda, R.C. A gain-of-function mutation of JAK2 in myeloproliferative disorders. *N. Engl. J. Med.* **2005**, *352*, 1779–1790. [CrossRef]

38. Ben-Batalla, I.; Erdmann, R.; Jorgensen, H.; Mitchell, R.; Ernst, T.; von Amsberg, G.; Schafhausen, P.; Velthaus, J.L.; Rankin, S.; Clark, R.E.; et al. Axl Blockade by BGB324 Inhibits BCR-ABL Tyrosine Kinase Inhibitor-Sensitive and -Resistant Chronic Myeloid Leukemia. *Clin. Cancer Res. Off. J. Am. Assoc. Cancer Res.* **2017**, *23*, 2289–2300. [CrossRef]
39. Pearson, S.; Blance, R.; Somerville, T.C.P.; Whetton, A.D.; Pierce, A. AXL Inhibition Extinguishes Primitive JAK2 Mutated Myeloproliferative Neoplasm Progenitor Cells. *HemaSphere* **2019**, *3*, e233. [CrossRef] [PubMed]
40. Singh, S.K.; Hawkins, C.; Clarke, I.D.; Squire, J.A.; Bayani, J.; Hide, T.; Henkelman, R.M.; Cusimano, M.D.; Dirks, P.B. Identification of human brain tumour initiating cells. *Nature* **2004**, *432*, 396–401. [CrossRef]
41. Mao, P.; Joshi, K.; Li, J.; Kim, S.H.; Li, P.; Santana-Santos, L.; Luthra, S.; Chandran, U.R.; Benos, P.V.; Smith, L.; et al. Mesenchymal glioma stem cells are maintained by activated glycolytic metabolism involving aldehyde dehydrogenase 1A3. *Proc. Natl. Acad. Sci. USA* **2013**, *110*, 8644–8649. [CrossRef] [PubMed]
42. Sadahiro, H.; Kang, K.D.; Gibson, J.T.; Minata, M.; Yu, H.; Shi, J.; Chhipa, R.; Chen, Z.; Lu, S.; Simoni, Y.; et al. Activation of the Receptor Tyrosine Kinase AXL Regulates the Immune Microenvironment in Glioblastoma. *Cancer Res.* **2018**, *78*, 3002–3013. [CrossRef] [PubMed]

Article

Inhibition of FABP6 Reduces Tumor Cell Invasion and Angiogenesis through the Decrease in MMP-2 and VEGF in Human Glioblastoma Cells

Feng-Cheng Pai ¹, Hsiang-Wei Huang ², Yu-Ling Tsai ³ , Wen-Chiuan Tsai ³ , Yu-Chen Cheng ², Hsin-Han Chang ^{2,*}  and Ying Chen ^{2,*} 

- ¹ Department of Emergency Medicine, Tri-Service General Hospital, National Defense Medical Center, Taipei 11490, Taiwan; ssbb15@gmail.com
- ² Department of Biology and Anatomy, National Defense Medical Center, Taipei 11490, Taiwan; m860502@yahoo.com.tw (H.-W.H.); plokmiizz@gmail.com (Y.-C.C.)
- ³ Department of Pathology, Tri-Service General Hospital, National Defense Medical Center, Taipei 11490, Taiwan; c909228@gmail.com (Y.-L.T.); ab95057@hotmail.com (W.-C.T.)
- * Correspondence: albertchang1008@gmail.com (H.-H.C.); ychen0523@mail.ndmctsgh.edu.tw (Y.C.); Tel.: +886-2-8792-3100 (ext. 18740) (H.-H.C.); +886-2-8792-3100 (ext. 18739) (Y.C.)



Citation: Pai, F.-C.; Huang, H.-W.; Tsai, Y.-L.; Tsai, W.-C.; Cheng, Y.-C.; Chang, H.-H.; Chen, Y. Inhibition of FABP6 Reduces Tumor Cell Invasion and Angiogenesis through the Decrease in MMP-2 and VEGF in Human Glioblastoma Cells. *Cells* **2021**, *10*, 2782. <https://doi.org/10.3390/cells10102782>

Academic Editors: Javier S. Castresana and Bárbara Meléndez

Received: 6 September 2021
Accepted: 13 October 2021
Published: 17 October 2021

Publisher's Note: MDPI stays neutral with regard to jurisdictional claims in published maps and institutional affiliations.



Copyright: © 2021 by the authors. Licensee MDPI, Basel, Switzerland. This article is an open access article distributed under the terms and conditions of the Creative Commons Attribution (CC BY) license (<https://creativecommons.org/licenses/by/4.0/>).

Abstract: Malignant glioma is one of the most lethal cancers with rapid progression, high recurrence, and poor prognosis in the central nervous system. Fatty acid-binding protein 6 (FABP6) is a bile acid carrier protein that is overexpressed in colorectal cancer. This study aimed to assess the involvement of FABP6 expression in the progression of malignant glioma. Immunohistochemical analysis revealed that FABP6 expression was higher in glioma than in normal brain tissue. After the knockdown of FABP6, a decrease in the migration and invasion abilities of glioma cells was observed. The phosphorylation of the myosin light chain was inhibited, which may be associated with migration ability. Moreover, expression levels of invasion-related proteins, matrix metalloproteinase-2 (MMP-2) and cathepsin B, were reduced. Furthermore, tube formation was inhibited in the human umbilical vein endothelial cells with a decreased concentration of vascular endothelial growth factor (VEGF) in the conditioned medium after the knockdown of FABP6. The phosphorylation of the extracellular signal-regulated kinase (ERK), c-Jun NH2-terminal kinase (JNK), and p65 were also decreased after FABP6 reduction. Finally, the bioluminescent images and immunostaining of MMP-2, cluster of differentiation 31 (CD31), and the VEGF receptor 1 (VEGFR1) revealed attenuated tumor progression in the combination of the FABP6-knocked-down and temozolomide (TMZ)-treated group in an orthotopic xenograft mouse tumor model. This is the first study that revealed the impact of FABP6 on the invasion, angiogenesis, and progression of glioma. The results of this study show that FABP6 may be a potential therapeutic target combined with TMZ for malignant gliomas.

Keywords: FABP6; invasion; angiogenesis; glioblastoma

1. Introduction

Gliomas account for the majority of primary tumors that arise within the brain parenchyma and are the most common intracranial neoplasms [1]. According to the 2016 edition of the World Health Organization's (WHO) revised classification, high-grade gliomas include glioblastoma, anaplastic astrocytoma, and anaplastic oligodendroglioma [2]. The initial treatment for high-grade gliomas is surgical resection, if accessible, combined with adjuvant post-operative temozolomide (TMZ)-based chemoradiotherapy. However, due to the infiltration of tumor cells, complete resection and adjuvant therapy are elusive, resulting in a higher percentage of recurrence and worse prognosis in patients with high-grade gliomas than in patients with low-grade gliomas [3].

Fatty acid-binding proteins (FABPs) modulate the metabolism of fatty acids, cell growth, and proliferation. In 2000, Jing et al. revealed that the dysregulation of FABP

plays important roles in carcinogenesis as well as the progression and metastasis of cancer [4]. In carcinoma cell lines, distinct differences were observed in the FABP expression patterns of cells derived from different tumors [5]. FABPs affect tumor progression via specific pathways. In hepatocellular carcinoma (HCC), the upregulated fatty acid-binding protein 1 (FABP1) interacts with the VEGF receptor and Src via the focal adhesion kinase (FAK) and enhances the expression of the angiogenic vascular endothelial growth factor A (VEGF-A) [6]. In addition, FABP4 promotes tumor progression by altering the activities of matrix metalloproteinases (MMPs), especially MMP-2 and MMP-9, in prostate cancer [7]. FABP4 is also associated with the mechanistic target of rapamycin complex 1 (mTORC1) in the human umbilical vein endothelial cells (HUVECs) as well as pro-angiogenic signals including mitogen-activated protein kinase (MAPK), endothelial nitric oxide synthase (eNOS), and stem cell factor (SCF)/c-kit [8]. Accordingly, tumor cells can obtain more oxygen and nutrients and clear waste products, which leads to the growth, progression, and metastasis of cancer.

FABP6, also known as gastrotropin or ileal FABP, can transport bile acids and is highly expressed in the ileum. FABP6 has a higher affinity for bile acids than fatty acids. Previous studies have revealed a link between bile acids, FABP6, and colorectal carcinogenesis in animal models [9]; however, whether the effect of FABP6 on glioma remains unknown. In the central nervous system, fatty acids and FABPs impact the growth and function of the brain [10]. This implies that lipid dysregulation may play a role in glioma development [11]. Accordingly, this is the first study to investigate the role of FABP6 in the progression of glioma.

2. Materials and Methods

2.1. Immunohistochemical Staining of Human Glioma Specimens

A glioma tissue microarray (GL807a; US Biomax Inc, Derwood, MD, USA) was incubated in 5% non-fat milk and with a rabbit anti-human FABP6 monoclonal antibody (Abcam) at 4 °C overnight. After 16 h of incubation, the specimens were incubated with biotin-labeled secondary immunoglobulin and 3-amino-9-ethylcarbazole substrate chromogen (DAKO, Glostrup, Denmark) to observe peroxidase activity.

2.2. Cell Culture

Two human glioma tumor cell lines, LN229 and U87MG, were obtained from American Type Culture Collection (ATCC). The glioma cells were cultured in Roswell Park Memorial Institute (RPMI) 1640 medium supplemented with 10% fetal bovine serum (FBS). HUVECs were obtained from the Bioresource Collection and Research Center in Taiwan and cultured with an endothelial cell medium (ScienCell Research Laboratories, Carlsbad CA, USA). All cells were cultured in an incubator at 37 °C with 5% carbon dioxide (CO₂).

2.3. Antibodies

The information on antibodies is shown in Table 1.

Table 1. Information on the antibodies.

Name	Species	Brand	Catalog Number
Cathepsin B	Rb	Abcam	ab125067
CD31	Rb	Abcam	ab28364
ERK	Rb	Cell Signaling Technology	9102s
FABP6	Rb	Novus	NBP1-32482
FAK	Rb	Cell Signaling Technology	71433s
GAPDH	Rb	Cell Signaling Technology	5174s
JNK	Rb	Cell Signaling Technology	9252s
MLC 2	Rb	Cell Signaling Technology	8505s
MMP2	Rb	Cell Signaling Technology	13132s
MMP9	Rb	Cell Signaling Technology	13667s
P65	Rb	Cell Signaling Technology	8242s

Table 1. Cont.

Name	Species	Brand	Catalog Number
Paxillin	Ms	BD Biosciences	610051
p-ERK	Rb	Cell Signaling Technology	4377s
p-FAK (Y397)	Ms	BD Biosciences	611723
p-JNK	Rb	Cell Signaling Technology	4668s
p-MLC (Ser19)	Rb	Cell Signaling Technology	3671
p-p65	Rb	Abcam	Ab185619
p-paxillin	Rb	Cell Signaling Technology	2541s
TIMP-1	Rb	Abcam	ab109125
TIMP-2	Ms	Millipore	MAB13446
VEGFR1	Rb	Abcam	ab32152
VEGFR2	Rb	Cell Signaling Technology	2479s

Rb and Ms indicated anti-rabbit and anti-mouse, respectively.

2.4. Stable Expression of shRNAs

The shRNA clones (TRCN0000059723, TRCN0000059724, TRCN00000419834, and TRCN00000447012) and lentiviral package vectors (pCMV-dR8.91 and pMD2.G) were obtained by the National RNAi Core Facility at Academia Sinica in Taiwan. The LN229 and U87MG glioma cells were infected with the virus and incubated with puromycin to select the stably infected cells.

2.5. Real-Time Polymerase Chain Reaction (RT-PCR)

Cells were seeded in 12-well plates and treated with a transfection reagent. After 72 h, the culture medium was removed from the plates. Following the cells were lysed by GENEzol™ Reagent, and purified the total RNA by the GENEzol™ TriRNA Pure Kit from Geneaid in Taiwan. Up to 500 ng of total RNA could be reverse transcribed in the reaction mixture, and synthesis of cDNA template was performed using the PrimeScript™ RT reagent Kit (TAKARA Bio Inc, Shiga, Japan) according to the manufacturer's instructions. Real time RT-PCR was carried out by LightCycler® 480 Instrument (Roche, Basel, Swiss) using SensiFAST SYBR (Meridian Bioscience, Cincinnati, OH, USA).

2.6. 3-(4,5-Dimethylthiazol-2-yl)-2,5-diphenyltetrazolium Bromide (MTT) Assay

Both 5×10^3 shScramble and shFABP6 stably expressing LN229 and U87MG glioma cells were cultured in a 96-well plate. The MTT assay was performed after 24, 48, and 72 h to determine the viabilities of cells. The absorbance was measured at 590 nm after 4 h of MTT application.

2.7. Cell Migration and Invasion Assays

Wound healing and transwell assays were performed to assess the migration abilities of tumor cells. In the wound healing assay, LN229 and U87MG glioblastoma cells were seeded in a 6-well plate. Thereafter, a P200 pipette tip was used to scrape cells for imaging after 16 h. The wound area was analyzed using ImageJ software. The transwell migration assay was conducted by seeding 2×10^5 LN229 or U87MG glioblastoma cells in the upper chamber of a Transwell insert (Corning, Midland, NC, USA). After 16 h of incubation, the cells on the lower side were stained and examined under a microscope. The transwell invasion assay was performed by seeding 2×10^4 LN229 or U87MG cells in the upper chamber of the insert. Before seeding, Matrigel (BD, Franklin Lakes, NJ, USA) was added to the upper chamber of a medium for 24 h. After 16 h of incubation, the cells in the lower chamber were fixed and stained with the Coomassie blue dye. The invaded cells were counted in three randomly selected fields from each membrane in six independent experiments.

2.8. Western Blotting

The glioma cells were homogenized by a protein extraction buffer (GE Healthcare Life Sciences, Chicago, IL, USA) applied with proteinase and phosphatase inhibitors (MedChemExpress, Monmouth Junction, NJ, USA). Electrophoresis was performed on a 10% sodium dodecyl sulphate-polyacrylamide gel electrophoresis (SDS-PAGE) gel, and the protein samples were transferred to a nitrocellulose membrane (Bio-Rad, Berkeley, CA, USA). Strips from the membrane were incubated with 5% non-fat milk in Tris-buffered saline (pH 7.4) containing 0.1% Tween (TBS-Tween). The membranes were then incubated in blocking solution with the primary antibodies overnight at 4 °C. After washing, the strips were incubated with a 1:5000 or 1:10,000 dilution of the horseradish peroxidase (HRP)-conjugated anti-rabbit or anti-mouse immunoglobulin G (IgG) antibodies from Cell Signaling Technology. Subsequently, the blots were incubated in the developing solution with the electrochemiluminescence (ECL) substrate (Bio-Rad). The densities of the bands on the membrane were captured and quantified by the ImageJ software. The density of the control sample was set as 100% and the densities of the test samples were relative to that of the internal control. At least six independent experiments were performed.

2.9. Tube Formation Assay

Matrigel (50 µL/well) was added to a 96-well plate and incubated for 1 h at 37 °C before the assay. Thereafter, 1×10^4 HUVECs were incubated with the conditioned medium collected from the 5×10^5 LN229 or U87MG cells in 6-well plates for 48 h. The number of nodes and tubes of the tubular structures after 6 h of incubation was recorded and analyzed using the AngioTool online software. VEGFA121 and VEGFA165 were obtained from Sino Biological Inc in Beijing, China.

2.10. Orthotopic Xenograft Animal Model

All animal experiments were approved by the experimental animal center of the National Defense Medical Center of Taiwan (IACUC No. 19-157). Nude mice with an average weight of 20–25 g were used. After administration of anesthetics, 1×10^5 FABP6 knockdown (clone 724)- or shScramble control (clone 004)-Luc2 cells were implanted into the right hemisphere of mice. Five days after implantation, they were divided into the following four groups: shScramble control, shScramble control plus TMZ, FABP6 knockdown, and FABP6 knockdown group plus TMZ. Body weight was measured every three days, and the tumor size was detected by IVIS spectrum (PerkinElmer, Waltham, MA, USA). TMZ was administered orally on the 6th day lasting for 9 days. After sacrifice, the brain was dissected out and fixed with 10% formalin, embedded in paraffin, and sectioned. The samples were then stained with hematoxylin and eosin (HE).

2.11. Histological and Immunohistochemical Examination

The brain tissues were excised, rinsed twice in phosphate-buffered saline (PBS), and fixed in 10% formaldehyde. Thereafter, the tissues were frozen and sliced into 5 µm thick sections. Then, HE stain was applied to facilitate the histological evaluation. The expression levels of MMP2, cluster of differentiation 31 (CD31), and VEGFR1 were detected in the brain tumors of nude mice by immunohistochemical (IHC) staining. The IHC staining was conducted by Ventana BenchMark ULTRA system (Roche, Basel, Swiss). The primary antibody was diluted in Antibody Dilution Buffer (Ventana). The antigen retrieval was performed according to the manufacturer's standard protocol. The secondary goat anti-rabbit antibodies (Jackson ImmunoResearch Laboratories, West Grove, PA, USA) were used. The aforementioned protein expression was observed in 10 random fields in each group.

2.12. Terminal Deoxynucleotidyl Transferase (TdT) dUTP Nick-End Labeling (TUNEL) Assay

The TUNEL staining was performed according to the manufacturer (In Situ Cell Death Detection Kit, Fluorescein (Roche, Basel, Swiss)). The pictures were photographed with BX51 (Olympus, Tokyo, Japan).

2.13. Enzyme-Linked Immunosorbent Assay (ELISA) for VEGF in Condition Medium

The concentration of VEGF-A was measured by the ELISA Kit (R&D Systems, Minneapolis, MN, USA) according to the manufacturer's instructions. The values detected by ELISA were corrected using a dilution factor and expressed as pg/mL.

2.14. Statistical Analysis

The overall survival data sets obtained from The Cancer Genome Atlas (TCGA) database were analyzed using the Kaplan–Meier method on the Gene Expression Profiling Interactive Analysis (GEPIA) website. All experiments were performed at least three times, and the results are expressed as the mean \pm standard error of the mean (SEM). The differences between means were assessed by the Kruskal–Wallis test. The Mann–Whitney U test was applied for post-hoc analysis. Statistical significance was estimated at $p < 0.05$.

3. Results

3.1. FABP6 Had Higher Expression in Glioma

As shown in Figure 1A, the expression levels of FABP6 were noted in the normal and tumor tissues. The expression of FABP6 was found to be elevated in the neoplastic brain tissue and was not proportional to the grade of the glioma. FABP6 expression was significantly higher in the glioma cell lines (Figure 1B). The relationship between the survival and expression of FABP6 was also analyzed by GEPIA and TCGA database (Figure S1).

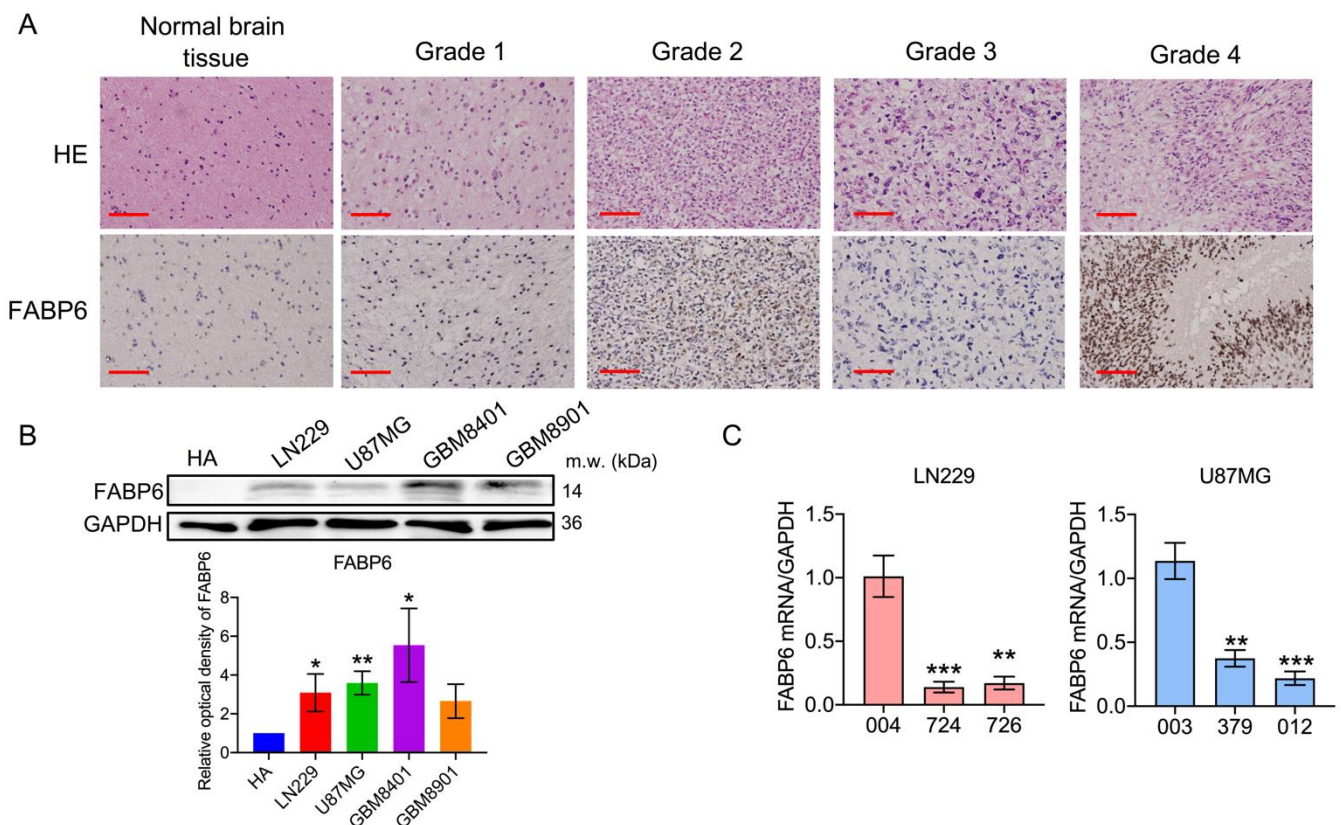


Figure 1. Fatty acid-binding protein 6 (FABP6) expression in human glioblastoma cells: (A) Hematoxylin and eosin (HE) staining (left column) of the normal brain tissue, pilocytic astrocytoma, diffuse astrocytoma, anaplastic astrocytoma, and glioblastoma multiforme. Immunohistological analysis of FABP6 in the right column (original magnification was $\times 400$). Scale bar = 50 μ m. (B) The expression levels of FABP6 in the glioma cell lines were analyzed by Western blotting. GAPDH was used as a loading control. * $p < 0.05$; ** $p < 0.01$ compared with the human astrocytes group. (C) Reverse transcription-polymerase chain reaction (RT-PCR) was used to analyze the mRNA expression of FABP6 after knockdown with shFABP6. ** $p < 0.01$; *** $p < 0.001$ compared with the shScramble control group (004 in LN229 cells and 003 in U87MG cells).

3.2. Analysis of the Expression of FABP and Establishment of shRNA (shFABP6) Stable Clones in Glioma Cell Lines

Stable clones were then established in two cell lines, LN229 and U87MG. The knock-down effects of shFABP6 in the LN229 (724 and 726) and U87MG (379 and 012) cells were confirmed by reverse transcription-polymerase chain reaction (RT-PCR) (Figure 1C). In addition, the protein expression levels of FABP6 in the LN229 and U87MG cells were found to be reduced (Figure S2A). However, cell growth was unaffected between FABP6 knockdown and scramble control groups by MTT assay (Figure S2B) and colony formation (Figure S2C,D).

3.3. Knockdown of FABP6 Decreased the Migration and Invasion Abilities of Invasion-Related Proteins in the LN229 and U87MG Cells

The wound healing assays demonstrated that the cell migration abilities were reduced in glioma cells compared with those in control cells (Figure 2A). In the transwell assays, the migration and invasion abilities decreased significantly after shFABP6 knockdown (Figure 2B). Interestingly, after FABP6 inhibition, the phosphorylation of FAK and paxillin increased. Simultaneously, the expression levels of the phospho-myosin light chain (p-MLC) were significantly reduced in both LN229 and U87MG cells (Figure 3). These results suggested that the decrease in migration abilities by FABP6 knockdown may be associated with the inhibition of MLC in glioma cells.

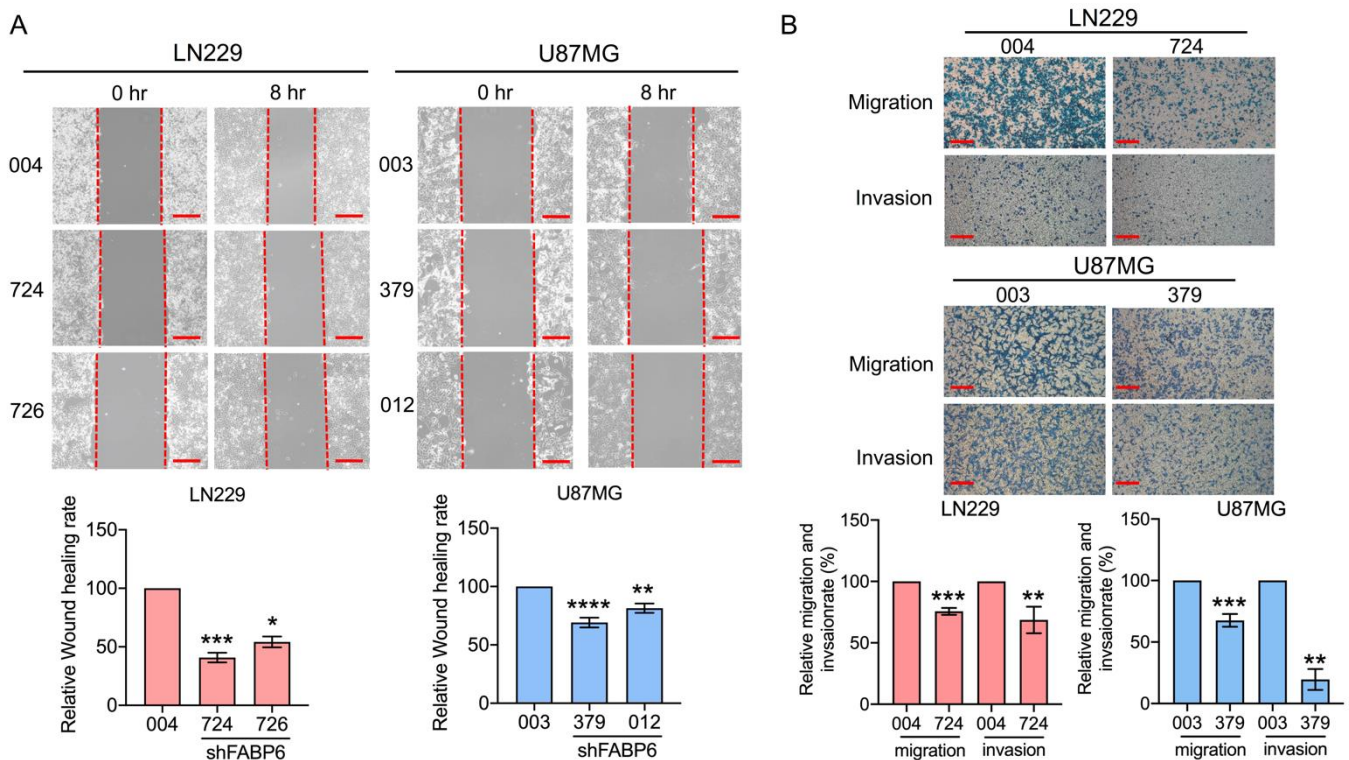


Figure 2. The migration and invasion abilities after the inhibition of FABP6: (A) Wound healing migration assays were performed in two human glioma cell lines, LN229 ($n = 6$) and U87MG ($n = 7$), after 8 h scratch. (B) Transwell migration assays were performed in the LN229 and U87MG cells after 16 h incubation. Thereafter, the cells were stained and captured. * $p < 0.05$; ** $p < 0.01$; *** $p < 0.001$; **** $p < 0.0001$ compared with the shScramble control group (004 in LN229 cells and 003 in U87MG cells). The lower panel displays the relative rate of the transwell migration ability compared to that of the control: 004 and 003 are the shScramble control groups in LN229 and U87MG, 724 and 726 in LN229 cells, and 379 and 012 in U87MG cells were the shFABP knockdown groups. Scale bar = 200 μm .

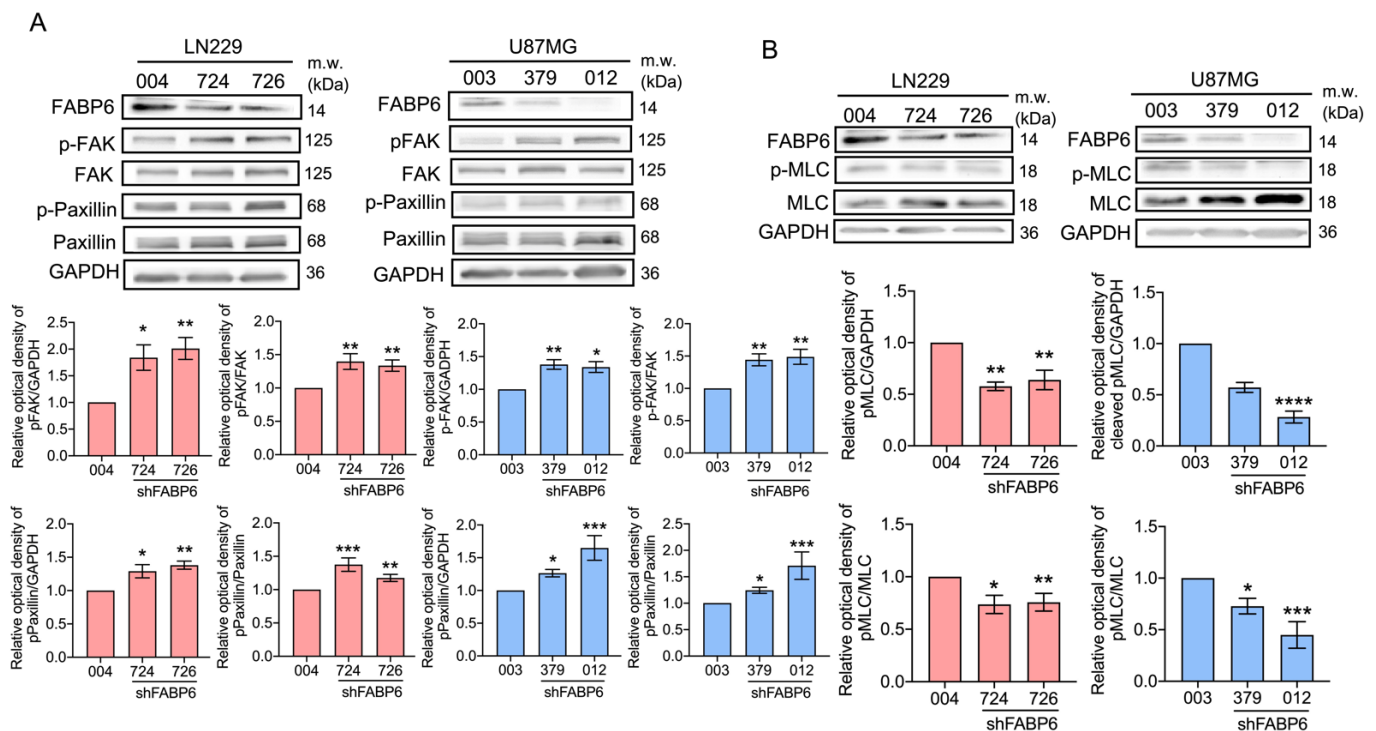


Figure 3. Effects of shFABP6 on the expression levels of the focal adhesion-related proteins in glioma cells: (A) focal adhesion kinase (FAK), phospho-focal adhesion kinase (p-FAK), paxillin, and phospho-paxillin (p-paxillin); (B) myosin light chain (MLC) and phospho-myosin light chain (p-MLC) were analyzed by Western blotting in the LN229 and U87MG cells using the shScramble control group (004 in LN229 cells and 003 in U87MG cells) and shFABP6. Glyceraldehyde-3-phosphate dehydrogenase (GAPDH) was used as the endogenous control. The plotted graphs show the relative quantitative analysis of the aforementioned proteins. * $p < 0.05$; ** $p < 0.01$; *** $p < 0.001$; **** $p < 0.0001$ compared with the shScramble control group.

The invasion-related proteins were investigated after the attenuation of FABP6. After the knockdown of FABP6, there was a significant decrease in the expression levels of active MMP-2 and cathepsin B (Figure 4). In addition, the levels of the tissue inhibitors of metalloproteinases (TIMP)-1 and TIMP-2 decreased after FABP6 reduction in glioma cells (Figure 4). These results implied that the decrease in the migration and invasion abilities after FABP6 knockdown may be due to the reductions in the levels of MMPs and cathepsin B and the enhancement of the TIMPs in glioma cells.

3.4. Tube Formation of Endothelial Cells Was Attenuated by the Knockdown of FABP6 in Glioma Cells

Next, the endothelial network formation was analyzed after FABP6 knockdown in glioma cells. As shown in Figure 5A, angiogenesis ability, including branch points and tube length, was reduced in the shFABP6 groups. Furthermore, the expression levels of VEGF in the glioma conditioned medium (CM) were examined. The concentration of VEGF in CM decreased significantly after FABP6 inhibition compared to that in the scramble control (Figure 5B). Moreover, the expression levels of VEGFR1 and VEGFR2 were significantly reduced after FABP6 inhibition in glioma cells (Figure 5C). The addition of VEGFA reversed the tube formation ability in shFABP6 group (Figure S3). These results indicated that the angiogenic ability of endothelial cells was decreased by FABP6 knockdown in glioma cells, which might be due to the decrease in VEGF secretion in glioma cells.

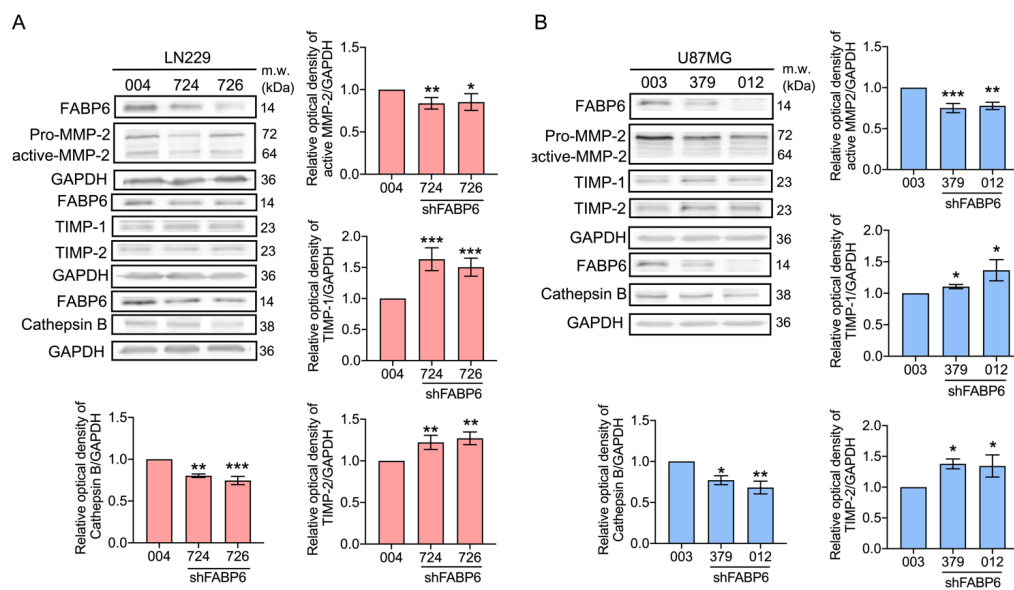


Figure 4. Effects of shFABP6 on the expression levels of the extracellular matrix (ECM) degradation-associated proteins in LN229 and U87MG cells. The expression levels of matrix metalloproteinases-2 (MMP-2), tissue inhibitor of metalloproteinase-1 (TIMP-1), tissue inhibitor of metalloproteinase-2 (TIMP-2), and cathepsin B were analyzed by Western blotting in the LN229 (A) and U87MG cells (B) using the shScramble control group (004 and 003) and shFABP6. GAPDH was used as the loading control. The plotted graphs show the relative quantitative analysis of the aforementioned proteins. * $p < 0.05$; ** $p < 0.01$; *** $p < 0.001$ compared with the shScramble control group.

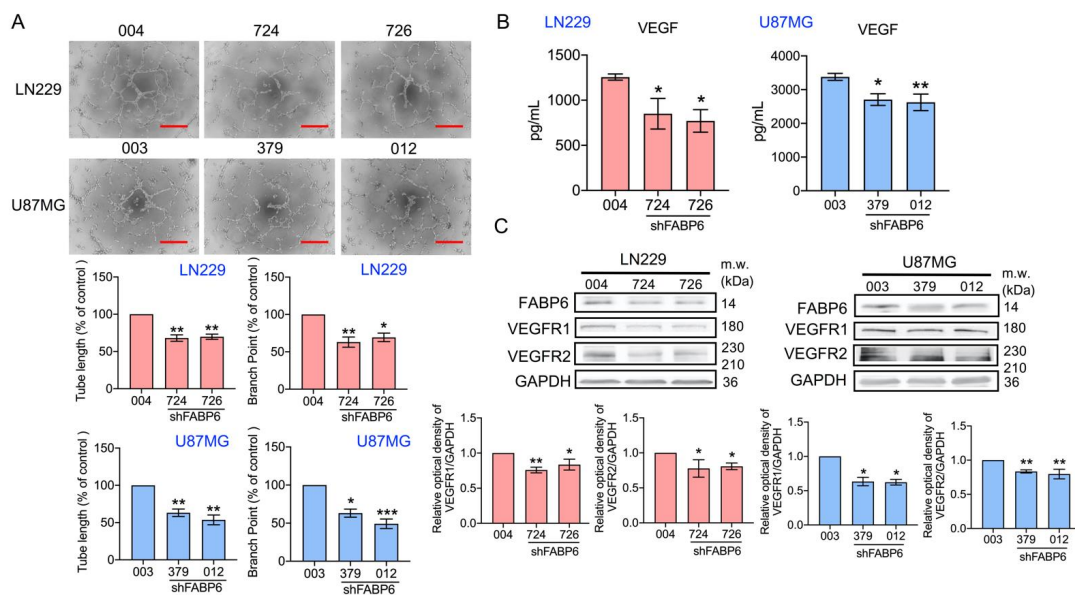


Figure 5. The effect of the knockdown of FABP6 on angiogenesis. The human umbilical vein endothelial cells (HUVECs) were cultured with an FABP6 knockdown conditioned medium (CM) or scramble control CM of glioma cells for 6 h. (A) The formation of an endothelial cell network was observed and the number of branch points and tube length in the LN229 and U87MG CM were analyzed. The plotted graphs show the relative attenuation of branch points and tube lengths in the FABP6 knockdown CM compared with those in the scramble control group. Scale bar = 200 μ m. (B) The concentration levels of vascular endothelial growth factors (VEGFs) in the CM of LN229 and U87MG cells were analyzed by the enzyme-linked immunosorbent assay (ELISA). (C) The expression levels of the vascular endothelial growth factor receptor 1 (VEGFR1) and vascular endothelial growth factor receptor 2 (VEGFR2) were analyzed by Western blotting in the LN229 and U87MG cells using the shScramble control group and shFABP6. GAPDH was used as the loading control. The plotted graphs show the relative quantitative analysis of the aforementioned proteins. * $p < 0.05$; ** $p < 0.01$; *** $p < 0.001$ compared with the shScramble control group.

3.5. The Reduced Phosphorylation of JNK, ERK, and p65 Was Caused by FABP6 Inhibition

As the phosphorylation of extracellular signal-regulated kinase (ERK) and c-Jun NH2-terminal kinase (JNK) promotes glioma cell invasion and migration [12], we examined the p-ERK and p-JNK expression after FABP6 knockdown. In both the LN229 and U87MG cell lines, p-JNK and p-ERK decreased with FABP6 attenuation (Figure 6A). NF- κ B is activated in malignant glioma and anti-p65 antibodies inhibit invasion and angiogenesis in glioma cells [13,14]. The p-p65 expression decreased significantly after FABP6 inhibition in the LN229 and U87MG cells (Figure 6B). The decreased expression levels of p-JNK, p-ERK, and p-p65 may attenuate invasion and angiogenesis in glioma cells.

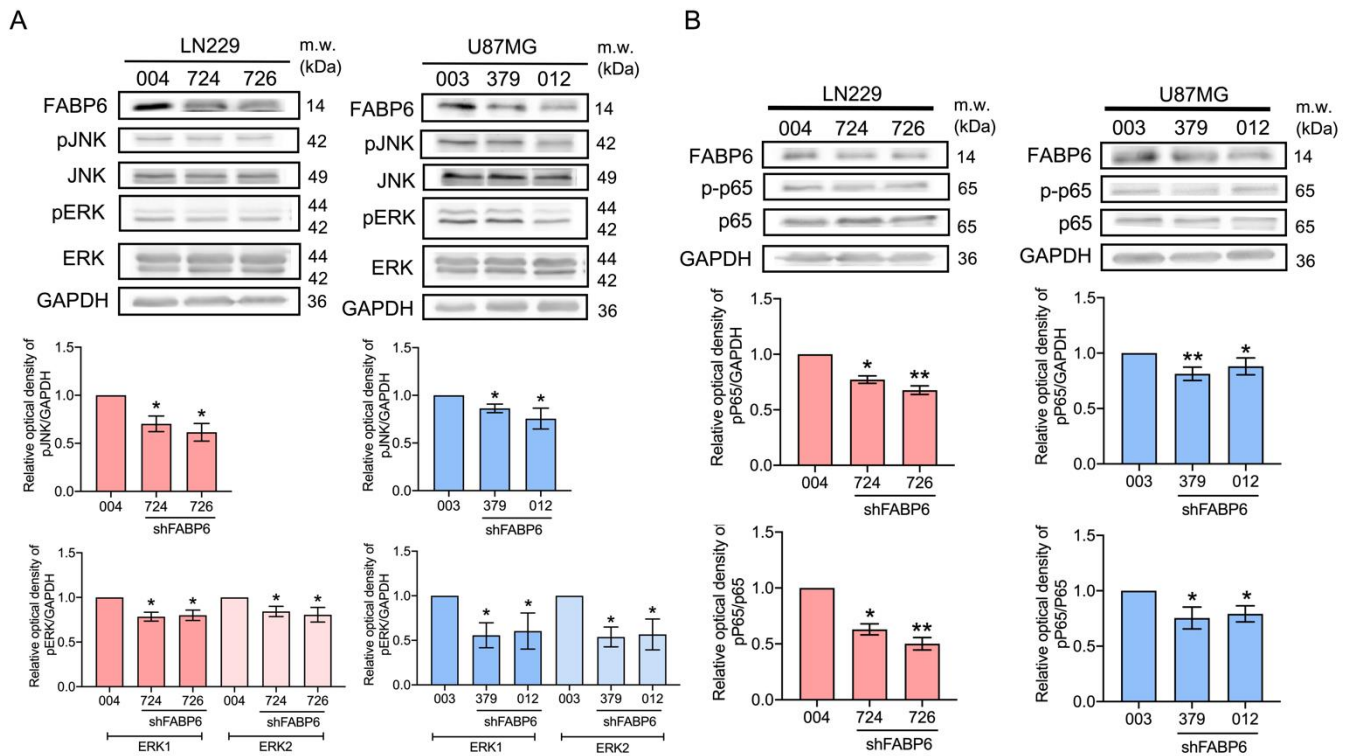


Figure 6. Effects of c-Jun NH2-terminal kinase (JNK), extracellular signal-regulated kinase (ERK), and p65 after FABP6 knockdown. The expression levels of phospho-c-Jun NH2-terminal kinase (p-JNK), JNK, phospho-extracellular signal-regulated kinase (p-ERK), ERK (A), phospho-p65 (p-p65), and p65 (B) were analyzed by Western blotting in the LN229 and U87MG cells using the shScramble control group and shFABP6. GAPDH was used as the loading control. The plotted graphs show the relative quantitative analysis of the aforementioned proteins. * $p < 0.05$ and ** $p < 0.01$ compared with the shScramble control group.

3.6. FABP6 Knockdown Combined with TMZ Application Attenuated Tumor Progression in the Orthotropic Xenograft Model

FABP6 reduction did not affect the survival rate of LN229 glioma cells compared to that of control cells. When FABP6 knockdown combined with 100 μ M TMZ for 48 h, the survival rate declined significantly compared with the CTL + TMZ group, indicating a synergistic effect of FABP6 inhibition and TMZ application (Figure 7A). An orthotropic xenograft mouse model was then used to verify the in vitro findings. The average body weight did not differ between the different groups (Figure 7B). After 15 days, the bioluminescence images were captured using an IVIS system (Figure 7C). When FABP6 knockdown was combined with TMZ treatment, the tumor regressed significantly compared to the CTL group (Figure 7D). Moreover, the expression of MMP-2, CD31, and VEGFR1 decreased in the FABP6 knockdown combined with the TMZ group (Figure 7E). In addition, FABP6 inhibition combined with TMZ induced more apoptotic cells than those in the control

group by TUNEL staining (Figure S4). These results indicated that FABP6 knockdown combined with TMZ attenuates tumor progression in animal models.

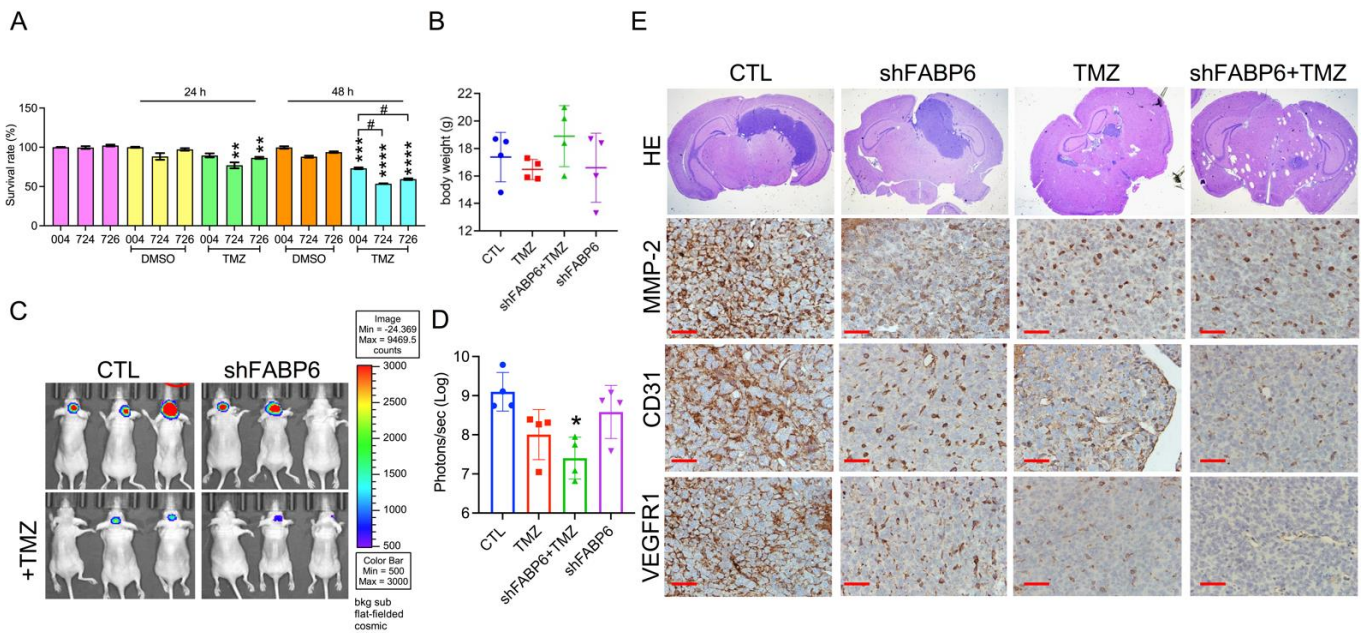


Figure 7. The effect of FABP6 knockdown on the tumor progression of LN229 cells in an orthotopic xenograft mouse model: (A) the survival rates of the glioma cell line in scrambled cytotoxic T lymphocyte (CTL) and shFABP6 combined with or without 100 μ M temozolomide (TMZ) for 24 and 48 h ($n = 6$); (B) the body weights of animals are shown; (C) the effects of different groups on the size and growth of tumors were observed using bioluminescent imaging with an in vivo imaging system (IVIS); (D) quantification of the bioluminescence data in different groups; (E) HE staining of the xenograft orthotopic brain tissues. * $p < 0.05$; ** $p < 0.01$; *** $p < 0.001$; **** $p < 0.0001$ compared with the DMSO control group. # $p < 0.05$ compared with shScramble control + TMZ group. Scale bar = 50 μ m.

4. Discussion

A FABP6 has been reported to be a cancer-related protein in colorectal cancer [9,15]. According to our results, the expression of FABP6 in gliomas was higher than normal tissue. Therefore, further investigation of the role of FABP6 in malignant glioma is imperative. However, most studies of fatty acid binding protein in glioma were limited to FABP7, which was found to be overexpressed and thought to be involved in tumor proliferation, invasion, and migration [10]. The significance of FABP6 attracts researcher’s interest as a regulator of cholesterol metabolism in gastrointestinal cancer [15]. Recently, targeting a cholesterol pathway has been proposed in anti-glioblastoma therapy [16]. Elsherbiny et al. reveals that these glioma properties might be related to fatty acid metabolism [17]. Therefore, the knockdown of FABP6 blocked migration, invasion, and angiogenesis, which may be associated with bile acid metabolism.

The attenuation of FABP6 inhibited the migration of malignant glioma cells. Herein, we analyzed the migration-related proteins to determine the impact of FABP on tumor migration. It is known that the regulation of MLC affects cell migration [18]. Further, the expression of phosphorylated MLC and ERK decreased after knocking down FABP6. This implies that tumor migration might be enhanced via ERK and myosin light-chain phosphorylation pathways. In breast cancer, the activation of myosin light-chain kinase (MLCK) leads to MLC phosphorylation, which promotes cancer cell migration via the ERK signaling pathway [19]. Notably, even the expression levels of phosphorylated FAK and paxillin, which are associated with cell motility and adhesion [20], increased after FABP6 knockdown. Further, the migration ability of the neoplasm was still inhibited. Such finding indicated that phosphorylation of paxillin may inhibit cell motility, which is similar to another study that investigated the role of phosphorylated paxillin in normal murine

mammary gland epithelial cells [21]. These contradictory results indicate that FABP6 may regulate cell migration through other signaling molecules or cascades, and further research is required.

As mentioned earlier, the expression of MMP-2 and cathepsin B was significantly reduced after FABP6 knockdown in our study. Conversely, TIMP-1 expression was increased. These proteins are known to be associated with tumor invasion. MMPs mediate the breakdown of the basal membrane, degrade the extracellular matrix, and create a microenvironment that enhances tumor cell survival [22]. On the other hand, TIMPs serve as inhibitors of MMPs. In oral squamous cell carcinoma, FABP5 regulates MMP-9 expression and tumor invasion [23]. Overexpression of FABP4 in prostate cancer results in the upregulation of MMP-2 and MMP-9, which promotes the invasion of cancer cells [7]. In a cerebral ischemia injury model, FABP4 promotes MMP-9 expression through JNK/c-Jun signaling [24]. In colon cancer, FABP4 enhances epithelial–mesenchymal transition and the associated proteins, including MMP-2, MMP-9, and E-cadherin via the AKT pathway [25]. Cathepsin B, which plays a role in neoplastic invasiveness and neovascularization, can be activated by NF- κ B in osteosarcoma [26]. In addition, inhibition of NF- κ B in glioma cells decreases MMP-9 and VEGF expression, leading to invasion and angiogenesis blockade [14]. In our study, p-JNK and p-p65 were decreased as FABP6 was reduced, which may inhibit MMP-2 and cathepsin B expression in glioma. Collectively, the reduction in p-ERK, p-JNK, and p-65 impaired tumor progression in FABP6 inhibition.

The combination of FABP6 inhibition and TMZ reduced cell survival in LN229 cells (Figure 7A). Perazzoli et al. has been reported that TMZ treatment induced cell cycle arrest at G2/M phase in LN229 cells [27]. In addition, by causing DNA damage, TMZ treatment leads to apoptosis in LN229 cells [28]. The possible combination effect on cell survival reduction may be due to the apoptosis by cleaved PARP expression (data not shown) and TUNEL positive cells in FABP6 knockdown combined with TMZ group (Figure S4). These results suggest that FABP6 inhibition may enhance the sensitivity of TMZ treatment in GBM cells.

Conventional GBM therapies lack potent drugs targeting the lipid metabolism pathway [16]. Our results suggest targeting FABP6 combined with TMZ can ameliorate glioma proliferation and migration. Pharmacological agents to modify FABP function has been proposed with tissue-specific or cell-type-specific control of lipid pathways [29]. In addition, targeting cholesterol synthesis in brain tumors might render their proliferation without compromising cell viability in other organs [16]. However, only inhibitors for FABP4 are available for research [29]. Animal studies reveal ideal response to FABP4 inhibitors in asthma, obesity, and type 2 diabetes mellitus without significant toxicity [30,31]. For targeting FABP6 in glioma patient therapy, specific FABP6 inhibitors or research into other modulators of the FABP6 pathway is recommended.

After knockdown of FABP6, angiogenesis was attenuated in HUVECs, accompanied by the decreased expression levels in VEGF in the CM and VEGFRs in glioma cells. A previous study indicated that FABP5 promotes tumor angiogenesis and activates the VEGF-A pathway in HCC via the peroxisome proliferator-activated receptor α (PPAR α)-dependent pathway [32]. In addition, liver FABP1 interacts with VEGFR2 in HCC, further activating specific pathways, and results in VEGF-A upregulation, thereby promoting angiogenesis and tumor migration [33]. Moreover, FABP4 has been reported to serve as a target of the VEGF/VEGFR2 signaling pathway in endothelial cells and affects vascular sprouting in ovarian cancer [34]. Taken together, the results of this study indicate that FABP6 may interact with the VEGF/VEGFR signaling pathway to control angiogenesis in gliomas; however, this needs to be investigated in future studies.

5. Conclusions

This is the first study to investigate the role of FABP6 in malignant glioma. In our study, the knockdown of FABP6 resulted in the inhibition of the invasion, migration, and

angiogenesis in glioma. These findings indicated that FABP6 may serve as a potential target for therapeutic strategies in gliomas in the future.

Supplementary Materials: The following are available online at <https://www.mdpi.com/article/10.3390/cells10102782/s1>, Figure S1: The correlation of FABP6 expression and survival time; Figure S2: Establishment of the fatty acid-binding protein 6 (FABP6)-attenuated glioma cell lines; Figure S3: The effect of VEGFA application on tube formation in FABP6 knockdown LN229 cells; Figure S4: TUNEL staining of the xenograft orthotropic brain tissues.

Author Contributions: All authors have contributed to this article significantly. Writing—original draft preparation, F.-C.P. and H.-W.H.; Methodology, Y.-C.C., H.-H.C., Y.-L.T. and W.-C.T.; Supervision, H.-H.C. and Y.C.; Funding Acquisition, Y.C. All authors have read and agreed to the published version of the manuscript.

Funding: This research was funded by the Ministry of National Defense—Medical Affairs Bureau (grant number: MND-MAB-110-001 and -003).

Institutional Review Board Statement: All animal experiments were approved by the experimental animal center of the National Defense Medical Center of Taiwan (IACUC No. 19-157).

Informed Consent Statement: Not applicable.

Data Availability Statement: The data presented in this study are available on request from the corresponding author.

Acknowledgments: We appreciate the Instrument Center and Animal Center at the National Defense Medical Center in Taiwan for the technical assistance and animal care. We also thank the National RNAi Core Facility at Academia Sinica in Taiwan for offering the shRNA reagents and related services.

Conflicts of Interest: All authors declare no conflict of interest.

References

- Ostrom, Q.T.; Bauchet, L.; Davis, F.G.; Deltour, I.; Fisher, J.L.; Langer, C.E.; Pekmezci, M.; Schwartzbaum, J.A.; Turner, M.C.; Walsh, K.M.; et al. The epidemiology of glioma in adults: A “state of the science” review. *Neuro-Oncology* **2014**, *16*, 896–913. [CrossRef]
- Louis, D.N.; Perry, A.; Reifenberger, G.; von Deimling, A.; Figarella-Branger, D.; Cavenee, W.K.; Ohgaki, H.; Wiestler, O.D.; Kleihues, P.; Ellison, D.W. The 2016 World Health Organization Classification of Tumors of the Central Nervous System: A summary. *Acta Neuropathol.* **2016**, *131*, 803–820. [CrossRef]
- Das, S.; Marsden, P.A. Angiogenesis in glioblastoma. *N. Engl. J. Med.* **2013**, *369*, 1561–1563. [CrossRef]
- Jing, C.; Beesley, C.; Foster, C.S.; Rudland, P.S.; Fujii, H.; Ono, T.; Chen, H.; Smith, P.H.; Ke, Y. Identification of the messenger RNA for human cutaneous fatty acid-binding protein as a metastasis inducer. *Cancer Res.* **2000**, *60*, 2390–2398.
- Tolle, A.; Suhail, S.; Jung, M.; Jung, K.; Stephan, C. Fatty acid binding proteins (FABPs) in prostate, bladder and kidney cancer cell lines and the use of IL-FABP as survival predictor in patients with renal cell carcinoma. *BMC Cancer* **2011**, *11*, 302. [CrossRef]
- Amiri, M.; Yousefnia, S.; Seyed Forootan, F.; Peymani, M.; Ghaedi, K.; Nasr Esfahani, M.H. Diverse roles of fatty acid binding proteins (FABPs) in development and pathogenesis of cancers. *Gene* **2018**, *676*, 171–183. [CrossRef]
- Huang, M.; Narita, S.; Inoue, T.; Koizumi, A.; Saito, M.; Tsuruta, H.; Numakura, K.; Satoh, S.; Nanjo, H.; Sasaki, T.; et al. Fatty acid binding protein 4 enhances prostate cancer progression by upregulating matrix metalloproteinases and stromal cell cytokine production. *Oncotarget* **2017**, *8*, 111780–111794. [CrossRef]
- Elmasri, H.; Ghelfi, E.; Yu, C.W.; Traphagen, S.; Cernadas, M.; Cao, H.; Shi, G.P.; Plutzky, J.; Sahin, M.; Hotamisligil, G.; et al. Endothelial cell-fatty acid binding protein 4 promotes angiogenesis: Role of stem cell factor/c-kit pathway. *Angiogenesis* **2012**, *15*, 457–468. [CrossRef] [PubMed]
- Ohmachi, T.; Inoue, H.; Mimori, K.; Tanaka, F.; Sasaki, A.; Kanda, T.; Fujii, H.; Yanaga, K.; Mori, M. Fatty acid binding protein 6 is overexpressed in colorectal cancer. *Clin. Cancer Res.* **2006**, *12*, 5090–5095. [CrossRef] [PubMed]
- De Rosa, A.; Pellegatta, S.; Rossi, M.; Tunici, P.; Magnoni, L.; Speranza, M.C.; Malusa, F.; Miragliotta, V.; Mori, E.; Finocchiaro, G.; et al. A radial glia gene marker, fatty acid binding protein 7 (FABP7), is involved in proliferation and invasion of glioblastoma cells. *PLoS ONE* **2012**, *7*, e52113. [CrossRef] [PubMed]
- Martin, D.D.; Robbins, M.E.; Spector, A.A.; Wen, B.C.; Hussey, D.H. The fatty acid composition of human gliomas differs from that found in nonmalignant brain tissue. *Lipids* **1996**, *31*, 1283–1288. [CrossRef]
- McCubrey, J.A.; Steelman, L.S.; Chappell, W.H.; Abrams, S.L.; Wong, E.W.; Chang, F.; Lehmann, B.; Terrian, D.M.; Milella, M.; Tafuri, A.; et al. Roles of the Raf/MEK/ERK pathway in cell growth, malignant transformation and drug resistance. *Biochim. Biophys. Acta* **2007**, *1773*, 1263–1284. [CrossRef] [PubMed]

13. Wang, H.; Wang, H.; Zhang, W.; Huang, H.J.; Liao, W.S.; Fuller, G.N. Analysis of the activation status of Akt, NFkappaB, and Stat3 in human diffuse gliomas. *Lab. Investig.* **2004**, *84*, 941–951. [CrossRef] [PubMed]
14. Puliyappadamba, V.T.; Hatanpaa, K.J.; Chakraborty, S.; Habib, A.A. The role of NF-kappaB in the pathogenesis of glioma. *Mol. Cell Oncol.* **2014**, *1*, e963478. [CrossRef] [PubMed]
15. Zhang, Y.; Zhao, X.; Deng, L.; Li, X.; Wang, G.; Li, Y.; Chen, M. High expression of FABP4 and FABP6 in patients with colorectal cancer. *World J. Surg. Oncol.* **2019**, *17*, 171. [CrossRef] [PubMed]
16. Ahmad, F.; Sun, Q.; Patel, D.; Stommel, J.M. Cholesterol metabolism: A potential therapeutic target in glioblastoma. *Cancers* **2019**, *11*, 146. [CrossRef]
17. Elsherbiny, M.E.; Emara, M.; Godbout, R. Interaction of brain fatty acid-binding protein with the polyunsaturated fatty acid environment as a potential determinant of poor prognosis in malignant glioma. *Prog. Lipid Res.* **2013**, *52*, 562–570. [CrossRef] [PubMed]
18. Totsukawa, G.; Wu, Y.; Sasaki, Y.; Hartshorne, D.J.; Yamakita, Y.; Yamashiro, S.; Matsumura, F. Distinct roles of MLCK and ROCK in the regulation of membrane protrusions and focal adhesion dynamics during cell migration of fibroblasts. *J. Cell Biol.* **2004**, *164*, 427–439. [CrossRef]
19. Zhou, X.; Liu, Y.; You, J.; Zhang, H.; Zhang, X.; Ye, L. Myosin light-chain kinase contributes to the proliferation and migration of breast cancer cells through cross-talk with activated ERK1/2. *Cancer Lett.* **2008**, *270*, 312–327. [CrossRef]
20. Lopez-Colome, A.M.; Lee-Rivera, I.; Benavides-Hidalgo, R.; Lopez, E. Paxillin: A crossroad in pathological cell migration. *J. Hematol. Oncol.* **2017**, *10*, 50. [CrossRef]
21. Yano, H.; Uchida, H.; Iwasaki, T.; Mukai, M.; Akedo, H.; Nakamura, K.; Hashimoto, S.; Sabe, H. Paxillin alpha and Crk-associated substrate exert opposing effects on cell migration and contact inhibition of growth through tyrosine phosphorylation. *Proc. Natl. Acad. Sci. USA* **2000**, *97*, 9076–9081. [CrossRef]
22. Deryugina, E.I.; Quigley, J.P. Tumor angiogenesis: MMP-mediated induction of intravasation- and metastasis-sustaining neovasculature. *Matrix. Biol.* **2015**, *44–46*, 94–112. [CrossRef]
23. Fang, L.Y.; Wong, T.Y.; Chiang, W.F.; Chen, Y.L. Fatty-acid-binding protein 5 promotes cell proliferation and invasion in oral squamous cell carcinoma. *J. Oral. Pathol. Med.* **2010**, *39*, 342–348. [CrossRef]
24. Liao, B.; Geng, L.; Zhang, F.; Shu, L.; Wei, L.; Yeung, P.K.K.; Lam, K.S.L.; Chung, S.K.; Chang, J.; Vanhoutte, P.M.; et al. Adipocyte fatty acid-binding protein exacerbates cerebral ischaemia injury by disrupting the blood-brain barrier. *Eur. Heart J.* **2020**, *41*, 3169–3180. [CrossRef]
25. Tian, W.; Zhang, W.; Zhang, Y.; Zhu, T.; Hua, Y.; Li, H.; Zhang, Q.; Xia, M. FABP4 promotes invasion and metastasis of colon cancer by regulating fatty acid transport. *Cancer Cell Int.* **2020**, *20*, 512. [CrossRef]
26. Hamer, I.; Delaive, E.; Dieu, M.; Abdel-Sater, F.; Mercy, L.; Jadot, M.; Arnould, T. Up-regulation of cathepsin B expression and enhanced secretion in mitochondrial DNA-depleted osteosarcoma cells. *Biol. Cell* **2009**, *101*, 31–41. [CrossRef]
27. Perazzoli, G.; Prados, J.; Ortiz, R.; Caba, O.; Cabeza, L.; Berdasco, M.; Gonzalez, B.; Melguizo, C. Temozolomide Resistance in Glioblastoma Cell Lines: Implication of MGMT, MMR, P-Glycoprotein and CD133 Expression. *PLoS ONE* **2015**, *10*, e0140131. [CrossRef]
28. Hermisson, M.; Klumpp, A.; Wick, W.; Wischhusen, J.; Nagel, G.; Roos, W.; Kaina, B.; Weller, M. O6-methylguanine DNA methyltransferase and p53 status predict temozolomide sensitivity in human malignant glioma cells. *J. Neurochem.* **2006**, *96*, 766–776. [CrossRef] [PubMed]
29. Furuhashi, M.; Hotamisligil, G.S. Fatty acid-binding proteins: Role in metabolic diseases and potential as drug targets. *Nat. Rev. Drug Discov.* **2008**, *7*, 489–503. [CrossRef] [PubMed]
30. Furuhashi, M.; Tuncman, G.; Görgün, C.Z.; Makowski, L.; Atsumi, G.; Vaillancourt, E.; Kono, K.; Babaev, V.R.; Fazio, S.; Linton, M.F. Treatment of diabetes and atherosclerosis by inhibiting fatty-acid-binding protein aP2. *Nature* **2007**, *447*, 959–965. [CrossRef]
31. Sulsky, R.; Magnin, D.R.; Huang, Y.; Simpkins, L.; Taunk, P.; Patel, M.; Zhu, Y.; Stouch, T.R.; Bassolino-Klimas, D.; Parker, R. Potent and selective biphenyl azole inhibitors of adipocyte fatty acid binding protein (aFABP). *Bioorganic Med. Chem. Lett.* **2007**, *17*, 3511–3515. [CrossRef] [PubMed]
32. Pan, L.; Xiao, H.; Liao, R.; Chen, Q.; Peng, C.; Zhang, Y.; Mu, T.; Wu, Z. Fatty acid binding protein 5 promotes tumor angiogenesis and activates the IL6/STAT3/VEGFA pathway in hepatocellular carcinoma. *Biomed. Pharm.* **2018**, *106*, 68–76. [CrossRef] [PubMed]
33. Ku, C.Y.; Liu, Y.H.; Lin, H.Y.; Lu, S.C.; Lin, J.Y. Liver fatty acid-binding protein (L-FABP) promotes cellular angiogenesis and migration in hepatocellular carcinoma. *Oncotarget* **2016**, *7*, 18229–18246. [CrossRef]
34. Harjes, U.; Bridges, E.; Gharpure, K.M.; Roxanis, I.; Sheldon, H.; Miranda, F.; Mangala, L.S.; Pradeep, S.; Lopez-Berestein, G.; Ahmed, A.; et al. Antiangiogenic and tumour inhibitory effects of downregulating tumour endothelial FABP4. *Oncogene* **2017**, *36*, 912–921. [CrossRef]

MDPI AG
Grosspeteranlage 5
4052 Basel
Switzerland
Tel.: +41 61 683 77 34

Cells Editorial Office
E-mail: cells@mdpi.com
www.mdpi.com/journal/cells



Disclaimer/Publisher's Note: The title and front matter of this reprint are at the discretion of the Guest Editors. The publisher is not responsible for their content or any associated concerns. The statements, opinions and data contained in all individual articles are solely those of the individual Editors and contributors and not of MDPI. MDPI disclaims responsibility for any injury to people or property resulting from any ideas, methods, instructions or products referred to in the content.



Academic Open
Access Publishing

mdpi.com

ISBN 978-3-7258-2935-4